SDC-91-104

SDC
SOLENOIDAL DETECTOR NOTES

CENTRAL AND FORWARD TRACKING COLLABORATION PROGRESS REPORT FOR FY 1991

September 13, 1991

R. Foster, G. Hanson, F. Luehring, X. Luo, B. Martin, H. Ogren, D. R. Rust and E. Wente
Indiana University

B. Adrian, D. Alexander, F. Ells, E. Erdos, W. T. Ford, D. Johnson, M. Lohner, P. Rankin and G. Schultz
University of Colorado

F.M. Newcomer, R. Van Berg and H.H. Williams
University of Pennsylvania

Y. Arai
KEK National Laboratory

D. Hess, J.A. Kadyk, A. P. T. Palounek and J. Wise
Lawrence Berkeley Laboratory & University of California, Berkeley

J.W. Chapman and A. Dunn
University of Michigan

M. Edwards, J.W. Hiddleston and B. T. Payne
Rutherford Appleton Laboratory

C.A. Amery, J.M. Bailey, J.B. Dainton, E. Gabathuler, S.J. Maxfield, J.M. Morton, A. Muir, G.D. Patel and P. Sanders
University of Liverpool

C. Raine and D.H. Saxon
University of Glasgow

D.T. Hackworth and R.L. Swensrud
Westinghouse Science and Technology Center

J. Mayhall, T. Ryan, J. Shaffer and D. Vandergriff
Oak Ridge National Laboratory

S. Newfield and C. Sadler
Los Alamos National Laboratory

J. Va'vra
Stanford Linear Accelerator Center

OUTLINE OF PROGRESS REPORT

I. INTRODUCTION

The goal of this subsystem R&D project is to carry out a detailed study and design of a complete wire chamber tracking system covering pseudorapidity $|\eta| \leq 2.5$ in a solenoidal detector for the SSC. Most of our group are now part of the Solenoidal Detector Collaboration (SDC), so the work has evolved into developing a tracking system conceptual design for the SDC detector.

The tracking system requirements are the measurement of momentum and fast triggering over $|\eta| \leq 2.5$. The project includes drift cell designs, engineering of a precise mechanical support structure, evaluation of front end and triggering electronics, design of connections for high voltage, gas and electronics, and computer simulation of the tracking system. The collaboration consists of physicists and engineers from Indiana University, the University of Colorado, the University of Pennsylvania, KEK National Laboratory (Japan), Lawrence Berkeley Laboratory (LBL) and the University of California, Berkeley, University of Michigan, Rutherford Appleton Laboratory (U.K.), University of Liverpool (U.K.), University of Glasgow (U.K.), Westinghouse Science and Technology Center (WSTC), Oak Ridge National Laboratory (ORNL), Los Alamos National Laboratory (LANL), and the Stanford Linear Accelerator Center (SLAC).

The design discussed in this report uses straw tube drift chambers for the central tracking region. Because of the high rates in the SSC environment, a small cell design is needed for wire chambers in the central region. Straw tubes as small cells offer many advantages because the sense wire is enclosed in a continuous cathode, and the wire tension due to the sense wire only can be supported without a massive structure. The straw tubes are grouped together to form superlayers in order to provide local track segments. The superlayers are composed of modules consisting of about two hundred straw tubes enclosed in a carbon fiber composite shell. Straw tubes have been used in previous experiments for small vertex drift chambers. However, they have never before been used for a large tracking system.

During the past year we have built several prototype straw modules. These allow us to develop all aspects of the design and construction. We are presently carrying out the design and fabrication of a full-scale module. The prototype modules are under test at several of the institutions (Indiana University, KEK, University of Colorado, University of

Michigan, and University of Pennsylvania). We are measuring positioning accuracy of the wires, chamber spatial resolution, attenuation length, effects of aging and radiation damage, and evaluating designs for interfacing of the wires to the electronics.

This tracking system design requires the novel use of materials, such as carbon fiber composites, on a large scale in order to provide the necessary structural rigidity and alignment with as little material as possible. Our group includes engineers at the Westinghouse Science and Technology Center and Oak Ridge National Laboratory, who are carrying out design work in this area. The engineering work also includes design of the structure to support the modules, as well as costing and scheduling activities for constructing an SDC tracking system.

We are evaluating prototypes of front end and triggering electronics, developed at the University of Pennsylvania, KEK, the University of Michigan, and the University of Colorado, on prototype wire chambers. We are investigating the layout and interfacing of the electronics on the chamber, including any on-chamber signal processing.

The U.K. groups are developing tracking detection for the intermediate angle region ($1.6 < |\eta| < 2.5$). During the past year a radial wire chamber wedge prototype was built and tested.

We are continuing our computer simulation studies of the tracking system. As is well known, tracking at the SSC will be difficult because of the high rates and small bunch spacing. For these studies we include the integration of a silicon detector at smaller radius. Computer simulation studies were carried out by groups at Indiana University, University of Colorado, LBL, University of Michigan, and the University of Liverpool. During the past year we investigated stereo layers, pattern recognition algorithms, and track fitting procedures. We also included our simulation software in the SDC simulation/analysis package and studied effects of material in and near the tracking volume. The performance of the trigger algorithm was studied using the complete simulation package. The performance of the intermediate angle tracking system was also simulated.

We are working towards the goal of fabricating full-scale prototypes of sections of the tracking system for beam tests in 1993 (test beams will then be available at Fermilab). These prototypes will test all of the designs for the full tracking system - chamber design and construction, mechanical support and alignment, and electronics.

II. CENTRAL TRACKING R&D

Institutions: Indiana University, University of Colorado, Los Alamos National Laboratory, Lawrence Berkeley Laboratory and University of California, Berkeley, Stanford Linear Accelerator Center

II.1. Central Tracking System Overview

The central tracking system is composed of cylindrically concentric superlayers of straw tubes.[1] Each superlayer is made up of 6-8 layers of straw tubes. The straw tubes are arranged in modules of approximately trapezoidal cross section each containing about 200 straws. Each straw module is essentially an independent tracking chamber with its own gas and power connections and its own electronics. The superlayers have straws running either parallel to the beam direction (axial superlayers) or at a small angle to this direction (stereo superlayers) in order to measure the coordinate (z) along the wire.

As an independent tracking system, the central outer tracker would need more superlayers. However, as part of the SDC Collaboration we have been studying a straw tracker that is part of an integrated system including a silicon inner tracker. For cost and material reasons neither part of the tracking system can be complete. One such system is the engineering baseline design,[2] which was defined to provide a basis for the mechanical engineering studies. The baseline design is shown in Fig. II-1, and the numerical data are given in Table II.1 for the four outer superlayers, which are composed of straw tubes (the inner two superlayers are made of scintillating fibers).

Table II.1 Straw Section of Engineering Baseline Design

Superlayer	Radius (m)	Straws/Layer	Layers/Super layer	z_{min} (m)	z_{max} (m)	Stereo Angle (°)
3	1.21722	1912	6	0.03	3.550	-3
4	1.34963	2120	6	0.03	3.900	0
5	1.48205	2328	6	0.03	3.950	+3
6	1.61447	2536	9	0.03	3.950	0

Total number of straws (both ends): 121,968.

Current cost estimates indicate that the engineering baseline system exceeds the guidelines given to SDC by the SSC Laboratory. A possibility for the SDC proposal, which is due April 1, 1992, is an all-straw central tracking system[3] with a future upgrade to scintillating fibers for the inner superlayers at higher than design luminosity. The cost of such a system is within the target goal for the descoped SDC detector, and, with the silicon inner tracker, it should provide a complete integrated tracking system that will perform well at luminosities at least up to the design value. The conceptual design of such a system consists of five straw superlayers, three axial and two stereo. The outer three superlayers are positioned as in the engineering baseline design. The inner two will be positioned radially so as to provide the best linking to the silicon detector. The two outer axial superlayers are trigger layers and have 8 straws per superlayer. We are also considering using the outer stereo superlayer in the trigger, which could be useful to provide z information, particularly at higher than design luminosities. The other superlayers have 6 straws per superlayer. The amount of material in the outer tracking system near 90° is 3.5% of a radiation length including all supports (but not including the last superlayer). (A detailed description of the material in the tracking volume is given in Section IV.) The components of this tracking system are listed in Table II.2 (the radial positions and lengths given are nominal and will be determined by simulation studies), and the design is presented in Fig. II-2. We are currently studying the performance of this tracking system design and reviewing the cost estimates for it.

Table II.2. Descoped Central Outer Tracker Design

Superlayer	Radius (m)	Straws/Layer	Layers/Superlayer	z_{min} (m)	z_{max} (m)	Stereo Angle (°)
1	0.708	1112	6	0.03	2.80	0
2	1.04	1640	6	0.03	3.20	+3
3	1.35	2120	8 (trigger)	0.03	3.90	0
4	1.48	2328	6	0.03	3.95	-3
5	1.61	2536	8 (trigger)	0.03	3.95	0

Total number of straws (both ends): 1.35×10^5.

II.2. Straw Tube Studies

In the past year there have been several studies of straw tube operation under conditions which would be expected in the SDC detector. The tubes will be about 4 meters long and therefore the attenuation per unit length of the electrical pulse as it travels along the straw must be small. Also the radiation level and the accumulated dose of radiation in each straw tube are expected to be larger than those that have been experienced before in straw tube trackers, so possible difficulties arising from these higher radiation levels must be investigated. These studies continue the work that had been done in the year before.[4]

II.2.1. Attenuation

The attenuation of the signal pulse from the collection of electrons at some point along the wire depends upon the resistance of the cathode walls and the wire and, to a smaller degree, upon the rise time of the pulse because of the skin effect. In the past our tubes were found to have an attenuation length of about 4 meters.[5] The resistance of the 25.4 μm gold plated tungsten wire was 113 Ω/m. The surface resistivity of the aluminized polycarbonate cathode material was about 1 Ω/square leading to a resistance[6] of about 90 Ω/m. In the past year we have obtained tubes made with a much thicker coating of aluminum so that the resistivity of the cathode material is about 0.3 Ω/square leading to a resistance of about 30 Ω/m. Two types of material were used. One was the same polycarbonate material as before but this time it was processed according to our specifications. We asked for as thick a layer of aluminum as possible while still maintaining the integrity of the material and the coating. The second type of material was based on Kapton. We asked for and obtained 2500 Å of aluminum. Both types of material had the same surface resistivity. Measurements of the attenuation length of the pulses from an Fe^{55} source made in the same way as for the old material but now with the new Kapton aluminized material for the cathode resulted in a value of 5.7 m with a 25.4 μm wire for the anode and a value of 6.9 m with a 51 μm wire.[7] Although a 51 μm wire may be too big, a 38 μm wire would be satisfactory and with that we can obtain at least 6 m for an attenuation length so that the amount of variation in pulse height with respect to the middle in a 4 m tube would be about 28%.

II.2.2. Radiation Effects

The behavior of the tubes in a radiation environment is rather a complex topic. Two types of measurements have been carried out to determine how stable the operation of straw tubes will be in the radiation environment of the SSC. One measure is the change in gain as a function of the accumulated charge per unit length of tube. The other is the change in the breakdown voltage limit as a function of accumulated charge and radiation level. The breakdown voltage in particular must be high enough so that the chamber does not trip off on overcurrent except under extraordinary conditions. If the effect is sufficiently severe, the lowering of the breakdown voltage as time goes on could make the straw tube detector unusable at some late time in the future of the SDC.

It has been shown that operation of tube chambers with a gas mixture containing 20% isobutane in tetrafluoromethane is very stable with respect to changes to the anode wire after large amounts of charge have been collected.[8] These studies, however, were not done with aluminized plastic straw tubes. If the same type of anode, namely gold-plated tungsten wire, and the same gas mixture are used in a straw tube with a metalized plastic cathode, break down and gain change effects are observed after a large amount of charge has been collected.[9] This points to the cathode as the source of the problem. One obvious effect that is observed is that the material is constantly being ablated as the current of positive ions keeps hitting the cathode surface. The rate of ablation is probably dependent on the type of material, how it is deposited, its thickness and perhaps other variables. During the course of ablation the surface properties change as the outer layers of the material are eroded away and the underlying layers are exposed perhaps to react with the chamber gas. The electric field at the cathode is about 2 kV/cm and at these energies ions may be implanted into the metallic surface. In short, there are many possibilities for changing the properties of the cathode as charge is accumulated.

In our tests the radiation levels are drastically increased over those expected at the SSC in order to accumulate enough charge on the wire and the cathode to make a meaningful test in a reasonably short time. The tendency to break down increases as the radiation level increases, and this is the reason that breakdown problems were observed. In order to measure the dependence on radiation level several data points were taken on a sample straw tube chamber with a source of 2 MeV electrons at varying distances from the straw. This is shown in Fig. II-3. The straw had previously been exposed to 0.2 C/cm of accumulated charge. The vertical axis is $(\mathrm{GAIN})^{-1}$ where the GAIN is the gain at the breakdown voltage and the gain is related to the voltage across the tube. The horizontal axis is proportional to the radiation level. Note that the full-scale horizontal axis corresponds to 500 times the normal SSC radiation level at the design luminosity. The gain should attain at least 10^5 for an inner straw layer for normal SSC radiation levels. The dependence of $(GAIN)^{-1}$ on the accumulated dose is shown in Fig. II-4. The increase is linear as a function of accumulated charge density.

The ablation rate imposes a minimum value of the thickness of the conductive coating. There must be enough that the pulse transmission properties are not too severely reduced after a nominal 10 year operation at design luminosity. The total accumulation of charge is estimated to be about 0.1 C/cm at about 80 cm from the beam using a gas gain of 2×10^4. Our studies show that this would result in a loss of about 500 Å of copper or aluminum. One would want to have, therefore, at least 1500 Å of copper or 2500 Å of aluminum at the beginning of operation.

All these results are valid only if there are never any sustained breakdowns. A breakdown that maintains itself over a fairly short time will damage the tube more than the full ten year radiation induced current.

II.2.3. Wire Aging Studies

There have been several areas of investigation concerning aging of wires with CF_4-based gases: a) accelerated radiation aging test, b) investigation of plasma chemistry processes leading to wire aging, and c) surface analysis of aged wires. This work also continues the studies made in previous years.[10]

• The gas CF_4/isobutane (80/20) (abbreviated as CF/IB), generally regarded as the most radiation-hard and "stable" wire chamber gas, actually shows a small (≈10%) initial transitory gain loss.

• The gas CF_4 results in rapid aging using gold-plated wires quite contrary to expectations.

• The CF/IB mixture, which works well with gold-plated wires, causes moderate to rapid aging when used with resistive wires, such as Nicotin, Stablohm and stainless steel.

• Strong evidence was found for the model of competitive ablation and polymerization (CAP), which is characterized by an equilibrium between deposition and removal of wire deposits, resulting in a finite avalanche gain, and a corresponding finite asymptotic value of current measured during tests.

Trace impurities occurring in the single constituent gas CF_4 were removed by passing the gas through a tube undergoing avalanche discharges induced by a strong radioactive source (Fe^{55}). This was observed using our cryotrap system. This is, to our knowledge, the first time such an "electrostatic" filter has been conclusively demonstrated. (This did not, however, prevent wire aging when subsequently used in a chamber as a purified gas.)

• Pre-coating of anode wires using established plasma techniques modified significantly the initial wire aging behavior suggesting the possibility (in the CAP model) of precoating the wire to the equilibrium coating level to circumvent gain loss.

• Trace contaminants $CFCl_3$ (Freon-11) and NH_3 (ammonia), two contaminants which produce wire aging behavior, were added to a chamber operating with argon/ethane gas. The effluent gas was found to contain compounds with CCl_3 and NH_2 attached to a benzene ring (benzotrichloride or aniline, respectively). These are electronegative and could be drawn to the anode wire resulting in deposits on the wire.

Studies have been made of the effect of wall and cathode material in aging and high voltage breakdown tests using CF/IB gas and also argon/ethane (50/50), and measured amounts of water vapor known to inhibit breakdown:

- Cathode materials tested: nickel, gold, copper and aluminum
- Wall materials used: Mylar, Kapton and polycarbonate (Lexan)
- Gases tested: CF_4/isobutane (80/20), argon/ethane (50/50)
- Water vapor concentrations: ≈ 0 to 4000-6000 ppm.

No important differences were observed among the cathode materials, but the polycarbonate wall resulted in much poorer aging performance than Mylar or Kapton. A significant suppression of breakdown was observed with water vapor added. Water vapor outgassing from plastic tubing was measured to be about 3000 ppm, which explains the suppression of breakdown observed when using these tubings for gas plumbing (e.g., Nylon).

II.3. Straw Tube Modules

The basic module design is shown in Fig. II-5. Three important areas for development are the carbon composite shell, the endplate, and the attachment of the module to the superstructure.[11] The outer shell holds the straws in position and maintains alignment along the length of the module. At the points where the straws have an internal wire support (every 80 cm) they will be forced into a rigid close-packed array and bonded before insertion into the shell. The unsupported 4 meter external shell does not have to be straight to 50 μm, since it is only between the 80 cm attachment points that it will be a free span. An independent alignment method will be used to attach the modules to the structure and provide the overall straightness. Also the trapezoidal cross section must be maintained between the 80 cm support points by the shell. The endplate structure and the bonded straw positions maintain this shape at the support points.

One of the goals for the past year was to construct several working straw tube modules using the shell concept. This project served the needs of other groups who wanted a small straw tube chamber for trigger and electronics studies and for gas studies and also allowed us to test some of the expected benefits of modular construction such as self centering of the straw tube array by close packing them in a precisely-made shell. These modules contained 64 straw tubes. Also, a module with 228 tubes was begun recently and will be completed in the near future.

Several composite modules of 30 cm length were constructed by Composites Horizons of Covina, California. The dimensions of these carbon shells are shown in Fig. II-6. These were made with 4 layers of 0.0025 in. prepreg carbon fiber tape (38 Million modulus). Measurements of these modules show that the intrinsic straightness over 80 to 100 cm can be held within the 50 μm accuracy limit. Working with Composites Horizons, several tests of the expansion or contraction of the composite structure with respect to the room temperature mandrel (mold) size have been performed. By using the computer program GENLAM, the final product size was accurately predicted. In particular, it was confirmed that the expansion coefficient along the fiber direction is very slightly negative. This shows that we can produce a final shell to the required specifications.

The composite shell also takes the compressional load of the wire tension, which is about 12 kg force for 240 straws. An analysis of a 240 straw module by Oak Ridge indicates that a 0.010 in. (250 μm) wall will support the tension, as explained in the ORNL Appendix.

An assembly view of the 64-straw module is shown in Fig. II-7. The 64 straw tubes are arranged in a close-packed rhombus-shaped array of 8 rows and 8 straws to a row with an offset of half a tube between rows. Connections to the cathodes are made by dipping the ends of the 64 straws into conductive epoxy. A connection is thus made from one tube to the next, and on the two opposite sides of the module the connection is carried outside with copper foil. The wires are positioned in the center of each straw with a so-called double-vee, one at each end of the tube. The double-vees, shown in Fig. II-8, are made for us by RTI Plastics to a design by R. Foster.[12] The double-vee centers the wire in the center of the tube. The wires are tensioned and soldered to clips inserted into the endplates, one at each end of the shell. Connection to the anodes is made via spring-loaded contacts (pogo sticks) stuck in the endcap, which covers the endplate. The pogo sticks press against the clips to which the wires are soldered. A gas manifold is also formed when the endcap is attached to the endplate. The outside ends of the pogo sticks are soldered on one end into a PC board which supplies the high voltage to each wire through a resistor and on the other end to another PC board which holds the blocking capacitors and connectors to carry the signals to a set of amplifiers. The modules were made at Indiana University and the PC boards at the University of Colorado.

A total of six modules of this type were constructed. One each has been sent to KEK in Japan, University of Colorado, University of Michigan and University of Pennsylvania. Two remain in Indiana. These prototype modules are or will be undergoing extensive testing to investigate and optimize their operating characteristics. One of the setups (at Colorado) incorporates a cylindrical drift chamber from an earlier experiment in conjunction with the prototype 64-tube module to study the performance (resolution, efficiency, etc.) of the module as part of an overconstrained tracking system. A full complement of FASTBUS TDCs is operating and cosmic ray tracks can be displayed. A track finding and fitting program has been produced and the residuals of the fits are being studied. Such tests on the module alone are also being carried out at Indiana.

Various tests of the accuracy of the module construction technique have been made both in the course of building the modules and after their completion. Before the wires were strung the positions of the double-vees were measured. The positions were then fit to an ideal close-packed array. The result was that the standard deviation in each of two orthogonal directions was less than 50 μm where the error of measurement was probably the largest contribution. After completion the module was tested with cosmic rays. The difference between fitted and measured positions of the tracks indicated that the deviations from a close-packed array were about 20 μm. Another test of the placement of the wires in the 64-tube module was performed by X-raying the module with a very small X-ray source at a large distance. The module was placed at an angle with respect to the X-ray flux so that the image of each wire was separated from the image from the wire in front or in back of it. In this way all 64 wires can be clearly resolved. The errors here also indicate about a 25 μm error from an ideal close-packed array in one plane.

The results of the placement error measurements of the 64-tube module led us to consider ways to improve the centering accuracy, and a new method was developed for use in the construction of the 228 straw tube module. The new method consists of clamping the straw tubes with their double-vee inserts inside precisely-machined steel clamps and gluing them. The shells then do not determine the close-packing of the wire pattern but they do keep the straws in line between the points along the straw where the clamp points are. The measurements of the placement accuracy were made on an optical comparator, and after fitting to a close-packed form, the result was that the standard deviation was 30 μm.[13] See Fig. II-9 for a plot of the deviations. Although the placement errors are not significantly better than for the 64-straw module, it seems clear that without this clamping method the errors on the 228 straw module would have been larger.

The proposed end structure assumes that the sense wire can be forced, on an air column or following a stiff leader, through a 3-4 m long tube loaded with wire supports at 80 cm intervals. The injection-molded double-vee supports used in current prototypes do not allow use of this technique; a design from Duke University works rather well from this perspective but has not yet been adapted to mass production with precisely controlled dimensions. We have procured prototype supports made to our second-generation design shown in Fig. II-10. It is a double-vee modified to funnel the wire through its aperture. We are encouraged by the performance of this model and expect to order injection-molded versions as soon as we are fully satisfied with the prototype evaluation.

We are now in the process of assembling two 1-meter-long and one 4-meter-long prototype modules. The design of the carbon fiber composite shell is discussed in Section IV.

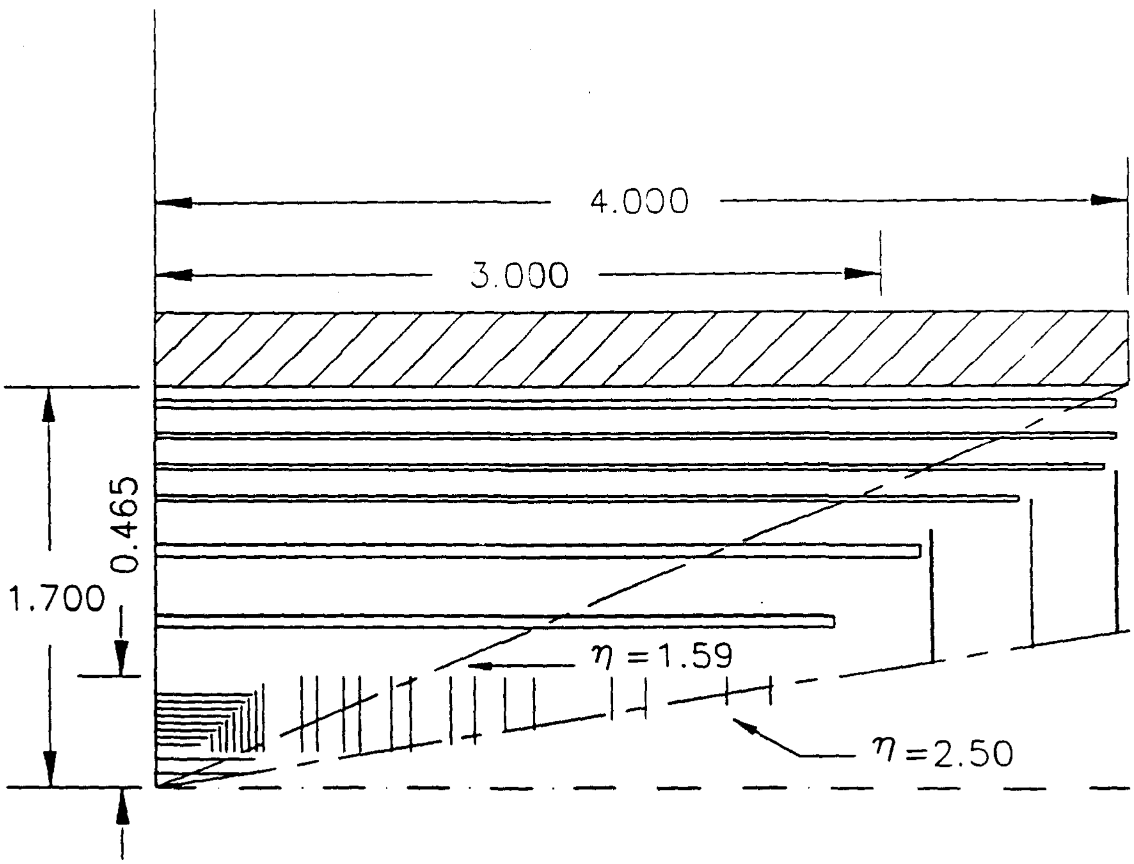

Fig. II-1. A section through one quadrant of the tracking system of the baseline design.

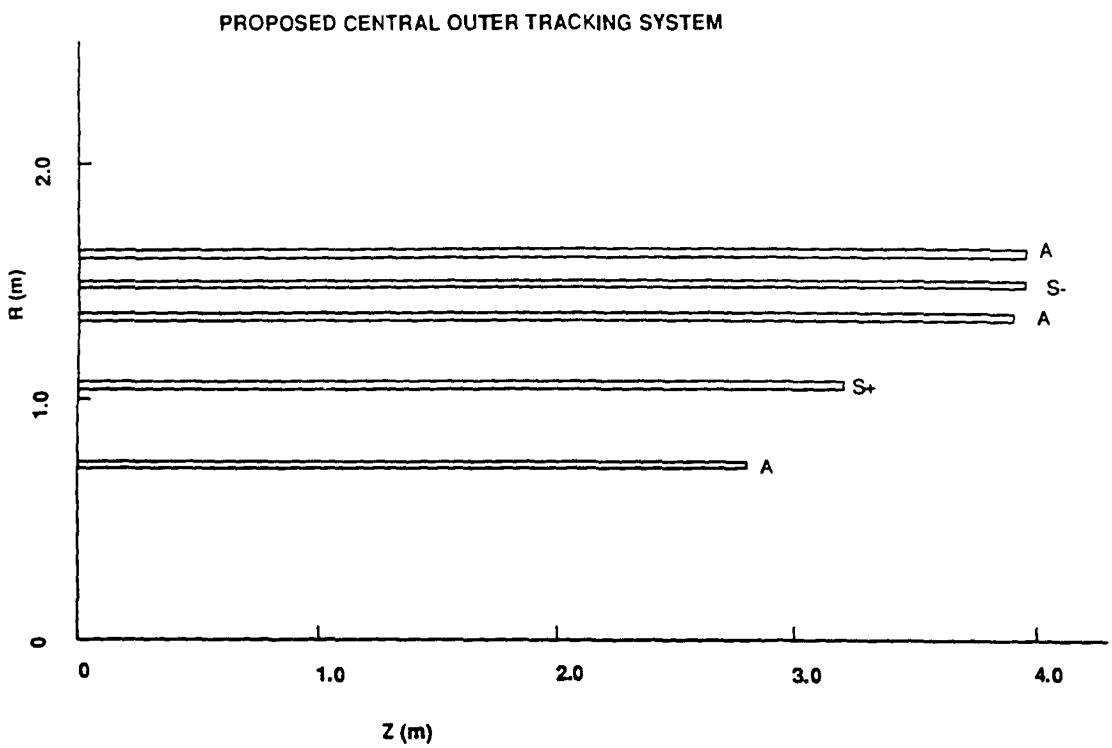

Fig. II-2. A section through one quadrant of the descoped all-straw central outer tracking system.

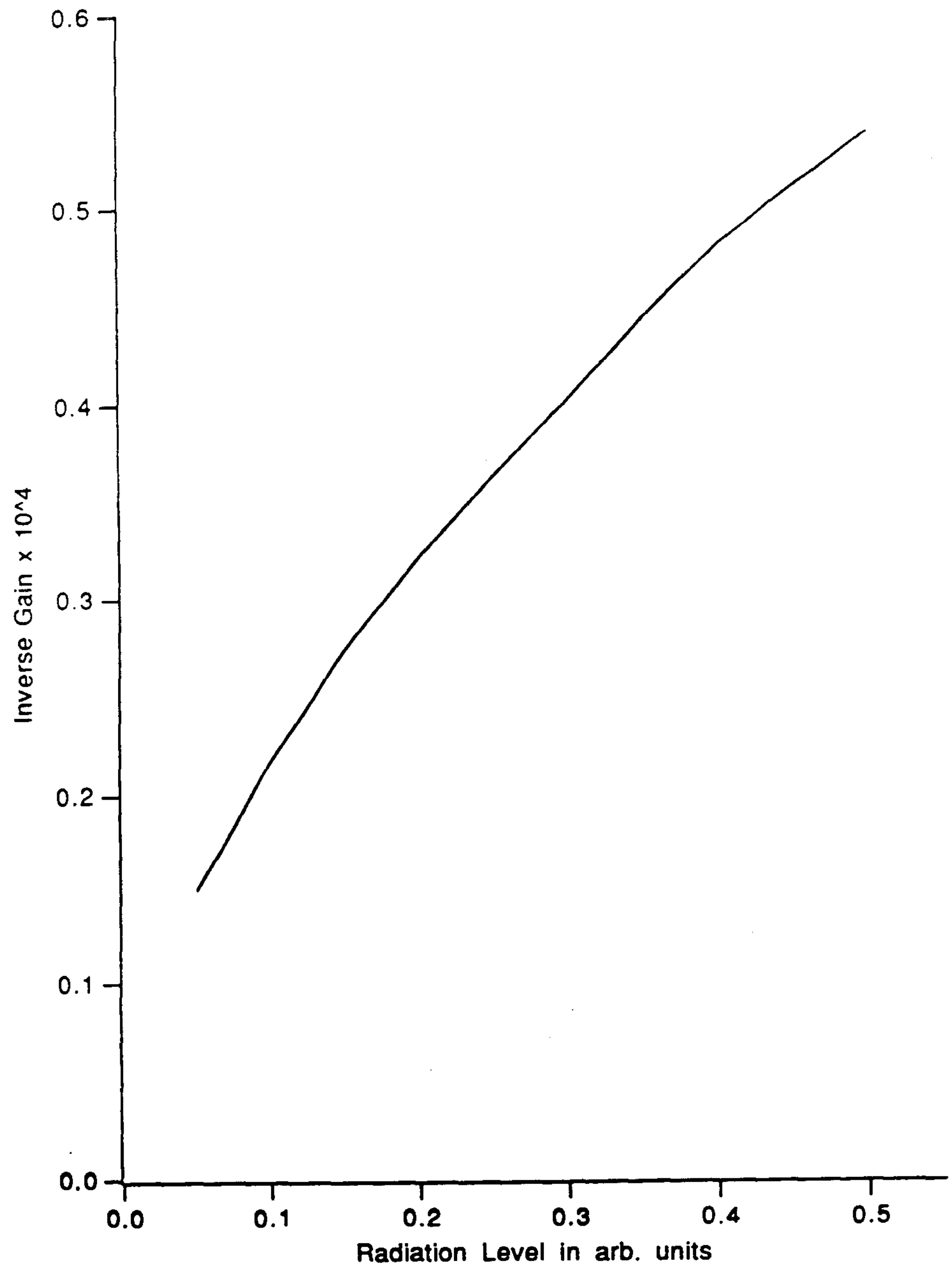

Fig. II-3. The limiting inverse gain vs. radiation level for a straw after exposure resulting in 0.2 C/cm of charge deposited on the wire. Full scale is 500 times the radiation level at design luminosity for a tube 70 cm from the beam.

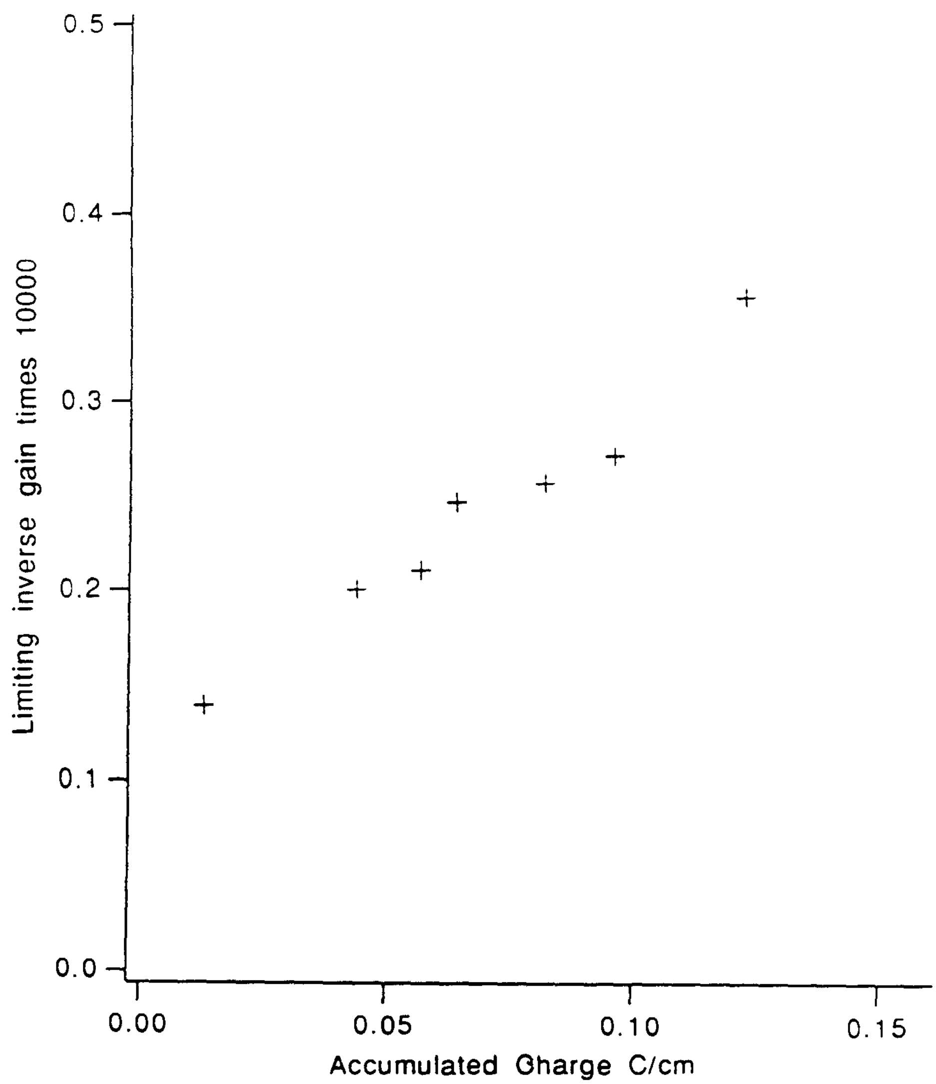

Fig. II-4. The dependence of the limiting inverse gain on the total exposure at a level of radiation 300 times the level expected at design luminosity for a tube 70 cm from the beam.

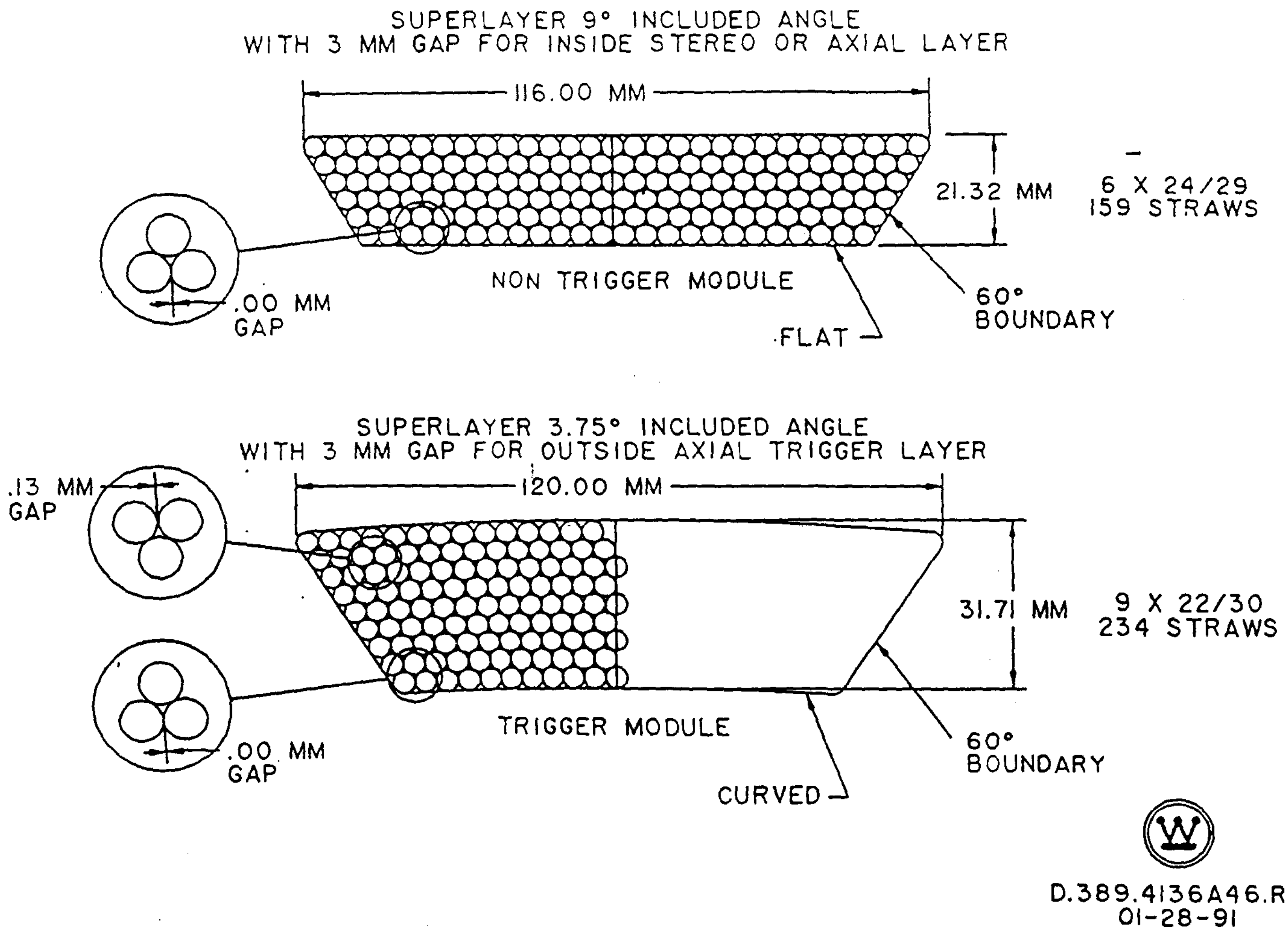

Fig. II-5. Cross sections of two proposed module designs.

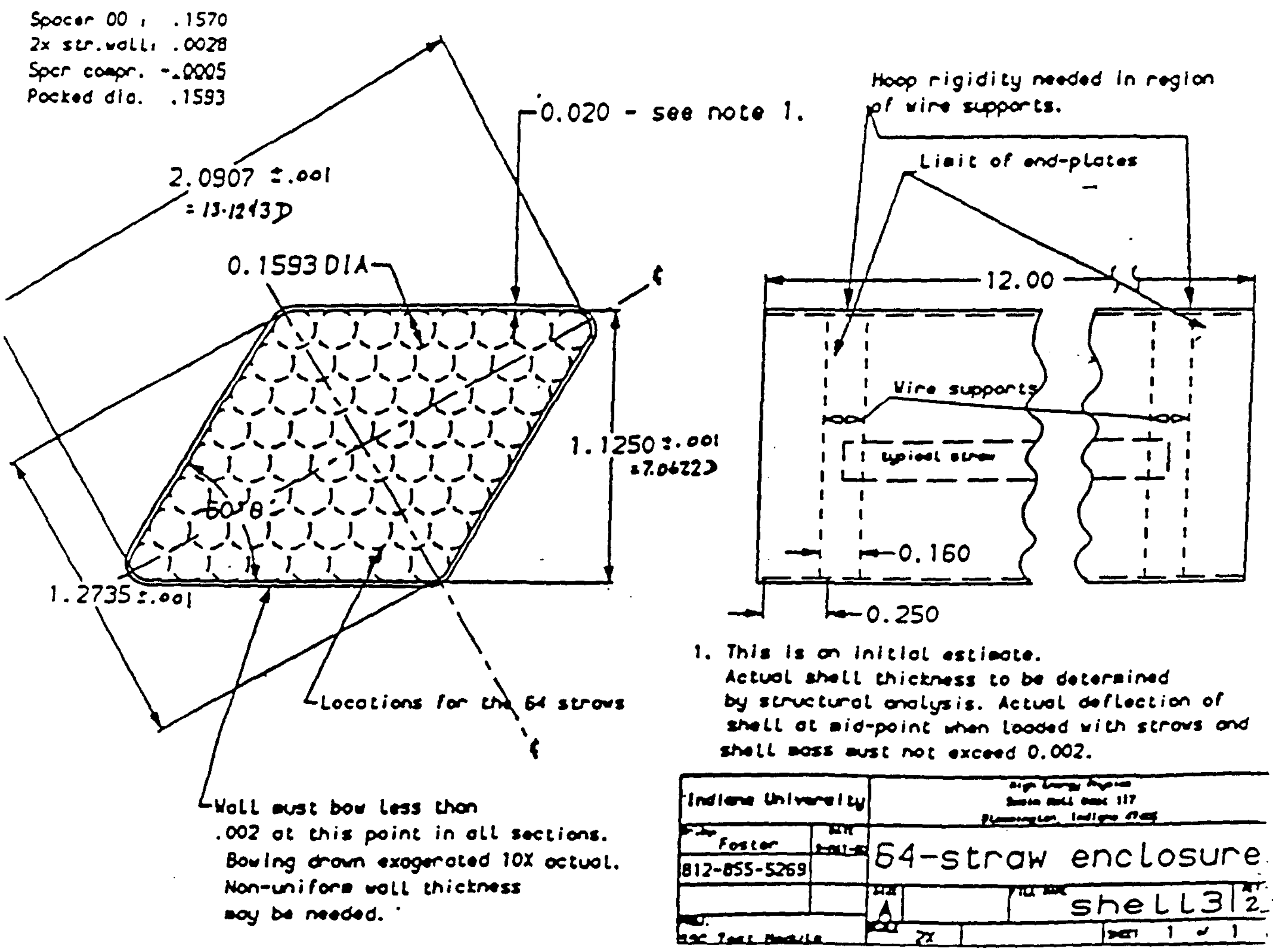

Fig. II-6. Drawing of the 64-tube prototype carbon fiber shells.

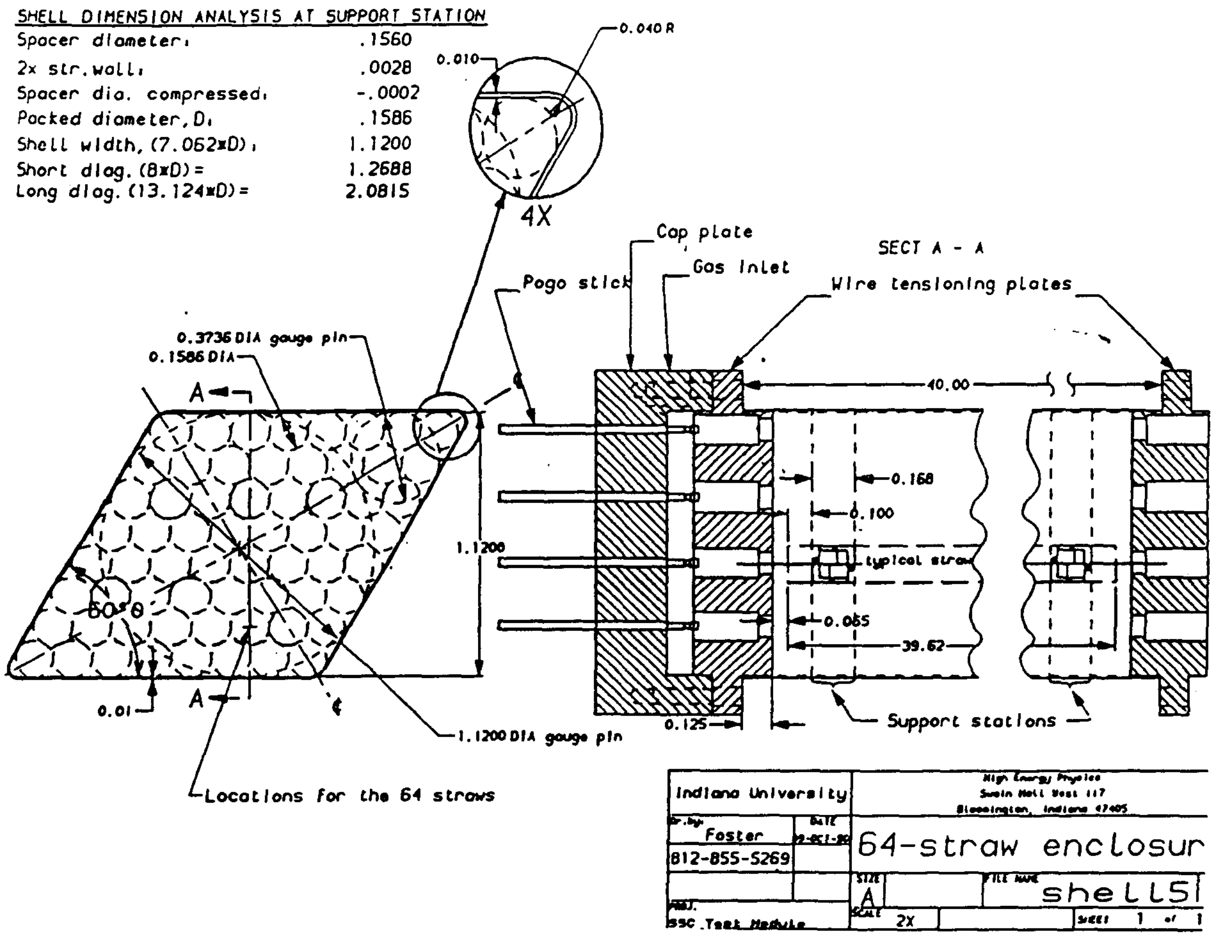

Fig. II-7. Assembly of the 64-tube prototype module.

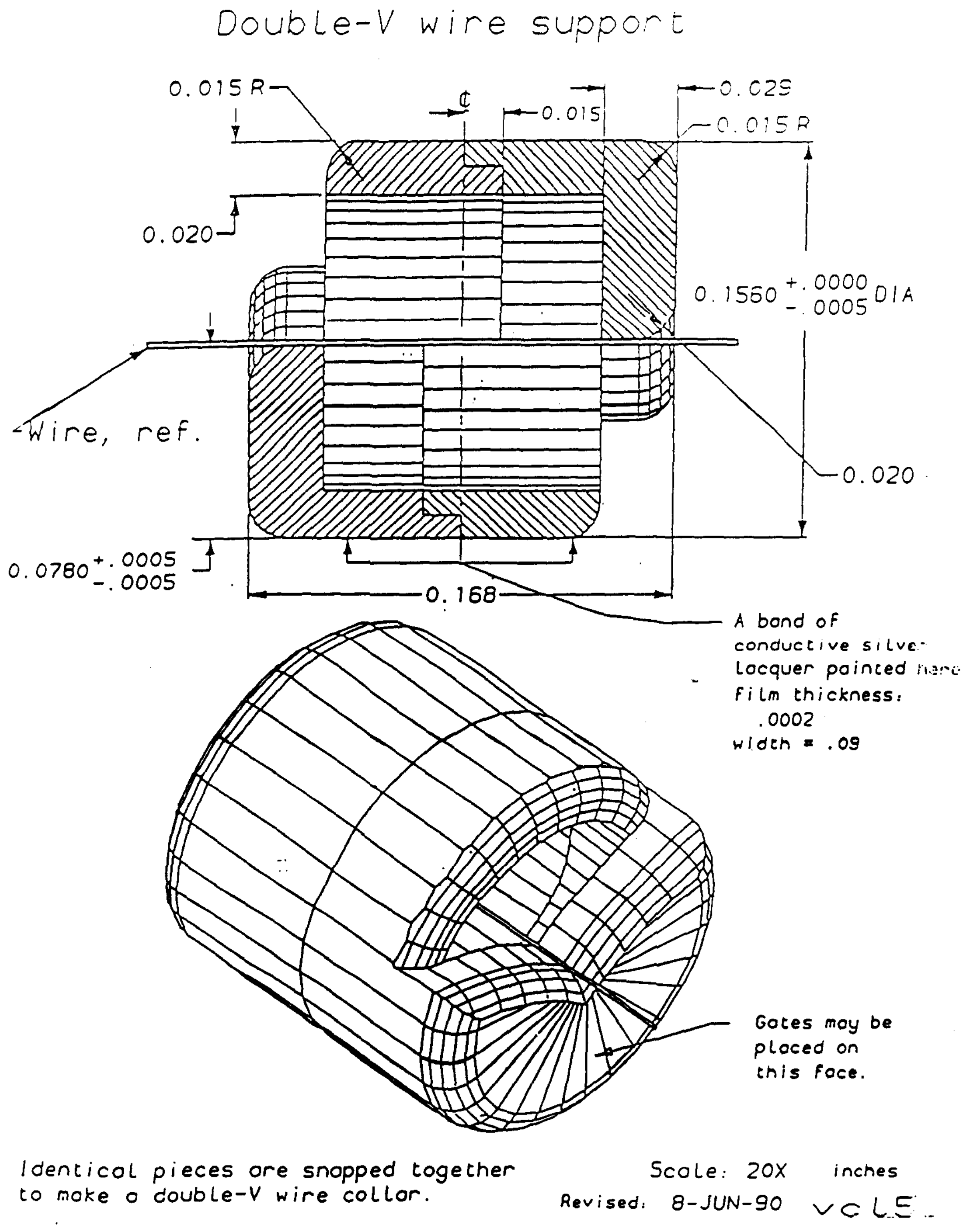

Fig. II-8. Detail of double-vee wire support.

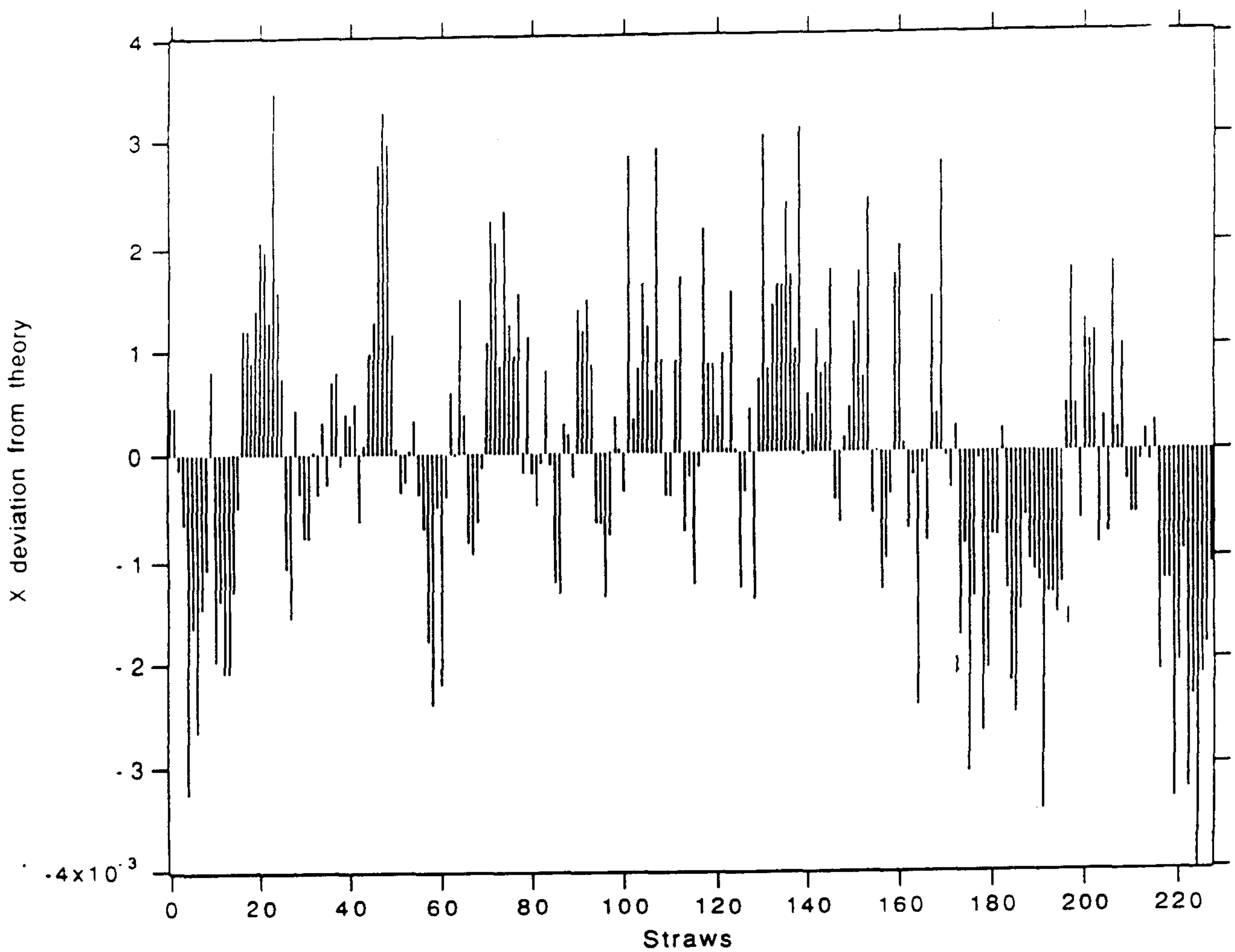

Fig. II-9. Deviation from an ideal close packed array as measured on an array of 228 straws glued in a trapezoidal clamp.

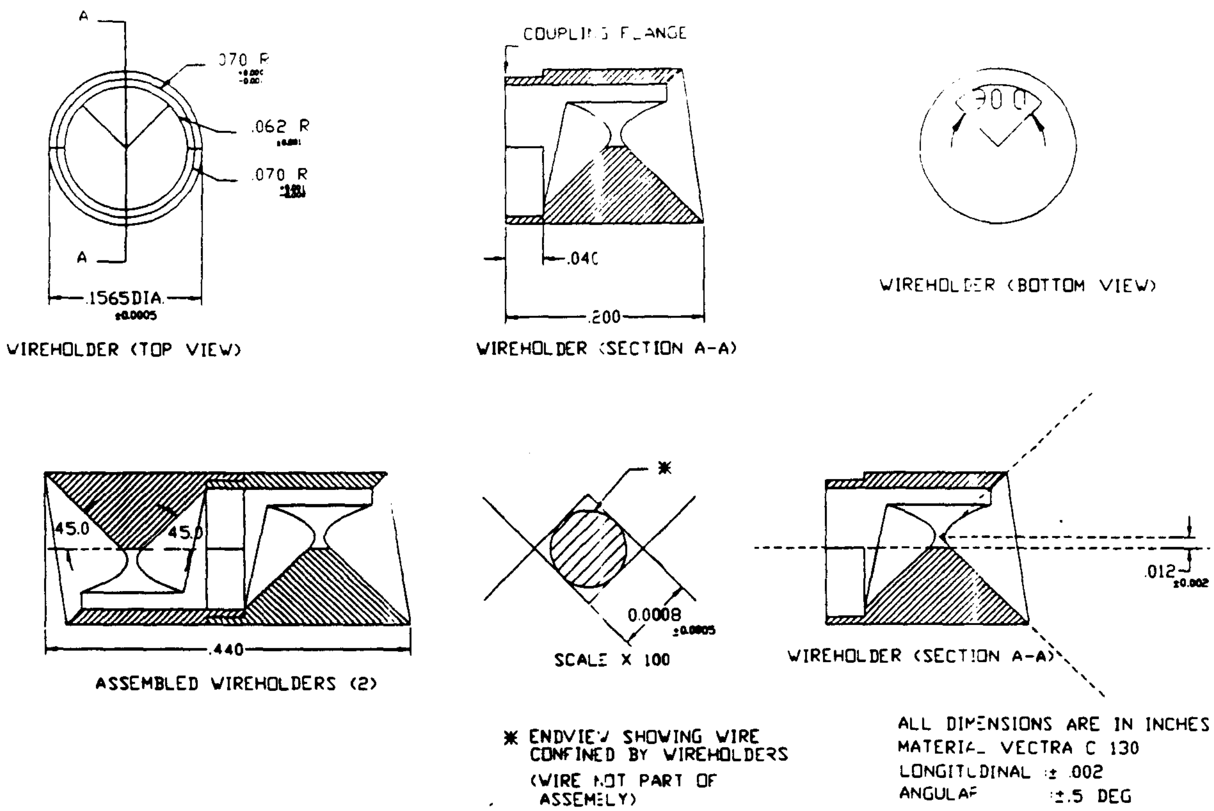

Fig. II-10. Molded plastic wire support for location of the sense wire between spans.

III. INTERMEDIATE ANGLE TRACKING R&D

Institutions: University of Liverpool, Rutherford Appleton Laboratory, University of Glasgow

The intermediate angle region of the outer tracking system in a supercollider experiment is important if rapidity coverage is to be adequate for good acceptance for production of new heavy particles, for example, the Higgs boson. Using gaseous charged track detection, the intermediate rapidity ranges $-2.3 < |\eta| < -1.2$ and $1.2 < |\eta| < 2.3$ are best covered using anodes (wires or microstrips) in planes perpendicular to the beam axis.[14] The SDC experiment presently has plans to include two Intermediate angle Track Detectors (ITDs) to cover these end rapidity regions.

The initial technique proposed for the ITDs used modules of radial wire drift chambers, similar in concept to those now installed in the H1 experiment at HERA. At supercollider luminosity ($\leq 10^{33}$ cm^{-2} s^{-1}) such chambers must have sufficiently small drift cell aperture and must be operated with the fastest possible drift gas. A "standard" design of radial wire drift chamber gives rise to two areas of concern for use in the SDC detector at a luminosity of 10^{33} cm^{-2} s^{-1}:

1. Current Draw
The current draw, which is expected to be 0.5 μA per sense wire at a luminosity of 10^{33}, will induce a similar current in the voltage graded cathode plane which will cause voltage sag if a resistive divider is used. The consequences are intolerable drift velocity and gas gain variations as a function of radius. An alternative approach, which is now favoured, is to supply each cathode strip, via a distribution network, from a set of ganged power supplies, one for each different voltage in the chamber. Such a system introduces no new conceptual design problems other than the large number of voltage lines needed to supply the drift chamber. This solution has the additional advantage of permitting the inner radius of sensitivity of the chamber to be increased to cope with unexpected background levels.

2. Occupancy

Occupancy, as presently used to evaluate the performance of straw tubes with single hit electronics, is misleading when multi-hit electronics are used. It is necessary to distinguish "memory time" and "busy time." Memory time is the maximum drift time, in this case 157 ns or 10 beam crossings. Busy time is twice the two hit resolution divided by the drift velocity, 2×2 mm divided by 100 μm/ns, or 40 ns. Using the busy time in the calculation, the effective occupancy is 12% at a luminosity of 10^{33} cm^{-2} s^{-1}. This is comparable to the occupancy of straws in the barrel outer tracker, as expected when one considers that the rapidity range and phi segmentations are similar.

The operational characteristics of the radial wire drift chambers at the SSC can be summarized by the following:

1. In the simulation at a luminosity of 10^{33} cm^{-2} s^{-1} the loss of hits due to the busy time of the anticipated two hit resolution (2 mm) is only 7%.

2. The proposed inclusion of a "crossing tagger" with a time resolution conservatively estimated at 3 beam crossings has been demonstrated by simulation to reduce the fraction of minimum bias background hits per trigger in the ITD from 79% to 27% of the total. This gives confidence that the pattern recognition problems could be manageable.

A "single wedge" radial wire chamber prototype of suitable size was constructed in Liverpool and tested in a CERN test beam. Figure III-1 shows some details of the construction of the prototype. In attempting to establish acceptable operating conditions in new fast drift gas mixtures (see below), problems were encountered with distribution of the necessary sense and field HV to this small (relative to H1) drift wedge. They have now been solved by means of modifications to the construction of the prototype, and the modified version is now operating quietly with conventional slow drift gas. The spatial resolution and pulse height uniformity are under investigation using X-rays and cosmic rays. This work is being continued to a conclusion which will establish how well such a radial wedge chamber operates in fast CF_4-based gas mixtures.

In parallel with this work, we have carried out a series of measurements of the drift characteristics of fast gas mixtures which include CF_4.[15] In radial, or for that matter other isochronous drift chambers which are suitable for ITDs, it is essential for design work to have a good understanding of both the drift velocity and the Lorentz angle as a function of the electric field. A series of measurements is continuing, after initial chemical and physical damage to our test chamber due to the action, both chemical and physical, of the CF_4 gas mixtures used. As an example of these measurements, Fig. III-2 shows the results for a mixture with which we can achieve a suitable drift velocity and manageable (< 45°) Lorentz angle, albeit at relatively high electric field.

As our design work for the SDC experiment at the SSC has progressed, the need for a fast Level 1 trigger from the ITDs has become one of the most important criteria in their design. Radial drift wires with multi-hit readout and thus large occupancy, but with low busy time, cannot meet this requirement. We are now also considering ITDs which include gaseous microstrip chambers for fast signals. At first our approach was to construct a hybrid of radial wires with gas microstrips in which the latter played the combined role both of tagging the bunch crossing to eliminate unwanted hits in the radial chambers and of providing a Level 1 trigger. It is now becoming clear that the excellent spatial resolution of the microstrips can be used to provide adequate track reconstruction precision, thereby removing a major reason for the radial drift wires and in doing so also enhancing the luminosity capability of each ITD to 10^{34} cm^{-2} s^{-1}. Simulation design work is now progressing well to fix the layout of an ITD based on microstrip "tiles." R&D is also underway to establish the reliable operation of suitably sized tiles in both Liverpool and RAL. This work is now becoming the main activity of these groups in the SDC experiment.

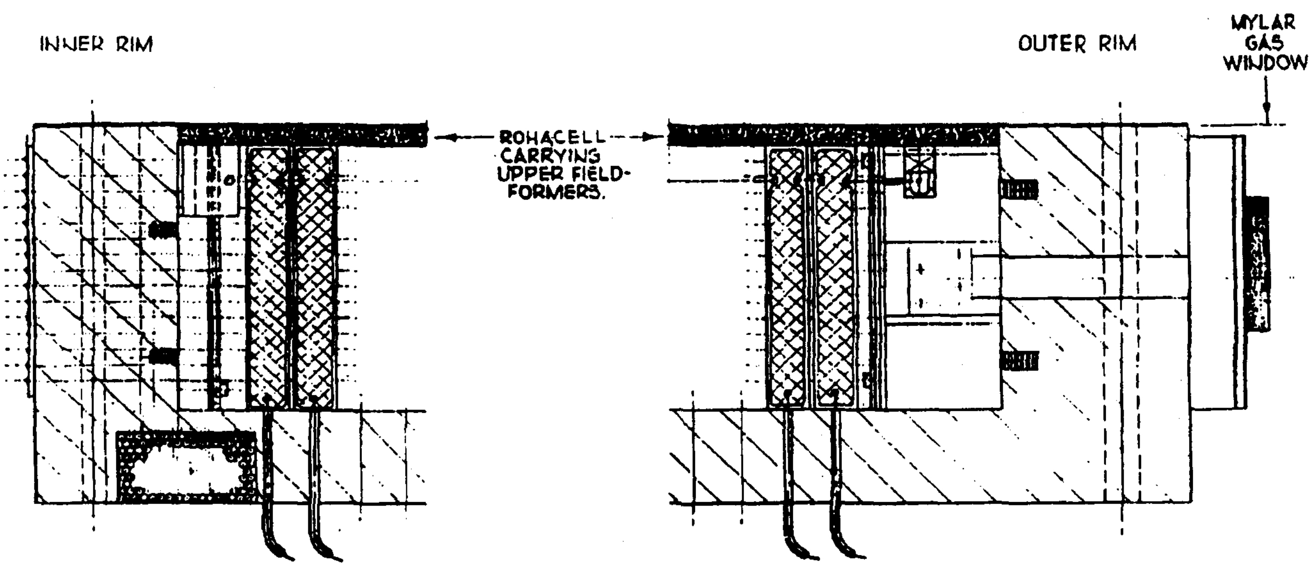

Fig. III-1. A side view of the inner and outer radius regions of a "wedge," showing details of the HV graded cathodes supported inside a composite structure.

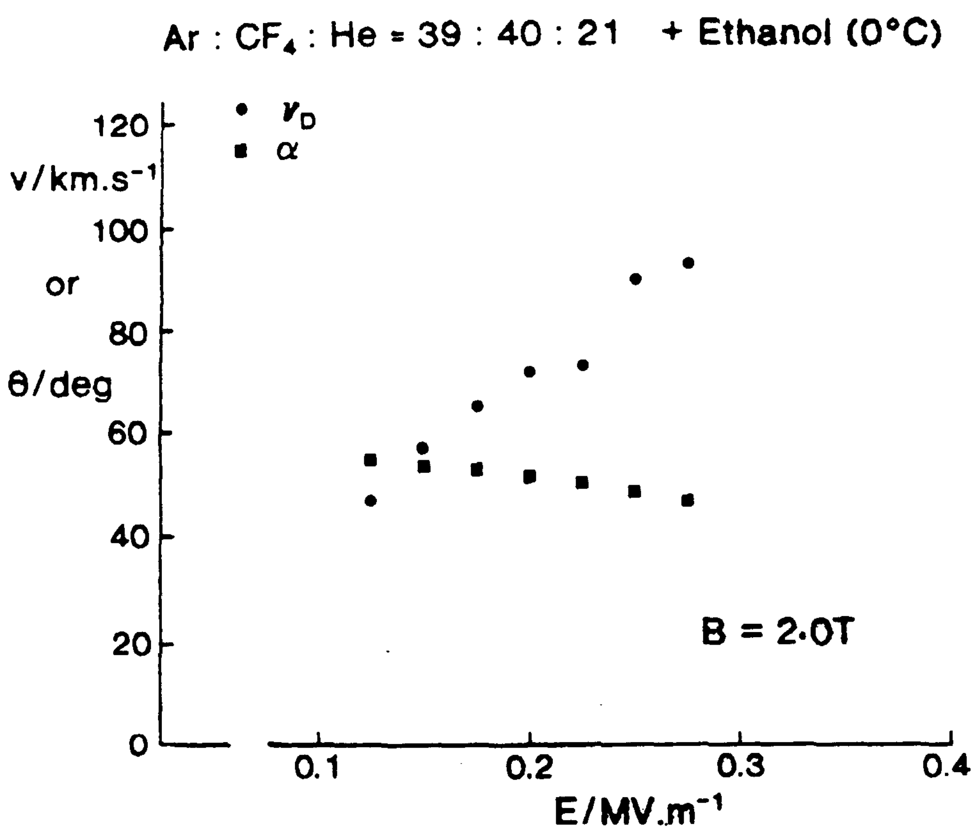

Fig. III-2. Drift velocity and Lorentz angle for a fast gas suitable for radial wires in an ITD: $Ar/CF_4/He$ 39/40/21.

IV. ENGINEERING R&D

Institutions: Indiana University, Oak Ridge National Laboratory, and Westinghouse Science and Technology Center

IV.1. Introduction

This report contains the results of the second year of engineering development on the modules, the superlayers, and the support structure for the SDC tracking system. The goal of this study was to develop a detailed concept for a modular charged particle tracking system based on small cell drift chambers.

The initial design of the tracking system has made significant progress in all major areas:

1. A one-meter-long prototype module with 228 cells
2. The cylindrical support for the modules
3. The space frame for the support of all the cylindrical superlayers and the silicon inner tracker.

There has also been a growing effort to complete the engineering studies of these systems. This has included:

1. A finite element analysis of nested cylindrical superlayers
2. A study of several space frame designs for holding the superlayers
3. A series of studies of the modules, including buckling calculations, transverse stiffness, and effects of composite orientation.

In addition, detailed manufacture and assembly studies have started on the following:

1. The large cylindrical mandrel for the carbon composite-Rohacell foam cylinders
2. The module support shim rings on each cylinder
3. Space frame support system
4. The four-meter-long modules.

Finally, in preparation for the full design report for the SDC, the cost and schedule for the straw tracking system have been analyzed. This includes engineering and design as well as labor and materials for construction and assembly.

We believe that a module-based central tracker using straw tube technology would have advantages such as simplicity, stability and repairability. The Straw Tube Placement Engineering Review Committee,[16] which met in June, has indicated that the modular concept should be chosen for the SDC if a 4-meter module can be demonstrated by the end of the year. Much of the modular work we report here is directly related to the construction of this proof of principle module. We are confident that this can be accomplished.

Figures and supporting documents referred to in this section are representative of the work completed. More detailed work reports from Indiana University, Oak Ridge National Laboratory, and Westinghouse Science and Technology Center can be found in the appendices.

IV.2. Concept

The module is the basic building block of the outer straw tracking system. A nontrigger module consists of six layers of 4-mm-diameter straws surrounded by a trapezoidal shell of graphite composite of 0.010-in.-thick wall. There are 29 straws in the widest layer, as shown in Fig. IV-1. The trigger module will have eight layers of straws in a shell with a transverse cross section that conforms to the superlayer radius. In the engineering baseline design, these modules, ranging in length from 2.7 to 4 meters, are arranged in four cylindrical superlayers distributed between 0.70 and 1.7 meter radius. The modules have positioning keys that are attached by shim rings to thin cylinders spanning the entire length of the eight-meter-long tracker. Each of the cylindrical superlayers is attached by an end flange to a space frame that keeps the superlayers coaxial and supports the tracker inside the magnet, as shown in Fig. IV-2.

IV.3. Modules

During this reporting period, a design of the graphite/epoxy straw module has been completed to request prototype fabrication bids. Detailed design calculations on the module were performed, and specifications and detail drawings produced to define completely the module for fabrication. The design is shown in Fig. IV-3 and is described in the ORNL Appendix. During this design work it was found that the major loads on the module were the thermal loads that develop as it cools back to room temperature from the maximum curing temperature. The stress-free temperature of a cured composite is close to the maximum cure temperature at which most of the cross-linking occurs in the polymer used for the matrix. Because of the high coefficient of thermal expansion (CTE) of the epoxy, which is about $21 \times 10^{-6}/°F$, and the negative CTE of the graphite, which is about $-1.38 \times 10^{-6}/°F$, compressive buckling stresses can be induced in the thin graphite laminates.

The induced compressive stresses in the thin laminates would cause warping and waviness of the modules. Such warping and waviness are unacceptable in the module; consequently a design was found which involves laying up the thin laminates on a polyimid foam. This enormously increases the flexural modulus and buckling strength of the laminate while imposing very little weight penalty on the module. In fact, the design using the foam core saves weight over that of the solid laminate for the case of designing to prevent buckling due to the tungsten-wire forces; i.e., only 0.009-in. thickness of graphite is required to prevent wire-force buckling, whereas six plies of 0.0025 in. per ply (0.015-in. of graphite) would have been required in a solid laminate.

Our studies have indicated all layups of thin laminates should be reinforced by foam or other means. This has implications for the cylinder design. Also, the layups should be balanced and symmetric, and the effects of the flexibility of the foam on the symmetry and balance should be assessed. These effects have been incorporated in the prototype shell design. The specifications and design drawings to be used for fabrication are given in the ORNL Appendix.

In addition to the detailed module design, the layout of the modules has been optimized for gapless azimuthal coverage by the active straw layers. This involved developing a program to optimize the size, position and separation of each module in a superlayer. In particular, the study investigated ways in which the modules could be positioned so that high momentum particles have a minimum number of lost hits in the boundary regions of modules. One way that this can be accomplished is to stagger alternate modules in the radial direction. The unequal radial spacing between modules reduces the required spacing between modules while maintaining a maximum number of hit straws. Configurations have been found that should allow high momentum tracks to have the full complement of hits. A typical layout is shown in Fig. IV.4. See the ORNL Appendix or the WSTC report for more pictures and details concerning missed hits.

The engineering baseline design incorporates stereo modules in two of the superlayers of the tracking system. We have worked out a stereo configuration of the modules that gives full coverage for all tracks using the nontrigger modules positioned at 3° to the axis of the cylinder. This is shown in Fig. IV.5. Details of this layout are in the WSTC Appendix.

IV.4. Support Cylinder

Each superlayer of modules is supported on a cylinder that spans the entire length of the tracker. The support cylinders are shown in Fig. IV-6. The structural stability of such a system has been studied. The assembly sequence has been developed. The materials to meet the stringent alignment and stability specifications exist.

The cylinders have shim rings that hold the modules at points separated by 80 cm along their length. The module shells are fitted with key type attachments along their length where they attach to the support structure. The keys are precisely located with respect to the inside surface of the module. These keys lock into the shim rings on each cylinder.

The design studies of the cylinders have indicated that the structure should be a graphite composite laminate composed of two 0.006 in. (3 ply) laminates sandwiching a 1 inch polyimid foam core. This satisfies the material constraints of the tracking system as well as the strength and stability requirements. The largest of these cylinders is 8 meters in length and 1.6 meters in radius. A design for shim rings made of polyimid foam is under way. It appears to meet the precision tolerance of 50 microns. Such a cylinder and shim ring is shown in Fig. IV-7.

The manufacturing procedure for the cylinders will require the construction of large steel mandrels. The carbon composite laminates will be laid up on the mandrel, then covered with foam panels. The foam can be machined to tolerance before covering with an additional 0.010-in. carbon laminate. Before removal of the cylinder from the mandrel the shim rings will be bonded and machined to tolerance for holding the modules, and end flanges for the cylinder would be attached.

Several finite element analysis studies have been carried out on the cylindrical superlayer design. An early study by WSTC looked at the displacements of the edge-coupled cylinders when supported horizontally at two points on the outer cylinder. This study showed that while the cylinders themselves show very little catenary sag, they can become distorted and displaced downward. Details are in the WSTC Appendix. Clearly the method of holding the cylinders is crucial. This is the topic of the next section.

IV.5. Space Frame

The most critical alignment issue is the stability of the internal silicon tracker with respect to the outer tracker superlayers. The two systems must remain fixed with respect to each other within 25 μm. A finite element analysis study of the cylinders shows that the cylinders themselves will be stiff enough to be within tolerance. What is needed is an end support that can hold the cylinders rigidly and with the required stability. To this end a space frame constructed from composite elements has been designed. It is shown in Fig. IV-8. It will attach to the SDC calorimeter and support the cylindrical superlayers and the silicon system. The truss framework is very strong and should be stable against torques that would rotate one cylinder with respect to the other. The individual strut members would be made from carbon fiber composites and be joined with carbon fiber fixtures at the joints. The conceptual design is shown in the WSTC report. A finite element analysis is in progress to study the distortions introduced by supporting the frame at four horizontal points. The design is also being studied by a carbon fiber composites company to determine the assembly sequence and estimate the cost.

IV.6. Material in the Particle Path

The amount of material in the tracking system is an important design consideration. We have taken taken considerable effort to keep it as small as possible. The basic straw material represents a total thickness of $\pi \times$ wall thickness for each straw. For a six layer system this is 697 mm of mylar. We take into account the internal wire supports by increasing this by 10% giving a total of 0.32% of a radiation length for each straw layer.

The external carbon composite shell will have a thickness of 250 μm. The entire shell will then have an equivalent thickness of about 600 μm per superlayer or about 0.24% of a radiation length at normal incidence. The support cylinder will have about 0.24% of a radiation length at normal incidence. There will also be a small amount of Rohacell in the support structure for attaching modules on the cylinder. The material is shown in Table IV-1 for the engineering baseline tracking system.

The endplates can be quite thin. The endplates for the prototype 64-straw module have an effective thickness of less than about 0.5 cm of plastic. This would contribute a thickness of about 2% of a radiation length normal to the ends. To this must be added the printed circuit board, electronics, cooling, cabling, and the cylinder support struts. Figure IV-9 shows the effect of these items at the end of each superlayer. Figure IV-10 shows the material for the whole tracking system in the engineering baseline design.

IV.7. Cost and Schedule

In preparation for the SDC design report the cost of the straw tracking system has been studied. This study has covered all aspects of manufacture, assembly, and installation. The work has been carried out over the past year by WSTC in close collaboration with Indiana University. The full costing document is shown in the WSTC Appendix. We are continuing to work with vendors to get better estimates of the component costs and to follow the changes in the tracking system as the tracking design evolves.

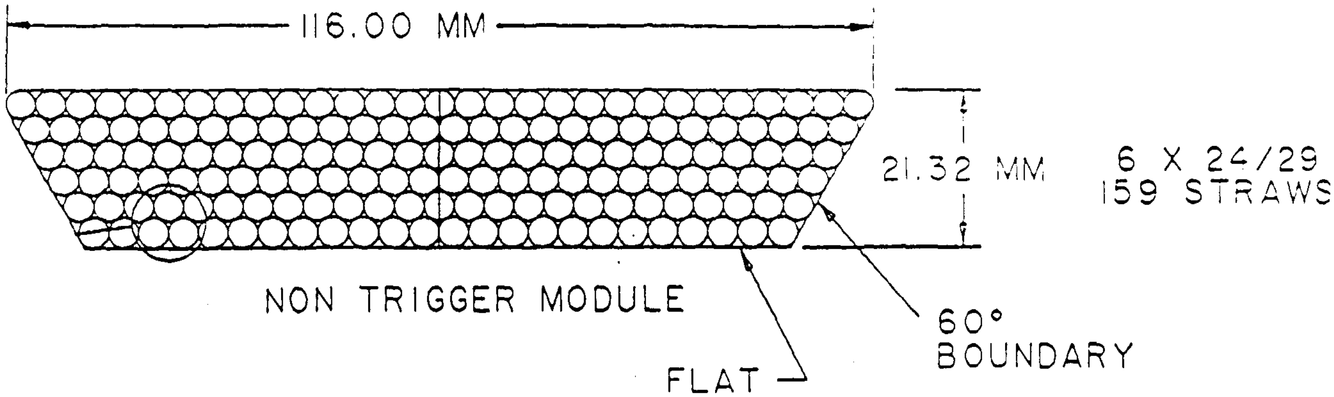

Fig. IV-1. A nontrigger six-layer module.

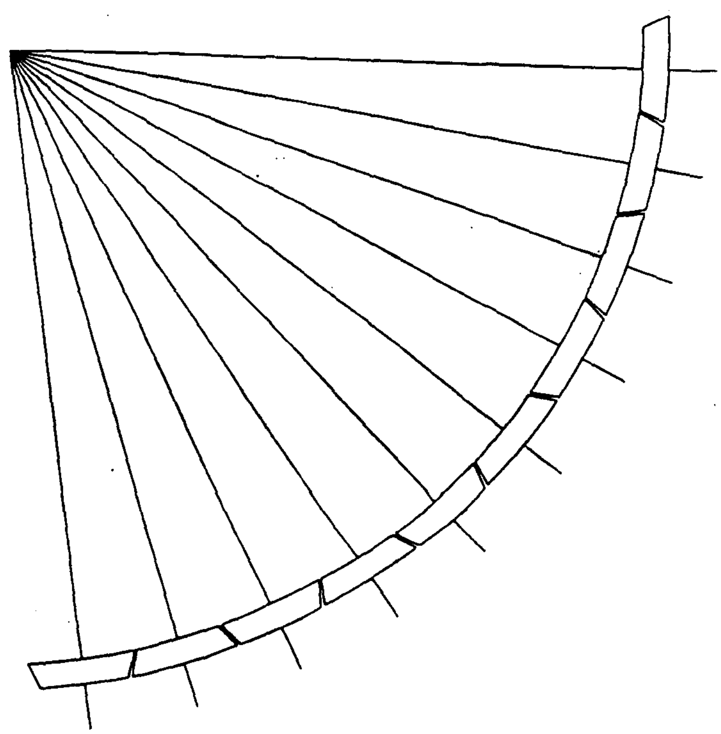

Fig. IV-2. A typical layout of modules to form a superlayer.

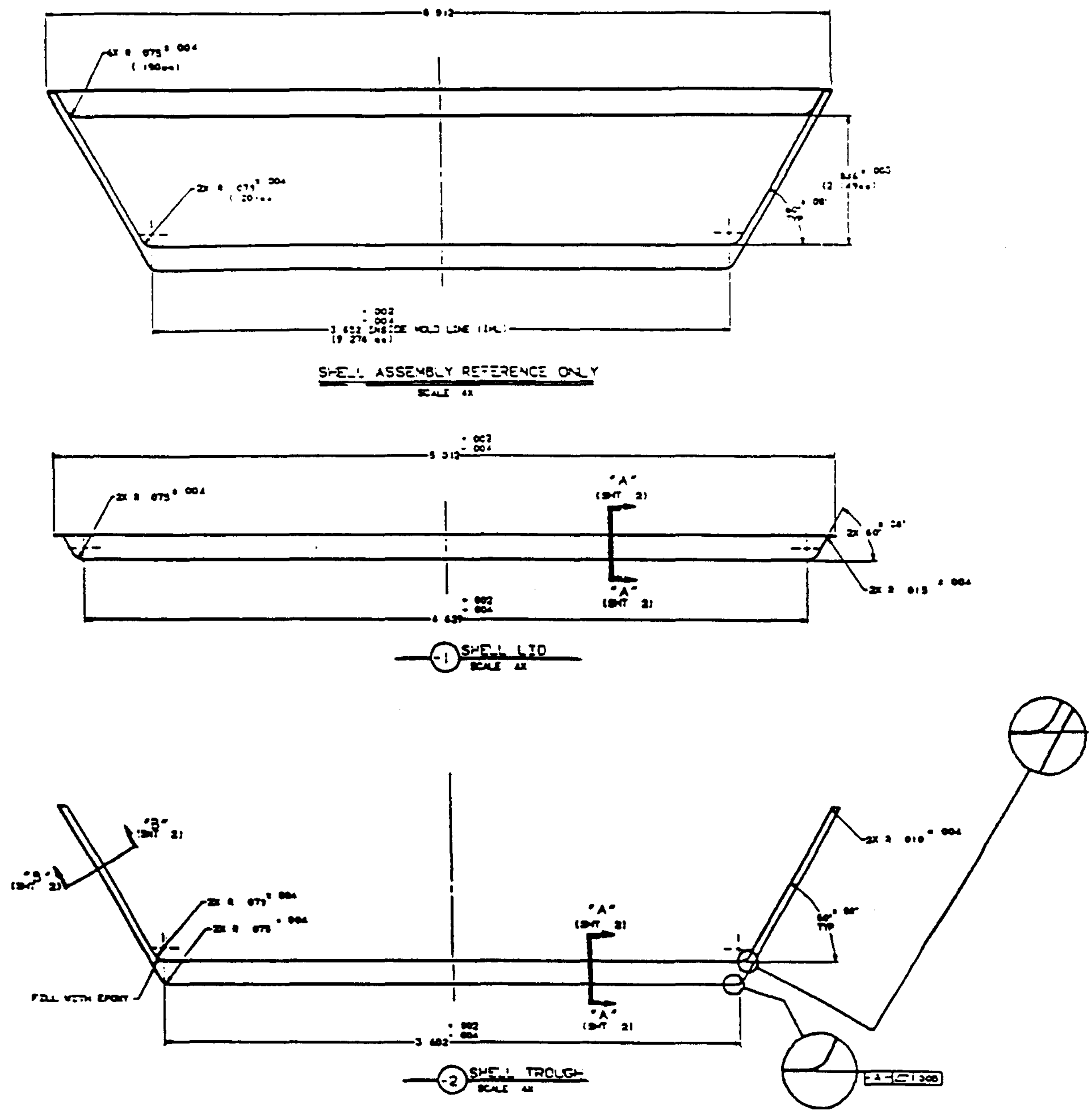

Fig. IV-3. The design of a trapezoidal shell using Rohacell foam on the lid and base sections. The completed module is shown at the top.

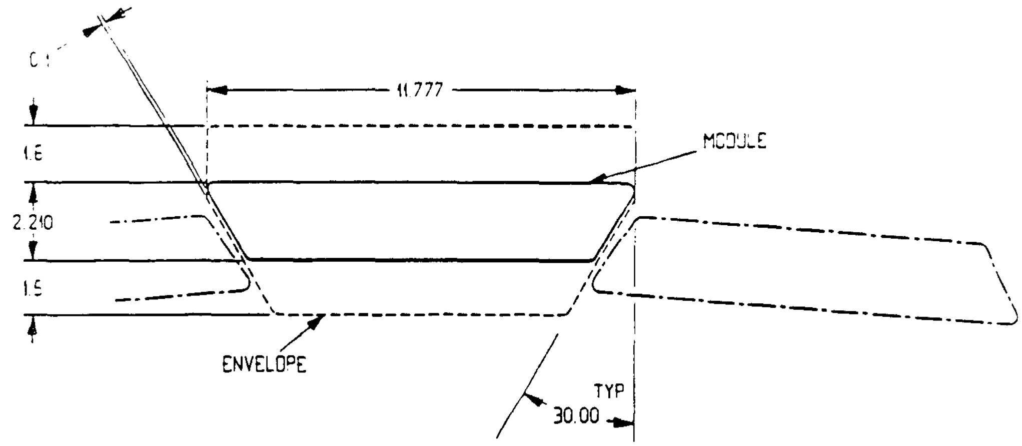

Fig. IV-4. A typical layout of axial modules.

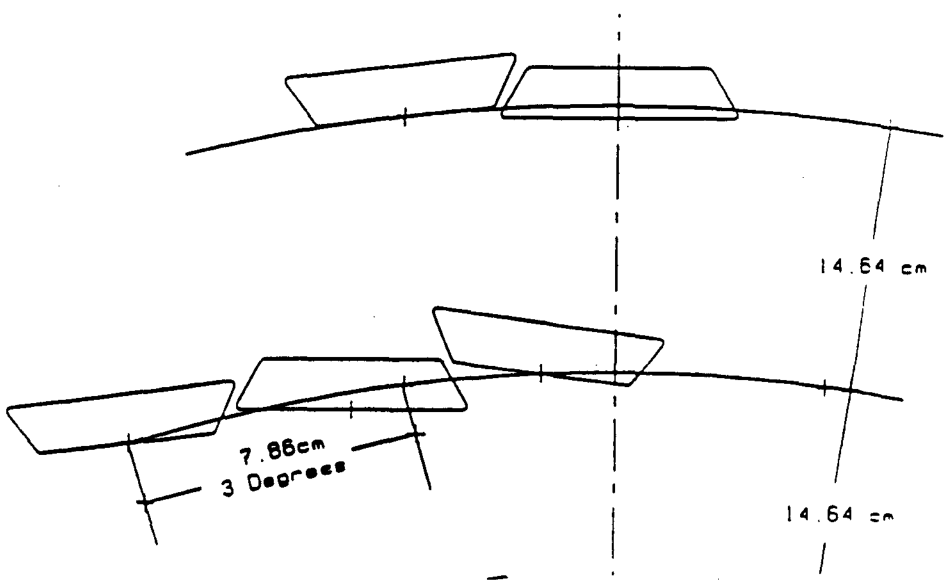

Fig. IV-5. The stereo module layout, showing the effect of radial staggering.

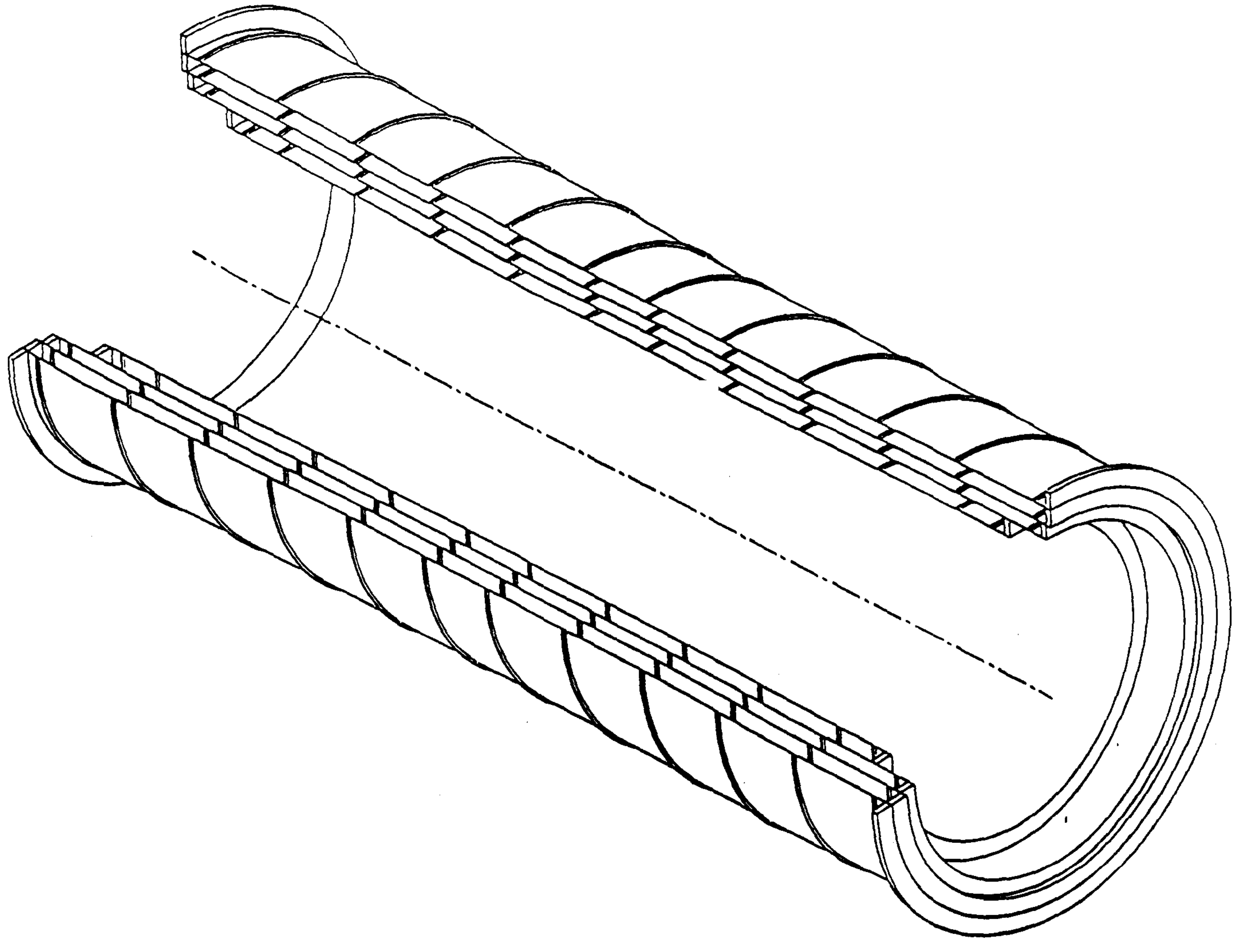

Fig. IV-6. The support cylinders for four superlayers in the engineering baseline design.

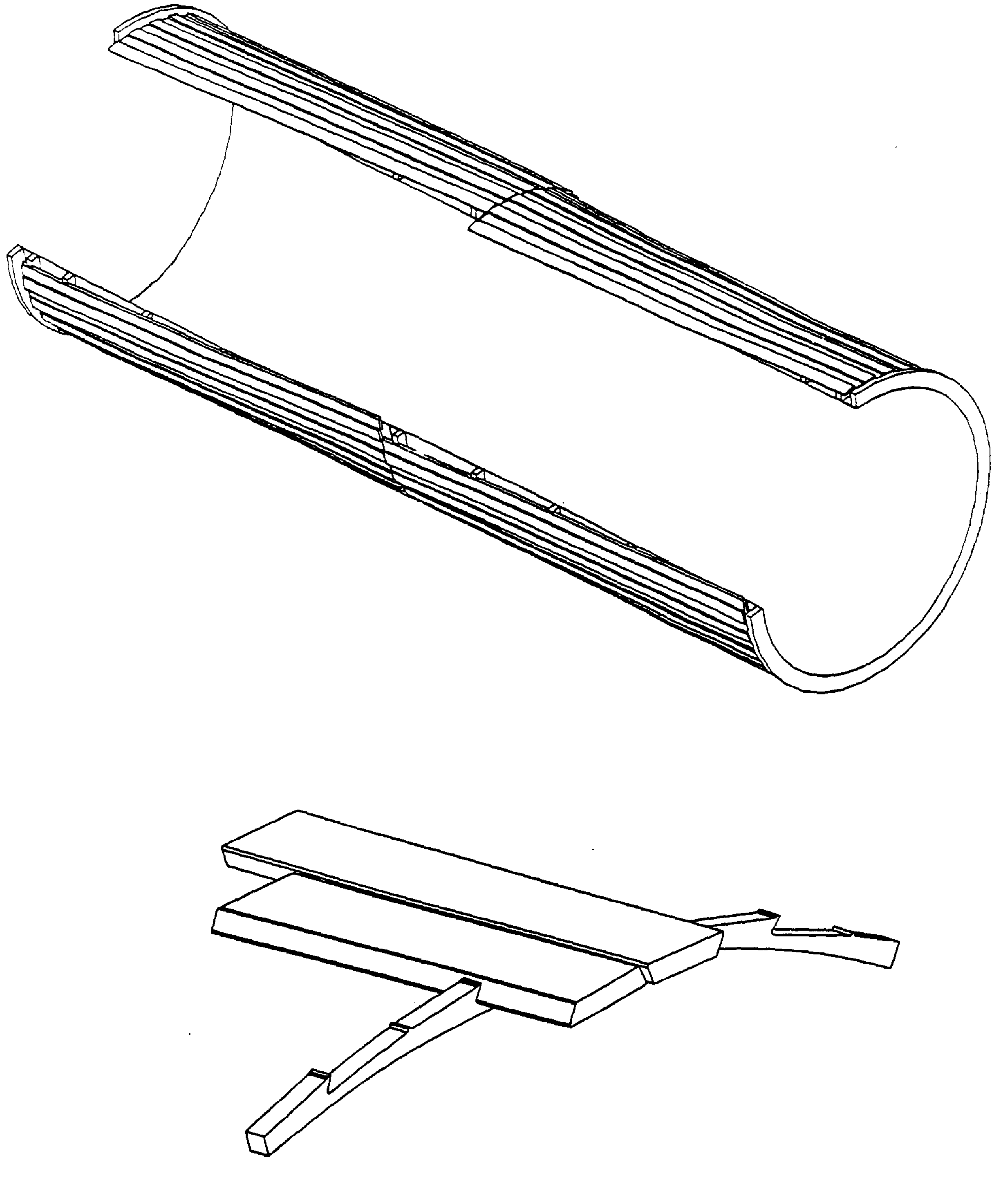

Fig. IV-7. The attachment of the stereo modules to the support structure using the shim rings. A close-up detail is also shown.

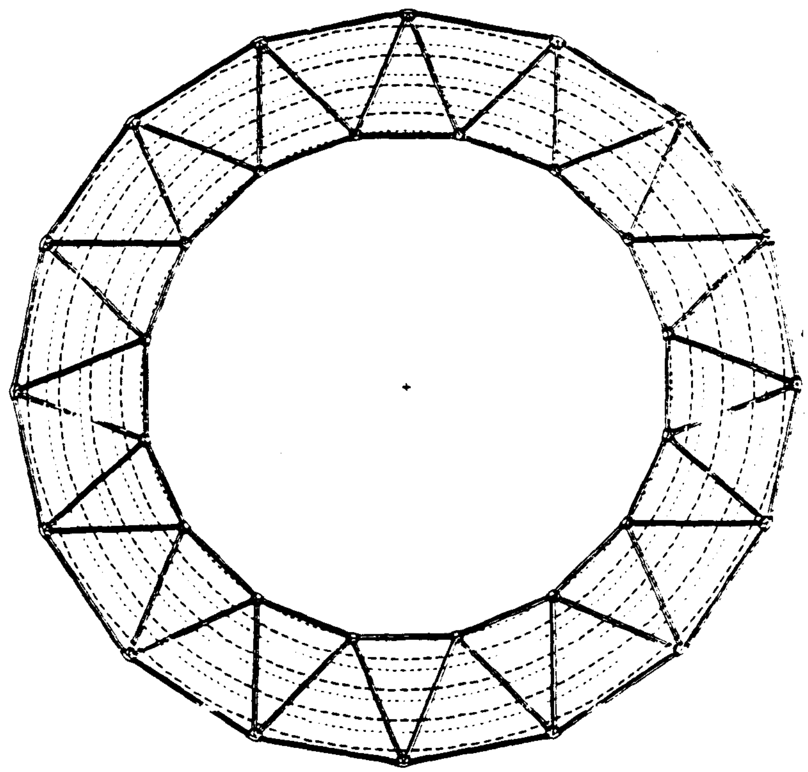

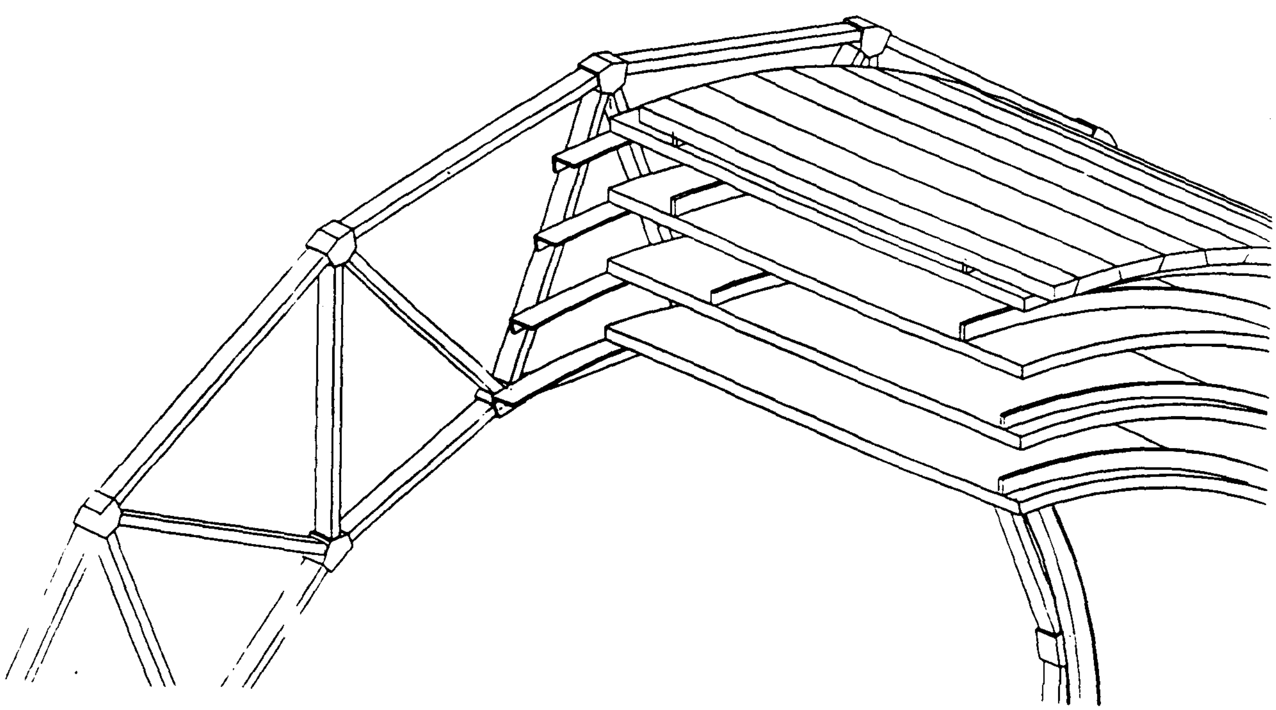

Fig. IV-8. Two views of the support structure, showing the end view as well as a more detailed view showing the cylinder and module attachment.

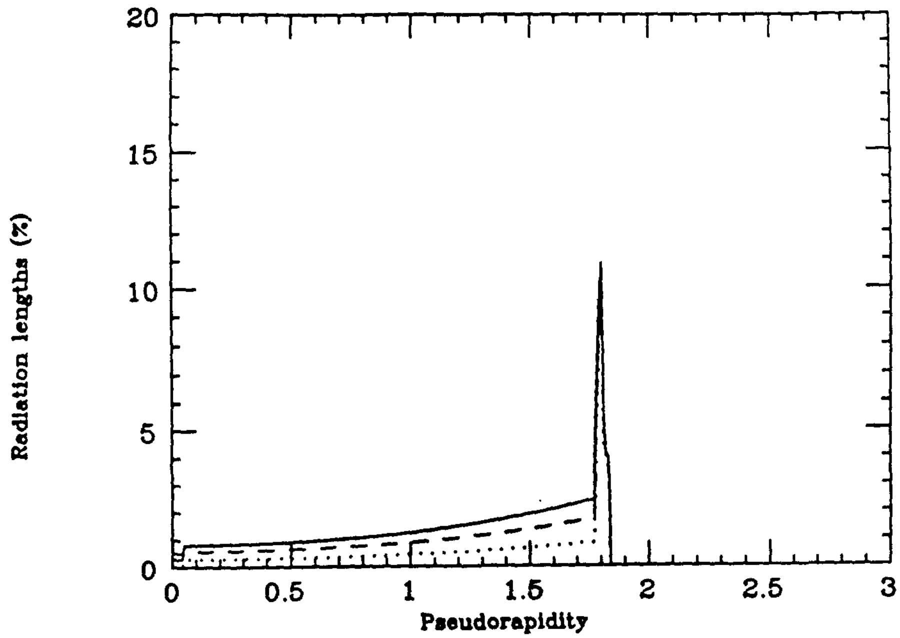

Fig. IV-9. The amount of material in radiation lengths as a function of η due to the straw tracking system. Dotted line: straws and electronics; dashed lines: adds the support structure; solid line: adds the modular shells.

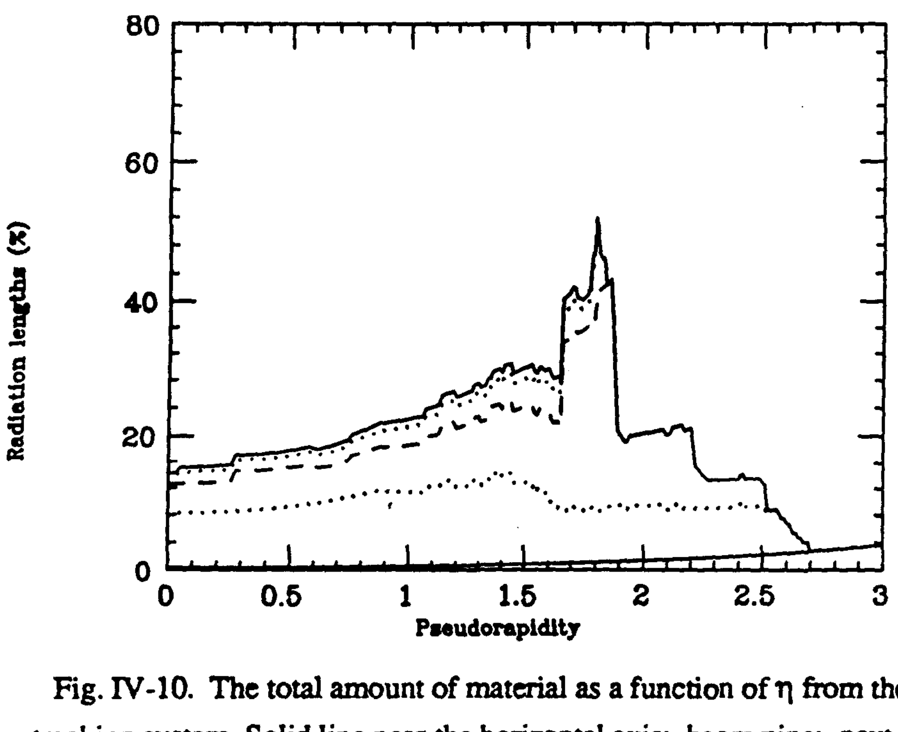

Fig. IV-10. The total amount of material as a function of η from the beam through the tracking system. Solid line near the horizontal axis: beam pipe; next dotted line: adds the silicon system; dashed line: adds the scintillating fiber system; dotted line adds the straw system with no shells; solid line: adds the modular shells.

tracker component	radiation length(%) at 90 degrees	sum with modules shell
Silicon system + beam pipe	8.0	8.0
fiber system+ supports	5.0	13.0
support cylinder	0.29	
module shell (10 mil wall)	0.24	
straws and supports	0.32	
support cylinder	0.29	
module shell (10 mil wall)	0.24	
straws and supports	0.32	
support cylinder	0.29	
module shell (10 mil wall)	0.24	
straws and supports	0.32	15.6
support cylinder	0.29	
module shell (10 mil wall)	0.24	
straws and supports	0.48	

Table IV-1. The material budget as a function of superlayer.

V. FRONT END AND TRIGGERING ELECTRONICS

Institutions: University of Pennsylvania, University of Colorado, University of Michigan, KEK, Indiana University, Oak Ridge National Laboratory

V.1. Introduction

During the past year the front end and triggering electronics efforts have been concentrated on developing and testing prototypes of the electronics. We have developed a conceptual design[17] for the electronics for a straw tube tracking system. We have fabricated prototypes of the preamplifier/shaper, the Time Memory Cell (TMC), and the triggering circuit (synchronizer). We have begun to be confronted with the detailed electrical and mechanical issues involved in testing the electronics prototypes on real straw tube modules and have designed an interface board to connect the sense wires to the prototype preamplifier/shaper circuits. We have completed the designs for an eight-channel preamplifier, shaper, tail cancellation and discriminator circuit and for the Time-to-Voltage Converter/Analog Memory Unit (TVC/AMU), and are continuing tests of the various radiation-hard processes.

V.2. Front End Electronics

Technical details of the progress during the past year of straw electronics research and development effort are contained in the report of the Front End Electronics Subsystem Collaboration, H. H. Williams, Spokesperson (September 1, 1991). Highlights from that effort are listed here, and some discussion of integration and system issues is attempted.

During the past year we have:

1. Fabricated, tested, packaged, and distributed the low noise, fast shaping time (5 ns) single channel preamplifier and shaper in large size (> 600) sample lots. This preamplifier/shaper is:

a. Constructed using the AT&T complementary bipolar process

b. Designed with fully differential inputs to allow pickup cancellation

c. Packaged in a small outline 16 pin package suitable for surface mounting

d. Available with yields before packaging of ~ 95% and after packaging of ~ 90%

e. Radiation-hard to doses in excess of 5 Mrad; i.e., a 10% shift in gain after 5 Mrad has been measured and there was no change in the signal/noise.

2. Designed, fabricated, tested, and distributed a small multilayer printed circuit test board[18] to house four of the AT&T single channel amplifiers.

3. Finished the design and nearly finished the layout of an eight channel preamplifier, shaper, tail cancellation, and discriminator[19] circuit. This circuit is:

a. Designed using the Tektronix *SHPi* high speed bipolar process, which has lower parasitic capacitances than the AT&T process, but lacks the fully complementary (PNP as well as NPN) transistors of the AT&T process

b. Laid out using *Quick Tiles* as a compromise between the very high densities possible with a full custom design and the predictability and high yield of a fully characterized fixed array. We should note that even with this *compromise* density we are apparently limited by the number of pins rather than the actual silicon area needed for devices and connections.

c. Likely to be capable of triggering reliably on a few femto-coulombs of charge generated by a single electron avalanche - the noise floor is set largely by the 300 Ω resistance needed to properly terminate long straw tubes

d. Designed using a process that is also radiation hard (at least in terms of gain and offset voltage variations - noise figures have not been measured yet) to better than 5 Mrad.

4. Finished the complete redesign of the TVC/AMU.[20]

   a. All cells have been examined and, where necessary, redesigned and re-laid out and re-simulated to operate properly at above the design rate

   b. The most complex parts of the logic (the *transfer* block) have been fabricated in a 2 μm non-rad-hard process and have been tested and shown to work properly at > 60 Mhz

   c. Blocks which were inefficient in terms of area or power have been redesigned to make better use of the silicon - most notably the Delay Logic which is sensitive to changes in the length of the Level 1 (L1) Trigger Time

   d. The complete, single channel, TVC/AMU up through L1 logic and including eight L1 and four L2 memory units has been tied together for simulations[21] at both the schematic and layout level.

5. Extensive measurements have been undertaken on the UTMC 1.2 μm CMOS process to characterize DC and noise behavior before and after radiation. These measurements indicate that this process is likely to be capable of producing TVC/AMUs and other analog objects capable of operating successfully well past the 1 MRad region.

6. Layout and fabrication of test structures in the IBM 1.0 and 0.5 μm CMOS processes has begun with the expectation of having parts to measure this Fall.

The tasks remaining include:

1. Fabrication and test of the eight channel preamp/shaper/discriminator.

2. Fabrication and test of the single channel TVC/AMU.

3. Layout of the full (L2 logic) TVC/AMU.

4. Layout of four or eight channel TVC/AMUs.

5. Transfer of the TVC/AMU design to a radiation hard process.

But, probably most importantly, the difficult issues will center around packaging of a complete system and interactions between the detectors, front end signal processing, and back end trigger and DAQ signals. The test chips and the test modules that are just beginning to be available are vital to a beginning understanding of the complex set of interactions that will occur in the full scale detector, but the present single channel devices fall far short of the densities actually necessary in the final detector. As multi-channel preamps become available in the Fall or Winter, it will be possible to begin making nearly full density mock-ups of electronics packaged directly onto the straw ends as is presently envisaged (see the Preliminary Conceptual Design Report for SDC Straw Electronics[17]). This will require closer co-ordination of mechanical and electronic efforts over the coming year.

V.3. Time Memory Cell

The Time Memory Cell (TMC)[22] utilizes low-power and high-density characteristics of a CMOS memory cell. A four-channel 1024-bit Time-to-Digital Converter chip, which records input signals to memory cells at 1 ns intervals, has been developed at KEK. To achieve 1 ns precision, the chip incorporates a feedback stabilized delay element. The chip was fabricated on a 5.0 mm by 5.6 mm die using 0.8 μm CMOS technology. It dissipates only 7 mW/channel under typical operating conditions. Tests show that overall linearity and stability are very good. Several prototype modules have been built and distributed to groups making measurements on straws.

V.4. Triggering Electronics

V.4.1. Introduction

We have continued the work on triggering with superlayers of straw tubes. The work is proceeding in both the simulation and the development of Application Specific Integrated Circuits (ASICs).[23] The first all digital implementation has been designed and fabricated, and initial tests are underway. Results to date indicate that the unit functions as designed. A cosmic-ray test stand to exercise the chips with the 64-straw prototype module is complete and will be used to inject actual straw tube signals into the trigger chips.

V.4.2. Chip Development

The circuit that is being tested is a single stage synchronizer based on 2 ns delay elements. It has 15 delay elements in the momentum selection portion of the circuit and 30 delay elements in the total drift time section. This gives it a range of up to 30 ns in the timing difference of radial wires and up to 60 ns of maximum drift time. Values less than these extremes are programmable within the chip. The locking of the delay element timing to an external clock is provided as well as numerous diagnostic points. We have tested the delay cell and locking circuits and have found them to function over the range of 1.3 ns to 4.0 ns, consistent with the CAD simulations. The mean timers have been found to work, and the drift time and momentum restriction circuitry has been partially tested. No design errors have so far been found. Testing is continuing.

V.4.3. Trigger Algorithm Simulation

We have continued to work on trigger simulation in the framework of GEANT, a fast emulation of a stiff track trigger, and with the parametrized global trigger being simulated at Chicago. The utility of a stiff track signal for electron identification has been demonstrated (namely that a 10 fold reduction of the QCD 2 jet rate of false electrons can be effected) and the stiff track momentum resolution requirements (approximately 10% or better) have been shown. This matches the characteristics of the proposed straw track trigger well. We have assessed the effect of material on the trigger with regard to occupancy and additional false rate. At the level of material proposed no significant variations in false rate have been seen. The uncertainty rests with the low statistics inherent in the slow GEANT simulations. This work is continuing along with a program to determine the triggering efficiency for electrons which show significant losses as the amount of material is increased ahead of the trigger. We continue to pursue a trigger based on 8 straw tubes per superlayer. Numerous connection arrangements are being investigated as a means of optimizing the trigger characteristics and fabrication ease for the ASICs.

V.4.4. Cosmic-ray Test Stand

The cosmic-ray test stand is mechanically complete with scintillator trigger counters, straw tube layer, amplifier-discriminators, and cabling. We plan to connect this stand to a LeCroy 1879 Fastbus TDC in the near future and begin testing the straw tube pattern. Our plan for testing trigger chips is to use the auxiliary card connection of the LeCroy TDC for pickoff of the straw outputs, form the trigger with one of several options, and reconnect the trigger results back into unused channels of the 1879. We will first exercise the chips that arrived in July. Later versions will also be tested. The auxiliary cards that we plan to use are already in hand.

V.5. Interface Between Straw Module and Electronics

We have worked out a number of refinements to the design reflected in the prototype modules that will be appropriate to a wire detector for the SSC. The connection of the detector sense wire to its readout electronics requires special care to minimize noise and crosstalk in view of the low gas gain and high amplifier sensitivity at which the detectors will be operated at the SSC. At the same time the burden of material placed in the path of the particles being detected is of concern, as is the management of failures (e.g., wire breakage) under conditions of limited accessibility. We plan to supply high voltage to the sense wire via the same connection from which the signal is extracted, through an end structure which must also provide gas supply or return. A potentially bulky decoupling capacitor must also be accommodated. The electronics board is to be removable for servicing. Space around the close-packed 4-mm-diameter tubes is extremely tight.

As mentioned previously, the 64-detector short prototypes have passive connector boards to feed high voltage at one end and to extract signals from the other. Decoupling capacitors in this version are surface mounted on the boards. Constraints resulting from the presence of high voltage on the board limit options for mitigating crosstalk. We are designing a second generation connection board which will incorporate in-line capacitors perpendicular to the board arranged in the footprint of the module end. Besides improving crosstalk, this design brings us closer to the high density layout ultimately required.

A conceptual design of the end structure is shown in Fig. V-1. Again the coupling capacitor is placed in-line between the sense wire and its preamp, while the cathode attachment is maintained locally and, as nearly as possible, in a coaxial configuration to avoid ground loops and coupling to neighboring channels. We have obtained quotes for fabrication of the parts which indicate that, with some further refinements in the design, a cost in the neighborhood of $1 per channel or less should be possible. We have not, however, invested the $30,000 startup cost for making prototypes at this time.

V.5.1. Prototype Front End Electronics Board

We have generated the layout (Fig. V-2) for a multilayer printed circuit board to contain 16 channels of the custom amplifier/shaper chips together with commercial comparators for use in prototype evaluation. The first boards have been made and are being loaded with components at this time.

Our planned next step will be to prepare a layout incorporating next generation eight-channel amplifier-shaper-discriminator chips, currently about to be submitted for production by the Tektronix *SHPi* high-speed bipolar process. This will be implemented first as surface-mount packaged chips, and subsequently as bare die on the board substrate to increase the density and approach the close-packed footprint to mate with the straw tube modules.

Figure V-3 shows a conceptual layout[24] for a board to service a module. This was made as an exercise to help understand the requirements for trace dimensions, substrate and bonding techniques, etc.

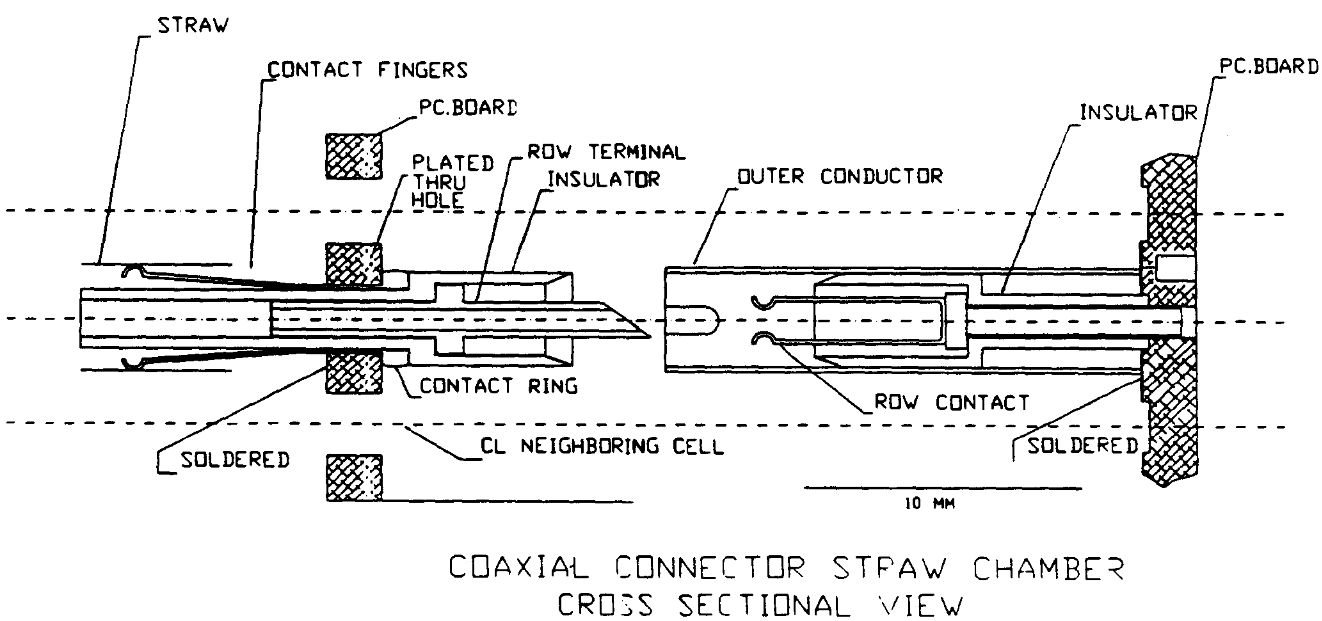

Fig. V-1. A scheme for anode wire and cathode tube electrical connection to the readout board. The sliding spring contacts permit ready attachment and removal of the board.

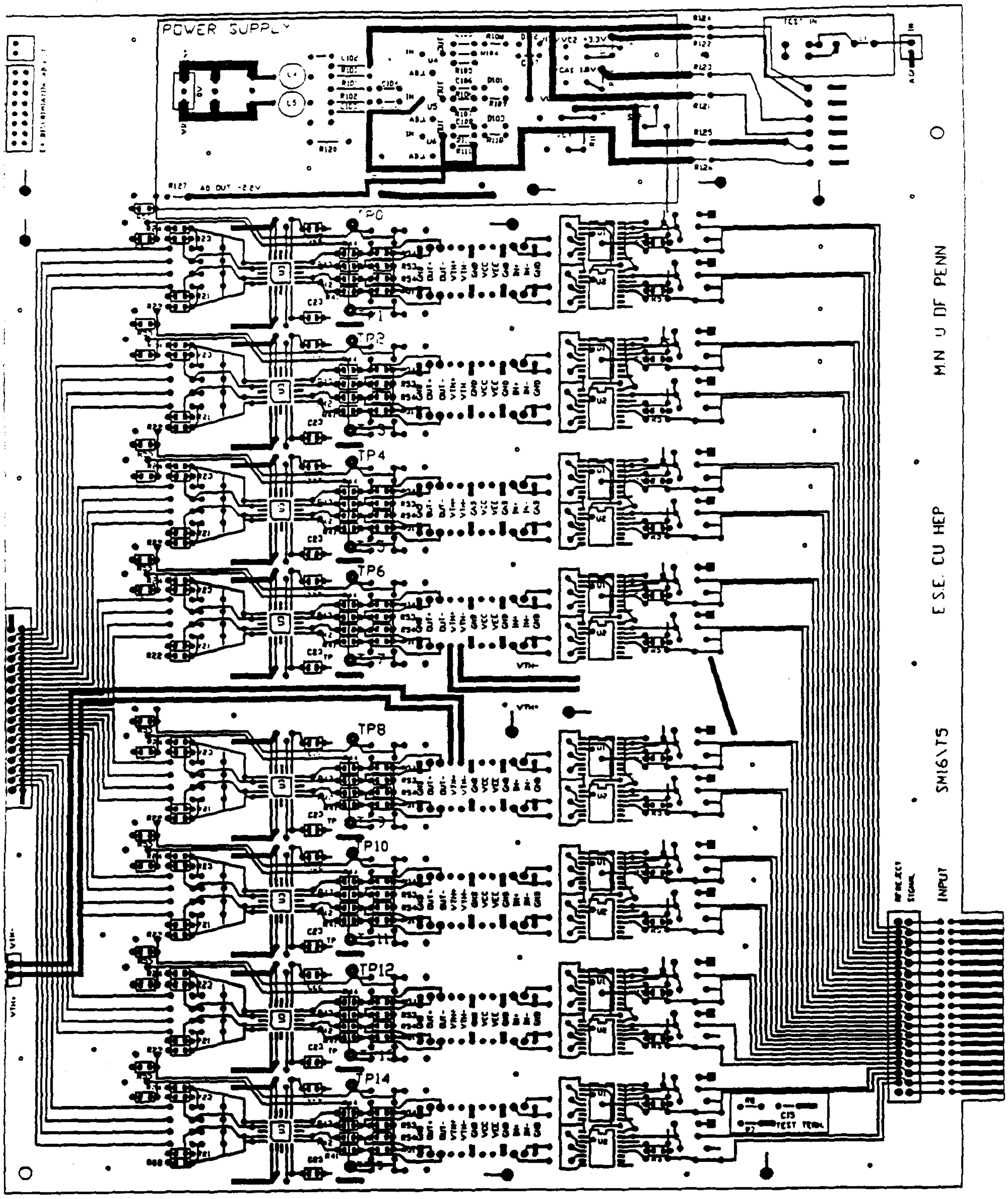

Fig. V-2. Sixteen channel readout board containing custom amplifier-shaper chip and tail cancellation piggyback board, with a commercial comparator.

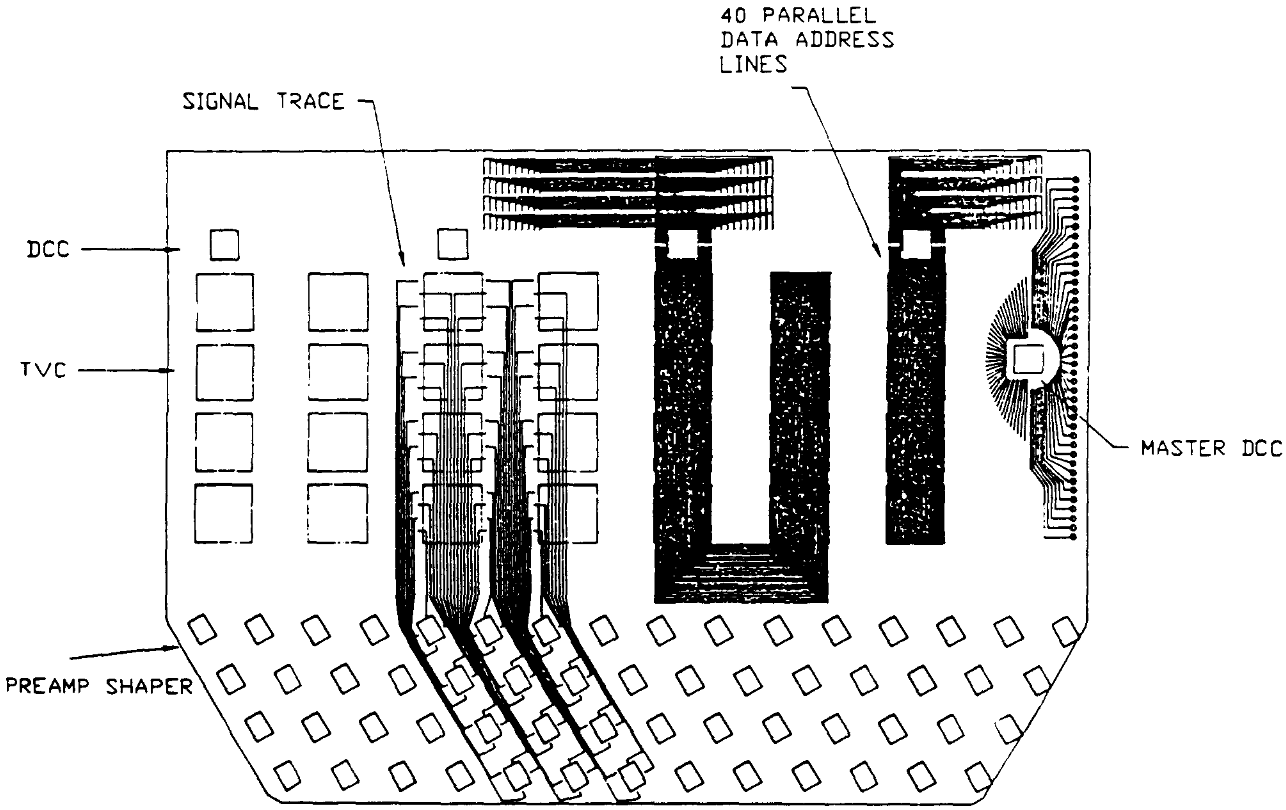

Fig. V-3. Preliminary layout for a front-end electronics circuit board for connection to about 240 straw tubes.

VI. COMPUTER SIMULATION

Institutions: Indiana University, University of Colorado, Lawrence Berkeley Laboratory

VI.1. Introduction

The simulation program for the central tracking system has advanced greatly in the last year. A detailed GEANT-based model of the central region straw tube tracking system has been developed. This simulation effort was initially made using GEANT only, but now the GEANT models have been successfully incorporated into the SDC standard simulation/analysis program, the SDCSIM SHELL (which is commonly referred to as "the SHELL"). The SHELL is intended to provide an organizing superstructure for both the GEANT simulation and the online/offline analysis code for the SDC detector. Fixed versions of the SHELL are distributed to the entire collaboration via electronic computer networks to insure that a detailed simulation of the entire detector is rapidly available to the entire collaboration. As a service to the SDC collaboration, part of this distribution process was developed by the straw tube tracking group. This group also contributed greatly to the development of data structure banks for recording the hits within the SHELL and in development of the SHELL software. This year the straw tube simulation was expanded to contain a number of additional details: a model of the adjacent parts of the SDC detector (beam pipe, silicon tracking system, and magnet coil), a description of the cylindrical carbon support structures for each superlayer, an accurate model of the materials within the straw tube system, properly distributed background (minimum bias) events, stereo detector layers, and a detailed model of the readout of the detector based on the timing of hits within the system. Preliminary occupancy, segment finding, and pattern recognition studies were made in the central region using the improved simulation. Much progress has been made to integrate the outer barrel tracker with the inner silicon tracking system and to study pattern recognition algorithms that take advantage of the integrated tracking system. We have also begun to study the descoping issues related to the central tracker particularly in the context of a combined silicon-straw system. The straw tube simulation has also been used as the basis for studies of the first level straw tube trigger, described in Section V.4.3. Much of this work has been done on a variety of UNIX-based workstations that execute the code much more quickly than the SLAC main frame and VAX computers used previously.

Converting the code to run correctly in an UNIX environment required a major investment of time and is now complete.

VI.2. Simulation Details

The description of the overall SDC detector geometry has been greatly improved. The simulation is now run as part of the SHELL and consequently we automatically have access to the geometries of parts of the detector located near the central tracking system: the beam pipe, the silicon tracker, and the magnet coil (see Fig. VI-1 for a picture of the combined system). Each SDC detector subsystem group has spent a great deal of effort to create a model of their detector compatible with the other detector subsystem models and the rules of the SHELL. The straw tube simulation is now made completely within the SHELL and as a result is available to the whole collaboration. Use of the SHELL automatically includes the effects of the materials in the other parts of the SDC detector. Also for explicitly studying the effects of materials, a simple set of commands can be used to turn on and off the use of the model of each part of the SDC detector (within the SHELL).

The proposed straw tube detector tracking geometry (which we are simulating) consists of a number of cylindrical detectors made from a support cylinder covered with a layer of straw tube modules that actually detect the charged particles. These structures are called superlayers and are spaced throughout the outer tracking volume. For simplicity and to reduce computer time consumption, the simulation does not introduce individual straws and modules; instead, the simulation uses a homogeneous volume of material with appropriate density to represent the modules. Within the simulation, the superlayer is divided into layers and during the tracking of the simulated particles, user-written code records which straws were struck. A layer is the smallest volume introduced. Both the real detector and the simulation are divided into two halves along the beam directions. See Figs. VI-2a and VI-2b for end and oblique views of this geometry. For each track, a superlayer measures a cluster of hits (known as a segment) which contains information about the track momentum. While a track follows a curved path, the curvature of the tracks with rather high transverse momenta (p_T) is small over the thin superlayers (2-3 cm), and the hits recorded fall on essentially straight lines within the superlayer. The angle of the segment relative to the superlayer depends on the curvature of the track which in turn depends on the p_T of the track. High p_T tracks produce segments that are perpendicular to the superlayer, and lower p_T tracks produce lower angle segments. Figure VI-3 shows an end view of a straw tube tracker containing the hits from four tracks; lines are drawn through a low and a high p_T track to illustrate the relationship between segment angle and p_T. Each high p_T (stiff) track passes through several superlayers so that a redundant measure of track momentum is obtained, and the process of assigning detector hits to tracks is facilitated.

For the straw tube system, a detailed description of the detector material and geometry is read from an external file. The wires in straw tubes run parallel or nearly parallel to the central axis of the detector and hence provide an azimuthal measurement (ϕ) of the track. The support cylinder is made of a carbon fiber material and is modeled using the GEANT material "carbon" to match the parameters given in the straw tube placement report.[11] The straw tube layers also contain an accurate allowance of material for the straws and the carbon fiber outer shells of the straw modules. This amount of material can be set within the geometry file. The geometry file inputs define the number of superlayers (8 before descoping, perhaps 5 after) and the number of layers within the superlayer (normally 6 for nontrigger and 8 for trigger layers). Since the straw tube detector description is read from a file, testing of multiple geometries for descoping and material studies is easily possible. The external file can also contain statements that activate debugging code. The external file can also contain a command to turn off the straw tube hit recording algorithm; this allows other subsystems to use our geometry as material only, without waiting for a full straw tube hit analysis.

The geometry description includes the full use of both stereo and axial layers. Axial layers have their wires running exactly parallel the central axis of the support cylinder, while stereo layers have their wires tilted at a 3° angle to the central axis of the superlayer. When axial and stereo layers are analyzed in conjunction with each other, the z position of the track along the superlayer can be calculated (z is the direction of the central axis of the superlayer). The use of stereo layers required the introduction into GEANT of a new volume shape, the "HYPE". The HYPE is the surface created by rotating a hyperbola around a cylindrical axis which is the geometrical shape of an ideal stereo layer. The superlayer description can have any amount of support material (including none). The straw tube geometry file allows any layer to be defined with any stereo angle or to be axial.

The simulation includes a detailed model of the way the straw system records the hits caused by the combined effect of an event of interest and background minimum bias events occurring in crossings before, during, and after the event of interest. Low energy tracks both from the event of interest and the minimum bias events can spend hundreds of nanoseconds spiraling through the detector and affect the readout of events tens of crossings after the track was generated. Figure VI-4a contains a time distribution for the hits caused by 25 minimum bias events in an accurate model of the SDC detector, and for comparison Fig. VI-4b shows the time distribution of hits with a very low mass SDC detector. Clearly while the mass of the detector causes a slight increase in the number of hits, it also has the desirable effect of clipping the long tail of late hits. The late hits are caused by low energy tracks that helically spiral (loop) around in limited areas of the detector and are consequently known as loopers. Loopers will strongly interfere with the readout of the detector along their trajectories. It is important to realize that these looper hits are not uncorrelated because the loopers affect groups of closely spaced straws. The background hits can either mask or supersede the hits from the event of interest and also produce legitimate stiff tracks which are not related to the event of interest. As the luminosity of the SSC increases, the detector experiences an increasing level of minimum bias hits, and the probability of losing a track or creating a false track from unrelated hits grows.

To study the effect of loopers, our simulation records the hits over a wide time window (as wide as -20 to +4 beam crossings) and models how hits would be recorded. The minimum bias events are modeled using the programs PYTHIA 5.4 and JETSET 7.3 to generate minimum bias tracks with an accurate rapidity distribution. The simulation stores all hits generated over this wide time region (in addition to the hits from the event of interest) and calculates which hits would actually be recorded by the front end electronics. The recording algorithm is blind to whether the hits it records are from the event of interest or a minimum bias event. The hits that are recorded must be in a 50 ns gate defined by the timing of the event of interest. The recorded hits must also not be blocked by a hit just before the event of interest because the front end electronics will not respond to the second of two closely-spaced signals. A realistic 40 ns dead-time for this effect is included. The hit recording algorithm considers the time offset (from the event of interest) of the bunch crossing producing the particle, the flight time of the particle producing the track, the drift time of the electrons to the sense wire, and the propagation time of the resulting signal to the front end electronics. Kinematical information about the track causing each hit is recorded for later use in understanding how well event reconstruction algorithms worked. All of the parameters for the model described above can be read from the external straw tube geometry configuration file.

VI.3. Event Reconstruction Algorithms

Two separate and independent superlayer-based segment finding and pattern recognition algorithms were developed and tested for the straw tube system. Work was begun to extend these algorithms to encompass a combined system of silicon and straws. Each algorithm has the same goals: (1) locating clusters of hits (segments) caused by individual tracks within a superlayer, (2) linking the segments into tracks, and (3) fitting the tracks to assign ϕ, p_T, p_z, and impact parameter to each track.

The first algorithm is based on a "road" algorithm. In a road algorithm, hits are searched for along a set of trajectories within the detector. The test trajectories are calculated using a set of predefined curvatures (essentially p_T's). This type of algorithm can be used to both find segments and to link segments from one layer to the next. In the segment finding case, hits in the outer layers of a superlayer are used as starting points for the roads. The starting hits are known as anchor hits. The anchor hit has the effect of defining the azimuthal position (ϕ) of the segment. For each of the curvature bins, the algorithm calculates using a straight line (the segments are essentially straight lines) which straws would be hit based on the track passing through the anchor hit; these sets of straws form the roads. Each road is examined to see if its straws are hit. Provided a minimum number of hits are found, a new segment is recorded for the path with the most hits. The ϕ and curvature for the segment are also recorded using the hit drift time to improve spatial resolution of the hit. A similar algorithm is then used to do the pattern recognition needed to link segments from different superlayers into overall tracks. In segment linking, segments are currently linked using outer superlayer segments as anchors (much as segments are formed using outer layer hits as anchors). This algorithm first links the axial layers to define the track in ϕ/curvature space and then links the stereo layer segments into the track to find the z of the stereo segments and ultimately the polar angle of the track. The algorithm is currently being modified to use a non-anchor segment approach for the linking in order to combine and link silicon and straw segments on an equal basis.

The second segment finding algorithm starts a search for hits with the outermost and innermost layers of a superlayer, proceeding from pairs that would give a reasonable crossing angle. For all left/right ambiguity combinations with these hits, it searches each remaining layer in turn for a compatible hit. For either ambiguity choice of the candidate hit, a fit of a line tangent to all of the drift isochrons is made. Solutions meeting a chi-squared test are used to interpolate to the next layer to continue the search for new hits. The code works its way through the superlayer until all layers are exhausted, updating the segment fit with all accumulated information at each stage.

Track segments found by this algorithm are then linked with one another and with hits in the inner silicon detectors using an algorithm developed by ALEPH. Starting from the outermost superlayer, this algorithm uses the vector quality of a found segment to point to a location in the next inner superlayer. If a track segment there has similar parameters, the algorithm looks inward for segments. It continues in this fashion until all superlayers of the straw tracker and all layers in the inner silicon have been searched. The final track fit then comes from fitting the segment parameters. Ultimately, the final track fit will have to be a refit of all the individual hits found to belong to the same track. The maximum number of superlayers that can be skipped while searching for segments to link together is controlled by a parameter, currently set to one.

Although the segment finding algorithm works well on stereo layers, the segment linking and track fitting are not yet optimized when stereo layers are included. Better utilization of the stereo information will be installed in the next few months.

VI.4. Simulation Results

The simulation results fall into two main categories: occupancy results for the design luminosity using minimum bias events and pattern recognition results for Higgs events with and without a minimum bias background. Most of these results use hits from an eight-layer straw tube system where the silicon contributes only dead material to the result. The work on the descoped, combined silicon and straw tube system is at an early stage and will produce results in the coming year.

The occupancy results for an eight-layer straw tube system are shown in Fig. VI-5a (straws with no other material) and Fig. VI-5b (a full system of beam pipe, silicon, coil, and straw). Even with a full set of material (except pixels) within the straw tube system, the innermost layer has an occupancy of about 10%. Conversions from the beam pipe/silicon slightly raise the occupancy of the inner superlayers. The greatest increase in occupancy caused by material is in the outer superlayers of the straw tube system. In this outer region, the occupancy almost doubles (going from the 1.5% to 2.5%) when the material of the coil is included. These results must be considered preliminary because the magnetic field was taken to be uniform over the entire thickness of the coil.

The pattern recognition results are at a somewhat more rudimentary stage. Figure VI-6a shows the raw hits for a system of eight superlayers and Fig. VI-6b shows the hits found on stiff tracks using the road-type algorithm. Figure VI-7 shows the number of possible matching stereo segments found for this system when all four axial segments are found. This plot used ISAJET simulated Higgs events and PYTHIA minimum bias events. We see that there is apparently a quite low inefficiency since there is almost always at least one possible segment (the right-most bin shows the number of times zero segments were found in the search region within a superlayer). Work still remains to improve the algorithm for selecting the correct stereo segment, especially when the background rate is high. Using a modified version of this algorithm, we hope to reconstruct hits in the entire silicon/straw tube tracking system to assist in defining the scope of the tracking system. A paper[25] was presented at the Fort Worth Symposium showing preliminary segment finding efficiencies with a considerably different system than is now proposed to be built. This paper used the second track finding algorithm described above.

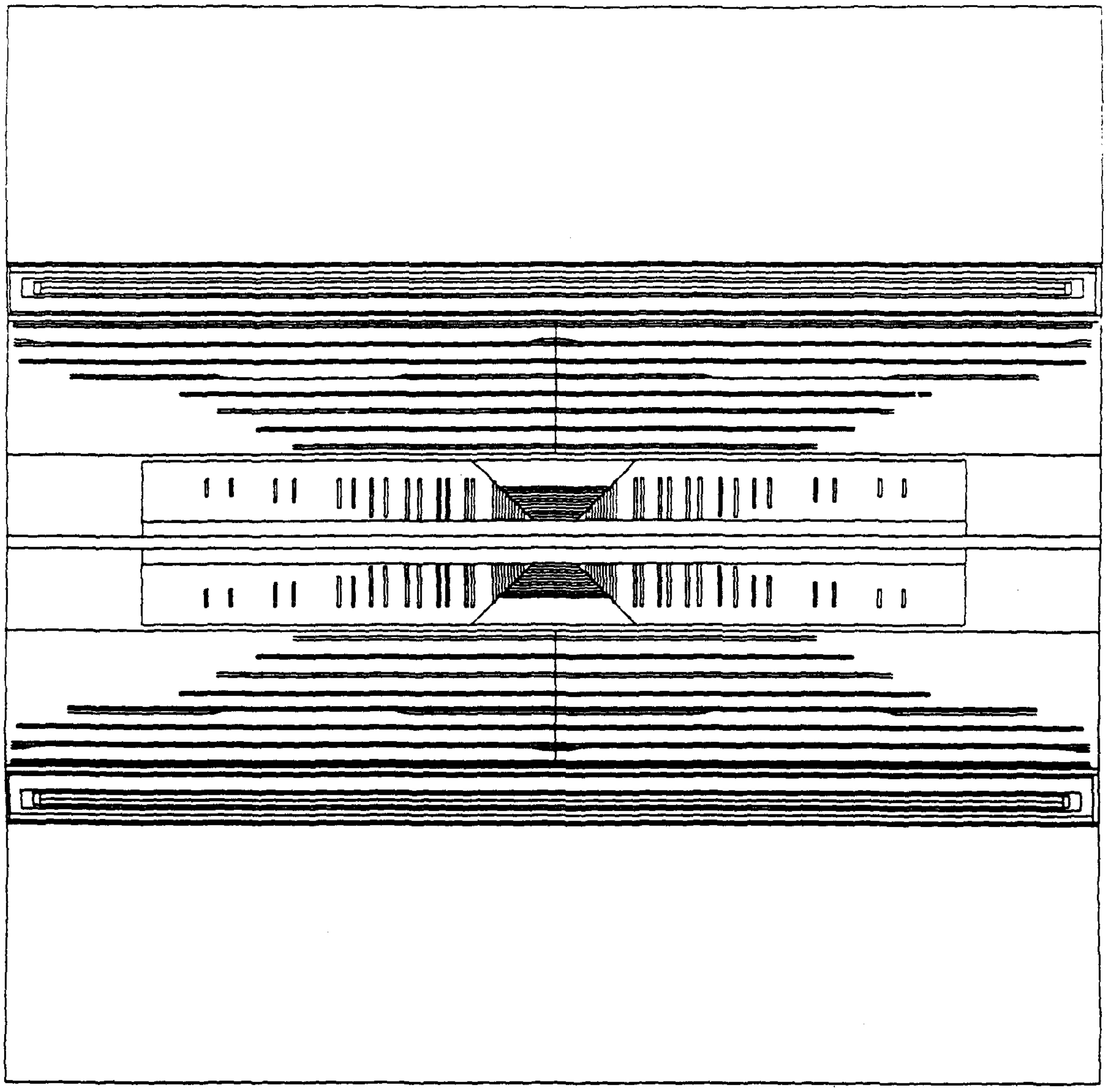

Fig. VI-1. A side view of the of the SDC tracking region detector geometry (as defined in the SHELL). The figure shows the beam pipe, a full silicon detector, a full (eight superlayer) straw tube system, and the solenoidal magnet.

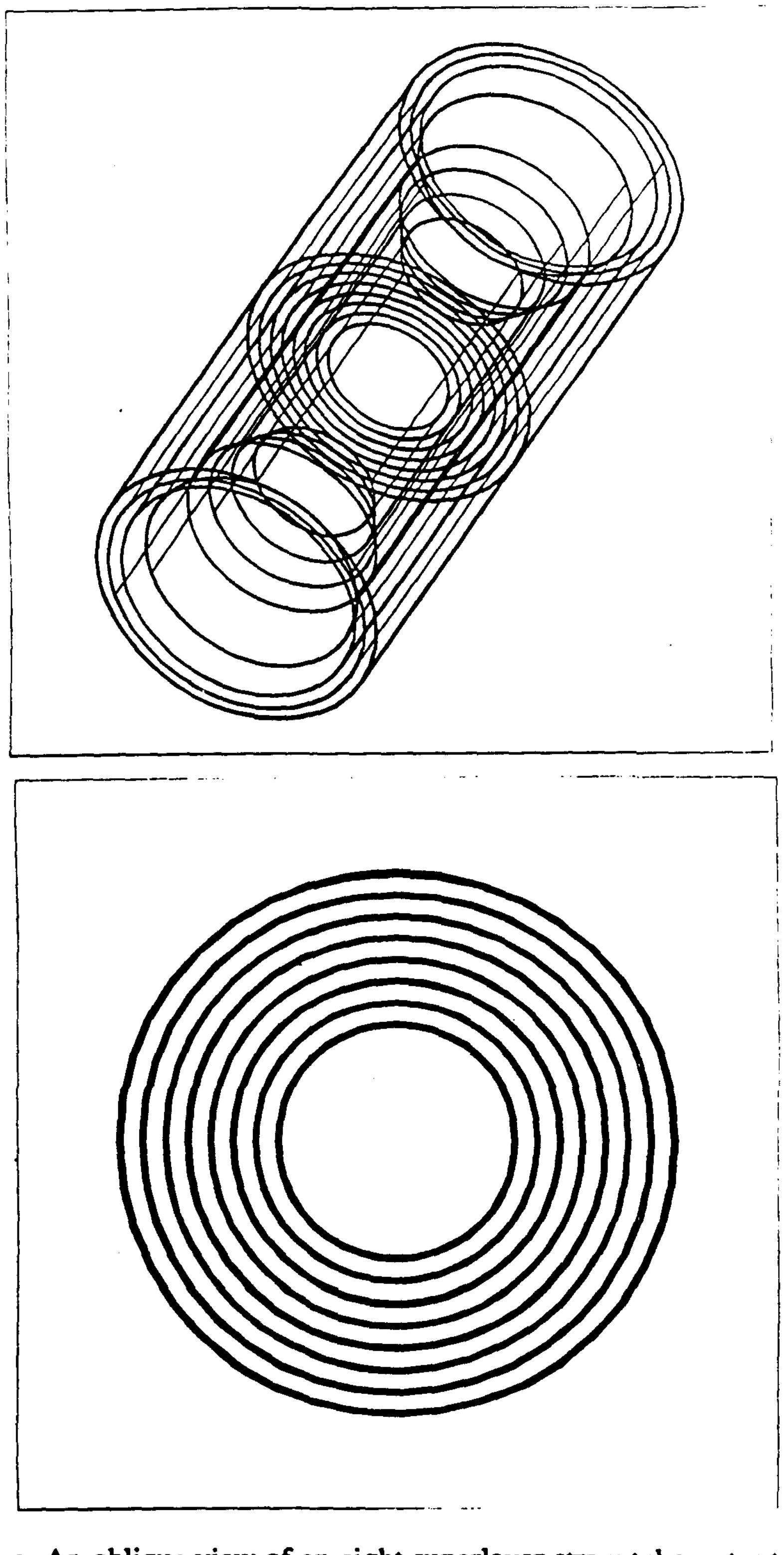

Fig. VI-2. a. An oblique view of an eight superlayer straw tube outer tracker. While not visible because of the scale of the drawing, this geometry includes individual volumes for each layer-half and carbon support cylinder.

b. An end view of an eight superlayer straw tube outer tracking system.

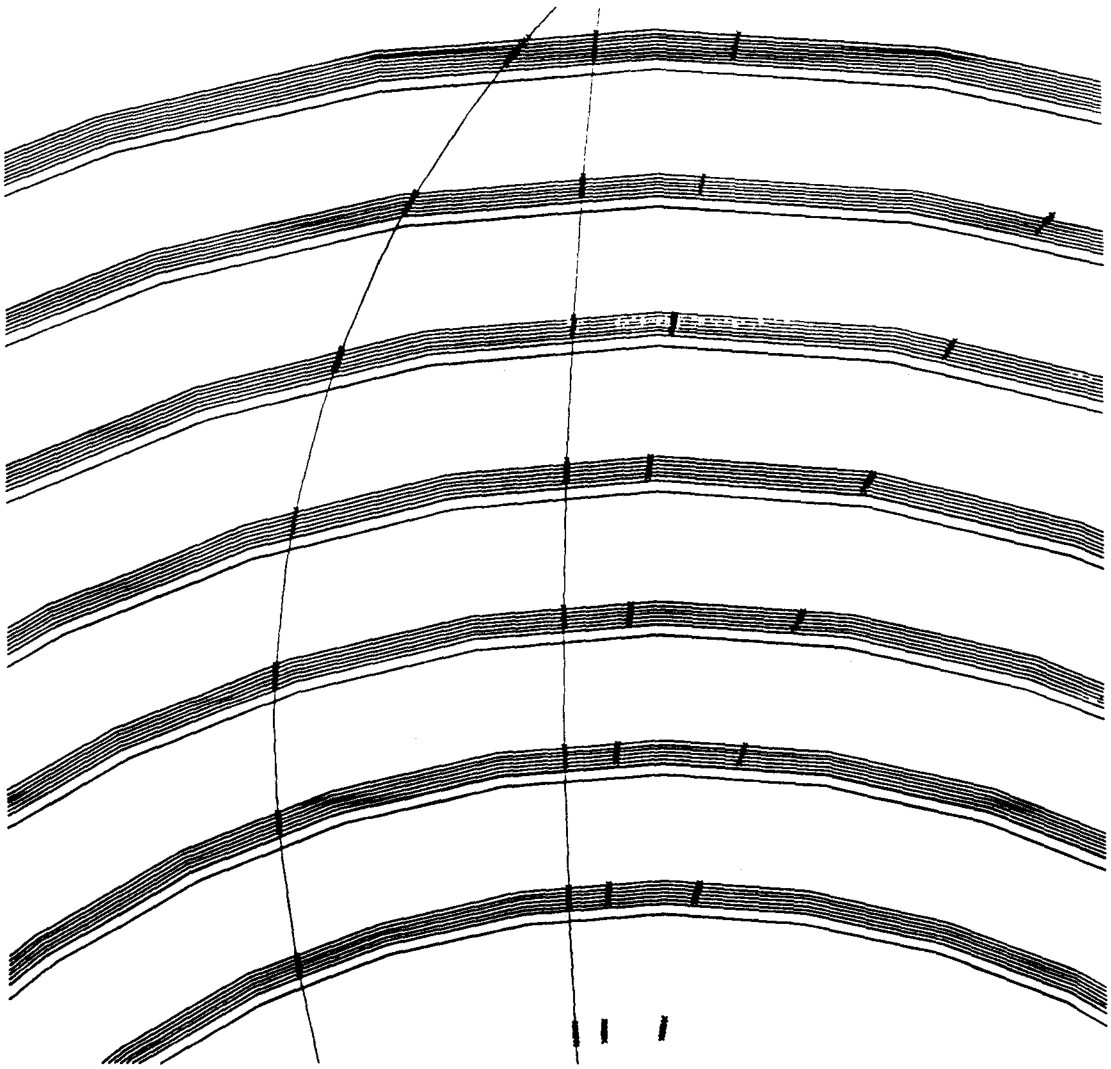

Fig. VI-3. A close-up end view of an eight layer straw tube tracker illustrating the difference between higher and lower p_T tracks. The small x's represent hits caused by four tracks. The flight path of the highest p_T track is almost a straight line and its hit segments are essentially perpendicular to the superlayers. The low p_T track follows a circular arc with its hit segments tilted at an angle to the superlayers.

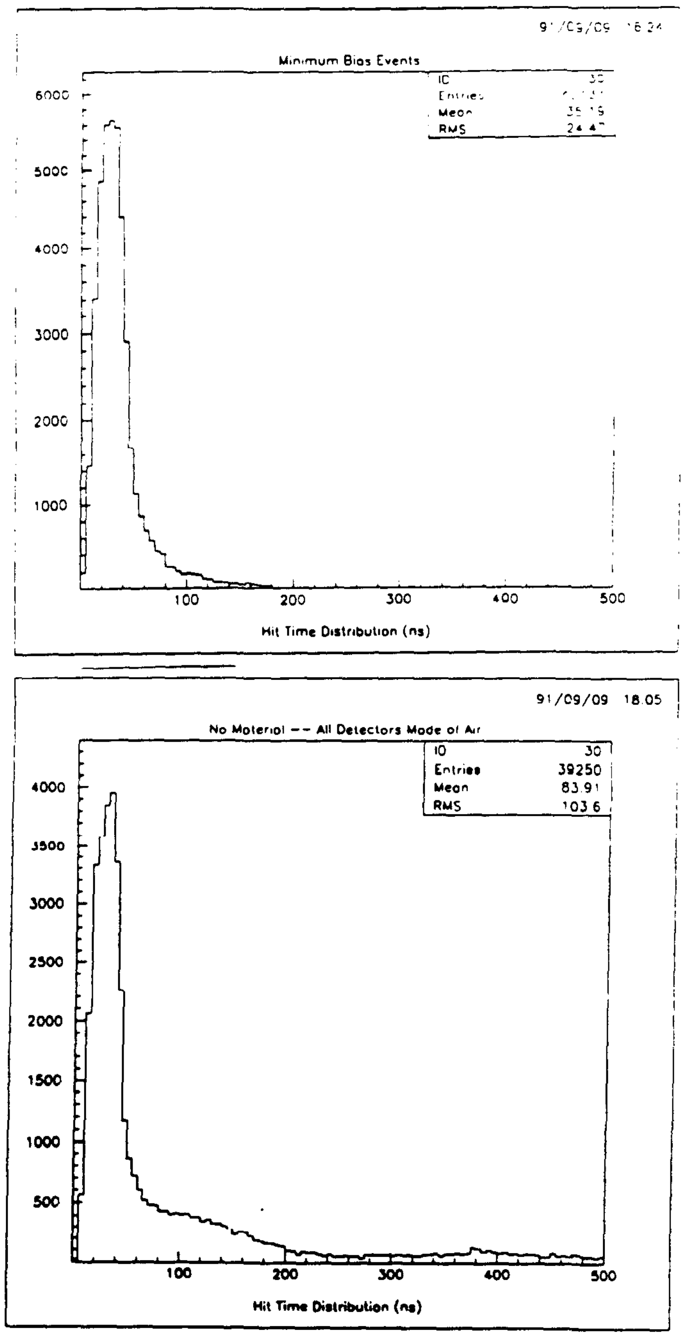

Fig. VI-4. a. The distribution of hit times recorded in an eight layer straw tube tracker. The plot shows the hit times recorded for 25 PYTHIA minimum bias events tracked through a full simulation of the SDC tracker system including beam pipe, a full silicon detector, and magnet coil.

b. The distribution of hit times for a simulated SDC tracker identical to the one in figure VI-4a except all parts of the detector are made of air (essentially a zero mass detector). Again hit times are recorded for 25 PYTHIA minimum bias events. Note: Fig. VI-4b shows fewer total hits but more late hits than Fig. VI-4a.

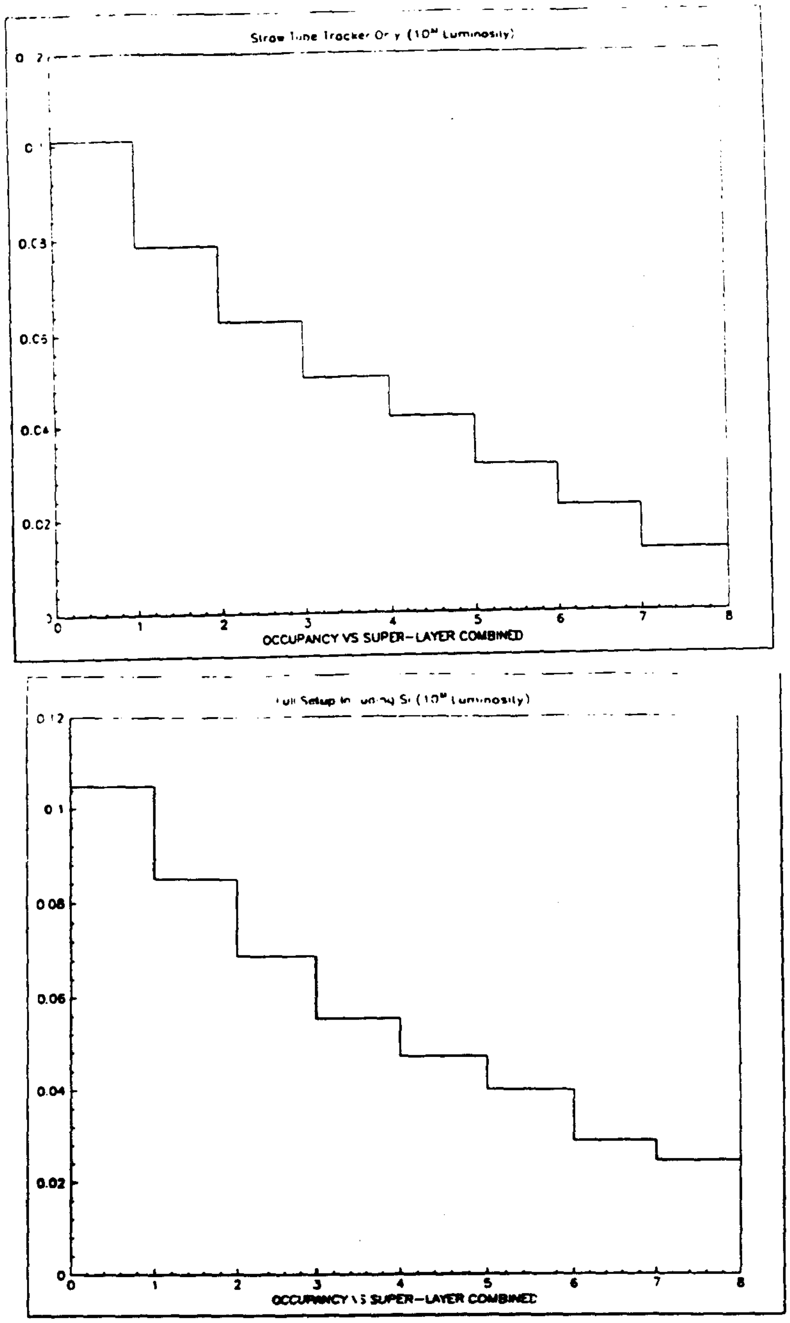

Fig. VI-5. a. The occupancy fraction (fraction of wires with a hit) vs. superlayer in a simulation of the straw tube tracker by itself. The innermost superlayer is at a radius of about 0.7 m and the outermost is at 1.6 m. The occupancy is calculated using minimum bias events only and considers in-time hits from the previous 20 and the next 4 beam crossings.

b. The same plot as Fig. VI-5a, except the material of the beam pipe, silicon tracker, and magnet coil is included. The occupancy rises slightly except for on the outer superlayer where backscatters from the magnet coil increase occupancy considerably (see the text).

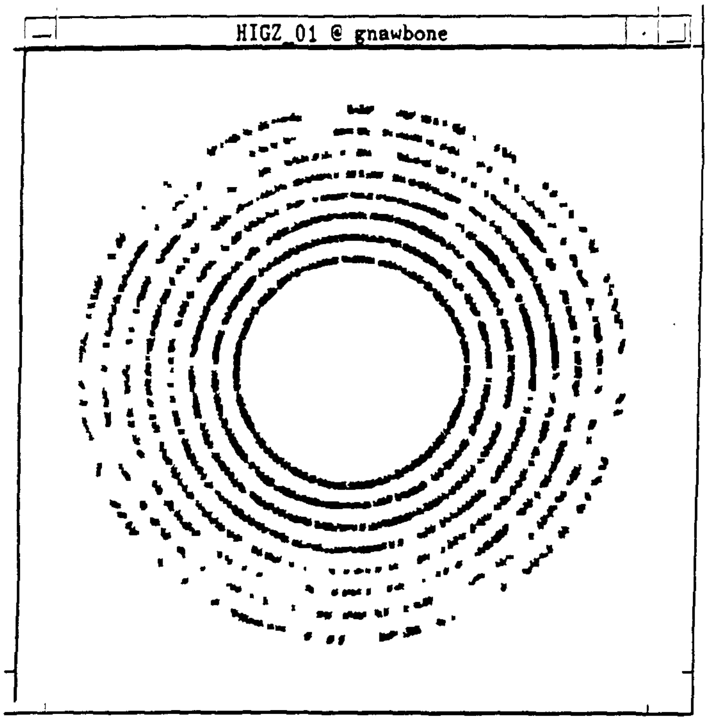

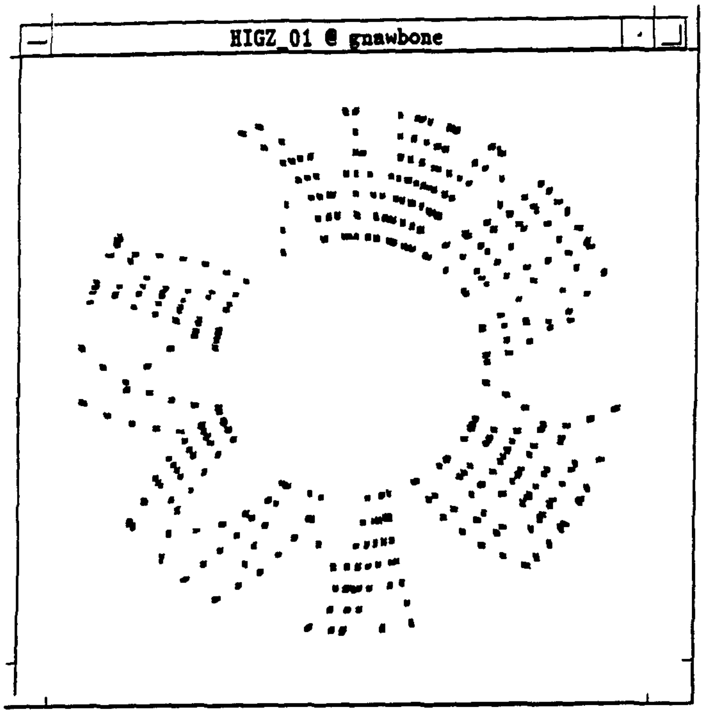

Fig. VI-6. a. End view of the hits in an eight layer straw tube tracker. The hits are caused by Higgs event in a design luminosity background of minimum bias events.

b. The same picture as Fig. VI-6a except only hits on the found tracks are shown. For this plot, a track had to have a reconstructed p_T of 0.8 GeV/c to be found. and plotted.

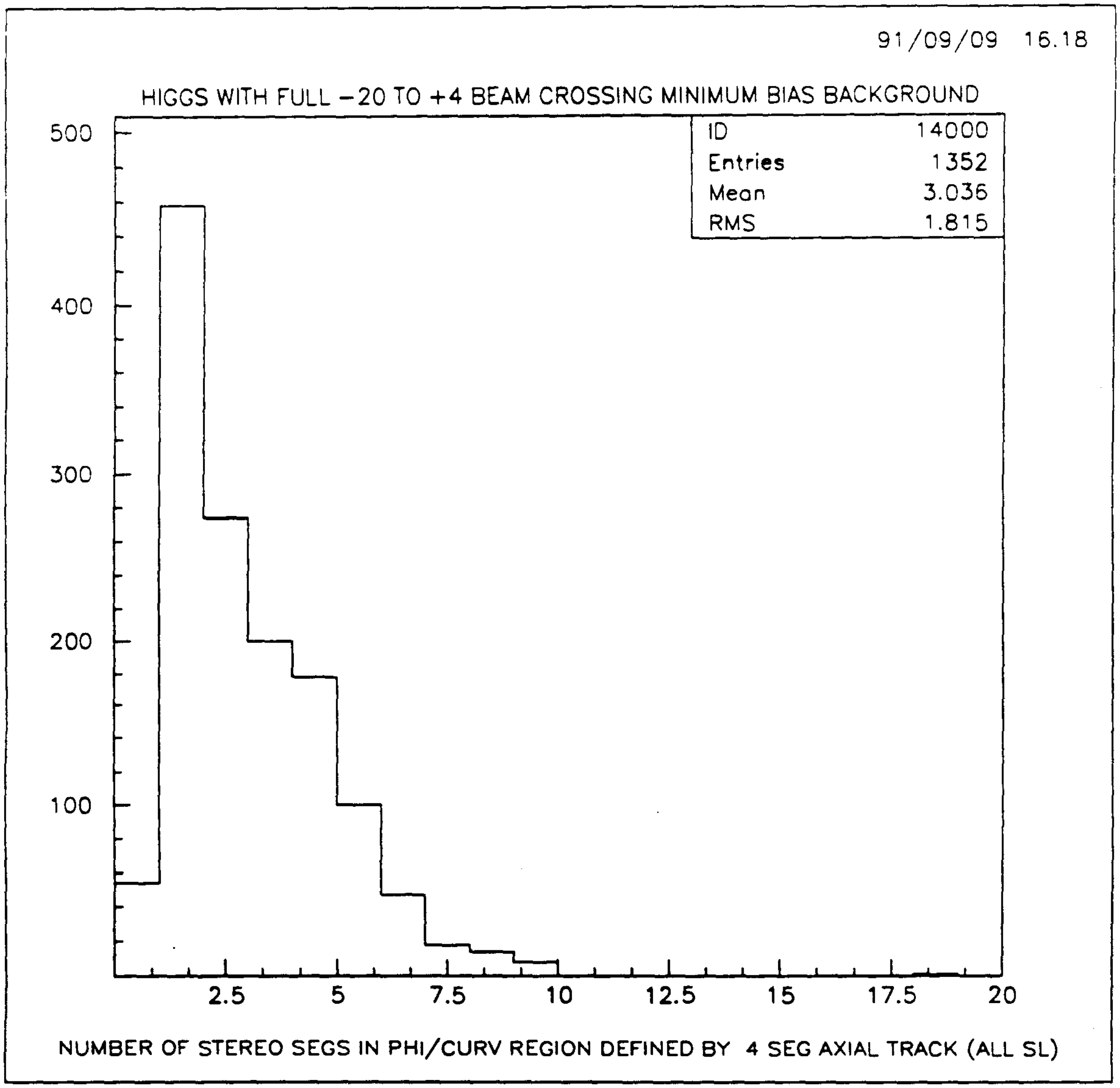

Fig. VI-7. A plot of the number of possible stereo segments when linking a stereo layer's segments into a track previously found using axial segments. The left-most bin contains the number of times 0 candidate segments were found, the next bin 1 segment, the next bin 2 segments, and so forth.

VII. CONCLUSIONS AND FUTURE PLANS

VII.1. Central Tracking R&D

The studies of the past year have been directed towards the goal of ascertaining whether the straw tube tracking idea is compatible with the SSC environment. The problem of pulse attenuation in long tubes was found to be sufficiently small as long as the cathode coating was made sufficiently thick. The material to be used as the cathode coating can be copper instead of aluminum and therefore the attenuation can be reduced even farther. Attenuation lengths in excess of 7 m can be attained. The problem of straw tube deterioration with time while operating in the radiation environment of the SSC is still under study but the difficulties which have been encountered appear to be at much higher radiation levels than the SSC environment. Operation at the design luminosity over a ten year period does not damage the tubes sufficiently to degrade their performance as long as sufficient care is taken to avoid breakdowns from occurring. Although the problem of gain change occurs to a limited extent as charge accumulates on the wire, the amount of change with the mixture of 20% isobutane in tetrafluoromethane is small (≈10%) and occurs only at the beginning of the radiation exposure. Any problem with the radiation hardness of the straw tube materials would be at radiation levels much higher than what would be encountered at the SSC.

The method of using modules to enclose the straws and hold them straight and in a regular array has been demonstrated in short sections. Measurements of the regularity of the arrays of straws in modules and in gluing clamps give deviations with a standard deviation of about 20 μm. The wire centering spacers appear to center the wires with a precision which is again about 25 μm while still permitting the wire to be removed and replaced if need be. At the same time they do not present a dead region more than about 4 mm apiece. Without these spacers, the concept of a narrow, thin but long straw tube chamber would be impossible.

We are pursuing a vigorous program of research and development on the straw tubes, which includes the following:

1. A program at LBL and Indiana University on chamber aging and radiation effects. This will allow us to proceed with confidence on the final selection of

the straw material and coatings. We have begun to concentrate on copper coatings on a Kapton substrate since there are indications that these are more resistant to damage.

2. We will select a wire support system from among the several existing prototypes. This will allow us to pursue a study of the most cost-effective way to produce them in the future.

3. In the next few months we will complete construction of an eight-layer, 1-meter-long test chamber to verify our assembly techniques.

4. We will also complete a 1-meter six-layer prototype using the final design for the modular shell. This shell will use a foam sandwich and the same construction techniques as the final 4-meter design.

5. We will complete and test a four-meter-long composite shell, which will be tested for straightness and flatness and then used to construct a four-meter-long proof-of-principle chamber. The shell is scheduled to be completed by December 15, 1991.

6. We will design and build an eight-layer 4-meter-long trigger module.

7. We will begin the prototyping of a resistive termination.

VII.2. Intermediate Tracking Angle Tracking R&D

A prototype radial wire drift chamber with dimensions scaled to match the crossing time and occupancy of the SSC at design luminosity has been constructed and tested at CERN. These tests were done with standard gas mixtures but will soon be done with CF_4-based mixtures. Studies of the drift properties in a magnetic field of gas mixtures containing CF_4 have been carried out in a small test chamber. These studies are continuing but it appears that a suitable gas exists.

The requirement of a Level 1 trigger in the forward region is very difficult with a detector like the radial wire drift chamber. Gas microstrip detectors could be used to provide a trigger. It also appears that given the good resolution of these detectors that they may be able to supplant the radial wire drift chambers.

The intermediate angle tracking group will be concentrating on gaseous microstrip chambers for the intermediate angle tracking region. Future work will include:

1. Simulation studies to fix the optimum layout of the microstrip tiles.

2. Prototype systems of tiles will be constructed to establish maximum sizes for reliable operation.

3. A final intermediate tracker design will be proposed for the SDC design report in April, 1992.

VII.3. Engineering R&D

One of the main conclusions of the engineering study is that a very rigid and light module can be built to hold the straws in position and to withstand the compressive load of the wire tension. This concept of module construction includes walls made of a sandwich of polyimid foam between two carbon fiber-epoxy composite layers.

Another important conclusion is that a cylindrical support structure can be built that is sufficiently light and strong that the modules in a superlayer can be mounted precisely and stably with respect to each other. The total material of the modules and the supports would then amount to about 3.5% of a radiation length for an outer tracking system consisting of five superlayers of straw tubes.

The mounting of the cylinders on a space frame which then connects to some fixed rigid structure such as the calorimeter has been studied.

A number of activities will need to be actively pursued for the SDC design report:

1. We will complete a finite element analysis study of the support frame. The carbon composite truss structure will be studied for deflection due to support positions and the full gravity load of the tracker.

2. We will complete a finite element analysis of the cylindrical superlayers. The 1-inch-thick Rohacell design will be examined in detail in this study.

3. The trigger module design will be completed for a proof-of-principle module construction.

4. The utilities for the outer tracker will be designed and costed.

5. The gas recovery system will be designed and costed.

6. Assembly details will be worked out for the tracker, including the alignment procedures.

VII.4. Front End and Triggering Electronics

The circuit for the differential, low-noise fast-shaping preamplifier for use on the straw tubes has been tested in a single channel package and works very well. The discriminator circuit has been designed but awaits incorporation with the preamplifier into an eight-channel amplifier-shaper-discriminator chip.

The time-to-voltage converter and analog memory chip has been completely designed and is ready for prototype production. The UTMC rad-hard CMOS process has been evaluated and found suitable for the TVC/AMU.

We are actively working towards a final electronics design. During the next year, several milestones should be reached:

1. The first Penn chip will be tested on a ASD (amplifier, shaper, discriminator) board now under construction. This will allow all of the groups to test the 64-straw modules that we have for resolution and for cross talk with the low threshold Penn amplifier.

2. We will complete a new interface board with in-line capacitors. This 8×8 board will be used for both the eight and six layer prototype chambers as well as for the four-meter proof-of-principle chamber. Tests of the ability to reduce cross talk will be made.

3. The eight-channel amplifier/shaper/discriminator chip will be mounted and used for chamber tests and for the first attempt to simulate the close packing geometry required on the chambers.

4. The TVC/AMUs will be tested both on the bench and on prototype straw modules.

5. The performance of the TMC in conjunction with the Penn front end electronics will be studied.

VII.5. Computer Simulation

The SDCSIM SHELL, the standard program for simulation of the SDC detector within GEANT, has been improved over the past several months to the point where it is generally useful to the members of the collaboration. After these improvements were made, both within the straw system and outside it, preliminary studies of occupancy, segment finding, and pattern recognition were made. The stereo layers are now treated correctly.

The simulation results for an eight-superlayer straw system with the silicon system presenting only mass show that the occupancy in the innermost straw tube layer is only about 10% and the efficiency for linking stereo segments is high.

The simulation effort will evaluate the performance of the tracking system design chosen for the SDC design report due in April, 1992. This will include:

1. The completion of the pattern recognition studies using the silicon and straw outer tracker system. The goal is to be able to treat the silicon and straw tracker on a more equal footing in the pattern recognition algorithms.

2. Use the pattern recognition and track fitting studies to settle on a tracking system design for the design report. For the selected design examine the dominant physics processes with the assumed background events present in order to look at momentum resolution, angular resolution (with stereo), mass resolution, and ability to track inside jets.

3. Over the next few months incorporate the data structures and data display algorithms in the working Monte Carlo package for all groups working on simulation.

4. The intermediate angle tracking system will be included in the simulation when the design is completed.

We have attached a copy of the Outer Tracker Section of the draft of the 1992 Research and Development and Engineering Plan for the Solenoidal Detector Collaboration, SDC-91-00036, July 8, 1991.

REFERENCES

1. Gail G. Hanson, "Design of a Tracking System for a Solenoidal Detector," *Proceedings of the Symposium on Detector Research and Development for the Superconducting Super Collider, Fort Worth, Texas, Oct. 15-18, 1990, World Scientific Publishing Co.*, p. 241.

2. Report of the Task Force on R&D Directions for Tracking, SDC-91-00055, April, 1991.

3. G. Hanson, F. Luehring, H. Ogren, and D. Rust, "Proposal for Central Outer Tracking System," IUHEE 91-8, SDC 91-00061, August 21, 1991.

4. H. Ogren, "Wire Drift Chamber Tracking at the SSC," IUHEE 90-17, SDC-90-00138, *Proceedings of the Symposium on Detector Research and Development for the Superconducting Super Collider, Fort Worth, Texas, Oct. 15-18, 1990, World Scientific Publishing Co.*, p. 202.

5. C. Neyman, B. Martin, and H. Ogren, "Attenuation Studies of 3.5m Straw Tubes," IUHEE-7, (1990).

6. David R. Rust, "Some Facts Concerning the Electrical Resistance of Straw Tube Chambers," IUHEE-90-11 (1990).

7. E. Wente, D. R. Rust, B. Martin, H. O. Ogren, G. Hanson, and R. Foster, "Attenuation Studies of Straw Drift Tubes," IUHEE 91-9 (1991).

8. J. A. Kadyk, J. Va'vra, and J. Wise, Nucl. Inst. and Meth. **A300,** 511 (1990).

9. David R. Rust, "Effects on Straw Drift Tubes of Extended Operation in a High Radiation Environment," IUHEE-91-1 (1991).

10. J. A. Kadyk, D. W. Hess, J. Va'vra, and J. Wise, "Recent Work on Radiation-Hard Gases and Straw Tubes," *Proceedings of the Symposium on Detector Research and Development for the Superconducting Super Collider, Fort Worth, Texas, Oct. 15-18, 1990, World Scientific Publishing Co.*, p. 236.

11. Straw Tube Superlayer Design Concepts, Prepared for SDC Tracker Review, University of Colorado, Duke University, Indiana University, Oak Ridge National Laboratory and Westinghouse Science and Technology Center, SDC-91-00062, May 20, 1991.

12. Harold Ogren, "Progress Report on 4 mm Straw Chambers," IUHEE-90-9 (1990).

13. R. Foster *et al.*, "Self Centering Measurement for an 8 Layer Trapezoid," IUHEE 91-7, SDC 91-0056 (1991).

14. J. M. Bailey *et al.*, "Forward Tracking with Enhanced Electron Identification," *Proceedings of the Symposium on Detector Research and Development for the Superconducting Super Collider, Fort Worth, Texas, Oct. 15-18, 1990, World Scientific Publishing Co.*, p. 202.

15. J. M. Bailey *et al.*, "Measurements of Electron Drift in Fast Gases with Crossed Electric and Magnetic Fields," *Proceedings of the Symposium on Detector Research and*

Table 4
Scintillating fiber R&D and engineering

Milestones and Goals	Date
1. Scintillating fiber R&D	
Selection of scintillator composition	6/92
Selection of active cladding material	6/92
Resolution of oxygen/radiation issue	4/92
2. Waveguide R&D	
Selection of the waveguide composition	1/92
Selection of cladding material	1/92
3. Splicing R&D	
Selection of splicing technique and sequence	8/92
4. Fiber manufacturing engineering	
Optimization of fabrication process	9/92
Development of automated Q/A apparatus	1/93
Production of significant quantities of fiber	2/93
5. Ribbon fabrication engineering	
Selection of ribbon fabrication technique	8/92
Engineering design of production facility	1/93
Determination of Q/A procedures and equipment	1/93
6. Readout engineering	
Engineering design for the readout system	12/91
Fully functional pre-production prototype	10/92
Operation of a 1 K fiber/VLPC prototype system	1/93
Operation of a 10 K fiber/VLPC prototype system	1/94
7. Fiber placement onto superlayers	
Stable-base cylinder prototype development and construction	9/92
Engineering of placement concept	6/92
Construction of placement facility	1/93
Placement of fibers onto superlayers of prototype cylinder	6/93

field for fast drift mixtures based on CF_4 should be complete by September 1991 In July 1991, the radial wire cell will be tested in a CERN test beam with fast drift gas mixtures. Design of a full-size 300-wedge radial wire drift chamber module is proceeding, and is now at the stage that manufacturing techniques for individual components are under discussion with industry.

Small gas microstrip devices of both planar and non-planar (knife-edge) design are under construction and test. Excellent (12% FWHM) pulse height resolution at rates up to 10^7 $cm^{-2}s^{-1}$ has been achieved for planar electrode geometry on glass substrates. Other substrates such as silicon, plastics, and different glass formulations are also under study. All of the above work has been done by SDC collaborating institutions. In addition, there are many institutions and universities throughout Europe, the US, and Japan also engaged in such work, one of whom (Pisa) already has a system operational in a CERN experiment. We are in close contact with most of them and are collaborating with some of them.

Simulation work is being undertaken in parallel with hardware development to achieve an optimal layout of either a microstrip system or a hybrid of microstrips and radial wire chambers in conjunction with the inner silicon tracker. The use of radial wire chambers alone has now been ruled out because of the prohibitively large occupancy in the full (single hit) memory time of a chamber with a feasible number of drift cells, and because of the need for a fast Level 1 trigger in p_t at intermediate angles. A hybrid system in which both the speed and the spatial accuracy of microstrips are used to tag the long radial chamber memory time into a time slice associated with an interesting bunch crossing remains a possibility. If simulation demonstrates that the advantages of precision drift measurements for track finding and reconstruction are no longer significant when considered in conjunction with the microstrips and inner silicon tracker, then a gas microstrip system alone could be chosen for the ITD. Furthermore at high luminosity ($\gg 10^{33}$ cm^{-2} s^{-1}), only a microstrip-based system remains a feasible option.

Engineering of a full scale detector design and R&D to determine the appropriateness of each technology option for use in the SDC detector are the main themes for our FY1992 plan. We propose to continue to develop working elements of the detectors with the actual cell dimensions required for the detector, and to complete initial design of a set of gaseous intermediate tracking detectors including engineering support, alignment, cooling and detector integration.

The milestones and goals for ITD development work are shown in Tables 5 and 6. They include overall engineering studies to specify support and infra-structure of two ITD's in the SDC detector.

Table 5
Milestones and goals for radial drift chambers

Goal	Date
Fast gas measurements in $B = 2$ T	10/91
Prove operation of full size radial cell with fast gas	10/91
Design full scale module (prototype)	12/91
First layout drawings	1/92
First cost estimate	1/92
Design and prototype electronics	7/92
Build full scale module	8/92
Layout of support structure	8/92
Refine cost estimate	8/92
Commence testing of full scale module (prototype)	10/92

Table 6
Milestones and goals for gas microstrip detectors

Goal	Date
Find stable and thin substrates	1/92
Choose optimum metallization thickness	1/92
Develop bonding to front-end electronics	1/92
Measure pulse shape from min I.	1/92
First measurement of efficiency	1/92
First layout drawings	1/92
First cost estimate	1/92
E-CAD design front-end electronics	4/92
Radiation hardness and aging	8/92
Optimize gas composition	8/92
Working devices $\approx 15\times20$ cm	8/92
Detailed layout of support structure (includes gas, cooling etc.)	8/92
Refine cost estimate	8/92
Measure efficiency, rate capability, resolution	8/92
Tested front-end electronics	10/92
Final E-CAD design for front-end electronics	10/92
Completed engineering study	10/92

5.3.4. Outer tracker engineering plan

We summarize here our plans for mechanical engineering and alignment work to be done for the outer tracker in FY1992.

The engineering projects are divided into three categories: 1) the basic support structure for the outer tracker, including considerations of interfaces with the silicon tracker and intermediate tracker and overall support and assembly of the detector; 2) issues related specifically to the placement and alignment of straw tubes into superlayers; and 3) the issues related to the assembly of scintillating fibers into superlayers. Tasks (2) and (3) are discussed in the respective technology sections above.

Basic support structure

The following list of tasks have been identified as critical to meet the schedule for the SDC outer tracker.

- Cylinder design—analysis of support cylinders for the tracking elements, determination of precision limitation (finite element analysis), and development of fabrication techniques for stable support cylinder.
- Cylinder prototype fabrication—fabrication of one prototype carbon-based composite cylinder, 6 to 8 m long and 1.5 m in diameter.
- Support structure design—design and analysis of the support structure designated to attach the superlayers to one another and to the exterior mounting interfaces.
- Support structure prototype—fabrication and assembly of a prototype of the support structure and mock-up of the cylinder and mounting interfaces.
- Assembly concepts—analysis and research into fabrication methods and assembly sequence for the central tracking chamber structure.
- Alignment methods—development of techniques for alignment of the CTC components to the required tolerances and for maintaining those tolerances.
- Tooling design—design of tooling necessary to allow construction of the CTC.
- Fixturing design—design of fixturing necessary for handling and manipulating the CTC during fabrication and installation.
- Development of silicon tracker support from outer tracker
- Development of intermediate tracker support
- Development of alignment techniques for intermediate-central tracker registration
- Development of 3D model of entire structure.

Table 7
FY1992 tracking system budget

Tracking design task	Institution	Requested (K$)
1. Silicon strip detector		
Front-end electronics	KEK,* LBL, U. Oxford,* RAL,* and UC Santa Cruz	970
Mechanical design and prototype construction	LANL and LBL	2050
Detector development	Hiroshima U.,* Johns Hopkins U., KEK,* U. New Mexico, U. Pittsburgh, UC Riverside, UC Santa Cruz, and others	210
Management and cost/schedule estimates	LBL and LANL	240
	Subtotal	*3470*
2. Pixel detector		
Mechanical design and tests	UC Davis, LBL, and others	380
Electronics design	Hughes, LBL, and others	650
	Subtotal	*1030*
3. Barrel tracker		
a. Straw tubes		
Basic drift tube R&D	Duke U., U. Indiana, and others	170
Prototype construction and test	Duke U., U. Indiana, and others	540
Straw placement engineering and manufacture	ORNL, WSTC, and others	340
Termination, endplate design, and prototypes	U. Colorado, ORNL, and others	110
Aging studies	LBL, TRIUMF,* and others	75
Support structure and system engineering (common to straws and fibers)	ORNL and WSTC	700
Management and cost/schedule estimates	ORNL and WSTC	180
	Subtotal	*2115*
b. Scintillating fibers		
Scintillating fiber and clear fiber R&D	FNAL, Florida State U., U. Illinois at Chicago, Northeastern U., U. Notre Dame, Purdue U., and industry	370
Fiber and ribbon manufacturing	Bicron, FNAL, Northeastern U., U. Notre Dame, ORNL, and Purdue U.	530
Fiber placement and prototype fabrication	U. Notre Dame, ORNL, Purdue U., and WSTC	310
VLPC system engineering	UT Dallas, UC Los Angeles, FNAL, Purdue U., and Rockwell	495
Support structure and system engineering (common to straws and fibers)	ORNL and WSTC	700
Management and cost/schedule estimates	ORNL and WSTC	180
	Subtotal	*2585*
4. Intermediate tracker		
Work on plastic substrates for microstrip detectors	Carlton U.,* CRPP (Ottawa),* KEK,* LANL, U. Liverpool,* RAL,* U. Rochester, and Texas A&M	75
	Total	*9275*

*Foreign budget not included.

IUHEE-90-17
SDC-90-00138

Recent Developments in Wire Chamber Tracking at SSC

Harold Ogren
Department of Physics, Indiana University
Bloomington, Indiana 47405

Abstract

All of the major SSC proposed detectors use wire chambers in their tracking systems. The feasibility of wire chambers in an SSC detector has now been established by a number of groups planning detectors at SSC.The major advances during the past year in understanding straw tube drift chambers are presented and several innovations in gaseous wire chambers are discussed.

Introduction

I will try to review the work that has gone on during the past year on wire chambers at SSC. The major part of this will have to do with straw drift chambers, since they are present in all three major detectors proposed at SSC. This talk is divided into two major parts. I will quickly review the wire chambers being planned for SSC detectors and then outline the major areas of research and development for the SSC environment. The R&D section will concentrate on progress in drift cell design, electronics and signal processing, and engineering aspects of the tracking designs.

Wire Chambers at SSC

SDC

The wire chamber tracking system that is being planned for SDC is shown in Fig. 1. It consists of a central tracking system built from straw drift tubes contained in modules as shown in Fig. 2. This design has been worked on primarily by the Wire Tracking Subsystem Group. [1] The central tracker uses 4 mm diameter straws with lengths varying from 4 meters to 2 meters from the outside radius of 1.7 meters to the inside 0.70 meter layers. The total number of modules in the two z halves is 1088 and the total number of straws is about 188,000. As we will see, a good deal of the R&D concerns itself with producing a simple construction and assembly scheme for this large number of straws. The modular approach for the construction will allow each module to be tested with final electronics before insertion into the tracker. The modules also group the straws in precise position and support the wire load of approximately 12 Kg per module. The tracking system in the intermediate region is a radial wire chamber as shown in Fig. 3. The tracking in the intermediate region is being worked on primarily by the groups from the United Kingdom. The present intermediate tracker consists of a radial wire chamber module with a wire "bunch tagger chamber" immediately in front. This tagger has sufficient timing resolution to select the proper crossing time for each event and tag the event for the somewhat slower radial wire chambers. There would be five radial modules required for a precise measurement of the track momentum in the forward direction.

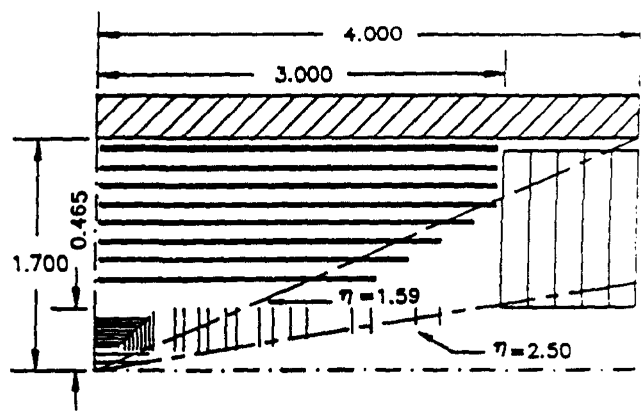

Fig.1. Tracking system for the SDC detector. The straw chamber superlayers surround the silicon system and radial wire chambers are used in the intermediate angle region.

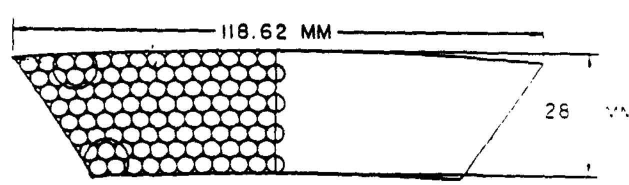

Fig.2. Straw module holding 196 straws. The module walls are constructed from a 250 μ carbon fiber composite.

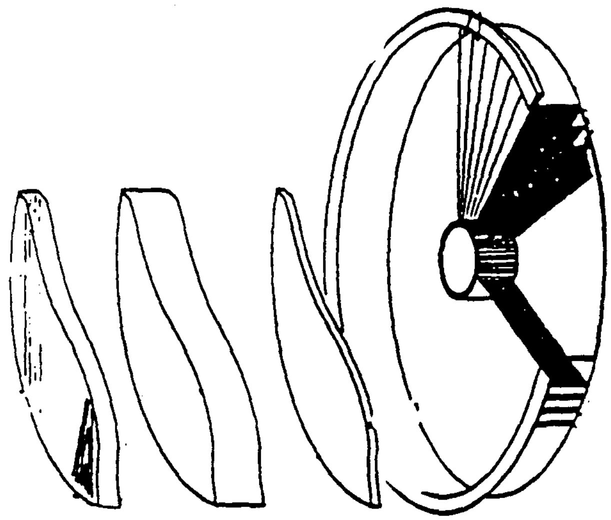

Fig. 3. An exploded view of the radial wire chamber with a bunch tagger and a transition radiation section in front.

Work is also being done on a "Hybrid" detector, consisting of axial straw superlayers and scintillating fiber stereo layers. This has been pursued in some detail by the Hybrid Tracking Subsystem Group.[2] The Hybrid tracker is shown in Fig. 4. The straw layers are glued to a precision cylinder, supported from each end by a conical support. Stereo scintillating fibers are attached to a separate support-cylinder on the outer 2 or 3 superlayers. The tracker would use 4 mm straws and 750 micron scintillating fibers.

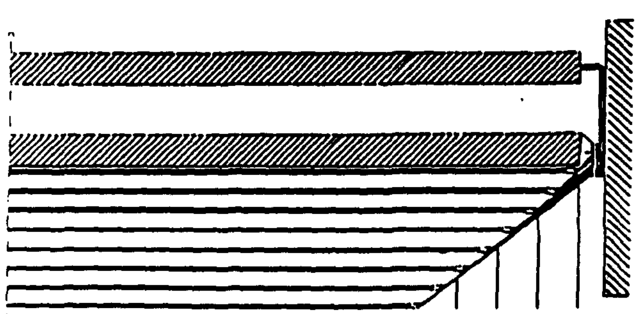

Fig. 4. Superlayer structure for the Hybrid Chamber.

EMPACT

The EMPACT tracker is shown in Fig. 5. As shown in the detailed close-up, straw chambers are used for tracking and transition radiation detectors. These drift tubes are arranged in modules that span a small delta phi, delta z region. There are a total of 385K readout channels for this straw tracker. Although TDCs will not be used for each channel, the pulse height will be digitized for electron id. This wire tracking and electron id work is being pursued by Boston University and Brookhaven National Laboratory.

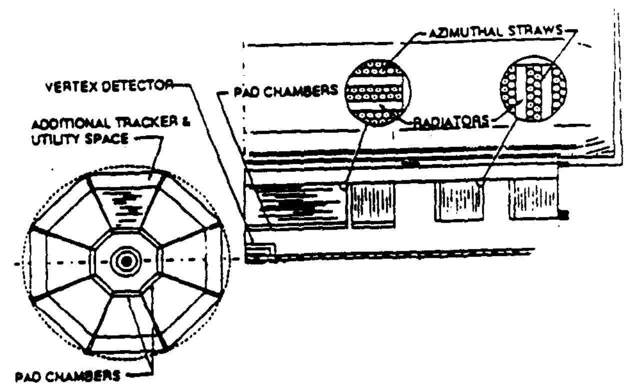

Fig. 5. End and side views of the EMPACT detector. The TRD chambers use straw tubes.

LSTAR

The central wire and scintillating fiber tracker for the LSTAR detector can be seen in Fig. 6. The straw tube chamber fills the region from a radius of 40 cm out to 75 cm and is about 2.8 meters long. The straw tracking system has about 75K channels with TDCs on all wires. As in the Hybrid system, the stereo tracking is done with scintillating fibers. The groups working on the straw chambers are from Boston University, New Mexico University, Indiana University and Los Alamos National Laboratory.

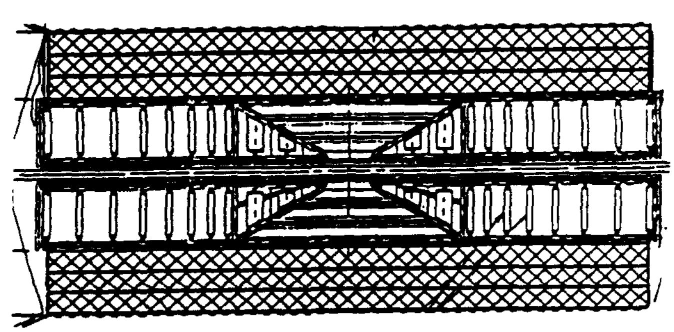

Fig. 6. The tracker for the LSTAR detector. The outer straw and scintillating fiber modules surround a silicon system.

Major Areas of R&D for the SSC Environment

Drift Cell Research

One of the central concerns in tracking at the SSC with straw chambers is shown in Fig. 7. This plot shows the occupancy, hit rate, and current for a straw drift cell in the SDC detector as a function of the radius. The cells were assumed to be half the length of the detector. The calculation was was carried out at KEK[3] and used a PYTHIA particle generator, and GEANT for detector simulation. All known materials were included in the model, and looping tracks in the magnetic field were used. We see that we can expect occupancies near 16% at the inner radius, and currents of up to .6 μ amps. Similar calculations have been carried out by other groups[4] and are in agreement with these basic numbers.

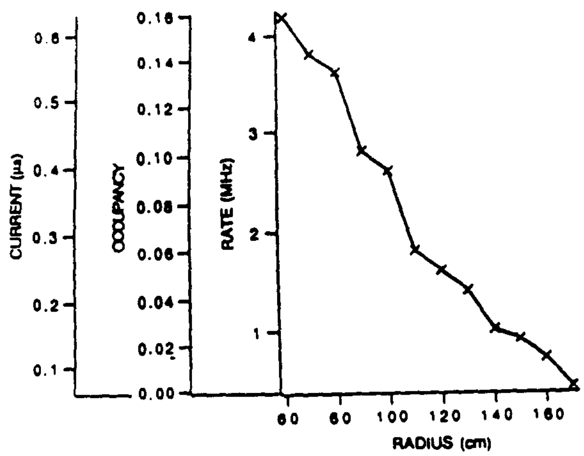

Fig. 7. The radial dependence of the hit rate, occupancy, and current draw versus radius of superlayers.

Although the occupancy is high, a Monte Carlo study at Colorado[5] has shown that the number of hits found in a superlayer remains very high even in the inner super- layers. The number of good 7 hit segments in a super- layer with 8 layers is about 90% at design luminosity at 75 cm radius and climbs to about 98% at the outer super- layer. This is is a very encouraging study and is being continued with more realistic tube efficiencies to determine the optimal number of straw layers.

These simulation studies show us what we can expect at SSC and what sort of detectors will be required. However, what must now be addressed is whether such detectors exist or can be built. This past year there has been a considerable amount of work on straw drift chamber R&D.

Gas selection:

CF_4-Isobutane(20%) appears we can be the most promising gas for use at SSC. In Fig. 8 the drift time distribution for a 4 mm straw drift tube filled with CF_4-Isobutane(20%) is shown. It has a drift time of about 19 ns. Additional measurements with 20% Isobutane show that straw chambers are fully efficient above 1900 volts.

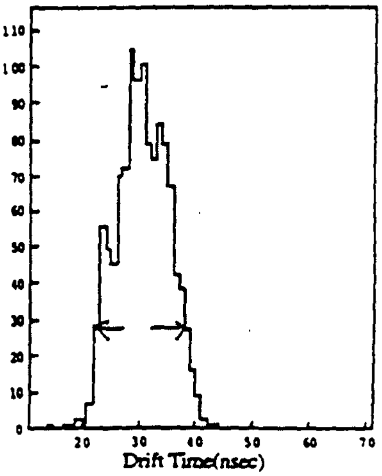

Fig. 8. Drift time distributions in a 4 mm straw for CF_4-Isobutane (20%).

Detailed measurements of the gain have been made by several groups[6]. As shown in Fig. 9, the gain of the CF_4-Isobutane chambers is about 30,000 at 1900 volts for 4 mm straws and 25 μ wire diameter. The measurements shown in the figure were made on a 3.5 meter straw system. At Princeton University the single cluster timing distributions have been measured.[7] These were used to determine the diffusion limit of spatial resolution for 3.5 mm drifts. As can be seen from Fig. 10, the diffusion limit for CF_4-Isobutane is about 40 μ. All of these measurements indicate that a fast efficient gas with good resolution in already in hand for the design of straw chambers.

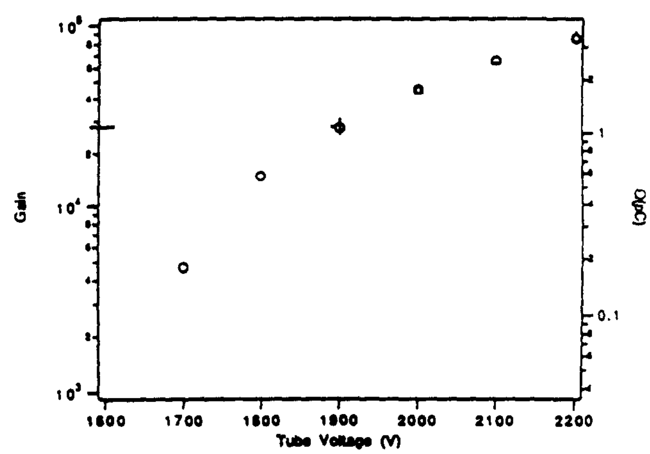

Fig. 9. Gain measurement on 3.5 meter straw chamber for CF_4-Isobutane (20%) 4 mm straw 25 m wire.

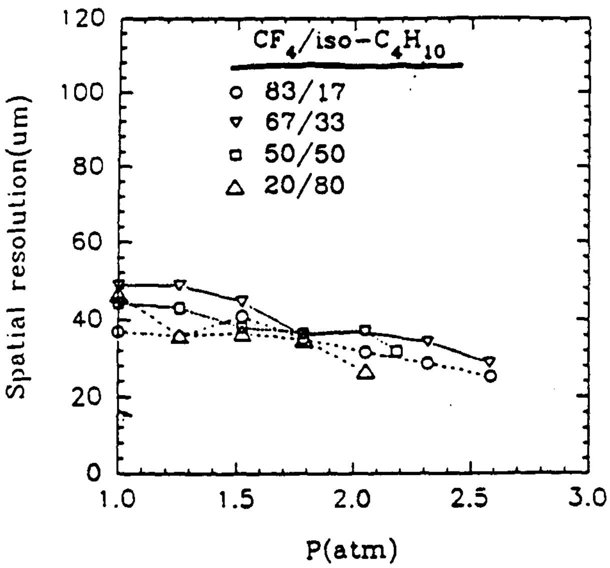

Fig. 10. Diffusion limit for CF_4-Isobutane for 3.5 mm drift.

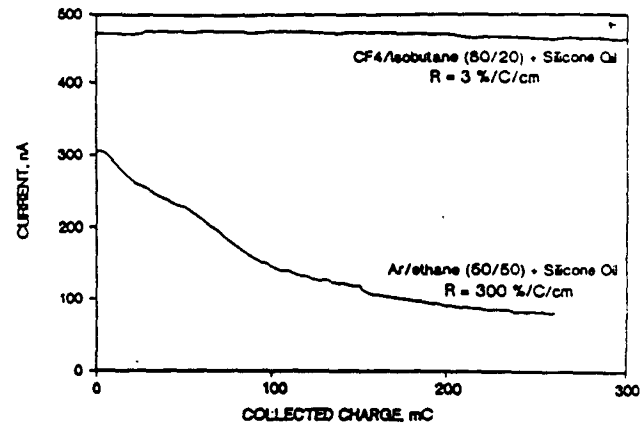

Fig. 11. The gain of a contaminated straw chamber system with CF4- Isobutane(20%) and Ar-ethane (50%) as a function of total charge.

Wire lifetimes

There are a number of questions to be addressed concerning the lifetime of straw chambers at SSC. It is expected that wire gain and long term contamination will be a function of the gas used in the drift cell. However, the other area of concern is the mechanical or structural damage due to the high radiation dose of components. During this past year there has been considerable progress in this areas.

In Fig. 11 we show some of the work that has been done at LBL.[8] The wire gain of CF_4 - Isobutane(20%) is compared to Ar/ethane with a known contaminant injected in the chamber. The CF_4 gas show little sign of damage , but the Ar/ethane gain is seriously degraded. It appears that the CF_4/Isobutane mixture has the ability to clean the signal wires. This has been also reported by a group at TRIUMF.[9] In Fig. 12 a previously contaminated chamber running on Argon/Ethane is shown to return to its original state when running in CF4-Isobutane. The damaged area was isolated to a small region in the middle of the wire. After an accumulated charge of about 1 C/cm it had completely recovered.

These measurements give us confidence that wire gain should remain constant at the SSC over the lifetime of the experiment for luminosities far above the design.

Neutron Damage

There were two reports at this conference on neutron damage to straw chambers. The North Carolina State reactor PULSTAR [10] was used to irradiate mylar straws and glued straws in chamber arrays with thermal neutron fluences up to 10^{16} cm^{-2} and fast neutrons fluences up to 10^{15} cm^{-2}. The basics straw components are confirmed to survive at much higher fluences than those expected at SSC.

A dramatic test of an operating straw chamber has been reported by a group at Boston University.[11] A 25 straw array was subjected to a 0.5 MeV neutron flux of 7×10^7 / cm^2/ sec . The straw chambers used CF4 gas and was running typically at 5 MHz. and drawing 15 μa of current. The total fluence of neutrons was 6.5×10^{14}/ cm^2 and no damage or gain loss was reported. Both of these tests give us confidence that the radiation levels predicted for SSC will present no obstacle to the operation of straw chambers.

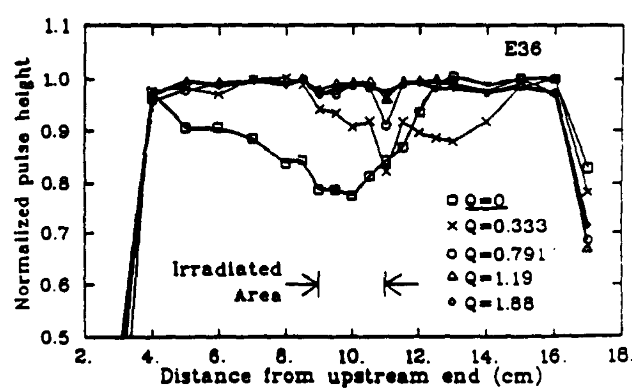

Fig. 12. The pulse height of a straw drift chamber with a contaminated central region (10 cm) for different amounts of total charge deposited.

High Rate tests

The principle long range activity of the groups working on straw chambers is to demonstrate that tracking in a high rate beam is possible. Ideally this should be with a full length (3 meter) straw system. Preparations are underway for such tests.

At Indiana University construction has started on a number of short 64 straw modules. These can be used for trigger and electronics tests by members of the SDC collaboration. A full length module is now under design at Oak Ridge and Indiana University. By next summer a full scale module should be ready for testing. At Duke University a full length cylinder of radius 0.8 meters is being constructed. This prototype superlayer can be used for high rate tests, and for verifying construction techniques.

Electronic related R&D

Signal size

There are a large number of electronics related issues under study. These include measurements of the signal size, effects of straw capacitance and attenuation in the straw chambers. There is also design of the preamps, shapers and fast TDC underway with an emphasis on high density, low power consumption, and radiation hardness. Finally, a design for a fast level one trigger has been worked out and will soon be tested on a straw module.

Detailed calculations of the signal size expected with 3 meter straw chambers have been carried out at KEK[12] for a 7 mm straws with a slow gas (Ar/ Ethane). It is expected that a 4 mm straw diameter and a fast gas like CF4- Isobutane will give more that twice the signal size. From these calculations we can estimate the time jitter and time walk expected in a 3 meter straw at SSC. There does not seem to any difficulty in principle to attaining 100-150 micron position resolution.

In Fig. 13 a pulse in a 3.6 meter straw chamber is shown along with the reflection pulse from the unterminated end.

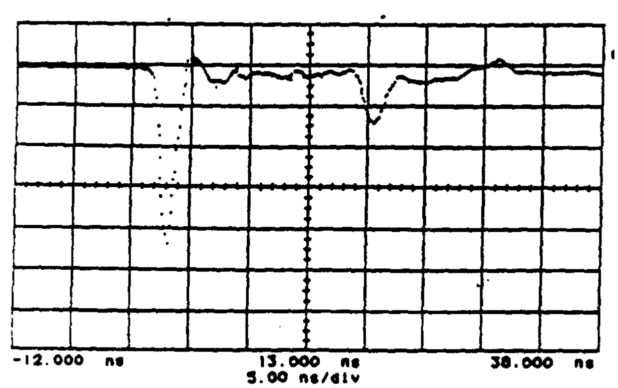

Fig. 13. The signal from an Fe 55 source for a 3.6 meter straw system. The reflection pulse can be seen to be attenuated.

Termination has also been applied to eliminate the reflected signal.The attenuation of reflected pulse in the figure indicates one of the areas of interest in R&D. This attenuation comes about due to the resistivity of the cathode material and the signal wire. The resistance of both wire and cathode were about 100 ohm/meter in the test shown in the figure, whereas the coaxial impedance of the straw is about 300 ohms.

The signal attenuation in straw chambers has been measured by several groups[13] and is shown in Fig. 14. The average attenuation length is about 5 meters. There are several ways to increase the attenuation length. Work is in progress on with lower resistance cathodes and larger diameter wires. The effect of appreciable attenuation would require an increase of gain in the straws and might require a more elaborate analysis to attain the desired time resolution.

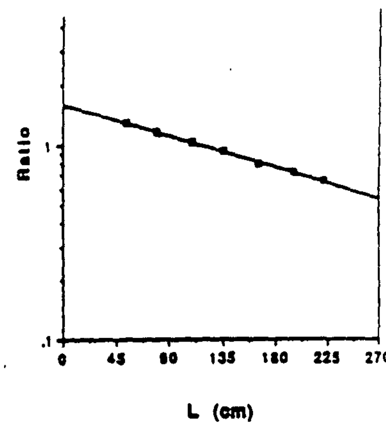

Fig. 14. Measurements of the signal attenuation for a 2.3 meter straws.

Signal electronics

The drift chamber electronics has been worked on by groups from University of Pennsylvania[14] and the Japanese laboratory, KEK[15]. The system that is being designed by the group from the US is shown in Fig. 15. It consists of a preamplifier, shaper, discriminator, and time to voltage convertor, and an analog memory for the Level 1 and Level 2 triggers. Their design has progressed significantly in the past year. They now have prototype chips with low threshold, low power and radiation hardness sufficient for SSC. The prototype preamplifiers have been used on several of the straw chambers, in fact they were crucial in the measurements of the single cluster characteristic presented by Princeton University. We anticipate that in the next year we will have a sufficient quantity of the amplifiers and shapers to test several straw modules. The time to voltage converters (TVC) and the analog storage are shown in somewhat more detail in Fig. 16. We anticipate that the first prototypes of this will also be available next year. KEK is working on an alternative method (the TMC) of measuring the time and storing it for a level 1 trigger.

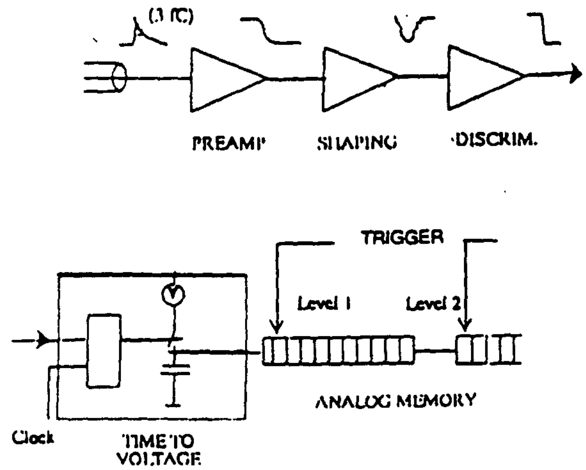

Fig. 15. A diagram of the straw chamber electronics.

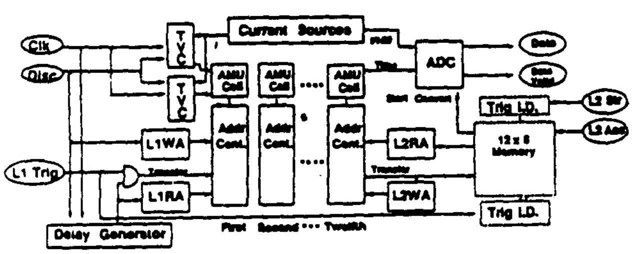

Fig. 16. Details of the TVC and level 1 and 2 triggers.

This Time Memory Converter or TMC is shown in Fig. 17. The chip has progressed to the fabrication stage, and should be available to test in a chamber by the end of the year. At University of Colorado there has been an attempt to design the layout for all of the front end electronics for a straw module. The resulting board layout is shown in Fig. 18. This is an existence proof that a compact layout of preamplifiers, shapers TVC along with all data and read out lines will fit in the modular scheme. The trigger electronics has also made real progress this year. At the University of Michigan[16] a real time trigger has been designed to find stiff tracks in a straw superlayer. The technique and the circuit is shown in Figure 19. The scheme relies on the layout of straw wires along radial rays from the intersection region. In this case a stiff track will produce a fixed relationship between the drift times in three successive straw layers. A synchronizer circuit will trigger on a stiff track within 30 ns of the arrival of the last pulse. The circuit has been designed and constructed. Testing will begin this fall.

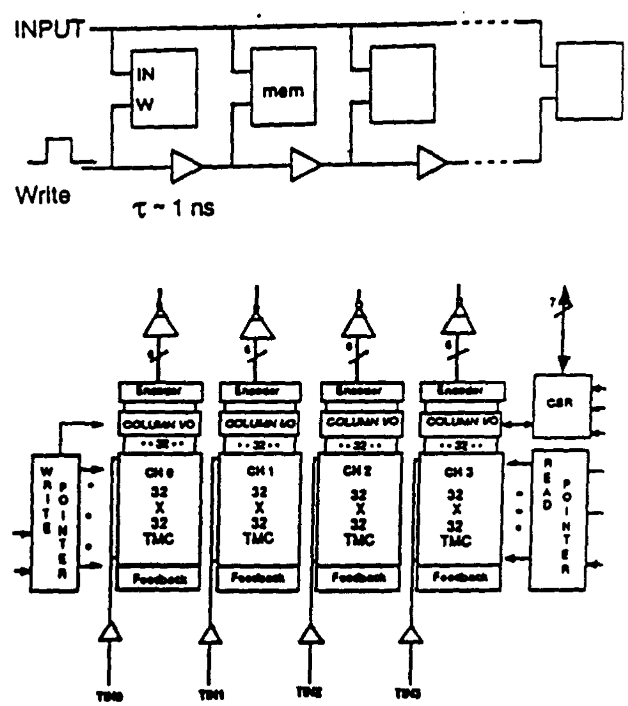

Fig. 17. The Time Memory Chip for recording and storing timing information from the straw chambers.

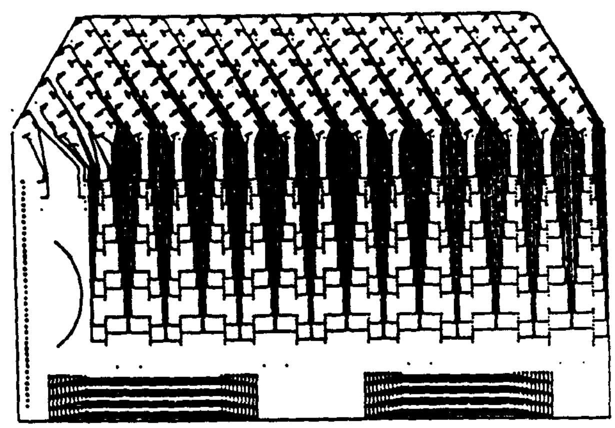

Fig. 18. A prototype layout of the front end electronics for a straw module.

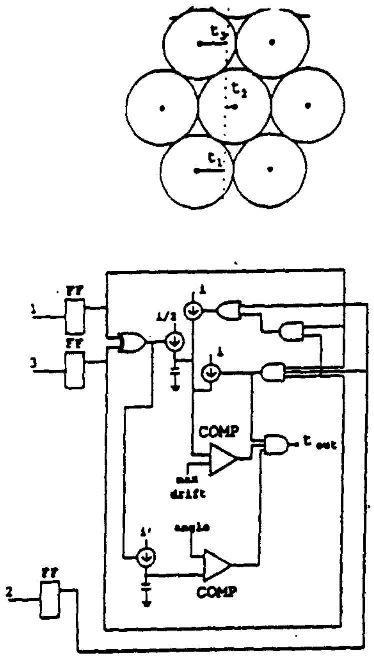

Fig. 19. The synchronizer circuit for triggering on triads of straw in the straw superlayer.

This has been a very productive year for the electronics R&D. Many circuits are now in the prototype stage and are ready for testing. The next step is to measure the high rate capabilities of the electronics and to confront the important details of chamber design such as proper straw resistance, proper wire attenuation, problems of capacitance, shielding and grounds.

Engineering R&D

Prototype Construction

Straw chamber prototypes have been built at Indiana University, Duke University, Boston University, and Princeton University. The problems of wire support and straw support have been solved in a number of different ways. At Duke a 25 straw system has been constructed. The straws were laid out and glued together on a flat grooved substrate. The straw length was 2.7 meters and the diameter was 4 mm. Measurements of the horizontal position in various rows show that the straws position for this configuration could be held to about 2 mils. This same system was instrumented and run at high voltage successfully. There is an ongoing program to study ways to accurately layout and glue the straws to the support cylinders in this hybrid scheme. A large prototype full length cylinder of 0.8 meter radius is being worked on. At Princeton University there is also work on building large structures of 7 mm diameter straws for a BCD experiment. Several straw clusters have been constructed and a novel method of pressurizing the straws to handle them has been worked out.[17] At Indiana University a 6 straw 3.6 meter long assemble was tested with electronics from University of Pennsylvania and attenuation in the system measured.[18] The major work at Indiana now, however, is the construction of modular arrays to hold the straws in position. A 64 straw module shown in Fig. 20 has been constructed and is now under testing. The support shell is $300\ \mu$ thick carbon fiber composite. The end plates have been designed to have very little material. The positioning of the straws and wires is accomplished by self centering of the wire supports within the shell. This wire support is shown in Fig. 21. It consisted of two identical molded pieces that snap together to form a cylinder with opposing V shaped passages at either end. It has the added advantage that the straw chamber can be strung after being assembled, or can be rewired if there is wire breakage.

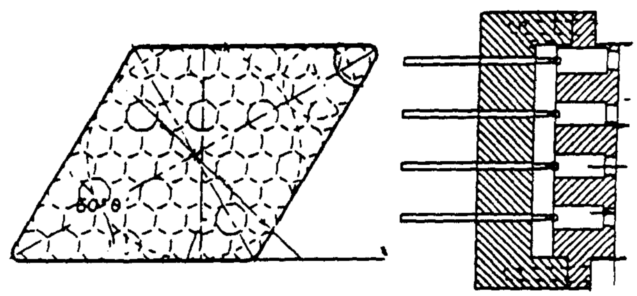

Fig. 20. Detail of the end and side view of a 64 straw module.

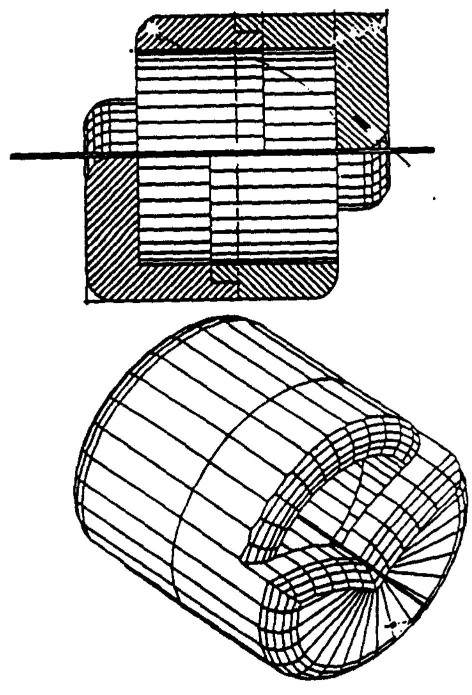

Fig. 21. Two view of a "double V" wire support.

Design Studies

Modular Tracker

All of the tracker engineering construction techniques are driven by the two somewhat incompatible considerations: First the amount of material must be kept small and second the straws and wires must be aligned with about 50 micron precision and be stable in that configuration.

The calculation of the radiation length versus eta for the SDC tracking system shows that in the region of the endplate of the central tracker there is more that 20% of a radiation length. It is difficult to reduce this significantly, since each superlayer has less than 1% of a radiation length for perpendicular traversals, and about 1/2 of this is from the straws themselves. The engineering challenge is to design a support system with 60-75 m tolerance with light weight materials. One support scheme that has been designed by Westinghouse[19] is shown in Fig. 22. The modules are held in position by a rigid support frame at three points. These frames have to only support the modules and not the wire tension, so they can be very light. They would be made from light weight carbon composites. Each module has a set of alignment pins that locate and hold it in position in the support disks. Four of the eight superlayers would be stereo layers. These are constructed by using the same modules as in the axial layers, but rotating them by 3 degrees. Modules could be assembled into the frame as the final operation after all electronics testing was complete and modules could be replaced in the case of accidental damage.

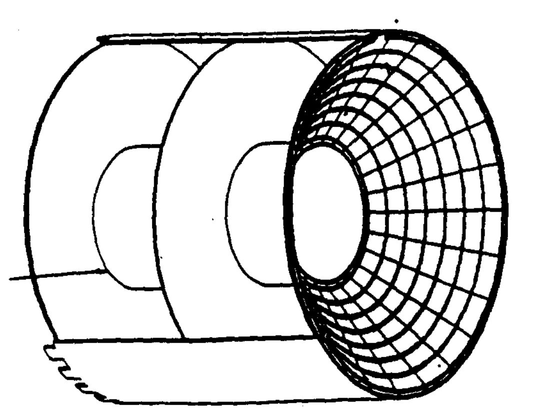

Fig. 22. An assembly drawing of one half of the modular drift chamber tracker showing the support system.

Hybrid Tracker

The hybrid central tracker is shown in Fig. 4. The design work on this tracker has been done at Oak Ridge National Laboratory.[20] In this concept the straws are supported on full length cylinders that are held on the ends by a cone and ring support. The details of the endplate with utilities are shown in Fig.23. This endplate must support wire tension for the entire cylinder, and also serve as the precision wire positioner. The amount of material in the support cylinder is comparable to the modular approach, however, there would need to be extra cylinders for the scintillating fiber layers. During this coming year both techniques will be designed in much more detail.The major R&D for reduction of material is in the endplates and utilities. This is being worked on at ORNL.

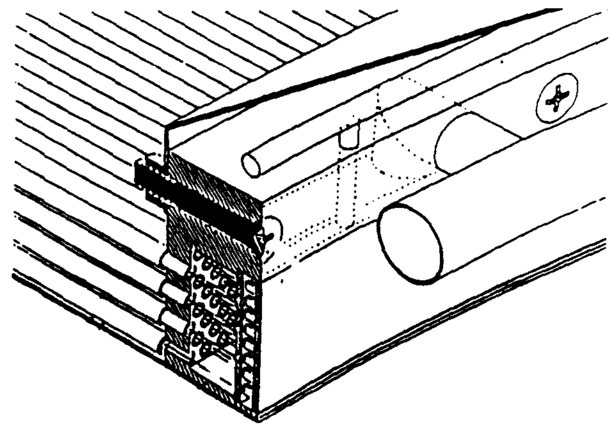

Fig. 23. Details of the endplate for the Hybrid design, showing utilities.

TRD Tracker

At CERN [21] there have been several very impressive tests of a straw tracking system coupled with TRD possibilities. A large array of straw tubes was tested in a CERN beam line to verify that the TDR tracking cell would give the resolution required by EMPACT. They found that using only the cell hits (and not drift time) they were able to achieve an position resolution of 0.4 mm. At Boston University a strawless detector is being developed.[22] The idea is to combine two foam molds with cylindrical depressions into a straw chamber. This has the advantage of low mass, ease of construction, and economy of handing. It may well be excellent solution to the short straw arrays required for EMPACT.

Intermediate Tracker

Radial Chamber

The intermediate tracker design is being worked on by several groups in the United Kingdom.[23] The design is based on the radial chambers being built for the H1 experiment at HERA. The details of the design are shown in Fig. 3. and Fig. 24. The present design involves 5 radial chambers position along the z axis. They each span a 50 cm to 150 cm radial space. Each has 300 azimuthal cells with a maximum drift distance of 15.7 mm. Within each module there are 8 layers of drift cells. The long drift times could be a problem at SSC where the bunch crossing is 16 ns., so a plane of tagging counters is placed in front of each radial chamber. These " bunch tagging counters" are shown in Fig. 25. The tagging counter time resolution is about three crossing times. This has been shown to be sufficient to result in good pattern recognition in the radial chamber. The R&D effort at present is concentrating on current draw in the voltage grading resistors. Because of the higher currents in the chambers at SSC this could be a difficult problem. Also the Lorentz angle for the drift gas (CF4) must be measured[24]. This work is already underway and first results were presented at this conference. One of the primary advantages of the radial wire chamber is that the geometry matches the physics in the forward region and an excellent tracking system can be built with very few electronics channels. It is anticipated that the total channel count from both ends will be less than 50K. There is also an active design program on electronics for radial chambers at Rutherford Laboratory. Alternative devices such as microstrip chambers are also under study.

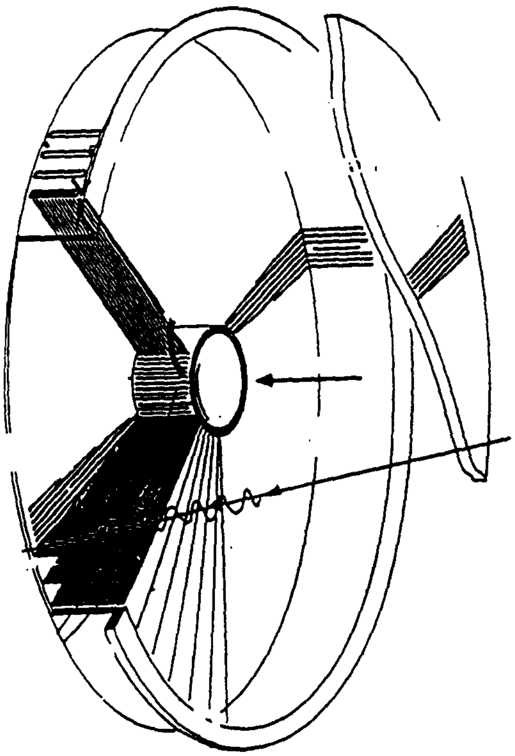

Fig. 24. Details of a radial wire chamber. The SDC version would have larger inner and outer radii and 300 sectors.

New Gaseous Chambers

In the intermediate region there have been a number of proposed detectors in addition to the radial wire chambers. Groups from Japan [25]and Texas[26] have been developing a new type of gaseous discharge chamber called the knife edge chamber with a signal and cathode structure printed on silicon. Reports from both groups were presented at this conference. In the case of the Texas design, an intermediate tracker has been proposed and the design started. Another technique being looked into at University of Rochester[27] is a resistive cathode drift cell. This scheme effectively uses a drift pad with hexagonal pads to fill the forward area. Each pad has a graded voltage for electron to drift toward the center pin where they avalanche. Scanning Tunneling Microscope points could be use for the discharge pins. Work is under way to design in intermediate tracker with such a system.

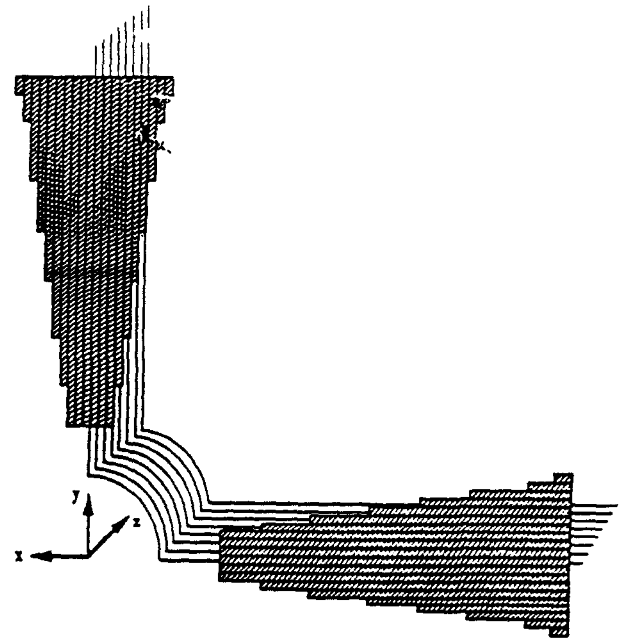

Fig. 25. Details of the bunch tagger counter which covers each sector and tags the proper bunch crossing time.

Summary

Wire chambers can play an important role at the SSC. Although straw drift chamber are a mature technique, there have been a number of innovations in straw drift chambers during the past year. All of the principle SSC detectors have been developing straw chambers and have concluded that such systems are feasible. The counting rates in the straws are high, but Monte Carlo studies indicate that tracking looks promising at and above design luminosity. The chamber lifetimes with CF_4 gases look very good.and radiation effects appear to be no problem at SSC for CF_4 gas mixtures.

In the intermediate region there is a radial wire chamber design under study and there are newer gaseous chambers that look promising.

Full scale tests are being planned to verify tracking at high rates and to confirm the triggering aspect of straw chambers.

[1] The members of the Wire tracking Subsystem group are Indiana University, University of Colorado, University of Pennsylvania, University of Liverpool, University of Glasgow, Rutherford Laboratory, KEK, Westinghouse Science and Technology Center, LBL and Oak Ridge National Laboratory.

[2] The members of the Hybrid Tracking subsystem are CBAF, Duke University, Florida State University, General Electric Canada, KEK, North Carolina State University, Northeastern University, Oak Ridge National Laboratory, Quantum Research Services, Supercomputer Calculations Research Institute, TRIUMF, and University of Pennsylvania.

[3] Asai- International Workshop on detectors for SSC, April, 1990, p260. The original plot was only for hit rate, which was scaled for the other parameters based on calculations at Indiana University.

[4] M. Corden, Proceeding of this conference. He predicts 17% at the first superlayer, and 3% at the final superlayer.

[5] W. Ford.and M Lohner "Track Reconstruction in Straw Superlayrs", Proceedings of this conference.

[6] C. Neyman, "Gain of a 3.65 m Straw Drift Tube", IUHEE-90-12.

[7] C. Lu "Investigations of a Single electrons' behavior in a proportional drift tube." Proceedings of this conference..

[8] J. Kadyk, J. Vavra. and J. Wise " Use of Straw tubes in High-Radiation Environments" Slac-pub 5306, and J. Kadyk,Proceedings of this conference.

[9] R.Henderson " Etching of Anode Wire Deposits with CF_4/Isobutane" Proceeding of this conference.

[10] W. Dunn " Radiation Damage Studies of Straw Tube and Scintillating Fiber components" Proceedings of this conference,

[11] B. Zhou " New Results on SSC Tracking Studies" WorkShop on Major SSC Detectors , Tuscon, Ar. ,Feb. 18,1990 ; S.Ahlen Private communication.

[12] H. Iwosaki " A time resolution study of Straw Chambers.". Kek, 89-158

[13] C. Neyman Attenuation Studies of 3.5 meter Straw Tubes" IUHEE-90-7 ; S. Oh, "Performance of a Prototype 3 meter Straw chamber", Proceedings of this conference.

[14] F. Newcomer et. al "A fast Monolithic Preamp and Shaper for High Rate Gas Tracking Detectors", Penn electronics Publication to appear in IEEE Trans. Nuclear Physics

[15] Y. Arai, "Development of TMC Chip and On-Chip Processing" " Proceeding of International Workshop on Solenoidal Detectors for the SSC, 1990 p 453.

[16] J. Chapman, " Synchronizer Development Update" Proceedings of this conference.

[17] J. Armitage, "A Straw Tracking System", Proceedings of this conference.

[18] Ogren "Progress Report on 4 mm Straw chambers" International Workshop on Solenoidal Detectors for the SSC, 1990 p 302.

[19] R. Swensrud, " Design of a modular Straw tracking chamber", Proceedings of this conference.

[20] T. Ryan, " Design of the Hybrid Tracker and Utilities" Proceedings of this conference.

[21] V. Polychronakos "Particle Identification and Tracking with Transition Radiation Detectors", Proceedings of this conference.

[22] S. Whitaker, Private communication

[23] University of Liverpool, University of Glasgow, and Rutherford Laboratory are working on this design. D. Saxon " Forward Tracking with Enhanced Electron Indentification", Proceedings of this conference.

[24] J. Baily, " A measurement of the Electron Drift in Fast Gases" Proceeding of this conference.

[25] A.Maki, " The knife edge chamber R&D at KEK" , Proceedings of this conference.

[26] P. McIntyre, "Knife Edge chambers", High resolution tracking for he SSC detectors." Proceedings of this conference.

[27] Sills, "Advanced Field Shaping Drift Chambers for SSC Muon Tracking", Proceedings of this conference.

June 3,1991
IUHEE-91-1

Effects on Straw Drift Tubes of Extended Operation in a High Radiation Environment

David R. Rust
Physics Dept. Indiana University
Bloomington IN 47405

Introduction

In the last few weeks we have been testing our straw tube modules and also individual straw tubes in a flux of electrons from Sr^{90}. This has been in response to the concerns of some people in the SDC that the straw tubes are not sufficiently robust to withstand the radiation environment of the SSC. There are two concerns: one is that the coating is so thin that it can be etched away during the lifetime of the SDC detector; the other is that experience with aluminum cathodes has shown that breakdowns can develop under certain conditions. With the sources at our disposal we could in a day or two expose small sections of the tubes to a dose that was equivalent to a full ten years accumulation at the SSC. This is a report of some observations to date.

Apparatus

The apparatus consisted of a single tube in a holder with a fixture at each end to allow the gas to be introduced and the voltage to be connected between the anode and the cathode. The anode was a 25.4 μm gold plated tungsten wire stretched to 50 grams of tension. The tube was 4 mm in diameter with either aluminum, copper or gold deposited on a plastic substrate. A 2 mCi Sr^{90} source was used to irradiate the tube and a plastic collimator limited the extent of the exposure along the length of the tube.The amount of radiation was varied by changing the distance of the source from the tube. The High voltage supply furnished monitor outputs of the current and voltage. It also incorporated a trip on a certain level of current or a rapid rate of rise of current. If a discharge started to occur the voltage was turned off immediately.

Loss of Cathode Material

The erosion or ablation of material from the cathode due to ion bombardment has been observed in two ways. First an electron micrograph of a 500 Å gold coating on kapton showed that after exposure the irregularities of the coating resulted in uncoated areas. A rough estimate from this indicated that about half the coating was removed during an exposure of 0.25 C/cm. A more quantitative measurement consisted of measuring the resistance of a strip of a tube after exposure and comparing it with an unexposed strip. The observation was that for a mylar strip with a 1000 Å coating of copper about half of it had disappeared after an exposure of 0.09±0.02 C/cm. The surface resistivity changed from 0.19 Ω/square to 0.40 Ω/square. The copper coating was also partially transparent. There is about a factor of 5 difference between the amount of gold and the amount of copper removed for a given amount of accumulated charge deposited on the cathode. There was some excess discharge current with the copper but only about as much as the normal current and that for a small fraction of the exposure. The gold was deposited by sputtering and the copper was applied by vacuum deposition and that may make a difference. So far the evidence for aluminum is consistent with both levels of ablation.

Alteration of the Surface Properties of the Cathode

Some measurements were made of the progressive damage to an aluminum cathode under heavy current from 2 MeV electrons passing through a straw tube. Figure 1 shows the results of the exposure. The amount of current drawn in the exposed region of the tube was 0.46 μa/cm up to an accumulated charge of 0.175 C/cm. The vertical axis is a quantity which characterizes the alteration or damage to the cathode surface. It is 1/G where G is the gain at the anode at which breakdown occurs. The gain is determined from the high voltage value. For the standard mixture of CF_4 with 20% isobutane the shape of the gain as a function of voltage is shown in Figure 2. The absolute value of the gain may be off by as much as 20% but the relative gain as a function of voltage is given quite accurately by this curve. The gain is the appropriate variable because something is happening to pull electrons out of the cathode in response to ions landing on the cathode. When the gain times the probability of releasing an electron for each ion is more than 1, a self sustaining discharge occurs. 1/G at breakdown is then equal to this probability. The tendency for the cathode to eject electrons must be reduced as much as possible. From Figure 1 it is seen that the accumulation of charge results in a uniform increase in 1/G.

The people who have been doing aging and lifetime tests at Berkeley have seen breakdowns of this same type.[1] They say also that adding 0.1% water to the gas has eliminated these breakdowns. Water was therefore added to the gas in this test also to the level of 0.13% vapor pressure by bubbling a fraction of the CF_4 through iced water. The breakdown occurred at a higher voltage when the water was added but as soon as the water was turned off the breakdown voltage returned gradually to the point it would have reached if no water had been added (see Fig. 1). It seems that damage occurs to the cathode with the water present in the gas but the effect of the damage on the operation of the chamber is not as great with the water present.

The tendency to breakdown is also very much influenced by the radiation level. In these tests the radiation level is about a hundred times more intense than in typical operation of the SDC detector at the SSC. It is primarily because of this accelerated irradiation schedule that we have discovered this tendency of the tubes to breakdown. In order to measure the dependence on irradiation, several data points of 1/G were taken with the source at different distances from the tube. This dependence is shown in Figure 3. The horizontal axis is the current at the trip point corresponding to the gain on the vertical axis shown by the solid line. The trip current is in microamperes but the current density in microamperes per centimeter can be obtained by multiplying by 1.4. The trip current is the product of the gain and a number proportional to the radiation level; therefore the limiting inverse gain as a function of radiation level on an arbitrary scale is obtained by scaling the horizontal axis to obtain the dashed line curve. There are no measurements at low radiation levels so that the extrapolation towards zero is only a guess. Still it is clear that the gain can be raised beyond 10^5 at low enough levels of radiation. The radiation level at the SSC is between the vertical axis and the first minor division.

Some observations of gold and copper surfaces have also been made. With the gold surface the gain went up to 3×10^5 without breaking down even after and exposure of 0.25 C/cm. The copper tube after an exposure of .23 C/cm broke down at a gain of 2×10^5. Both of these were at radiation levels causing 0.64 μa/cm at a gain of 4×10^4 and therefore more than 100 times the radiation level expected at the SSC at design luminosity.

Conclusions

The loss of material from the cathode is at a level which must be considered when specifying the thickness of the coating. More work needs to be done to see which materials ablate the least while still being good conductors and having a long radiation length. One would like to have coatings of 2000 Å or more of either aluminum or copper to provide enough material to sacrifice over the lifetime of the detector (assumed to be 10 years) while still maintaining good electrical conductivity of the cathode

Although aluminum probably would work sufficiently well at SSC radiation levels, the extra margin of safety provided by a copper surface makes that material very attractive.The amount of material in radiation lengths of a 2000 Å coating of various materials is given in the following table. It appears that copper is not a large additional amount in relation to the mylar material and even less considering all the other material in the outer tracking system.

35 μm mylar is 1.22×10^{-4} R. L.

Compared with this 2000 Å of	aluminum	is	2.25×10^{-6} R. L.
	chromium	is	1.00×10^{-5} R. L.
	copper	is	1.40×10^{-5} R. L.
	silver	is	2.4×10^{-5} R. L.
	gold	is	6.2×10^{-5} R. L.

These are the only reasonably common solid elements with resistivity below 3 μΩ cm. (Aluminum coatings, however, have a resistivity about double the bulk value.)

[1] J. Kadyk, J. Va'vra and J. Wise, Use of Straw Tubes in High Radiation Environments, Nucl. Inst. and Methods **A300** 511 (1991)

FIG.1

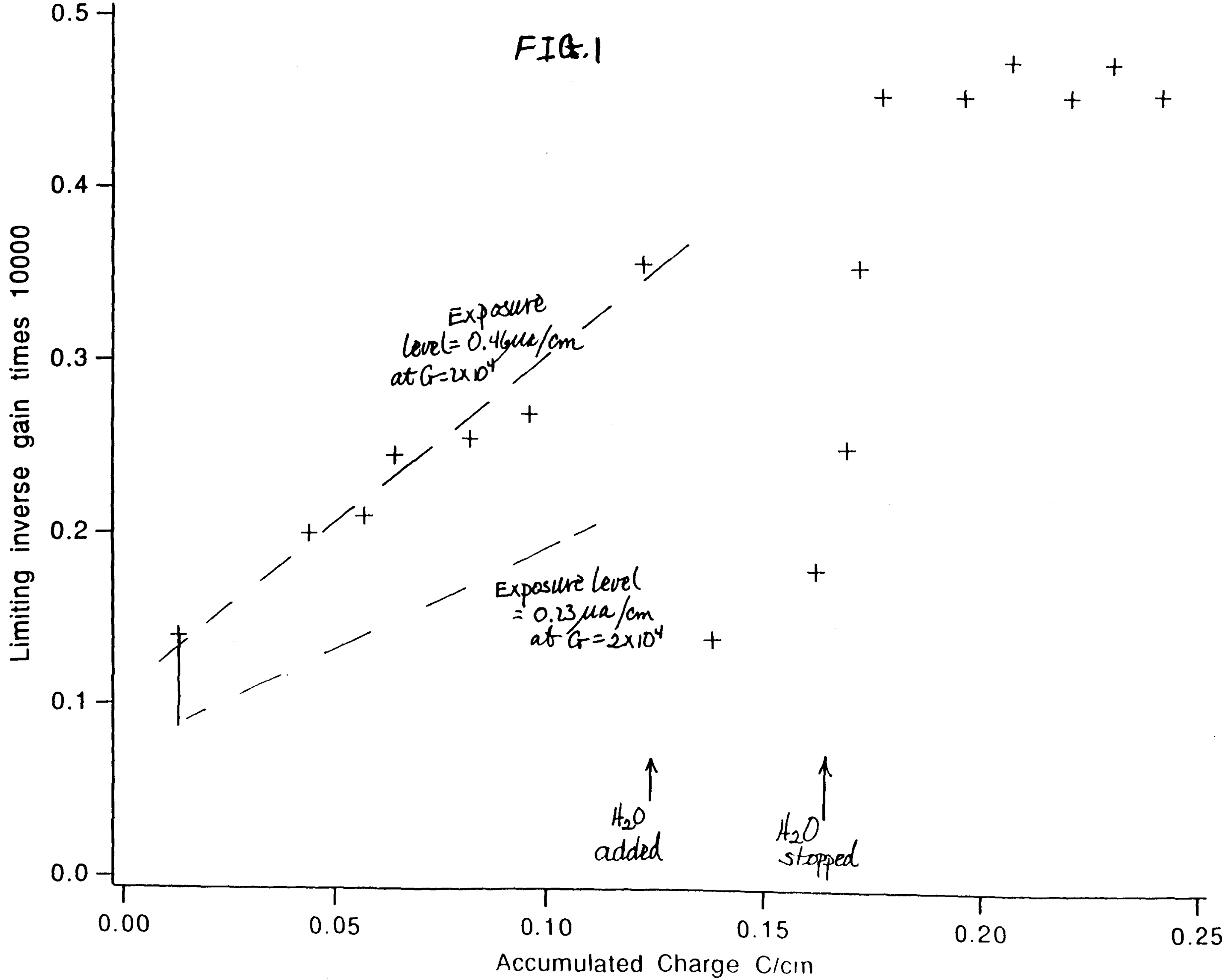

0.5
0.4
0.3
0.2
0.1
0.0
Limiting inverse gain times 10000
Exposure level= 0.46ua/cm at G=2x10^4
Exposure level = 0.23 ua/cm at G=2x10^4
H2O added
H2O stopped
0.00
0.05
0.10
0.15
0.20
0.25
Accumulated Charge C/cm

FIG. 2

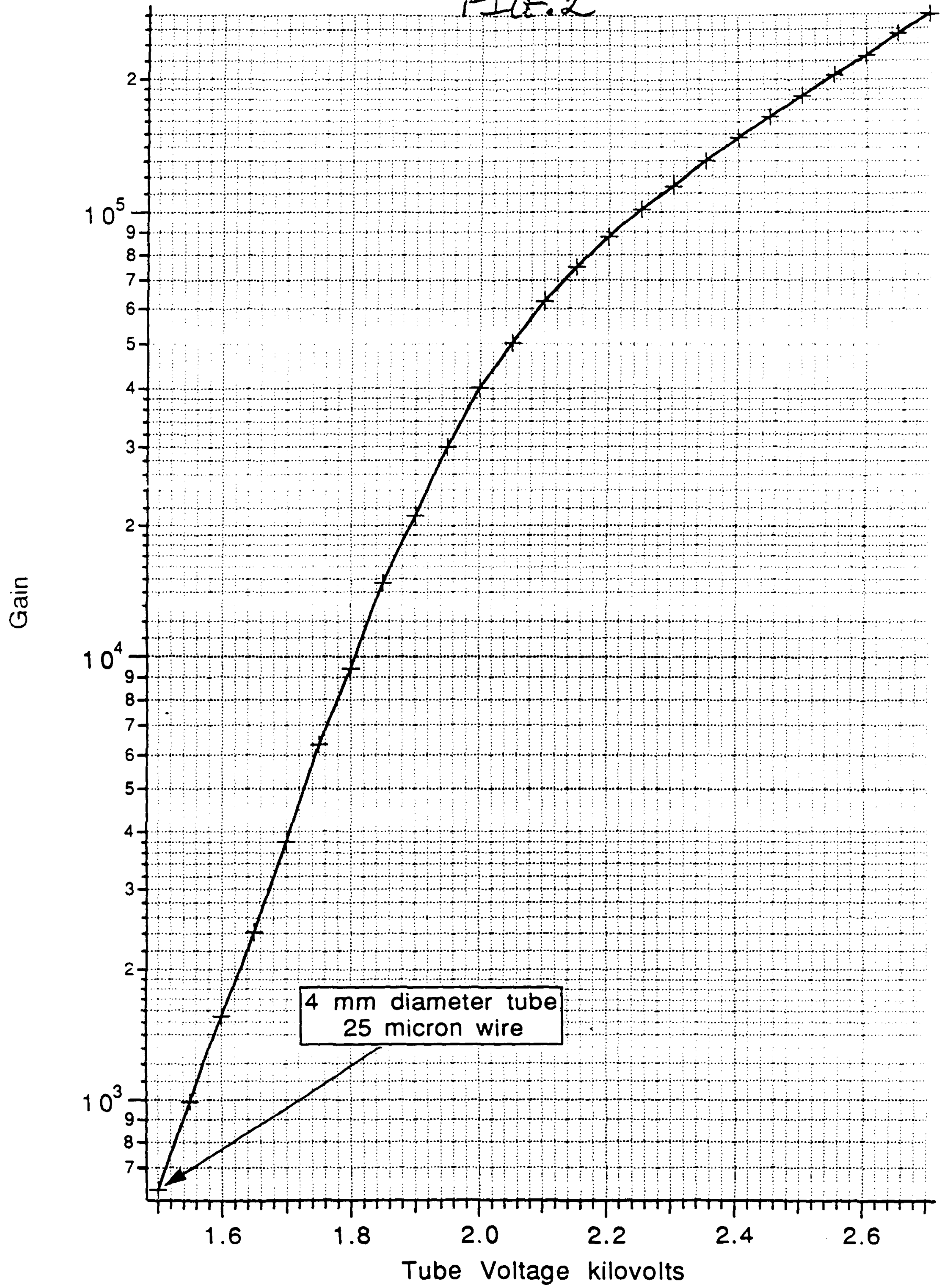
Gain
Tube Voltage kilovolts
1.6
1.8
2.0
2.2
2.4
2.6
10^5
10^4
10^3
2
3
4
5
6
7
8
9
4 mm diameter tube
25 micron wire

FIG. 3

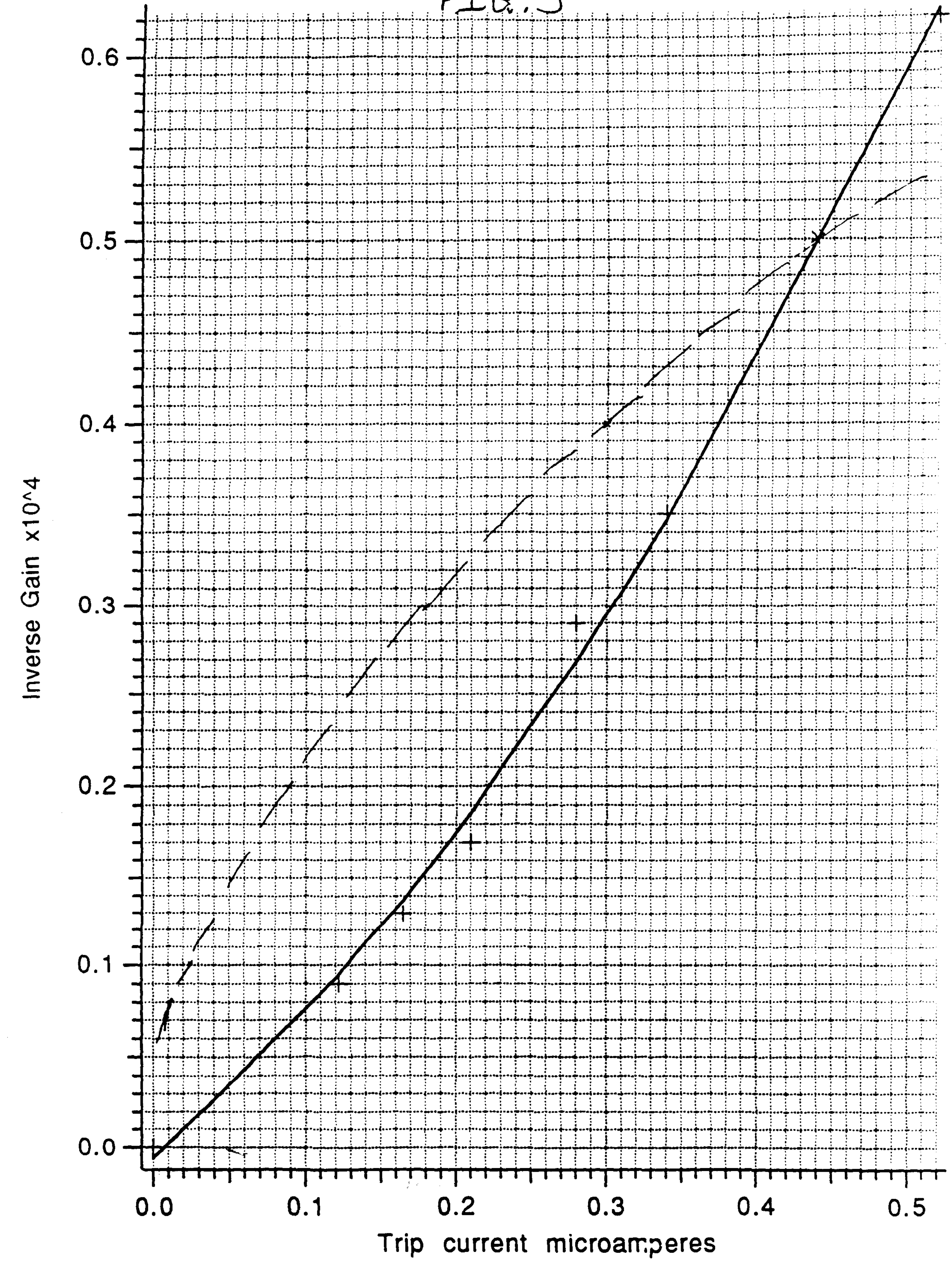

0.6
0.5
0.4
0.3
0.2
0.1
0.0
Inverse Gain x10^4
0.0
0.1
0.2
0.3
0.4
0.5
Trip current microamperes

IUHEE 91-7
SDC 91-00056

Self centering measurement for 8 layer trapezoid

R. Foster, G. Hanson, F. Luehring,
B. Martin, H. Ogren, D. Rust, E. Wente

Physics Department, Indiana University
Bloomington, Indiana 47405

Straw Chambers

The basic drift cell is constructed with a plastic based cylindrical cathode structure and a 0.025 mm diameter wire along the axis. The straws are formed by winding several centimeter strips of the plastic wrap on a mandrel and then overlaying and gluing a second layer. This results in a rather uniform overall straw, but tension variations and gluing variation result in a diameter variation of about ± 25 microns and a deviation from circularity of about ± 50 microns. All methods proposed for using the straws for drift chambers require that the straws be held straight in some manner and be formed in regular array by some means. These two aspects of the design of a straw module are critical. The ultimate precision of the drift chamber is obtained by knowing the positions both at the ends of the wire positions and at the intermediate wire support points.

The proposed scheme for positioning the straws with respect to each other requires clamping and gluing the straws at the points along the straw where the internal wire supports are located. The layout is shown in Fig. 1. This technique relies on the wire supports (double V's) close packing in a regular array when clamped and glued. The array must maintain this configuration when freed from the clamp.

The design of the wire support (Double V) is shown in Fig. 2. The diameter has been measured to be 3.972 mm (0.1564 in.) The double V's are injection molded and are uniform to about 0.005 mm.

This memo reports on the first series of tests we have carried out on a 8 layer trapezoidal array that we are preparing for a one meter test module.

Description of the clamp

The clamp is shown in Fig. 3. It is designed to be used along with 4 other identical pieces in a linear array to clamp 228 straws in a one meter module. In this test, however, we used short (about 2 cm) sections of straws with the double V's inserted and then clamped in only one clamp. The clamp dimensions are set by assuming a straw + double V diameter of 4.043 mm (0.1592 inches). The wall thickness is taken to be 0.035 mm (1.4 mils). The reference blanks were cut by Liberty Advanced Machining of Columbus IN, using a numerically controlled mill. The clamps were then precision cut using a electrodischarge cutting technique at Wirecut Technologies in Indianapolis, IN. The drawing tolerance of 0.013 mm (0.5 mil) appears to have been achieved by this technique.

Clamping and gluing tests

Two types of tests were performed. First, the straws and wire spacers were clamped without gluing. This array was measured while still inside the clamp. The positions of the double V's were determined by using a Nikon optical comparator with a measuring accuracy of about 0.005 mm (0.2 mil). However, it is estimated that the location of the vertex of the double V could be found to about 0.025 mm (1 mil).

The second measurement was made on an array of straw sections that had been be glued with Eccobond 45 epoxy. This particular array was formed layer by layer with a bead of glue applied on the surface of each layer before the next was laid down. The bottom, top and sides (in contact with the clamp) were not glued. After the array had dried it was removed from the clamp and measured in the same manner as the first array.

Determination of the self centering errors

The determination of the self centering errors of the double V's was made by fitting the measurements to an ideal close packed cylindrical array. This was done using MINUIT and using the x, y centroid, the rotation angle, and the close packed diameter as fitting parameters in a chi squared minimization procedure. The details were reported in IUHEP 91-6.

The resulting fits gave the following results:

Clamped array (no glue)

fitted diameter- 4.044 ± 0.00025 mm (0.15921 inches)

Sigma- 35 microns (1.33 mils)

The deviations of the fit in both X and Y are shown in Fig. 4 a, b.

Unclamped glued array

Fitted diameter 4.046 ± 0.001 mm (0.15930 inches)

Sigma 30 microns (1.2 mils)

The deviation of the fit in both X and Y is shown in Fig. 5 a, b.

Conclusions

The resulting fits showed several interesting effects. For the clamped array the fitted diameter was 4.046 mm (0.15921 inches) which corresponds to a midline width of 115.2525 mm (4.5375 inch.) The unclamped, glued array had a fitted straw + Double V diameter of 4.044 mm (0.15930 inches.) Along the midline of the trapezoid this corresponds to a width of 115.3185 mm (4.5401 inches). So, it appears that the array expanded when unclamped by less than 0.066 mm (2.5 mils). We suspect that this is the effect of the elasticity of the double V. Depending on how reproducible the gluing procedure is we can compensate for this when designing the shell structure.

The more important result is the self-centering error we have determined. We conclude that the unclamped array can be modeled by a perfect array with an error at each wire position of less than 0.030 mm (1.2 mils). (We believe that much of this error is measurement error due to a lack of precision in determining the vertex of the double V.) This error is well with in the requirements set for the tracking precision in the SDC. We intend to use this modeling technique for the final modules, so that a rather restricted number of parameters will be used to determine the wire position at the four wire support points along a module.

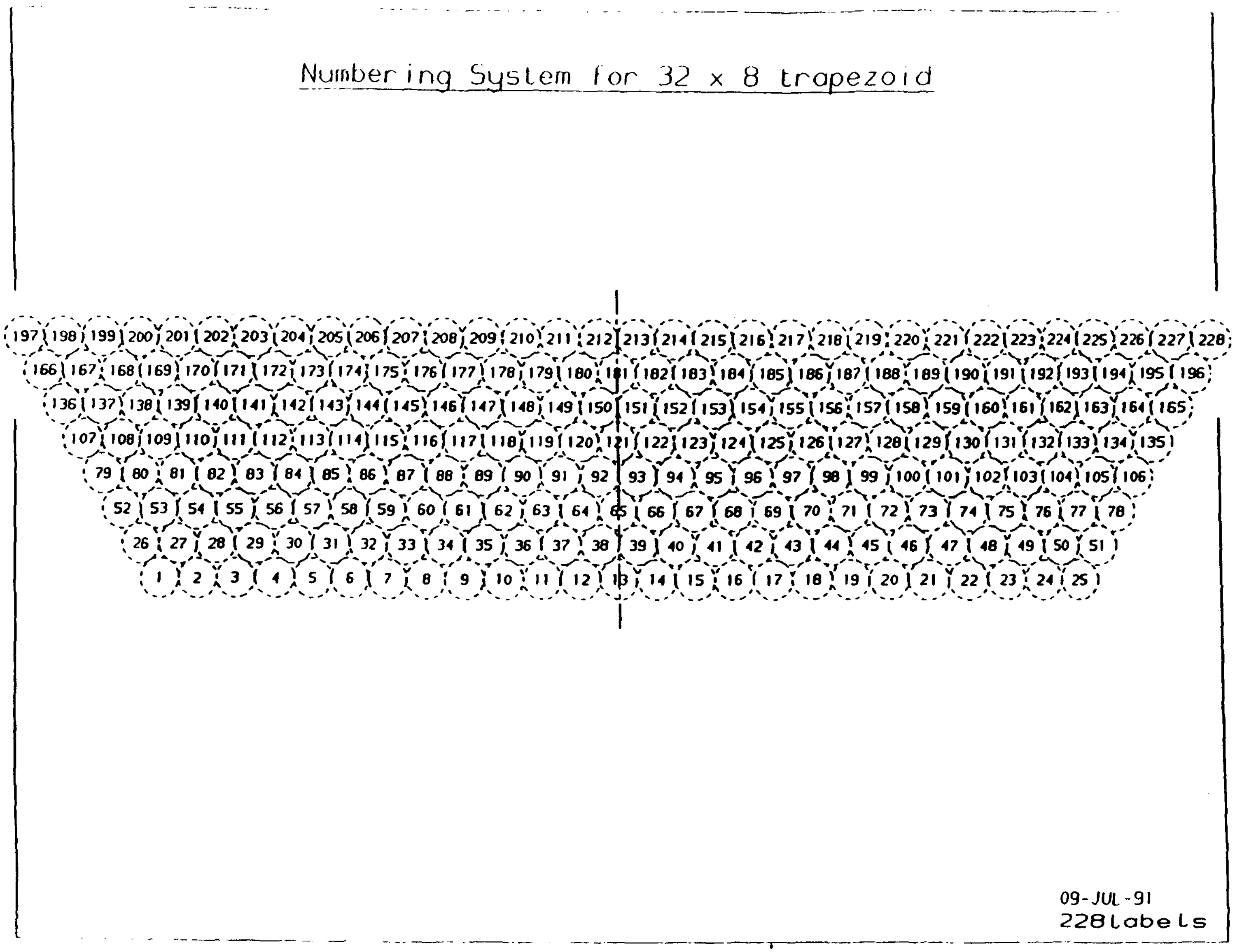

Fig. 1 Eight Layer array convention

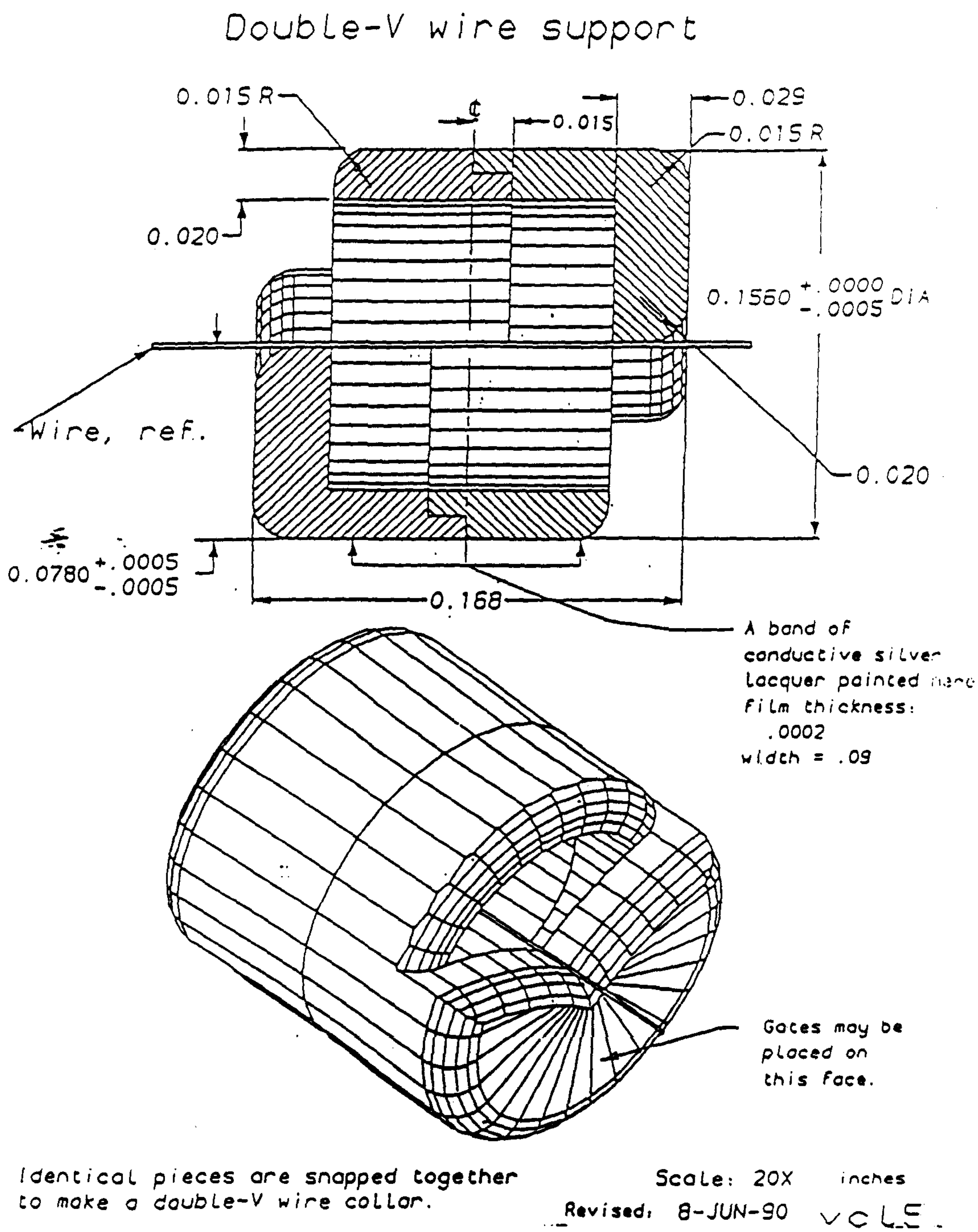

Fig. 2 Double V dimensions

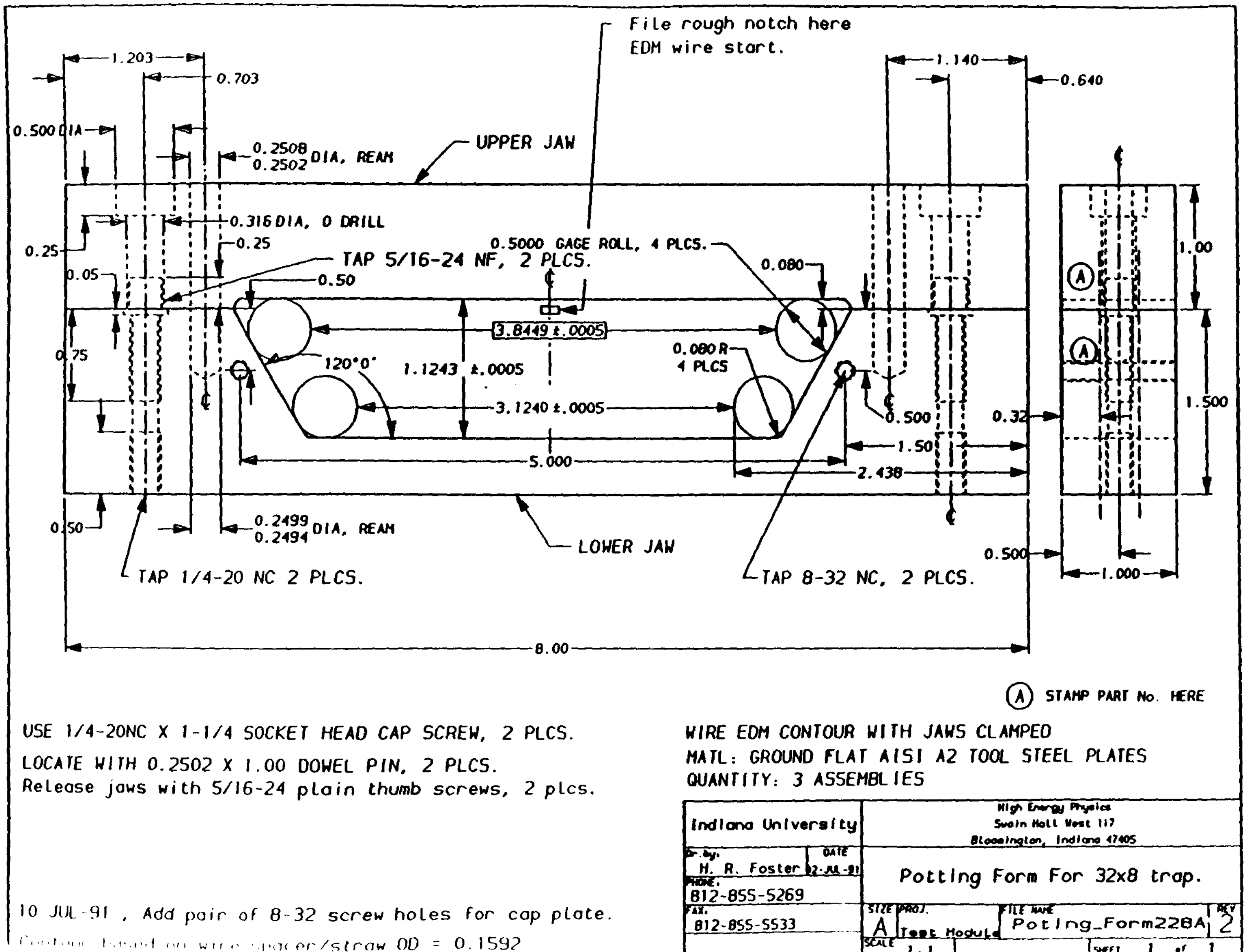

Fig. 3 Clamp design

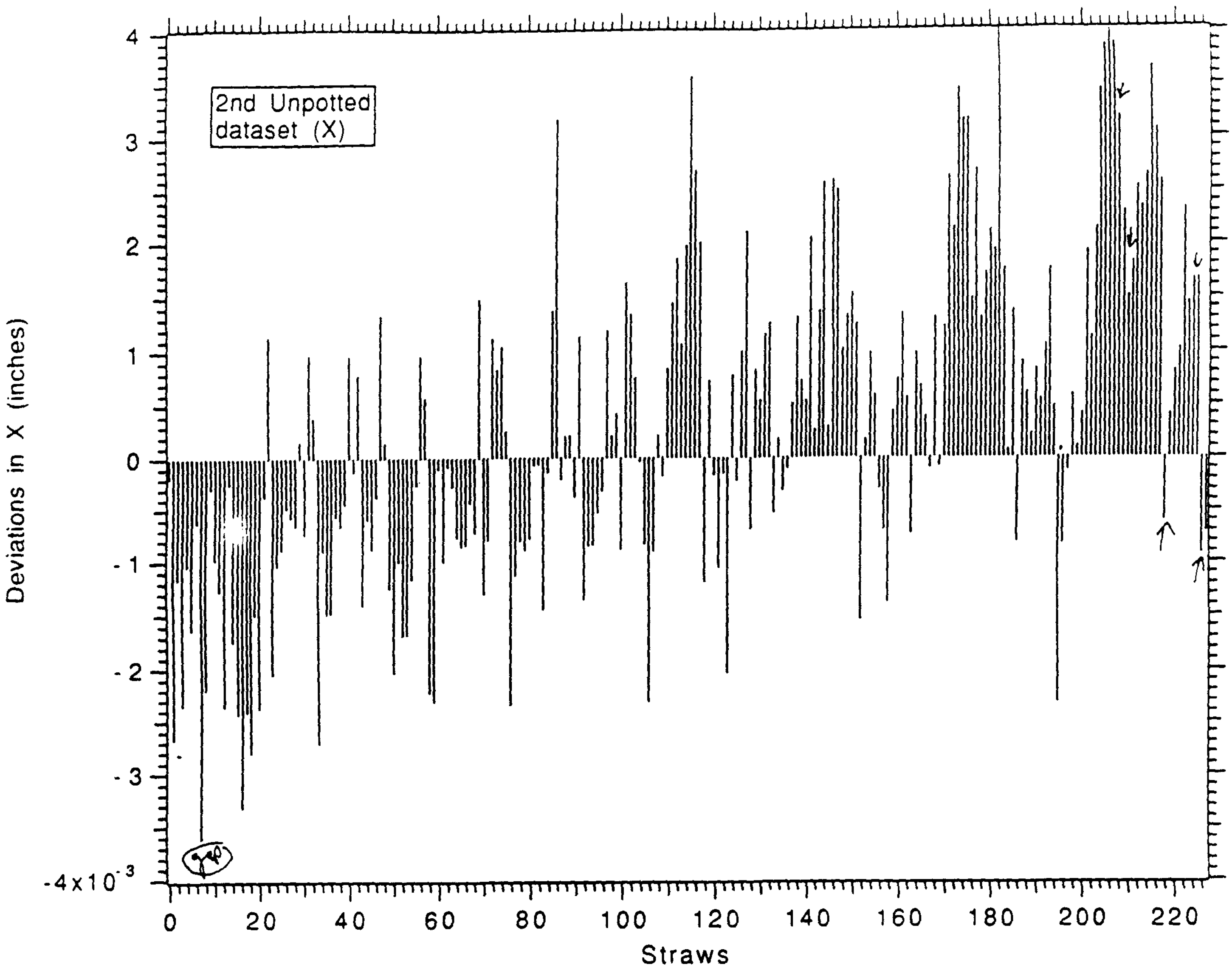

Fig. 4 a X deviations for clamped array

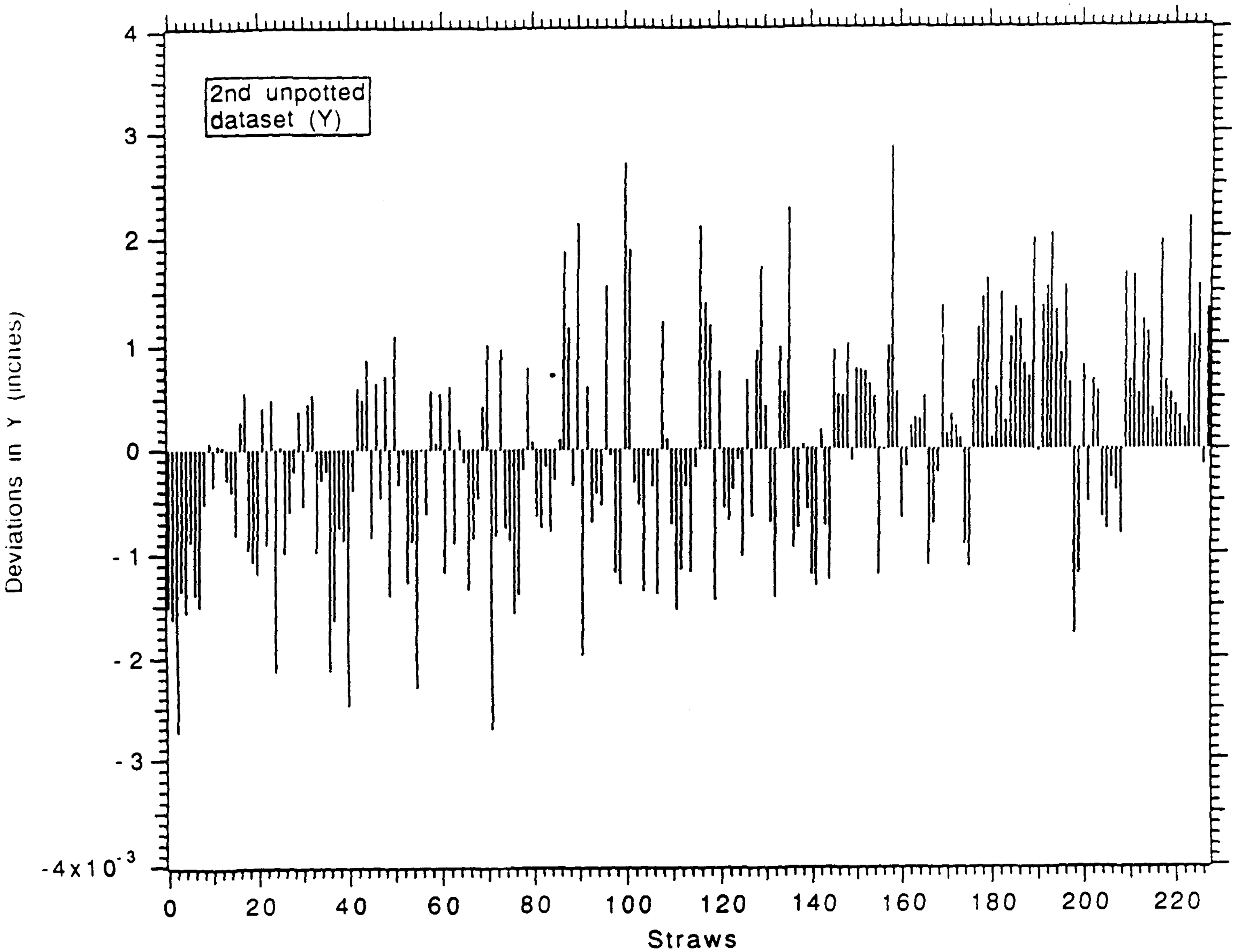

Fig. 4 b. Y deviations for clamped array

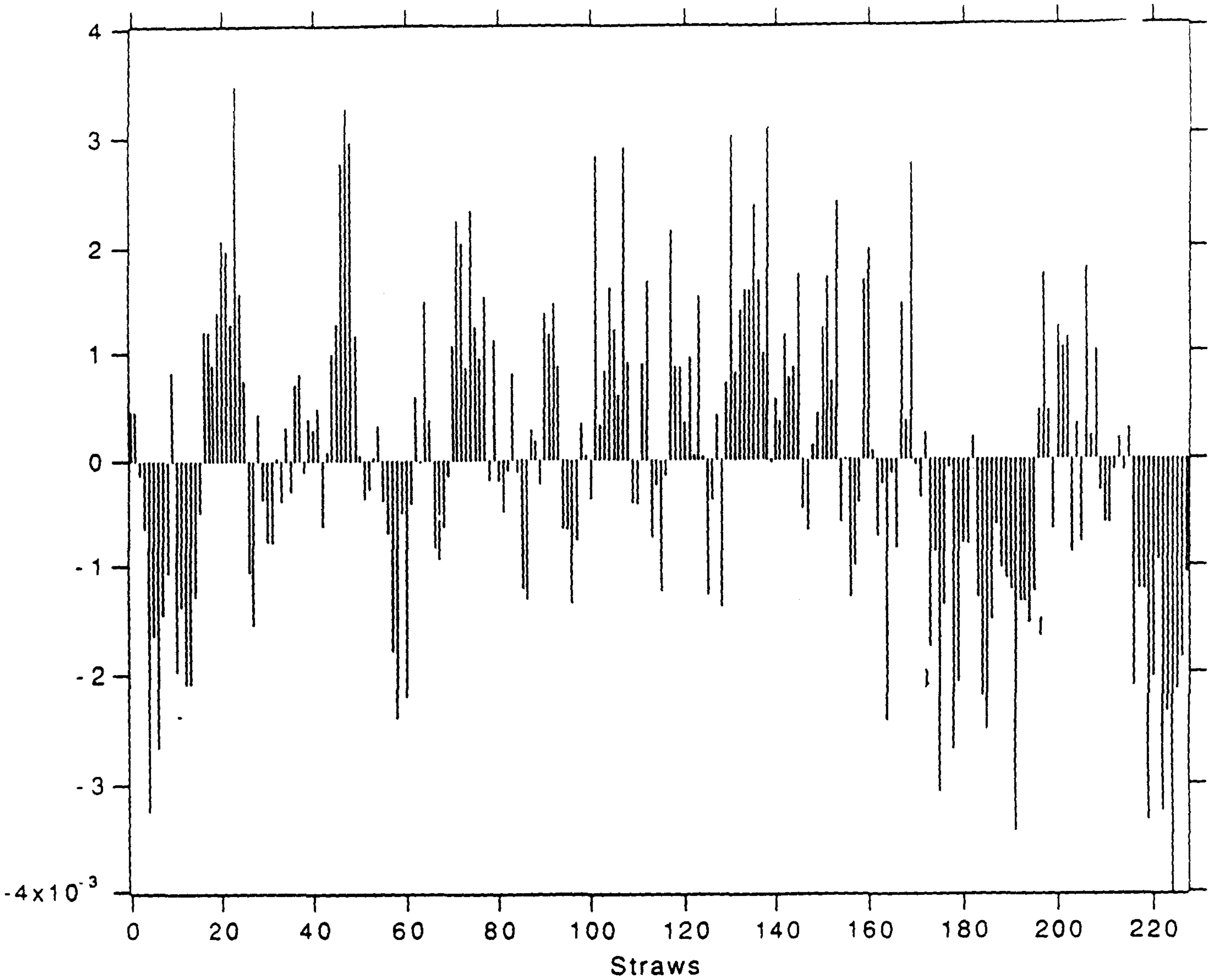

Fig. 5 a X deviations for glued,unclamped array

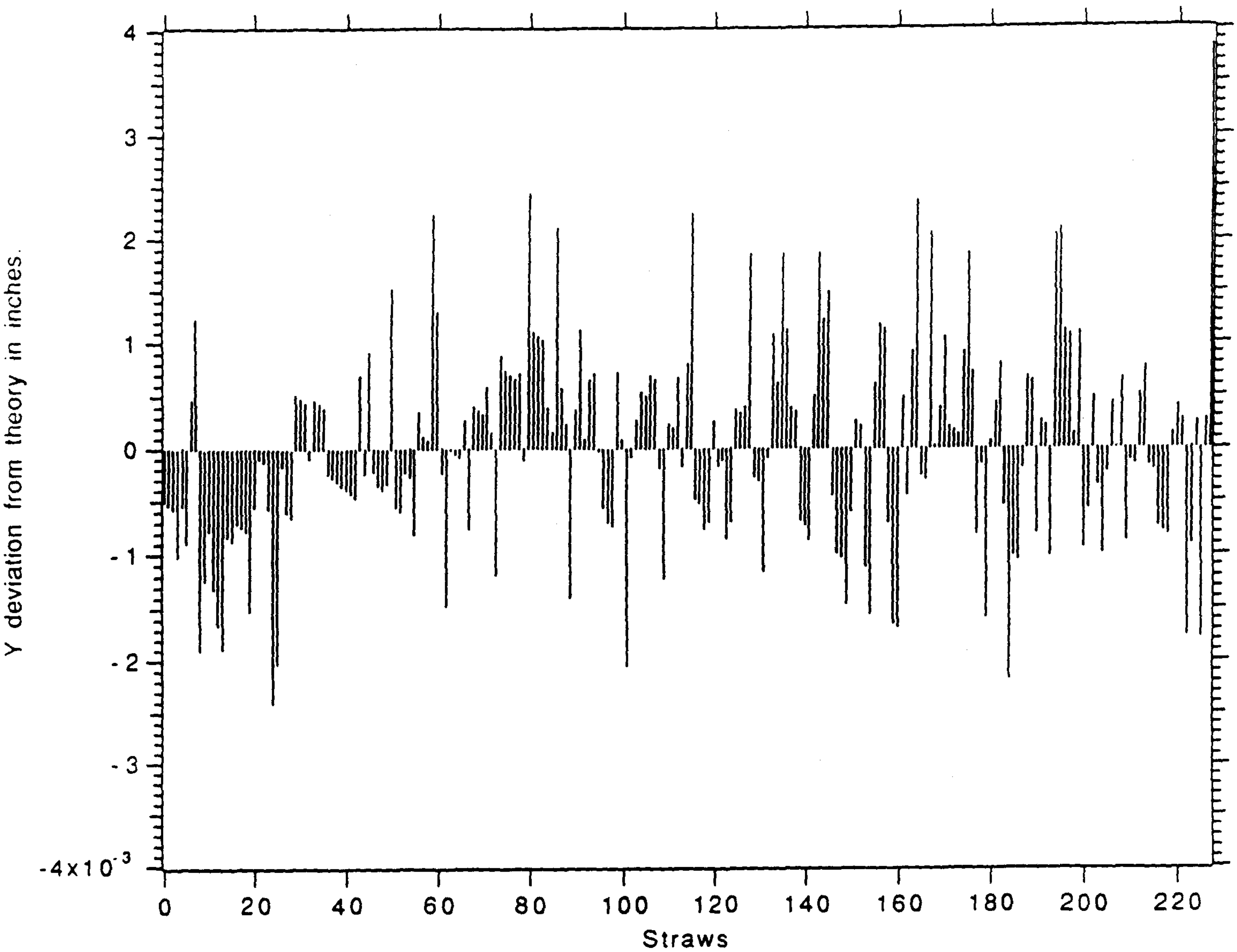

Fig. 5 b. Y deviations for glued,unclamped array

IUHEE # 91-4
SDC
Harold Ogren
Indiana University
April 23,1991

Straw and module placement

(Presented at ORNL on Feb 11, 1991)

I will begin by discussing support structure stability. I assume that Abe Seiden's numbers on correlated errors for the tracking layers are a statement of stability requirements for the structure. I will discuss module placement in a second section. In this report the numbers I will quote for errors are sigmas of the assumed gaussian errors. ie. +-sigma = +- 15 microns In order to be conservative we will assume that this should be interpreted as construction tolerances ie. +- 15 microns. (all points on the part within this window), with 1 mil = 25.4 microns.

Support stability:

1) the centroids of the Si and the Straw system must not vary by more than +- 15 microns. This will require monitoring the relative position of the silicon with respect to the outer tracker.

2) The rotational stability of the Si with respect to Straw layers is Δ phi = +_ 10^{-5} radians= +_ 0.00057 degrees. This also should be monitored continuously.

3) Each superlayer must have a circumferential stability (phi rotation with respect to other superlayers) that is about +- 50 microns. (actually the requirement is less strict for the inner layers of the straws, but lets be conservative). This will require a good understanding of the long term stability of support materials, but may not require continuous monitoring.

4) The radial stability is much less stringent. The purely radial stability is +_1.5 mm. However, this assumes that the circumference position (phi) does not change. So, I don't think this really allows us much design flexibility. Abe reduces this to +- 200 microns.

1) Placement of each end of the system with respect to other end. (hard to say, needs more work, probably close to the rotational requirement for each module, ie. +- 50 microns.) Will be fixed at assembly time using optical alignment techniques.

2) Placement of the entire tracking system with respect to the beam is , in part set by the amount of beam movement we expect. (+-1 mm?)
It is also set by the triggering requirements in the Si system., so it should be smaller than a strip size , say +- 100 microns. This may require local (Si) adjustment. This can be done to high accuracy during initial installation, and then monitored each down time, and perhaps adjusted with the kinematic constraints.

3) Assuming that the modules are aligned after the support structure is complete, the construction of the gross support frame need not be more accurate than +- 500 microns. This is an engineering detail of how the support cylinders are made.

Module requirements:

1) Placing modules on the cylinders (module placement)

Assuming that we have monolithic support rings or cylinders for the modules in each superlayer, then the over all angular error requirement should result in a maximum placement error of +_ 50 microns for each module.(this is the total placement error for the mean position of the module, ie placement of fiducial points at say 8 positions on the module.) To be conservative I will assume that each of the 8 module attachment positions has this precision.

2) Module intrinsic straightness.

From our limited tests on a 1 meter, smaller section, carbon composite shell, the bowing should amount to less than +_50 microns between support points (80 cm). I will assume +- 50 conservatively. This is one place where the reduced radial requirement helps us, since the modules are thinner radially, and might have more built-in bowing in this direction.

3) Straw placement within a module

The wire placement error will add in quadrature with the intrinsic wire resolution, assuming that they are random , uncorrelated errors. We have attempted to determine the size of such placement errors by optical measurements of straw center (double vee) positions at the end of a 64 straw rhombus. The x-y positions were measured using a milling machine and an optical telescope. Our estimated reading error was about +- 1 mil. The measurements were done with the endplate inserted in the rhombus shell. These measurements were then fitted to a close packed pattern with arbitrary center, rotation, and straw radius. The individual deviations from a perfect close packed geometry are shown in Fig. 1.This resulted in a 65 micron average sigma. determination of wire centers .(So a good part of this may be our measurement error.) But again, I will take 65 microns as the deviation from true close packing. The best fit straw separation was 3984 +- 7 microns.

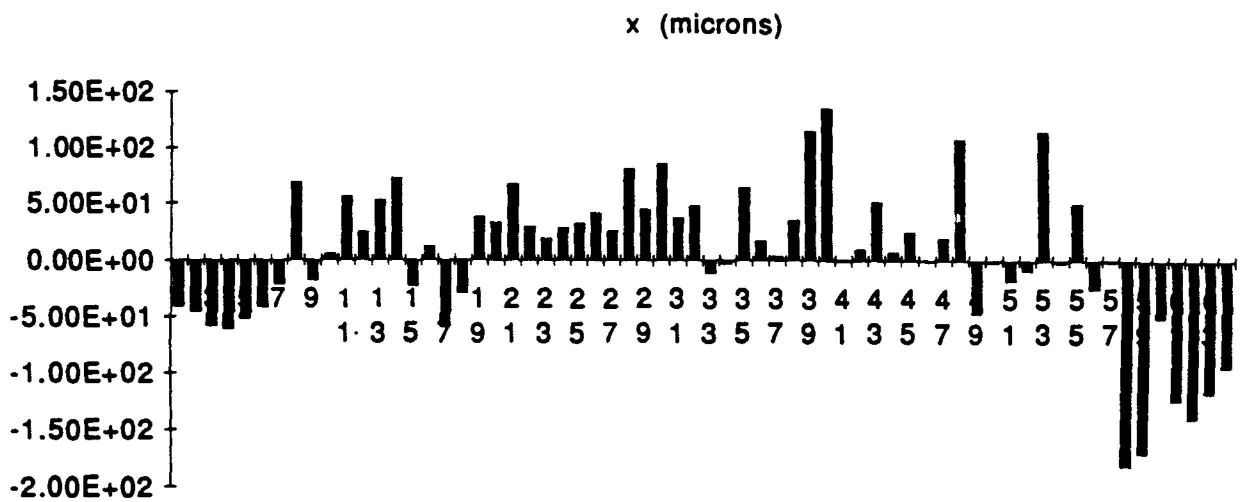

Fig. 1 Wire displacements from best fit of close packed geometry

In order to determine the effects of correlated errors in the straw and wire positions, the difference matrix from the above fit was used to fit vertical tracks. (see Figure 2). Correlation effects would show up as significant deviations from a "Zero "crossing. These were found to be small < 30 microns for all x positions. So we conclude that correlated displacements are not a problem. We will assume a straw placement error of 65 micron wire placement, however we feel that this can this can be improved considerably in our final module design.

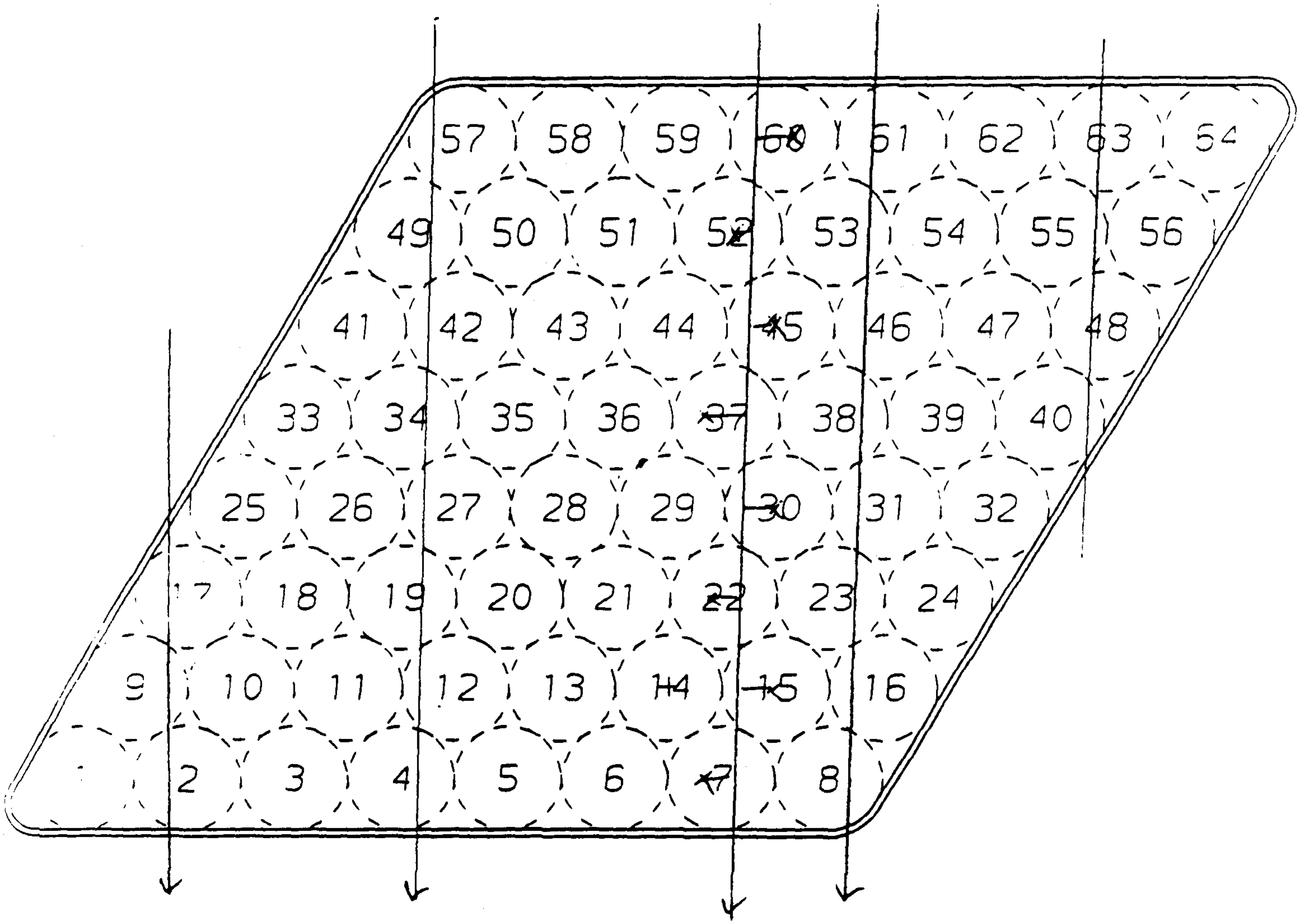

Fig. 2 Fitting wire displacements with vertical tracks

If we use an intrinsic wire resolution of 100 microns, wire placement error of 65 microns, module placement error of 50 microns, and module intrinsic error of 50 microns. then we get get micron total superlayer error of 83 microns. I take this to indicate that we can build and align a modular system that will give us the required momentum resolution.

Notice that unlike Abe, we conclude that the major part of the error in the superlayer measurement comes from alignment not intrinsic error in the straw.

October, 1990
IUHEE-90-16

DESIGN OF A TRACKING SYSTEM FOR A SOLENOIDAL DETECTOR*

Gail G. Hanson
Indiana University
Bloomington, Indiana 47405

Abstract

The design of an integrated tracking system for a solenoidal detector will be presented. The tracking system consists of a silicon pixel and microstrip detector at smaller radii from the beam collision point and wire chambers at larger radii. The tracking system provides momentum measurements and a fast trigger for all charged particles with p_T above a few GeV/c and for $|\eta| \leq 2.5$. Research and development issues will be discussed.

Introduction

The goals of a tracking system for the SSC are to provide momentum measurement and a fast trigger for charged particles with p_T above a few GeV/c and $|\eta| \leq 2.5$. In addition, the tracking system should provide a precise vertex measurement in order to identify long-lived tracks, for example, from *B* decays, and detect separated vertices from multiple *p-p* interactions. Since the tracking system is only a part of the complete detector, it must provide these functions in an economical manner. The tracking system must operate in the high-rate environment of the SSC at and above the design luminosity.

We are engaged in detailed design studies of an integrated tracking system[1] for a solenoidal detector for the SSC. The tracking system consists of a silicon pixel and microstrip detector[2] at small radii from the beam collision point and wire chambers at larger radii. The R&D includes wire chamber detector design for straw tubes and intermediate angle tracking detectors with wires transverse to the beam direction, engineering R&D including support structure and alignment, front end and triggering electronics, and computer simulation.

Tracking System Design

A conceptual design of the tracking system, contained inside a 2 Tesla solenoidal magnetic field, is shown in Fig. 1. The inner radius of the coil is located at a radius of 1.7 m, and the tracking volume half-length is 4.0 m. In order to aid the pattern recognition in the high-rate SSC environment, the entire tracking system design, except for the pixel detector, is based on the concept of track segments, rather than individual track hits. Track segments in the outer tracking system (radius > 50 cm) are used in the first level trigger. Track segments in the superlayers are linked to form tracks.

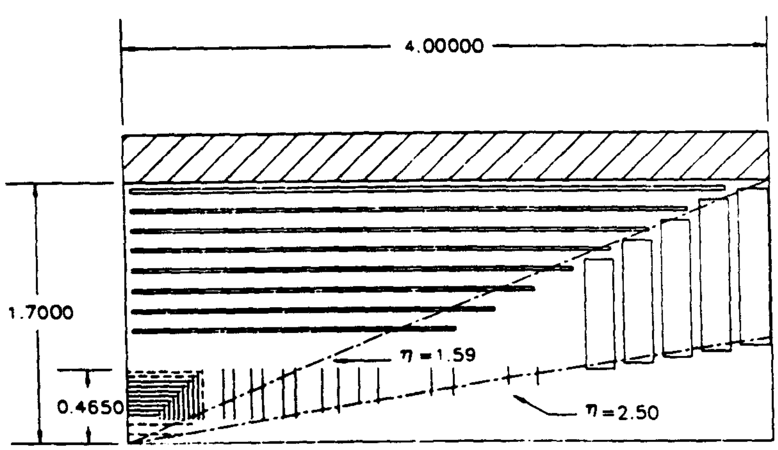

Fig. 1. Conceptual design for a silicon and wire chamber tracking system for a solenoidal detector.

The silicon tracking detector, inside 50 cm radius, consists of an array of high-resolution two-dimensional pixel detectors and segmented microstrip detectors; these provide vertex measurement and pattern recognition capability even in the cores of dense jets.[3] Some of the microstrip layers are double-sided silicon with axial strips on one side and stereo on the other. Track segments are found in superlayers consisting of two layers of silicon.

Wire chambers are used for tracking between 70 and about 163 cm radius. The central tracking system, covering the region $|\eta| \leq 1.5$, consists of superlayers of 4 mm diameter straw tubes[4], as shown in Fig. 2. In order to reduce radiation damage and current draw, the straws are made as small as practical and run at low gas gain, $\sim 2 \times 10^4$. Occupancy is reduced by the small straw diameter and the use of a fast gas, such as mixtures containing CF_4.[4,5] The half-cell stagger between layers permits resolution of left-right and crossing-time ambiguities. The coordinate along the wire is measured by means of small-angle (~3°) stereo. With a spatial resolution of 100-150 μm per wire in the r-ϕ projection, the expected resolution in z is 2-3 mm. The superlayers alternate axial and stereo. Local track segments are found in each superlayer.

The intermediate angle tracking system[6] covers the region of radius > 50 cm and $|\eta| > 1.5$. It is composed of drift chambers with wires transverse to the beam direction and "crossing taggers," as shown in Fig. 3. A crossing tagger is set of planes of gaseous proportional detector with cathode strip readout. Crossing taggers are used to associate a wire chamber hit to within 3 or 4 bunch crossings and could be used for the trigger. The wire chambers are presently envisaged to be radial wire chambers.

The performance of the tracking system is shown in Fig. 4.

Engineering R&D

The tracking system will be supported and aligned using a structure of graphite fiber composites.[7] There are inner and outer support cylinders for structural stability. The superlayers in the central tracking system are made up of modules of straws with an outer graphite composite shell to provide rigidity and positioning. The replaceable modules are positioned and supported by an open framework. The intermediate angle and silicon tracking systems are supported by the same structure.

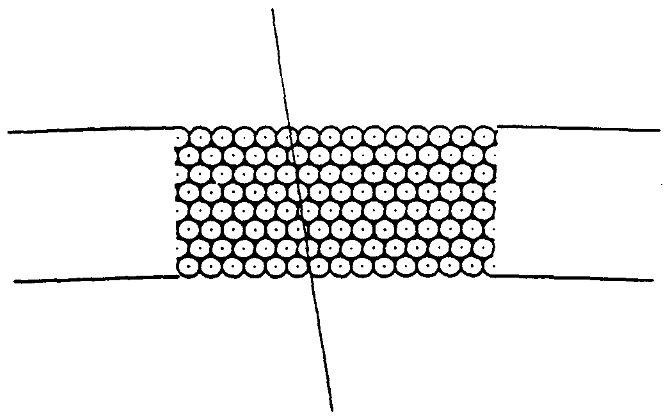

Fig. 2. Cross sectional view of a superlayer of straw tubes.

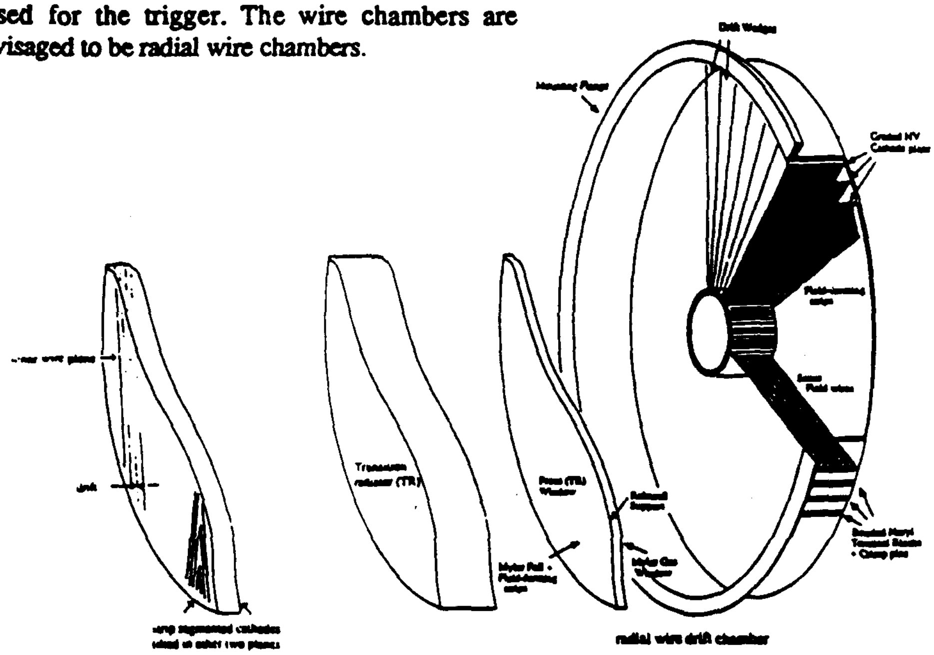

Fig. 3. Intermediate angle tracking supermodule layout.

Front End and Triggering Electronics

Custom integrated circuits for the front end and triggering electronics are being developed both as part of this subsystem effort and as part of separate electronics subsystem R&D projects. A low-power radiation-hard integrated preamp, shaper, discriminator and time-to-voltage converter are being developed as part of an R&D program centered at the University of Pennsylvania.[8] Similar developments are taking place in Japan. Circuits for triggering on track segments in superlayers using drift time (synchronizers) are being developed at the University of Michigan.

R&D Issues

The R&D issues involved in the design of the tracking system are being addressed by design and prototyping, as well as computer calculations and simulations. Some of these R&D issues are summarized below.

In the design of the tracking system, we must minimize material (primarily because of the problem of photon conversions) and cost. Materials issues include sufficient rigidity and structural support in the module walls and support structure, and connections to the wires at the endplates, including terminations, wire-holding devices, interface boards, electronics, and cabling. Finite element analyses are carried out to optimize the designs of the module walls and the support structure. Design and prototyping are being carried out to minimize material at the wire connections.

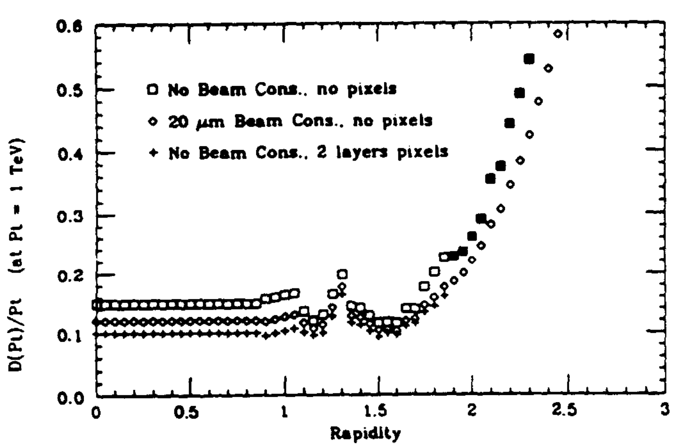

Fig. 4. Momentum resolution in a 2 Tesla magnetic field as a function of $|\eta|$ for the tracking system.

Wire chamber design and prototyping are being carried out for both the straws and the radial wire chambers. These studies include minimizing the resistance of the straws and determining the optimum technique for supplying graded high voltage to the cathodes for the radial wire chambers. Tests of suitable fast gases are being carried out. In addition, there are many construction and assembly problems to be solved.

We are building prototypes for all of the components of the design: straw modules, radial wire chamber sectors, connections, electronics, and support structure. These will be tested in a beam when possible.

Many crucial design issues are being addressed by computer simulation of the response of the detector to SSC background and physics events. With 16 ns between bunch crossings and 1.6 interactions per bunch crossing at the SSC design luminosity, high occupancy and its result, lost hits, are a major issue for wire chambers. We are using simulations to determine the best configuration for triggering on track segments in the outer superlayers of the central tracking and in the crossing taggers of the intermediate angle tracking. We need to continue to trigger on track segments as the luminosity increases beyond the design value, and we must do this with a sufficiently robust trigger using a minimum number of channels and at a minimum outer radius for the tracking system. We are also carrying out studies of pattern recognition for finding tracks.[9]

*Work supported by the Department of Energy, contract DE-AC02-84ER40125.

Presented at the Symposium on Detector Research and Development for the Superconducting Super Collider, Fort Worth, Texas, October 15 - 18, 1990.

REFERENCES

1. "SSC Detector Subsystem Summary Report and Proposal for FY 1991," Central and Forward Tracking Collaboration, G. Hanson, contact person.
2. "Subsystem R&D Proposal to Develop a Silicon Tracking System," A. Seiden, contact person.
3. A. Seiden, "Silicon Tracking," in these Proceedings.
4. H. Ogren, "Wire Chamber Tracking," in these Proceedings.
5. J.A. Kadyk *et al.*, in these Proceedings.
6. J.B. Dainton *et al.*, in these Proceedings; D.H. Saxon *et al.*, in these Proceedings.
7. R. Swensrud, in these Proceedings.
8. L. Callewaert *et al.*, in these Proceedings.
9. W.T. Ford, "Pattern Recognition in Tracking Systems with Small Drift Cell Arrays," in these Proceedings.

REPORT of the REVIEW COMMITTEE on STRAW TUBE PLACEMENT in the SDC
June 1991

INTRODUCTION

The SDC Technical Coordinator had charged the Committee to review the technical options of straw tube placement in the SDC tracking system. Appendix A lists the members of the committee. The committee submitted to the proponents of the SDC straw tracking system a list of criteria by which to decide on a preferred technical solution (Appendix B). A report describing the options and proposed mile stones and R&D plans was assembled by the proponents of the straw tube tracking system and a draft was submitted to the committee on May 16, 1991. The final report (Appendix E) was distributed to the committee on May 28–29 1991. In the report the proponents do not select a preferred solution but describe the alternatives and propose a date of October 1991 for a decision between two basically different approaches to the straw tube placement onto the support structure.

The Committee met on May 29, 1991 at the SSC Lab and listened to presentations of physicists and engineers as outlined in the agenda appended as Appendix C. After discussions with the proponents present (Appendix D), the committee decided to forward the following recommendations.

EXECUTIVE SUMMARY

Aside from small variants, the proponents proposed basically two alternative designs for the straw tube placement onto the support structure:

a) "single straw" approach where single straw tubes are assembled and placed one by one on the support structure,

b) "modular" approach where about 200 straws are placed in rigid shells forming modules which are then placed onto the support structure.

It is important to note that there are many R&D issues common to the two solutions. One of them is the support structure design which is envisioned to be a stable base composite cylinder.

The Committee determined that several tasks must be completed to allow a choice to be made based on sound engineering results. It seems unlikely that the envisioned milestones can be met before January, 1992. These milestones are:

a) for the single straw concept: an 8m straw must be constructed and tested with sense wires and mid terminations in place. A straw placement device of appropriate length (~3m) has to be constructed for proof of principle to demonstrate quick and efficient glueing with low mass.

b) for the module design: it is necessary to demonstrate that a 4m shell can be fabricated with the required 50 micron straightness after loading with straws. Time and funds must be made available for possibly two attempts.

For both concepts, the consequences of the differential expansion and swelling of the tubes relative to their constraints (cylinders or shells) have to be evaluated.

The above tasks should carry the highest priority even to the extent of displacing present planned FY91 activities. Should additional funding be required to complete the above specific tasks, a request should be made immediately.

If a 4m shell can be constructed with the required tolerances, it is further recommended that this configuration be selected as the central tracker straw baseline design. Within the time and funding available, the single straw activities should continue until the module design proves workable. If the module design proves unworkable within a finite amount of time (e.g., 6 months) then the single straw configuration should be adopted.

We do not recommend construction of a full-size stable base support cylinder at this time. Instead we recommend that a vigorous program in Finite Element Analysis (FEA) should be undertaken to assess the effects of stresses, temperature and humidity on the complete structure of straw tubes/modules, supports and cylinders. Special attention should be given to the end flanges and the supports.

The committee is concerned about the very sketchy costing.

DISCUSSION OF CONCEPTS

Physics

The performance of the two configurations appear to be nearly equal. The gaps required by the modules both at $z = 0$ and between modules would introduce small inefficiencies in track reconstruction and triggering. Single straws might require larger spacing between the straws. It is expected that the support cylinders are basically the same for all designs with the expected loads about equal. The module design will add about 0.24% of a radiation length per superlayer due to the 10mil shells, about the same amount again than either the straws or the cylinders. In addition there will be end plates for gas containment and for distribution of the wire tension both at $\pm z$ max and at $z = 0$. The added material appears to be a disadvantage of the modular concept. Single straws will need thicker, but yet unspecified end flanges. Stereo straws are possible using any of the discussed configurations, but their support seems to be more matured in the modular concept.

Straws

Several types of straws were discussed. The outside diameter selected is 4 mm. A 3m straw made of two 0.5 mil Kapton tapes wound over a mandrel was shown. Aluminum had been deposited on the inner surface. Since some reports indicate that aluminum may have an ageing problem, copper is being considered as a replacement cathode material and its increase in the radiation length budget has to be considered. Although the details of wire connections at the ends were different for the two designs, it was agreed that the basic straw will be the same for all concepts. All straw designs use internal supports to accurately locate the wires. The preferred design seems to be a short rod with a helix cutout that allows the sense wire to be blown through and still provide accurate placement. A tube vendor to provide the large number required has not been found, but this is not seen as a problem. The groups are also developing a unique wire resistive/capacitive termination rod.

Wire tension and connections

The tension in the sense wires is held ultimately by a support cylinder end ring in the single straw design and by the module shell in the module concept. Deflection and buckling calculations indicate that no problems are expected for either case.

Several means of connecting the sense wire electrically and mechanically were presented. The final design should be able to incorporate the best features of each of the suggested connections.

Single straw design

A truly single straw design and a bundled design were presented. We did not consider the bundled concept separately but judged that as a modular design it was inferior to the "modular" concept. The major advantage of the single straw concept is the reduction of the material inventory in the tracker. One of the major disadvantages of this design is that most of the assembly steps must be scheduled in series as the support cylinder is also the local support for the straws. Only after completion and shipping of the cylinders to the assembly location can the final assembly of the straws begin. If several locations are used for assembly, they all must have the capability to handle the very large cylinders and high precision tooling has to be replicated. Another possible disadvantage is that the straws will follow distortions of the support cylinder and this may not be stable enough over the long term. There will be a different coefficient of expansion between the straws and the cylinder. A method of straw attachment must be developed that solves this possible problem. Possible distortions of the cylinder due to the load of the wire tension have to be evaluated. After assembly of the straws and the support cylinder, the ability to repair and maintain individual or groups of straws appears very difficult.

The straws are pretested and then individually placed upon the support cylinder. A special machine is being designed that will accurately place the straws. The final location of the wires is then determined after attachment to the cylinder. The sense wire tension is carried by a flange attached to the end of the cylinders. No problems are anticipated with the proposed method of obtaining the required tension and the application of those loads onto this flange. Tests using a flat table have shown that the straws can be placed within the required tolerances. It is anticipated that the straw placement machine will be stationary and the cylinders will be rotated and accurately indexed so that there is no accumulation of errors as each layer is placed.

The design calls for 8m wires to be used with a mid-tube termination. The present design of this item allows gas to pass through it. Prototypes of 2.7m have been made and look promising. One area of concern is the gas tightness of individual tube assemblies.

Module design

The design using modules was thought to allow the greatest flexibility of the concepts discussed. Tests have indicated that, using x-rays, the location of each wire can be determined after module assembly. This method could be automated and its accuracy improved by existing centroid-finding measuring machines. Construction of the various parts can be accomplished in parallel. Each module can be completely characterized both mechanically and electrically prior to attaching to the support cylinder. For use in the trigger, overlapping modules have to be interconnected. The number of modules used is small enough to allow manual placement using external fiducials and fairly simple equipment such as microscopes and manipulators, if necessary. About 1000 modules are required and with a rate of about 10/day placed, only about 100 days for assembly would be required. If necessary, module assembly could be carried out at several facilities.

The modules/cylinder attachment design may allow for tie down only on one end and some form of slip joint at the other. This minimizes the effect of cylinder movement due to possible creep or thermal gradients.

The possible ability to remove and replace a module from the support cylinder after SDC installation was viewed as a very desirable feature of this design. Spare modules can be characterized and held as spares during the total assembly process and after installation in Texas. If modules are to be replaceable, a method of accurate indexing on the cylinders must be developed. The present suggested method of glueing the modules to the cylinders does not appear practical.

The accuracy of module placement on the cylinder is a strong function of the straightness of the 4m shell. It also depends upon the ability of the shell to hold the internal wire positioners in place. For these reasons, a 4m shell must be fabricated in the near future, prior to a choice of design.

Costs

The cost estimate available for the module design was that of the LOI. If costs should enter into the decision, a more reliable base for the costing should be attempted. Taking the LOI numbers at face value, it seems that nearly all the costs for the two designs were the same except an additional cost for module shells. This was estimated to be about $2.2M. This increment is well within the cost uncertainty of different tooling, etc., required for both concepts and thus the selection of a concept has been made for other reasons.

Areas of concern

There was much discussion of the effects of non-round support cylinders and the method of attachment of the tracker to the calorimeter. It was assumed that the cylinders will have a CTE of zero, but the movement of the calorimeter support points was not known. This possible difference of movement may cause stresses in the cylinder that affect their locations after turn on. Some form of kinematic mount may be required.

The concept of a very thin support cylinder held round by stiff end caps should be pursued only if the planned "thick" cylinder is shown to have severe problems. Although such a thin design is possibly feasible with some R&D, it is a much more riskier concept. The thin skin would be vulnerable to radial point loading which could be encountered during shipment and/or assembly. The "thick" design is much more robust and is the preferred concept. Also, the "precision" cylinder is not seen to be an advantage over the "imprecise" design and is seen as much riskier.

We consider it essential that modules be replaceable in situ without removal of the entire tracking system. Careful attention to the layout of the ends, including cabling, gas lines and power feeds, should preserve this option. The overall detector design should accommodate such a replacement in about one weeks time.

The schedules for fabrication of the tracker did not include the necessary approval periods prior to the purchase of items in excess of $100K. The schedules need to be modified to include time for DOE approval (6 weeks), advertising the bid in the Congressional Register (4 weeks), bidding (6 weeks) and final approval of contracts by the DOE (6 weeks). These processes could add 4 to 6 months to the schedule for the acquisition of large, expensive items (e.g., the cylindrical shells).

Design suggestion

As with any review panel, some real-time design will take place and this panel was no exception. The straw review panel suggests that two support cylinders may be adequate instead of the four presently planned. This reduces the material inventory and costs. The deflection of the present cylinders under the expected loads are very small and with little increase in size, if any, one cylinder should be able to carry two layers of straws. The maximum radius difference is about 14 cm, therefore, intermediate support rings will be fairly short and contribute little material.

Additional R&D

Committee members with experience in building large tracking devices pointed out the following areas which need attention soon:

A. Mechanical testing of all materials and assemblies

B. Radiation testing of all materials and assemblies

C. Quality control of all materials and processes

D. Assembly and test procedures (or how they will be determined)

E. Costing that is determined by the actual procedures proposed

F. Some indication that this is being treated as a manufacturing problem (100k straws) and not a lab project

APPENDIX A

MEMBERS of the
MEMBERS of the SDC COMMITTEE on STRAW PLACEMENT

Morris Binkley (FNAL)	BINKLEY@FNAL	(708) 840 3112
Richard Boyce (SLAC)	RFB@SLACVM	(415) 926 2932
Richard Kadel (LBL)	KADEL@LBL	(415) 486 7360
Hartmut Sadrozinski (UCSC)	HFWS2@SLACVM	(408) 459 4670 (Chair)
Roger Stone (LBL)	RSTONE@LBL	(415) 486 7360

APPENDIX B

CRITERIA to DECIDE between
DIFFERENT STRAW PLACEMENT SOLUTIONS

1) Structural integrity
2) Ease of assembly, alignment and servicing
3) Amount of material (expressed in radiation length)
4) Cost
5) Ease of manufacturing
6) Compatibility with stereo layers
7) Ease of interfacing with electronics (grounds) and cooling

APPENDIX C

AGENDA for the SDC STRAW REVIEW
MAY 29, 1991, SSC Lab

8:30	Executive Session
9:00	Discussion of Scope and Ground Rules of Review
9:10	Presentation by Physicists & Engineers
	Al Goshaw (Duke): Introduction
9:20	Straw Modules
	Harold Ogren (Indiana U.)
	Roger Swensrud (WSTC)
	John Mayhall (ORNL)
11:00	Single Straws
	Seog Oh (DUKE U.)
	David Vandergriff (ORNL)
13:00	Working Lunch with Speakers
13:50	Executive Session
14:15	Al Goshaw (Duke): R&D Plan
14:30	Recall Engineers and Physicists for Open Floor Questions
	(Oh, Ogren, Goshaw)
15:30	Executive Session - Write Report
17:00	Adjourn

APPENDIX D

STRAW TUBE PROPONENTS ATTENDING the REVIEW MEETING

Institution	Person	Technical Background
Colorado	Bill Ford	physicist
Duke	Al Goshaw	physicist
	Seog Oh	physicist
	Joe Simpkins	mechanical engineer
Indiana	Gail Hanson	physicist
	Harold Ogren	physicist
	David Rust	physicist
	Randy Foster	programmer/designer
ORNL	Tony Gabriel	physicist
	John Mayhall	mechanical engineer
	Ted Ryan	mechanical engineer
	John Shaffer	mechanical engineer
	David Vandergriff	mechanical engineer
WSTC	Roger Swensrud	mechanical engineer

STRAW TUBE SUPERLAYER DESIGN CONCEPTS

Prepared for SDC Tracker Review

May 20, 1991

University of Colorado, Duke University, Indiana University,

Oak Ridge National Laboratory and Westinghouse Science and Technology Center

ABSTRACT

The purpose of this report is to review the procedures which have been proposed for the construction of straw tube superlayers and to evaluate them against various physics, mechanical and cost requirements. In the process of this evaluation, critical R&D issues have been identified which need to be resolved before a final decision on superlayer construction is made. A plan to reach this decision in a timely manner is proposed. The plan makes maximum use of ongoing FY 1991 R&D and focuses the effort for FY 1992 on the construction of a full-scale multi-superlayer or single superlayer prototype.

OUTLINE

1. INTRODUCTION

1.1. Physics Requirements for Outer Central Tracking

The tracking system plays a major role in exploratory physics, lepton and heavy quark identification, mass reconstruction, and in the formation of the trigger. We put emphasis on reliable pattern recognition capability, and in conjunction with the silicon inner tracking and the outer intermediate angle tracking, precise momentum and vertex resolution over pseudorapidity $|\eta| < 2.5$. At 1 TeV/c transverse momentum (p_T), the design goal for momentum resolution is $\sigma(p_T)/p_T < 25\%$ for $|\eta| < 1.5$. In order to achieve the design goal for momentum resolution, the spatial resolution must be < 150 μm per wire. The intrinsic straw chamber resolution is ~ 100 μm. Added to this are the errors due to alignment and electronics resolution on the drift time measurement. The alignment requirements are the following [A.Seiden, "Systematic Errors and Alignment", unnumbered memo, H. O. Ogren, "Straw and Module Placement", IUHEE 91-4 (1991)]:

$\Delta\phi < 35 - 50$ μm

$\Delta r < 1$ mm

$\Delta z < 0.5$ mm.

The pattern recognition requirement is the reconstruction with high efficiency of all relatively high p_T (> 1 GeV/c) charged particle tracks for $|\eta| < 1.6$. The outer central tracking system must provide level 1 or 2 trigger information for tracks with $p_T >$ about 10 GeV/c. The amount of material in the tracking system must be minimised, since it will have several negative effects on the physics performance of the detector. Photons will convert, producing an increased trigger rate for high p_T electrons and interfering with identification of electrons from decays of interest. The extra charged particles will increase the tracking system occupancy, making pattern recognition more difficult. Charged particles will lose energy in the material, degrading the momentum measurement performance. However, there is significant material in front of the outer tracking system, about 8% of a radiation length at 90° incidence, due to the beam pipe and silicon tracking system.

1.2. Engineering Baseline Design

The engineering baseline design for the outer tracking system has been defined to provide a basis for mechanical engineering. This baseline has not been optimised for either engineering or physics concerns, but rather represents a "zeroth" order layout used to define the engineering concepts needed for a complete outer tracker design regardless of which tracking technology is finally chosen. The baseline design is shown in Fig. 1.1, and the numerical data is given in Table 1.1 for the four outer superlayers, which are composed of straw tubes.

Table 1.1. Straw Section of Engineering Baseline Design.

Superlayer	Radius (m)	Number of Straws/Layer	Number of Layers/Superlayer	z_{min} (m)	z_{max} (m)	Stereo Angle (°)
3	1.21722	1912	6	0.03	3.550	-3
4	1.34963	2120	6	0.03	3.900	0
5	1.48205	2328	6	0.03	3.950	+3
6	1.61447	2536	9	0.03	3.950	0

Total number of straws (both ends): 121,968.

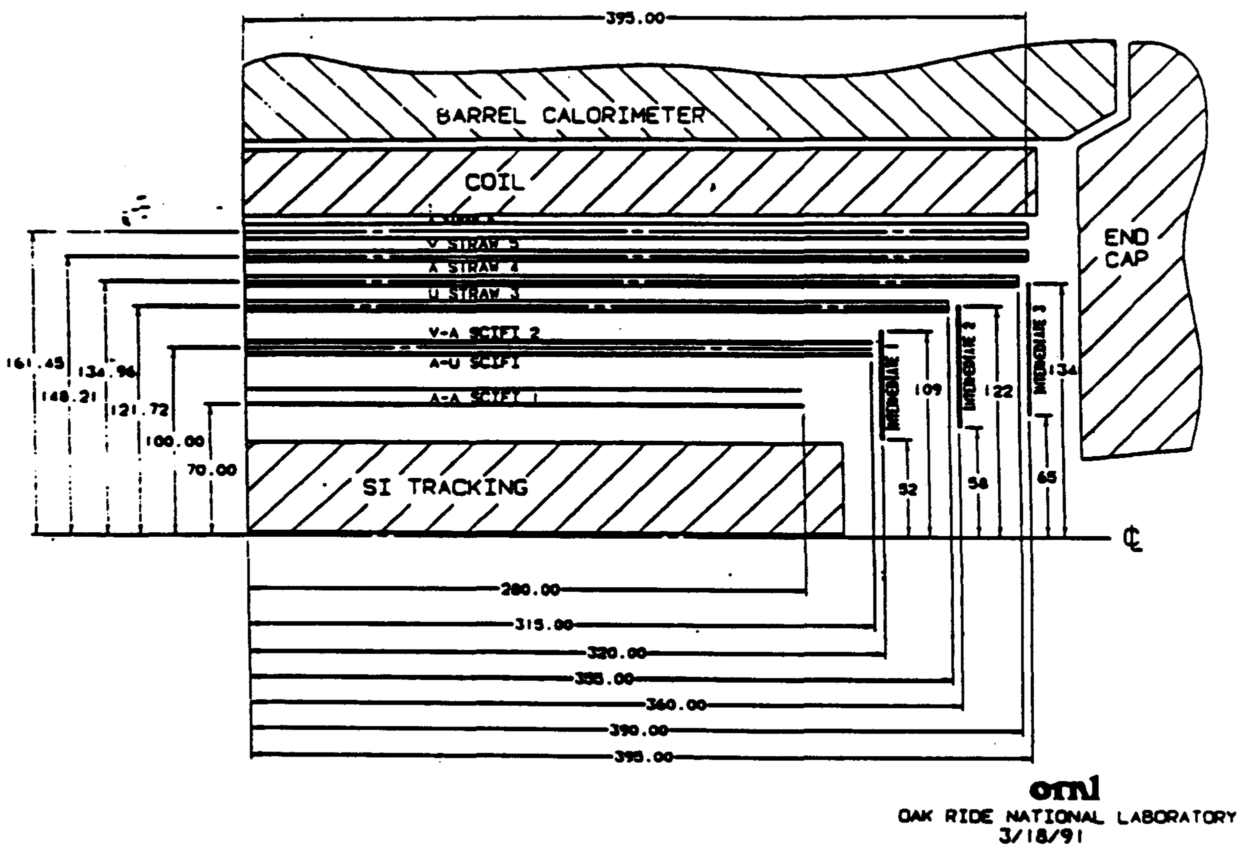

Fig. 1.1. A section through one quadrant of the tracking system of the baseline design

2. GENERAL DESCRIPTION OF STRAW TUBE SUPERLAYERS

2.1. Support Structure

The support structure for a straw tube superlayer will be a cylinder composed of a carbon-fiber epoxy material. The cylinder will span the full length of the superlayer (6 to 8 meters) and provide the primary precision support for the straw tubes, either directly or by means of thin rings attached to the cylinders. The cylinders will be supported only by means of end rings bonded to their ends. Calculations carried out at ORNL show that cylinders as thin as 0.3% X_0 can support the gravitational and wire tension loads of a straw tube superlayer.

2.2. Generic Superlayer Structure

All of the straw placement schemes discussed in this report involve the placement of straws in superlayers of six, eight, or nine (for the trigger superlayer) straws. Within each superlayer, the layers are staggered by the straw radius in order to resolve left-right ambiguities locally and allow hits from out-of-time bunch crossings to be rejected. Locally identifiable track segments can be obtained at the pattern recognition stage and for the trigger. Track segments in superlayers can be characterised as local straight line segments. Assuming that the track originates at the center of the tracking system, the slope of the line segment relative to the radial direction gives a measurement of the curvature, and therefore the transverse momentum, of the track. A tracking system design based on finding local track segments provides a powerful method for rejecting background from extra hits from any source (e.g., out-of-time bunch crossings, but this scheme was found to be useful in the Mark II central drift chamber at the SLC where the source of extra hits was synchrotron radiation). Local track segment finding also simplifies the pattern recognition, although sufficient redundancy within a superlayer and in the number of superlayers must be maintained to keep the efficiency high. The central tracking systems of many detectors have been designed to make use of local track segments – JADE, Mark III, Mark II (SLC upgrade), CDF, OPAL. A superlayer structure also simplifies the mechanical support. Single long straws are not self-supporting. However, several layers of straws held together in superlayers (probably at least six are needed) can form a rigid, mechanically stable structure. The mechanical support problem is then reduced to supporting the superlayers and aligning them spatially. There is also the possibility of supporting the wire tension within a subdivision of a superlayer. In the SDC detector, all of the elements of the tracking system – inner silicon system, outer central tracking, and probably also the outer intermediate angle tracking – are organised into superlayers, with each superlayer measuring the space coordinate and the local slope of the track segments. Track segments in each part of the tracking system will be linked to find tracks in the complete tracking system.

3. OPTIONS FOR THE CONSTRUCTION OF STRAW TUBE SUPERLAYERS

This section describes in some detail two proposed procedures for the construction of straw tube superlayers. Section 3.1 discusses a design based on the construction of straw tube modules which are self contained units providing support for wire tension, gas flow and electronics. Section 3.2 discusses an approach in which individual straw tube drift cells are pre-assembled and then transferred directly into superlayers on the support cylinders. This section describes the fabrication procedures, and Section 4 evaluates them based upon various physics and engineering criteria.

The basic 4 mm diameter straw tube is common to all superlayer construction methods. A brief description of this drift cell is given below.

The basic drift cell is constructed with a plastic based cylindrical cathode structure and a 25 μm diameter wire along the axis. Most of the straws that have been built are formed from an outer mylar wrap 12 μm thick and a 15 μm aluminised polycarbonate film inner layer. We have been using straws manufactured by Precision Paper Tubes, Wheeling, Illinois, and Stone Industrial, College Park, Maryland. The tubes are 4 mm in diameter with a 37 μm wall thickness. The standard aluminised coating is typically 1000 Å thick. The tubes have a DC resistance of 80 ohms/meter, the 25 μm wire has a 100 ohm/m resistance, and the characteristic impedance of the transmission line is 350 ohms. The weight of a straw is 0.5 grams/meter. Straws have also been made with an aluminised Kapton inner layer. These have the advantage that a thicker aluminum coating is possible (2000 Å). The resistance is about 24 ohms/meter, and the signal attenuation length is increased to about 7 meters. The straws are formed by winding a continuous 1 centimeter wide strip of aluminised plastic on a mandrel and then gluing the overlapping edges. This results in a rather uniform overall straw, but tension variations and gluing variations result in a diameter variation of about $\pm$ 25 μm and a deviation from circularity of about $\pm$ 50 μm. These variations can be important considerations when assembling a multistraw structure. The tubes are not naturally straight, with average bowing of 200 to 500 μm for a 50 cm length and 2-4 cm bowing at the 3-4 meter length. They also have very weak bowing resistance and will not support the wire tensional loads, even if glued in larger arrays. All methods proposed for using the straws for drift chambers must confront these properties of the straws. That is, the straws must be held straight in some manner, must be formed into regular arrays by some means, and the wire tension load must be transferred to some external support structure. Two options for accomplishing this are described below.

3.1. Straw Tube Modules (Units Providing Support for Wire Tension and Electronics)

3.1.1. Basic Module

The basic module design is shown in Fig. 3.1. Three important areas for development are the carbon composite shell, the endplate, and the attachment of the module to the superstructure. The outer shell holds the straws in position and maintains the alignment along the length of the module. Since the straws have an internal wire support every 80 cm, they probably will be be forced into a rigid close packed array at this point and bonded before insertion into the shell. The unsupported 4 meter external shell does not have to be straight to 50 μm, since it is only between the 80 cm attachment points that it will be a free span. An independent alignment method will be used to attach the modules to the structure and provide the overall straightness. Also the trapesoidal cross section must be maintained between 80 cm support points by the shell. The endplate structure and the bonded straw positions maintain this shape at the support points.

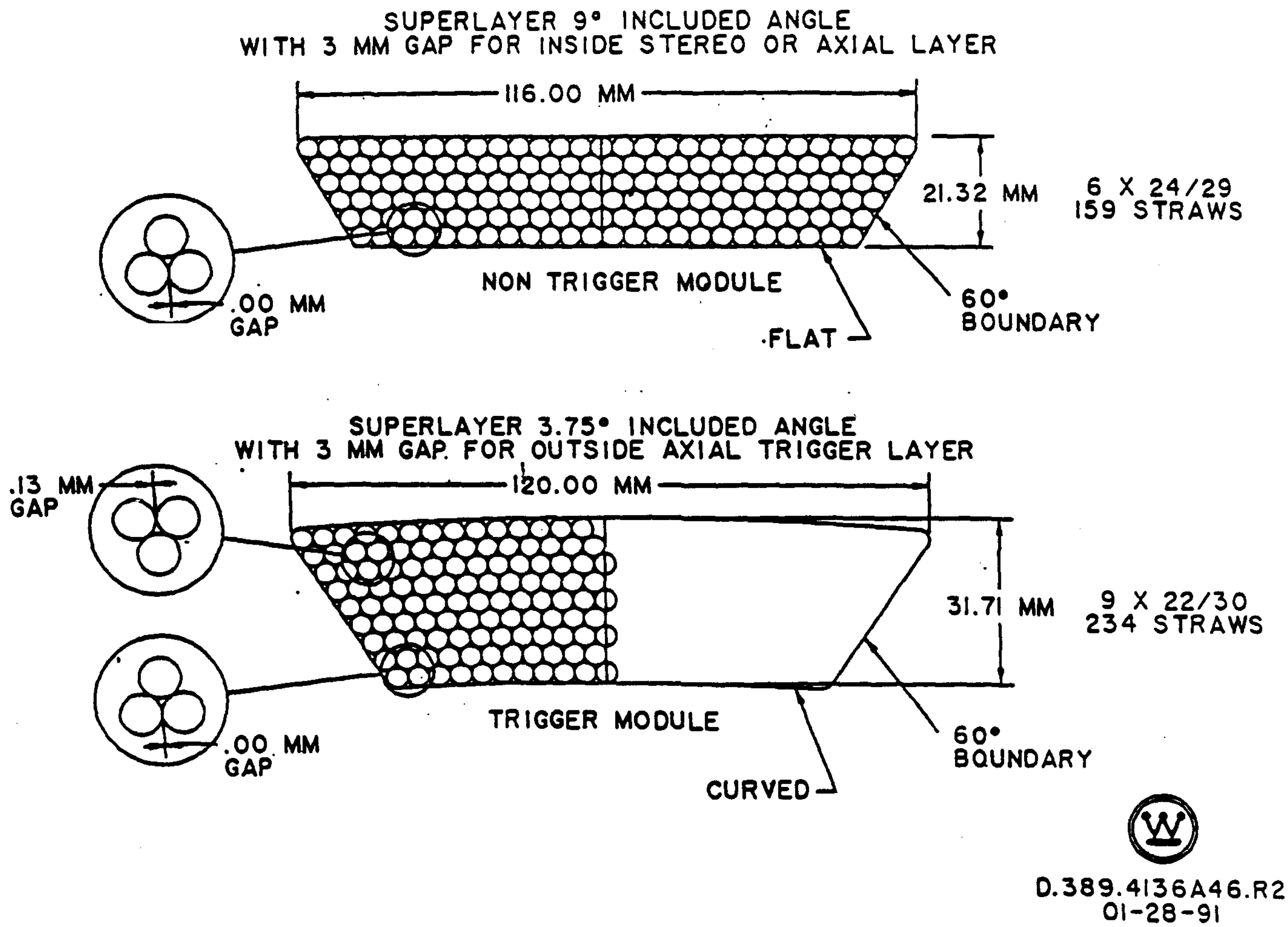

Fig. 3.1. Cross sections of two proposed module designs, one for layers 3,4 or 5, the other for layer 6.

Several carbon composite modules of 30 cm and 1 meter lengths have been constructed by Composite Horizons of Covina, California. The dimensions of these carbon shells are shown in Fig. 3.2. These were made with 4 layers of 2.5 mil prepreg carbon fiber tape (38 Million modulus). Measurements of these modules show that the intrinsic straightness over 80 to 100 centimeters can be held within the 50 μm accuracy limit.

Working with Composite Horizons, several tests of the expansion or contraction of the composite structure with respect to the room temperature mandrel (mold) size have been performed. By using the computer program, GENLAM, the final product size was accurately predicted. (See memo by R.Foster, May 6, 1991). In particular, it was confirmed that the expansion coefficient along the fiber direction is very slightly negative. This shows that we can produce a final shell to the required specifications.

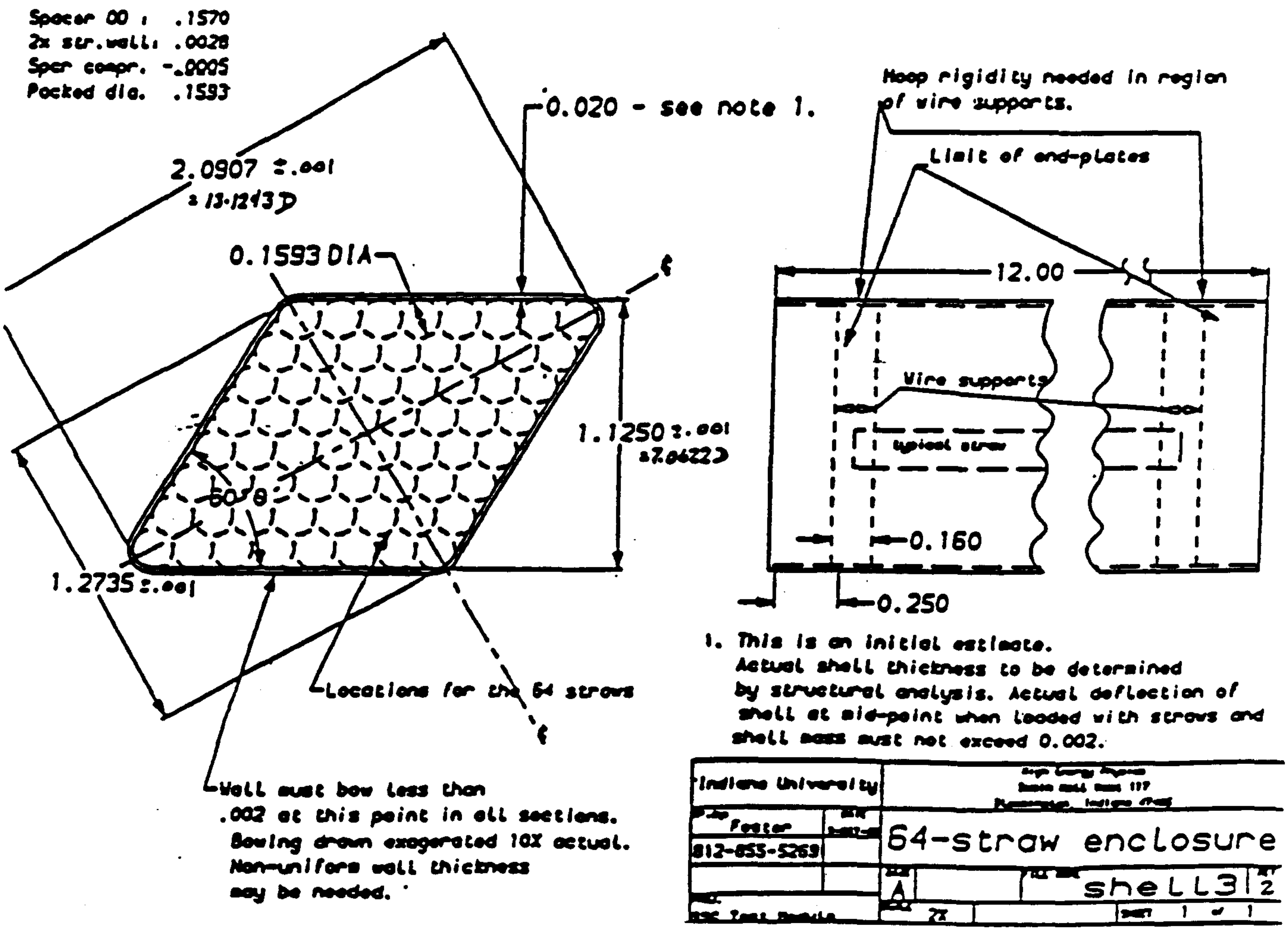

Fig. 3.2. Detail of the carbon shell for a 64 straw prototype.

The composite shell also takes the compressional load of the wire tension which is about 12 kg force for 240 straws. An analysis of the 240 straw module by Oak Ridge indicates that a 10 mil (250 μm) wall will support the tension. This is explained in a memo by J. Mayhall, Jan. 23, 1991. The molds for a 1 meter long module of this type are being fabricated, and it is expected that by June that shells will be available for loading with straws.

A total of four 30 cm long 64 straw modules have been built and tested using the 30 cm composite shells, and two additional modules of the same sise are being produced. Groups at Indiana, Colorado, University of Michigan, KEK, and Pennsylvania are using them to understand multistraw tracking systems. An assembly view of this module is shown in Fig. 3.3. We have measured the straw positions at the end of the short module and found them to be within the specified ± 2 mil tolerance, as discussed in the memo by H. Ogren, April 29, 1991.

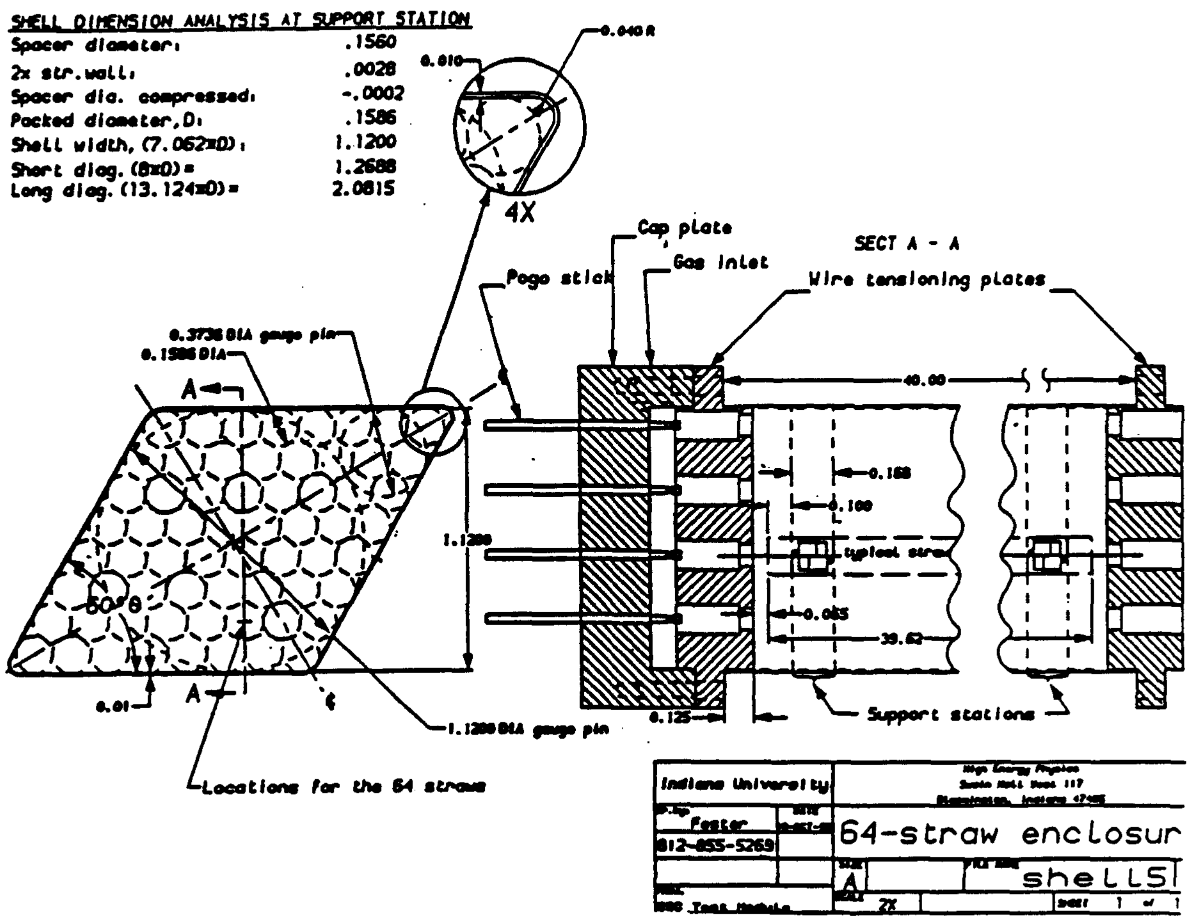

Fig. 3.3. Assembly drawing of the 64 straw prototype module.

A considerable amount of design and engineering work remain to be done on the 4 meter module. At the present time no fundamental difficulties with the concept are foreseen.

3.1.2. Endplate

Each module is capped with an endplate, as shown in Fig. 3.4. This endplate has multiple functions. It holds the signal wires and transfers the wire tension to the shell. It is also a gas manifold and provides an electrical connection to the preamplifier for each signal wire. Prior to attaching the endplate during assembly, the straws and the wire supports will be premounted in the shell. The electrical connection to the inside metalised cathode at the ends of the module will be made by dip coating the ends of the straws with conducting epoxy. (An alternative spring contact cathode connector is also being studied.) The endplate will then be inserted into the shell but will not touch the ends of the straws. The straws can then be threaded with the signal wires, which are attached and tensioned with a solder connection to a clip in the endplate. (A solderless method of wire connection is being developed.) The endplate also acts as one side of a gas manifold. The drift chamber gas enters each straw through the same hole that holds the solder clip. The other side of the gas manifold is a plate that contains signal feedthroughs, which extend through the gas manifold and make contact with the solder clips. The printed circuit board for the electronics is attached to the feedthrough plate. This construction results in a very short end section on each module and a very low mass connection. The goal is not to allow the material in the endplate to exceed a few percent of a radiation length. The gas seal for the module is the two-piece endplate. This results in a simple leak tight unit and eliminates the necessity of forming a gas seal for each straw. The module shell itself becomes the gas barrier.

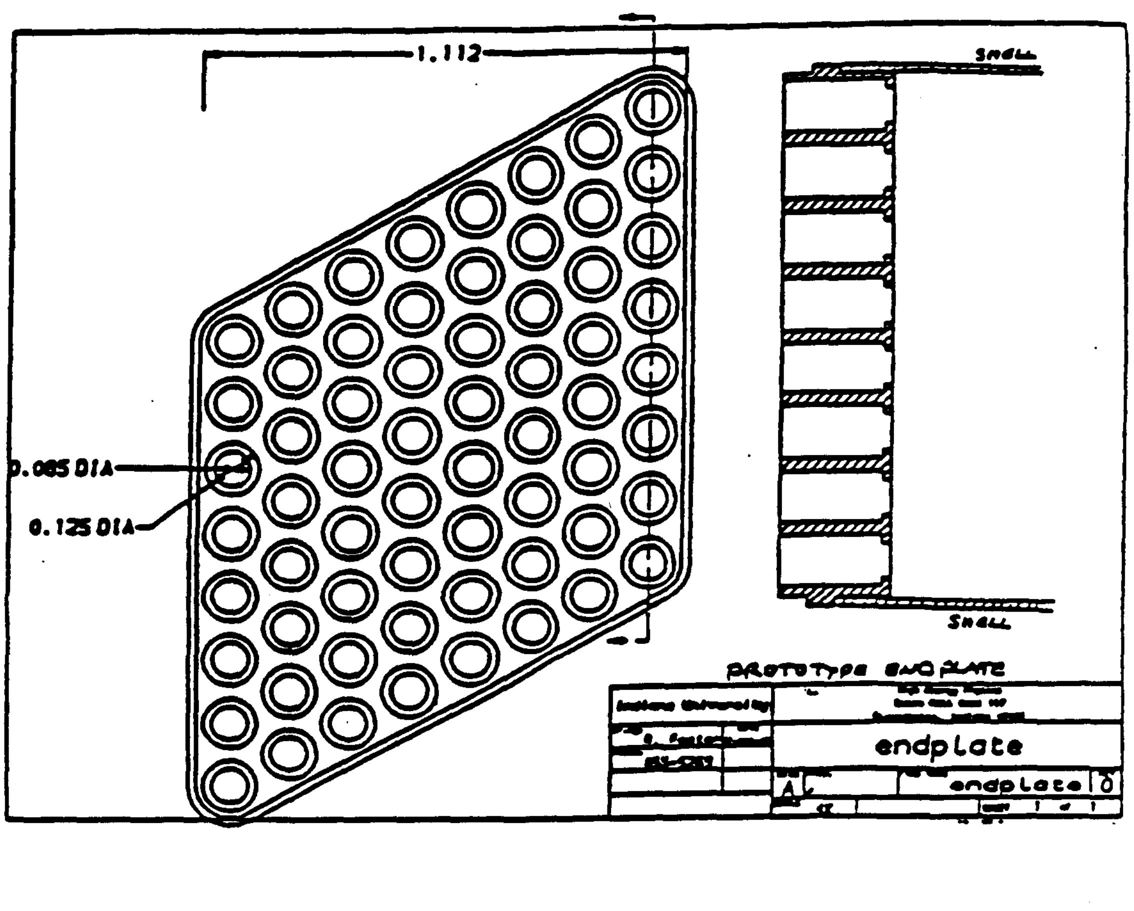

Fig. 3.4. Endplate design for the 64 straw prototype module.

A module together with the appropriate electronics becomes an independent operating drift chamber similar to a Sauli hexagonal chamber [R. Bouclier, *et al.*, Nucl. Instr. and Methods, A283, 509 (1989)]. It is anticipated that each module will be completely tested and measured before insertion into the tracking structure. This is an important step in the assembly. Each module can be mapped using X-rays to assure that placement tolerances are met with respect to the attachment fiducial points at each wire support position. The ultimate precision of the drift chamber is obtained by knowing the positions of the wires both at the ends of the modules and at the intermediate wire support points.

3.1.3. Module Attachment to the Support Structure

There are a number of methods that have been proposed for attaching the modules to the support structure.

a) Simple bonding to the support cylinder. This has the advantage of simplicity. It might require the construction of a module holder that maintains the module in alignment and rigidly positions it for bonding on the cylinder. There are a couple of disadvantages to this scheme. One is that it requires the cylinders and the modules to be assembled as a unit, so that each must be ready early in the construction sequence. There might be as many as eight such cylinders to construct, which would require careful coordination and might preclude construction of the modules at several sites. Another disadvantage is that it does not allow for easy repair if the module is damaged or needs replacement. It would require disassembling the entire structure to gain access to and replace the module. As an alternative in this scheme, the modules could be bonded to support rings spaced along the cylinder axis or directly to the cylinder. The gap between the cylinder and its required position could be filled with a thickness of bonding agent.

b) Bonding of support sleeves to the cylinder. The support sleeves are positioned on an alignment mandrel that positions them on the cylinder. The mandrel then is removed by slipping it axially out of the sleeves. The advantage of this method is that the final modules do not have to be bonded to the cylinder early in the assembly sequence. This is important both from scheduling considerations and for safety reasons, since it reduces the possibility of damage during construction. At a later stage in the assembly sequence, perhaps as late as the reassembly at SSCL, the tested modules could be installed, by sliding them in axially. At that time an alignment check would be made at several points on each module. This allows the option of bonding the modules in the sleeve at this point or designing an unlocking scheme that would allow the module to be removed at a later date. If the latter option were taken, it would be possible to replace a module quite easily during an extended shutdown, without disassembling the entire array of superlayers. There is one design under consideration that builds these sleeves as as integral part of the cylinder.

c) Attaching a module supporting device to the cylinder. This is more complicated than a sleeve. The module support device is bonded or mechanically attached to the cylinder using an alignment mandrel as in the case of the sleeve. It has the advantages of the sleeve design, but could be made so that the module could be installed by directly clipping it in radially, rather than sliding it along its entire length. This has the advantage that radial obstructions in the internal support structure do not prevent a module from being removed and would in principle allow the interchange of a module at any time.

3.1.4. Stereo Modules

The axial modules and the stereo modules will be 4 meters long (half the length of the full tracking cylinder support). This makes the construction of the modules less cumbersome and keeps the occupancy low. It also reduces the module end displacement during rotation about the module center.

The stereo modules are rotated approximately 3° about their centers. This corresponds to a tangential shift of the end of each module by about 10 cm (the module width is about 12 cm). The radial shift of the end of the module from the reference circle due to this translation is 0.34 cm. In order to reduce interference of the corners of the modules, alternate modules would be radially shifted by about 0.5 cm as shown in Fig. 3.5 and 3.6. The final configuration gives complete coverage for all tracks.

The attachment of the stereo modules to the support cylinder can be done in any of the three schemes listed above.

3.1.5. Advantages of Modules

The straw modules are independent tracking units that can be assembled in parallel and completely pretested before insertion into the superlayer. They can be calibrated and tested with the final electronics. The modules are also repairable and replaceable as units. The envelope construction also simplifies the gas containment, which has safety advantages. The final alignment of the modules on the superlayers also is easier and less time consuming, since there will typically be only about 100 modules to place around the circumference of one superlayer at each end.

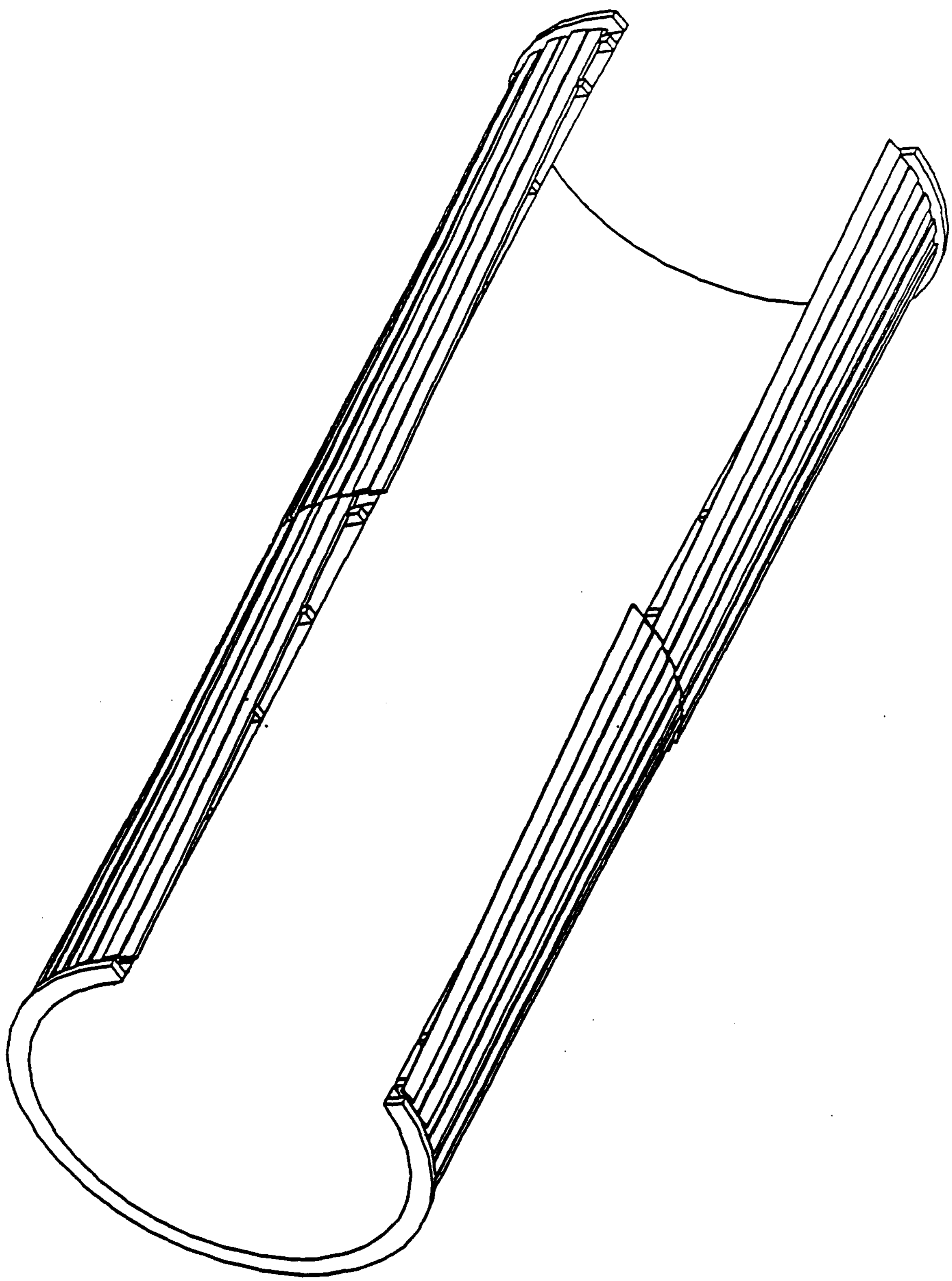

Fig. 3.5. A cut-away view of the stereo module superlayer.

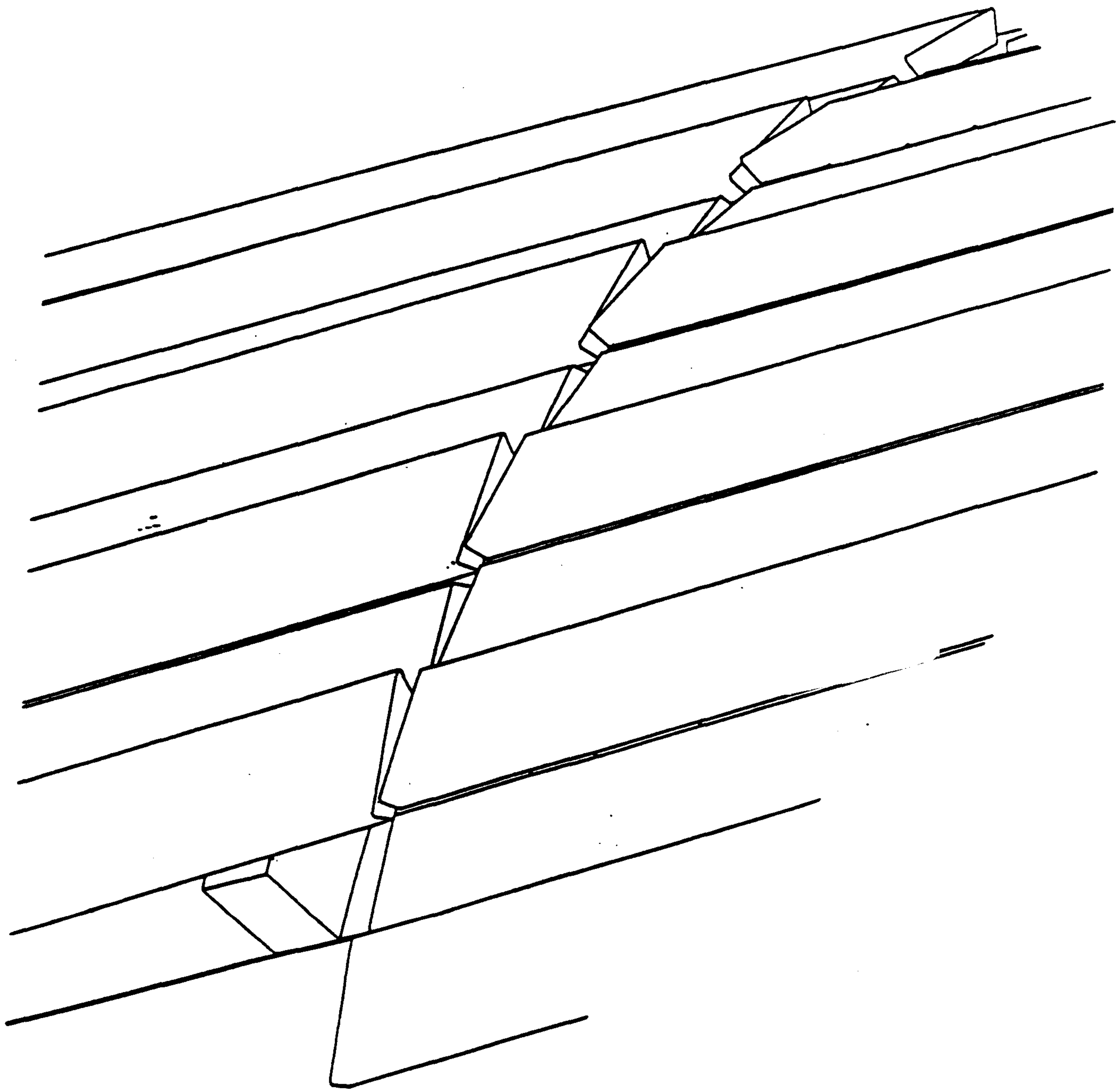

Fig. 3.6. A view at z=0 for the stereo superlayer showing the angles and radial displacements of the modules.

3.2. Straw Tube Bundles or Single Straws (Support for Wire Tension and Electronics Provided by Support Cylinder End Rings)

3.2.1. General Concept and Prototype Performance

The goal of the straw tube bundle/single straw approach is to design a straw tube superlayer using simple, low risk engineering principles. By constructing and operating a 2.7 meter long prototype over the past 12 months, a technique for superlayer fabrication based on bonding individual straws to a stable base surface has been developed. This fabrication procedure provides the required precision and is simple to implement. Figure 3.7 shows data recorded from this prototype using cosmic rays, the details of which are described in SDC Note 90-00119. The SDC barrel tracker can be fabricated using the concepts developed in the construction of the 2.7 meter prototype.

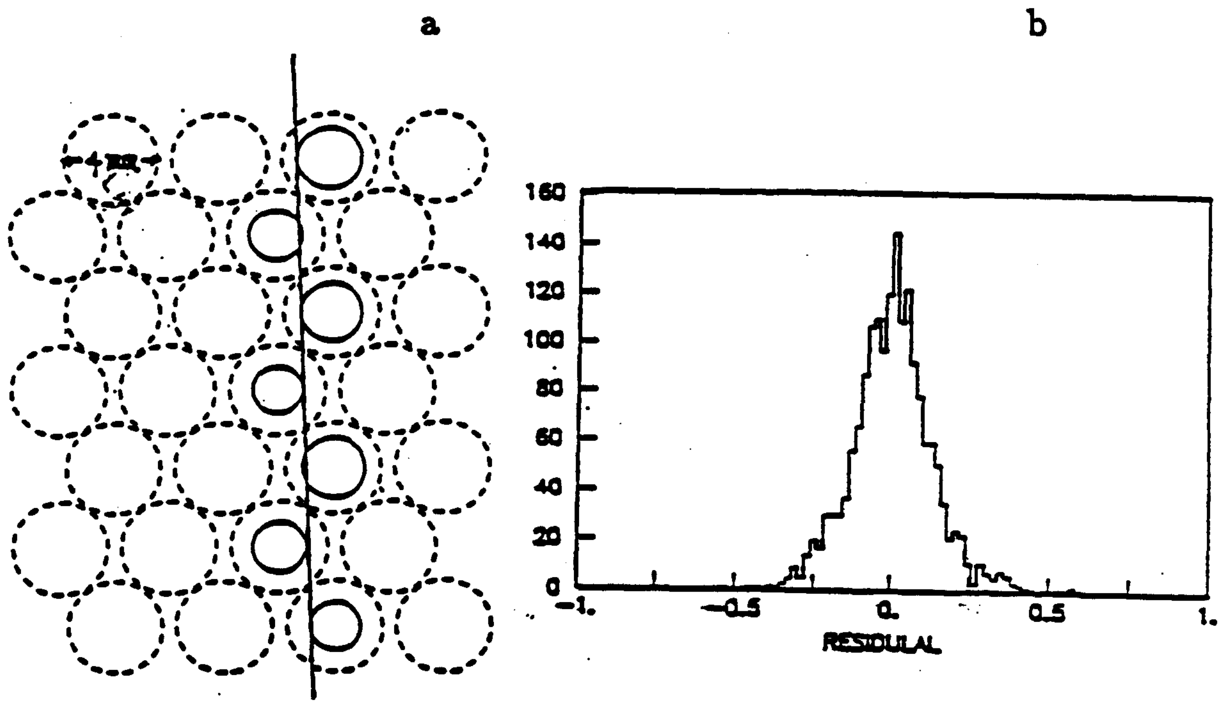

Fig. 3.7. Performance of a 2.7 m long superlayer constructed of individual straw tube drift cells. a) A triggered cosmic ray track traversing a superlayer. b) Distribution of the residuals in millimeters obtained using cosmic ray tracks. A standard deviation of 110 μm is calculated from a gaussian fit to the histogram.

Two straw tube superlayer designs are described in this document. In both, the tubes are placed onto a cylindrical support structure either individually or in groups. The primary structural difference between the single straw concept and the modular approach is the method by which the wire tensile loads are transmitted to the base cylinder. The single straw approach transmits this load to the cylinder through rings on each end of the cylinder. Calculations done at ORNL (David Vandergriff) have shown that a carbon fiber cylinder with thickness less than 0.3% radiation length can support the wire tensile and gravitational loads of the straw superlayer. For this design, the straw tubes span the full 6 to 8 meter length of the cylinder with no support structure at $\eta = 0$. An intra-tube terminator, centered in the straw, divides it into two drift cells read out at each end. The terminator and sense wire supports allow gas to flow through the full length of the tube, and permit wire stringing after the cell is assembled.

3.2.2. Assembly of Pretested Drift Cells

Figures 3.8 and 3.9 illustrate the assembly and testing sequence for a single straw tube cell. Wire supports and end plugs are inserted into the straw tubes and the assembled unit placed on a temporary holding fixture (see steps 1 to 3 in Fig. 3.8). This fixture is mounted on a flat surface containing a jig which aligns the tubes using a series of "combs". This technique has been perfected using the operating 2.7 m prototype. Approximately 50 tubes would be mounted at a time. The sense wires are blown through the tubes using the feed mechanism shown in step 4 in Fig. 3.9. Experimental tests show that this procedure can be used to blow a wire through a tube 5 meters long with up to 6 wire supports. It is simple and reliable.

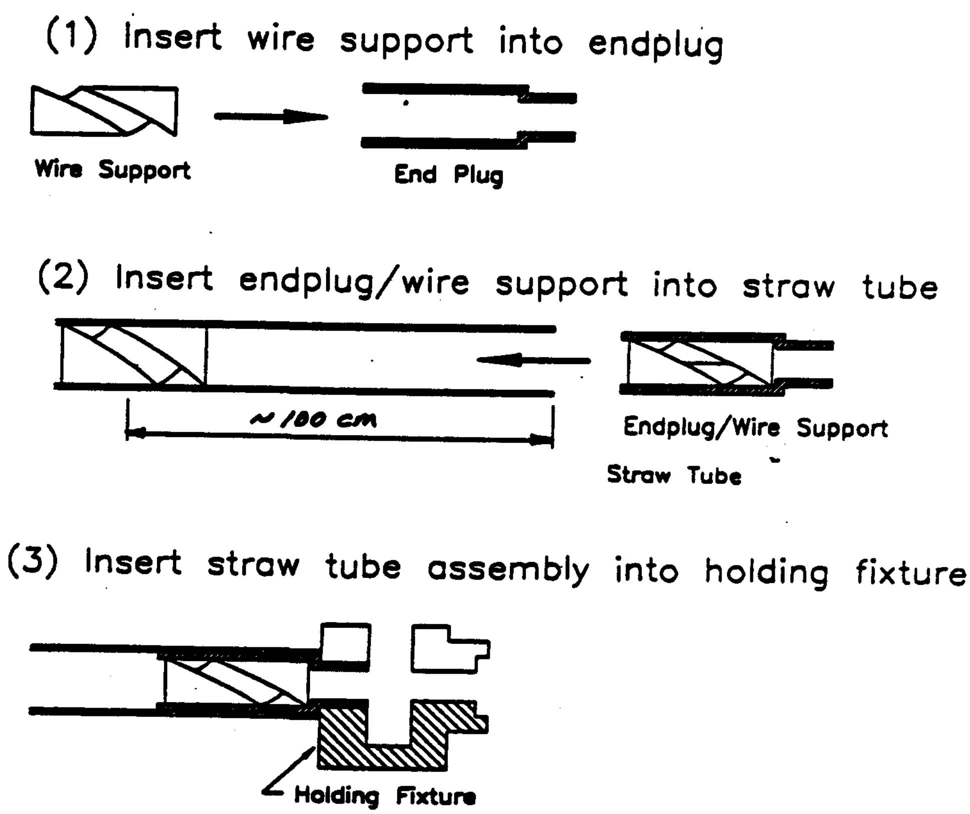

Fig. 3.8. Assembly sequence for a single straw cell: preparation of the tube and wire support.

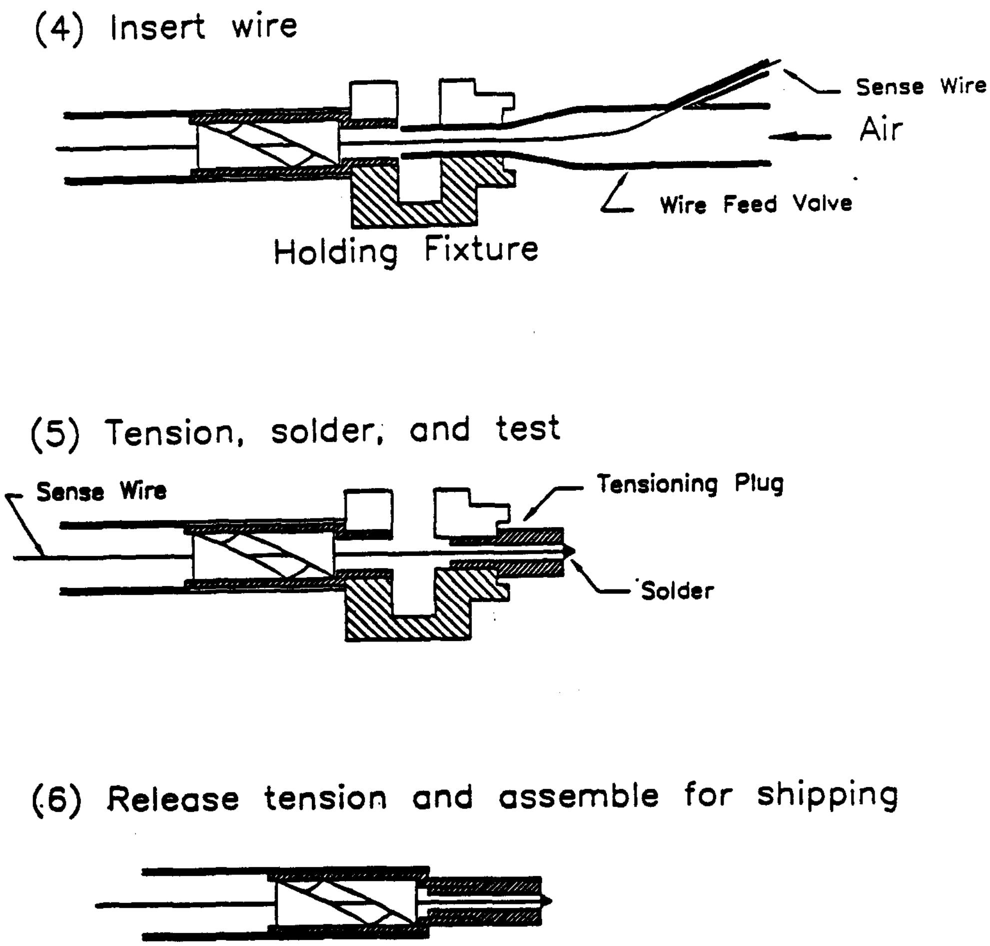

Fig. 3.9. Assembly sequence for a single straw cell: wire insertion and testing.

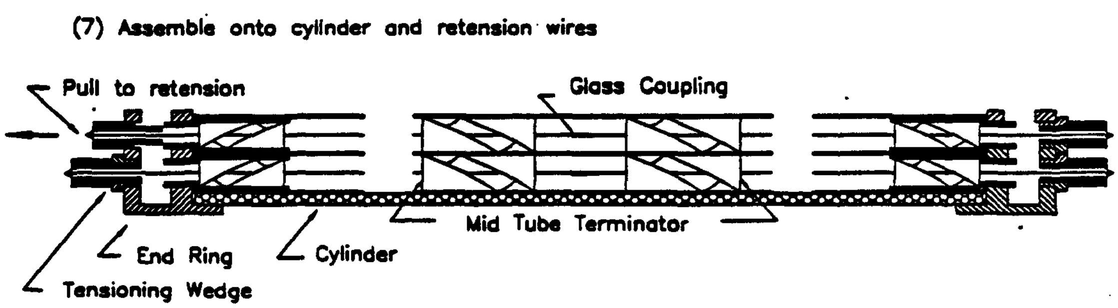

Fig. 3.10. Assembly of tested straw tube drift cell onto the support cylinder.

Next, the wire is tensioned and secured in a clamping plug. The drift cell can now be fully tested (gas, high voltage and readout with a radioactive source). After these tests, the wire tensioning plug is released and slips into a recess in the tube end plug (step 6 in Fig. 3.9). The wire elasticity is sufficient to hold the tensioning plug in the tube. These pretested drift cells are now ready for mounting on the support cylinder. Completed straw tube cells on the support cylinder are shown in Fig. 3.10.

The details of wire support construction are discussed in Section 4.1.5. A solution for the fabrication of a mid-tube terminator and insulating wire break is presented in Section 4.1.8.

3.2.3. Superlayer Assembly Concept

Assembly of the straw tube tracking system into superlayers is accomplished by placing individual straws on a support structure. The first construction step is to assemble each straw tube drift cell as described above. The straw assemblies consist of wire supports, mid-termination, end plugs and a sense wire. The tested and certified straw drift cell is ready for further assembly into superlayers.

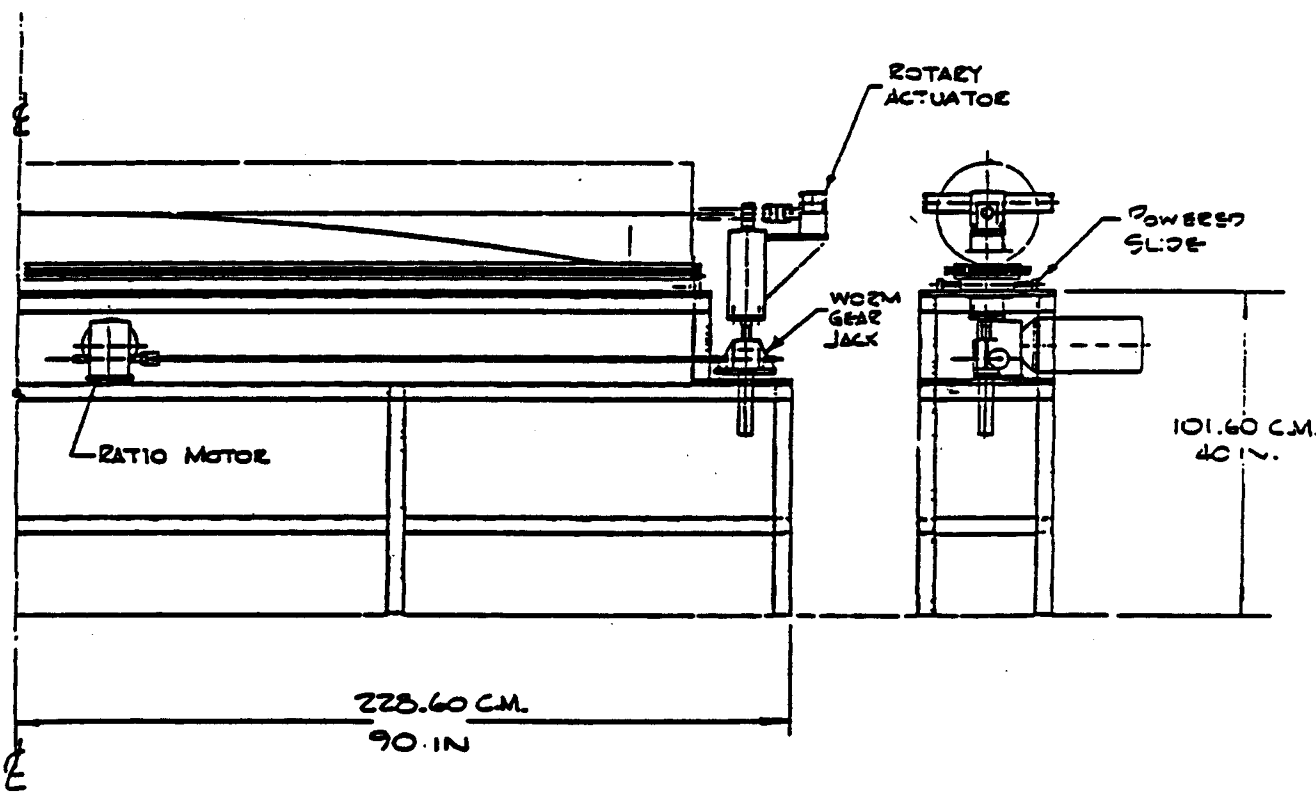

Fig. 3.11. Prototype straw tube placement machine.

The certified straw tubes are packaged and shipped to final assembly sites. They are assembled onto the support cylinder individually or in groups. The single straw concept is preferred at this time, but both concepts are being evaluated. An automatic straw laying device is being developed to apply individual straws to the support cylinder (Fig. 3.11). The FY 1991 R&D effort places high priority on automation of the straw laying procedure. This will verify that precision and speed requirements have been met. A superlayer is completed by laying a full complement of straws onto the cylinder (Fig. 3.12). The sense wires are re-tensioned by pulling the wire clamp into position in the end plate. The wire tension is transferred to the support cylinder through the endplates. Each endplate consists of two plates separated by a few millimeters, with the space between the two plates serving as a manifold to provide gas to groups of tubes (Fig. 3.13).

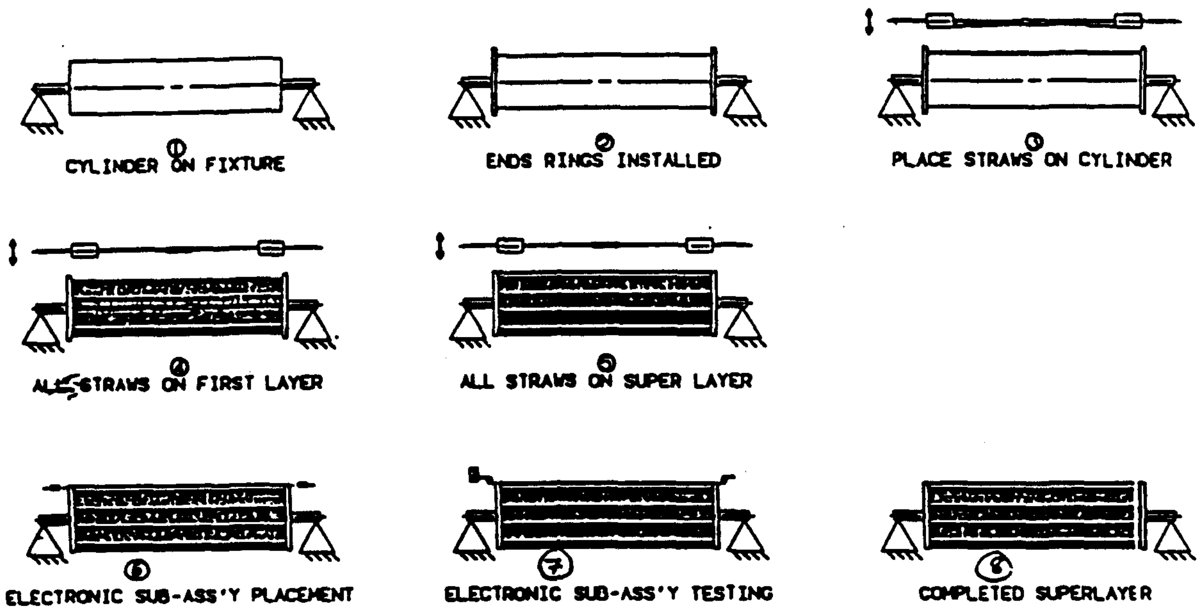

Fig. 3.12. Placement of straw tubes onto support cylinder.

The straw tube is aligned relative to the support cylinder by a placement fixture. The tubes are glued at about 30 cm intervals, which locates them with respect to a fixed reference point on the cylinder. The position of the wires at the wire support locations will be mapped using a Sr-90 or X-ray source after construction. At final assembly of the tracking superlayers into the full tracking detector, the fiducial reference marks on the cylinder are aligned with respect to each other. This provides corelation of the entire central tracking components.

The assembly goal is to automate the straw laying and alignment procedure so that a single straw is placed on the stable-base cylinder in 5 to 10 minutes. This rate allows 50K to 100K straw drift cells to be mounted per year at each assembly site. This final step would be performed at only two sites due to the relative sophistication of the environmental control and placement tooling required for the assembly.

3.2.4. Stereo Straw Tube Superlayers

Straw tubes can be formed into hermetic, simple geometry in axial superlayers. For stereo layers the straw tube geometry can be no longer uniform or hermetic and a tracking solution using scintillating fibers, which can be wound in a low pitch spiral on the surface of a cylinder, is more desirable. However, a solution using the straw tube construction described in this section is also possible. This requires replacing the simple cylindrical support structure with a hyperbolic support surface. The straws would be laid with small angle stereo using the same fabrication technique described above for the axial straw layers.

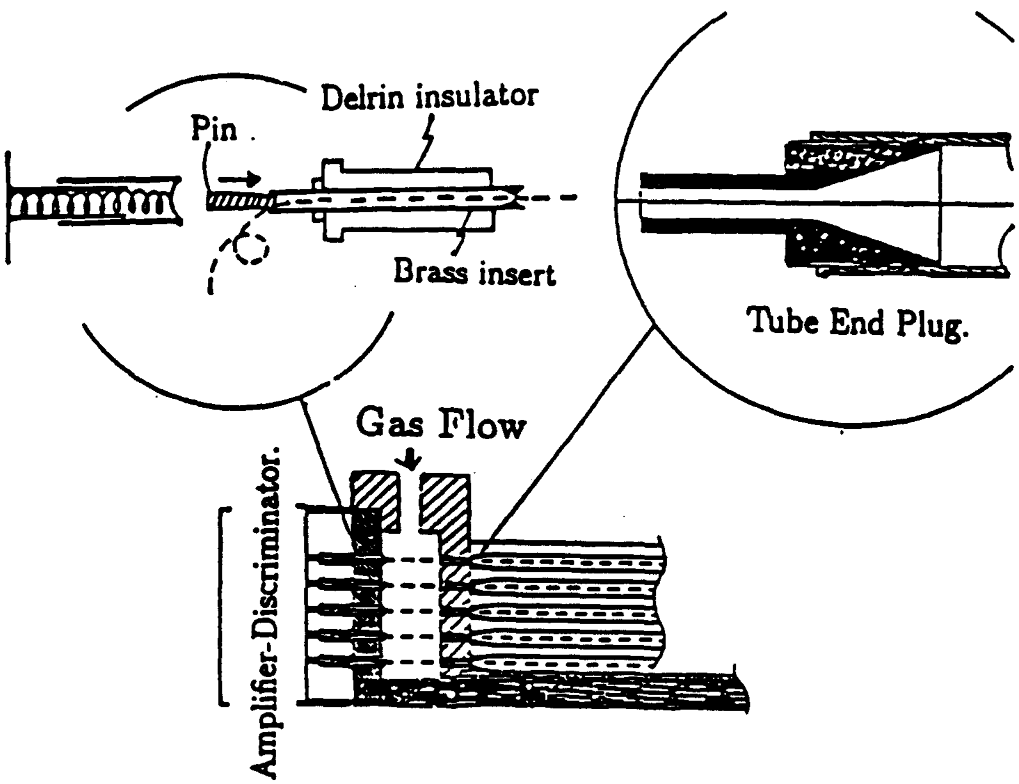

Fig. 3.13. End ring detail showing an assembled superlayer.

3.2.5. Conclusions for the Single Straw Approach

The advantages of this procedure for straw tube superlayer construction stem from the utilization of low risk and simple engineering. The resulting detector has very low mass construction and results in an isotropic and hermetic superlayer construction, advantageous for triggering and track reconstruction. By pretesting the individual straw tube drift cells at many sites, the advantages of mass production can be realised. To insure quality control of the final superlayers, only a few sites (probably two) would be used for the environmentally controlled straw tube placement and alignment. This fabrication procedure will allow the complete assembly of approximately two cylindrical superlayers per year at each assembly site.

4. EVALUATION OF DIFFERENT APPROACHES

4.1. Engineering and Manufacturing Feasibility

In the outer tracking system, we can divide the feasibility into two different areas. One is the feasibility of producing straw elements, whether they are single cells or modules. The other is the feasibility of placing elements on a support cylinder to make a superlayer. The superlayers are combined to form the tracking system. There are many overlap areas of the two approaches we have discussed so far. The design of the cylinder and structure to support them is one. Another common area is the components used to complete a single straw cell, such as a wire support.

In the following subsection, we will discuss not only the common areas but also the differences between the two approaches and their consequences.

For a feasibility study of constructing the outer tracking system, there have been several prototype systems built. One is based on a modular concept, and the other is based on a single straw concept.

The construction of four 64 straw modules each 30 cm long has been completed. The experience in dealing with these multistraw systems has given us an understanding of the engineering feasibility of extending the design to 4 meters. We are using them to study alignment, resolution, electronics prototypes and interfaces to them. We have designed and built three different molds for forming the composites and worked closely with Composite Horizons and ORNL in understanding the final shells. The design of a composite mold for a trapezoidal module 1 meter in length has been completed. The construction of this mold is now in its final phase, and the first trapezoidal shell should be finished by the end of May, 1991. The design for a full-length, 4 meter trapezoidal mold should be started in June, 1991.

For a prototype employing a single straw placing concept, a 2.7 meter long 64 channel chamber was constructed in September, 1990, on a flat surface (which simulates the support structure). The chamber has been operating since then. Using the prototype, studies such as resolution as a function of high voltage and gas mixture, attenuation length, and performance of different electronics have been performed. A test to simulate the SSC rate is being set up using several high radiation sources (Sr^{90}). Electronic responses, space charge, and resolution are some of the tests to be conducted.

4.1.1. Support Cylinder

Straw elements, whether they are modules or single straws, are held in place by support cylinders. Studies carried out at ORNL and WSTC show that the support cylinder can be constructed with the desired thickness and the tolerance we want and at reasonable cost. The cylinder is made of carbon fiber composite. The construction is 1 cm of Rohacell foam sandwiched between two 10-mil layers of carbon fiber composite. Calculation shows that an 8 meter cylinder with a radius of 1.5 meter deflects less than 10 microns at the middle when end rings are attached. Extensive cost estimates were done by ORNL and WSTC, and Table 4.1 shows the summary of the cost estimates for manufacturing the cylinders. Smaller size cylinders are routinely constructed, and no great difficulties are expected. We have already proposed to construct a smaller size (about 4 meters in length and 0.75 meter in radius) cylinder in FY 1992.

TOTAL COST ($K)

CYLINDRICITY REQUIREMENT (IN.)

CYL. O.D. (FT)	.001	.002	.005	.010	.020
4.4	660	330	182	173	145
5.2	1870	390	315	205	170
6.6	2375	1190	400	258	216
7.8	2810	1405	585	450	255
9.2	3310	1655	1380	635	442
10.5	3780	1890	1575	722	590

R&D REQUIRED

EXPENSIVE

AFFORDABLE

MACHINING REQUIRED

Table 4.1. Cost of large cylinders of several diameters and for several grades of precision.

4.1.2. Placement Tooling

The next important issue is to develop a technique to place straw elements accurately and reasonably quickly onto the support cylinder. This requires an indexing mechanism and placing equipment. Like the base cylinder, tooling is required for both approaches although the details may be a little different. The design of the tooling is in progress.

4.1.3. Supporting Structure

There have been some conceptual designs from ORNL and WSTC on how to support the several superlayers once they are constructed and how the outer tracker will be supported. Although there is a great deal of detailed work required, no really difficult problems have been identified.

4.1.4. Straws

The basic drift cell is constructed with a plastic based cylindrical cathode structure and a 25 μm diameter wire along the axis, as described in Section 3. Most of the straws that have been built up to now are formed from an outer mylar wrap 12 μm thick and a 15 μm aluminised polycarbonate film inner layer. We have been using straws manufactured by Precision Paper Tubes, Wheeling, Illinois, and Stone Industrial, College Park, Maryland. The tubes are 4 mm in diameter with a 37 μm wall thickness. Straws up to 3 meters have been constructed. The manufacturers have indicated that longer lengths are possible. A more detailed discussion will be required if lengths up to 8 meters are required. We also need to negotiate cost and schedule for manufacturing runs of very large numbers of straws.

4.1.5. Wire Supports

Due to electrostatic instability, a wire support is required about every 80 cm. Several designs for wire supports have been carried through to fabrication. Over 2400 pieces of the "double V" design (Fig. 4.1) have been produced by RTI plastics. Other companies are now bidding on the project in order to establish costs for large scale manufacture.

Another design is the "Twister," which has a spiral hole inside a plastic cylinder as shown in Fig. 4.2. The wire supports are made by first extruding a long solid plastic rod of the appropriate diameter. The rod then is passed through a special fixture for machining out a spiral groove along the length of the rod. As the rod exits the fixture, 1 cm long sections are sliced off the rod. Strict quality control will be used to ensure the depth of the spiral groove and the diameter of the rod are within tolerance. This method for mass producing wire supports has been shown to be reliable and easy to implement at very low cost.

4.1.6. Shell

For a modular concept, an external carbon composite shell holds the straws in alignment and supports the wire tension. For the engineering baseline design, for example, at least 672 composite shells would be fabricated. The number of modules would be disposed as follows:

a) Trigger layer #6 would have 192 modules. There would be two types of molds required, one for the in-facing and one for the out-facing modules.
b) Stereo layer #5 – 176 identical modules
c) Axial layer #4 – 160 identical modules as in layer #5
d) Stereo layer #3 – 144 identical modules as in layer #5.

Thus three different types of modules would be required. The module design and manufacture would represent the most significant aspect of the engineering work in this approach. As part of the preparation of the 1 meter long mold design, we have compared the mold and part sizes for a 8 × 8 inch test panel of a six layer panel using Hercules UHMS3501-6 prepreg tape with a 38 million modulus. The report (R. Foster, April, 1991) is included, and the results agree well with a simple calculation using the GENLAM program. The tests on the the 1 meter module will help us understand the problems in increasing the length to 4

meters. Design of a full-scale module shell will begin about June, 1991, and the first prototype should be available in Fall, 1991.

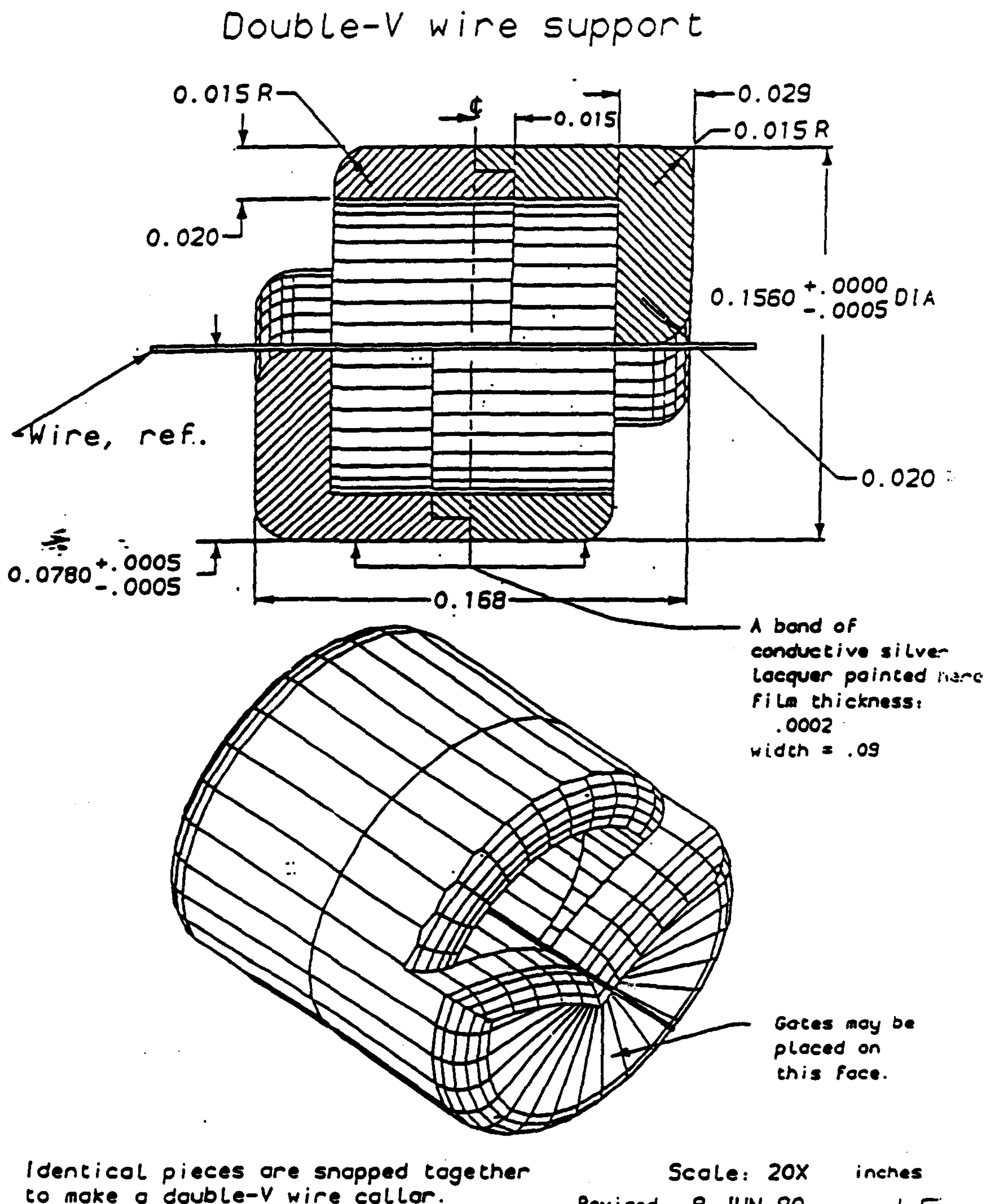

Fig. 4.1. Drawing of the "double-vee" wire support.

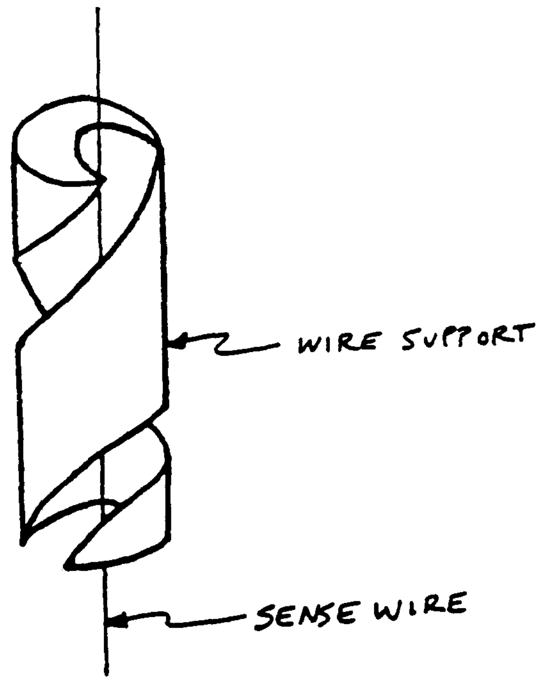

Fig. 4.2. Conceptual drawing of the "twister" wire support.

4.1.7. Endplates

The endplate designs are different for the different approaches. For the modular concept, an endplate which fits into the end of the module is required. For the single straw concept, the straw tube termination plate and gas manifold is part of the end ring used to support the cylinder.

For small size endplates, manufacturing has been carried out for the 64 straw modules using numerically controlled milling techniques. For the straw tracking system of the engineering baseline design, about ~~2500~~ pieces are required and would probably be done in a similar manner, although molding techniques are being examined.

For a large continuous endplate, the plates would be made of carbon composite material. The holes on the plates would be drilled after the endplates are mounted on the base cylinder using a precision indexing mechanism. There are two plates on each end of the cylinder, one of which is the end ring for the support cylinder.

4.1.8. The Mid-tube Termination and the Wire Coupling

One way to reduce the material at the middle of the straw tube tracker is to terminate the sense wires inside the tubes, as shown in Fig. 3.10. The termination permits gas flow. For this scheme there are two requirements. One is the terminator itself, and the other is the wire coupling through an insulator at the middle.

The manufacturing of the mid-tube termination will employ many of same techniques used in manufacturing the wire supports. First, a long composite rod with an inner core of conductive plastic with the proper resistivity with a coating of dielectric skin will be made. The rod is then passed through a fixture identical to the one used for the wire supports. A spiraled groove (with a depth slightly less than cut in the wire supports) will be machined out of the rod. As the rod exits the fixture, 1 cm slices are cut. Strict quality control will be used to ensure the electrical properties of the composite rod meet specifications.

A mechanically continuous wire with an electrically insulating coupling will be manufactured using a borosilicate hard glass to couple to the ends of 25 μm gold plated tungsten wire. The ends of the wire are inserted into a small glass tube which is held in a carbon base fixture. The fixture is heated enough to allow the fusing of the wire ends to the glass. This method allows current automation techniques used for handling small diameter wire to be employed to mass produce the wire couples. The glass coupling provides good mechanical strength and good electrical insulation with very little mass and at a very small cost. This technique has already been demonstrated satisfactorily.

4.1.9. Straw Tube End Plugs

The end plugs are necessary for the single straw concept. The end plugs for the straw tubes serve three purposes:

1. They provide a path to ground for the straw tube.
2. They provide an access for gas into and out of the straw tube.
3. They provide for wire support at the extreme ends of the straw tube.

The end plug will be a stepped (in outside diameter) hollow cylinder 2 cm long made by injected molded conductive plastic. The inner surface of the end plug will be coated with an insulator or have an insulating ceramic sleeve around which the conductive plastic is molded. A small diameter wire support will then be inserted in the large diameter end of the end plug (see Fig. 3.8).

4.2. Ease of Assembly, Alignment and Servicing

The basic assembly of the straw tracking system consists of 4 steps. The first is quality control of individual straws. The second is to prepare them for placement on the support cylinder either individually or by assembling them into multistraw elements. At this stage the basic straw tube elements will undergo testing and quality evaluation. The third is placing and aligning the elements on the cylinder. The last is the overall test of the superlayer including electronics.

4.2.1. Ease of Assembly

Depending on the approach, the individual straw test steps will be a little different. For one approach (for example, the single straw approach), the testing will be extensive since it is somewhat difficult to replace tubes once they are placed on the support cylinder. For another approach (for example, the modular approach), the testing may not have to be as extensive since the testing will be performed after a module is constructed.

Here are some scenarios showing how to assemble the outer tracker using different concepts.

For the single straw concept, the following steps are required. After the straw tubes are inspected by eye and the necessary components, such as the wire support and end plugs, are placed inside the tubes, the tubes are placed in a jig shown in Fig. 3.9. We expect to mount about 50 cells at one time. The jig is placed on a optical table or an equally flat surface. The sense wire is strung and tensioned.

The wire is inserted using the special Y shaped valve, shown in Fig. 3.9. As air passes through the primary branch of the valve, the wire is pulled along and follows the path of the air flow through the wire supports and out the other end. This technique has been reliable for quickly inserting wires into horisontally oriented 5 m straws with 6 wire supports. This technique can be easily adapted for automation. The length of wire inserted into the straw could be measured by a low friction tracking wheel that rotates as the wire is passed over the wheel.

After the sense wire is strung, gas will be introduced into the tube for gas leak, high voltage and source test. After selecting good cells, the tension in the wire is relieved by taking out the feedthrough from the second plate and inserting it into the end plug (Fig. 3.9). These tubes are then ready to be placed on the cylinder. These pretest steps can be done in several locations independent of support cylinder preparation. The 8 meter long assembled single straw cells can then be transported to the site for placing them on the cylinders.

After they are placed on the cylinder, the wire is retensioned by simply moving the feedthrough to the second plate (Fig. 3.10). Of course, if any wire breaks at this point, it can be replaced easily. The gas sealing is not done tube by tube. It is accomplished by pouring a thin layer of low viscosity silicon glue on the endplates. The glue will flow around the end plug (or feedthrough). This technique was used in earlier chambers that we constructed and found very effective.

In the modular approach the individual straws would pass an initial quality check and then have wire supports bonded at locations separated by 80 cm. Groups of 240 straws would be held in a jig clamped and bonded at the wire support positions to lock in an accurate close packed structure, as shown in Fig. 4.3. These units would then be placed in the carbon shells and bonded. After making the electrical connection to the straw cathodes, the endplates would be added and the wires would be strung. At this point the entire module could be tested and calibrated.

In the baseline design, a total of about 700 modules would be produced. It is anticipated that the assembly could be done at several different sites over a two year period. As a separate assembly step the modules would be attached to the superlayer support and aligned as shown in Fig. 3.5. In one of the assembly scenarios this final step could be done at the SSCL.

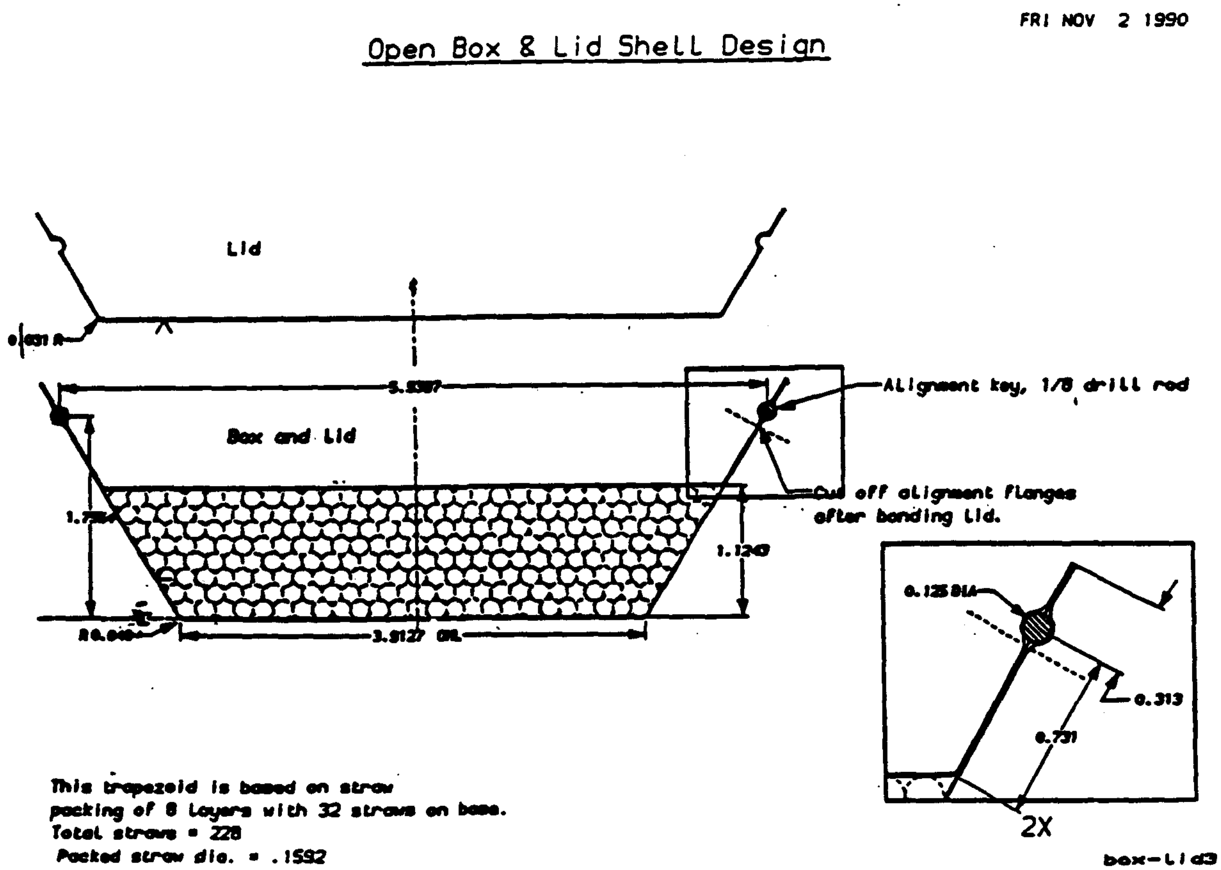

Fig. 4.3. Diagram of the box and lid modular design.

4.2.2. Alignment

For the modular concept, alignment takes place in three steps. They are the alignment of straw tubes with respect to the shell, the alignment of shell with respect to base cylinder, and the alignment of cylinders with respect to each other. In the first step, the wire position will be checkeded using X-ray sources once they are strung. This step can be carried out on the modules in parallel. The alignment of shells to cylinder requires a placement tooling as discussed earlier. A low mass structural support between the module and cylinder is necessary for both axial and stereo modules. This final alignment step should be much less time consuming than in the single straw concept.

For the individual straw concept, only two steps are required for detector alignment. First, once the tubes are mounted on the cylinder, the position of wires will be surveyed using a Sr^{90} source and slits. This procedure has been used in prototype tests and found to be effective. The second step, alignment of superlayers with respect to each other, is the same as for the modular approach.

4.2.3. Servicing

Although a wire chamber is quite reliable once it is made operational and stable, some kind of servicing will be still required. For electronics and gas leaks, the proposed designs are equally effective since gas supply and electronics are modular. If a situation where a section of tubes has to be removed occurs, it is very likely the repair would be done during a long shut down where the chamber has to be moved out to an open area. However it may be possible to carry out this repair without removing the entire superlayer, depending on the design of the module support. One design requires removal, replacement, and realigning the bad module. In the other design it is necessary to remove the bad section of tubes, and then restack the straws. This procedure has been developed. The superlayer cylinder must be removed for this operation.

4.2.4. Stereo Superlayers

Modules can be held in place on the support cylinder by attaching them to the support rings. This approach can also be used for the stereo modules. In order to keep the transverse shift of the ends of the modules small, each 4 meter module is rotated about its center by about 3°. The difference in radial positions (resulting from this rotation) along the length of the stereo module is made up by the low mass attachment fixture at each ring. The interference between the corners of the modules at each end is eliminated by displacing alternate modules by a small (0.5 cm) radial offset. This displacement is also taken up by the attachment fixture. The resulting stereo superlayer, as shown in Figs. 3.5 and 3.6, is quite similar in appearance to the axial superlayer. Track coverage for the stereo layer over the whole length is complete.

For the single straw tube approach, a stereo superlayer is to be constructed on a tapered cylinder which has a smaller radius at the center compared to the ends. A detailed cost estimation of this type of cylinder has not been done.

4.3. Long Term Structural Integrity

4.3.1. Radiation Resistance

All of the straw tube components are radiation resistant. Carbon fiber, mylar and tungsten wire are very radiation resistant. The straws have also been tested and present no problems. The effects of anode and cathode aging due to high currents are also well studied and documented. The mixtures of CF_4 with a hydrocarbon (such as Isobutane) are well studied. Nevertheless, the radiation resistance of all final components must be established by testing.

4.3.2. Thermal Effects

Because of the large amount of heat generated by the electronics and nearby cryogenics and the requirements on alignment and stability, very good environmental control is necessary for the whole tracking system. However, it is expected that there will be some temperature variation during construction and operation.

The support cylinder made of carbon has virtually zero thermal expansion coefficient. The 8 meter long mylar changes about 2mm in length under a temperature change of 5° C. Since the tubes are glued on the cylinder, there will be some small stress on the glue joint. In the modular option, the straws would expand lengthwise in the module, but not touch the endplates.

4.3.3. Long Term Structural Integrity

All material creeps, especially plastics. Because of this, in all designs, it is important that the tubes are not under stress. The material which takes up the most of the stress in the outer tracking is the carbon fiber. Since carbon fiber is excellent against creep, no problem is anticipated because of creep. Mylar has low moisture absorption. Immersed in water for 1 week at 25° C, it absorbs 0.3% of its weight. Moreover, the difference in the thermal expansion coefficient changes by about 5–10% when the relative humidity changes by 10%. The behavior of the carbon fiber cylinder of the shell may be more complex due to moisture absorption than that of the mylar because it involves fibers in different angles and glues. A careful study has to be done.

4.4. Interface with Electronics and Cooling

A module is a stand-alone drift chamber with its own gas, high voltage, and electronics. The basic interfacing is via the endplate structure. Several designs have been proposed.

In the individual or bundled straw design, although the endplate is one continuous plate, the electronics and gas supply are provided for every 200–300 channels such that a bad electronic card can be removed and replaced and the gas supply turned off to a set of tubes so a leak can be isolated. Because the endplate provides a good support for mounting electronics and providing gas, one does not have to worry about the misalignment while working on the ends. The cooling gas lines run around the endplate providing the cooling for electronics. Again the endplate provides a good support for the cooling gas lines.

4.5. Material in the Particle Path

The basic straw material represents a total thickness of $\pi \times$ wall thickness for each straw. For a six layer system this is 697 μm of mylar. We take into account the internal wire supports by increasing this by 10% giving a total of 0.32% of a radiation length for each straw layer.

In the modular version the carbon shell thickness will be 250 μm. The entire shell will then have an equivalent thickness of about 600 μm per superlayer or about 0.24 percent of a radiation length at 90° incidence. The support cylinder will have about 0.24% of a radiation at 90° (Table 4.2). There may also be a small amount of extra material in the support structure for attaching modules on the cylinder. The endplates can be quite thin. The endplates for the prototype 64 straw module have an effective thickness of less than about 0.5 cm of plastic. This would contribute a thickness of about 2% of a radiation length normal to the ends. To this must be added the printed circuit board, electronics, cooling, cabling, and cylinder support struts. Figure 4.4 shows the effect of these items. Figure 4.5 shows the material for the whole tracking system in the baseline design.

tracker component	radiation length(%) at 90 degrees	sum with modules shell	sum without modules shell
Silicon system + beam pipe	8.0	8.0	8.0
fiber system+ supports	5.0	13.0	13.0
support cylinder	0.29		
module shell (10 mil wall)	0.24		
straws and supports	0.32		
support cylinder	0.29		
module shell (10 mil wall)	0.24		
straws and supports	0.32		
support cylinder	0.29		
module shell (10 mil wall)	0.24		
straws and supports	0.32	15.6	14.8
support cylinder	0.29		
module shell (10 mil wall)	0.24		
straws and supports	0.48		

Table 4.2. The material budget for both the single straw and modular approach near 90°.

For the design where tension is taken up by the stable cylinder rather than by the shell, the amount of material at 90° is less than the modular design by about 30%, which is about 0.3% of a radiation length. The thickness of the support cylinder is about the same for all designs because compression load is not the determining factor of the thickness of the cylinder.

The material in the region of the endplates may be slightly higher when the compression load of the wire tension is transferred through the endplates to the base cylinder. However, since a base cylinder requires an end ring for its support, and the end ring will be one of two plates, the increment of the material would be small compared to the modular design. The present design scheme calls for continuous straw tubes without a breakage at $\eta = 0.0$. The sense wires are terminated at the middle. This design provides the minimum material near and at $\eta = 0.0$.

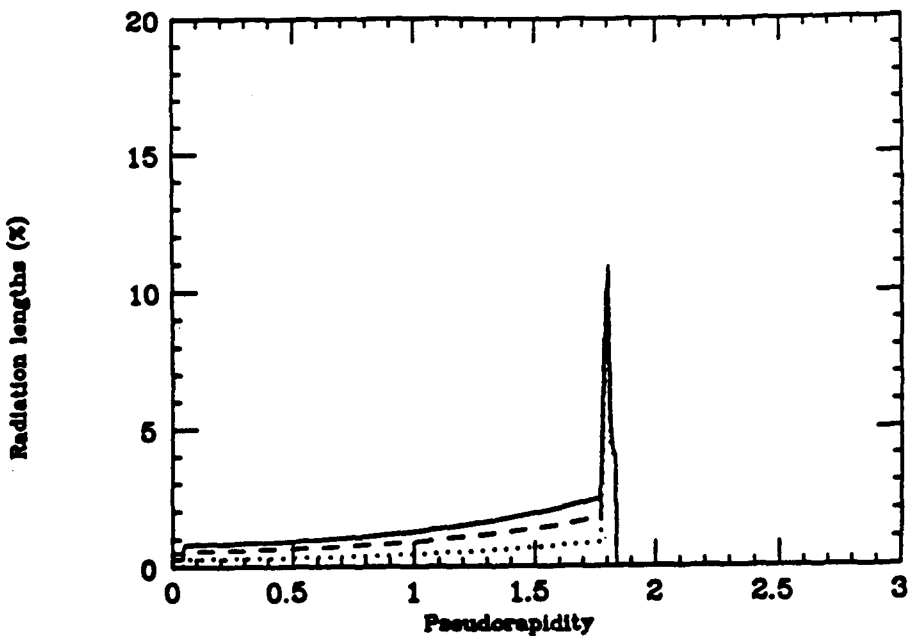

Fig. 4.4. The amount of material in radiation lengths as a function of η due to the straw tracking system. Dotted line: straws and electronics; dashed line: adds the support structure; solid line: adds the shells.

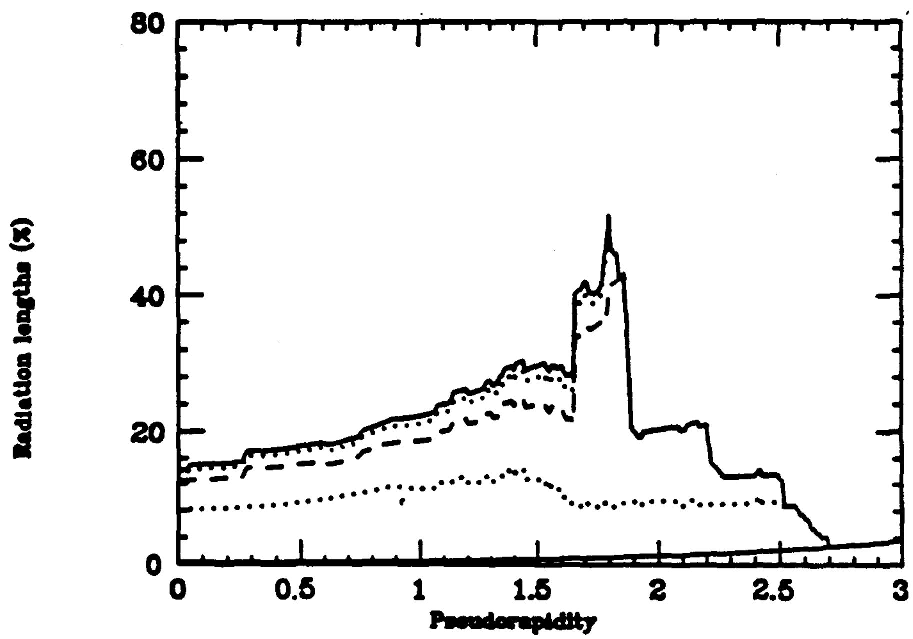

Fig. 4.5. The total amount of material as a function of η from the beam through the tracking system. Solid line near horizontal axis: beam pipe; next higher dotted line: adds the silicon system; dashed line: adds the scintillating fiber system; dotted line adds the straw system with no shells; solid line: adds the shells in the modular approach.

4.6. Triggering Considerations

Both approaches use superlayer structures, so the differences are really in detail. Triggering on straws in both the KEK 3/4 coincidence and synchronisers makes use of the drift time difference for radially aligned wires. The curvature determined from local track segments, assuming the tracks pass through the origin, is used to make a cut in transverse momentum. Modules for axial superlayers need to be curved to follow the circumference of a cylinder in order to keep the wires radial. Since the stereo superlayers in the module approach cannot have wires which are exactly aligned radially, we plan to use only axial superlayers in the trigger. Perhaps the stereo superlayers could be used with a looser curvature cut, and in coincidence with an axial superlayer trigger. If stereo straws could be placed in superlayers directly on a precise hyperbolic cylinder, the wires would be radially aligned and could be used in the trigger in the same way as for axial superlayers, but it is not clear that this warrants the mechanical complexity of such a design. Computer simulations of the trigger are under way and will provide information as to the number of superlayers needed. If one or two axial superlayers are sufficient, the nonradial stereo wires will not cause a problem. Because of cost, we do not expect to implement the trigger for all superlayers in any case.

Another possible problem for the trigger with the module approach is the trigger connection across module boundaries. This can be accomplished without inefficiency, in principle, since the modules overlap. The wiring and logic, however, will be more complicated with modules.

An advantage for the module approach is that the trigger electronics can be an integral part of the front end electronics and mounted directly on the module. The front end electronics, including the trigger, can then be tested for each module separately as part of a parallel construction and testing procedure.

4.7. Pattern Recognition Considerations

The pattern recognition approach for all schemes, since they involve superlayer structures, is to find track segments locally in superlayers and then link them. The segments from all parts of the tracking system, the silicon inner tracker, the outer central tracker, and the outer intermediate angle tracker, are linked to reconstruct complete charged particle tracks. Pattern recognition for the trigger is discussed in the previous section.

As for the trigger, a module approach will involve complications due to module boundaries and nonradial wires. These complications would not be present in the scheme with superlayers of wires placed on precise cylinders. However, the problems of pattern recognition in crossing boundaries have been solved before for jet cell chambers, such as the Mark II and CDF central drift chambers. As long as module boundaries do not line up radially, a track which crosses a boundary in one superlayer will be found without complication in a neighboring superlayer. As long as there is sufficient redundancy in the tracking system, module boundaries should not be a problem. The algorithm could also be written so that track segments crossing boundaries would be found in the first pass. The geometry of nonradial wires can be calculated in software. The first pass of the pattern recognition should be able to find track segments without correction (this should be investigated in the computer simulation). For axial superlayers the effect is small since the displacement is radial and so has little effect on the curvature determination. Track segments will probably be found first in the axial superlayers and then linked to those in the stereo superlayers. Stereo superlayers are somewhat more complicated since the radial displacement is coupled to the determination of the coordinate along the wire.

5. CONCLUSIONS AND RECOMMENDATIONS

The support structure for the straw tube superlayers has evolved to a design which can accommodate all the straw tube superlayer options discussed in this report (see Section 2.1). The main remaining issue to be resolved deals with the detailed procedure to be used to construct the superlayers. The institutions working on this problem (Colorado, Duke, Indiana, ORNL and WSTC) have formed an integrated straw tube group which will pursue a coordinated R&D program leading to the best, most cost effective solution. The program we have developed will insure that a straw tube tracker is available for the turn on of SDC. Section 5.1 describes the straw tube placement concept and Section 5.2 presents the R&D work required to arrive at the detailed solution.

5.1. Proposed Straw Tube Placement Concept

The procedure for fabrication of a superlayer has three main steps.

STEP ONE: Assembly and quality control of individual straw tube cells. This step is common to all approaches we are considering for the construction of superlayers. The straws could have wire supports inserted and wires strung, high voltage, and gas flow, and be completely tested for gas leaks and with a radioactive source, or simply be visually inspected. After this quality control, the drift cells would be passed on to assembly stage two or three.

STEP TWO: Fabrication of multi-straw tube elements. The drift cells would next be assembled into multi-straw elements. These elements could be self contained (e.g., see the modular description in Section 3.1) or an intermediate fabrication stage which would be used to transfer the multi-straw elements directly to the support cylinder. In either case, the multi-straw element would be subjected to testing and quality control before passing to the next assembly stage. Note that steps one and two can be performed at multiple assembly sites.

STEP THREE: Placement of straw tube elements onto support cylinders. At this stage in the assembly process the pretested straw tube elements would be placed on the support cylinders, aligned and attached. A final check of wire placement and quality control of the superlayer section would be performed. This step is in common to each of the options being considered.

Step one is necessary for all methods of straw tube superlayer construction and will be pursued as a cooperative effort. Step three, the placement of straw tube elements onto support cylinders, is required for all methods of superlayer construction, but will differ in detail if the elements are single straws, straw tube bundles, or self-contained modules. For the single straw approach, step three is most time critical. Step two is most time critical for the modular approach.

This R&D program will lead to a single design of a superlayer or sector in time for the construction of a 2000 tube prototype by the end of 1992. This prototype will be used to establish in detail the superlayer construction procedure and will demonstrate the measurement precision attainable. This plan requires a decision on the straw placement technique by about October, 1991. In order to make this decision, we have established minimum R&D milestones that must be met for a given superlayer fabrication procedure if it is to remain as an alternative. The general FY 1991 R&D plan with the milestone requirements is presented in Section 5.2.

5.2. Critical R&D Milestones for Straw Tubes

The R&D program needed to determine the best straw tube superlayer structure is described in this section. The critical issues in the design will be alignment tolerance, the assembly techniques needed to achieve it, and the resulting cost. The R&D will be directed towards these issues.

The R&D program is outlined below.

1. Single cell Q. C. and testing
   - Wire supports
   - Terminators
   - Cathode integrity
   - Wire insertion and holding
   - Gas seal
   - Electrical connections
   - Straw handling techniques
2. Prototype multistraw element
   - Support shell engineering
   - Assembly sequence
   - Relative straw/wire alignment
   - Q. C. testing and acceptance
3. Front end and triggering electronics
   - Testing and evaluation of prototypes, interface boards
   - Cooling, utilities
4. Placement of straw tube elements on support cylinders
   - Support cylinder
   - End ring design
     - Structural
     - Wire, gas connections
   - Element placement tooling
     - Handling
     - Bonding

- Alignment

5. Cost and schedule

The critical milestones leading to a decision are:

	Milestone	Date
MODULES		
	Construction and evaluation of a 1 meter module. Evaluation items: alignment, precision, temperature/humidity, gas tightness, cost, assembly procedure	10/91
	Design of 4 meter carbon fiber shell	7/91
	Fabrication of 4 meter shell	11/91
	Evaluation of 4 meter module. Evaluation items as above.	1/92
	Detailed conceptual design of modular superlayers (axial and stereo)	10/91
SINGLE STRAW		
	Construction and testing of 6 meter drift cells, to evaluate: wire support, stringing two piece wire, mid-tube terminator, gas tightness	10/91
	Detailed conceptual design of superlayers (axial and stereo)	10/91
	Development of detailed schedule for superlayer construction	10/91

Prototype 3 meter straw tube placement device; straw placement studies	**10/91**
Begin construction of 3 meter superlayer with endplates	**1/92**
Conceptual design of 8 meter straw tube placement tool and fabrication of 8 meter straw	**3/92**

Critical dates:

1 Oct 91 - Internal design review: Straw placement decision

1 Jan 92 - Internal design review: Just before beginning construction of multi-superlayer prototype.

6. COST AND SCHEDULE

There has been a detailed schedule and cost estimate of the central tracking system for the LoI. This work was done by Westinghouse Science and Technology Center and Oak Ridge National Laboratory. The modular tracking system was chosen for the cost estimate for the LoI, but it had an alternate support assembly, so we expect that there will be some differences in both costs and schedule between the present design and that of the LoI. The LoI estimate of the cost for the central outer tracking system was $50.0M, of which $20.8M were electronics costs. We will try to have more up-to-date costs and schedules for the designs discussed in this document by the time of the engineering review.

IUHEE 91-8
SDC 91-00061
August 21, 1991

PROPOSAL FOR CENTRAL OUTER TRACKING SYSTEM

G. Hanson, F. Luehring, H. Ogren and D. Rust
Indiana University

Introduction

We need to decide on a central outer tracking design for the proposal since there is a great deal of work to be done - engineering, simulation, and costing. The decision will also influence the use of the FY 1992 R&D money, which is very limited. This note describes some of the thinking behind the conceptual design proposed by Gail Hanson at the Tracking Group Meeting at the SDC Collaboration Meeting at LBL. At this meeting it was proposed that the decision on outer tracking technology be made by a panel consisting of members of the tracking groups and collaboration members outside the tracking groups. We feel that it would be much better if the tracking groups could come to a consensus first and then have the decision reviewed by the panel.

Fibers vs. Straws

Scintillating fibers offer an advantage at high luminosity because of their finer segmentation and therefore lower occupancy. However, there is still proof-of-principle R&D to be done, as well as costing information for the VLPCs. It is likely that we will not have enough information at the time the decision must be made for the proposal to be able to decide on an all-fiber outer tracker. An affordable all-fiber outer tracker may not have enough layers for adequate pattern recognition and stereo measurement. Since fibers introduce more material per superlayer, they are best used where really needed in regions of high occupancy for straws at high luminosity.

A system of both fibers and straws could offer some advantages, but the cost will undoubtedly be higher because of carrying out both technologies. The Hybrid Tracking Group claims that this is not the case; both groups are reviewing costs.

We would like to maintain the capability of upgrading to scintillating fibers for the inner superlayer(s) if needed for high luminosity, either later in the design of the detector so that we could have scintillating fibers at turn-on, or a few years after turn-on. It is expected that it will take two to three years for the SSC to reach design luminosity. Meanwhile straw inner superlayers should perform well. It seems likely that the SSC will reach a maximum luminosity of ~ 5×10^{33} cm $^{-2}$ s^{-1} rather than 10^{34} cm $^{-2}$ s^{-1}, and in any case that will take several years. Our proposal encourages the scintillating fiber R&D to continue, with funding from several sources (SSC, HEP, TNRLC).

How Many Superlayers?

The minimum number of superlayers needed can be determined from the following requirements for the outer tracking system:

1. High-p_T track segment trigger
2. Momentum measurement in conjunction with the silicon inner tracking system
3. Sufficient pattern recognition capability to link track segments in the inner and outer tracking systems
4. Measurement of the coordinate along the beam direction (z), in conjunction with the silicon tracker.

In order to provide the high-p_T track segment trigger, we need at least one axial superlayer at the outer radius. At higher luminosities we may require two axial superlayers for the trigger. There is also the possibility of including one of the stereo superlayers so as to obtain the z-coordinate for a high-p_T track in the trigger, although we haven't included this in our proposal. *We propose two axial superlayers at large radius for the trigger.*

Momentum measurement is accomplished by using both the inner and outer tracking systems in an integrated manner. In order to do this, track segments have to be linked between the two systems. This is the main focus of the tracking simulation effort. Indications are that we will need an axial superlayer relatively close to the silicon tracker. The exact radius cannot be determined until we have progressed further with the simulation studies. This inner superlayer might be upgraded to scintillating fibers at high luminosity, if needed. *Thus we propose a third axial superlayer at a radius of about 70 cm.*

The minimum number of stereo superlayers is two, one with wires running at about +3° to the beam direction, the other at -3°. The best choice would probably be to have both of them at large radius so as to obtain the best resolution in angle and the best coordinate measurement for linking to the calorimeter and muon system. However, some information about the z-coordinate may prove useful in linking to the silicon tracker, since it also provides z information. Note that with the present very small angle stereo (1 mrad) in the silicon tracker, the resolution per measurement in z is about the same (3 mm) in the inner and outer tracking systems The exact location of this superlayer needs to be determined from the simulation studies. *We propose two stereo superlayers, one between the outer two axial superlayers and one at an intermediate radius of about 1 m.*

The conclusion is that *five superlayers* would provide a minimal system with reasonable performance and essentially no redundancy, especially for the z measurement. It has been suggested that due to budgetary constraints four superlayers would be enough. In that case, two would be axial and two stereo. There are two possibilities: two axial superlayers at the outer radius for the trigger, or one at the outer radius and one at the inner radius to provide linking to the silicon. In the former case, linking to the silicon would probably be difficult, although more simulation studies are needed to substantiate this. In the latter case, we would not have the possibility of using two outer axial layers in the trigger, which could be needed at higher luminosities.

It has also been suggested that we reduce the number of straw layers in each superlayer, allowing more superlayers. However, this would increase the material and the cost. Most of the material is in the supports for the straws, not in the straws themselves. The cost is dominated by a fixed cost and then by a cost per superlayer. The incremental cost per channel or module is relatively small compared with these.

The Proposal

The Table lists the components of the proposed outer tracking system, which consists of five superlayers of straw tubes, three axial superlayers and two stereo. The design is also shown in the figure. The three outer superlayers are placed as in the engineering baseline design. The inner superlayer is placed at about 70 cm radius, consistent with the envelope for the outer tracking system. The second superlayer is equidistant from the inner superlayer and the three outer superlayers. The radial positions of the superlayers and the exact arrangement (axial vs. stereo) are rather arbitrary here and are the subject of simulation studies. The lengths of the superlayers are in agreement with the η coverage as in the engineering baseline design and would be adjusted to accommodate the intermediate angle tracking system. The two outer axial superlayers are trigger layers and have 8 straws per superlayer. The other superlayers have 6 straws per superlayer. The amount of material in the outer tracking system at 90° is 3.5% of a radiation length including all supports (not including the last superlayer). A preliminary cost estimate, based on the costing structure developed by Westinghouse Science and Technology Center and Indiana University, is $34.8M. The cost is being reviewed, and there is some possibility of reduction. There are a total of 1.35×10^5 straws.

We would like to continue the scintillating fiber R&D so that the inner superlayer(s) could be upgraded to scintillating fibers if needed at higher luminosity or even by turn-on if technology progress and funds permit.

Conclusions

This proposal offers a central outer tracker that, with the silicon inner tracker, forms a complete tracking system that should perform well at luminosities up to at least the design value, which is important for presentation in the proposal. The amount of material is minimal. The cost is within the target value for the tracking system. The proposal also offers the possibility of continuing the scintillating fiber R&D for upgrading the inner superlayers, where occupancy could be a problem with straws for higher luminosity, on a time scale consistent with the foreseen turn-on schedule for the SSC. We can use this proposal to plan future R&D, carry out definite simulation studies, and do the design, engineering, and costing needed for the SDC proposal. We would like our proposal to receive serious consideration.

Table. Central Outer Tracker Design

Superlayer	Radius (m)	Straws/Layer	Modules	Layers/Super layer	z_{max} (m)	Stereo Angle (°)
1	0.708	1112	84	6	2.80	0
2	1.04	1640	124	6	3.20	+3
3	1.35	2120	160	8 (trigger)	3.90	0
4	1.48	2328	176	6	3.95	-3
5	1.61	2536	192	8 (trigger)	3.95	0

PROPOSED CENTRAL OUTER TRACKING SYSTEM

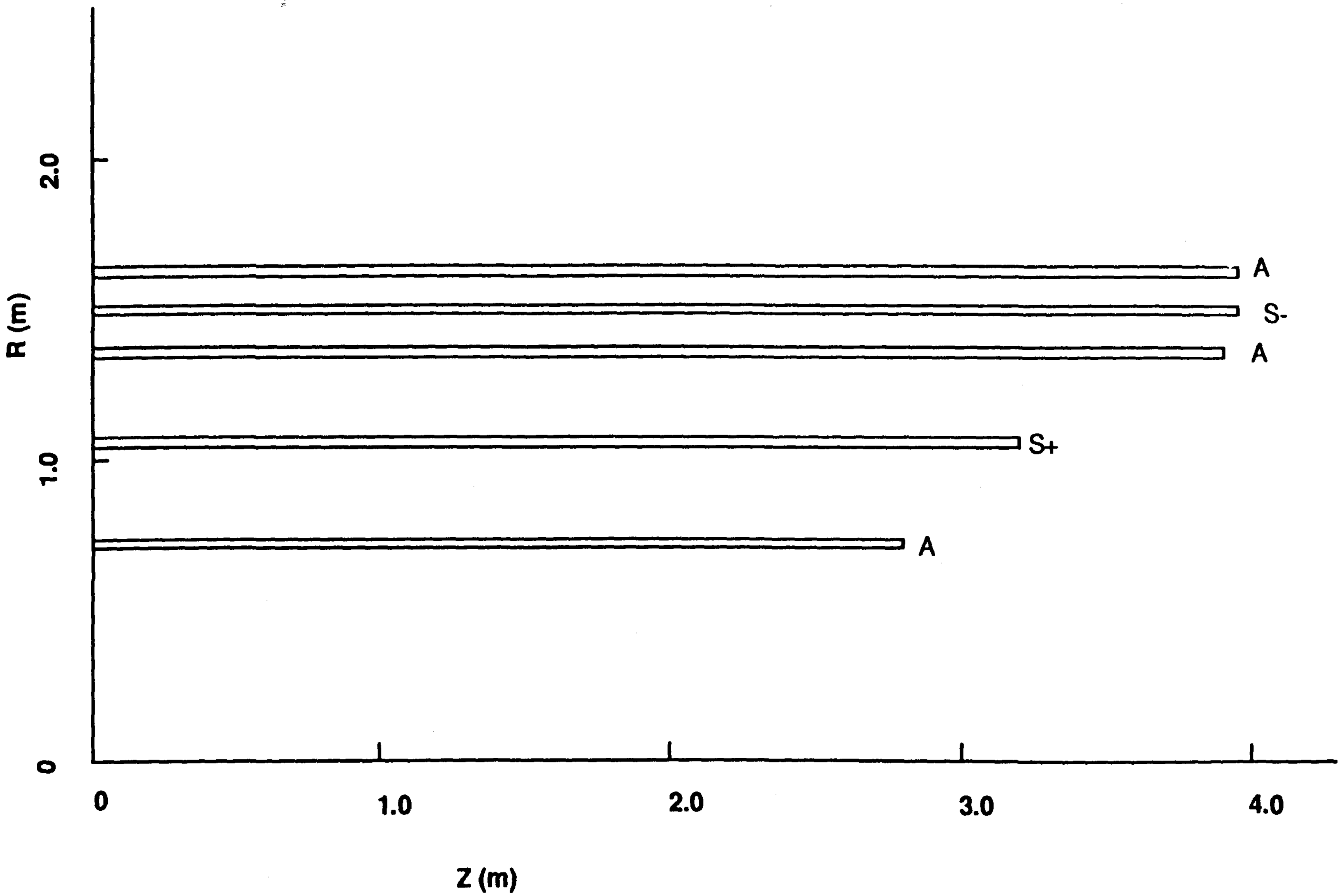

SLAC-91-00273

EFFECTS OF CATHODE AND WALL MATERIALS AND WATER VAPOR ON STRAW TUBE AGING*

J. KADYK
J. WISE
Physics Division, Lawrence Berkeley Laboratory
1 Cyclotron Rd., Berkeley, California 94720, USA

and

J. VA'VRA
Stanford Linear Accelerator Center
Stanford, California 94309,USA

ABSTRACT

Nine short straw tube with different cathode and wall materials have been used for accelerated aging tests and high-voltage breakdown tests. The gases used were argon/ethane (50/50) and CF_4/isobutane. The effect of adding water vapor in each type of test has been investigated. All but one of the tubes performed well in aging and HV breakdown tests, and water vapor was found to be effective in suppressing discharges during aging tests, but had no noticeable effect in the HV breakdown tests.

1. Introduction

Nine straw tube prototypes about 15 cm long by 4 mm diameter have been used for accelerated aging tests and high-voltage breakdown tests, as a function of several variables: HV or gain, principal gas mixture (two types), water vapor to quench discharges, and current densities. The tube wall materials are Mylar, Kapton, polycarbonate, and aluminum, and cathode materials are aluminum, copper, nickel, and gold. The anode wire was 38 μm diameter gold-plated tungsten, except for one tube which used a carbon fiber of 33 μm diameter. The gases were: (1)argon/ethane (50/50), and (2)CF_4/Isobutane(80/20). The latter has properties that appear very attractive for use in high radiation environments, such as at an SSC experiment.[1] Aging studies of this gas mixture and of related gases will be

---

*This work was supported by the Director, Office of Energy Research, Office of High Energy and Nuclear Physics, Division of High Energy Physics, of the U.S. Department of Energy under Contract No. DE-AC03-76SF00098.

1 Use of Straw Tubes In High-Radiation Environments, J. Kadyk, et al., NIM A300(1991)511.

reported in an accompanying paper. The parameters used to measure aging are: (1)the current drawn by the straw tube vs. the charge transfered; (2)gain uniformity using pulse-height analysis. (3)spontaneous breakdown during aging tests; (4) measurement of the high voltage necessary to induce breakdown of the tube by deliberately raising the voltage.

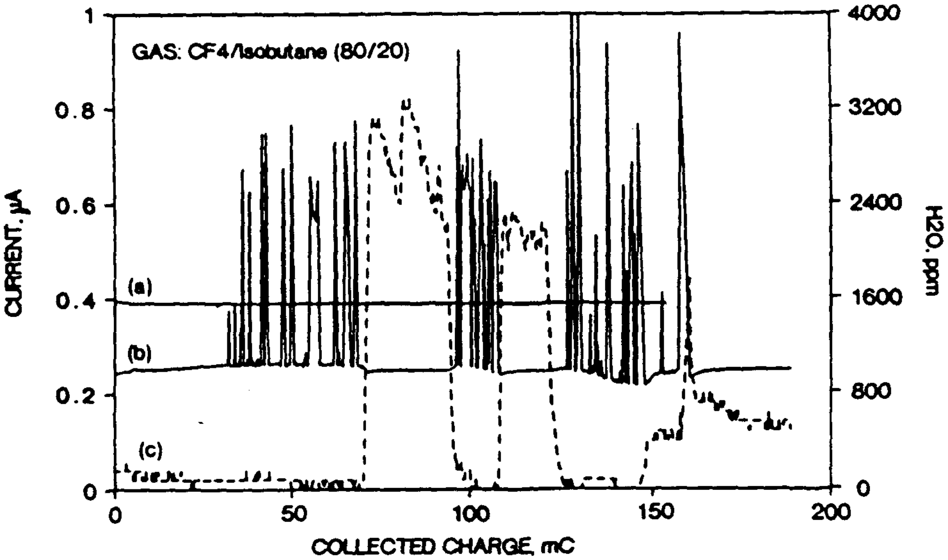

Fig. 1. Two examples of aging tests (see Table 1): (a)gold-plated Al tube, and (b) Mylar tube. The latter went into discharge mode after 0.1 C/cm, and subsequently recovered when H_2O was added, as shown by the graph (c). As can be seen, the cycle of removing and adding H_2O vapor was repeated with similar results.

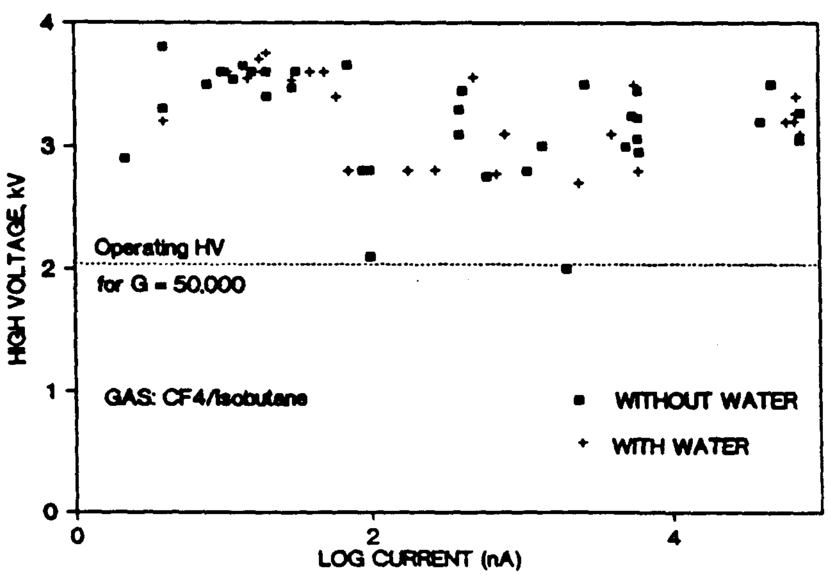

Fig. 2. High voltage breakdown tests on nine straw tubes, using CF_4/isobutane gas. Plotted are the HV and current when breakdown occurred, with and without H_2O vapor. The tests were performed at three radiation levels:a)no source, b)200µCi, and c)2mCi sources.

During an aging test, the current is induced by exposure to a relatively intense Fe^{55} source, which results in an avalanche region of about 3 mm along the wire. Measurements of the current vs. charge are shown in Fig. 1, with examples of a small aging rate (a), and tube discharges (b). Breakdown resulting in large current "spikes" is typically a result of cathode surface coating by a thin insultating layer. Measurements of deliberately induced HV breakdown are summarized in Fig. 2. HV tests were done with and without the addition of water vapor at the level of 3000-6000 ppm; previous reports[2] have indicated that breakdown and other aging effects can be suppressed by the addition of similar amounts of water into the gas. We have used a permeation device to control the amount of water vapor injected into the gas stream and also have monitors to measure continuously the amount of water vapor and oxygen.

2. Result from Accelerated Aging Tests

Table 1 summarizes the results from accelerated aging tests. The fractional gain decrease is parameterized by:

$$R = - (1/G)dG/dQ, \%/(C/cm), \quad (1)$$

where G is the tube gain, assumed to be proportional to current, and Q is the linear charge transfer in coulombs. The total charge accumulated during each test is given, as are the wall and cathode materials of each tube. General parameters applying to all the tests, unless otherwise noted, are: 1) G is near 50,000; 2) the wire is gold-plated tungsten of 38μm diameter; 3) the current density is about 0.6 - 1.2 μA/cm. Under "Comments" are found other relevant observations or departures from these general parameters.

Under the most extreme conditions anticipated for use in SSC experiments, wire chambers might be expected to sustain a current of about one μA per meter.[3] Assuming this current over a period of "five years", or 5×10^7 sec, then the total charge transfer during the lifetime of the experiment is 10nA/cm x 5×10^7 sec = 0.5 coulombs/cm. The tube should not lose gain more than, say, 10%, requiring $R < 20\%/(C/cm)$. This then sets the scale by which the results in Table 1 can be measured, assuming that accelerated aging tests can be scaled to lower radiation intensities. The general picture is that nearly all results are compatible with the required performance.The one test which has resulted in poor performance is that of the tube with a polycarbonate wall.[4] There is some evidence that the aluminum cathode film does not adhere well to the wall in this case.[5]

---

[2] Wire Chamber Aging, J. Kadyk, NIM A300(1991), p. 448 and references 24-29.
[3] See, for example, p. 25 of Radiation Effects At The SSC;SR-1035, SSC Central Design Group, M.G.D. Gilchriese, Editor, June 1988.
[4] Private communication with B. Dolgoshein at the Pisa Instrumentation Conference, Elba, May 1991; he has said that he used similar tubes successfully.
[5] Private communication with D. Rust of University of Indiana, which supplied much of the tubing we used to fabricate the test counters.

Table 1. Accelerated Aging Test Results

Gas	Gain Loss, R (%/(C/cm))	Linear Charge Transfer (C/cm)	Materials: Wall/Cathode	Comments
Ar/Eth. (50/50)	5	1.2	Mylar/Al	33μm carbon fiber anode
"	3	0.5	Al/Al	
"	8	0.6	Al/Ni	
"	5	0.6	Al/Cu	
"	12	0.2	Al/Au	
"	8	0.4	Mylar/Al	2 discharges, then recovery
CF_4/Iso butane (80/20)	3	0.5	Mylar/Al	Discharges quenched by H_2O (Fig. 1)
"	6	1.0	Kapton/Al	gain=1.5×10^5
"	200	0.06	polycarbonate/ Al	Rapid gain loss and discharges; gain=1.5×10^5
"	<1	0.5	Al/Au	Very stable, Sr^{90} (Fig. 1)
"	2	0.2	Al/Ni	Sr^{90}
"	10	0.2	Al/Cu	Sr^{90}
"	9	0.1	polycarbonate/ Al	gain=1.5×10^5
"	4	0.4	Kapton.Al	gain=1.5×10^5
"	9	0.2	Mylar/Al	gain=1.5×10^5
+1000 ppm H_2O	5	0.4	Mylar/Al	Same as above, with H_2O added.

Such a defect might lead to charging by positive ions of the plastic surface where the aluminum has come off, resulting in "Malter-like" discharges. It was found that all discharges could be suppressed by the addition of sufficient amounts of water vapor. In the case of the polycarbonate tube, which underwent both rapid decrease of gain and breakdown, between 4000 and 5000 ppm of H_2O were needed to suppress the discharges; in the case of a Mylar/Al tube, a smaller amount, <1000ppm, seemed to suffice (see Fig. 1).

3. High Voltage Test Results

The capability of a straw tube to reach a level of high voltage momentarily does not appear to be correlated with its integrity over a longer time period, or its history of aging. The nine straw tubes were tested at three different radiation levels, both with and without addition of water vapor. Each tube was tested to find its maximum voltage before discharge (1)without a source, (2)with a 200μCi source, and (3)with a 2mCi source. For each of these, tests were done with a low (about 200ppm) and high (3000-6000ppm) water content.

Fig. 2 summarizes the HV tests: each test is represented by a point having the HV at breakdown plotted on the vertical axis, and $\log_{10}(I_b)$ on the horizontal axis, where I_b is the current at breakdown. Two points lying near 2.0 kV are from the tests of a damaged Mylar tube that subsequently recovered to about 3.0 kV when water vapor was added. The remainder of the points cluster in the neighborhood of 3.0 - 3.6 kV, where there is no apparent effect of the water vapor! It is of interest that a typical breakdown HV far exceeds the operating voltage for our standard gain of 50,000 (2050 kV), and yet some of the same tubes that breakdown at 3.0 kV or more will enter the discharge mode operating at only 2050 volts during aging tests. It becomes clear that the momentary HV breakdown test has only limited utility in identifying damaged tubes.

4. Water Vapor From Gas Tubing

Since it is confirmed that water vapor is influential in suppressing discharges during aging runs, it is interesting to measure the "natural" outgassing which occurs from tubing commonly used for gas plumbing. The results of Table 2 were obtained by flowing argon/ethane (50/50) at a rate of 20 cc/min through a 3m length of the tubing; the gas was pre-filtered to remove the H_2O and O_2 in the supply gas:

Table 2. Outgassing From Gas Tubing

Tubing	H_2O Content, ppm	O_2 Content, ppm
0.25" Nylon	3000	10
0.25" polyethylene	300	70
0.125" copper	4	2

5. Summary

Using CF_4/isobutane(80/20) and argon/ethane (50/50), the potential influence of cathode and wall materials on straw tube performance have been studied. All of the tubes performed well in aging tests except the one with polycarbonate wall. Water vapor added to the gas suppressed discharges occurring during aging runs, but did not significantly affect the HV at which a deliberate breakdown was induced. The HV test was found to have little usefulness in identifying damaged tubes. All tubes but one were compatible with anticipated running in an extended SSC experiment.

LBL-31-00274

CHEMICAL MODELING OF AGING PROCESSES IN CF_4/ISOBUTANE GASES*

J. WISE and J.A. KADYK
Lawrence Berkeley Laboratory, University of California, Berkeley, CA 94720

and

D.W. HESS
Department of Chemical Engineering, University of California, Berkeley, CA 94720

ABSTRACT

We are investigating the chemistry that leads to wire aging transients that we have observed in various CF_4/isobutane gas mixtures including the well-studied 80% CF_4 + 20% isobutane mixture. Aging tests using such mixtures exhibit transients resulting in loss of gain. The magnitude and duration of these transients are dependent on the CF_4/isobutane ratio and the wire material, and are sufficiently large to affect the gain stability during the early operation of an experiment. Film formation on the wire may explain these observations.

1. Introduction

The very good aging properties of the CF_4/isobutane (80/20) mixture have been known for some time,[1,2] and there has recently been a report that hydrocarbon deposits were etched away by using this mixture.[3] However, in aging tests using the 80/20 as well as other mixtures of CF_4/isobutane, we observe transients in which the wire current changes (almost) exponentially towards a nonzero steady-state value, a result that may be interpreted as a competitive ablation and polymerization process.[4]

This investigation is along three lines: 1) monitoring of the aging of the wire, 2) analysis of the aged wire surface, and 3) analysis of condensible species in the proportional tube effluent, presumed to be associated with the gas-phase chemical reactions that may have led to the aging. Only the first two parts are discussed in this report.

2. Experimental

In this series of experiments, wire aging has been investigated as a function of gas composition and wire material. Gases used were CF_4 and isobutane, both individually and in mixtures with each other. Wire materials used were gold-plated tungsten,

*This work was supported by the Director, Office of Energy Research, Office of High Energy and Nuclear Physics, Division of High Energy Physics, of the U.S. Department of Energy under Contract No. DE-AC03-76SF00098

Table 1: Decay constants and gain changes for some wires and gases.

Gas	*Wire*	τ, *mC*	I_∞/I_0
CF_4	Au/W	1.9 ± 0.5	0.6 ± 0.1
CF_4	Stablohm	1.1 ± 0.1	0.75 ± 0.06
CF_4	Nickel	0.9 ± 0.2	0.4 ± 0.1
CF_4	Copper	1.2 ± 0.2	0.7 ± 0.1
CF_4	Carbon	1.2 ± 0.2	0.75 ± 0.1
80/20	Au/W	7.7 ± 2.3	0.96 ± 0.04
80/20	Stablohm	25 ± 5	0.59 ± 0.14

Stablohm, nickel, copper, and carbon. The techniques used to collect aging data have already been described.[2]

3. Exponential Curve Fits

In aging tests using different mixtures of CF_4/isobutane, we observe transients in which the wire current approaches a nonzero value. We model these transients a a constant plus an exponential. The two parameters used are the gain change (I_∞/I_0) and the decay constant. Although not always a good fit ($\chi^2/n \sim 100$), this procedure nevertheless gives a consistent basis for comparison of different aging tests.

Although the experiments are still in progress and little data is presently available for gas mixtures containing more than 20% isobutane, indications are that the decay constant increases with increasing isobutane content, but that the gain change shows no distinct trend. For CF_4 alone, the decay constant is independent of the wire material. For CF_4/isobutane mixtures, however, the decay constants for Stablohm wires are much longer than those for gold-plated wires, suggesting that the two types of wires age by different mechanisms. The decay constant for CF_4 alone is also much smaller than for CF_4/isobutane mixtures. Gain changes and decay constants for some of the aging tests in this study are summarized in Table 1.

4. Surface Analysis

Wire surfaces are analyzed using secondary electron microscopy (SEM) and Auger spectroscopy combined with argon ion milling of the surface so that a composition-depth profile can be obtained. Hydrogen is not detectable with the Auger technique, so hydrocarbons appear only as carbon. This technique has been used previously by Williams,[5] and an example of an Auger depth profile is illustrated in that work.

4.1. Aged Gold-Plated Wires

Aging deposits on gold-plated wires are predominantly carbonaceous: little or no fluorine is observed, suggesting that the gold surface is not significantly chemically attacked. This is so even for wires aged in CF_4 without admixture of isobutane, in which case the source of the hydrogen presumed to be in the deposits is unclear. There is, however, evidence from other investigations that we have done on CF_4 indicating that significant hydrocarbon contamination exists in this gas. The carbonaceous deposits appear to be an agglomeration of spheres with diameters typically $1\mu m$.

4.2. Aged Stablohm, Nickel, and Copper Wires

In contrast to gold-plated wires, aged Stablohm, nickel, and copper wires show deposits containing significant amounts of fluorine. These deposits are thinner than the carbonaceous deposits, and are not always easily seen at 1500x magnification. Heavy carbonaceous deposits, which are readily identified by Auger analysis and by their distinctive appearance under SEM observation, are sometimes present in addition to the fluorinated deposits.

5. Discussion

The fact that fluorine is a major component of deposits on non-gold-plated wires while carbon is the major component of deposits on gold-plated wires suggests that different aging mechanisms are in effect and that the surface plays a role in the determination of which mechanism dominates. This interpretation is supported by the observation that different wire materials have different aging decay constants.

A possible explanation for these observations is that metals more active than gold react with the F• and/or CF_3• radicals expected to be produced in the avalanche to form an insulating metal fluoride. After the wire surface is passivated by this fluoride, hydrocarbon or fluorocarbon deposits may also form, at a rate dependent on the CF_4/isobutane ratio of the counter gas.

In the avalanche environment, we expect that fluorine radicals will react with carbon on the wire surface to form volatile species (e.g., CF_4). However, fluorine radicals will also react with hydrogen to form HF, leaving behind carbon-rich species that will tend to polymerize and deposit onto the wire. The necessary factors for a competitive ablation and polymerization process are thus present, and the fact that the aging curves approach nonzero asymptotes suggests that this process indeed occurs: a steady-state film thickness results from the two competing processes.

Unresolved questions about this work that remain under investigation include 1) How does isobutane affect CF_4 so that the CF_4/isobutane mixture ages less rapidly than CF_4 alone, and 2) Why is the decay constant for aging of CF_4 essentially independent of the wire surface material.

References

1. (a) R. Henderson *et al.*, *IEEE Trans. Nucl. Sci.*, **NS-35** (1988) 477, (b) R. Openshaw *et al.*, *IEEE Trans. Nucl. Sci.*, **NS-36** (1989) 567.
2. J. Kadyk *et al.*, *IEEE Trans. Nucl. Sci.*, **NS-37** (1990) 478.
3. R. Openshaw *et al.*, presented at 1990 IEEE Nuclear Science Symposium.
4. H. Yasuda, Plasma Polymerization (Academic Press, New York, 1985), p. 178.
5. K. Kwong *et al.*, *Nucl. Instr. and Meth.*, **A238** (1985) 265.

John Kadyk

J. Va'vra, Pisa, 26.5.1991

Measurement of Electron Drift parameters for He and CF4 based gases.

J.Va'vra

Stanford linear Accelerator Center, Stanford University, Stanford, CA 94309, U.S.A.

P.Coyle

Santa Cruz Institute for Particle Physics, University of California, Santa Cruz, CA 95064, U.S.A.

J.Kadyk and J.Wise

Lawrence Berkeley Laboratory, University of California, Berkeley, CA 94720, U.S.A.

WHY THESE TYPES OF GASES ?

- CF4 GASES ARE FAST(AT RELATIVELY LOW FIELDS) WHICH IS IMPORTANT ESPECIALLY FOR HADRON COLLIDERS.

- He GASES HAVE BEEN SUGGESTED FOR USE IN CHARM-TAU AND B-FACTORIES WHERE THE IMPORTANT PHYSICS IS MORE SENSITIVE TO MULTIPLE SCATTERING IN THE GAS RATHER THAN TO INTRINSIC WIRE RESOLUTION.

SUMMARY :

- Measured the electron drift velocity and the single electron longitudinal diffusion in the following gas mixtures :
  CF4 only, 80% CF4+20% C4H10, 95%CF4+5%DME, 78%He+15%CO2+7%C4H10, 82%He+18%DME, 91%He+9%DME, 95%He+ 5%DME, 93%He+7%C3H8, 95%He+5%C2H6 and 50%Ar+50%C2H6.

- Effect of water addition on the electron velocity and diffusion.
- Impurities in the CF4 based gas mixtures.
- Single electron pulse height spectra.
- Comments on relative breakdowns.
- Measurement of the near wire diffusion.
- Wire aging in CF4 gas.

- Macintosh controlled CAMAC and GPIB system :

  1. Steps the laser beam using a stepping motor
  2. Measures temperature, pressure, O2,H2O level, etc.
  3. A lot of on-line and off-line fitting.
  4. Monitor probability per event (P < 5-10 %)
  5. MAC-UAJ software with our improvements.

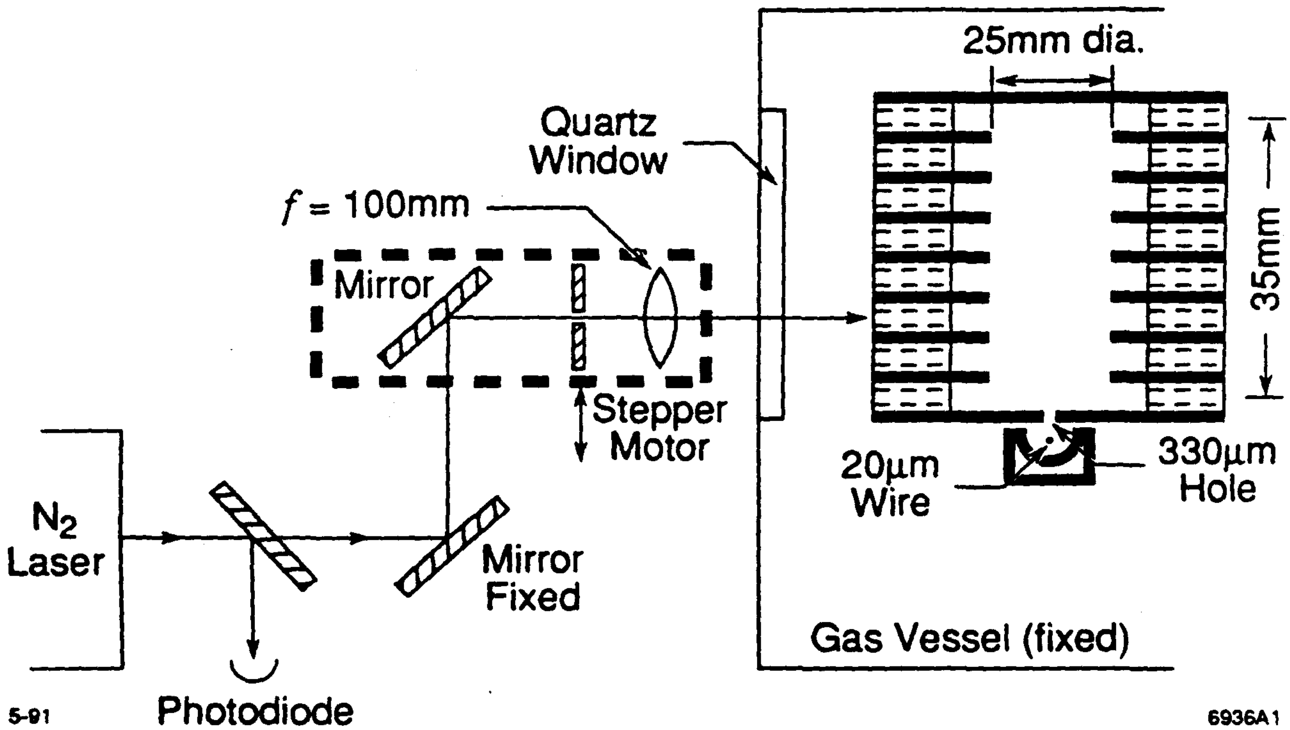
25mm dia.
Quartz
Window
f = 100mm
Mirror
35mm
Stepper
Motor
20µm
Wire
330µm
Hole
N2
Laser
Mirror
Fixed
Gas Vessel (fixed)
5-91
Photodiode
6936A1

DOUBLE THRESHOLD TIMING

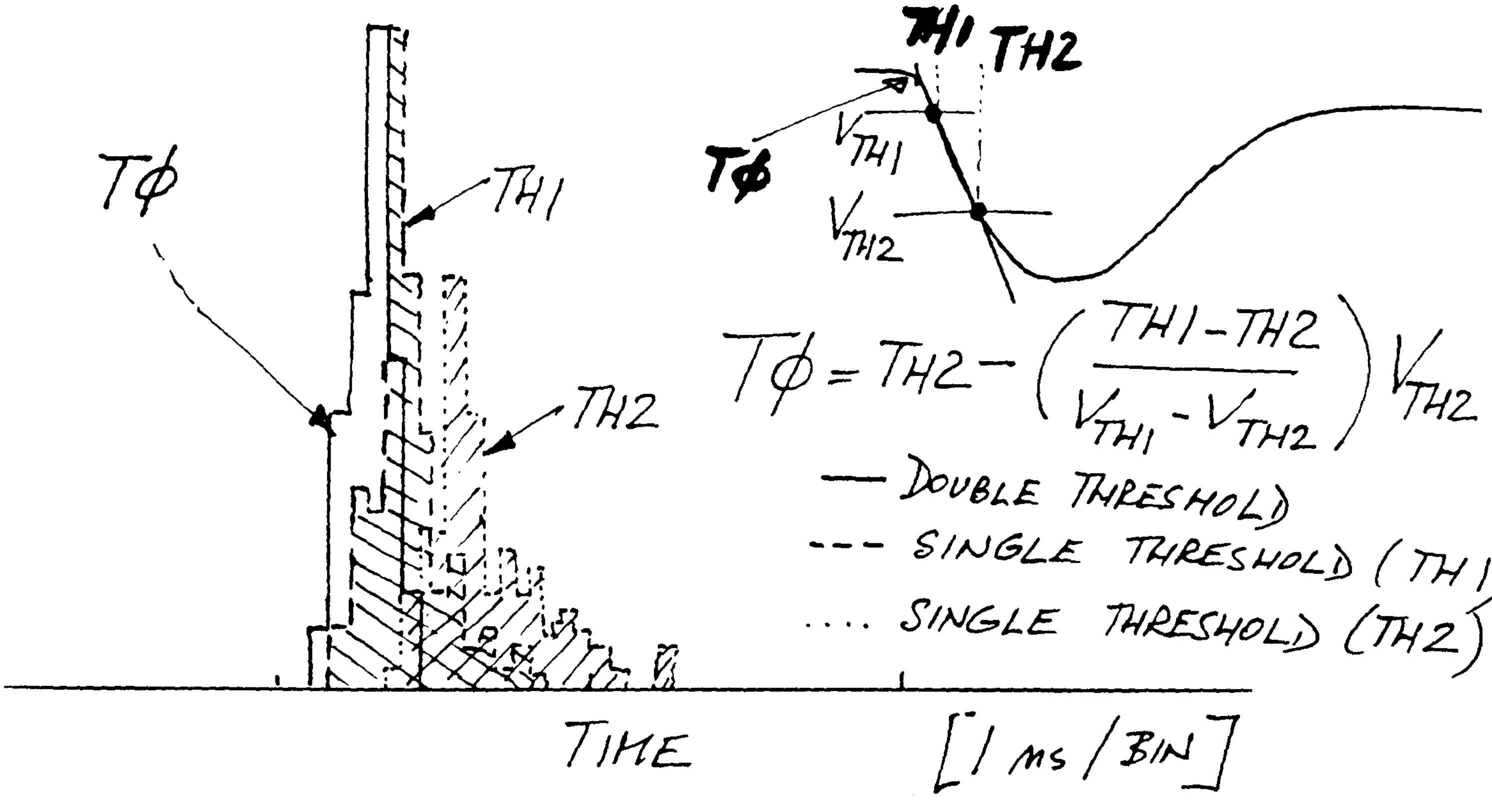

$$T\phi = TH2 - \left(\frac{TH1 - TH2}{V_{TH1} - V_{TH2}}\right) V_{TH2}$$

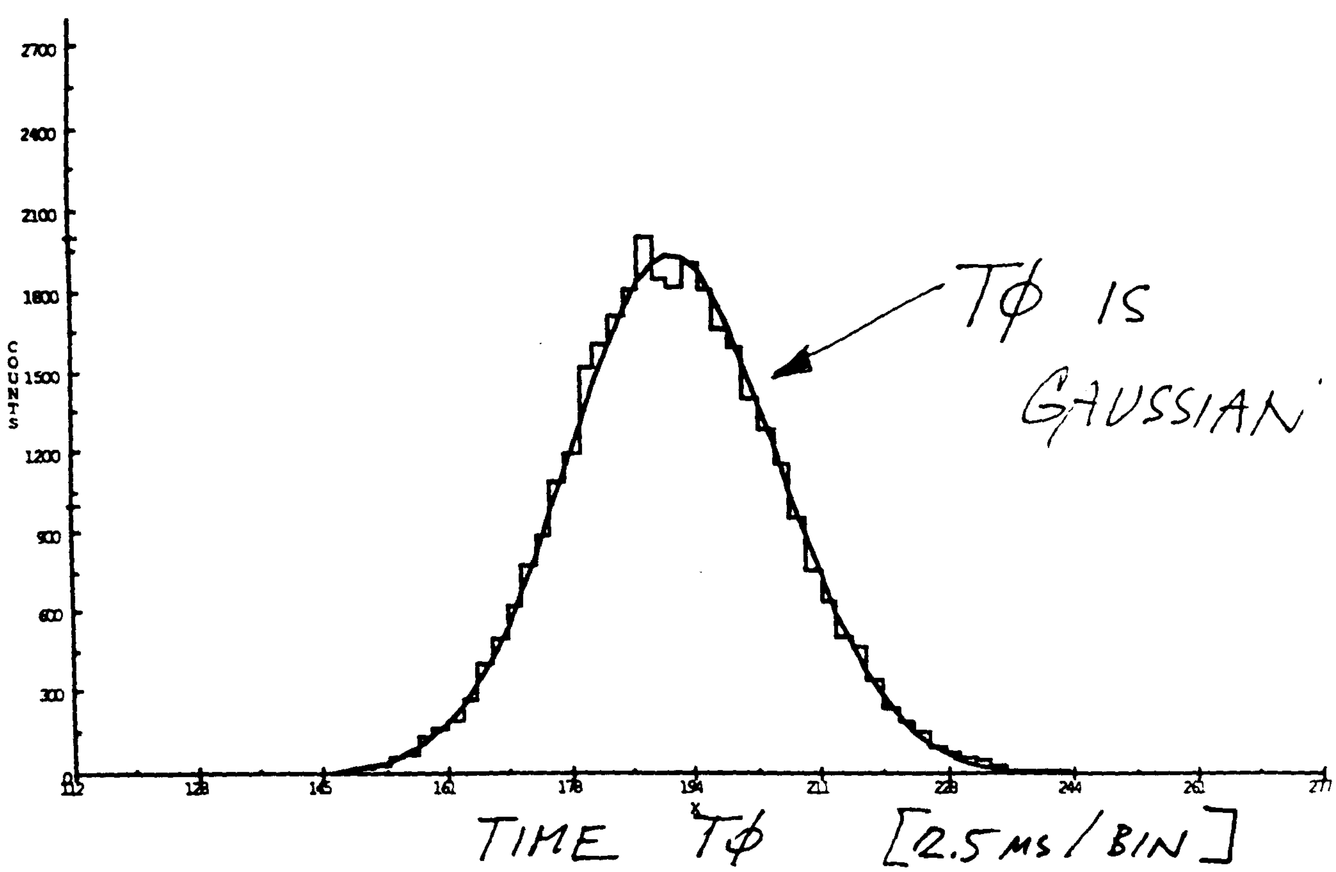

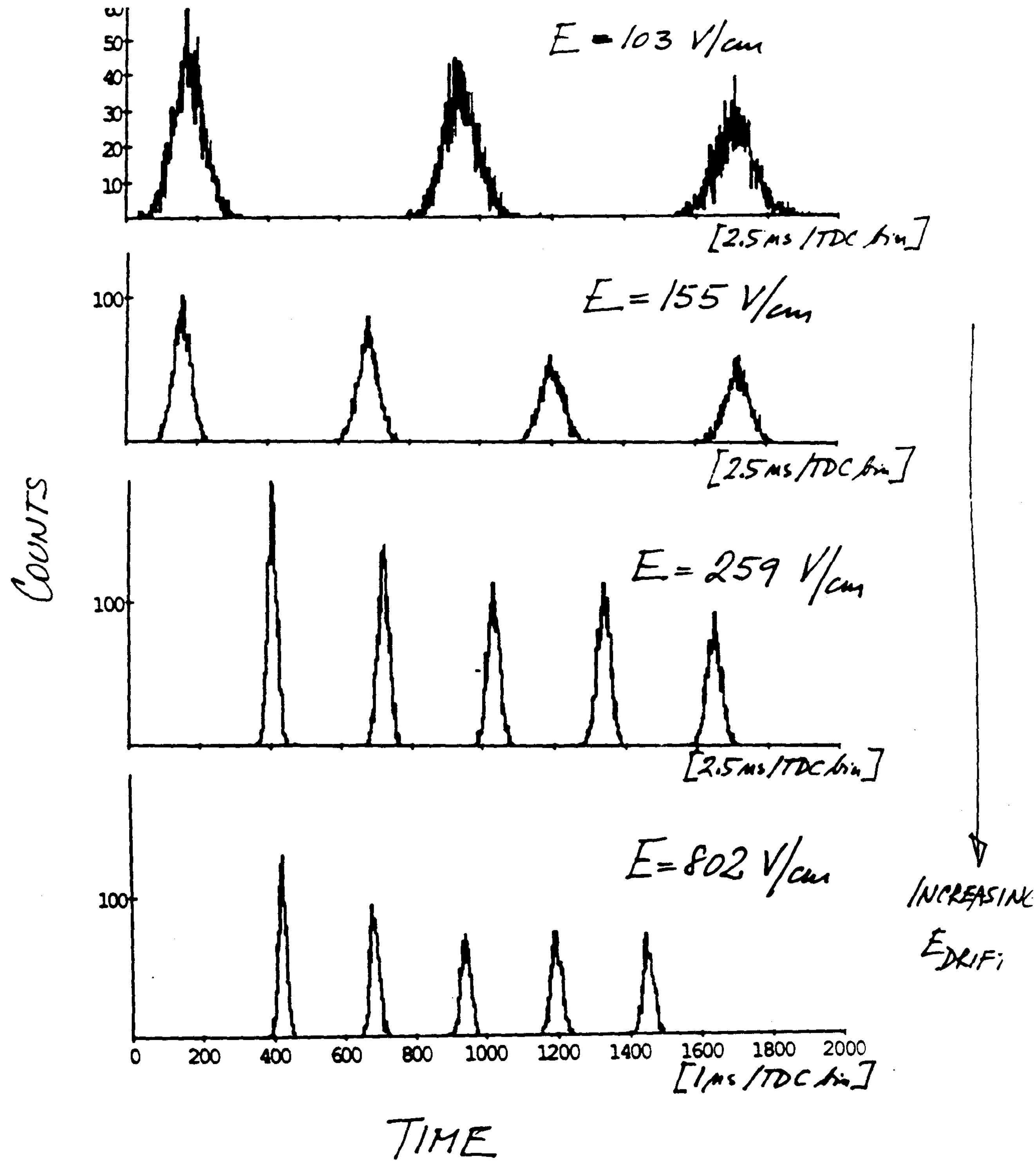

E = 103 V/cm
10
20
30
40
50
[2.5ms/TDC bin]
E = 155 V/cm
100
[2.5ms/TDC bin]
E = 259 V/cm
100
[2.5ms/TDC bin]
E = 802 V/cm
100
0
200
400
600
800
1000
1200
1400
1600
1800
2000
[1ms/TDC bin]
COUNTS
TIME
INCREASING
EDRIFT

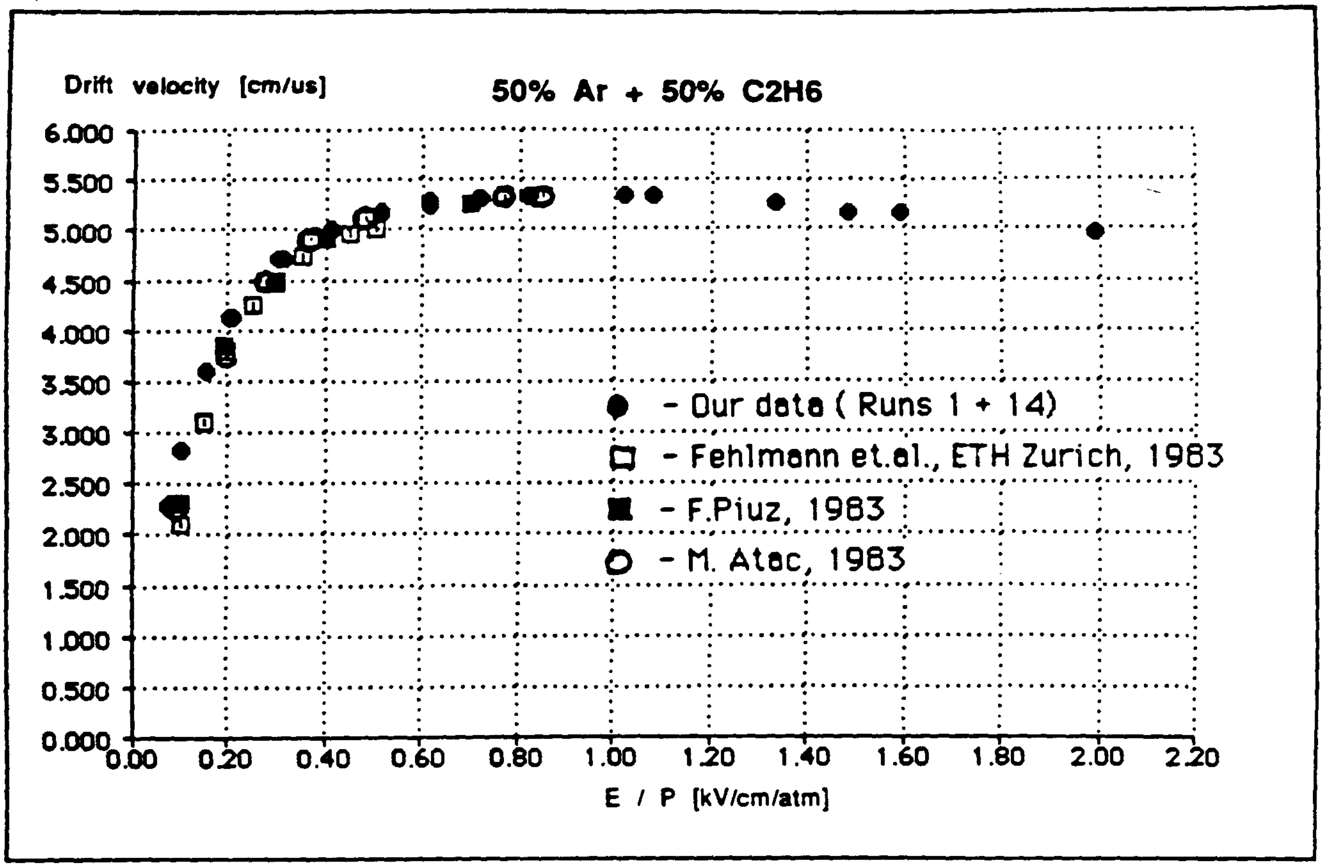
Drift velocity [cm/us]
50% Ar + 50% C2H6
6.000
5.500
5.000
4.500
4.000
3.500
3.000
2.500
2.000
1.500
1.000
0.500
0.000
0.00
0.20
0.40
0.60
0.80
1.00
1.20
1.40
1.60
1.80
2.00
2.20
E / P [kV/cm/atm]
- Our data (Runs 1 + 14)
- Fehlmann et.al., ETH Zurich, 1983
- F.Piuz, 1983
- M. Atac, 1983

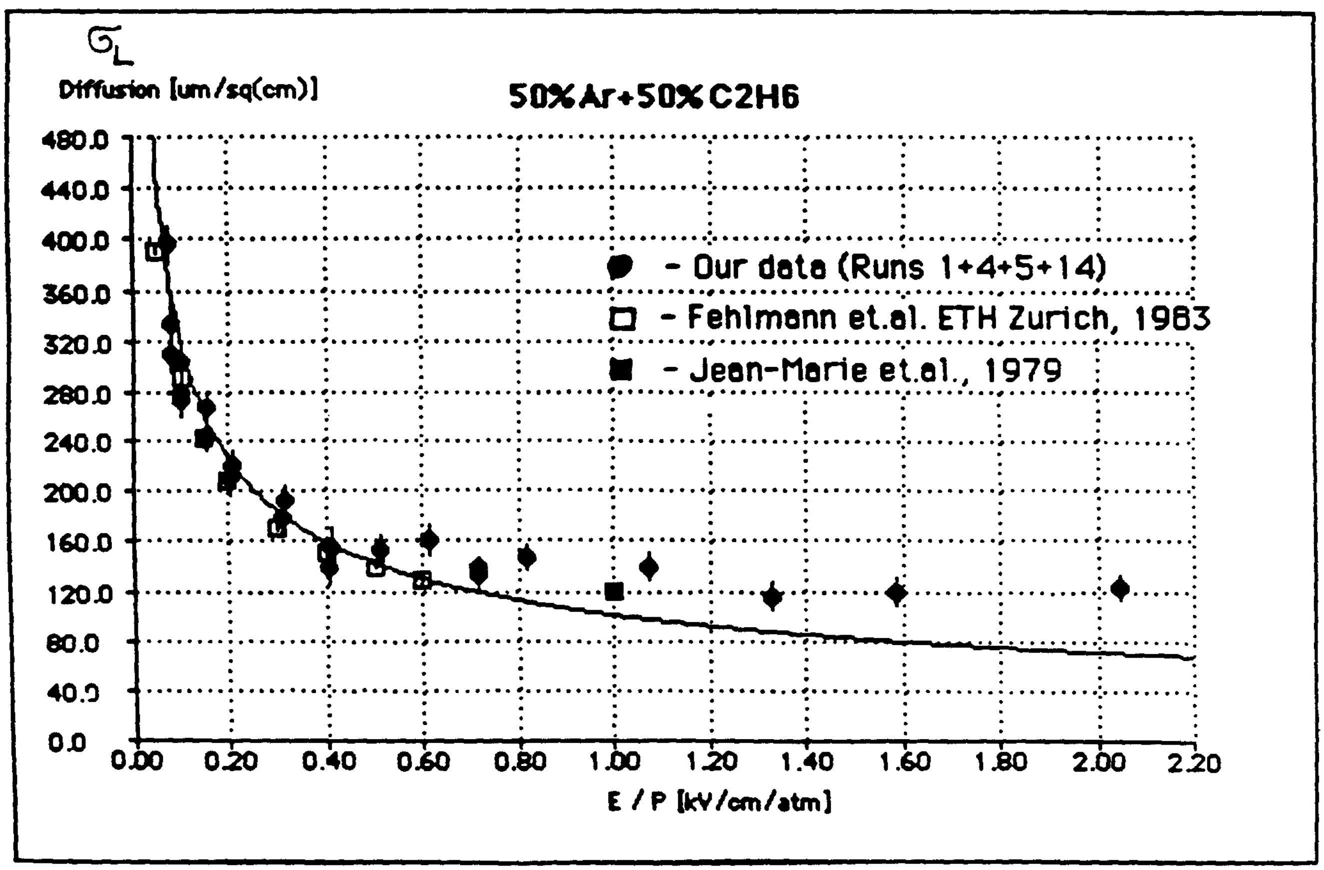
σL
Diffusion [um/sq(cm)]
50%Ar+50%C2H6
480.0
440.0
400.0
360.0
320.0
280.0
240.0
200.0
160.0
120.0
80.0
40.0
0.0
0.00
0.20
0.40
0.60
0.80
1.00
1.20
1.40
1.60
1.80
2.00
2.20
E / P [kV/cm/atm]
- Our data (Runs 1+4+5+14)
- Fehlmann et.al. ETH Zurich, 1983
- Jean-Marie et.al., 1979

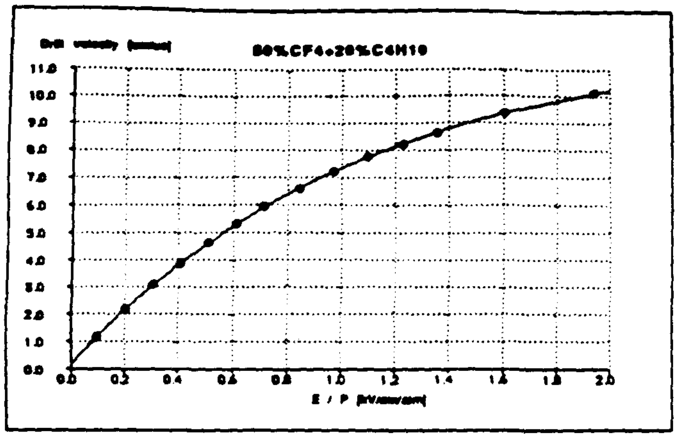
80%CF4+20%C4H10
E / P

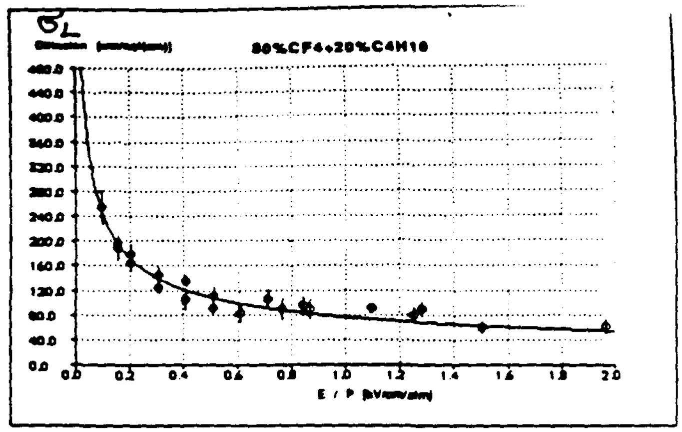
80%CF4+20%C4H10
E / P

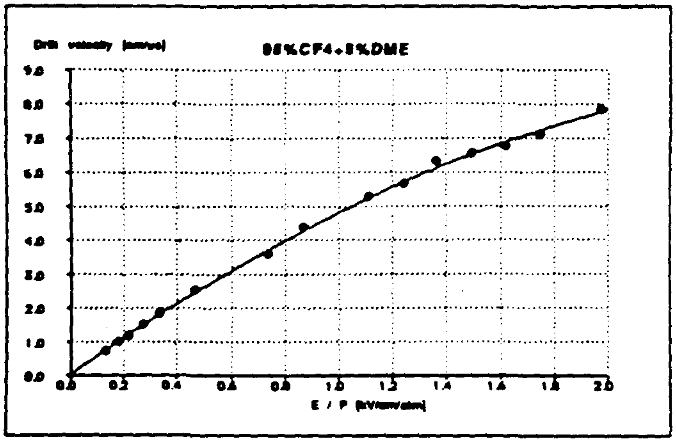
95%CF4+5%DME
E / P

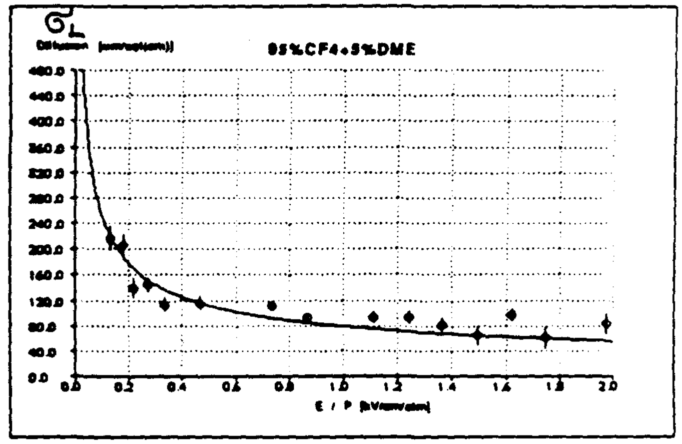
95%CF4+5%DME
E / P

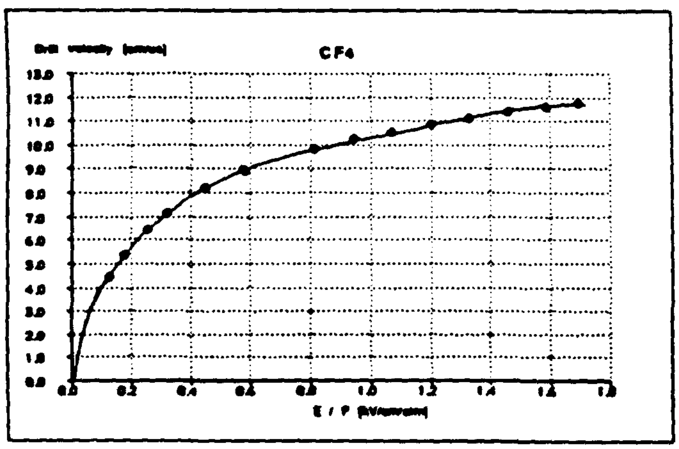
CF4
E / P

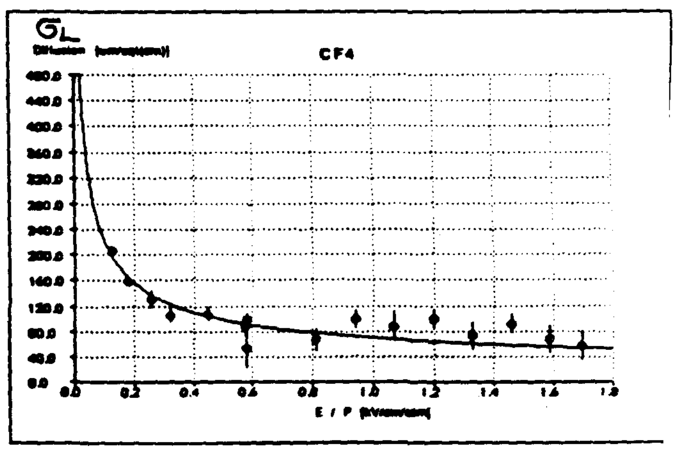
CF4
E / P

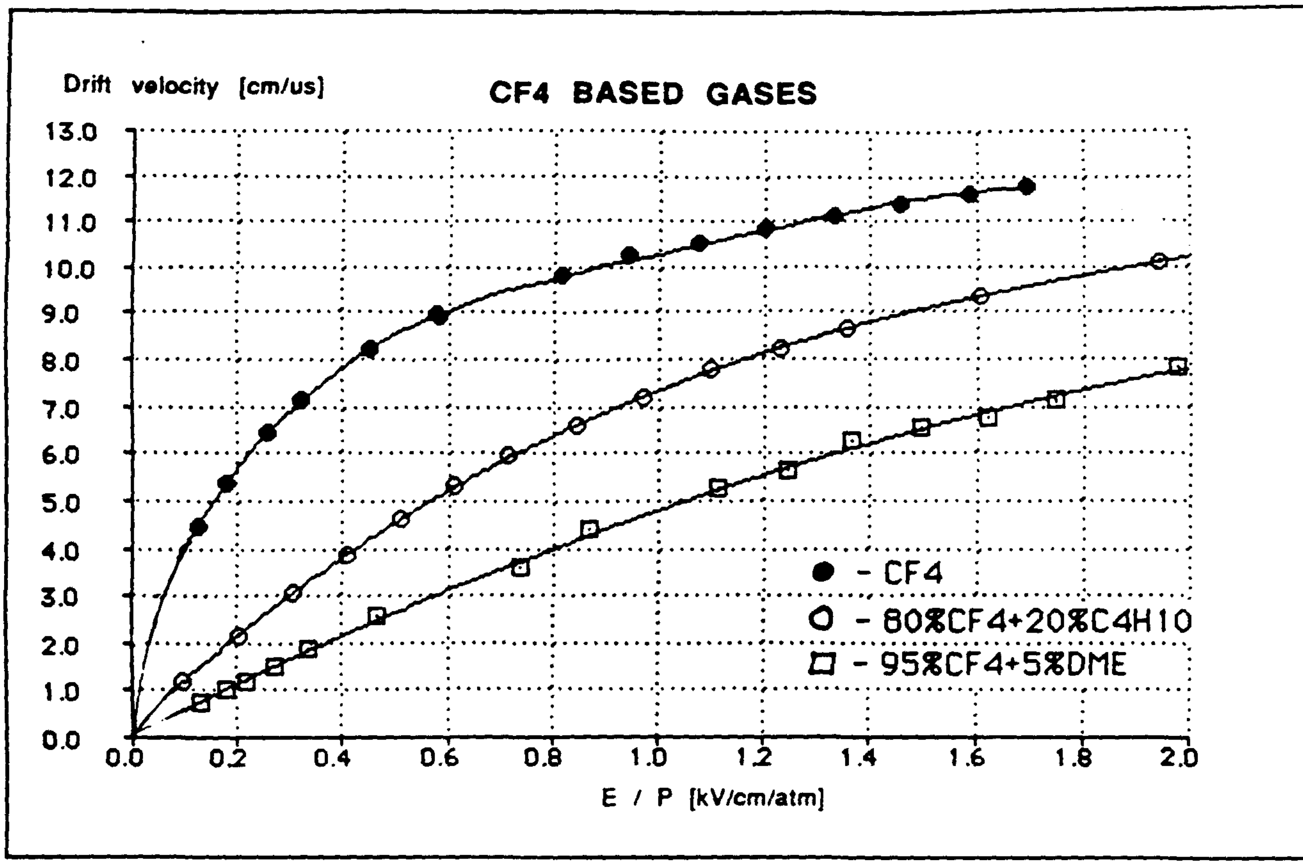

- EVEN SMALL AMOUNT OF DME WILL CONSIDERABLY SLOW DOWN THE VELOCITY.

- CF_4 QUENCHES AT LOW ENOUGH GAINS ($\lesssim 5 \times 10^5$)

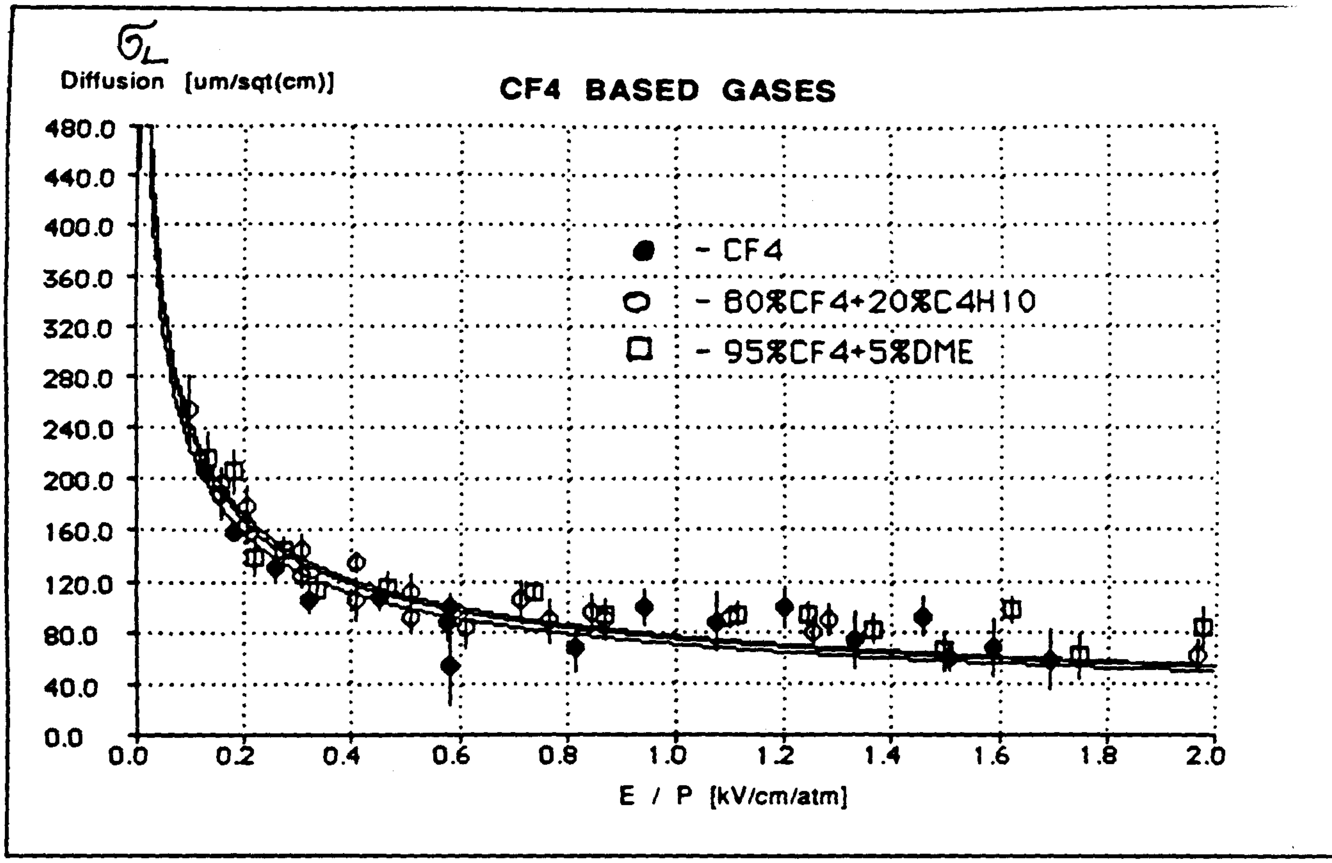

GAS	FIT
● – CF_4	$(70.0 \pm 1.5)/\sqrt{E/p}$
□ – 95% CF_4 + 5% DME	$(74.6 \pm 2.7)/\sqrt{E/p}$
○ – 80% CF_4 + 20% C_4H_{10}	$(76.6 \pm 1.9)/\sqrt{E/p}$

S.R. HUNTER, J.G. CARTER AND L.G. CHRISTOPHOROU
(J. APPL. PHYS. 58 (8) 1985)

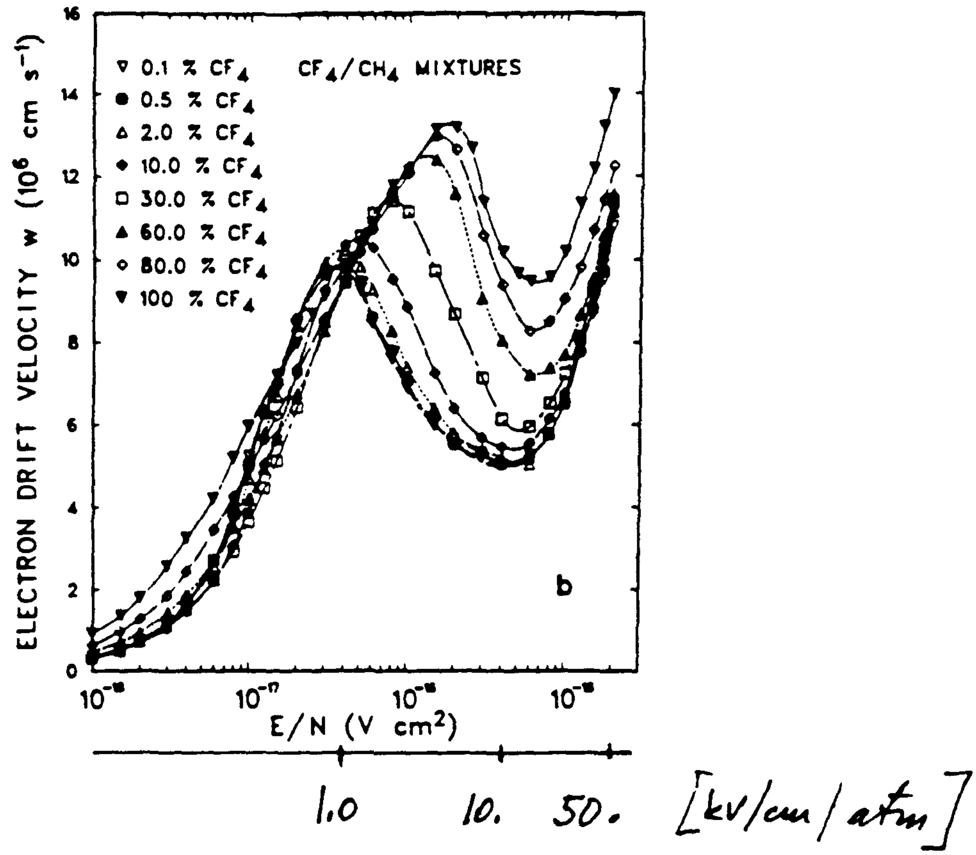

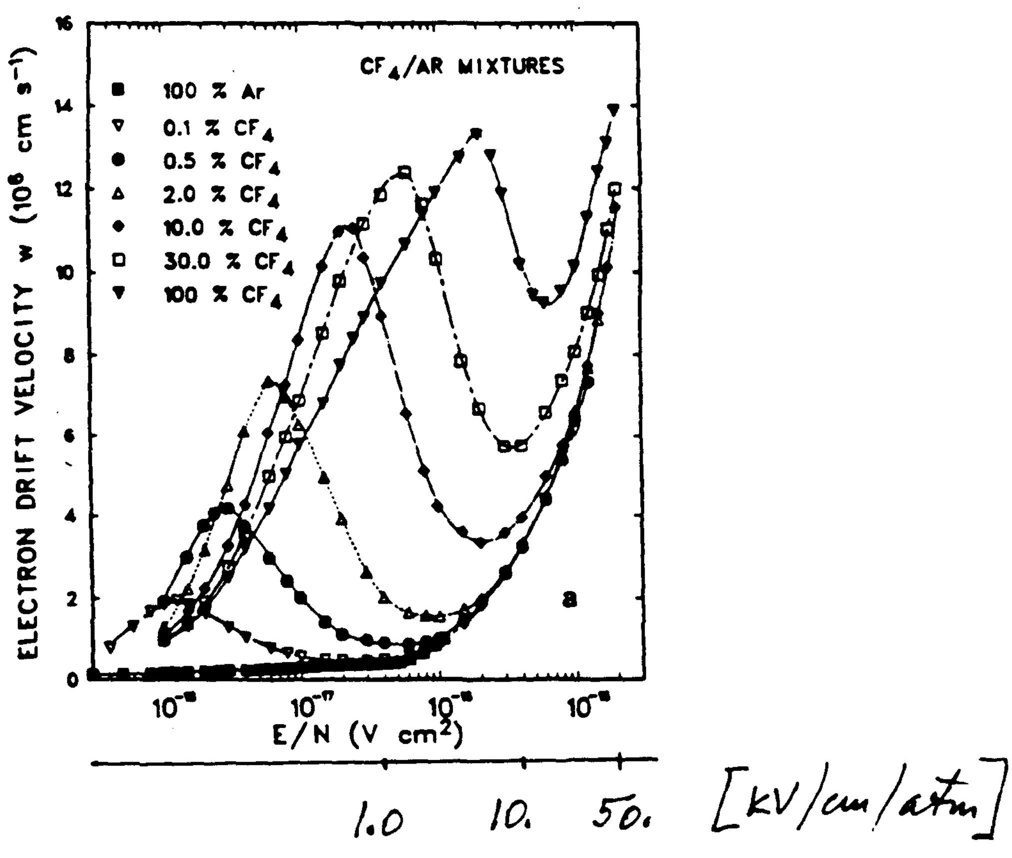

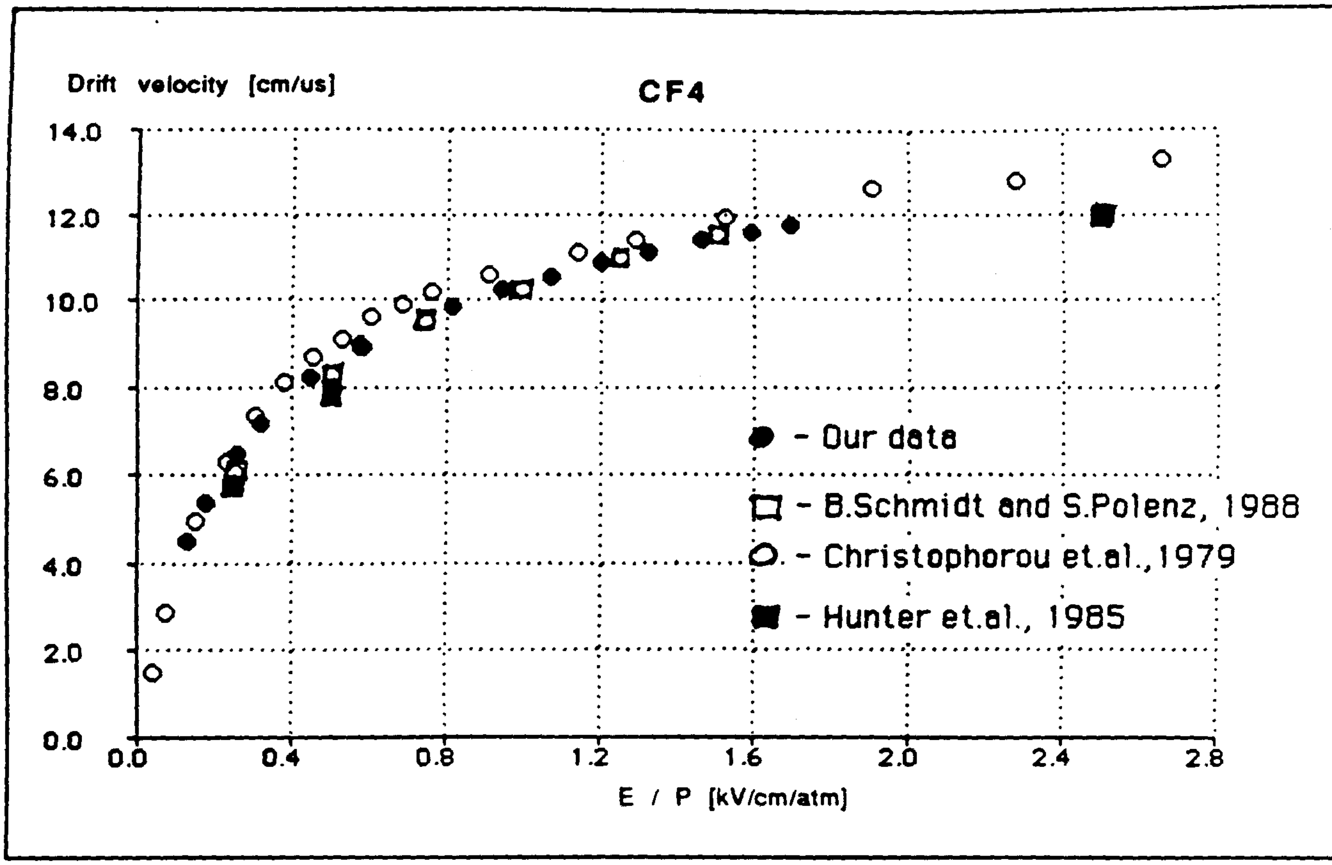
Drift velocity [cm/us]
CF4
14.0
12.0
10.0
8.0
6.0
4.0
2.0
0.0
0.0
0.4
0.8
1.2
1.6
2.0
2.4
2.8
E / P [kV/cm/atm]
- Our data
- B.Schmidt and S.Polenz, 1988
- Christophorou et.al.,1979
- Hunter et.al., 1985

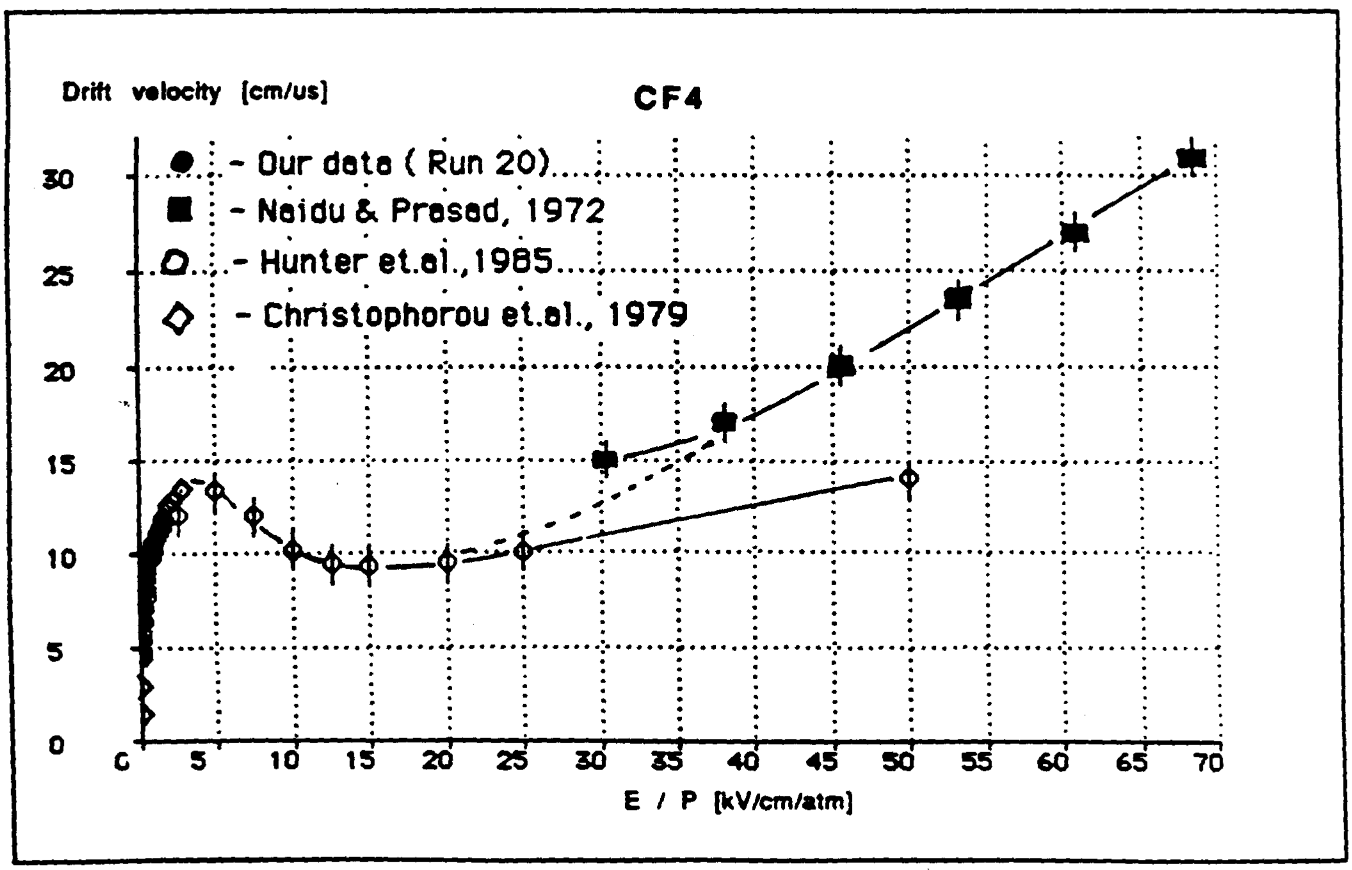
Drift velocity [cm/us]
CF4
- Our data (Run 20)
- Naidu & Prasad, 1972
- Hunter et.al.,1985
- Christophorou et.al., 1979
30
25
20
15
10
5
0
0
5
10
15
20
25
30
35
40
45
50
55
60
65
70
E / P [kV/cm/atm]

INFLUENCE OF INTRINSIC WIRE RESOLUTION AND MULTIPLE SCATTERING IN THE GAS ON VARIOUS PHYSICS ANALYSES

– P. BURCHAT WORK

Intrinsic Wire Resolution:	150 μm	300 μm	150 μm
Radiation Length:	600 m (He)	600 m (He)	100 m (Ar)
ν_τ mass limit			
$\tau \to 5\pi^\pm\nu_\tau$:	3.8 MeV	4.1 MeV	5.3 MeV
$\tau \to KK\pi\nu_\tau$:	4.9 MeV	5.9 MeV	7.0 MeV
$B \to \pi^+\pi^-$			
Invariant mass resolution:	23 MeV	30 MeV	35 MeV
$B \to J/\psi K_S$			
Reconstruction efficiency:	44%	42%	40%
Δz resolution:	59 μm	62 μm	64 μm
$B \to D^+D^-$, $D \to K\pi\pi$			
D mass resolution:	4.6 MeV	4.9 MeV	8.1 MeV
B mass resolution:	6.6 MeV	7.5 MeV	12 MeV
Signal-to-noise ratio:	40	30	7

⇒ PHYSICS ANALYSES ARE MORE SENSITIVE TO MULTIPLE SCATTERING IN THE GAS THAN TO INTRINSIC WIRE RESOLUTION.

[NOTE: DME NOT TRIED!]

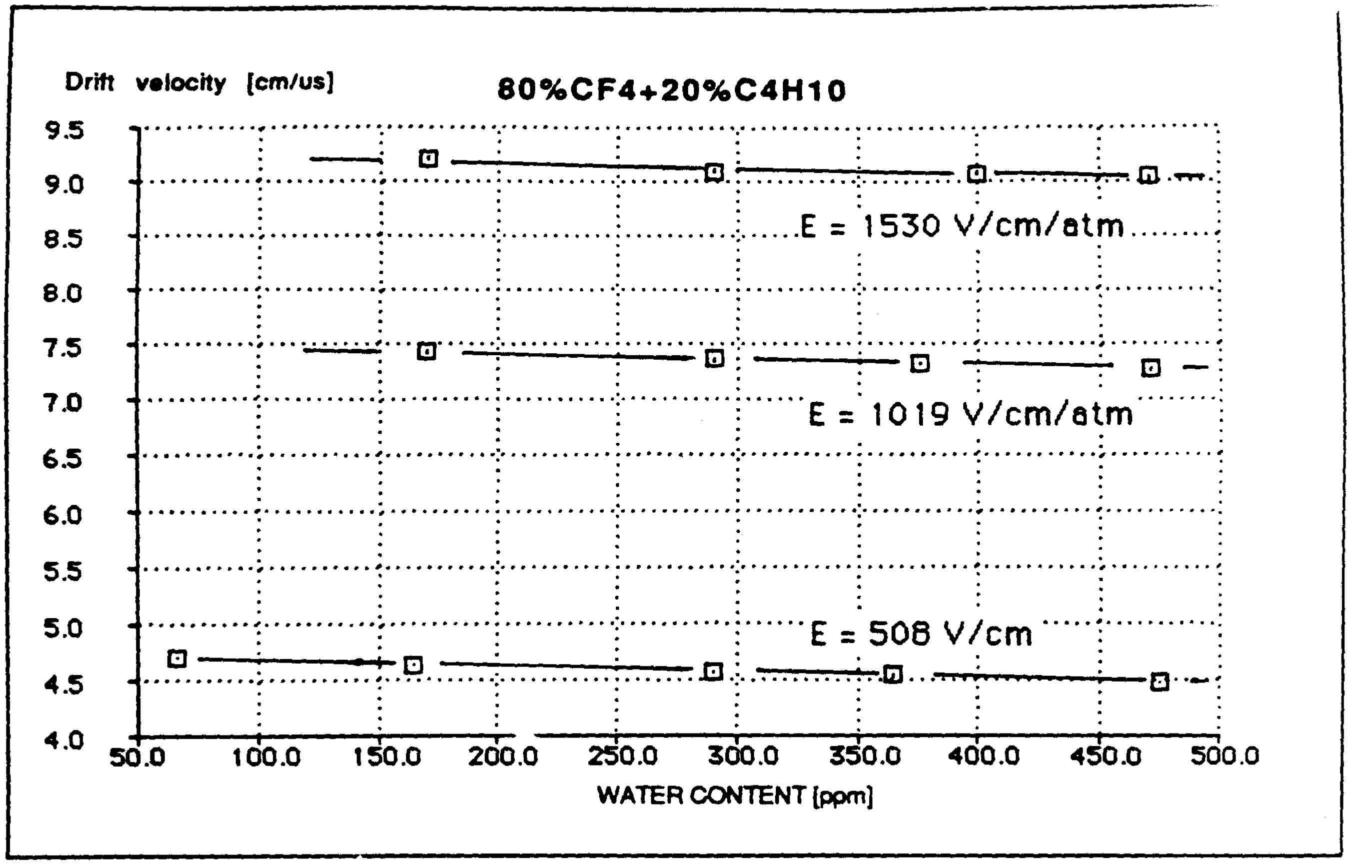
Drift velocity [cm/us]
80%CF4+20%C4H10
9.5
9.0
8.5
8.0
7.5
7.0
6.5
6.0
5.5
5.0
4.5
4.0
E = 1530 V/cm/atm
E = 1019 V/cm/atm
E = 508 V/cm
50.0
100.0
150.0
200.0
250.0
300.0
350.0
400.0
450.0
500.0
WATER CONTENT [ppm]

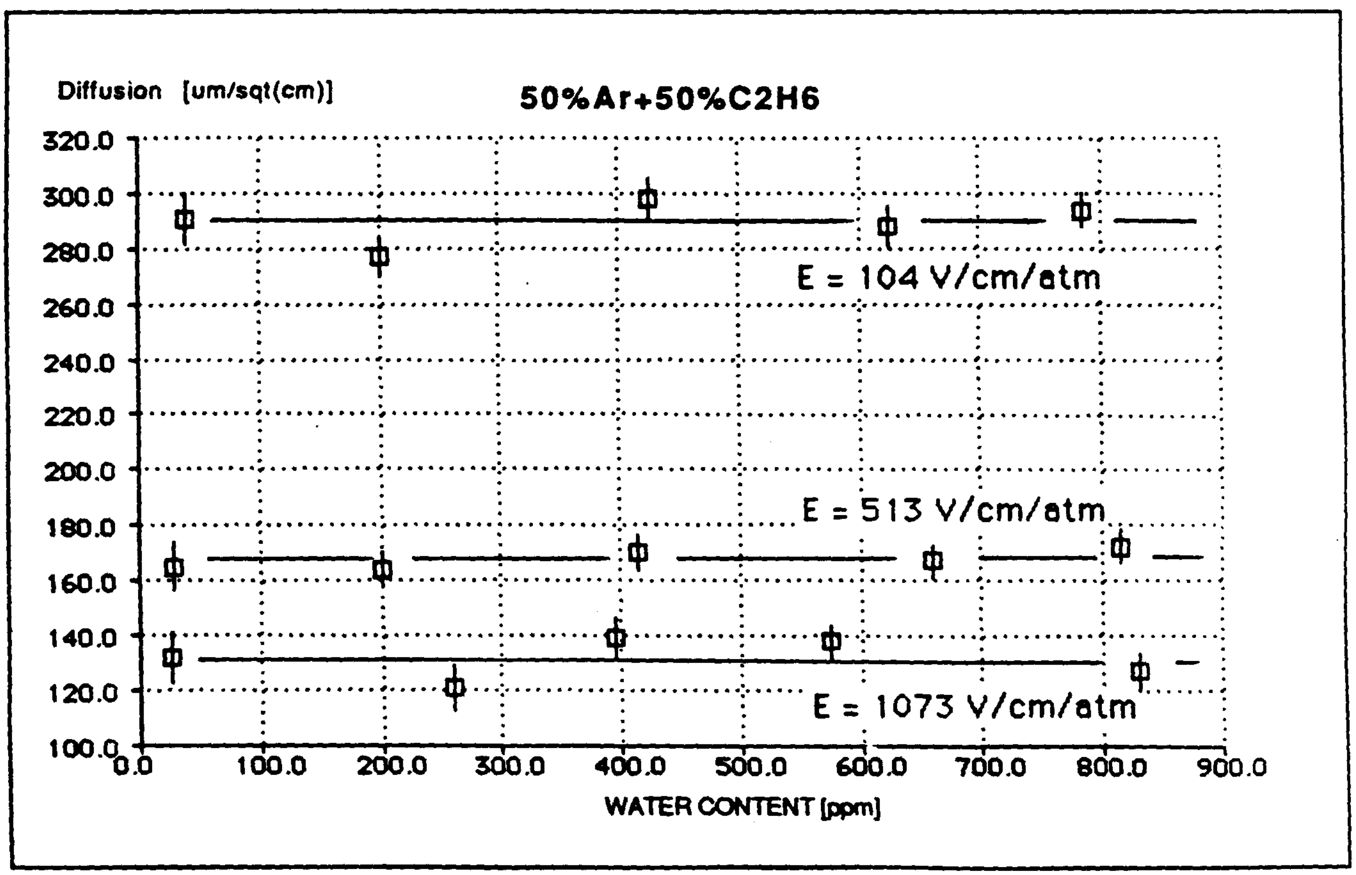
Diffusion [um/sqt(cm)]
50%Ar+50%C2H6
320.0
300.0
280.0
260.0
240.0
220.0
200.0
180.0
160.0
140.0
120.0
100.0
E = 104 V/cm/atm
E = 513 V/cm/atm
E = 1073 V/cm/atm
0.0
100.0
200.0
300.0
400.0
500.0
600.0
700.0
800.0
900.0
WATER CONTENT [ppm]

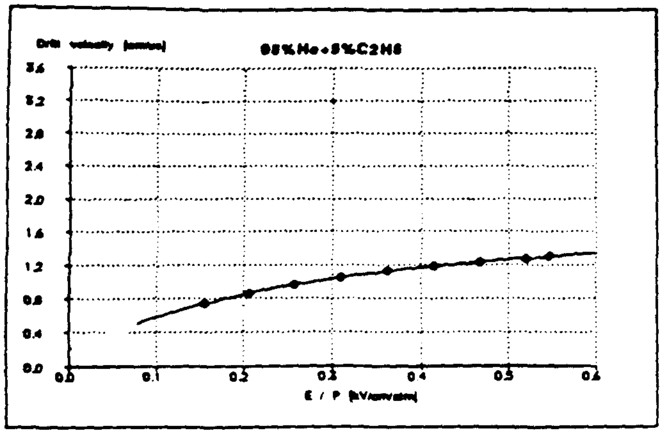
Drift velocity (cm/us)
95%He+5%C2H6
E / P (kV/cm/atm)

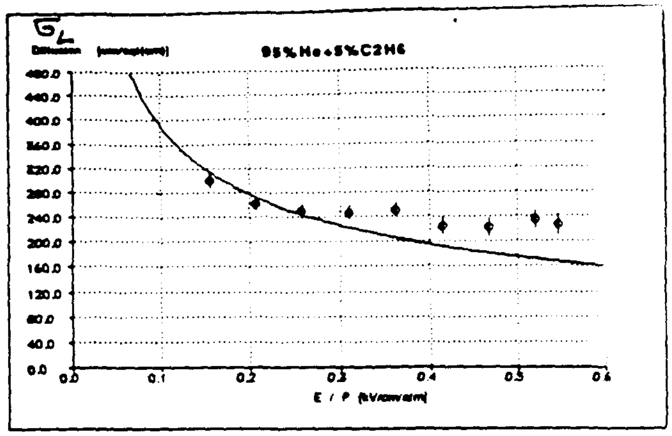
σL
Diffusion (um/sqrt(cm))
95%He+5%C2H6
E / P (kV/cm/atm)

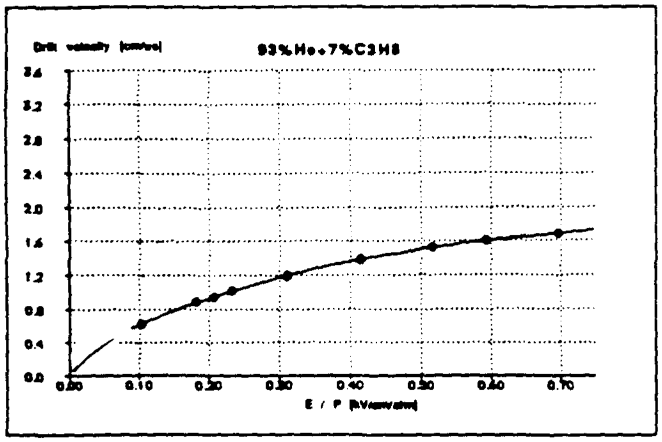
Drift velocity (cm/us)
93%He+7%C3H8
E / P (kV/cm/atm)

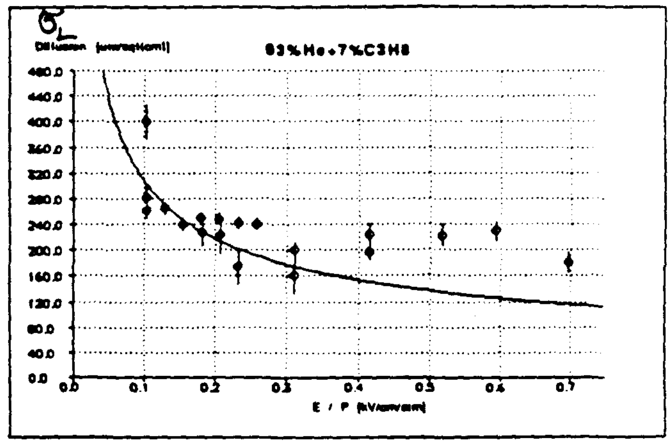
σL
Diffusion (um/sqrt(cm))
93%He+7%C3H8
E / P (kV/cm/atm)

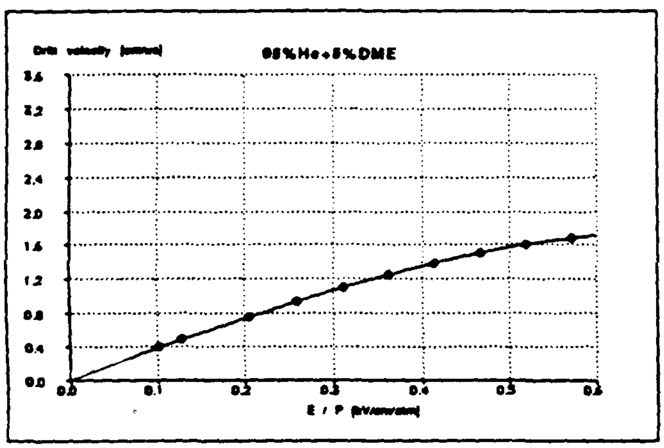
Drift velocity (cm/us)
95%He+5%DME
E / P (kV/cm/atm)

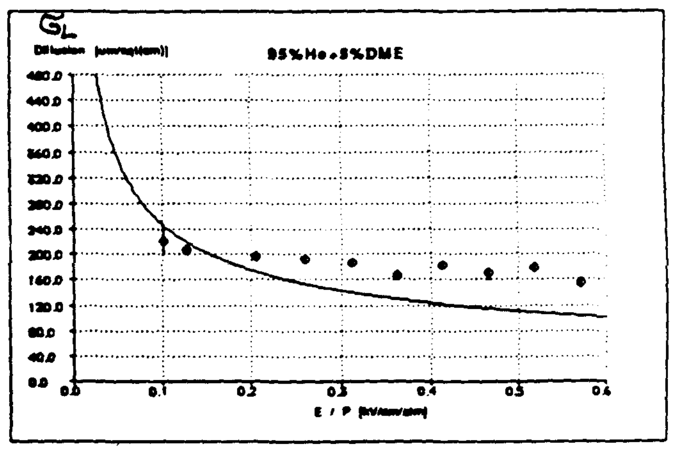
σL
Diffusion (um/sqrt(cm))
95%He+5%DME
E / P (kV/cm/atm)

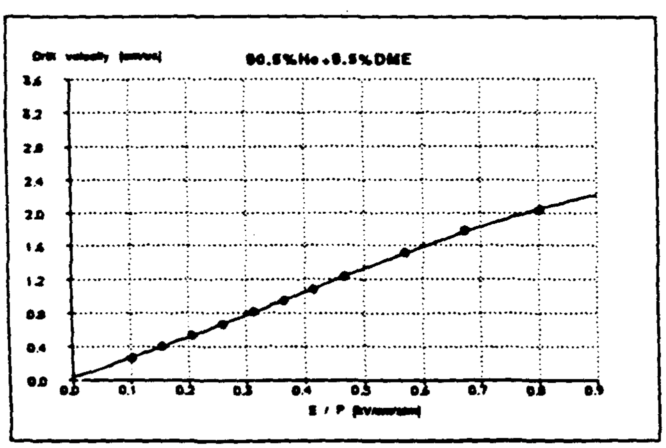
Drift velocity (cm/us)
90.5%He+9.5%DME
E / P (kV/cm/atm)

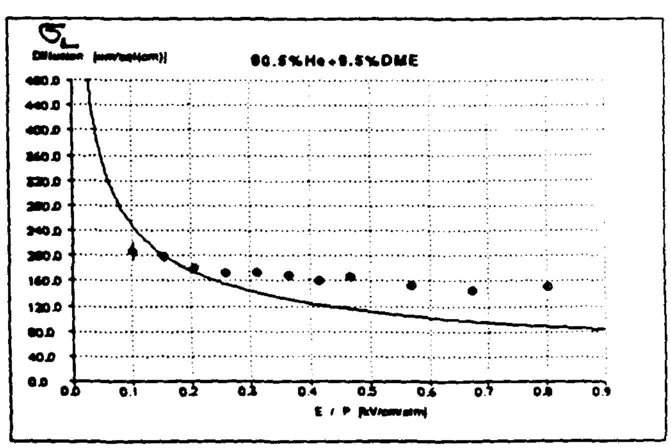
σL
Diffusion (um/sqrt(cm))
90.5%He+9.5%DME
E / P (kV/cm/atm)

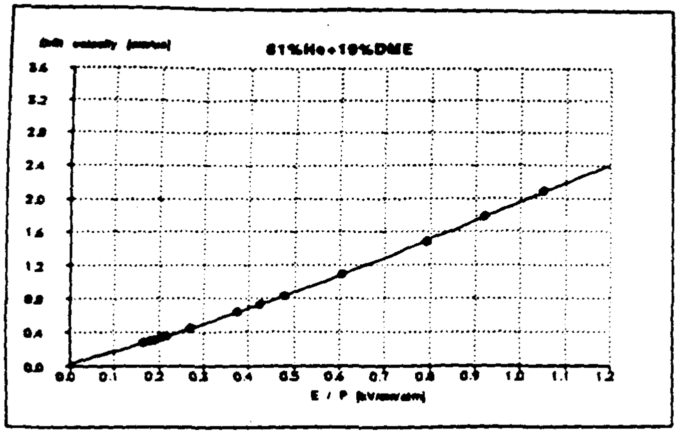
81%He+19%DME

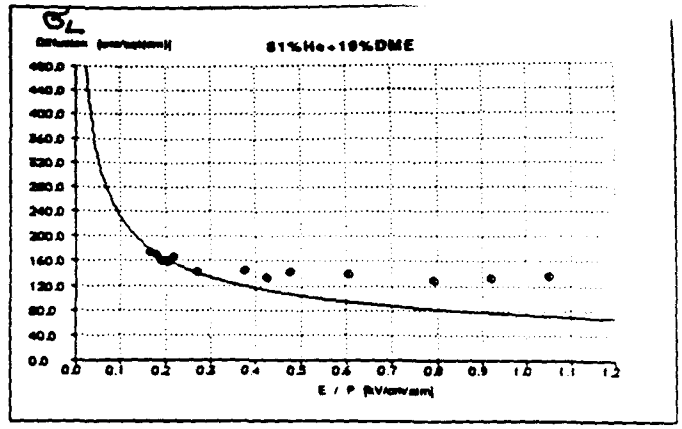
81%He+19%DME

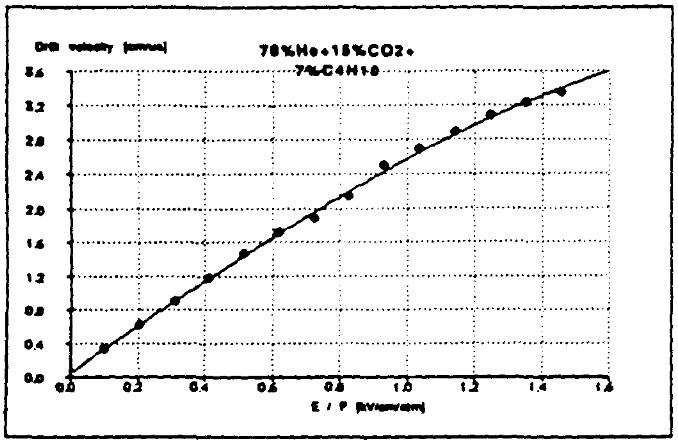
78%He+15%CO2+
7%C4H10

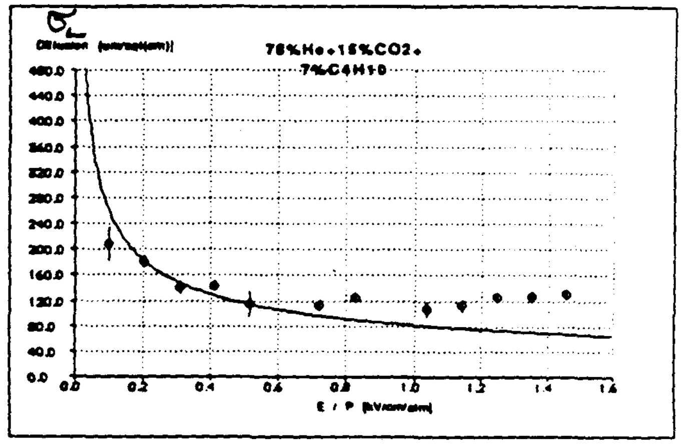
78%He+15%CO2+
7%C4H10

CHARACTERISTIC ELECTRON ENERGY.

- It is a measure how much an electron heats up while drifting relative to a "cool" gas behavior.

$$\varepsilon_{L,T} = \frac{e D_{L,T}}{\mu} = \frac{e D_{L,T} E}{v} \geq kT \cong 0.025\,eV$$

$D_{L,T}$ – DIFFUSION CONSTANT

μ – ELECTRON MOBILITY

v – ELECTRON VELOCITY

E – ELECTRIC FIELD

POSITION RESOLUTION:

$$\sigma = \sqrt{2 D_{L,T}\, t} = \sqrt{\frac{2 D_{L,T}\, x}{v}} = \sqrt{\frac{2 \varepsilon_{L,T}\, x}{e E}}$$

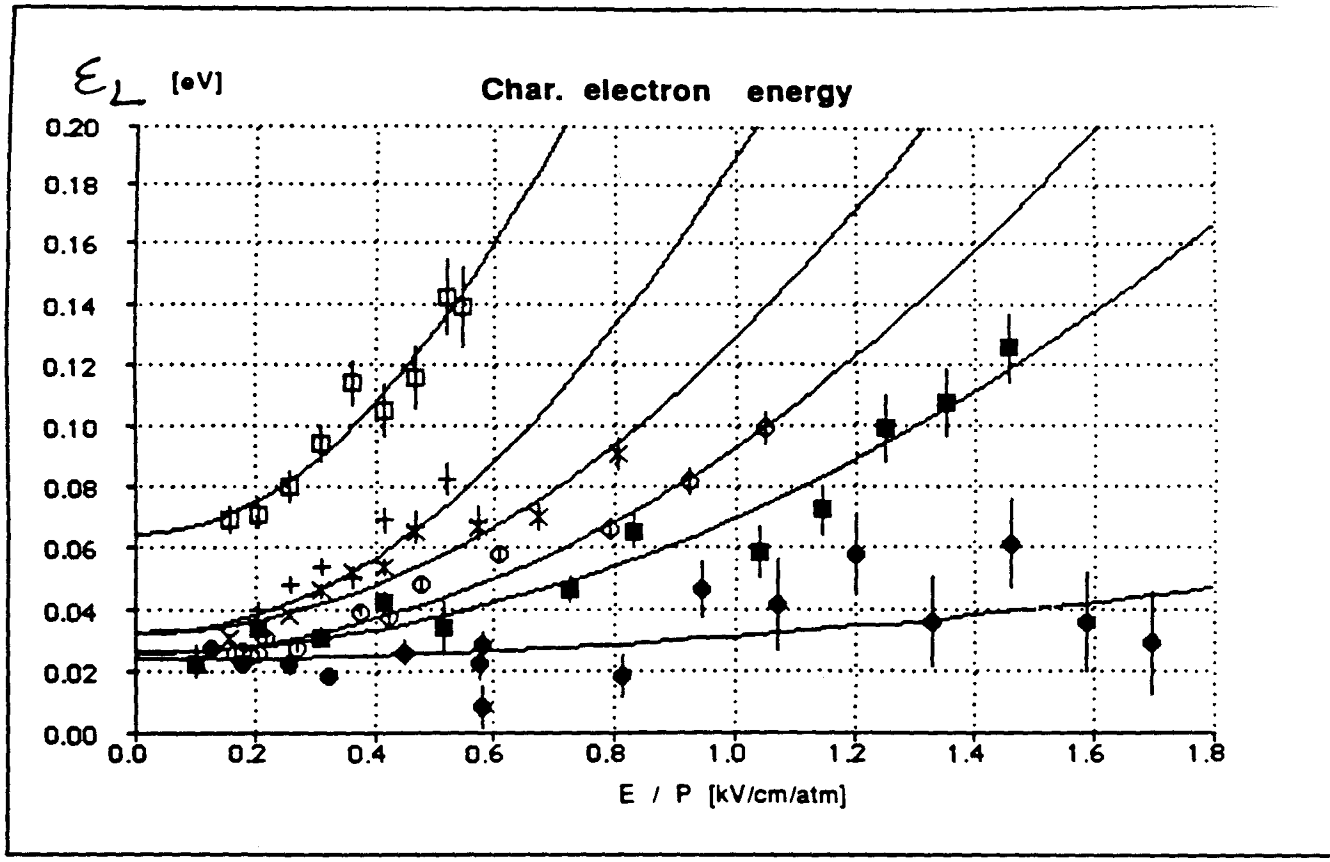

GAS	FIT
□ - 95% He + 5% C_2H_6	$0.063 + 0.282 \times (E/p)^2$
+ - 95% He + 5% DME	$0.028 + 0.195 \times (E/p)^2$
× - 90.5% He + 9.5% DME	$0.030 + 0.117 \times (E/p)^2$
○ - 81% He + 19% DME	$0.024 + 0.075 \times (E/p)^2$
■ - 78% He + 15% CO_2 + 7% C_4H_{10}	$0.026 + 0.044 \times (E/p)^2$
● - CF_4	$0.024 + 0.0072 \times (E/p)^2$

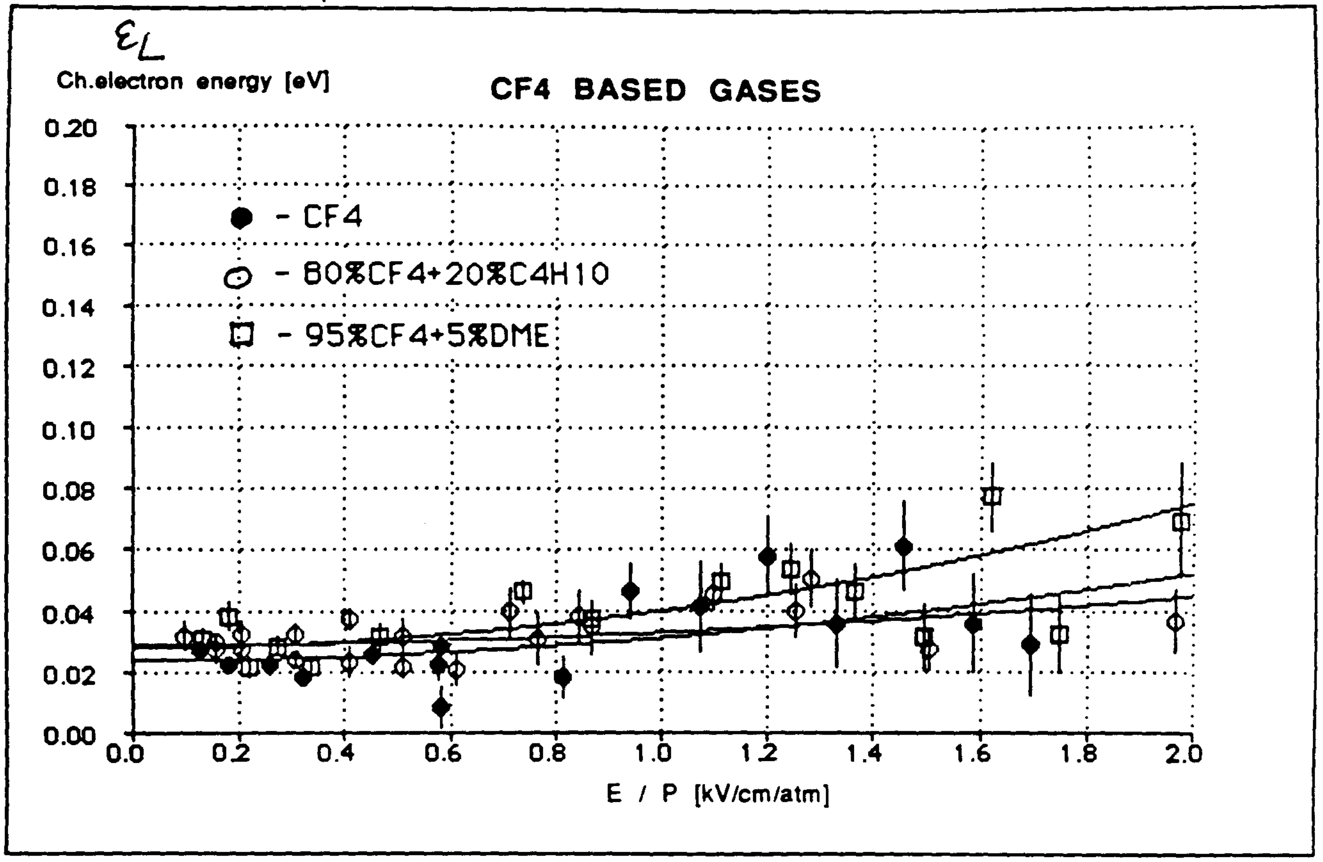

GAS	FIT
● - CF_4	$0.024 + 0.0072(E/p)^2$
○ - 80% CF_4 + 20% C_4H_{10}	$0.029 + 0.004(E/p)^2$
□ - 95% CF_4 + 5% DME	$0.028 + 0.0119(E/p)^2$

RELATIVE CATHODIC BREAKDOWN IN OUR STRUCTURE

IN VARIOUS GASES.

GAS	E_{drift} [kV/cm/atm]	
50% Ar + 50% C2H6	> 2.0	LIMITED BY P.S.
95% CF4 + 5% DME	> 2.0	LIMITED BY P.S.
80% CF4 + 20% C4H10	> 2.0	LIMITED BY P.S.
CF4	1.7	
78%He+15%CO2+7%C4H10	1.45	
81% He + 19% DME	1.05	
90.5% He + 9.5% DME	0.8	
95% He + 5% DME	0.58	
95% He + 5% C2H6	0.55	
93% He + 7% C3H8	0.7	

Note :

The numbers are to be taken only in relative sense !!!

POLYA FUNCTION:

$$P(q) = \frac{1+\theta}{\bar{q}\,\Gamma(1+\theta)}\left[(1+\theta)\frac{q}{\bar{q}}\right]^{\theta} e^{-(1+\theta)q/\bar{q}}$$

$q = ne^-$

$\bar{q}$ – MEAN CHARGE

FOR $\theta = 0$ $\quad P(q) = \frac{1}{\bar{q}}\, e^{-q/\bar{q}}$

FOR $\theta < 0$ $\quad P(q)$ FALLS FASTER THAN EXPONENTIAL FUNCTION

FOR $\theta > 0$ $\quad P(q)$ GETS A "TURNOVER" SHAPE.

SINGLE ELECTRON PULSE HEIGHT SPECTRA

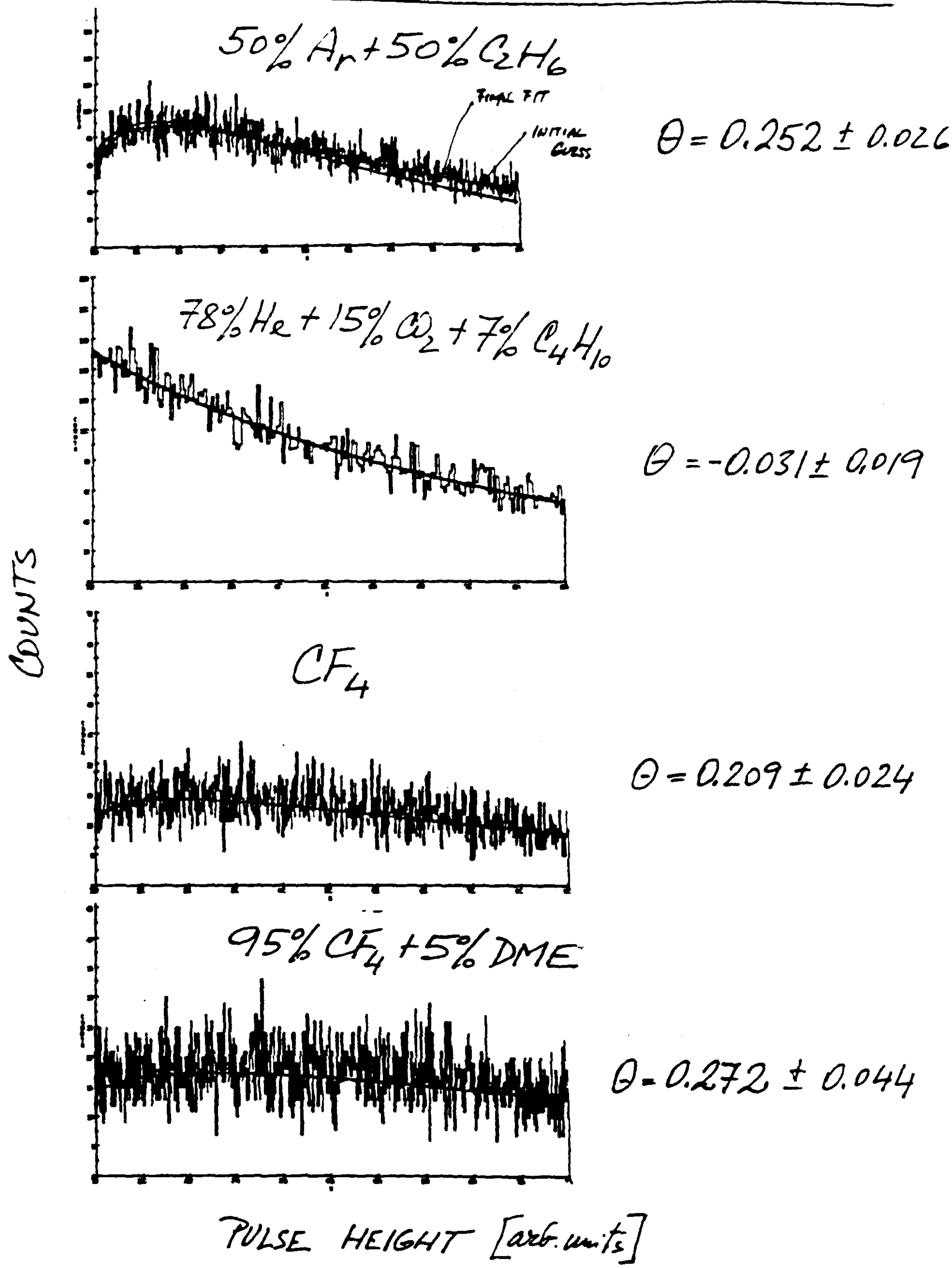

SUMMARY OF <u>POLYA FITS</u> TO SINGLE ELECTRON PULSE HEIGHTS.

GAS	V_c [kV]	Appr. $r_a \cdot E_a$ [V]	$\overline{q}$ MEAN VISIBLE GAIN	Θ	χ^2/n_D
50% Ar+50% C2H6	-1.5	311	2.5×10^5	0.252 ± 0.026	1.05
CF4	-1.95	396	3.8×10^5	0.209 ± 0.024	1.02
95% CF4 + 5% DME	-1.85	377	4.5×10^5	0.272 ± 0.044	1.04
80% CF4 + 20% C4H10	-1.7	349	3.4×10^5	0.624 ± 0.043	1.15
95% He + 5% C2H6	-0.85	188	$\approx2.6\times10^4$	-0.9 ±	1.25
93% He + 7% C3H8	-0.97	211	$\sim5.5\times10^4$	-0.537 ± 0.008	1.15
95% He + 5% DME	-0.85	188	$\sim10^4$	-0.897 ±	1.59
90.5% He + 9.5% DME	-1.0	216	$\sim6.5\times10^4$	-0.532 ± 0.013	1.18
81% He + 19% DME	-1.15	245	–	–	–
78%He+15%CO2+ +7%C4H10	-1.35	283	$\sim2.9\times10^5$	-0.031 ± 0.019	1.01

DIFFUSION NEAR THE ANODE WIRE

- F.Villa has suggested in 1983 that it might be an important contribution to resolution for some gases.

$$\epsilon_k = a + b E^2 \Rightarrow \sigma_x = \sqrt{\frac{2 \epsilon_k x}{E}}$$ CAN BE LARGE AT HIGH E

- To my knowledge nobody has addressed it since.

- IN OUR GEOMETRY:

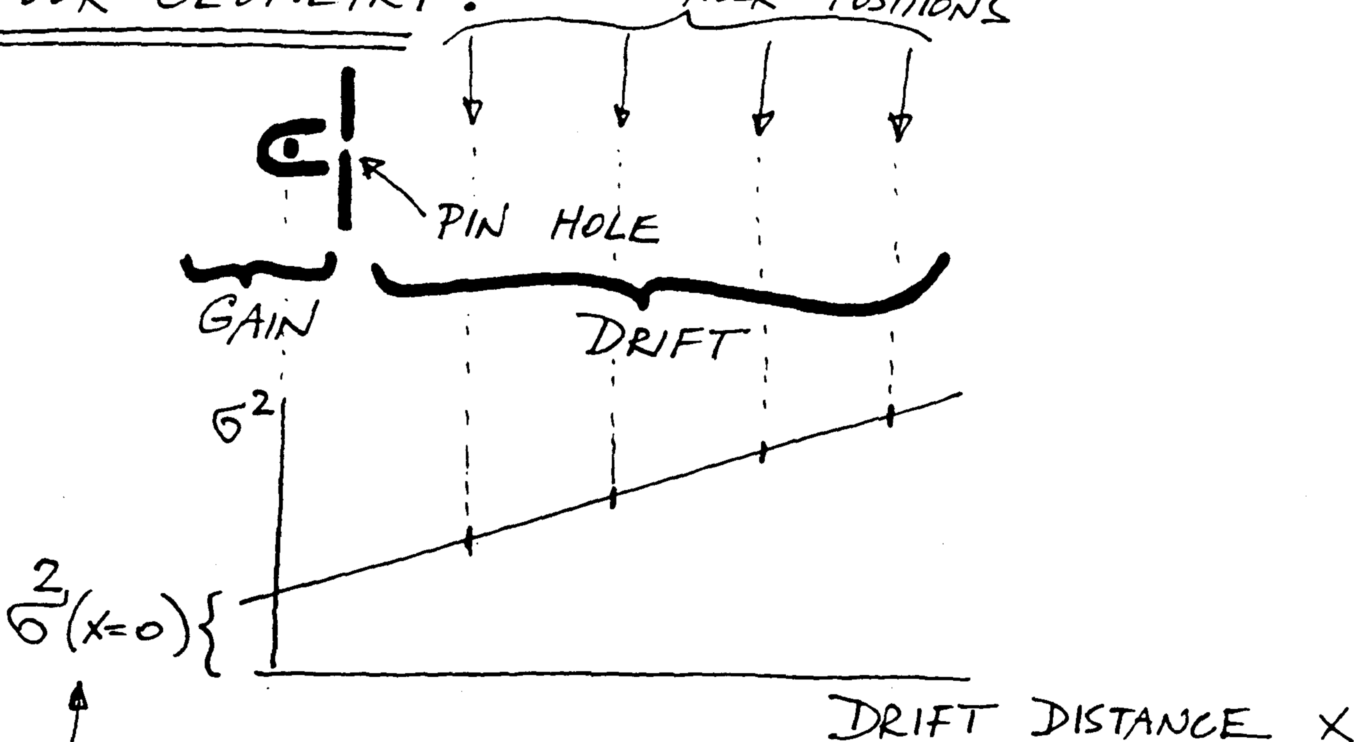

HAS TWO MAJOR CONTRIBUTIONS:

a) $\sigma_{ELECTRONICS}$ (& ITS RESPONSE TO AVALANCHE FLUCTUATIONS, ION. STATISTICS, GEOMETRY ETC)

b) $\sigma_{NEAR\ WIRE\ DIFFUSION}$

ESTIMATE OF $\sigma_{ELECTRONICS}$ & $\sigma_{NEAR\ WIRE\ DIFFUSION}$

$\sigma_{NEAR\ WIRE\ DIFFUSION}$ – CALCULATE NUMERICALY

a) IF WE KNOW v_{DRIFT} & ε_L AT HIGH E

- STEP IN 100 psec STEPS
- IN EACH STEP EVALUATE

$$\sigma_x = \sqrt{2Dt} = \sqrt{2t\frac{\varepsilon_L v}{E}}$$

b) DETERMINE $\varepsilon_L = a + b E^2$ AT LOW E

- STEP IN 10 μm STEPS
- EVALUATE $\sigma_x = \sqrt{\dfrac{2\varepsilon_L x}{E}}$

$\sigma_{ELECTRONICS}$ – CALIBRATE USING A PULSER

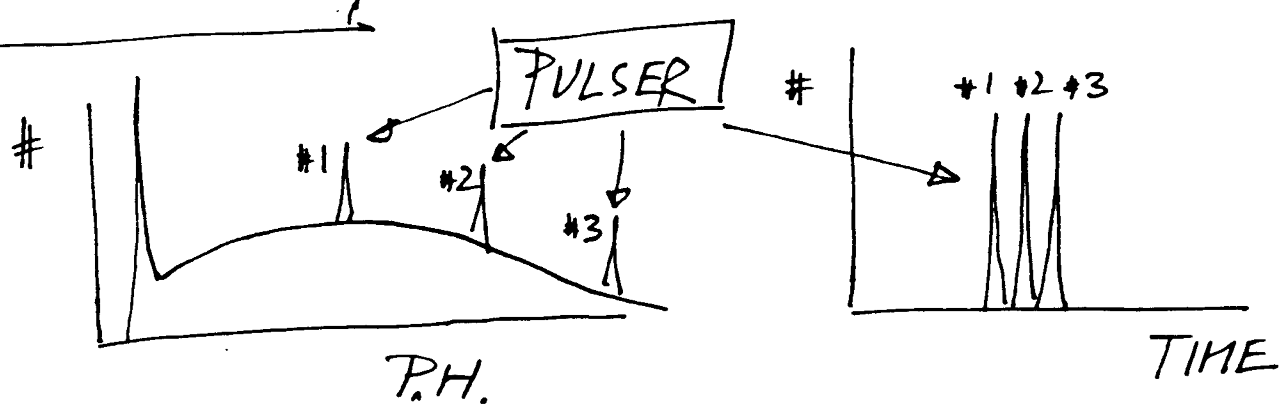

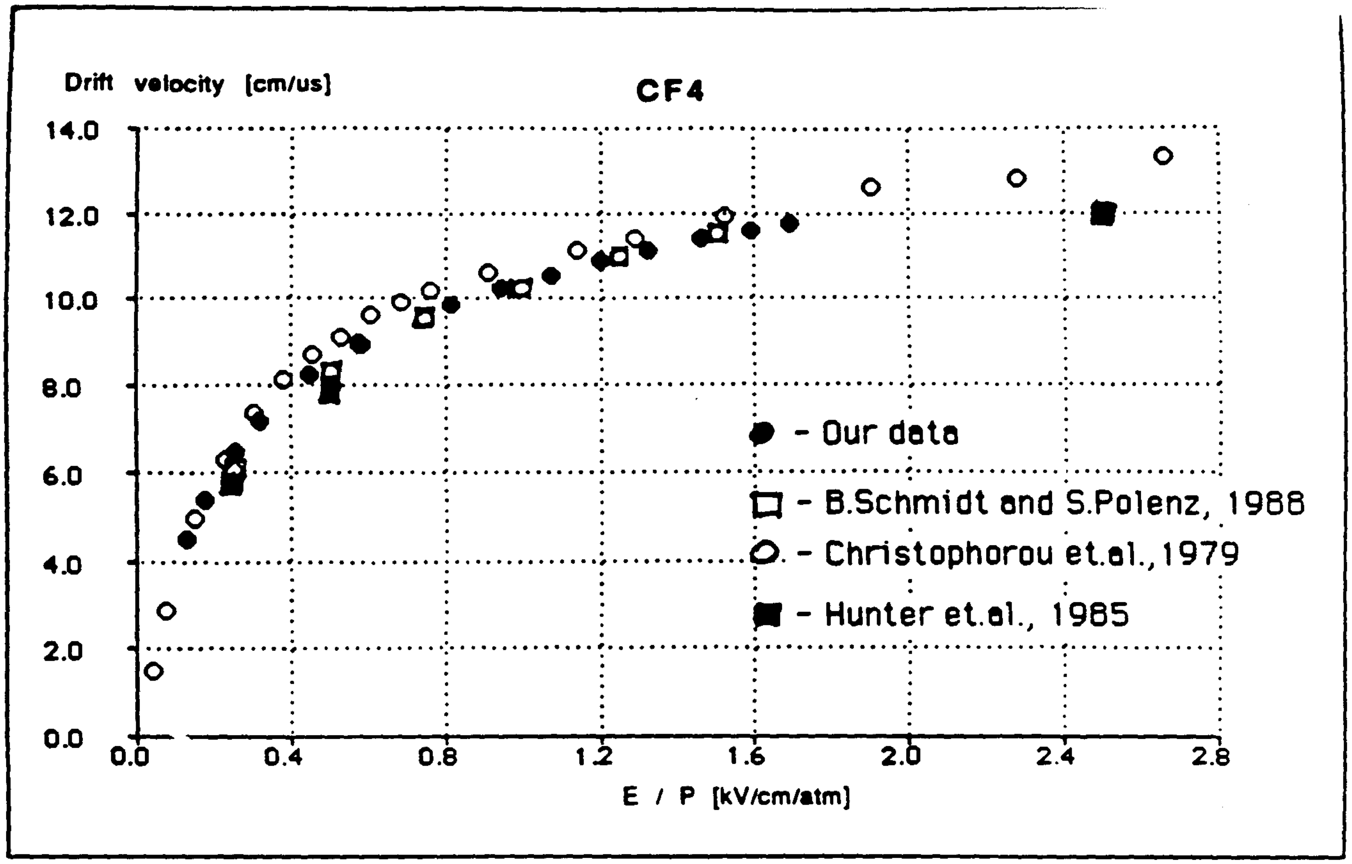

Drift velocity [cm/us]
CF4
14.0
12.0
10.0
8.0
6.0
4.0
2.0
0.0
0.0
0.4
0.8
1.2
1.6
2.0
2.4
2.8
E / P [kV/cm/atm]
- Our data
- B.Schmidt and S.Polenz, 1988
- Christophorou et.al.,1979
- Hunter et.al., 1985

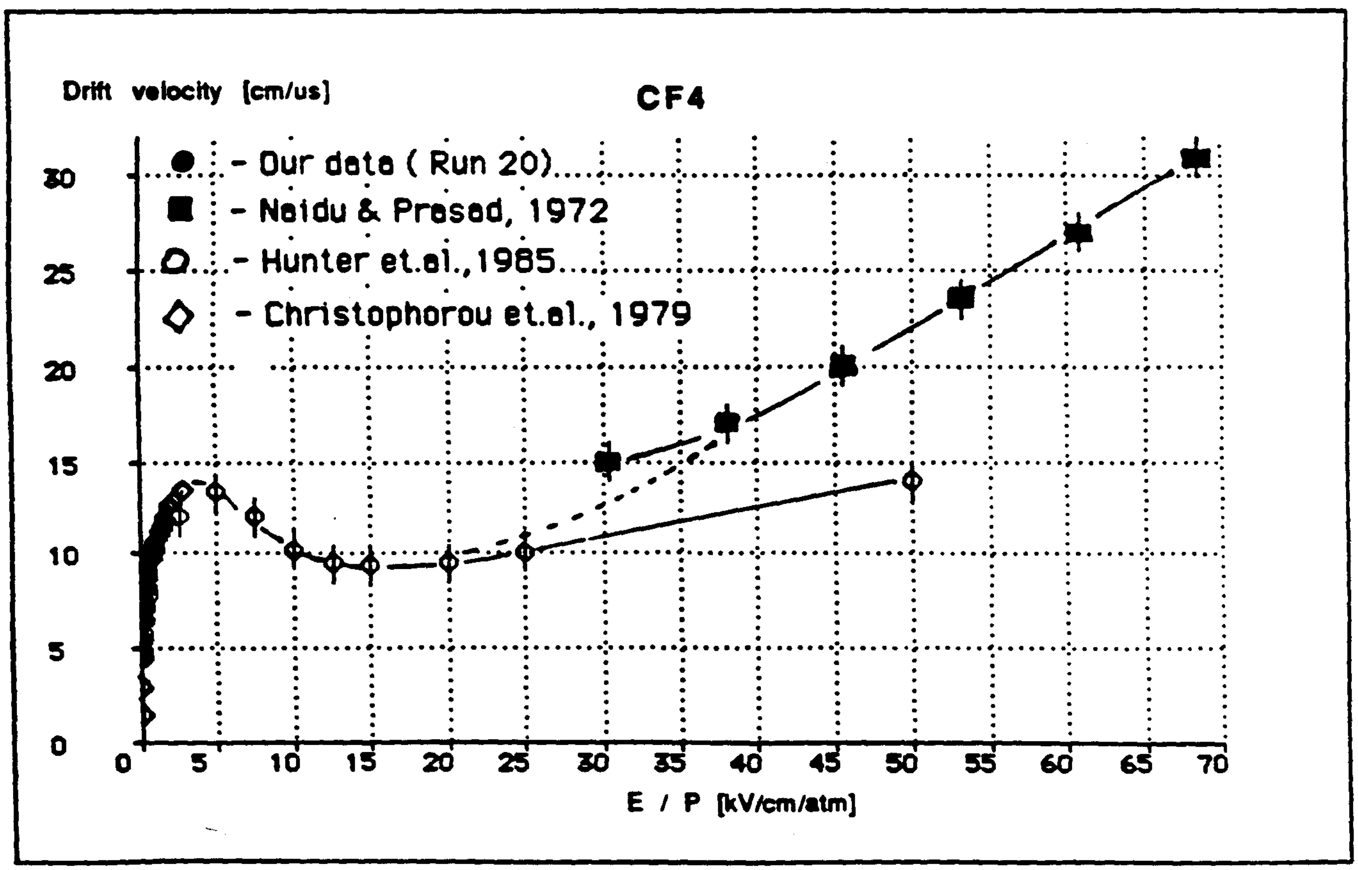

Drift velocity [cm/us]
CF4
- Our data (Run 20)
- Naidu & Prasad, 1972
- Hunter et.al.,1985
- Christophorou et.al., 1979
30
25
20
15
10
5
0
0
5
10
15
20
25
30
35
40
45
50
55
60
65
70
E / P [kV/cm/atm]

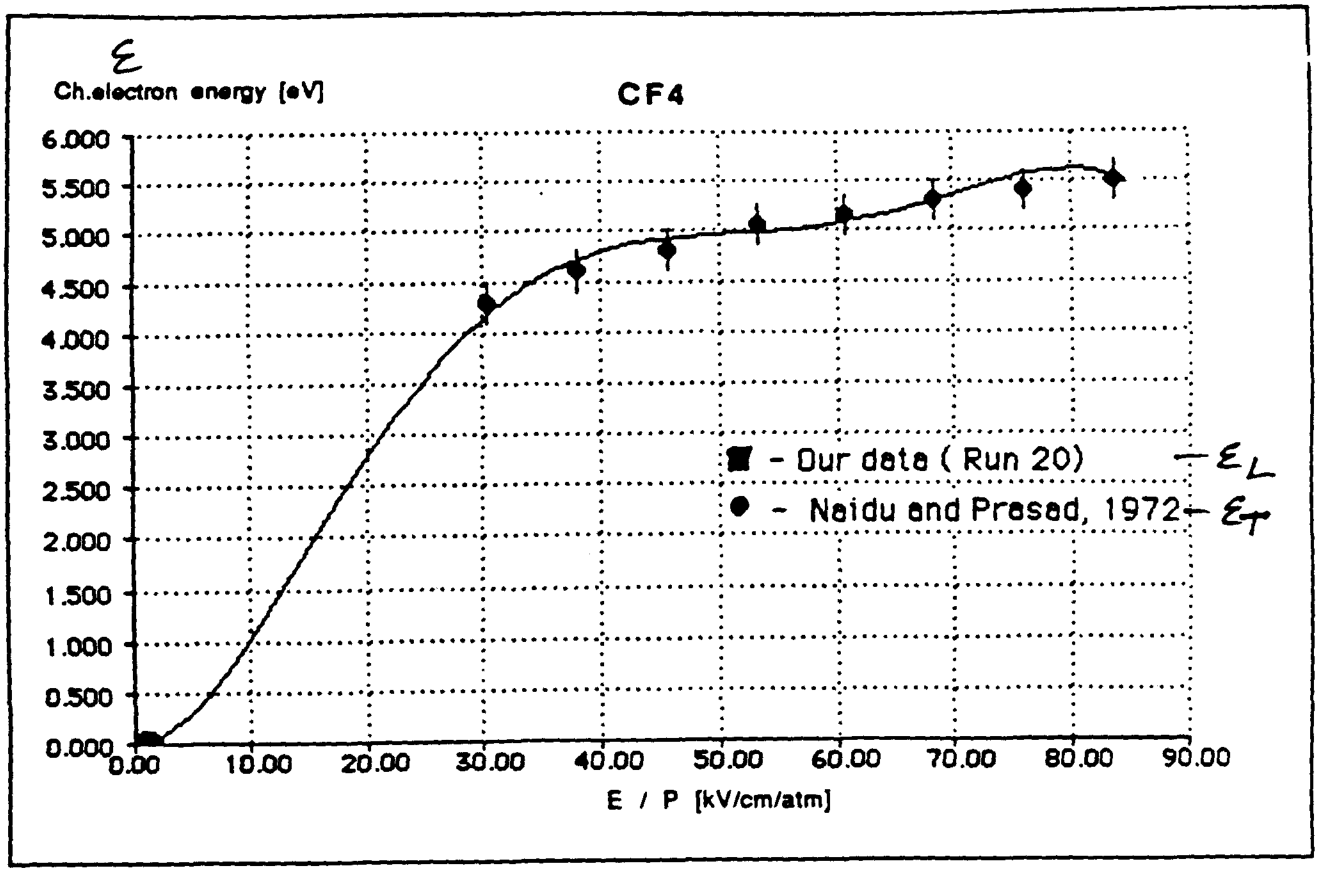

ε
Ch.electron energy [eV]
CF4
6.000
5.500
5.000
4.500
4.000
3.500
3.000
2.500
2.000
1.500
1.000
0.500
0.000
0.00
10.00
20.00
30.00
40.00
50.00
60.00
70.00
80.00
90.00
E / P [kV/cm/atm]
- Our data (Run 20) — ε_L
- Naidu and Prasad, 1972 — ε_T

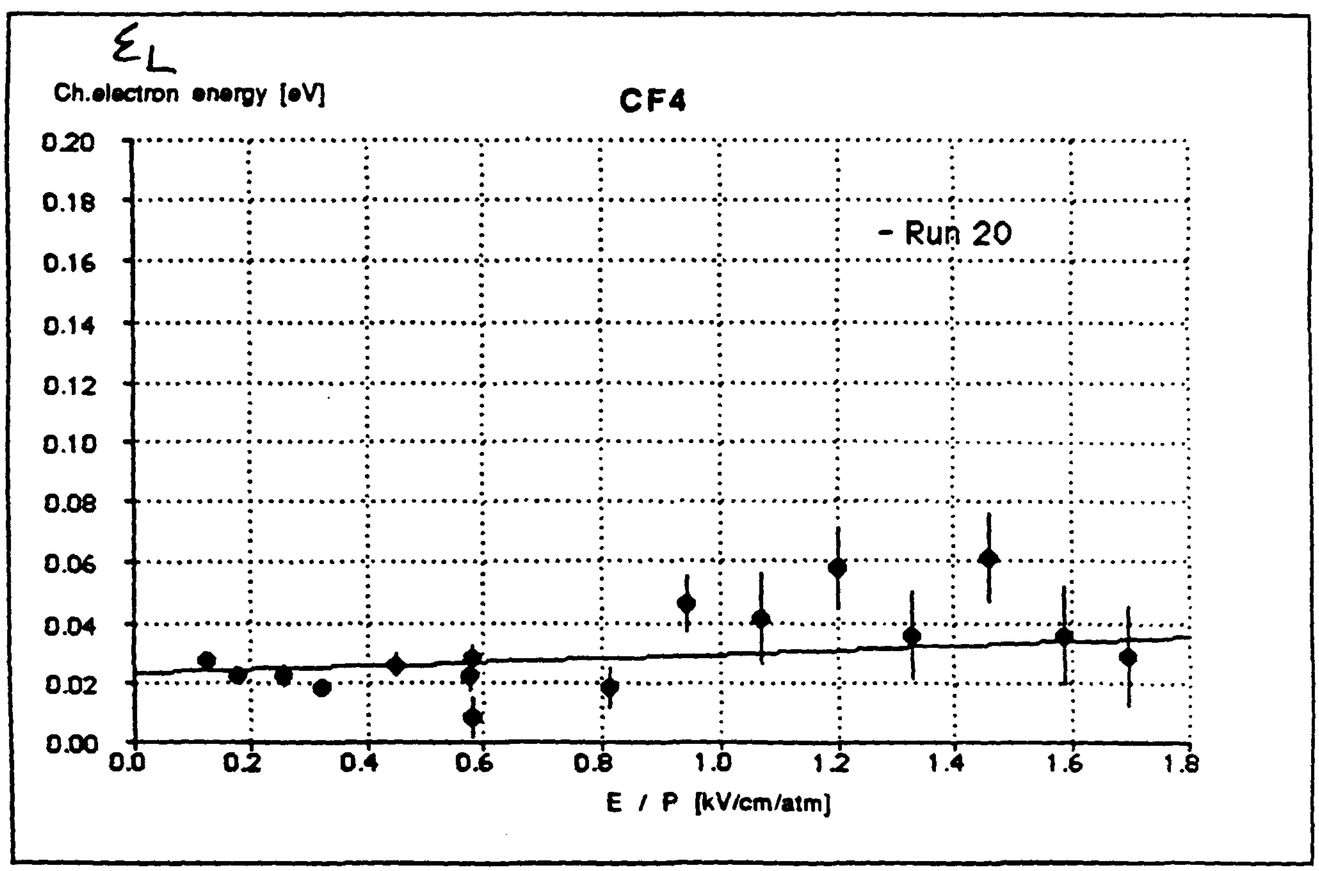

ε_L
Ch.electron energy [eV]
CF4
0.20
0.18
0.16
0.14
0.12
0.10
0.08
0.06
0.04
0.02
0.00
0.0
0.2
0.4
0.6
0.8
1.0
1.2
1.4
1.6
1.8
E / P [kV/cm/atm]
- Run 20

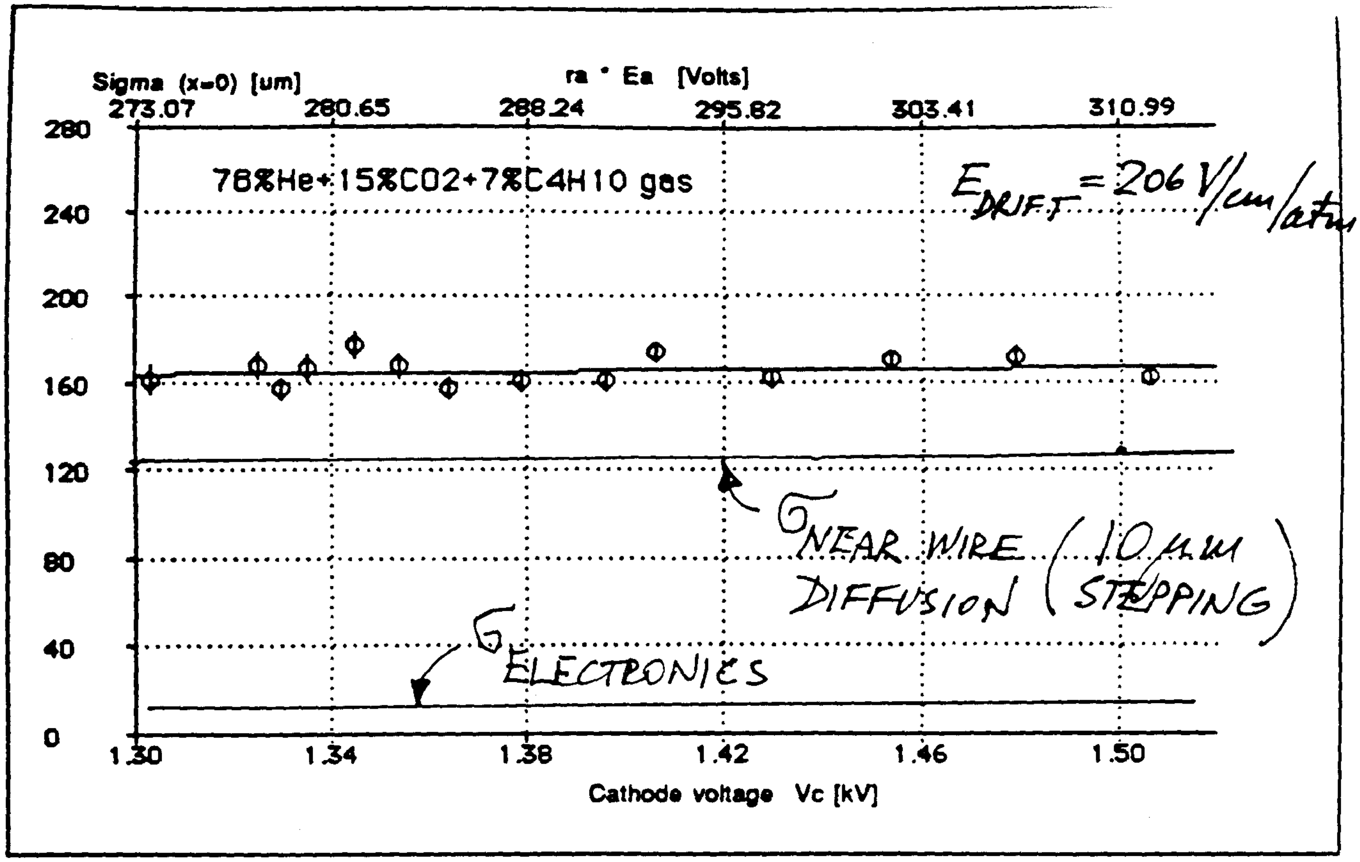
Sigma (x=0) [um]
ra * Ea [Volts]
273.07 280.65 288.24 295.82 303.41 310.99
78%He+15%CO2+7%C4H10 gas
E DRIFT = 206 V/cm/atm
σ NEAR WIRE DIFFUSION (10 μm STEPPING)
σ ELECTRONICS
280 240 200 160 120 80 40 0
1.30 1.34 1.38 1.42 1.46 1.50
Cathode voltage Vc [kV]

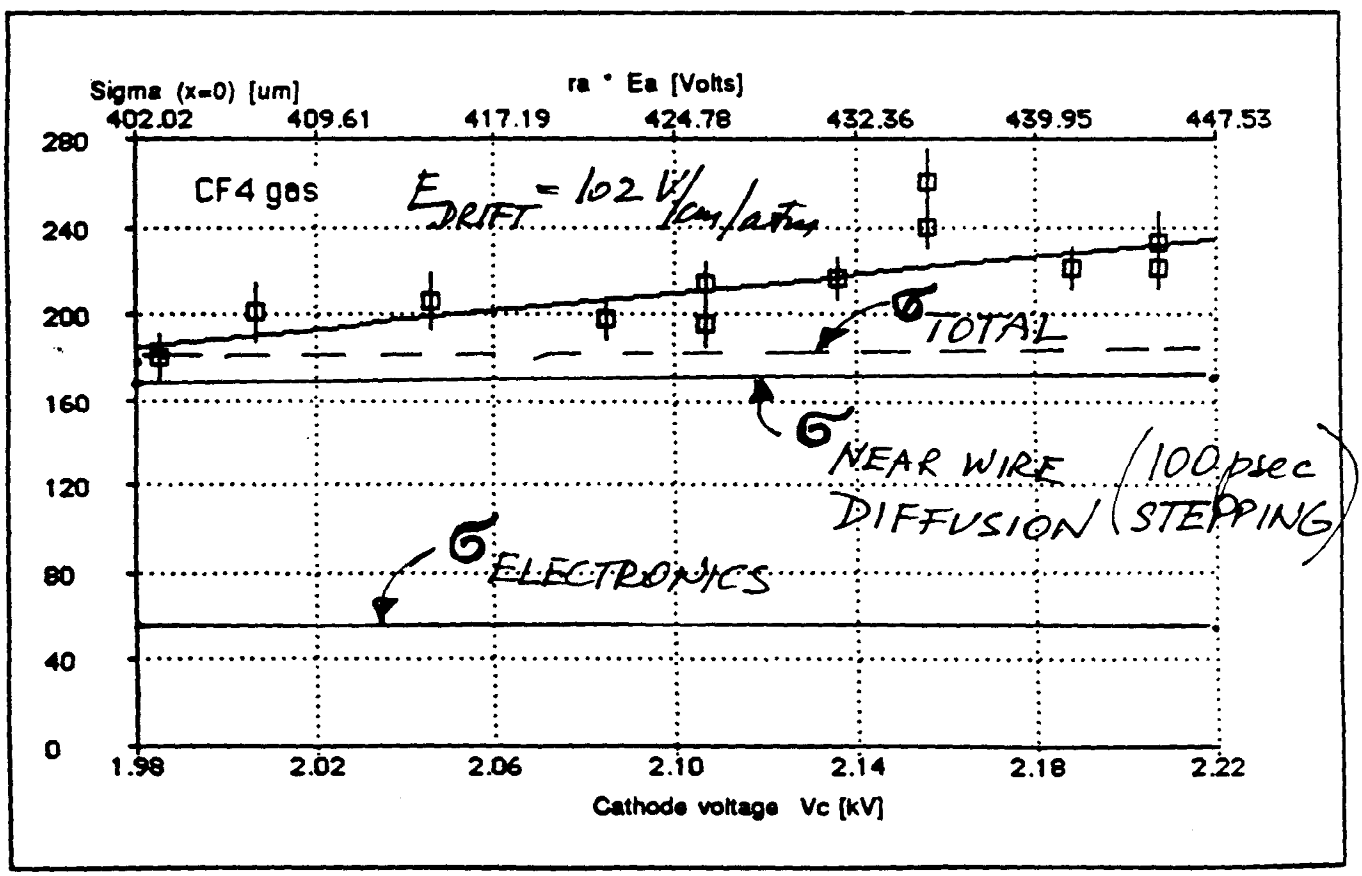
Sigma (x=0) [um]
ra * Ea [Volts]
402.02 409.61 417.19 424.78 432.36 439.95 447.53
CF4 gas
E DRIFT = 102 V/cm/atm
σ TOTAL
σ NEAR WIRE DIFFUSION (100 psec STEPPING)
σ ELECTRONICS
280 240 200 160 120 80 40 0
1.98 2.02 2.06 2.10 2.14 2.18 2.22
Cathode voltage Vc [kV]

CONCLUSIONS :

A) CF4 GASES :

- CF4 gases are fast and their diffusion is near thermal.
- CF4 data agrees well with Schmidt, but only to 5-10% level with Christophorou et.al.
- CF4 alone quenches well for low enough gains.
- 5 % addition of DME to CF4 slows it down considerably, more so than 20% of C4H10.
- **CF4 gases are prone to be dirty !!** We found that NANOCHEM filter will clean it to allow a long electron drift time.
- **CF4 alone wire ages surprisingly fast** in the 1-st mC/cm !!! NANOCHEM filter doesn't help. Effect being studied.
- CF4 gases single electron pulse height spectra looks fine.
- Water addition studied.

B) He GASES :

- He gases are slower and electrons tend to heat up quickly.
- Longitudinal diffusion is not that large in these gases. Final resolution will be determined with poor ionization statistics.
- **Cathodic breakdown is a problem to watch.**
- Single electron pulse height spectra indicate that an admixture of a streamer mode is possibly present even at low gains.
- Near wire diffusion is a larger contribution in He based gases than other typical gas mixtures.

FORWARD TRACKING WITH ENHANCED ELECTRON IDENTIFICATION[+]

EHIT Collaboration

J.M.Bailey[a], G.A.Beck[a], P.J.Bussey[b], P.Colrain[b], J.B.Dainton[a], E.Gabathuler[a], J.C.Hart[c], J.W.Hiddleston[c], S.J.Maxfield[a], N.A.McCubbin[c], J.M.Morton[a], G.D.Patel[a], B.T.Payne[c], C.Raine[b], E.J.Romans[c], D.P.C.Sankey[a], D.H.Saxon[b], I.O.Skillicorn[b], D.J.White[c]

[+]Supported by the UK SERC and the US DoE through SSClab R & D project SSC-PC-024.

[a] Department of Physics, University of Liverpool, P O Box 147, Liverpool L69 3BX, England
[b] Department of Physics and Astronomy, University of Glasgow, Glasgow G12 8QQ, Scotland
[c] Rutherford Appleton Laboratory, Chilton, Didcot, Oxon OX11 0QX, England

Abstract

Design concepts and developments are described for the construction and use of charged particle tracking detectors in the intermediate pseudorapidity range ($1.4 < \eta < 2.4$). Electron identification is enhanced by simultaneous detection of transition radiation X-rays and ionisation energy loss.

Physics Agenda and Detector Concept

The physics agenda set the detector requirements. A representative range of processes to consider includes Higgs searches, t-quark physics (Wb, Ws, H^+b, $\tilde{t}\tilde{\gamma}$, $\tilde{W}\tilde{b}$, Z^0c decays), Z' search and triple gauge boson vertex studies [1].

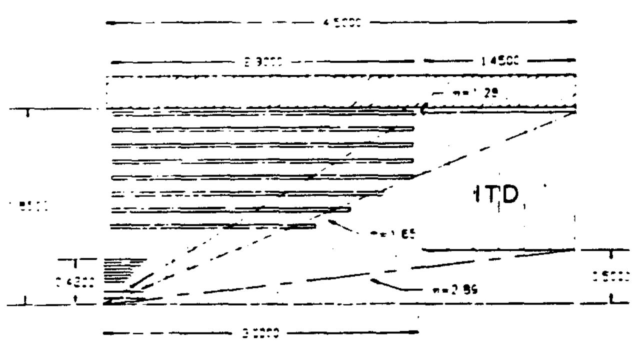

Figure 1 a) Charged track detector layout for use in 2T solenoidal magnetic field; 6 ITD modules are shown [2,3]

The (s)fermion channels have "large" cross-sections and detailed signatures, and the boson channels have low rates (at high masses) and simple signatures. Both types of process identify tracking, $e^{\pm}$ identification and charge sign determination over an angular range exceeding ±2 units of rapidity as prime requirements. In congested events it is a great benefit to have $e^{\pm}$ identification (dE/dx + TRD) located on the electron track, as well as calorimeter signatures.

Figure 1 shows a detector concept for an Intermediate angle Track Detector (ITD) [2,3] using detectors that measure $\phi.r$ (150 μm accuracy) and r (2 cm accuracy) at fixed z (beam direction) in a 2T solenoid. The momentum resolution is compared to that of a dipole detector in figure 2. The accuracies are comparable but a solenoid is preferred because of azimuthal uniformity, advantages in systematic errors and track matching to an inner track/vertex detector (e g silicon in SDC, see figure 1), and in suppression of background caused by (very) low momentum secondaries produced in the beam pipe [4]. The measurement is obtained using radial-wire drift chambers that measure ϕ-differences directly. To obtain given a momentum error the number of sense planes needed is only half that of a Cartesian grid of the same cell-size. Because the radial-wire cell size is better matched to the varying hit density ($d^2N/drd\phi \sim 1/r$ in endcaps) the advantage grows to a factor of three.

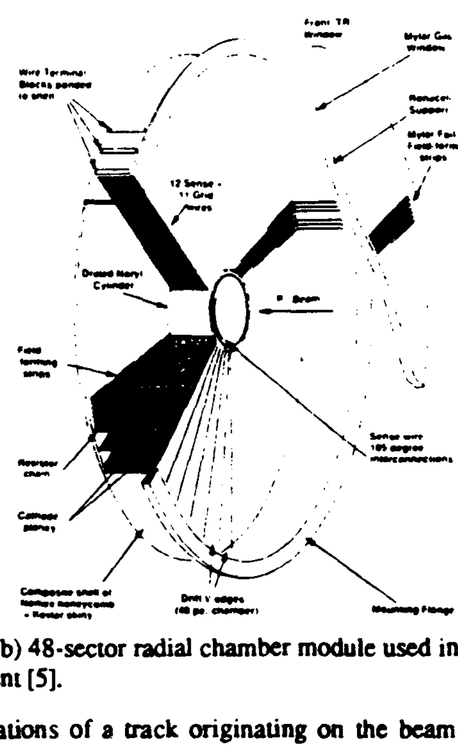

Figure 1 b) 48-sector radial chamber module used in the H1 experiment [5].

The equations of a track originating on the beam line at $r = z = 0$ in a uniform magnetic field are

$$\phi = \phi_0 + eBz/2p_z$$
$$r = 2p_T . \sin(eBz/2p_z)/eB$$

Event associated tracks are thus exactly straight lines in the ϕ-z plane. This makes for easy track-finding within and between modules.

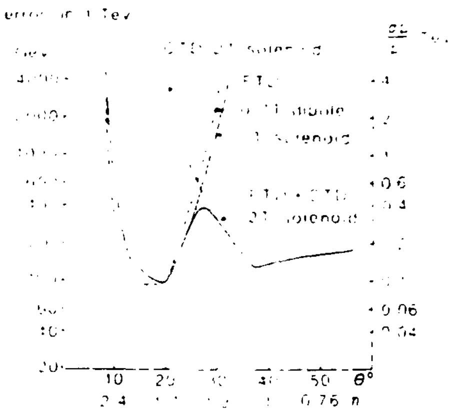

Figure 2: Comparative momentum resolutions for solenoidal and dipole intermediate angle tracking detectors (FTD) [4].

Detector Layout and Performance

The ITD in figure 1 has 6 (or 5) modules per end-cap with 300 sectors ($50 \le r \le 150$ cm). The maximum drift distance varies with radius from 5.2 to 15.7 mm. Each module has eight radial wire sense-layers giving a modest total of 14400 (or 12000) channels per end-cap. For readout, each sense wire is joined to another well separated in azimuth (105^o in H1). Using resistive sense wire, charge division readout gives 2 cm position resolution in r. The whole detector is constructed of light composite materials. The z-space between modules is filled with suitable transition radiator (TR) material (polypropylene foils in H1). Traversing electrons emit ~1.4 collinear X-ray photons ($<E_X> \sim 6$ keV) which convert in the chamber gas (30% Xe) in each module. Deposited charge ($^{dE}/_{dx}$ + TR) is used to distinguish e from hadrons.

With a gas gain of 2.10^4 the sense wire irradiation dose is 0.08 C cm^{-1} y^{-1} at $\mathcal{L} = 1.10^{33}$ cm^{-2} s^{-1} and the occupancy, (hit rate/cell) x (busy time), is 0.12. The busy time is equal to 2 x (two hit resolution)/(drift velocity). The H1 forward tracker has already achieved 1.5 mm two-hit resolution [5]. Given radial wire sense wire geometry and azimuthal electric drift fields in a solenoidal magnetic field, the component of drift velocity perpendicular to the wire cannot exceed

$$v_{perp} = {}^{E}/_{2kB} \cdot \sin(2\theta_L)$$

where θ_L is the Lorentz angle of rotation of the electron drift relative to $\underline{E}$, and $k = {}^{E}/(vB \sin\theta_L)$. $k \sim 1.1$ for most gas mixtures. We therefore design our chamber for a fast gas with E = 3 - 4 kV cm^{-1}, B = 2T, $\theta_L = 45^o$, $v_{perp} \sim 100$ µm ns^{-1}. (See [6] by J.M.Bailey for our work on gas mixtures).

The occupancy and lifetime figures indicate that the detector is viable up to $\mathcal{L} = 3.10^{33}.cm^{-2}$ s^{-1}. Detector congestion and pattern recognition is discussed below. The major technical concern is the maintenance of the cathode-plane voltage gradient in the presence of the high anode current draw.

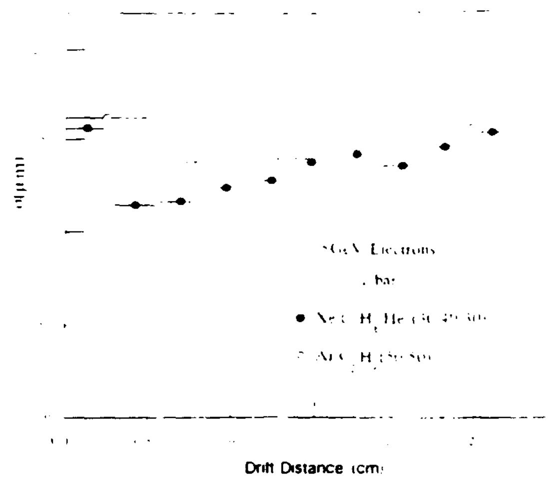

Figure 3 a) Position resolutions in ϕ.r as a function of drift distance in an H1 48 sector radial wire chamber [5]

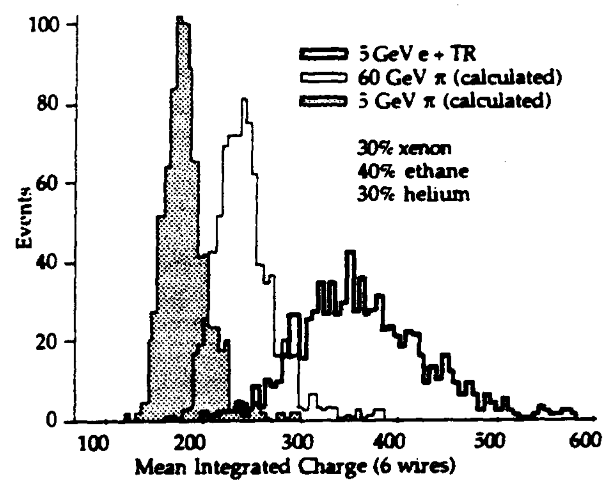

Figure 3 b) Integrated charge measurement for three 12 wire modules in the H1 configuration for 5 GeV e with preceding radiator; also shown are π spectra calculated from measurement of 5 GeV e without radiator [5].

The 48-sector H1 forward tracker [5] acts as a prototype for this device. Mechanical construction provides wire position accuracy of 38 µm rms. Pulse height measurement is independent of position along the sense wire to within 2% and is very uniform between sense wires. Figure 3(a) shows position resolution as a function of drift distance (everywhere better than 150 µm) and figure 3(b) the integrated charge measurement for electrons and pions. At 90% electron efficiency these provide a pion rejection of 200 at 5 GeV/c and 25 at 40 GeV/c. Similar precision is anticipated in each case for the SSC ITD as described. The ϕ.r and r measurements are naturally correlated by the readout (8-bit nonlinear FADC in this case). The device therefore provides three-dimensional space points with deposited charge information.

MEASUREMENTS OF ELECTRON DRIFT IN FAST GASES WITH CROSSED ELECTRIC AND MAGNETIC FIELDS†

EHIT Collaboration

J.M.Bailey[a], G.A.Beck[a], S.F.Biagi[a], P.J.Bussey[b], P.Colrain[b], J.B.Dainton[a], E.Gabathuler[a], J.C.Hart[c], J.W.Hiddleston[c], S.J.Maxfield[a], N.A.McCubbin[c], J.M.Morton[a], B.T.Payne[c], C.Raine[b], E.J.Romans[c], D.P.C.Sankey[a], D.H.Saxon[b], I.O.Skillicorn[b], D.J.White[c]

†Supported by the UK SERC and the US DoE through SSClab R & D project SSC-PC-024

[a] Department of Physics, University of Liverpool, P O Box 147, Liverpool L69 3BX, England
[b] Department of Physics and Astronomy, University of Glasgow, Glasgow G12 8QQ, Scotland
[c] Rutherford Appleton Laboratory, Chilton, Didcot, Oxon. OX11 0QX, England

Abstract

Results are presented from theoretical and experimental studies of electron drift in gas mixtures which aim for high drift speed and good X-ray detection. Implications for the design of an Intermediate Track Detector at a supercollider are briefly considered.

Introduction

This paper reports progress in establishing the optimum gas mixture for an intermediate angle gaseous chamber system at an experiment at a future proton supercollider (SSC or LHC). The detector (Intermediate Track Detector ITD) will be designed to reconstruct charged tracks, and possibly also to identify electrons by means of transition radiation (TR) detection in the pseudo-rapidity range $1.2 < \eta < 2.2$ [1]. The foreseen technique follows closely that of the forward track detector at the H1 experiment at HERA [2,3,4,5]. An essential ingredient for the proper design of an ITD is an understanding of the electron drift properties of potentially suitable gas mixtures.

Preliminary Considerations

Theoretical and experimental studies of various gas mixtures are under way. Interaction rates at a proposed luminosity (10^{33} cm^{-2} s^{-1}) of future supercolliders together with the nature and configuration of drift cells in an ITD at a "magnetic detector" (e g the SDC experiment at SSC [6]) pose the following minimum set of requirements on choice of gas mixture if optimal drift chamber operation is to be possible:

- high drift velocity for minimal cell occupancy with minimal drift Lorentz angle;
- good spatial accuracy in proportional mode;
- minimal depreciation with radiation exposure;
- manageable physical and chemical properties;
- X-ray sensitivity for efficient TR detection.

Figure 1 shows a compilation of measurements of the electron drift velocity as a function of drift field for the six fastest known pure gases [7]. When mixed with noble gases for comfortable HV operation (Ar for cheapness, He for low density, Kr and Xe for TR X-ray absorption), high drift speed is still to be expected. Other components may also be included as quenchers, ionization increasers, or fillers.

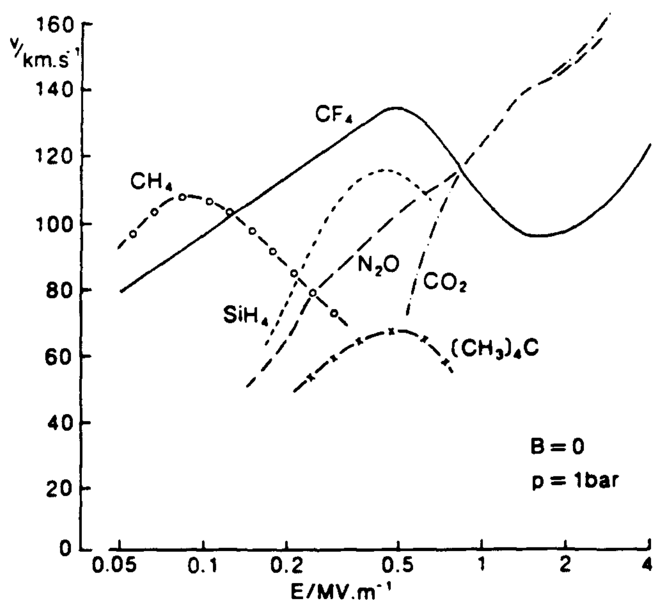

Fig 1: Electron drift velocities in fast polyatomic gases.

Admixtures of the gases of figure 1 to the noble gases also cool electron drift by virtue of their (inelastic) vibrational degrees of freedom. Nitrous oxide (N_2O) and neo-pentane ($(CH_3)_4C$) have further good properties. For example N_2O contains no C atoms, so can never polymerize, while $(CH_3)_4C$ absorbs the UV emission of Kr or Xe better than iso-C_4H_{10} or other quenchers. Kr or

In choosing a particular mix we try of course also to minimize the toxicity and explosion risk. In what follows, we present first\ measurements of mixtures containing the cheapest nooie gas (Ar) and the fastest pure gas (CF_4).

Experiment

A multi-wire drift cell designed and constructed specifically for the purpose is used to measure drift velocity and Lorentz angle. The chamber follows closely the design of Atac et al [8]. Drift time in a constant electric field is measured over perpendicular distances of a 16, 32 or 48 mm from a sense wire. Drift direction is measured using the known position of irradiation by a collimated ^{90}Sr source (β end-point energies 0.55 MeV ^{90}Sr, 2.23 MeV ^{90}Y) and the position of gas avalanche along the sense wire by means of the induced signal on adjacent cathode strips. The chamber itself is operated in the uniform magnetic field of a C-magnet ($B \leq 2$ T) with the plane of ionisation drift and sense wire perpendicular to the magnetic field direction.

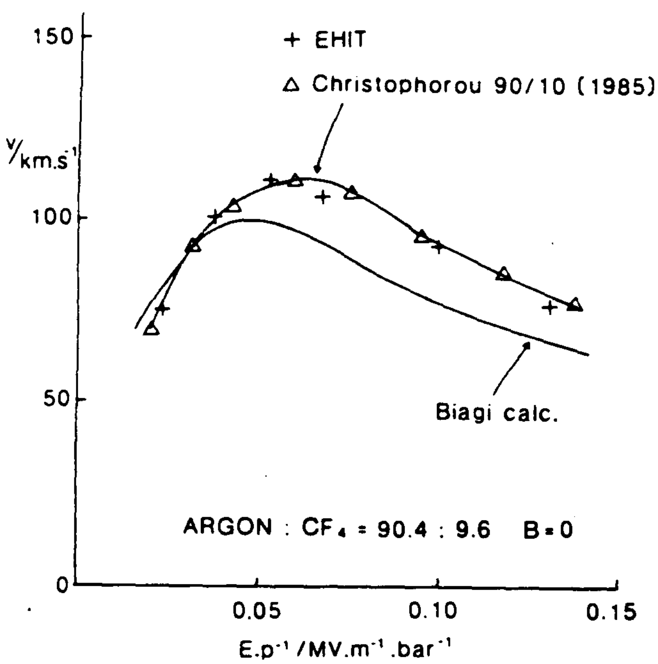

Fig 2: Drift velocity measurement in an Ar:CF_4 90:10 mixture with B=0; previous measurements and calculation are also shown [9,11,12].

Results of drift velocity measurements for CF_4:Ar mixtures in zero magnetic field are shown in figure 2 together with preliminary calculations [9,10]. In zero field our drift velocity measurements agree with previous measurements [11,12]. Systematic errors of measurement are of order 10%, and may be reduced after further study.

In finite applied magnetic fields (examples are shown in figures 3 and 4), where our measurements are unique, there is however some discrepancy of drift speed and angle with calculation. These calculations involving CF_4, and the parametrisations of input cross sections which they use, are new so the discrepancies should not yet be regarded as established.

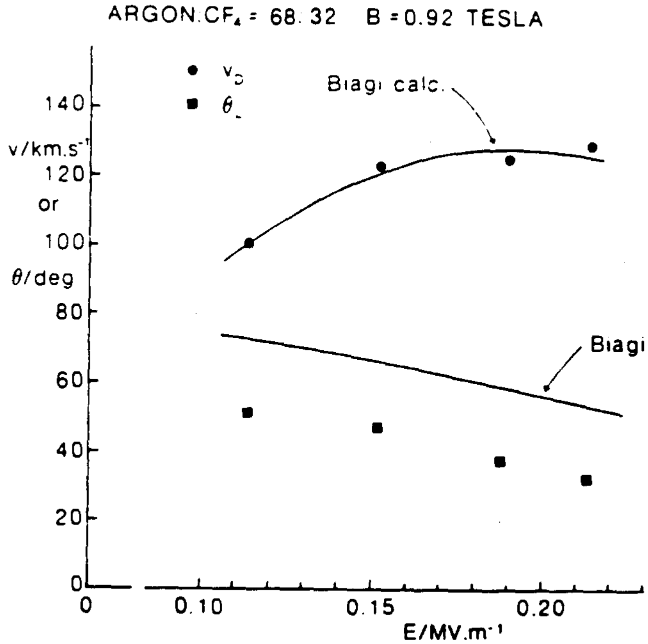

Fig 3: Drift velocity and angle measurements in an Ar:CF_4 68:32 mixture and crossed B field of 0.92 T; theoretical calculation is also shown [9].

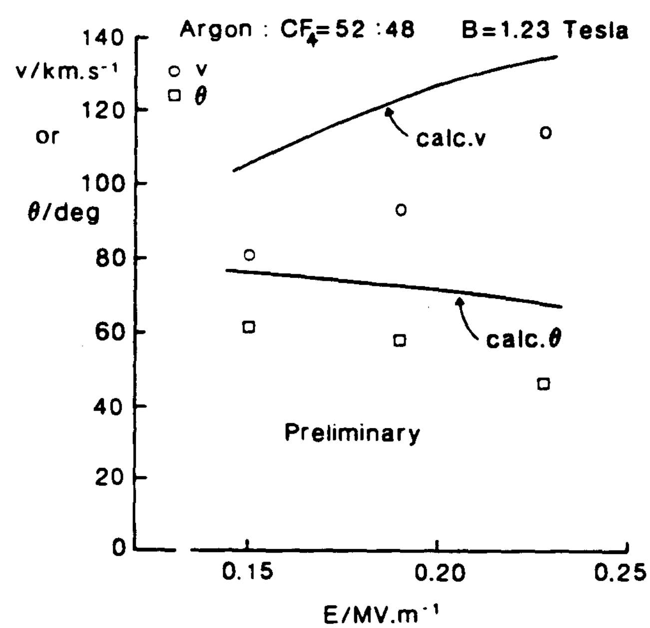

Fig 4: Drift velocity and angle measurements in an Ar:CF_4 52:48 mixture and crossed B field of 1.23 T; theoretical calculation is also shown [9].

It is already clear however that the use of CF_4 as a major component of drift chamber gas for the purpose of increasing ionisation drift velocity to at least 100 μm ns^{-1} is confirmed and for the first time demonstrated in substantial crossed magnetic field. Nevertheless its use in a magnetic field of ~1.8 T (likely in the SSC experiment SDC) with a suitable drift electric field may involve Lorentz angles substantially greater than 45° unless the chamber can be operated with a high drift field ≥ ~2 kV cm^{-1}.

A major problem associated with the use of CF_4 is the chemical effect it has on materials familiar to us in the construction of low mass drift chambers, e g foam, phenolic and epoxy based composites. At least one of our insulating materials, probably phenolic-bonded fabric ("Tufnol"), and perhaps also epoxy-bonded fabric ("G10"), had shrunk significantly due to absorbing CF_4.

We are therefore now carrying out measurements of mixtures with N_2O, which on paper looks also to be a suitable gas for drift velocities of 100 μm ns^{-1}, as quencher while we prepare a new prototype using CF_4 resistant materials. To date it is not yet clear that we can achieve adequate avalanche gas gain in the externally applied magnetic field for the hitherto possible electric drift fields.

Implications for ITD Chamber Design

The requirement of high drift field and thus acceptable Lorentz angle (~ 45°) is easily achieved with modest applied voltage for the small chamber aperture which is essential at high rate supercollider experiments. Any significant Lorentz angle increases the memory time of a drift cell and thus increases the occupancy. One possible way of reducing this effect is to string the ITD sense wires to follow as closely as possible to equiangular (logarithmic) spirals (figure 5).

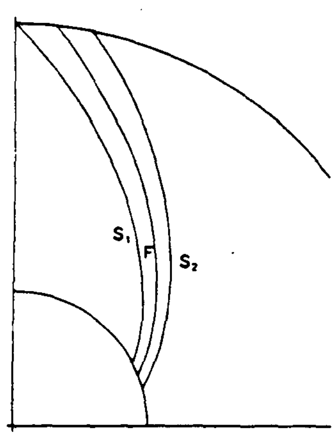

Fig 5: Equiangular spirals for 45°.

The problems experienced with the deformation, chemical and/or physical, of the construction materials used dictate the following:

- pre-shrinkage by long immersion in CF_4 gas, or perhaps other CFCs
- identification and use of low mass, inert materials which also have the necessary mechanical properties, e g Teflon (PTFE)

and they are being pursued.

Conclusions

First measurements have been made of electron drift characteristics in substantial crossed magnetic fields with gas mixtures which appear suitable theoretically for gaseous drift chambers at high rate supercolliders. It is possible to achieve acceptable drift velocities (>~100 km s^{-1}) in Ar:CF_4 mixtures, but with the disadvantage of substantial drift angles for values of drift electric fields used hitherto (~0.12 MV m^{-1}). At higher drift field (> ~0.3 MV m^{-1}) the drift angle can probably be reduced to 45° or less. Present theoretical calculations of drift velocity and angle for these mixtures are not yet of adequate precision for chamber design.

A serious drawback of the mixtures so far investigated is their deleterious effects on the materials traditionally used for low mass construction.

References

1 EHIT collaboration, J.M.Bailey *et al.*, "Forward Tracking with Enhanced Electron Identification", presented at this conference by D.H.Saxon.

2 G.A.Beck *et al.*, Nucl.Inst.Meth **A283** 471 (1989).

3 H.Gräßler *et al.*, Nucl.Inst.Meth **A283** 622 (1989).

4 H.Gräßler *et al.*, "Precision Reconstruction of Charged Tracks with Simultaneous Electron Identification in a Gaseous Detector using Transition Radiation", to be published in *Proceedings of the 2nd London conference on Position Sensitive Detectors, Imperial College of Science Technology and Medicine, London*, September 4-7 1990.

5 J.B.Dainton, in *Proceedings of the Workshop on Tracking Systems for the SSC, Triumf Laboratory, Vancouver, Canada*, ed W Frisken, July 24-28 1989.

6 SDC Expression of Interest, SSClab May 1990.

7 J.M.Bailey, "Compilation of Electron Drift Velocity Measurements", in preparation and references therein.

8 M.Atac *et al.*, Nucl Inst Meth **A249** 265 (1986).

9 S.F.Biagi, Nucl Inst Meth **A283** 716 (1989).

10 M.Yousfi, private communication.

11 L.G.Christophorou *et al.*, Nucl Inst Meth **163** 141 (1979).

12 L.G.Christophorou *et al.*, J Appl Phys **58** 3001 (1985).

OAK RIDGE NATIONAL LABORATORY
OPERATED BY MARTIN MARIETTA ENERGY SYSTEMS, INC.

POST OFFICE BOX 2009
OAK RIDGE, TENNESSEE 37831

August 27, 1991

Dr. Gail Hanson
Dr. Harold Ogren
Indiana University
Swain Hall West, 117
Bloomington, IN 47405

Progress Report for SDC

1.0 Background

During this reporting period, the design of the graphite/epoxy straw module has been completed in detail to put out requests for fabrication bids. Detailed design calculations were performed, and specifications and detail drawings produced to completely define the module for fabrication.

2.0 Detailed Calculations

Attachment A contains the detailed calculations upon which the detailed design was based. These calculations led to the following conclusions:

2.1 **Loads**

The loads that designed the module were found to be the thermal loads due to cooling the module back to room temperature from the maximum curing temperature. The stress-free temperature of a cured composite is close to the maximum cure temperature at which most of the cross-linking occurs in the polymer used for the matrix. Because of the high coefficient of thermal expansion (CTE) of the epoxy (about $21.(10)^{-6}/°F$), and the negative CTE of the graphite (about $-1.38(10)^{-6}/°F$), compressive buckling stresses are induced in the graphite filament.

2.2 Stresses

The induced compressive stresses in the thin laminates, due to cooling from cure, result in various modes of buckling, which cause warping and waviness of the modules. Such warping and waviness are unacceptable in the module; consequently a design fix was found which involves laying up the thin laminates on a polyimide foam, which enormously increases the flexural modulus and buckling strength of the laminate while imposing very little weight penalty on the module. In fact, the design using the foam core saves weight over that of the solid laminate for the case of designing to prevent buckling due to the tungston-wire forces; i.e., only .009-in. thickness of graphite (3 plies of .0015-in. per ply layed up on each side of foam core) are required to prevent wire-force buckling, whereas six plies of .0025 in. per ply (.015-in. of graphite) are required in a solid laminate to prevent wire-force buckling. However, the latter point is mute, since curing compressive stresses would cause buckling of the solid laminate.

2.3 Required Layup on Foam

In general, for curing temperatures over 150°F, thin laminates will buckle if there is no stabilization provided by foam or other reinforcements. Therefore, all layups of thin laminates should be reinforced by foam or other means. Also the layups should be balanced and symmetric, and the effects of the flexibility of the foam on the symmetry and balance, should be assessed.

3.0 Specifications and Drawings

Attachment B shows the developed specifications and design drawings to be used for fabrication.

Prepared by: John A. Mayhall

Approved by: Ted L. Ryan

ATTACHMENT A.

SANDWICH MODULE

Problem

There are residual stresses generated in graphite-epoxy composites which can cause buckling in thin, unsupported layups. These stresses are zero at temperature near the maximum curing temperature, but the stresses develop during cooling back to room temperature.

Types of Residual Stresses

There are two types of residual stresses, as follows:

1. Shearing Residual Stresses Between Plies

   There are residual stresses due to each ply of the laminate being differently oriented (e.g., ±30° layup), and, consequently each ply has different coefficients of thermal expansion in different directions. These differences induce shearing forces between plies and would cause warpage if the layup is not balanced and symmetric about the centroidal center line of the layup. If balanced and symmetric, however, the forces sum to zero and generally cause no trouble. Additionally, these stresses can be determined using finite-element laminated analysis, usually using the maximum curing temperature as zero stress temperature, and cooling back to room temperature, and reading out the resulting residual stresses.

2. Shearing Residual Stresses Between Epoxy Matrix & Graphite Filament

   These stresses result due to the enormous differences between graphite filament COE (coefficient of thermal expansion) and the epoxy COE. Again, these stresses do not cause warpage, providing the layup is symmetric and balanced about the centroidal plane. These stresses can not be determined by laminated finite-element analysis. One would need to perform a "micro-finite-element" analysis, modeling individual elements of epoxy and elements of graphite in order to determine these stresses. These stresses can cause buckling of thin elements, because of the net compressive forces which they produce in the graphite filaments. The following example can aid in this understanding. Our current layup is as follows:

   [0/+30/-30/-30/+30/0] .0025" per ply. The properties of this layup have been determined by finite element analysis to be:

   $E_0 = 20.0(10)^6$ psi

   $E_{90} = 2.14(10)^6$ psi

   $G = 5.29(10)^6$ psi

   COE $= \alpha$

   $$\alpha_0 = \frac{-1.382(10)^6}{°F}$$

$$\alpha_{90} = \frac{6.315(10)^{-6}}{°F}$$

For an approximate analysis, we will treat the layup as two bars, one is graphite with a COE of α_0 and the other will be epoxy with a COE of

$\frac{21.0(10)^{-6}}{°F}$, α_e.

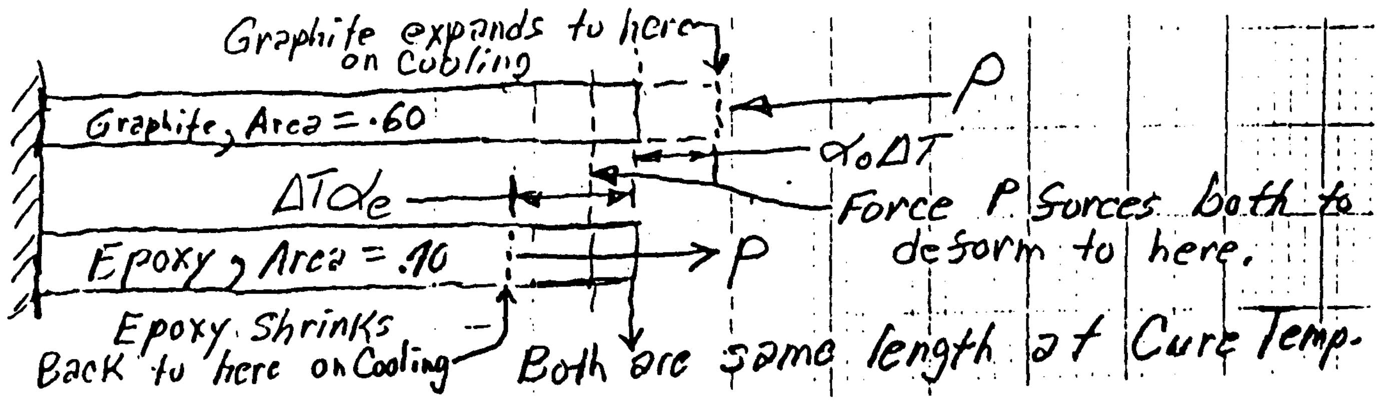

The equation that expresses the behavior of the two bars during cooling is as follows:

$$\Delta T(\alpha_e - \alpha_0) = \frac{P}{A_g E_g} + \frac{P}{A_e E_e}$$

Where

ΔT = Cure Temperature – Room Temperature

P = induced compressive force in graphite, equal to tensile force in epoxy

A_g = cross sectional area of graphite

A_e = cross sectional area of epoxy

(A_g =.60 ; A_e =.40)

E_g = Modulus of graphite = $E_0 = 20(10)^6$

E_e = Modulus of epoxy = $1.0(10)^6$ psi

In actuality, the induced forces will be shear as follows:

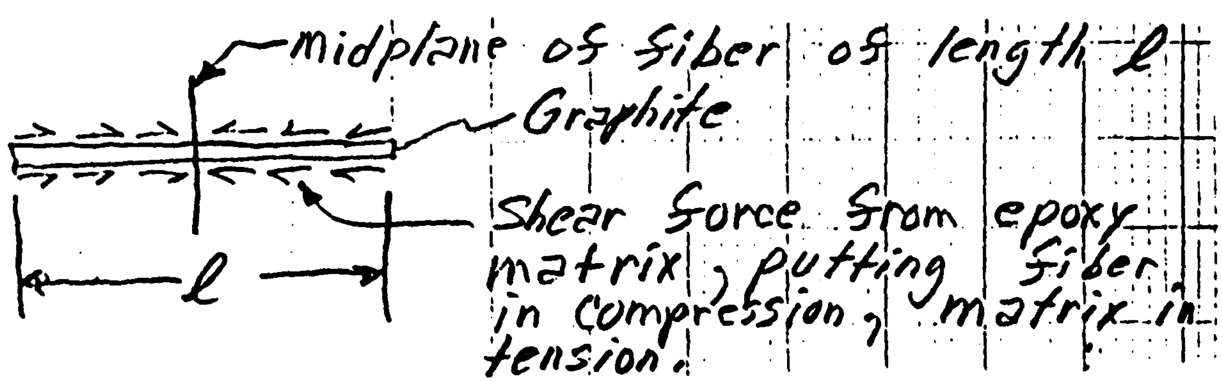

However, the shear behavior will induce a force of P (equation 1) and we can use Equation 1 to determine the compressive stresses in the graphite. Using Equation 1,

$$10^{-6}(350-70)[21.0-(-1.382)] = P\left[\frac{1}{.4(10)^6} + \frac{1}{.6(20)10^6}\right]$$

or $\quad P = 2426$ lb

$$\text{Compressive Stress in Graphite} = \frac{P}{A_g} = \frac{-2426}{.6} = -4043 \text{ psi}$$

We consider that this longitudinal compressive stress exists everywhere in the trough and lid.

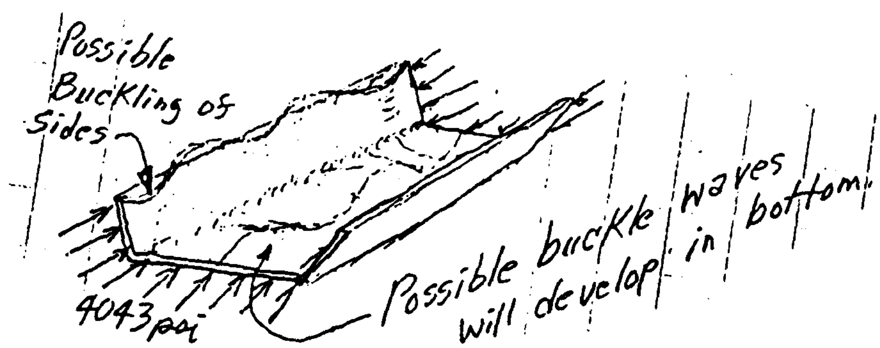

We see that the equation

$$\frac{P}{A_g} \approx \Delta T \quad 14.0$$

will give a good estimate of the compressive stresses (that tend to buckle) that will be induced in the curing ΔT. Obviously, we would like ΔT to be as low as possible.*

Such residual compressive stresses would be no problem in thick laminates or in supported thin laminates; i.e., thin face sheets bonded to honeycomb or foam sandwich.

Thus, we must worry about buckling or crippling during cure. Let us examine our current design.

---

* We should use a 200°F curing epoxy; this will reduce ΔT from the current 280°F to 130°F.

1.0 Buckling of Sides of Trough

From Timushenko's Theory of Elastic Stability, 1st Edition, 1936, page 339,

$$\sigma_{cr} = \frac{K\pi^2 D}{b^2 h}$$

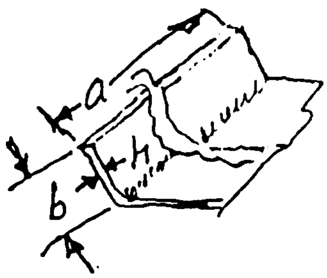

$$\sigma_{cr} = \frac{K\pi^2 D}{b^2 h} \tag{2}$$

$$K = .456 + \left(\frac{b}{a}\right)^2 = .456 + \left(\frac{1.403}{39.37}\right)^2 = .457$$

Where

$$D = I\sqrt{(E_0 E_{90})} \cdot I$$

I = Bending moment of Inertia of cross section per running inch.

For our 6-ply $[0/30/-30]_S$ layup,

h = .015 in ;

$$I = \frac{(.015)^3}{12} = 2.81(10)^{-7}\frac{in^4}{in}$$

and E_0 and E_{90} are the flexural moduli in the 0° direction [20(10)^6 psi] and 90° direction [2.14(10)^6 psi], respectively.

Thus from Equation 2

$$\sigma_{cr} = \frac{.457\pi^2\sqrt{20(2.14)}\,10^6(2.81)10^{-7}}{(1.403)^2(.015)} = 281 \quad \text{psi}$$

Thus, since the residual compressive stress is 4043 psi, the side will buckle badly. Let's try the following design:

$$I = (.005)\left(\frac{h'}{2}\right)^2 2 + \frac{(.005)^3}{6} = .0025h'^2 + 2.08(10)^{-7} = .0025\left[h'^2 + 8.33(10)^{-6}\right]$$

h ≡ Thickness of Rohacell Foam 3 lb/ft³

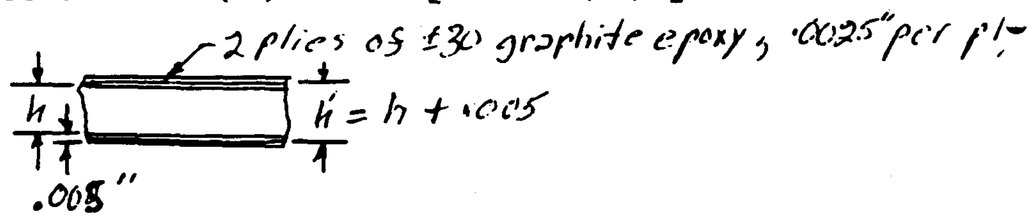

$E_{90} = 3.5(10)^6$

Solve for h' required to give factor of safety of 2.

$$2(4043) = \frac{.457\pi^2\sqrt{19.8(3.5)}\,10^6(.0025)\left[h'^2 + 8.33(10)^{-6}\right]}{(1.403)^2(.010)}$$

$h' = .0411$

$h = .0411 - .005 = .0361$

Rohacell's thinnest foam is 1 mm, or .0394-in. We will use this.

2. <u>Buckling of LID TOP</u>

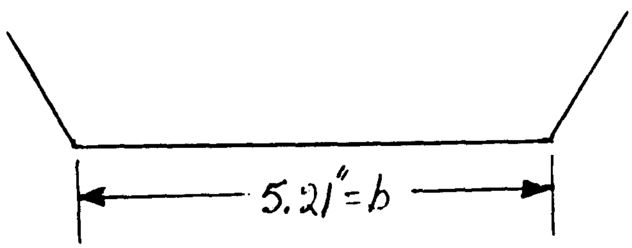

Treat as plate, a inches long, b inches wide, simply supported all around, with axial compressive stresses of 4043 psi (page 2), use Timoshenko reference, page 329, eqn. 213, K = 4.

$$\sigma_{cr} = \frac{(N_x)_{cr}}{h} = \frac{4\pi^2 D}{b^2 h}$$

or

$$\sigma_{cr} = \frac{4\pi^2\sqrt{E_0 E_{90}}\,h^3}{b^2 h\ 12} = \frac{\pi^2\sqrt{E_0 E_{90}}}{3}\left(\frac{h}{b}\right)^2$$

or our cure,

$$\sigma_{cr} = \frac{\pi^2}{3}\sqrt{20(2.14)}\,10^6\left(\frac{.015}{5.21}\right)^2 = 178 \text{ psi}$$

Since the residual compressive stress is 4043 psi, the plate will buckle. Now see what thickness foam with the design $I = .0025\left[h'^2 + 8.33(10)^{-6}\right]$ and with the layup [30/-30/foam/-30/30] .0025 in. per ply, and with the cure temperature 200°F, producing a stress $(\sigma = 14\Delta T)$ of -1820 psi. Equation 2 becomes:

$$2(1820) = \frac{4\pi^2\sqrt{19.8(3.5)}(.0025)\left[h'^2 + 8.33(10)^{-6}\right]10^6}{(5.21)^2(.010)}$$

or $\quad h'^2 + 8.333(10)^{-6} = .0012026$

$h' = .0346$

$h = .0296$

Thus .030-in foam would be required to prevent this buckling.

Now, we will examine what thickness of foam will prevent bulging.

3. Bulging Due to Straw Pressure

The straws will be squeezed between the lid top and the trough bottom. The straws will be squeezed down against the m-m's, which are spaced every 80 cm (approximately), 31.5". While, clamped in this squeeze, the lid will be bonded onto the trough. Because of compliance of the st raw, it will exert pressure back against the lid and trough (after removal from the bonding fixture) causing bulging, analyzed as follows:

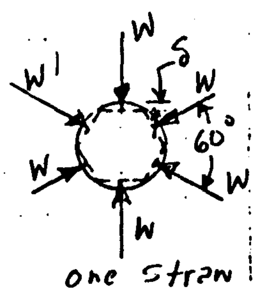

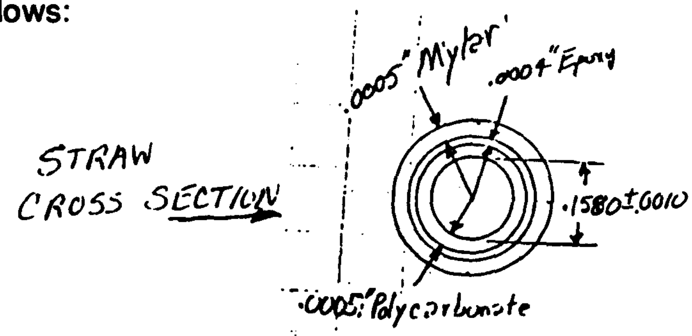

The force W (applied on 6 sides) can be determined versus deflection, δ from Roark, 5th Edition, page 226, case 7 as follows:

$$\delta = \frac{WR^3}{EI}\left[\frac{1}{4\sin^2\theta}\left(\theta K_1 + \frac{\sin^2\theta}{2}K_3\right) - \frac{1}{2\theta}\right] \qquad (4)$$

The properties of the straw materials are as follows:

Material	Mylar	Epoxy	Polycarbonate
Specific Gravity	.920	1.35	1.20

CONTINUED NEXT PAGE

Young's Modulus, psi	25,000	200,000	330,000
Ultimate Strength, psi	1,500	5,000	9,000
Elongation, %	--	--	100
CTE	$\frac{90(10)^{-6}}{°F}$	$\frac{30(10)^{-6}}{°F}$	$\frac{37.5(10)^{-6}}{°F}$

Determine EI of Wall of straw in bending for a 1" section

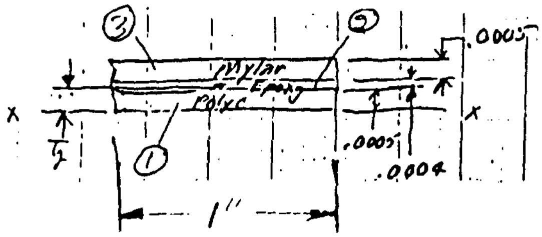

E	Item	A	EA	$\bar{y}$	$E\bar{y}A$	$E\bar{y}^2A$	$E\bar{I}$
330,000	1	.0005	165.0	.00025	.04125	.0000103125	$3.4375(10)^{-6}$
200,000	2	.0004	80.000	.0007	.0560	.0000392	$1.0666(10)^{-6}$
25,000	3	.0005	12.50	.00115	.014375	.00001653125	$2.60417(10)^{-6}$
			257.5		.111625	$6.604(10)^{-5}$	$4.7646(10)^{-6}$

$$\bar{Y} = \frac{\Sigma E\bar{y}A}{\Sigma EA} = .0004335;$$

$$R = \frac{.1580}{2} + \bar{y}; \text{or}$$

$$R = .07943''$$

$$E\bar{I} = \Sigma E\bar{I} + \Sigma \bar{y}^2 AE - (\Sigma EA)\bar{y}^2$$

$$E\bar{I} = 2.242(10)^{-5} \text{lb} - \text{in}^2$$

Equation 4 becomes as follows:

$$\theta = 30°$$

$$\alpha = \frac{I}{AR^2} = \frac{2.242(10)^{-5}}{257.5(.07943)^2} = 1.38(10)^{-5}; K_1 = 1$$

$$\beta = \frac{FEI}{GAR^2} \simeq \frac{1.5(2.242)10^{-5}}{\left[10^5(1.4)(.07943)^2\right]} = 3.8(10)^{-8}; K_3 = 1.0$$

$$\delta = W\frac{(.07943)^3}{2.242(10)^{-5}}\left[\frac{1}{4\sin^2 30°}\left(\frac{\pi}{6} + \frac{\sin 60}{2}\right) - \frac{1}{\frac{\pi}{3}}\right] = .0376W - \text{in}$$

$$W = K\delta = 25.6\delta$$

Where K = constant of straw.

Amount that straw will be squeezed $\delta = .00160 = \frac{.1590 - .1558}{2}$

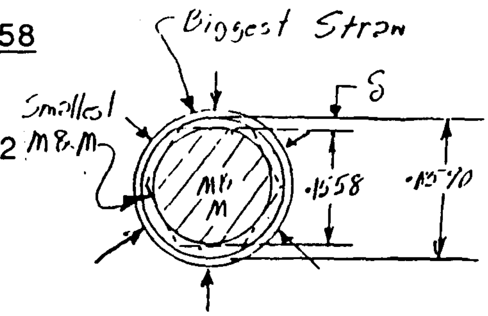

Pressure on shell of Module due to straw squeeze will be q lb/in2

$$q = \frac{W}{\text{strawpitch}} = \frac{26.6(.00160)}{[.1558 + .0014(2)]} = .268\,\text{psi}$$

First determine bulge of 4 ply, $(\pm 30)_s$, without foam, and then with foam:

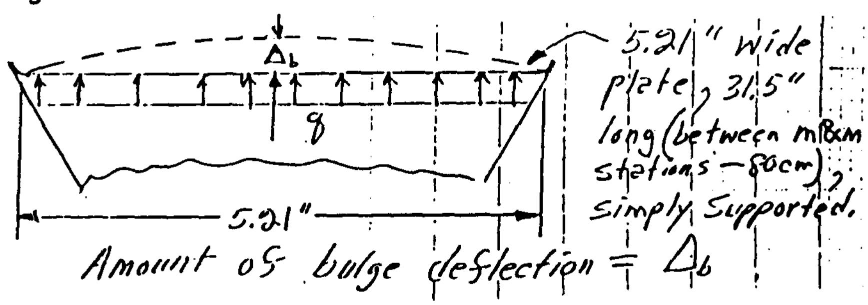

Roark, 5th Edition, pg. 386, case 1a,

$$\frac{a}{b} = \frac{31.5}{5.21} = 6.05$$

$$\Delta_b = \frac{\alpha q b^4}{E_{90} t^3} 5;$$

$$E = E_{90} = 3.51(10)^6$$

$$\alpha = .142$$

$$\Delta_b = \frac{.142(.268)(5.21)^4}{3.51(10)^6(.010)^3} = 7.97 - \text{in}$$

This is too flexible. But make the correction as follows:

$\Delta_b = (7 \sin 60 + 1)\delta$ for 8 rows of straws.

So, when $\delta = .0016$, Δ_b should be no more than (7 sin 60 + 1).0016 = .0113
Thus use enough foam so that this condition is achieved.

Replace t in Equation 3 with t*, where

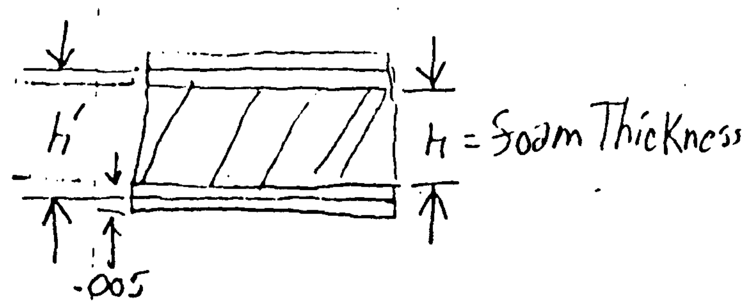

$$\frac{(t^*)^3}{12} = \frac{h'^2(.010)}{4}$$

$$t^{*3} = .030h'^2$$

$$\Delta_b = .0113 = \frac{.142(.268)(5.21)^4}{3.51(10)^6(.030)h'^2}$$

$$h' = .1535 \text{ in}$$

Thus we see that .154-in of foam would reduce the flexibility by a factor of 7.99/.0113 or 707. (over 700 times as stiff as without the foam).

Using the 1.9 lb/ft^3 Ruhacell WF Grade, .150 in of foam weighs the same as 1.07 plies of graphite epoxy. Thus, we solve the terrible transverse flexibility problem with a minimum cost in weight.

Thus, we solve the problem of the sides buckling and top and bottom excessively bulging by placing .015-in. foam in sides of trough and .150-in of foam in bottom and top of module. Now there is one more problem of instability to solve; i.e., because of one side of trough (or lid) buckling before the other side does, a form of twist-bend buckling occurs.

We will check the lid first.

Check the lid for twist-bend buckling. See appendix (see J.P. Den Hartog's <u>Advanced Strength of Materials</u>, page 283) for explanation of this buckling mode.

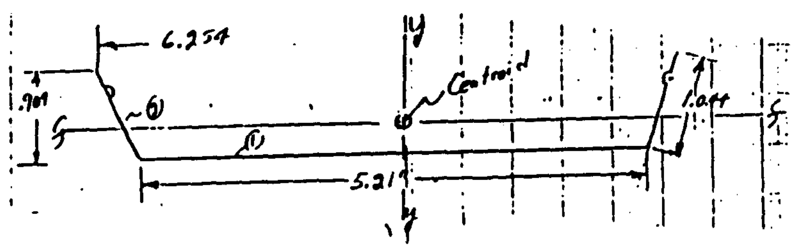

From the appendix, $M_{o_{critical}} \equiv M_o$, where

$$M_o = \frac{\pi\sqrt{EI_f \cdot C}}{l}$$

Determine If :

Item	A	$\bar{y}$	$A\bar{y}$	$A\bar{y}^2$	I
1	.0521	.005	$2.605(10)^{-4}$	$1.3025(10)^{-6}$	$4.3417(10)^{-7}$
2	.02088	.452	.0094378	.0042659	.0014218
			.0096983	.0042672	.0014222

analyzed for $[\pm 30]_s$ .0025in/ply

$A = .07298$

$\bar{y} = .13289$ in

$I_f = .0014222 + .0042672 - .0096983\,(.13289)$
$= .00440\ \text{in}^4$

$C\theta = T$; or twist angle per in of length $= \frac{\theta}{L} = \frac{T}{C}$

See Roark, 5th Edition, page 300, case 1., C=KG

$$K = \frac{t^3}{3}(h + 2b) = \frac{(.010)^3}{3}[5.21 + 2(.904)] = 2.34(10)^{-6}$$

G of $[\pm 30]_s$ layup $= 6.39(10)^6$

$\therefore\ C = KG = 14.95\ \text{in}^2 - \text{lb}$

Equation 4 becomes:

$$M_o = \frac{\pi}{32''}\sqrt{20(10)^6(.00440)14.95}$$

$$M_o = 112.6\ \text{in} - \text{lb}$$

What differential stress and strain in the turned-up legs would produce this buckling moment:?

Determine I_{yy} from Figure above

$$I_{yy} = .010\frac{(5.21)^3}{12} + (1.044)(.010)2(2.866)^2 = .289\ \text{in}^4$$

$$\sigma = \frac{M_o C}{I} = \frac{(112.6)2.87}{.289} = 1{,}118\ \text{psi}$$

$$\text{Strain} = E = \frac{\sigma}{E} = \frac{1118}{20(10)^6} = .0000559\frac{\text{in}}{\text{in}}$$

Now, we should estimate what possible differential stress exists in the cured graphite epoxy.

Cured Graphite Epoxy Cools from 350°F to 70°F

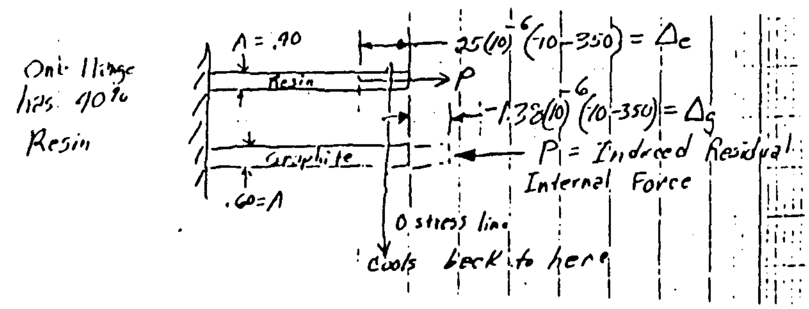

$$E_{epoxy} = 1(10)^6 \text{ psi}$$

$$E_{graphite} = 60(10)^6 \text{ psi}$$

$$\Delta_e - \Delta_g = P_A\left[\frac{1}{A_eE_e} + \frac{1}{A_gE_g}\right]$$

$$P_A = \left(\frac{\Delta_E - \Delta_g}{\frac{1}{A_eE_e} + \frac{1}{A_gE_g}}\right) = \frac{(25 + 1.38)10^{-6}(-280)}{\left[\frac{1}{.40(10)^6} + \frac{1}{.60(60)10^6}\right]}$$

$$P_{.4} = -2922 \text{lb}$$

$$\text{stress in graphite} = \frac{P_{AO}}{.60} = \sigma_g$$

$$\sigma_g^{.4} = -4{,}870 \text{ psi compression}$$

$$\text{Differential Stress in Flanges} = \sigma^{.5}_g - \sigma^{.4}_g = -2395 \text{ psi}$$

Also note that if one flange buckled before the other, twist-bend buckle would occur. The -2395 psi is more than twice the value required to buckle the lid in twist-bend.

Now, we will see if the foam will solve the twist-bend buckling problem.

To determine K(C=GK); use Roark, 5th Edition, a combination of case 1 (pg. 300) and case 16 (pg. 293):

Treat the case as two springs in parallel

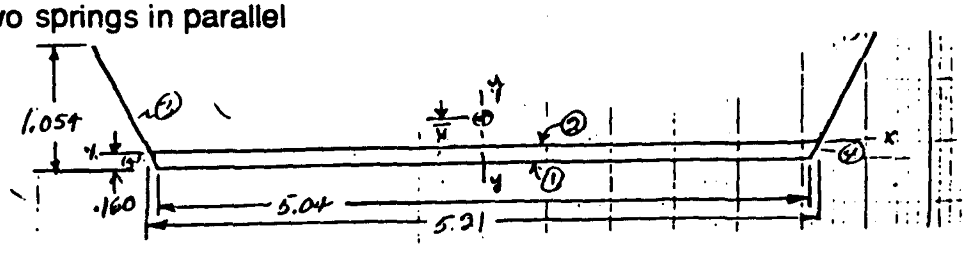

$(T = KG\theta)$

$T_1 + T_2 = T$

$T_T = GK_T = G(K_1 + K_2)$

$K_T = K_1 + K_2$

$$K_1 = \frac{(.010)^3}{3} \cdot 2(.904) + \frac{(.005)^3(5.21)2}{3}$$

or $K_1 = 6.027(10)^{-7} + 4.342(10)^{-7}$

$$K_2 = \frac{2(.005)(5.125 - .005)^2(.16 - .005)^2}{(5.125 + .160 - .010)} = 1.19394(10)^{-3}$$

$K_T = K_1 + K_2 = 1.1945(10)^{-3}$

$G = 6.39(10)^{-6}$

$C = GK_T = 7630\ in^2/lb$

If I_f were the same,

$$M_o = \frac{\pi}{32}\sqrt{20(10)^6 .00440(7,630)}$$

$=2544$

and the critical differential stress would be $\left(\sigma = \frac{MC}{I}\right)$25,300 psi

Thus, whereas the design without foam would buckle (twist bend) at a defferential stress of only 1,118 psi, the design with .150-in of foam between the face sheets (of ±30 plies on each side), would require 25,300 psi differential stress. Thus, it is proven that the .150-in of foam needed for minimizing bulging will also eliminate twist-bend buckling.

Therefore, it is proven here in that .039-in foam in side walls and .150-in foam in the bottom and top of module (trough and lid), there will be no buckling or excessive bulging in the module.

ADVANCED STRENGTH OF MATERIALS

J. P. Den Hartog

Professor of Mechanical Engineering
Massachusetts Institute of Technology

New York Toronto London
McGRAW-HILL BOOK COMPANY, INC.
1952

Twis d B ng (ams a t is v stiff ast bending in one plane and very flexible in a perpendicular plane, like a ruler or T square, and if that beam is loaded in the stiff plane, it has been observed to buckle out in the flexible direction, and this bending buckling in the flexible plane is always associated with a twist. Consider the case of Fig. 190, where the beam of cross section ht (the height h being many

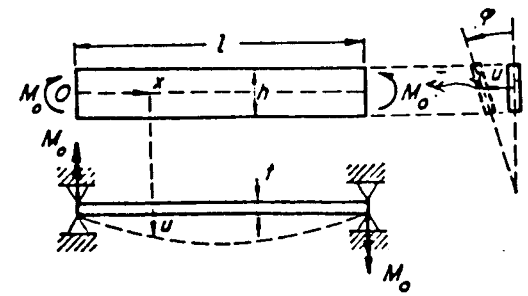

FIG. 190. A beam with $h \gg t$, supported at its ends so that the angle φ is zero there, subjected to bending moments M_0 in its stiff plane. When M_0 reaches the critical value [Eq. (150)], the beam buckles out in a combination of bending u in the flexible plane and torsion φ.

times the thickness t) is simply supported on its ends between flat guides so that it cannot twist-turn at those ends. The beam is loaded by two equal and opposite bending moments at the ends in the stiff plane, which puts the upper fiber in compression and the lower fiber in tension. When these stresses get sufficiently high, the upper fiber can buckle out sidewise, while the lower fiber roughly remains straight. This means a sidewise bending u of the middle line $h/2$ of the beam together with a twist, because in the center of the span the h is no longer vertical, while at the ends h is held in place by the end guides.

A similar situation exists with the cantilever beam of Fig. 192 (page 286). The bending deflection in the stiff plane is very small, and when the load P gets large enough, the beam can be in indifferent equilibrium in a condition of sidewise bending combined with twist. This type of problem was solved in 1899 independently by Prandtl in Germany and by Michell in England.

Twist-bend Instability by Bending Moments. This is the simplest case in this class of problems, and the system is shown in Fig. 190. We call u the sidewise displacement of the *center line* $h/2$ of the beam. If the angle φ were zero throughout, then this u would also be the sidewise displacement of the upper and lower fibers of the beam. In the buckled shape however, there will be an angle $\varphi = \varphi(x)$, and $u = u(x)$, so that then u is not the displacement of any fibers except the center one. [The top-fiber curve displaces by $u + (h\varphi/2)$.] The bending moments M_0 are represented in the plane sketch of Fig. 190 as double-headed straight arrows, related to the curved arrows by a right-hand screw convention.

The differential equations are found from considering the equilibrium of a piece of the beam from O to x (Fig. 191). In the plane view of Fig. 191*a* the moment exerted on the beam for equilibrium must be M_0, as shown. The M_0 at point O is called a bending moment in the stiff plane, but the same moment M_0 at x can no longer be called that. We first break up M_0 into two components in the horizontal plane, as shown. The moment $M_0(du/dx)$ is called a twisting moment, since it is directed along the center line. The magnitude of the other component M_0^- differs from M_0 only in quantities of the second order. Now we proceed to the other projection (Fig. 191*b*). The moment vector M_0^- in the horizontal plane is again

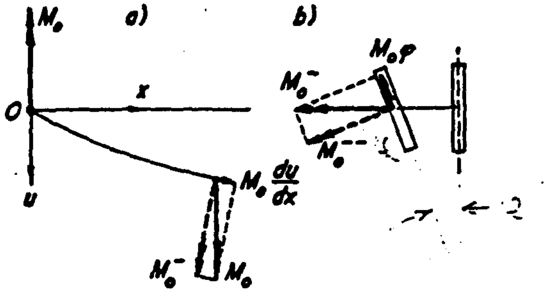

FIG. 191. Left-hand portion of the beam of Fig. 190 in the buckled state. The moment M_0 is resolved into three components: M_0^{--} in the stiff bending direction, $M_0\varphi$ in the flexible bending direction, and M_0u' in the twisting direction.

resolved into components; $M_0\varphi$ is called the bending moment in the flexible plane, and M_0^{--} (differing from the magnitudes of M_0 and M_0^- by second-order quantities only) is the true local bending moment in the stiff plane.

Now consider a small element dx of the beam at x and write the deformation equations in the flexible bending plane and in the twisting direction:

$$EI_f u'' = -M_0\varphi \qquad\qquad C\varphi' = M_0 u' \tag{149}$$

Here C is the torsional stiffness $Ght^3/3$ (see page 15); EI_f is the flexible bending stiffness $Eht^3/12$. The bending moment $M_0\varphi$ is so directed as to tend to cause a negative curvature u'' in the beam; hence the negative sign in Eqs. (149). The twist moment M_0u' tends to increase φ locally, so that in the second equation the sign is positive. Here then we have a *pair* of equations in two variables u, φ, whereas in the simple Euler-column problem we had one equation,

$$EIy'' = -Py$$

We are now ready to solve Eqs. (149). Differentiating the second one, we find u'' from it and substitute into the first one, thus eliminating u:

$$\frac{EI_f \cdot C}{M_0}\varphi'' = -M_0\varphi$$

or

$$\varphi'' + \frac{M_0^2}{EI_f \cdot C}\varphi = 0$$

The general solution is

$$\varphi = C_1 \sin\left(x\frac{M_0}{\sqrt{EI_f \cdot C}}\right) + C_2 \cos\left(x\frac{M_0}{\sqrt{EI_f \cdot C}}\right)$$

At the left boundary $x = 0$, we have $\varphi = 0$, and as a consequence $C_2 = 0$:

$$\varphi = C_1 \sin\left(x\frac{M_0}{\sqrt{EI_f \cdot C}}\right)$$

At the other end $x = l$, we again have $\varphi = 0$. This can be done in two ways. One possibility is $C_1 = 0$, which gives us a true but uninteresting solution: a non-buckled straight beam. The other possibility is that C_1 has an arbitrary value φ_{max} and that the sine is zero or

$$\frac{M_0 l}{\sqrt{EI_f \cdot C}} = \pi,\ 2\pi,\ 3\pi, \text{ etc.}$$

We are interested in the lowest buckling load only, which is

$$(M_0)_{crit} = \frac{\pi\sqrt{EI_f \cdot C}}{l} \tag{150}$$

The shape of the buckling then is $\varphi = \varphi_{max} \sin (\pi x/l)$, a half sine wave. From the second of Eqs. (149) we then conclude that

$$\varphi = \varphi_{max} \sin\frac{\pi x}{l} \qquad\qquad u = \frac{C}{M_0}\varphi_{max} \sin\frac{\pi x}{l} = \frac{l}{\pi}\sqrt{\frac{C}{EI_f}}\,\varphi_{max} \sin\frac{\pi x}{l} \tag{151}$$

The reader is advised to work Problem 200 to get a better visualization of the deformed shape.

If the beam is not sufficiently flexible either in bending or in torsion [Eq. (150) contains the product of the two], then the critical bending moment becomes large and the possibility exists that the beam will yield before it buckles. Assuming $E = 2\frac{1}{2}G$ and a yield stress of $E/1{,}000$, this occurs when

$$\text{Yields before buckling for } \frac{hl}{t^2} \leq 2{,}000 \tag{152}$$

approximately. The derivation of this result is left to the reader as Problem 199.

ATTACHMENT B

CARBON FIBER SHELL SPECIFICATION

1.0 SCOPE

This specification describes the requirements for the design, analysis, fabrication, testing, and inspection of carbon fiber shell parts to be furnished to Indiana University, hereinafter referred to as the buyer.

2.0 APPLICABLE DOCUMENTS

Drawing No. X2E021147A001 - SDC Central Tracker Straw Module Shell.

3.0 SHELL PART REQUIREMENTS

The Seller (subcontractor) shall fabricate one "one-meter" and one "four-meter" shell body and lid to meet the requirements of this specification and drawing X2E021147A001. Prior to fabrication of the shell parts the Seller shall furnish to the buyer, for review, a process specification that shall identify shell part and mold materials of construction, processing equipment, lay-up, and fabrication procedures. In addition, an analysis shall be provided detailing the anticipated buckling strengths, deflections and wall thickness of the completed shell parts.

3.1 Materials Materials used directly in the shell parts shall have carbon fiber as the reinforcement. The Seller is responsible for the selection of the particular carbon fiber, matrix and mold materials used in the fabrication of the shell parts. The completed shell parts shall be physically stable over a period of ten years within an operating temperature range of 70° to 110°F, and function efficiently after exposure to about three Mrad of radiation.

3.2 Fabrication The same fabrication process shall be used to produce the one meter and four meter shell parts.

3.3 Cutting, Trimming, and Finishing All cutting, trimming, and finishing of the completed shell parts shall be defined and shall not have any degrading effects on material properties.

3.4 Defects All reasonable measures will be taken to minimize defects during the fabrication of the shell parts. The following are maximum allowable and repairable defects. For defects which are beyond the limits shown, repair procedures shall be written by the Seller and submitted to the buyer for approval prior to repair of the defect.

Defect	Maximum Allowable
Overlaps, Wrinkles, and Ridges	Must be within flatness limits of Drawing No. X2E021147A001
Voids, Delaminations, and Resin Starvation	Non Visible

3.5 Mechanical and Physical Requirements

3.5.1 The following information is provided to the Seller in order to clarify the design goals and requirements for the shell assembly which were used to arrive at the design of Drawing No. X2E021147A001. The main goals of the design are to minimize the amount of material while using low atomic number materials and meet the structural strength and stability criteria stated below. The Seller is encouraged to suggest any means determined to achieve these goals which improve the design, final product, its producibility, or reduce cost and fabrication time.

3.5.2 The module will consist of a trough and lid cured separately, which will later be filled with straws, and subsequently, the lid will be bonded to the trough to make up the finished module. The wall thicknesses of lid and trough can have a maximum total cured graphite-epoxy composite (50% minimum by volume fiber) thickness of .010 ± .003 inches. However, the total thickness of the top of the lid or bottom of the trough can be .166 ± .006 inches. The total thickness of the sides of the trough can be .0484 ± .005 inches. These total thicknesses are comprised of graphite composite and Rohacell foam, 3.1 lb./ft^3. The graphite layup comprising each face sheet must each be symmetric and balanced about its midplane.

When individually cured, all elements of the trough and lid must have a buckling (crippling) strength to resist a residual compressive longitudinal stress of 14.0 (ΔT) psi, with a safety factor of 2.0 on critical stress, where ΔT = Max. Cure Temperature -70°F. The lid and bottom of the trough shall have a plate-bending modulus D, where D = $\sqrt{E_0 E_{90}}\, I$; where E_0 = Young's modulus in bending in longitudinal direction, psi; E_{90} = Young's modulus in bending in transverse direction, psi; I = bending moment of inertia per running inch of cross section; and D = 884. lb.-in. minimum. This value is required to prevent excessive transverse bulging due to straw compression. Each side wall of the trough must have a D of 64.0 lb-in. minimum.

Additionally, the completed module must be able to sustain a longitudinal compressive force (wire load) of 18.2 lbs, uniformly applied to the cross section, without buckling, using a factor of safety of 2.0.

Drawing X2E021147A001 depicts the dimensions and tolerances of the module, with the inside mold line to be considered the fixed surfaces. The allowable thicknesses listed herein in this specification will determine the outer mold line as shown in the drawing.

4.0 SHELL PART INSPECTION AND ACCEPTANCE

All completed shell parts shall be inspected for conformance to this specification and drawing no. X2E021147A001 requirements using visual, nondestructive test (NDT) methods, and dimensional inspection techniques. The inspection techniques, NDT methods and equipment used shall be fully described by the Seller in the proposal. The buyer or their designated representative will witness the inspection for the purpose of accepting the parts.

5.0 OTHER REQUIREMENTS

5.1 All tooling specific to the fabrication of the shell parts becomes the property of the buyer at the completion of the subcontract.

5.2 The Seller shall package and ship the shell parts in a manner affording sufficient protection so as not to damage the parts during transit.

5.3 At the time of delivery, the Seller shall furnish the following quality documentation:

a. Manufacturer's certification documents for all materials used directly in the parts.

b. Inspection and final test reports for all inspections and tests performed by the Seller.

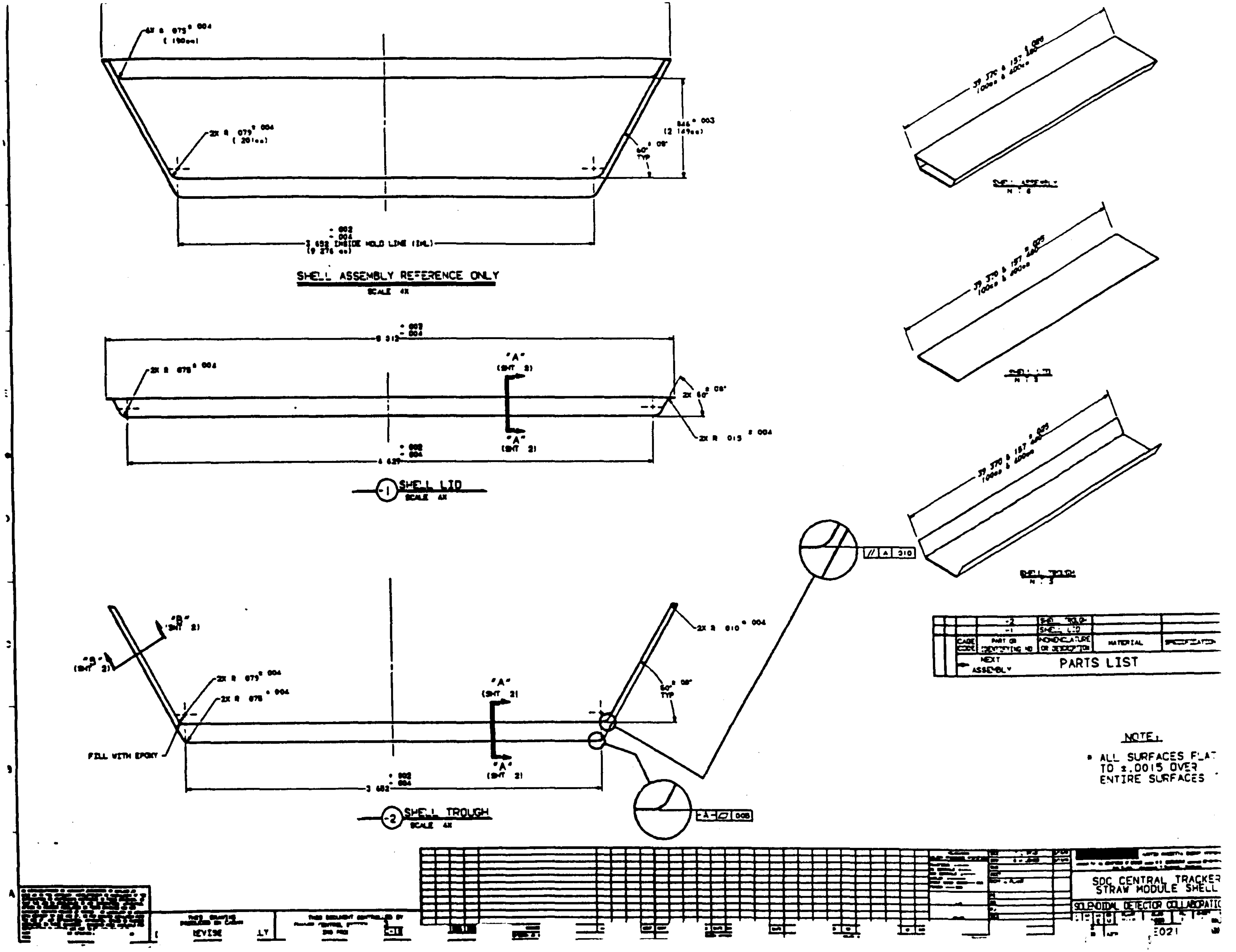
SHELL ASSEMBLY REFERENCE ONLY
SCALE 4X
3.652 INSIDE MOLD LINE (IML)
(9.276 cm)
60° TYP
SHELL LID
SCALE 4X
"A" (SHT 2)
SHELL TROUGH
SCALE 4X
FILL WITH EPOXY
"B" (SHT 2)
PARTS LIST
-2 SHELL TROUGH
-1 SHELL LID
CAGE CODE
PART OR IDENTIFYING NO
NOMENCLATURE OR DESCRIPTION
MATERIAL
SPECIFICATION
NEXT ASSEMBLY
NOTE:
* ALL SURFACES FLAT TO ±.0015 OVER ENTIRE SURFACES
SDC CENTRAL TRACKER STRAW MODULE SHELL
SOLENOIDAL DETECTOR COLLABORATION

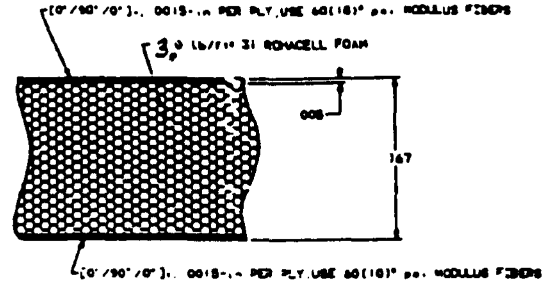

SECTION "A"-"A"

SCALE 20X

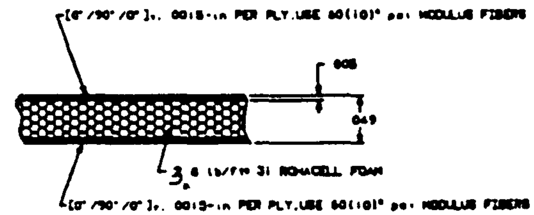

SECTION "B"-"B"

SCALE 20X

SDC CENTRAL TRACKER
STRAW MODULE SHELL

CENTRAL AND FORWARD TRACKING SUBSYSTEM
FY1991 PROGRESS REPORT

PROJECT # 9TM3-IUTDB
REPORT #3
COVERING MAY 1991 TO AUGUST 1991

AUGUST 28 1991

WESTINGHOUSE ELECTRIC CORPORATION
(W)STC
PITTSBURGH, PA

Westinghouse
Science & Technology Center

CENTRAL AND FORWARD TRACKING SUBSYSTEM

TABLE OF CONTENTS

CENTRAL AND FORWARD TRACKING SUBSYSTEM

TABLE OF CONTENTS CONTINUED

Westinghouse
Science & Technology Center

CENTRAL AND FORWARD TRACKING SUBSYSTEM

INTRODUCTION

The material presented in this final Fiscal Year 1991 Engineering Report on the Central Tracker for SDC is intended to represents the major areas of work that were pursued, under the direction of the High Energy Physics (HEP) Department of Indiana University, since the Interim Reporting period covering the first quarter of FY1991.

The material presented is in view graph form, which is the standard reporting document format used by the HEP community, and in many cases, consists of documents presented as status reports to the Physicists throughout the subject period. This material represents the the key areas of work performed during the period and thus does not include all efforts that have been undertaken at (W)STC. This material was selected to be representative and is intended to present many of the key points that it was felt needed to be highlighted.

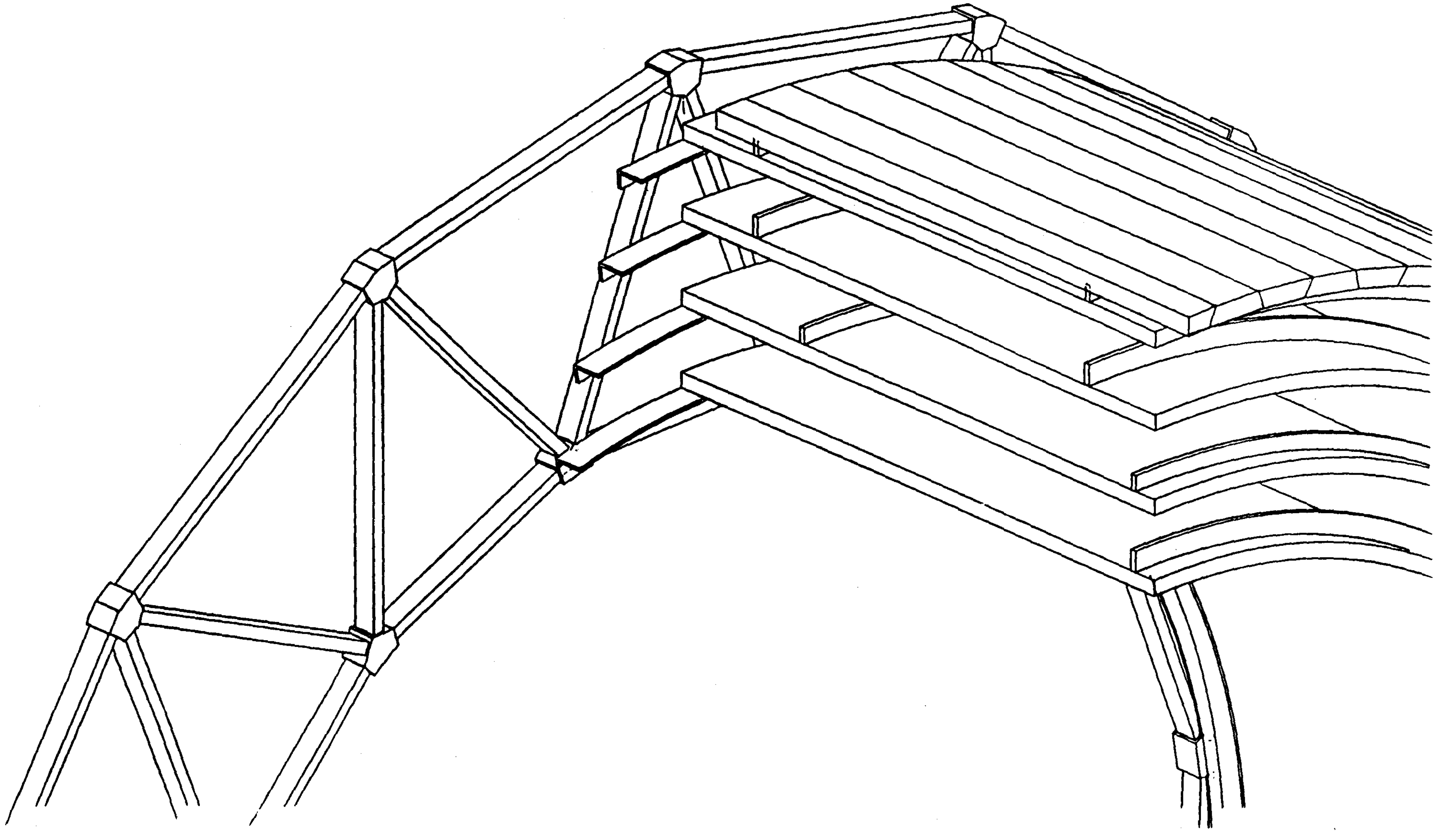

CENTRAL AND FORWARD TRACKING SUBSYSTEM

CENTRAL STRAW SUPPORT DESIGN

Support Cylinders

End Flanges

Shim Rings

Module Attachments

CENTRAL AND FORWARD TRACKING SUBSYSTEM

SUPPORT CYLINDERS

THE DESIGN USES:

Support Cylinders

1) Selected Graphite Composite Cylinders
2) Selected Two 0.10 Inch 4 Ply Layups with Rohacell Core

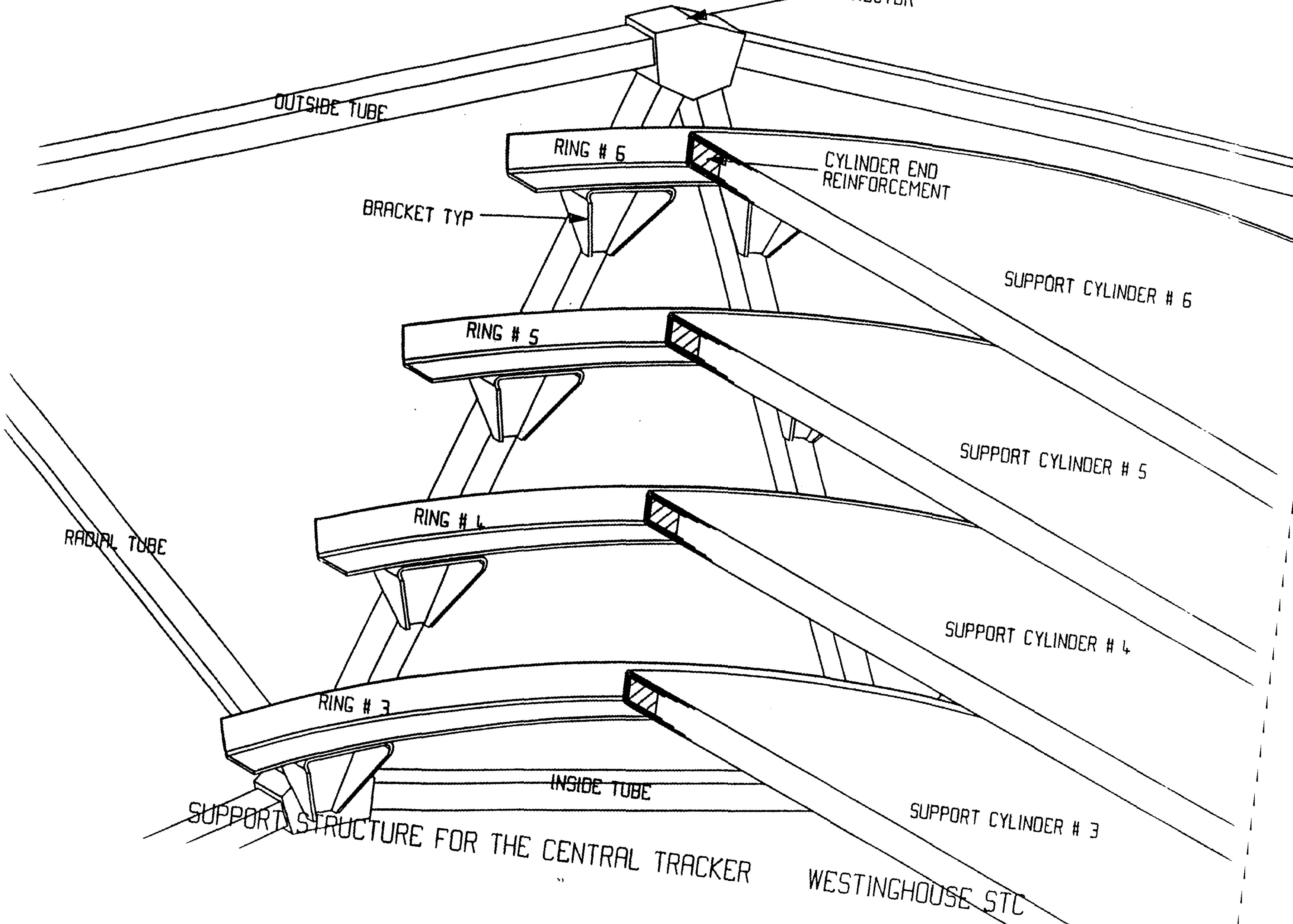

SUPPORT STRUCTURE FOR THE CENTRAL TRACKER WESTINGHOUSE STC

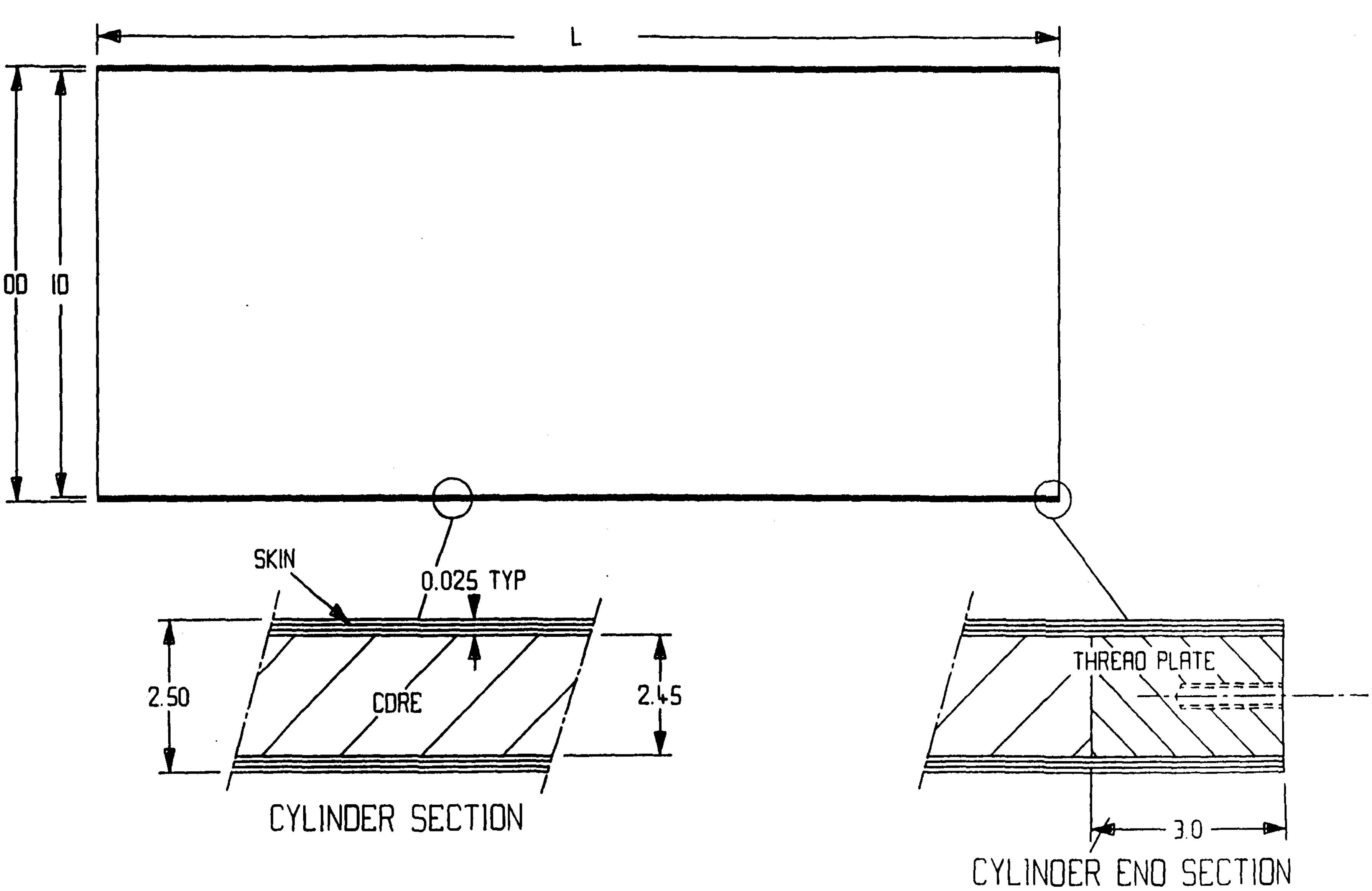

CYL	ID	OD	L
1	--	--	--
2	--	--	--
3	232.0	237.0	820
4	258.6	263.6	820
5	284.8	289.8	820
6	311.2	316.2	820

ALL DIMENSIONS ARE IN CM

SUPPORT CYLINDER DIMENSIONS WESTINGHOUSE STC

SUPPORT CYLINDER LAYUP MATERIALS

TABLE 1

CANDIDATE MATERIALS

HERCULES AS4, 0.0025" DIAM @ $600. / LB.
AMOCO P75, 0.001" DIAM @ $2200. / LB.
MODULUS 75 MILLION FOR BOTH ABOVE MATERIALS

			HERCULES AS4			AMOCO P75		
CYL	RADIUS, M	LENGTH	# PLYS	LBS	COST $	# PLYS	LBS	COST $
1	0.704	2.80	4	38.41	23,046.	6	34.6	76,120.
2	1.04	3.20	4	64.80	38,880.	6	58.3	128,260.
3	1.34	3.90	4	101.8	61,080.	6	91.6	201,520.
4	1.48	3.95	4	113.6	68,160.	6	102.4	225,280.
5	1.61	3.95	4	123.9	74,340.	6	111.5	254,100.
				TOTAL	$265,506		TOTAL	$885,280.

WESTINGHOUSE STC

DM 8-20-91

CYLINDER SKIN CONSTRUCTION MATERIALS
UNIDIRECTIONAL B-STAGE
TABLE 2

DATE	CANDIDATES	# PLYS	ANGLES	VENDOR	TYPE	DIAM.	MODULUS	RESIN SYS
	1							
	2							
	3							
	4							
	5							
	6							
	7							
	8							
	9							
	10							

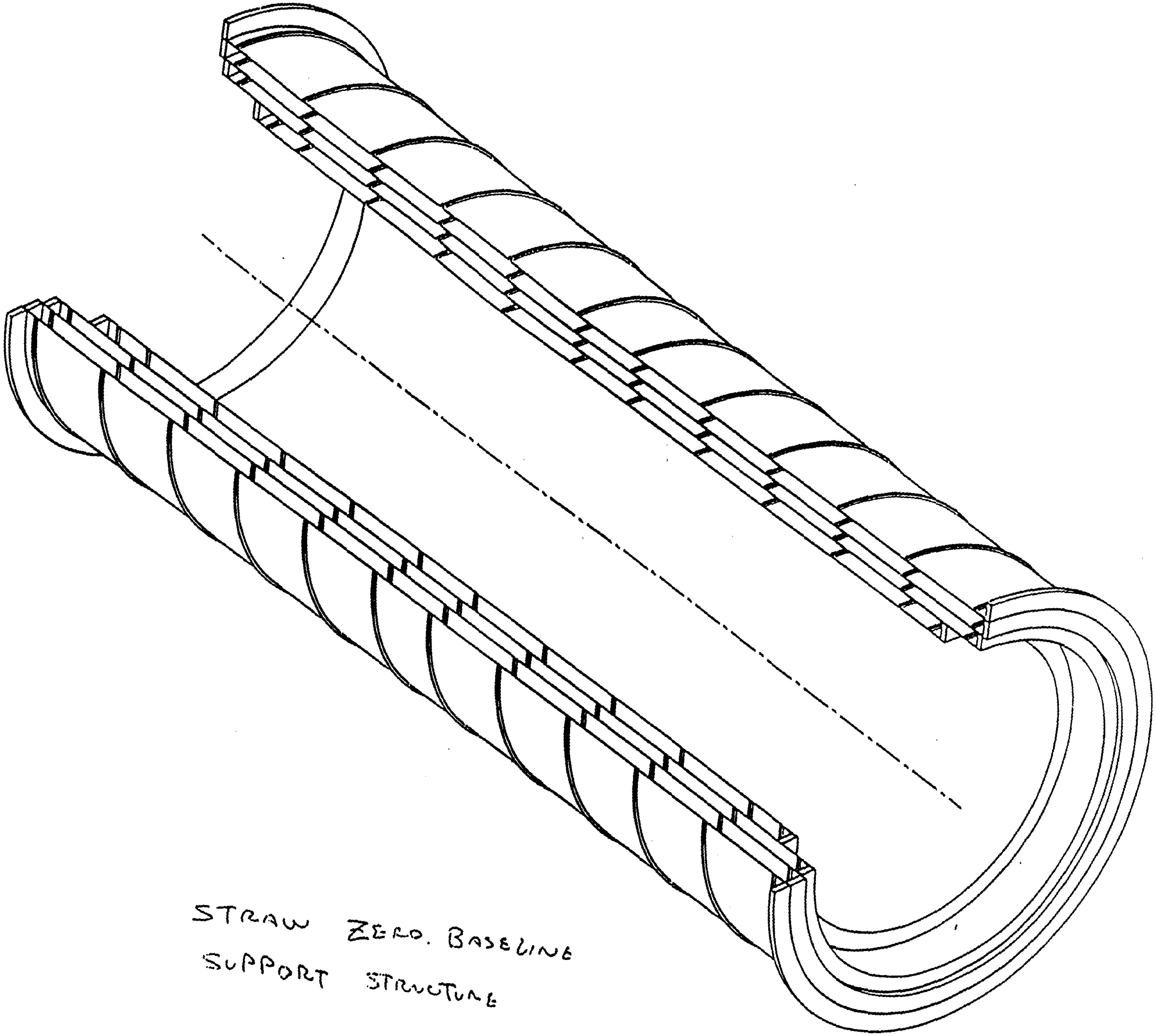

STRAW ZERO. BASELINE
SUPPORT STRUCTURE

CENTRAL AND FORWARD TRACKING SUBSYSTEM

END FLANGES

THE DESIGN USES:

End Flange Rings

1) Selected Complex Space Frame
2) Graphite Hardware (Bolts) at the Machined Cylinder Interface

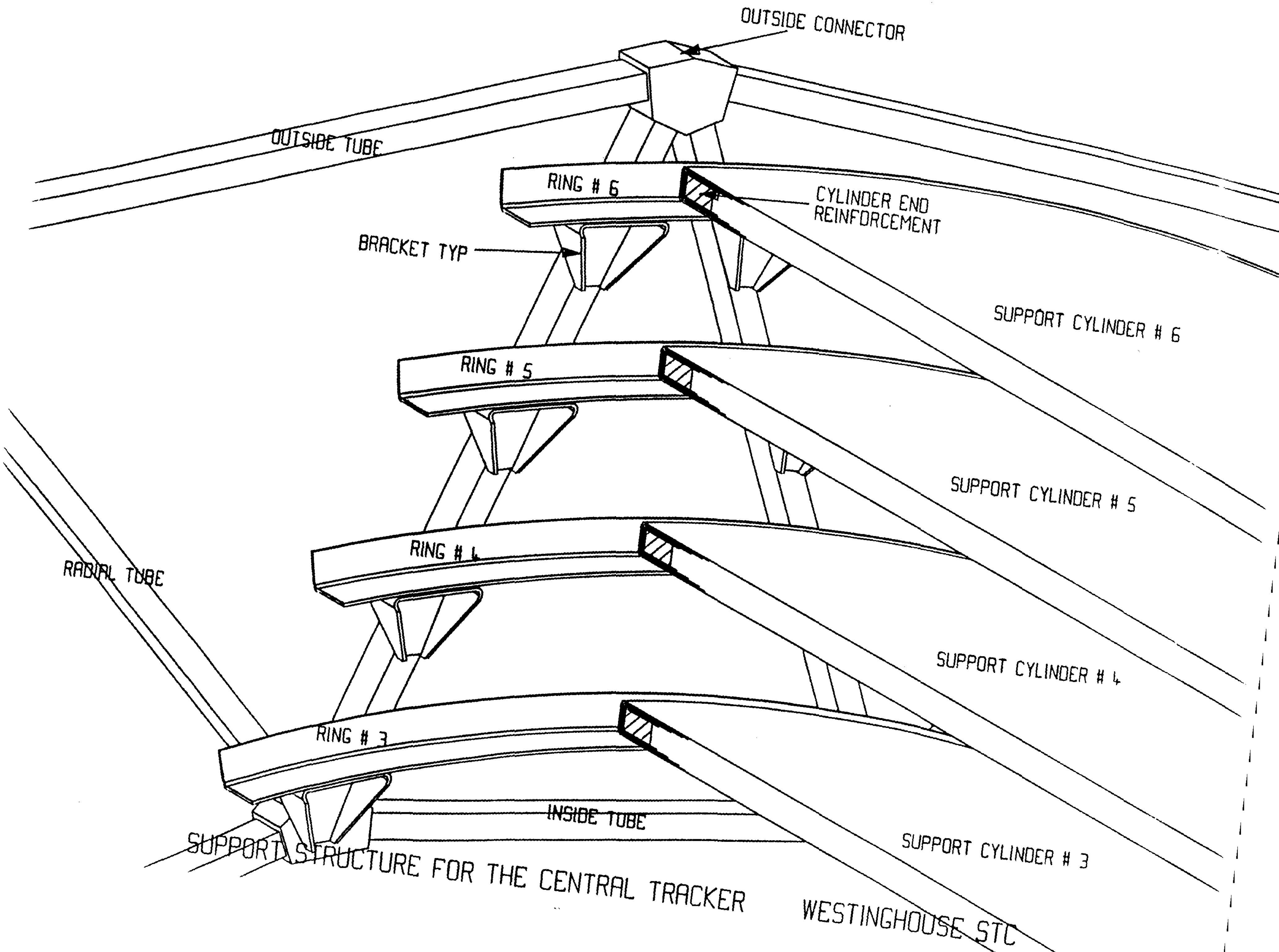

SUPPORT STRUCTURE FOR THE CENTRAL TRACKER WESTINGHOUSE STC

CENTRAL AND FORWARD TRACKING SUBSYSTEM

CENTRAL TRACKER MOUNTING

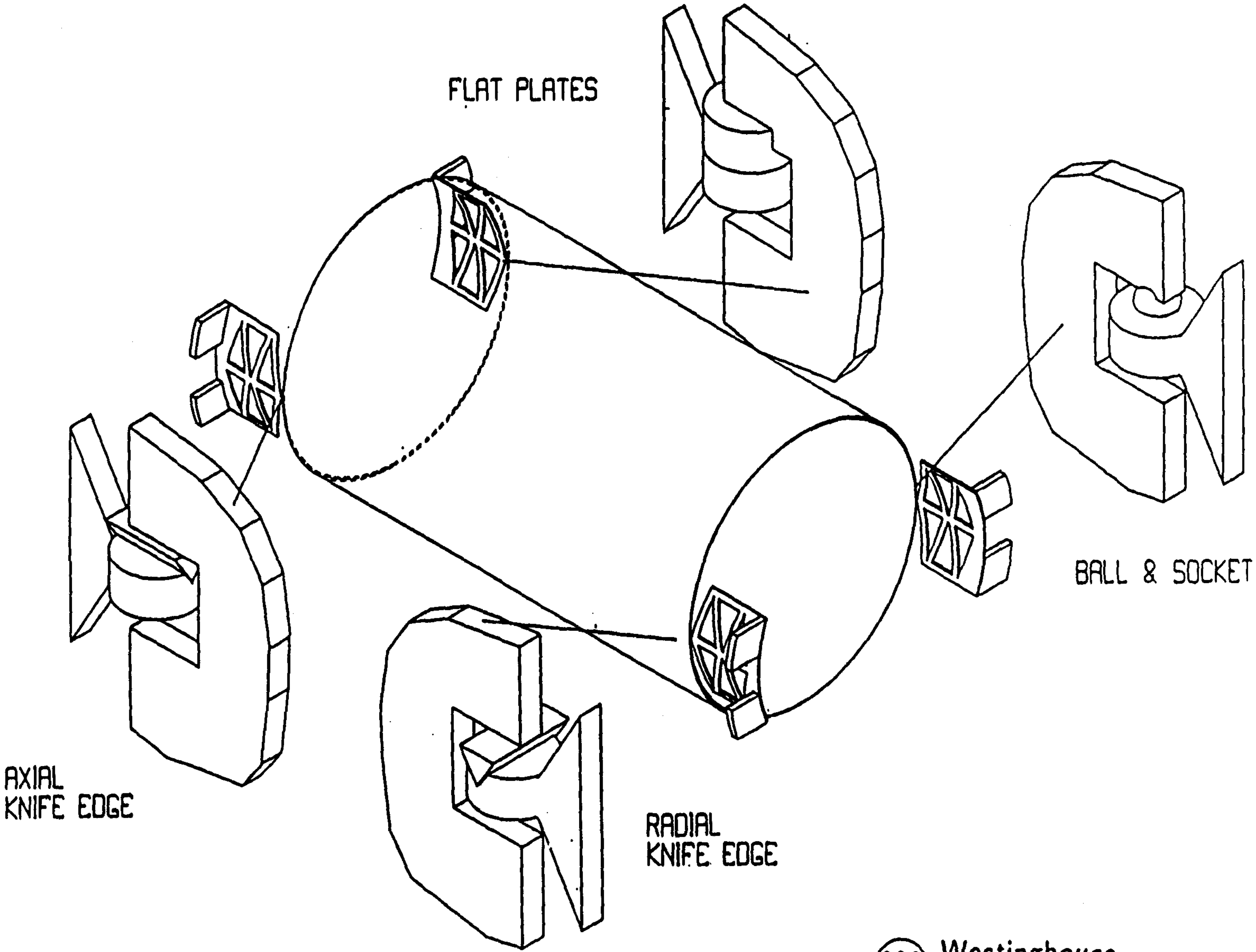

Westinghouse
Science & Technology Center

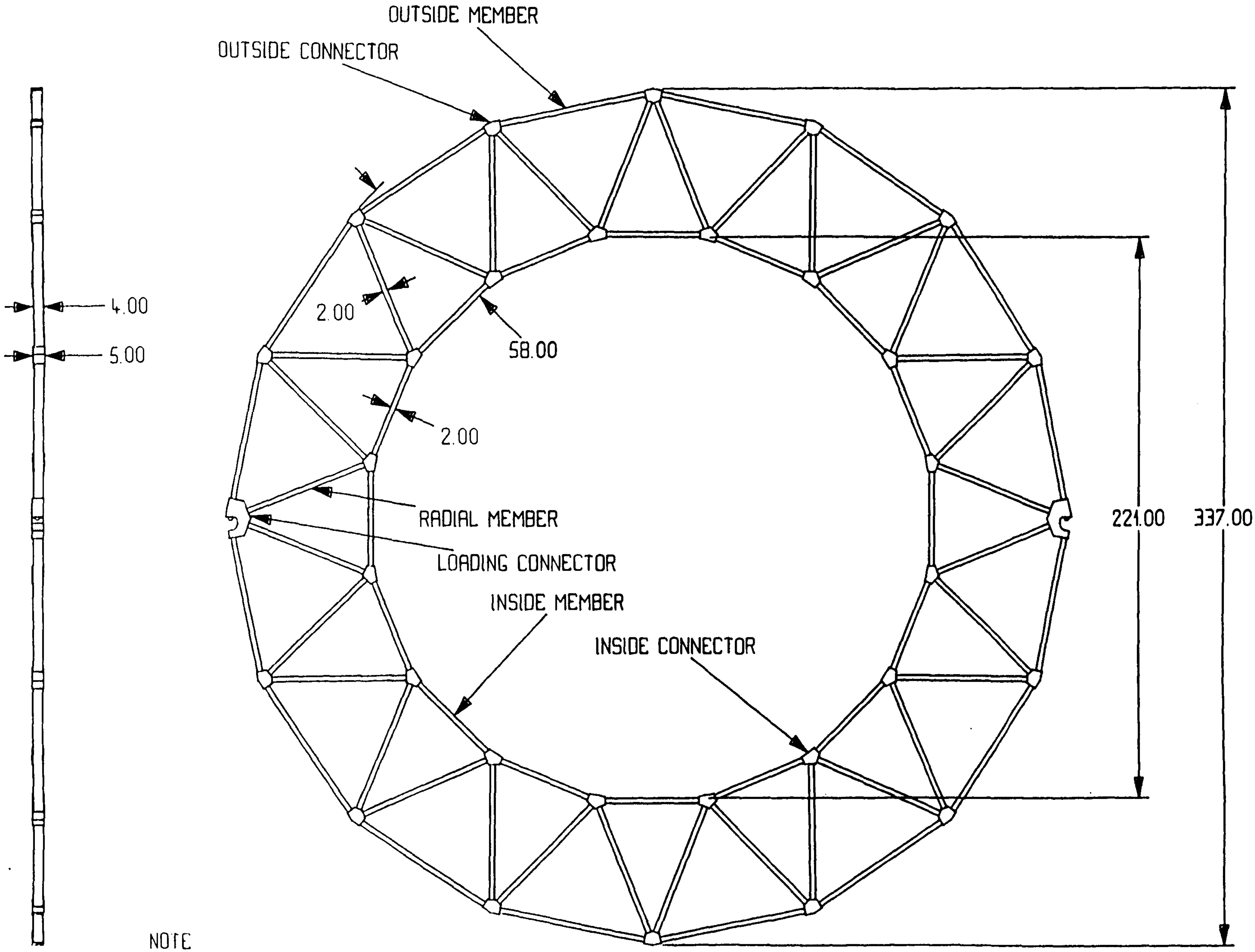

NOTE
1 ALL DIMENSIONS ARE IN CM

STRUCTURAL TUBING QUANITIES FOR TWO SUPPORT FRAMES

TUBE #	L,CM	QUAN/FRAME	TOTAL
1	43.45	16	32
2	54.36	2	4
3	53.19	2	4
4	55.92	28	32
5	58.91	2	4
6	61.91	2	4
7	64.55	12	24

		TOTAL	128 PCS.

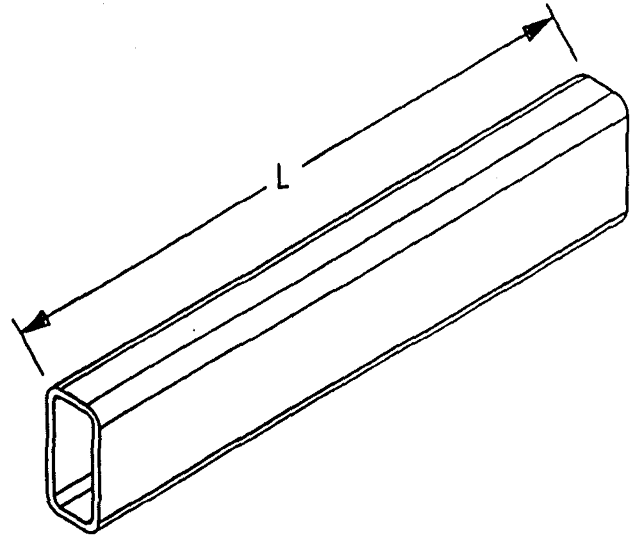

MATERIAL GRAPHITE - EPOXY COMPOSITE

ALL DIMENSIONS IN CM.

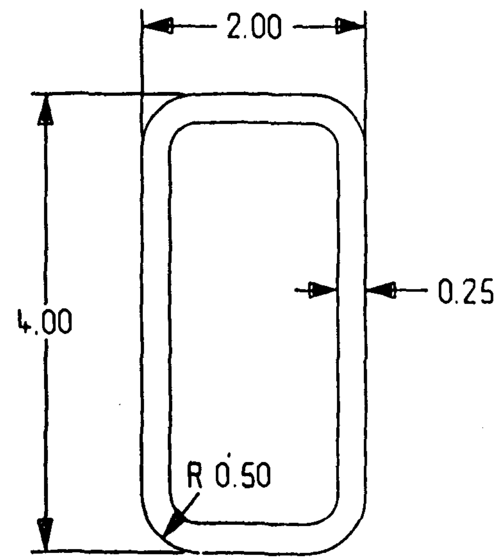

SUPPORT FRAME STRUCTURAL TUBING WESTINGHOUSE STC

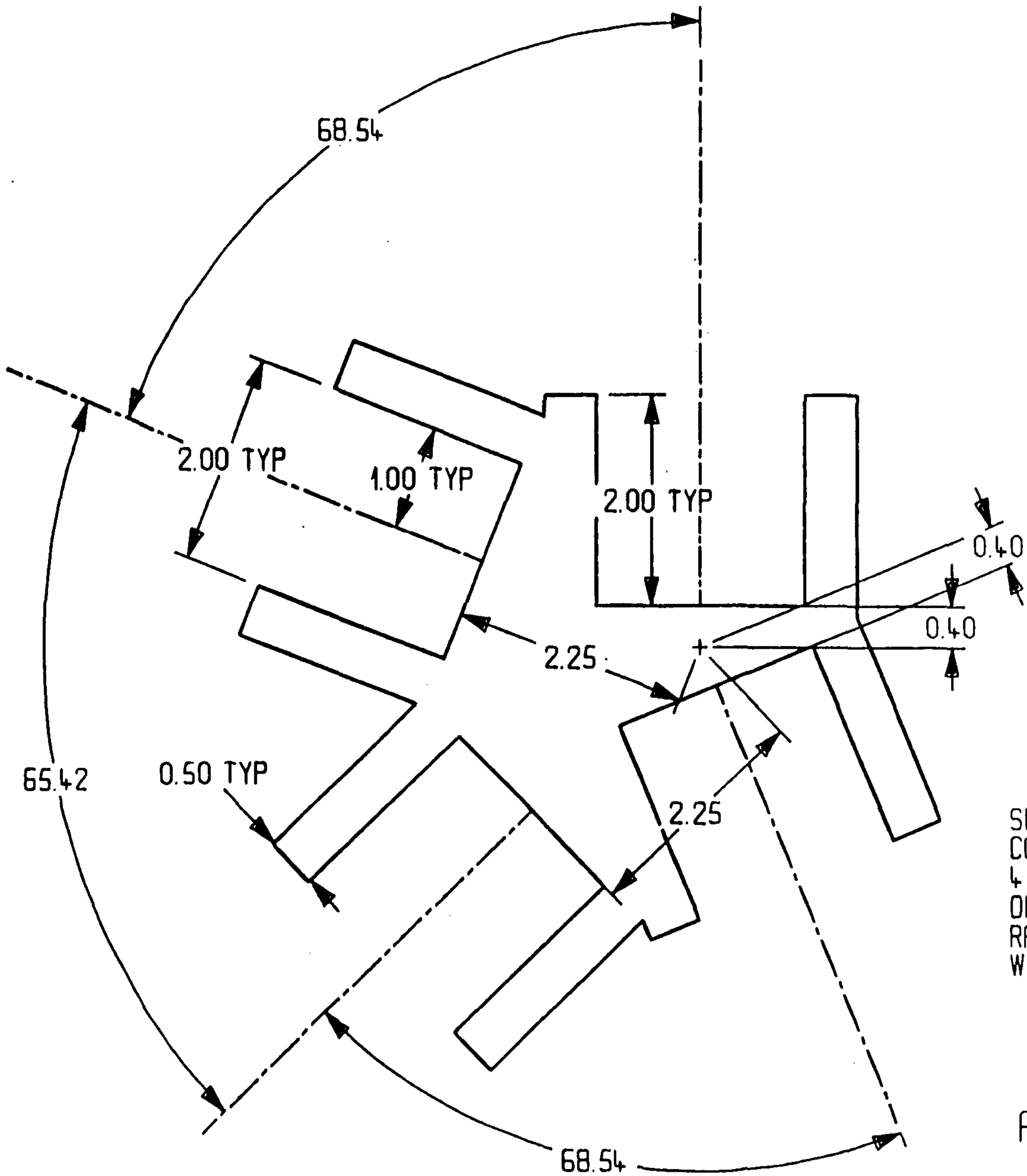

SECTION OF SUPPORT FRAME INSIDE CONNECTOR, THIS CONNECTOR CONNECTS 4 RECTANGULAR TUBES HAVING A SECTION OF 2.00 X 4.00 CM WITH 0.50 CM OUTSIDE RADIUS AT ALL CORNERS, MINIMUM WALL THICKNESS = 0.50 CM

ALL DIMENSIONS IN CM

INSIDE CONNECTOR SECTION

WESTINGHOUSE STC

DM 8-2-94

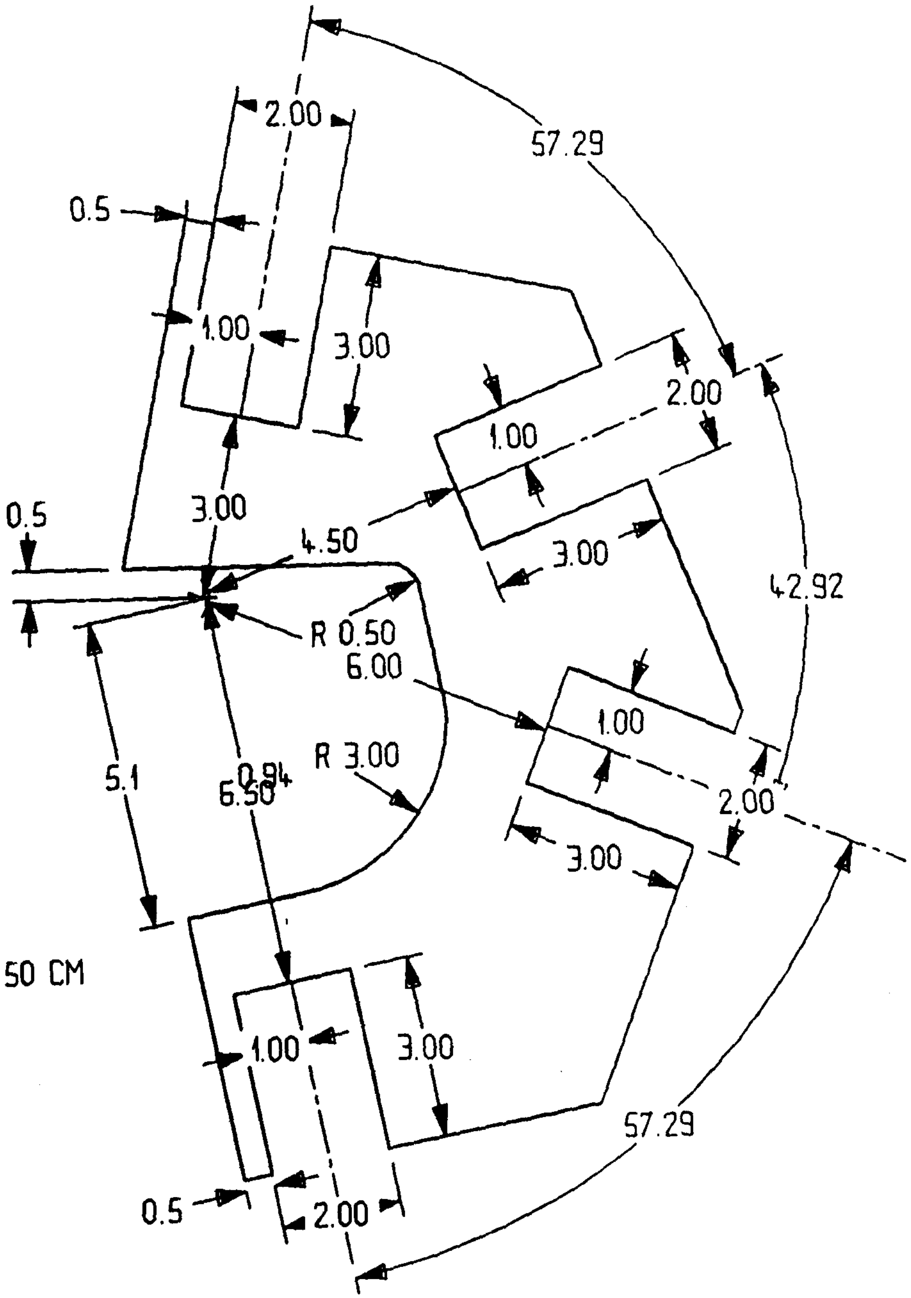

SECTION OF THE SUPPORT FRAME LOAD CONNECTOR
THIS CONNECTOR CONNECTS 4 RECTANGULAR TUBES
HAVING A 2.00 X 4.00 CM SECTION AND 0.50 CM RADIUS
AT ALL OUTSIDE CORNERS. MINIMUM WALL THICKNESS = 0.50 CM

LOAD CONNECTOR SECTION WESTINGHOUSE STC

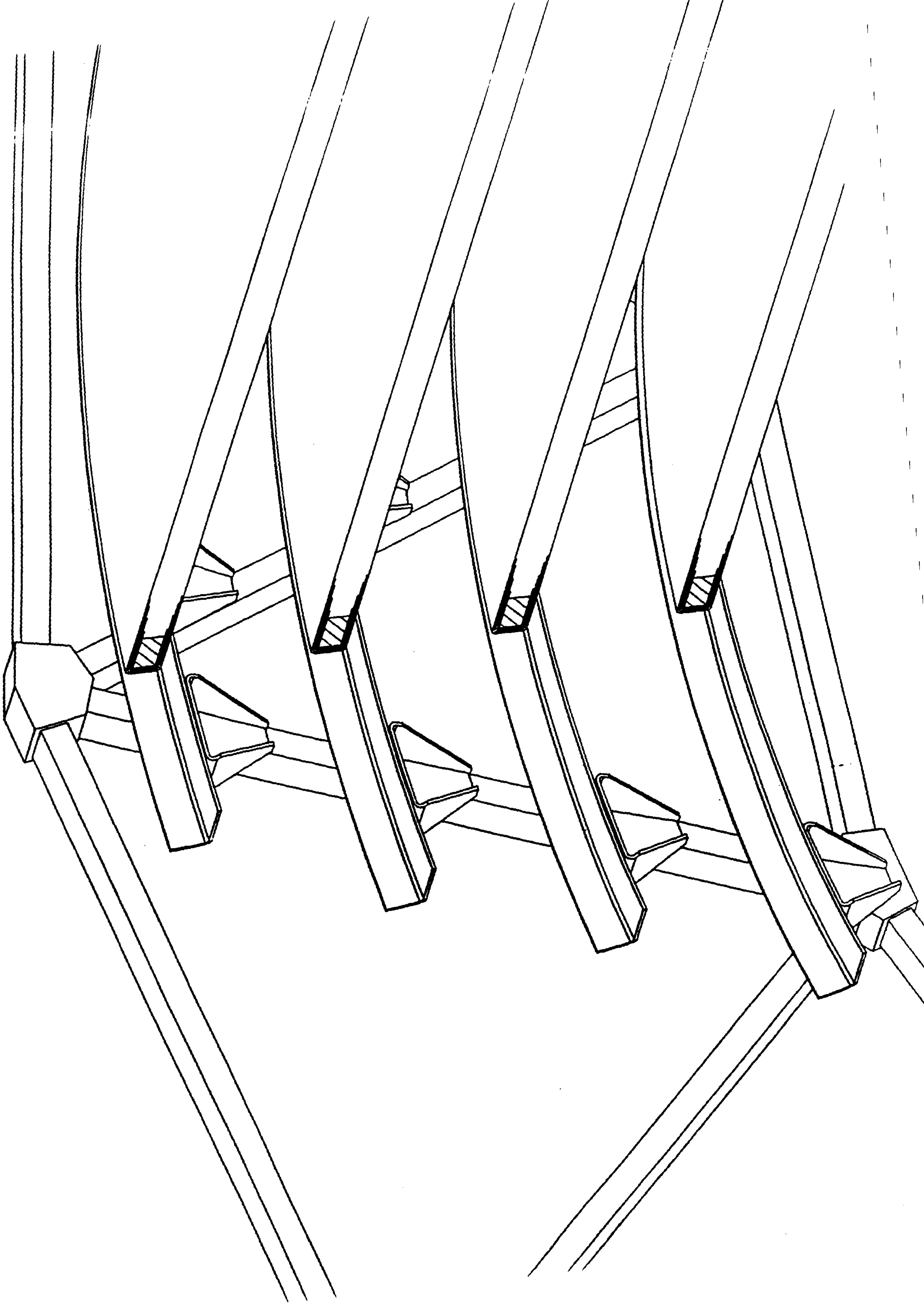

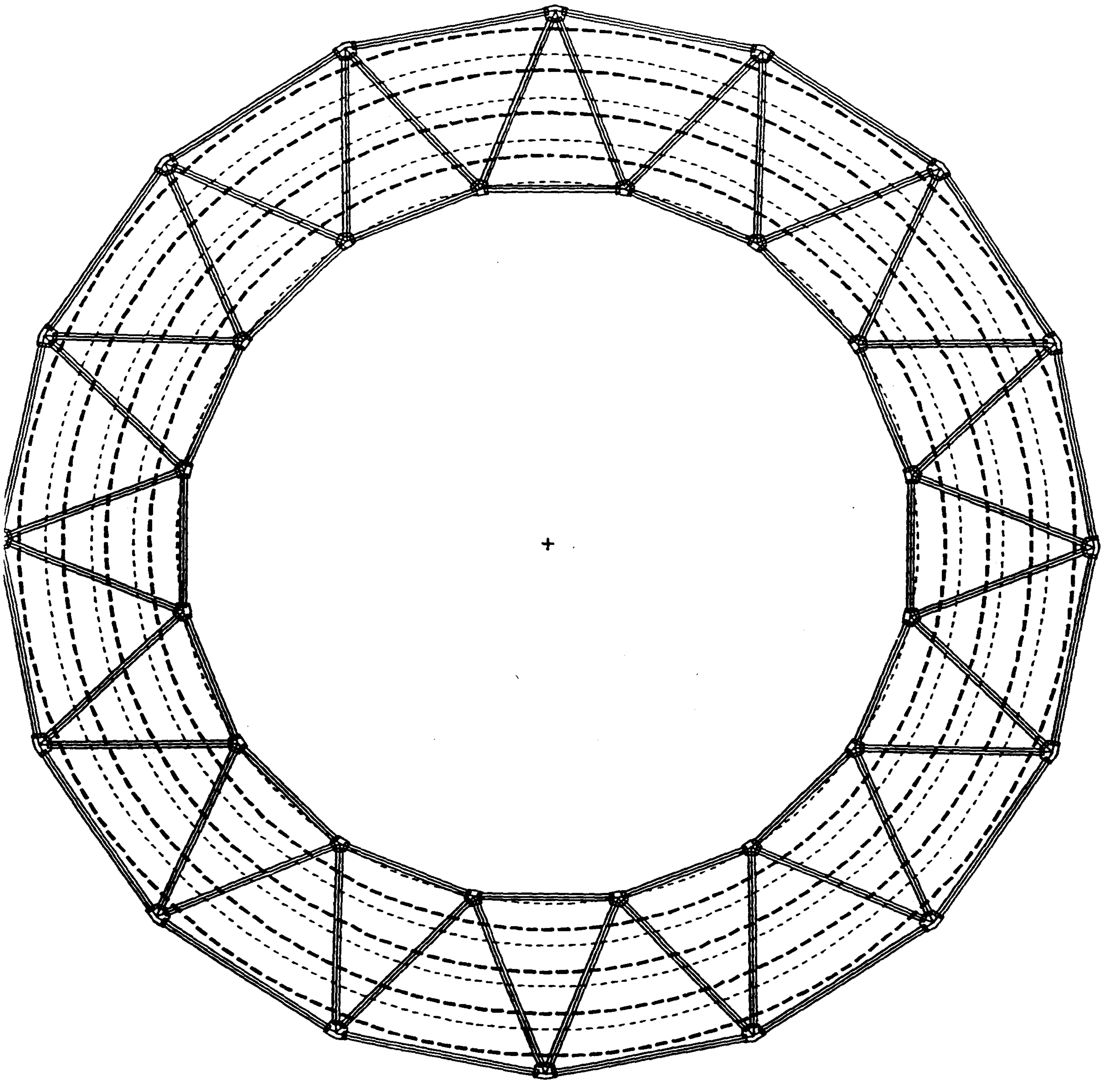

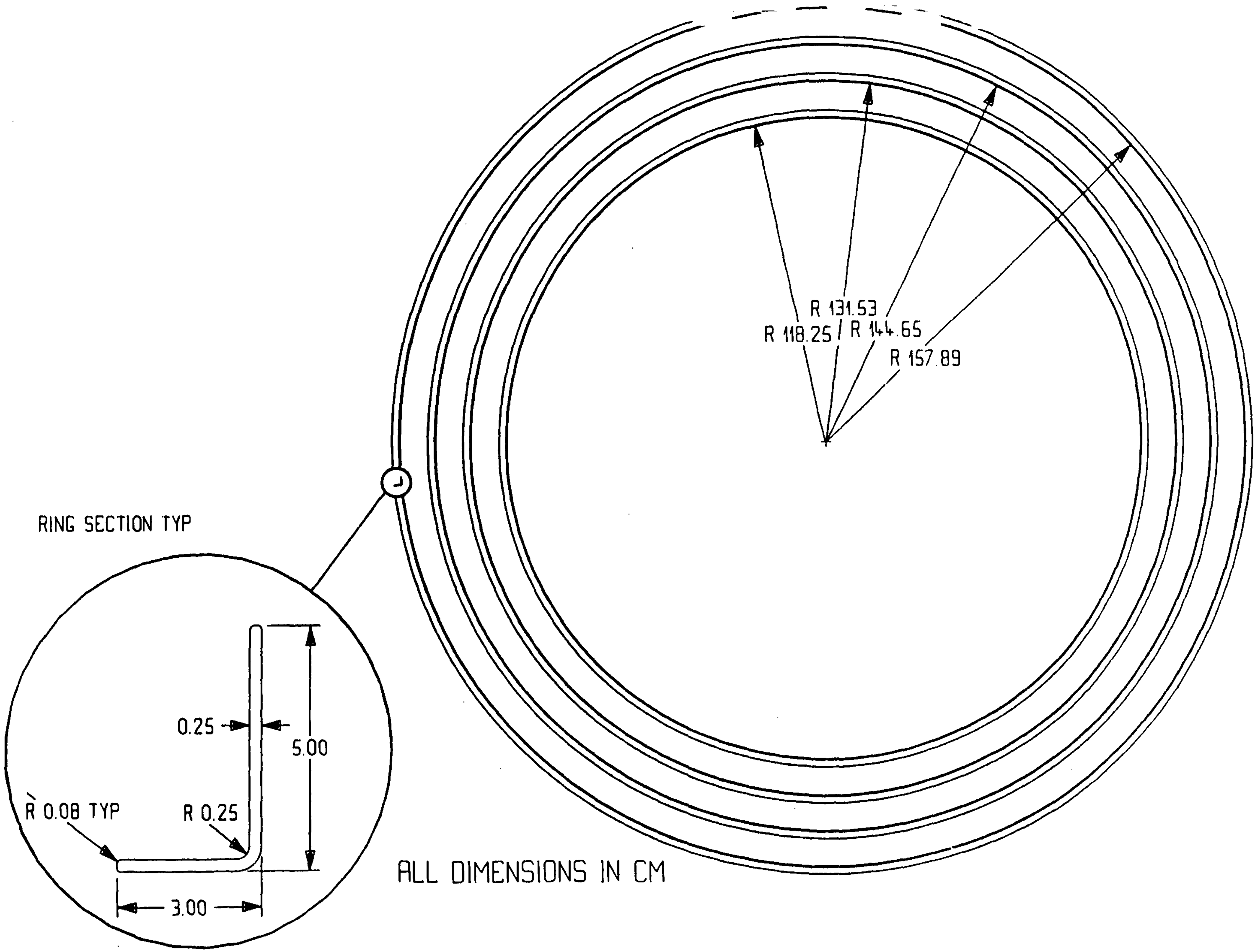

COMPOSITE SUPPORT RINGS WESTINGHOUSE STC

DM 8-5-91

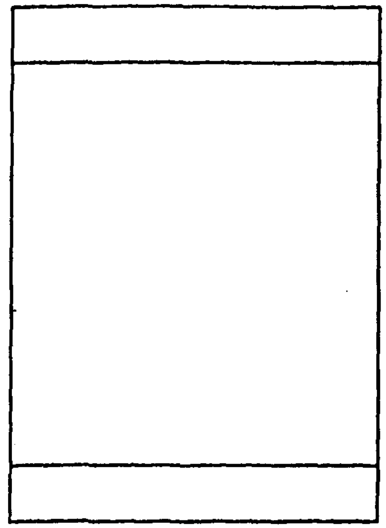

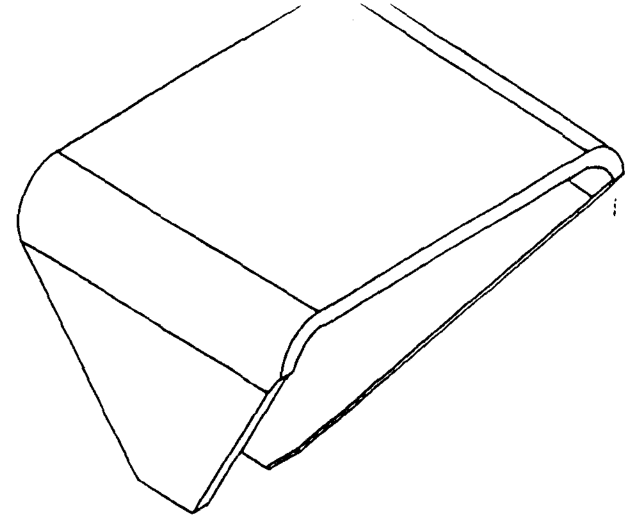

NOTE

1 SUPERLAYER 3 R = 115.75
SUPERLAYER 4 R = 129.04
SUPERLAYER 5 R = 142.16
SUPERLAYER 6 R = 155.39

2 ALL DIMENSIONS IN CM

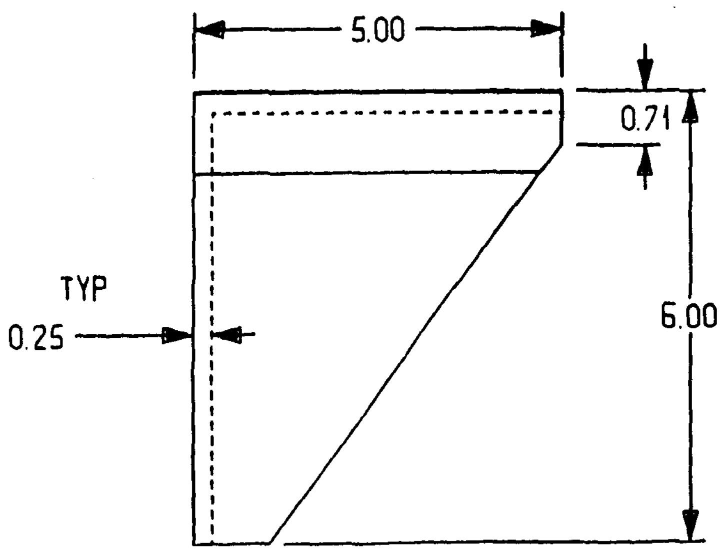

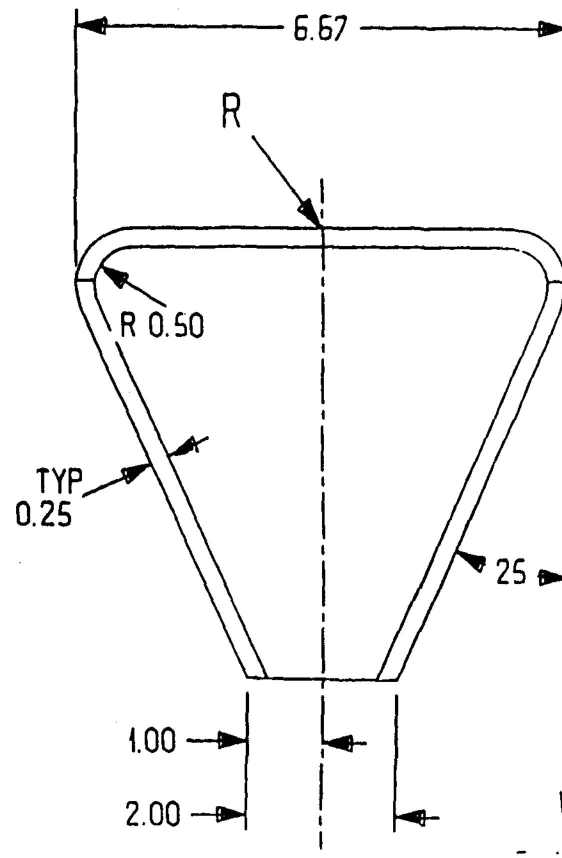

RING SUPPORT BRACKET

W STC

7-2

CENTRAL AND FORWARD TRACKING SUBSYSTEM

SHIM RINGS

THE DESIGN USES:

Shim Rings

1) Selected Rohacell Rings as Simple Way to Get Precision Cylinders
2) Required for Stereo

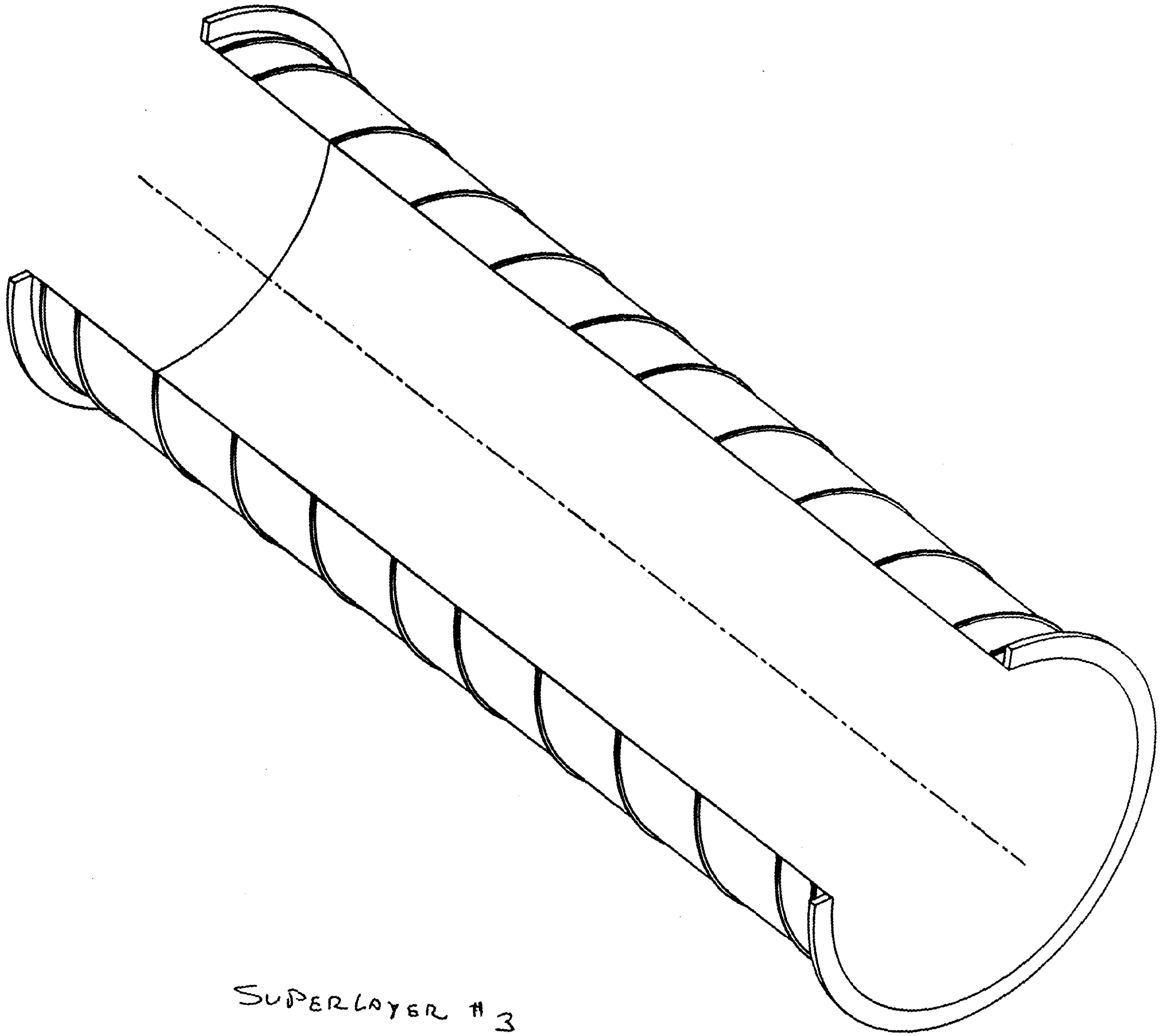

SUPERLAYER #3
SUPPORT CYLINDER

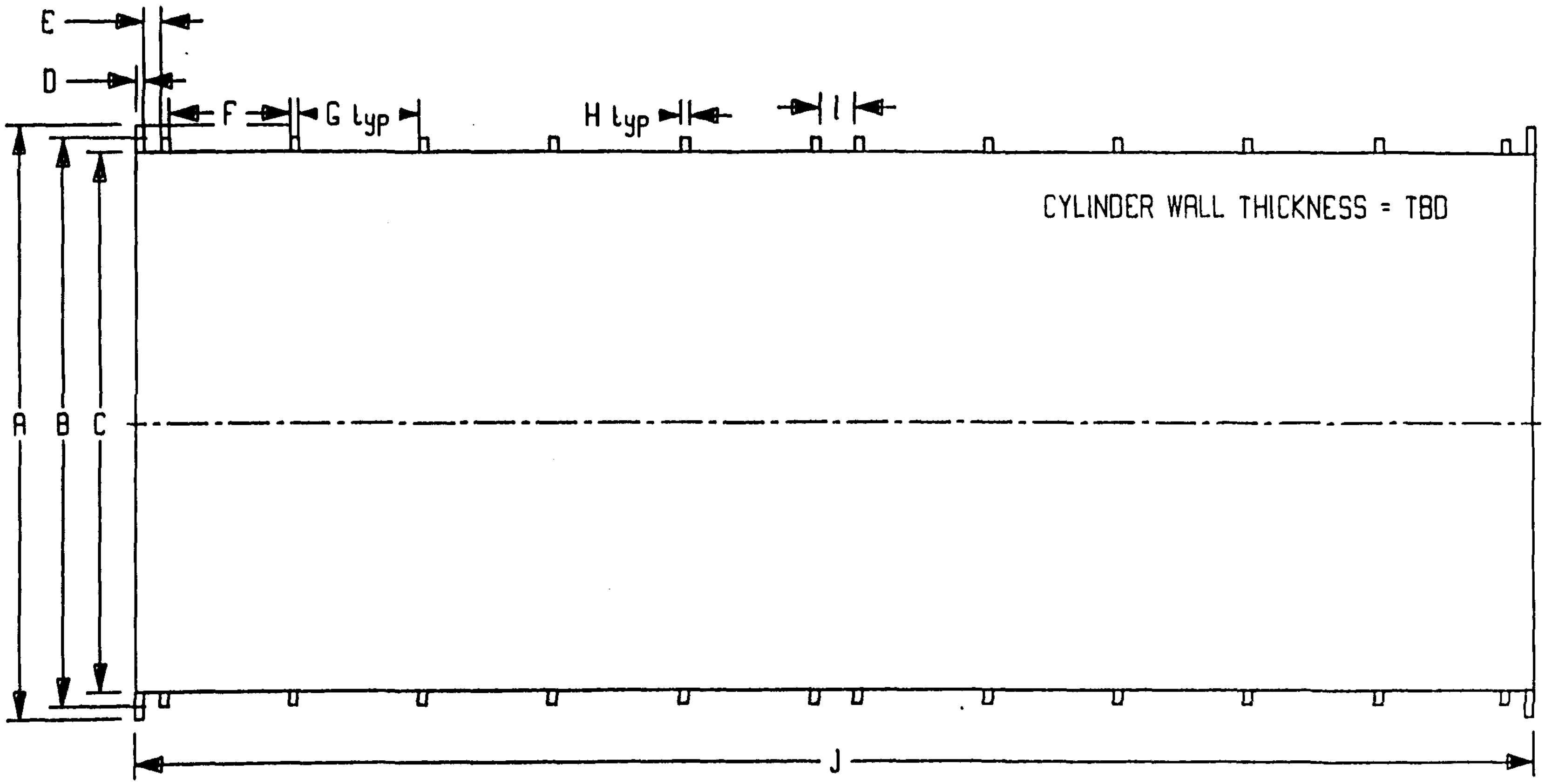

DIMENSIONS OF CENTRAL TRACKER SUPPORT CYLINDERS

SUPRLYR	A	B MIN	B MAX	C	D	E	F	G	H	I	J	
6	335.0	319.5	320.5	317.5	5.0	10.0	70.0	70.0	2.50	20.0	810.0	CM
5	317.5	290.8	295.4	288.8	5.0	10.0	70.0	70.0	2.50	20.0	810.0	CM
4	288.8	266.2	267.2	264.2	5.0	10.0	65.0	70.0	2.50	20.0	800.0	CM
3	264.2	237.9	242.8	235.9	5.0	10.0	30.0	70.0	2.50	20.0	730.0	CM

CENTRAL AND FORWARD TRACKING SUBSYSTEM

STEREO SHIM RING

FEATURES

- o Machined in Place on Cylinder on Mandrel
- o Relatively Simple to Skew Machining Axis to Mandrel Cylinder Axes
- o Single Setup Produces All Module Locations Therefore Initial Setup Not Critical

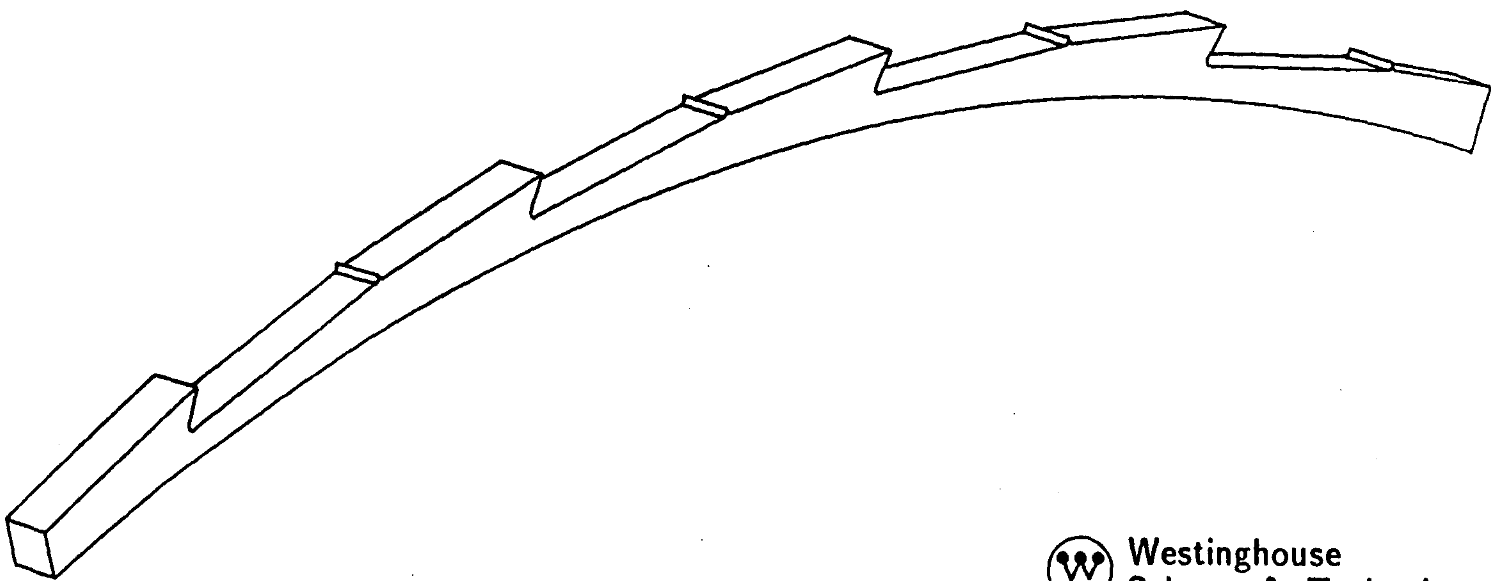

Westinghouse
Science & Technology Center

CENTRAL AND FORWARD TRACKING SUBSYSTEM

MODULE ATTACHMENT

THE DESIGN USES:

Mechanical Attachment

1) Selected to Attach Modules Directly to Shim Rings
2) Uses Precision Machined or Formed Rohacell Blocks as an Interface or
3) Locations are Machined Directly into Shim Rings

MODULE POSITIONING

MODULE WITH SPACER ATTACHED

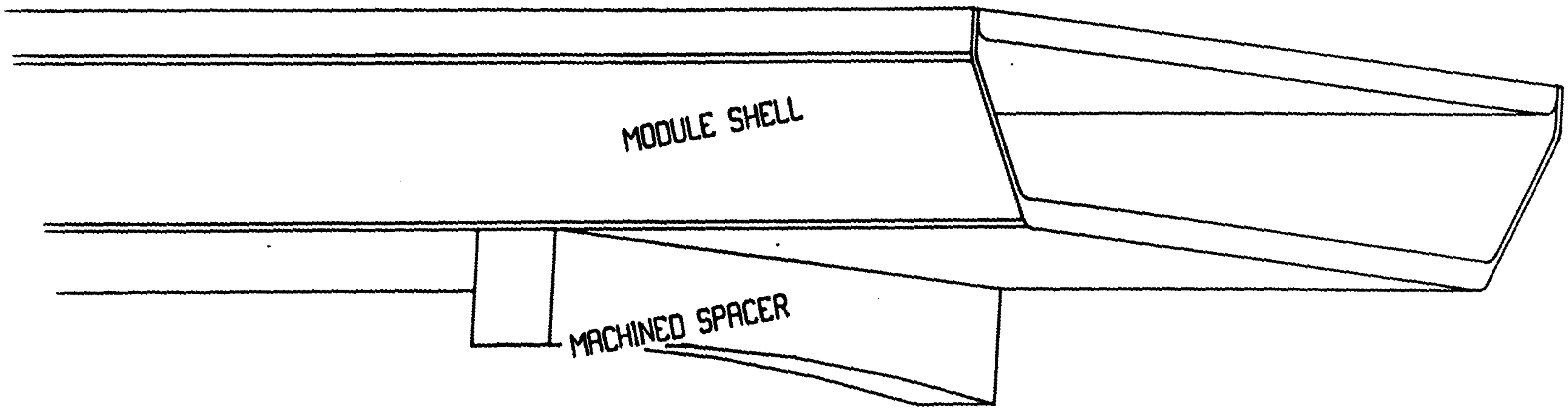

MODULE POSITIONING

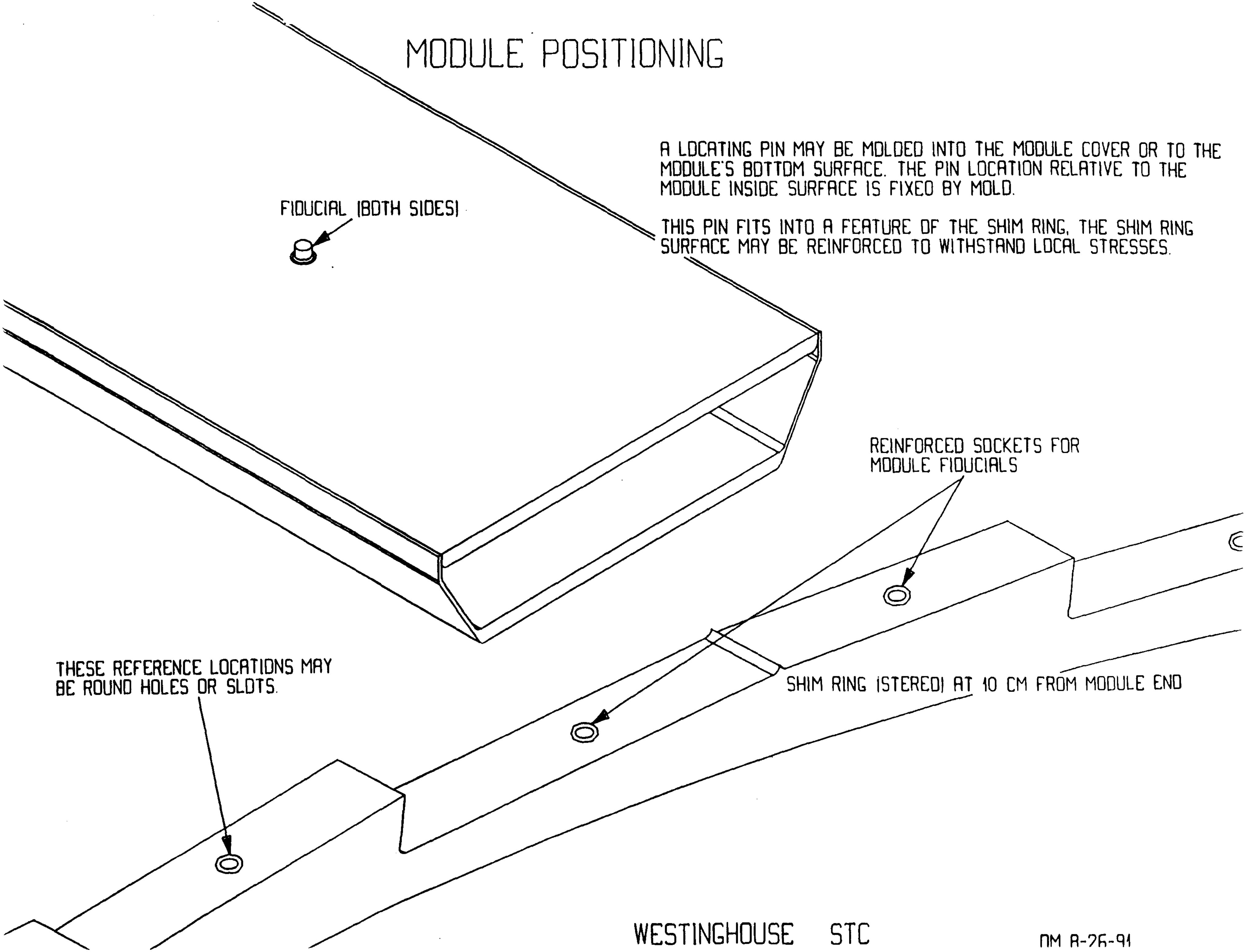

CENTRAL AND FORWARD TRACKING SUBSYSTEM

COMPONENT MANUFACTURING AND COSTS

- Support Cylinders
- End Flanges
- Shim Rings
- Module Placement

Westinghouse
Science & Technology Center

CENTRAL AND FORWARD TRACKING SUBSYSTEM

SUPPORT CYLINDERS

THE MANUFACTURING PROCESS USES:

Support Cylinders

1) Large Steel Mandrels to Form Graphite Composite Cylinders
2) Large Custom Machine Tool to Apply Ply Layups and Rohacell Core

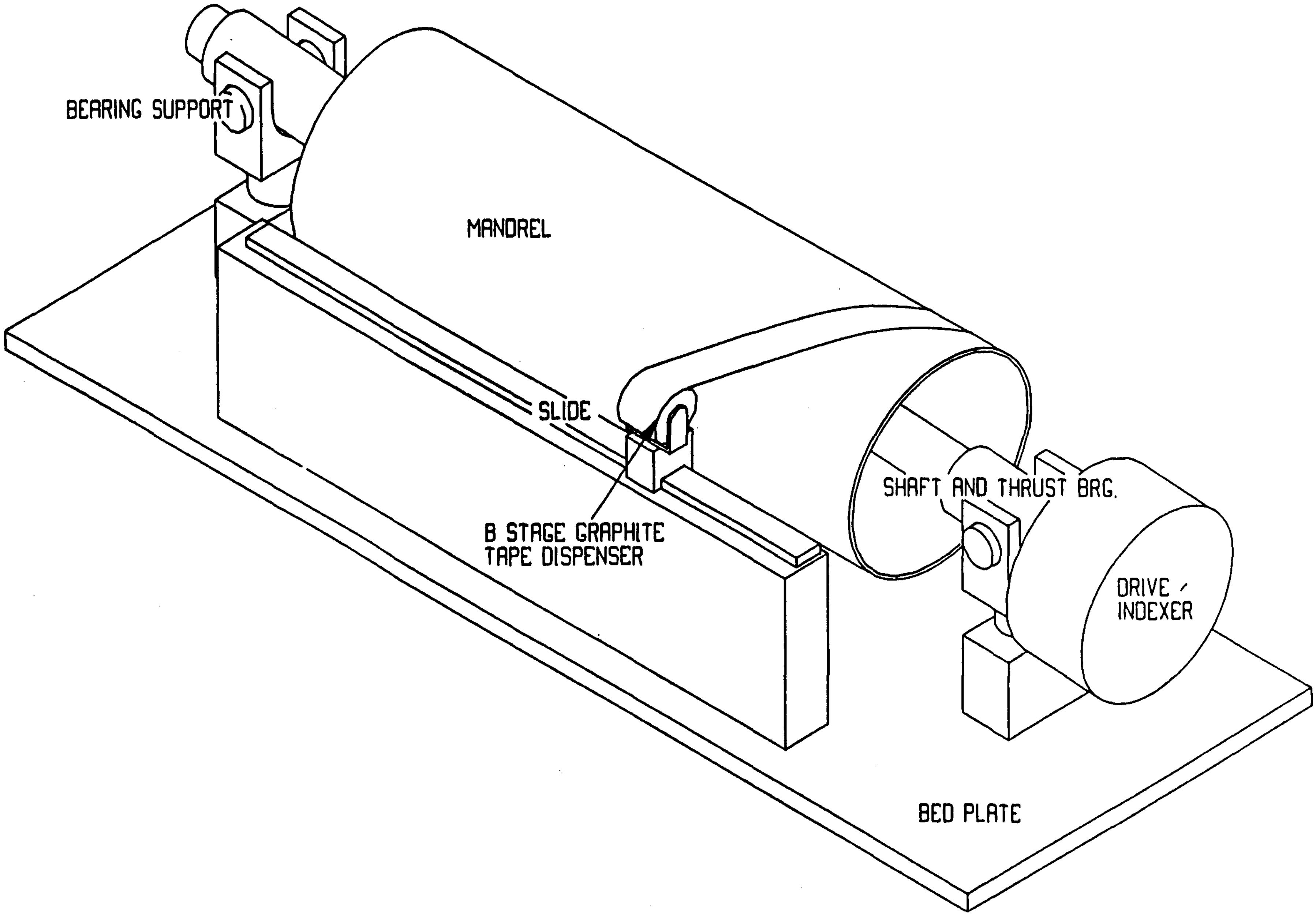

SYSTEM FOR TAPE FABRICATION OF SUPPORT CYLINDERS

MACH1.WK3 TAPING STATION 6-14-91

ITEM	SUPPLIER	COMMENT	PURCHASE $	DESIGN HRS	DESIGN $	DRAFTING HRS	DRAFTING $	MACHINING HRS	MACHINING $	LABOR HRS	LABOR $	TOTAL
BED PLATE PEDESTAL ASSY.	LAKESHORE INC	10 FT X 20 FT X 2 PCS	$30,000.00	24.00	$1,560.00	20.00	$1,000.00					$32,560.00
BLANK END PEDESTAL												
BASE ASSY												
BURNOUTS		PURCHASED MATERIALS	$1,800.00	30.00	$1,950.00	40.00	$2,000.00	20.00	$1,000.00			$6,750.00
WELDING		TIME & MATERIALS								32.00	$1,600.00	$1,600.00
STRESS ANNEALING		TRANSPORTATION & TIME	$400.00									$400.00
MACHINING		TIME						60.00	$3,000.00			$3,000.00
ASSY		TIME								24.00	$1,200.00	$1,200.00
COLUMN ASSY												
BURNOUTS		PURCHASED MATERIALS	$1,200.00	30.00	$1,950.00	40.00	$2,000.00			20.00	$1,000.00	$6,150.00
WELDING		TIME & MATERIALS								20.00	$1,000.00	$1,000.00
STRESS ANNEALING		TRANSPORTATION & TIME	$400.00									$400.00
MACHINING		TIME						32.00	$1,600.00	16.00	$800.00	$2,400.00
ELEVATING MECHANISM		PURCHASED MATERIAL	$2,000.00	24.00	$1,560.00	32.00	$1,600.00			12.00	$600.00	$5,760.00
ASSY		TIME								40.00	$2,000.00	$2,000.00
TRUNNION BRG HOUSING ASSY												
BURNOUTS		PURCHASED MATERIALS	$1,600.00	32.00	$2,080.00	40.00	$2,000.00	24.00	$1,200.00	16.00	$800.00	$7,680.00
WELDING		TIME								24.00	$1,200.00	$1,200.00
STRESS ANNEALING		TRANSPORTATION AND TIME	$400.00									$400.00
MACHINING		TIME						32.00	$1,600.00	12.00	$600.00	$2,200.00
BEARING ASSY		PURCHASED MATERIALS	$600.00	16.00	$1,040.00	16.00	$800.00			16.00	$800.00	$3,240.00
ASSEMBLY TIME		TIME								32.00	$1,600.00	$1,600.00
SHAFT BRG HOUSING ASSY												
BURNOUTS		PURCHASED MATERIALS	$300.00	12.00	$780.00	16.00	$800.00					$1,880.00
WELDING		TIME								12.00	$600.00	$600.00
STRESS ANNEALING		TRANSPORTATION AND TIME	$300.00									$300.00
MACHINING		TIME						32.00	$1,600.00	8.00	$400.00	$2,000.00
BEARING ASSY		PURCHASED MATERIALS	$2,000.00	12.00	$780.00	12.00	$600.00			8.00	$400.00	$3,780.00
ASSEMBLY TIME		TIME								16.00	$800.00	$800.00
DRIVEN END PEDESTAL												
BASE ASSY												
BURNOUTS		PURCHASED MATERIALS	$1,800.00	30.00	$1,950.00	40.00	$2,000.00	20.00	$1,000.00			$6,750.00
WELDING		TIME								32.00	$1,600.00	$1,600.00
STRESS ANNEALING		TRANSPORTATION AND TIME	$400.00									$400.00
MACHINING		TIME						60.00	$3,000.00			$3,000.00
ASSY		TIME								24.00	$1,200.00	$1,200.00
COLUMN ASSY												
BURNOUTS		PURCHASED MATERIALS	$1,200.00	30.00	$1,950.00	40.00	$2,000.00	40.00	$2,000.00	20.00	$1,000.00	$8,150.00
WELDING		TIME								20.00	$1,000.00	$1,000.00
STRESS ANNEALING		TRANSPORTATION AND TIME	$400.00									$400.00
MACHINING		TIME						32.00	$1,600.00	16.00	$800.00	$2,400.00
ELEVATING MECHANISM		PURCHASED MATERIALS	$2,000.00	24.00	$1,560.00	32.00	$1,600.00			12.00	$600.00	$5,760.00
ASSY		TIME								40.00	$2,000.00	$2,000.00
TRUNNION BRG HOUSING ASSY												
BURNOUTS		PURCHASED MATERIALS	$1,600.00	32.00	$2,080.00	40.00	$2,000.00	24.00	$1,200.00	16.00	$800.00	$7,680.00
WELDING		TIME								24.00	$1,200.00	$1,200.00
STRESS ANNEALING		TRANSPORTATION AND TIME	$400.00									$400.00
MACHINING		TIME						32.00	$1,600.00	12.00	$600.00	$2,200.00
BEARING ASSY		PURCHASED MATERIALS	$800.00	16.00	$1,040.00	24.00	$1,200.00			16.00	$800.00	$3,840.00
ASSEMBLY TIME		TIME								32.00	$1,600.00	$1,600.00
SHAFT BRG HOUSING ASSY												
BURNOUTS		PURCHASED MATERIALS	$300.00									$300.00
WELDING		TIME						12.00	$600.00	12.00	$600.00	$1,200.00
STRESS ANNEALING		TRANSPORTATION AND TIME	$300.00									$300.00
MACHINING		TIME						32.00	$1,600.00	8.00	$400.00	$2,000.00
SHAFT BEARING ASSY		PURCHASED MATERIALS	$2,000.00	12.00	$780.00	12.00	$600.00			8.00	$400.00	$3,780.00
THRUST BEARING ASSY		PURCHASED MATERIALS	$3,200.00	24.00	$1,560.00	32.00	$1,600.00			12.00	$600.00	$6,960.00
DRIVE												
ROTARY ENCODER		PURCHASED MATERIALS	$1,800.00	16.00	$1,040.00	24.00	$1,200.00			12.00	$600.00	$4,640.00
BRAKE ASSY		PURCHASED MATERIALS		12.00	$780.00	12.00	$600.00			18.00	$900.00	$2,280.00
ASSEMBLY TIME		TIME								24.00	$1,200.00	$1,200.00
MATERIAL SUPPLY STATION												
CUTTING TABLE		PURCHASED MATERIALS	$2,000.00	12.00	$780.00	12.00	$600.00	10.00	$500.00	32.00	$1,600.00	$5,480.00
LINEAR WAYS		PURCHASED MATERIALS	$3,200.00	16.00	$1,040.00	24.00	$1,200.00	24.00	$1,200.00	20.00	$1,000.00	$7,640.00
LINEAR DRIVE SYSTEM		PURCHASED MATERIALS	$2,500.00	18.00	$1,170.00	24.00	$1,200.00	40.00	$2,000.00	18.00	$900.00	$7,770.00
FEEDBACK ENCODER SYSTEM		PURCHASED MATERIALS	$1,200.00									$1,200.00
TAPING HEAD		PURCHASED MATERIALS	$4,000.00	36.00	$2,340.00	32.00	$1,600.00	60.00	$3,000.00	48.00	$2,400.00	$13,340.00
CONTROL SYSTEM		PURCHASED MATERIALS	$10,500.00	120.00	$7,800.00	60.00	$3,000.00	40.00	$2,000.00	120.00	$6,000.00	$29,300.00
		TOTALS	$80,300.00	578.00	$37,570.00	624.00	$31,200.00	626.00	$31,300.00	904.00	$45,200.00	$225,870.00

CENTRAL AND FORWARD TRACKING SUPPORT CYLINDER TAPE LAYUP MANDREL

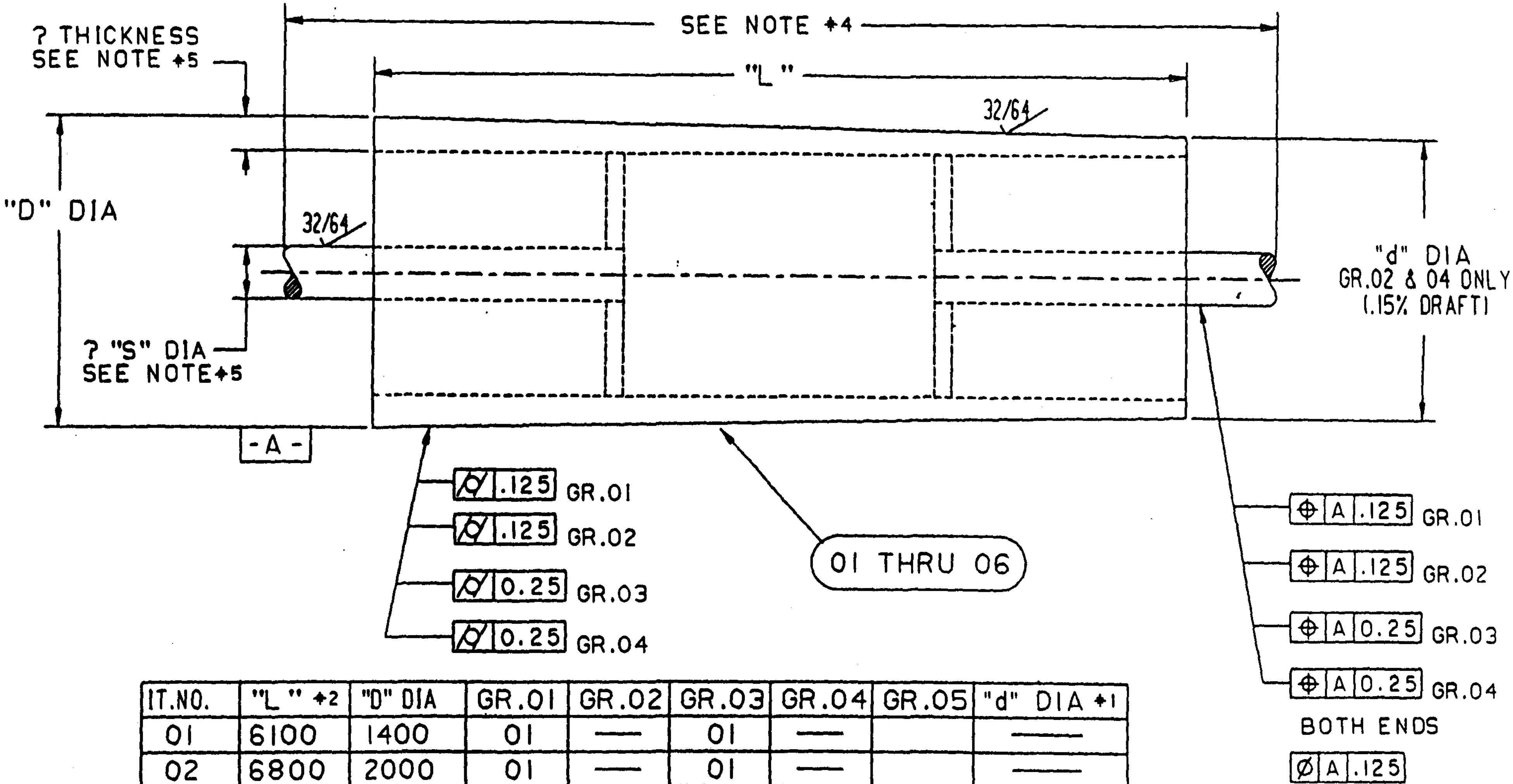

IT.NO.	"L" #2	"D" DIA	GR.01	GR.02	GR.03	GR.04	GR.05	"d" DIA #1
01	6100	1400	01	—	01	—		—
02	6800	2000	01	—	01	—		—
03	7600	2268	01	01	01	01		7589
04	8300	2532	01	01	01	01		8288
05	8400	2790	01	01	01	01		8387
06	8400	3064	01	01	01	01		8387

#1- USE .15% TO CALCULATE ACTUAL DIAMETER AT "d" END
#2- ="L" INCREASED BY .5 m FOR "AIR FLANGE" AND TEST COUPONS
#3- INCLUDE ONE SET SHAFT AND BEARING SEPARATE QUOTE
#4- SUPPLY BEARING CENTERLINE AND TOTAL SHAFT LENGTH
#5- SUPPLY SHAFT DIA AND SHELL THICKNESS
#6- ALL ITEMS TO BE BALANCED

D.389.4136A84.R1
DIMS. IN MILLIMETERS
KEPES 5-10-91

!ROMIUM INDUSTRIES, INC. • 4645 West Chicago Avenue, Chicago, Illinois 60651-3385 • (312) 287-3716 • FAX (312) 287-5792

CHROMIUM

June 4, 1991

Mr. Roger Swensrud
Westinghouse Electric Corporation
1310 Beulah Rd.
Pittsburgh, PA 15235

Dear Roger:

Thank you for your time and patience as we review and prepare this proposal. The mandrels really are not complicated but the raw size of these and establishing tolerances is the difficulty.

Below is a basic summary of what we have considered, followed by the pricing estimates. We would imagine that the prices are accurate within 10% but changes could impact the price significantly. The considerations such as material type, wall thickness, and the taper have not only an impact on costs but in manufacturing techniques which can cause additional costs.

MATERIALS - The shells would be made of grade A-36 plate that would be rolled and welded into tubing. Both circumferential and longitudinal weld seams will exist.

WALL THICKNESS - For quoting purposes, we have assumed a .75 inch wall. This would have to be reviewed for deflection and deformation so not to "collapse". Also, the shell thickness is critical to the manufacturing processes. A thin wall could cause machining problems.

WALL THICKNESS VARIATION - This is difficult to establish at this point but we currently beleive a specification of ±.125 inch is appropriate.

BALANCING - The mandrels are to be statically balanced for manufacturing reasons.

SHAFTS AND BEARINGS - Shafts and bearings will be supplied for manufacturing and handling reasons. The bearings and shafts will be made so to be removable. The shaft diameters are assumed to be 8" diameter for this quote.

PRICING

GROUP 1

1400mm dia x 6100mm lth	= $114,970
2000mm dia x 6800mm lth	= 171,210
2268mm dia x 7600mm lth	= 223,260
2532mm dia x 8300mm lth	= 265,100
2790mm dia x 8400mm lth	= 309,250
3064mm dia x 8400mm lth	= 347,125

GROUP 2

2268mm dia x 7600mm lth	= $245,590
2532mm dia x 8300mm lth	= 291,500
2790mm dia x 8400mm lth	= 339,900
3064mm dia x 8400mm lth	= 381,700

GROUP 3

1400mm dia x 6100mm lth	= $105,775
2000mm dia x 6800mm lth	= 157,515
2268mm dia x 7600mm lth	= 205,400
2532mm dia x 8300mm lth	= 243,892
2790mm dia x 8400mm lth	= 284,510
3064mm dia x 8400mm lth	= 319,355

GROUP 4

2268mm dia x 7600mm lth	= $225,940
2532mm dia x 8300mm lth	= 268,180
2790mm dia x 8400mm lth	= 312,708
3064mm dia x 8400mm lth	= 351,100

DELIVERIES - A delivery schedule can be established based on your requirements. We would expect a period between twenty-eight (28) and fifty-two (52) weeks depending on quanitites.

TERMS - We would negotiate the terms with you at a point closer to establishing the actual requirements. We would need to have a downpayment for engineering and materials purchase. We would also like to have a progress payment schedule developed.

We appreciate the opportunity to work with you. If Chromium Industries or I may be of further assistance, please call.

Sincerely,

CHROMIUM INDUSTRIES, INC.

Scott Patterson
General Manager

SP/pf

SDC COST AND SCHEDULE INTEGRATION

UNIDIRECTIONAL PREPREG GRAPHITE

VENDOR: AMOCO

NUMBER	P100
THICKNESS	5 MIL
MODULES	100 MILLION
RESIN SYSTEM	HYSOL MY720
COST/LB	$2200.

NUMBER	P75
THICKNESS	1 MIL
MODULES	75 MILLION
RESIN SYSTEM	HYSOL MY720
COST/LB	$2200.

SDC COST AND SCHEDULE INTEGRATION

UNIDIRECTIONAL PREPREG GRAPHITE

VENDOR: HERCULES

NUMBER	AS4
THICKNESS	5 MIL
MODULES	30 MILLION
RESIN SYSTEM	3501-6
COST/LB	$300.

NUMBER	AS4
THICKNESS	2.5 MIL
MODULES	75 MILLION
RESIN SYSTEM	3501-6
COST/LB	$600.

COMP1.WK3 6-14-91

TRACKER SUPPORT STRUCTURE MATERIAL COST

ITEM	MATERIAL	OD, IN.	ID, IN.	THKNESS,IN.	LENGTH IN.	VOL. CU.IN.	# / IN. CU.	WT. LBS.	COST $ /LB.	MATERIAL $
SUPPORT CYL. SUPERLAYER #3										
OUTSIDE SKIN	GRAPHITE-EPOXY	92.91		0.01	287.4	838.86	0.05	41.94	$2,400.00	$100,665.43
INSIDE SKIN	GRAPHITE-EPOXY	90.91		0.01	287.4	820.82	0.05	41.04	$2,400.00	$98,498.48
FOAM CORE	ROHACELL 71 IG	92.91	90.91		287.4	82985.16	0.0027	224.06	$50.00	$11,203.00
SHIM RINGS (12 PCS)	ROHACELL 71 IG	94.91	92.91		1	295.03	0.0027	9.56	$50.00	$477.94
ENDFLANGES (2 PCS)	ROHACELL P190 /	101.21	92.91	1	2	2530.87	0.007	35.43	$50.00	$1,771.61
	GR-EPXY	101.21	92.91	0.02*3*2		75.93	0.05	7.59	$2,400.00	$18,222.24
SUPPORT CYL. SUPERLAYER #4										
OUTSIDE SKIN	GRAPHITE-EPOXY	103.27		0.01	314.96	1021.83	0.05	51.09	$2,400.00	$122,619.63
INSIDE SKIN	GRAPHITE-EPOXY	101.27		0.01	314.96	1002.04	0.05	50.10	$2,400.00	$120,245.08
FOAM CORE	ROHACELL 71 IG	103.27	101.27		314.96	101183.65	0.0027	273.22	$50.00	$13,661.18
SHIM RINGS (12 PCS)	ROHACELL 71 IG	105.27	103.27		1	327.57	0.0027	10.61	$50.00	$530.67
ENDFLANGES (2 PCS)	ROHACELL P190 /	114.63	103.27	1	2	3888.27	0.007	54.44	$50.00	$2,721.79
	GR-EPXY	114.63	103.27	0.02*3*2	2	116.65	0.05	11.66	$2,400.00	$27,995.55
SUPPORT CYL. SUPERLAYER #5										
OUTSIDE SKIN	GRAPHITE-EPOXY	116.69		0.01	318.89	1169.03	0.05	58.45	$2,400.00	$140,283.20
INSIDE SKIN	GRAPHITE-EPOXY	114.69		0.01	311	1120.56	0.05	56.03	$2,400.00	$134,467.42
FOAM CORE	ROHACELL 71 IG	116.69	114.69		311	113033.48	0.0027	305.19	$50.00	$15,259.52
SHIM RINGS (12 PCS)	ROHACELL 71 IG	118.69	116.69		1	369.73	0.0027	11.98	$50.00	$598.97
ENDFLANGES (2 PCS)	ROHACELL P190 /	128.09	116.69	1	2	3178.43	0.007	44.50	$50.00	$2,224.90
	GR-EPXY	128.09	116.69	0.02*3*2	2	95.35	0.05	9.54	$2,400.00	$22,884.71
SUPPORT CYL. SUPERLAYER #6										
OUTSIDE SKIN	GRAPHITE-EPOXY	127.12		0.01	311	1242.01	0.05	62.10	$2,400.00	$149,040.86
INSIDE SKIN	GRAPHITE-EPOXY	125.12		0.01	311	1222.47	0.05	61.12	$2,400.00	$146,695.99
FOAM CORE	ROHACELL 71 IG	127.12	125.12		311	123223.98	0.0027	332.70	$50.00	$16,635.24
SHIM RINGS (12 PCS)	ROHACELL 71 IG	129.12	127.12		1	402.50	0.0027	13.04	$50.00	$652.05
ENDFLANGES (2 PCS)	ROHACELL P190 /	132.66	127.12	1	2	2269.00	0.007	31.77	$50.00	$1,588.30
	GR-EPXY	132.66	127.12	0.02*3*2	2	68.07	0.05	6.81	$2,400.00	$16,336.91
									TOTAL	$1,148,943.97

TRACKER SUPPORT STRUCTURE LABOR COST

ITEM	LAYUP DESIGN HRS ENGR	PURCHASING ENGR	MATL CUTTING TECH	LAYUP HRS ENGR	LAYUP HRS TECH	MACHINING HRS	INSPECTION HRS			
SUPPORT CYL. SUPERLAYER #3										
OUTSIDE SKIN	120.00	20.00	40	233.02	466.04					
INSIDE SKIN	120.00	20.00	40	228.01	456.01					
FOAM CORE	160.00	20.00	200	58.26	233.02					
SHIM RINGS (12 PCS)	60.00	20.00	60	49.69	99.38	72.00	180.00			
ENDFLANGES (2 PCS)	40.00	20.00	40							
SUPPORT CYL. SUPERLAYER #4										
OUTSIDE SKIN	40.00	10.00	40	283.84	567.69					
INSIDE SKIN	40.00	10.00	40	278.35	556.69					
FOAM CORE	55.00	10.00	200	70.96	283.84					
SHIM RINGS (12 PCS)	20.00	10.00	60	55.12	110.24	78.00	190.00			
ENDFLANGES (2 PCS)	16.00	10.00	40							
SUPPORT CYL. SUPERLAYER #5										
OUTSIDE SKIN	40.00	10.00	40	324.73	649.46					
INSIDE SKIN	40.00	10.00	40	311.27	622.54					
FOAM CORE	55.00	10.00	200	79.17	316.70					
SHIM RINGS (12 PCS)	20.00	10.00	60	62.15	124.29	80.00	200.00			
ENDFLANGES (2 PCS)	16.00	10.00	40							
SUPPORT CYL. SUPERLAYER #6										
OUTSIDE SKIN	40.00	10.00	40	345.00	690.01					
INSIDE SKIN	40.00	10.00	40	339.57	679.15					
FOAM CORE	55.00	10.00	200	86.25	345.00					
SHIM RINGS (12 PCS)	20.00	10.00	60	67.61	135.21	84.00	210.00			
ENDFLANGES (2 PCS)	16.00	10.00	40							

CENTRAL AND FORWARD TRACKING SUBSYSTEM

END FLANGES

THE MANUFACTURING PROCESS USES:

End Flanges

1) Commercial Graphite Components to Fabricate End Flange Rings
2) Components Fabricated into a Space Frame
3) Machining to Form a Precision Cylinder Interface

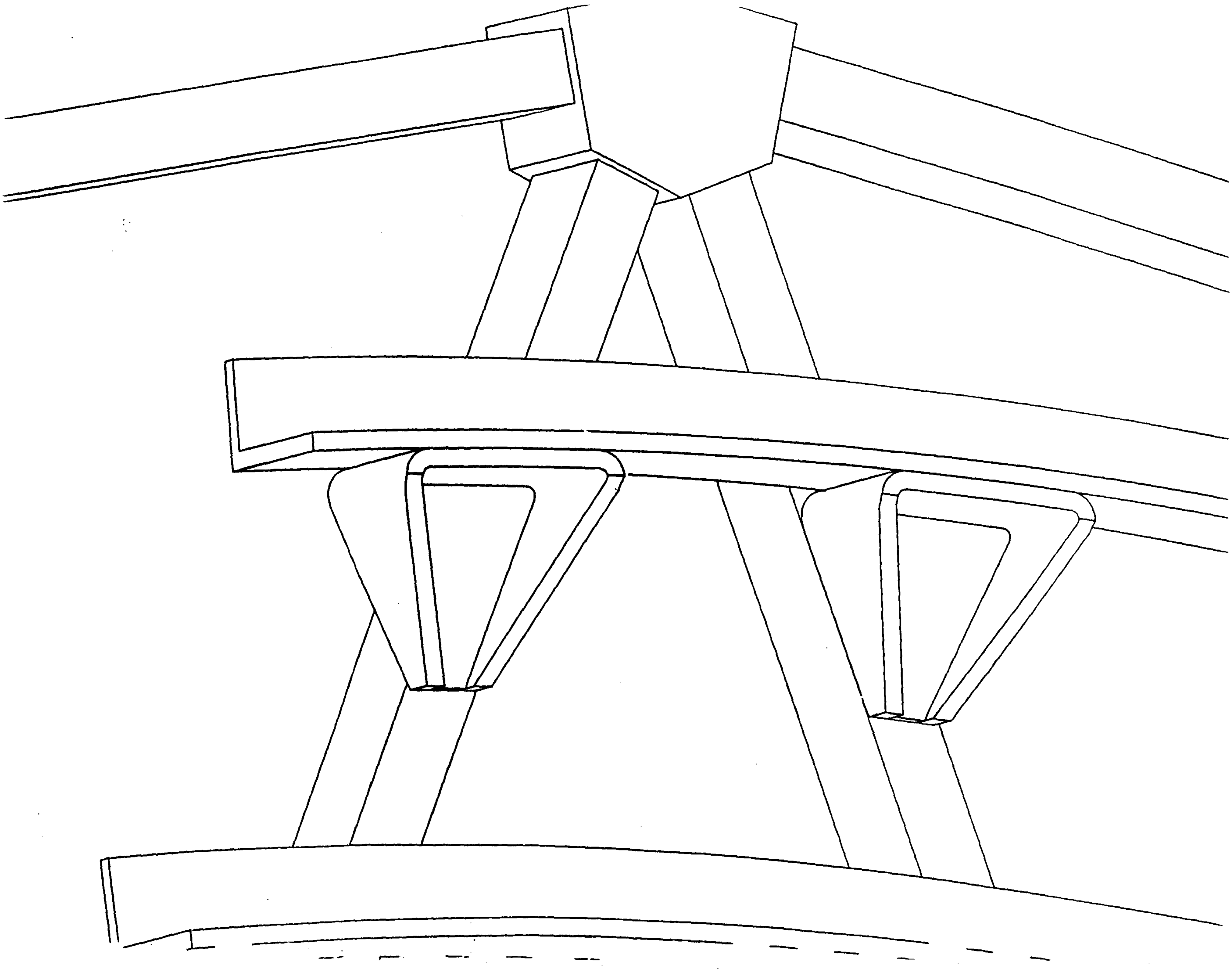

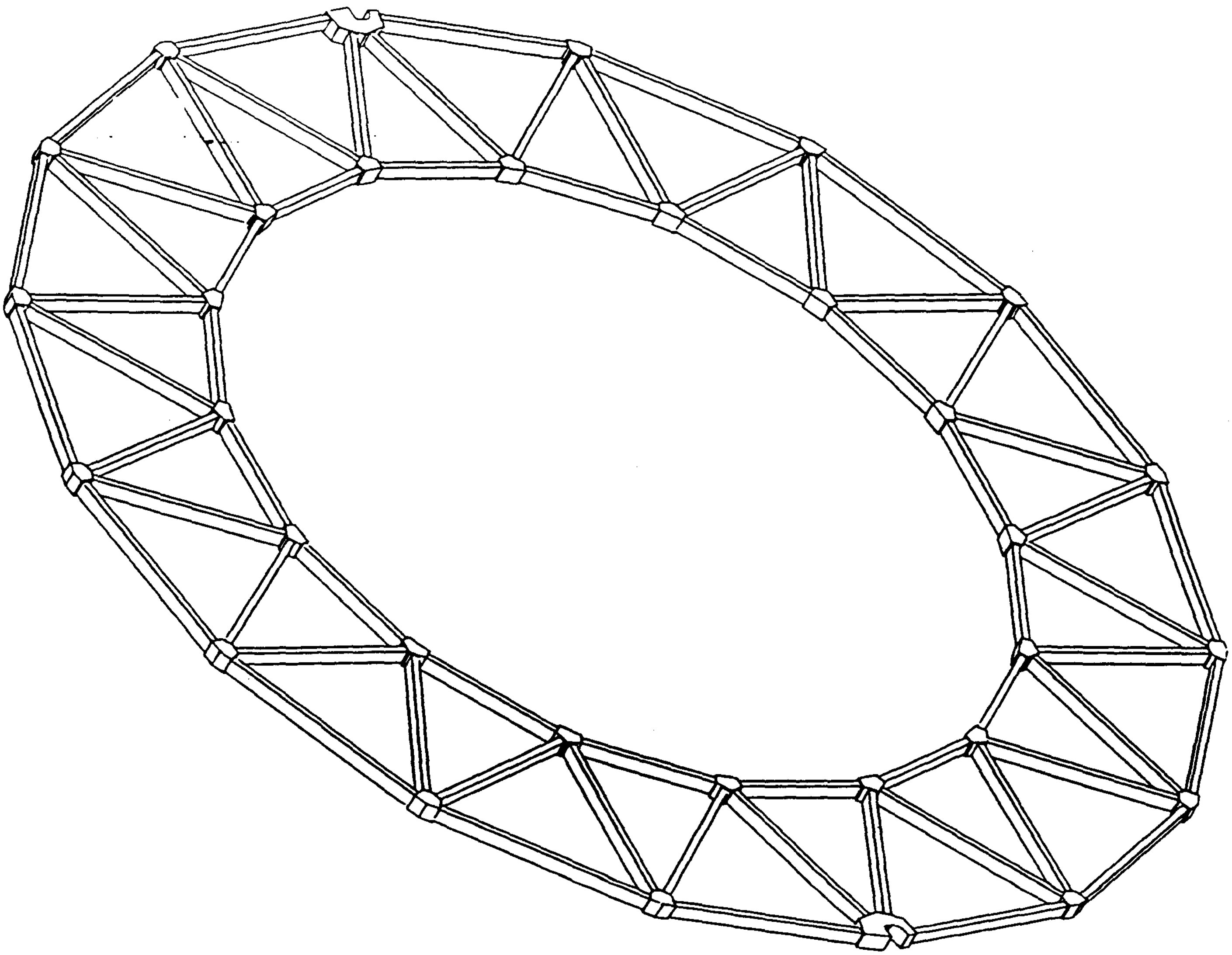

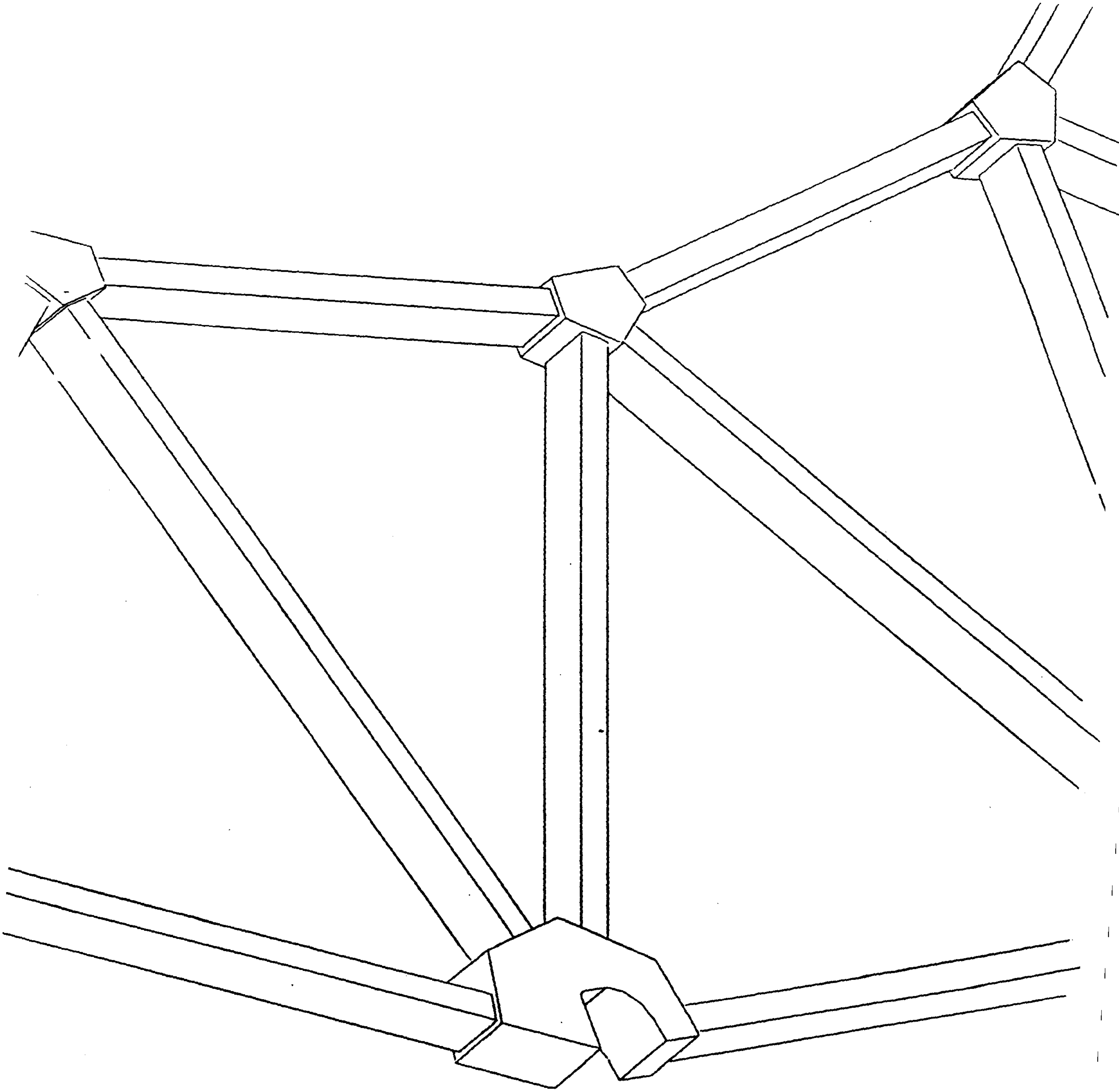

CENTRAL AND FORWARD TRACKING SUBSYSTEM

SHIM RINGS

THE MANUFACTURING PROCESS USES:

1) Large Steel Mandrels for Support During Machining
2) Large Custom Machine Tool to Manipulate Router Type Spindle For Milling Precision Shape Rohacell Rings

THE MANUFACTURING PROCESS MUST PRODUCE:

1) Precision Diameter Required For Trigger and Axial Superlayers
2) Precision Shape Required For Stereo Superlayers to Form Alternating Plus Minus 3 Degree Angles
3) The Use of Machining Manufacturing Process Makes Possible Stereo and Thus Axial Position Measurement With Straws

Westinghouse
Science & Technology Center

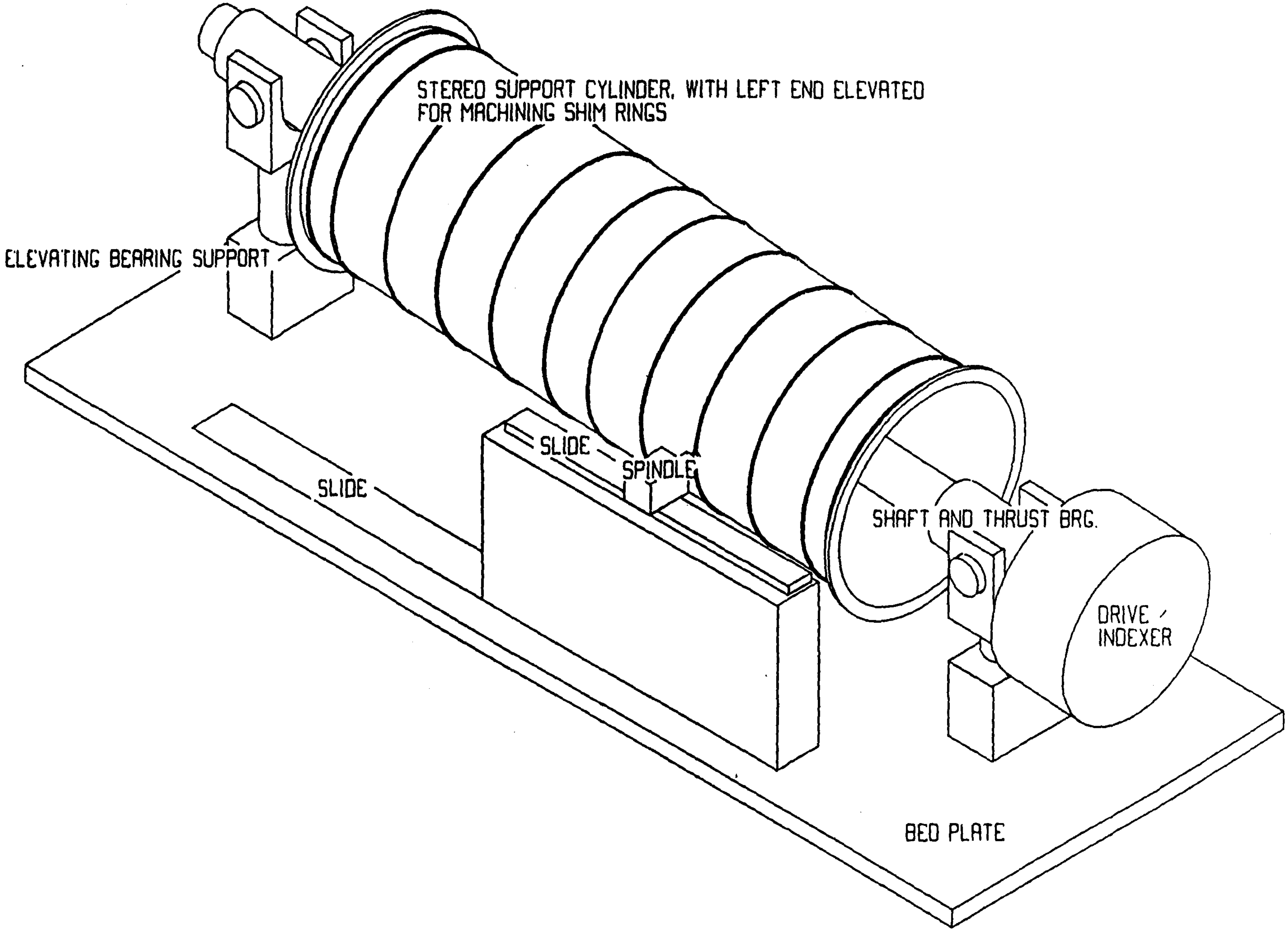

SYSTEM FOR MACHINING SUPPORT CYLINDER SHIM RINGS

WESTINGHOUSE STC

MACH2.WK3 MACHINING STATION 6-14-91

ITEM	SUPPLIER	COMMENT	PURCHASE $	DESIGN HRS	DESIGN $	DRAFTING HRS	DRAFTING $	MACHINING HRS	MACHINING $	LABOR HRS	LABOR $	TOTAL
BED PLATE PEDESTAL ASSY.	LAKE SHORE INC	16 FT X 20 FT X 2 PCS	$30,000.00	24.00	$1,560.00	20.00	$1,000.00					$32,560.00
BLANK END PEDESTAL												
BASE ASSY												
BURNOUTS		PURCHASED MATERIALS	$1,800.00	30.00	$1,950.00	40.00	$2,000.00	20.00	$1,000.00			$6,750.00
WELDING		TIME & MATERIALS								32.00	$1,600.00	$1,600.00
STRESS ANNEALING		TRANSPORTATION & TIME	$400.00									$400.00
MACHINING		TIME						60.00	$3,000.00			$3,000.00
ASSY		TIME								24.00	$1,200.00	$1,200.00
COLUMN ASSY												
BURNOUTS		PURCHASED MATERIALS	$1,200.00	30.00	$1,950.00	40.00	$2,000.00			20.00	$1,000.00	$6,150.00
WELDING		TIME & MATERIALS								20.00	$1,000.00	$1,000.00
STRESS ANNEALING		TRANSPORTATION & TIME	$400.00									$400.00
MACHINING		TIME						32.00	$1,600.00	16.00	$800.00	$2,400.00
ELEVATING MECHANISM		PURCHASED MATERIAL	$2,000.00	24.00	$1,560.00	32.00	$1,600.00			12.00	$600.00	$5,760.00
ASSY		TIME								40.00	$2,000.00	$2,000.00
TRUNNION BRG HOUSING ASSY												
BURNOUTS		PURCHASED MATERIALS	$1,800.00	32.00	$2,080.00	40.00	$2,000.00	24.00	$1,200.00	16.00	$800.00	$7,880.00
WELDING		TIME								24.00	$1,200.00	$1,200.00
STRESS ANNEALING		TRANSPORTATION AND TIME	$400.00									$400.00
MACHINING		TIME						32.00	$1,600.00	12.00	$600.00	$2,200.00
BEARING ASSY		PURCHASED MATERIALS	$800.00	16.00	$1,040.00	16.00	$800.00			16.00	$800.00	$3,440.00
ASSEMBLY TIME		TIME								32.00	$1,600.00	$1,600.00
SHAFT BRG HOUSING ASSY												
BURNOUTS		PURCHASED MATERIALS	$300.00	12.00	$780.00	16.00	$800.00					$1,880.00
WELDING		TIME								12.00	$600.00	$600.00
STRESS ANNEALING		TRANSPORTATION AND TIME	$300.00									$300.00
MACHINING		TIME						32.00	$1,600.00	8.00	$400.00	$2,000.00
BEARING ASSY		PURCHASED MATERIALS	$2,000.00	12.00	$780.00	12.00	$600.00			8.00	$400.00	$3,780.00
ASSEMBLY TIME		TIME								16.00	$800.00	$800.00
DRIVEN END PEDESTAL												
BASE ASSY												
BURNOUTS		PURCHASED MATERIALS	$1,800.00	30.00	$1,950.00	40.00	$2,000.00	20.00	$1,000.00			$6,750.00
WELDING		TIME								32.00	$1,600.00	$1,600.00
STRESS ANNEALING		TRANSPORTATION AND TIME	$400.00									$400.00
MACHINING		TIME						60.00	$3,000.00			$3,000.00
ASSY		TIME								24.00	$1,200.00	$1,200.00
COLUMN ASSY												
BURNOUTS		PURCHASED MATERIALS	$1,200.00	30.00	$1,950.00	40.00	$2,000.00	40.00	$2,000.00	20.00	$1,000.00	$6,150.00
WELDING		TIME								20.00	$1,000.00	$1,000.00
STRESS ANNEALING		TRANSPORTATION AND TIME	$400.00									$400.00
MACHINING		TIME						32.00	$1,600.00	16.00	$800.00	$2,400.00
ELEVATING MECHANISM		PURCHASED MATERIALS	$2,000.00	24.00	$1,560.00	32.00	$1,600.00			12.00	$600.00	$5,760.00
ASSY		TIME								40.00	$2,000.00	$2,000.00
TRUNNION BRG HOUSING ASSY												
BURNOUTS		PURCHASED MATERIALS	$1,800.00	32.00	$2,080.00	40.00	$2,000.00	24.00	$1,200.00	16.00	$800.00	$7,880.00
WELDING		TIME								24.00	$1,200.00	$1,200.00
STRESS ANNEALING		TRANSPORTATION AND TIME	$400.00									$400.00
MACHINING		TIME						32.00	$1,600.00	12.00	$600.00	$2,200.00
BEARING ASSY		PURCHASED MATERIALS	$800.00	16.00	$1,040.00	24.00	$1,200.00			16.00	$800.00	$3,840.00
ASSEMBLY TIME		TIME								32.00	$1,600.00	$1,600.00
SHAFT BRG HOUSING ASSY												
BURNOUTS		PURCHASED MATERIALS	$300.00									$300.00
WELDING		TIME						12.00	$600.00	12.00	$600.00	$1,200.00
STRESS ANNEALING		TRANSPORTATION AND TIME	$300.00									$300.00
MACHINING		TIME						32.00	$1,600.00	8.00	$400.00	$2,000.00
SHAFT BEARING ASSY		PURCHASED MATERIALS	$2,000.00	12.00	$780.00	12.00	$600.00			8.00	$400.00	$3,780.00
THRUST BEARING ASSY		PURCHASED MATERIALS	$3,200.00	24.00	$1,560.00	32.00	$1,600.00			12.00	$600.00	$6,960.00
DRIVE												
ROTARY ENCODER		PURCHASED MATERIALS	$1,600.00	16.00	$1,040.00	24.00	$1,200.00			12.00	$600.00	$4,440.00
BRAKE ASSY		PURCHASED MATERIALS		12.00	$780.00	12.00	$600.00			16.00	$800.00	$2,180.00
ASSEMBLY TIME		TIME								24.00	$1,200.00	$1,200.00
MACHINING STATION		PURCHASED MATERIALS										
BEDPLATE WAYS		PURCHASED MATERIALS	$4,400.00	40.00	$2,600.00	32.00	$1,600.00	60.00		24.00	$1,200.00	$9,800.00
MACHINE TABLE		PURCHASED MATERIALS	$16,000.00	120.00	$7,800.00	120.00	$6,000.00	60.00		40.00	$2,000.00	$31,800.00
MACHINE TABLE WAYS		PURCHASED MATERIALS	$2,000.00	16.00	$1,040.00	24.00	$1,200.00	20.00		20.00	$1,000.00	$5,240.00
SPINDLE CARRIER		PURCHASED MATERIALS	$4,500.00	60.00	$3,900.00	32.00	$1,600.00	40.00		20.00	$1,000.00	$11,000.00
SPINDLE		PURCHASED MATERIALS	$2,500.00	16.00	$1,040.00	16.00	$800.00	20.00		12.00	$600.00	$4,940.00
CONTROL SYSTEM		PURCHASED MATERIALS	$10,500.00	40.00	$2,600.00	20.00	$1,000.00	40.00		48.00	$2,400.00	$16,500.00
		TOTALS	$95,900.00	688.00	$45,420.00	716.00	$35,800.00	452.00	$22,800.00	830.00	$41,500.00	$235,220.00

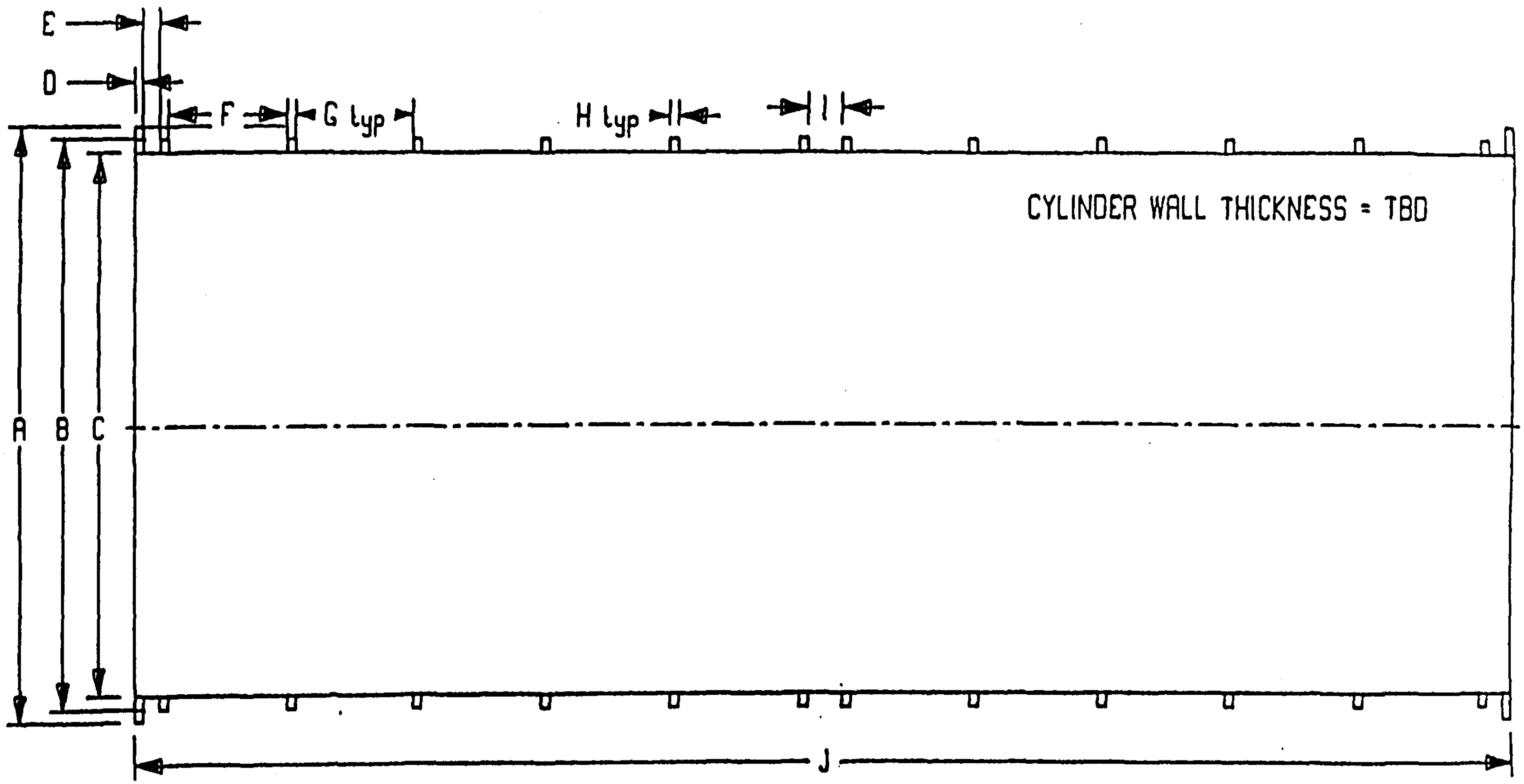

DIMENSIONS OF CENTRAL TRACKER SUPPORT CYLINDERS

SUPRLYR	A	B MIN	B MAX	C	D	E	F	G	H	I	J	
6	335.0	319.5	320.5	317.5	5.0	10.0	70.0	70.0	2.50	20.0	810.0	CM
5	317.5	290.8	295.4	288.8	5.0	10.0	70.0	70.0	2.50	20.0	810.0	CM
4	288.8	266.2	267.2	264.2	5.0	10.0	65.0	70.0	2.50	20.0	800.0	CM
3	264.2	237.9	242.8	235.9	5.0	10.0	30.0	70.0	2.50	20.0	730.0	CM

CENTRAL AND FORWARD TRACKING SUBSYSTEM

STEREO SHIM RING

FEATURES

- o Machined in Place on Cylinder on Mandrel
- o Relatively Simple to Skew Machining Axis to Mandrel Cylinder Axes
- o Single Setup Produces All Module Locations Therefore Initial Setup Not Critical

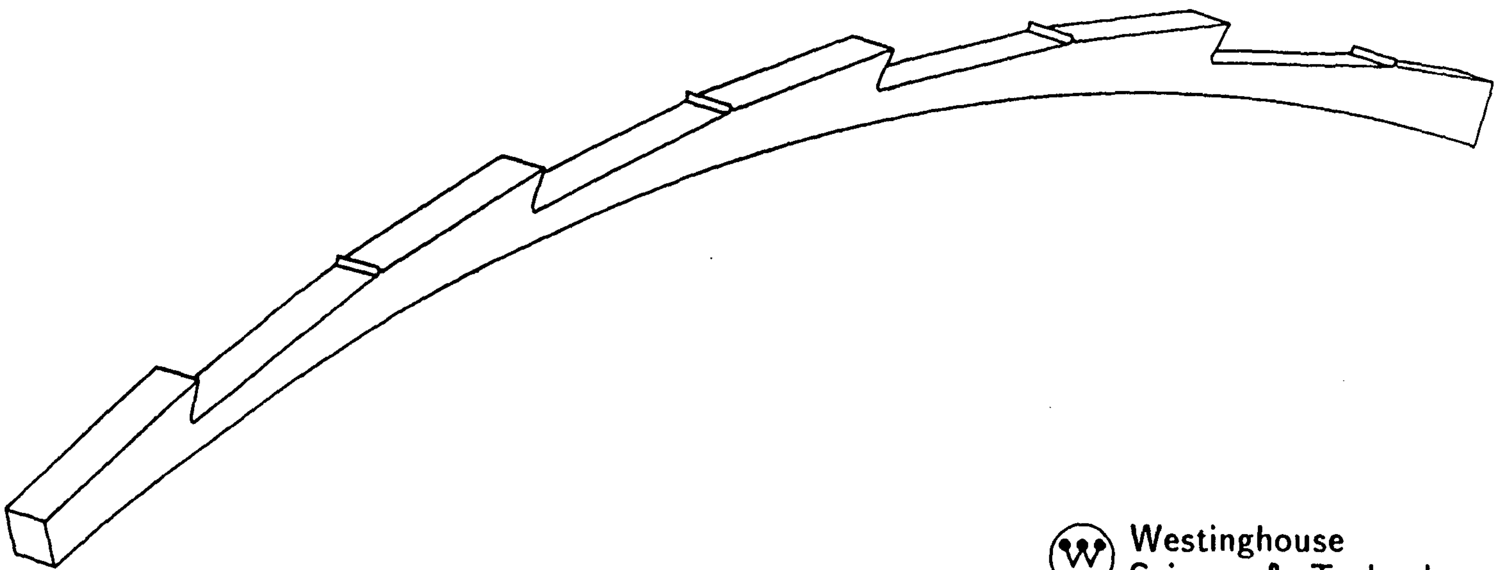

Westinghouse
Science & Technology Center

CENTRAL AND FORWARD TRACKING SUBSYSTEM

MODULE PLACEMENT

THE MANUFACTURING PROCESS USES:

Mechanical Precision Locating

1) The Large Steel Mandrels for Support During Placement
2) Large Laser Optical Aligned Custom Machine Tool to Locate and Confirm Locations of Modules on Rohacell Rings

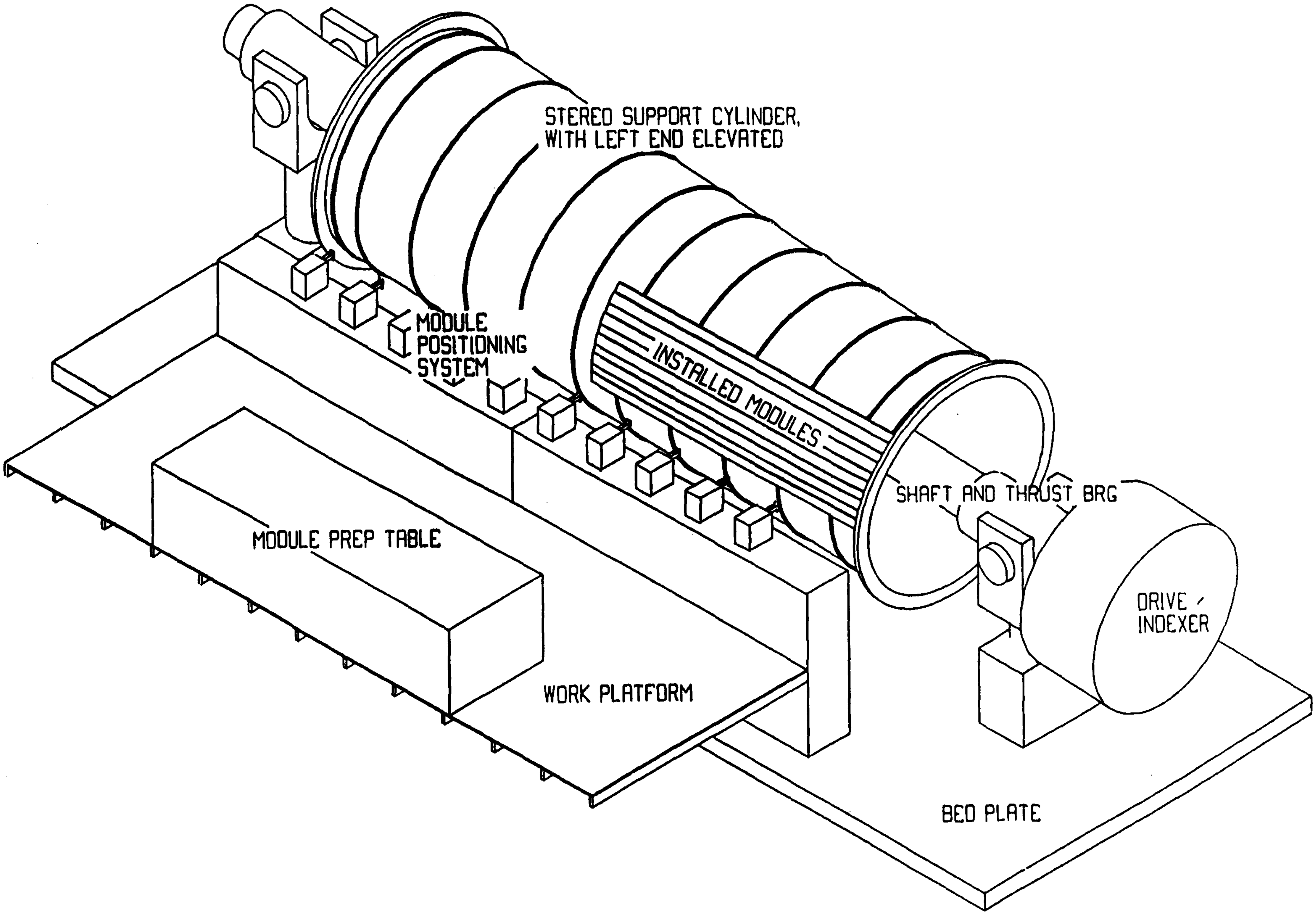

MODULE INSTALLATION SYSTEM

WESTINGHOUSE STC

MACH3.WK3 MODULE INSTALLATION STATION 6-14-91

ITEM	SUPPLIER	COMMENT	PURCHASE $	DESIGN HRS	DESIGN $	DRAFTING HRS	DRAFTING $	MACHINING HRS	MACHINING $	LABOR HRS	LABOR $	TOTAL
BED PLATE PEDESTAL ASSY.	LAKE SHORE INC	10 FT X 20 FT X 2 PCS	$30,000.00	24.00	$1,560.00	20.00	$1,000.00					$32,560.00
BLANK END PEDESTAL												
BASE ASSY												
BURNOUTS		PURCHASED MATERIALS	$1,800.00	30.00	$1,950.00	40.00	$2,000.00	20.00	$1,000.00			$6,750.00
WELDING		TIME & MATERIALS								32.00	$1,600.00	$1,600.00
STRESS ANNEALING		TRANSPORTATION & TIME	$400.00									$400.00
MACHINING		TIME						60.00	$3,000.00			$3,000.00
ASSY		TIME								24.00	$1,200.00	$1,200.00
COLUMN ASSY												
BURNOUTS		PURCHASED MATERIALS	$1,200.00	30.00	$1,950.00	40.00	$2,000.00			20.00	$1,000.00	$6,150.00
WELDING		TIME & MATERIALS								20.00	$1,000.00	$1,000.00
STRESS ANNEALING		TRANSPORTATION & TIME	$400.00									$400.00
MACHINING		TIME						32.00	$1,600.00	16.00	$800.00	$2,400.00
ELEVATING MECHANISM		PURCHASED MATERIAL	$2,000.00	24.00	$1,560.00	32.00	$1,600.00			12.00	$600.00	$5,760.00
ASSY		TIME								40.00	$2,000.00	$2,000.00
TRUNNION BRG HOUSING ASSY												
BURNOUTS		PURCHASED MATERIALS	$1,500.00	32.00	$2,080.00	40.00	$2,000.00	24.00	$1,200.00	16.00	$800.00	$7,580.00
WELDING		TIME								24.00	$1,200.00	$1,200.00
STRESS ANNEALING		TRANSPORTATION AND TIME	$400.00									$400.00
MACHINING		TIME						32.00	$1,600.00	12.00	$600.00	$2,200.00
BEARING ASSY		PURCHASED MATERIALS	$600.00	16.00	$1,040.00	16.00	$800.00			16.00	$800.00	$3,240.00
ASSEMBLY TIME		TIME								32.00	$1,600.00	$1,600.00
SHAFT BRG HOUSING ASSY												
BURNOUTS		PURCHASED MATERIALS	$300.00	12.00	$780.00	12.00	$600.00					$1,680.00
WELDING		TIME								12.00	$600.00	$600.00
STRESS ANNEALING		TRANSPORTATION AND TIME	$300.00									$300.00
MACHINING		TIME						32.00	$1,600.00	8.00	$400.00	$2,000.00
BEARING ASSY		PURCHASED MATERIALS	$2,000.00	12.00	$780.00	12.00	$600.00			8.00	$400.00	$3,780.00
ASSEMBLY TIME		TIME								16.00	$800.00	$800.00
DRIVEN END PEDESTAL												
BASE ASSY												
BURNOUTS		PURCHASED MATERIALS	$1,800.00	30.00	$1,950.00	40.00	$2,000.00	20.00	$1,000.00			$6,750.00
WELDING		TIME								32.00	$1,600.00	$1,600.00
STRESS ANNEALING		TRANSPORTATION AND TIME	$400.00									$400.00
MACHINING		TIME						60.00	$3,000.00			$3,000.00
ASSY		TIME								24.00	$1,200.00	$1,200.00
COLUMN ASSY												
BURNOUTS		PURCHASED MATERIALS	$1,200.00	30.00	$1,950.00	40.00	$2,000.00	40.00	$2,000.00	20.00	$1,000.00	$8,150.00
WELDING		TIME								20.00	$1,000.00	$1,000.00
STRESS ANNEALING		TRANSPORTATION AND TIME	$400.00									$400.00
MACHINING		TIME						32.00	$1,600.00	16.00	$800.00	$2,400.00
ELEVATING MECHANISM		PURCHASED MATERIALS	$2,000.00	24.00	$1,560.00	32.00	$1,600.00			12.00	$600.00	$5,760.00
ASSY		TIME								40.00	$2,000.00	$2,000.00
TRUNNION BRG HOUSING ASSY												
BURNOUTS		PURCHASED MATERIALS	$1,500.00	32.00	$2,080.00	40.00	$2,000.00	24.00	$1,200.00	16.00	$800.00	$7,580.00
WELDING		TIME								24.00	$1,200.00	$1,200.00
STRESS ANNEALING		TRANSPORTATION AND TIME	$400.00									$400.00
MACHINING		TIME						32.00	$1,600.00	12.00	$600.00	$2,200.00
BEARING ASSY		PURCHASED MATERIALS	$600.00	16.00	$1,040.00	24.00	$1,200.00			16.00	$800.00	$3,640.00
ASSEMBLY TIME		TIME								32.00	$1,600.00	$1,600.00
SHAFT BRG HOUSING ASSY												
BURNOUTS		PURCHASED MATERIALS	$300.00									$300.00
WELDING		TIME						12.00	$600.00	12.00	$600.00	$1,200.00
STRESS ANNEALING		TRANSPORTATION AND TIME	$300.00									$300.00
MACHINING		TIME						32.00	$1,600.00	8.00	$400.00	$2,000.00
SHAFT BEARING ASSY		PURCHASED MATERIALS	$2,000.00	12.00	$780.00	12.00	$600.00			8.00	$400.00	$3,780.00
THRUST BEARING ASSY		PURCHASED MATERIALS	$3,100.00	24.00	$1,560.00	32.00	$1,600.00			12.00	$600.00	$6,860.00
DRIVE												
ROTARY ENCODER		PURCHASED MATERIALS	$1,600.00	16.00	$1,040.00	24.00	$1,200.00			12.00	$600.00	$4,440.00
BRAKE ASSY		PURCHASED MATERIALS		12.00	$780.00	12.00	$600.00			16.00	$800.00	$2,180.00
ASSEMBLY TIME		TIME								24.00	$1,200.00	$1,200.00
MODULE INSTALLATION STATION		PURCHASED MATERIALS										
WORK PLATFORM			$18,000.00	140.00	$9,100.00	160.00	$8,000.00	120.00	$6,000.00	120.00	$6,000.00	$47,100.00
MODULE PREP TABLE			$6,500.00	20.00	$1,300.00	24.00	$1,200.00	40.00	$2,000.00	20.00	$1,000.00	$12,000.00
MODULE POSITIONING SYSTEM			$35,000.00	320.00	$20,800.00	240.00	$12,000.00	400.00	$20,000.00	240.00	$12,000.00	$99,800.00
OPTICAL ALIGNMENT SYSTEM			$12,500.00	60.00	$3,900.00	80.00	$4,000.00	120.00	$6,000.00	320.00	$16,000.00	$42,400.00
X-RAY INSPECTION SYSTEM		PURCHASED MATERIALS	$120,000.00	160.00	$10,400.00	160.00	$8,000.00	80.00	$4,000.00	60.00	$3,000.00	$145,400.00
CONTROL SYSTEM		PURCHASED MATERIALS	$10,500.00	40.00	$2,600.00	20.00	$1,000.00	40.00	$2,000.00	160.00	$8,000.00	$24,100.00
		TOTALS	$268,400.00	1116.00	$72,540.00	1156.00	$57,800.00	1252.00	$62,600.00	1506.00	$75,300.00	$531,640.00

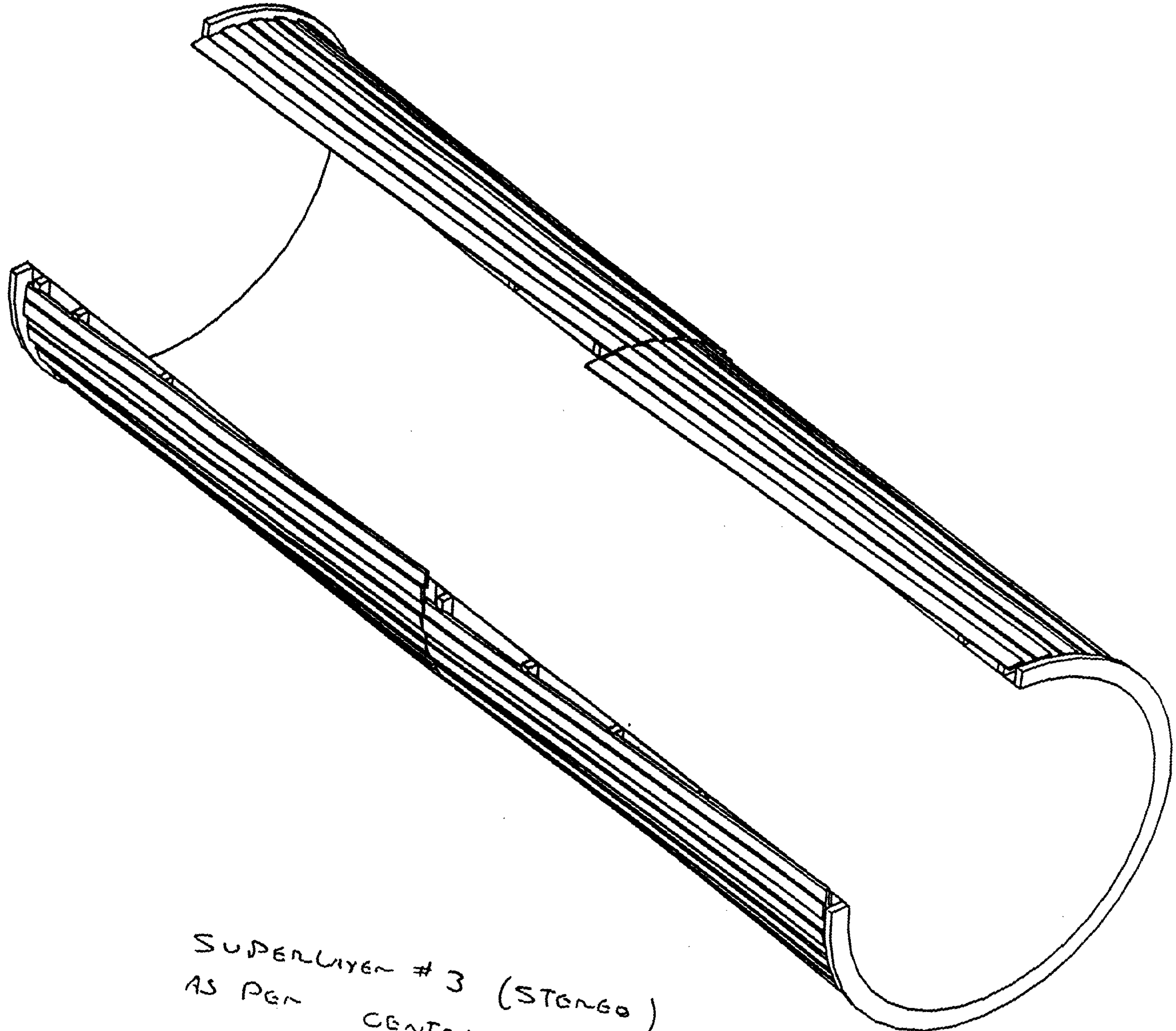

SUPERLAYER #3 (STEREO)
AS PER CENTRKIS 4-26-90

CENTRAL AND FORWARD TRACKING SUBSYSTEM

STEREO MODULE SHIM RING PLACEMENT DETAIL

FEATURES

- o Relatively Simple to Skew Placement Axis to Mandrel Cylinder Axes
- o Single Setup Produces All Module Locations Therefore Initial Setup Not Critical

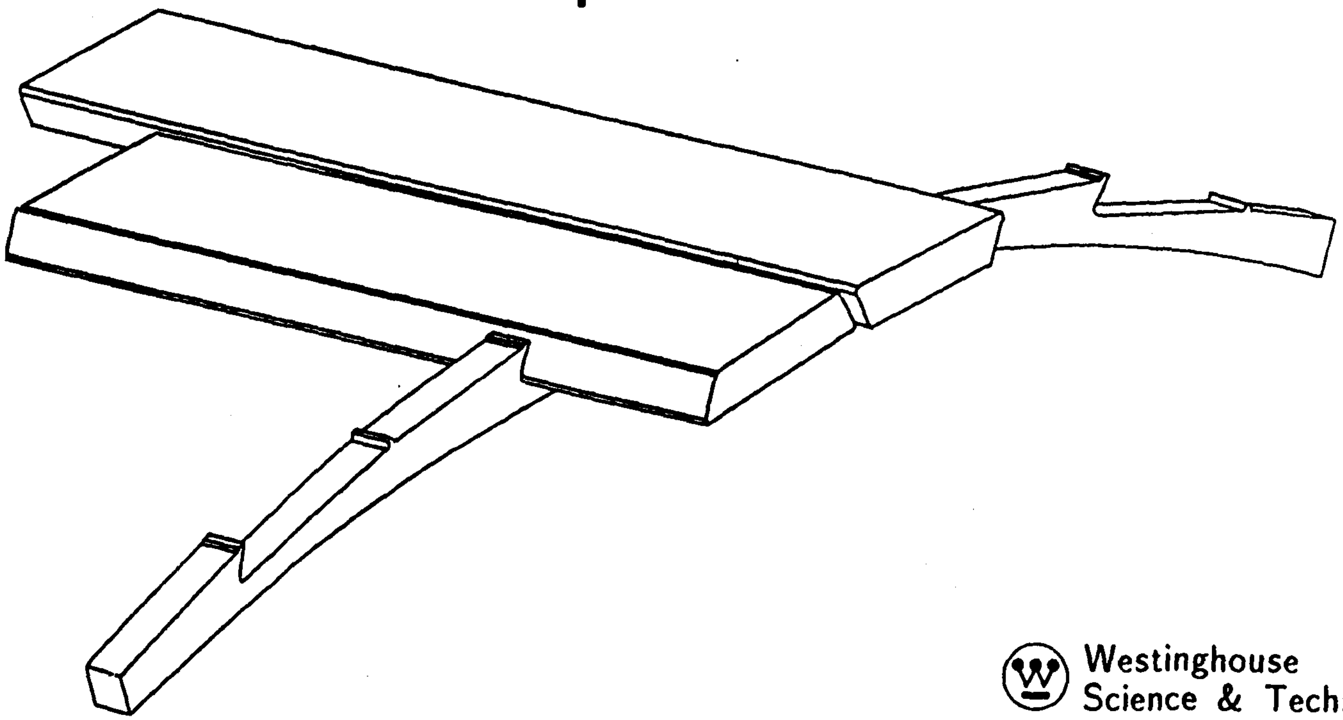

Westinghouse
Science & Technology Center

CENTRAL AND FORWARD TRACKING SUBSYSTEM

REVISED TECHNICAL DATA ON TRACKER GEOMETRY

Westinghouse
Science & Technology Center

Revised Outer Tracker Parameters

This revision is composed of a combination of four outer superlayers of straws and two inner superlayers of fibers. This program is to define the outer straw superlayers with minimum radial displacement and minimum module side clearance, this attempt has the modules mounted to rings located on concentric cylinders.

Baseline information from Bill Ford relating to the Straw Section

Suprlyr	Radius cm	straws/lyr	rows/mod	zmin	zmax	stereo
#3	121.722	1912	6	0.30	355.0	-3 deg
#4	134.963	2120	6	0.30	390.0	0 deg
#5	148.205	2328	6	0.30	395.0	+3 deg
#6	161.447	2536	9	0.30	395.0	0 deg

Maximum Tracker radius = 168.5 cm
Total straws both ends, 121,968. (baseline)
Point of rotation for stereo layers is now defined as (zmax - zmin) /2.

Superlayer #6 Trigger layer, axial, curved modules, nine straws high
Superlayer #5 Stereo layer, + 3 degrees, flat modules, six straws high
Superlayer #4 Axial layer, flat modules, six straws high
Superlayer #3 Stereo layer, - 3 degrees, flat modules, six straws high

Description of Flat, Axial Trapezoidal section modules, (superlayer #4)

Each trapezoid is (N) straws wide on the long side and each succeding layer contains one straw less. The height is (L) straws high with the straws nested. The module has a epoxy-graphite wrapper (T) cm thick. The straw diameter is d) cm. These trapezodial modules are alternated in position and are spaced (sp) cm from the adjoining modules. Both the radial position (D) of the alternate modules and the number of straws (N) may be varied to change the superlayer radius. Trapezodial modules must be added in groups of two to make large radius changes such as between superlayers. Each module contains (CH) straws.

Flat Axial Element Definations (superlayer #4)

$sp := 0$ (space between modules, cm)
$d := .40437$ (straw diameter, cm)
$D := 1.03$ (radial difference of alternating modules, cm)
$T := 0.025$ (Wrapper thickness. cm)
$N := 29$ (number of straws, long side)
$L := 6$ (number of straws high)
$H := ((L - 1)\cdot d\cdot .866) + d + (2\cdot T)$ (height of module, cm
$LS := N\cdot d + (2\cdot T)$ (length of module long side, cm)
$SS := (N - (L - 1))\cdot d + (2\cdot T)$ (length of module short side, cm)
$U := LS + SS + sp - (D\cdot .5774)$ (total length of module pair, cm)

$CH := L\cdot\left[N - \frac{L-1}{2}\right]$ $CH = 159$ (straws per module)

$LS = 11.777$
$SS = 9.755$
$H = 2.205$

Description of Curved Trapezoidal Elements, (superlayer #6)

Superlayer #6 is a trigger layer and the module is nine straws high. The long and short sides, (top and bottom) are curved to the same radius as their distance from the beam centerline. Other than the curved top and bottom and increased layers of straws these modules are simular to the flat Ones and will be incorporated into the tracker like other axial layers.

Curved Axial Element Definitions that may be different from above.

$spc := 0.03$ (space between modules, cm)

$Dc := 0.45$ (radial difference of alternating modules, cm)

$Nc := 30$ (number of straws, long side)

$Lc := 9$ (number of straws high)

$Hc := ((Lc - 1) \cdot d \cdot .866) + d + (2 \cdot T)$ (height of module, cm)

$LSc := Nc \cdot d + (2 \cdot T)$ (length of module, long side cm)

$SSc := (Nc - (Lc - 1)) \cdot d + (2 \cdot T)$ (length of module, short side)

$Uc := LSc + SSc + spc - (Dc \cdot .5774)$ (total length of module pr cm)

$$CHc := Lc \cdot \left[Nc - \frac{Lc - 1}{2} \right] \qquad CHc = 234 \qquad \text{(straws per module)}$$

$LSc = 12.181$

$SSc = 8.946 \qquad Hc = 3.256$

Description of Trapezodial Stereo Elements, (superlayers #3 & #5)

The need is to generate stereo modules that have a trapezodial cross section and provide uniform spacing between modules.

The rotation of the stereo module is on a line starting at the beam axis and passing through the center of the module. To achieve uniform stereo module spacing the modules with the long side up are rotated 3.00 degrees and the modules with the short side up are rotated 2.714 degrees.

Definitions that may apply only to this set of modules.

$sps := 0$ (space between modules, cm)

$Ds := 1.30$ (radial difference of alternating modules, cm)

$Ns := 29$ (number of straws, long side)

$Ls := 6$ (number of straws, high)

$Hs := ((Ls - 1) \cdot d \cdot .866) + d + (2 \cdot T)$ (height of module, cm)

$LSs := Ns \cdot d + (2 \cdot T)$ (length of module, long side, cm)

$SSs := (Ns - (Ls - 1)) \cdot d + (2 \cdot T)$ (length of module short side, cm)

$Us := LSs + SSs + sps - (Ds \cdot .5774)$ (total length of module pr cm)

$$CHs := Ls \cdot \left[Ns - \frac{Ls - 1}{2} \right] \qquad CHs = 159 \qquad \text{(straws per module)}$$

$LSs = 11.777$

$SSs = 9.755$

$Hs = 2.205$

Superlayer #3 Stereo angle (ac)

BEFORE ROTATION ac := 0.0524 radians, (3.00 degrees)

c := 36 module pairs

$is3 := \frac{c \cdot Us}{2 \cdot \pi}$

inside radius (is3), short side up is3 = 119.066 cm

outside radius (os3), short side up os3 := is3 + Hs os3 = 121.272 cm

inside radius (il3), long side up il3 := is3 + Ds il3 = 120.366 cm

outside radius (ol3), long side up ol3 := il3 + Hs ol3 = 122.572 cm

mean radius (m3) m3 := .5·(ol3 − is3) + is3 m3 = 120.819 cm

Superlayer #3 (AFTER ROTATION, DIMENSIONS AT MODULE ENDS)

module length mlc := 354.7 cm

distance from module center line to max radius after rotation (ABc)

$ABc := \frac{LSs}{2} + \frac{mlc}{2} \cdot \tan(ac)$ ABc = 15.19 cm

outside radius, (olr), long side up $olr := \sqrt{(ol3)^2 + (ABc)^2}$

olr = 123.509 cm

delc := olr − ol3 delc = 0.938 cm

inside radius (ilr), long side up ilr := il3 + delc ilr = 121.304 cm

inside radius (ir3), short side up ir3 := is3 + delc ir3 = 120.004 cm

outside radius (or3), short side up or3 := os3 + delc or3 = 122.209 cm

mean radius (mr3) mr3 := m3 + delc mr3 = 121.757 cm

Number of straws in this superlayer STc := CHs·(4·c)

= (ST) both halfs of tracker. STc = 22896 straws

Superlayer #4 Axial

d := 40 module pairs

module length mld := 389.7 cm $is4 := \frac{d \cdot U}{2 \cdot \pi}$

inside radius (is4), short side up is4 = 133.288 cm

outside radius (os4), short side up os4 := is4 + Hc os4 = 136.544 cm

inside radius (il4), long side up il4 := is4 + Dc il4 = 133.738 cm

outside radius (ol4), long side up $ol4 := \sqrt{(il4 + Hc)^2 + \frac{LS}{2}}$

ol4 = 137.016 cm

mean radius (m4) m4 := .5·(ol4 − is4) + is4 m4 = 135.152 cm

number of straws in this superlayer STd := CH·(4·d)

= (STd), both halfs of the tracker STd = 25440 straws

Superlayer #5 Stereo angle (ac)

ac = 0.0524 radians

BEFORE ROTATION

E := 44 module pairs

$is5 := \frac{E \cdot Us}{2 \cdot \pi}$

inside radius (is5), short side up is5 = 145.525 cm

outside radius (os5), short side up os5 := is5 + Hs os5 = 147.731 cm

inside radius (il5), long side up il5 := is5 + Ds il5 = 146.825 cm

outside radius (ol5), long side up ol5 := il5 + Hs ol5 = 149.031 cm

mean radius (m5) m5 := .5·(ol5 − is5) + is5 m5 = 147.278 cm

Superlayer #5 (AFTER ROTATION, DIMENSIONS AT MODULE ENDS)
module length mde := 394.7 cm
distance from module center line to max radius after rotation (ABe)

$$ABe := \frac{LSs}{2} + \frac{mde}{2} \cdot \tan(ac) \qquad ABe = 16.239 \quad cm$$

$$ore := \sqrt{(ol5)^2 + (ABe)^2}$$

outside radius, (ore), long side up
dele := ore - ol5   dele = 0.882 cm   ore = 149.913 cm
inside radius (ire), long side up ire := il5 + dele   ire = 147.708 cm
inside radius (ir5), short side up ir5 := is5 + dele   ir5 = 146.408 cm
outside radius (or5), short side up or5 := os5 + dele   or5 = 148.613 cm
mean radius (mr5)   mr5 := m5 + dele   mr5 = 148.16 cm
Number of straws in this superlayer   STe := CHs·(4·E)
= (STe) both halfs of the tracker   STe = 27984 straws

Superlayer #6 Axial Trigger Layer, curved modules
f := 48 module pairs

$$is6 := \frac{f \cdot Uc}{2 \cdot \pi}$$

inside radius (is6), short side up   is6 = 159.644 cm
outside radius (os6), short side up os6 := is6 + Hc   os6 = 162.9 cm
inside radius (il6), long side up il6 := is6 + Dc   il6 = 160.094 cm
outside radius (ol6), long side up ol6 := il6 + Hc   ol6 = 163.35 cm
mean radius (m6)   m6 := .5·(ol6 - is6) + is6   m6 = 161.497 cm
Number of straws in this superlayer   STf := CHc·(4·f)
= (STf) both halfs of the tracker   STf = 44928 straws

Total number of straws in superlayers #3 to #6 (both ends)
Total_straws := STc + STd + STe + STf
Total_straws = 121248

Total number modules, (both ends)
stereo := 2·c + 2·E   stereo = 160
axial := 2·d   axial = 80
trigger := 2·f   trigger = 96
Total_Modules := 2·(stereo + axial + trigger)   Total_Modules = 672

Mean radius of superlayers

Superlayer #3			Delta cm
#3	mr3 = 121.757	cm*	m4 - mr3 = 13.395
#4	m4 = 135.152	cm	mr5 - m4 = 13.008
#5	mr5 = 148.16	cm*	m6 - mr5 = 13.337
#6	m6 = 161.497	cm	

Space betweem superlayers cm

#6 - #5	is6 - ore = 9.732	cm
#5 - #4	ir5 - ol4 = 9.392	cm
#4 - #3	is4 - olr = 9.779	cm

Support Structure Summary

Superlayer #3 (stereo)

Mean Radius (after rotation)		mr3 =	121.757	cm
	Maximum Radius	olr =	123.509	cm
	Minimun Radius	ir3 =	120.004	cm
Shim Ring Maximum Radius	sr3m := ilr + 1	sr3m =	122.304	cm
Minimun Radius	sr3n := ir3 - 1.5	sr3n =	118.504	cm
Support Cyl outside rad	sc3or := ir3 - 1.5	sc3or =	118.504	cm
inside rad	sc3ir := sc3or - 2.5	sc3ir =	116.004	cm

Superlayer #4 (axial)

	Mean Radius	m4 =	135.152	cm
	Maximum Radius	ol4 =	137.016	cm
	Minimun Radius	is4 =	133.288	cm
Shim Ring Maximum Radius	sr4m := il4 + 1	sr4m =	134.738	cm
Minimun Radius	sr4n := is4 - 1.5	sr4n =	131.788	cm
Support Cyl outside rad	sc4or := is4 - 1.5	sc4or =	131.788	cm
inside rad	sc4ir := sc4or - 2.5	sc4ir =	129.288	cm

Superlayer #5 (stereo)

	Mean Radius	m5 =	147.278	cm
	Maximum Radius	ore =	149.913	cm
	Minimun Radius	ir5 =	146.408	cm
Shim Ring Maximum Radius	sr5m := ire + 1	sr5m =	148.708	cm
Minimun Radius	sr5n := ir5 - 1.5	sr5n =	144.908	cm
Support Cyl outside rad	sc5or := ir5 - 1.5	sc5or =	144.908	cm
inside rad	sc5ir := sc5or - 2.5	sc5ir =	142.408	cm

Superlayer #6 (axial, trigger)

	Mean Radius	m6 =	161.497	cm
	Maximum Radius	ol6 =	163.35	cm
	Minimum Radius	is6 =	159.644	cm
Shim Ring Maximum Radius	sr6m := il6 + 1	sr6m =	161.094	cm
Minimun Radius	sr6n := is6 - 1.5	sr6n =	158.144	cm
Support Cyl outside rad	sc6or := is6 - 1.5	sc6or =	158.144	cm
inside rad	sc6ir := sc6or - 2.5	sc6ir =	155.644	cm

Radial Clearance between Superlayers and Support Cylinders.

Superlayer #3 and Support Cylinder #4				
	d34 := sc4ir - olr	d34 =	5.779	cm
Superlayer #4 and support Cylinder #5				
	d45 := sc5ir - ol4	d45 =	5.392	cm
Superlayer #5 and support Cylinder #6				
	d56 := sc6ir - ore	d56 =	5.732	cm
Superlayer #6 and coil ID				
	d6c := 168.5 - ol6	d6c =	5.15	cm

W STC

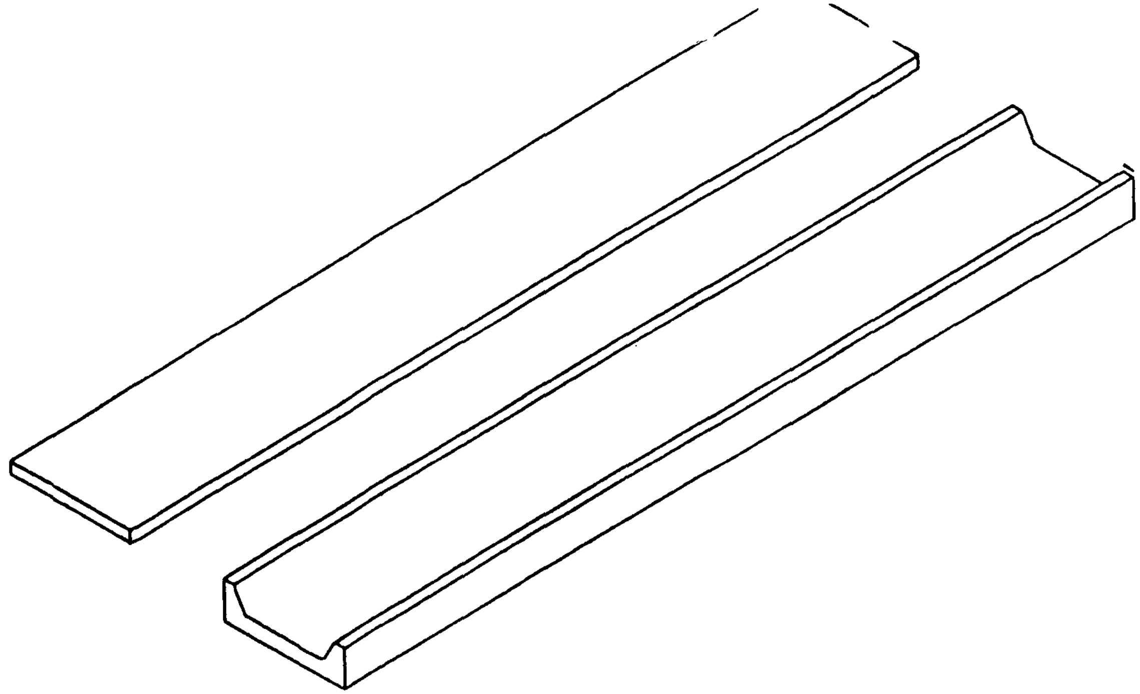

LENGTH OF BASE AND COVER 100.0 CM

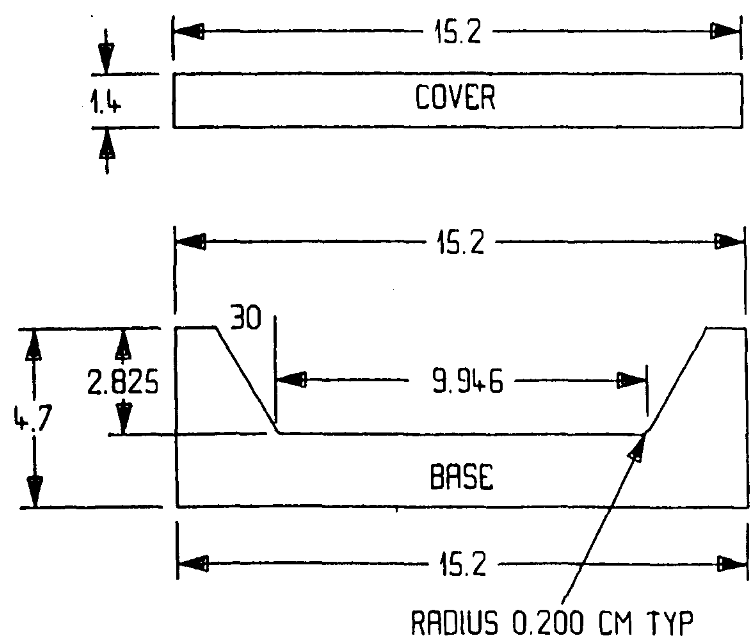

228 STRAW MODULE FORM
32 STRAWS WIDE X 8 LAYERS

MATERIAL ALUNINUM 6061-T6

DAGDAC - PGH, PA
PER DAVE WILLIAMS 07-12-91
$1195 - 2 WKS
DELIVERY

ALL DIMENSIONS IN CM
TOLERANCE 3 PLACES HELD TO A MIL

DM 07-10-91-2

W STC

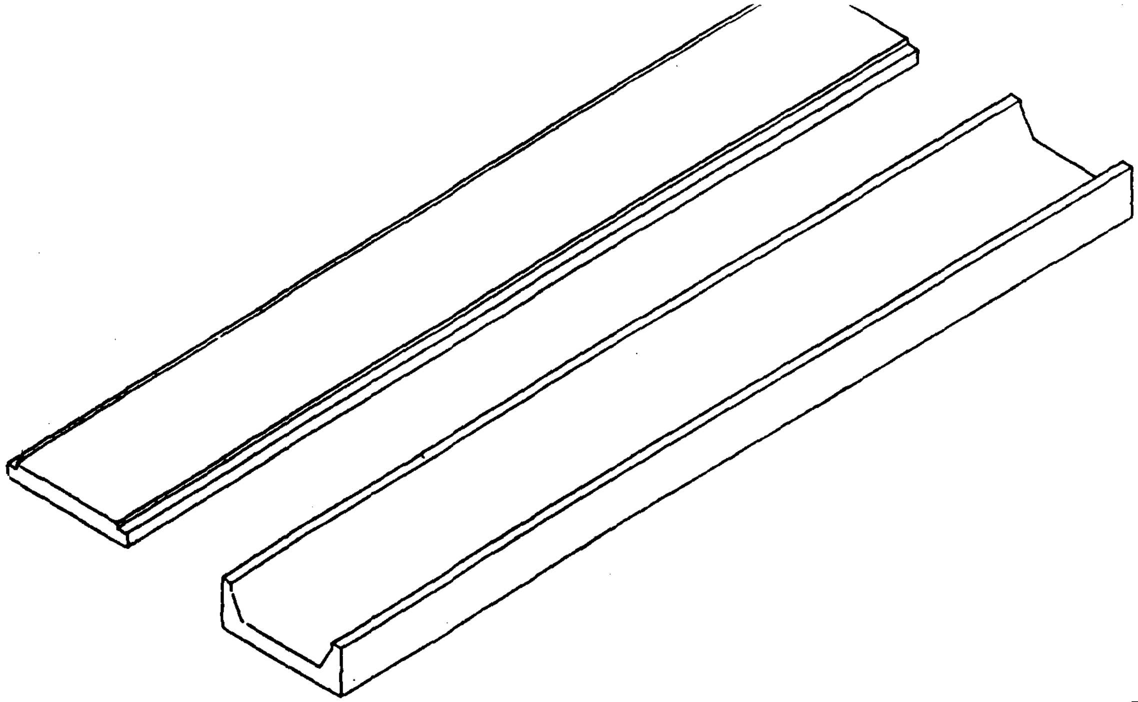

LENGTH OF BASE AND COVER 100.0 CM

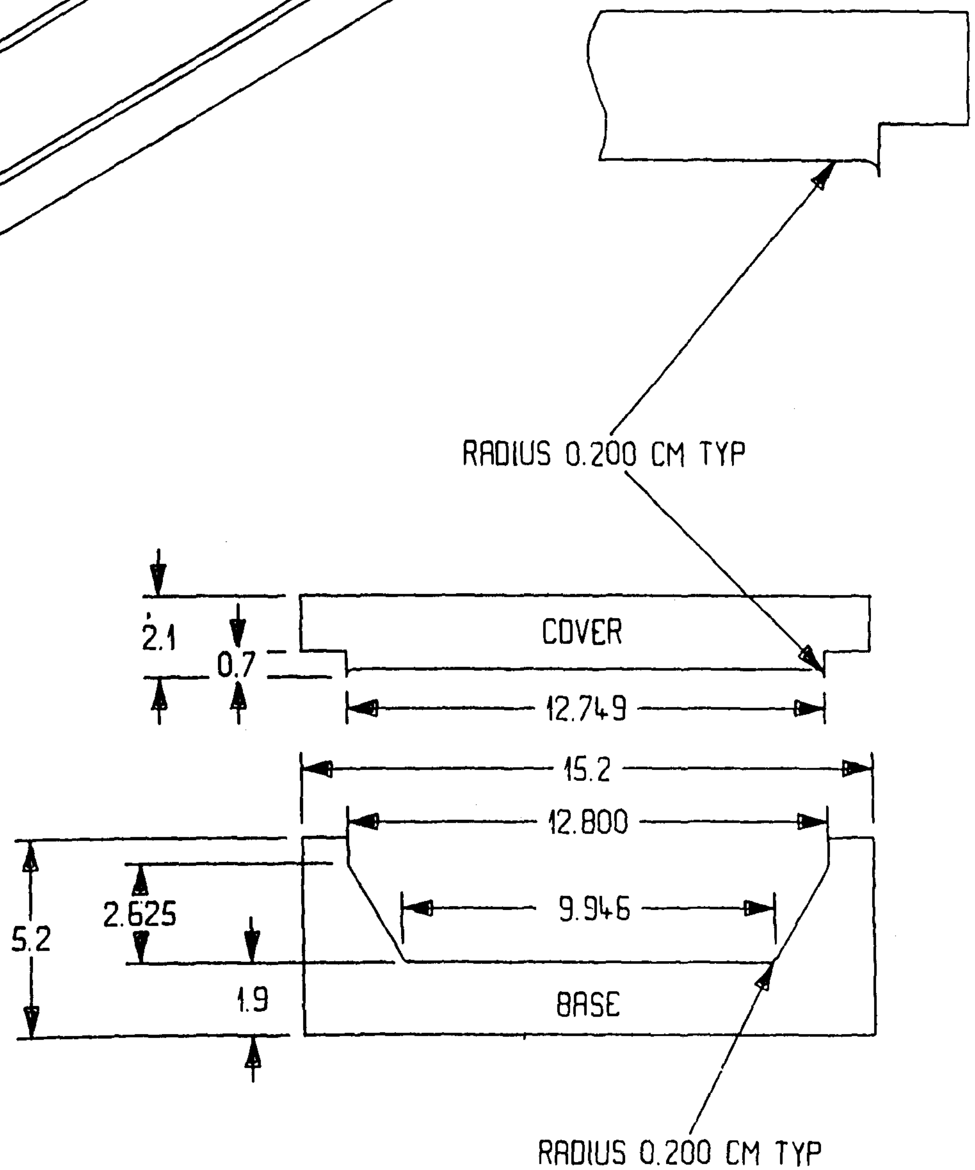

228 STRAW MODULE FORM
32 STRAWS WIDE X 8 LAYERS

MATERIAL ALUNINUM 6061-T6

ALL DIMENSIONS IN CM

DM 07-10-91-1

SE[illegible]ION[illegible] OF [illegible]ER[illegible]YER [illegible]UM[illegible] 3, [illegible] CE[illegible]RK[illegible] RE[illegible]-20-[illegible]

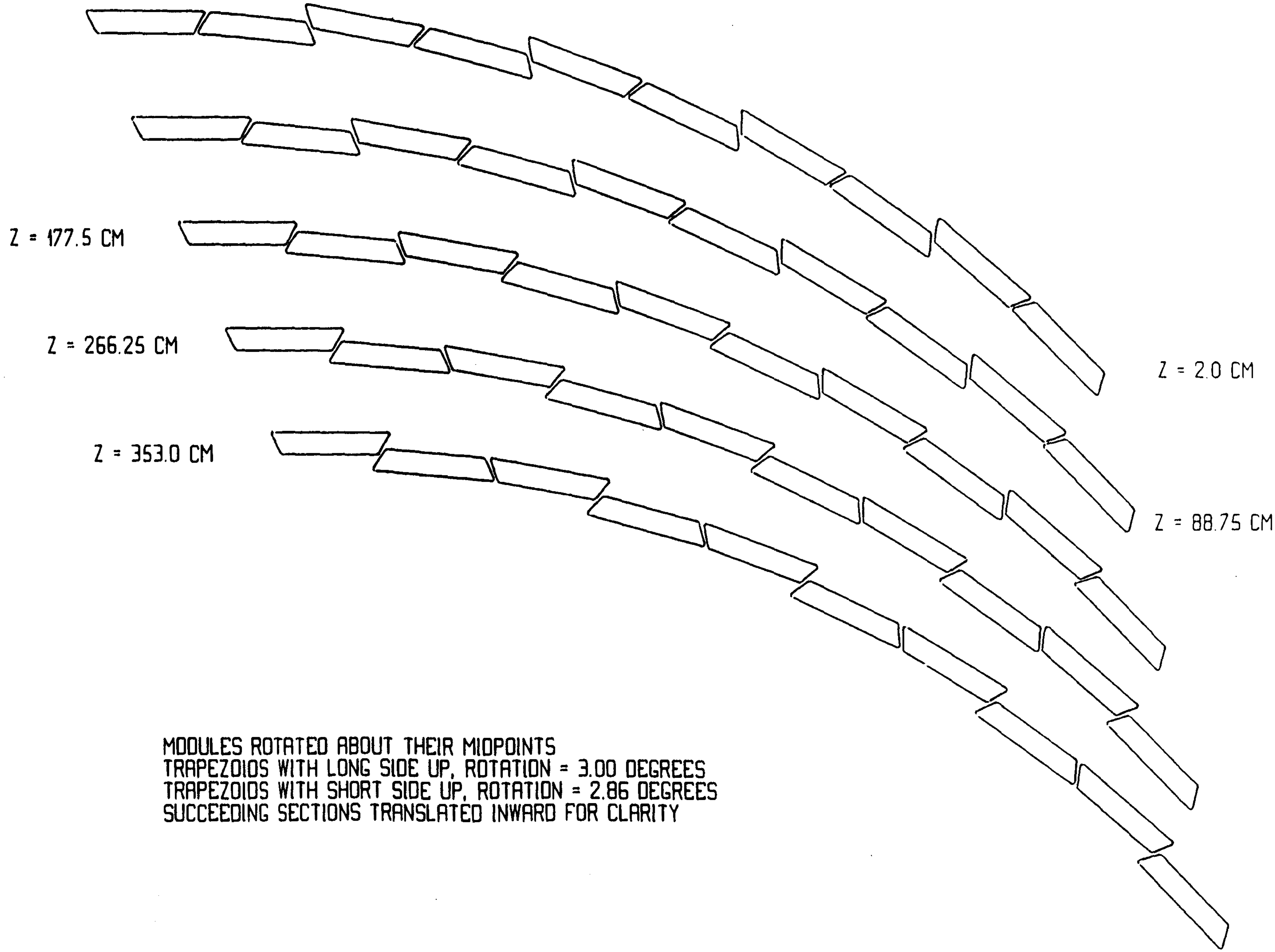

CENTRAL AND FORWARD TRACKING SUBSYSTEM

BASELINE DESIGN

THE DESIGN USES:

Four Outer Superlayers of Straw Modules

Westinghouse
Science & Technology Center

MODULAR STRAW TUBE TRACKING SYSTEM
EXPLODED VIEW

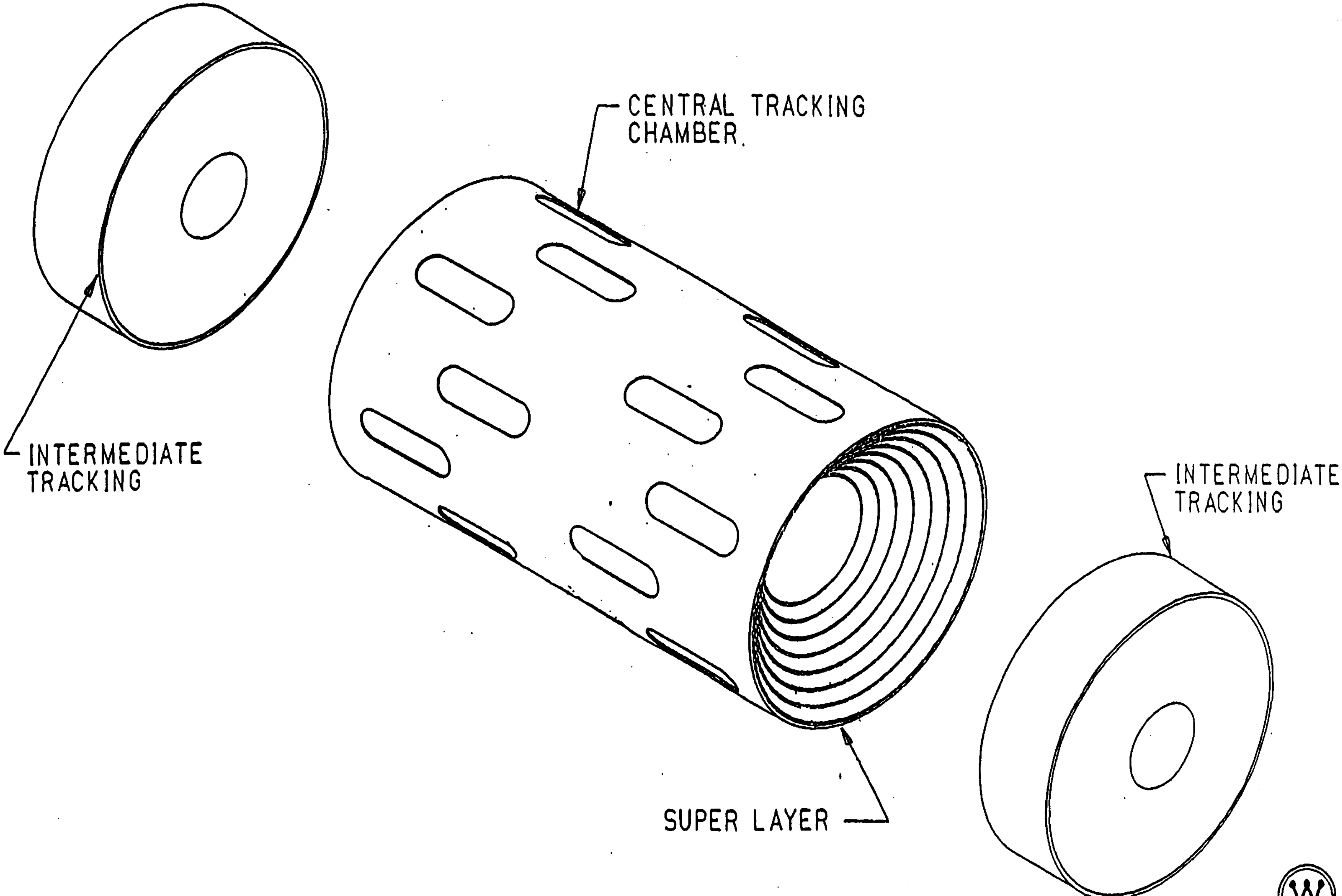

D.389.4136A44.R1
KEPES 12-4-90

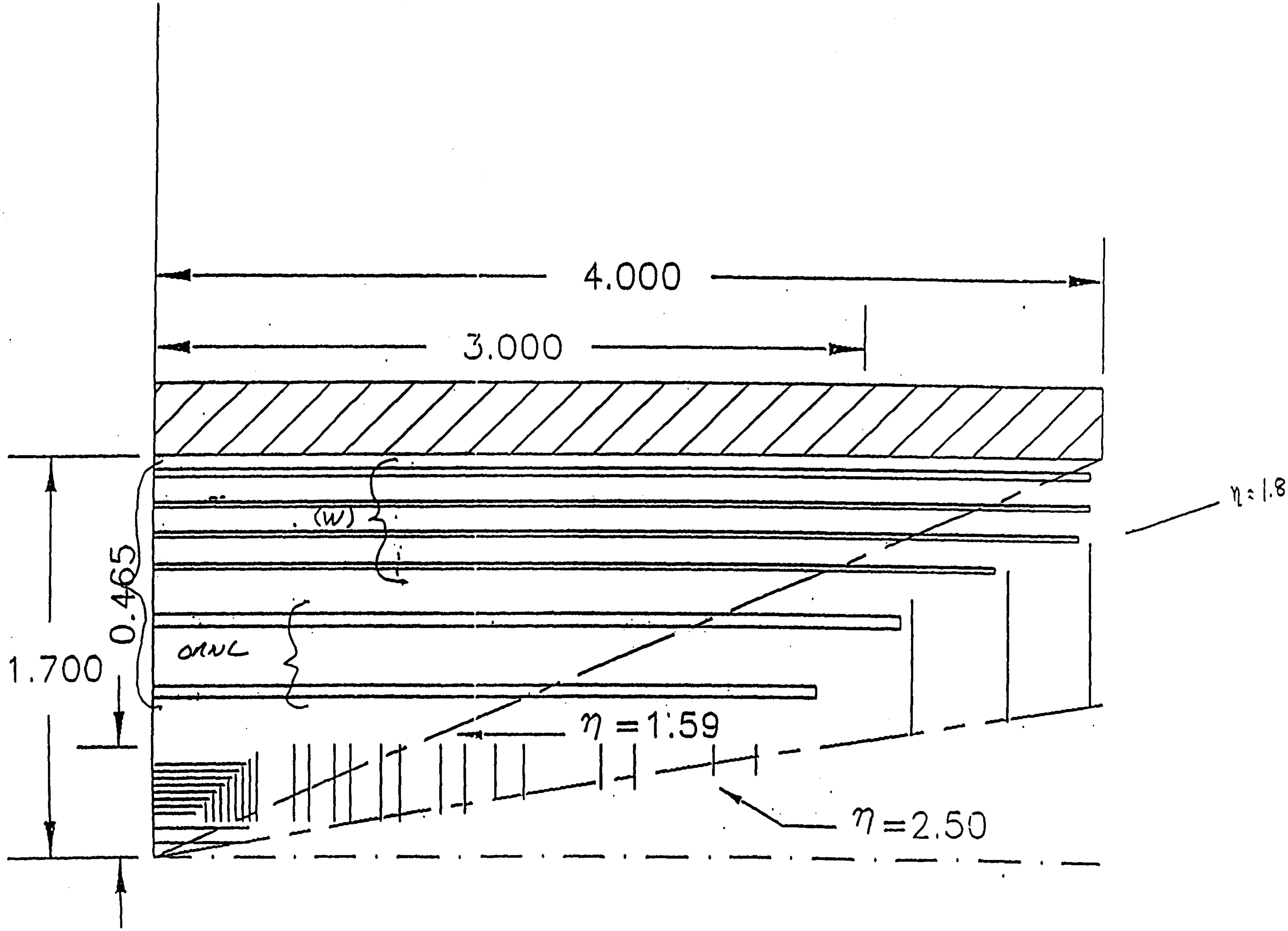

4.000
3.000
1.700
0.465
(W)
ORNL
η = 1.8
η = 1.59
η = 2.50

Baseline layout:

Central outer barrel.

Fiber section:

superlr	layer	<r>	Nfiber	half length	stereo	
1	1	0.700−0.0235	22670	2.80	0	5.6 + .5 = 6.1
	2	0.700+0.0235	24245	2.80	0	
2	1	1.000−0.0235	32723	3.15	0	
	2	1.000−0.0205	32823	3.15	−4.5 deg	6.3 + .5 = 6.8
	3	1.000+0.0205	34197	3.15	3 deg	
	4	1.000+0.0235	34298	3.15	0	
total (both ends)			361912			

Straw section:

superlr	r_1	Nstraws/lr	Nlr/sl	zmin	zmax	stereo	
3	1.21722	1912	6	0.03	3.550	−3 deg	7.1 + .5 = 7.6
4	1.34963	2120	6	0.03	3.900	0	7.8 + .5 = 8.3
5	1.48205	2328	6	0.03	3.950	+3 deg	7.9 + .5 = 8.4
6	1.61447	2536	9	0.03	3.950	0	7.9 + .5 = 8.4
total (both ends) 121968							

Intermediate angle fiber tracker.

disk	downstream z	r_inner	r_outer	Nfiber
1	3.20	0.52	1.09	34851
2	3.60	0.585	1.22	39207
3	3.95	0.65	1.34	43563
	total (both ends)			235242

CENTRAL AND FORWARD TRACKING SUBSYSTEM

BASELINE COSTS

Westinghouse
Science & Technology Center

TABLE NUMBER 1[illegible]
STRAW TUBE CENTRAL TRACKER
MAN DAY SUMMARY 08-06-91

WBS	TASK	EN	ENM	EA	EAM	DR	DRM	TE	TEM	LA	LAM
1.2.1.1	TRIGGER MODULES(192)	744	0	0	0	255	0	0	2856	0	0
1.2.1.2	AXIAL(160) & STEREO(320) MODULES	1271	0	0	0	410	0	0	10098	0	0
1.2.2	SUPPORT COMPONENTS	278	441	121	0	295	54	232	1398	0	0
1.2.3	SUPERLAYER(S/L) ASSEMBLY	175	123	1	0	120	30	296	828	0	0
1.2.4	S/L TO S/L ASSEMBLY	150	72	12	0	180	46	45	231	0	0
1.2.5	EQUIPMENT,TOOLING,& FIXTURES	971	200	154	152	1299	175	304	296	0	0
1.2.6	FINAL FACTORY ASSEMBLY	309	0	14	17	485	56	10	545	0	0
1.2.7	FINAL FACTORY TESTING	43	10	2	4	44	7	10	354	0	0
1.2.8	TRACKER TRANSPORTATION	15	0	0	0	20	3	0	0	0	0
1.2.9	SURFACE ERECTION AT SSCL	165	51	50	0	112	29	10	145	0	0
1.2.10	FACILITIES	22	1500	14	0	44	757	0	1500	0	0
1.2.11	PROGRAM MANAGEMENT	2454	500	875	0	630	0	0	0	0	0
1.2.12	R & D EFFORT	400	0	0	0	800	0	480	0	0	0
8.2	INSTALLATION & TEST	106	152	2	5	81	42	104	277	0	35
	SUBTOTAL	7103	3049	1245	178	4775	1199	1491	18528	0	35

TABLE NUMBER 18
STRAW TUBE CENTRAL TRACKER
LABOR SUMMARY CALCULATIONS 08-06-91

		EDIA		KFAL	
WBS	TASK	(MD)	(MY)	(MD)	(MY)
1.2.1.1	TRIGGER MODULES(192)	999	4.0	2856	11.4
1.2.1.2	AXIAL(160) & STEREO(320) MODULES	1681	6.7	10098	40.4
1.2.2	SUPPORT COMPONENTS	694	2.8	2125	8.5
1.2.3	SUPERLAYER(S/L) ASSEMBLY	296	1.2	1277	5.1
1.2.4	S/L TO S/L ASSEMBLY	342	1.4	394	1.6
1.2.5	EQUIPMENT,TOOLING,& FIXTURES	2424	9.7	1127	4.5
1.2.6	FINAL FACTORY ASSEMBLY	808	3.2	628	2.5
1.2.7	FINAL FACTORY TESTING	89	0.4	385	1.5
1.2.8	TRACKER TRANSPORTATION	35	0.1	3	0.0
1.2.9	SURFACE ERECTION AT SSCL	327	1.3	235	0.9
1.2.10	FACILITIES	80	0.3	3757	15.0
1.2.11	PROGRAM MANAGEMENT	3959	15.8	500	2.0
1.2.12	R & D EFFORT	1200	4.8	480	1.9
8.2	INSTALLATION & TEST	189	0.8	615	2.5
	TOTAL	13123	52.5	24480	97.9

STRAW TUBE CENTRAL TRACKER
COST SUMMARY CALCULATIONS 07-30-91

TABLE NUMBER 1

							PERCENT OF ITS OWN TOTAL					PERCENT OF TASK BASE TOTAL			
WBS	TASK	EDIA	MFAL	TMAT	BASE	BAS+CON	%EDIA	%MFAL	%TMAT	%BASE	%BAS+CON	%EDIA	%MFAL	%TMAT	%BASE
1.2.1.1	TRIGGER MODULES(192)	425859	833952	959000	2218811	3013414	6.81	9.62	8.12	8.30	8.39	19.19	37.59	43.22	100.00
1.2.1.2	AXIAL(160) & STEREO(320) MODULES	293322	2114664	1931000	4338986	5444456	4.69	24.40	16.36	16.24	15.16	6.76	48.74	44.50	100.00
1.2.2	SUPPORT COMPONENTS	421987	1134037	1990000	3546024	5367600	6.75	13.09	16.86	13.27	14.94	11.90	31.98	56.12	100.00
1.2.3	SUPERLAYER(S/L) ASSEMBLY	191972	657681	10000	859653	1104987	3.07	7.59	0.08	3.22	3.08	22.33	76.51	1.16	100.00
1.2.4	S/L TO S/L ASSEMBLY	207620	206996	165000	579616	858505	3.32	2.39	1.40	2.17	2.39	35.82	35.71	28.47	100.00
1.2.5	EQUIPMENT,TOOLING,& FIXTURES	1428895	574638	4456000	6459533	8981661	22.85	6.63	37.75	24.17	25.00	22.12	8.90	68.98	100.00
1.2.6	FINAL FACTORY ASSEMBLY	444536	255303	237000	936839	1184219	7.11	2.95	2.01	3.51	3.30	47.45	27.25	25.30	100.00
1.2.7	FINAL FACTORY TESTING	44093	139917	93000	277010	378898	0.70	1.61	0.79	1.04	1.05	15.92	50.51	33.57	100.00
1.2.8	TRACKER TRANSPORTATION	21040	1364	10000	32404	47958	0.34	0.02	0.08	0.12	0.13	64.93	4.21	30.86	100.00
1.2.9	SURFACE ERECTION AT SSCL	146273	101119	475000	722392	1058805	2.34	1.17	4.02	2.70	2.95	20.25	14.00	65.75	100.00
1.2.10	FACILITIES	45737	2096405	630000	2772142	3548512	0.73	24.19	5.34	10.37	9.88	1.65	75.62	22.73	100.00
1.2.11	PROGRAM MANAGEMENT	1955840	334136	379000	2668976	3304137	31.27	3.86	3.21	9.99	9.20	73.28	12.52	14.20	100.00
1.2.12	R & D EFFORT	627310	214989	470000	1312299	1627252	10.03	2.48	3.98	4.91	4.53	47.80	16.38	35.82	100.00
	TOTAL	6254484	8665201	11805000	26724685	35920404	100.00	100.00	100.00	100.00	100.00	23.40	32.42	44.17	100.00
8.2	INSTALLATION & TEST	102416	268682	67500	438598	590039	1.61	3.01	0.57	1.61	1.62	23.35	61.26	15.39	100.00
	TOTAL	6356900	8933883	11872500	27163283	36510443	100.00	100.00	100.00	100.00	100.00	23.40	32.89	43.71	100.00

TABLE NUMBER 2

							PERCENT OF BASE COST					PERCENT OF BASE PLUS CONTINGENCY COST				
WBS	TASK	EDIA	MFAL	TMAT	BASE	BAS+CON	%EDIA	%MFAL	%TMAT	%BASE	%BAS+CON	%EDIA	%MFAL	%TMAT	%BASE	%BAS+CON
1.2.1.1	TRIGGER MODULES(192)	425859	833952	959000	2218811	3013414	1.59	3.12	3.59	8.30	11.28	1.19	2.32	2.67	6.18	8.39
1.2.1.2	AXIAL(160) & STEREO(320) MODULES	293322	2114664	1931000	4338986	5444456	1.10	7.91	7.23	16.24	20.37	0.82	5.89	5.38	12.08	15.16
1.2.2	SUPPORT COMPONENTS	421987	1134037	1990000	3546024	5367600	1.58	4.24	7.45	13.27	20.08	1.17	3.16	5.54	9.87	14.94
1.2.3	SUPERLAYER(S/L) ASSEMBLY	191972	657681	10000	859653	1104987	0.72	2.46	0.04	3.22	4.13	0.53	1.83	0.03	2.39	3.08
1.2.4	S/L TO S/L ASSEMBLY	207620	206996	165000	579616	858505	0.78	0.77	0.62	2.17	3.21	0.58	0.58	0.46	1.61	2.39
1.2.5	EQUIPMENT,TOOLING,& FIXTURES	1428895	574638	4456000	6459533	8981661	5.35	2.15	16.67	24.17	33.61	3.98	1.60	12.41	17.98	25.00
1.2.6	FINAL FACTORY ASSEMBLY	444536	255303	237000	936839	1184219	1.66	0.96	0.89	3.51	4.43	1.24	0.71	0.66	2.61	3.30
1.2.7	FINAL FACTORY TESTING	44093	139917	93000	277010	378898	0.16	0.52	0.35	1.04	1.42	0.12	0.39	0.26	0.77	1.05
1.2.8	TRACKER TRANSPORTATION	21040	1364	10000	32404	47958	0.08	0.01	0.04	0.12	0.18	0.06	0.00	0.03	0.09	0.13
1.2.9	SURFACE ERECTION AT SSCL	146273	101119	475000	722392	1058805	0.55	0.38	1.78	2.70	3.96	0.41	0.28	1.32	2.01	2.95
1.2.10	FACILITIES	45737	2096405	630000	2772142	3548512	0.17	7.84	2.36	10.37	13.28	0.13	5.84	1.75	7.72	9.88
1.2.11	PROGRAM MANAGEMENT	1955840	334136	379000	2668976	3304137	7.32	1.25	1.42	9.99	12.36	5.44	0.93	1.06	7.43	9.20
1.2.12	R & D EFFORT	627310	214989	470000	1312299	1627252	2.35	0.80	1.76	4.91	6.09	1.75	0.60	1.31	3.65	4.53
	TOTAL	6254484	8665201	11805000	26724685	35920404	23.40	32.42	44.17	100.00	134.41	17.41	24.12	32.86	74.40	100.00
8.2	INSTALLATION & TEST	102416	268682	67500	438598	590039	0.38	0.99	0.25	1.61	2.17	0.28	0.74	0.18	1.20	1.62
	TOTAL	6356900	8933883	11872500	27163283	36510443	23.40	32.89	43.71	100.00	134.41	17.41	24.47	32.52	74.40	100.00

..RAH ... ENTR ... TRACKER
COST SUMMARY CALCULATIONS 08-06-91

TABLE NUMBER 11

BS	TASK	EDIA	MFAL	TMAT	BASE	BAS+CON	PERCENT OF ITS OWN TOTAL %EDIA	%MFAL	%TMAT	%BASE	%BAS+CON	PERCENT OF TASK BASE TOTAL %EDIA	%MFAL	%TMAT	%BASE
.2.1.1	TRIGGER MODULES(192)	425859	833952	959000	2218811	3013414	9.00	12.51	8.12	9.56	9.65	19.19	37.59	43.22	100.00
.2.1.2	AXIAL(160) & STEREO(320) MODULES	293322	2114664	1931000	4338986	5444456	6.20	31.73	16.36	18.70	17.43	6.76	48.74	44.50	100.00
.2.2	SUPPORT COMPONENTS	263358	696811	1990000	2950169	4499381	5.57	10.45	16.86	12.72	14.41	8.93	23.62	67.45	100.00
.2.3	SUPERLAYER(S/L) ASSEMBLY	120000	394661	10000	524661	673770	2.54	5.92	0.08	2.26	2.16	22.87	75.22	1.91	100.00
1.2.4	S/L TO S/L ASSEMBLY	131550	128734	165000	425284	631121	2.78	1.93	1.40	1.83	2.02	30.93	30.27	38.80	100.00
1.2.5	EQUIPMENT,TOOLING,& FIXTURES	919856	373675	4456000	5749531	8008411	19.45	5.61	37.75	24.78	25.64	16.00	6.50	77.50	100.00
1.2.6	FINAL FACTORY ASSEMBLY	304624	182535	237000	724159	915898	6.44	2.74	2.01	3.12	2.93	42.07	25.21	32.73	100.00
1.2.7	FINAL FACTORY TESTING	34773	114473	93000	242246	332308	0.74	1.72	0.79	1.04	1.06	14.35	47.25	38.39	100.00
1.2.8	TRACKER TRANSPORTATION	13415	975	10000	24390	36097	0.28	0.01	0.08	0.11	0.12	55.00	4.00	41.00	100.00
1.2.9	SURFACE ERECTION AT SSCL	128715	78196	475000	681911	1002130	2.72	1.17	4.02	2.94	3.21	18.88	11.47	69.66	100.00
1.2.10	FACILITIES	28992	1375525	630000	2034517	2604291	0.61	20.64	5.34	8.77	8.34	1.43	67.61	30.97	100.00
1.2.11	PROGRAM MANAGEMENT	1620419	230500	379000	2229919	2764549	34.26	3.46	3.21	9.61	8.85	72.67	10.34	17.00	100.00
1.2.12	R & D EFFORT	444400	140160	470000	1054560	1307656	9.40	2.10	3.98	4.55	4.19	42.14	13.29	44.57	100.00
	TOTAL	4729283	6664861	11805000	23199144	31233482	100.00	100.00	100.00	100.00	100.00	20.39	28.73	50.89	100.00
8.2	INSTALLATION & TEST	75841	200799	67500	344140	468094	1.58	2.92	0.57	1.46	1.48	22.04	58.35	19.61	100.00
	TOTAL	4805124	6865660	11872500	23543284	31701576	100.00	100.00	100.00	100.00	100.00	20.41	29.16	50.43	100.00

TABLE NUMBER 12

WBS	TASK	EDIA	MFAL	TMAT	BASE	BAS+CON	PERCENT OF BASE COST %EDIA	%MFAL	%TMAT	%BASE	%BAS+CON	PERCENT OF BASE PLUS CONTINGENCY COST %EDIA	%MFAL	%TMAT	%BASE	%BAS+CON
1.2.1.1	TRIGGER MODULES(192)	425859	833952	959000	2218811	3013414	1.84	3.59	4.13	9.56	12.99	1.36	2.67	3.07	7.10	9.65
1.2.1.2	AXIAL(160) & STEREO(320) MODULES	293322	2114664	1931000	4338986	5444456	1.26	9.12	8.32	18.70	23.47	0.94	6.77	6.18	13.89	17.43
1.2.2	SUPPORT COMPONENTS	263358	696811	1990000	2950169	4499381	1.14	3.00	8.58	12.72	19.39	0.84	2.23	6.37	9.45	14.41
1.2.3	SUPERLAYER(S/L) ASSEMBLY	120000	394661	10000	524661	673770	0.52	1.70	0.04	2.26	2.90	0.38	1.26	0.03	1.68	2.16
1.2.4	S/L TO S/L ASSEBLY	131550	128734	165000	425284	631121	0.57	0.55	0.71	1.83	2.72	0.42	0.41	0.53	1.36	2.02
1.2.5	EQUIPMENT,TOOLING,& FIXTURES	919856	373675	4456000	5749531	8008411	3.97	1.61	19.21	24.78	34.52	2.95	1.20	14.27	18.41	25.64
1.2.6	FINAL FACTORY ASSEMBLY	304624	182535	237000	724159	915898	1.31	0.79	1.02	3.12	3.95	0.98	0.58	0.76	2.32	2.93
1.2.7	FINAL FACTORY TESTING	34773	114473	93000	242246	332308	0.15	0.49	0.40	1.04	1.43	0.11	0.37	0.30	0.78	1.06
1.2.8	TRACKER TRANSPORTATION	13415	975	10000	24390	36097	0.06	0.00	0.04	0.11	0.16	0.04	0.00	0.03	0.08	0.12
1.2.9	SURFACE ERECTION AT SSCL	128715	78196	475000	681911	1002130	0.55	0.34	2.05	2.94	4.32	0.41	0.25	1.52	2.18	3.21
1.2.10	FACILITIES	28992	1375525	630000	2034517	2604291	0.12	5.93	2.72	8.77	11.23	0.09	4.40	2.02	6.51	8.34
1.2.11	PROGRAM MANAGEMENT	1620419	230500	379000	2229919	2764549	6.98	0.99	1.63	9.61	11.92	5.19	0.74	1.21	7.14	8.85
1.2.12	R & D EFFORT	444400	140160	470000	1054560	1307656	1.92	0.60	2.03	4.55	5.64	1.42	0.45	1.50	3.38	4.19
	TOTAL	4729283	6664861	11805000	23199144	31233482	20.39	28.73	50.89	100.00	134.63	15.14	21.34	37.80	74.28	100.00
8.2	INSTALLATION & TEST	75841	200799	67500	344140	468094	0.32	0.85	0.29	1.46	1.99	0.24	0.63	0.21	1.09	1.48
	TOTAL	4805124	6865660	11872500	23543284	31701576	20.41	29.16	50.43	100.00	134.65	15.16	21.66	37.45	74.27	100.00

	OUR	%	SUMMARY OESCRIPTION / BUDGET	EARNED	SCHEDULEO START	FINISH
121	1527	0	1.2.1 MODULES 6557797.00	.00	1OCT92	5DEC96
122	1107	0	1.2.2 SUPPORT STRUCTURE 3546016.71	.00	1OCT92	12OCT95
123	923	0	1.2.3 SUPERLAYER (S/L) ASSEMBLY 859654.10	.00	29DEC94	8JUL97
124	1748	0	1.2.4 TRACKER S/L TO S/L ASSEMBLY 579613.40	.00	9APR93	20JAN98
125	1784	0	1.2.5 EQUIPMENT,TOOLING,& FIXTURES 6459542.11	.00	1OCT92	19AUG97
126	1836	0	1.2.6 FINAL FACTORY ASSEMBLY 936835.01	.00	25MAR93	3APR98
127	1884	0	1.2.7 FINAL FACTORY TESTING 277010.41	.00	25MAR93	21MAY98
128	1016	0	1.2.8 TRACKER TRANSPORTATION SYSTEM 32404.50	.00	10AUG95	21MAY98
129	1875	0	1.2.9 SURFACE ASSY AT SUPERCOLLIDER SITE 722391.28	.00	21MAY93	8JUL98
12A	1878	0	1.2.10 FACILITIES 2772141.00	.00	30NOV92	20JAN98
128	1583	0	1.2.11 PROGRAM MANAGEMENT 2668973.42	.00	1OCT92	18JAN99
12C	900	0	1.2.12 R & D EFFORT 1312299.60	.00	15JUL91	30DEC93
821	1268	0	8.2.1 SUBSYSTEM INSTALLATION IN HALL 335295.48	.00	28OCT93	9NOV98
822	895	0	8.2.2 SUBSYSTEM AND SYSTEM TEST IN HALL 103304.20	.00	27JUN95	18JAN99
REPORT TOTAL			27163278.22	.00		

ENGINEERING MANPOWER

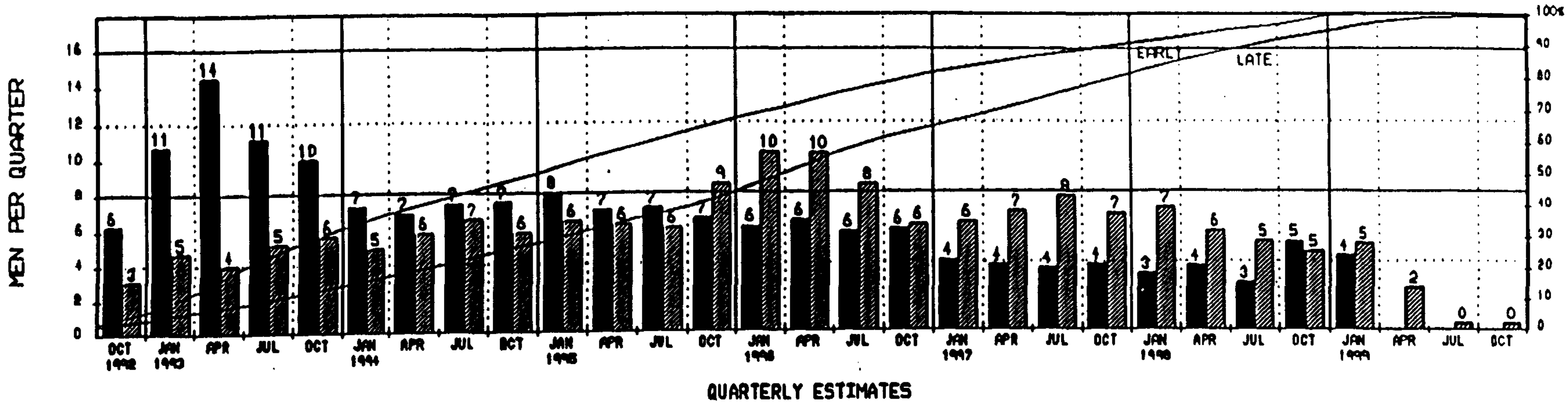

DRAFTING MANPOWER

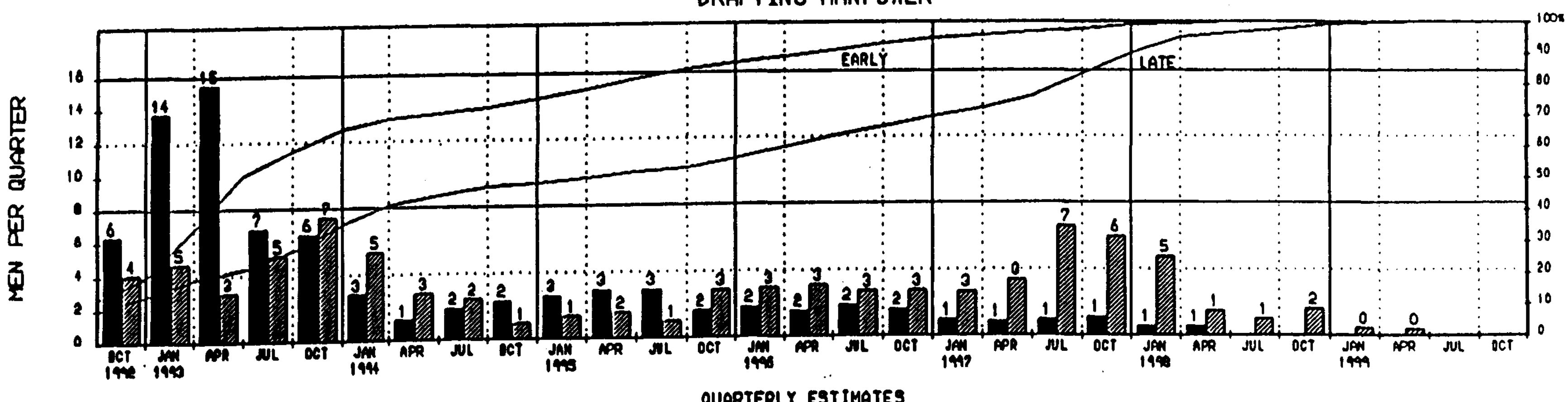

Early dates
Late dates

Primavera Systems, Inc. 1984-1990

Project Start: 1JUL91
Project Finish: 10JAN99

WESTINGHOUSE DEPARTMENT TMO
1.2 CENTRAL TRACKER
ENGINEER, DRAFTING, TECHNICIAN, LABORER

Sheet 1 of 1

Data Date: 1JUL91
Plot Date: 9AUG91

TRAK-SSC DETECTOR CENTRAL TRACKER

Date	Revision	Checked	Approved

TECHNICIAN MANPOWER

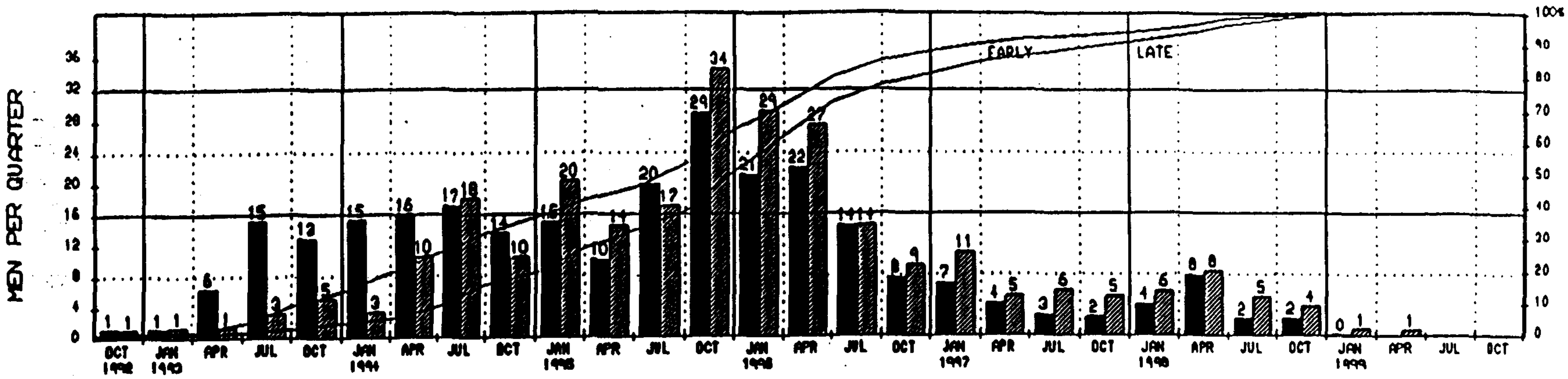

QUARTERLY ESTIMATES

LABORER MANPOWER

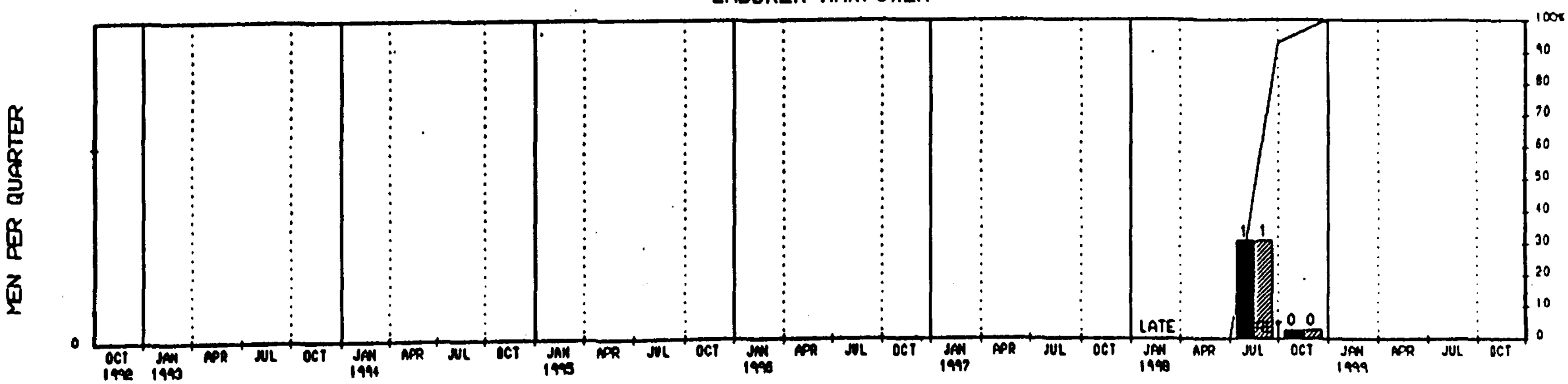

QUARTERLY ESTIMATES

Early dates Late dates Primavera Systems, Inc. 1984-1991	WESTINGHOUSE DEPARTMENT TMO 1.2 CENTRAL TRACKER ENGINEER, DRAFTING, TECHNICIAN, LABORER Project Start: 1JUL91 Project Finish: 1OJAN99	Sheet 2 of 2 Data Date: 1JUL91 Plot Date: 1AUG91	TRAK-SSC DETECTOR CENTRAL TRACKER Date / Revision / Checked / Approved

TOTAL MANPOWER COSTS

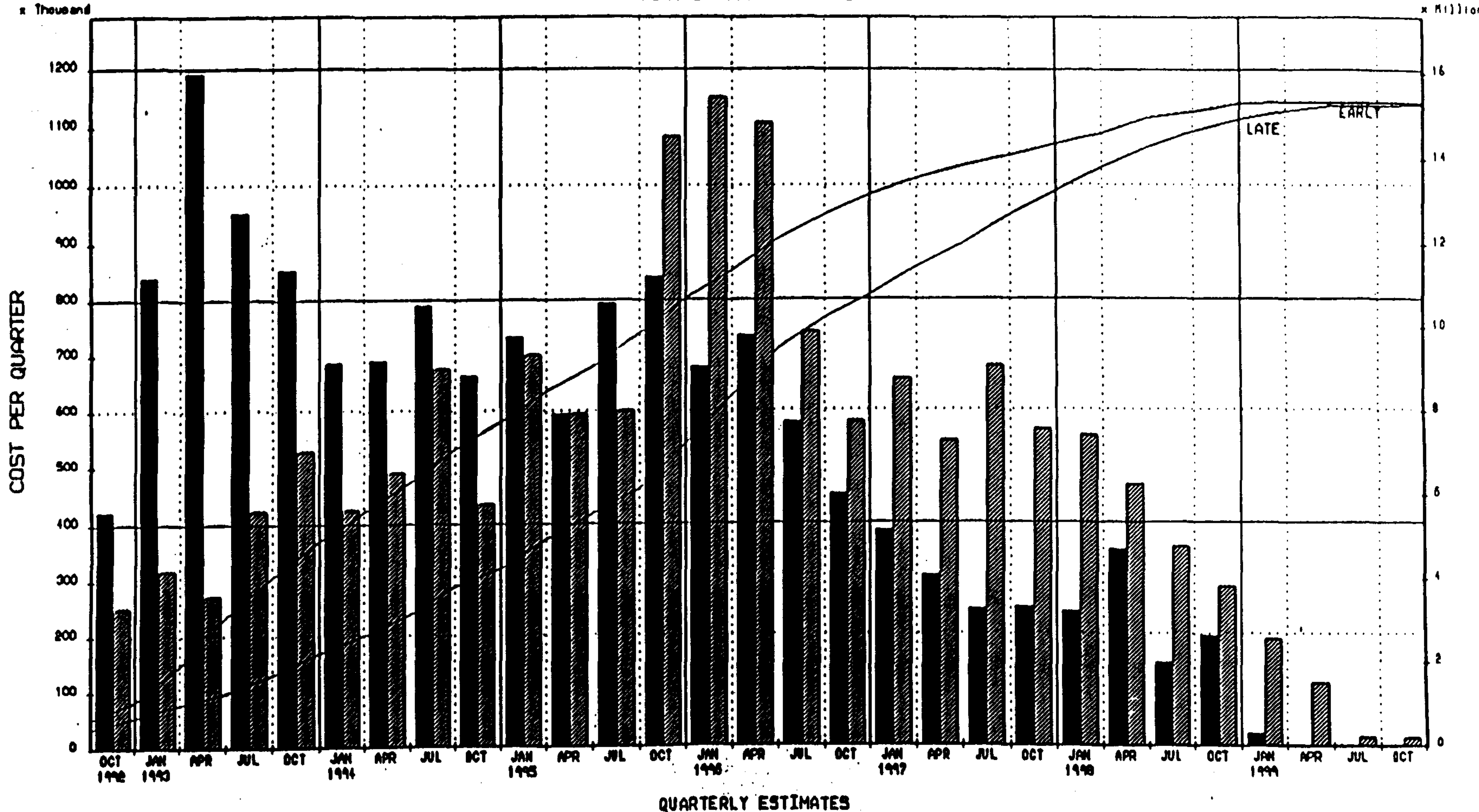

Early dates
Late dates

Primavera Systems, Inc. 1984-1990

WESTINGHOUSE DEPARTMENT TMO
1.2 CENTRAL TRACKER
SUMMARY MANPOWER & MATERIAL COSTS

Sheet 1 of 1

Project Start: 1JUL91
Project Finish: 10JAN99

Data Date: 1JUL91
Plot Date: 9AUG91

TRAK-SSC DETECTOR CENTRAL TRACKER

Date	Revision	Checked	Approved

(TIUSUM12 FILE 1 OF 2/FSIA CALCULAT SUMMARIZE FILES TIUSUM11:
TABLES 11 TO 19 USE ONLY UNIVERSITY LABOR RATES

TABLE NUMBER 13
INPUT DATA 08-06-91

WBS	TASK	EDIA	MFAL	TMAT	BASE	BAS+CON
1.2.1.1	TRIGGER MODULES(192)	425859	833952	959000	2218811	3013414
1.2.1.2	AXIAL(160) & STEREO(320) MODULES	293322	2114664	1931000	4338986	5444456
1.2.2	SUPPORT COMPONENTS	263358	696811	1990000	2950169	4499381
1.2.3	SUPERLAYER(S/L) ASSEMBLY	120000	394661	10000	524661	673770
1.2.4	S/L TO S/L ASSEMBLY	131550	128734	165000	425284	631121
1.2.5	EQUIPMENT,TOOLING,& FIXTURES	919856	373675	4456000	5749531	8008411
1.2.6	FINAL FACTORY ASSEMBLY	304624	182535	237000	724159	915898
1.2.7	FINAL FACTORY TESTING	34773	114473	93000	242246	332308
1.2.8	TRACKER TRANSPORTATION	13415	975	10000	24390	36097
1.2.9	SURFACE ERECTION AT SSCL	128715	78196	475000	681911	1002130
1.2.10	FACILITIES	28992	1375525	630000	2034517	2604291
1.2.11	PROGRAM MANAGEMENT	1620419	230500	379000	2229919	2764549
1.2.12	R & D EFFORT	444400	140160	470000	1054560	1307656
8.2	INSTALLATION & TEST	75841	200799	67500	344140	468094
	SUBTOTAL	4805124	6865660	11872500	23543284	31701576

TABLE NUMBER 14
STRAW TUBE CENTRAL TRACKER 08-06-91
SCALING CONSTANTS INCLUDING CONTINGENCY

	FIXED COSTS	(K$)
1.2.5	EQUIPMENT,TOOLING,& FIXTURE	8008
1.2.7	FINAL FACTORY TESTING	332
1.2.8	TRACKER TRANSPORTATION SYST	36
1.2.9	ERECTION AT SUPERCOLLIDER S	1002
1.2.10	FACILITIES	2604
1.2.11	PROGRAM MANAGEMENT	2765
1.2.12	R & D EFFORT	1308
8.2	INSTALLATION & TEST	468
	TOTAL:	16524
	SUPPORT STRUCTURE COSTS	
1.2.2	SUPPORT STRUCTURE	4499
1.2.3	SUPERLAYER (S/L) ASSEMBLY	674
1.2.4	TRACKER SUB ASSEMBLY	631
1.2.6	FINAL FACTORY ASSEMBLY	916
	4 SUPERLAYERS	6720
	ONE SUPERLAYER SUPPORT:	1680
	TRIGGER MODULES COSTS	
1.2.1.1	192 TRIGGER MODULES	3013
	ONE TRIGGER MODULE	15.695
	STEREO OR AXIAL MODULE COSTS	
1.2.1.2	176 STEREO	
	160 AXIAL	
	144 STEREO	
	480 TOTAL	5444
	ONE AXIAL OR STEREO MODULE	11.343

TABLE NUMBER 15
SCALING TABLE FOR NUMBER OF MODULES VS.
SUPERLAYER DIAMETER (REF 1.7 M DIA. DESIGN)

DIAM IN METERS		NO. REQUIRED
NOMINAL	ACTUAL	
1.7	1.61	192.00
	1.48	176.00
	1.34	160.00
	1.22	144.00

TABLE NUMBER 16
SCALING TABLE FOR COST VS. TRACKER LENGTH
(REF 1.7 M DIAM.)(683 K$ * AVER 1.3 CONTINGENCY)

LENGTH IN METERS	COST (K$)
EACH METER	-887.9
8	31702
7	30814
6	29926
5	29038

CHECK
TOTAL BASE COST 31702

TABLE NUMBER 19
STRAW TUBE CENTRAL TRACKER 08-08-91
SCALING CONSTANTS INCLUDING CONTINGENCY
(THIS TABLE USES UNIVERSITY LABOR RATES)

A) FOR DIAMETER CHANGES USE THE FOLLOWING:

BASE COST (K$)=(A)(FIXED COSTS) +
(B) * (# OF SUPERLAYERSL) +
(C) * (# OF TRIGGER MODULES) +
(D) * (# OF AXIAL MODULES) +
(E) * (# OF STEREO MODULES)

FOR THE REFERENCE (BASE) TRACKER:

	(# OF SUPER LAYERS)=		4	
	DIAMETER		3.4	
LAYER#6	(# OF TRGGER MODULES)=		192	
LAYER#5	(# OF STEREO MODULES)=		176	
LAYER#4	(# OF AXIAL MODULES)=		160	
LAYER#3	(# OF STEREO MODULES)=		144	
	(A)=	(K$)	16524	FIXED
	(B)=	(K$)	1680	LAYERS
	(C)=	(K$)	15.695	TRIGGER
	(D)=	(K$)	11.343	AXIAL
	(E)=	(K$)	11.343	STEREO

B) FOR LENGTH CHANGES USE THE FOLLOWING:

FINAL COST (K$)=(BASE COST K$) - (F) * (# OF METERS REDUCTION)

FOR THE REFERENCE (BASE) TRACKER:

(# OF METERS LONG)=		8
(# OF METERS REDUCTION)=		0
(F)=	(K$)	-887.9

DESCOPE 1 (BASE TRACKER)

DATA		BEFORE	AFTER	FACTOR	COST(K$)	EXAMPLE
	(FIXED COSTS)	16524	16524	0	16523	% (-10)
	DIAMETER CHANGE	3.4	3.4	N/A	(BELOW)	N/A
	(EFFECTS LAYER & MOD COSTS)	-	-	-	-	N/A
	(# OF SUPER LAYERS)=	4	4	N/A	6720	N/A
LAYER#6	(# OF TRIGGER MODULES)=	192	192	0	3013	# (-192)
LAYER#5	(# OF STEREO MODULES)=	176	176	0	1996	# (-192)
LAYER#4	(# OF AXIAL MODULES)=	160	160	0	1815	# (-192)
LAYER#3	(# OF STEREO MODULES)=	144	144	0	1633	# (-192)
	(# OF METERS LONG)=	8	8	N/A	0	# (-192)
	TOTAL COST				31701	

DESCOPE 2 (REDUCED DIAMETER TRACKER)

DATA		BEFORE	AFTER	FACTOR	COST(K$)
	(FIXED COSTS)	16524	16524	0	16523

	DIAMETER CHANGE	3.4	3	N/A	(BELOW)
	(EFFECTS LAYER & MOD COSTS)	-	-	-	-
	(# OF SUPER LAYERS)=	4	4	N/A	5930
LAYER#6	(# OF TRIGGER MODULES)=	192	169	0	2659
LAYER#5	(# OF STEREO MODULES)=	176	155	0	1761
LAYER#4	(# OF AXIAL MODULES)=	160	141	0	1601
LAYER#3	(# OF STEREO MODULES)=	144	127	0	1441
	(# OF METERS LONG)=	8	8	N/A	0
	TOTAL COST				29915

DESCOPE 3 (REDUCED LENGTH TRACKER)

DATA		BEFORE	AFTER	FACTOR	COST(K$)
	(FIXED COSTS)	16524	16524	0	16523
	DIAMETER CHANGE	3.4	3.4	N/A	(BELOW)
	(EFFECTS LAYER & MOD COSTS)	-	-	-	-
	(# OF SUPER LAYERS)=	4	4	N/A	6720
LAYER#6	(# OF TRIGGER MODULES)=	192	192	0	3013
LAYER#5	(# OF STEREO MODULES)=	176	176	0	1996
LAYER#4	(# OF AXIAL MODULES)=	160	160	0	1815
LAYER#3	(# OF STEREO MODULES)=	144	144	0	1633
	(# OF METERS LONG)=	8	6	N/A	-1776
	TOTAL COST				29925

DESCOPE 4 (REDUCED DIAMETER & LENGTH TRACKER)

DATA		BEFORE	AFTER	FACTOR	COST(K$)
	(FIXED COSTS)	16524	16524	0	16523
	DIAMETER CHANGE	3.4	3	N/A	(BELOW)
	(EFFECTS LAYER & MOD COSTS)	-	-	-	-
	(# OF SUPER LAYERS)=	4	4	N/A	5930
LAYER#6	(# OF TRIGGER MODULES)=	192	169	0	2659
LAYER#5	(# OF STEREO MODULES)=	176	155	0	1761
LAYER#4	(# OF AXIAL MODULES)=	160	141	0	1601
LAYER#3	(# OF STEREO MODULES)=	144	127	0	1441
	(# OF METERS LONG)=	8	6	N/A	-1776
	TOTAL COST				28140

DESCOPE 5 (REDUCED TO 3 SUPERLAYERS TRACKER)

DATA		BEFORE	AFTER	FACTOR	COST(K$)
	(FIXED COSTS)	16524	16524	0	16523
	DIAMETER CHANGE	3.4	3.4	N/A	(BELOW)
	(EFFECTS LAYER & MOD COSTS)	-	-	-	-
	(# OF SUPER LAYERS)=	4	3	N/A	5040
LAYER#6	(# OF TRIGGER MODULES)=	192	192	0	3013
LAYER#5	(# OF STEREO MODULES)=	176	176	0	1996
LAYER#4	(# OF AXIAL MODULES)=	160	160	-160	0
LAYER#3	(# OF STEREO MODULES)=	144	144	0	1633
	(# OF METERS LONG)=	8	8	N/A	0
	TOTAL COST				28206

DESCOPE 6 (REDUCED TO 3 SUPERLAYERS, DIAMETER, LENGTH, & 25% FIXED COST TRACKER)

DATA		BEFORE	AFTER	FACTOR	COST(K$)
	(FIXED COSTS)	16524	16524	-25	12392
	DIAMETER CHANGE	3.4	3	N/A	(BELOW)
	(EFFECTS LAYER & MOD COSTS)	-	-	-	-
	(# OF SUPER LAYERS)=	4	3	N/A	4447
LAYER#6	(# OF TRIGGER MODULES)=	192	169	0	2659

LAYER#5	(# OF STEREO MODULES)=	176	155	0	1761
LAYER#4	(# OF AXIAL MODULES)=	160	141	-160	-214
LAYER#3	(# OF STEREO MODULES)=	144	127	0	1441
	(# OF METERS LONG)=	8	6	N/A	-1776
	TOTAL COST				20712

DESCOPE 7 (INCREASED TO 5 SUPERLAYERS AND DECREASED INSIDE DIAMETER OF TRACKER)

NEW SUPERLAYER DATA:

#	DIAM(M)	Z(U)	STEREO	# MODULES	
1	1.408	2.80	0	84	84.06
2	2.08	3.20	3	124	123.68
3	2.68	3.90	0	160	
4	2.96	3.95	-3	176	
5	3.22	3.95	0	192	

DATA		BEFORE	AFTER	FACTOR	COST(K$)
	(FIXED COSTS)	16524	16524	0	16523
	DIAMETER CHANGE	3.4	3.4	N/A	(BELOW)
	(EFFECTS LAYER & MOD COSTS)	-	-	-	-
	(# OF SUPER LAYERS)=	4	5	N/A	8400
LAYER#5	(# OF TRIGGER MODULES)=	192	192	0	3013
LAYER#4	(# OF STEREO MODULES)=	176	176	0	1996
LAYER#3	(# OF TRIGGER MODULES)=	160	160	0	2511
LAYER#2	(# OF STEREO MODULES)=	124	124	0	1406
LAYER#1	(# OF AXIAL MODULES)=	84	84	0	953
	(# OF METERS LONG)=	8	8	N/A	0
	TOTAL COST				34803

CENTRAL AND FORWARD TRACKING SUBSYSTEM

BASELINE DESIGN REVISED SCHEDULE

Westinghouse
Science & Technology Center

WBS1	MAJOR ITEM	EARLY START	EARLY FINISH
121	1.2.1 MODULES	1OCT92	5DEC96
122	1.2.2 SUPPORT STRUCTURE	1OCT92	12OCT95
123	1.2.3 SUPERLAYER (S/L) ASSEMBLY	29DEC94	8JUL97
124	1.2.4 TRACKER S/L TO S/L ASSEMBLY	9APR93	20JAN98
125	1.2.5 EQUIPMENT, TOOLING, & FIXTURES	1OCT92	19AUG97
126	1.2.6 FINAL FACTORY ASSEMBLY	25MAR93	3APR98
127	1.2.7 FINAL FACTORY TESTING	25MAR93	21MAY98
128	1.2.8 TRACKER TRANSPORTATION SYSTEM	10AUG95	28MAY98
129	1.2.9 SURFACE ASSY AT SUPERCOLLIDER SITE	21MAY93	8JUL98
12A	1.2.10 FACILITIES	30NOV92	20JAN98
12B	1.2.11 PROGRAM MANAGEMENT	1OCT92	18JAN99
12C	1.2.12 R & D EFFORT	15JUL91	30DEC93
821	8.2.1 SUBSYSTEM INSTALLATION IN HALL	28OCT93	18JAN99
822	8.2.2 SUBSYSTEM AND SYSTEM TEST IN HALL	27JUN95	18JAN99

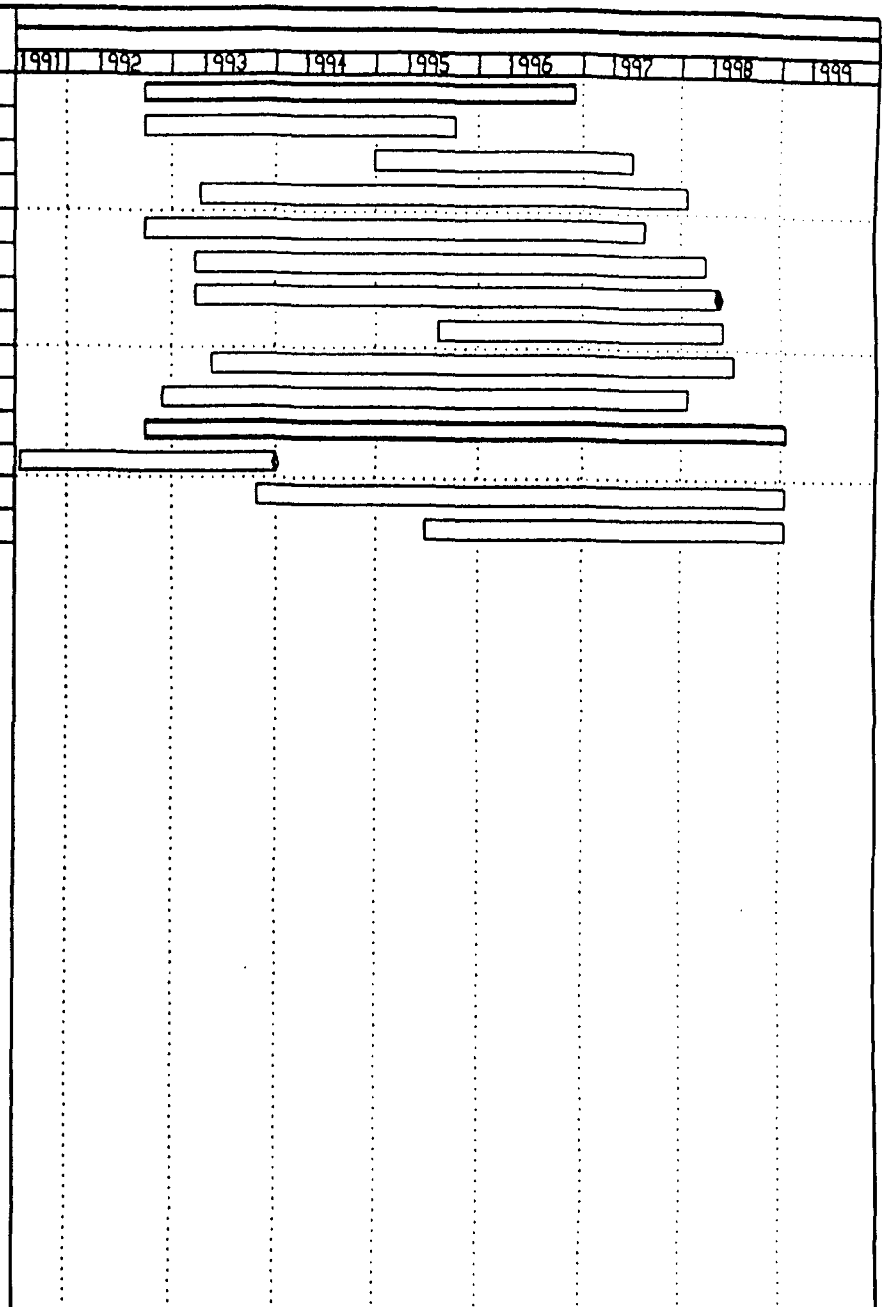

Summary Bar/ Early Dates
Critical Designator
Progress Bar

Primavera Systems, Inc. 1984-1991

Project Start : 1JUL91
Project Finish: 18JAN99

WESTINGHOUSE DEPARTMENT TMO
1.2 CENTRAL TRACKER
WBS LEVEL 3 SUMMARY

Sheet 1 of 1

Data Date: 1JUL91
Plot Date: 16AUG91

TRAK-SSC DETECTOR CENTRAL TRACKER REV. 2

Date	Revision	Checked	Approved

WESTINGHOUSE DEPARTMENT TMO
1.2 CENTRAL TRACKER
MILESTONES

ACTIVITY ID	ACTIVITY DESCRIPTION	EARLY START	EARLY FINISH
S001	START MODULE DESIGN	1OCT92	
S004	START MODULE PURCHASING	28JAN93	
S005	START ASSY OF MODULES	28APR93	
F003	FINISH MODULE PURCHASING		6JUL94
F002	FINISH MODULE DSGN ACTIVITIES		14JUN95
F001	FINISH MODULE ASSY ACTIVITIES		18OCT96
F004	FINISH SHIPMENT OF MODULES		5DEC96
S006	START STRUCTURE SUPPORT DESIGN	1OCT92	
S009	START STRUCTURE SUPPORT PURCHASING	15SEP93	
S008	START STRUCTURE SUPPORT FABRICATION	17JAN94	
F009	FINISH STRUCTURE SUPPORT PURCHASING		25FEB94
S007	START STRUCTURE SUPPORT ASSY	12APR94	
F006	FINISH STRUCTURE SUPPORT DESIGN		28DEC94
F007	FINISH STRUCTURE SUPPORT ASSY		9AUG95
F008	FINISH STRUCTURE SUPPORT FABRICATION		5OCT95
S010	START SUPERLAYER ASSY	6DEC96	
F010	FINISH SUPERLAYER ASSEMBLY		8JUL97
S011	START TRACKER S/L TO S/L ASSEMBLY	9JUL97	
F011	FINISH S/L TO S/L ALIGNMENT		20JAN98
S013	START EQUIP, TOOLING DESIGN	1OCT92	
S014	START TOOLING PROCUREMENTS	28JAN93	
S012	START TOOLING ASSY	26APR93	
F014	FINISH TOOLING PROCUREMENTS		16SEP93
F013	FINISH EQUIP, TOOLING DESIGN		21DEC94
F012	FINISH TOOLING & FIXTURES ASSY		2JUN97
S015	START FINAL FACTORY PERIPHERAL ASSY	1MAY96	
F015	FINISH FINAL FACTORY PERIPHERAL ASSY		1APR98
S016	START FINAL FACTORY TESTING	14MAY98	
F016	FINISH FINAL FACTORY TESTING		21MAY98
F017	RECEIVE TRACKER AT SITE		28MAY98
S018	START UNPACKING TRACKER FOR SURFACE ASSY	1JUN98	
F018	COMPLETE CENTRAL TRACKER SURFACE ASSY		8JUL98
B10000.07	#7 MFG,TOOLING & TESTING PRELIM.DESIGN REVIEW	11FEB93	12FEB93
B10000.04	#4 SUPPORT STRUCT,PREL.DSGN REVIEW	11MAR93	12MAR93

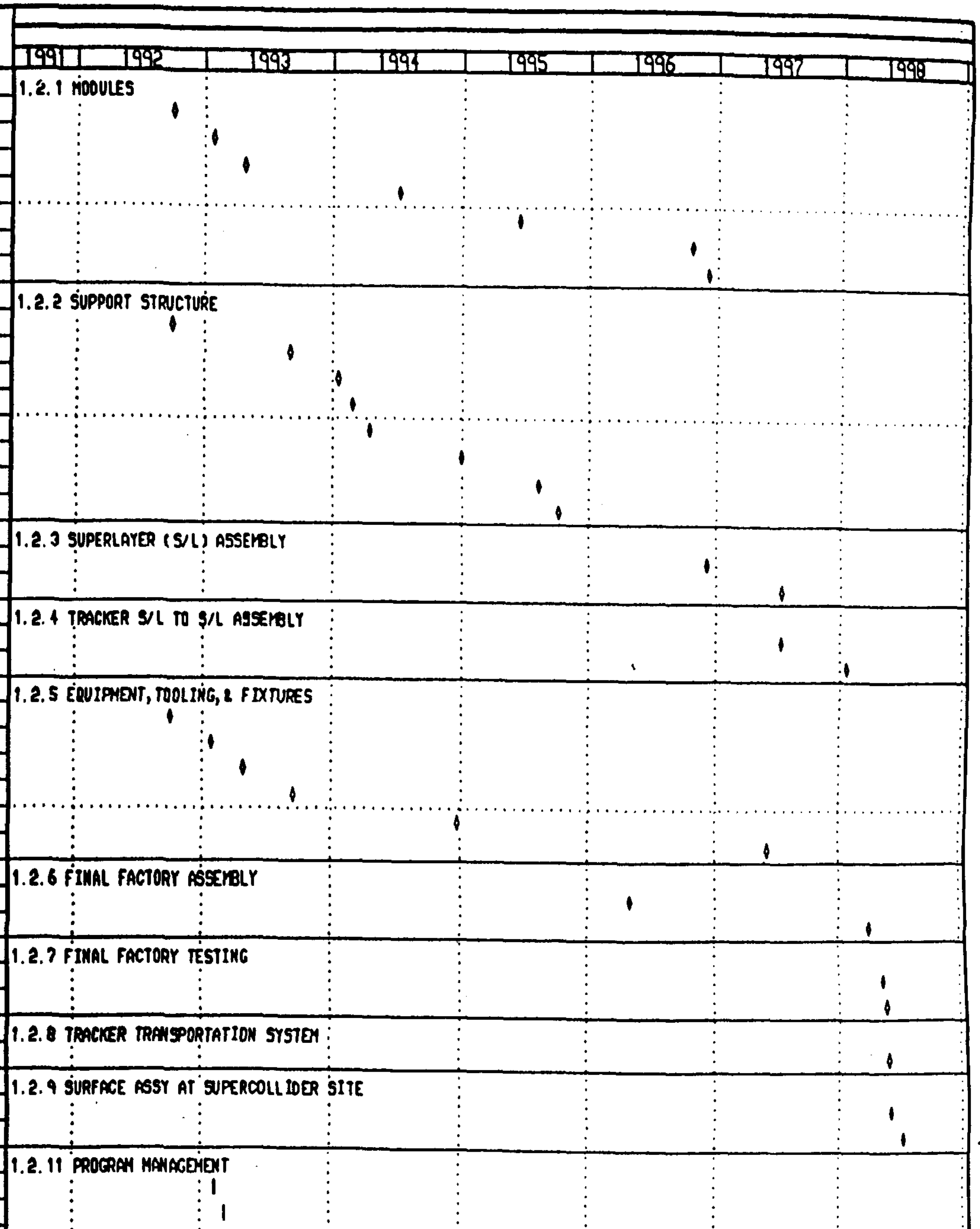

Activity Bar/Early Dates
Critical Activity
Progress Bar

Project Start : 1JUL91
Project Finish: 18JAN99

Sheet 1 of 2

TRAK-SSC DETECTOR CENTRAL TRACKER REV.2

Date	Revision	Checked	Approved

Data Date: 1JUL91
Plot Date: 16AUG91

ACTIVITY ID	ACTIVITY DESCRIPTION	EARLY START	EARLY FINISH
B10000.01	#1 MODULE PREL.DESIGN REVIEW	25MAR93	26MAR93
B10000.05	#5 SUPPORT STRUCT. INTERIM DESIGN REVIEW	27APR93	28APR93
B10000.02	#2 MODULE INTERIM DESIGN REVIEW	11MAY93	12MAY93
B10000.08	#8 MFG,TOOLING & TESTING INTERIM DESIGN REVIEW	9JUN93	10JUN93
B10000.06	#6 SUPPORT STRUCT. FINAL DESIGN REVIEW	21JUN93	22JUN93
B10000.03	#3 MODULE FINAL DESIGN REVIEW	18AUG93	19AUG93
B10000.09	#9 MGF,TOOLING & TESTING FINAL DESIGN REVIEW	6OCT93	7OCT93
B10000.10	#10 TRACKER INST./TEST PREL.DESIGN REVIEW	19DEC95	20DEC95
B10000.11	#11 TRACKER INST./TEST INTERIM DESIGN REVIEW	5FEB96	6FEB96
B10000.12	#12 TRACKER INST./TEST FINAL DESIGN REVIEW	14JUN96	17JUN96
C12000	Dsgn Prototype Modules	15JUL91	23SEP91
S000	START PROTOTYPE DSGN	15JUL91	
C11000	Dsgn Prototype Cylinder	24SEP91	2MAR92
C13000	Dsgn Prototype Cylinder Module Interface	24SEP91	20JAN92
C14000	Dsgn Prototype Support Structure	24SEP91	17FEB92
C1200A	Assy & Test Prototype Modules	23DEC91	30SEP92
C1400A	Assy Prototype Support Structure	18MAY92	30DEC93
C1300A	Assy & Test Prototype Cylinder Module Interface	1OCT92	31AUG93
F000	COMPLETE PROTOTYPES		30DEC93
S020	START OF INSTALLATION	1MAY97	
F020	END CENTRAL TRACKER INSTALLATION & TEST		18JAN99
S021	START SETUP FOR TRACKER TESTING	28OCT98	
F021	FINISH FOR TRACKER TESTING		18JAN99

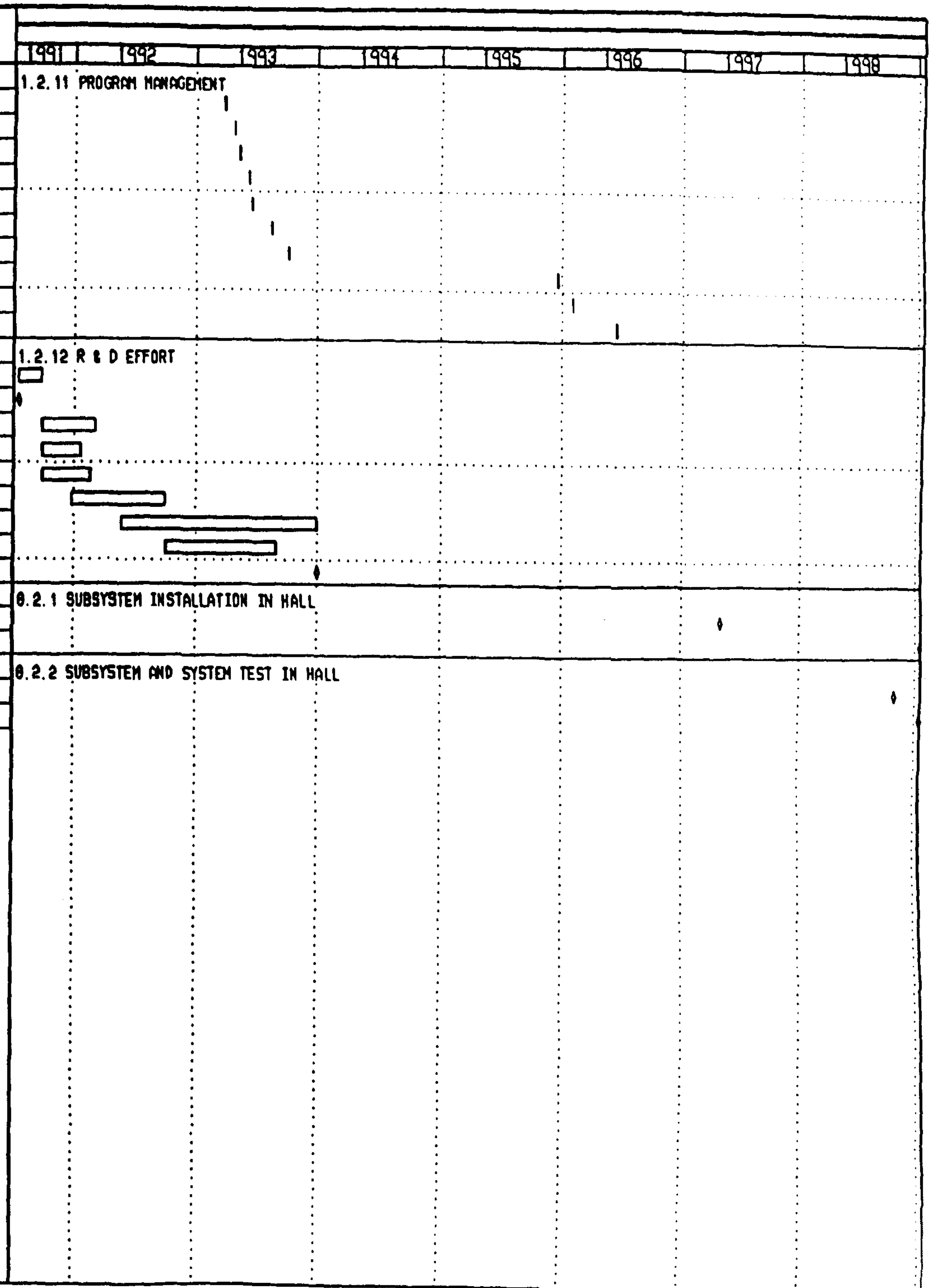

ACTIVITY ID	ACTIVITY DESCRIPTION	REM DUR	EARLY START	EARLY FINISH
121DSGN		680	1OCT92	14JUN95
121PURC		661	28JAN93	12SEP95
121ASSY		877	28APR93	18OCT96
121INSP		907	28APR93	3DEC96
121SHIP		787	21OCT93	5DEC96
122DSGN		563	1OCT92	28DEC94
122PURC		247	15SEP93	23AUG94
122FAB		435	17JAN94	5OCT95
122ASSY		335	12APR94	9AUG95
122INSP		370	26APR94	12OCT95
123DSGN		382	29DEC94	2JUL96
123FAB		80	20JUN95	12OCT95
123PURC		61	5JUL96	30SEP96
123ASSY		227	12AUG96	8JUL97
123INSP		192	1OCT96	8JUL97
124DSGN		240	9APR93	22MAR94
124PURC		62	26SEP95	22DEC95
124FAB		505	26DEC95	26DEC97
124ASSY		135	9JUL97	20JAN98
124INSP		130	16JUL97	20JAN98
125DSGN		560	1OCT92	21DEC94
125PURC		1148	28JAN93	19AUG97
125ASSY		1033	26APR93	2JUN97
125INSP		1026	10MAY93	5JUN97
125FAB		30	8JUL93	18AUG93
125SHIP		131	9JUL93	14JAN94
126DSGN		180	25MAR93	10DEC93
126PURC		259	18DEC95	27DEC96
126FAB		71	1MAY96	12AUG96
126ASSY		482	1MAY96	1APR98
126INSP		454	13JUN96	3APR98
127DSGN		598	25MAR93	9AUG95
127PURC		345	10AUG95	20DEC96
127INSP		34	6APR98	21MAY98

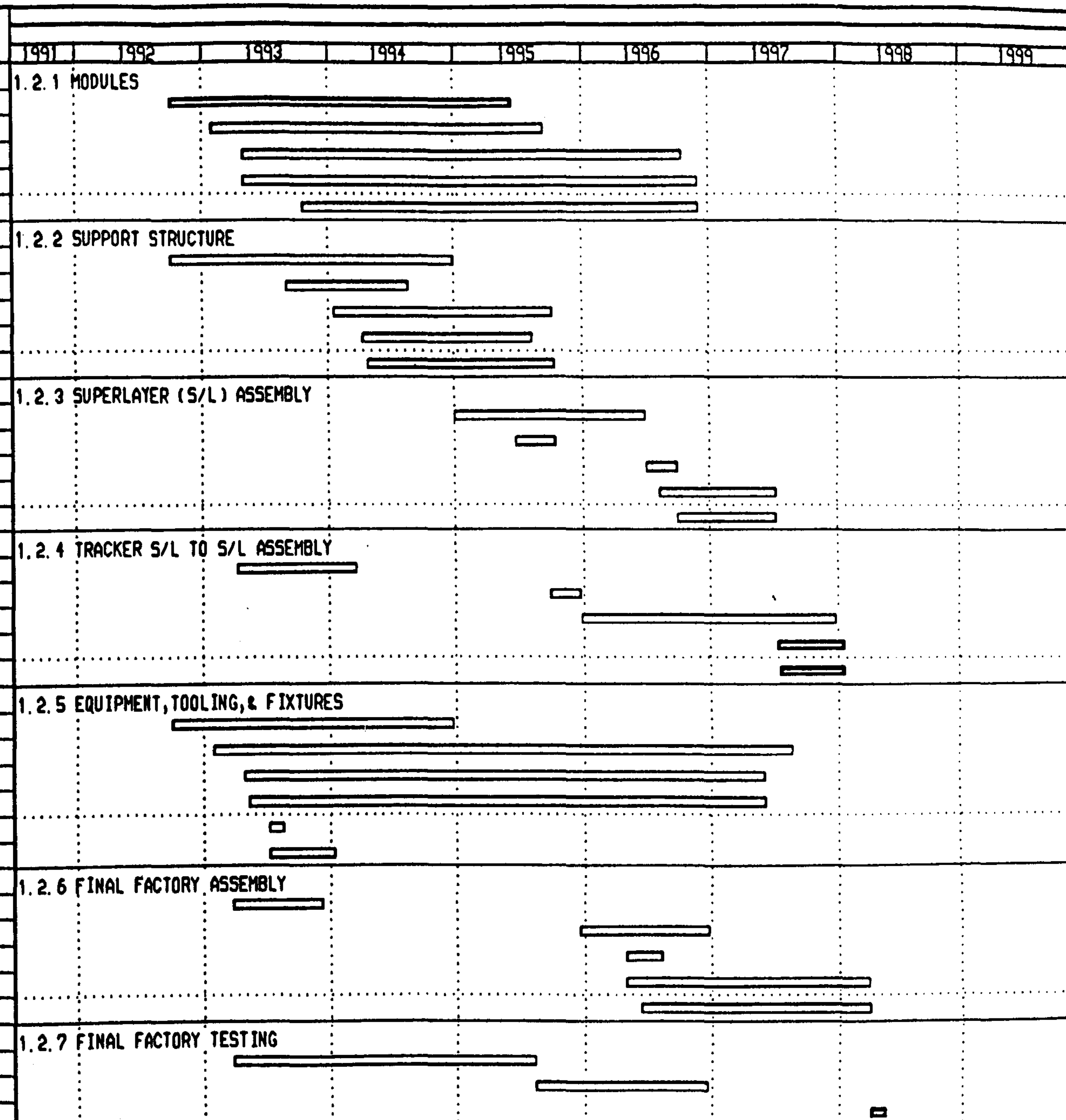

Activity Bar/Early Dates
Critical Activity
Progress Bar

Primavera Systems, Inc. 1984-1991

Project Start : 1JUL91
Project Finish: [illegible]

WESTINGHOUSE DEPARTMENT TMO
1.2 CENTRAL TRACKER
WBS LEVEL 3 SUMMARY BY FUNCTION, ES

Sheet 1 of 2

Data Date: 1JUL91
Plot Date: 16[illegible]

TRAK-SSC DETECTOR CENTRAL TRACKER REV.2

Date	Revision	Checked	Approved

ACTIVITY ID	ACTIVITY DESCRIPTION	REM DUR	EARLY START	EARLY FINISH
1.2.7 FINAL FACTORY TESTING				
127TST		0	14MAY98	13MAY98
127ASSY		4	14MAY98	19MAY98
127TEST		0	22MAY98	21MAY98
1.2.8 TRACKER TRANSPORTATION SYSTEM				
128DSGN		30	10AUG95	21SEP95
128PURC		63	23FEB98	21MAY98
128SHIP		5	22MAY98	28MAY98
1.2.9 SURFACE ASSY AT SUPERCOLLIDER SITE				
129DSGN		608	21MAY93	19OCT95
129PURC		367	24SEP96	10MAR98
129FAB		90	26NOV96	4APR97
129INSP		284	1MAY97	16JUN98
129ASSY		129	6JAN98	8JUL98
1.2.10 FACILITIES				
12ADSGN		150	30NOV92	6JUL93
12APURC		262	26APR93	9MAY94
12AFAB		50	29JUL93	7OCT93
12AMGMT		1092	17SEP93	20JAN98
1.2.11 PROGRAM MANAGEMENT				
128MGMT		1583	1OCT92	18JAN99
128DSGN		1040	11FEB93	31MAR97
1.2.12 R & D EFFORT				
12CDSGN		160	15JUL91	2MAR92
12CPURC		172	24SEP91	28MAY92
12CASSY		509	23DEC91	30DEC93
12CFAB		0	3JAN94	30DEC93
8.2.1 SUBSYSTEM INSTALLATION IN HALL				
821DSGN		1128	28OCT93	22APR98
821FAB		50	7NOV96	22JAN97
821ASSY		431	1MAY97	18JAN99
821PURC		90	28NOV97	8APR98
821INSP		155	2APR98	9NOV98
8.2.2 SUBSYSTEM AND SYSTEM TEST IN HALL				
822DSGN		180	27JUN95	13MAR96
822ASSY		14	28OCT98	16NOV98
822TST		54	28OCT98	18JAN99
822INSP		49	4NOV98	18JAN99

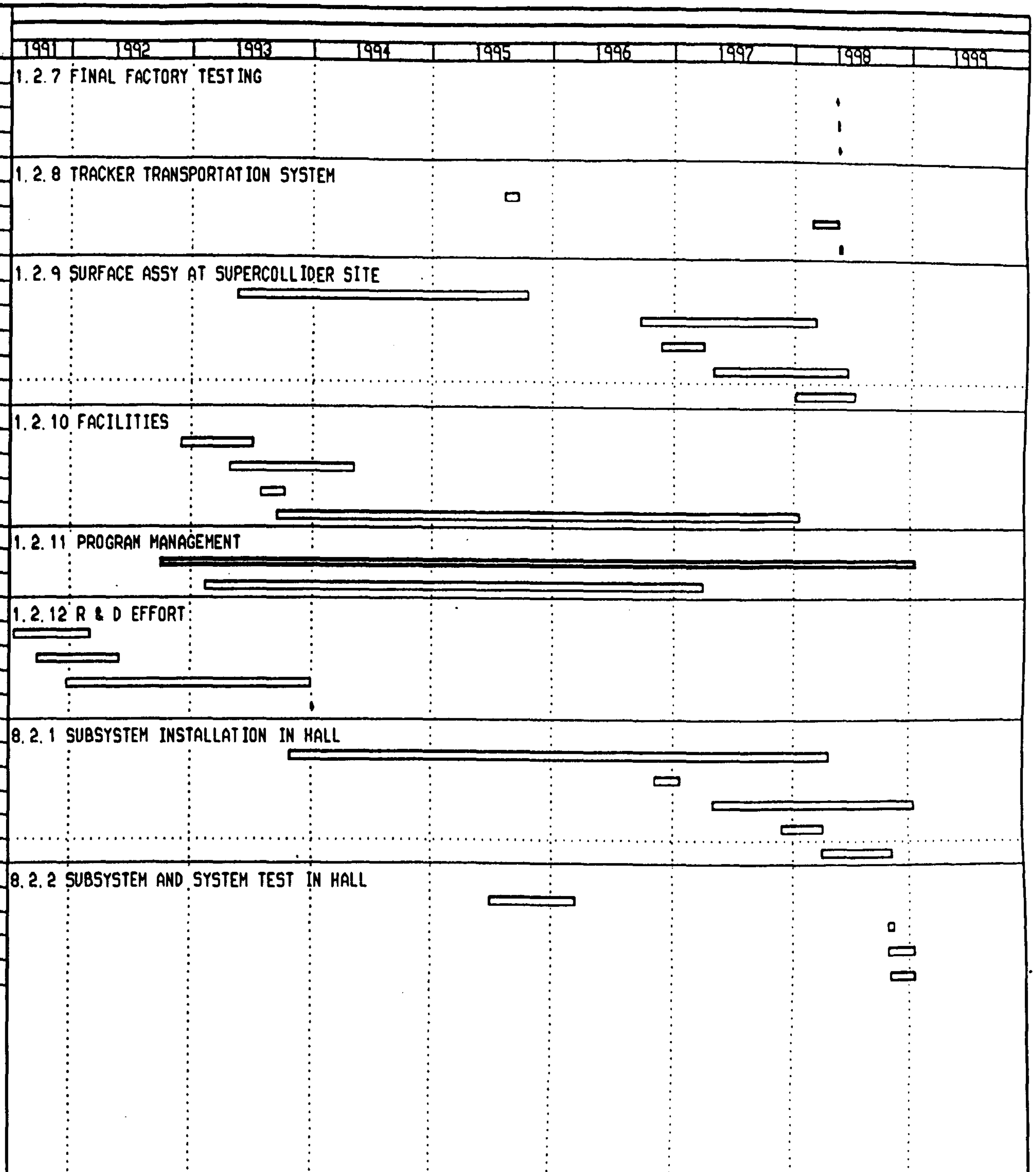

G. Hanson

Contract-Required Document. Internal Distribution Only.

STC Document No.

UISTD-02-0591

Interim Mechanical Engineering Design Effort Report for the Central Tracker SDC Subsystem

Roger L. Swensrud
Advanced Electromechanical Systems

May 3, 1991

Progress Report #2 Covering the Period
October 1990 to April 1991

Prepared for

Indiana University
Physics Department
Swain West 117
Bloomington, IN 47405

Under Contract No. 20107-0647
General Order No. IN-12410-CE
Project No. 9E83-UISD

by

Westinghouse Electric Corporation
Science & Technology Center
1310 Beulah Road
Pittsburgh, PA 152135

Westinghouse STC
1310 Beulah Road
Pittsburgh, Pennsylvania 15235

STC Document No.

UISTD-02-0591

Interim Mechanical Engineering Design Effort Report for the Central Tracker SDC Subsystem

Roger L. Swensrud
Advanced Electromechanical Systems

May 3, 1991

Progress Report #2 Covering the Period
October 1990 to April 1991

Prepared for

Indiana University
Physics Department
Swain West 117
Bloomington, IN 47405

Under Contract No. 20107-0647
General Order No. IN-12410-CE
Project No. 9E83-UISD

by

Westinghouse Electric Corporation
Science & Technology Center
1310 Beulah Road
Pittsburgh, PA 152135

Westinghouse STC
1310 Beulah Road
Pittsburgh, Pennsylvania 15235

Report prepared by

Roger L. Swensrud
Electromechanics

D. Marschik
Electromechanics

D. A. Hoecker
Electromechanics

F. P. Beninati
Advanced Electromechanical Systems

Approved by

Donald T. Hackworth, Manager
Electromechanics

TABLE OF CONTENTS

1. SUMMARY

Westinghouse is working on the second phase of a preliminary conceptual design, evaluation, and analysis of the feasibility of building a modular type straw tube central tracker for use in the Superconducting Super Collider at the SSC Laboratory. The following list summarizes the status, results, and conclusions of that work:

- Concept layouts of the following have been developed:
  - Several conceptual versions of the tracker
  - Several module cross sectional geometries
  - Fabrication and assemblies for modules and support structures
  - Proposed alignment equipment and methods for obtaining required alignments
  - Module design and fabrication for needed automation

- Module sizing and spacing geometrical calculations have been done.

- Conceptual evaluation indicated that for several reasons, including potential for automation fabrication and assembly, ability to accommodate maintenance and repair, and potential for good alignment, the design is very attractive.

- Finite element analysis of the deadweight deflection of a cylinder support structure including eight "superlayers" of a detector-straw module with attachment to a rigid external structure.

- Scheduling and cost estimating of a complete central tracker using straw tube technology was developed from technical information and input from a wide cross section of individuals.

- A module based central tracker using straw tube technology would have advantages such as simplicity, stability and reparability. With respect to mechanical engineering design issues, conceptual feasibility has been demonstrated, but many conceptual and preliminary design, and analysis tasks remain to be addressed.

2. INTRODUCTION

This report contains the results of the interim phase of a conceptual design study. The goal of the conceptual study was to develop a concept for a structural support system for small cell straw tubes used for charged particle tracking. This charge particle tracking detector would ultimately be a subsystem of an overall detector for use in the superconducting super collider at the SSC Laboratory near Dallas, Texas.

Figures and supporting documents referred to in this report are but a few of the many generated during the course of the study. These attached documents are intended to be representative. To prevent this report from becoming burdensome, the majority of the balance of the material in the form of approximately 100-page hardcopy viewgraph presentation is attached but is only a reference document with respect to this report.

3. STEREO CENTRAL TRACKER SUPERLAYER STUDIES

The method by which the straw modules are shaped and positioned to accomplish the stereo requirements of the central tracker were studied. Eight different cases were studied and listed in Table 3.1 and Figures 3.1 through 3.10.

Table 3.1 — Case Summary

Case	Module Shape	Figure #
#1	Alternating Trapezoids.............................	3.1
#2	Parallelograms.....................................	3.2
#3	Radial Modules.....................................	3.3 - 3.5
#4	Rectangular Modules...............................	3.3 - 3.5
#5	Overlapping Rectangular Modules...................	3.6 & 3.7
#6	Twisted Alternating Trapezoids.....................	3.8 & 3.9
#7	Overlapping Alternating Trapezoids.................	None
#8	Dual Angle Alternating Trapezoids..................	3.10

The goal has been to create a tracker geometry using as few style modules as possible. The above stereo schemes with the exception of cases #3, #4 and #6 may be accomplished with a single module style; however, triggering, channel count, and other factors have deemed multiple styles necessary.

Alternating trapezoids, rectangular and radial modules allow for symmetry in the radial portion of the support structure. Parallelogram modules bias the direction of the radial support structure, thus reducing its stiffness. All the above cases except Case #6 (Twisted Trapezoid) generate larger radial superlayer dimensions, thus reducing the support structure sections and stiffness.

Alternating Trapezoids, with dual angles of rotation (Case #8) offer uniform module spacing with minimum radial build and the best overall selection to date. The eight cases listed in the above table are described below.

Attached at the end of this memo is a program (A:Centkll). This program and earlier versions were used to generate the support structure geometry used for these studies.

The software used is Mathcad 2.5 from Mathsoft, Inc., Cambridge, MA.

Case Explanations

Case #1, Figure 3.1, (Alternating Trapezoids). This was the first stereo option studied. Figure 3.1 illustrates the result of rotating superlayer #2 three degrees about the mid-point of the 300-cm length module. In this case the side spacing was 0.20 cm. with all modules identical and all modules of a given superlayer at the same radius. The result is not suitable because of the alternating interference and large gaps generated at the non-radial side surfaces after rotation. The section shown in the figure is the surface nearest to us, Z = 300 cm, at the far end, Z = 0 cm. The interference takes place between the modules that show large gaps at the near end.

The disadvantages of this configuration are non-uniformity, module to module interference side spacing and increased radial dimension after rotation.

Advantages: symmetrical radial support structure.

Case #2, Figure 3.2, (Parallelograms). Parallelograms suffer the same difficulties as alternating trapezoids above plus the additional problem that the support structure radial members through the superlayer, between modules are biased in one direction reducing the support structure stiffness. The series of radial lines passing through each module to the origin are the axis of rotation for each module.

Case #3, Figures 3.3, 3.4, & 3.5 (Radial and Rectangular Modules). Radial modules have sides that are parallel to lines radiating from the origin, rectangular modules have a rectangular section. Both radial and rectangular modules respond similarly during rotation. There is no advantage to making radial modules over

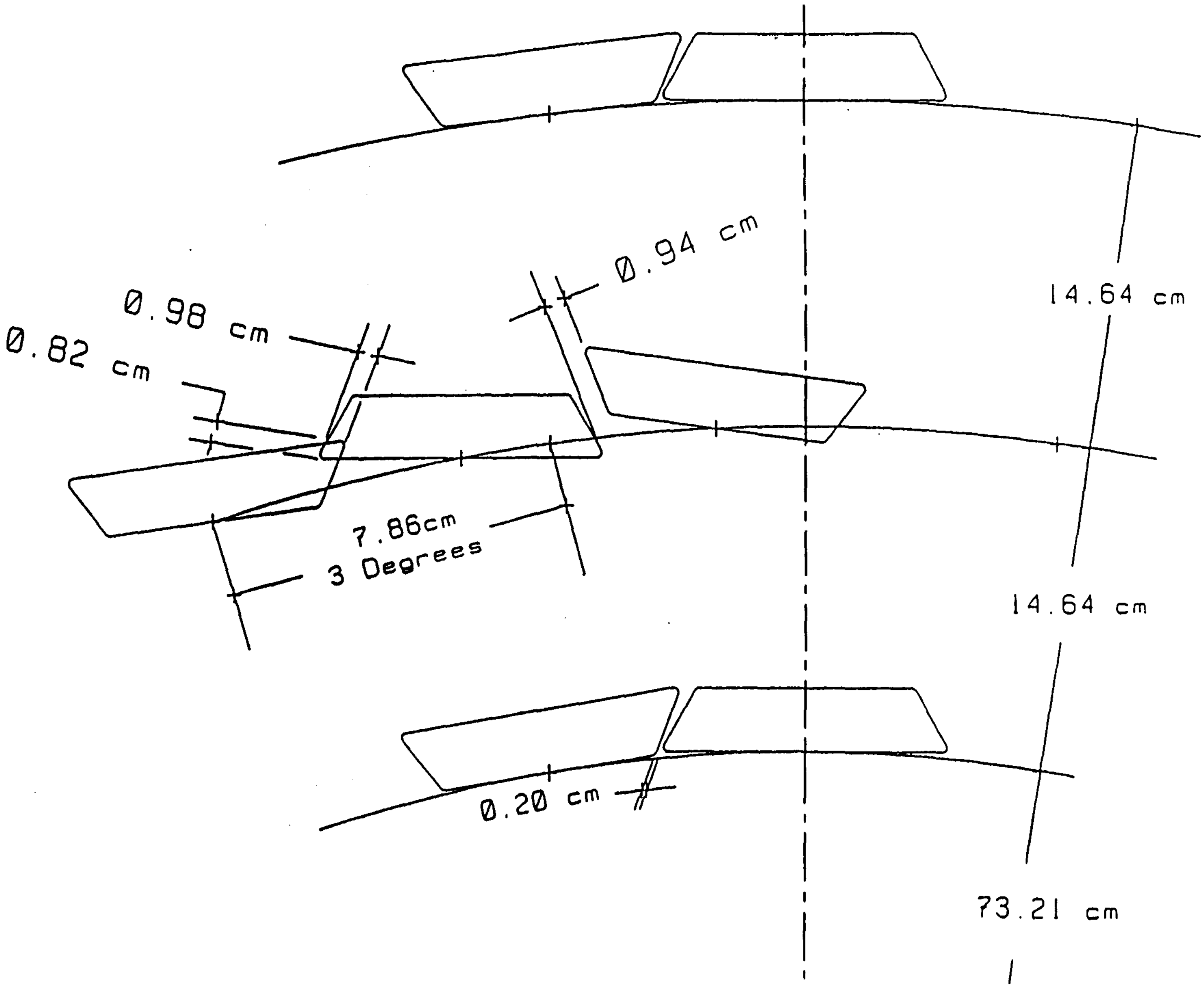

Figure 3.1 — Alternating trapezoids, superlayer #1 rotated 3.00 degrees.

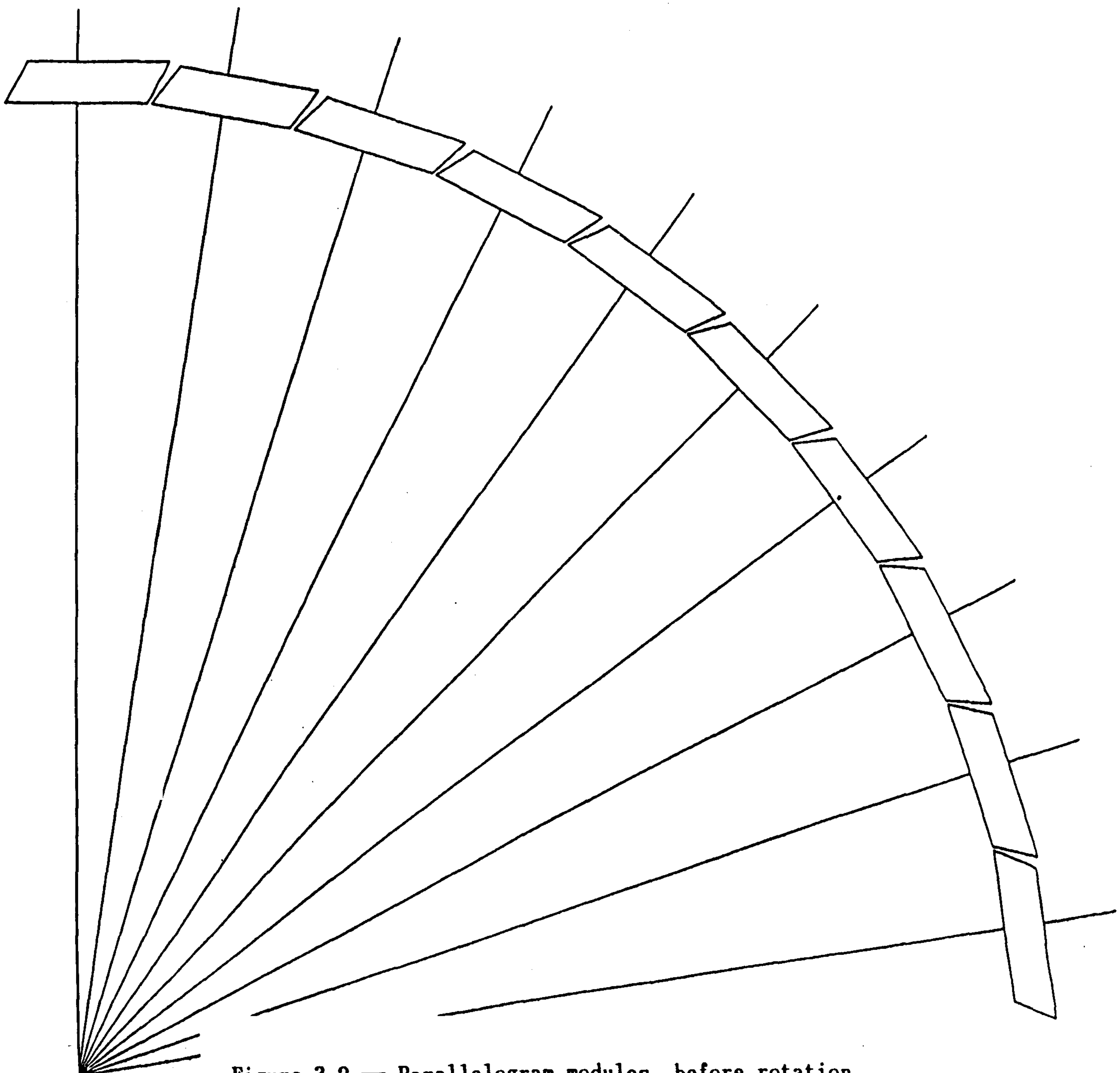

Figure 3.2 — Parallelogram modules, before rotation.

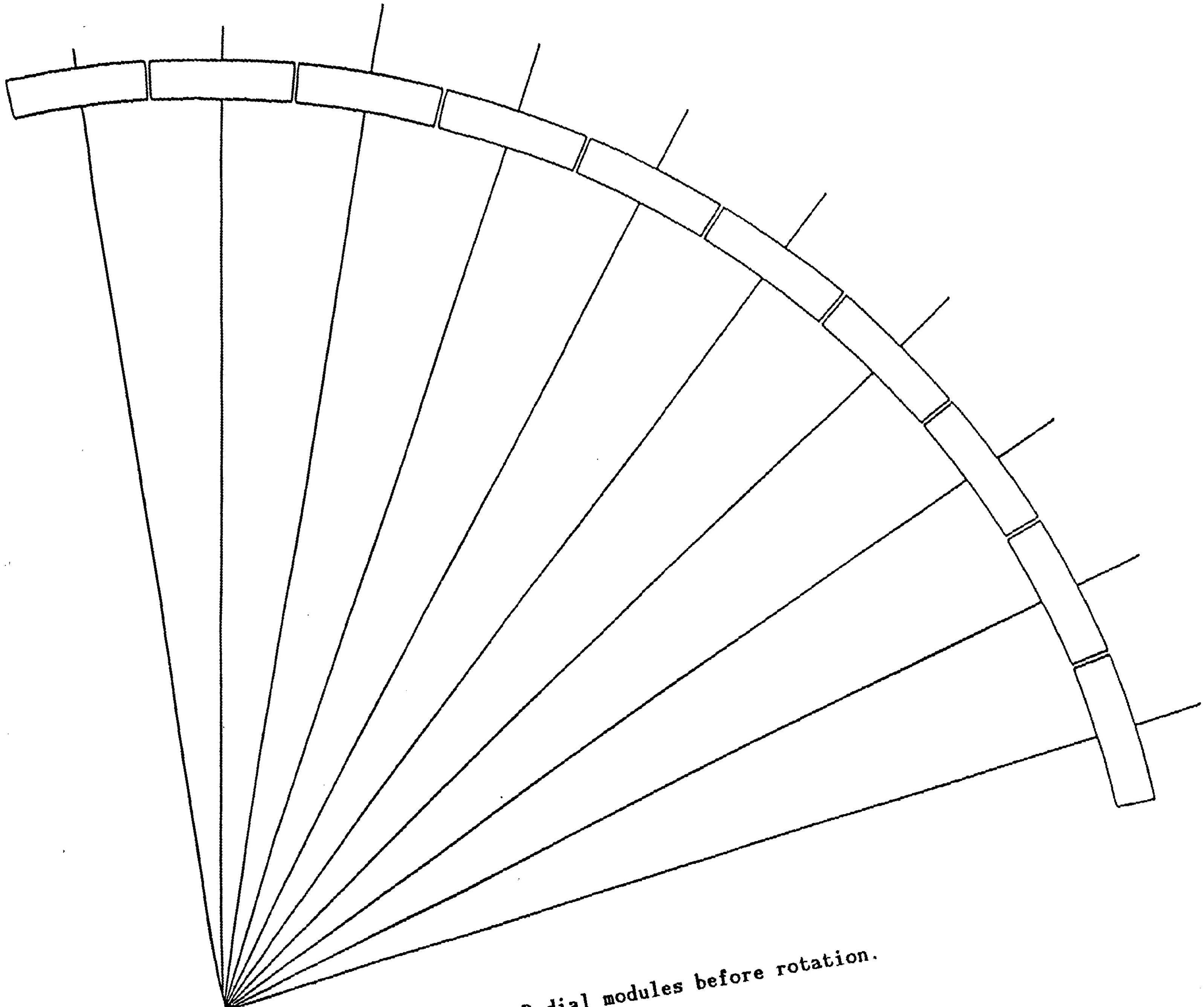

Figure 3.3 — Radial modules before rotation.

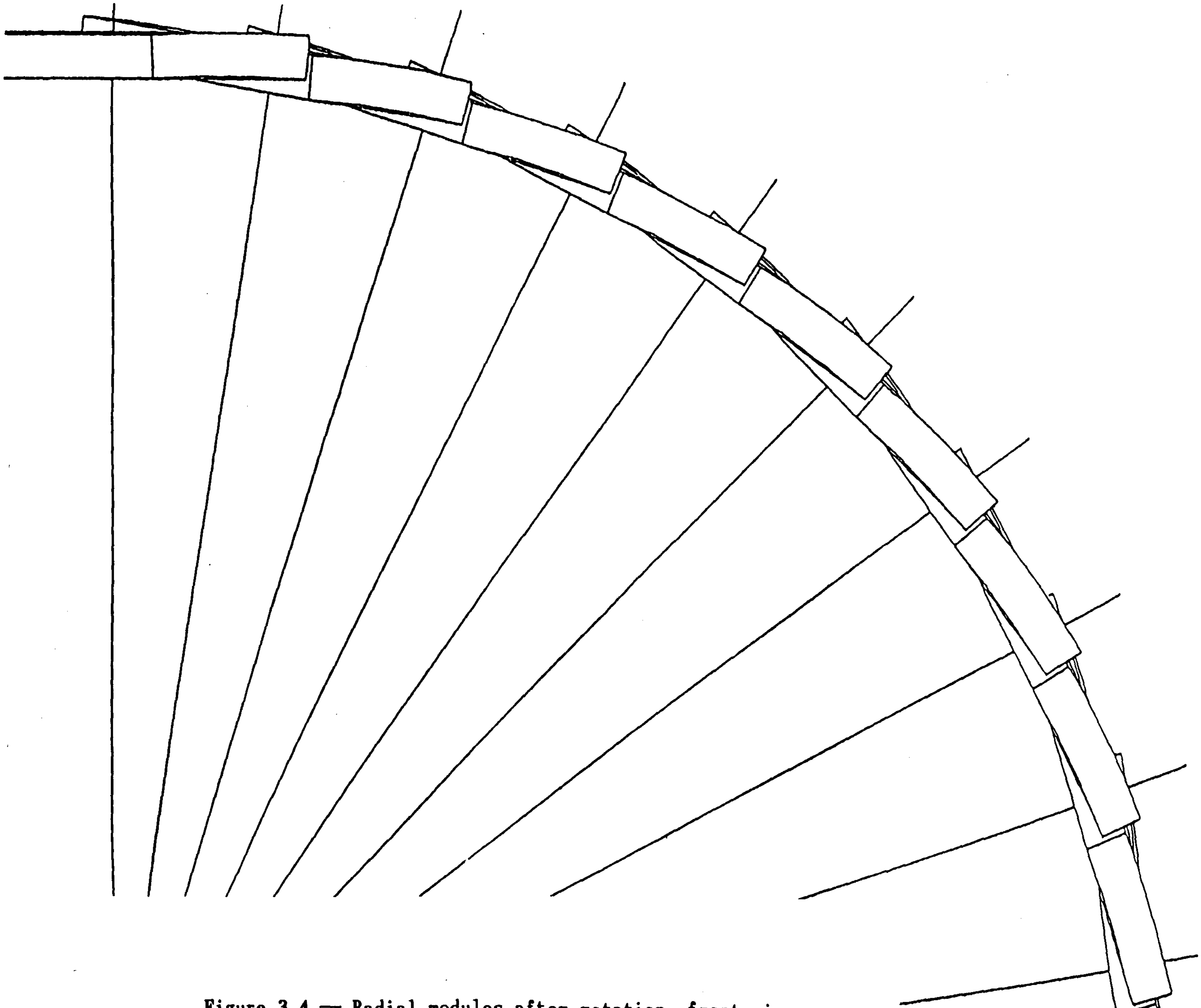

Figure 3.4 — Radial modules after rotation, front view.

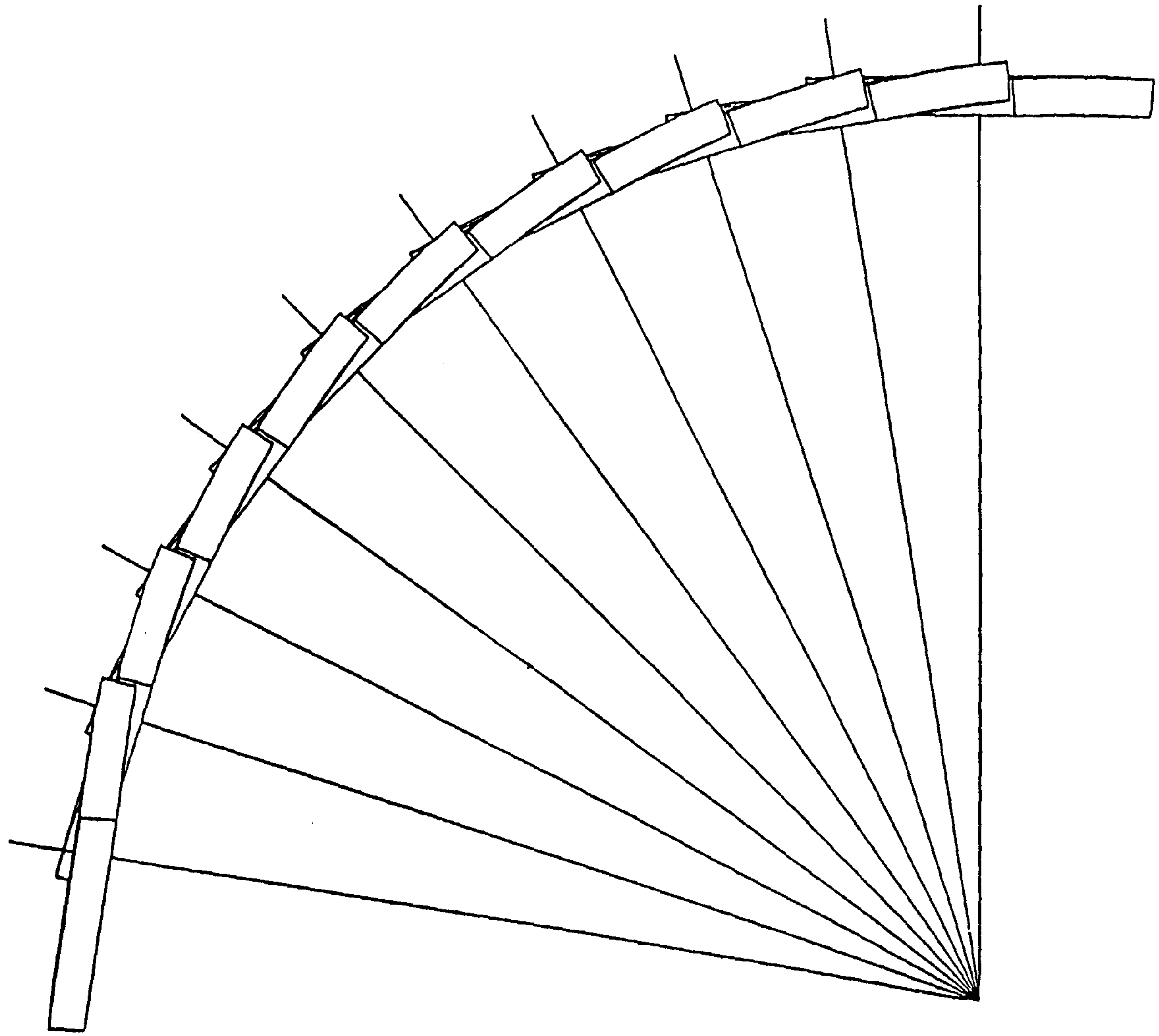

Figure 3.5 — Radial modules after rotation, rear view.

rectangular in respect to straw count. Figure 3.3 shows radial modules before rotation, Figure 3.4 the front surface after rotation and Figure 3.5 the rear surface. With both radial and rectangular modules the side spacing remains almost uniform. The radial increases are not serious but the major difficulty is missed hits caused by the radial spaces between modules. Another difficulty is that this geometry does not lend itself to fine tuning superlayer spacing as well as alternating trapezoids at different radiuses.

Case #5, Figures 3.6 and 3.7 (Overlapping Rectangular Modules). This was an attempt to avoid missed hits. Figure 3.6 shows the radial space necessary to avoid contact after rotation. Figure 3.7 shows the modules after rotation. This configuration would leave very little space for the support structure, which becomes more complex and less rigid.

Case #6, Figure 3.8 (Twisted Alternating Trapezoidal Modules). This configuration offers the best of the above with one big negative. The twisted module produces a small cross sectional area change from the module ends to the point of rotation; however, the module side gaps remain almost constant end to end.

Case #6, Figure 3.9. Measurements of the twisted module show the amount of cross sectional change for a full length module. None of the stereo superlayers are full length, and the axis of rotation is at what would be the center of full length module. The measurements shown on this figure are a worst case since they are made at the intersection of line segments, not the center of the extreme straws.

Case #7, (Overlapping Alternating Trapezoids). This case does not offer any more advantages than Case #5.

Case #8, Figure 3.10 (Dual Angles for Stereo Modules). This method illustrates the uniformity in geometry generated by this system. The three module sections shown and their gaps show almost uniform

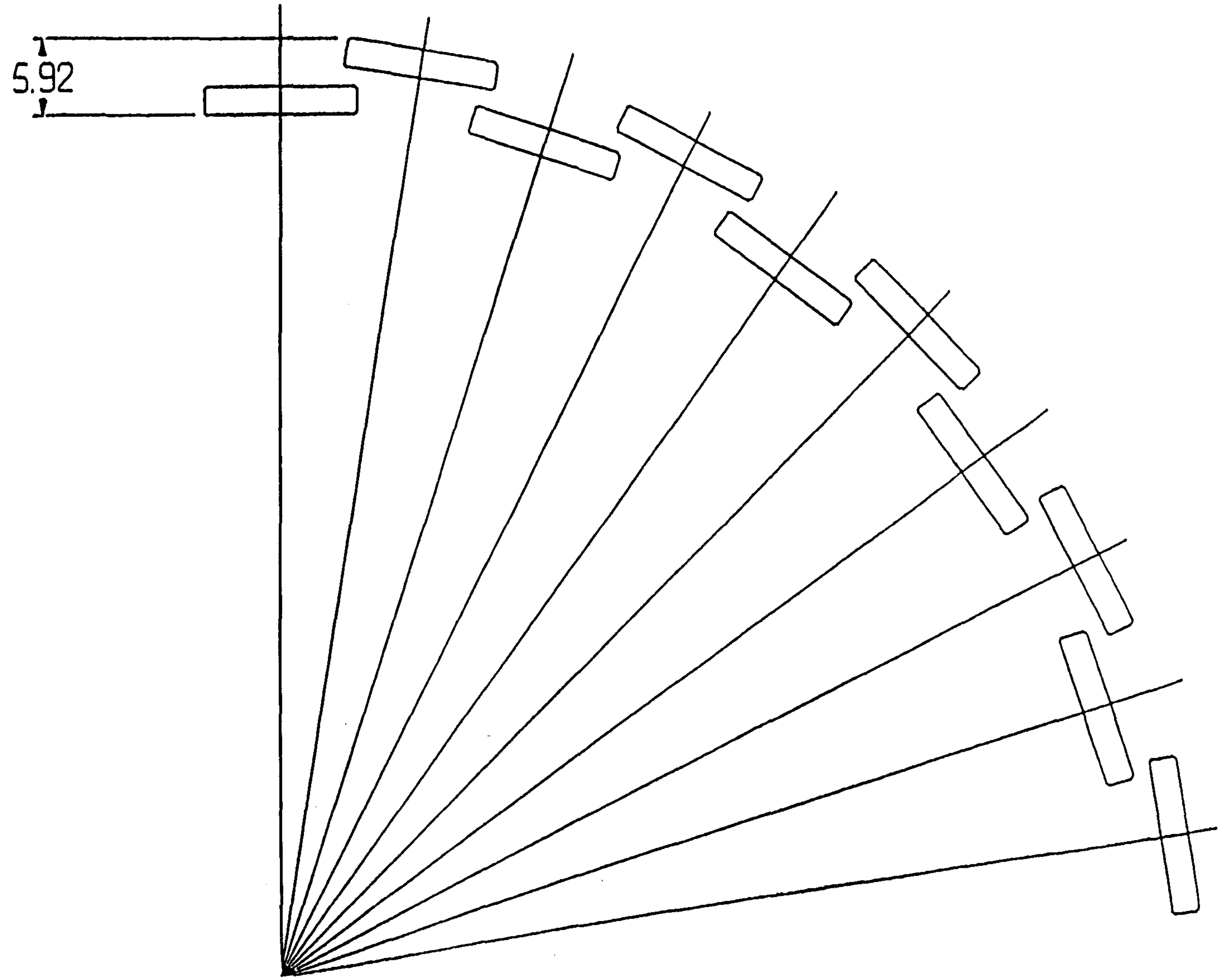

Figure 3.6 — Overlapping rectangular modules, before rotation.

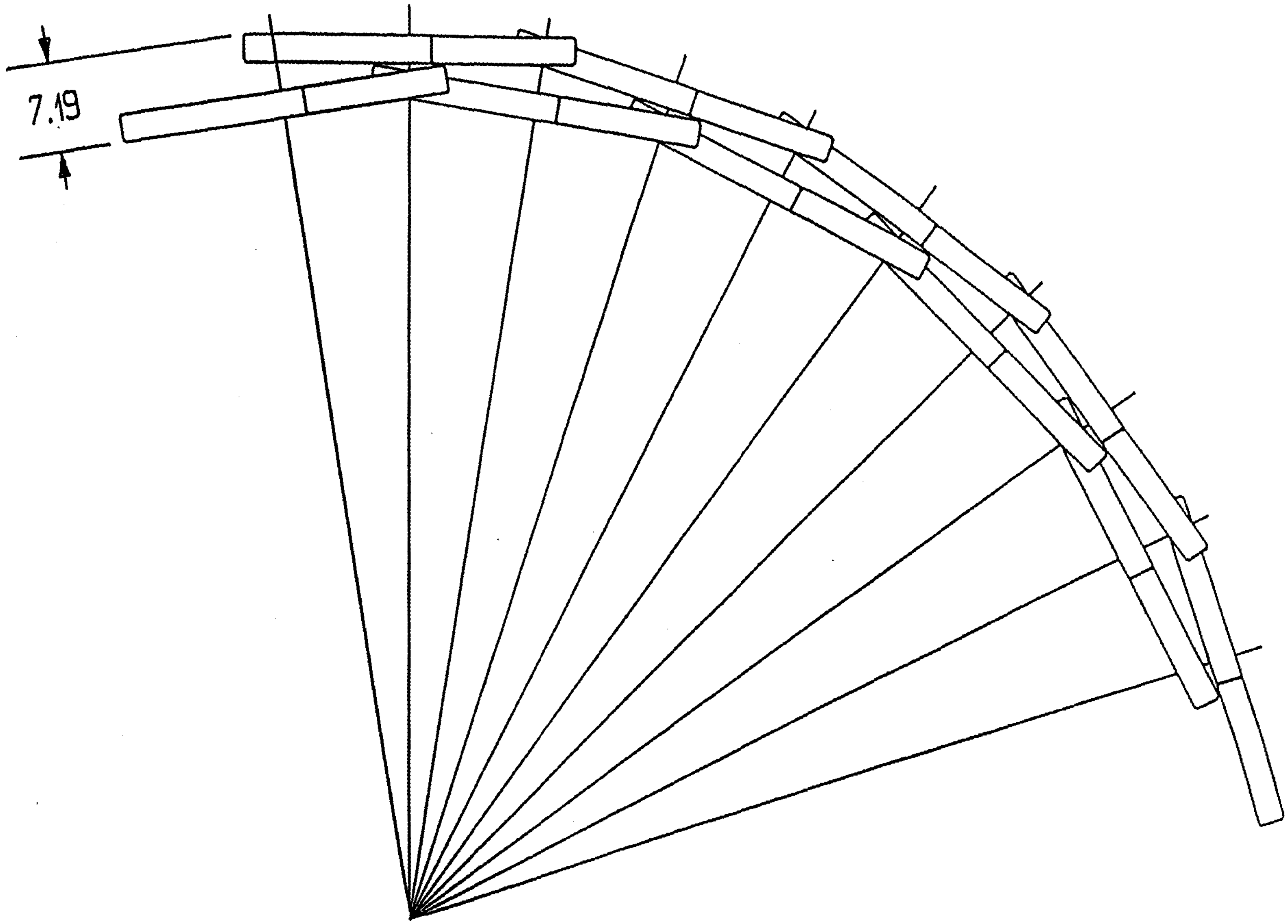

Figure 3.7 — Overlapping rectangular modules, after rotation.

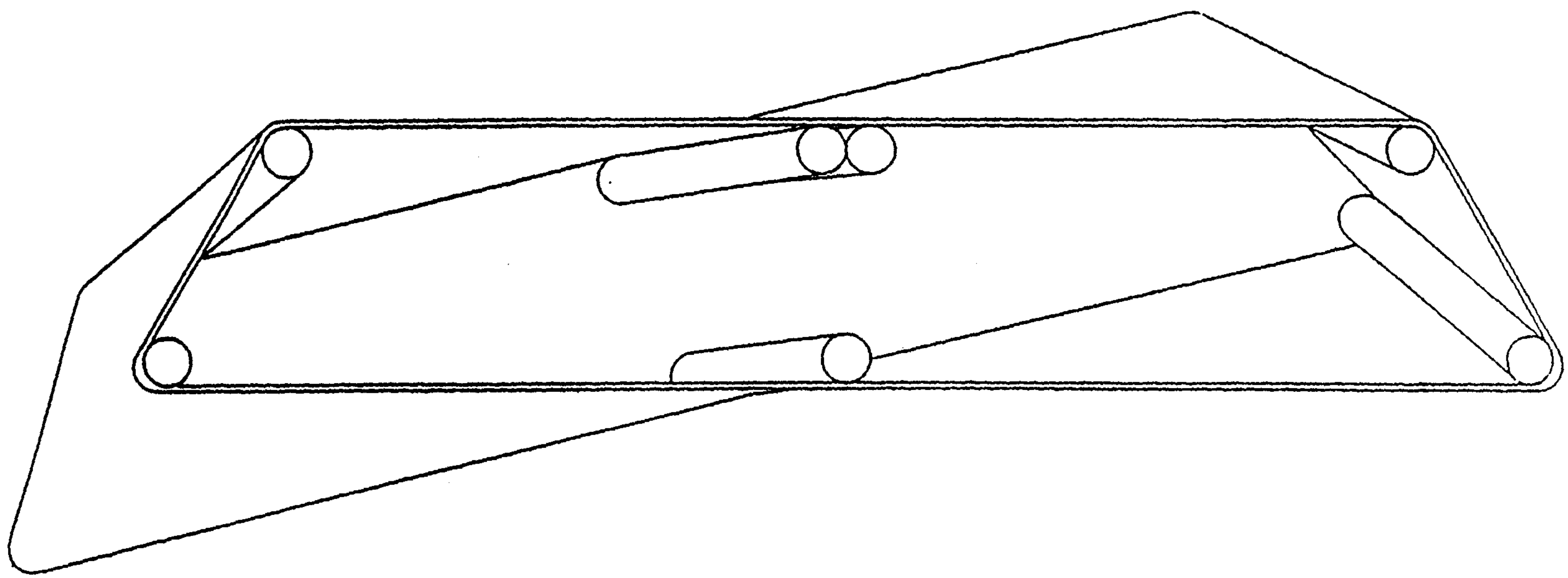

Figure 3.8 — Twisted alternating trapezoid module with selected straws.

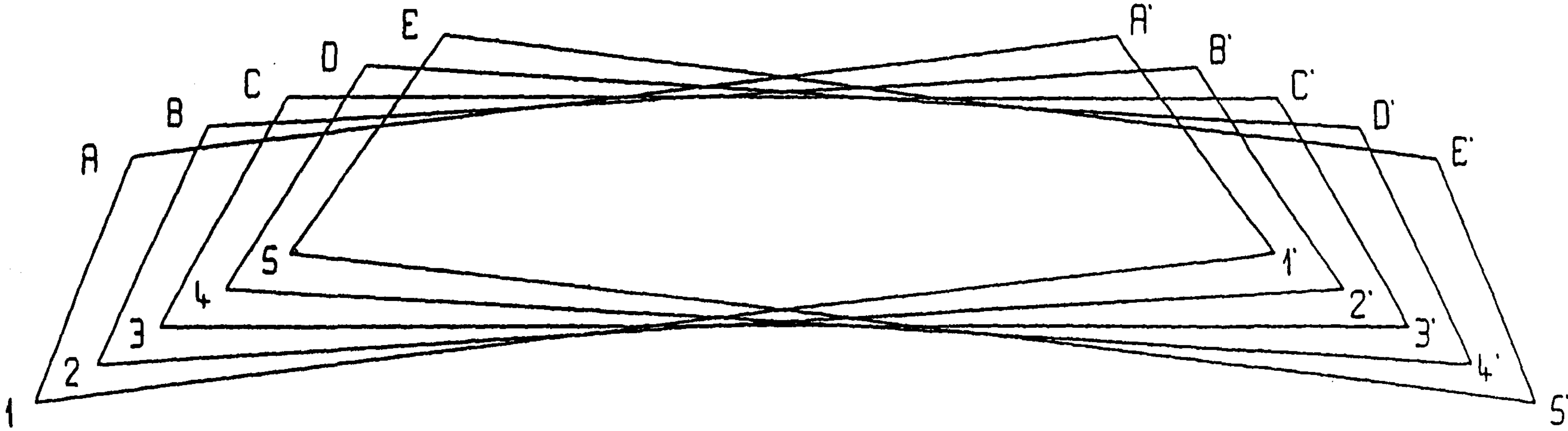

LEFT SIDE	SHORT SIDE	LONG SIDE	RIGHT SIDE
1-A = 2.461 CM	A-A' = 9.417 CM	1-1' = 11.876 CM	1'-A' = 2.460 CM
2-B = 2.448 CM	B-B' = 9.369 CM	2-2' = 11.816 CM	2'-B' = 2.448 CM
3-C = 2.444 CM	C-C' = 9.353 CM	3-3' = 11.795 CM	3'-C' = 2.444 CM
4-D = 2.448 CM	D-D' = 9.369 CM	4-4' = 11.816 CM	4'-D' = 2.448 CM
5-E = 2.460 CM	E-E' = 9.417 CM	5-5' = 11.875 CM	5'-E' = 2.461 CM

POSITION OF SECTIONS
A = Z=0 CM
B = Z=75 CM
C = Z=150 CM (POINT OF ROTATION)
D = Z=225 CM
E = Z=300 CM

MEASUREMENT OF TWISTED STEREO MODULE SECTIONS

Figure 3.9 — Twisted alternating trapezoid module, sections.

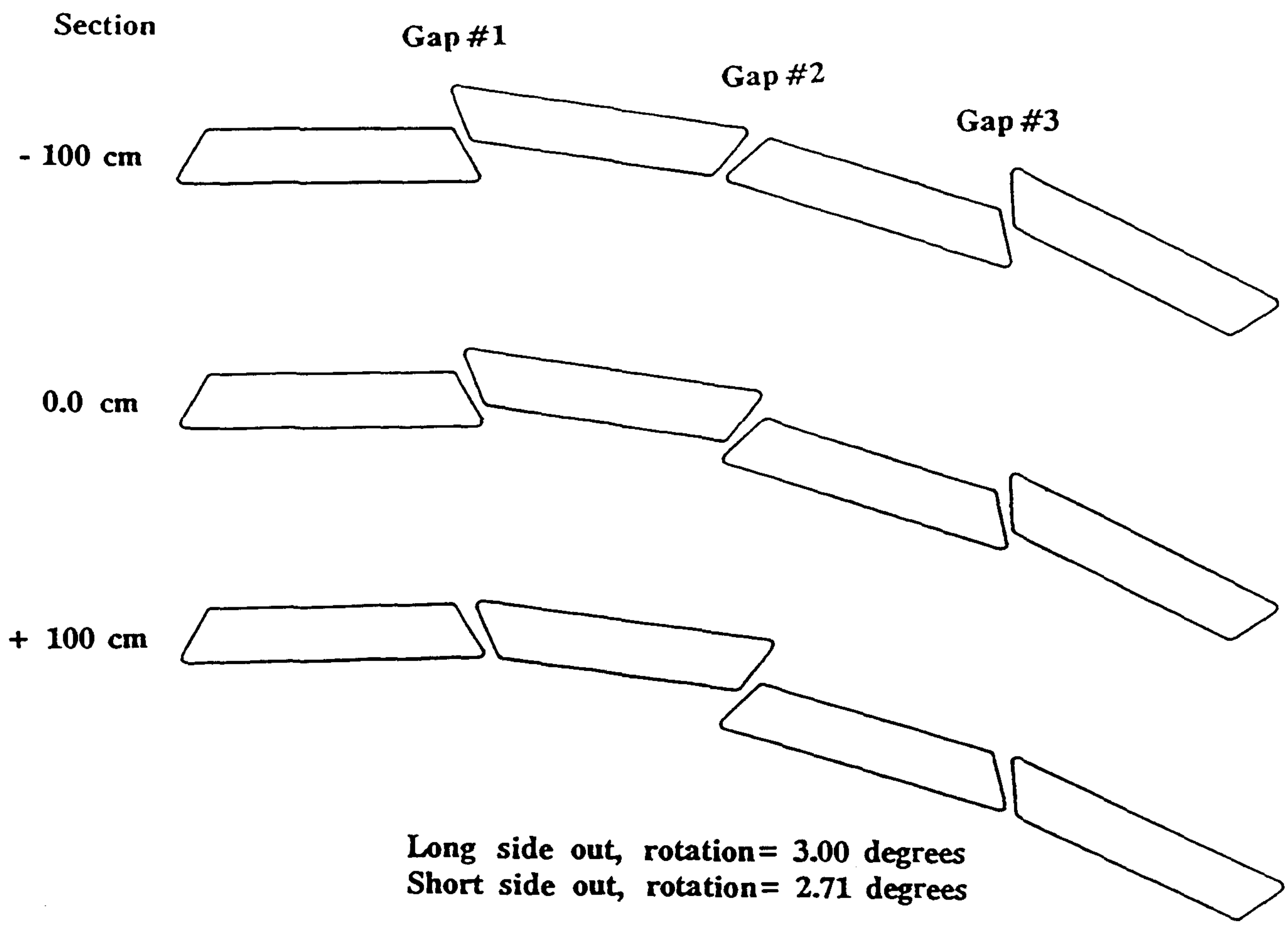

Section	Gap #1	Gap #2	Gap #3
- 100 cm	.442	.455	.442
0.0 cm	.415	.415	.415
+ 100 cm	.455	.442	.455

Figure 3.10 — Stereo study using dual angles for alternating trapezoids.

spacing for angles of 3.00 and 2.71 degrees. Calculating the above table errors show the second angle should be 2.714 degrees for uniform spacing.

The advantages of the dual angle system are uniform radial structural elements and minimal radial build. The main disadvantage is requiring two alternating stereo angles. This will be handled by calculating the alternating module positions separately.

Conclusion

At this time the arrangement for stereo superlayer modules should be straight alternating dual angle trapezoids. Within any given superlayer the modules with the long side toward the outside will be at some greater radius than the modules with their long side inward.

Approximate Radial Space Required for Several Geometry Cases

Module Geometry	Required Radial Space cm	Radial Displacement of Alternating Modules cm
Alter. Trapezoids	6.38	1.8
Parallelograms	3.75	0
Radial Sides	3.55	0
Rectangular	3.55	0
Overlapping Rectangular	7.19	5.0
Twisted Trapezoidal	4.60	1.1
Dual Angle Trap	3.85	1.1

The above table reflects geometry as per Centrak10 dated 1-8-91, for superlayer #1, stereo + 3.00 degrees. The dual angle trapezoid case was generated using 3.00 and 2.71 degrees.

STEREO STUDY USING DUAL ANGLES FOR ALTERNATING MODULES IN A SUPERLAYER

The Tracker as presently defined consists of eight modular concentric superlayers. Four of the superlayers will be aligned with the beam axis. The other four superlayers are stereo layers; two are set at an angle of plus three degrees and the other two are set at minus three degrees to the beam. Alternating modules within a given stereo superlayer are set slightly different angles to accomplish a more uniform module spacing.

The outermost two axial superlayers, layers #8 and #6 are trigger layers, these trapezodial modules have curved tops and bottoms, these modules also are nine straws deep. The remaining layers have trapezoidal modules that are six straws deep, with flat tops and bottoms.

Superlayer	#1	stereo + 3	degrees	flat	trapezoid	(inside superlayer)	
"	#2	axial 0	"	"	"		
"	#3	stereo - 3	"	"	"		
"	#4	axial 0	"	"	"		
"	#5	stereo + 3	"	"	"		
"	#6	axial 0	"	curved	"	trigger	
"	#7	stereo - 3	"	flat	"		
"	#8	axial 0	"	curved	"	trigger	(outside)

The Central Tracker support structure is to be manufactured from light weight graphite epoxy composite. The system requirements for the structure are minimum radiation length, high stability and provide precision positioning of the modules and easy module replacement.

The major support structure components are

1. Inside torsion cylinder
2. Disk, (intermediate radial supports
   Keystones, (radial structure through superlayers)
   Rings, (ring beams between superlayers)
3. Cones, (radial supports at the Tracker ends
   Keystones, (radial structure through superlayers)
   Cylinders, (cylinder beams between superlayers, longer that rings)
4. Outside torsion cylinder

Description of Flat Trapezoidal modules, (layers #2 and #4)

Each trapezoid is (N) straws wide on the long side and each layer contains one straw less. The height is (L) straws high, (H) cm high (straws nested) and has a epoxy, graphite wrapper (T) cm thick. The straw diameter is (d) cm. These trapezoidal modules are alternated in position and are spaced (sp) from the adjoining modules. Both radial position of the alternate modules (D) and the number of straws (N) may be varied to change the superlayer radius. Trapezoid modules must be added in groups of two to make large radius changes such as between superlayers. The module contains (CH) straws.

$sp := .3$ (space between modules cm)

$d := .4$ (straw diameter, cm)

$D := 1.1$ (radial difference of alternating modules, cm)

$T := .025$ (wrapper thickness, cm)

$N := 29$ (number of straws, long side)

$L := 6$ (number of straws high)

$H := ((L - 1)\cdot d\cdot .866) + d + (2\cdot T)$ (height of module, cm)

$LS := N\cdot d + (2\cdot T)$ (length of module long side, cm)

$SS := (N - (L - 1))\cdot d + (2\cdot T)$ (length of module short side cm)

$U := LS + SS + sp - (D\cdot .5774)$ (total length of module pair cm)

$$CH := L\cdot\left[N - \frac{L-1}{2}\right] \qquad CH = 159$$ (straws per module)

Description of Curved Trapezoidal Modules, (layers #6 and #8)

Layers #6 and #8 are trigger layers and are nine straws high. The long and the short sides, (top and bottom) are curved to the same radius as their distance from the beam center line. Other than the curved top and bottom and the increased layers of straws these modules are simular to the flat modules and will be incorporated into the tracker like the other axial layers.

Listed below are the definitions that may be different from the flat modules above.

spc := .3	(space between modules cm)
Dc := .5	(radial difference of alternating modules, cm)
Nc := 30	(number of straws, long side)
Lc := 9	(number of straws high)
Hc := ((Lc − 1)·d·.866) + d + (2·T)	(height of module, cm)
LSc := Nc·d + (2·T)	(length of module long side, cm)
SSc := (Nc − (Lc − 1))·d + (2·T)	(length of module short side cm)
Uc := LSc + SSc + spc − (Dc·.5774)	(total length of module pair cm)

$$CHc := Lc\cdot\left[Nc - \frac{Lc - 1}{2}\right] \qquad CHc = 234 \qquad \text{(straws per module)}$$

Description of Trapezodial Stereo Modules (layers #1,#3,#5 and #7)

The idea here is to generate stereo modules that will have a trapezoidal cross section, provide close to uniform spacing between modules and straight solid support for each straw. The stereo module point of rotation is on a line starting at the beam axis and passing through the center of the module.

Rotation of modules to achieve uniform stereo spacing, the modules with the long side up are rotated 3.00 degrees and the short side up modules are rotated 2.68 degrees.

Listed below are some definitions that may apply only to this set of modules.

sps := .3	(space between modules cm)
Ds := 1.1	(radial difference of alternating modules, cm)
Ns := 29	(number of straws, long side)
Ls := 6	(number of straws high)
Hs := ((Ls − 1)·d·.866) + d + (2·T)	(height of module, cm)
LSs := Ns·d + (2·T)	(length of module long side, cm)
SSs := (Ns − (Ls − 1))·d + (2·T)	(length of module short side cm)
Us := LSs + SSs + sps − (Ds·.5774)	(total length of module pair cm)
Hs = 2.182 cm	

$$CHs := Ls\cdot\left[Ns - \frac{Ls - 1}{2}\right] \qquad CHs = 159 \qquad \text{(straws per module)}$$

Defined geomentry limits for the Central Tracker

The size of the central tracker and it·s support structure are presently defined as having a maximum outside radius of 168.5 cm and a minimum inside radius of 60.0 cm.

The mean superlayer radius as defined by Bill Ford 10-1-89 are as follows

superlayer	radius	
#1	72.0	cm
#2	85.2	cm
#3	98.5	cm
#4	111.7	cm
#5	124.9	cm
#6	138.1	cm
#7	151.4	cm
#8	164.6	cm

The length of the superlayers as defined at this time are as follows, measured from Z = 0.

superlayer	length	
#1	200.0	cm
#2	225.0	cm
#3	250.0	cm
#4	275.0	cm
#5	300.0	cm
#6	300.0	cm
#7	300.0	cm
#8	300.0	cm

The point of rotation for each stereo superlayer is now defined as the module mid point.

superlayer	point of rotation	
#1	100.0	cm
#3	125.0	cm
#5	150.0	cm
#7	150.0	cm

Definition of the Superlayers

Superlayer #1 Stereo +3 degrees

a := 20 module pairs

$$is1 := \frac{a \cdot Us}{2 \cdot \pi}$$

inside radius (is1), short side up		is1 = 66.733	cm
outside radius (os1), short side up	os1 := is1 + Hs	os1 = 68.915	cm
inside radius (il1), long side up	il1 := is1 + Ds	il1 = 67.833	cm
outside radius (ol1), long side up	ol1 := il1 + Hs	ol1 = 70.015	cm
mean radius (m1) m1 := .5·(ol1 − is1) + is1		m1 = 68.374	cm

Superlayer #2 Axial

b := 24 module pairs

$$is2 := \frac{b \cdot U}{2 \cdot \pi}$$

inside radius (is2), short side up		is2 = 80.08	cm
outside radius (os2), short side up	os2 := is2 + H	os2 = 82.262	cm
inside radius (il2), long side up	il2 := is2 + D	il2 = 81.18	cm
outside radius (ol2), long side up	ol2 := il2 + H	ol2 = 83.362	cm
mean radius (m2) m2 := .5·(ol2 − is2) + is2		m2 = 81.721	cm

Superlayer #3 Stereo -3 degrees

c := 28 module pairs

$$is3 := \frac{c \cdot Us}{2 \cdot \pi}$$

inside radius (is3), short side up		is3 = 93.427	cm
outside radius (os3), short side up	os3 := is3 + Hs	os3 = 95.609	cm
inside radius (il3), long side up	il3 := is3 + Ds	il3 = 94.527	cm
outside radius (ol3), long side up	ol3 := il3 + Hs	ol3 = 96.709	cm
mean radius (m3) m3 := .5·(ol3 − is3) + is3		m3 = 95.068	cm

Superlayer #4 Axial

d4 := 32 module pairs

$$is4 := \frac{d4 \cdot U}{2 \cdot \pi}$$

inside radius (is4), short side up		is4 = 106.773	cm
outside radius (os4), short side up	os4 := is4 + H	os4 = 108.955	cm
inside radius (il4), long side up	il4 := is4 + D	il4 = 107.873	cm
outside radius (ol4), long side up	ol4 := il4 + H	ol4 = 110.055	cm
mean radius (m4) m4 := .5·(ol4 − is4) + is4		m4 = 108.414	cm

Superlayer #5 Stereo +3 degrees

e := 36 module pairs

$$is5 := \frac{e \cdot Us}{2 \cdot \pi}$$

inside radius (is5), short side up		is5 = 120.12	cm
outside radius (os5), short side up	os5 := is5 + Hs	os5 = 122.302	cm
inside radius (il5), long side up	il5 := is5 + Ds	il5 = 121.22	cm
outside radius (ol5), long side up	ol5 := il5 + Hs	ol5 = 123.402	cm
mean radius (m5) m5 := .5·(ol5 − is5) + is5		m5 = 121.761	cm

Superlayer #6 Axial curved

f := 40 module pairs

$$is6 := \frac{f \cdot Uc}{2 \cdot \pi}$$

inside radius (is6), short side up		is6 = 133.125	cm
outside radius (os6), short side up	os6 := is6 + Hc	os6 = 136.347	cm
inside radius (il6), long side up	il6 := is6 + Dc	il6 = 133.625	cm
outside radius (ol6), long side up	ol6 := il6 + Hc	ol6 = 136.847	cm
mean radius (m6) m6 := .5·(ol6 − is6) + is6		m6 = 134.986	cm

Superlayer #7 Stereo -3 degrees

$g := 44$ module pairs

$is7 := \frac{g \cdot Us}{2 \cdot \pi}$

inside radius (is7), short side up	$is7 := \frac{g \cdot Us}{2 \cdot \pi}$	$is7 = 146.813$	cm
outside radius (os7), short side up	$os7 := is7 + Hs$	$os7 = 148.995$	cm
inside radius (il7), long side up	$il7 := is7 + Ds$	$il7 = 147.913$	cm
outside radius (ol7), long side up	$ol7 := il7 + Hs$	$ol7 = 150.095$	cm
mean radius (m7)	$m7 := .5 \cdot (ol7 - is7) + is7$	$m7 = 148.454$	cm

Superlayer #8 Axial curved

$h := 48$ module pairs

inside radius (is8), short side up	$is8 := \frac{h \cdot Uc}{2 \cdot \pi}$	$is8 = 159.751$	cm
outside radius (os8), short side up	$os8 := is8 + Hc$	$os8 = 162.972$	cm
inside radius (il8), long side up	$il8 := is8 + Dc$	$il8 = 160.251$	cm
outside radius (ol8), long side up	$ol8 := il8 + Hc$	$ol8 = 163.472$	cm
mean radius (m8)	$m8 := .5 \cdot (ol8 - is8) + is8$	$m8 = 161.611$	cm

Definition of the support structure

Radius of Torsion Cylinders, Rings and Cylinders

Inside Torsion Cylinder

inside band (a1)	$a1 := m1 - .5 \cdot (m2 - m1)$	$a1 = 61.701$	cm
outside band (a2)	$a2 := a1 + 2.5$	$a2 = 64.201$	cm

Ring, Cylinder 1-2

inside band (b1)	$b1 := m2 - .5 \cdot (m2 - m1) - 2.5$	$b1 = 72.548$	cm
outside band (b2)	$b2 := m2 - .5 \cdot (m2 - m1) + 2.5$	$b2 = 77.548$	cm
mean radius (bm)	$bm := .5 \cdot (b2 - b1) + b1$	$bm = 75.048$	cm

Ring, Cylinder 2-3

inside band (c1)	$c1 := m3 - .5 \cdot (m3 - m2) - 2.5$	$c1 = 85.894$	cm
outside band (c2)	$c2 := m3 - .5 \cdot (m3 - m2) + 2.5$	$c2 = 90.894$	cm
mean radius (cm)	$cm := .5 \cdot (c2 - c1) + c1$	$cm = 88.394$	cm

Ring, Cylinder 3-4

inside band (d1)	$d1 := m4 - .5 \cdot (m4 - m3) - 2.5$	$d1 = 99.241$	cm
outside band (d2)	$d2 := m4 - .5 \cdot (m4 - m3) + 2.5$	$d2 = 104.241$	cm
mean radius (dm)	$dm := .5 \cdot (d2 - d1) + d1$	$dm = 101.741$	cm

Ring, Cylinder 4-5

inside band (e1)	$e1 := m5 - .5 \cdot (m5 - m4) - 2.5$	$e1 = 112.587$	cm
outside band (e2)	$e2 := m5 - .5 \cdot (m5 - m4) + 2.5$	$e2 = 117.587$	cm
mean radius (em)	$em := .5 \cdot (e2 - e1) + e1$	$em = 115.087$	cm

Ring, Cylinder 5-6

inside band (f1)	$f1 := m6 - .5 \cdot (m6 - m5) - 2.5$	$f1 = 125.873$	cm
outside band (f2)	$f2 := m6 - .5 \cdot (m6 - m5) + 2.5$	$f2 = 130.873$	cm
mean radius (fm)	$fm := .5 \cdot (f2 - f1) + f1$	$fm = 128.373$	cm

Ring, Cylinder 6-7

inside band (g1)	$g1 := m7 - .5 \cdot (m7 - m6) - 2.5$	$g1 = 139.22$	cm
outside band (g2)	$g2 := m7 - .5 \cdot (m7 - m6) + 2.5$	$g2 = 144.22$	cm
mean radius (gm)	$gm := .5 \cdot (g2 - g1) + g1$	$gm = 141.72$	cm

Ring, Cylinder 7-8

inside band (h1)	$h1 := m8 - .5 \cdot (m8 - m7) - 2.5$	$h1 = 152.533$	cm
outside band (h2)	$h2 := m8 - .5 \cdot (m8 - m7) + 2.5$	$h2 = 157.533$	cm
mean radius (hm)	$hm := .5 \cdot (h2 - h1) + h1$	$hm = 155.033$	cm

Outside Torsion Cylinder RADIUS

inside band (i1)	i1 := ol8 + (is1 - a2)	i1 = 166.004	cm
outside band (i2)	i2 := i1 + 2.5	i2 = 168.504	cm

Summary

Superlayer mean radius cm.		Delta cm.	Space between superlayers cm.	
lay 1	m1 = 68.374		Cyl-lay1	is1 - a2 = 2.532
lay 2	m2 = 81.721	m2 - m1 = 13.347	Lay 1-2	is2 - ol1 = 10.065
lay 3	m3 = 95.068	m3 - m2 = 13.347	Lay 2-3	is3 - ol2 = 10.065
lay 4	m4 = 108.414	m4 - m3 = 13.347	Lay 3-4	is4 - ol3 = 10.065
lay 5	m5 = 121.761	m5 - m4 = 13.347	Lay 4-5	is5 - ol4 = 10.065
lay 6	m6 = 134.986	m6 - m5 = 13.225	Lay 5-6	is6 - ol5 = 9.724
lay 7	m7 = 148.454	m7 - m6 = 13.468	Lay 6-7	is7 - ol6 = 9.966
lay 8	m8 = 161.611	m8 - m7 = 13.157	Lay 7-8	is8 - ol7 = 9.655
			Lay8-Cyl	i1 - ol8 = 2.532

Space between components

Tor cyl and superlayer 1	is1 - a2 = 2.532	cm
Superlayer 1 and ring 1	b1 - ol1 = 2.532	cm
Ring 1 and superlayer 2	is2 - b2 = 2.532	cm
Superlayer 2 and ring 2	c1 - ol2 = 2.532	cm
Ring 2 and superlayer 3	is3 - c2 = 2.532	cm
Superlayer 3 and ring 3	d1 - ol3 = 2.532	cm
Ring 3 and superlayer 4	is4 - d2 = 2.532	cm
Superlayer 4 and ring 4	e1 - ol4 = 2.532	cm
Ring 4 and superlayer 5	is5 - e2 = 2.532	cm
Superlayer 5 and ring 5	f1 - ol5 = 2.472	cm
Ring 5 and superlayer 6	is6 - f2 = 2.252	cm
Superlayer 6 and ring 6	g1 - ol6 = 2.373	cm
Ring 6 and superlayer 7	is7 - g2 = 2.593	cm
Superlayer 7 and ring 7	h1 - ol7 = 2.438	cm
Ring 7 and superlayer 8	is8 - h2 = 2.218	cm
Superlayer 8 and tor cyl	i1 - ol8 = 2.532	cm

Inside radius of inner torsion cyl	a1 = 61.701	cm	spec minimum = 60.0
Outside radius of outer torsion cyl	i2 = 168.504	cm	spec maximum = 168.5

Number of Modules (Total System).
Modules, full system **mod := 4·(a + b + c + d4 + e + f + g + h)**
mod = 1088 modules

Number of channels (Total System).
tch := 4·(CHs·a + CH·b + CHs·c + CH·d4 + CHs·e + CHc·f + CHs·g + CHc·h)
tch = 199392 channels

Number of Axial channels (Total System).
ach := 4·(CH·b + CH·d4 + CHc·f + CHc·h)
ach = 117984 channels
Number of Stereo channels (Total System)
sch := 4·(CHs·a + CHs·c + CHs·e + CHs·g)
sch = 81408 channels
Number of Trigger channels (Total System)
tch := 4·(CHc·f + CHc·h)
tch = 82368 channels

4. FINITE-ELEMENT ANALYSIS OF DEADWEIGHT DEFLECTIONS OF FIVE-CYLINDER CENTRAL TRACKER SUPPORT STRUCTURE

ABSTRACT

The gravity-induced deflections of the five-cylinder central tracker support structure were calculated using the ANSYS package. The loading included the eight "superlayers" of detector-straw modules, but omitted the silicon tracker inside the innermost cylinder.

4.1 INTRODUCTION

The deflections of the central tracker under its own weight have been estimated for the design shown in Figure 4.1. This design is composed of five concentric structural cylinders which support eight "superlayers" of trapezoidal modules which are packed with straw-shaped detectors. The five cylinders are made of identical sandwiches of foam core symmetrically sandwiched between layers of graphite-epoxy skin.

The entire structure is supported at the four corner points indicated in Figure 4.1: the points where the circular ends of the outermost cylinder intersect the horizontal plane through the axis of the structure. Each of the four inner cylinders is supported at each end by a ring-shaped plate which connects it to the next-outer cylinder; these end rings are of the same sandwich construction as the cylinders, but with the foam core twice as thick. Figure 4.2 shows the structure in cross-section.

The detector modules which are supported by the structure are shown in cross-section in Figure 4.3. An arc of one superlayer made up of these modules is sketched in Figure 4.4. Each superlayer is attached to its supporting cylinder by a number of "hanger" rings which can be seen in Figures 4.1 and 4.2. The modules pass more or less loosely through trapezoidal holes in these rings (and in the structural end-rings). Since the modules are not connected to each other and are not

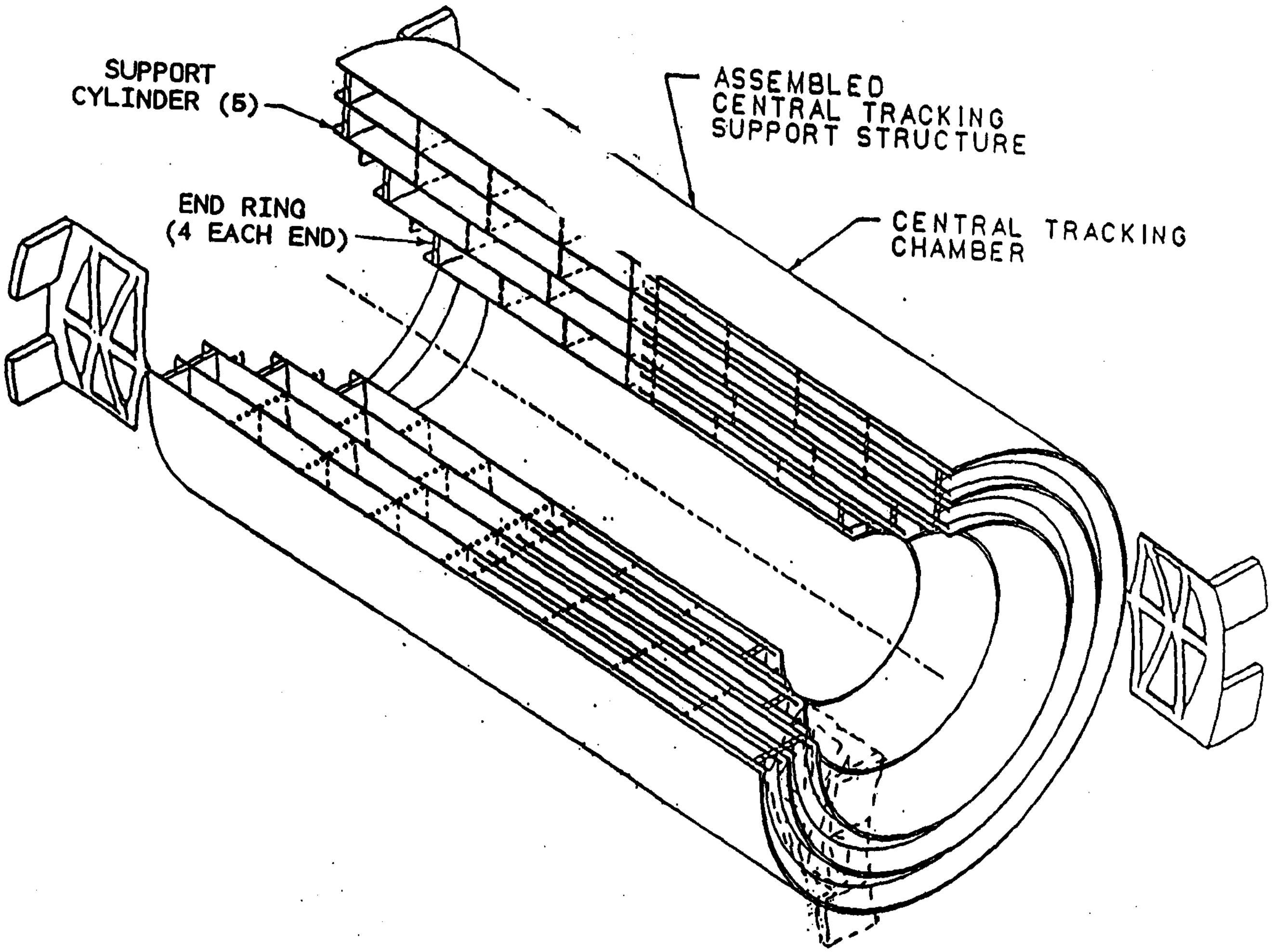

Figure 4.1 — Isometric sketch of tracker structure, including corner support points; module superlayers have been omitted from the left half to show the structural elements more clearly.

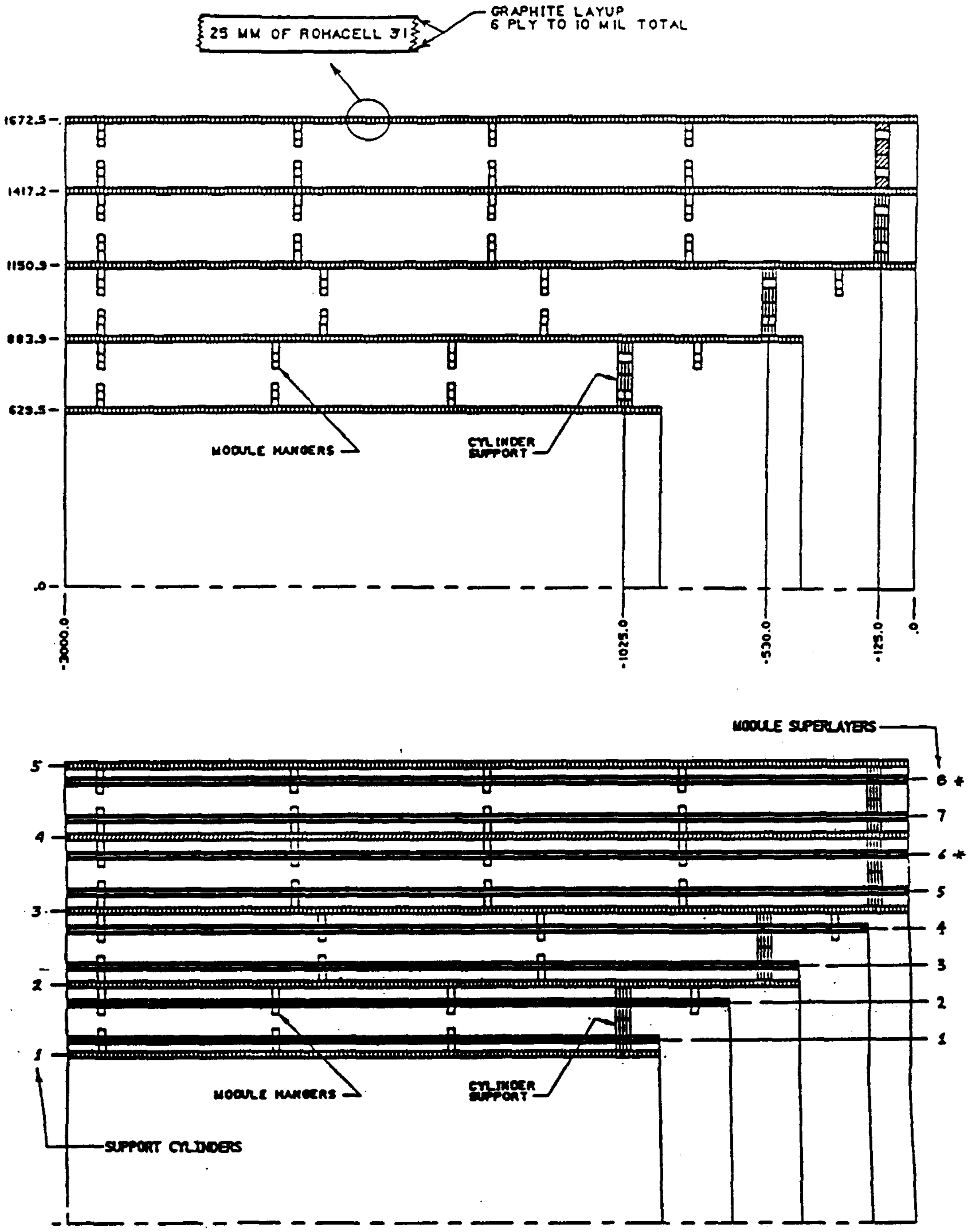

Figure 4.2 — Cross-section of the tracker structure.

Upper: Dimensions of structural elements.
Lower: Attachment of superlayers to structure; layes 6 and 8 (*) contain the heavier trigger modules.

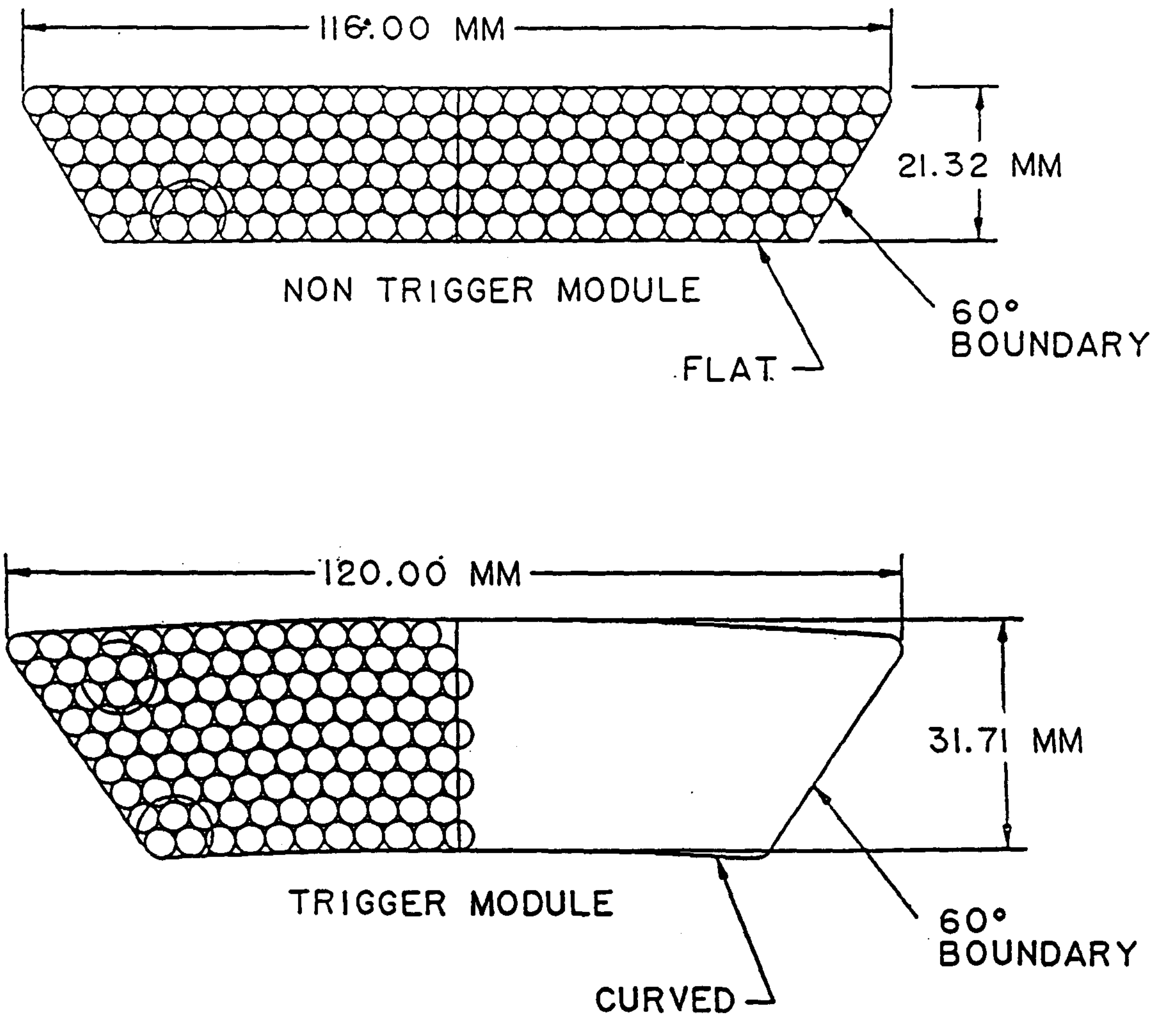

Figure 4.3 — Cross-sections of the modules incorporated in the superlayers.

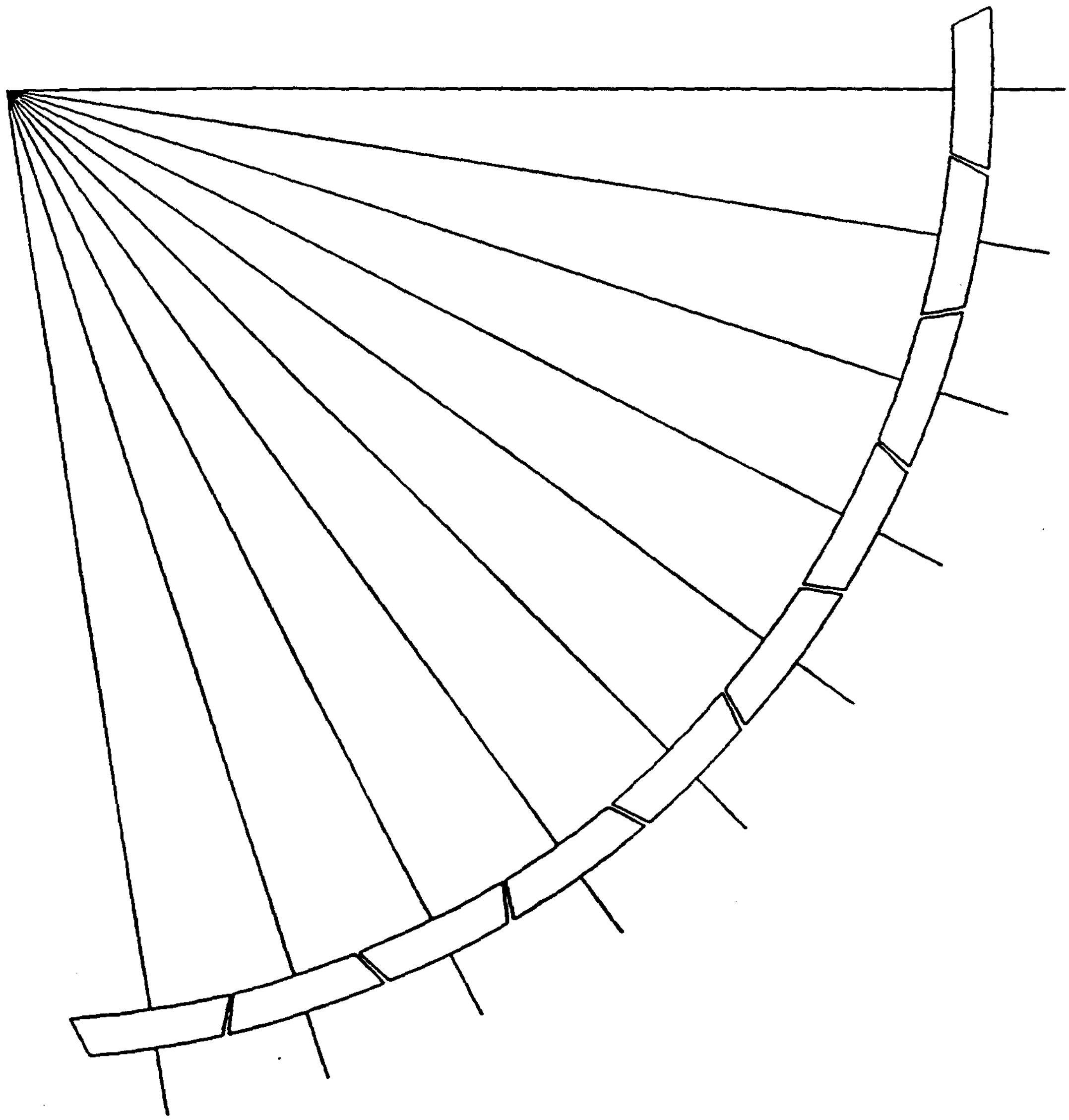

Figure 4.4 — Schematic cross-section of a superlayer arc.

firmly attached to the cylinders, their contribution to the stiffness of the structure is negligible when compared to the stiffness of the cylinders. They can therefore be treated as non-structural mass whose deadweight contributes to the loading of the structure. The modules shown in Figure 4.3 are estimated to weigh 0.0100 lb/in (non-trigger module) and 0.0125 lb/in (trigger module).

To assess the static deflections of this structure due to gravity loading, a finite-element model was constructed using the ANSYS package. This model will be described in the following section.

4.2 FINITE-ELEMENT MODEL

Figure 4.1 shows that the structure has two vertical planes of mirror symmetry, dividing it end-to-end and side-to-side. Because of this symmetry, only a quarter of the structure needed to be modeled; the model mesh (using curved shell elements) is shown in Figure 4.5. The symmetry of the structure is enforced in this partial model by applying appropriate constraints to the nodes lying in the two vertical symmetry planes. As the figure indicates, the model has been constructed with the origin of global coordinates at the geometrical center of the structure, so that the symmetry planes are the global X-Y and Y-Z planes.

The single-point support indicated in Figure 4.1 is spread into a vertical constraint applied to five nodes along the edge of the outermost cylinder, in order to avoid the unrealistic creation of a point-load singularity in the problem.

The model mesh is relatively coarse because only displacements are being sought, and not stresses. This is why the simple five-node representation of the corner support is acceptable. Similarly, the application of the deadweight of the modules at the discrete locations of the hanger rings has not been considered. Each superlayer has been incorporated into the model of its support cylinder as a sort of non-structural (but heavy) "cladding." Thus, each superlayer is considered to be exactly as long as its support cylinder. The short extensions of

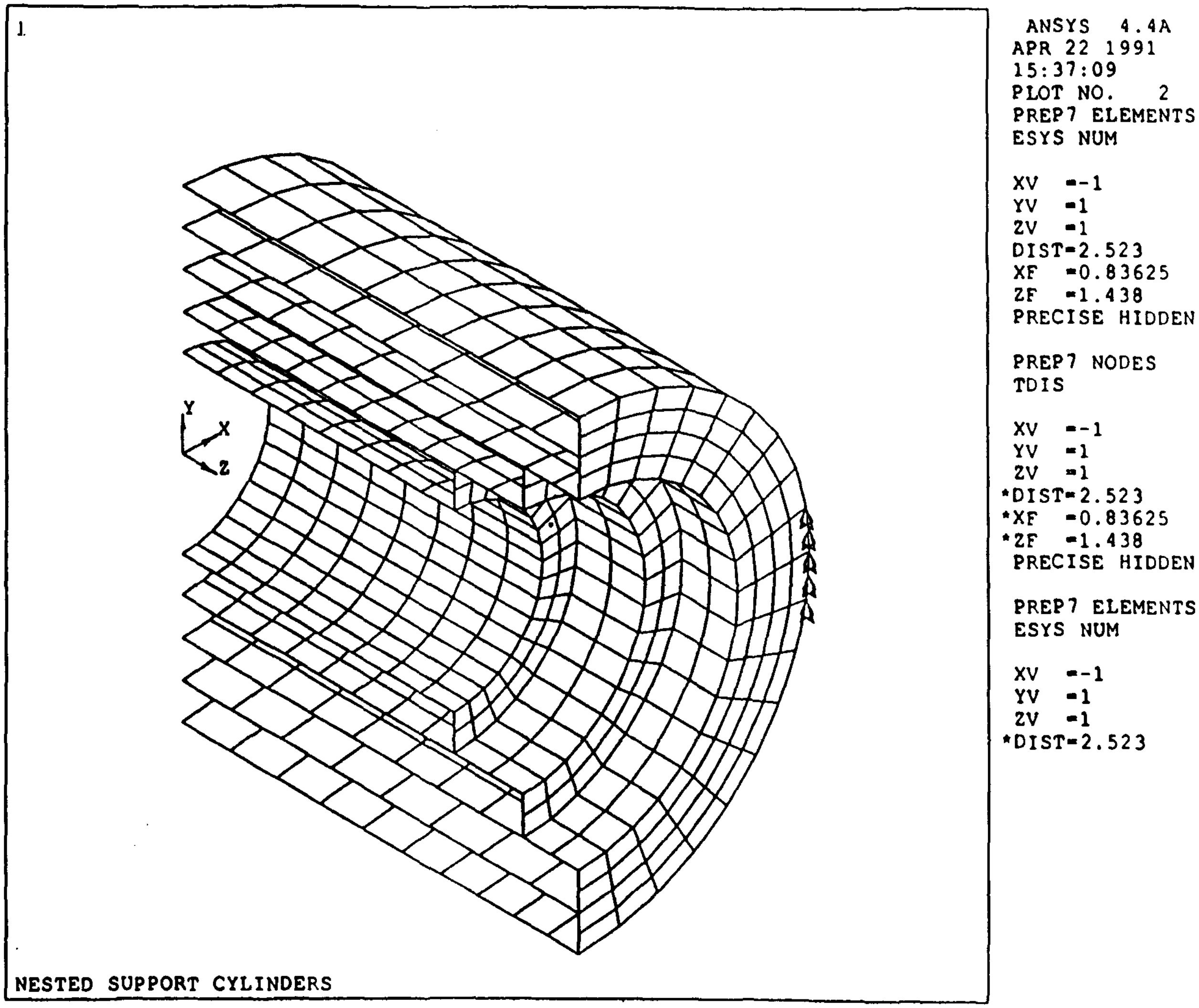

Figure 4.5 — ANSYS shell-element model of the tracker, representing one quadrant of the structure shown in Figure 4.1.

the cylinders beyond the structural end-rings, which can be seen in Figures 4.1 and 4.2, were omitted from the model.

The elements shown in Figure 4.5 are the ANSYS "Layered Shell Element" STIF91, which models a sandwich of various materials all with different thicknesses and material properties. The sandwich for the most general cylinder element, with a superlayer "cladding" both inside and outside, is shown in Figure 4.6. It contains a symmetrical sequence of seven materials. The center (No. 4) layer is the structural foam core of the cylinder, a 25-mm layer of "Rohacell 31." The centerline of this layer corresponds to the nominal radius assigned to the shell element, using the values shown in Figure 4.2. Attached to either surface of the foam (i.e., material layers 3 and 5) are the graphite-epoxy skins of the cylinders, with a 0.229-mm (9-mil) thickness and incorporating the combined elastic properties of a six-ply filament-wound layup with filaments oriented along the zero-degree (circumferential) direction, +60 degrees, and -60 degrees.

Each superlayer of modules is modeled by a two-layer sandwich of non-structural (very compliant) materials. Just outboard of the skins (material layers 2 and 6) are dummy standoff layers whose density is negligible as well as its stiffness. These layers are present only to space the layers representing the modules themselves to the correct midline radius, and in most cases are 67 mm thick.

The module layers (material layers 1 and 7) are given a nominal density of 1678 kilograms per cubic meter; non-trigger module layers have a nominal thickness of 1.00 mm, while the heavier trigger module layers (numbered 6 and 8 in Figure 4.2) are assigned 1.256 mm thickness.

The innermost and outermost cylinders are modeled by a slightly different shell element; since these cylinders each support only one module superlayer, they need only a five-layer shell element. The stand-off layer is also reduced in thickness from 67 mm to 53 mm; this closer separation between cylinder and superlayer can be seen in the lower half of Figure 4.2.

The end rings are modeled with a three-layer STIF91 element, using materials 3, 4, and 5 from Figure 4.6, but with the thickness of the foam doubled to 50 mm.

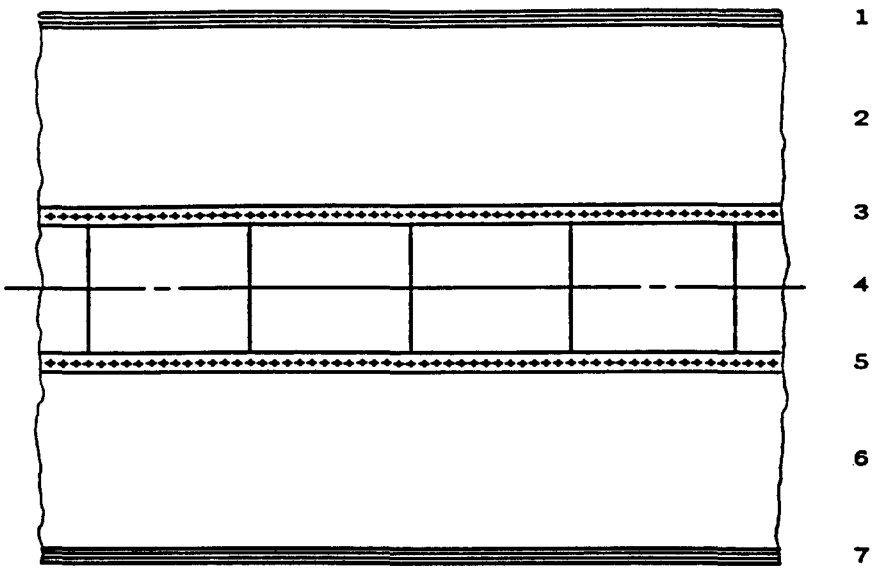

Figure 4.6 — Sandwich of materials specified for layered shell element modeling a general case (numbered 2, 3, or 4 in Figure 4.2) structural cylinder with its attached module superlayers.

1 & 7: Nonstructural superlayer of modules with mass included.
2 & 6: Dummy nonstructural standoff layer.
3 & 5: Six-ply filament-wound epoxy-graphite skin.
4: "Rohacell-31" foam core.

4.3 DISPLACEMENT RESULTS

Figures 4.7 - 4.9 display the element displacements calculated by ANSYS for gravity loading on the model described in the previous section. The original element positions are indicated in dashed lines, and the deflected elements are drawn in solid lines. The displacements have been exaggerated by a factor ("DSCA") which ANSYS selects automatically for each display; as appears in the annotations to the right of the plot frame, its value varies between 2126 and 2626. The value "DMX" gives the vector-sum displacement (in meters) of the largest nodal displacement associated with the display; the value 0.899E-04 shown in Figures 4.7 and 4.8 corresponds to 0.0899 mm, or about 3.6 mils. As the end-view in Figure 4.7 suggests, the displacements are predominantly in the vertical direction.

Figures 4.7 and 4.8 exhibit significant local deformation around the five-node support constraint, which contributes to the absolute vertical motion of the rest of the structure. These figures also show some warping of the outermost cylinder and end-ring in the vicinity of their common edge. This is the only area where any of the cylinders depart noticeably from their original circular shape.

Figure 4.9 displays only the displacements in the Y-Z symmetry plane, and has been annotated with the values of downward vertical displacement at the corner and end nodes. Examining these values gives an idea of how much each cylinder sags out of its original straight profile. For example, the innermost cylinder sags about (0.0859 - 0.0692) = 0.0167 mm, or about 0.67 mil. Similarly, the inner span of the second cylinder sags (0.0878 - 0.06905) = 0.01875 mm, while the stub end of that same cylinder, which carries a shear load of most of two cylinders including three superlayers, undergoes a relative displacement of (0.06905 - 0.05545) = 0.0136 mm over a rather short length.

The maximum-displacement ("DMX") value in this figure is given as 0.878E-04 meters, or 0.0878 mm, and occurs at the top and bottom nodes in the mid-section of the second cylinder. The maximum displacement in the whole model, the 0.0899 mm mentioned above, also occurs in this cross-section, but in the horizontal X-Z plane; its direction is almost exactly vertical.

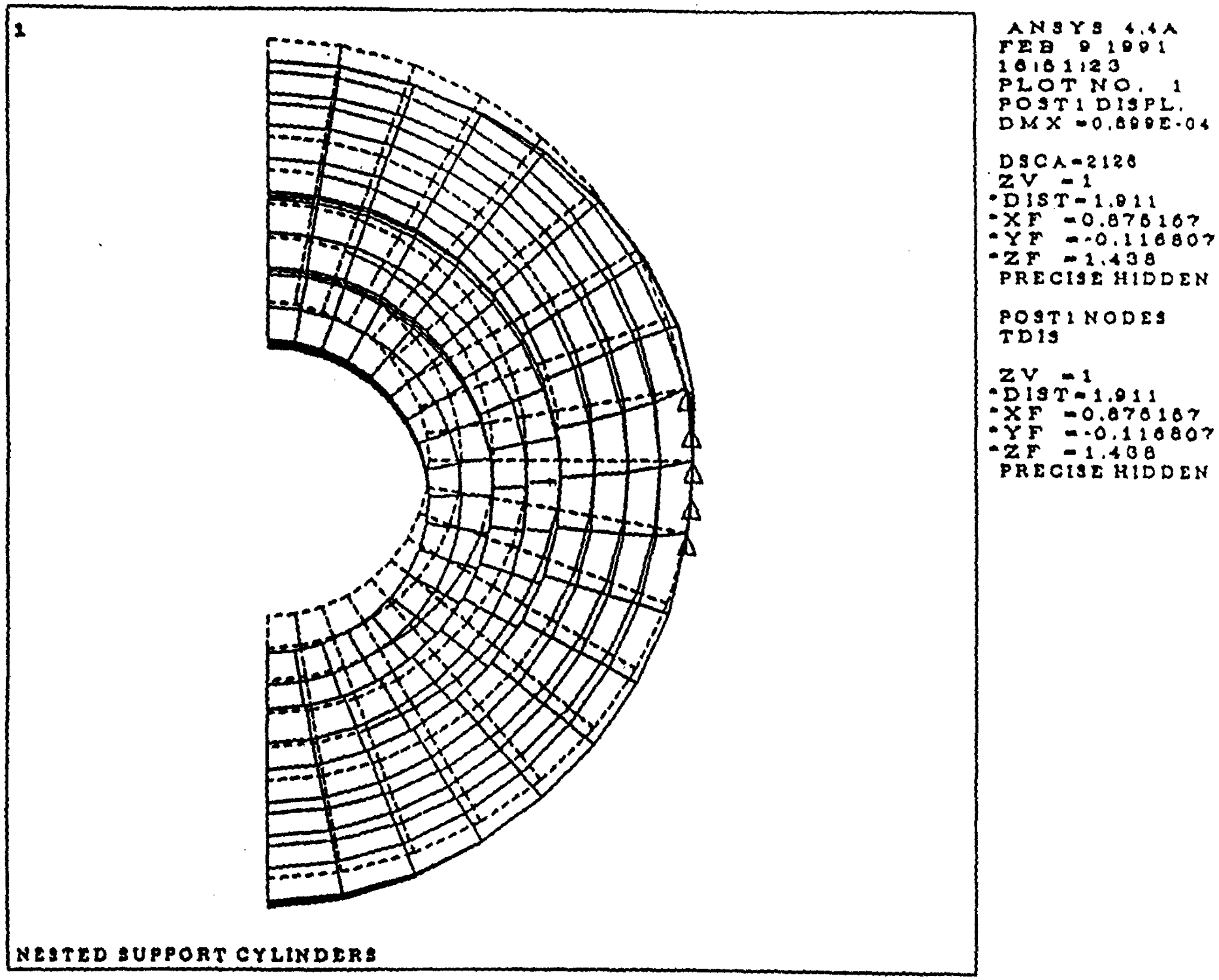

Figure 4.7 — End view of elements displaced by gravity load.

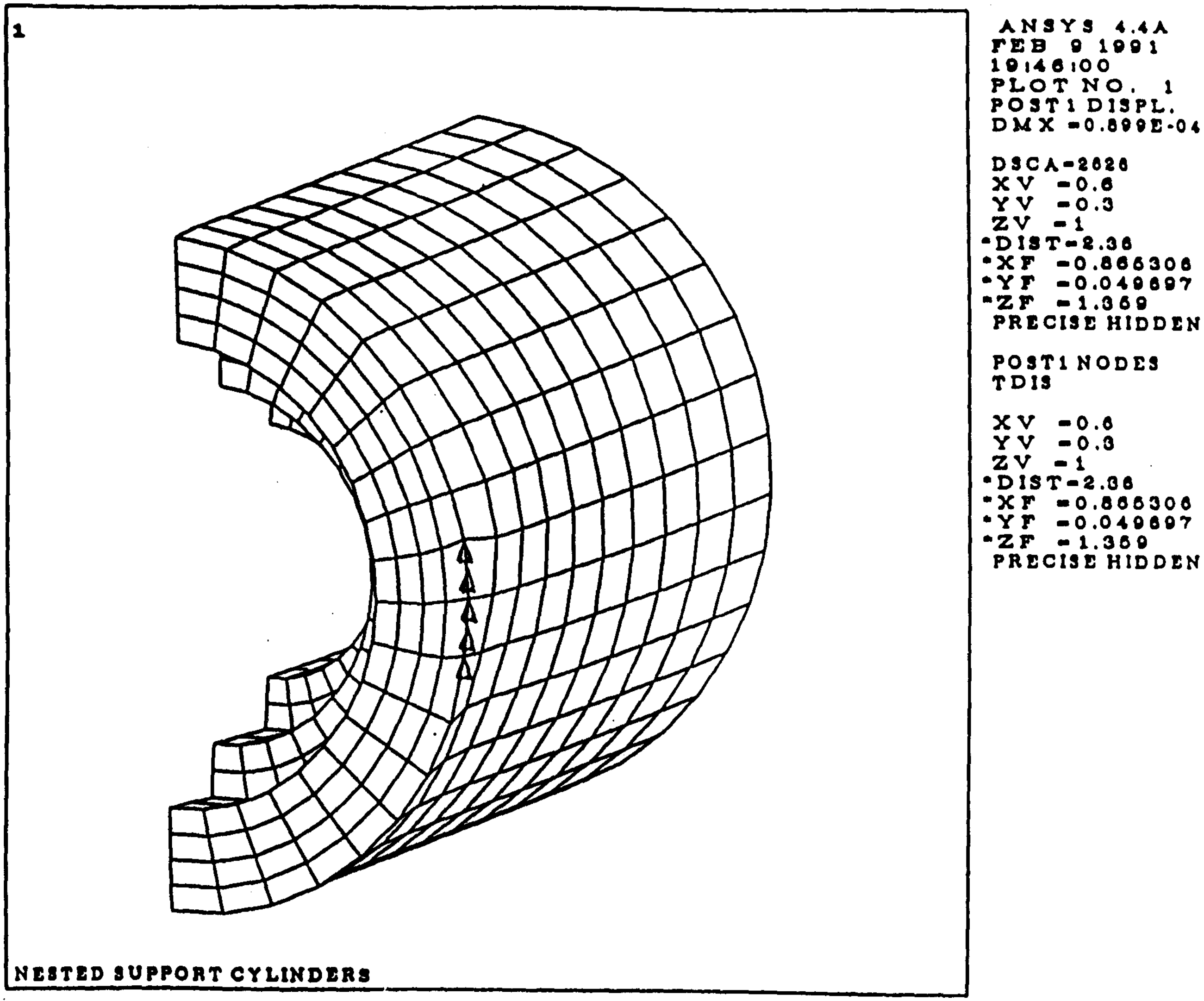

Figure 4.8 — Isometric view of elements displaced by gravity load.

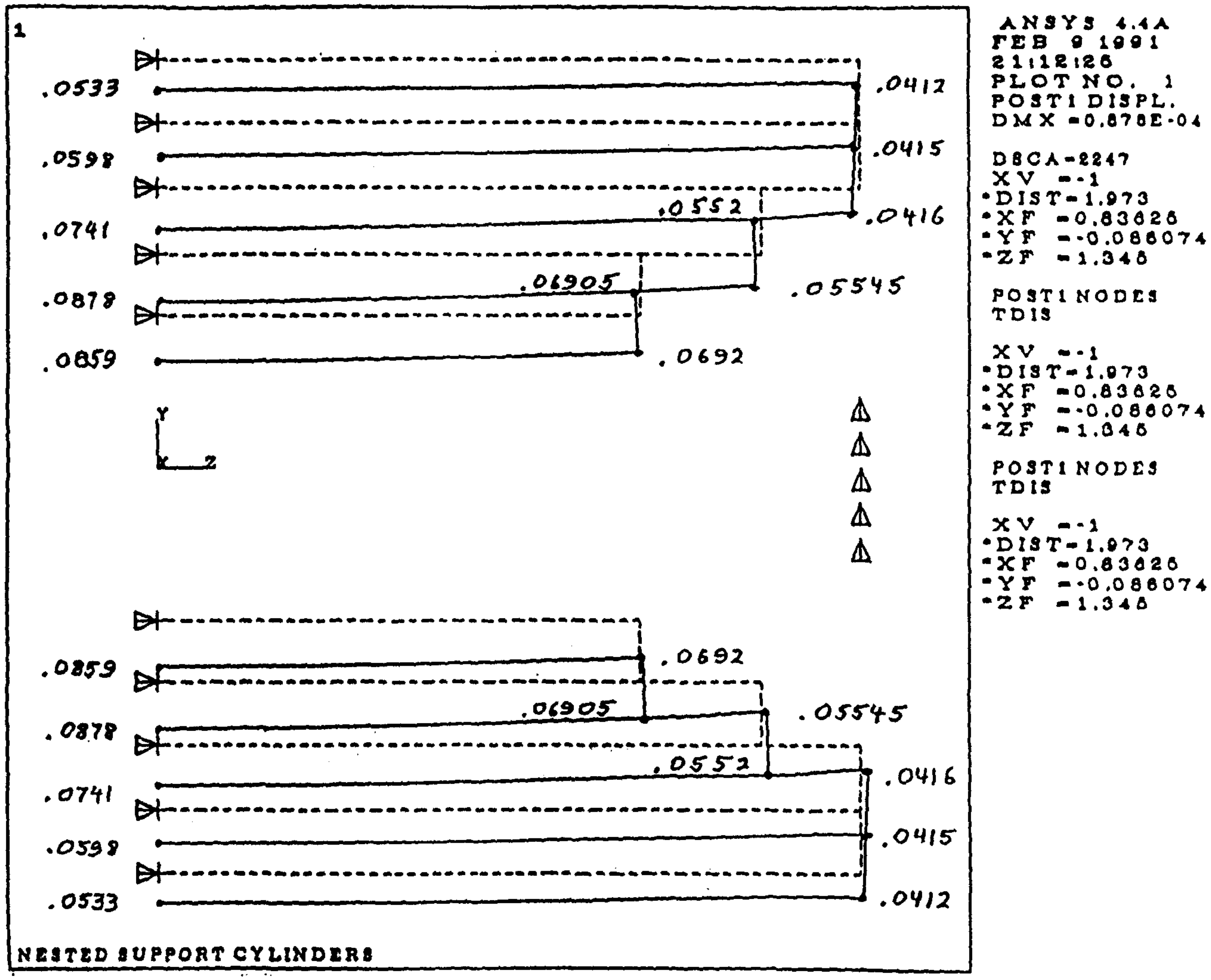

Figure 4.9 — Deadweight displacements in the Y-Z plane.

5. INTEGRATED COST/SCHEDULE DATA

Attached is the integrated cost and schedule data created from the Central Tracker Work Breakdown structure. To provide a meaningful presentation of the data we grouped the work packages according to a set of functions. This helped us to see the span of time required to complete each function. The schedule is made using precedence diagramming method assuming a product life cycle for each component with its scheduled calendar time estimated from the labor and material estimates and/or supplier delivery times. Purchases are free float (as late as possible) with material spending at the end of each work package. The expected spending curve for the Central Tracker effort lies between the early and late date curves on the summary of costs profile. More specifically, we expect to level the resources so that a smoother labor loading is achieved for the first 2.5 years of the program.

Attached are the following:

BAR CHARTS

- Summary of TARGET versus Planned network
- Grouped by Function, early start

LOGIC DIAGRAMS

- Critical Path
- Conceptual Design & Prototype Devel Assy
- Component Design
- Elect. Design
- Tooling Design
- Manufacturing (Subassy)
- Tooling Fabrication

RESOURCE AND COST PROFILES

- Engineering and Dsgn/Drafting Manpower
- Technician and Labor Manpower
- Labor and Material Costs
- Summary of costs

SUMMARY WBS

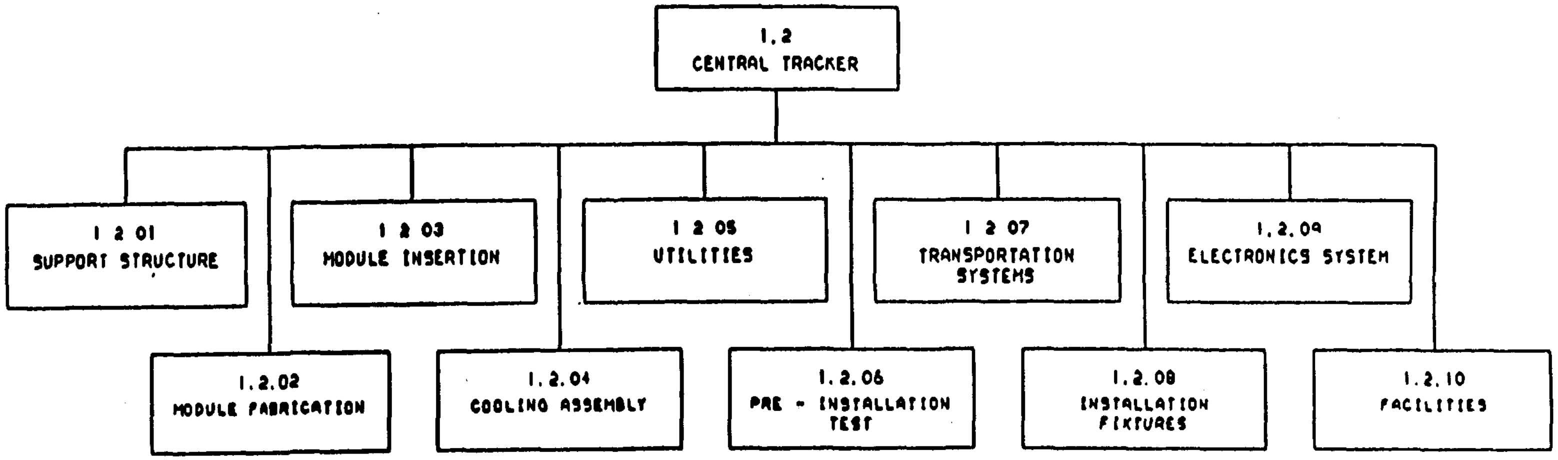
1.2
CENTRAL TRACKER
1 2 01
SUPPORT STRUCTURE
1.2.02
MODULE FABRICATION
1 2 03
MODULE INSERTION
1.2.04
COOLING ASSEMBLY
1 2 05
UTILITIES
1.2.06
PRE - INSTALLATION TEST
1 2 07
TRANSPORTATION SYSTEMS
1.2.08
INSTALLATION FIXTURES
1.2.09
ELECTRONICS SYSTEM
1.2.10
FACILITIES

SUMMARY
BAR CHART

- TARGET
- ACTUALS vs. TARGET

FUNCTION	EARLY START	EARLY FINISH
CONCEPTUAL DESIGN (R&D)	3JAN91	30SEP94
COMPONENT DESIGN	2JUL92	28FEB95
PURCHASE SUPPORT STRUCTURE	1OCT93	19DEC96
TOOLING FABRICATION	1OCT93	29SEP95
MANUFACTURE SUPPORT STRUCTURE COMPONENTS	1JUL94	29APR97
FABRICATE ASSEMBLY SUPPORT STRUCTURE	1MAR96	29SEP97
FACTORY TESTING	1OCT97	2FEB98
SHIPPING	3FEB98	1MAY98
UNPACK AND TEST	4MAY98	8MAY98
INSTALLATION	11MAY98	31AUG98
FINAL PLUMBING & CABLING	1SEP98	28JAN99
FINAL CHECKOUT	29JAN99	30SEP99
OPERATION-TURN IT ON !	1OCT99	1OCT99

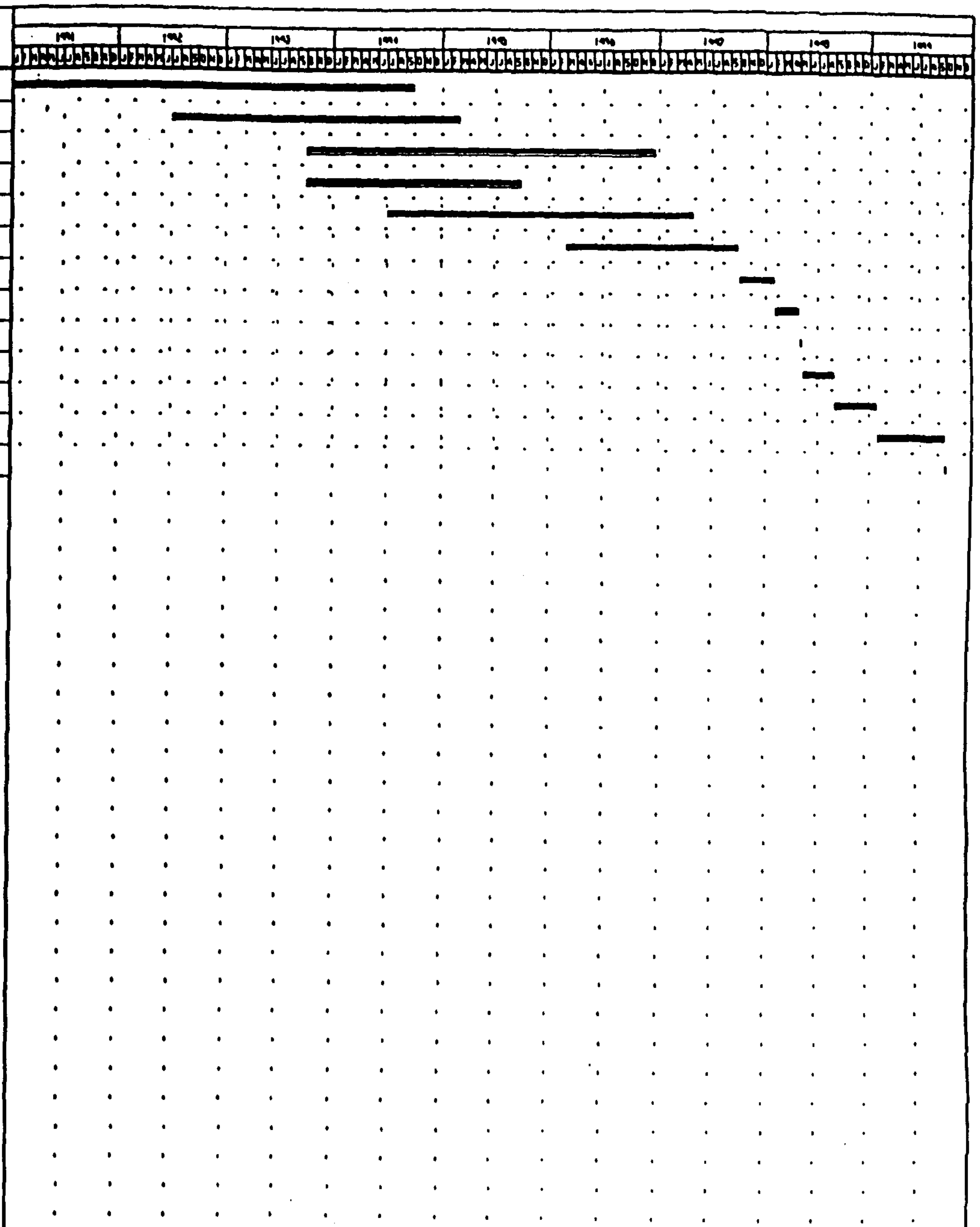

Project Start: 1DEC90
Project Finish: 31DEC99

SOLENOIDAL DETECTOR COLLABORATION
CENTRAL TRACKER REV 1 NETWORKED
TARGET MASTER SCHEDULE

Sheet 1 of 1

Data Date: 3JAN91
Plot Date: 18MAR91

Primavera Systems, Inc.

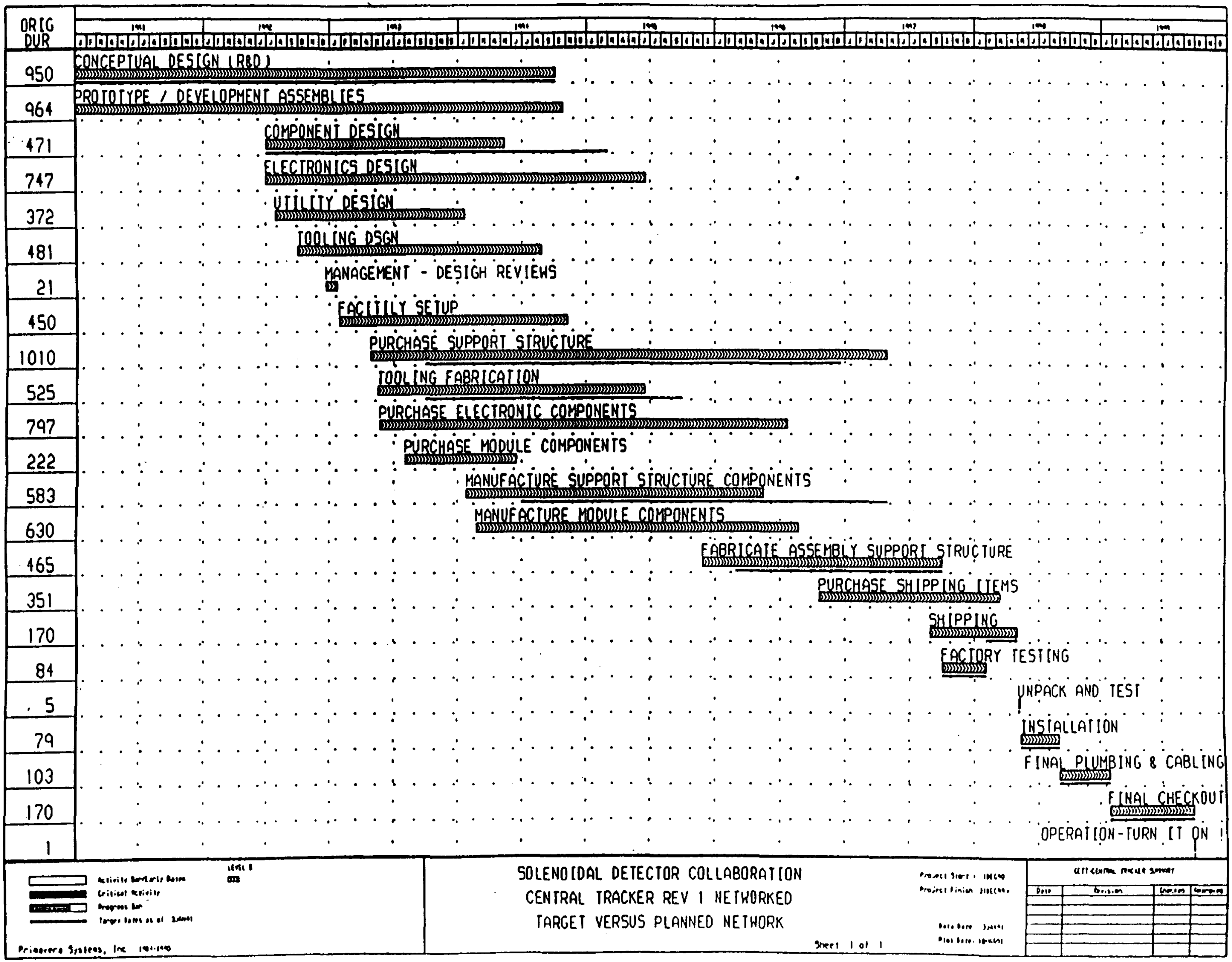
ORIG DUR
950 CONCEPTUAL DESIGN (R&D)
964 PROTOTYPE / DEVELOPMENT ASSEMBLIES
471 COMPONENT DESIGN
747 ELECTRONICS DESIGN
372 UTILITY DESIGN
481 TOOLING DSGN
21 MANAGEMENT - DESIGH REVIEWS
450 FACITILY SETUP
1010 PURCHASE SUPPORT STRUCTURE
525 TOOLING FABRICATION
797 PURCHASE ELECTRONIC COMPONENTS
222 PURCHASE MODULE COMPONENTS
583 MANUFACTURE SUPPORT STRUCTURE COMPONENTS
630 MANUFACTURE MODULE COMPONENTS
465 FABRICATE ASSEMBLY SUPPORT STRUCTURE
351 PURCHASE SHIPPING ITEMS
170 SHIPPING
84 FACTORY TESTING
5 UNPACK AND TEST
79 INSTALLATION
103 FINAL PLUMBING & CABLING
170 FINAL CHECKOUT
1 OPERATION-TURN IT ON !
SOLENOIDAL DETECTOR COLLABORATION
CENTRAL TRACKER REV 1 NETWORKED
TARGET VERSUS PLANNED NETWORK
Sheet 1 of 1

BAR CHART

CRITICAL PATH WITH FABRICATION TASKS

ACTIVITY ID	ACTIVITY DESCRIPTION	EARLY START	EARLY FINISH
M005	START DESIGN	2JUL92	1JUL92
A144	CONES INSIDE BAND QTY 4 DSGN.	2JUL92	30JUL92
A198	DISKS INSIDE BAND (QTY 2) DSGN.	31JUL92	19AUG92
A204	RING #1 (QTY 4) DSGN.	20AUG92	29SEP92
A210	RING #2 (QTY 4) DSGN.	30SEP92	13NOV92
A216	RING #3 (QTY 4) DSGN.	16NOV92	29DEC92
A222	RING #4 (QTY 4) DSGN.	30DEC92	11FEB93
A228	RING #5 (QTY 4) DSGN.	12FEB93	2APR93
A234	RING #6 (QTY 4) DSGN.	5APR93	25MAY93
A240	RING #7 (QTY 4) DSGN.	26MAY93	23JUL93
A096	KEYSTONE STYLE #1 DSGN.	26JUL93	20AUG93
A098	PURCH KEYSTONE STYLE #1	21AUG93	28DEC93
A104	PURCH.KEYSTONE STYLE #2	31JAN94	9JUN94
A110	PURCH.KEYSTONE STYLE #3	21APR94	28AUG94
A116	PURCH.KEYSTONE STYLE #4	10JUL94	16NOV94
A122	PURCH.KEYSTONE STYLE #5	28SEP94	4FEB95
A128	PURCH KEYSTONE STYLE #6	17DEC94	25APR95
A134	PURCH KEYSTONE STYLE #7	7MAR95	14JUL95
A140	PURCH KEYSTONE STYLE #8	26MAY95	20CT95
A142	KEYSTONE STYLE #8 ASSEMBLY	30CT95	27NOV95
A054	PURCH ANTISAG FIXTURE TOOLING	15NOV95	2MAY96
A080	ASSY OUTER SUPPORT CONES QTY 2	28NOV95	24JAN96
A526	PURCH TEST EQUIPMENT	15DEC95	2MAY96
A074	ASSY SUPPORT DISKS INTERMEDIATE QTY 2	25JAN96	13MAR96
A490	PREPARE MODULES FOR INSTALLATION IN STRUCTURE	22FEB96	20AUG96
M025	START FABRICATION	1MAR96	29FEB96
S025	FABRICATION	1MAR96	29SEP97
A068	ASSY SUPPORT DISKS Z=0 QTY 2	14MAR96	2MAY96
A088	PRE-INSTALL ALIGN SEGMENTS ON RINGS & CONES	18APR96	16MAY96
A028	SETUP OUTER TORSIONAL CYLINDER	3MAY96	16MAY96
A032	BUILD MODULE SUPPORT STRUCTURE (HAMMOCK)	3MAY96	30SEP97
A026	INSTALL INNER DISCS IN OUTER TORSIONAL CYL	17MAY96	28JUN96
A024	INSTALL CONES IN OUTER TORSIONAL CYL	1JUL96	13AUG96
A094	INSTALL INNER TORSIONAL CYLINDER IN STRUCTURE	14AUG96	25SEP96
A050	ASSEMBLE ALIGNMENT RIG	4SEP96	25SEP96
A042	ALLIGN SEGMENTS	26SEP96	7JAN97
A040	LOCK SEGMENTS IN STRUCTURE QTY 336	30CT96	14JAN97

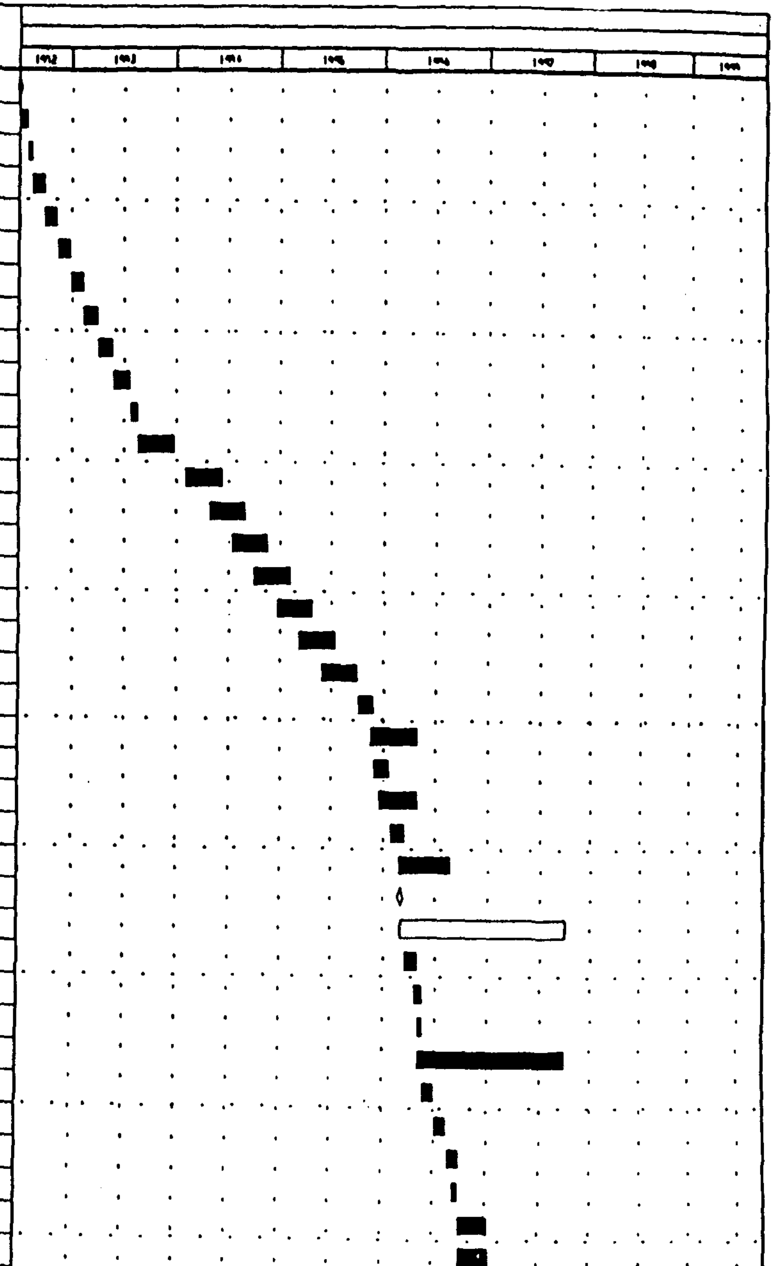

Critical Activity
Progress Bar

Primavera Systems, Inc

Project Start · 1DEC90

SOLENOIDAL DETECTOR COLLABORATION
CENTRAL TRACKER REV 1 NETWORKED
CRITICAL PATH AND FABRICATION TASKS

Sheet 1 of 2

ACTIVITY ID	ACTIVITY DESCRIPTION	EARLY START	EARLY FINISH
A016	FINISH MODULE SUPPORT STRUCTURE		14JAN97
A492	INSTALL MODULES IN SUPPORT STRUCTURE	15JAN97	7JUL97
A512	ASSEMBLE ELECTRONICS COOLING COMPONENTS	26FEB97	7JUL97
A564	ASSEMBLY MOUNTING FIXTURES	26FEB97	7JUL97
A502	PURCH FITTINGS	2MAR97	30APR97
A498	ASSEMBLY MANIFOLD	1MAY97	7JUL97
A540	PURCH SHIPPING CONTAINER	15JUN97	22SEP97
A018	CONNECT MANIFOLD TO STRAW TUBE MODULES	8JUL97	30SEP97
A020	INSTALL MOUNTING FIXTURES ON SUPPORT STRUCTURE	8JUL97	30SEP97
A022	INSTALL ELECTRONIC COOLING SYSTEM	8JUL97	30SEP97
A544	DESIGN SHIPPING ATMOSPHERE SYSTEM	28AUG97	4SEP97
A546	PURCH ATMOSPHERE SYSTEM FOR SHIPMENT	8SEP97	22SEP97
A536	ASSEMBLE SHIPPING SUPPORT	23SEP97	2FEB98
A542	ASSEMBLE SHIPPING CONTAINER	23SEP97	2FEB98
A548	ASSEMBLE ATMOSPHERE SYSTEM	23SEP97	2FEB98
M030	START FACTORY TESTING	1OCT97	30SEP97
A530	PERFORM TRACKER FUNCTIONAL TEST	1OCT97	2FEB98
M035	START TO PREPARE TRACKER FOR SHIPMENT	3FEB98	2FEB98
A554	PREPARE TRACKER FOR SHIPMENT	3FEB98	2APR98
M040	START SHIPMENT TRACKER	3APR98	2APR98
A558	SHIP TRACKER	3APR98	1MAY98
M045	START UNPACK AND TEST TRACKER	4MAY98	1MAY98
S045	UNPACK TRACKER	4MAY98	8MAY98
M050	START INSTALLATION OF TRACKER	11MAY98	8MAY98
S050	ASSEMBLE TRACKER PARTS FOR INSTALLATION IN COIL	11MAY98	31JUL98
M052	START INSTALL TRACKER IN COIL	3AUG98	31JUL98
S052	INSTALL TRACKER IN COIL	3AUG98	31AUG98
M055	START FINAL PLUMBING AND CABLING	1SEP98	31AUG98
S055	FINAL PLUMBING AND CABLING	1SEP98	28JAN99
M060	START TO PERFORM FINAL CHECKOUT	29JAN99	28JAN99
S060	PERFORM FINAL CHECKOUT	29JAN99	30SEP99
M065	START DETECTOR TURN ON	1OCT99	30SEP99
S065	DETECTOR TURN ON	1OCT99	1OCT99

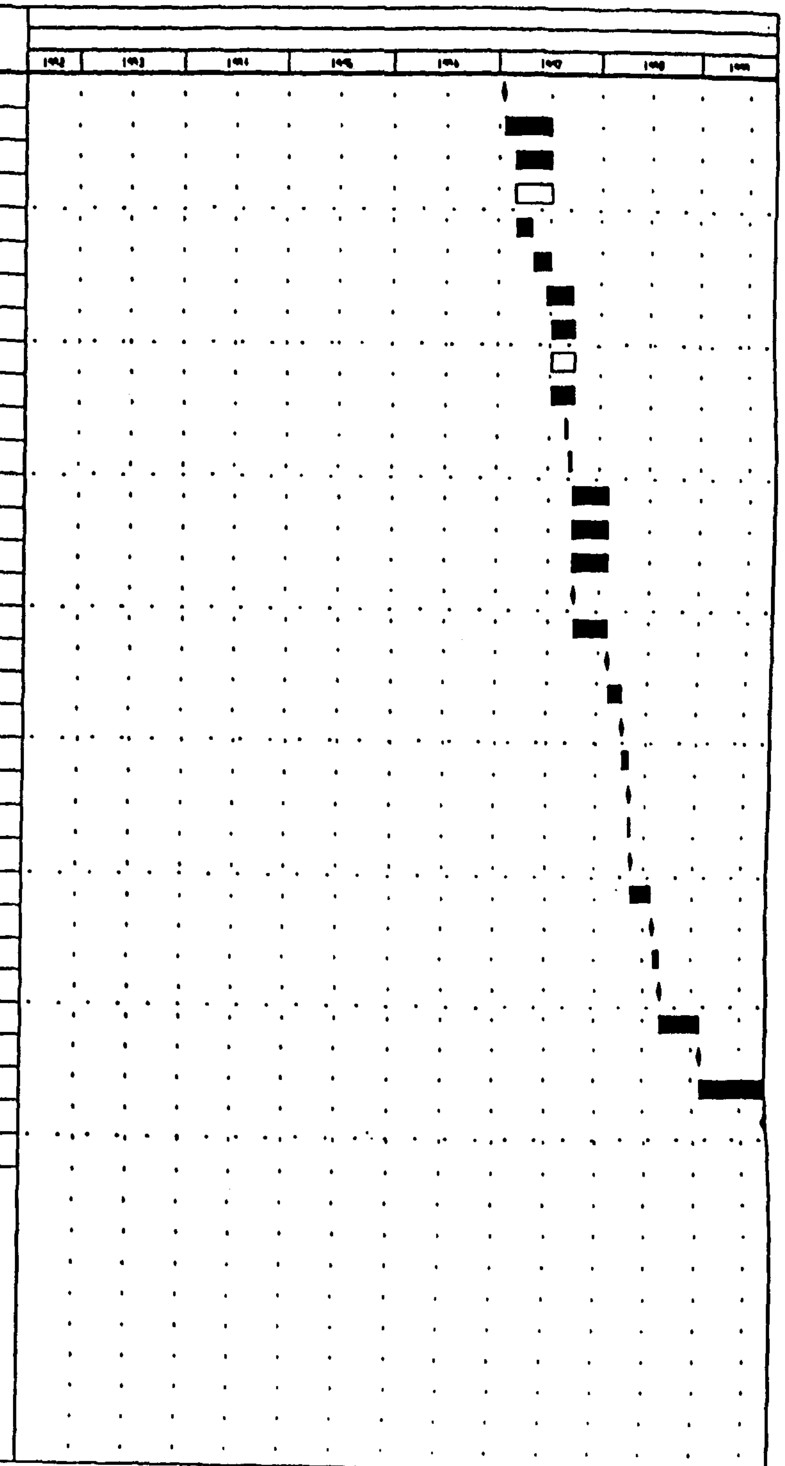

BAR CHART

FUNCTION BY EARLY START

ACTIVITY ID	WBS#	ACTIVITY DESCRIPTION	REM DUR	EARLY START	EARLY FINISH
S		START PROGRAM	0	3JAN91	
E		END OF PROGRAM	0	4OCT99	1OCT99
A090	0201020101	INNER TORSIONAL CYLINDER DSGN	23	2JUL92	4AUG92
A144	0201020301	CONES INSIDE BAND QTY 4 DSGN	20	2JUL92	30JUL92
M005	TARGET	START DESIGN	0	2JUL92	1JUL92
S005	TARGET	DESIGN	670	2JUL92	28FEB95
A150	0201020302	CYLINDER #1 (QTY 2) DSGN.	18	31JUL92	25AUG92
A198	0201020401	DISKS INSIDE BAND (QTY 2) DSGN.	14	31JUL92	19AUG92
A300	0201020601	OUTSIDE TORSIONAL CYLINDER DSGN	240	5AUG92	19JUL93
A430	02020101	STRAW TUBE MODULE DESIGN	125	5AUG92	2FEB93
A204	0201020402	RING #1 (QTY 4) DSGN	28	20AUG92	29SEP92
A156	0201020303	CYLINDER #2 (QTY 2) DSGN	20	26AUG92	23SEP92
A162	0201020304	CYLINDER #3 (QTY 2) DSGN	21	24SEP92	22OCT92
A210	0201020403	RING #2 (QTY 4) DSGN	33	30SEP92	13NOV92
A168	0201020305	CYLINDER #4 (QTY 2) DSGN	26	23OCT92	30NOV92
A216	0201020404	RING #3 (QTY 4) DSGN.	29	16NOV92	29DEC92
A174	0201020306	CYLINDER #5 (QTY 2) DSGN.	30	1DEC92	14JAN93
A222	0201020405	RING #4 (QTY 4) DSGN	31	30DEC92	11FEB93
A180	0201020307	CYLINDER #6 (QTY 2) DSGN	32	15JAN93	1MAR93
A228	0201020406	RING #5 (QTY 4) DSGN	35	12FEB93	2APR93
A186	0201020308	CYLINDER #7 (QTY 2) DSGN	35	2MAR93	20APR93
A234	0201020407	RING #6 (QTY 4) DSGN	37	5APR93	25MAY93
A192	0201020309	CONES OUTSIDE BAND QTY 4 DSGN	3	21APR93	23APR93
A240	0201020408	RING #7 (QTY 4) DSGN.	40	26MAY93	23JUL93
A532	020701	DSGN SHIPPING SUPPORT	24	20JUL93	20AUG93
A096	0201020201	KEYSTONE STYLE #1 DSGN	20	26JUL93	20AUG93
A246	0201020409	DISKS OUTSIDE BAND (QTY 2) DSGN	15	26JUL93	13AUG93
A254	0201020501	ALIGNMENT SEGMENT, STYLE 1, QTY 5X6 DSGN	6	16AUG93	23AUG93
A102	0201020202	KEYSTONE STYLE #2 DSGN	18	23AUG93	16SEP93
A538	020702	DESIGN SHIPPING CONTAINER	42	23AUG93	20OCT93
A260	0201020502	ALIGNMENT SEGMENT, STYLE 2, QTY 6X6 DSGN	6	24AUG93	31AUG93
A266	0201020503	ALIGNMENT SEGMENT, STYLE 3, QTY 7X6 DSGN	6	1SEP93	9SEP93
A272	0201020504	ALIGNMENT SEGMENT, STYLE 4, QTY 8X6 DSGN.	6	10SEP93	17SEP93
A108	0201020203	KEYSTONE STYLE #3 DSGN.	21	17SEP93	15OCT93
A278	0201020505	ALIGNMENT SEGMENT, STYLE 5, QTY 9X6 DSGN	6	20SEP93	27SEP93
A284	0201020506	ALIGNMENT SEGMENT, STYLE 6, QTY 10X6 DSGN	6	28SEP93	5OCT93
A290	0201020507	ALIGNMENT SEGMENT, STYLE 7, QTY 11X6 DSGN	6	6OCT93	13OCT93
A296	0201020508	ALIGNMENT FASTENERS QTY 206X4 DSGN.	16	14OCT93	4NOV93
A114	0201020204	KEYSTONE STYLE #4 DSGN	23	18OCT93	17NOV93
A120	0201020205	KEYSTONE STYLE #5 DSGN	26	18NOV93	28DEC93
A126	0201020206	KEYSTONE STYLE #6 DSGN	29	29DEC93	8FEB94
A132	0201020207	KEYSTONE STYLE #7 DSGN.	32	9FEB94	24MAR94
A138	0201020208	KEYSTONE STYLE #8 DSGN.	35	25MAR94	13MAY94

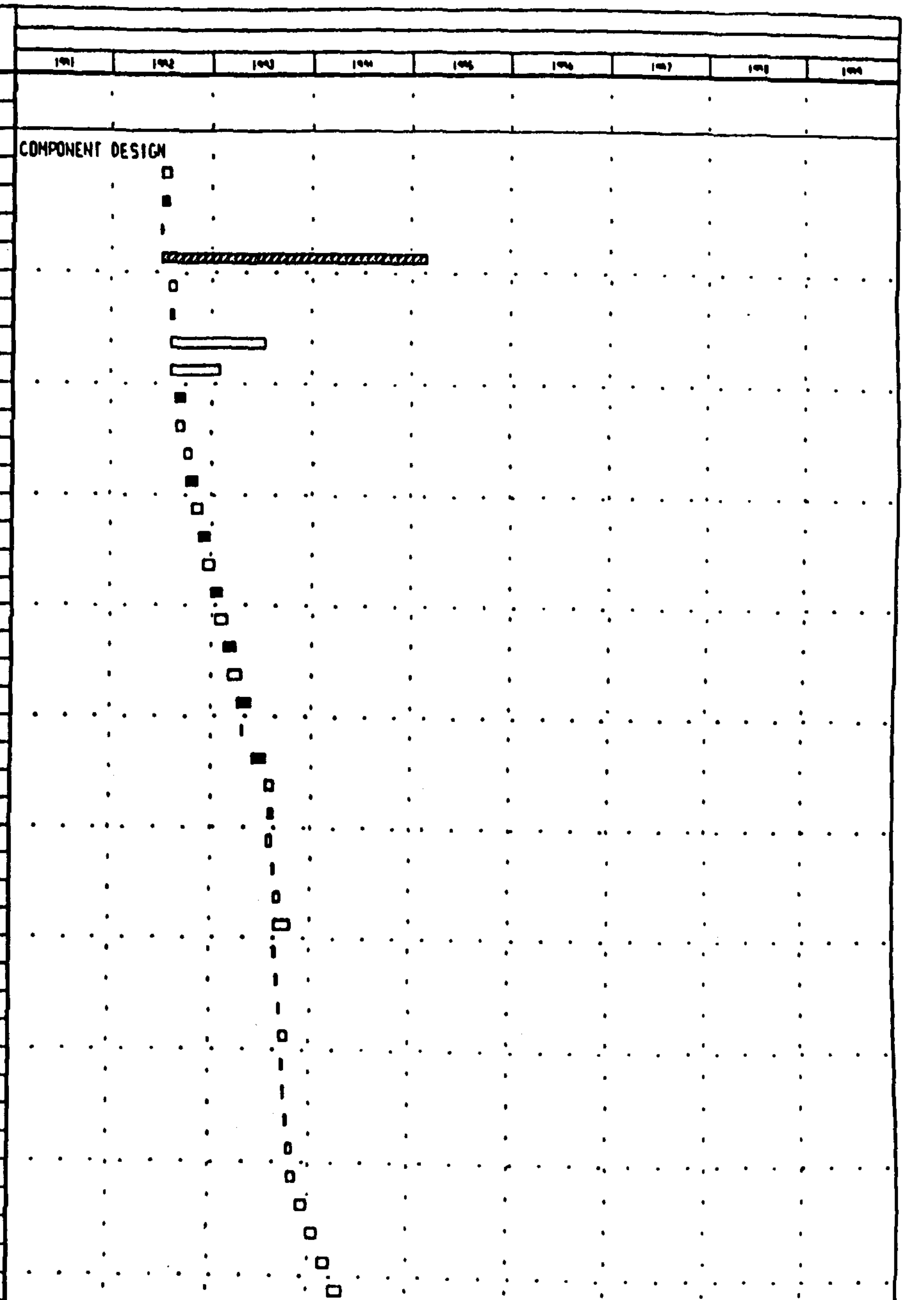

Activity Bar/Early Dates
Critical Activity
Progress Bar

Primavera Systems, Inc.

SOLENOIDAL DETECTOR COLLABORATION
CENTRAL TRACKER REV 1 NETWORKED
FUNCTION BY EARLY START

Sheet 1 of 4

ACTIVITY ID	WBS#	ACTIVITY DESCRIPTION	REM DUR	EARLY START	EARLY FINISH
A614	02090114	CONNECTOR DEVELOPMENT	28	2JUL92	11AUG92
A628	02090204	TVCAMU OR TMC DEVELOPMENT	405	2JUL92	9FEB94
A656	02090214	SUBSTRATE DEVELOPMENT	272	2JUL92	30JUL93
A670	02090304	DRIVER DEVELOPMENT DSGN	203	2JUL92	21APR93
A680	02090403	TRIGGER INTERFACE DEVELOPMENT	135	2JUL92	14JAN93
A602	02090110	HV DECOUPLING CAPACTOR DEVELOPMENT DSGN	28	12AUG92	21SEP92
A608	02090112	HV CABLE DEVELOPMENT	28	12AUG92	21SEP92
A690	02090503	DEVELOP CALIBRATION SYSTEM	203	15JAN93	2NOV93
A664	02090302	SYNCHRONIZER CHIP DEVELOPMENT	180	22APR93	10JAN94
A650	02090212	CONNECTOR DEVELOPMENT	59	6MAY93	30JUL93
A640	02090208	LV DC DEVELOPMENT	13	7FEB94	23FEB94
A622	02090202	P/S/D DEVELOPMENT DSGN	203	24FEB94	13DEC94
A584	02090104	LOW VOLTAGE DEVELOPMENT	89	26OCT94	6MAR95
A592	02090107	HIGH VOLTAGE DEVELOPMENT	89	26OCT94	6MAR95
A634	02090206	DATA COLLECTION CHIP DEVELOPMENT	150	11NOV94	19JUN95
B002	02020001	DESIGN PT STRAW TUBE MODULE (QTY 64 X 1 FT)	0		2JAN91
B010	02020002	DESIGN PT STRAW TUBE MODULE (QTY 240 X 1 M)	61	3JAN91	28MAR91
B040	02020005	SIMULATE PATTERN RECOGNITION-SET 1	250	3JAN91	30DEC91
M001	TARGET	START R&D DESIGN	0	3JAN91	2JAN91
S001	TARGET	R&D DESIGN	947	3JAN91	30SEP94
B050	02020005	SIMULATE DESIGN PARAMETERS-SET 1	230	31JAN91	30DEC91
B038	02020005	SIMULATE TRIGGER RESPONSE	105	1MAR91	31JUL91
B020	02020003	DESIGN PT STRAW TUBE MODULE (QTY 240 X 3 M.)	85	1APR91	31JUL91
B030	02020004	DESIGN PARTIAL SUPERLAYER STRUCTURE	105	1AUG91	31DEC91
B042	02020005	SIMULATE PATTERN RECOGNITION-SET 2	250	31DEC91	22DEC92
B052	02020005	SIMULATE DESIGN PARAMETERS-SET 2	250	31DEC91	22DEC92
B044	02020005	SIMULATE PATTERN RECOGNITION-SET 3	250	23DEC92	21DEC93
B054	02020005	SIMULATE DESIGN PARAMETERS-SET 3	250	23DEC92	21DEC93
B046	02020005	SIMULATE PATTERN RECOGNITION-SET 4	200	22DEC93	5OCT94
B056	02020005	SIMULATE DESIGN PARAMETERS-SET 4	200	22DEC93	5OCT94
M002	TARGET	COMPLETE R&D DESIGN	0	6OCT94	5OCT94
A306	0201020701	INNER TORSION CYLINDER MANDREL DSGN.	44	1OCT92	2DEC92
A312	0201020702	DSGN EXTERNAL SIZING RINGS (QTY 6) TOOL	11	3DEC92	17DEC92
A318	0201020703	DESIGN INSIDE BAND TOOL	8	18DEC92	31DEC92
A436	02020102	MODULE ASSEMBLY AUTOMATION DSGN	125	3FEB93	2AUG93
A444	02020104	MODULE TOOLING DSGN.	250	3FEB93	31JAN94
A330	0201020705	CYLINDER #1, RING #1, TOOLING DSGN.	13	21APR93	7MAY93
A342	0201020707	CYLINDER #2, RING #2, TOOLING DSGN.	12	10MAY93	25MAY93
A354	0201020709	CYLINDER #3, RING #3, TOOLING DSGN.	12	26MAY93	11JUN93
A366	0201020711	CYLINDER #4, RING #4, TOOLING DSGN.	12	14JUN93	29JUN93
A378	0201020713	CYLINDER #5, RING #5, TOOLING DSGN.	12	30JUN93	19JUL93
A052	0201010303	ANTISAG FIXTURE TOOLING DSGN	32	20JUL93	1SEP93
A390	0201020715	CYLINDER #6, RING #6, TOOLING DSGN.	12	20JUL93	4AUG93
A420	0201020720	OUTSIDE TORSION CYLINDER MANDREL DSGN	23	20JUL93	19AUG93
A402	0201020717	CYLINDER #7, RING #7, TOOLING DSGN.	12	5AUG93	20AUG93
A414	0201020719	OUTSIDE BAND TOOLING DSGN	6	16AUG93	23AUG93

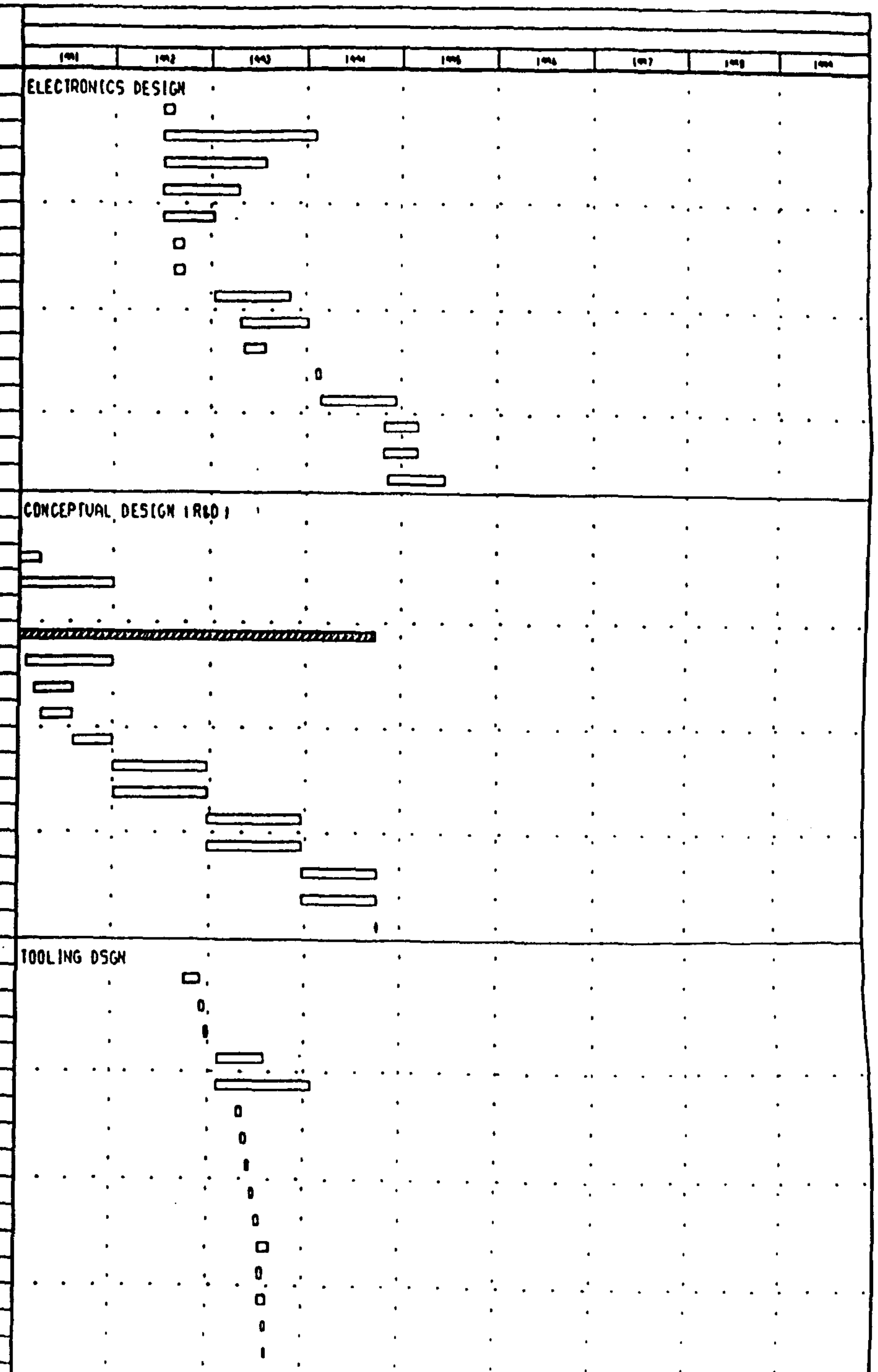

ACTIVITY ID	WBS#	ACTIVITY DESCRIPTION	REM DUR	EARLY START	EARLY FINISH
A048	0201010302	DESIGN ALIGNMENT RIG	40	2SEP93	28OCT93
A560	020801	MOUNTING FIXTURES DSGN	24	2SEP93	6OCT93
A566	020802	DESIGN INSTALLATION TOOLING FIXTURES	23	7OCT93	8NOV93
A034	0201010102	DISC LOCATING TOOLING DSGN	20	14OCT93	10NOV93
A070	0201010502	PLATTEN AND Z-D ADAPTER TOOLING DSGN.	22	14OCT93	12NOV93
A064	0201010405	WINDING MACHINE DSGN	12	29OCT93	15NOV93
A572	020803	DESIGN FINAL TEST EQUIPMENT	17	9NOV93	3DEC93
A044	0201010301	ALIGN MANIPULATOR DSGN.	5	11NOV93	17NOV93
A082	0201010506	CONE PLATTEN TOOLING DSGN	30	15NOV93	29DEC93
A076	0201010504	INTERMEDIATE ADAPTER TOOLING DSGN	22	16NOV93	17DEC93
A324	0201020704	KEYSTONE STYLE #1 TOOLING DSGN	22	16MAY94	15JUN94
A336	0201020706	KEYSTONE STYLE #2 TOOLING DSGN	7	16JUN94	24JUN94
A348	0201020708	KEYSTONE STYLE #3 TOOLING DSGN	7	27JUN94	6JUL94
A360	0201020710	KEYSTONE STYLE #4 TOOLING DSGN	8	7JUL94	18JUL94
A372	0201020712	KEYSTONE STYLE #5 TOOLING DSGN	8	19JUL94	28JUL94
A384	0201020714	KEYSTONE STYLE #6 TOOLING DSGN.	7	29JUL94	8AUG94
A396	0201020716	KEYSTONE STYLE #7 TOOLING DSGN.	7	9AUG94	17AUG94
A408	0201020718	KEYSTONE STYLE #8 TOOLING DSGN	7	18AUG94	26AUG94
A514	020502	DRIFT GAS SUPPLY DSGN.	188	31JUL92	28APR93
A508	020501	DESIGN ELECTRONICS COOLING SYSTEM	125	3FEB93	2AUG93
A504	020403	HOSES DSGN	50	29APR93	12JUL93
A500	020402	FITTINGS DSGN	40	13JUL93	7SEP93
A494	020401	MANIFOLD DSGN.	63	8SEP93	7DEC93
A518	020503	GAS LEAK DETECTION SYSTEM DSGN.	63	21OCT93	21JAN94
A522	020504	INERTING SYSTEM DSGN	63	21OCT93	21JAN94
A080	0201010505	ASSY OUTER SUPPORT CONES QTY 2	40	28NOV95	24JAN96
A074	0201010503	ASSY SUPPORT DISKS INTERMEDIATE QTY 2	35	25JAN96	13MAR96
A490	020302	PREPARE MODULES FOR INSTALLATION IN STRUCTURE	125	22FEB96	20AUG96
M025	TARGET	START FABRICATION	0	1MAR96	29FEB96
S025	TARGET	FABRICATION	398	1MAR96	29SEP97
A068	0201010501	ASSY SUPPORT DISKS Z-D QTY 2	35	14MAR96	2MAY96
A028	0201010101	SETUP OUTER TORSIONAL CYLINDER	10	3MAY96	16MAY96
A032	0201010101	BUILD MODULE SUPPORT STRUCTURE (HAMMOCK)	355	3MAY96	30SEP97
A026	0201010101	INSTALL INNER DISCS IN OUTER TORSIONAL CYL	30	17MAY96	28JUN96
A024	0201010101	INSTALL CONES IN OUTER TORSIONAL CYL.	30	1JUL96	13AUG96
A094	0201020101	INSTALL INNER TORSIONAL CYLINDER IN STRUCTURE	30	14AUG96	25SEP96
A050	0201010302	ASSEMBLE ALIGNMENT RIG	15	4SEP96	25SEP96
A042	0201010202	ALLIGN SEGMENTS	70	26SEP96	7JAN97
A040	0201010201	LOCK SEGMENTS IN STRUCTURE QTY 336	70	3OCT96	14JAN97
A016	0201010101	FINISH MODULE SUPPORT STRUCTURE	0		14JAN97
A492	020303	INSTALL MODULES IN SUPPORT STRUCTURE	120	15JAN97	7JUL97
A512	020501	ASSEMBLE ELECTRONICS COOLING COMPONENTS	90	26FEB97	7JUL97
A564	020801	ASSEMBLY MOUNTING FIXTURES	90	26FEB97	7JUL97
A498	020401	ASSEMBLY MANIFOLD	45	1MAY97	7JUL97
A018	0201010101	CONNECT MANIFOLD TO STRAW TUBE MODULES	60	8JUL97	30SEP97
A020	0201010101	INSTALL MOUNTING FIXTURES ON SUPPORT STRUCTURE	60	8JUL97	30SEP97

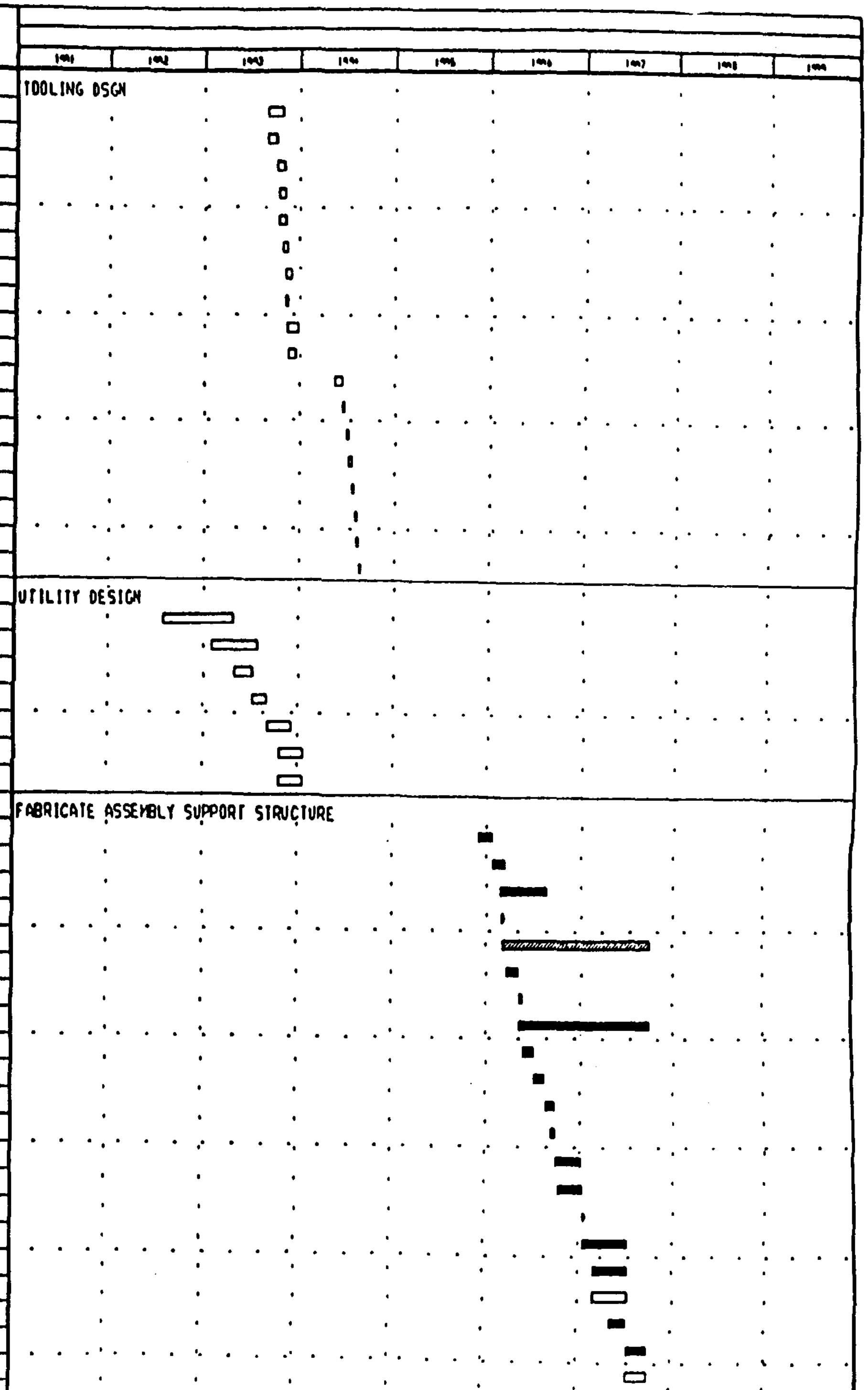

ACTIVITY ID	WBSX	ACTIVITY DESCRIPTION	REM DUR	EARLY START	EARLY FINISH
		FABRICATE ASSEMBLY SUPPORT STRUCTURE			
A022	0201010101	INSTALL ELECTRONIC COOLING SYSTEM	60	8JUL97	30SEP97
		PROTOTYPE / DEVELOPMENT ASSEMBLIES			
B004	02020001	FAB (10) PT STRAW TUBE MODULE (QTY 64 X 1 FT)	105	3JAN91	31MAY91
B012	02020002	FAB (3) PT STRAW TUBE MODULE (QTY 240 X 1 M)	168	3JAN91	30AUG91
B006	02020001	TEST (10) PT STRAW TUBE MODULE (QTY 64 X 1 FT)	231	31JAN91	31DEC91
B014	02020002	TEST (3) PT STRAW TUBE MODULE (QTY 240 X 1 M)	194	24JUN91	31MAR92
B022	02020003	FAB.(2) PT STRAW TUBE MODULE (QTY 240 X 3 M.)	210	2JUL91	30APR92
B024	02020003	TEST (2) PT STRAW TUBE MODULE (QTY 240 X 3 M.)	276	29AUG91	30SEP92
B032	02020004	FAB (10) PARTIAL SUPERLAYER STRUCTURES	170	2JAN92	31AUG92
B034	02020004	TEST (10) PARTIAL SUPERLAYER STRUCTURES	273	1SEP92	30SEP93
B036	02020004	TEST BEAM WITH SUPERLAYER STRUCTURE	255	28DEC92	30DEC93
A432	02020101	PURCH MODULE PROTOTYPES	100	10MAR93	2AUG93
A428	0201020901	PROTOTYPES	200	6APR93	20JAN94
A684	02090403	TRIGGER INTERFACE DEVELOPMENT ASSEMBLY	90	10FEB94	17JUN94
A674	02090304	DRIVER DEVELOPMENT ASSEMBLY	90	20JUN94	25OCT94
		FACILITY SETUP			
A702	02100101	LAYOUT SUPPORT ASSEMBLY FACILITIES	260	29JAN93	9FEB94
A706	02100103	ENGR (SUPERVISION)	260	29JAN93	9FEB94
A708	02100104	DESIGNER (REVISIONS)	260	29JAN93	9FEB94
A710	02100105	TECH (Q A)	260	29JAN93	9FEB94
A722	02100301	LAYOUT ELECTRONIC FACILITIES	260	2MAR93	11MAR94
A724	02100302	ENGR (SUPERVISION)	260	2MAR93	11MAR94
A726	02100303	DESIGNER (REVISIONS)	260	2MAR93	11MAR94
A728	02100304	TECH (ASSEMBLY)	260	2MAR93	11MAR94
A730	02100305	TECH (Q.A.)	260	2MAR93	11MAR94
A712	02100201	LAYOUT MODULE ASSEMBLY FACILITIES	260	29OCT93	8NOV94
A714	02100202	ENGR (SUPERVISION)	260	29OCT93	8NOV94
A716	02100203	DESIGNER (REVISIONS)	260	29OCT93	8NOV94
A718	02100204	TECH (Q A)	260	29OCT93	8NOV94
		FINAL CHECKOUT			
M060	TARGET	START TO PERFORM FINAL CHECKOUT	0	29JAN99	28JAN99
S060	TARGET	PERFORM FINAL CHECKOUT	170	29JAN99	30SEP99
		FACTORY TESTING			
A530	020602	PERFORM TRACKER FUNCTIONAL TEST	84	1OCT97	2FEB98
M030	TARGET	START FACTORY TESTING	0	1OCT97	30SEP97
S030	TARGET	FACTORY TESTING	84	1OCT97	2FEB98
		INSTALLATION			
M050	TARGET	START INSTALLATION OF TRACKER	0	11MAY98	8MAY98
S050	TARGET	ASSEMBLE TRACKER PARTS FOR INSTALLATION IN COIL	58	11MAY98	31JUL98
M052	TARGET	START INSTALL TRACKER IN COIL	0	3AUG98	31JUL98
S052	TARGET	INSTALL TRACKER IN COIL	21	3AUG98	31AUG98
		MANUFACTURE SUPPORT STRUCTURE COMPONENTS			
A304	0201020601	OUTSIDE TORSIONAL CYLINDER ASSEMBLY	90	26JAN94	2JUN94
A258	0201020501	ALIGNMENT SEGMENT, STYLE 1, QTY 5X6 ASSEMBLY	30	14FEB94	25MAR94
A694	02090503	ASSEMBLE CALIBRATION SYSTEM	84	14MAR94	12JUL94
A264	0201020502	ALIGNMENT SEGMENT, STYLE 2, QTY 6X6 ASSEMBLY	30	28MAR94	9MAY94
A270	0201020503	ALIGNMENT SEGMENT, STYLE 3, QTY 7X6 ASSEMBLY	30	10MAY94	21JUN94
A316	0201020702	EXTERNAL SIZING RINGS (QTY 6) ASSEMBLY	60	3JUN94	26AUG94

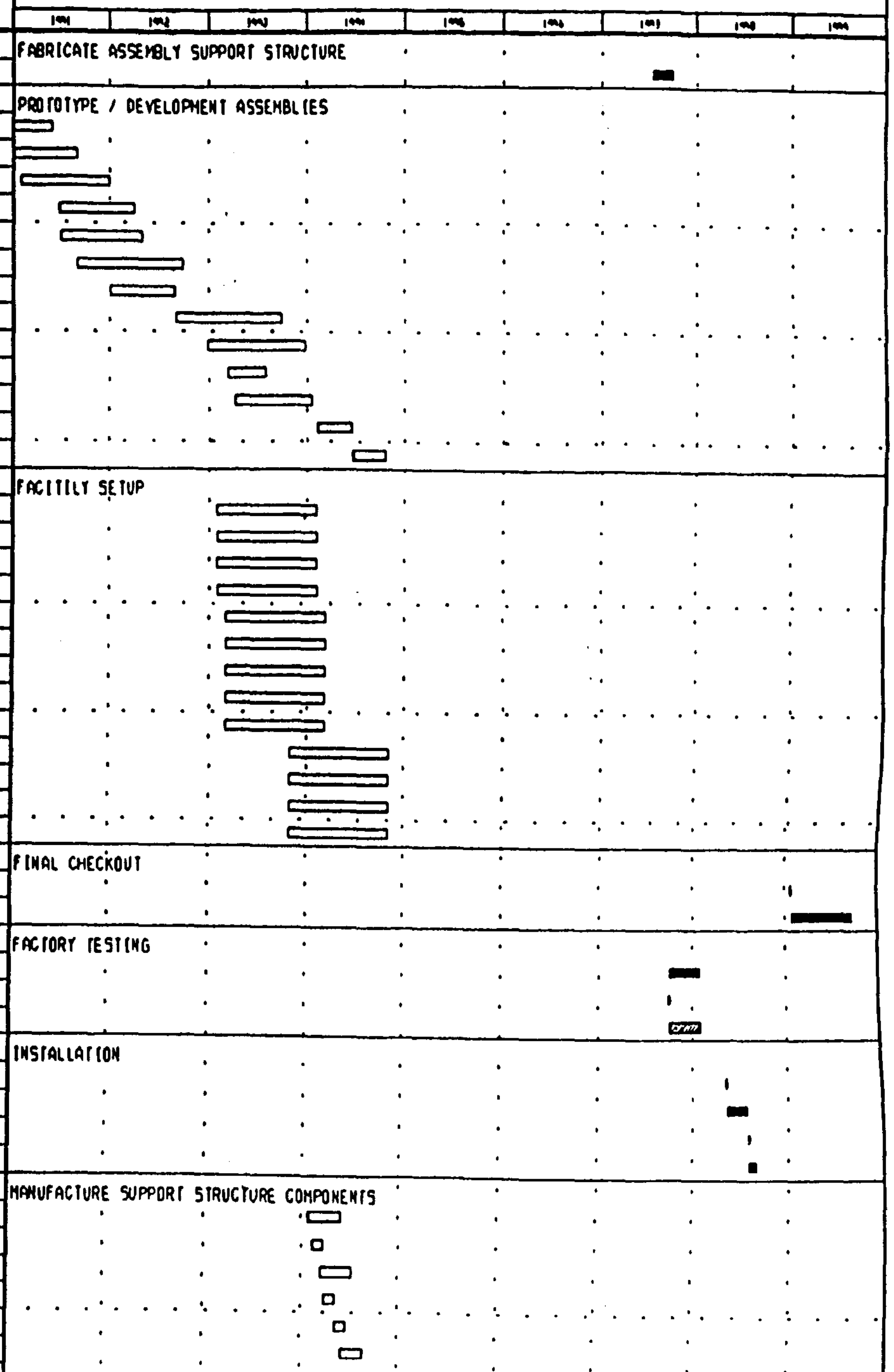

ACTIVITY ID	WBS	ACTIVITY DESCRIPTION	REM DUR	EARLY START	EARLY FINISH
A148	0201020301	CONES INSIDE BAND QTY 4 ASSEMBLY	5	13JUN94	17JUN94
A154	0201020302	CYLINDER #1 (QTY 2) ASSEMBLY	19	20JUN94	15JUL94
A276	0201020504	ALIGNMENT SEGMENT, STYLE 4, QTY 8X6 ASSEMBLY	30	22JUN94	3AUG94
M020	TARGET	START MANUFACTURING	0	1JUL94	30JUN94
S020	TARGET	MANUFACTURING	712	1JUL94	29APR97
A100	0201020201	KEYSTONE STYLE #1 ASSEMBLY	16	11JUL94	1AUG94
A160	0201020303	CYLINDER #2 (QTY 2) ASSEMBLY	22	18JUL94	16AUG94
A202	0201020401	DISKS INSIDE BAND (QTY 2) ASSEMBLY	2	19JUL94	20JUL94
A208	0201020402	RING #1 (QTY 4) ASSEMBLY	19	21JUL94	16AUG94
A106	0201020202	KEYSTONE STYLE #2 ASSEMBLY	19	2AUG94	26AUG94
A282	0201020505	ALIGNMENT SEGMENT, STYLE 5, QTY 9X6 ASSEMBLY	30	4AUG94	15SEP94
A214	0201020403	RING #2 (QTY 4) ASSEMBLY	22	17AUG94	16SEP94
A166	0201020304	CYLINDER #3 (QTY 2) ASSEMBLY	26	25AUG94	30SEP94
A112	0201020203	KEYSTONE STYLE #3 ASSEMBLY	22	29AUG94	28SEP94
A322	0201020703	INSIDE BAND ASSEMBLY	60	29AUG94	21NOV94
A288	0201020506	ALIGNMENT SEGMENT, STYLE 6, QTY 10X6 ASSY	24	16SEP94	19OCT94
A172	0201020305	CYLINDER #4 (QTY 2) ASSEMBLY	29	3OCT94	10NOV94
A294	0201020507	ALIGNMENT SEGMENT, STYLE 7, QTY 11X6 ASSY	30	20OCT94	2DEC94
A654	02090213	MFG SUBSTRATE FOR ELECTRONICS	120	26OCT94	19APR95
A178	0201020306	CYLINDER #5 (QTY 2) ASSEMBLY	32	15NOV94	4JAN95
A118	0201020204	KEYSTONE STYLE #4 ASSEMBLY	25	17NOV94	27DEC94
A220	0201020404	RING #3 (QTY 4) ASSEMBLY	.26	27DEC94	1FEB95
A184	0201020307	CYLINDER #6 (QTY 2) ASSEMBLY	35	5JAN95	22FEB95
A124	0201020205	KEYSTONE STYLE #5 ASSEMBLY	29	6FEB95	16MAR95
A190	0201020308	CYLINDER #7 (QTY 2) ASSEMBLY	39	6MAR95	28APR95
A130	0201020206	KEYSTONE STYLE #6 ASSEMBLY	32	26APR95	9JUN95
A226	0201020405	RING #4 (QTY 4) ASSEMBLY	29	4MAY95	14JUN95
A232	0201020406	RING #5 (QTY 4) ASSEMBLY	32	15JUN95	1AUG95
A196	0201020309	CONES OUTSIDE BAND QTY 4 ASSEMBLY	6	28JUN95	7JUL95
A136	0201020207	KEYSTONE STYLE #7 ASSEMBLY	35	17JUL95	1SEP95
A238	0201020407	RING #6 (QTY 4) ASSEMBLY	33	2AUG95	18SEP95
A244	0201020408	RING #7 (QTY 4) ASSEMBLY	39	19SEP95	10NOV95
A142	0201020208	KEYSTONE STYLE #8 ASSEMBLY	38	3OCT95	27NOV95
A250	0201020409	DISKS OUTSIDE BAND (QTY 2) ASSEMBLY	3	13NOV95	15NOV95
A088	0201010508	PRE-INSTALL ALIGN. SEGMENTS ON RINGS & CONES	21	18APR96	16MAY96
A476	0202030605	GAS CONNECTION	100	24FEB94	18JUL94
A478	0202030606	H V CONNECTION	100	24FEB94	18JUL94
A454	02020204	LOCATING KEY MOUNTS	100	20JUN94	8NOV94
A462	02020303	WIRE SUPPORT	180	1JUL94	20MAR95
A484	02020402	POGO STICK	90	1JUL94	7NOV94
A482	02020401	POGO PLATE	90	5JUL94	8NOV94
A468	0202030601	WIRE TENSION PLATE	180	19JUL94	5APR95
A448	02020201	GRAPHITE SHELL	180	14SEP94	1JUN95
A442	02020103	ASSEMBLE MODULES	450	9NOV94	23AUG96
A426	0201020801	DESIGN REVIEW	21	22DEC92	22JAN93

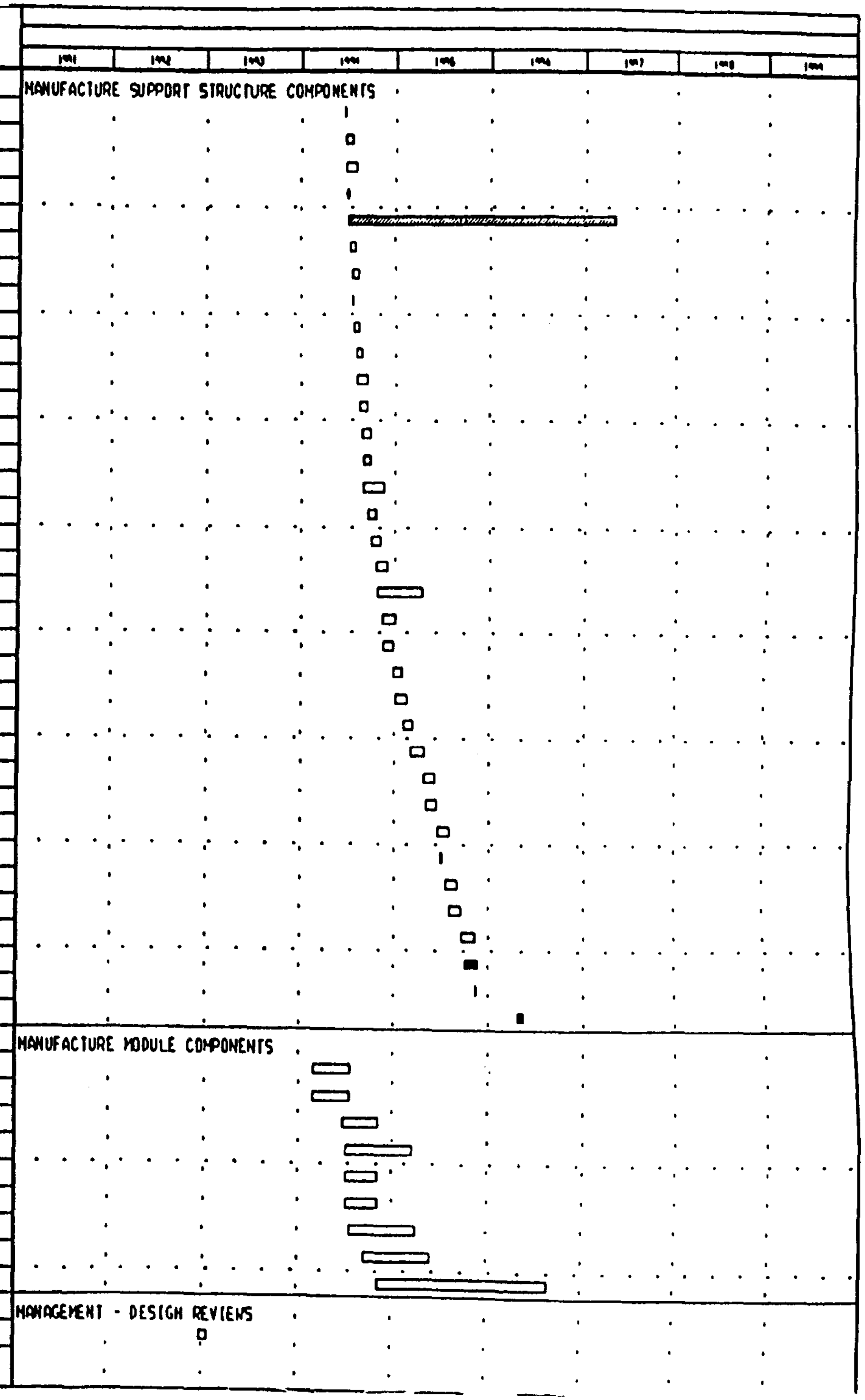

ACTIVITY ID	WBSX	ACTIVITY DESCRIPTION	REM DUR	EARLY START	EARLY FINISH
		OPERATION-TURN IT ON			
M065	TARGET	START DETECTOR TURN ON	0	1OCT99	30SEP99
S065	TARGET	DETECTOR TURN ON	1	1OCT99	1OCT99
		FINAL PLUMBING & CABLING			
M055	TARGET	START FINAL PLUMBING AND CABLING	0	1SEP98	31AUG98
S055	TARGET	FINAL PLUMBING AND CABLING	103	1SEP98	28JAN99
		PURCHASE ELECTRONIC COMPONENTS			
A646	02090210	PURCH.DRIVER FOR READOUT SIGNALS	130	23MAY93	29SEP93
A644	02090209	PURCH.RECEIVER - (FAST AND SLOW)	130	30SEP93	6FEB94
A604	02090110	PURCH HV DECOUPLING CAPACITOR DEVELOPMENT	130	1OCT93	7FEB94
A610	02090112	PURCH HV CABLE DEVELOPMENT	130	1OCT93	7FEB94
A668	02090303	PURCH DRIVER FOR TRIGGER SIGNALS OUT AND CABLE	130	1OCT93	7FEB94
A676	02090401	PURCH LEVEL 1 INTERFACE	130	1OCT93	7FEB94
A682	02090403	PURCH TRIGGER INTERFACE DEVELOPMENT	120	13OCT93	9FEB94
A648	02090211	PURCH CONNECTOR FOR INPUT SIGNALS	130	17OCT93	23FEB94
A692	02090503	PURCH CALIBRATION SYSTEM	130	3NOV93	12MAR94
A574	020803	PURCH.FINAL TEST EQUIPMENT	30	4DEC93	2JAN94
A666	02090302	PURCH.SYNCHRONIZER CHIP DEVELOPMENT	170	11JAN94	29JUN94
A600	02090109	PURCH HV DECOUPLING CAPACITORS	130	8FEB94	17JUN94
A606	02090111	PURCH HV CABLES ON END OF CHAMBER	130	8FEB94	17JUN94
A678	02090402	PURCH LEVEL 2 INTERFACE	130	8FEB94	17JUN94
A630	02090204	PURCH TVCAMU OR TMC DEVELOPMENT	170	10FEB94	29JUL94
A672	02090304	PURCH DRIVER DEVELOPMENT	120	20FEB94	19JUN94
A642	02090208	PURCH LV DC DEVELOPMENT	130	24FEB94	3JUL94
A598	02090108	PURCH.RESISTORS	130	18JUN94	25OCT94
A658	02090214	PURCH.SUBSTRATE	120	28JUN94	25OCT94
A632	02090205	PURCH DATA COLLECTION CHIP (1-2 PER 256 CHANNELS	170	30JUN94	16DEC94
A638	02090207	PURCH LOW VOLTAGE DECOUPLING CAPACITORS	130	4JUL94	10NOV94
A688	02090502	PURCH DISTRIBUTION FOR CALIBRATION	130	13JUL94	19NOV94
A626	02090203	PURCH TVCAMU OR TMC (4 - 8 CHANNELS PER CHIP)	170	30JUL94	15JAN95
A686	02090501	PURCH PULSERS	130	20NOV94	29MAR95
A624	02090202	PURCH P/S/D DEVELOPMENT	130	14DEC94	22APR95
A612	02090113	PURCH CONNECTORS	130	25FEB95	4JUL95
A586	02090104	PURCH.LOW VOLTAGE DEVELOPMENT	130	7MAR95	14JUL95
A594	02090107	PURCH.HIGH VOLTAGE DEVELOPMENT	120	7MAR95	4JUL95
A636	02090206	PURCH DATA COLLECTION CHIP	170	20JUN95	6DEC95
A590	02090106	PURCH HV DISTRIBUTION TO DETECTOR	130	5JUL95	11NOV95
A578	02090102	PURCH LV DISTRIBUTION TO DETECTOR	130	15JUL95	21NOV95
A580	02090103	PURCH LV DISTRIBUTION ON DETECTOR	130	15JUL95	21NOV95
A588	02090105	PURCH HV SUPPLIES	130	12NOV95	20MAR96
A576	02090101	PURCH LV SUPPLIES	130	22NOV95	30MAR96
A620	02090201	PURCH PREAMP, SHPR, & DISCRIM (4 - 8 CHANNELS)	130	16MAR96	23JUL96
		PURCHASE SUPPORT STRUCTURE			
A320	0201020703	PURCH. INSIDE BAND	10	28APR93	7MAY93
A152	0201020302	PURCH CYLINDER #1 (QTY 2)	130	29APR93	5SEP93
A332	0201020705	PURCH CYLINDER #1, RING #1, TOOLING	10	8MAY93	17MAY93
A302	0201020601	PURCH OUTSIDE TORSIONAL CYLINDER	190	20JUL93	25JAN94
A368	0201020711	PURCH CYLINDER #4, RING #4, TOOLING	10	23JUL93	1AUG93
A380	0201020713	PURCH CYLINDER #5, RING #5, TOOLING	10	2AUG93	11AUG93

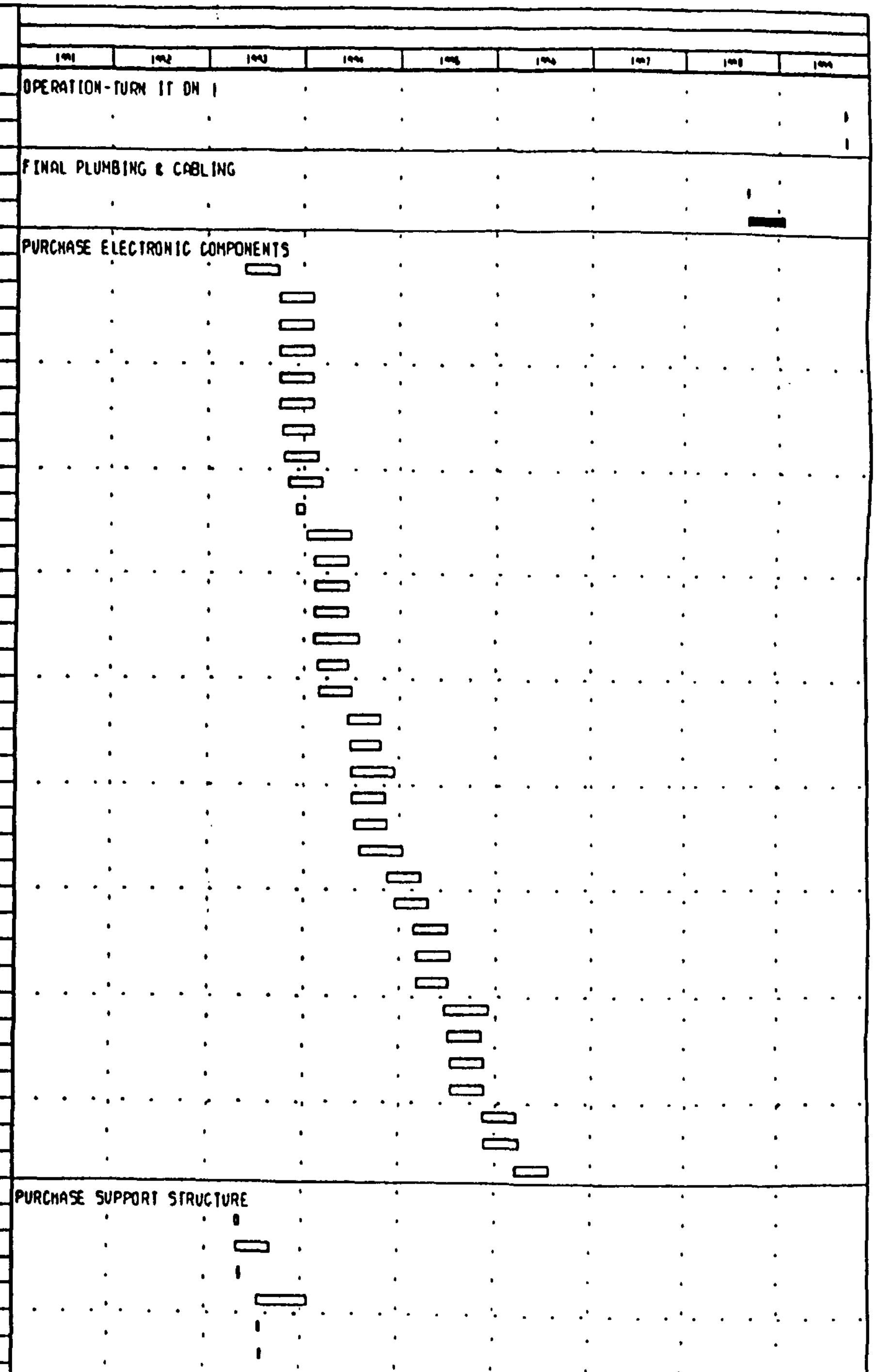

ACTIVITY ID	WBS	ACTIVITY DESCRIPTION	REM DUR	EARLY START	EARLY FINISH
A344	0201020707	PURCH CYLINDER #2, RING #2, TOOLING	10	3AUG93	12AUG93
A392	0201020715	PURCH CYLINDER #6, RING #6, TOOLING	10	12AUG93	21AUG93
A098	0201020201	PURCH KEYSTONE STYLE #1	130	21AUG93	28DEC93
A404	0201020717	PURCH CYLINDER #7, RING #7, TOOLING	10	22AUG93	31AUG93
A422	0201020720	PURCH OUTSIDE TORSION CYLINDER MANDREL	30	1SEP93	30SEP93
A158	0201020303	PURCH CYLINDER #2 (QTY 2)	130	6SEP93	13JAN94
A056	0201010401	PURCH.MANIPULATOR	140	1OCT93	17FEB94
A058	0201010402	PURCH.POSITION CONTROL	140	1OCT93	17FEB94
A060	0201010403	PURCH LASER INTERFEROMETER /TELESCOPE	140	1OCT93	17FEB94
A086	0201010507	PURCH ADHESIVE	10	1OCT93	10OCT93
A200	0201020401	PURCH DISKS INSIDE BAND (QTY 2)	60	1OCT93	29NOV93
A256	0201020501	PURCH ALIGNMENT SEGMENT, STYLE 1, QTY 5X6	35	1OCT93	4NOV93
M010	TARGET	START PROCUREMENT ACTIVITIES	0	1OCT93	30SEP93
S010	TARGET	PROCUREMENT ACTIVITIES	1176	1OCT93	19DEC96
A562	020801	PURCH MOUNTING FIXTURES	30	7OCT93	5NOV93
A092	0201020101	PURCH. INNER TORSIONAL CYLINDER	290	21OCT93	6AUG94
A356	0201020709	PURCH.CYLINDER #3, RING #3, TOOLING	10	29OCT93	7NOV93
A262	0201020502	PURCH ALIGNMENT SEGMENT, STYLE 2, QTY 6X6	35	5NOV93	9DEC93
A568	020802	PURCH INSTALLATION TOOLING FIXTURES	20	9NOV93	28NOV93
A036	0201010102	PURCH DISC LOCATING TOOLING	130	11NOV93	20MAR94
A038	0201010103	PURCH ADHESIVE	10	11NOV93	20NOV93
A072	0201010502	PURCH PLATTEN AND 2-D ADAPTER TOOLS	130	13NOV93	22MAR94
A066	0201010405	PURCH WINDING MACHINE	130	16NOV93	25MAR94
A510	020501	PURCH.ELECTRONICS COOLING	180	20NOV93	18MAY94
A206	0201020402	PURCH.RING #1 (QTY 4)	130	30NOV93	8APR94
A496	020401	PURCH MANIFOLD	180	8DEC93	5JUN94
A268	0201020503	PURCH ALIGNMENT SEGMENT, STYLE 3, QTY 7X6	35	10DEC93	13JAN94
A078	0201010504	PURCH INTERMEDIATE ADAPTER TOOLS	130	18DEC93	26APR94
A506	020403	PURCH HOSES	60	26DEC93	23FEB94
A084	0201010506	PURCH CONE PLATTEN TOOLS	130	30DEC93	8MAY94
A164	0201020304	PURCH CYLINDER #3 (QTY 2)	130	14JAN94	23MAY94
A274	0201020504	PURCH ALIGNMENT SEGMENT, STYLE 4, QTY 8X6	35	14JAN94	17FEB94
A298	0201020508	PURCH.ALIGNMENT FASTENERS QTY 336X4	40	14JAN94	22FEB94
A516	020502	PURCH.DRIFT GAS SUPPLY	130	22JAN94	31MAY94
A520	020503	PURCH GAS LEAK DETECTION SYSTEM	130	22JAN94	31MAY94
A524	020504	PURCH INERTING SYSTEM	130	22JAN94	31MAY94
A308	0201020701	PURCH INNER TORSION CYLINDER MANDREL	60	26JAN94	26MAR94
A104	0201020202	PURCH KEYSTONE STYLE #2	130	31JAN94	9JUN94
A280	0201020505	PURCH ALIGNMENT SEGMENT, STYLE 5, QTY 9X6	35	18FEB94	24MAR94
A286	0201020506	PURCH ALIGNMENT SEGMENT, STYLE 6, QTY 10X6	40	25MAR94	3MAY94
A314	0201020702	PURCH EXTERNAL SIZING RINGS (QTY 6)	15	27MAR94	10APR94
A212	0201020403	PURCH.RING #2 (QTY 4)	130	9APR94	16AUG94
A146	0201020301	PURCH.CONES INSIDE BAND QTY 4	60	14APR94	12JUN94
A110	0201020203	PURCH KEYSTONE STYLE #3	130	21APR94	28AUG94
A292	0201020507	PURCH ALIGNMENT SEGMENT, STYLE 7, QTY 11X6	35	4MAY94	7JUN94
A720	02100205	PURCH CLEAN ROOM	170	23MAY94	8NOV94
A170	0201020305	PURCH CYLINDER #4 (QTY 2)	130	24MAY94	30SEP94
A326	0201020704	PURCH KEYSTONE STYLE #1 TOOLING	20	16JUN94	5JUL94

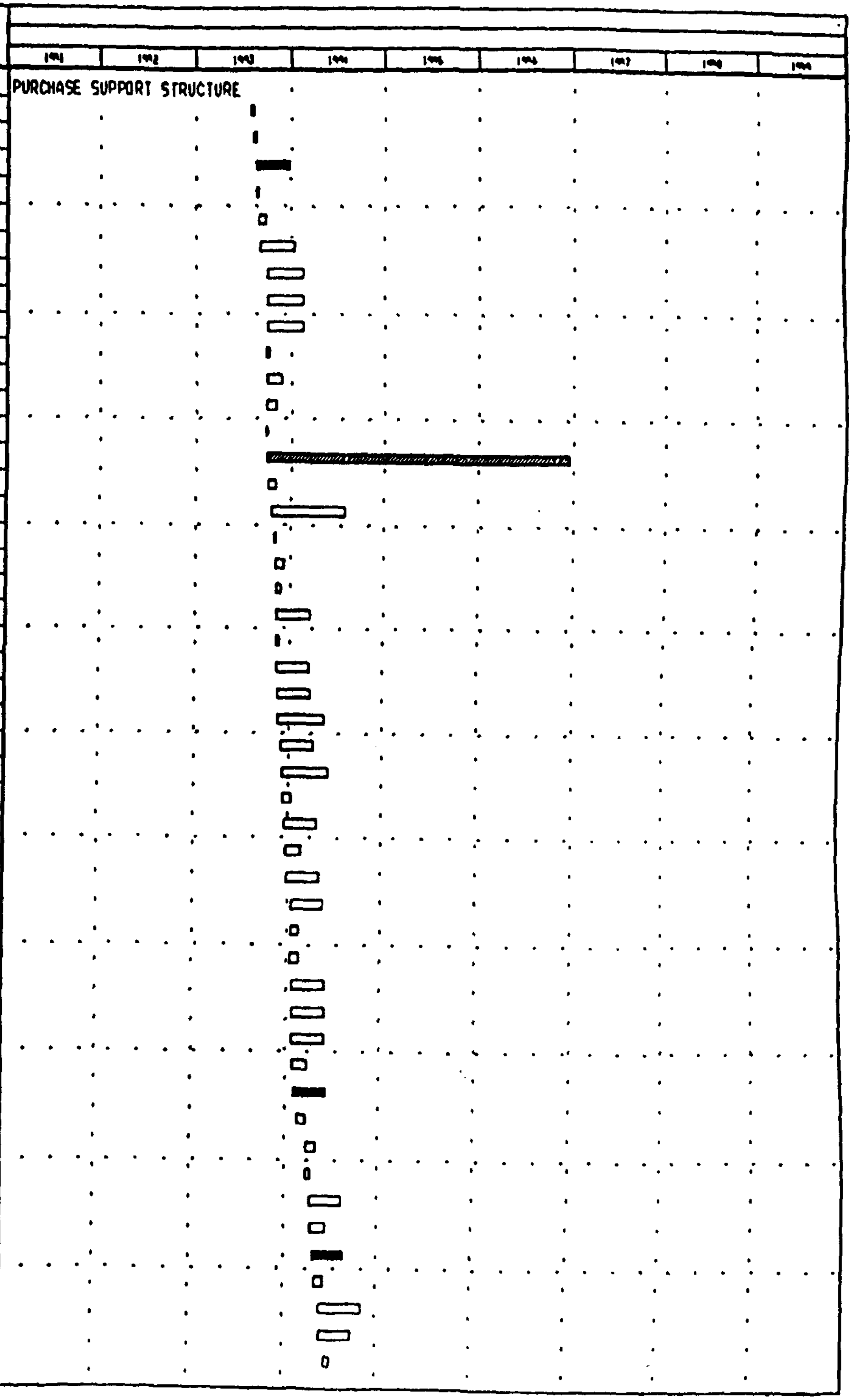

ACTIVITY ID	WBS#	ACTIVITY DESCRIPTION	REM DUR	EARLY START	EARLY FINISH
A338	0201020706	PURCH KEYSTONE STYLE #2 TOOLING	20	6JUL94	25JUL94
A176	0201020306	PURCH CYLINDER #5 (QTY 2)	130	8JUL94	14NOV94
A116	0201020204	PURCH KEYSTONE STYLE #4	130	10JUL94	16NOV94
A350	0201020708	PURCH KEYSTONE STYLE #3 TOOLING	15	26JUL94	9AUG94
A362	0201020710	PURCH KEYSTONE STYLE #4 TOOLING	15	10AUG94	24AUG94
A218	0201020404	PURCH RING #3 (QTY 4)	130	17AUG94	24DEC94
A182	0201020307	PURCH.CYLINDER #6 (QTY 2)	130	22AUG94	29DEC94
A374	0201020712	PURCH.KEYSTONE STYLE #5 TOOLING	15	25AUG94	8SEP94
A386	0201020714	PURCH KEYSTONE STYLE #6 TOOLING	15	9SEP94	23SEP94
A398	0201020716	PURCH KEYSTONE STYLE #7 TOOLING	15	24SEP94	8OCT94
A122	0201020205	PURCH KEYSTONE STYLE #5	130	28SEP94	4FEB95
A410	0201020718	PURCH KEYSTONE STYLE #8 TOOLING	15	9OCT94	23OCT94
A188	0201020308	PURCH CYLINDER #7 (QTY 2)	130	26OCT94	4MAR95
A128	0201020206	PURCH KEYSTONE STYLE #6	130	17DEC94	25APR95
A224	0201020405	PURCH RING #4 (QTY 4)	130	25DEC94	3MAY95
A230	0201020406	PURCH.RING #5 (QTY 4)	130	25DEC94	3MAY95
A416	0201020719	PURCH.OUTSIDE BAND TOOLING	10	9JAN95	18JAN95
A236	0201020407	PURCH RING #6 (QTY 4)	130	8FEB95	17JUN95
A134	0201020207	PURCH KEYSTONE STYLE #7	130	7MAR95	14JUL95
A242	0201020408	PURCH RING #7 (QTY 4)	130	25MAR95	1AUG95
A194	0201020309	PURCH CONES OUTSIDE BAND QTY 4	60	29APR95	27JUN95
A140	0201020208	PURCH KEYSTONE STYLE #8	130	26MAY95	2OCT95
A248	0201020409	PURCH DISKS OUTSIDE BAND (QTY 2)	60	2AUG95	30SEP95
A054	0201010303	PURCH.ANTISAG FIXTURE TOOLING	170	15NOV95.	2MAY96
A526	020601	PURCH.TEST EQUIPMENT	140	15DEC95	2MAY96
A502	020402	PURCH FITTINGS	60	2MAR97	30APR97
A438	02020102	PURCH MODULE MFG SYSTEM	90	3AUG93	31OCT93
A450	02020202	PURCH SHELL GLUE	60	1OCT93	29NOV93
A458	02020301	PURCH STRAW TUBES	260	1OCT93	17JUN94
A464	02020304	PURCH WIRE	140	1OCT93	17FEB94
A470	0202030602	PURCH SOLDER CLIP	140	1OCT93	17FEB94
A472	0202030603	PURCH.RESISTOR TERMINATION	140	1OCT93	17FEB94
A474	0202030604	PURCH.END PLATE GLUE	130	1OCT93	7FEB94
A534	020701	PURCH SHIPPING SUPPORT	60	21OCT96	19DEC96
A540	020702	PURCH SHIPPING CONTAINER	100	15JUN97	22SEP97
A546	020703	PURCH ATMOSPHERE SYSTEM FOR SHIPMENT	15	8SEP97	22SEP97
A552	020704	PURCH FREIGHT	40	3FEB98	14MAR98
A544	020703	DESIGN SHIPPING ATMOSPHERE SYSTEM	6	28AUG97	4SEP97
A536	020701	ASSEMBLE SHIPPING SUPPORT	90	23SEP97	2FEB98
A542	020702	ASSEMBLE SHIPPING CONTAINER	90	23SEP97	2FEB98
A548	020703	ASSEMBLE ATMOSPHERE SYSTEM	90	23SEP97	2FEB98
A550	020704	DETERMINE FREIGHT	30	18DEC97	2FEB98
A554	020705	PREPARE TRACKER FOR SHIPMENT	42	3FEB98	2APR98
M035	TARGET	START TO PREPARE TRACKER FOR SHIPMENT	0	3FEB98	2FEB98
S035	TARGET	PREPARE TRACKER FOR SHIPMENT	42	3FEB98	2APR98

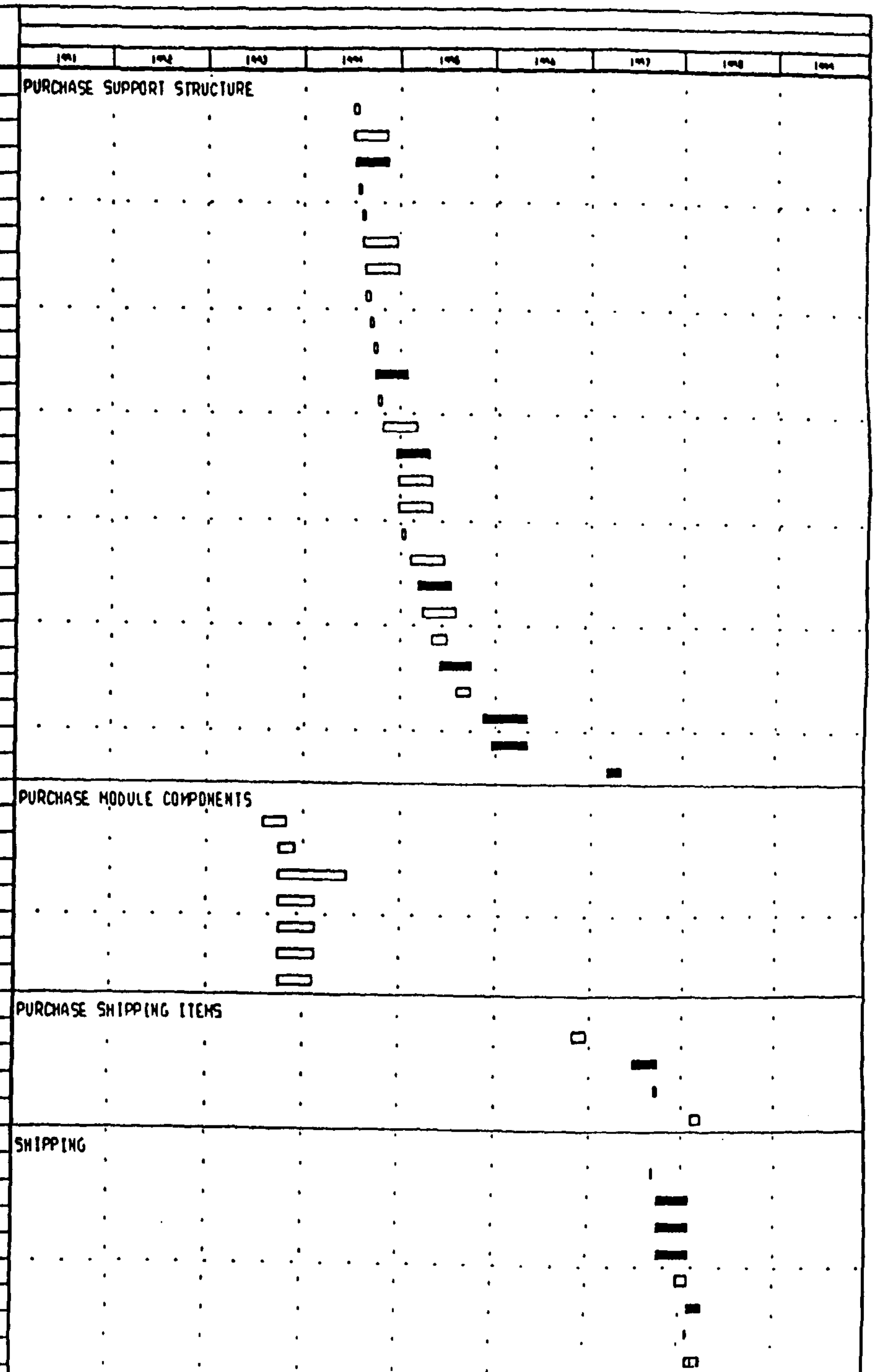

ACTIVITY ID	WBS	ACTIVITY DESCRIPTION	REM DUR	EARLY START	EARLY FINISH
A558	020705	SHIP TRACKER	21	3APR98	1MAY98
M040	TARGET	START SHIPMENT TRACKER	0	3APR98	2APR98
S040	TARGET	SHIP TRACKER	21	3APR98	1MAY98
A334	0201020705	CYLINDER #1, RING #1, TOOLING ASSEMBLY	60	18MAY93	12AUG93
A346	0201020707	CYLINDER #2, RING #2, TOOLING ASSEMBLY	60	13AUG93	5NOV93
A424	0201020720	OUTSIDE TORSION CYLINDER MANDREL ASSEMBLY	90	1OCT93	9FEB94
A452	02020203	MANDRELS (16)	180	1OCT93	17JUN94
A460	02020302	STRAW INSERTION MACHINE	180	1OCT93	17JUN94
A466	02020305	WIRE INSERTION MACHINE	180	1OCT93	17JUN94
A486	02020403	POGO STICK ASSEMBLY TOOLING	100	1OCT93	23FEB94
A488	020301	MODULE INSERTION TOOLING	90	1OCT93	9FEB94
A704	02100102	RESIN CURING OVEN	90	1OCT93	9FEB94
M015	TARGET	START TOOLING FABRICATION	0	1OCT93	30SEP93
S015	TARGET	TOOLING FABRICATION	503	1OCT93	29SEP95
A480	0202030607	END PLATE ASSEMBLY TOOLING	90	15OCT93	23FEB94
A440	02020102	ASSEMBLE MODULE MFG SYSTEM	90	1NOV93	10MAR94
A358	0201020709	CYLINDER #3, RING #3, TOOLING ASSEMBLY	60	8NOV93	3FEB94
A046	0201010301	ALIGN MANIPULATOR ASSEMBLY	5	18NOV93	26NOV93
A062	0201010404	ADJUSTMENT TOOLING	99	24NOV93	19APR94
A570	020802	ASSEMBLE INSTALLATION TOOLING FIXTURES	90	24NOV93	6APR94
A456	02020205	LOCATING FIXTURE	100	27JAN94	17JUN94
A446	02020104	MODULE TOOLING ASSEMBLY	100	1FEB94	22JUN94
A370	0201020711	CYLINDER #4, RING #4, TOOLING ASSEMBLY	60	4FEB94	29APR94
A310	0201020701	INNER TORSION CYLINDER MANDREL ASSEMBLY	90	28MAR94	3AUG94
A382	0201020713	CYLINDER #5, RING #5, TOOLING ASSEMBLY	60	2MAY94	26JUL94
A328	0201020704	KEYSTONE STYLE #1 TOOLING ASSEMBLY	60	6JUL94	28SEP94
A394	0201020715	CYLINDER #6, RING #6, TOOLING ASSEMBLY	60	27JUL94	19OCT94
A340	0201020706	KEYSTONE STYLE #2 TOOLING ASSEMBLY	60	29SEP94	27DEC94
A406	0201020717	CYLINDER #7, RING #7, TOOLING ASSEMBLY	60	20OCT94	18JAN95
A352	0201020708	KEYSTONE STYLE #3 TOOLING ASSEMBLY	60	27OCT94	25JAN95
A364	0201020710	KEYSTONE STYLE #4 TOOLING ASSEMBLY	60	28NOV94	22FEB95
A376	0201020712	KEYSTONE STYLE #5 TOOLING ASSEMBLY	60	28DEC94	22MAR95
A418	0201020719	OUTSIDE BAND TOOLING ASSEMBLY	60	19JAN95	13APR95
A388	0201020714	KEYSTONE STYLE #6 TOOLING ASSEMBLY	60	26JAN95	20APR95
A400	0201020716	KEYSTONE STYLE #7 TOOLING ASSEMBLY	60	23FEB95	18MAY95
A412	0201020718	KEYSTONE STYLE #8 TOOLING ASSEMBLY	60	23MAR95	16JUN95
M045	TARGET	START UNPACK AND TEST TRACKER	0	4MAY98	1MAY98
S045	TARGET	UNPACK TRACKER	5	4MAY98	8MAY98

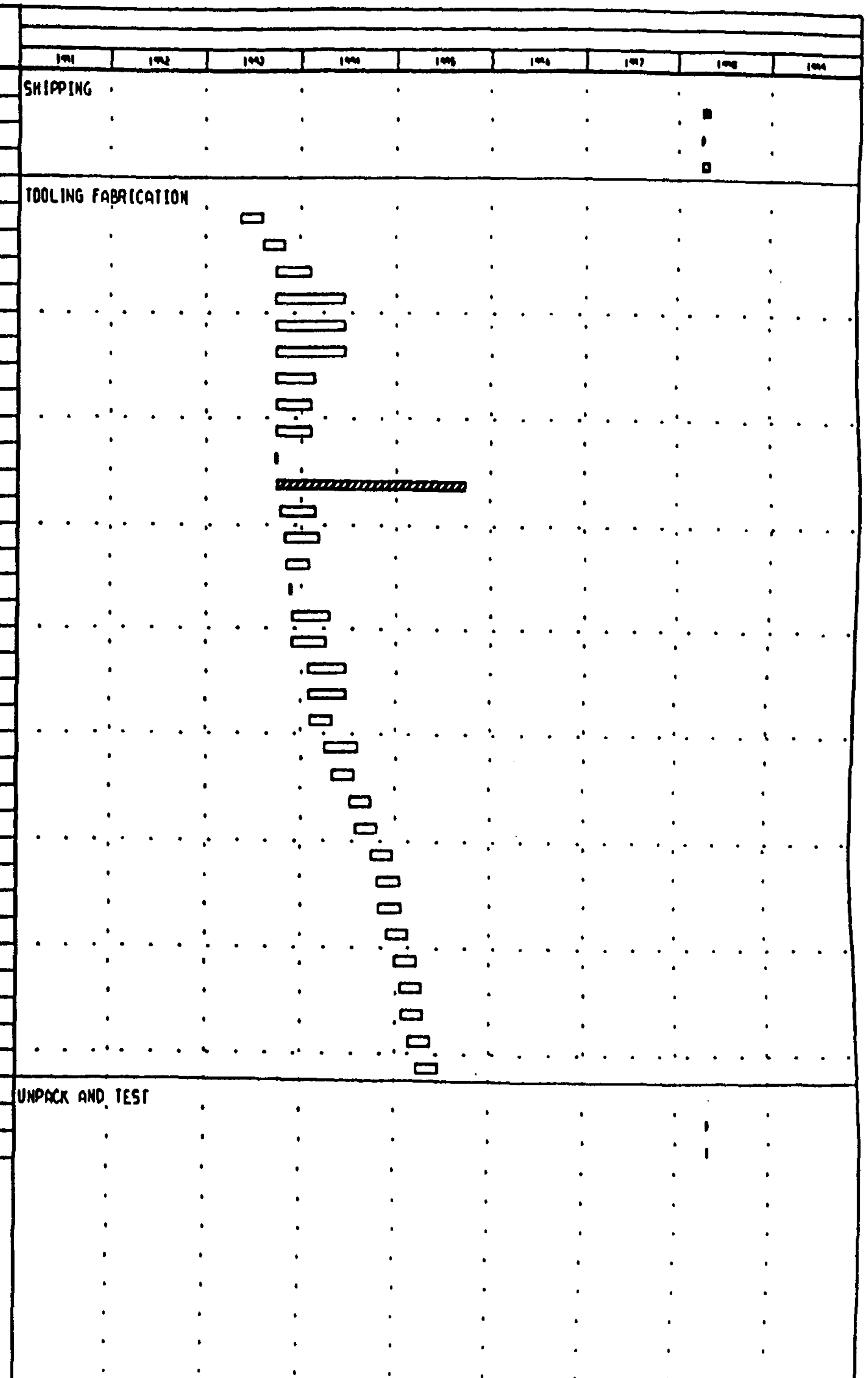

LOGIC DIAGRAMS

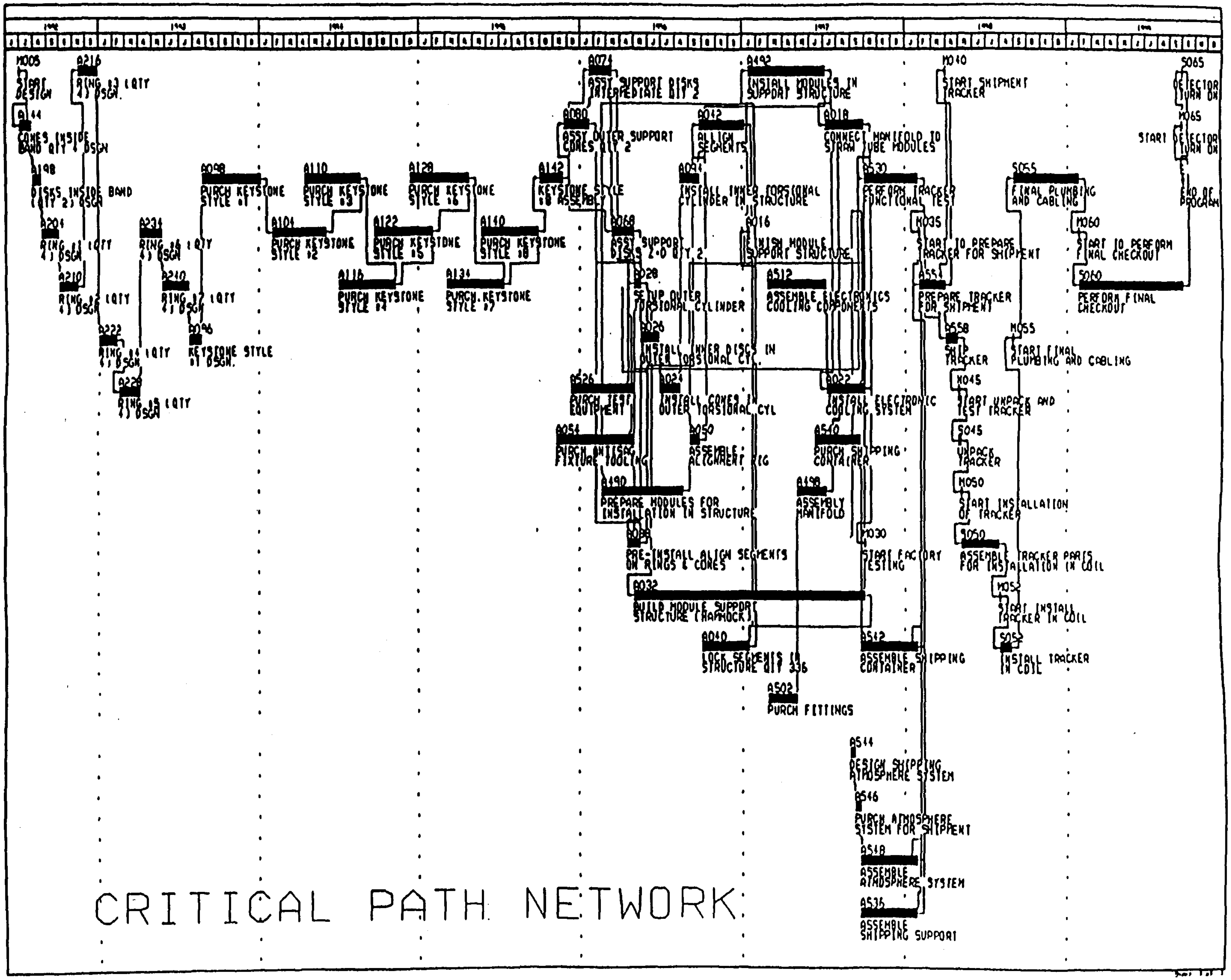
M005 START DESIGN
A216 RING #3 (QTY 4) DSGN.
A144 CONES INSIDE BAND QTY 4 DSGN
A198 DISKS INSIDE BAND (QTY 2) DSGN
A204 RING #1 (QTY 4) DSGN
A210 RING #2 (QTY 4) DSGN
A222 RING #4 (QTY 4) DSGN
A228 RING #5 (QTY 4) DSGN
A234 RING #6 (QTY 4) DSGN
A240 RING #2 (QTY 4) DSGN
A096 KEYSTONE STYLE #1 DSGN.
A098 PURCH KEYSTONE STYLE #1
A104 PURCH KEYSTONE STYLE #2
A110 PURCH KEYSTONE STYLE #3
A116 PURCH KEYSTONE STYLE #4
A122 PURCH KEYSTONE STYLE #5
A128 PURCH KEYSTONE STYLE #6
A134 PURCH KEYSTONE STYLE #7
A140 PURCH KEYSTONE STYLE #8
A142 KEYSTONE STYLE #8 ASSEMBLY
A074 ASSY SUPPORT DISKS INTERMEDIATE QTY 2
A080 ASSY OUTER SUPPORT CONES QTY 2
A068 ASSY SUPPORT DISKS Z-0 QTY 2
A028 SETUP OUTER TORSIONAL CYLINDER
A026 INSTALL INNER DISCS IN OUTER TORSIONAL CYL.
A526 PURCH TEST EQUIPMENT
A024 INSTALL CONES IN OUTER TORSIONAL CYL
A054 PURCH ANTISAG FIXTURE TOOLING
A050 ASSEMBLE ALIGNMENT JIG
A490 PREPARE MODULES FOR INSTALLATION IN STRUCTURE
A038 PRE-INSTALL ALIGN SEGMENTS ON RINGS & CONES
A032 BUILD MODULE SUPPORT STRUCTURE (HAMMOCK)
A040 LOCK SEGMENTS IN STRUCTURE QTY 336
A502 PURCH FITTINGS
A042 ALLIGN SEGMENTS
A034 INSTALL INNER TORSIONAL CYLINDER IN STRUCTURE
A492 INSTALL MODULES IN SUPPORT STRUCTURE
A016 FINISH MODULE SUPPORT STRUCTURE
A512 ASSEMBLE ELECTRONICS COOLING COMPONENTS
A018 CONNECT MANIFOLD TO STRAW TUBE MODULES
A022 INSTALL ELECTRONIC COOLING SYSTEM
A540 PURCH SHIPPING CONTAINER
A498 ASSEMBLY MANIFOLD
A530 PERFORM TRACKER FUNCTIONAL TEST
M030 START FACTORY TESTING
A542 ASSEMBLE SHIPPING CONTAINER
A544 DESIGN SHIPPING ATMOSPHERE SYSTEM
A546 PURCH ATMOSPHERE SYSTEM FOR SHIPMENT
A548 ASSEMBLE ATMOSPHERE SYSTEM
A536 ASSEMBLE SHIPPING SUPPORT
M040 START SHIPMENT TRACKER
M035 START TO PREPARE TRACKER FOR SHIPMENT
A554 PREPARE TRACKER FOR SHIPMENT
A558 SHIP TRACKER
M045 START UNPACK AND TEST TRACKER
S045 UNPACK TRACKER
M050 START INSTALLATION OF TRACKER
S050 ASSEMBLE TRACKER PARTS FOR INSTALLATION IN COIL
M052 START INSTALL TRACKER IN COIL
S052 INSTALL TRACKER IN COIL
S055 FINAL PLUMBING AND CABLING
M055 START FINAL PLUMBING AND CABLING
M060 START TO PERFORM FINAL CHECKOUT
S060 PERFORM FINAL CHECKOUT
S065 DETECTOR TURN ON
M065 START DETECTOR TURN ON
END OF PROGRAM
CRITICAL PATH NETWORK

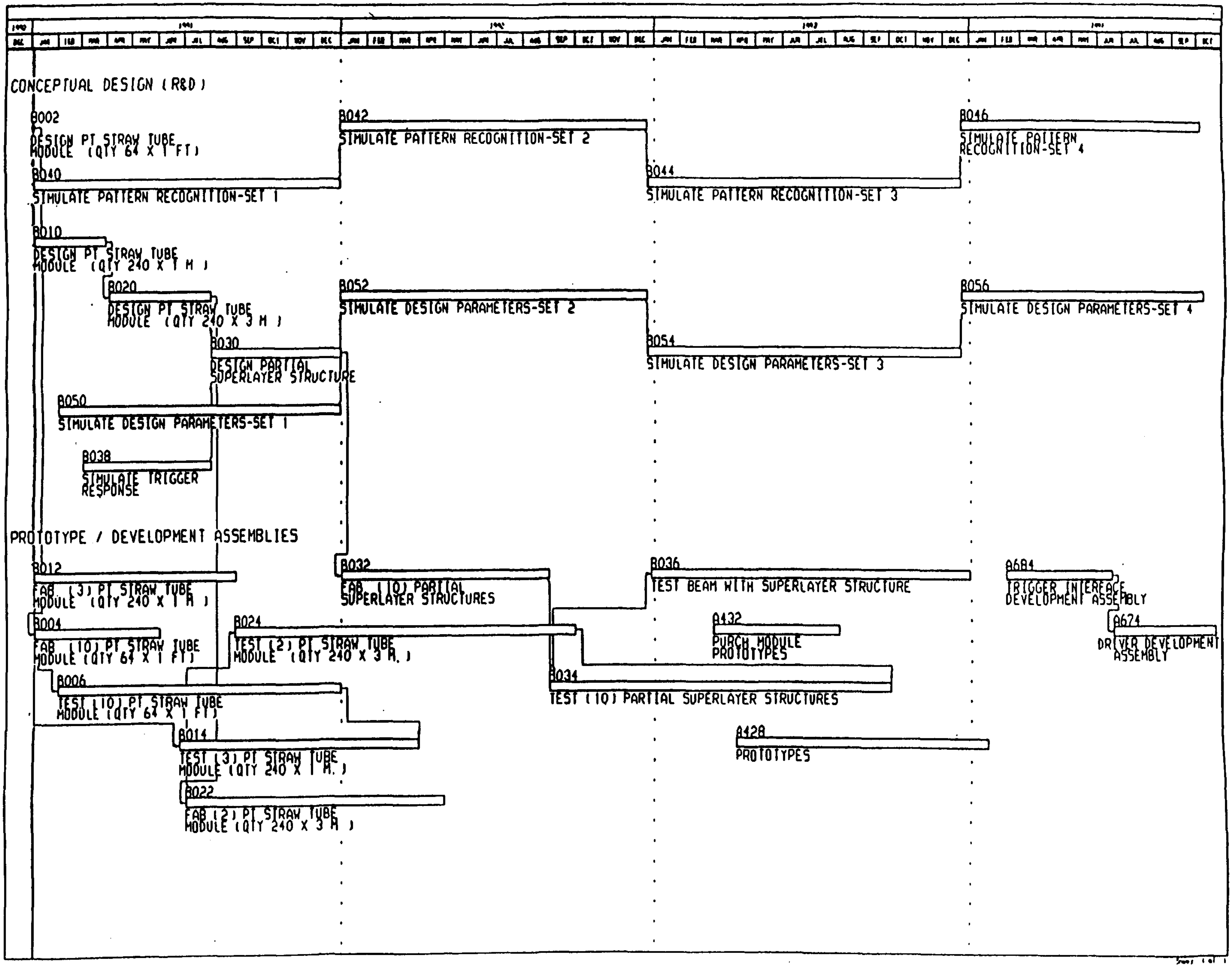
CONCEPTUAL DESIGN (R&D)
B002
DESIGN PT STRAW TUBE MODULE (QTY 64 X 1 FT)
B042
SIMULATE PATTERN RECOGNITION-SET 2
B046
SIMULATE PATTERN RECOGNITION-SET 4
B040
SIMULATE PATTERN RECOGNITION-SET 1
B044
SIMULATE PATTERN RECOGNITION-SET 3
B010
DESIGN PT STRAW TUBE MODULE (QTY 240 X 1 M)
B020
DESIGN PT STRAW TUBE MODULE (QTY 240 X 3 M)
B052
SIMULATE DESIGN PARAMETERS-SET 2
B056
SIMULATE DESIGN PARAMETERS-SET 4
B030
DESIGN PARTIAL SUPERLAYER STRUCTURE
B054
SIMULATE DESIGN PARAMETERS-SET 3
B050
SIMULATE DESIGN PARAMETERS-SET 1
B038
SIMULATE TRIGGER RESPONSE
PROTOTYPE / DEVELOPMENT ASSEMBLIES
B012
FAB (3) PT STRAW TUBE MODULE (QTY 240 X 1 M)
B032
FAB (10) PARTIAL SUPERLAYER STRUCTURES
B036
TEST BEAM WITH SUPERLAYER STRUCTURE
A684
TRIGGER INTERFACE DEVELOPMENT ASSEMBLY
B004
FAB (10) PT STRAW TUBE MODULE (QTY 64 X 1 FT)
B024
TEST (2) PT STRAW TUBE MODULE (QTY 240 X 3 M.)
A432
PURCH MODULE PROTOTYPES
A674
DRIVER DEVELOPMENT ASSEMBLY
B006
TEST (10) PT STRAW TUBE MODULE (QTY 64 X 1 FT)
B034
TEST (10) PARTIAL SUPERLAYER STRUCTURES
B014
TEST (3) PT STRAW TUBE MODULE (QTY 240 X 1 M.)
A428
PROTOTYPES
B022
FAB (2) PT STRAW TUBE MODULE (QTY 240 X 3 M)

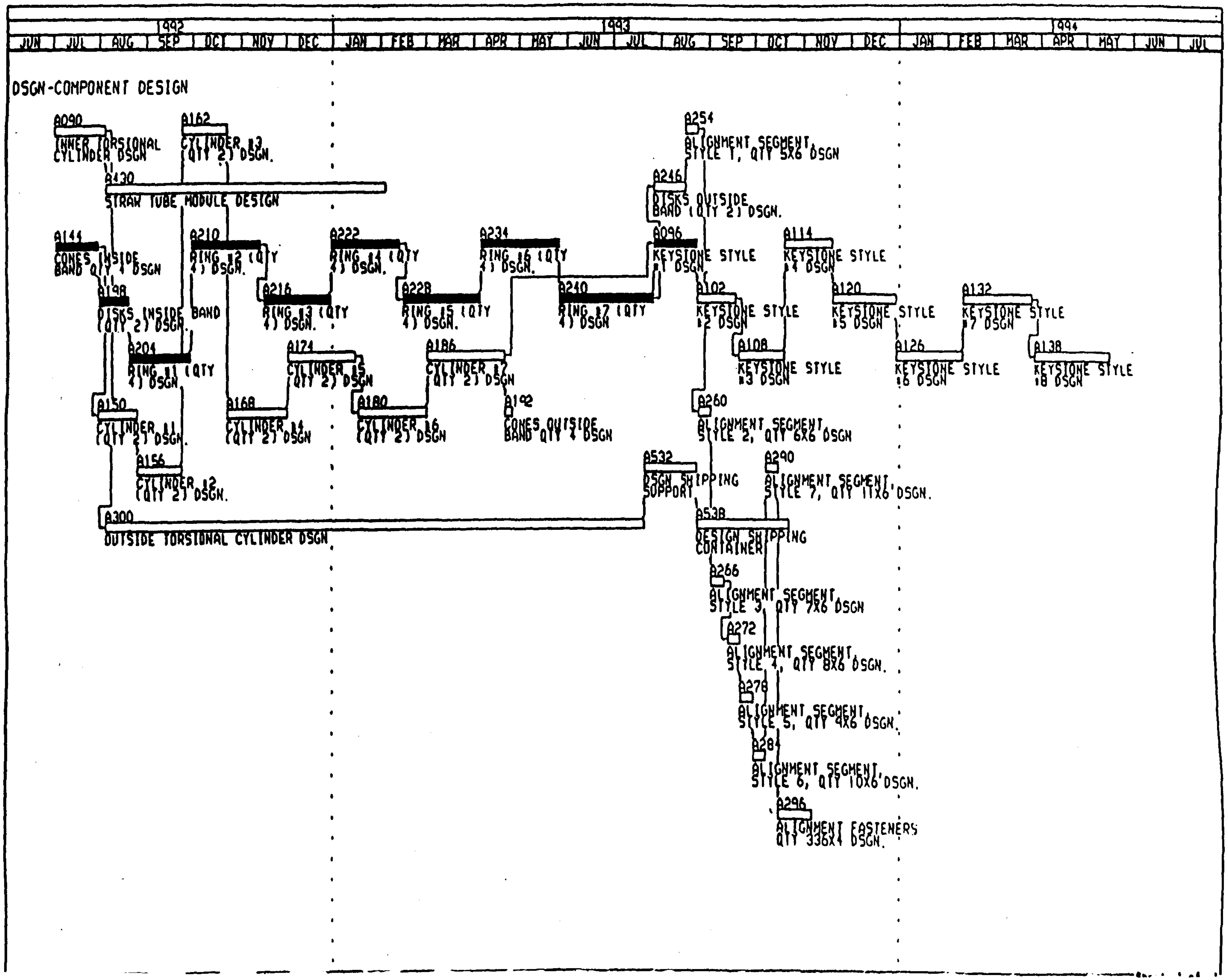
1992
1993
1994
JUN JUL AUG SEP OCT NOV DEC JAN FEB MAR APR MAY JUN JUL AUG SEP OCT NOV DEC JAN FEB MAR APR MAY JUN JUL
DSGN-COMPONENT DESIGN
A090 INNER TORSIONAL CYLINDER DSGN
A162 CYLINDER #3 (QTY 2) DSGN.
A130 STRAW TUBE MODULE DESIGN
A144 CONES INSIDE BAND QTY 4 DSGN
A198 DISKS INSIDE BAND (QTY 2) DSGN.
A204 RING #1 (QTY 4) DSGN
A210 RING #2 (QTY 4) DSGN.
A216 RING #3 (QTY 4) DSGN.
A222 RING #4 (QTY 4) DSGN.
A228 RING #5 (QTY 4) DSGN.
A234 RING #6 (QTY 4) DSGN.
A240 RING #7 (QTY 4) DSGN
A150 CYLINDER #1 (QTY 2) DSGN.
A156 CYLINDER #2 (QTY 2) DSGN.
A168 CYLINDER #4 (QTY 2) DSGN
A174 CYLINDER #5 (QTY 2) DSGN
A180 CYLINDER #6 (QTY 2) DSGN
A186 CYLINDER #7 (QTY 2) DSGN
A192 CONES OUTSIDE BAND QTY 4 DSGN
A300 OUTSIDE TORSIONAL CYLINDER DSGN
A254 ALIGNMENT SEGMENT, STYLE 1, QTY 5X6 DSGN
A246 DISKS OUTSIDE BAND (QTY 2) DSGN.
A096 KEYSTONE STYLE #1 DSGN
A102 KEYSTONE STYLE #2 DSGN
A108 KEYSTONE STYLE #3 DSGN
A114 KEYSTONE STYLE #4 DSGN
A120 KEYSTONE STYLE #5 DSGN
A126 KEYSTONE STYLE #6 DSGN
A132 KEYSTONE STYLE #7 DSGN
A138 KEYSTONE STYLE #8 DSGN
A260 ALIGNMENT SEGMENT, STYLE 2, QTY 6X6 DSGN
A532 DSGN SHIPPING SUPPORT
A290 ALIGNMENT SEGMENT, STYLE 7, QTY 11X6 DSGN.
A538 DESIGN SHIPPING CONTAINER
A266 ALIGNMENT SEGMENT, STYLE 3, QTY 7X6 DSGN
A272 ALIGNMENT SEGMENT, STYLE 4, QTY 8X6 DSGN.
A278 ALIGNMENT SEGMENT, STYLE 5, QTY 4X6 DSGN.
A284 ALIGNMENT SEGMENT, STYLE 6, QTY 10X6 DSGN.
A296 ALIGNMENT FASTENERS QTY 336X4 DSGN.

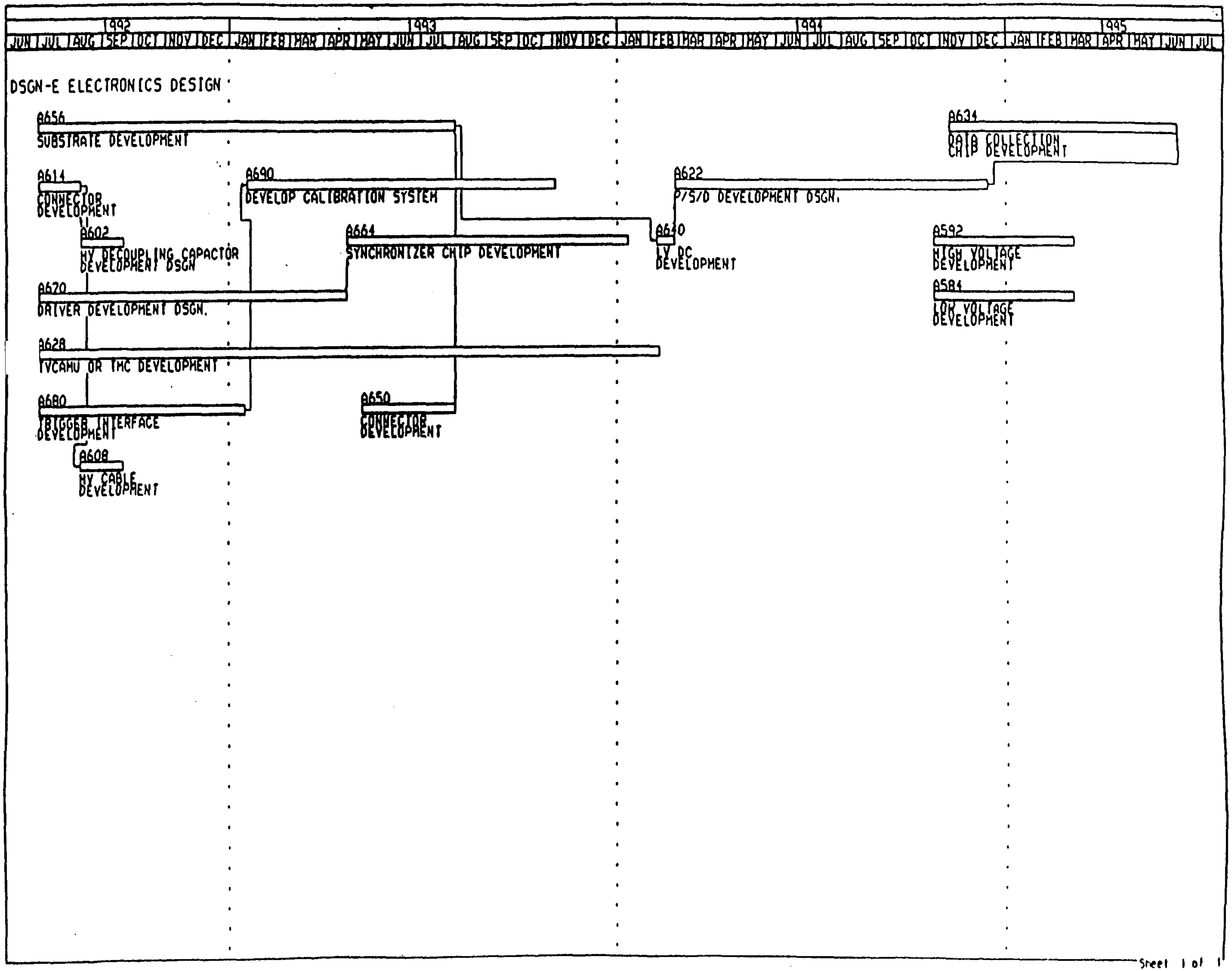
1992
1993
1994
1995
JUN JUL AUG SEP OCT NOV DEC JAN FEB MAR APR MAY JUN JUL AUG SEP OCT NOV DEC JAN FEB MAR APR MAY JUN JUL AUG SEP OCT NOV DEC JAN FEB MAR APR MAY JUN JUL
DSGN-E ELECTRONICS DESIGN
A656
SUBSTRATE DEVELOPMENT
A634
DATA COLLECTION CHIP DEVELOPMENT
A614
CONNECTOR DEVELOPMENT
A690
DEVELOP CALIBRATION SYSTEM
A622
P/S/D DEVELOPMENT DSGN.
A602
HV DECOUPLING CAPACTOR DEVELOPMENT DSGN
A664
SYNCHRONIZER CHIP DEVELOPMENT
A640
LV DC DEVELOPMENT
A592
HIGH VOLTAGE DEVELOPMENT
A620
DRIVER DEVELOPMENT DSGN.
A584
LOW VOLTAGE DEVELOPMENT
A628
TVCAMU OR TMC DEVELOPMENT
A680
TRIGGER INTERFACE DEVELOPMENT
A650
CONNECTOR DEVELOPMENT
A608
HV CABLE DEVELOPMENT
Sheet 1 of 1

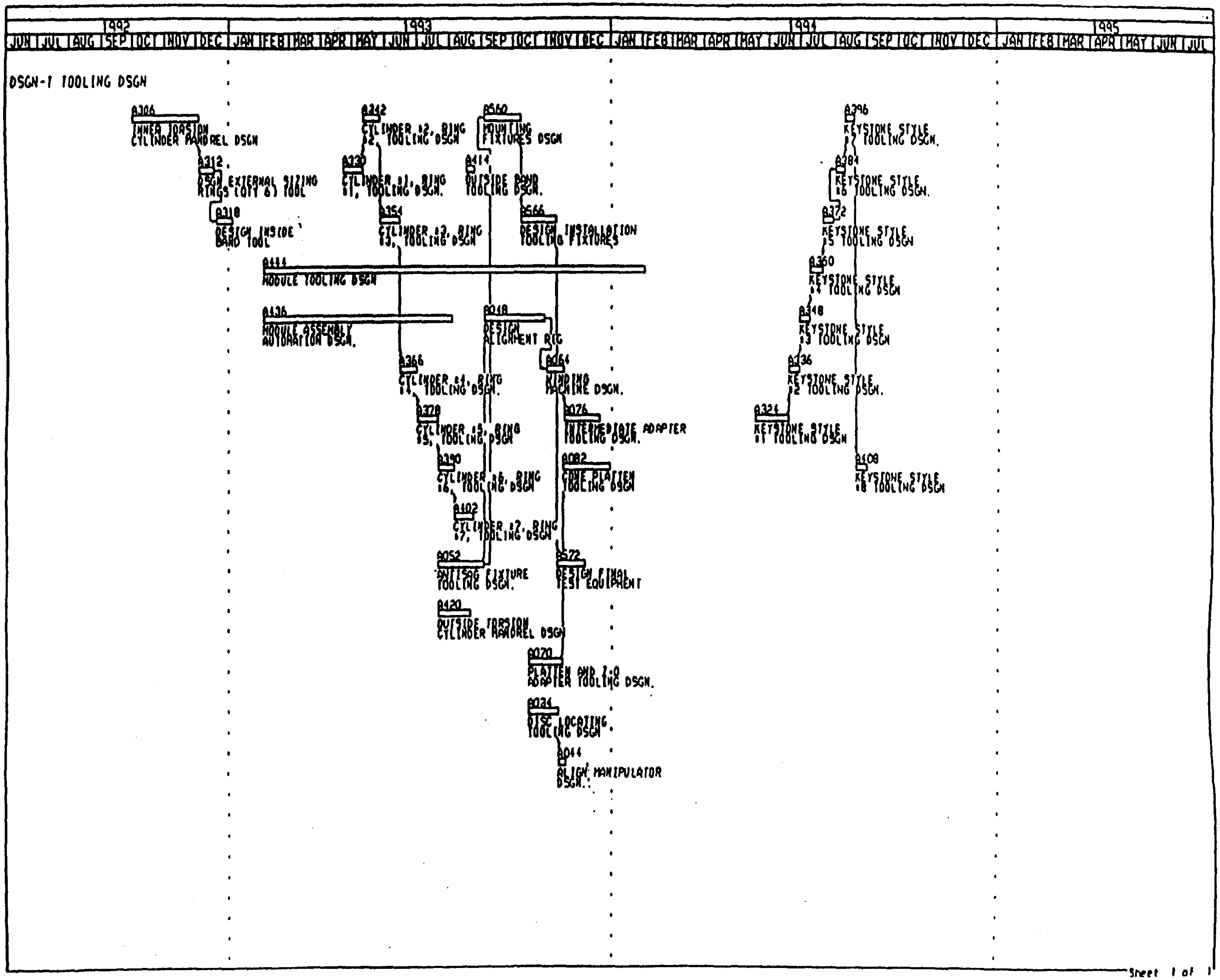
1992
1993
1994
1995
JUN JUL AUG SEP OCT NOV DEC JAN FEB MAR APR MAY JUN JUL AUG SEP OCT NOV DEC JAN FEB MAR APR MAY JUN JUL AUG SEP OCT NOV DEC JAN FEB MAR APR MAY JUN JUL
DSGN-T TOOLING DSGN
A306 INNER TORSION CYLINDER MANDREL DSGN
A312 DSGN EXTERNAL SIZING RINGS (QTY 6) TOOL
A318 DESIGN INSIDE BAND TOOL
A342 CYLINDER #2, RING #2, TOOLING DSGN
A330 CYLINDER #1, RING #1, TOOLING DSGN.
A354 CYLINDER #3, RING #3, TOOLING DSGN
A560 MOUNTING FIXTURES DSGN
A414 OUTSIDE BAND TOOLING DSGN.
A566 DESIGN INSTALLATION TOOLING FIXTURES
A444 MODULE TOOLING DSGN
A436 MODULE ASSEMBLY AUTOMATION DSGN.
A018 DESIGN ALIGNMENT RIG
A366 CYLINDER #4, RING #4, TOOLING DSGN.
A064 WINDING MACHINE DSGN.
A378 CYLINDER #5, RING #5, TOOLING DSGN
A076 INTERMEDIATE ADAPTER TOOLING DSGN.
A390 CYLINDER #6, RING #6, TOOLING DSGN
A082 CONE PLATTEN TOOLING DSGN
A402 CYLINDER #7, RING #7, TOOLING DSGN
A052 ANTISAG FIXTURE TOOLING DSGN.
A572 DESIGN FINAL TEST EQUIPMENT
A420 OUTSIDE TORSION CYLINDER MANDREL DSGN
A070 PLATTEN AND 7:0 ADAPTER TOOLING DSGN.
A034 DISC LOCATING TOOLING DSGN
A044 ALIGN MANIPULATOR DSGN.
A396 KEYSTONE STYLE #7 TOOLING DSGN.
A384 KEYSTONE STYLE #6 TOOLING DSGN.
A372 KEYSTONE STYLE #5 TOOLING DSGN
A360 KEYSTONE STYLE #4 TOOLING DSGN
A348 KEYSTONE STYLE #3 TOOLING DSGN
A336 KEYSTONE STYLE #2 TOOLING DSGN.
A324 KEYSTONE STYLE #1 TOOLING DSGN
A408 KEYSTONE STYLE #8 TOOLING DSGN
Sheet 1 of 1

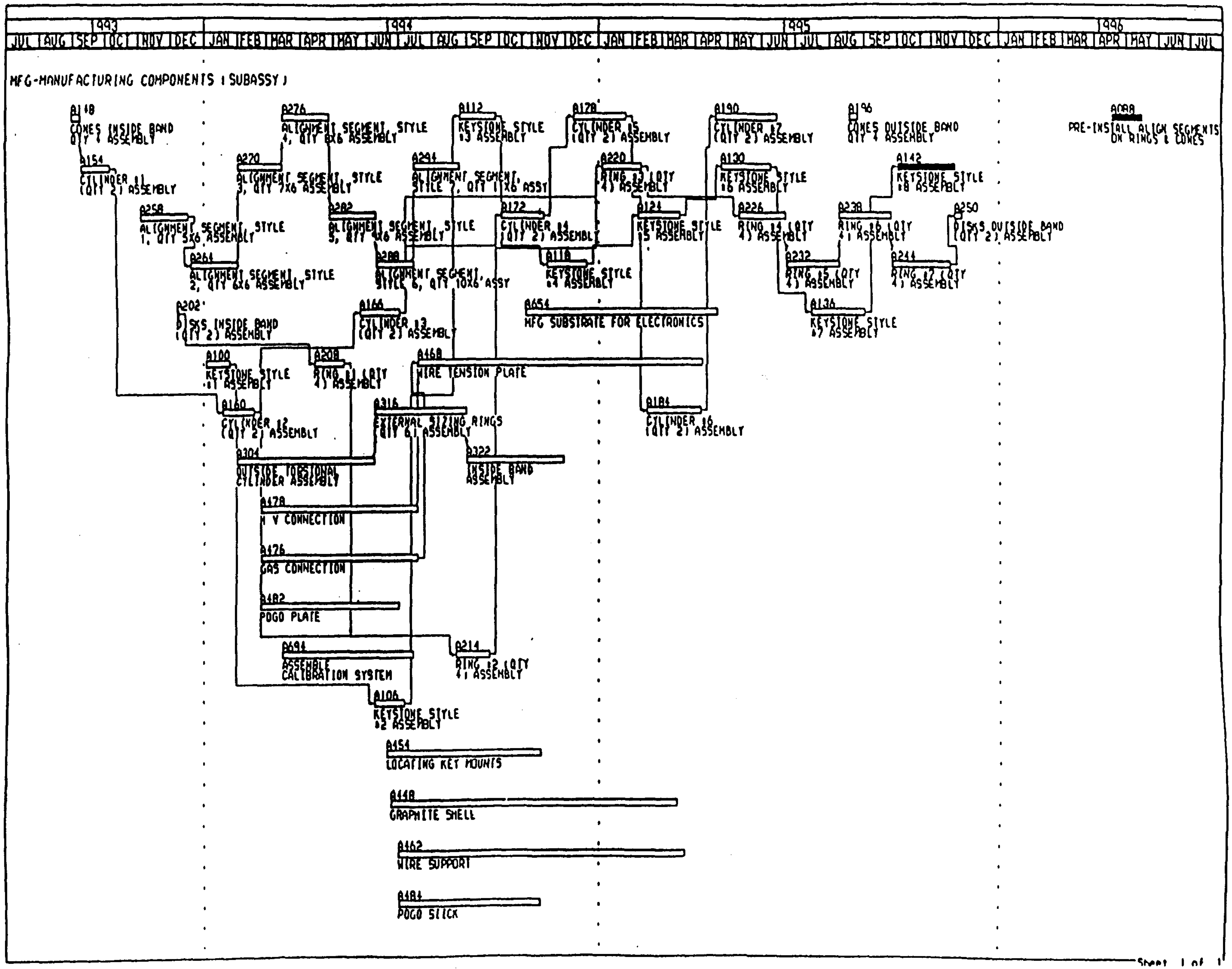
1993
1994
1995
1996
JUL AUG SEP OCT NOV DEC JAN FEB MAR APR MAY JUN JUL AUG SEP OCT NOV DEC JAN FEB MAR APR MAY JUN JUL AUG SEP OCT NOV DEC JAN FEB MAR APR MAY JUN JUL
MFG-MANUFACTURING COMPONENTS (SUBASSY)
A148 CONES INSIDE BAND QTY 4 ASSEMBLY
A154 CYLINDER #1 (QTY 2) ASSEMBLY
A258 ALIGNMENT SEGMENT, STYLE 1, QTY 5X6 ASSEMBLY
A264 ALIGNMENT SEGMENT, STYLE 2, QTY 6X6 ASSEMBLY
A202 DISKS INSIDE BAND (QTY 2) ASSEMBLY
A100 KEYSTONE STYLE #1 ASSEMBLY
A160 CYLINDER #2 (QTY 2) ASSEMBLY
A304 OUTSIDE TORSIONAL CYLINDER ASSEMBLY
A478 H V CONNECTION
A476 GAS CONNECTION
A482 POGO PLATE
A694 ASSEMBLE CALIBRATION SYSTEM
A106 KEYSTONE STYLE #2 ASSEMBLY
A454 LOCATING KEY MOUNTS
A448 GRAPHITE SHELL
A462 WIRE SUPPORT
A484 POGO STICK
A276 ALIGNMENT SEGMENT, STYLE 4, QTY 6X6 ASSEMBLY
A220 ALIGNMENT SEGMENT, STYLE 3, QTY 7X6 ASSEMBLY
A282 ALIGNMENT SEGMENT, STYLE 5, QTY 4X6 ASSEMBLY
A288 ALIGNMENT SEGMENT, STYLE 6, QTY 10X6 ASSY
A166 CYLINDER #3 (QTY 2) ASSEMBLY
A208 RING #1 (QTY 4) ASSEMBLY
A468 WIRE TENSION PLATE
A316 EXTERNAL SIZING RINGS (QTY 6) ASSEMBLY
A322 INSIDE BAND ASSEMBLY
A214 RING #2 (QTY 4) ASSEMBLY
A112 KEYSTONE STYLE #3 ASSEMBLY
A294 ALIGNMENT SEGMENT, STYLE 7, QTY 11X6 ASSY
A172 CYLINDER #4 (QTY 2) ASSEMBLY
A118 KEYSTONE STYLE #4 ASSEMBLY
A654 MFG SUBSTRATE FOR ELECTRONICS
A178 CYLINDER #5 (QTY 2) ASSEMBLY
A220 RING #3 (QTY 4) ASSEMBLY
A124 KEYSTONE STYLE #5 ASSEMBLY
A184 CYLINDER #6 (QTY 2) ASSEMBLY
A190 CYLINDER #7 (QTY 2) ASSEMBLY
A130 KEYSTONE STYLE #6 ASSEMBLY
A226 RING #4 (QTY 4) ASSEMBLY
A232 RING #5 (QTY 4) ASSEMBLY
A136 KEYSTONE STYLE #7 ASSEMBLY
A196 CONES OUTSIDE BAND QTY 4 ASSEMBLY
A142 KEYSTONE STYLE #8 ASSEMBLY
A238 RING #6 (QTY 4) ASSEMBLY
A244 RING #7 (QTY 4) ASSEMBLY
A250 DISKS OUTSIDE BAND (QTY 2) ASSEMBLY
A088 PRE-INSTALL ALIGN SEGMENTS ON RINGS & CONES
Sheet 1 of 1

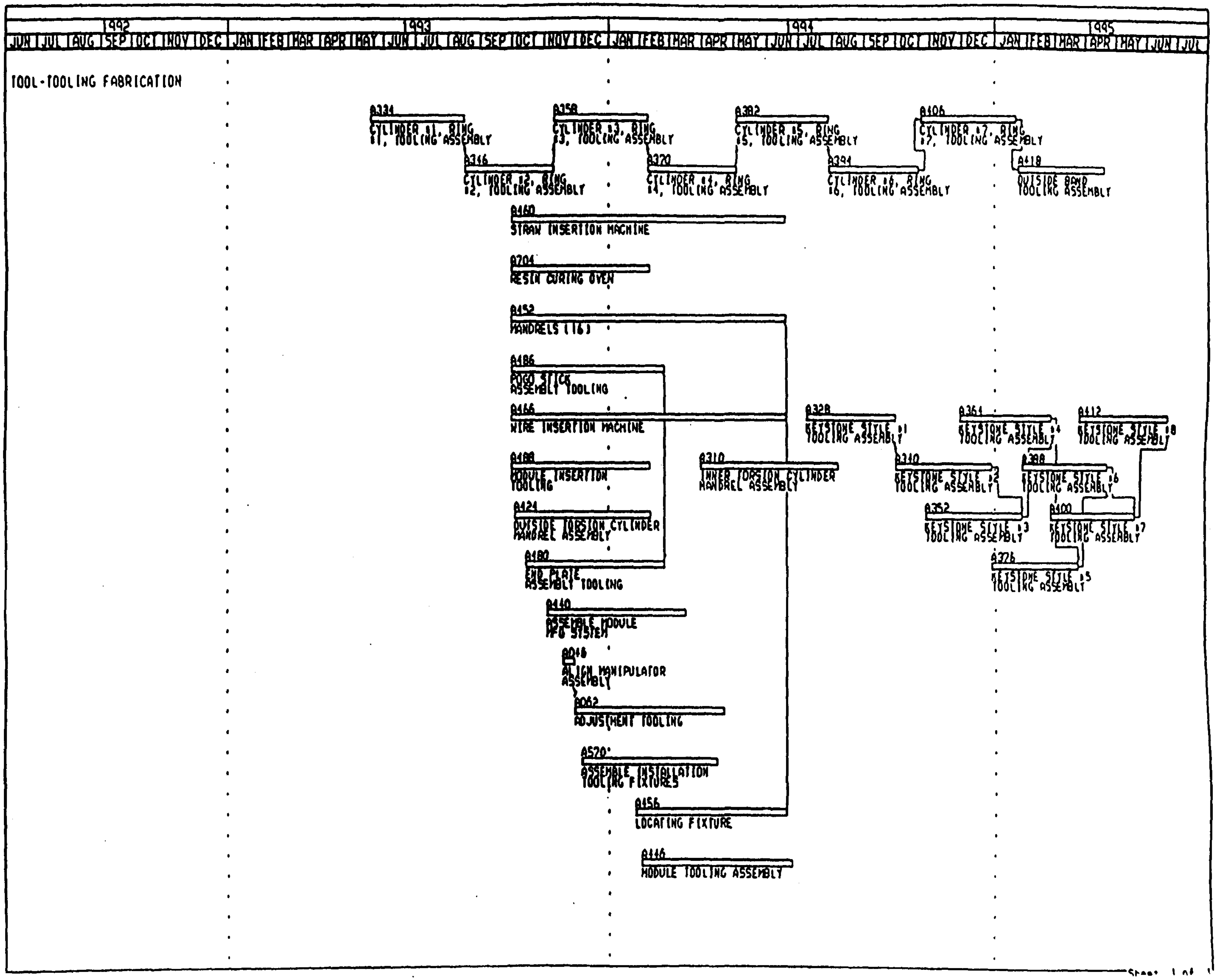
1992
1993
1994
1995
JUN JUL AUG SEP OCT NOV DEC JAN FEB MAR APR MAY JUN JUL AUG SEP OCT NOV DEC JAN FEB MAR APR MAY JUN JUL AUG SEP OCT NOV DEC JAN FEB MAR APR MAY JUN JUL
TOOL-TOOLING FABRICATION
A334
CYLINDER #1, RING #1, TOOLING ASSEMBLY
A358
CYLINDER #3, RING #3, TOOLING ASSEMBLY
A382
CYLINDER #5, RING #5, TOOLING ASSEMBLY
A406
CYLINDER #7, RING #7, TOOLING ASSEMBLY
A346
CYLINDER #2, RING #2, TOOLING ASSEMBLY
A370
CYLINDER #4, RING #4, TOOLING ASSEMBLY
A394
CYLINDER #6, RING #6, TOOLING ASSEMBLY
A418
OUTSIDE BAND TOOLING ASSEMBLY
A460
STRAW INSERTION MACHINE
A704
RESIN CURING OVEN
A452
MANDRELS (16)
A486
POGO STICK ASSEMBLY TOOLING
A466
WIRE INSERTION MACHINE
A328
KEYSTONE STYLE #1 TOOLING ASSEMBLY
A364
KEYSTONE STYLE #4 TOOLING ASSEMBLY
A412
KEYSTONE STYLE #8 TOOLING ASSEMBLY
A488
MODULE INSERTION TOOLING
A310
INNER TORSION CYLINDER MANDREL ASSEMBLY
A340
KEYSTONE STYLE #2 TOOLING ASSEMBLY
A388
KEYSTONE STYLE #6 TOOLING ASSEMBLY
A424
OUTSIDE TORSION CYLINDER MANDREL ASSEMBLY
A352
KEYSTONE STYLE #3 TOOLING ASSEMBLY
A400
KEYSTONE STYLE #7 TOOLING ASSEMBLY
A480
END PLATE ASSEMBLY TOOLING
A376
KEYSTONE STYLE #5 TOOLING ASSEMBLY
A440
ASSEMBLE MODULE MFG SYSTEM
A048
ALIGN MANIPULATOR ASSEMBLY
A062
ADJUSTMENT TOOLING
A520
ASSEMBLE INSTALLATION TOOLING FIXTURES
A456
LOCATING FIXTURE
A446
MODULE TOOLING ASSEMBLY

RESOURCE AND COST PROFILES

(UN-LEVELED)

ENGINEERING MANPOWER

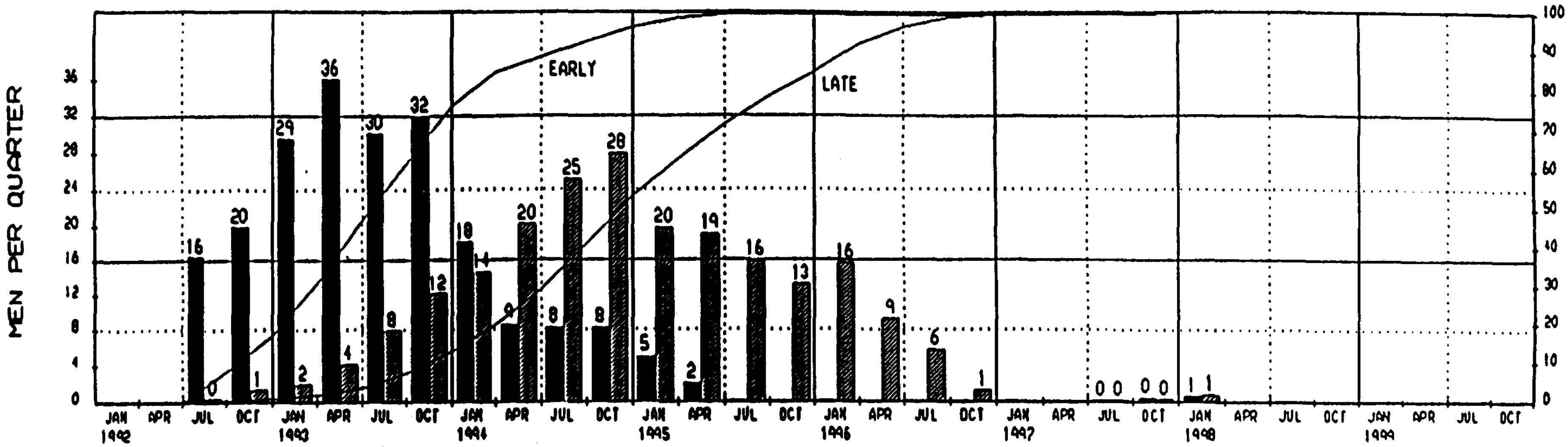

QUARTERLY ESTIMATES

DSGN / DRAFTING MANPOWER

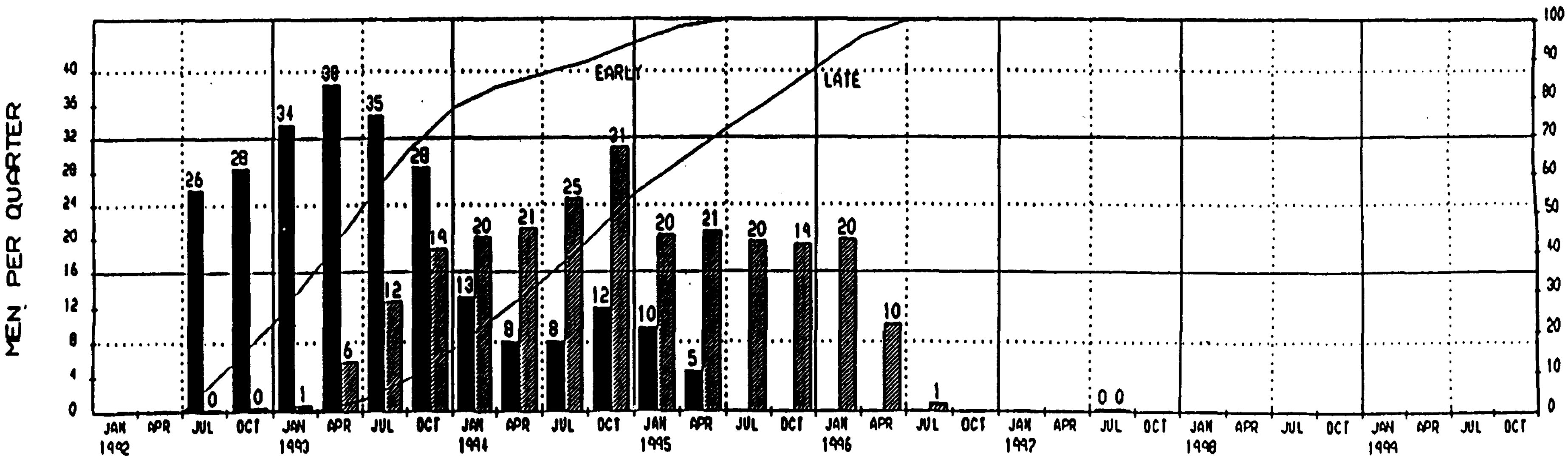

QUARTERLY ESTIMATES

Early dates Late dates Primavera Systems, Inc. 1981-1990	SOLENOIDAL DETECTOR COLLABORATION CENTRAL TRACKER REV 1 NETWORKED ENGINEERING AND DESIGN MANPOWER Project Start: 1DEC90 Project Finish: 30SEP99 Sheet 1 of 1 Data Date: 3JAN91 Plot Date: 11FEB91	CETA-MODULAR CENTRAL STRAW TUBE TRACKER SCHEDULE Date / Revision / Checked / Approved

TECHNICIAN MANPOWER

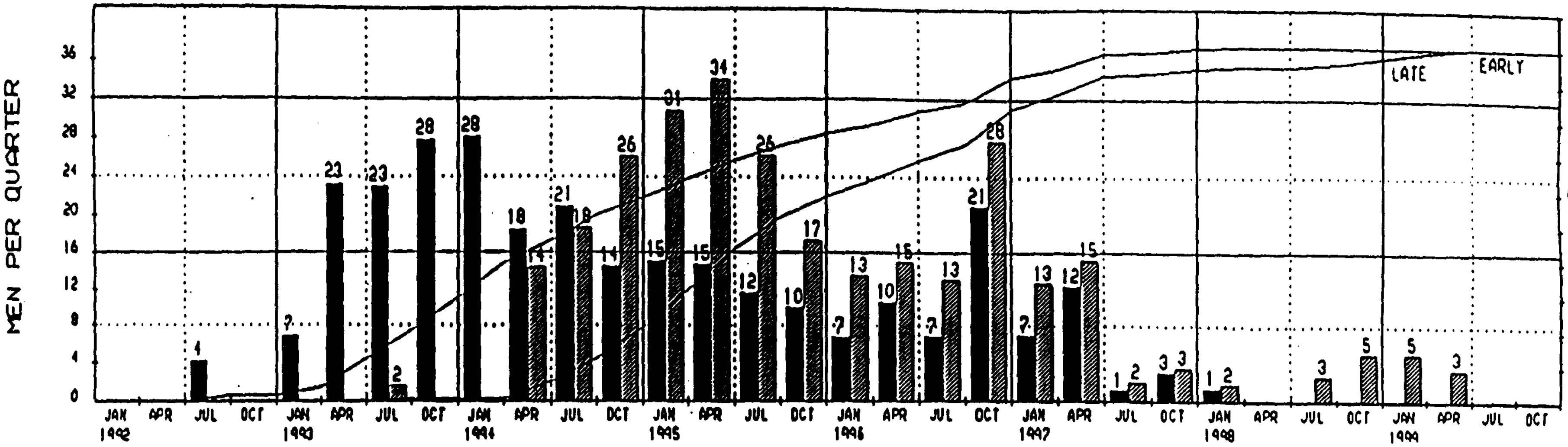

QUARTERLY ESTIMATES

LABOR MANPOWER

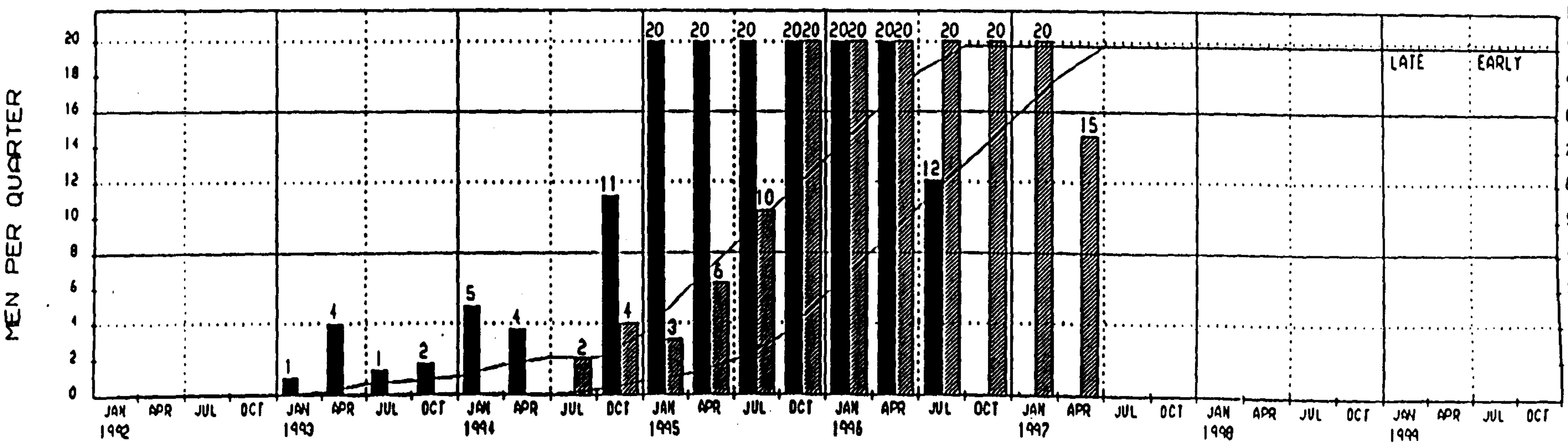

QUARTERLY ESTIMATES

Early dates Late dates Primavera Systems, Inc. 1981-1990	SOLENOIDAL DETECTOR COLLABORATION CENTRAL TRACKER REV 1 NETWORKED TECHNICIAN AND LABOR MANPOWER Project Start: 1DEC90 Project Finish: 30SEP99	Sheet 1 of 1 Data Date: 3JAN91 Plot Date: 11FEB91	CETA-MODULAR CENTRAL STRAW TUBE TRACKER SCHEDULE Date / Revision / Checked / Approved

LABOR COSTS

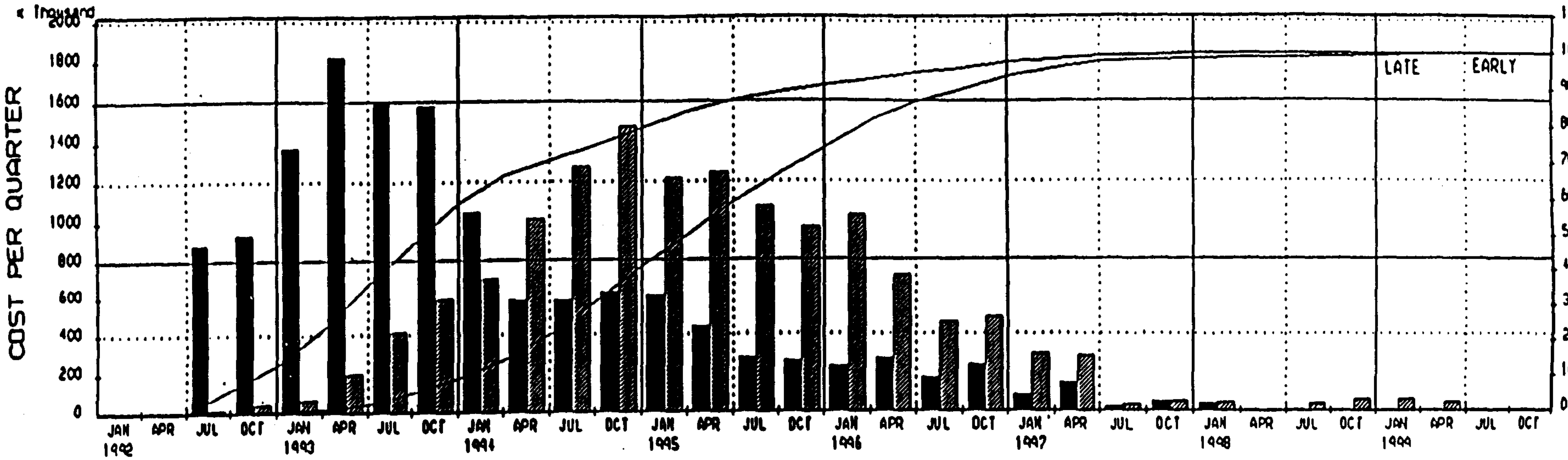

MATERIAL COSTS

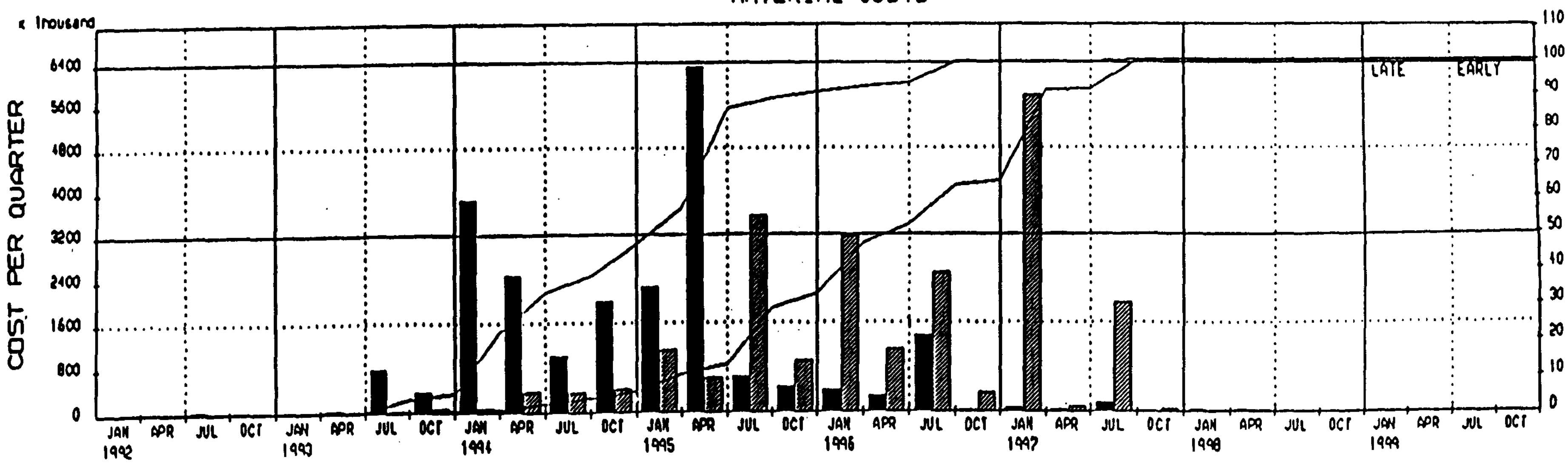

Early dates Late dates Primavera Systems, Inc. 1991-1990	SOLENOIDAL DETECTOR COLLABORATION CENTRAL TRACKER REV 1 NETWORKED LABOR & MATERIAL COSTS Project Start: 1DEC90 Project Finish: 30SEP99	Sheet 1 of 1 Data Date: 3JAN91 Plot Date: 11FEB91	CETA-MODULAR CENTRAL STRAW TUBE TRACKER SCHEDULE Date / Revision / Checked / Approved

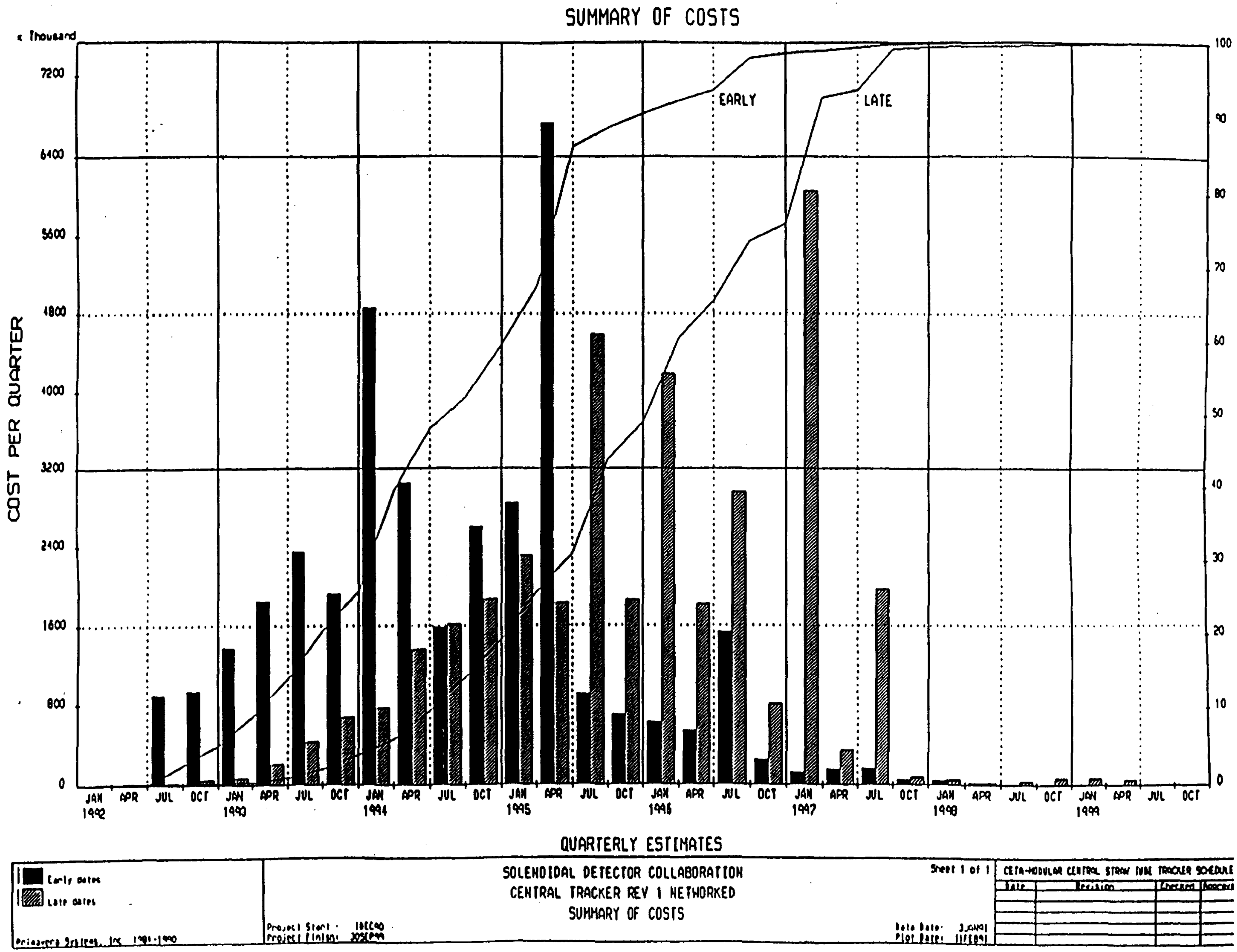
SUMMARY OF COSTS
$ Thousand
7200
6400
5600
4800
4000
3200
2400
1600
800
0
COST PER QUARTER
EARLY
LATE
100
90
80
70
60
50
40
30
20
10
0
JAN APR JUL OCT JAN APR JUL OCT JAN APR JUL OCT JAN APR JUL OCT JAN APR JUL OCT JAN APR JUL OCT JAN APR JUL OCT JAN APR JUL OCT
1992
1993
1994
1995
1996
1997
1998
1999
QUARTERLY ESTIMATES
Early dates
Late dates
Primavera Systems, Inc 1984-1990
SOLENOIDAL DETECTOR COLLABORATION
CENTRAL TRACKER REV 1 NETWORKED
SUMMARY OF COSTS
Sheet 1 of 1
Project Start: 18EC90
Project Finish: 30SEP99
Data Date: 3JAN91
Plot Date: 11FEB91
CETA-MODULAR CENTRAL STRAW TUBE TRACKER SCHEDULE
Date
Revision
Checked
Approved

APPENDIX

ORNL Presentation on Central Tracking

by R. L. Swensrud

CENTRAL AND FORWARD TRACKING

SOLENOIDAL DETECTOR COLLABORATION

Presentation

February 11, 1991

R. L. Swensrud (Roger)

RLS

Westinghouse
Science & Technology Center

CENTRAL AND FORWARD TRACKING

TABLE OF CONTENTS

Westinghouse
Science & Technology Center

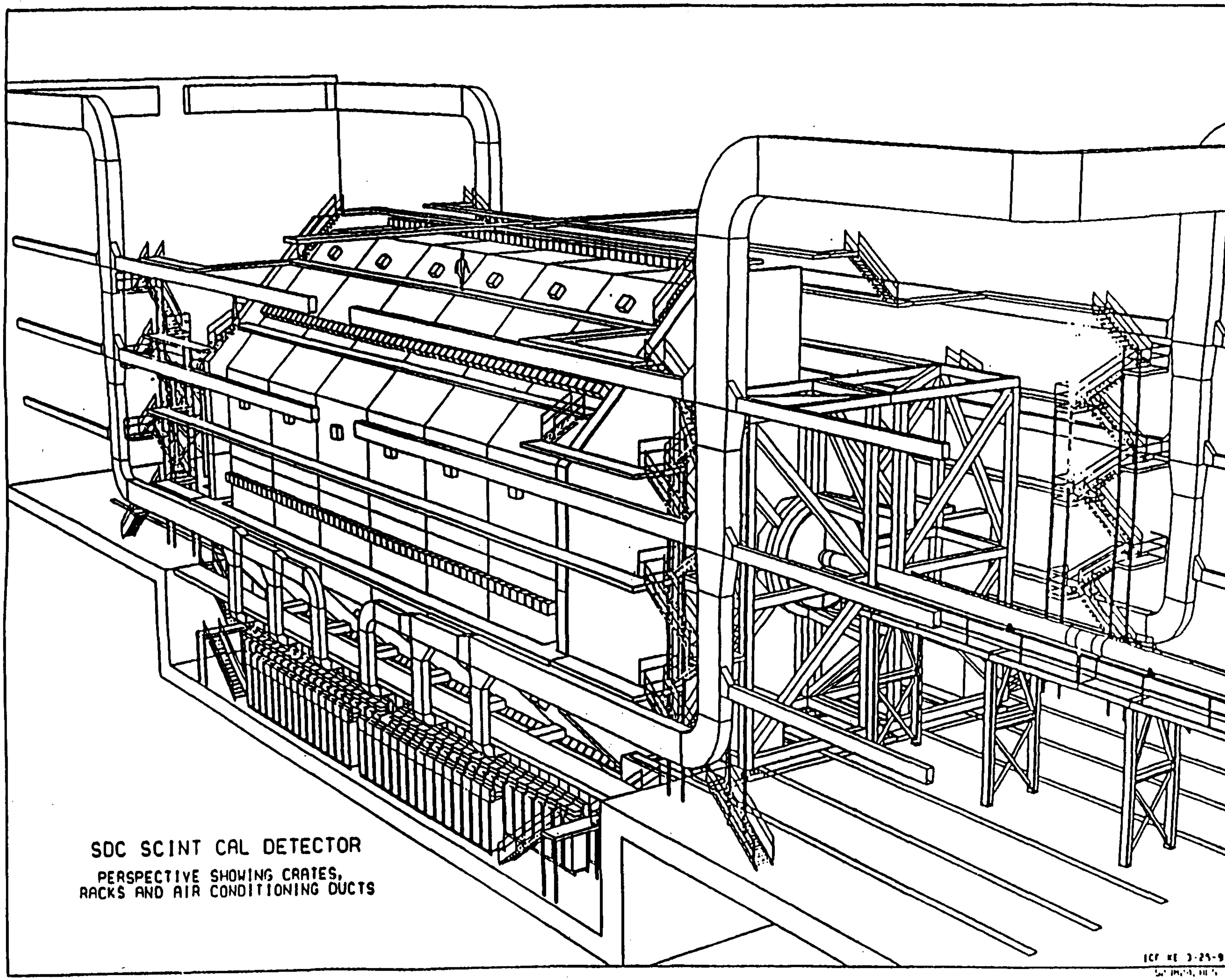
SDC SCINT CAL DETECTOR
PERSPECTIVE SHOWING CRATES,
RACKS AND AIR CONDITIONING DUCTS

FIG 3.1

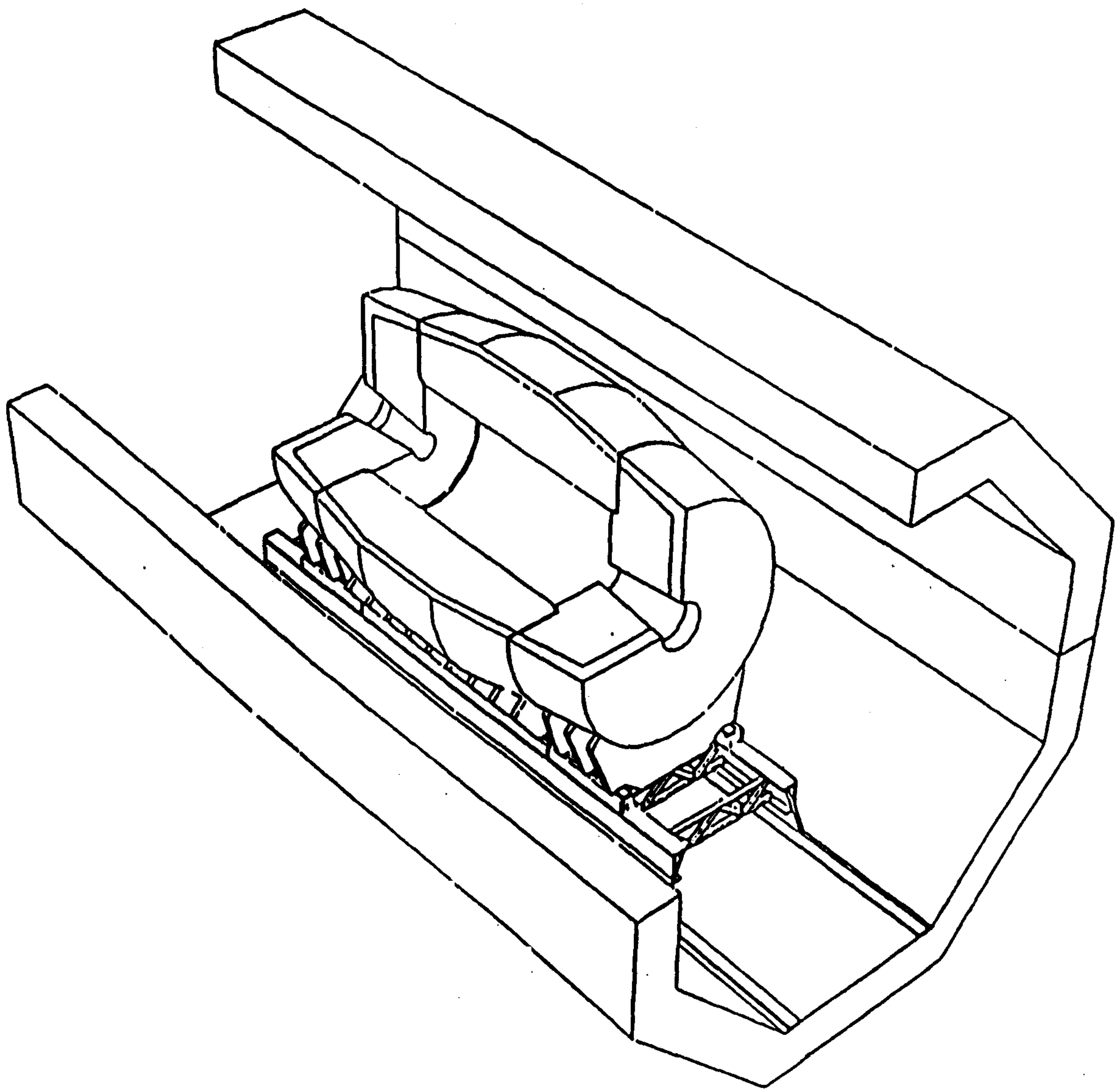

SCINT CAL DETECTOR

LEAD CALORIMETER AND SUPPORTS

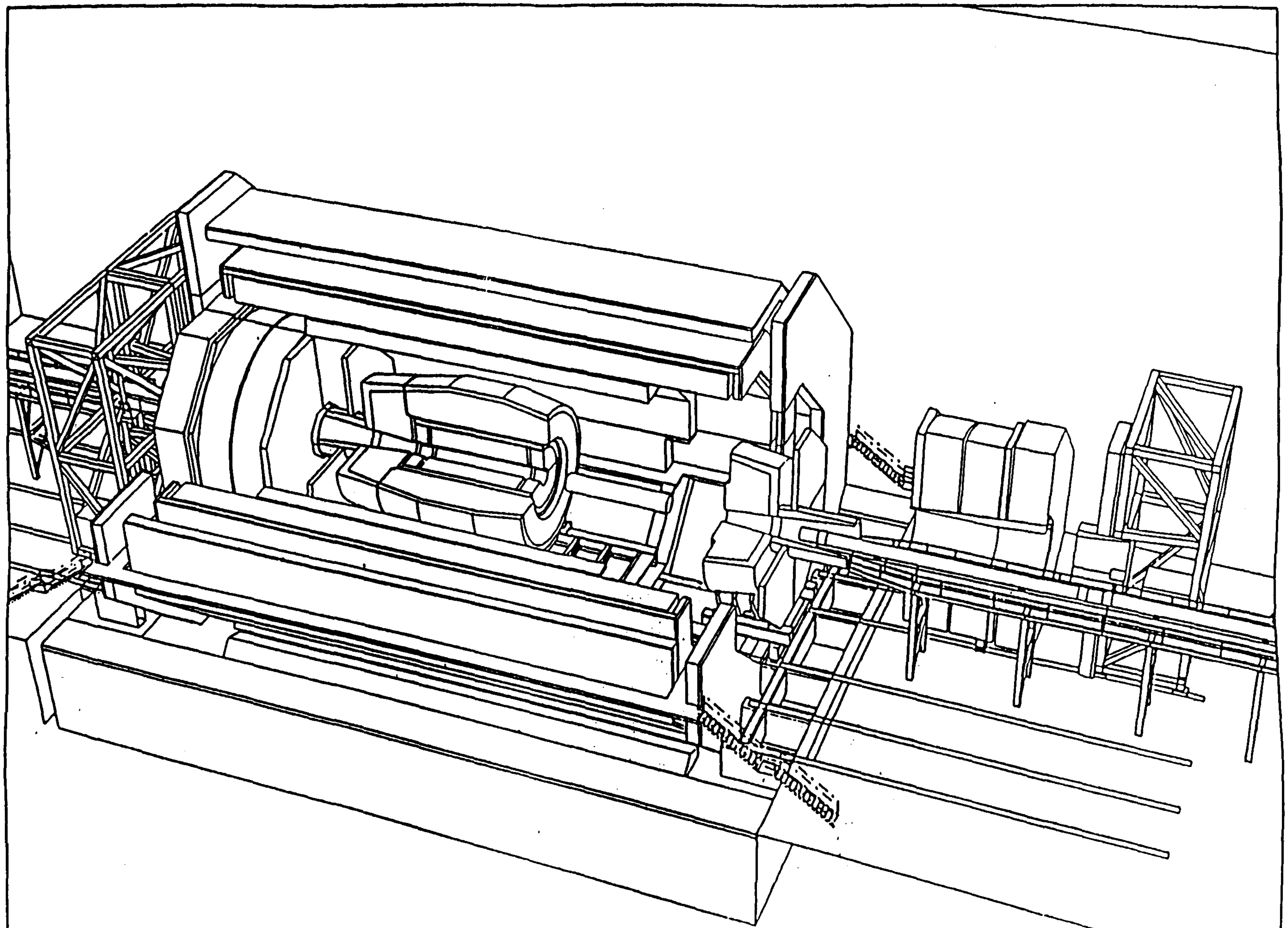

SDC SCINT CAL DETECTOR

FIG 3.14

CENTRAL AND FORWARD TRACKING

INTRODUCTION
CONCEPT

MODULAR STRAW TUBE TRACKING SYSTEM
EXPLODED VIEW

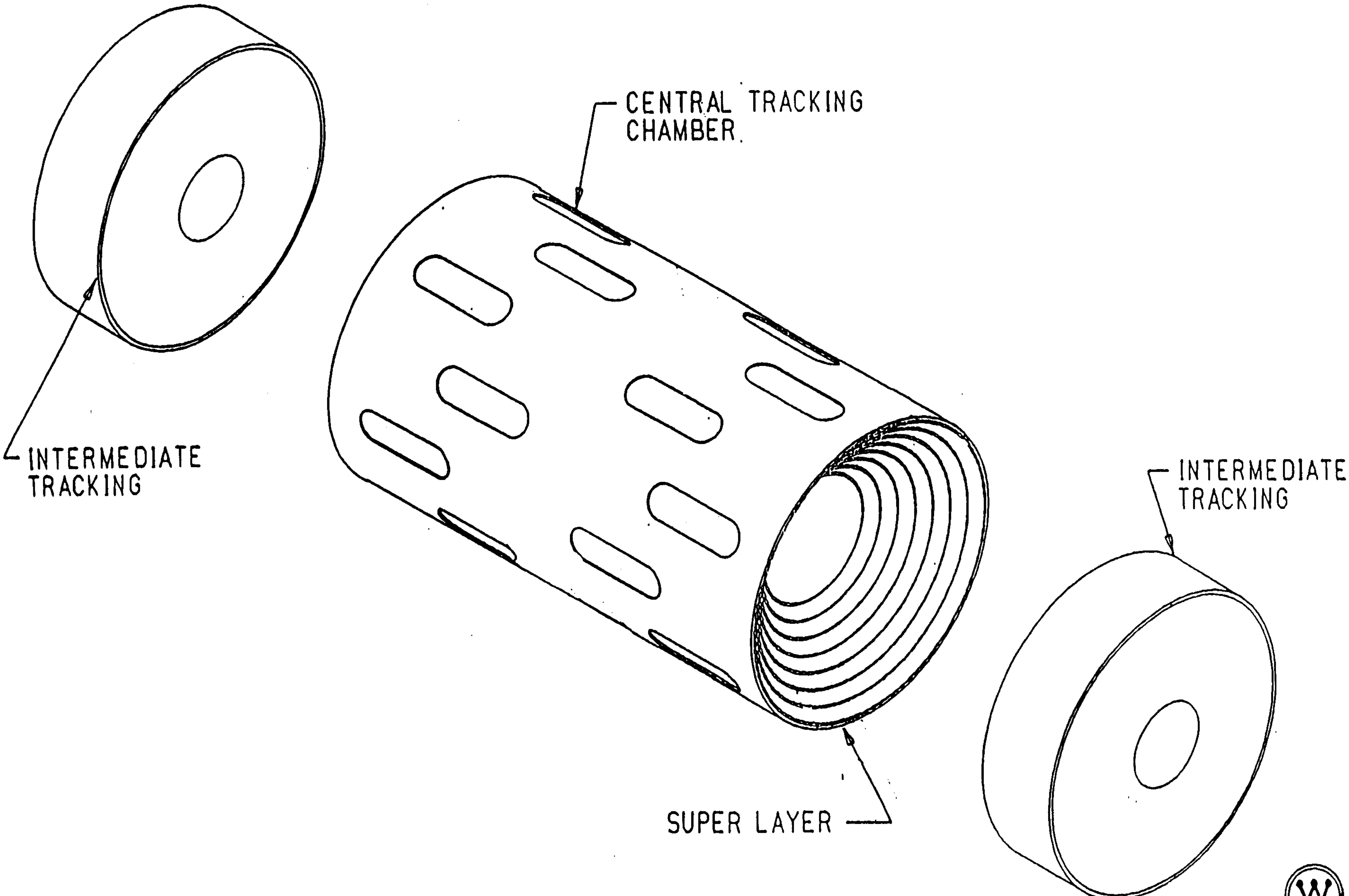

D.389.4136A44.R1
KEPES 12-4-90

CENTRAL AND FORWARD TRACKING

SOLENOIDAL DETECTOR COLLABORATION

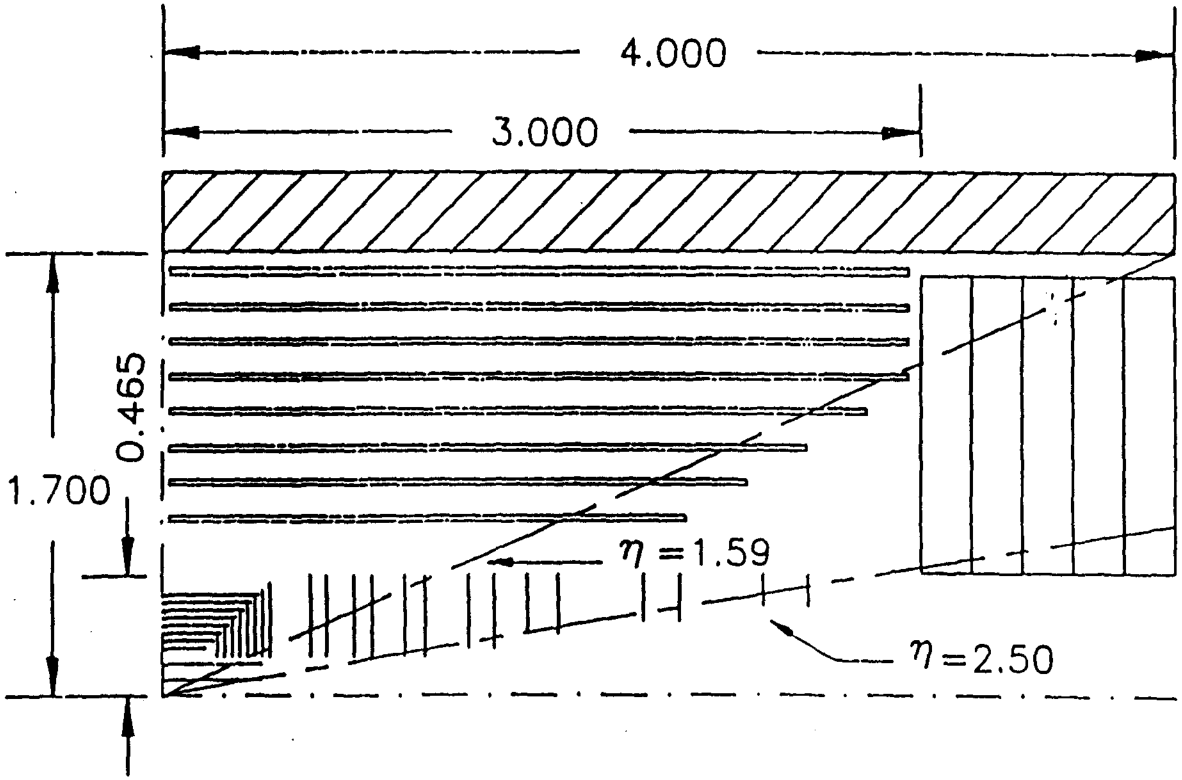

12-06-91 Bill Ford

Westinghouse
Science & Technology Center

RLS

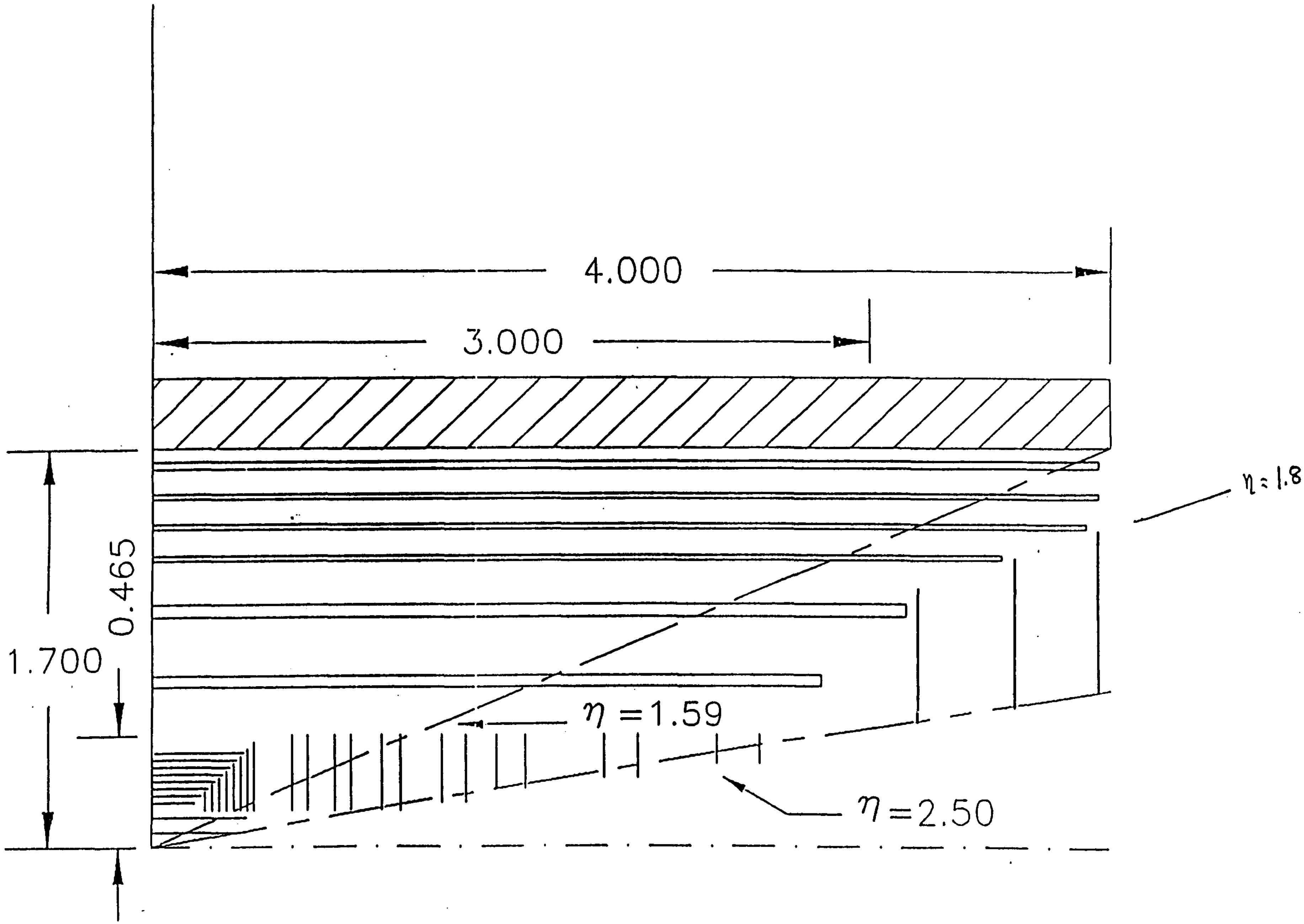
4.000
3.000
0.465
1.700
η = 1.8
$\eta = 1.59$
$\eta = 2.50$

CENTRAL AND FORWARD TRACKING

Summary

Superlayer mean radius cm.		Delta cm.	Space between superlayers cm.	
			Cyl-lay1	is1 - a2 = 2.532
lay 1	m1 = 68.374		Lay 1-2	is2 - ol1 = 10.065
lay 2	m2 = 81.721	m2 - m1 = 13.347	Lay 2-3	is3 - ol2 = 10.065
lay 3	m3 = 95.068	m3 - m2 = 13.347	Lay 3-4	is4 - ol3 = 10.065
lay 4	m4 = 108.414	m4 - m3 = 13.347	Lay 4-5	is5 - ol4 = 10.065
lay 5	m5 = 121.761	m5 - m4 = 13.347	Lay 5-6	is6 - ol5 = 9.724
lay 6	m6 = 134.986	m6 - m5 = 13.225	Lay 6-7	is7 - ol6 = 9.966
lay 7	m7 = 148.454	m7 - m6 = 13.468	Lay 7-8	is8 - ol7 = 9.655
lay 8	m8 = 161.611	m8 - m7 = 13.157	Lay8-Cyl	i1 - ol8 = 2.532

Space between components

Tor cyl and superlayer 1	is1 - a2 = 2.532	cm
Superlayer 1 and ring 1	b1 - ol1 = 2.532	cm
Ring 1 and superlayer 2	is2 - b2 = 2.532	cm
Superlayer 2 and ring 2	c1 - ol2 = 2.532	cm
Ring 2 and superlayer 3	is3 - c2 = 2.532	cm
Superlayer 3 and ring 3	d1 - ol3 = 2.532	cm
Ring 3 and superlayer 4	is4 - d2 = 2.532	cm
Superlayer 4 and ring 4	e1 - ol4 = 2.532	cm
Ring 4 and superlayer 5	is5 - e2 = 2.532	cm
Superlayer 5 and ring 5	f1 - ol5 = 2.472	cm
Ring 5 and superlayer 6	is6 - f2 = 2.252	cm
Superlayer 6 and ring 6	g1 - ol6 = 2.373	cm
Ring 6 and superlayer 7	is7 - g2 = 2.593	cm
Superlayer 7 and ring 7	h1 - ol7 = 2.438	cm
Ring 7 and superlayer 8	is8 - h2 = 2.218	cm
Superlayer 8 and tor cyl	i1 - ol8 = 2.532	cm

Inside radius of inner torsion cyl	a1 = 61.701	cm	spec minimum = 60.0
Outside radius of outer torsion cyl	i2 = 168.504	cm	spec maximum = 168.5

A:Centk11 1-30-91 D.M. Westinghouse STC
STEREO STUDY USING DUAL ANGLES FOR ALTERNATING MODULES IN A SUPERLAYER

RLS

Westinghouse
Science & Technology Center

CENTRAL AND FORWARD TRACKING

Number of Modules (Total System).

Modules, full system $mod := 4 \cdot (a + b + c + d4 + e + f + g + h)$

$mod = 1088$ modules

Number of channels (Total System).

$tch := 4 \cdot (CHs \cdot a + CH \cdot b + CHs \cdot c + CH \cdot d4 + CHs \cdot e + CHc \cdot f + CHs \cdot g + CHc \cdot h)$

$tch = 199392$ channels

Number of Axial channels (Total System).

$ach := 4 \cdot (CH \cdot b + CH \cdot d4 + CHc \cdot f + CHc \cdot h)$

$ach = 117984$ channels

Number of Stereo channels (Total System)

$sch := 4 \cdot (CHs \cdot a + CHs \cdot c + CHs \cdot e + CHs \cdot g)$

$sch = 81408$ channels

Number of Trigger channels (Total System)

$tch := 4 \cdot (CHc \cdot f + CHc \cdot h)$

$tch = 82368$ channels

A:Centk11 1-30-91 D.M. Westinghouse STC

STEREO STUDY USING DUAL ANGLES FOR ALTERNATING MODULES IN A SUPERLAYER

MODULAR CENTRAL TRACKING
SUPERLAYER MODULES
POST LOI

SUPERLAYER 9° INCLUDED ANGLE
WITH 3 MM GAP FOR INSIDE STEREO OR AXIAL LAYER

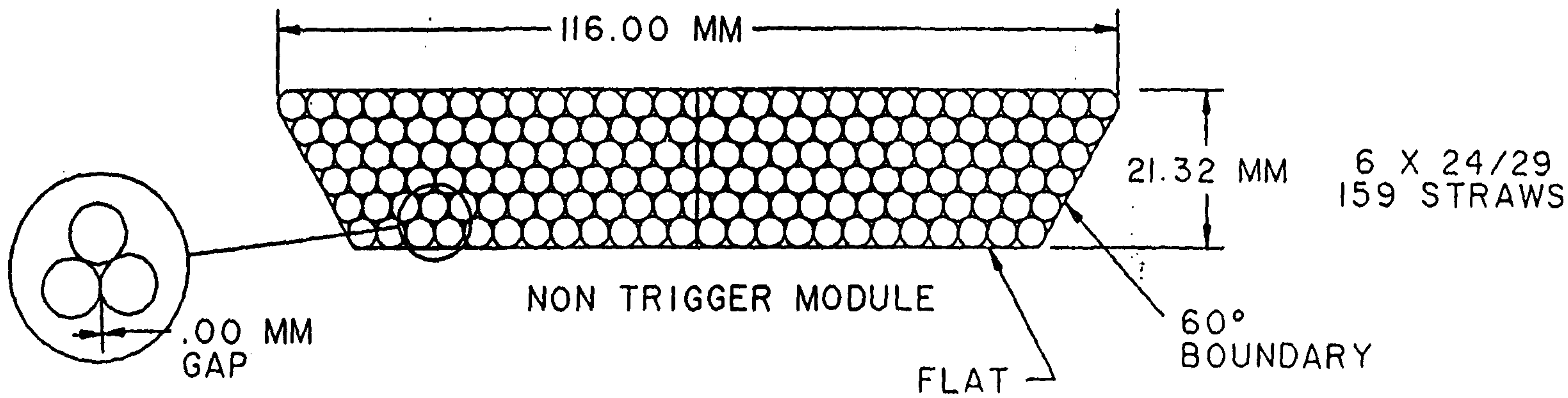

SUPERLAYER 3.75° INCLUDED ANGLE
WITH 3 MM GAP FOR OUTSIDE AXIAL TRIGGER LAYER

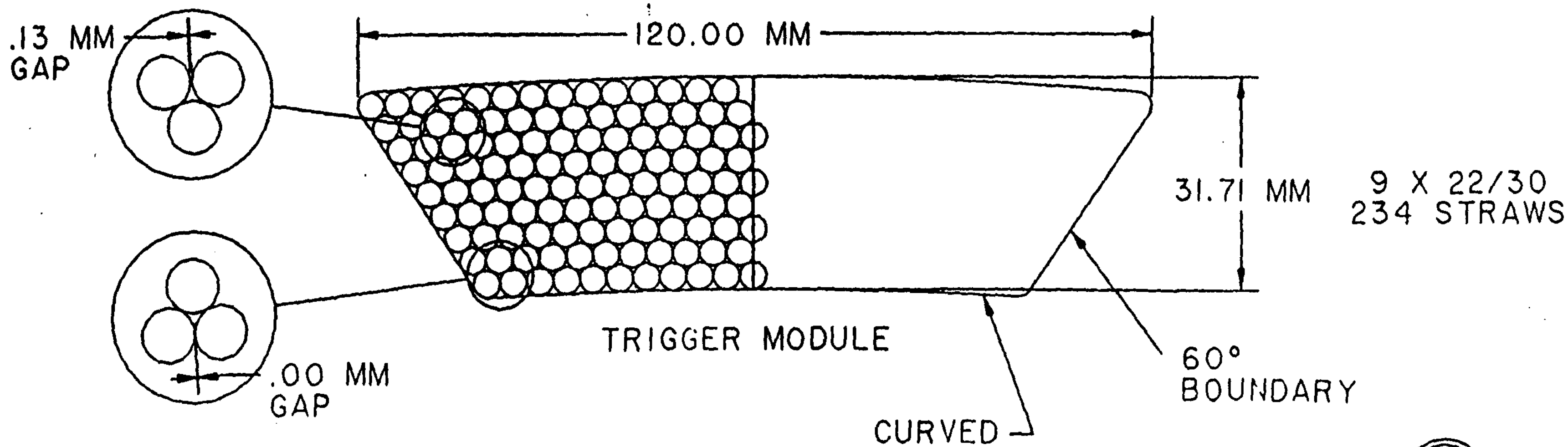

D.389.4136A46.R2

CENTRAL TRACKING SUBSYSTEM
COMPONENT MANUFACTURE
MODULE ASSEMBLY

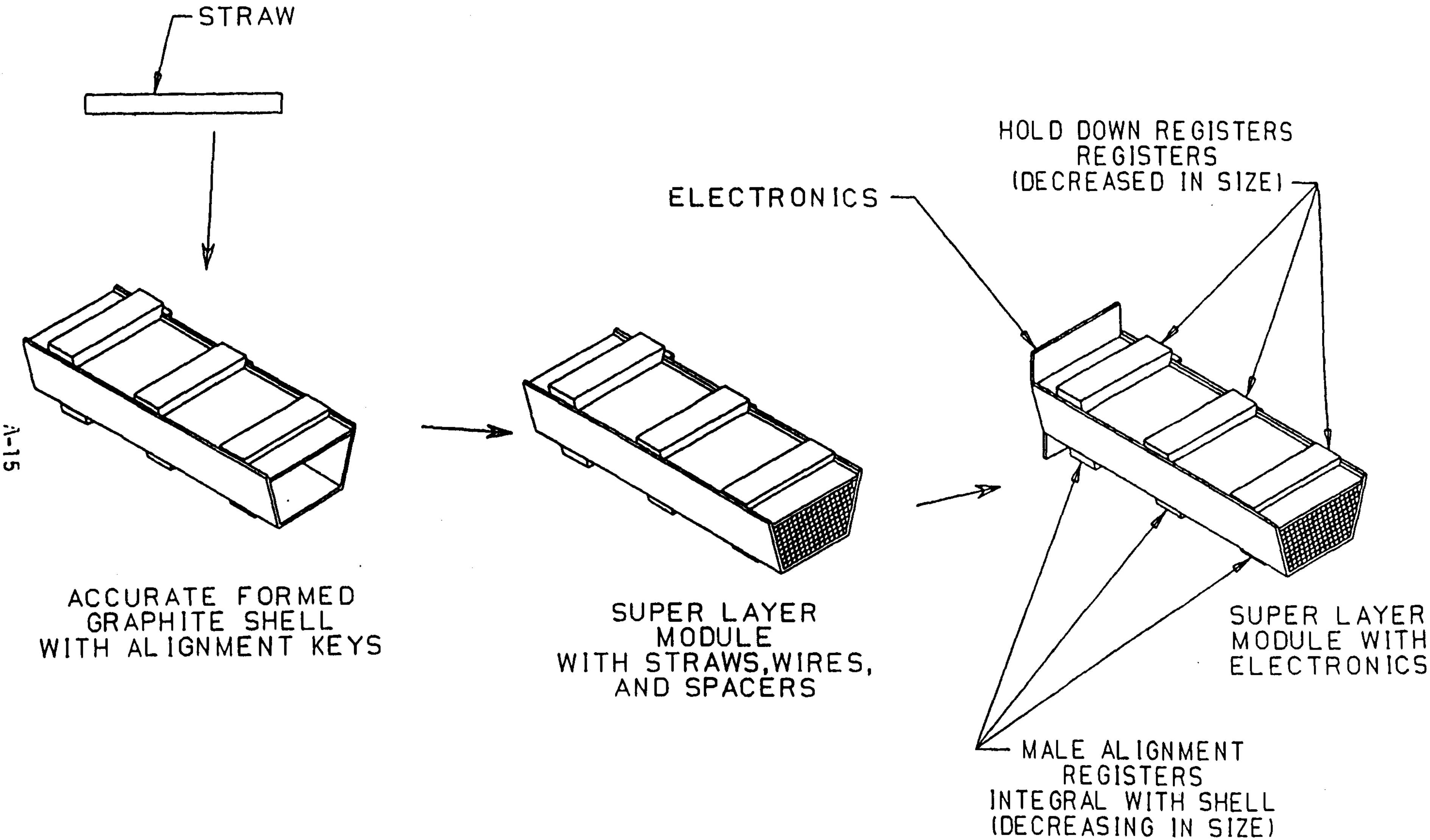

D.389.4136A58.R1
KEPES 1-30-91

CENTRAL AND FORWARD TRACKING SYSTEM
MODULE ATTACHMENT

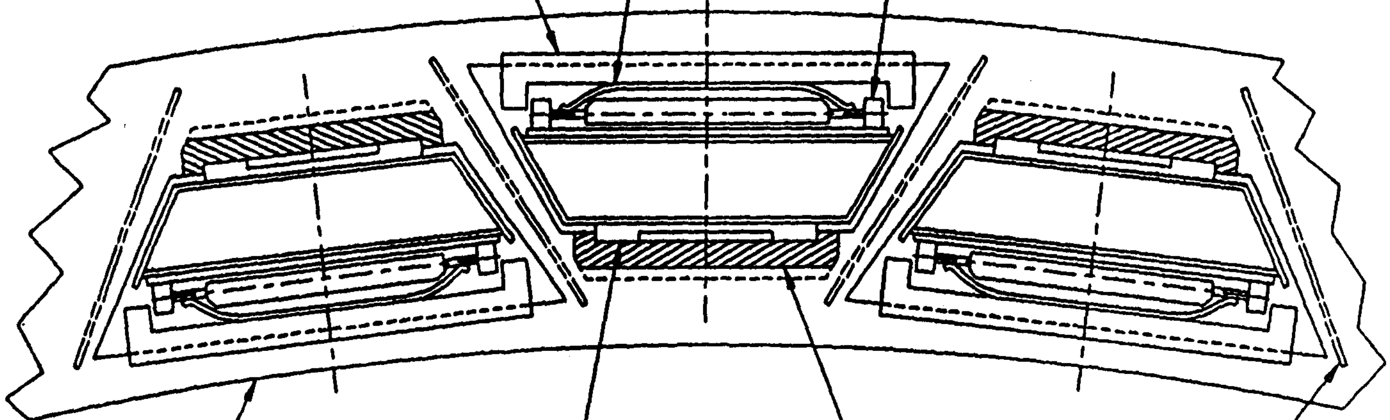

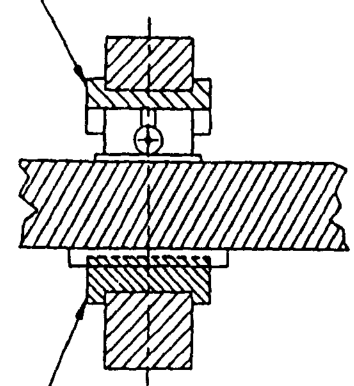

D.389.4136A66.R1
KEPES 2-9-91

CENTRAL AND FORWARD TRACKER
MODULAR STRAW DESIGN
CYLINDRICAL SUPPORT SYSTEM

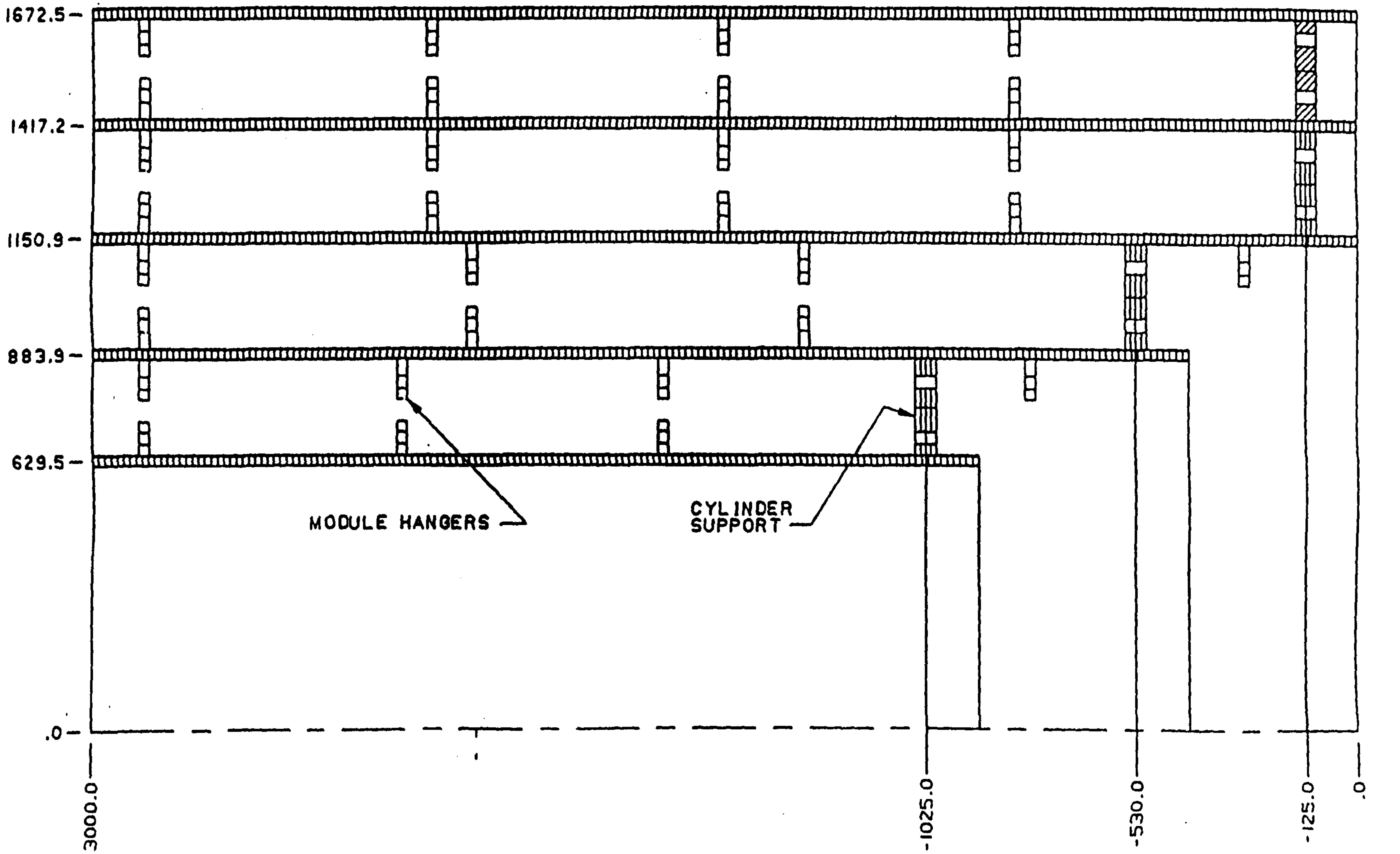

0.389.4136A61.R1
DIMS.IN MILLIMETERS
KEPES 2-1-91

CENTRAL AND FORWARD TRACKING SYSTEM

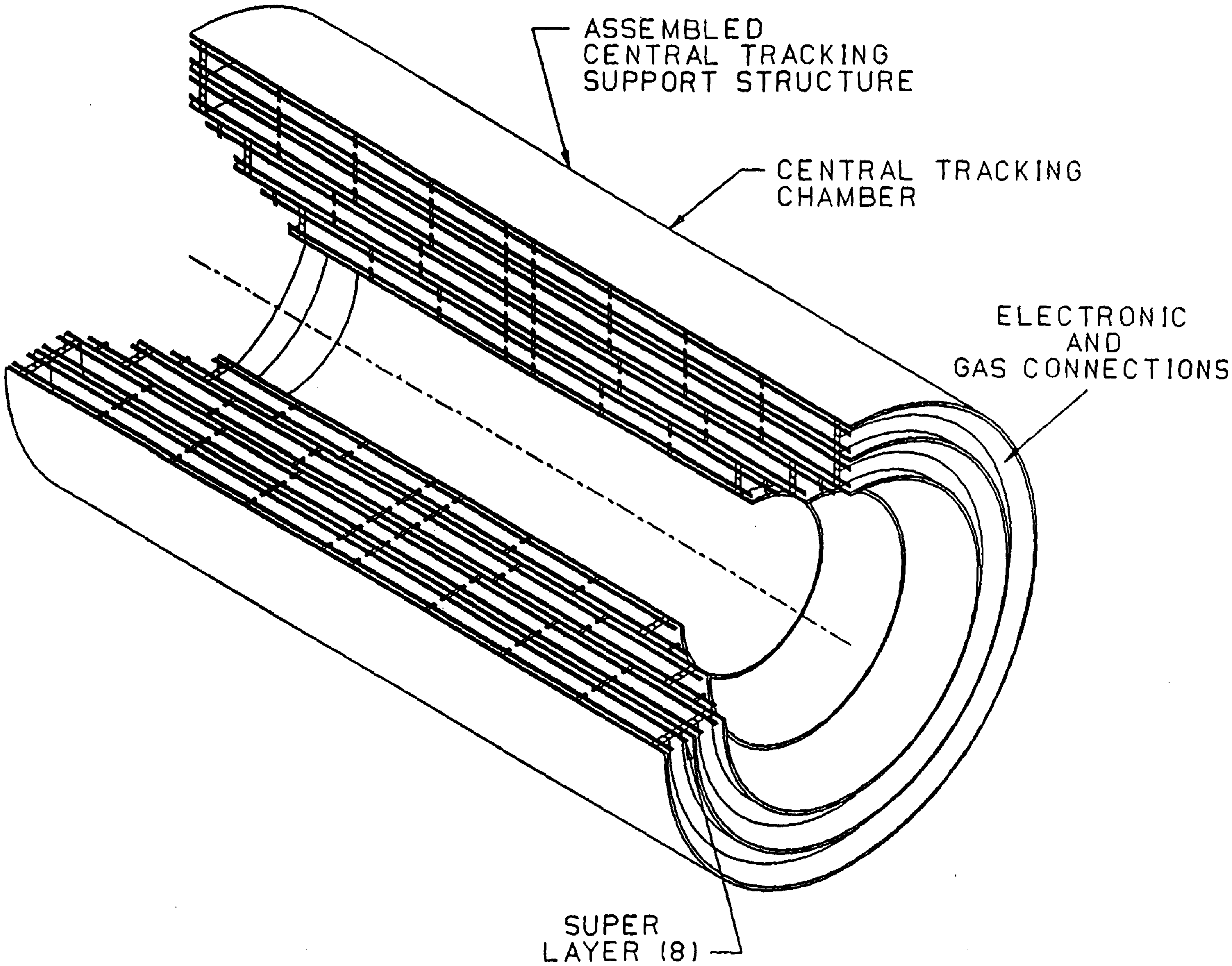

CENTRAL AND FORWARD TRACKING

STEREO STUDY USING DUAL ANGLES FOR ALTERNATING MODULES

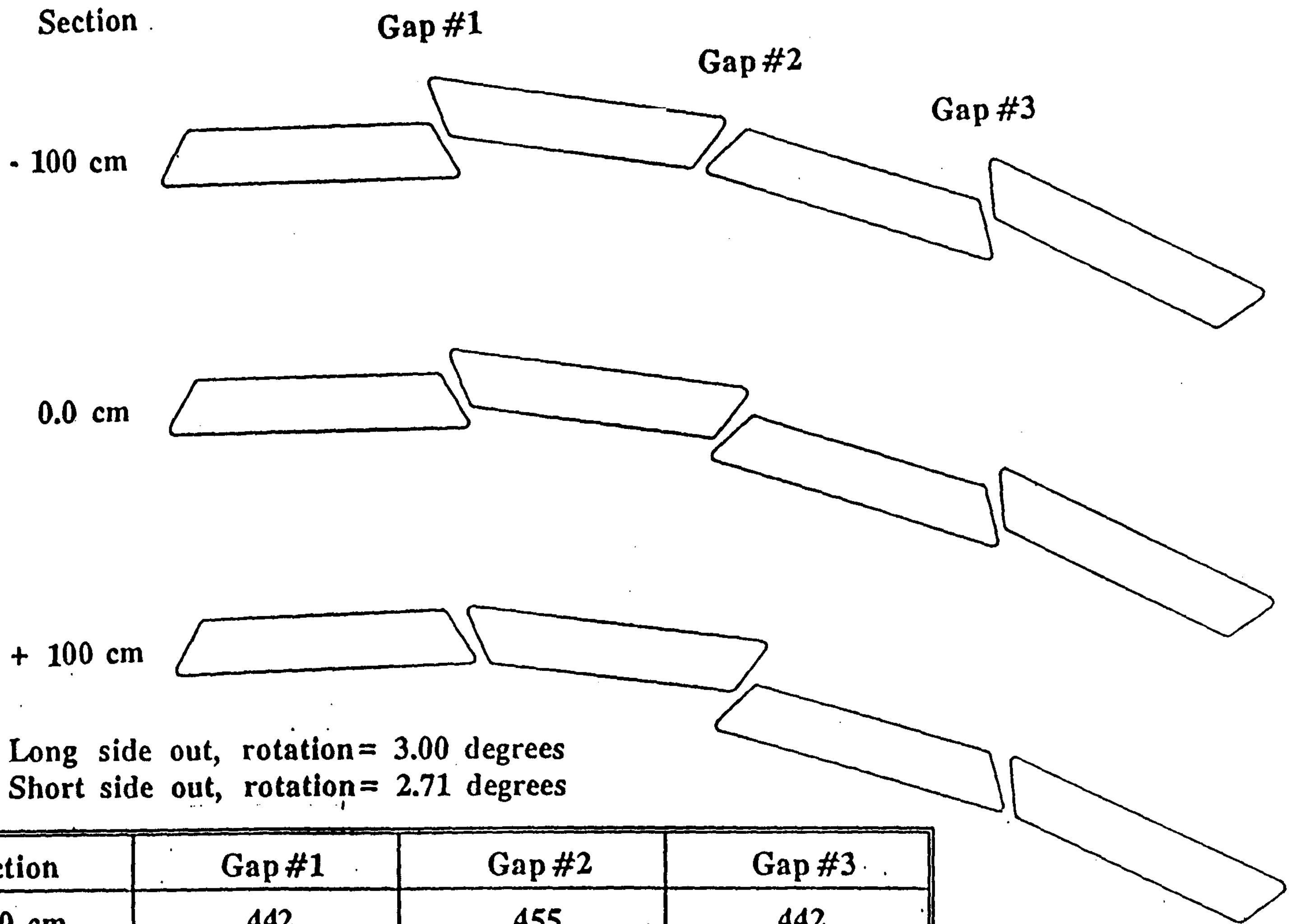

Long side out, rotation= 3.00 degrees
Short side out, rotation= 2.71 degrees

Section	Gap #1	Gap #2	Gap #3
- 100 cm	.442	.455	.442
0.0 cm	.415	.415	.415
+ 100 cm	.455	.442	.455

Westinghouse
Science & Technology Center

COST ESTIMATE OF CENTRAL STRAW TUBE TRACKER

DESC	NO.OF UNITS		COST/UNIT $		COST M$
STRUCTURE	2121	LBS.	3048		6.5
STRAW MODULES	905	LBS.	9320		8.4
	1088	MODULES	7752		
	188000	CHANNELS	45		
ELECTRONICS	188000	CHANNELS	85		16.0
FACILITIES	3	FACILITIES	1337417		4.0
FIXTURES,TRANS,MISC.	....		....		0.7
TOTAL INCLUDING BASE AND EDIA					35.7

REV3B120290

Table 6.16

BENEFITS OF USING MODULAR DESIGN FOR STRAW SUPERLAYERS

- Entire Compression Load is Taken by the Module Shell + Straws
  - 9 Kg Total Wire Load/Module (192 Straws)
  - Support Structure Can be Lightweight

- Mass Production Possible
  - Construct 1088 Modules
  - 188,000 Channels
  - Straw Size Identical
  - End Cap Design Identical, HV, Gas, Electronics

- Each Module Can be Tested, Calibrated, and Measured Prior to Assembly
  - HV and Gas Tests
  - Complete Electronics Assembly, Trigger

- Modular Structure Allows Repair and Replacement

- Modular Shell Aligns the Straws

- Support Structure Aligns the Modules

CENTRAL AND FORWARD TRACKING

ALIGNMENT REQUIREMENTS

CENTRAL AND FORWARD TRACKING

ALIGNMENT REQUIREMENTS

1. Module Location
   - Module Itself (Intrinsic)
     - Straightness +-75 Micron
     - Circumferential +-50 Micron
       - (X-Ray to Establish Map of Wire Position -With Respect to- Precision Located Module Register)
   - Structural Support Module Placement (Position)
     - Circumferential +-50 Micron
       - (Precision Located Male Module Register -Matched Fit With- Female Register Located with Optically Aligned Tooling in the Alignment Ring)
       - (Alignment Rings Which are Located with a Precision Calabrated
     - Radial +-400 Micron
2. Support Stability
   - Centroids of Si and Straw Systems +-15 Micron
   - Rotational Si with Respect to Straw System +- 0.00057 Degrees
   - Each Superlayer Circumferential +-50 Micron
   - Radial +-1.5 MM
3. Placement Support System
   - One End With Respect to Other End +-50 Micron
   - Entire Tracking System With Respect to Beam +-1 MM
   - Si System (Triggering System) +- 100 Micron

Westinghouse
Science & Technology Center

RLS
02-10-91

Harold Ogren
Indiana University
Feb. 11,1991

Support structure alignment and stability
and module and straw placement considerations

As a starting point, I assume that Abe's numbers on correlated errors are a statement of stability requirements for the structure. I will discuss initial placement later. The number I will quote for errors are sigma of the assumed gaussian errors. ie. +-sigma = +- 15 microns In order to be conservative we will assume that this should be interpreted as construction tolerances ie. +- 15 microns, where 1 mil = 25.4 microns.

Support stability:

1) the centroids of the Si and the Straw system must not vary by more than +- 15 microns. This will require monitoring.

2) The rotational stability of the Si with respect to Straw layers is Δ phi = +_ 10^{-5} radians= +_ 0.00057 degrees. This also should be monitored.

3) Each superlayer must have a circumferential stability (phi rotation with respect to other superlayers) that is about +- 50 microns. (actually the requirement is less strict for the inner layers of the straws, but lets be conservative). This will require a good understanding of the long term stability of support materials, but may not require continuous monitoring.

4) The radial stability is much less stringent. The purely radial stability is +_1.5 mm. However, this assumes that the circumference position (phi) does not change. So, I don't think this really allows us much design flexibility. Abe reduces this to +- 200 microns.

Placement errors:Support system:

1) Placement of each end of the system with respect to other end. (hard to say, needs more work, probably close to the rotational requirement for each module, ie. +- 50 microns.) Will be fixed at assembly time using optical alignment techniques.

2) Placement of the entire tracking system with respect to the beam is , in part set by the amount of beam movement we expect. (+-1 mm?)
It is also set by the triggering requirements in the Si system., so it should be smaller than a strip size , say +- 100 microns. This may require local (Si) adjustment. This can be done to high accuracy during initial installation, and then monitored each down time, and perhaps adjusted with the kinematic constraints.

3) Assuming that the module supports are aligned after the support structure is complete, the construction of the gross support frame need not be more accurate than +- 500 microns. This is a detail of how the support cylinders are made.

Module requirements:

1) Placing modules on the cylinders (mod placement)

Assuming that we have monolithic support rings for the modules in each superlayer, then the over all angular error should result in a maximum of +_ 50 microns for each ring.(this is the total placement error for the mean position of the ring, ie placement of fiducial points at say 8 positions of the ring.)(this keeps the correlated errors under control)
This is conservative, since we have 3-4 attachment points on each module.

2) Module intrinsic straightness.

From our limited tests on 1 meter, smaller section shells, the bowing should amount to less than +_50 microns between support points (80 cm). Take +- 50 conservatively. This is one place where the reduced radial requirement helps us, since the modules are thinner radially, and might have more built-in bowing in this direction.

The straw placement error will add in quadrature with the intrinsic wire resolution, assuming that they are random , uncorrelated errors. We have attempted to determine the size of such placement errors by optical measurements of straw center (double vee) positions at the end of a 64 straw rhombus. The x-y positions were measured using a milling machine and an optical telescope. Our estimated reading error was about +- 1 mil. The measurements were done with the endplate inserted in the rhombus shell. These measurements were then fitted to a close packed pattern with arbitrary center, rotation, and straw radius. This resulted in a 65 micron average sigma. determination of wire centers. So a good part of this may be our measurement error. The best fit straw separation was 3984 +- 7 microns.

In order to determine the effects of correlated errors in the straw positions, the difference matrix from the above fit was used to fit vertical tracks. (see Figure 1). Correlation effects would show up as significant deviations from a "Zero "crossing. These were found to be small < 30 microns for all x positions. We will assume a straw placement error of 65 micron wire placement, however this can be improved considerably.

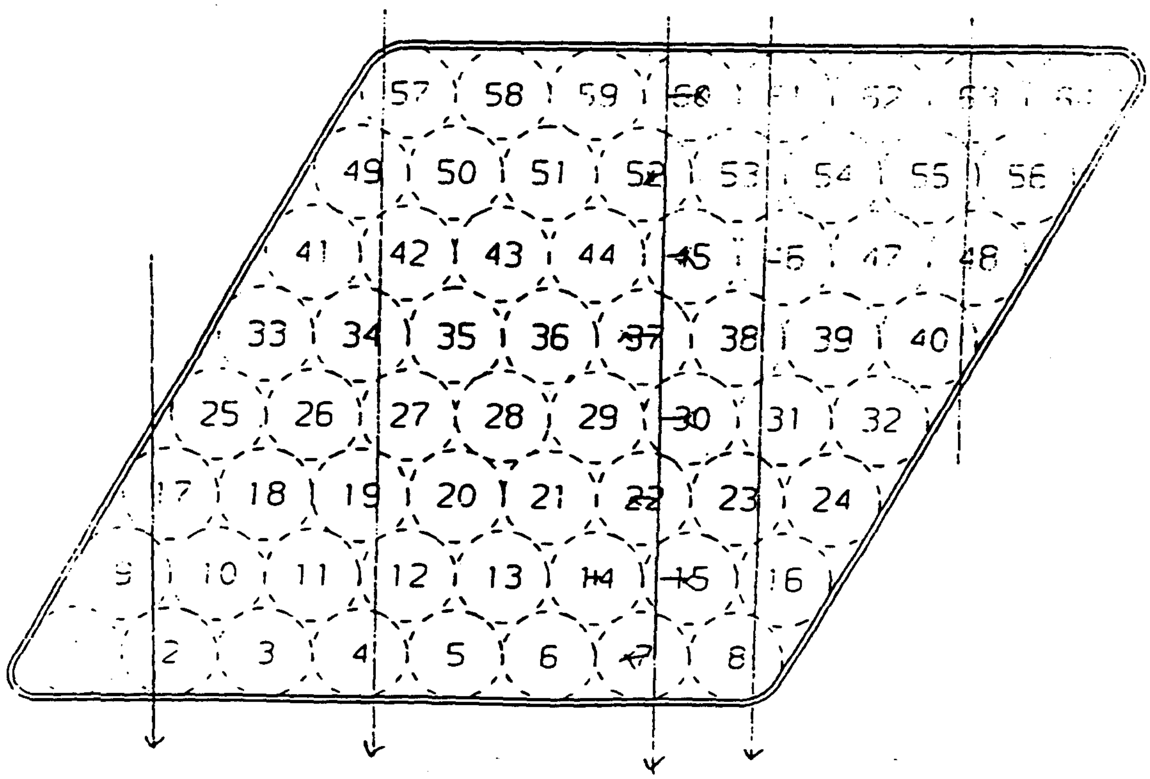

Fig. 1 Fitting tracks with wire displacements

For the trapezoidal modules the required straw placement precision will be obtained by fitting the wire positions as measured by x-rays to the fiducial points on the underside rails. (See Figure 2). We anticipate that these will be measured as the quality control step in fabrication, since it will also tell us if we have loose wires or irregular placement.

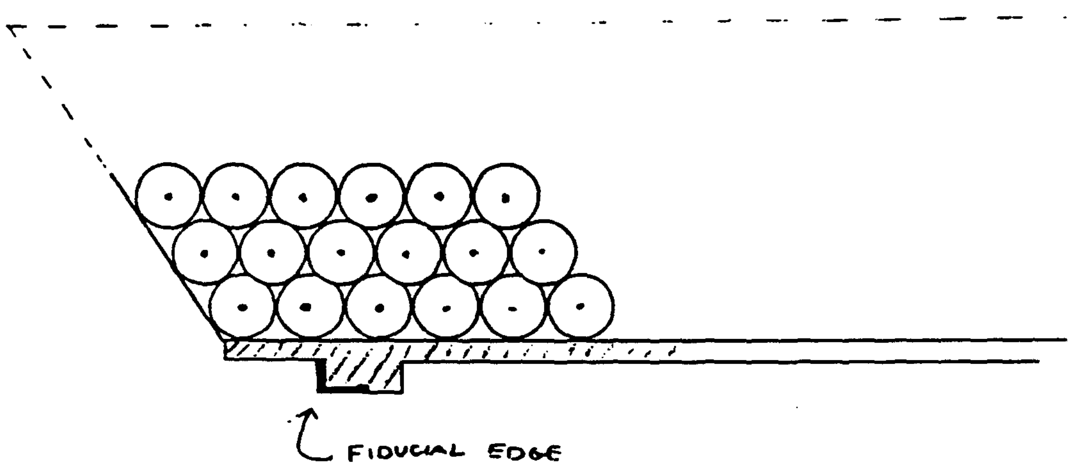

Fig. 2 Detail of Straw and Module fiducal

Intrinsic wire resolution

The intrinsic wire resolution for CF4- Isobutane is about 100 microns. Since this is not the limiting feature in the superlayer resolution, I will not go into the details of the measurement here.

Superlayer resolution

We will take the final superlayer resolution to be 80 microns.
So we can write (assuming 6 straw layers)

$$80^2 = (\sigma^2_{\text{wire in}} + \sigma^2_{\text{wire placement}})/6 \quad +\sigma^2_{\text{mod in}} \quad +\sigma^2_{\text{mod placement}}$$

If we use an intrinsic wire resolution of 100 microns, wire placement error of 65 microns, module placement error of 50 microns, and module intrinsic error of 50 microns. then we get get micron total superlayer error of 83 microns. I take this to indicate that we can build and align a modular system that will give us the required momentum resolution.

Notice that unlike Abe, we conclude that the major part of the error in the superlayer measurement comes from alignment not intrinsic error in the straw.

Silicon Tracking System

TYPICAL ALIGNMENT CAPABILITIES

- Angle
  - Alignment Telescopes ~ 15 μradians
  - Precision Theodolites ~ 3 μradians
  - Precision Electronic Levels ~ 3 μradians
  - Electronic Autocollimators ~ 0.05 μradians
- Length
  - Hewlett Packard Interferometer ~ 0.05 microns
- Position
  - Quadrant Detectors ~ 0.5 microns
  - Camera's & Centroid Software
    - ~ 1/100 - 1/200 of Pixel Spacing (25 microns)
    - ~ 0.25 - 0.1 microns
  - Misaligned Fibers 0.001 microns

A-31

Los Alamos

CENTRAL AND FORWARD TRACKING SUBSYSTEM

ALIGNMENT RING FABRICATION
Ring Blank

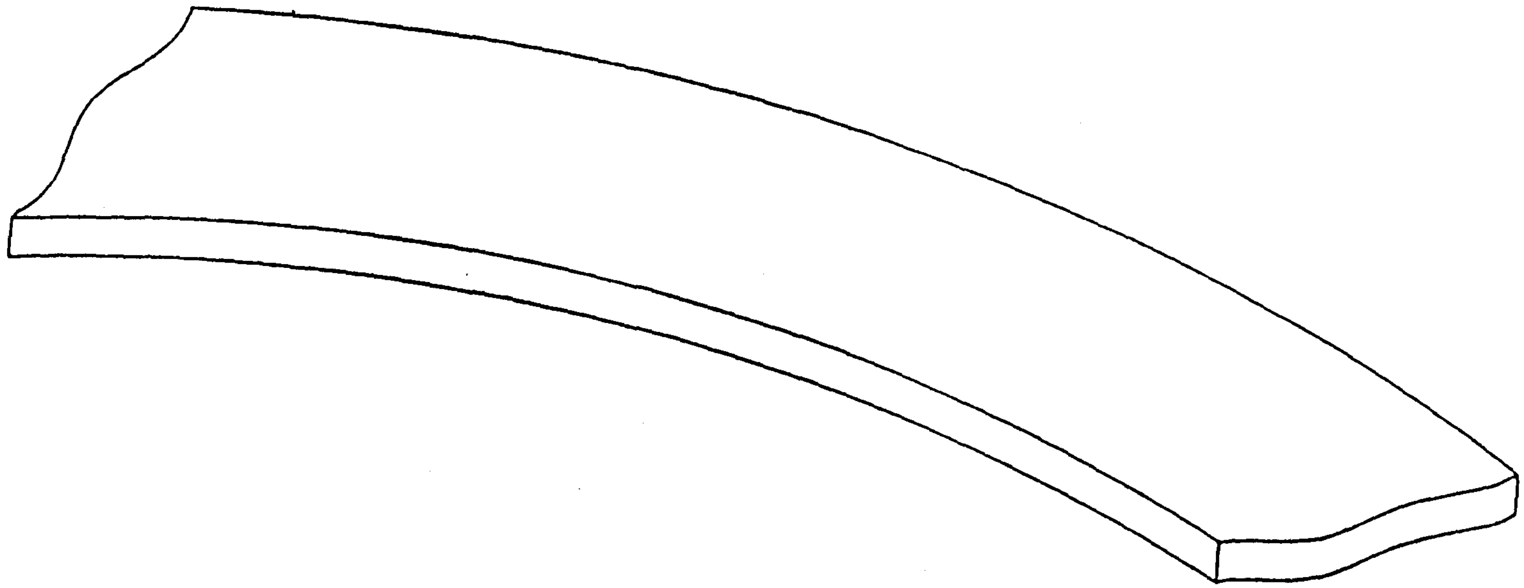

Westinghouse
Science & Technology Center

C IT AL R KI S B S
COMPONENT MANUFACTURE
SUPPORT RINGS

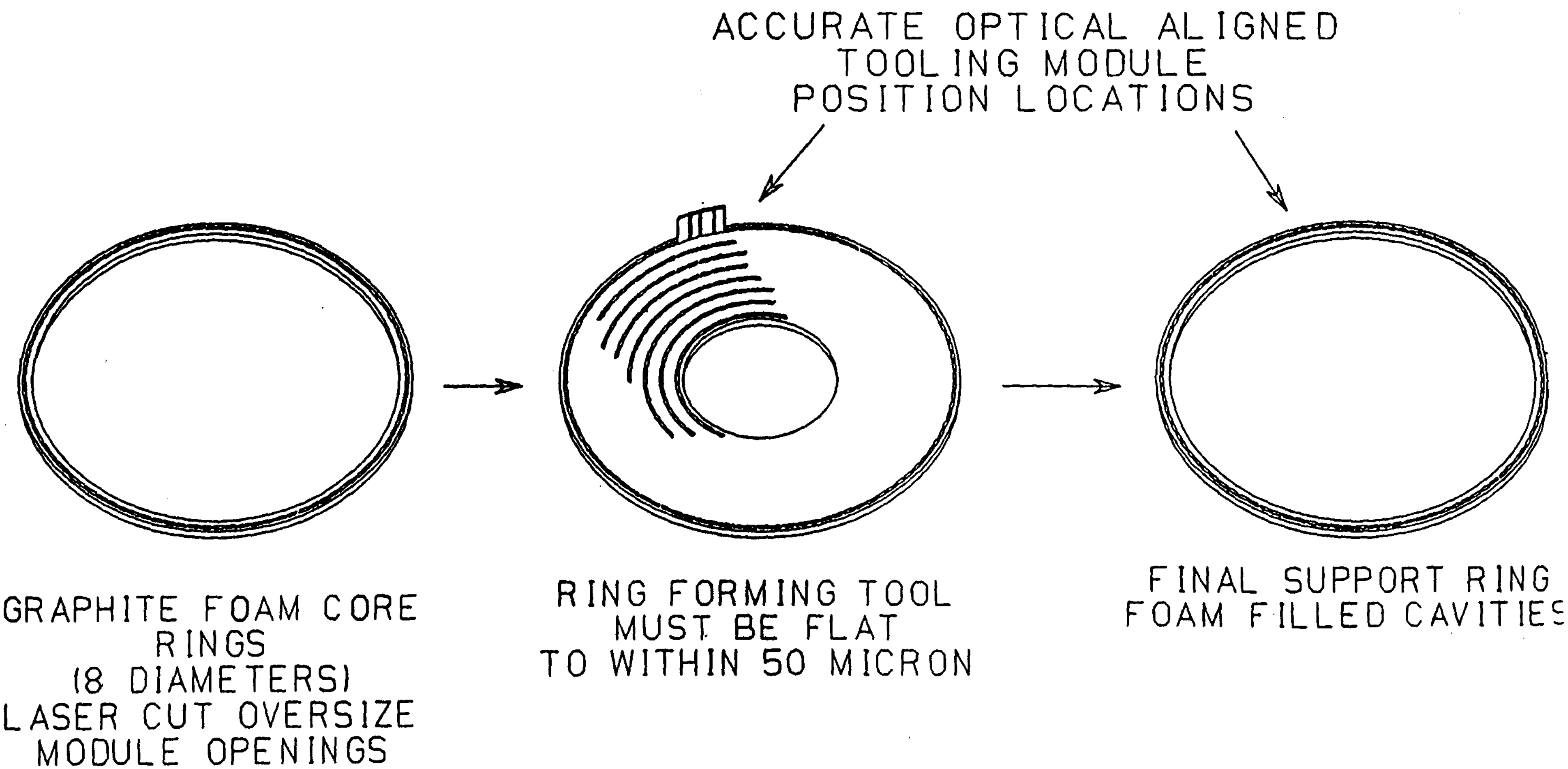

D.389.4136A59.R1
1-30-91

CENTRAL AND FORWARD TRACKING SUBSYSTEM

ALIGNMENT RING FABRICATION
Ring Blank

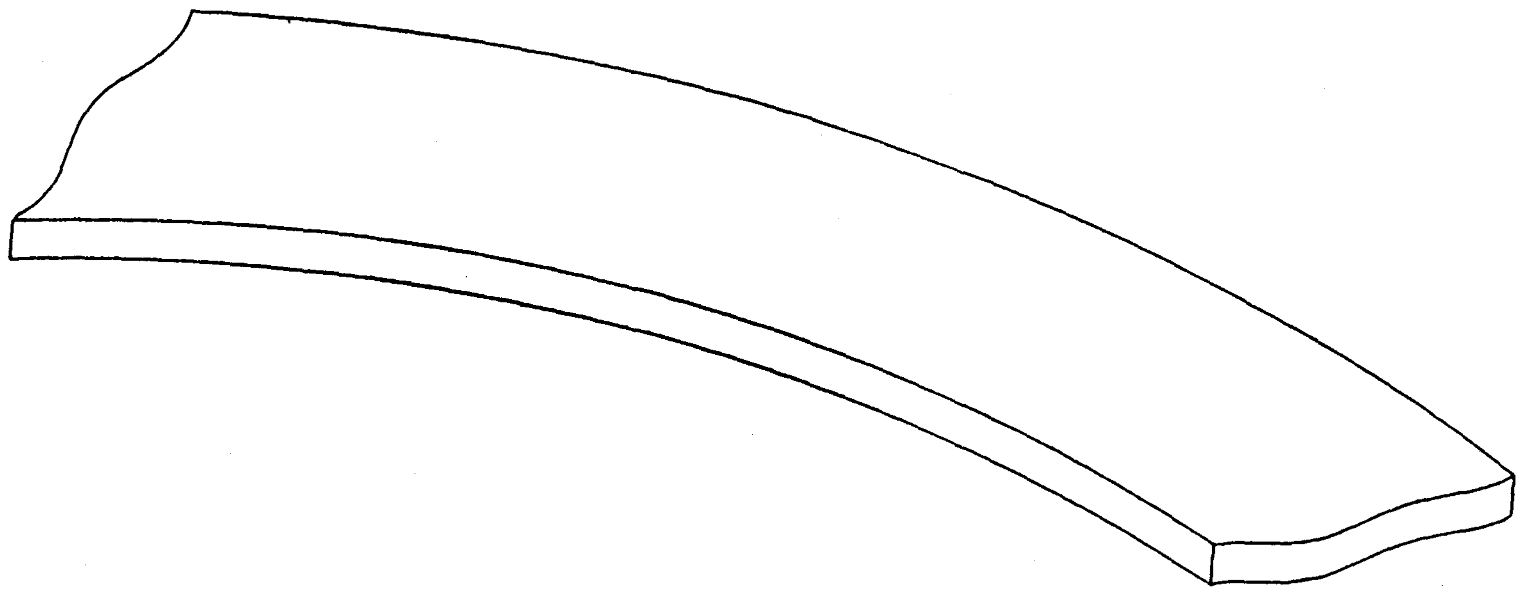

A-34

Westinghouse
Science & Technology Center

(N' AL 'R K.' ; . B' IS M

COMPONENT MANUFACTURE
SUPPORT RINGS

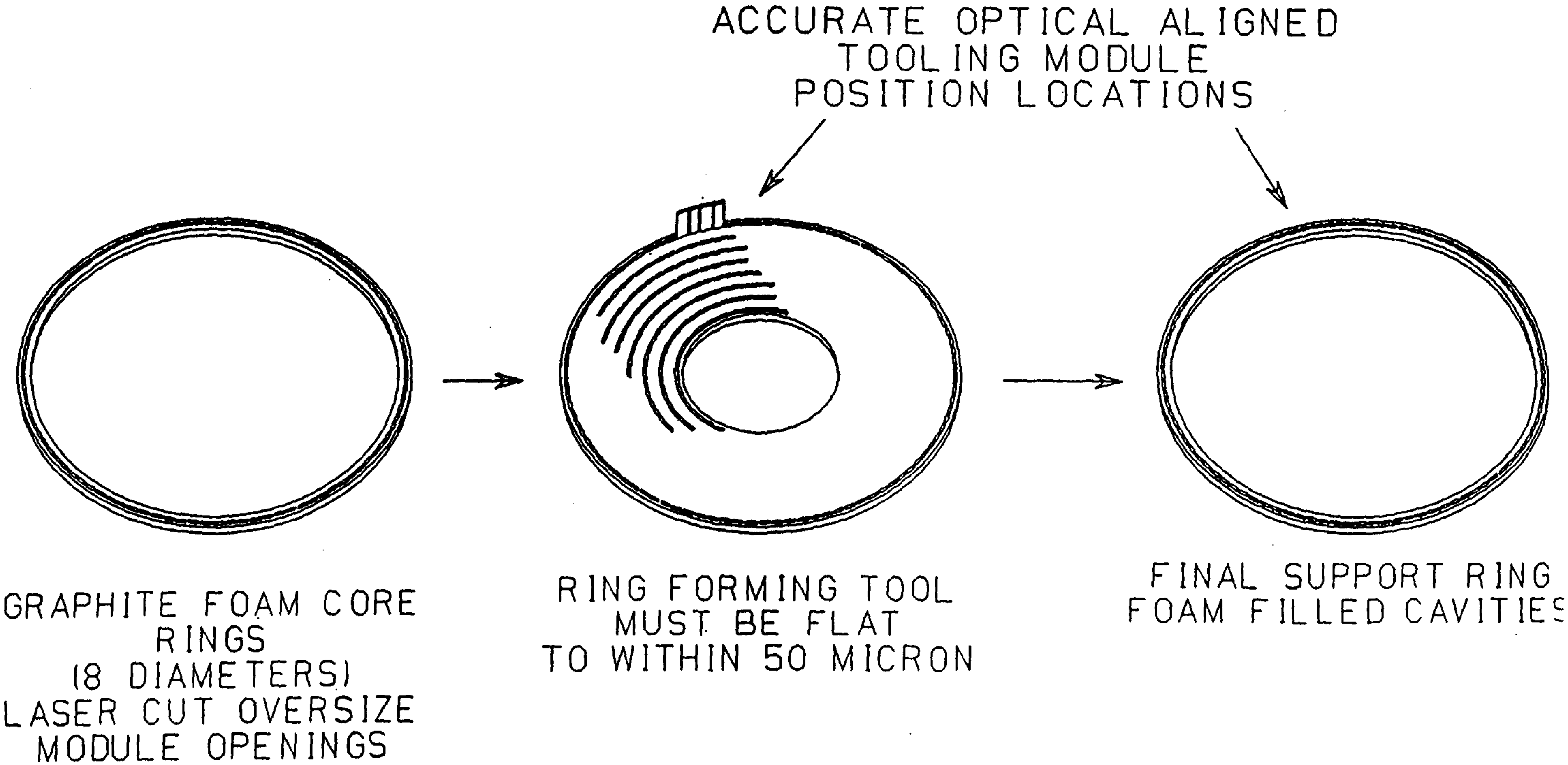

-D.389.4136A59.R1
1-30-91

CENTRAL AND FORWARD TRACKING SUBSYSTEM

ALIGNMENT RING FABRICATION
Ring Blank

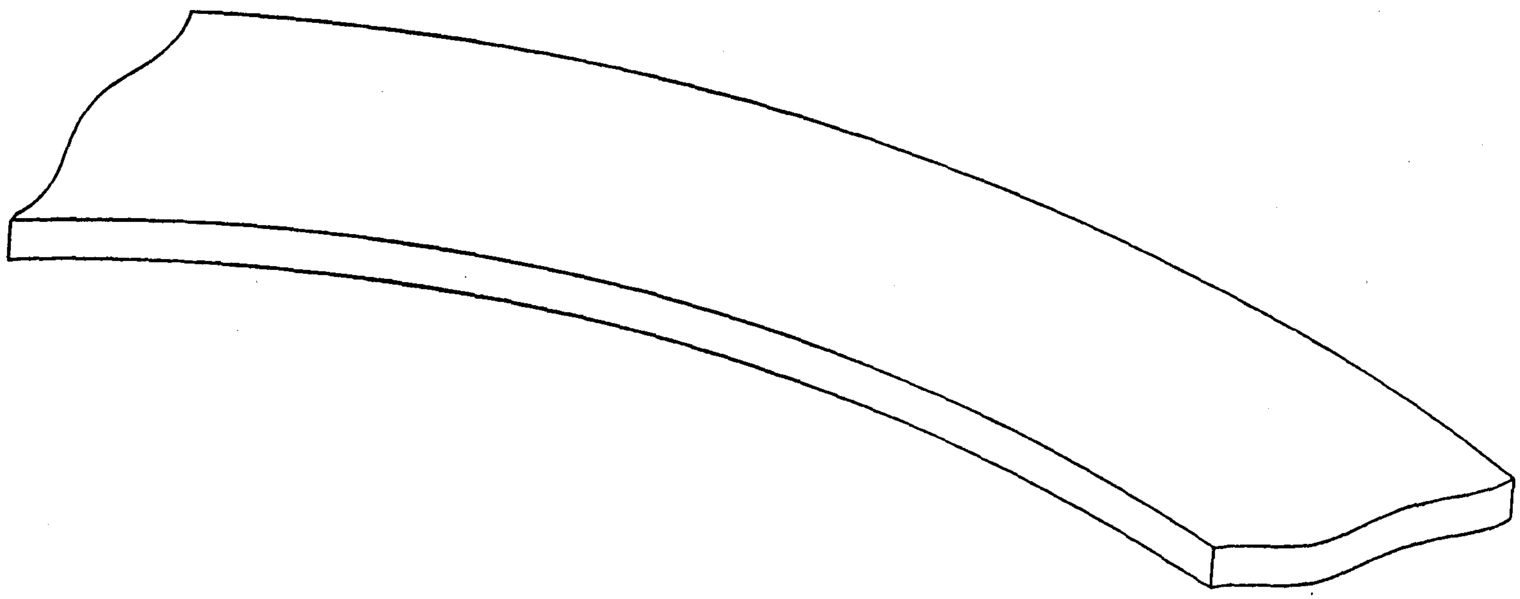

Westinghouse
Science & Technology Center

CENT..AL TR. KI G S B YS M
COMPONENT MANUFACTURE
SUPPORT RINGS

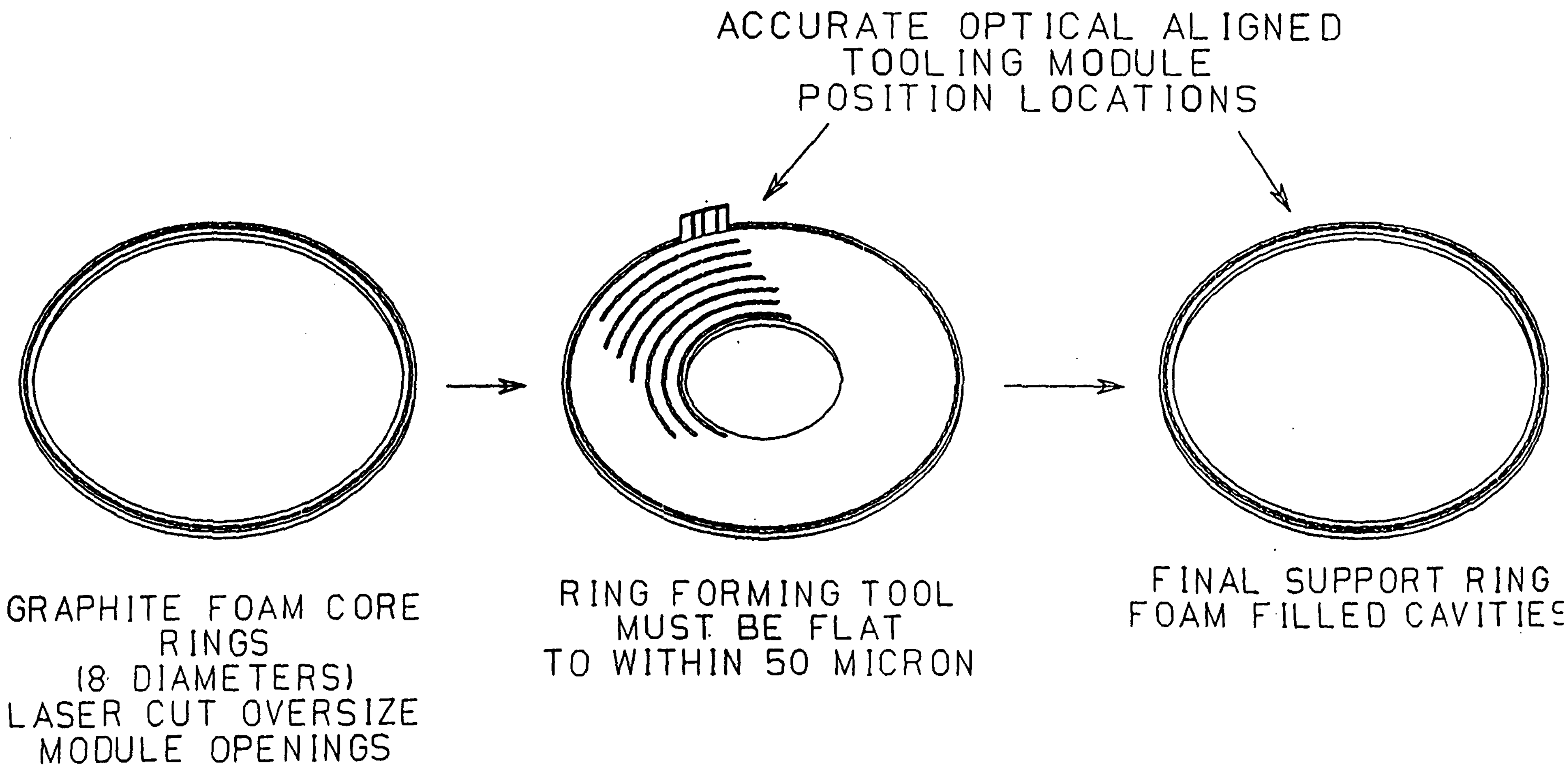

D.389.4136A59.R1
1-30-91

CENTRAL AND FORWARD TRACKING SUBSYSTEM

ALIGNMENT RING FABRICATION
Ring Blank

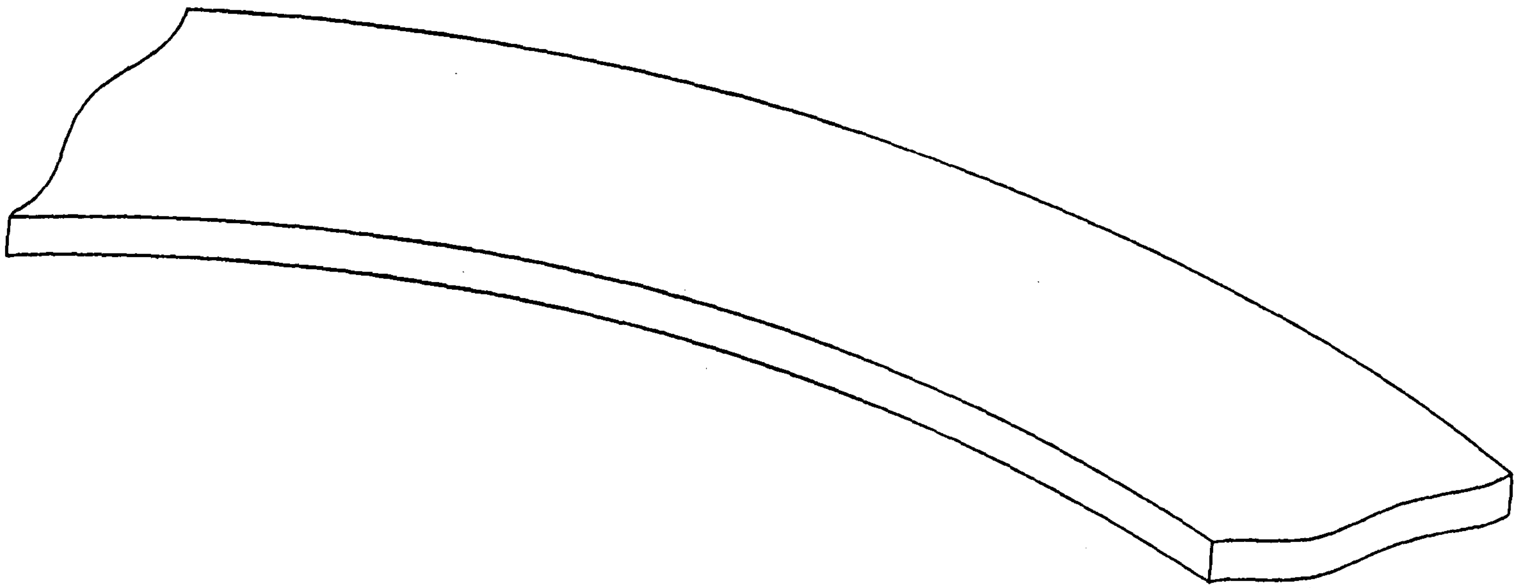

Westinghouse
Science & Technology Center

SILICON TRACKING SYSTEM

Detector Alignment Approaches	Considerations
● Visual and IR	● Convenient - personnel present during operation ● Commercially available instumentation ● Visual presentation - easier interpretation ● Fast rise time pulses ● Will pass through silicon, but blocked by metalization ● Good tools for assembly
● X-ray	● Particle like - smaller track ● Will pass through metal and G/E structure ● Inconvenient for assembly operation ● Electronic sensing required ● Good tool for assembled alignment/ electronic checkout

Los Alamos

SILICON TRACKING SYSTEM

GENERAL SILICON SYSTEM ALIGNMENT CONCEPT

- Use visual optics and IR laser sources for silicon tracker part - to part and sub-assembly - to sub-assembly pattern registration and therefore alignment. This requires close coordination between chip layout, chip manufacture and assembly/alignment teams

- Use x-ray source for final *in situ* alignment checks, registration of straw tubes to silicon tracker and final electronic check out. This requires an x-ray alignment system at Los Alamos for final assembly check prior to shipping and installation
  - Beam tube diameter may be a limiting factor

- Complementary techniques also give useful cross checks

Los Alamos

MODULE FABRICATION AND ASSEMBLY

Westinghouse
Science & Technology Center

CENTRAL AND FORWARD TRACKING

COMPONENT MANUFACTURING

Developed for Ease of Automation, Maintenance and Repair

1. Fabricate the Superlayer Module Shells
   - Manufacture the Module Shell Tops
     - Preplace Hold Down Registers Into the Precision Tooling
   - Manufacture the Module Shell Bottoms
     - Preplace Prefabricated Alignment Registers Into Precision Tooling

Westinghouse
Science & Technology Center

MODULE SHELL

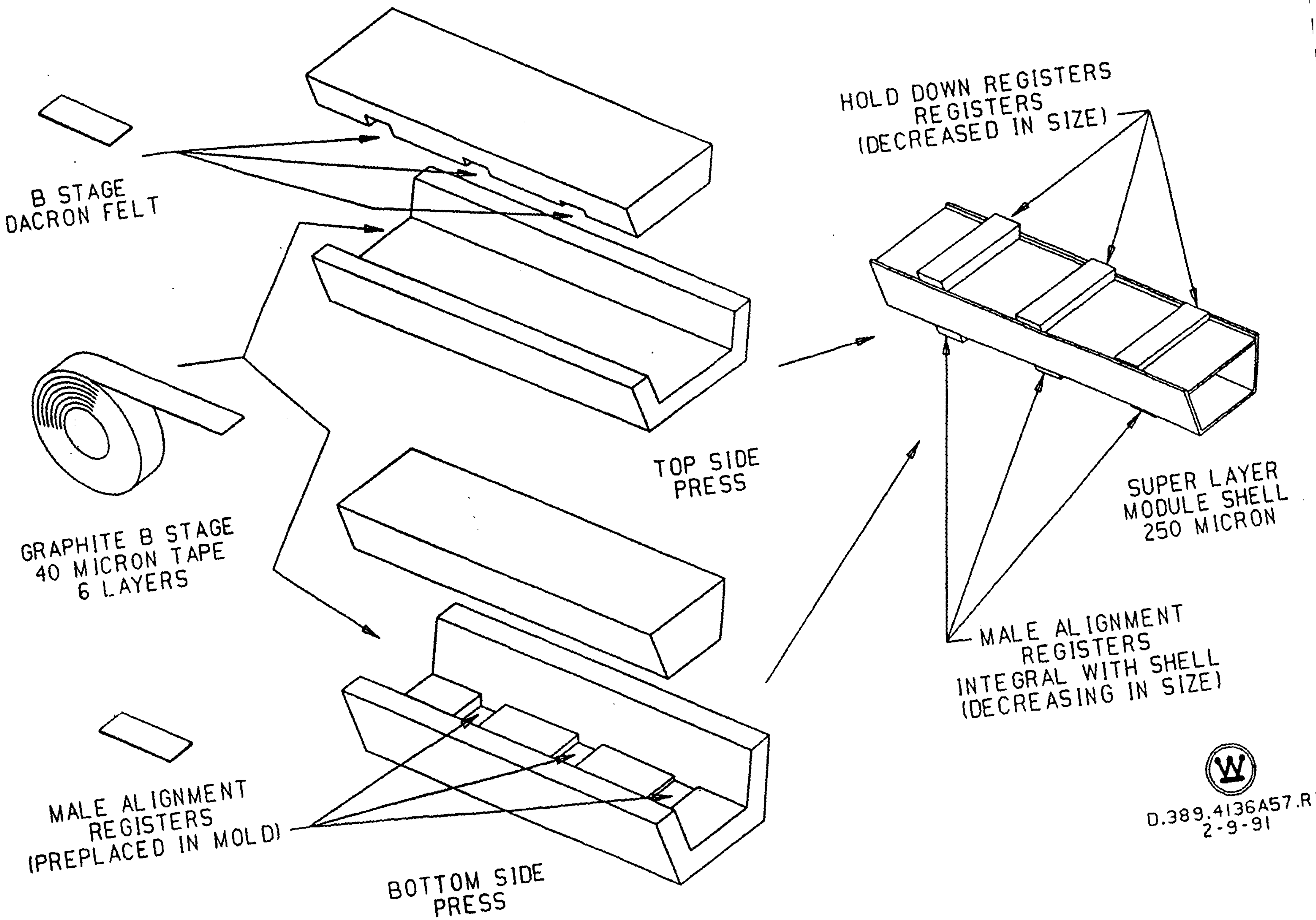

CENTRAL AND FORWARD TRACKING

COMPONENT MANUFACTURING

Developed for Ease of Automation, Maintenance and Repair

2. Assemble the Superlayer Modules (Designed for Manufacturing)
   - Machine Insert Support Spacers, End Caps and Wires Into Straws
   - Form to Desired Straightness in Tooling While Inserting Epoxy Potting at Discrete Locations?
   - Place Assembled Straws Into Module Shell Bottoms
   - Bond Shell Top Onto Shell Bottom in Tooling
   - Install Electronics
   - Test Straw Functionally (as a Complete Assembled Module)

Westinghouse
Science & Technology Center

CENTRAL TRACKING SUBSYSTEM
COMPONENT MANUFACTURE
MODULF ASSEMBLY

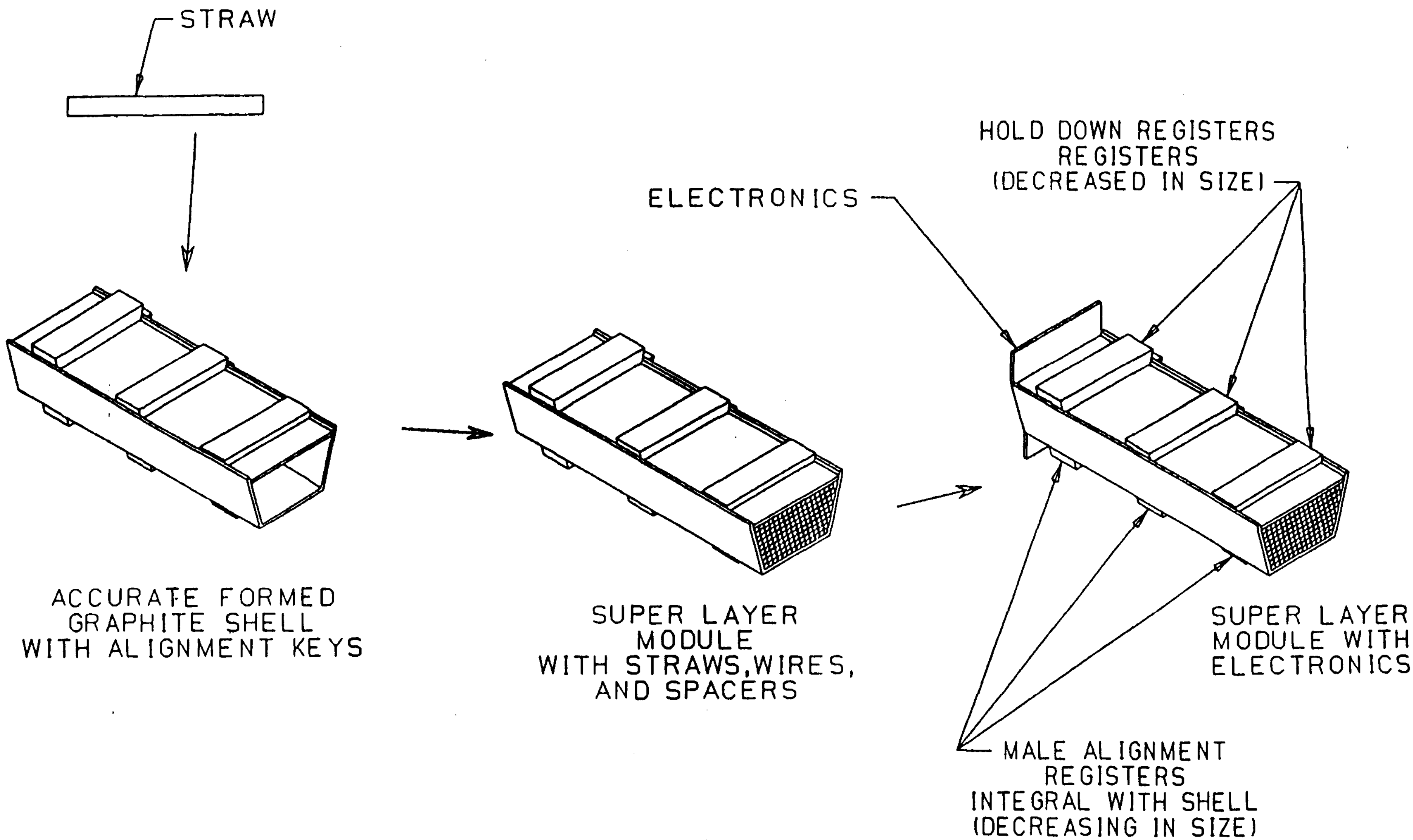

D.389.4136A58.R1
KEPES 1-30-91

CENTRAL AND FORWARD TRACKING SUBSYSTEM

SUPPORT STRUCTURE COMPONENT FABRICATION

Westinghouse
Science & Technology Center

COMPONENT MANUFACTURING

Developed to Accommodate Conventional Fabrication Tolerances

1. Manufacture the Inner, Outer and Three Intermediate Foam Core Torsion Cylinders
   - Layup Machine Tape Inner Skin on Mandrel
   - Add Foam Core Segments
   - Layup Machine Tape Outer Skin

CENTRAL TRACKING SUB SYSTEM
COMPONENT MANUFACTURE
TORSION CYLINDERS
FIVE TOTAL

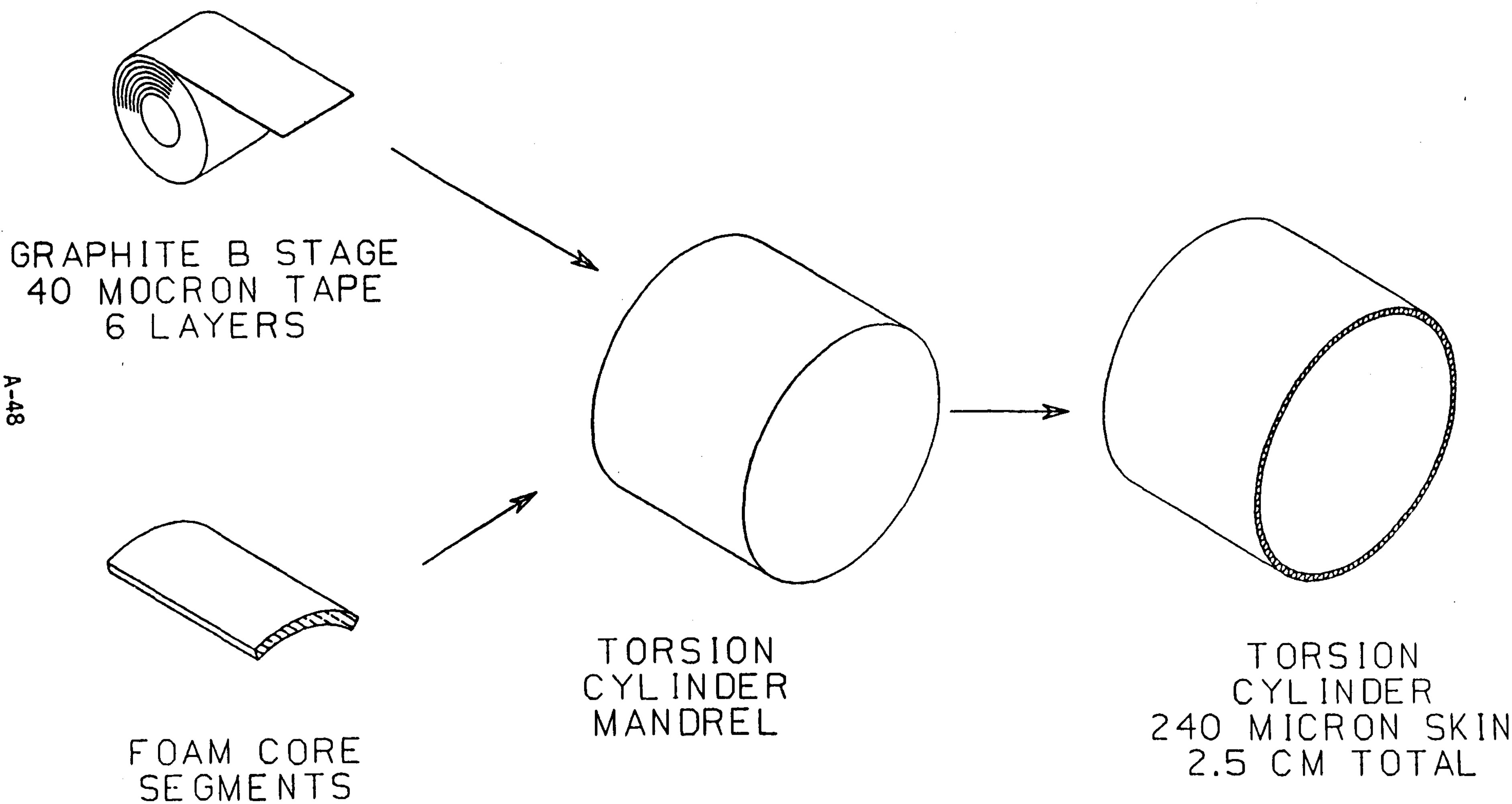

D.389.4135A96.R3
KEPES 2-4-91

CENTRAL AND FORWARD TRACKING

COMPONENT MANUFACTURING

Developed to Accommodate Conventional Fabrication Tolerances

2. Fabricate Alignment Ring Module Attachments
   - Mold in Accurate Tooling Matched Male and Female Alignment Registers
     - The Mold Component Will Be Attached to the Bottom of Module Shell
     - The Female Component Will Be Attached to the Alignment Rings
   - Mold and Assemble the Hold Down Registers
     - The Slight Spring Loaded Component Will Be Attached to the Alignment Ring
     - The Bearing Surface Will Be Attached to the Top of the Module Shell

Westinghouse
Science & Technology Center

CENTRAL AND FORWARD TRACKING SYSTEM
MODULE ATTACHMENT

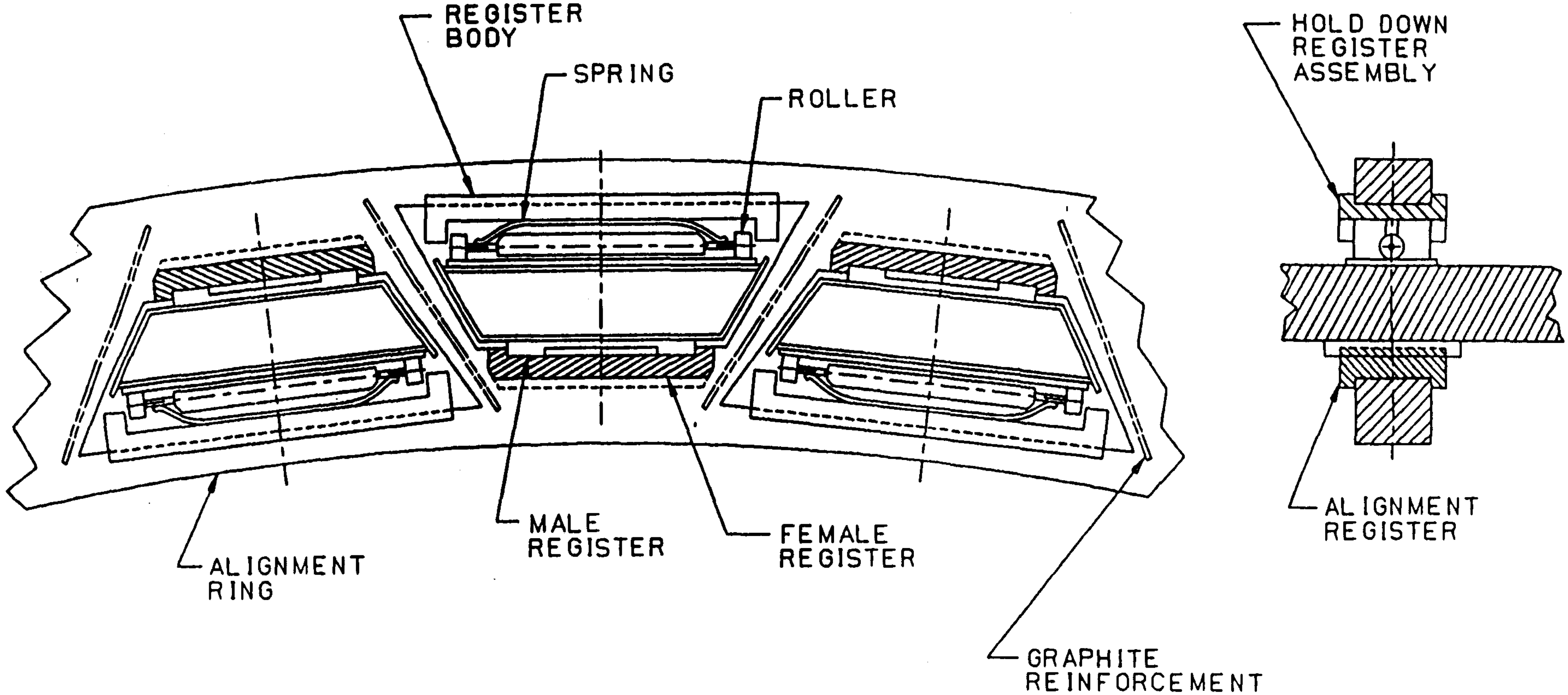

D.389.4136A66.R1
KEPES 2-9-91

CENTRAL AND FORWARD TRACKING

COMPONENT MANUFACTURING

Developed to Accommodate Conventional Fabrication Tolerances

3. Manufacture the Alignment Rings
   - Fabricate the Ring Components by Layup on Flat Tooling
   - Rough Laser Cut Openings
   - Optically Align Tooling
   - Preplace "Female Register" and "Hold Down Positioner" on Tooling; One at Each Module Support Location
   - Place Laser Precut Ring Over Tooling With Attached Registers
   - Bond Into Single Unit Producing a Very Accurate Alignment Ring
   - Remove From Tooling
   - Proceed to Manufacture Next Ring

Westinghouse
Science & Technology Center

CENTRAL TRACKING SUB SYSTEM
COMPONENT MANUFACTURE
SUPPORT RINGS

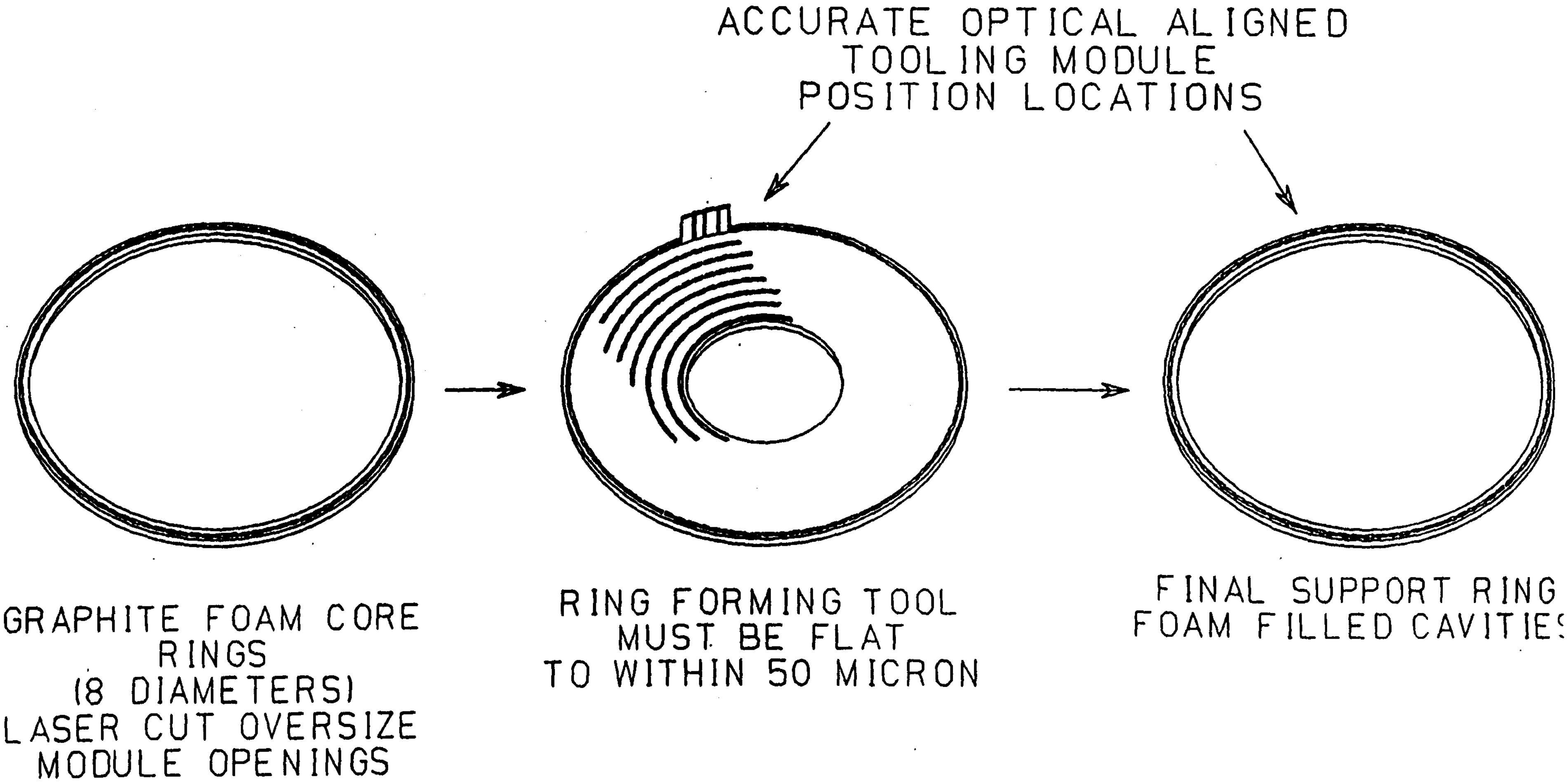

D.389.4136A59.R1
1-30-91

CENTRAL AND FORWARD TRACKING SUBSYSTEM

ALIGNMENT RING FABRICATION
Ring Blank

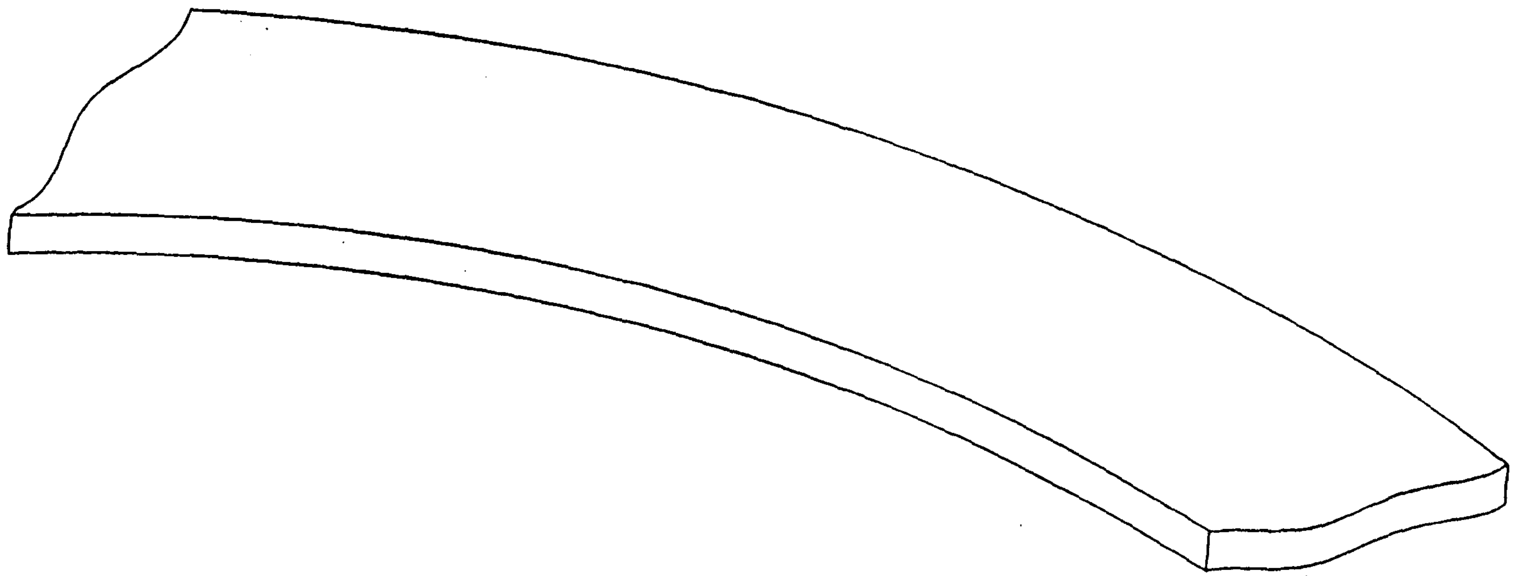

Westinghouse
Science & Technology Center

CENTRAL AND FORWARD TRACKING SUBSYSTEM

ALIGNMENT RING FABRICATION
Adhesively Joined Completed Alignment Ring

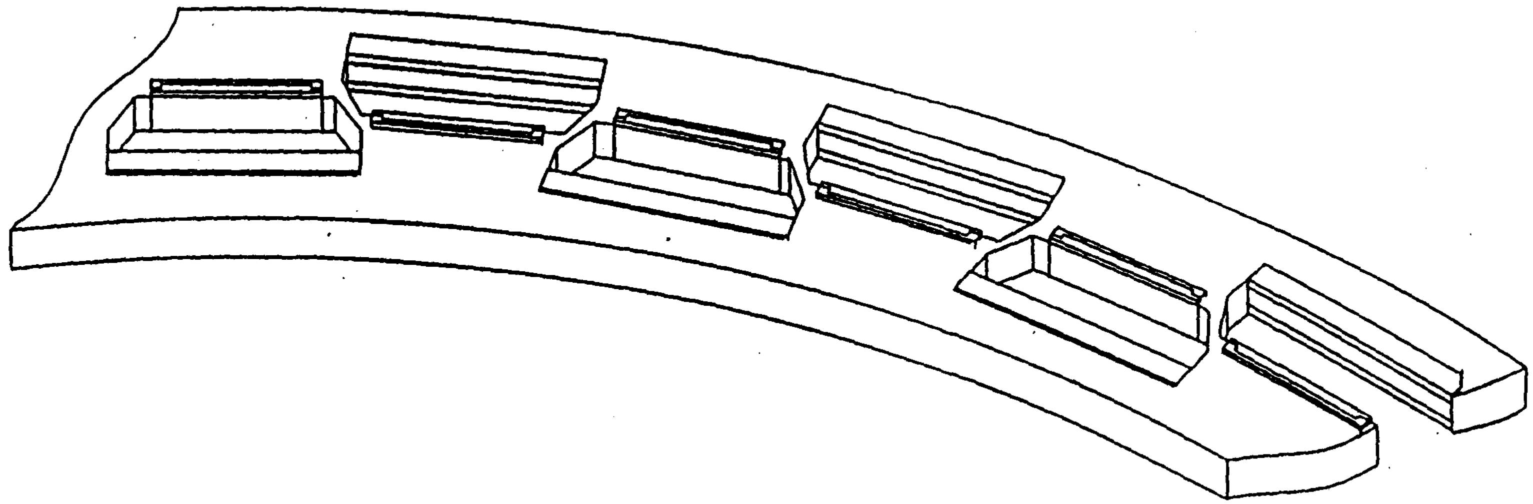

Westinghouse
Science & Technology Center

CENTRAL AND FORWARD TRACKING SUBSYSTEM

SUPPORT STRUCTURE ASSEMBLY AND ALIGNMENT

Westinghouse
Science & Technology Center

CENTRAL AND FORWARD TRACKING SYSTEM ASSEMBLY

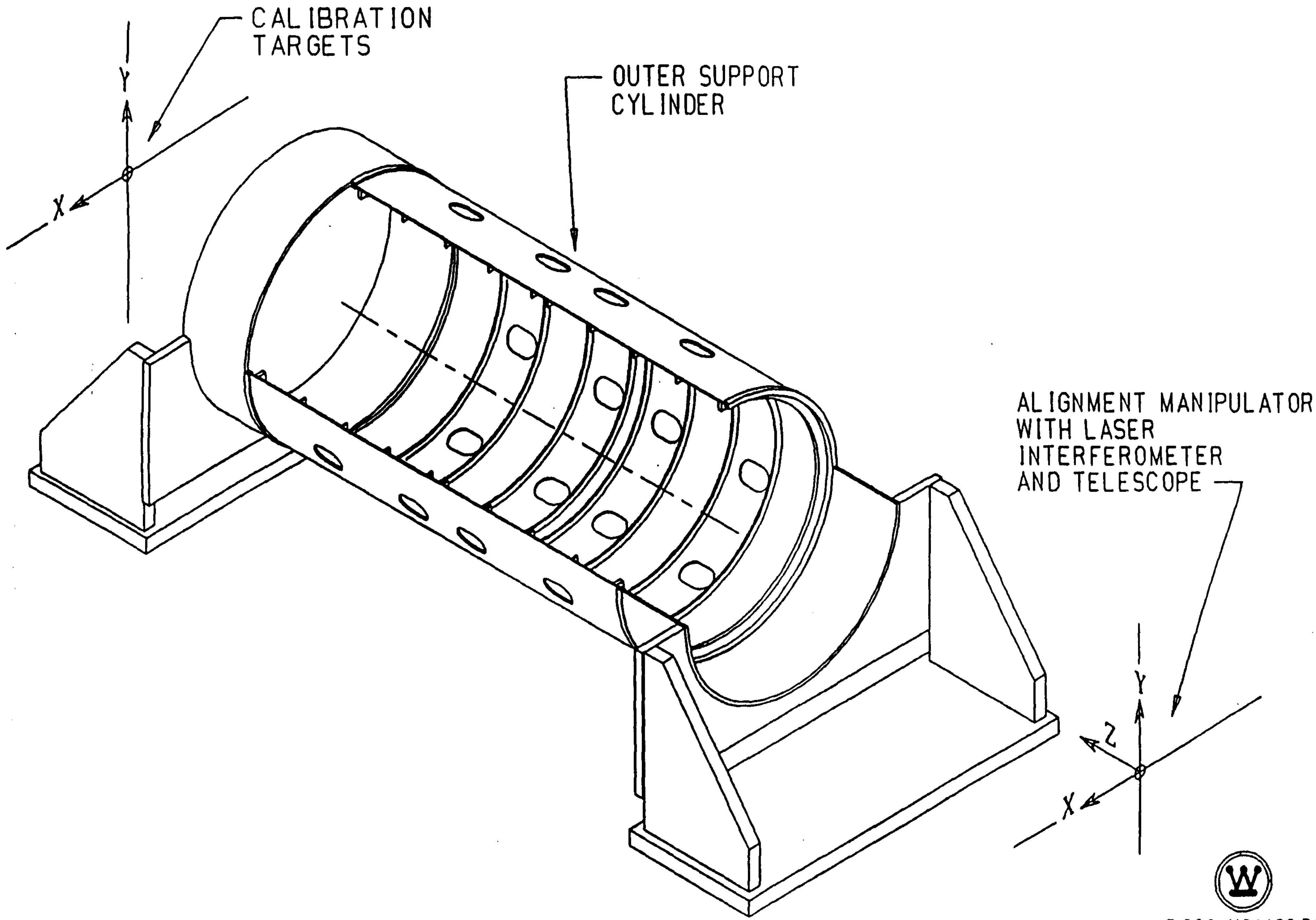

A-62

D.389.4136A63.R1
KEPES 2-8-91

ALIGNMENT SEQUENCE

Developed to Eliminate Gravity and Accumulated Fabrication Tolerances

2. Set Up and Calibrate the Alignment System
   - Place a XY Alignment Manipulator Fixed with a Laser Interferometer and a Precision Theodolite at One End of the Tracker
   - Set Up the Target With a Laser Interferometer
   - Calibrate the Alignment Manipulator and Theodolite Against the Target

Westinghouse
Science & Technology Center

CENTRAL AND FORWARD TRACKING SUBSYSTEM

ALIGNMENT

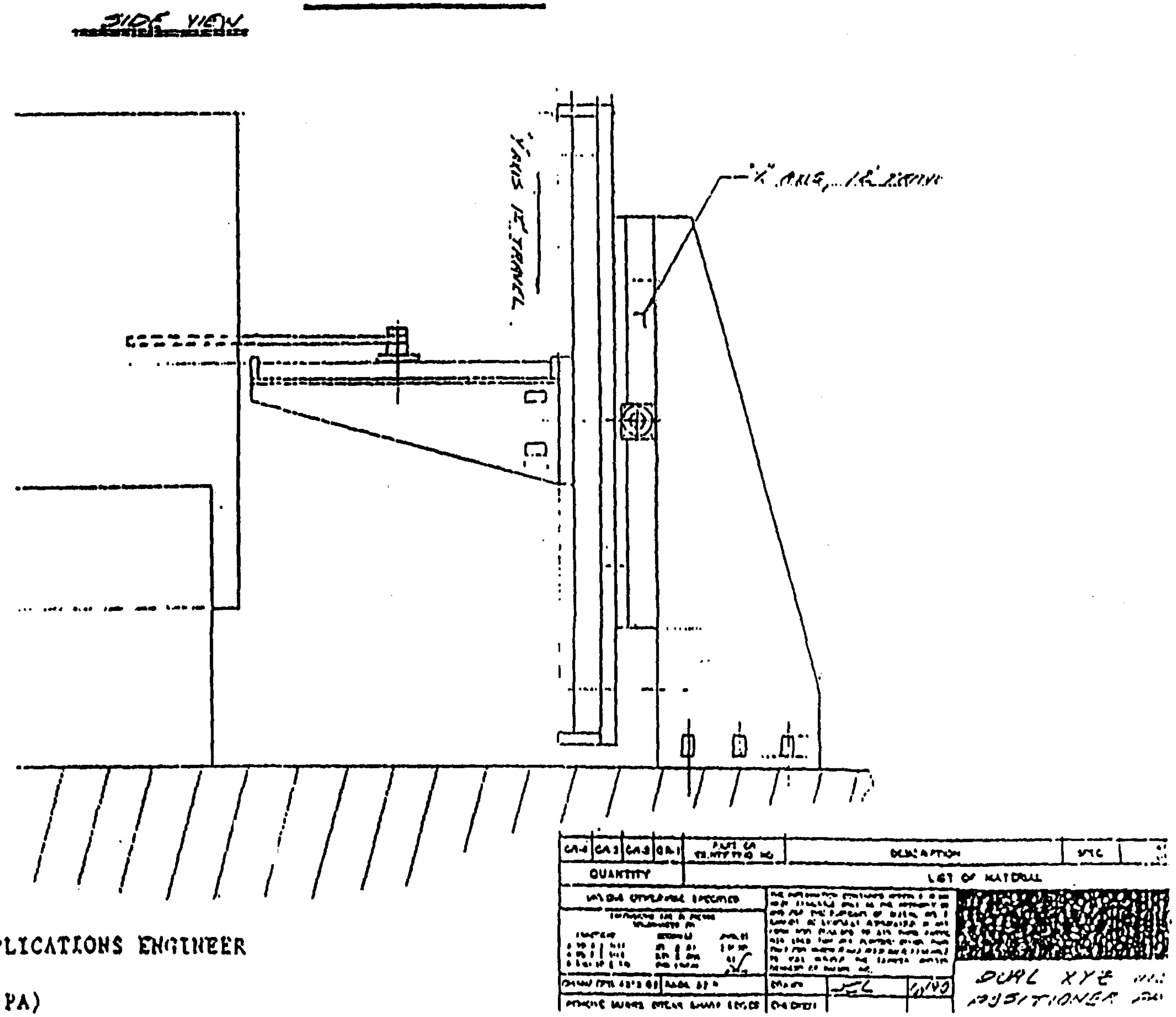

DAEDAL

Precision Positioning Equipment

FROM: FRANZ E. SIGE/APPLICATIONS ENGINEER

PHONE: 412-744-4451 (IN PA)
800-245-6903 (TOLL FREE)

FAX: 412-744-7626

Westinghouse
Science & Technology Center

[illegible] ASSEMBLY

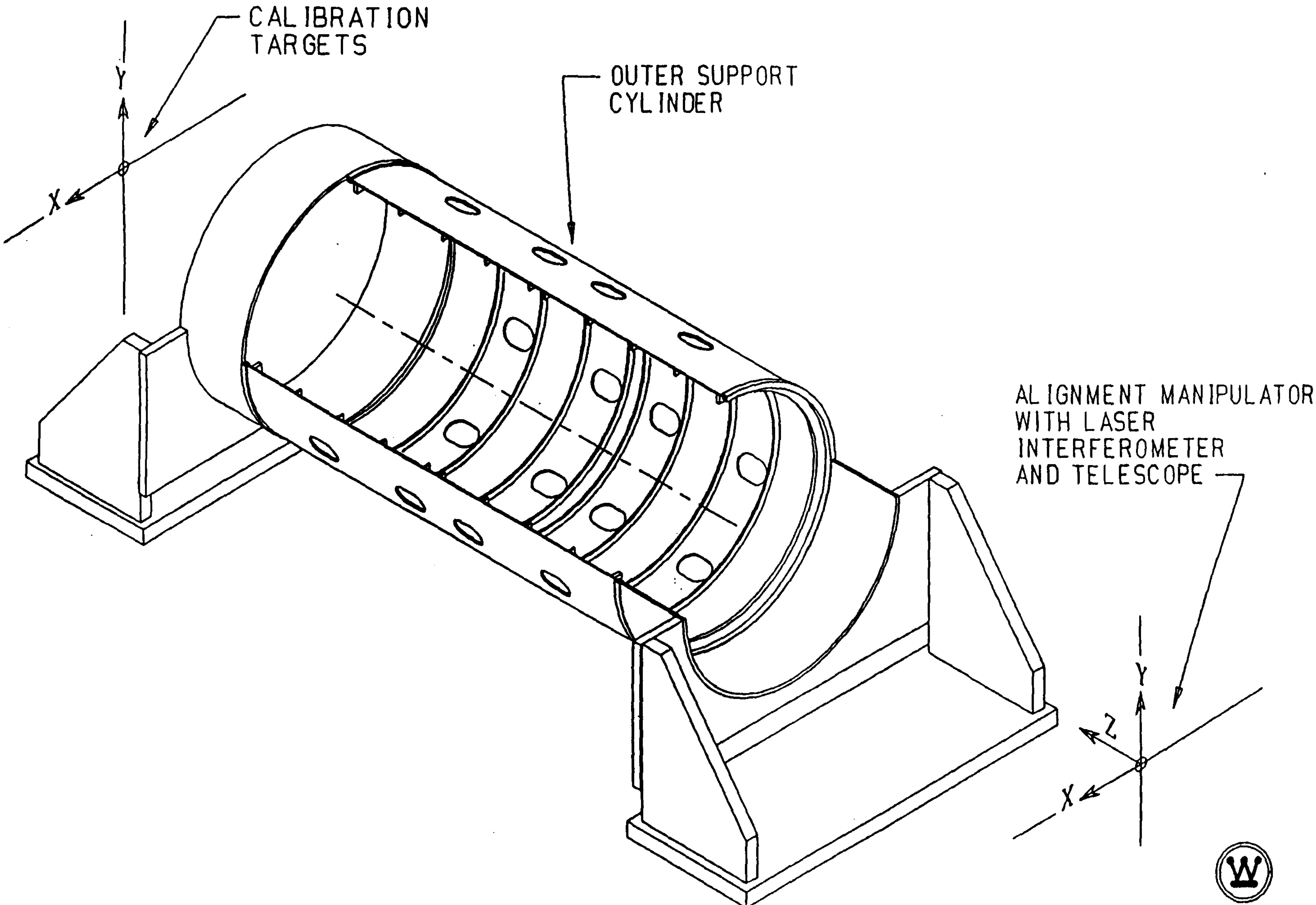

D.389.4136A63.R1
KEPES 2-8-91

CENTRAL AND FORWARD TRACKING

ASSEMBLY SEQUENCE

Developed to Eliminate Gravity and Accumulated Fabrication Tolerances

3. Sequentially, Globally Align and Fix the Position of Each Alignment Ring By:
   - Temporarily Mounting Optic Targets on Each Ring/Ring Attachment
   - Align the Ring Attachment Via the Laser Interferometer and the Ring Via the Precision Theodolite on the XY Precision Manipulator
     - First Fix the Longitudinal Position of Each Ring Attachment By Using the Interferometer
     - Second Fix the Radial and Circumferential Position of Each Ring Using the Precision Theodolite
   - Use Four Points at 90 Degrees for X&Y Precision Theodolite and Four Points for Z Alignment Interferometer
   - Repeat Steps 1 and 2 for All Five Cylinders
     - The Outer Cylinder Has Inner Modules Only
     - The Three Intermediate Cylinders Have Inner & Outer Modules
     - The Inner Cylinder Has Outer Modules Only

Westinghouse
Science & Technology Center

[illegible]

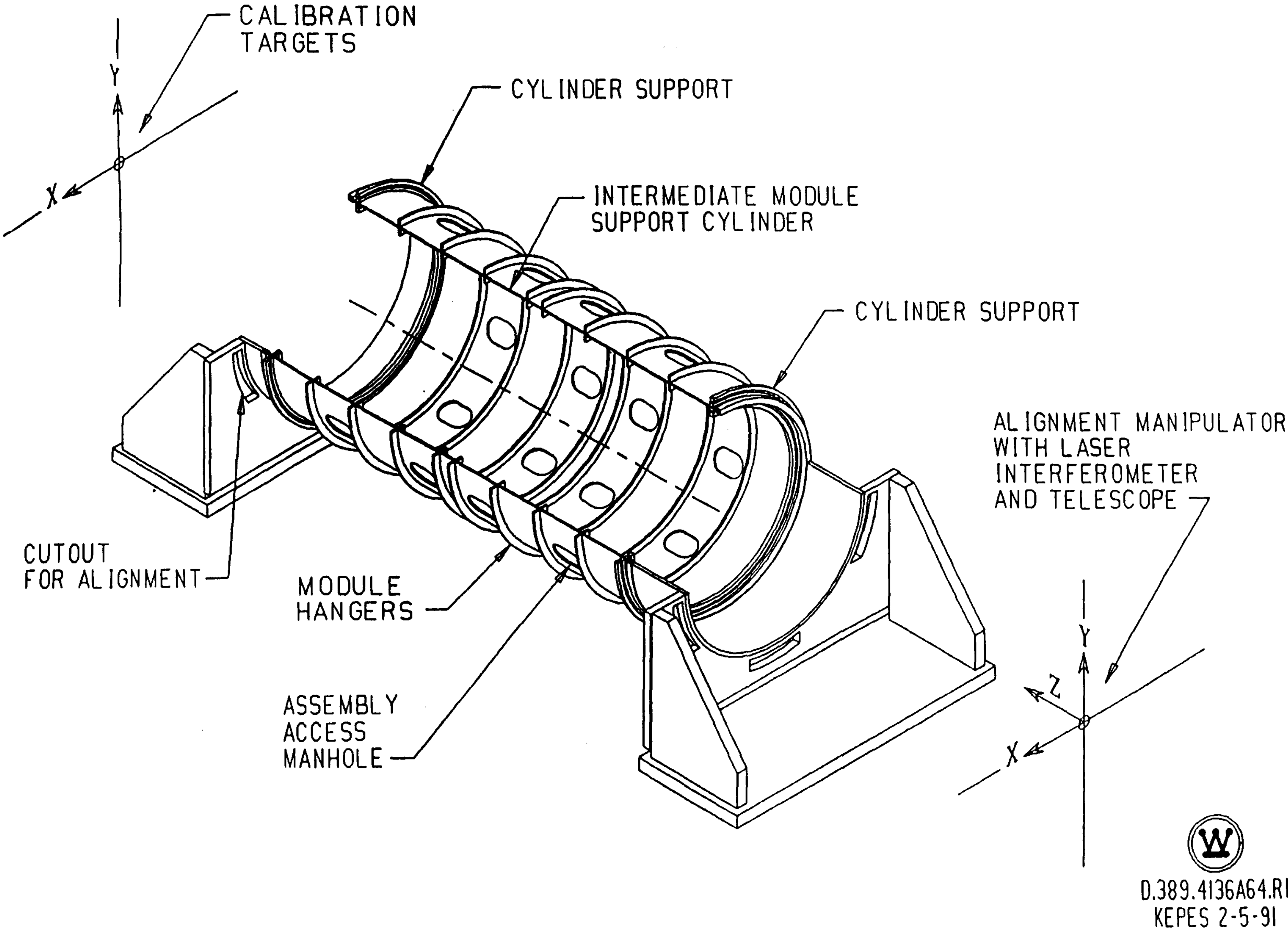
CALIBRATION TARGETS
Y
X
CYLINDER SUPPORT
INTERMEDIATE MODULE SUPPORT CYLINDER
CYLINDER SUPPORT
ALIGNMENT MANIPULATOR WITH LASER INTERFEROMETER AND TELESCOPE
CUTOUT FOR ALIGNMENT
MODULE HANGERS
ASSEMBLY ACCESS MANHOLE
Y
Z
X
D.389.4136A64.R1
KEPES 2-5-91

CENTRAL AND FORWARD TRACKING

ASSEMBLY SEQUENCE

Developed to Accommodate Conventional Fabrication Tolerances

4. Assemble the Support Structure
   - Assemble the Intermediate Module Support Cylinders Into the Outer Torsion Cylinder
   - Check Alignment While Fitting and Attaching the End Supports Between Each Cylinder
   - Adhesively Join All Components

Westinghouse
Science & Technology Center

CENTRAL AND FORWARD TRACKING SYSTEM

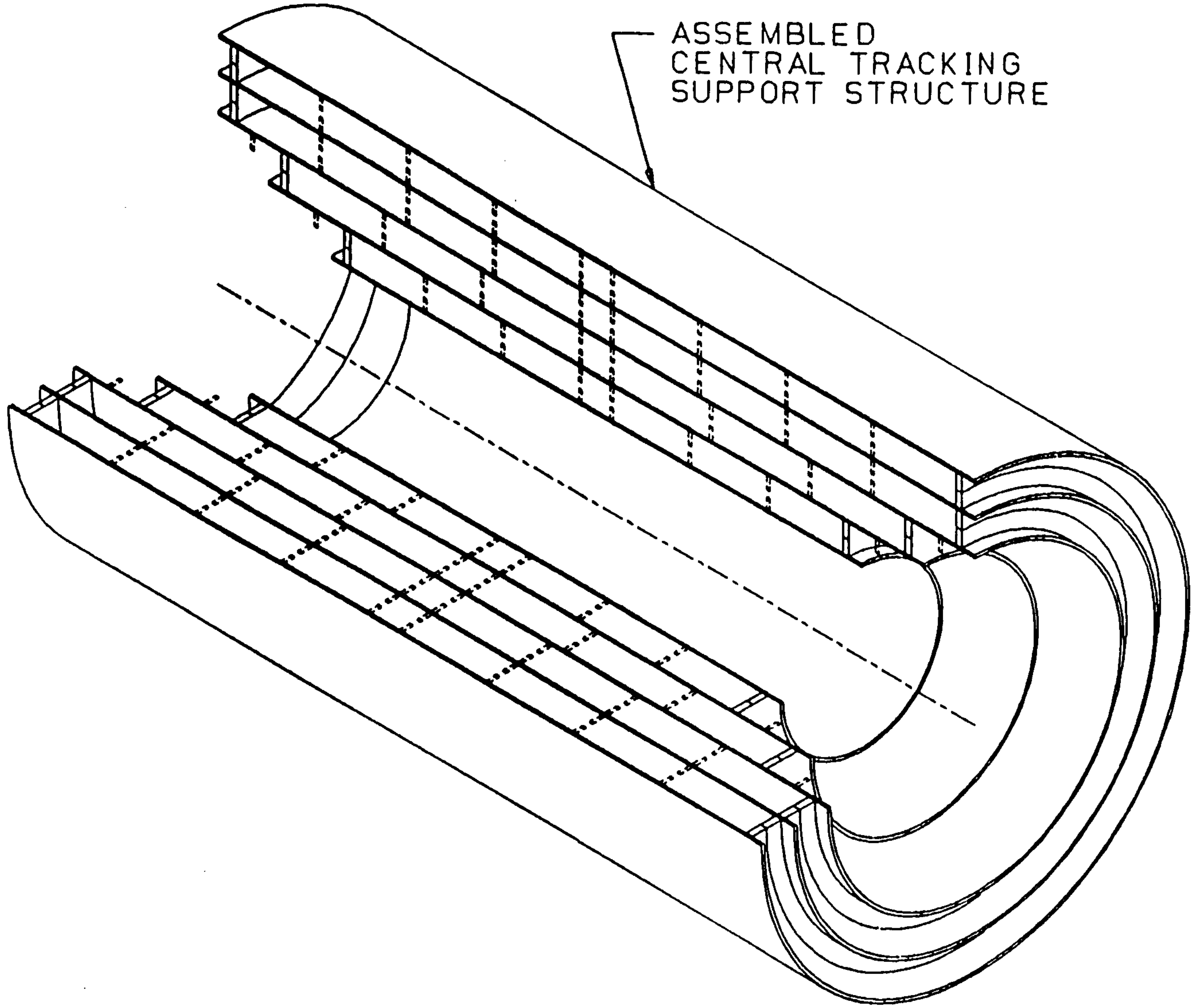

CENTRAL AND FORWARD TRACKING SUBSYSTEM

FINAL ASSEMBLY AND TEST

Westinghouse
Science & Technology Center

CENTRAL AND FORWARD TRACKING

SEQUENCE OF ASSEMBLY

1. Install Modules and Perform Functional Tests
   - Insert the Superlayer Modules Into the Support Structure
   - Connect Hoses and Cables
   - Test Straw Functionally

MODULE ASSEMBLY

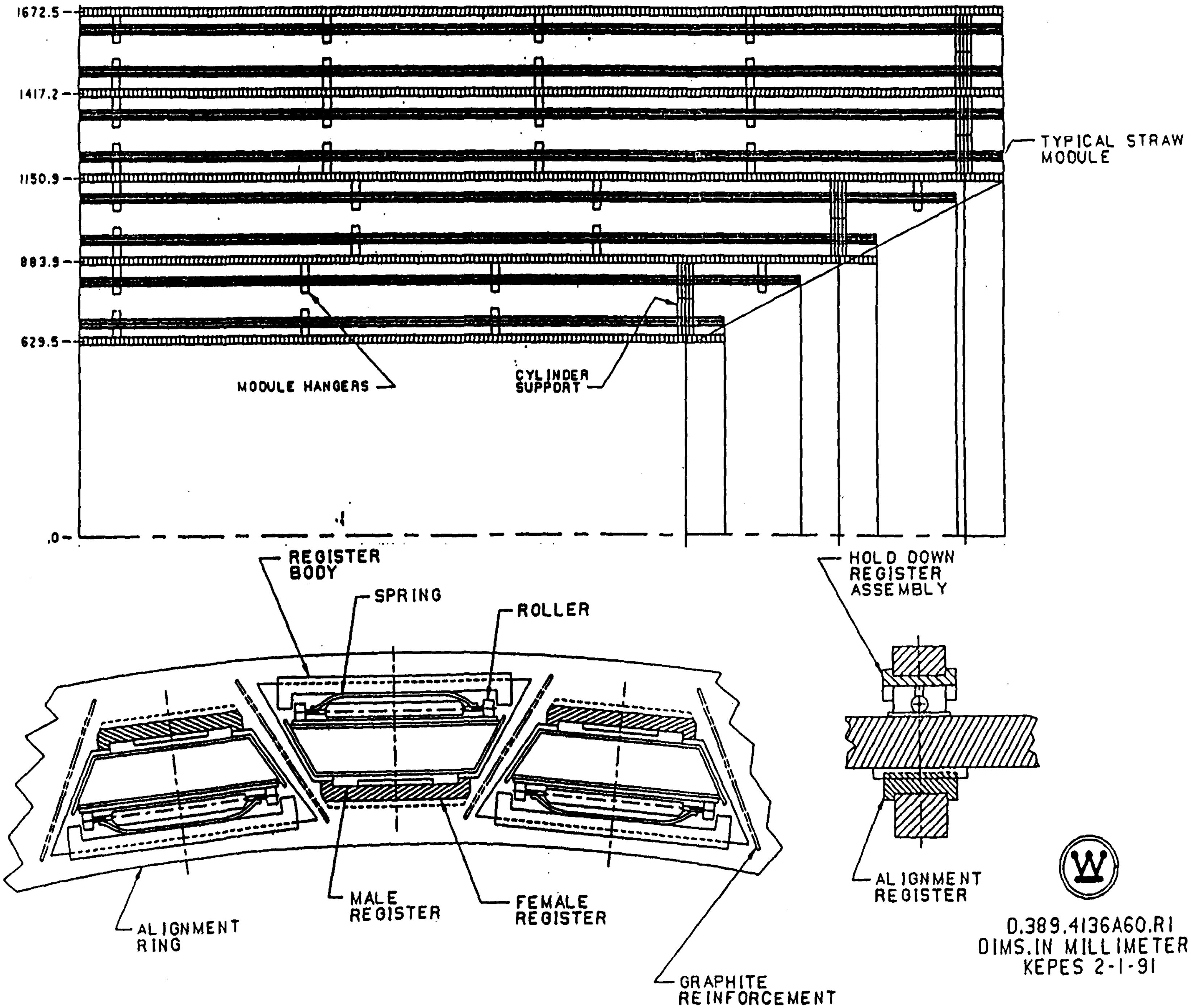

D.389.4136A60.R1
DIMS. IN MILLIMETERS
KEPES 2-1-91

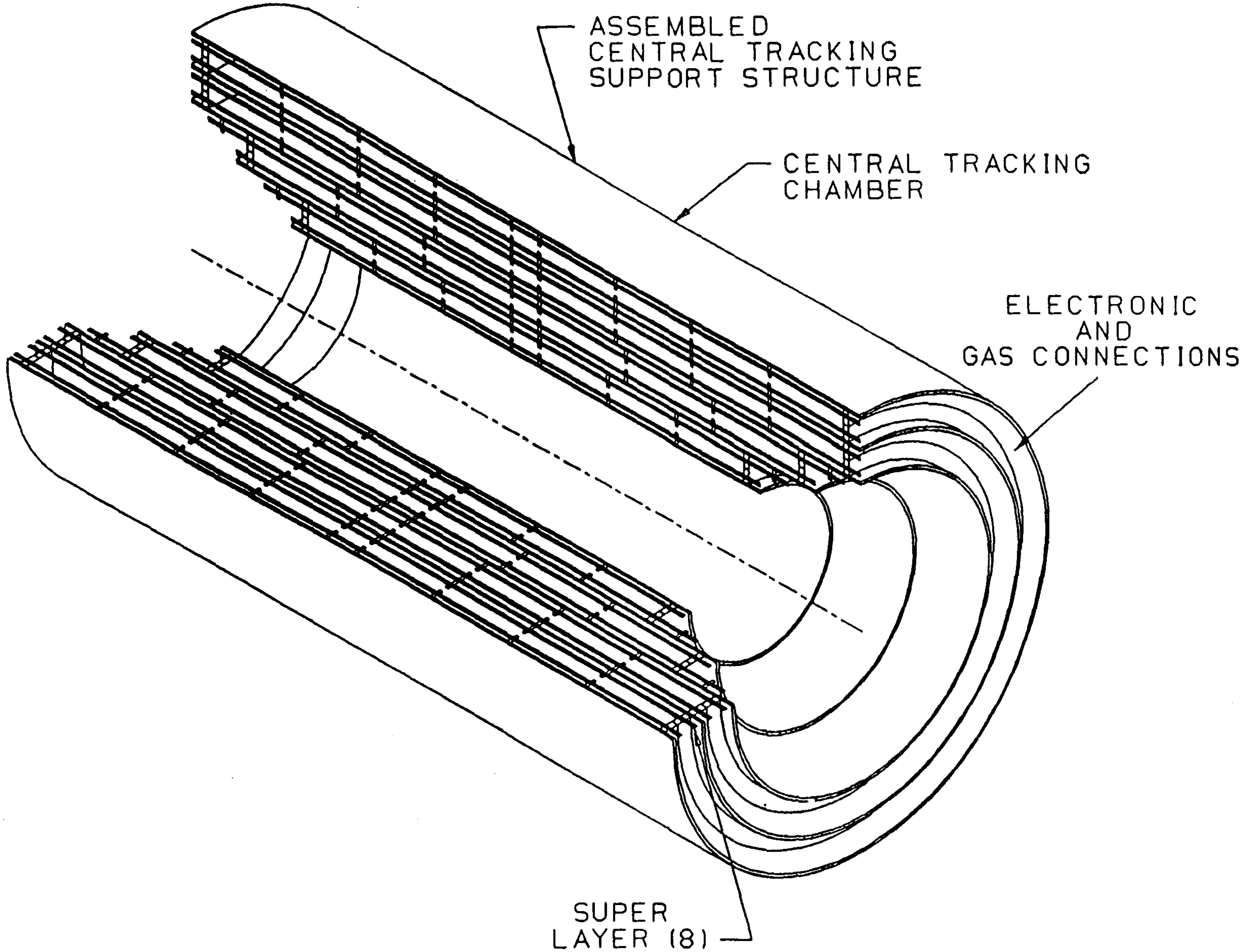
ASSEMBLED
CENTRAL TRACKING
SUPPORT STRUCTURE
CENTRAL TRACKING
CHAMBER
ELECTRONIC
AND
GAS CONNECTIONS
SUPER
LAYER (8)

CENTRAL AND FORWARD TRACKING

STEREO

Westinghouse
Science & Technology Center

CENTRAL AND FORWARD TRACKING

STEREO STUDY USING DUAL ANGLES FOR ALTERNATING MODULES

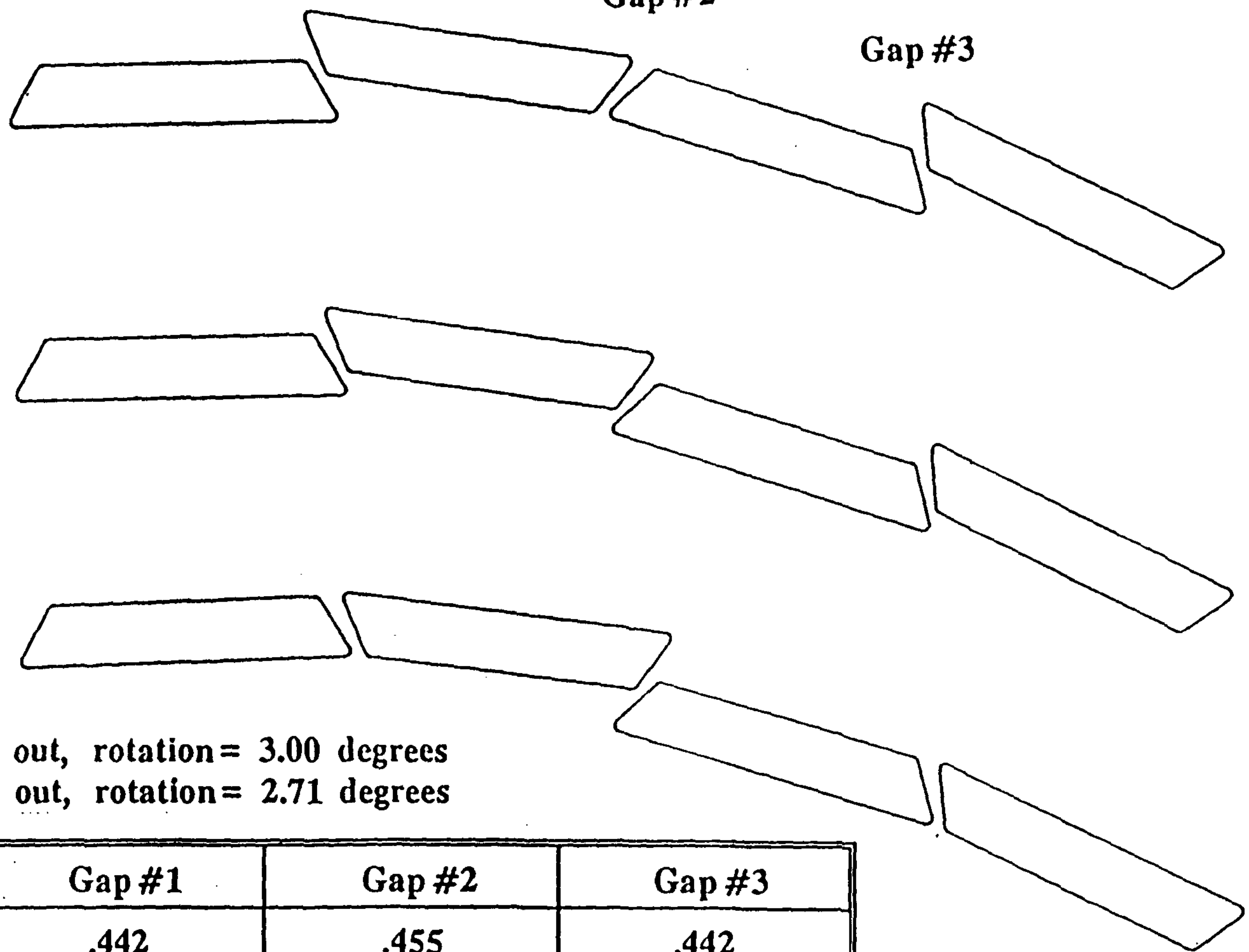

Long side out, rotation= 3.00 degrees
Short side out, rotation= 2.71 degrees

Section	Gap #1	Gap #2	Gap #3
- 100 cm	.442	.455	.442
0.0 cm	.415	.415	.415
+ 100 cm	.455	.442	.455

Westinghouse
Science & Technology Center

CENTRAL AND FORWARD TRACKING

FINITE ELEMENT ANALYSIS

Westinghouse
Science & Technology Center

ANALYSIS

1. The Mechanical Analysis Models
   - Classical Beam Theory Predicts Low Deflection from Gravity Load (ORNL on 01-24-91)
   - Finite Element Analysis by (W)STC Indicates the Same
     - Tried to Start Simple But!
     - Five Concentric Cylinders with Drum Type Composite Ends
     - Support at Four Corners
     - Weight/Density Increased to Account for Module Mass
     - Sophifticated Composite FEA Element Used

CENTRAL AND FORWARD TRACKING SUBSYSTEM

FINITE ELEMENT MODEL

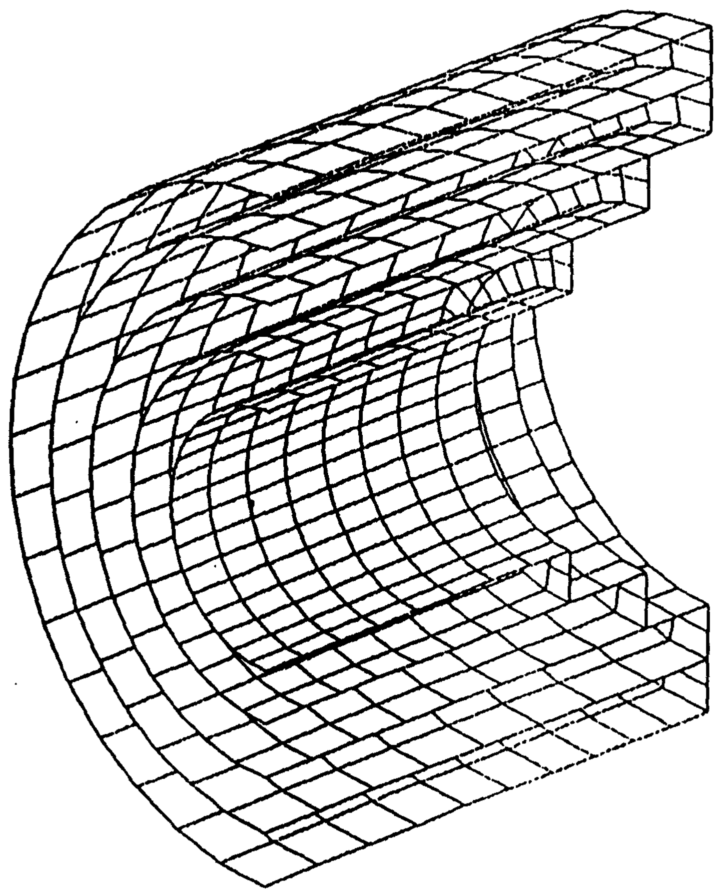

Westinghouse
Science & Technology Center

[illegible]
MODULAR STR[illegible] D[illegible]GN
SUPPORT CYLINDER

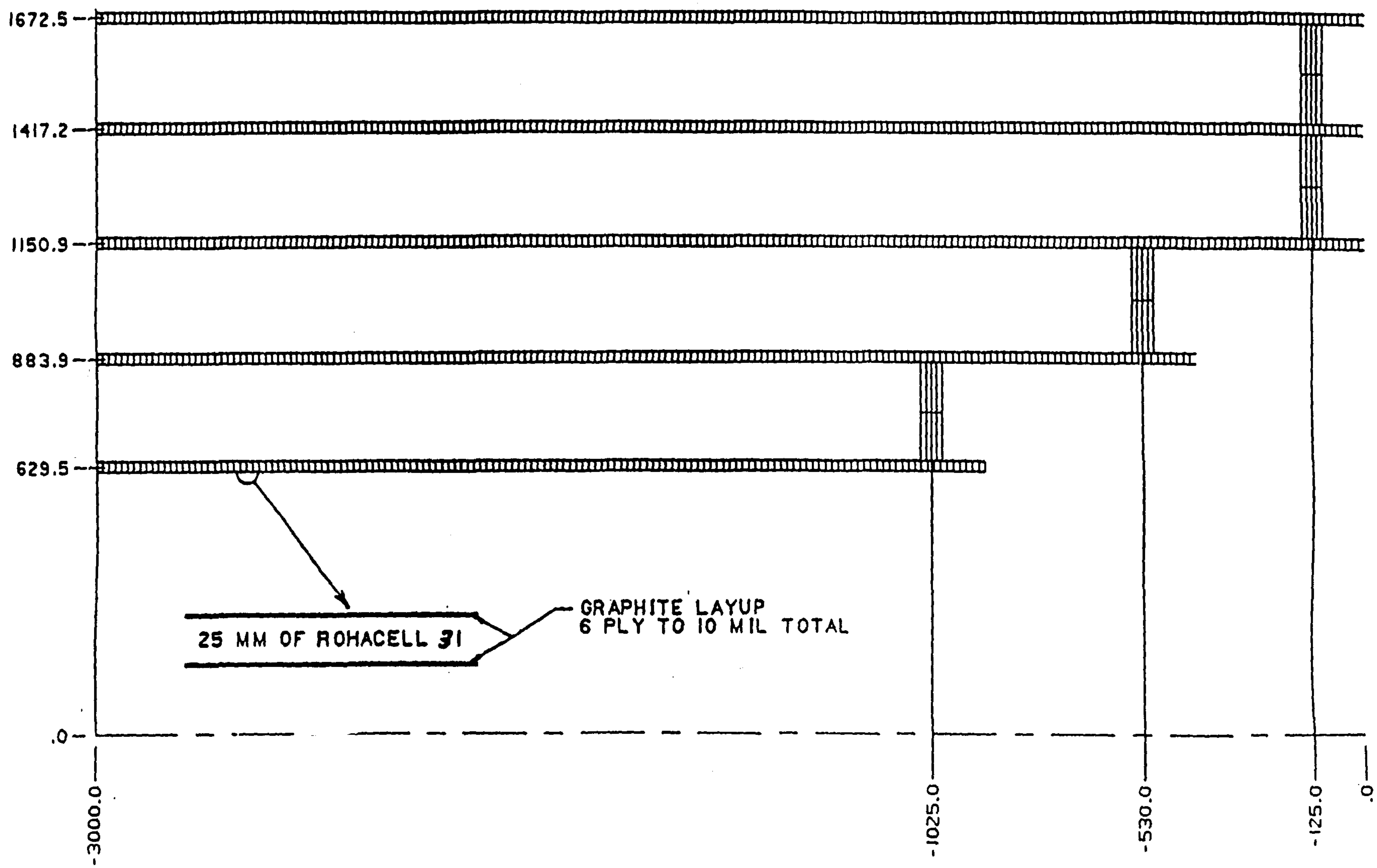

D.389.4136A62.R1
DIMS.IN MILLIMETERS
KEPES 2-1-91

CENTRAL AND FORWARD TRACKING SUBSYSTEM

ANALYSIS

2. Weights, Densities, and Stiffness

CENTRAL AND FORWARD TRACKING SUBSYSTEM

WEIGHT

	COMPONENT	WT.LBS
1.	Inside Torsional Cylinder	54.6
2.	Intermidiate Cylinder #1	95.9
3.	Intermidiate Cylinder #2	151.7
4.	Intermidiate Cylinder #3	186.7
5.	Outside Torsional Cylinder	220.4
6.	End Rings	55.5
7.	Alignment Rings	146.7
8.	Modules	1315.8
	TOTAL	2227.3

Westinghouse
Science & Technology Center

CENTRAL STRAW TUBE TRACKER

Wt of graphite epoxy module

Layer # = area sq in * length in. * density * # of modules * 2 halfs

$$L1 := .101 \cdot \left[\frac{200}{2.54}\right] \cdot .06 \cdot 40 \cdot 2 \qquad L1 = 38.173 \quad \text{lbs}$$

$$L2 := .101 \cdot \left[\frac{214.3}{2.54}\right] \cdot .06 \cdot 48 \cdot 2 \qquad L2 = 49.083 \quad \text{lbs}$$

$$L3 := .101 \cdot \left[\frac{228.6}{2.54}\right] \cdot .06 \cdot 56 \cdot 2 \qquad L3 = 61.085 \quad \text{lbs}$$

$$L4 := .101 \cdot \left[\frac{242.9}{2.54}\right] \cdot .06 \cdot 64 \cdot 2 \qquad L4 = 74.178 \quad \text{lbs}$$

$$L5 := .101 \cdot \left[\frac{257.2}{2.54}\right] \cdot .06 \cdot 72 \cdot 2 \qquad L5 = 88.363 \quad \text{lbs}$$

$$L6 := .101 \cdot \left[\frac{271.4}{2.54}\right] \cdot .06 \cdot 80 \cdot 2 \qquad L6 = 103.602 \quad \text{lbs}$$

$$L7 := .101 \cdot \left[\frac{285.9}{2.54}\right] \cdot .06 \cdot 88 \cdot 2 \qquad L7 = 120.051 \quad \text{lbs}$$

$$L8 := .101 \cdot \left[\frac{300}{2.54}\right] \cdot .06 \cdot 96 \cdot 2 \qquad L8 = 137.424 \quad \text{lbs}$$

Wt_module_wrappers := L1 + L2 + L3 + L4 + L5 + L6 + L7 + L8
Wt_module_wrappers = 671.96 lbs total

Wt straws lbs.
layer# * # straws * # modules * length m * .5 gm / m * (1/453.6) * 2 = lbs

```
lay1 := 159·40·2.00·.5·.0022·2        lay1 = 27.984
lay2 := 159·48·2.143·.5·.0022·2       lay2 = 35.982
lay3 := 159·56·2.286·.5·.0022·2       lay3 = 44.78
lay4 := 159·64·2.429·.5·.0022·2       lay4 = 54.379
lay5 := 159·72·2.572·.5·.0022·2       lay5 = 64.777
lay6 := 234·80·2.666·.5·.0022·2       lay6 = 109.797
lay7 := 159·88·2.801·.5·.0022·2       lay7 = 86.222
lay8 := 234·96·3.00·.5·.0022·2        lay8 = 148.262
```

Wt_straws := lay1 + lay2 + lay3 + lay4 + lay5 + lay6 + lay7 + lay8
Wt_straws = 572.182 lbs total

Wt_straws_plus_wrappers := Wt_straws + Wt_module_wrappers
Wt_straws_plus_wrappers = 1244.142 lbs total

CENTRAL AND FORWARD TRACKING

SUMMARY OF INPUT DATA (MATERIAL PROPERTIES)

AMOCO P-75 TAPE

MATL NO.		MODULUS OF ELASTICITY	POISSONS RATIO	COEF. OF THERMAL EXPANSION	SHEAR MODULUS OF ELASTICITY	TRANSVERSE MODULUS OF ELASTICITY	TRANSVERSE COEF. OF THERMAL EXPANSION
	1	0.490E+08	0.300	-0.540E-06	0.850E+06		
1	2	0.100E+07	0.300	0.167E-04	0.380E+06		
	3	0.100E+07	0.300	0.167E-04	0.850E+06		

MATL NO		THERMAL CONDUCTIVITY	DENSITY
	1	0.000E+00	0.620E-01
1	2	0.000E+00	
	3	0.000E+00	

SUMMARY OF LAYER CONSTANTS

LAYER NO.	MATERIAL NUMBER	AVERAGE THICKNESS	ANGLE OF ORIENTATION
1	1	0.150E-02	0.000E+00
2	1	0.150E-02	-60.0
3	1	0.150E-02	60.0
4	1	0.150E-02	60.0
5	1	0.150E-02	-60.0
6	1	0.150E-02	0.000E+00

RLS

Westinghouse
Science & Technology Center

CENTRAL AND FORWARD TRACKING

SUMMARY OF INDIVIDUAL LAMINA PROPERTIES

****
* IN-PLANE ENGINEERING CONSTANTS *
****

MATL. ID	ELASTIC MODULUS E1	E2	E3	SHEAR MODULUS G12	G23	G13
1	0.490E+08	0.100E+07	0.100E+07	0.850E+06	0.380E+06	0.850E+06

MATL. ID.	POISSON RATIO MU12	MU21	MU23	MU32	MU13	MU31
1	0.300	0.612E-02	0.300	0.300	0.300	0.612E-02

****
* THERMAL PROPERTIES   *
****

MATL. ID.	THERMAL EXPANSION COEFS. ALPHA-1	ALPHA-2	ALPHA-3	THERMAL CONDUCTIVITY K1	K2	K3
1	-0.540E-06	0.167E-04	0.167E-04	0.000E+00	0.000E+00	0.000E+00

****
*   DENSITY   *
****

MATL. ID.	DENSITY
1	0.620E-01

RLS

Westinghouse
Science & Technology Center

CENTRAL AND FORWARD TRACKING

MATERIAL STIFFNESS FOR MULTIPLE LAYERED COMPOSITE

[0 , +/-60]sym

****
* IN-PLANE ENGINEERING CONSTANTS *
****

ELASTIC MODULUS			SHEAR MODULUS		
0.174E+08	0.174E+08	0.109E+07	0.661E+07	0.615E+06	0.615E+06

POISSON RATIO

MUXY	MUYX	MUYZ	MUZY	MUXZ	MUZX
0.314	0.314	0.238	0.149E-01	0.238	0.149E-01

****
* THERMAL PROPERTIES *
****

THERMAL EXPANSION COEFS.				THERMAL CONDUCTIVITY		
ALPHA-X	ALPHA-Y	ALPHA-XY	ALPHA-Z	K1	K2	K3
-0.971E-07	-0.971E-07	0.173E-13	0.216E-04	0.000E+00	0.000E+00	0.000E+00

****
* TOTAL THICKNESS *
****

0.90000E-02

****
* DENSITY *
****

0.620E-01

RLS

Westinghouse
Science & Technology Center

CENTRAL AND FORWARD TRACKING

rohacell® IG

ROHACELL® IG is a lightweight, rigid, high-quality, polymethacrylimide foam. It is especially suited for use as a core material for composite construction.

Applications

ROHACELL IG has a variety of uses in composite construction as a core material, e.g.:

- Aircraft construction
- Radiation technology
- Electronics
- Construction of sporting goods, tennis rackets, canoe paddles, cross country and downhill skis, etc.
- Freight containers
- Marine construction such as: hulls, decks, bulk-heads, and rudders.
- Model building in industry and architecture
- Thermal expansion molding mandrels

Typical mechanical properties

Properties	Dimension	ROHACELL IG 31 IG	51 IG	71 IG	110 IG	ROHACELL® Pressed Grades P170	P190	ASTM Test Method
Density	Lbs./cu. ft.	2.0	3.2	4.7	6.9	10.6	11.9	D1622
Tensile strength	PSI	142	270	398	498	1,070	1,210	D638
Compressive strength	PSI	57	128	213	427	924 (398)[1]	1,110 (455)[1]	D1621
Flexural strength	PSI	114	228	356	640	1,490 (1,420)[1]	1,780 (1,710)[1]	D790
Shear strength	PSI	57	114	185	341	640 (427)[1]	782 (427)[1]	C273
Modulus of elasticity	PSI	5,120	9,950	13,100	22,700	45,500	54,000	D638
Shear modulus	PSI	1,990	2,990	4,270	8,250	17,000	26,300	D2236
Shear modulus	PSI	1,850	2,700	4,120	7,110	12,500	14,200	C273
Elongation at break	%	3.5	4	4.5	4.5	5	6	D638

CENTRAL AND FORWARD TRACKING SUBSYSTEM

ANALYSIS

3. What Have We Learned?
   - Deflections are Small- 100 Microns Size
   - Structure stayes Basically Round But:
     - End Support Rings Connecting Cylinders Have High Shear Strains Resulting From Center Cylinders Translating Downward
   - Structure Stays Basically Straight But:
     - Longitudinal Deformed Shape do to Gravity Load is Fundamental Pin-Pin Beam Mode
     - Appears to be a Lot of Shear Near Ends of Cylinder at Support
     - Limited Beam Bending Occurs

   Spreading Support Load (Restrain More Nodes) Simulating Reinforcement Results in:
     - Decreases Large Shear Strains Around Supports
     - Reduces Overall Deflection by 30%
     - Distorts Outer Cylinder Roundness

Westinghouse
Science & Technology Center

CENTRAL AND FORWARD TRACKING SUBSYSTEM

Finite Element Analysis

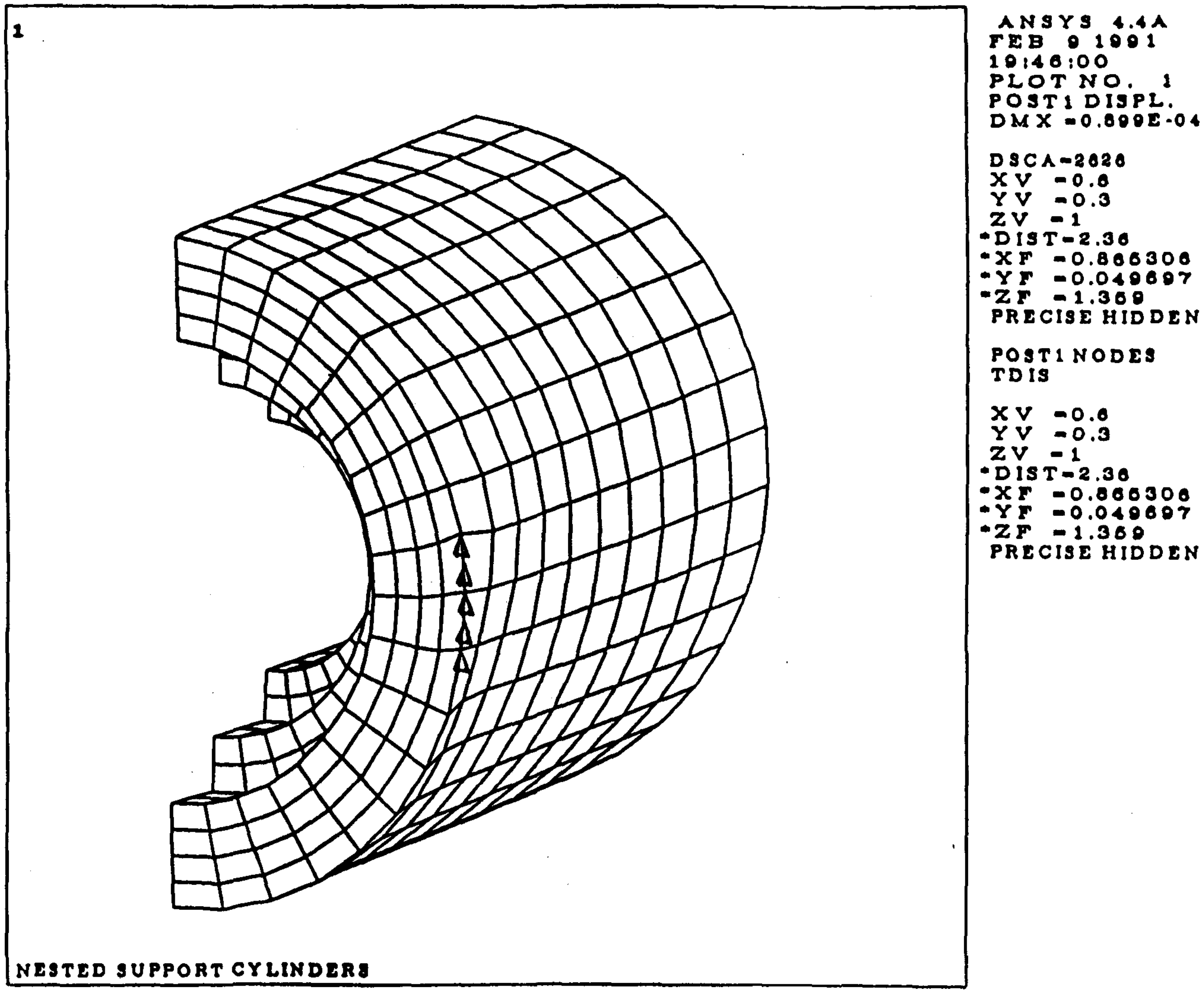

Westinghouse
Science & Technology Center

CENTRAL AND FORWARD TRACKING SUBSYSTEM

Finite Element Analysis

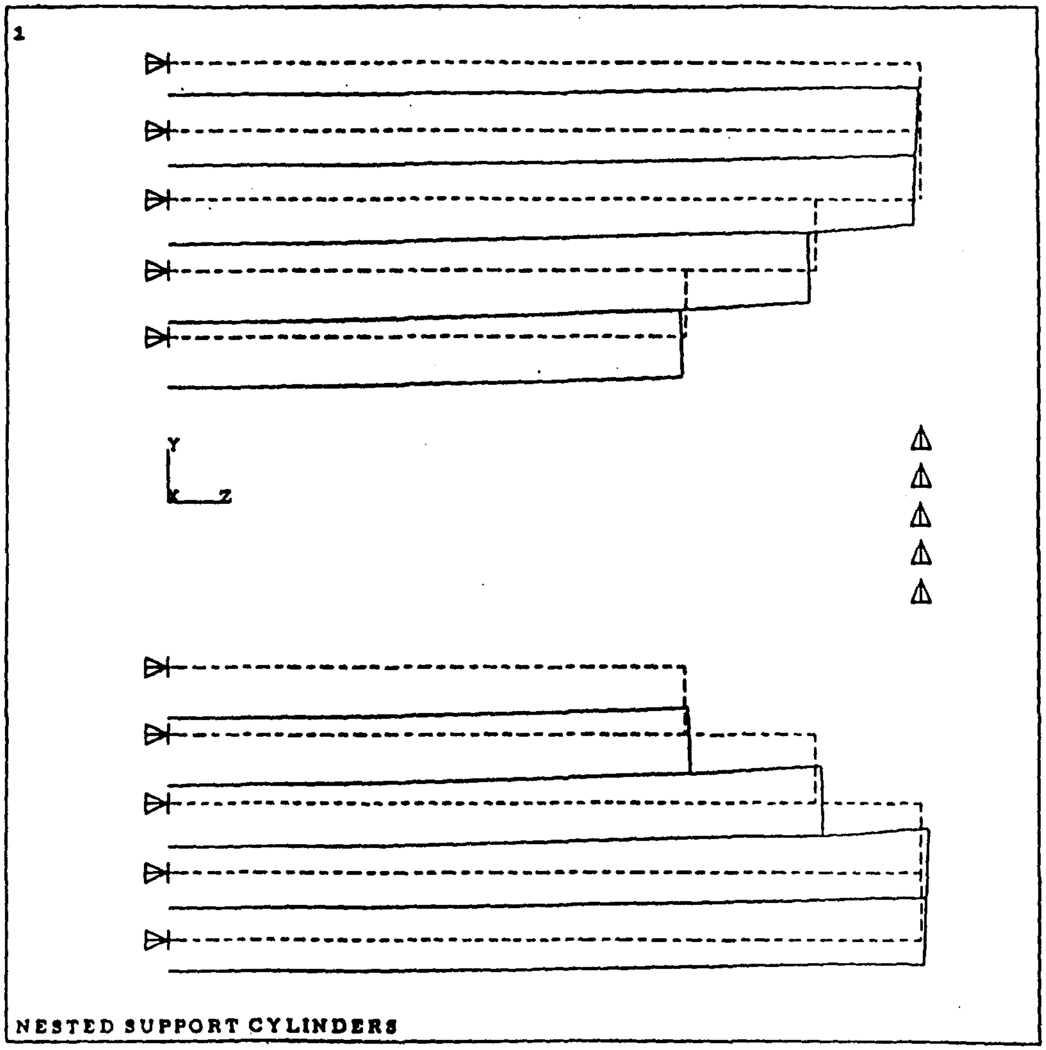

ANSYS 4.4A
FEB 9 1991
21:12:26
PLOT NO. 1
POST1 DISPL.
DMX =0.678E-04

DSCA=2247
XV =-1
*DIST=1.973
*XF =0.83626
*YF =-0.086074
*ZF =1.346

POST1 NODES
TDIS

XV =-1
*DIST=1.973
*XF =0.83626
*YF =-0.086074
*ZF =1.346

POST1 NODES
TDIS

XV =-1
*DIST=1.973
*XF =0.83626
*YF =-0.086074
*ZF =1.346

Westinghouse
Science & Technology Center

CENTRAL AND FORWARD TRACKING SUBSYSTEM

Finite Element Analysis

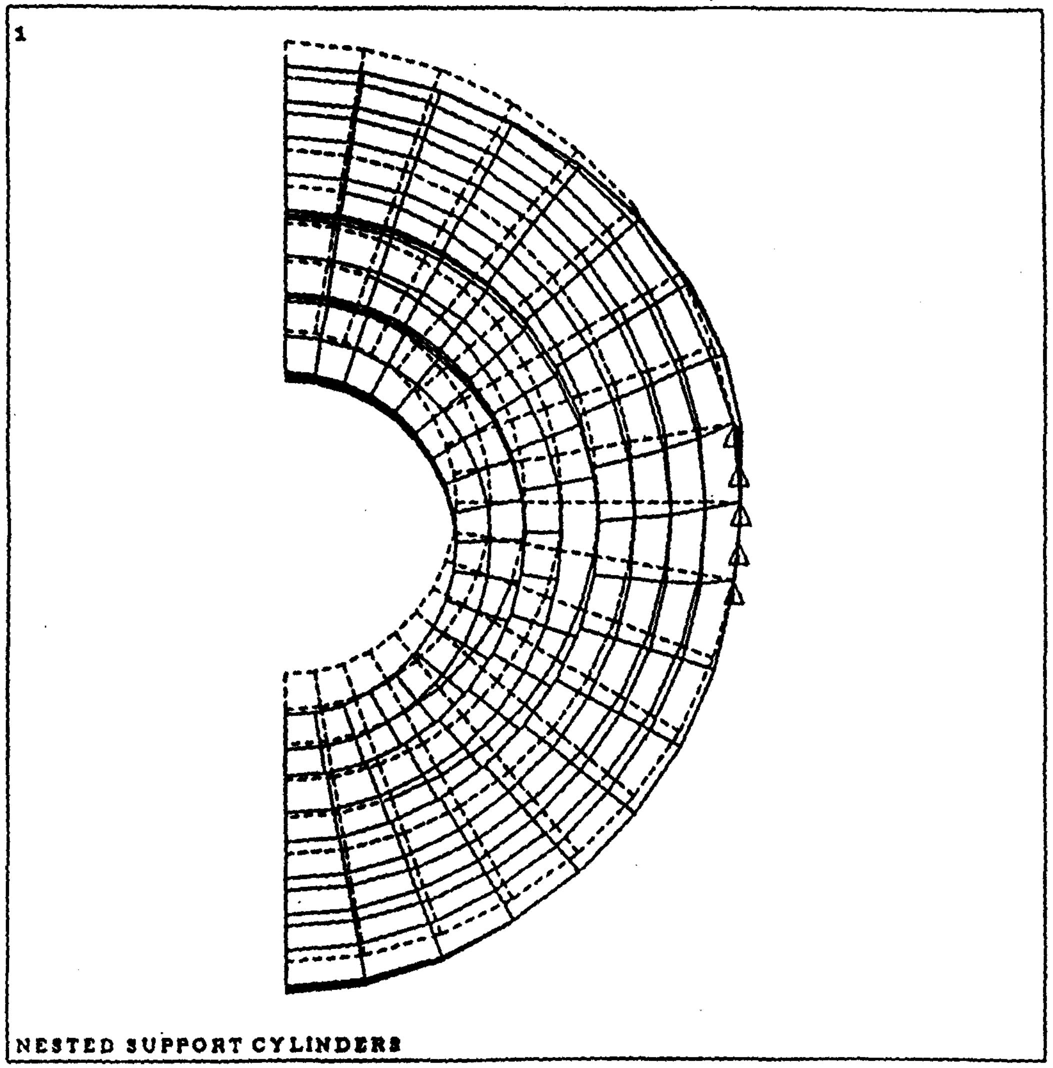

ANSYS 4.4A
FEB 9 1991
16:51:23
PLOT NO. 1
POST1 DISPL.
DMX =0.699E-04

DSCA=2128
ZV =1
*DIST=1.911
*XF =0.875157
*YF =-0.116807
*ZF =1.438
PRECISE HIDDEN

POST1 NODES
TDIS

ZV =1
*DIST=1.911
*XF =0.875157
*YF =-0.116807
*ZF =1.438
PRECISE HIDDEN

Westinghouse
Science & Technology Center

CENTRAL AND FORWARD TRACKING SUBSYSTEM

FUTURE PLANS

Westinghouse
Science & Technology Center

CENTRAL AND FORWARD TRACKING SUBSYSTEM

FUTURE PLANS

1. What Do We Do Next?
   - Study the Mechanics of Alignment
   - Continue to Ballpark the Design
   - Look Closer at Module Attachment and Build Prototype
   - Exercise and Analyze the FEA Model
     - Do Design Optimizing
     - Study Thermal Loads

Westinghouse
Science & Technology Center

CENTRAL AND FORWARD TRACKING

INTEGRATION SYSTEMS

Westinghouse
Science & Technology Center

CENTRAL AND FORWARD TRACKING

INTEGRATION SYSTEMS
SUBSYSTEM MOUNTING

1. Central Tracker Mounting
   - Concept Would:
     - Uses Aluminum Bracket at Four Corners of Central Tracker Mounted Off Calorimeter
     - Has Manual Adjustment in Elevation
     - Features Kinematic Mounts

Westinghouse
Science & Technology Center

LEAD IRON CALORIMETER WITH TRACKER SUPPORT

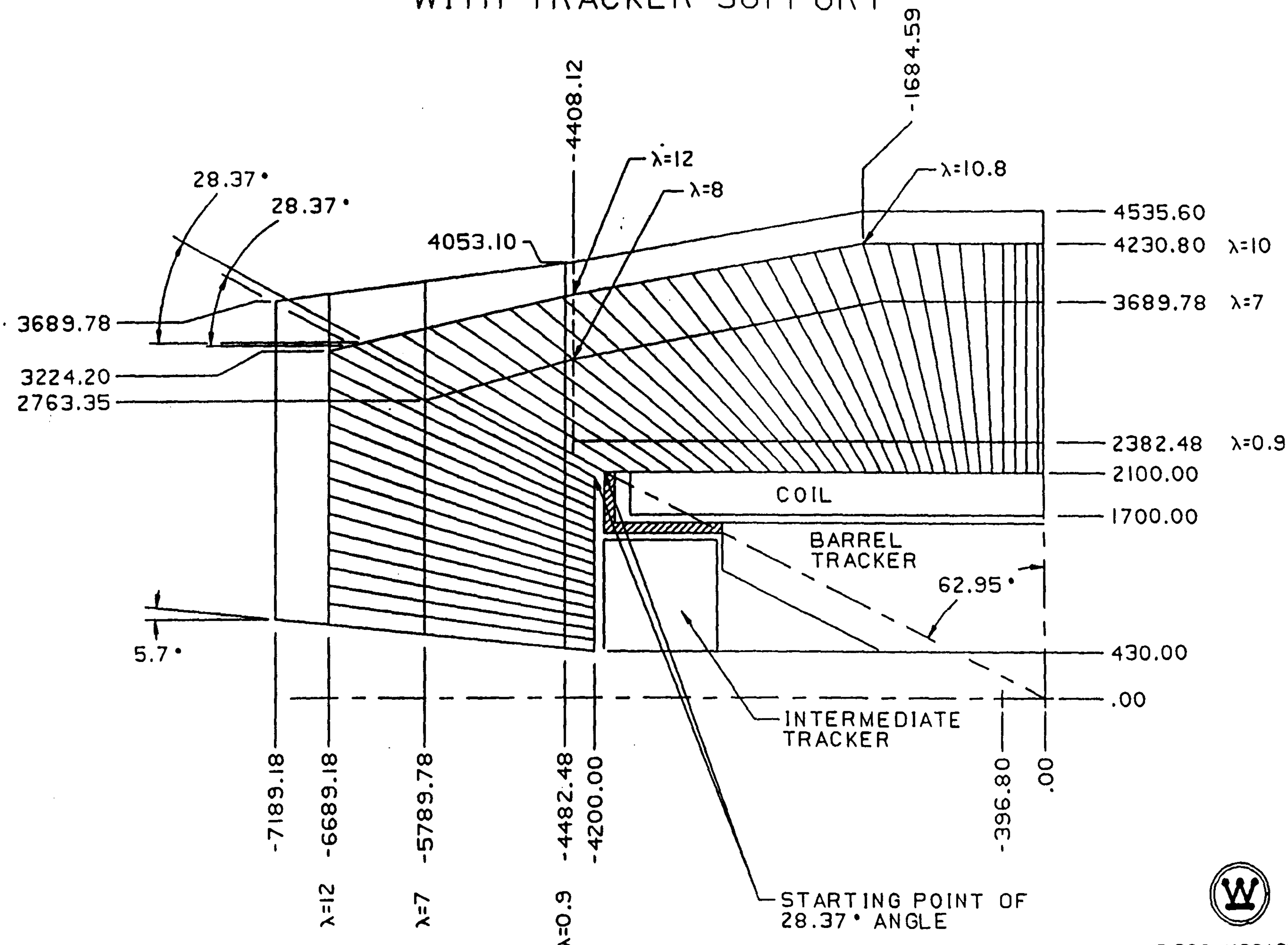

CALORIMETER VOLUME = 673 CUBIC METERS
CALORIMETER WEIGHT = 5837 SHORT TONS
5295 METRIC TONS

D.389.4136A65.R1
DIM.IN MILLIMETERS
SCALE:.02=1.00
KEPES 2-9-90

CENTRAL AND FORWARD TRACKING SUBSYSTEM

CENTRAL TRACKER MOUNTING

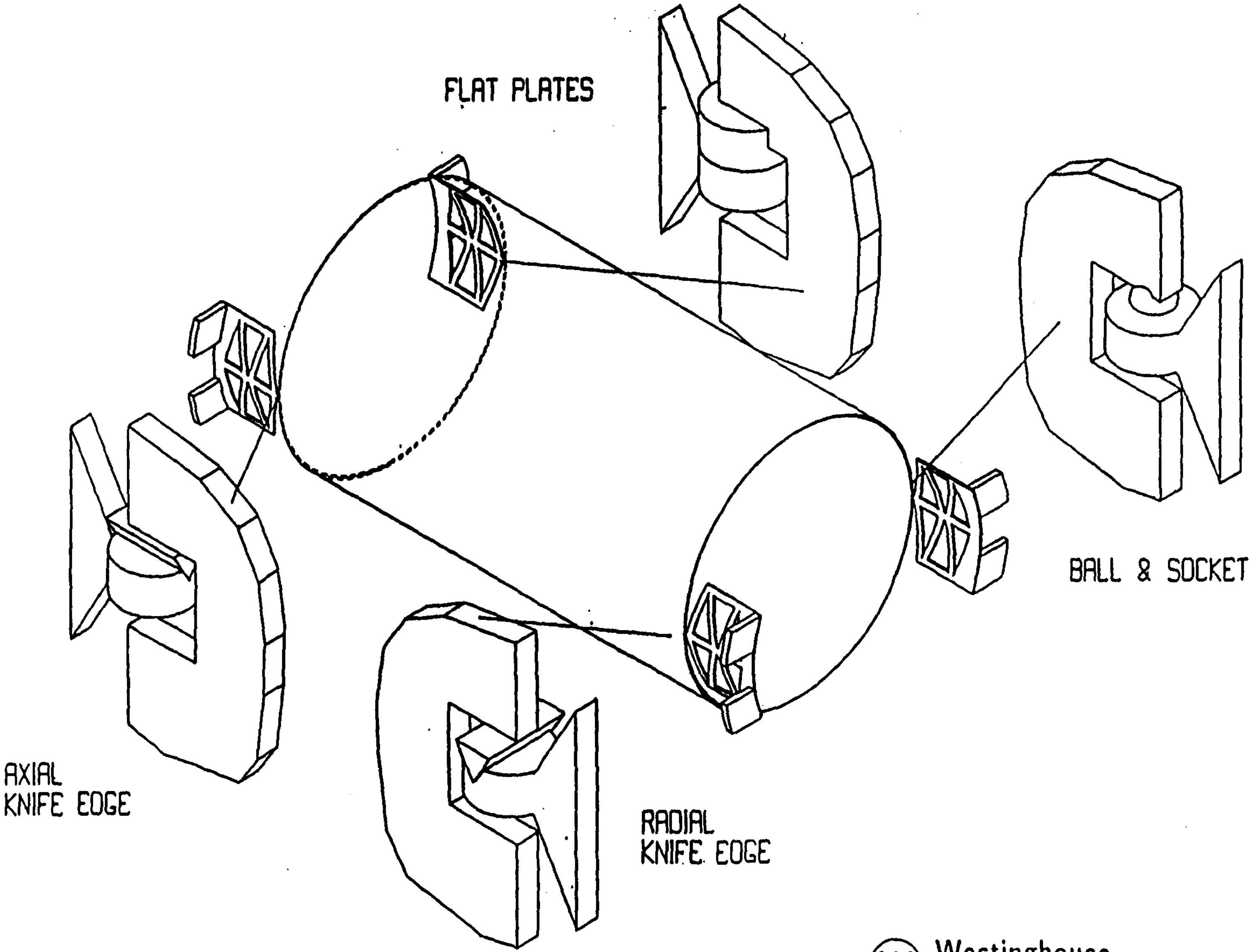

Westinghouse
Science & Technology Center

INTEGRATION SYSTEMS
SUBSYSTEM MOUNTING

2. Intermediate Tracker Support
   - Uses Aluminum Bracket at Top 90° of Intermediate Tracker Mounted Off Calorimeter
   - Concept Would Use:
     - Manual Adjustment in Elevation
     - Four Corner Kinematic Mount
     - Rail System for Longitudinal Movement
   - Requires Optic/Diode Position to Central Tracker Stability Monitor
   - Access to Central Tracker Electronics Would Require at Least 1-1/2 Meters Motion
     - Mounting of Tooling to Achieve This 1-1/2 Meters is Required
     - One Meter Motion to Clear Calorimeter
     - 1/2 Meter for Access

CENTRAL AND FORWARD TRACKING SUBSYSTEM

INTERMEDIATE TRACKER SUPPORT

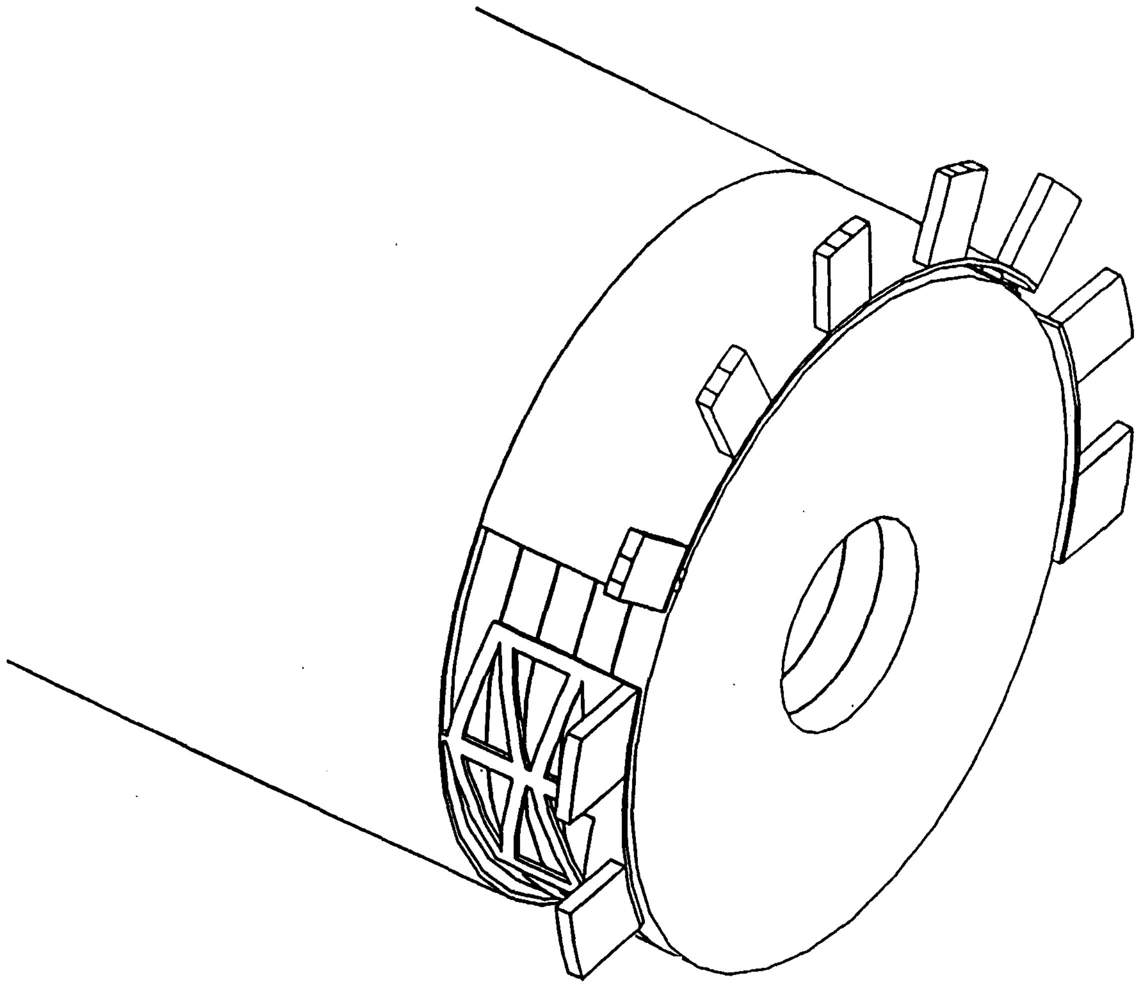

Westinghouse
Science & Technology Center

CENTRAL AND FORWARD TRACKING SUBSYSTEM

INTERMEDIATE TRACKER SUPPORT

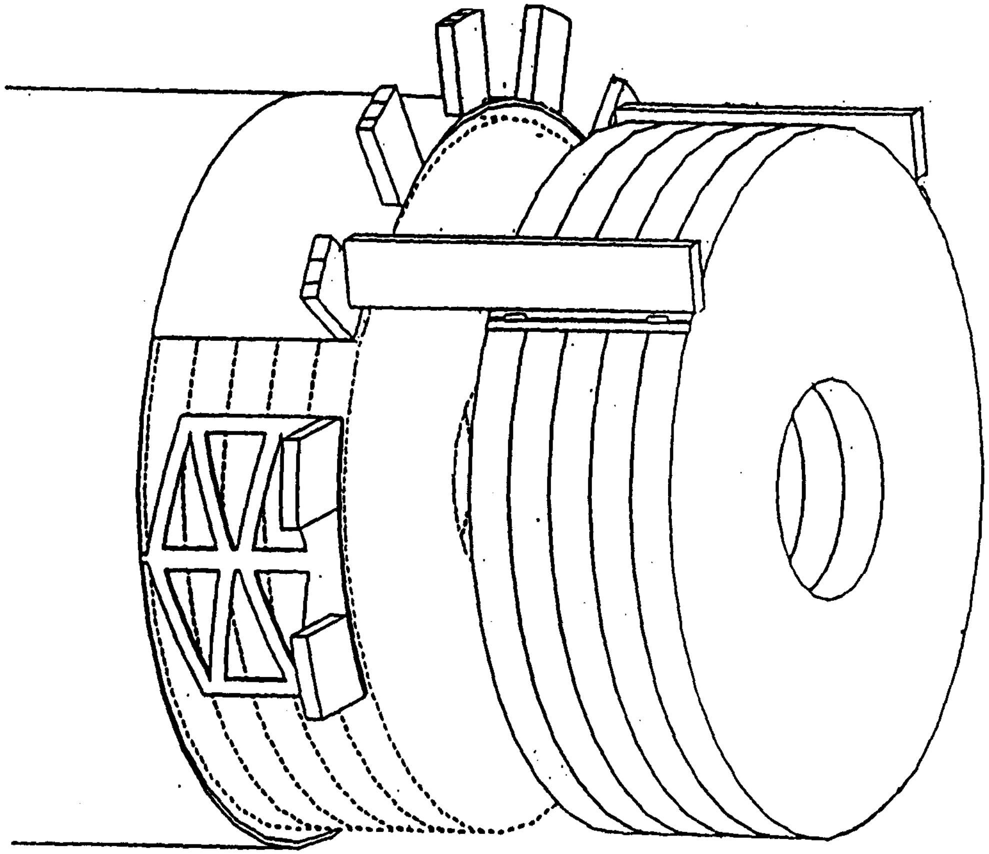

Westinghouse
Science & Technology Center

CENTRAL AND FORWARD TRACKING

INTEGRATION SYSTEMS
SUBSYSTEM MOUNTING

3. Silicon Tracker Support
   - Concept Would:
     - Mount Silicon at Four Corners on the Bore of the Central Tracker
     - Use Four Corner Kinematic Mount
   - Require Optic/Diode Position to Central Tracker Stability Monitor

Westinghouse
Science & Technology Center

CENTRAL AND FORWARD TRACKING SUBSYSTEM

SILICON TRACKER SUPPORT

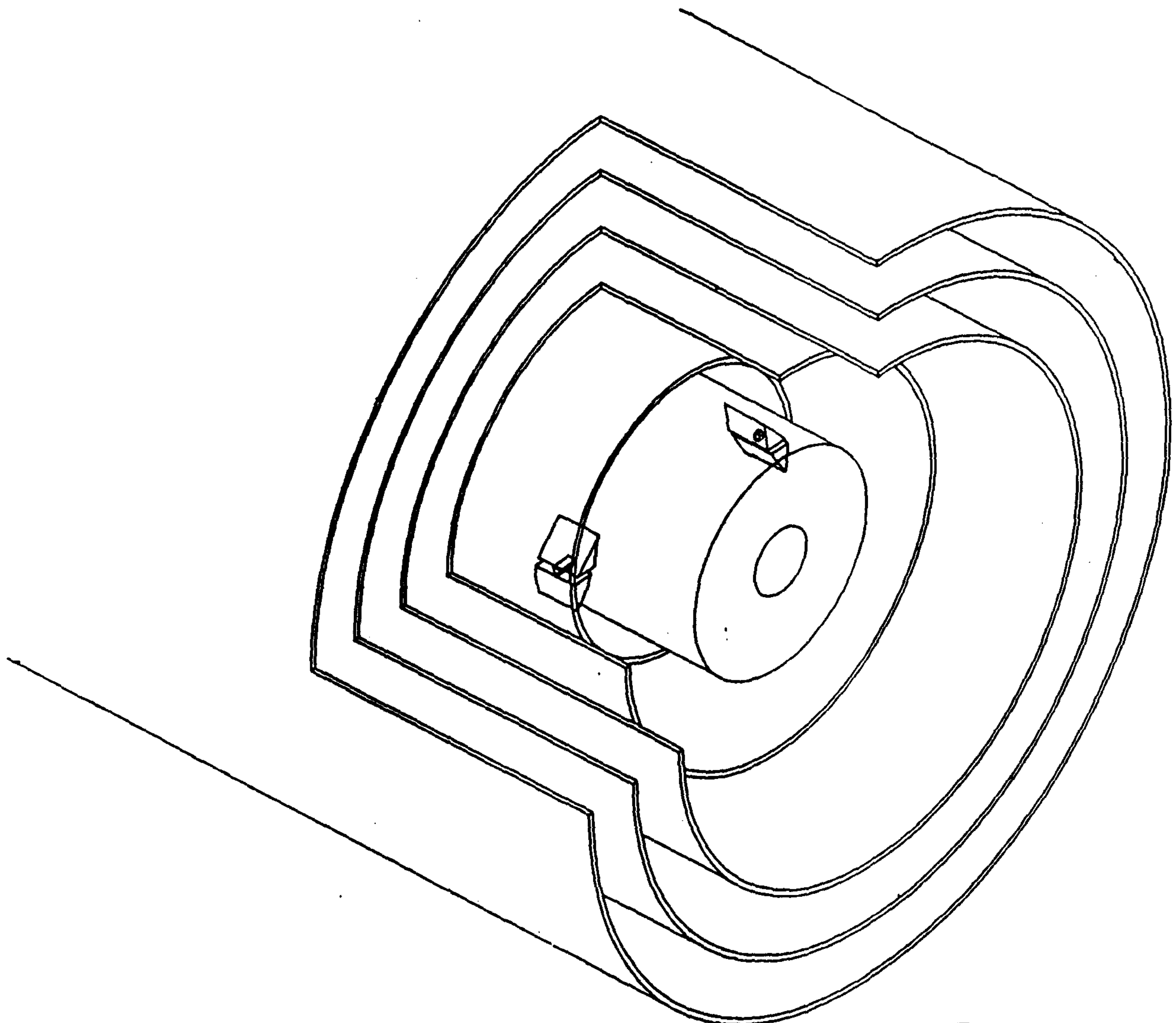

Westinghouse
Science & Technology Center

CENTRAL AND FORWARD TRACKING

INTEGRATION SYSTEMS
UTILITIES FOR CENTRAL TRACKER

1. Electronics Cables
   - Per Module
     - Power Cable Requires (Electronics)
       - 3 MM Diameter High Voltage (Jacketed?) Twisted Pair
     - Logical Signals Require (Module Control, Trigger and Data Output)
       - 50 MM Wide x 1 MM Thick Flat Kapton Cable
   - Per Tracker End
     - Power Cable Requires
       - 528-3 MM Diameter
     - Logic Signals Require
       - 528-50 MM x 1 MM

Westinghouse
Science & Technology Center

CENTRAL AND FORWARD TRACKING

INTEGRATION SYSTEMS
UTILITIES FOR CENTRAL TRACKER

2. Service Plumbing
   - Per Module
     - Drift Gas Requires
       - Two One-Inch Diameter Tubes
     - Electronics Cooling Requires
       - Two One-Inch Diameter Tubes
   - Per Tracker End
     - Drift Gas Requries
       - Sixteen One-Inch Diameter
     - Electronics Cooling Requires
       - Sixteen One-Inch Diameter

Westinghouse
Science & Technology Center

CENTRAL AND FORWARD TRACKING SUBSYSTEM

SCHEDULE

COST ESTIMATE OF CENTRAL STRAW TUBE TRACKER

TABLE 3

A-105

WBS	DESC	ENG	DSGN	TECH	LABOR	PROC	BASE	EDIA
		MAN DAYS	MAN DAYS	MAN DAYS	MAN DAYS	$	$	$
1.2.1	SUPPORT STRUCTURE							
1.2.1.1	SUPPORT ASSEMBLY							
1.2.1.1.1	STRUCTURAL SUPPORT ASSEMBLY	20	32	64	0	10936	22466	16980
1.2.1.1.2	MODULE LOCATING SEGMENT ALLIGNMENT	0	0	1449	0	0	280820	0
1.2.1.1.3	SUPPORT STRUCTURE SETUP	30	32	20	0	40000	43600	20210
1.2.1.1.4	PRECISION ALLIGNMENT TOOLING	12	28	0	0	380436	380436	11656
1.2.1.1.5	STRUCTURAL COMPONENT SUBASSEMBLY	74	160	139	0	325000	350020	68902
1.2.1.2	SUPPORT STRUCTURE COMPONENTS FABRICATION							
1.2.1.2.1	INNER TORSIONAL CYLINDER	23	7	100	0	76695	94767	11275
1.2.1.2.2	RADIAL SUPPORT COMPONENTS	196	63	862	0	789622	944782	97492
1.2.1.2.3	DISK COMPONENTS FABRICATION	185	60	826	0	756909	905481	92073
1.2.1.2.4	CONE COMPONENTS FABRICATION	188	57	801	0	742598	886706	92919
1.2.1.2.5	ALIGNMENT COMPONENT FABRICATION	31	50	338	0	27944	88424	24769
1.2.1.2.6	OUTSIDE TORSIONAL CYLINDER	480	624	537	0	490437	587025	349837
1.2.1.2.7	SUPPORT STRUCTURE COMPONENT TOOLING	220	474	439	0	603537	682550	204497
1.2.1.2.8	DESIGN REVIEW	80	64	0	0	0	0	48880
1.2.1.2.9	PROTOTYPES	0	0	1000	0	0	180000	0
1.2.2	MODULES FABRICATION							
1.2.2.1	MODULE DEVELOP AND FABRICATION							
1.2.2.1.1	MODULE DESIGN	500	500	100	400	100000	165600	329000
1.2.2.1.2	MODULE ASSEMBLY AUTOMATION	500	500	65	260	100000	142640	329000
1.2.2.1.3	MODULE ASSEMBLY	0	0	2250	9000	0	1476000	0
1.2.2.1.4	MODULE TOOLING	1000	1500	100	400	0	65600	775500
1.2.2.2	SHELL FABRICATION	0	0	0	0	2284800	2284800	0
1.2.2.3	STRAW COMPONENTS	0	0	0	0	1690752	1690752	0

COST ESTIMATE OF CENTRAL STRAW TUBE TRACKER

TABLE 3

A-106

WBS	DESC	ENG	DSGN	TECH	LABOR	PROC	BASE	EDIA
		MAN DAYS	MAN DAYS	MAN DAYS	MAN DAYS	$	$	$
1.2.3	MODULE INSERTION	0	0	1083	0	30000	221340	0
1.2.4	COOLING ASSEMBLY	215	0	250	0	4380	49380	90945
1.2.5	UTILITIES	813	0	250	0	425000	470000	343899
1.2.6	PRE-INSTALLATION TEST	20	0	31	0	180000	185625	8460
1.2.7	TRANSPORTATION SYSTEMS	165	278	250	0	177000	222000	130425
1.2.8	INSTALLATION FIXTURES	127	136	114	0	70000	90520	85681
1.2.9	ELECTRONICS SYSTEM							
1.2.9.1	ELECTRICAL POWER	403	701	334	0	1818479	1878599	335204
1.2.9.2	FRONT-END ELECTRONICS	2381	5165	167	0	8093533	8123593	2220938
1.2.9.3	DATA ACQUISITION INTERFACE	733	1351	167	0	1672419	1702479	627544
1.2.9.4	TRIGGER SYSTEM INTERFACE	233	541	187	0	319224	349284	225694
1.2.9.5	CALIBRATION SYSTEM	350	810	187	0	213900	243960	338400
1.2.10	FACILITIES							
1.2.10.1	SUPPORT ASSEMBLY	1600	750	760	0	225000	360000	810750
1.2.10.2	MODULE ASSEMBLY	1500	750	1500	0	225000	495000	810750
1.2.10.3	ELECTRONICS ASSEMBLY	1500	750	3750	0	50000	725000	810750

	ENG	DSGN	TECH	LABOR	PROC	BASE	EDIA
TOTAL MAN DAYS	13468	15380	18047	10060	21923600	26369238	9311431
TOTAL DOLLARS	6697037	3614394	3248498	1197140	21923600	26369238	9311431

GRAND TOTAL DOLLARS 35680668

REV3B120190

CENTRAL STRAW TUBE TRACKER
Design Estimated Manpower

90	91	92	93	94	95	96	97	98	99

Concept (90 → 92)

DESIGN (92 → 94.5), 2 yrs

Build (94.5 → 97.5), 3 yrs

Install (97.5 → 98.6)

DESIGN TRACKER
(Requires 50 People for 2 Yrs)

SUPPORT STRUCTURE

- Components

4 Engg	8
3 Design	6
1 Tech	2
	16 MYrs.

- Tooling

2 Engg	4
1 Design	2
1 Tech	2
	8 MYrs

ELECTRONICS

8 Engg	16
17 Design	34
2 Tech	4
	50 MYrs

STRAW MODULES

- Components

2 Engg	4
2 Design	4
1 Tech	2
	10 Yrs

- Tooling

2 Engg	4
3 Design	6
1 Tech	2
	12 MYrs

CENTRAL STRAW TUBE TRACKER
Build Estimated Manpower

90	91	92	93	94	95	96	97	98	99

Concept → (90–92)

Design → (92–94.5), 2 yrs

BUILD → (95–97.5), 3 yrs

Install → (97.5–99)

BUILD TRACKER

(Requires 40 People for 3 Yrs)

SUPPORT STRUCTURE

- Production

2 Engg	6
1 Design	3
9 Tech	27
1 Tech (QA)	3
	39 MYrs

STRAW MODULES

2 Engg	6
1 Design	3
14 Labor	42
2 Tech (QA)	6
	57 MYrs

ELECTRONIC

2 Engg	6
1 Design	3
3 Tech	9
2 Tech (QA)	6
	24 MYrs

Westinghouse
Science & Technology Center

Rev. 3A

A TIME TO VOLTAGE CONVERTER AND ANALOG MEMORY UNIT FOR STRAW TRACKING DETECTORS

L. Callewaert*, W. Eyckmans*, A. Stevens, W. Sansen*,
J. Van der Spiegel, R. Van Berg, H.H. Williams, T.Y. Yau
University of Pennsylvania
Philadelphia, Pa. 19104

Abstract

A low power, sub-nanosecond accuracy, quick recovery, data-driven, multiple sample Time to Voltage Converter suitable for use on high rate straw tracking detectors is described. The described TVC includes "virtual" storage of analog data in both Level 1 and Level 2 queues and an on board ADC with first order correction for capacitance variations and non- linearities.

Introduction

In a high precision drift tube or straw tracking system, one measures the time of arrival of the first electron at the anode. While many possible schemes exist, our initial judgement was that an analog time measurement would offer both lower power and greater resolution than an equally complex digital system. In addition, we believe that it will be necessary to incorporate *all* of the system features such as connection to the trigger and DAQ systems in any usable design in order to keep the power, mass and complexity of the final system under control.

Design Goals

The minimum set of specifications necessary for a successful time measuring device would seem to be:

- $<$ 0.5ns time accuracy, $\sim$ 0.2ns time resolution - in order to ensure spatial precision of $< 100\mu m$ without extensive (preferably without any) calibration.
- Deadtimeless continuous multihit operation - second hit or double track resolution better than any conceivable chamber (i.e. $\leq 30ns$).
- High rate capability - at the SSC average rates for a straw chamber near the inner radius of survivability approach 10 MHz.
- Local storage of data during the trigger decision time(s) - to keep cabling and power from dominating a detector design, it will be necessary to move data off the detector only after the trigger has had time to reject most of the uninteresting events.

Time to Voltage Conversion

In previous work, we have fabricated and measured a Time to Voltage Converter [1] [2] in a 1.6 μm digital CMOS process that easily met the first criterion as can be seen in the differential nonlinearity distribution, Figure 1.

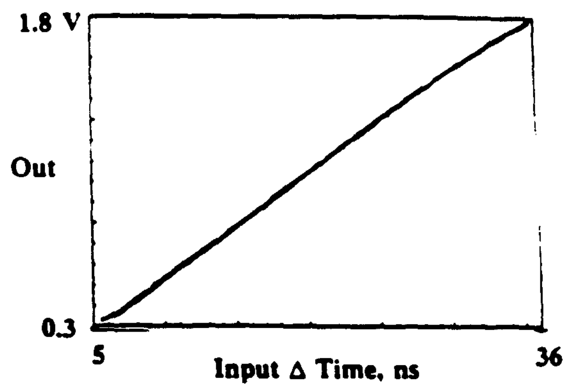

Figure 1: TVC Differential Non-Linearity from 7 to 31 ns. Note that 50 mV is equivalent to 1 ns.

This eight channel prototype TVC design depended upon careful matching of capacitance values from one sample to the next using common centroid layouts. It became obvious in this design that while the common centroid layout gave very good matching channel to channel, the cost in area and layout complexity for a much larger number of capacitors would be prohibitive. Because of this, we decided to pursue a charge–measurement scheme that would, to first order, be insensitive to capacitance values. In addition, we have attempted to include in the TVC/AMU all of the logic necessary for a full SSC compatible readout system. The block diagram in Figure 2 shows many of these features, the most salient of which will be discussed below. The first prototype of the TVC/AMU was also fabricated in a 1.6μm CMOS process, but a number of layout errors prevented full operation of the device. A second version of the TVC/AMU is now being readied for fabrication and measurement.

Any capacitor memory scheme capable of simultaneous reading and writing will have at least three switches around each individual capacitor – an input charging switch, an output discharge switch, and a reset switch. By placing charge on the capacitor at a constant input rate and then using the output switch to remove charge at a much

*Catholic University of Leuven, Belgium

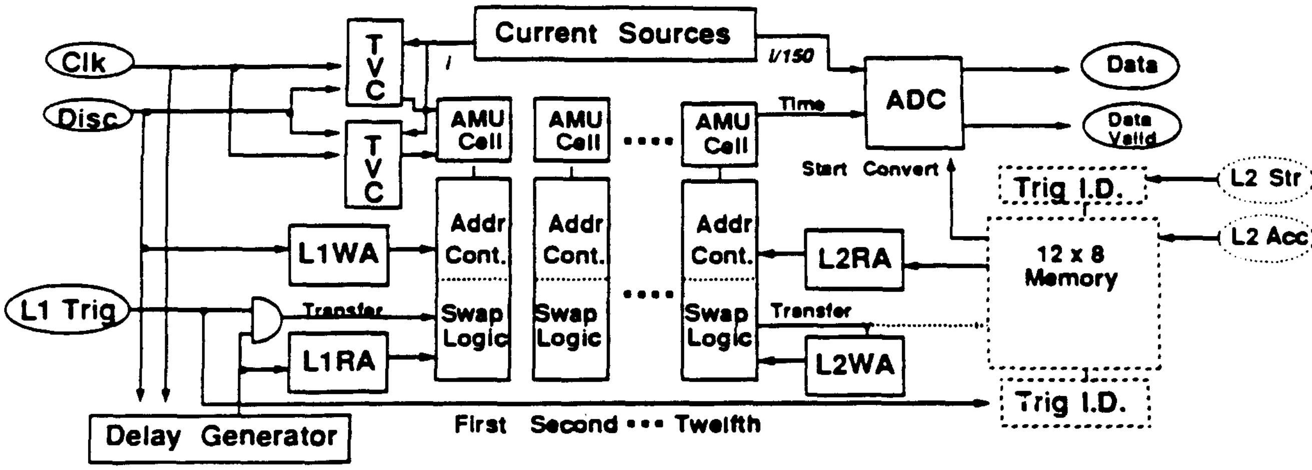

Figure 2: TVC/AMU Block Diagram. Dotted blocks associated with L2 Trigger identification are not implemented in the prototype version

lower rate, it is possible to measure the time *duration* of the input current to high precision with a relatively slow comparator. If the input and output currents are ratioed to each other, then the accuracy of the measurement can be kept high even with relatively large integrated circuit process and device variations since both the capacitance and the absolute values of the currents ratio out of the first order time equation, $\Delta t_{out} = \frac{\Delta t_{in} \times i_{in}}{i_{out}}$. We have chosen a ratio of $i_{in}/i_{out} \sim 150 :: 1$ in order to give $\sim 0.2ns$ resolution over a 16 ns (plus 8 ns pedestal) range.

Level 1 Storage

For a two to three μs Level 1 storage time it would be necessary to provide 128 to 192 storage locations for a simple synchronous system. However, by implementing a data driven system which uses a storage location only if new data is present, many fewer locations will suffice given the necessarily modest occupancies of any viable tracking system. Thus in the design of the prototype TVC/AMU, we have limited the number of Level 1 locations to eight which is more than enough for a 1 μs delay with a 5 MHz average input rate. This design may be expanded to 16 or more locations in Level 1 at the cost of additional silicon real estate.

Level 2 Storage

While a few microseconds of synchronous storage for Level 1 is conceivable, even if awkward, many tens of microseconds is clearly outside the realm of realisable circuits and thus Level 2 must also be implemented in a data driven fashion. For the TVC/AMU we have chosen to use a virtual Level 2 scheme in order to simplify the analog storage problems. The particular technique adopted is *address swapping* which is logically similar to minimum FIFO or pointer schemes, but minimizes the length of analog control signal lines - at the expense of longer control buses.

The Level 1 and Level 2 queues are implemented by using a write and read address counter for each queue. Thus the storage location next to be used is identified by the Level 1 Write Address (**L1WA**) counter which is incremented by the discriminator pulse, the **L1RA**, which is incremented by a delayed version of the discriminator pulse, identifies the next data to be tested for a valid Level 1 trigger. Similarly **L2WA** (incremented by a transfer from Level 1) and **L2RA** (incremented by an End of Convert) identify the beginning and end of the Level 2 queue. The output of these counters then serves to select the required capacitor by parallel comparison with the address contained in local address registers. The local address register is implemented as a five bit latch, the Level 1 counters (**L1WA**, **L1RA**) are implemented with four bits, and the Level 2 counters (**L2WA**, **L2RA**) are three bits wide, appropriate for a system with 16 Level 1 locations and 8 Level 2 locations even though the initial prototype TVC/AMU realises only 8 and 4 locations respectively.

Time Measurement Logic

To accurately reconstruct tracks, it is necessary to know the time of arrival of the first electron at each straw anode relative to some common time that relates all of the data for a given event. The TVC/AMU operates as a common-stop time measuring device - starting on an anode discriminator pulse and stopping on the positive going clock edge after the next negative going clock edge.

This scheme leaves a guaranteed minimum of one-half of a clock cycle for any time measurement and for a nominal 16 ns clock means that the actual time ramp in the TVC goes from 8 to 24 ns. This minimum time allows the TVC response to be linear in the range of interest and avoids the possible race conditions associated with a system that allows a zero minimum measuring time.

Event Delay

In a data driven architecture, there is no one-to-one correspondence between physical storage location and event time. Thus there must be some provision in the TVC/AMU to allow synchronisation of an event with a possible Level 1 Trigger signal. A simple 64 element shift register would allow about 1 μs of delay with a 16 ns clock period, but all 64 elements would be clocked at 60 MHz and significant power would be dissipated. In this design we have chosen to use a 64 element dynamic memory cell with read and write decoding done by a single decoder but with write select directed to the $(N)th$ element while read select is directed to the $(N+1)th$ element. One input line and one output line bussed to each of the elements then results in any input being delayed by 64 clock pulses before appearing on the output line.

Level 1 Trigger Interface

After a delayed data pulse exits from the delay generator, it is simply *AND*ed with the Level 1 Trigger signal and the resulting signal, **L1ok** is used to provide the transfer signal that logically moves data from Level 1 to Level 2. If the Level 1 Trigger signal remains high for more than one clock period, then the same simple logic will continue to transfer any existing Level 1 data to Level 2, thus providing for the case where the detector response time is greater than one clock period (in this case the electron drift in the straw detector). In order to differentiate data from different clock cycles within any one Level 1 Trigger time, a separate small counter must keep track of clock pulses.

Level 2 Trigger Interface

The Level 2 Trigger is asynchronous so that a delay line is not appropriate for providing the trigger-data synchronism. Since the Level 2 Trigger is monotonic, however, it is only necessary to provide two counters (**L2WA**, **L2RA**) to keep track of Level 2 inputs and outputs. Each new entry into Level 2 increments the **L2WA** counter and each read (or reset) of Level 2 increments the **L2RA** counter.

As the Level 2 Trigger is asynchronous, it must be accompanied by a timing signal. The Level 2 Strobe is used to clock a D-Flip Flop with the Level 2 Accept at the data input of the flip flop. For an accepted event, the ADC cycle is started, for a rejected event, the **L2RA** is simply incremented and the storage location is reset.

Event Identification

During normal SSC operation, individual detector elements and systems will be involved in simultaneous input processing, data storage, data conversion, and data output. Given the non-deterministic nature of multiple asynchronous devices, the data stream out of a detector will be disordered in time and it will be necessary to include in each data packet some time identifier.

The simplest time stamp, of course, would be a crossing counter - advancing every 16 ns. However, for Level 2 storage times of 50μs or more plus realistic DAQ pipeline delays of many tens of microseconds, a 13 or 14 bit crossing counter would be necessary in order to avoid ambiguity. We have chosen to count not the crossings at 60 MHz but the Level 1 Triggers at 1 to 100 KHz. Even at 100 KHz the eight bit Trigger I.D. Counter remains unambiguous for 2.5 ms.

Since the Level 1 Trigger may in many cases remain true for more than one crossing, to completely specify time it is necessary to have a small four bit Bunch Counter to keep track of bunches. This counter is enabled by Level 1 Trigger true and counts until Level 1 Trigger goes false.

Because the occupancy of a tracking system must be relatively low, most Level 1 and Level 2 Triggers will not have data in any given detector channel. For Level 1 Triggers, the Level 1 Trigger I.D. Counter advances on the L1 Accept, but the delayed data is *AND*ed with the L1 Accept and Level 2 data is stored only on a coincidence. At Level 2, it is necessary to tag each piece of data with the Level 1 Trigger I.D. and then, at each Level 2 Trigger, search the on chip memory for any relevant data.

The **L2WA** counter provides the write address for this memory and the **L2RA** provides the readout address. In order to skip over Level 2 Accepts not associated with stored data, the Trigger I.D. output of the present **L2RA** is compared with the value of the Level 2 Trigger I.D. Counter which is advanced by the Level 2 Strobe. If the memory-Level 2 Trigger I.D. Counter comparison is true and Level 2 Accept is true, the A/D converter is started and the **L2RA** is advanced on the end of the A/D conversion cycle. For events where Level 2 Accept is false, the **L2RA** is simply advanced on the Level 2 Strobe.

ADC

The Analog to Digital Converter is implemented as a Wilkinson run-down device with a capacitor (i_{out} discharge current ratioed (at 1/150) to the charging current (i_{in}). The capacitor voltage is then viewed by a comparator which trips when the voltage reaches the reset value. A 60 MHz counter that began counting when the discharge current began flowing is stopped when the comparator trips and the counter value is loaded into an output register. This value is then the relative time of the detector *hit* in units of about 0.2 ns per least significant bit.

Data Output

Data from the TVC/AMU prototype consists of the contents of the ADC register and the contents of the four bit Bunch Counter. The Data Present signal goes true at the beginning of the ADC cycle and the Data Valid line goes true at the end of the ADC cycle. For the production version, the data output must contain the ADC and Bunch Counter information, but also a geographic address of the *hit* wire (or element), and a temporal address in the form of the Trigger I.D. Number.

References

[1] A.E. Stevens et. al., *A Time to Voltage Converter for Colliding Beam Detectors*, IEEE Transactions on Nuclear Science, **36** No. 1, 517-21, (1989).

[2] A.E. Stevens et. al., *A Time-to-Voltage Converter and Analog Memory Unit for Colliding Beam Detectors*, Journal of Solid State Circuits, **24**, No. 6, 1748-51 (1989).

A LOW POWER TIMING DISCRIMINATOR FOR SSC APPLICATIONS

F.M. Newcomer, S. Tedja
University of Pennsylvania
Philadelphia, Pa., 19104

Abstract

A bipolar monolithic discriminator with programmable threshold and hysteresis is being developed for proportional drift tube tracking sensors. Design goals include low power(4-8mW), sub-nanosecond cluster detection accuracy, and uniform channel to channel response. Technology, circuit design and expected performance are discussed.

Introduction

In a proportional wire tracking detector each sensor is instrumented with a signal amplifier, shaper and discriminator. The discriminator serves the dual purpose of providing a logic pulse to indicate that an element has been triggered and a timing edge to determine the closest point of approach of the track to the wire.

Critical design parameters for an SSC wire chamber discriminator are power, time slewing and chip to chip threshold matching.

Technology

Silicon bipolar technologies offer the best choice of trade-offs in speed, power, matching and reliability. Bipolar transistors have the highest transconductance, g_m, per unit standing current of any available technology. The typical, on chip, matching of the base emitter, or controlling, voltage is $1mV$ or less. This low offset voltage allows the use of a simple emitter coupled pair as a discriminator input stage without trimming or the use of other offset cancellation techniques. It also may lead to a reduced the gain requirement in earlier signal processing stages which will directly affect the power.

Low values of collector substrate capacitance, C_{cs}, and collector base capacitance, C_{cb}, in the advanced bipolar processes allow the designer to depend more heavily on resistive elements for gain. In the Tektronix *SHPi* process C_{cb} is 39fF and C_{cs} is 24fF for a minimum size transistor. These values are the same or smaller than the expected interconnect capacitance. A direct benefit of low transistor capacitance is high bandwidth at low power. A minimum size *SHPi* transistor has an expected unity gain bandwidth of $3GHz$ at $100\mu A$ of collector current.

Design Considerations

Power

The fixed logic output swing and requirement for a nearly constant internal delay requires a circuit with both high gain and bandwidth. Typical commercial comparators with ECL outputs and good delay versus input overdrive characteristics, consume several hundred milliwatts per channel and require off chip components to provide threshold and hysteresis feedback. The power budget for an entire channel of SSC wire chamber electronics is less than $25mW$.

Power depends on technology, output logic levels, drive load capacity, input range requirements and the details of the circuit design.

Output Signal

The discriminator couples directly to a time conversion unit located a few cm away. Differential outputs will minimize feedback to the preamplifier. Since the electronics is expected to be fully custom, the output logic levels can be set to any convenient magnitude.

A bipolar differential pair, or CMOS line receiver with an internal gain stage, can be fully switched with an input voltage difference of $150mV$. We have chosen this as the minimum acceptable logic swing for modeling purposes. Open collector outputs in this design allow larger logic levels, at the expense of output rise time.

Gain

Given the $150mV$ logic levels described above, a conventional analog amplifier would require a gain-bandwidth of more than 50GHz to switch its outputs (10 to 90%) in 1ns with a $1mV$ input. High speed bipolar transistors, operating at low current, rarely have a unity gain

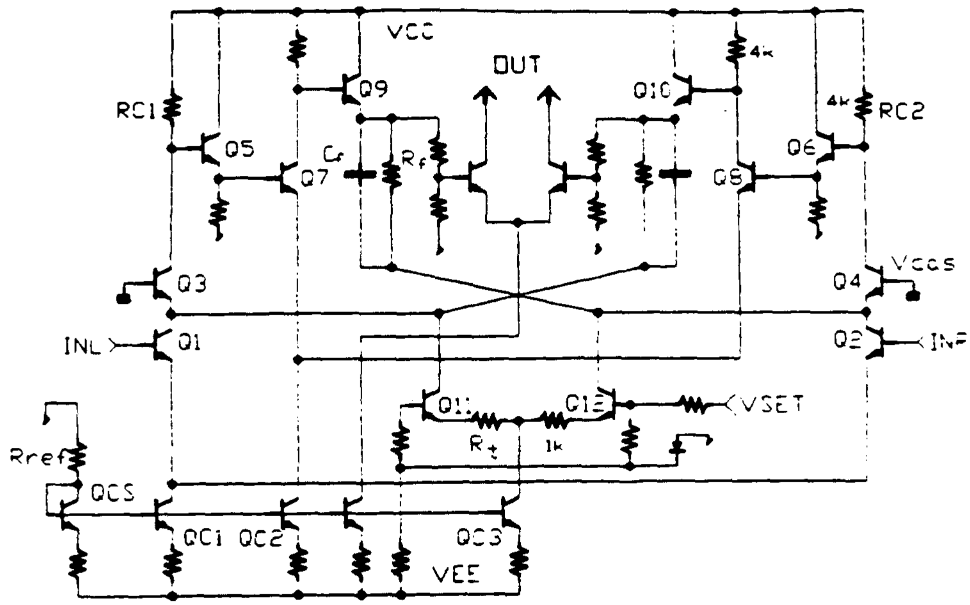

Figure 1: Prototype Wire Chamber Discriminator Circuit.

bandwidth, f_t, greater than 5GHz, so it is necessary to employ multiple gain stages to achieve a comparable level of performance. Since the objective is a digital output, positive feedback can be employed to boost the near crossing point gain.

Circuit Description

We have designed a prototype timing discriminator based on requirements for an intermediate tracking, proportional drift tube system at SSC. General characteristics based on known process variations and HSPICE simulations using model parameters for the Tektronix *SHPi* process are given below.

Performance Specification	
Power Dissipation	5mW
Time Slewing	Less than 1ns/decade of overdrive
Input offset	$1mV$ or less
Internal Threshold	Greater than $50mV$
Threshold Uniformity (chip to chip)	Better than 10% of setting

A simplified schematic is shown in figure 1. This design is similar to one previously developed for a fixed target silicon strip detector using the Tektronix *SHS* process. The major performance differences are in power and overdrive response [1].

Referring to the schematic, INL and INR are the differential inputs. If the outputs of the shaping stage are balanced to within an acceptable threshold error, they may be directly coupled to INL and INR. The DC level at the input may be between $\pm$ $600mV$.

Gain Stages

The input transistors, Q1 and Q2, operate at a quiescent current of $100\mu A$. They perform a voltage to current conversion with a gain, A_i, equal to the g_m of Q1 or Q2. This may be defined:

$$A_i \equiv \frac{i_o}{V_{in}} = \frac{I_c}{v_t}. \qquad (1)$$

I_c is the $100\mu A$ collector current and v_t is a constant equal to $26mV$ at room temperature.

Q1 and Q2, together with cascode transistors, Q3 and Q4, form the first stage amplifier. Similarly Q7 and Q8 with a quiescent current of $50\mu A$ each, form the second stage amplifier.

The small signal voltage gain of a differential pair with load resistors R_l is:

$$A_v = g_m R_l; \quad (g_m = I_c/v_t). \qquad (2)$$

In a monolithic design, semiconductor resistors offer the lowest capacitance choice for R_l, but process variations of up to $\pm30\%$ will directly affect A_v unless some form of compensation is applied.

The DC gain is stabilized by making the reference current in QCS depend on a resistance of the same type. This current is ratioed among QC1, QC2, and QC3, which contribute to the gain of the first two stages.

Assuming a small voltage drop across the emitter resistor of QCR and setting the current in QC1 to four times the reference current in QCR, the transconductance above may be expressed as follows:

$$g_m = 2\frac{VEE - v_{be}}{v_t Rref} \qquad (3)$$

effectively placing the same process dependent resistance in the denominator of A_v.

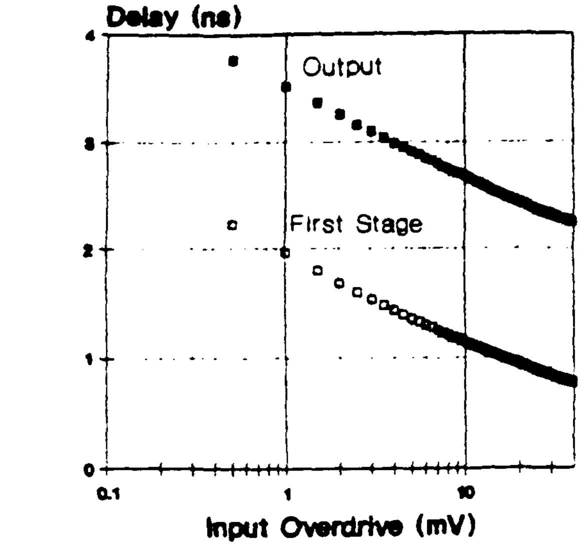

Figure 2: The plot above shows the delay from input to an output logic swing of 75% and the delay in the first stage from input to a $20mV$ cross over of the collector nodes.

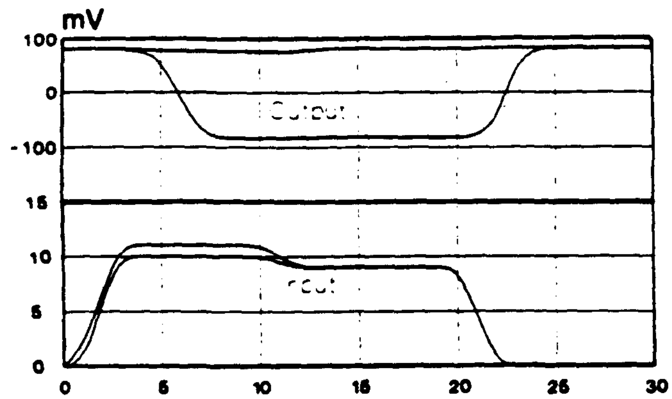

Figure 3: HSPICE simulation showing the effect of hysteresis.

The first and second stage gain is set to 15 and 7, respectively, by using 4kΩ collector resistors. Since the collector node time constant is nearly the same for both stages and the gain of the first stage is much larger than the second, the first stage dominates the overdrive delay. Figure 2 is a simulation result showing the elapsed time from input to a $20mV$ cross over in the first stage and from input to a 75% output transition, as a function of input overdrive. This plot clearly shows that the output overdrive characteristic is determined in the first stage.

Threshold and Hysteresis

The threshold and hysteresis circuits operate by supplying offset currents into resistors RC1 and RC2, shifting the differential voltage across the collector nodes.

The threshold input, VSET, is attenuated by a factor of ten and used to set a voltage difference across the transistor pair QTL and QTR. In the linear operating region, the current difference between QTL and QTR is approximately $VSET/10R_e$, where R_e is the sum of the resistor, Rt, and the emitter node impedance of one of the threshold setting transistors. Using A_i to relate this to an equivalent input voltage, V_{in}, defined in 1 and replacing the output signal, i_0, with the current difference in QTL and QTR, the effective threshold is:

$$V_{th} = \frac{v_t}{20}\frac{Rref}{R_e}\left(\frac{VSET}{VEE - v_{be}}\right) \tag{4}$$

where V_{in} has been re-labeled V_{th}. The threshold dependends on ratios of voltages, ratios of resistors and v_t . The inherent temperature of dependence v_t is partially compensated by the shift in v_{be}, resulting in an expected threshold shift of $.13\%/^oC$. Resistor ratioing errors are typically 1% or smaller for this process and should not contribute significantly to the chip to chip threshold variations.

Assuming an input offset error of $1mV$ or less, the gain of the shaper can be set so that a typical minimum signal will be 10 to $20mV$. The discriminator threshold setting would then be in the range of 5 to $15mV$ depending on amplifier and system noise. The prototype design maintains a linear response to the threshold reference, VSET, up to $60mV$ of equivalent input threshold.

A standard technique to eliminate output oscillation due to noise on near threshold signals, is to add a small amount of positive feedback, or hysteresis. This positive feedback may be tuned to greatly improve the gain of the input stage and therefore reduce the output delay for near threshold signals.

In this design, a resistor and capacitor pair, Rf and Cf, connect cross coupled from the emitter outputs of Q9 and Q10 to the cascode input nodes at Q3 and Q4. The capacitor and resistor are matched (within expected process variations) to provide the same level of positive feedback. Rf is chosen to provide a current difference equivalent to a few mV input offset. This value, added to V_{th}, determines the effective input threshold. When the output changes state, the hysteresis offset is reversed, lowering the threshold. Figure 3 shows an example this threshold shifting behavior. The two input pulses differ by only $1mV$ in their initial magnitude. After 10ns they both revert to a value $2mV$ below threshold. The output is triggered only once and remains *on* for the duration of the input pulse due to the lowering of the effective threshold.

This design is presently being prepared for fabrication in the Tektronix *SHPi* process.

References

[1] D. Christian et al., "The Development of two ASIC's for a Fast Silicon Strip Detector ", IEEE NS36, 507-511, (1989).

SIMULATION AND MODELLING STUDY OF AN SSC FRONT END ELECTRONICS ARCHITECTURE

K. J. Ragan
McGill University

P. K. Sinervo
University of Toronto

R. Van Berg and H. H. Williams
University of Pennsylvania

Abstract

An architecture and design for a front end electronics circuit intended for the readout of a wire tracking chamber at the SSC is described. A detailed high-level simulation has been developed and is being used to study the behavior of this circuit. Initial results from this simulation study are described.

Introduction

Proton-proton collisions at the SSC will occur at a rate of 60 MHz, but of this we estimate that the rate of "interesting" collisions will only be of order 100 to 1000 Hz. Thus, a detector will have to reduce the event rate by at least five orders of magnitude in order to obtain a reasonable readout rate of events. We also expect a typical SSC detector to have of order 10^7 channels of front end electronics, which means that these front end (FE) systems must have high channel density. In addition, they must have low power consumption and be resistant to radiation doses in excess of 1 MRad. These functional and technical requirements can only be met by electronics systems that employ the latest fabrication technologies and rather sophisticated control structures.

The behaviour of such systems is difficult to predict without detailed modelling and simulation. We have employed a high-level modelling language known as Verilog* to simulate the behaviour of a specific FE circuit designed for the readout of an SSC wire tracking detector (such as a "straw" chamber). Our simulation models the circuit by implementing each of its functional components and the control and logic signals required by each component (including signal delays). The simulation is driven by input signals from the wire chamber, the SSC beam clock and the Level 1 (L1) and Level 2 (L2) trigger system. We describe this model and report the preliminary results of a study using this simulation.

*Verilog is a product of Cadence Design Systems

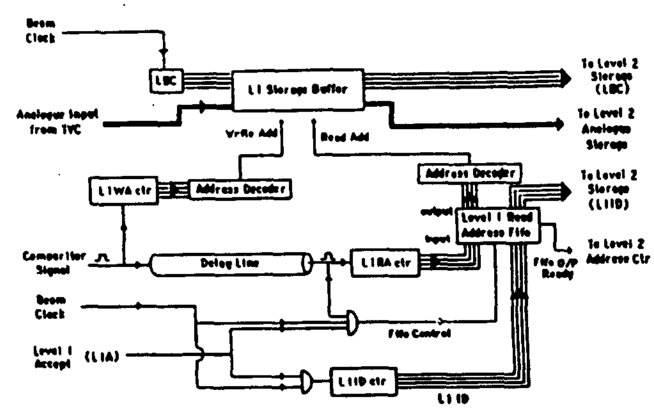

Figure 1: The block schematic of the portion of the FE circuit that manipulates the data prior to a L1 decision.

System Architecture

We show the schematic of the readout system in Figs. 1 and 2. Because of the inherently low channel occupancy of a wire tracking detector, we have taken a "data-driven" approach to buffering data on the FE circuit. The data consists of an analogue voltage signal produced by a time-to-voltage circuit (TVC) [1], which converts the time elapsed from the arrival of a hit on the wire chamber anode to the next crossing into a voltage signal. The edge of the discriminator pulse that starts the time-to-voltage conversion also signals that valid analogue data is available for storage. The circuit must store this data for a fixed delay time (on the order of several μs), during which time the L1 trigger has made a decision and a L1 Accept (L1A) signal has propogated to the FE circuit. Since the L1A signal is always delayed with respect to the interaction by a fixed number of crossings, this signal is synchronized to

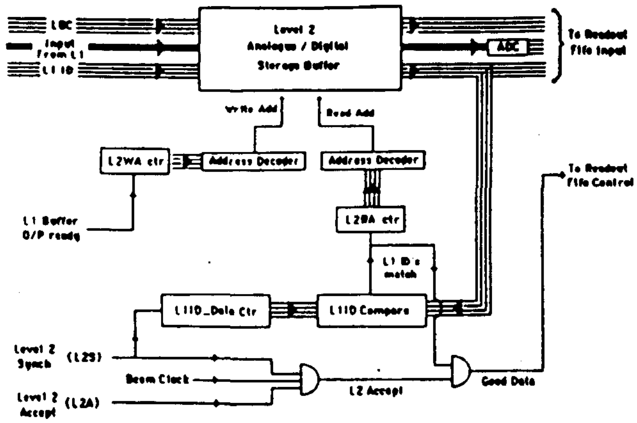

Figure 2: The block schematic of the portion of the FE circuit that manages the data prior to the L2 trigger decision.

the beam clock. This implies that only one signal is essential between the L1 trigger and the FE circuit (excluding the beam clock).

When the L1 trigger decides to accept a crossing, the FE circuit must store all data associated with the interaction that occurred on that crossing, which for a wire chamber system will be any data that is recorded by the circuit within some number of crossings of the interaction. The circuit then waits for a L2 trigger decision, which in our model may come at any time between a minimum and maximum time after the L1 trigger decision is made. When the L1 trigger rejects a crossing, any recorded data associated with that crossing are discarded by the circuit.

We expect the L2 trigger decision time to be of order 50 μs, and to vary considerably from event to event. We assume that the L2 trigger decisions will be made in the same order as the L1 trigger accepts, as otherwise the L2 trigger would have to identify to the FE circuit the L1 accept to which the L2 decision pertains; this would involve the distribution of a large number of signals from the L2 trigger to each FE circuit. The L2 trigger decision is communicated to the FE circuit using a pair of signals: the L2 Strobe signal (L2S) indicates to the circuit that a L2 trigger decision has been made, while the L2 Accept (L2A) signal is used to inform the circuit whether the L2 trigger accepted or rejected the L1 accept. The data associated with interactions rejected by the L2 trigger are then discarded by the circuit, while the data associated with a L2 accept are digitized and transferred to the data acquisition (DAQ) system.

Model for the FE Circuit Inputs

We have developed a Verilog module that provides as output a beam clock signal, a L1A signal, a L2S signal and a L2A signal. The behaviour of the L1 Accept signal is determined by two parameters: the L1 accept rate, and the L1 trigger delay. We define the L1 accept rate as the probability that the L1 trigger will generate a L1 accept for a crossing (a typical value would be 0.001). The L1 trigger delay is the number of crossings that is required before the L1 decision has propagated to the FE circuit (typically $\sim$ 120 crossings).

We specify the behaviour of the L2 trigger by (i) the fraction of those interactions passing the L1 trigger that are accepted by the L2 trigger; and (ii) the L2 trigger decision time, which in our model is a random variable that can have various distributions (we typically choose a Gaussian distributon with a mean and width of 40 μs and 25 μs, respectively. We also restrict the L2 decision time; typically we require that it be at least 5 μs and no more than 200 μs.

A separate Verilog module generates the input signal from the TVC circuit that prepares the analogue input and the hit signal. We characterize this signal by (i) the nominal hit rate, or wire occupancy, and (ii) the minimum time between hits, which is defined by the width of the signal pulse from the chamber. Typical values for these parameters are 0.05 hits/crossing and 30 ns, respectively. We note that we define the nominal wire occupancy to be the probability that a hit will occur in a given time, and does not reflect the deadtime experienced by the wire due to the finite pulse width (*i.e.*, the observed hit rate is less than the nominal rate).

Schematic of the Front End Circuit

The design of the FE circuit features (i) a L1 buffer, which stores all the analogue data during the time required for a L1 decision; (ii) a L2 buffer, which stores the analogue data associated with interactions accepted by the L1 trigger; (iii) a "buffered" L1-L2 transfer, in which the data transfer between the L1 and L2 buffers is performed by using an intermediate FIFO; and (iv) an output buffer, which holds the digitized data that will be transferred to the DAQ system. These components can be seen in the block diagrams shown in Figs. 1 and 2.

The L1 analogue buffer is implemented as a circular buffer, with a write address register (L1WA) that holds the address of the next L1 location into which data will be stored, and a read address register (L1RA) that points to the location that contains the oldest piece of data in the buffer. The TVC hit signal triggers the circuit to store the data in the next L1 buffer location and then increments the L1WA counter. The same hit signal is also fed into a delay line that stores the signal for the time required for the L1 decision.

The arrival of the L1 trigger decision is coincident with the arrival of the hit signal out of the delay line. Each hit signal increments the read address register (L1RA). If the L1 trigger accepts the crossing, each hit signal that comes out of the delay line during the time resolution of the detector is associated with the same L1 trigger and is transferred to the L2 buffer. In order to be able to associate each hit with a specific L1 trigger, it is necessary at this stage to tag each data with a L1 identification (L1ID). We do this by having a separate register that is

Parameter	Min	Max	Default
L1 Accept rate	0.0001	1.0	0.001
L1 Delay (ns)	480	3000	960
L2 Accept rate	0.001	1.0	0.02
L2 decision time (μs)	0.5	100	8
Hit rate (hits/crossing)	0.001	0.20	0.05
Minimum hit separation (ns)	20	50	30
Maximum readout time per event (ns)	16	500	50
Length of L1 buffer	8	32	16
Length of L2 buffer	2	32	4
Length of L1 Read Fifo	2	8	4
Time for writing into L2 (ns)	100	2000	100
Time for reading from L2 (ns)	100	5000	100

Table 1: The range of values used to specify the readout system.

incremented on each L1 accept. The data associated with a specific L1 accept is tagged with the L1ID value for that L1 trigger and this digital value is stored with each piece of analogue information that is transferred to the L2 buffer.

The data transfer from the L1 to L2 buffer is performed by storing the L1 address in the short address FIFO (L1RF). This can take place rapidly so several hits can be stored for the same interaction if necessary. The analogue data transfer to the L2 buffer can take place on a much slower time scale, even allowing for a low power analogue-to-digital conversion in the process if desired.

Simulation Results

We have begun a study of the performance of this buffered L1-L2 circuit using this simulation. We are varying the system parameters, as shown in Table 1, where we also indicate the default parameters for the readout system. Although the potential parameter space is large, it is significantly restricted by the demand that the overall L2 trigger rate be of order 10^3 Hz and that a significant fraction of the rejection be achieved in both trigger levels.

We show in Fig. 3 the measured "deadtime" of the circuit due to L1 and L2 buffer saturation as a function of the wire occupancy, keeping all other system parameters constant. We note that this deadtime (defined as the fraction of hits lost because the buffer was full) is small even for wire hit rates in excess of 0.20 hits/crossings. Since the actual wire efficiency is well below 0.90 in this case due to the width of the wire chamber pulse, the additional loss of efficiency because of the buffering on the circuit is acceptable.

The simulation executing on a SUN 4D/40 takes approximately 3 ms to perform a single 1 ns time-step (the time step we are currently using in the Verilog model). Thus, although it is possible to simulate a reasonable number of L1 and L2 triggers, the task of simulating 1 ms of actual operation requires approximately 1 hour of elapsed time.

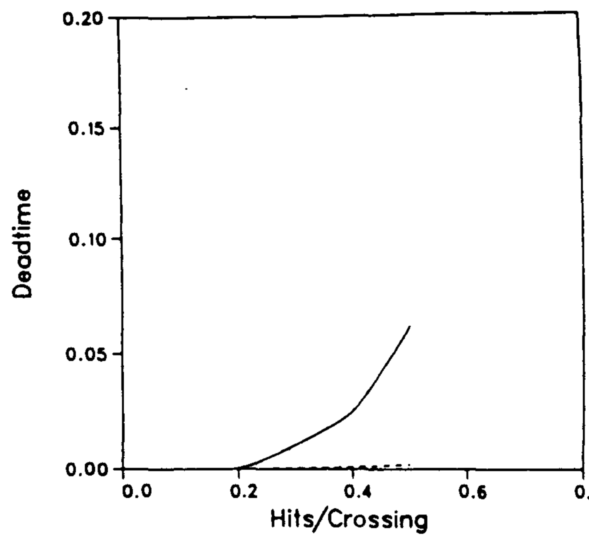

Figure 3: The deadtime of the the L1 buffer (solid line) and the L2 buffer (dashed line) in the as a function of the nominal wire occupancy (excluding the effects of the pulse width). Other system parameters are set to their default values.

Conclusions

We are continuing our simulation studies of this buffered L1-L2 data-driven circuit in order to fully characterize the behaviour of this circuit as a function of the salient system parameters such as input hit rate, L1 and L2 trigger rates and delays, and L1-L2 buffer transfer times. The simulation has already shown that the data-driven scheme explained here results in negligible excess deadtime for a sparsely occupied detector such as a wire tracking chamber.

We are also undertaking a simulation of the data collection network which will be responsible for collecting the data from each of the FE circuits after a L2 accept has been received. This requires us to take into account the correlations between nearby wire channels in a typical SSC event. We intend to do this by using as input to our hit generator the actual time structure of hits as predicted by a detailed simulation of the wire tracking detector in minimum-bias events.

References

[1] A. E. Stevens et al., *A Time-to-Voltage Converter and Analog Memory Unit for Colliding Beam Detectors*, IEEE Trans. Nucl. Sci., Vol. 36, No. 1 (1989).

Straw Preamp/Shaper Test Board

F.M. Newcomer, R. Van Berg
University of Pennsylvania

A four channel test board designed to support the second (and fully differential version) of the Penn AT&T preamplifier and shaper is described and various optional features are detailed.

This small four layer printed circuit board is designed as a test vehicle for investigating either the performance of the preamplifier/shaper chip or the behavior of detectors using the chip in a vanilla fashion. The board supports fully differential inputs, fully differential 50 Ω output drive capability, and very conservative shielding and decoupling design to try to allow the lowest noise environment possible.

MUP1343 Preamplifier/Shaper

The MUP1343 is a 16 pin small outline packaged version of the high speed, low noise, low power, bipolar preamplifier and shaper described in the attached NIM reprint.This version differs electrically only in having a fully differential input structure. The original design has a 3.3 pF capacitor on the reference side of the amplifier that serves to kill high frequency gain and thus reduces the equivalent input noise by a factor of $\sqrt{2}$. After some experience with the prototype, it became obvious that an ability to reject common mode noise might be more advantageous than a somewhat lower internal noise and the 3.3 pF capacitor was reduced to a symmetric 0.3pF.

Packaging

The MUP1343 is packaged in a plastic small outline surface mount package. An outline of the package is shown in Figure 1. Pins 7, 10 and 11 are not connected internally.

Single Channel Circuit

The individual channel circuit is shown in Figure 2. Several points are obvious -

1. There are a great many different power supply leads - this is partially because of the developmental nature of this circuit, it is, for instance, interesting (but non-essential) to move V_{cas} and watch the circuit turn off outside the 1.6 to 1.8 V operating range. The separation between the output power (VC4 and VE4) and the preamp and shaper power is, however, probably essential to avoid feedback. Later versions of this preamplifier and shaper will have fewer power lines.
2. The test pulse is injected via the A input using a 10:1 divider into a small coupling capacitor. This is also the normal signal input.
3. The differential inputs are negative In_A (pin 15) and positive In_B (pin 12).
4. The input reference (ground) is pin 14 (and 9).
5. The differential output pins (and their power) are on the opposite side from the input lines.

FIGURE 1 SOICL 16 Pin Package

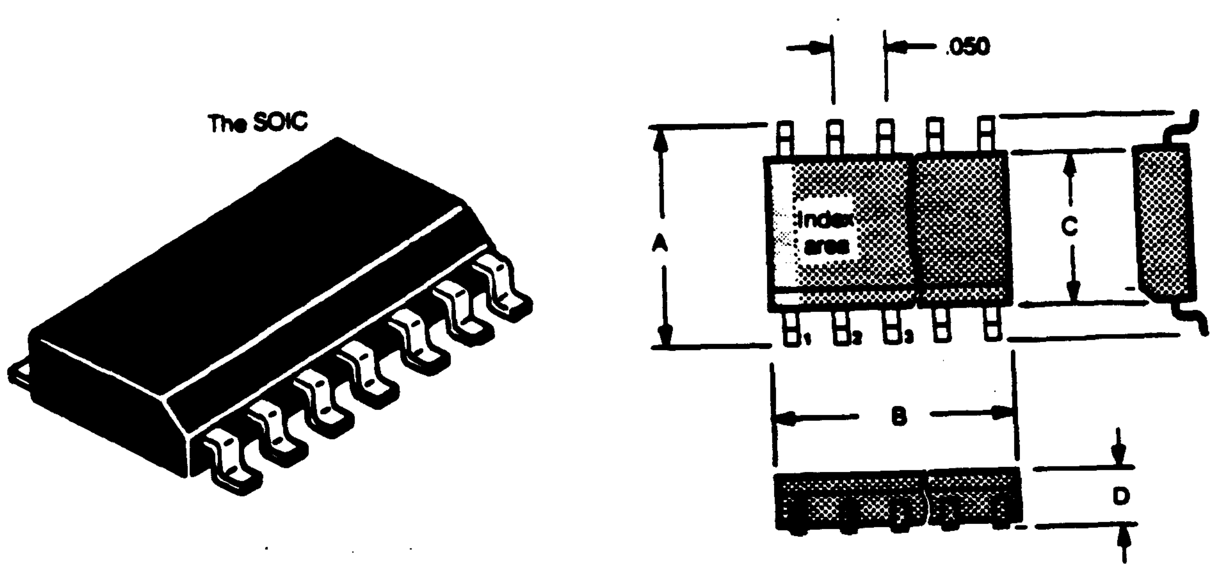

	SO 8	SO 14	SO 16	SO 16L	SO 20	SO 24	SO 28
A	.240	.240	.240	.415	.415	.415	.415
B	.195	.340	.390	.410	.510	.610	.710
C	.155	.155	.155	.295	.295	.295	.295
D	.070	.070	.070	.103	.103	.103	.103

FIGURE 2 Single Channel Circuit

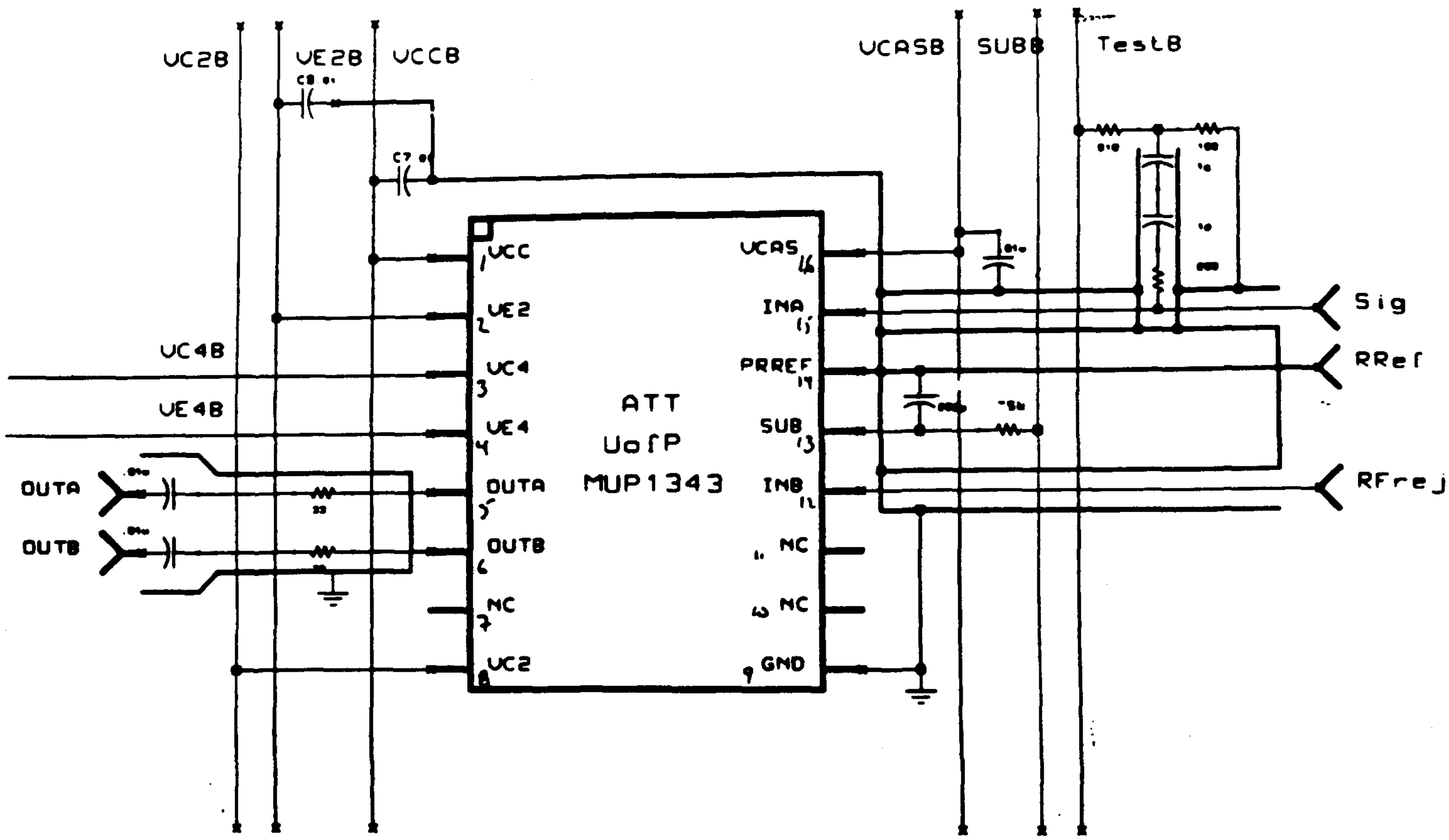

Four Channel Circuit

The circuit diagram of the full board is simply four of the above single chip circuits plus power supply, power distribution and filtering, test pulse distribution, input connector, output connector options, and voltage test points.

Power Supply

In order to be compatible with many different test set ups, the four channel board has on board positive and negative regulators capable of dealing with input power from $\pm 6V$ to $\pm 25V$. The regulators are set to provide about $\pm 4V$ which is then dropped via various diodes to give the required working voltages

Each voltage is distributed via a vertical bus with one or two test points and decoupling capacitors at both the top and bottom of the board.

FIGURE 3 Power input and regulator circuit

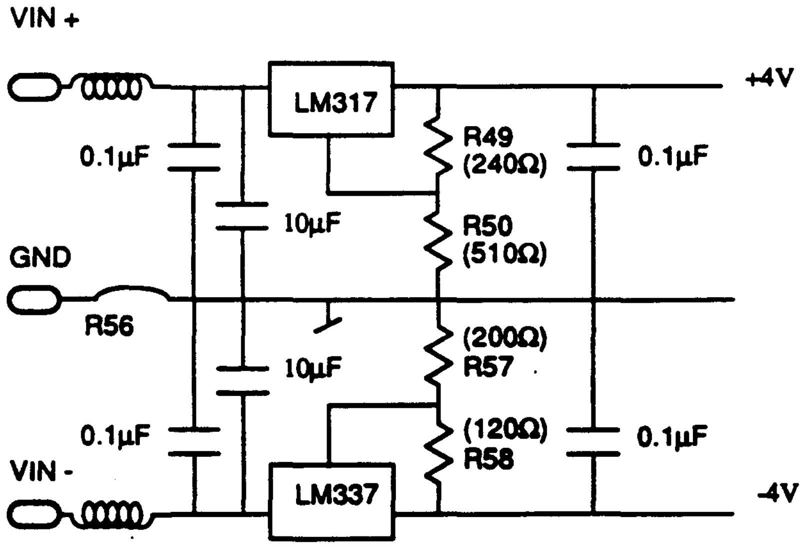

V_{CAS}

The cascode voltage is critical (1.6 to 1.8 V) and is developed by using the forward voltage drop of a single red LED (CR3) to ground, fed by R55 (33 Ω).

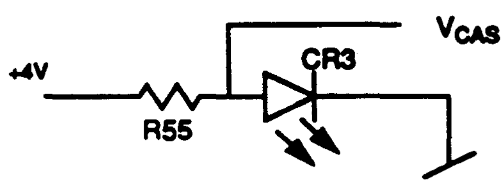

V_{C2}

The shaper collector voltage is made by taking a silicon diode forward voltage drop (CR2) plus a stopper resistor (R53) from the +4V bus.

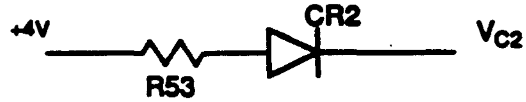

V_{CC}

The preamp collector voltage also uses a diode (CR1) and resistor (R51).

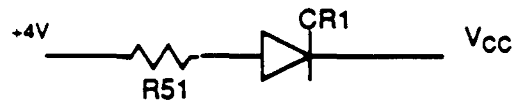

V_{C4}

The output collector voltage comes directly off the +4V bus.

V_{E2}

The preamp emitter voltage should be in the range of -1.6 to about -2.0 V and is derived by subtracting two diode drops (CR4 and CR5) from ground (or, as stuffed, one red LED) going through R59 (33 Ω) to -4V.

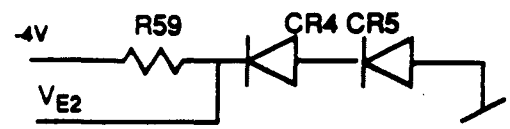

V_{SUB}

The substrate voltage is attached directly through R61 (33 Ω) to -4V, the most negative voltage - the substrate voltage is distributed through a printed circuit plane.

V_{E4}

The output emitter voltage is also connected directly to -4V.

Power Supply Decoupling

In an effort to provide an extremely conservative board design, each power supply input to each chip is decoupled via a stopper resistor (33 Ω) and a filter capacitor. It was clear after initial tests that the individual filter caps were a luxury and so stuffed versions of the board have a number (6) of unstuffed capacitor locations for each chip. Stopper resistors were, however, stuffed in order to get continuity - no experiments have been made as of yet to try a board with simple wire jumpers in place of the 33 Ω stoppers.

Test Pulse

The test pulse enters the board via the Lemo connector at the top, proceeds across the board and down the right (input) side of the preamp chips, and is terminated in a 51 Ω resistor, R52.

At each chip the pulse is attenuated via a resistive 10:1 divider - for U1, 910 Ω R7 and 100 Ω R12. After the attenuator a pair of 1 pF capacitors in series with a 200 Ω damping resistor (R6) join with the input. Because the 1 pF capacitors have relatively large variations (±25 %), it is not possible to use the test pulse to calibrate the relative gain of the channels - it is, however, useful to track gain changes.

FIGURE 4 Test Pulse Connection

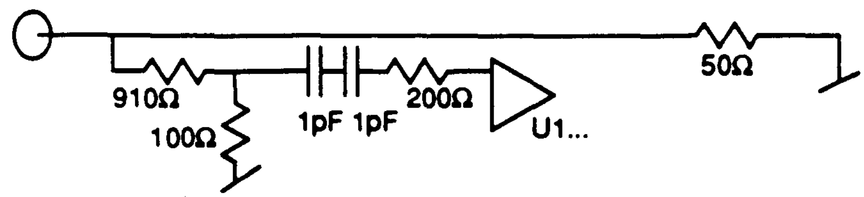

Inputs

The individual channel differential inputs are brought in on the right side of the board as a 16 position 0.1 x 0.1 inch grid with grounds interspersed between signal pairs - GSSGSSGSS... For use with straw detectors, it is probably useful to bring in both the Anode and Cathode signals (suitable decoupled from HV) as directly as possible to these inputs and take advantage of the common mode rejection offered by the fully differential inputs.Note that both inputs sit a V_{BE} above ground and should not be attached to any DC voltage point except by a blocking capacitor.

Input ground tie points are available at the top, bottom, and right edges of the board.

Outputs

The individual channel outputs are decoupled via a 33 Ω damping resistor and a 0.01 µF decoupling capacitor (required) - R8 and R13 to C62 and C64 for U1.

The outputs are available at either the 0.1 x 0.1 inch 16 pin connector footprint or on (unstuffed) Lemo connectors at the left hand board edge. At the 16 position connector the signals are interspersed with grounds - GSSGSSG... - to allow the use of flat ribbon cable for the outputs.

The outputs are all referenced to the output ground and V_{B4} and V_{C4} are both decoupled to the output ground which is a mesh of 0.25" traces on the top and bottom signal layers. This ground mesh is connected to the ground plane which serves as the reference for the input signals at only one point - just to the right of and below the Test Input signal. There are two jumper points for connecting the input and output grounds, one is stuffed with a solid jumper - it is possible that in some circumstances an inductive jumper would be advantageous.

Output ground tie points are available near the test input Lemo connector and below the bottom Lemo output connector.

Board Layers

In the following figures, the various design layers of the board are presented to allow tracing of circuits or analysis of possible odd behavior.

FIGURE 5 Silkscreen and Top Signal Layer -

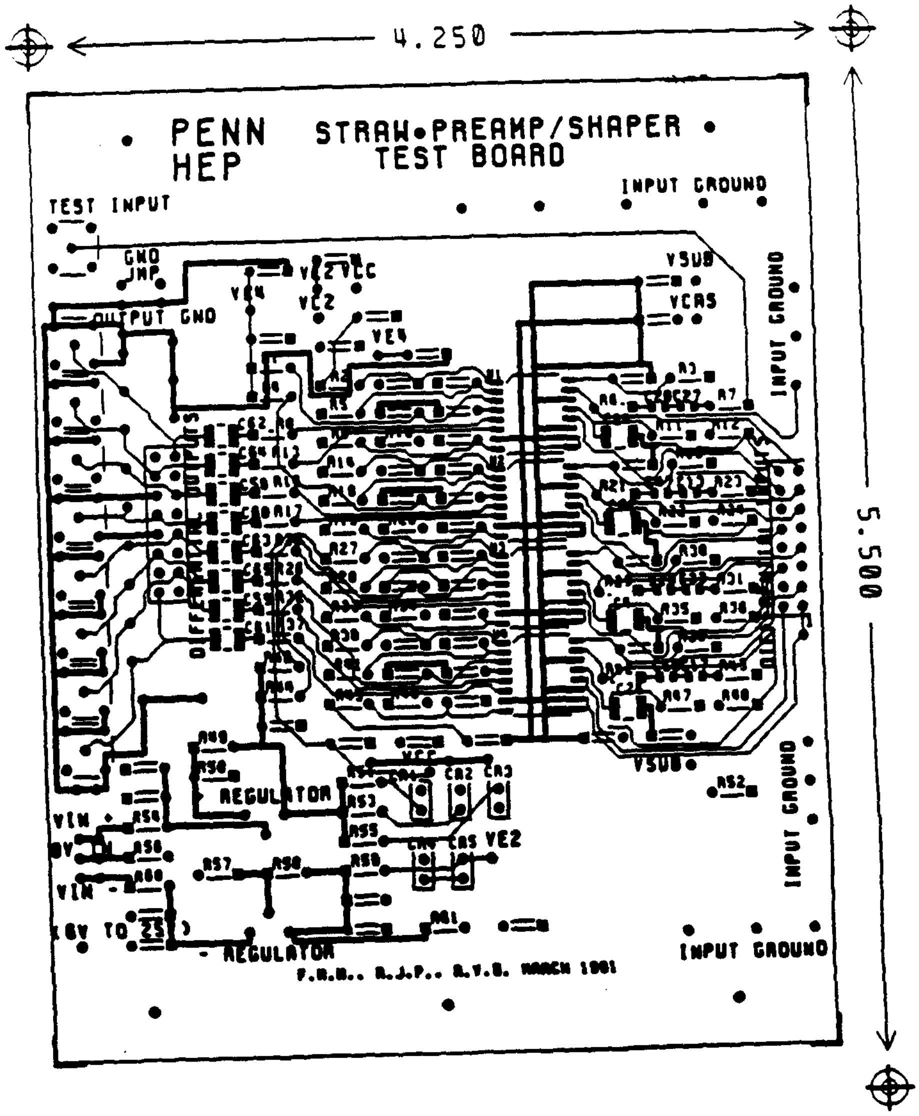

FIGURE 6 Top Signal Layer -

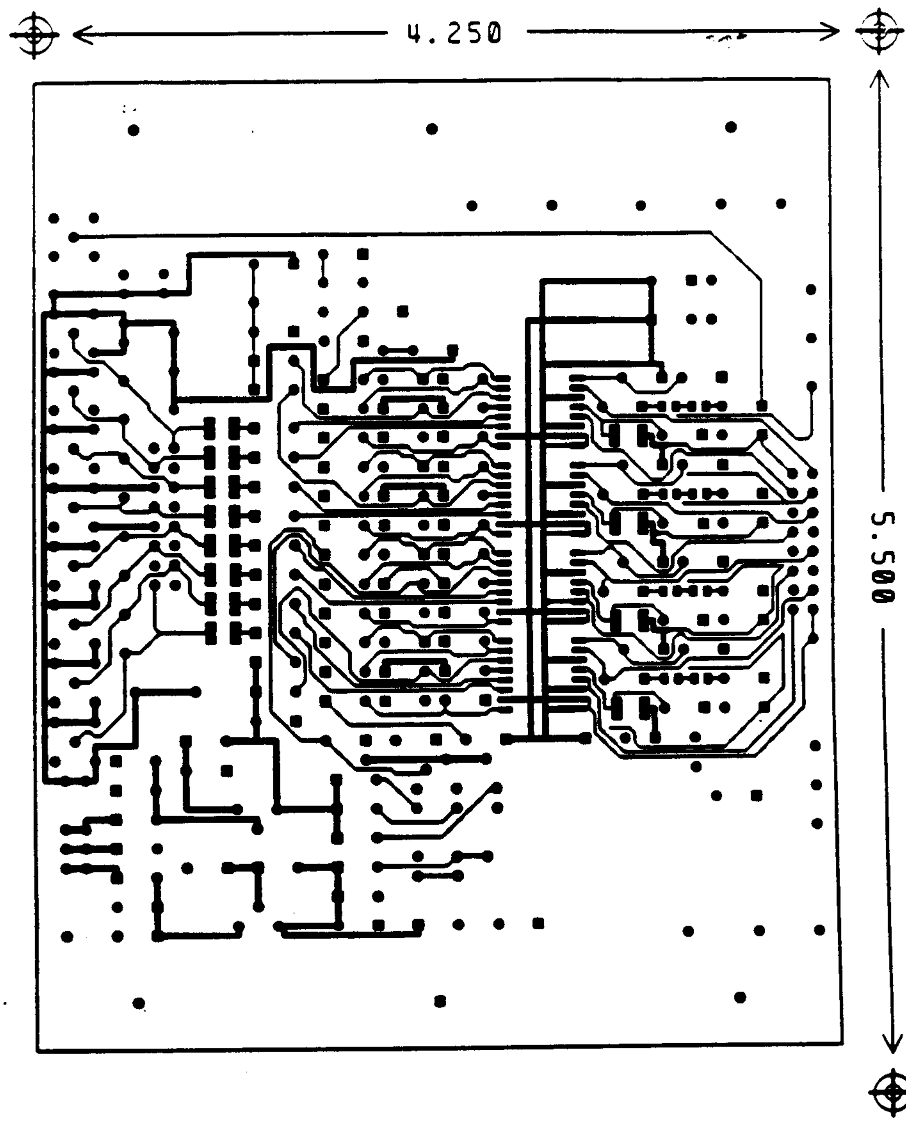

FIGURE 7 Bottom Signal Layer -

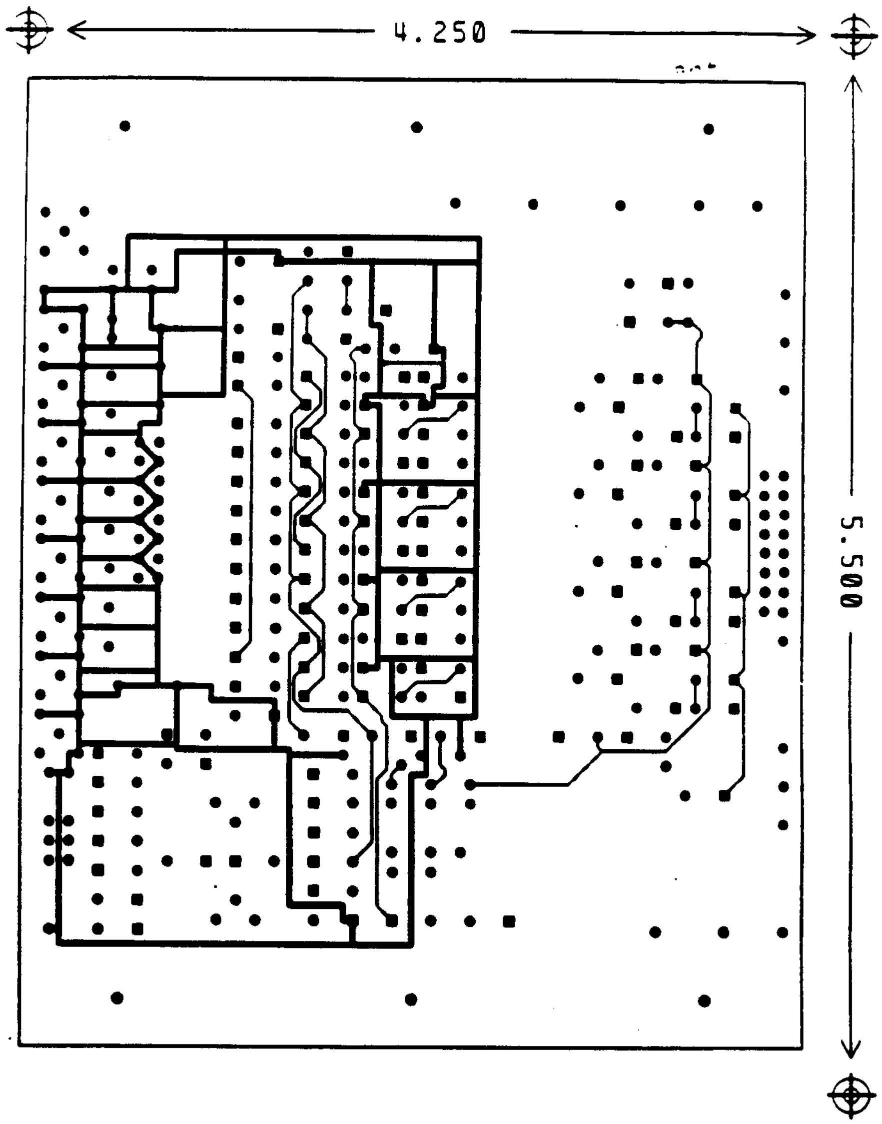

FIGURE 8 Ground Plane

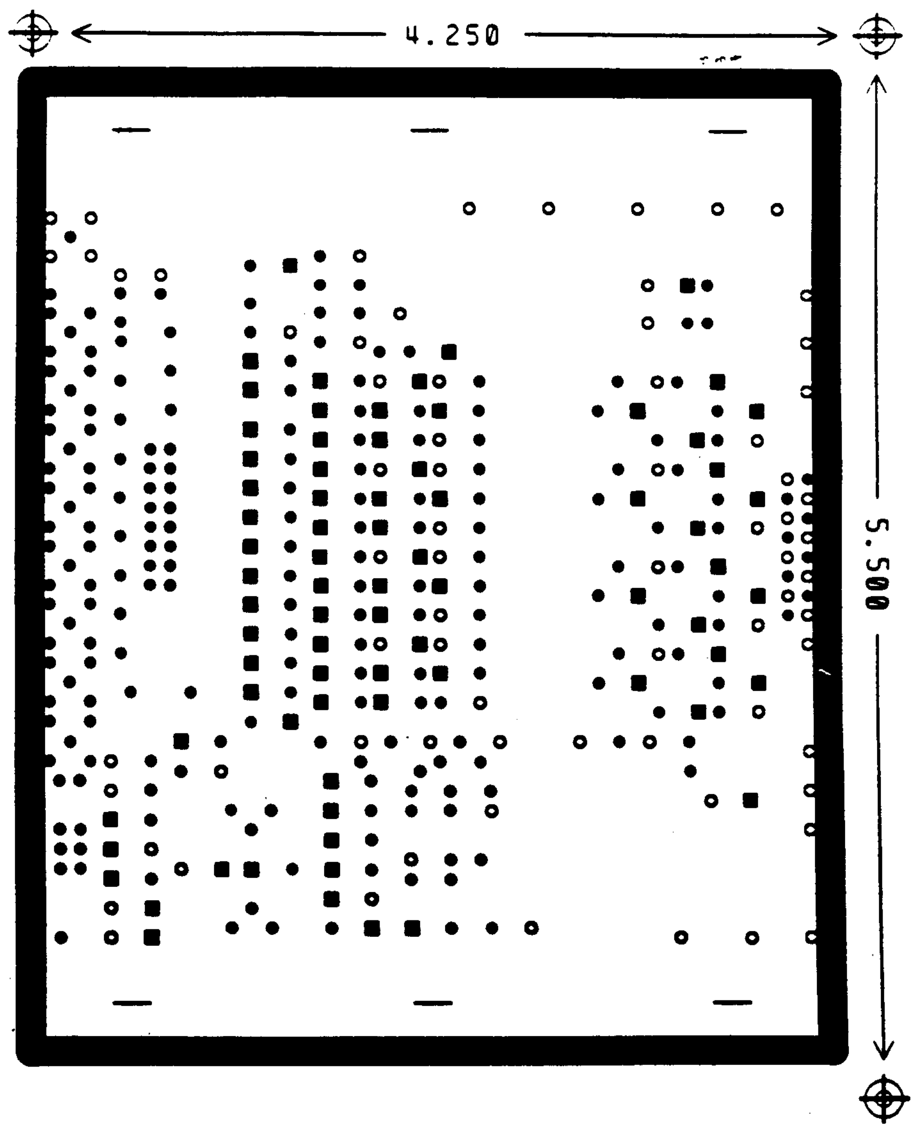

FIGURE 9 Assembly -

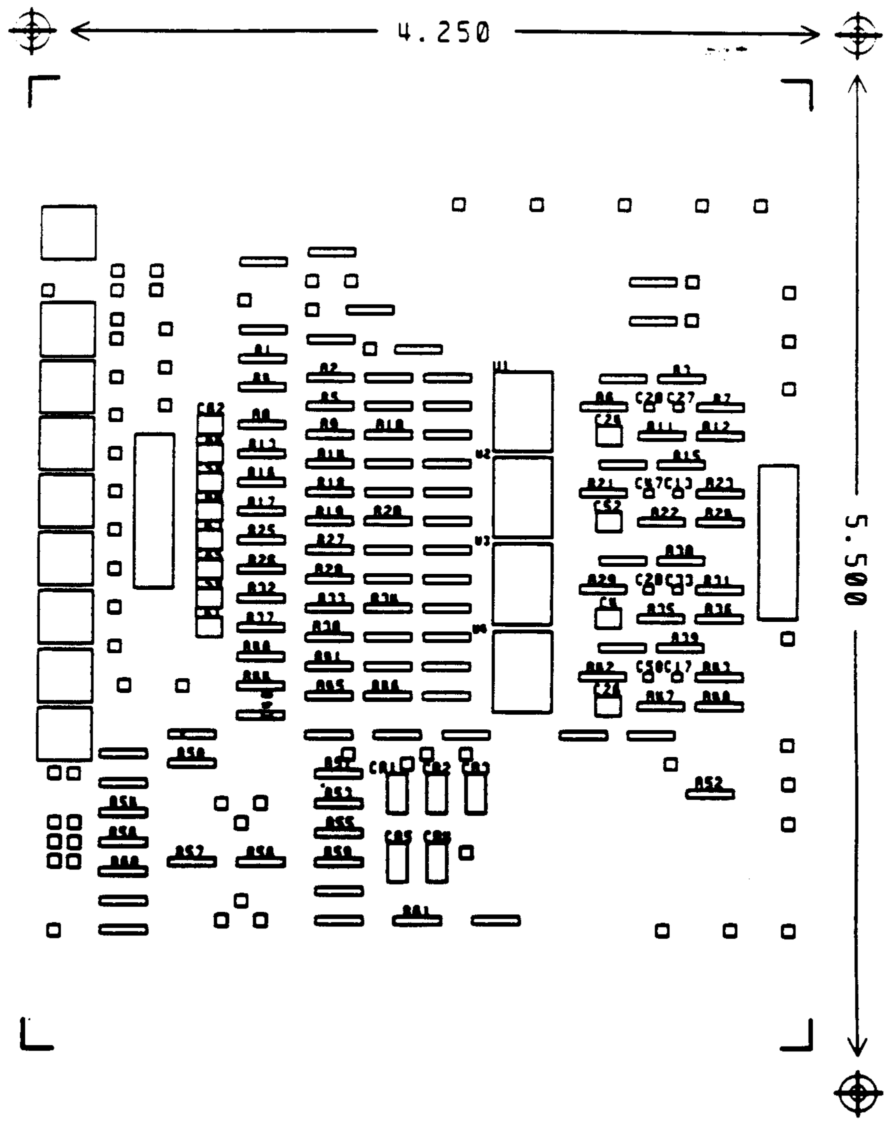

Nuclear Instruments and Methods in Physics Research A283 (1989) 806-809
North-Holland, Amsterdam

HIGH-SPEED BIPOLAR INTEGRATED CIRCUITS FOR SSC APPLICATIONS

F.M. NEWCOMER, R. VAN BERG, J. VAN DER SPIEGEL and H.H. WILLIAMS

University of Pennsylvania, Philadelphia, PA, USA

As part of our research and development program to investigate signal-processing electronics at high-luminosity machines we have studied the general problem of optimizing electronics for pad or wire chambers in a low-gain, high-rate environment. Using ATT's semi-custom monolithic bipolar process, we have designed a prototype amplifier/shaper to test our simulations and help gain insight into critical design constraints in the development of integrated circuits for proportional drift tube systems. Design considerations, comparisons among monolithic technologies and details of simulation results are presented.

1. Introduction

In the SSC environment the expected interaction rate of 10^8 events/s sets a difficult design constraint. The impact on readout electronics for proportional gas detectors is twofold. First, to minimize the effects of ageing, the gas gain will need to be low. The noise in the preamp may ultimately set the lowest value of allowed gain. Second, since the beam crossing rate is expected to be about 60 MHz, deadtime-less operation will require a double pulse resolution of about 15 ns. Since the shaping time for minimum noise is usually longer than this, the two requirements are in indirect competition. Optimal signal shaping in this case is a symmetric pulse [1].

A typical tracking detector proposed for SSC has 100000 4 mm diameter straw tubes assembled as six to eight *superlayers* starting at a radius of 0.5 m from the beam and extending to 1 m. To keep the heat dissipation at the end-caps below 100 mW/cm^2, the maximum power dissipation for each channel must be less than 25 mW, including readout, storage and triggering if required.

Table 1 summarizes design requirements for front-end readout electronics suitable for most gas tracking detector systems.

Table 1
Design parameters for preamp/shaper

Noise	< 2000 rms electrons E.N.C.
Power	5-20 mW per channel
Dynamic range	2-8 bits dependent on sensor type
Input impedance	100-300 Ω optimize for chamber impedance
Rise time	3-5 ns to minimize timing jitter
Double pulse resolution	< 20 ns
Packing density	4-16 channels/cm^3

0168-9002/89/$03.50

2. Noise

Noise in the tracking system modifies the true measurement in two ways. First, false triggering when there is no signal information may contribute extra, *in-time*, hits that can confuse tracking algorithims, or inefficiencies can result if a signal appears while a noise trigger is being processed. Second, the superposition of noise on the true signal will cause a timing jitter by changing the amount of signal required to fire the timing comparator. This can ultimately affect the position resolution. There are three sources of noise that require careful consideration:

(a) detector noise including significant leakage currents and rf pickup;
(b) amplifier shot and thermal noise;
(c) system noise induced by control logic and data conversion.

Reductions in pickup noise from the sensor are achieved by the addition of good high-frequency Faraday shielding and the provision for low-impedance reference connections to the sensor. Differential designs with perhaps dual anode readouts would be ideal, but are not generally used due to performance limitations.

Pickup from outputs and control logic is minimized by making all logic transitions only as fast as required, minimizing logic level swings and using differential transmission where signal edges must be fast.

Amplifier shot and thermal noise, including noise caused by terminations, can be modeled as noise currents which are summed and added *in parallel* with the input signal and noise voltages which are summed and connected *in series* with the input. An illustrative expression for the total equivalent input noise charge is given below. τ_s is proportional to the output signal rise and fall times and τ_p is proportional to the output signal duration for an impulse input. e_n represents the total *series* equivalent input noise voltage and i_n repre-

Table 2
Technology selection. Tabulated values are based on equivalent total drain or collector current of 1 mA; note that the large value of the input capacitance for the transistor in weak inversion is a result of the low current densities required to operate in the weak inversion region

Technology	BIPOLAR	CMOS strong inversion (W/L = 1000)	CMOS Weak inversion (W/L = 20000)
g_m [mS]	38	11	25
f_t [GHz]	1.6	1.1	0.077
R_{n_s} [Ω]	26	100	20–50
R_{n_p} [kΩ]	4.5	none	none
C_{in} [pF]	3.2	2.0	52

sents the total *parallel* equivalent input noise current [2].

$$(\mathrm{ENC})^2 = e_n^2 C_t^2/\tau_s + i_n^2 \tau_p.$$

In this form it can be easily seen that the *series* noise charge is proportional to detector capacitance and inversely proportional to the measurement time. *Parallel* noise charge, however, is proportional to the shaping time and therefore is not necessarily minimized in the design of fast, low-noise amplifiers. The optimal shaping time may be determined once e_n, i_n and the total input capacitance are known. For an optimized design using present technologies, this will usually be longer than the maximum allowed measurement time as set by occupancy requirements. In these designs, *series* noise dominates and *parallel* noise can be allowed to grow to satisfy other more critical design constraints. A thorough treatment of amplifier and detector noise is given in ref. [3].

3. Technology

Bipolar technology offers a clear advantage for low-power shaping amplifiers since for a fixed standing current it has the highest transconductance (gain) and for fixed transconductance it has the lowest *series* noise of any available transistor technology. It should be noted that base current in bipolar transistors adds *parallel* noise that is not present in FET technologies and therefore bipolar is a good choice for fast shaping only. Table 2 shows the performance of the ATT LA200 bipolar transistors compared with two examples of 1.6 μm *leff* CMOS transistors, first optimized for speed that rivals the bipolar and secondly optimized for noise performance similar to the bipolar.

Extensive modeling using parameters from commercially available bipolar processes (1.75–2.0 μm emitter width) has shown that for a 15 ns base-to-base shaping time and equivalent input noise charge of less than 1100e rms (CDET = 10 pF) can be achieved at a power requirement of less than 20 mW with a dynamic range of 50 : 1. The base-to-base time is taken as the interval during which the output exceeds the baseline by 5% for an impulse input.

Trends towards low-voltage, high-frequency transistors with lower substrate capacitance integrated resistors are leading to the development of commercially

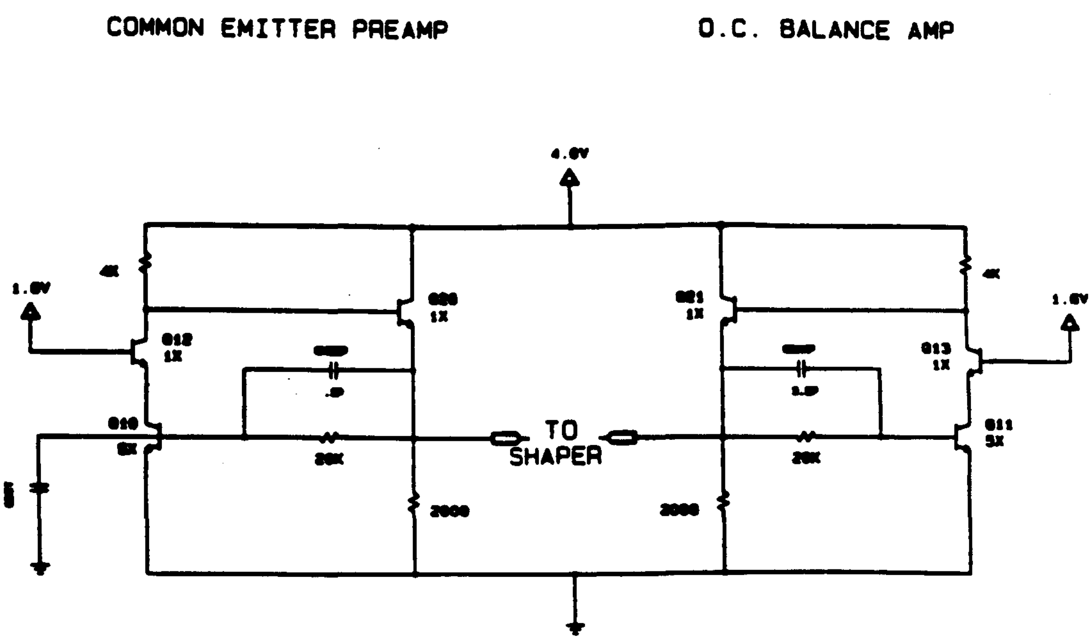

Fig. 1. Preamplifier section of the prototype circuit fabricated in the ATT ALA200 bipolar process.

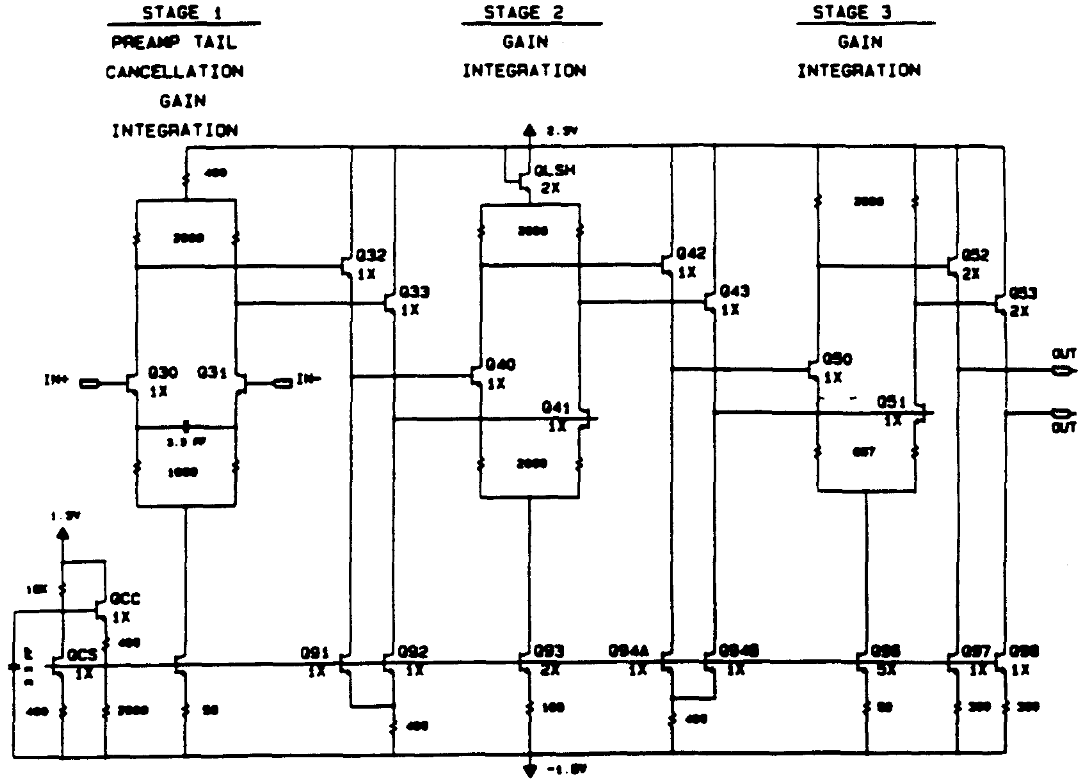

Fig. 2. Shaping amplifier section of the prototype circuit.

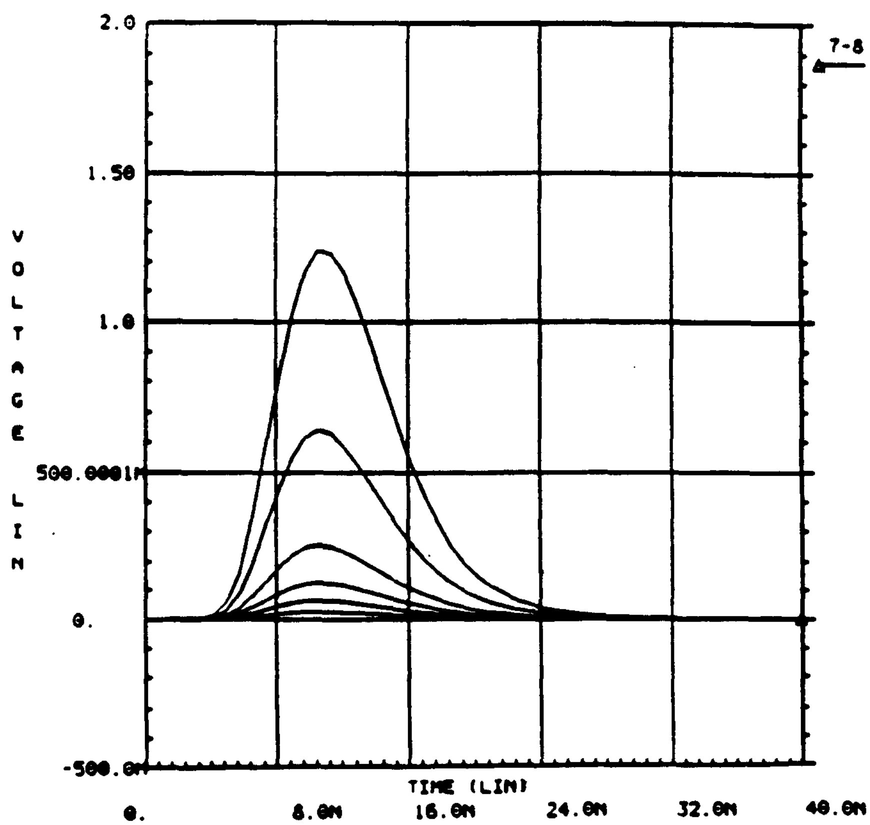

Fig. 3. Simulated response at the shaper output for 1, 2, 5, 10, 20 and 50 fC input pulses.

available processes from several vendors that will provide the same or better performance at a per-channel power dissipation of less than 10 mW.

4. Circuit design

We have studied in detail both common-base and common-emitter preamplifier circuits. Suitable signal-to-noise performance may be obtained from either configuration but the common-emitter one is clearly superior when power dissipation is a driving concern [4]. It requires lower voltage rails for the same value of transconductance. The common-emitter configuration (fig. 1) has good power supply rejection and can be designed to have a stable input impedance over frequency when the unity gain bandwidth of the transistors is much higher than the cutoff frequency of the amplifier.

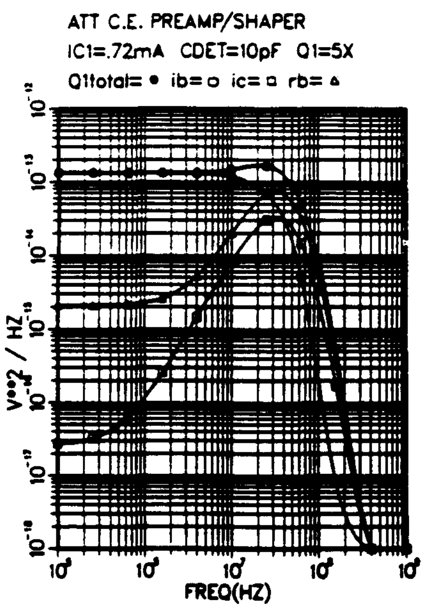

Fig. 4. Noise spectrum of the first transistor after signal processing by the shaper. $Q_{1\,total}$ is very nearly the sum of the other three curves, indicating that no other significant noise sources are associated with this transistor.

To shape the pulse we make use of a differential shortening filter that eliminates the preamp tail by providing a zero to cancel the dominant pole of the preamp. This is followed by three *R–C* integrations that symmetrize the output pulse (see shaper schematic, fig. 2). Fig. 3 shows the simulated pulse response for a series of input charge pulses ranging from 1 to 50 fC.

Noise contributions from the input transistor, measured at the shaper output, are broken down into component noise sources and plotted as a function of frequency in fig. 4. The increase in noise power at 20 MHz is due to the low impedance of the detector capacitance at this frequency and its resultant effect on the input noise voltage due to base resistance.

5. Implementation

A single-channel version of this circuit with additional test structures is in fabrication at ATT in the LA200 semi-custom bipolar process. Chips are being prepared for testing at this time and results will be publised at our earliest opportunity.

Previous experience leads us to expect that measurements on working devices should closely agree with simulation [5]

References

[1] L. Callewaert et al., IEEE Trans. Nucl. Sci. NS-36 (1989) 446.
[2] V. Radeka, IEEE Trans. Nucl. Sci. NS-21 (1974) 51.
[3] V. Radeka, Ann. Rev. Nucl. Part. Sci. 38 (1988) 217.
[4] E. Gatti and P.F. Manfredi, Nucl. Instr. and Meth. 226 (1984) 142.
[5] D. Christian et al., IEEE Trans. Nucl. Sci. NS-36 (1989) 507.

SDC Straw Tracking Electronics
Preliminary Conceptual Design Report

Draft Version 1.1

August 16, 1991

F.M. Newcomer, R. Van Berg, H.H. Williams
Pennsylvania

1 Introduction

In order to make reasonable estimates of dollar costs, design and manufacturing schedules, cable access needs, material budgets, cooling loads, and installation (and repair) strategies, it is necessary to have a complete conceptual design of the straw readout system. The following design is based upon the work that we have done in making a detailed electronic design for the straw readout. We are describing a system that goes from a contact at the straw anode (and cathode) and contains all of the DAQ and trigger functionality necessary for full SSC operation up to but not including the *SDC Standard* DAQ and Trigger boards and fiber optic transmission cable(s) going to the off-detector DAQ and Trigger systems While much of the following is fairly obvious or part of the *perceived wisdom* of the community, there are many places where we have had to make assumptions or extrapolations with little or no hard justification. In general we will try to note all such assumptions.

After a discussion of the technical and performance requirements demanded by the application and the particular implementation (including details of design, simulation, and test); we will then describe the necessary electrical connections and components followed by a description of a scheme for actually implementing the physical interconnections and support required. In all of the following, we are assuming a *module* of 200 active straws per readout assembly. A module is an independent subsystem that may be bench tested and verified independent of detector and central DAQ and Trigger connections.

The number 200 is close to the modularity (at least of electronics) of both the Duke and Indiana mechanical designs. Actual straw counts will depend upon super layer structure and whether or not a particular layer is included in the first level trigger. A final design will probably be divided at about the 200 straw level and we do not believe that any of the cost or material estimates depend strongly on this assumption.

A group of about 16 modules connects to a standard SDC crate via a Crate Interface Card (Straw System specific). The Crate will be located in the Electronics/Access area outside of the calorimeter as indicated in Fig. 30. The crate is also independently testable with or without Crate Interface Cards using the standard DAQ/Trigger interfaces. High Voltage is supplied to the Crate Interface Cards (and thence via the module cable to the module itself) either directly from the High Voltage Supplies (whereever they are) or indirectly via a Straw System Specific connection within the SDC standard Crate.

2 Systems Requirement and Overview of Electronics System

2.1 Design Requirements

For a high precision drift tube or straw tracking system, it is necessary to accurately measure the time of arrival of the first electron (or cluster of electrons) at the anode. This, combined with the desire of operating with as low a gas gain as possible, implies the use of a low noise preamplifier with risetime sufficiently fast to provide the desired time resolution, but sufficiently slow to provide acceptable signal-to-noise.

In addition, because of the high rate of pulses on individual wires - for the inner wires the rate will approach 5 - 6 MHz - excellent double pulse resolution is very important.

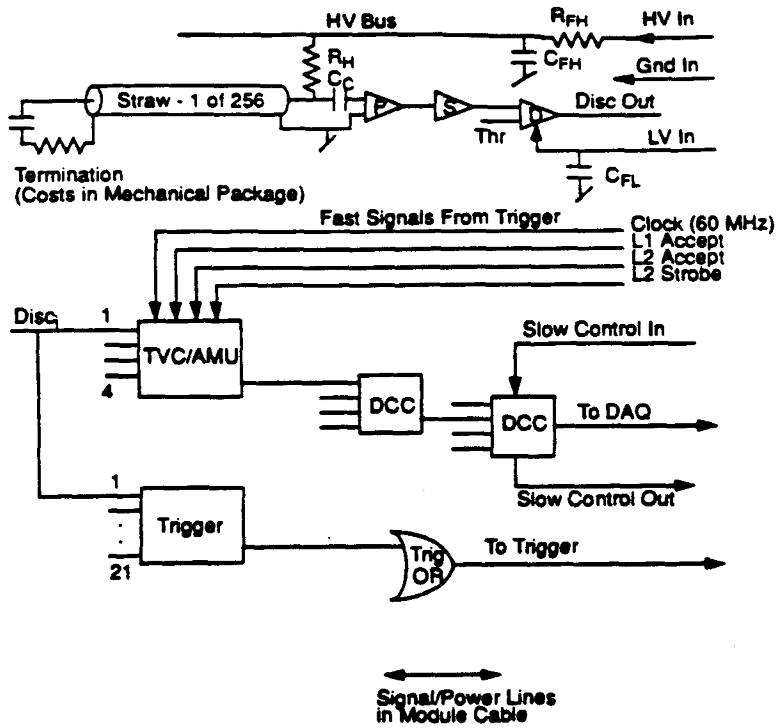

Figure 1: Block Diagram of the Straw Readout System

The basic design goals which seem reasonable are:

- $< 0.5ns$ time accuracy in order to ensure spatial precision of $< 100\mu m$
- Double pulse resolution of 20 - 30 nsec. We have adopted the specific goal of having the return to baseline for a single cluster be less than 15 nsec
- Semi-gaussian shaping to minimize baseline shifts and noise from parallel current sources
- On-chip Level 1 storage for 3 - 4 μsec and Level 2 storage for a latency interval of order 50 μsec
- Able to withstand > 1 MRad over the life of the experiment

2.2 System Overview

Figure 1 shows a simplified schematic of the key elements in the front end; to date it is these blocks which have been given the most attention and rightfully so since they are repeated for every straw tube and since they define the performance of the system as a whole. We discuss briefly the nature of the signal from the straws as this is important for optimizing the electronics.

2.3 Analog Signal Processing

Each straw sensor will require a preamplifier, shaper, discriminator, time converter and sparsification unit. Bipolar technology offers the optimal performance for the preamplifier, shaper and discriminator.

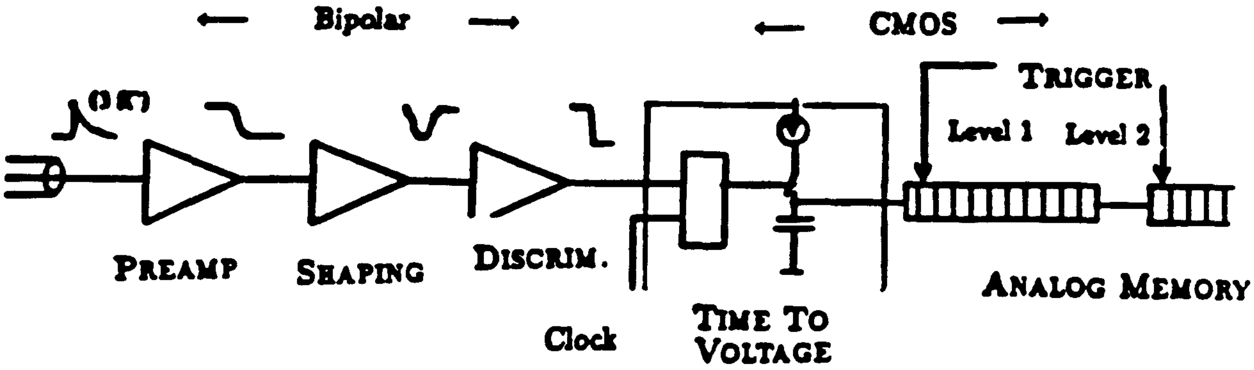

Figure 2: Block Diagram of the Straw Front End

It's high gain-bandwidth at low power is unmatched by any other commercially available technology as is the noise performance for shaping times of less than 20ns and the matching of the control voltage between transistors. CMOS is clearly the technology of choice for the time-to-voltage conversion, which includes analog memory for at least the Level 1 storage, and for the overall control logic due to its high density and low power.

Due to the high occupancy and low value of operational gain in the straw tube system, it is necessary to carefully consider the characteristics of the straw tube as part of the readout system.

2.3.1 Properties of the Straw Signal

The drift velocity for ionized electrons in CF_4, the *fast* gas being explored for use in straw tubes, is about $100\mu m/ns$. A position accuracy of $100\mu m$, therefore requires sub-nanosecond timing accuracy from the electronics. Since there is no plan to store charge information for off line analysis, it will be important to trigger on the avalanche from the first arriving drift electrons to get the most accurate timing information. This condition severely restricts the amount of charge available to trigger the electronics. Most of the signal from the straw is induced by the motion of positive ions towards the cathode, a process that takes about two hundred microseconds to complete; much of this signal must be truncated. The equation below gives the ratio of the total charge collected at the anode as a function of time for a straw tube of wire radius a and cathode radius b.

$$\frac{Q}{Q_m} = \frac{\ln(1 + t/t_0)}{2ln(b/a)} \tag{1}$$

For a typical straw tube t_0 is 2ns or less and $2ln(b/a)$ is about 10. After three t_0, about 6ns, only 14% of the induced charge has been collected. Adding 2% for the electron contribution only about 16% total charge for a single avalanche cluster has been collected. It becomes quickly apparent that the t_0 for a chamber directly affects the timing resolution when the gas gain must be limited. Extending the measurement time decreases the timing accuracy for signals of different amplitude due to time slewing. Decreasing the measurement time reduces the available signal and, in gain limited applications, may severely affect the signal to noise.

To estimate the timing resolution for a given charge collection, or shaping time, the input signal is convoluted with a preamplifier and shaper transfer function. Figure 2 shows a simulation result of the effects of intrinsic noise from the straw and preamplifier with multipole shaping on the timing resolution. These studies have led to the conclusion that a five to seven nanosecond shaping time gives reasonable signal to noise, without compromise to the goal of a locally determined sub-nanosecond timing accuracy.

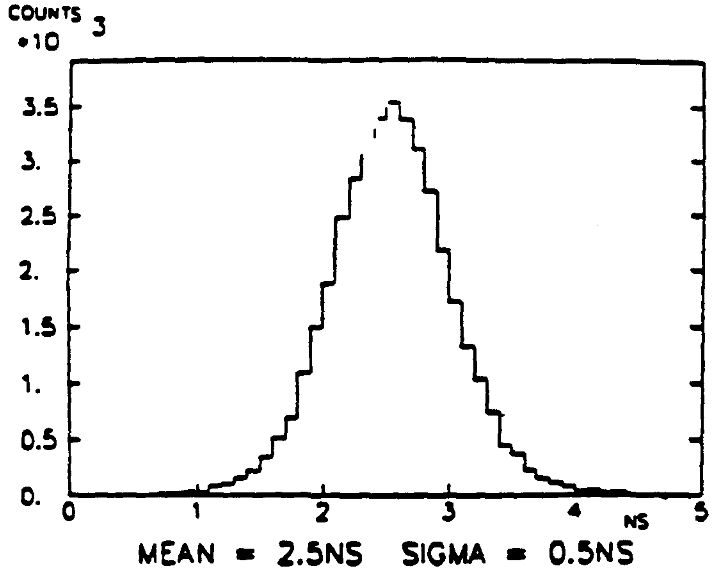

Figure 3: Simulated timing resolutiion showing of the effects of intrinsic noise from the straw, amplifier and shaper. The straw t_0 is 2ns, and electronic t_m, 5ns, S/N is 6:1 and the effective threshold is 3 times the RMS noise.

This gives an approximate available signal of .64fC (4000e) per drift electron for a terminated straw tube operated at a total gain of $5X10^4$.

We have developed and tested a lumped sum model of the straw tube as a lossy transmission line. Signal to noise for a straw tube with a transmission line termination requires careful analysis. The complex impedance of the lossy straw tube requires a complex rather than purely resistive termination. A suitable passive circuit is formed by adding a small capacitor in series with the termination resistor. The signal, of course, is absorbed at the termination end and therefore only half of the total charge is available to the readout amplifier. In addition, when formed with only passive components, the intrinsic noise in a measurement is dominated by the termination. (Assuming a well designed preamplifier.) In this situation, the choice of symmetric shaping may help reduce the noise. In figure 3 the shaping time is assumed to be 5ns and the the straw is assumed to be terminated with a 300Ω resistor. The R.M.S. equivalent noise in electrons is plotted as a function detector capacitance, (length of the straw tube) for different numbers of equivalent pole shaping stages. It can be seen that a considerable reduction in noise is achieved as the number of shaping stages is increased.

Simulations show that significant additional noise reduction is possible by replacing the passive components at the termination end with an active load, at a power cost of about 3mW per channel.

2.3.2 Bipolar Preamp and Shaper

Circuit Design For the preamplifier design, we have chosen a cascoded common emitter configuration with a dominant pole primarily determined by the feedback network. (Refer to figure 5) This self-biasing circuit allows the input transistor to be large and operate near it's noise optimum, while requiring only a modest supply voltage of 3 to 4 volts. The power dissipation is therefore relatively low and the circuit may be easily implemented in advanced, high speed technologies that characteristically have low breakdown voltages. As shown in the figure the common emitter structure is duplicated and forms a pseudo-differential input for the fully differential shaper.

A differential structure has been implemented in the shaper to help eliminate sensitivity to external

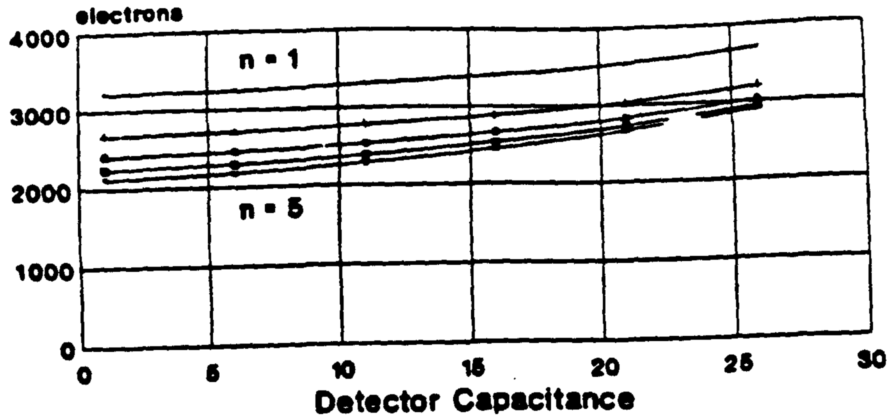

Figure 4: Calculated ENC_t for our prototype preamplifier as a function of detector capacitance for different numbers of shaping stages. The noise contribution due to a 300Ω termination resistor has been included.

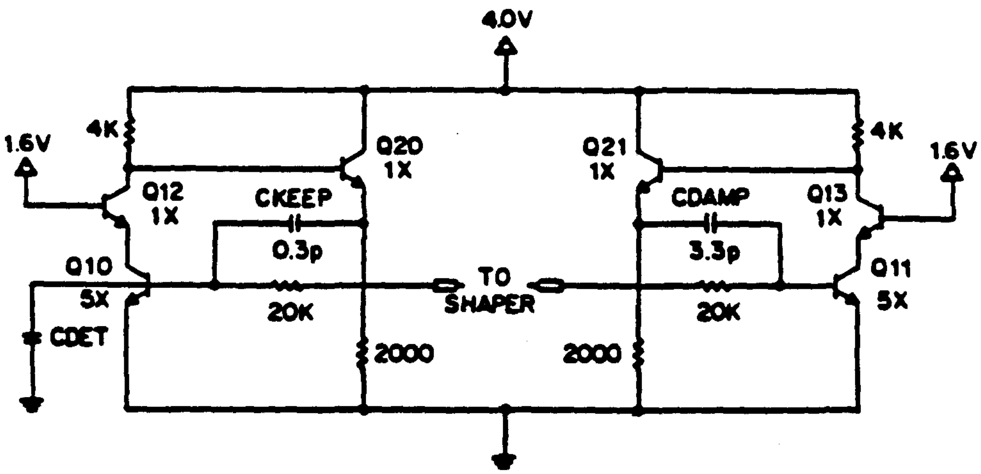

Figure 5: Schematic for prototype preamplifier.

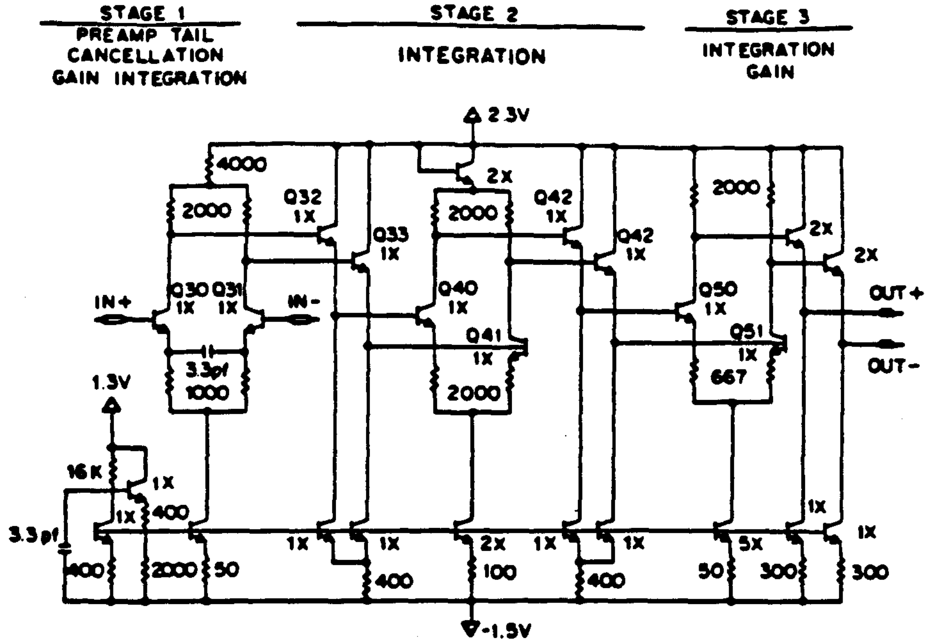

Figure 6: Schematic for prototype shaper.

sources of noise conducted in through power supply lines or radiated into the chip itself. In the original prototype version of the amplifier, fabricated in the AT&T ALA200 linear array, the "dummy" side of the preamplifier had a bandwidth limit of 3MHz. This helped to reduce the thermal noise, improving the S/N by about 15% in a realistic system with a 10pF detector capacitance. In a new version fabricated at AT&T in December 1990, the bandwidth of the balance side amplifier is matched to the input amplifier to provide fully differential inputs (other than the inherent asymmetry in the straw tube itself). While this increases slightly the thermal noise, it was felt that it would aid significantly in noise rejection (such as from RF pickup in connections to the straw tube) and would provide a more robust system, at least for initial field tests.

The shaper has one zero matched to cancel the dominant pole of the preamplifier and three equivalent integrations that limit the bandwidth and maintain pulse symmetry (Figure 6). Good matching is achieved in the pole-zero cancellation by choosing components of the same types to dominate the pole and the zero. The integration poles are formed in the collector nodes of each differential pair. The collector resistor times the stray capacitance at each node sets a time constant of about 1.7ns for each stage. These time constants match to within a few percent between stages, but are expected to vary chip to chip by as much as ±25%. We are investigating methods to *program* this shaping time, so that preamplifiers may be matched to each other and perhaps tuned for the best system S/N.

The semi-gaussian pulse symmetry realized by use of multiple pole shaping is demonstrated in figure 7 which shows the shaper response for a 1fC input pulse formed by injecting a 1mV signal into a 1pF capacitor. The amplitude of this pulse is within 15% of the value predicted by SPICE simulation and is well within range of uncertainty in the measurement.

The intrinsic amplifier noise is primarily determined by the size of the input transistor and it's quiescent current. In the design stage, the noise performance was optimized for an amplifier with a pure detector capacitance of 5 to 10pF. The quiescent current was set to about 0.5mA and an input transistor of 75μm emitter length was used to achieve a base resistance of about 15Ω. Noise performance in the prototypes was checked using a method suggested by Jarron where the threshold required for a discriminator efficiency of 12, 50 and 88 percent is recorded for a input pulse of known charge. The 12 and 88 percent points give the noise FWHM in terms of threshold voltage and the 50 percent point

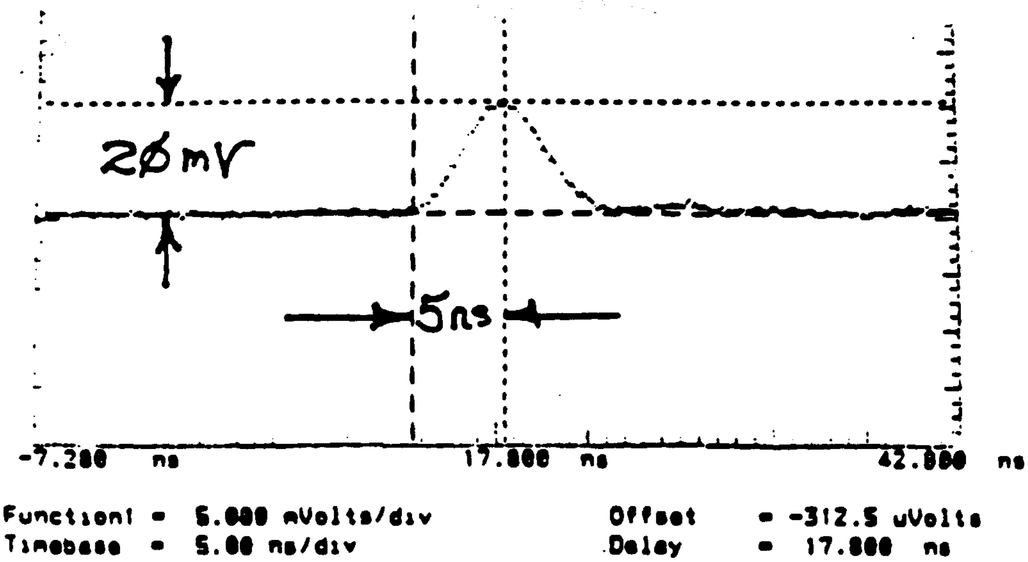

Figure 7: Shaper response for a 1fC impulse input , averaged over 40 pulses.

calibrates the threshold voltage in terms of input charge. A comparison of the measured results and SPICE calculations using transistor models provided by AT&T for several values of detector capacitance is shown in figure 8. The agreement between measurements and model based calculations encourages our reliance on SPICE based modeling to predict the performance of system blocks.

2.3.3 Measurements with Straw Tubes

The detector tail may be eliminated by adding a set of poles and zeroes to the shaping function determined by the t_0 of the chamber. In figure 10 the digitizing oscilliscope was triggered by a cosmic ray scintillator coincidence above and below the 2 meter straw discussed above. The waveform in this figure shows the output of the prototype amplifier when attached to a passive detector tail cancellation network. It is likely that this signal is due to a single ionization cluster. In this case the signal processing time is less than 15ns. In a more typical case, a minimum ionizing track passes near the center of the tube and leaves a trail of 20 to 30 clusters of ions. The electrons from these ionization clusters will drift in to the anode over a 30ns period. This implies that the double pulse resolution is the sum of the difference in drift time for all collected clusters and the single cluster processing time. It is clear that dead time depends critically on the ability to accurately cancel the detector tail and the use of a fast gas. The multichannel chip now being layed out in the Tektronix SHPI process (and discussed in more detail below) includes tail cancellation optimized for a 4 mm straw.

Independent measurements of the performance of the preamplifier/shaper circuit by other groups have confirmed the expected performance. In particular, a number of detailed tests have been carried out at Princeton University. Their measurements of the noise of the preamplifier as a function of the input capacitance lead them to conclude that the preamplifier is more than five times less noisy than the LeCroy TRA402; in addition they observed an ENC of about 2000 electrons when the amplifer was connected to a 2m long straw tube. These numbers could decrease somewhat further as the final system is refined, but are close to the performance expected and demonstrate that good results may be obtained in an actual system.

Measurements of the obtainable position resolution were also made. Figure 9 shows the measured spatial resolution, using the AT&T preamplifer/shaper, for single electrons emitted from near the wall of the straw tube.

A 200 channel prototype system is currently under construction at Princeton for tests at FNAL. It is very encouraging that the yield from the recent fabrication run at AT&T was 90% after packaging; (only those devices from the center half of the wafer were packaged). Four channel prototyping boards have been sent to a number of different groups and sixteen channel boards with a commercial discriminator

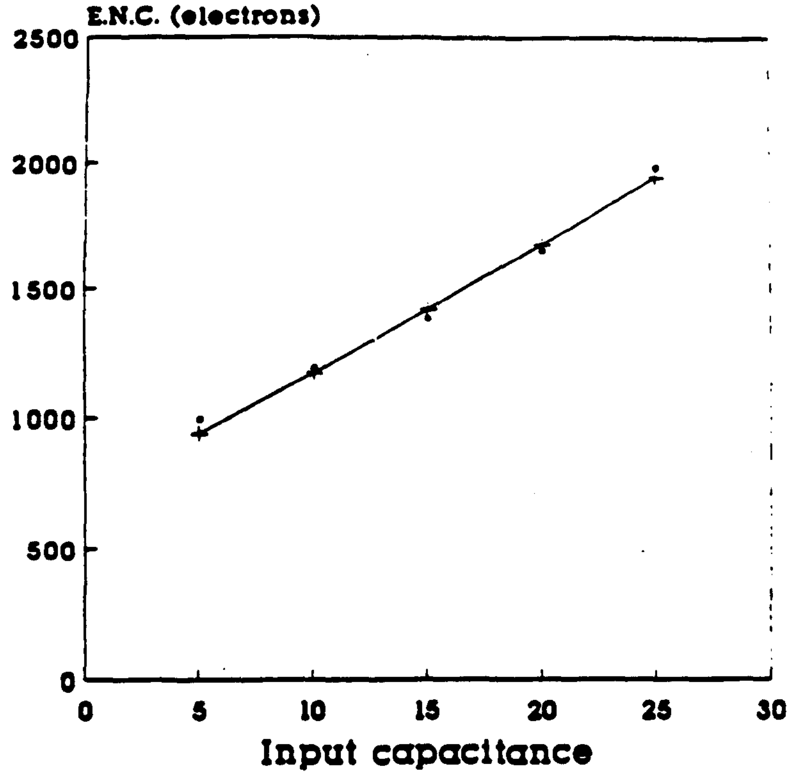

Figure 8: Comparison of simulated and measured noise.

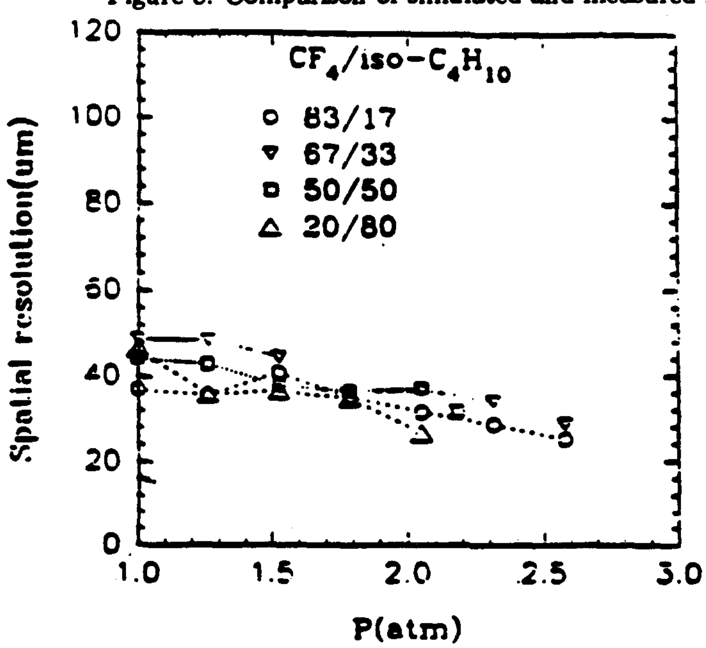

Figure 9: Measured position resolution in a 7mm straw tube using the the AT&T preamplifier for single electrons emitted from near the wall of the straw tube.

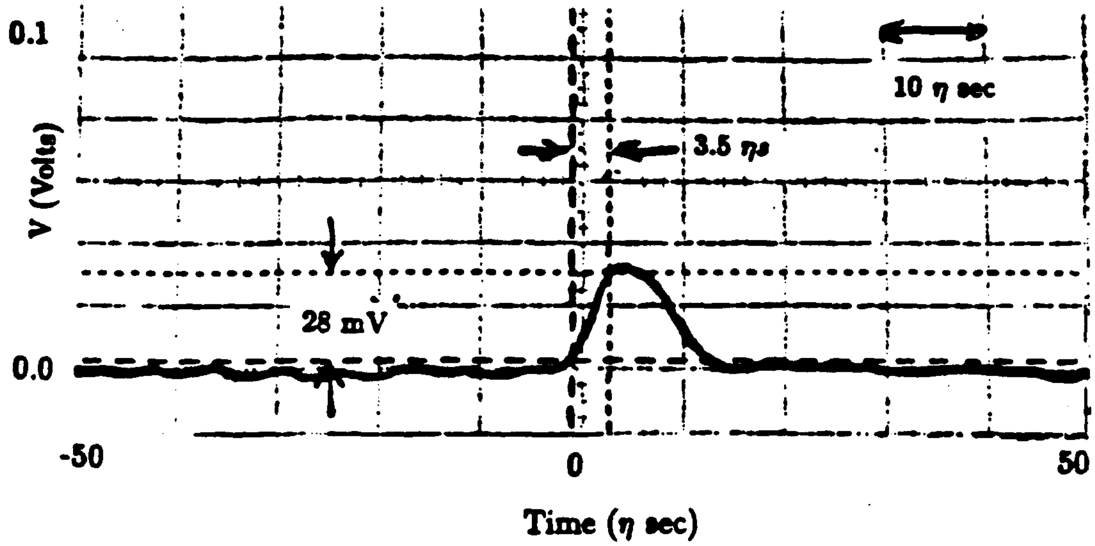

Figure 10: Signal from 2 meter straw tube filled with CF_4 The waveform shows the output of the prototype amplifier attached to a detector tail cancellation circuit.

will be available soon in quantity; the printed circuit board is presently being layed out at the University of Colorado.

2.3.4 Bipolar Discriminator

We are presently exploring the design of very low power timing discriminators intended for use with the preamp and shaper. The present design goals are:

Power	5 - 10mW
Minimum Threshold	10mV
Hysteresis	2mV
Time Slewing	1ns (3–300 mV overdrive)
Output Drive	150mV diff. into 5pF

Our designs attempt to take full advantage of the benefits of advanced bipolar technology. Since base emitter matching between transistors is about 1mV, it is possible to design for a reliable minimum input signal of 10mV or less without input trimming. High unity gain bandwidth transistors allow for the use of cascaded gain blocks with feedback to implement hysteresis and reduce time slewing. Drawing on previous experience in the design of differential discriminators, we have developed several possible configurations suited to particular bipolar technologies and are planning to implement a design in our next bipolar run. An example of the near threshold performance of one design, modeled using Tektronix SH-PI technology is shown in figure 11. The top part of the figure shows the response of the discriminator to inputs just below and just above threshold; the bottom half shows the change in the output timing as a function of the overdrive. From 3mV to 40mV, the largest overdrive used, the output delay shortens by about 1ns. From about $500\mu V$ to 3mV the output delay changes by nearly 2ns. With a power requirement of 7mW this circuit should easily satisfy our design goals.

2.3.5 New Prototypes

As noted above, a multi-channel (probably 8 channels per chip) preamp/shaper/discriminator with detector tail cancellation has been designed and will be fabricated in the Tektronix SHPi process (layout of the preamplifier and first shaper section is shown in Figure 12. The low stray capacitance of this process allows a much lower power dissipation that in previous designs, 7 mW in the preamp and shaper and 7

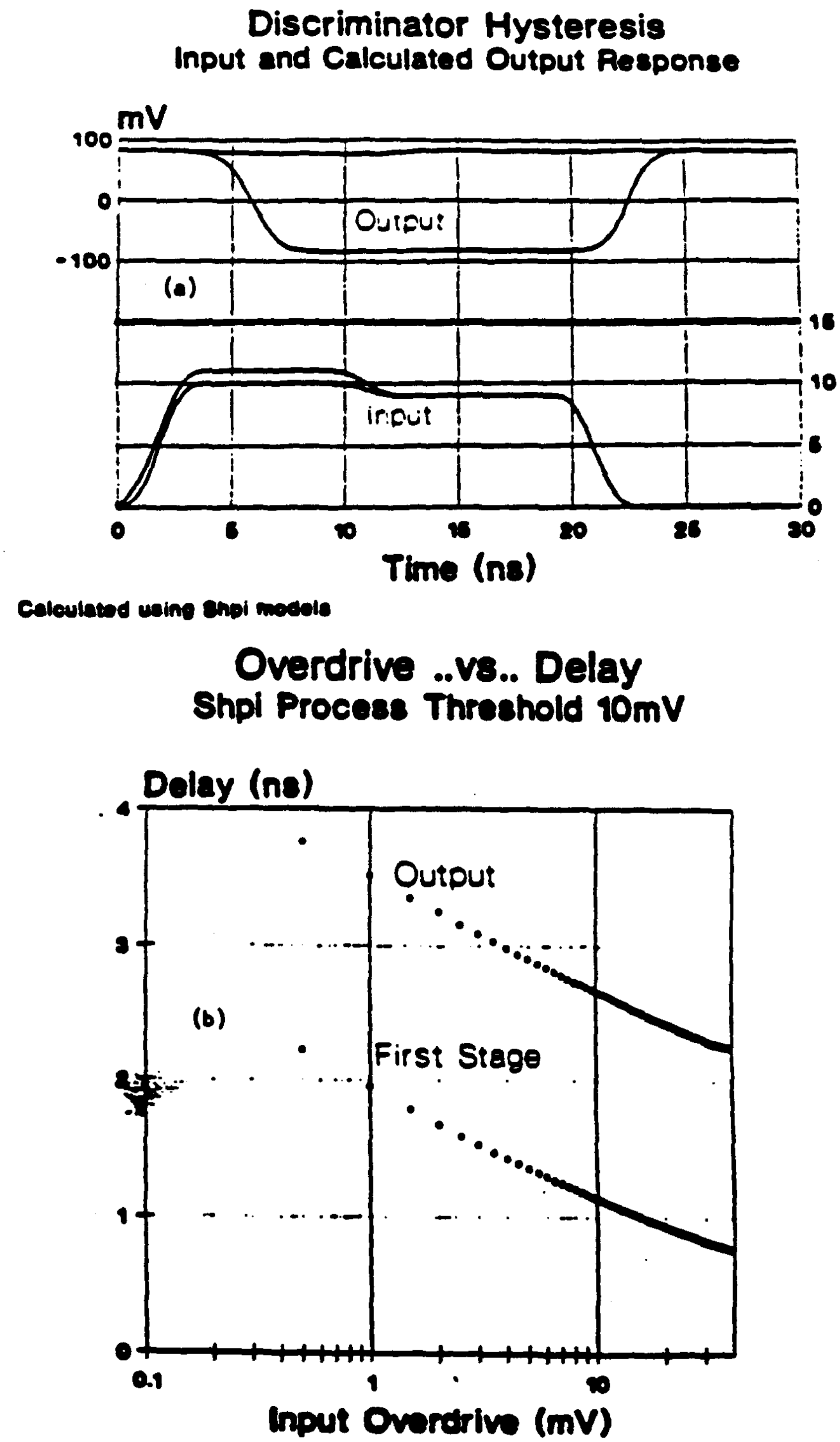

Figure 11: Low Power Discriminator (8mW) output waveforms for input pulses just above and below threshold (SPICE modeling result)

mW in the discriminator. Revision of the preamplifier, increasing the open loop gain has reduced it's sensitivity to the size of the detector capacitance. It is no longer necessary to optimize the preamp power supply voltage for input capacitance in the range of 0 - 20 pF. To satisfy impedance matching criteria for the muon group, the input impedance has been tuned to be approximately 120 ohms over the usefull bandwidth of the preamplifier, with a smooth rolloff at high freqency. The tail cancellation circuit is based on a design by John Oliver.

This second protyping amplifier will have current programmable analog outputs, before and after the detector tail cancellation, as well as current programmable differential discriminator outputs capable of driving 50 ohm lines. To make it easier to use in a variety of designs, only two power supplies are required.

2.3.6 Radiation Hardness of AT&T and other Processes

Given that it is possible to obtain the required performance with integrated circuits, the critical question is whether there exist available processes that are sufficiently radiation hard. While ultimately each individual circuit must be demonstrated to be sufficiently radiation resistant, two of the most critical parameters to be checked are the current gain, β, and the inherent noise of the transistors. Figure 13 presents measurements of β for transistors produced in the AT&T CBIC U process as a function of collector current, before and after 2 Mrad Co^{60} radiation. For NPN devices the current gain remains well above 100, which is quite suitable from the point of noise and circuit design, for integrated doses of 2 Mrads. For PNP the initial beta is significantly lower, but the decrease after radiation is again quite modest. Figure 14 presents results on the degradation of current gain as a function of n fluence; after an integrated fluence of $6 * 10^{13} n/cm^2$, the current gain remains above 100 for NPN devices except for operation at low $V_{ce}(1V)$ and very low currents ($< 10\mu A$). Figure 15 shows the percentage change in β due to both n and ionizing radiation for devices operated at a current of $100\mu A$.

The intrinsic noise of transistors in modern bipolar processes is quite insensitive to radiation. There is little if any increase for ionizing doses of up to 5 Mrads of Co^{60} irradiation.

2.3.7 Radiation Hardness of Complete Amplifier

Six channels of the AT&T preamplifier have been exposed to Co^{60} radiation at BNL. Three channels were exposed to 1 MRad and three to 2 MRad. A small gain loss of approximately 5% was measured for those channels exposed to 2 MRad and there was essentially no change in the noise (the measurements actually indicated a small decrease, but this is probably due to systematic uncertainties in the measurements). Rise time measurements indicate an increase of approximately 0.6 ns for all channels and only one channel out of six had more than a 1 mV shift in the DC output voltages.

2.4 Time to Voltage Converter/Analog Memory Unit (TVC/AMU)

While many possible schemes exist for making the precision time measurements, providing data to the Trigger, and providing data to the final DAQ readout, our judgement has been that a measurement scheme which takes advantage of the precision and simplicity of analog time ramps coupled with the great dynamic range of digital counters and the long precision storage available from CMOS capacitors will offer both lower power and greater resolution than an equally complex all digital system. In addition any system for SSC detectors is bound to have a significant digital component because it is necessary to incorporate all of the desired system features (connection to trigger and DAQ systems, for instance) directly into the custom silicon in order to keep power and mass of the final system as low as possible. The SLAC SLD detector serves as an example of a device where a great reduction in the volume and complexity of the electronics system was accomplished by using custom integrated circuits, but where the total gain was very much less than it might have been just because some of the simple interface and control functions were left as *off-chip* commercial devices.

Another serious potential limitation of any system may be the very high density required of the readout electronics coupled with the fact that the high rate environment requires that there are asynchronous data acquisition, data conversion, and data readout processes occurring simultaneously. Because self

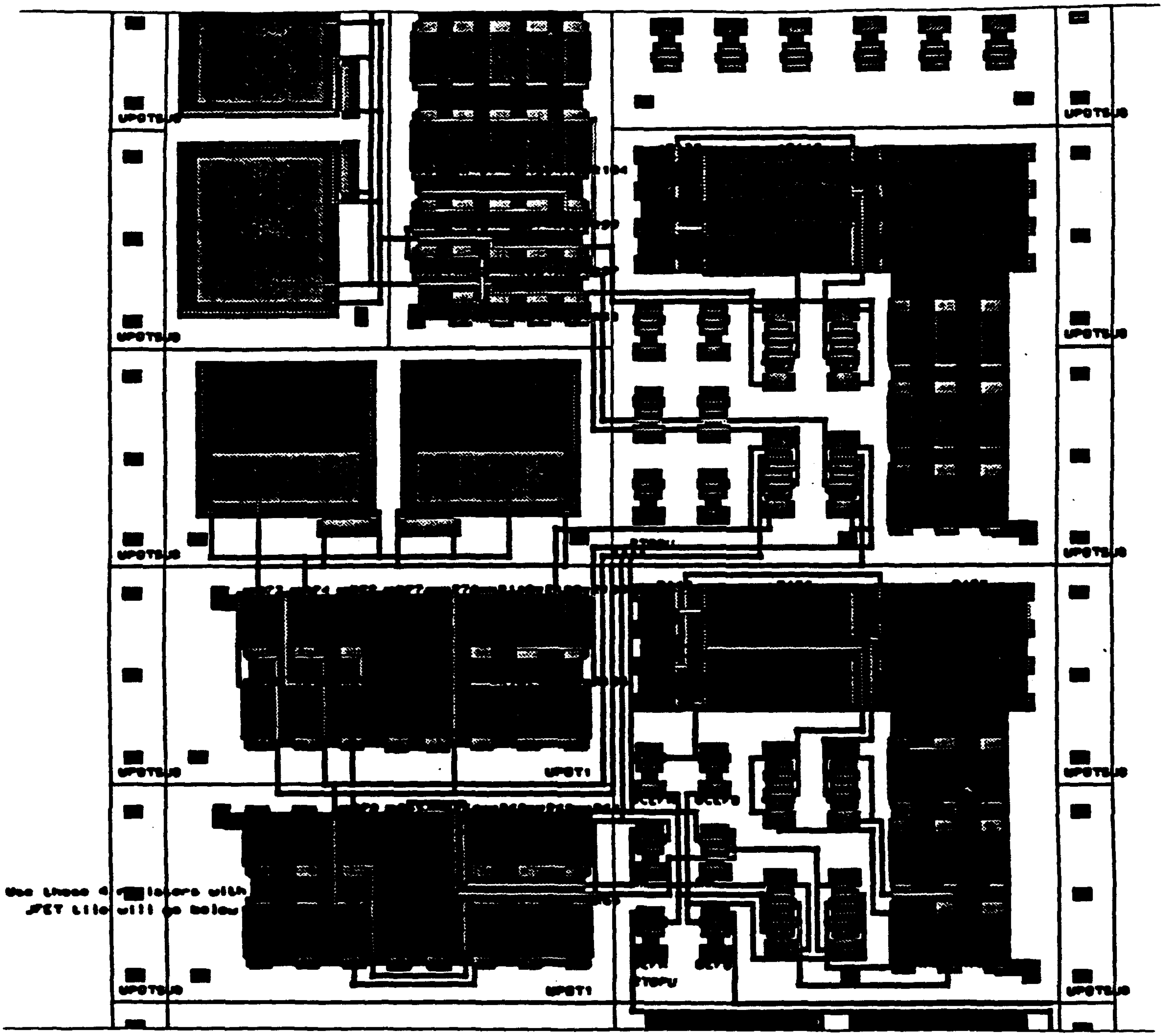

Figure 12: Layout of the preamplifer and first stage of shaping amplifier in the Tektronix SHPi Quick Tile process. Note the isolating substrate contacts along both sides of the amplifier chain.

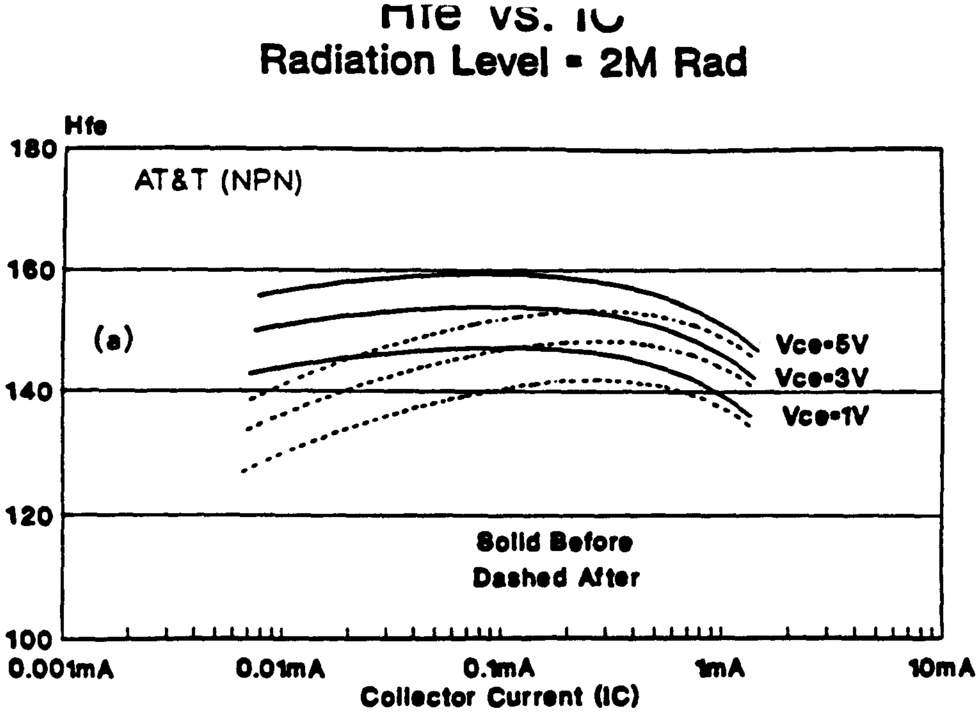

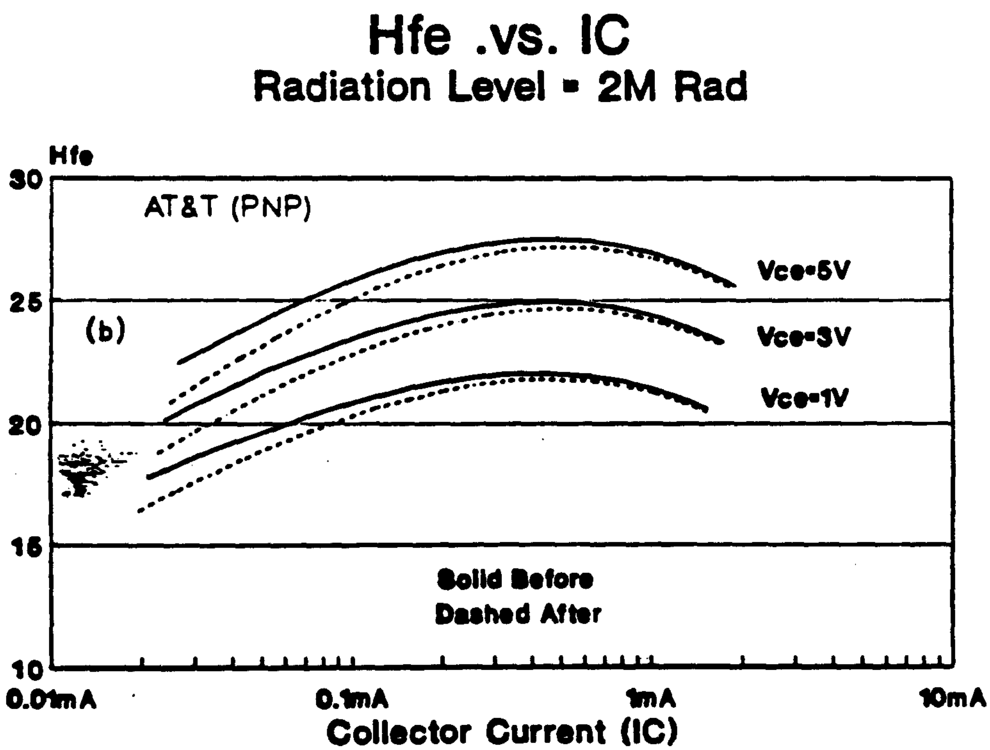

Figure 13: Beta of the AT&T CBIC-U transistors as a function of collector current before and after exposure to 2MRad of Co^{60}.

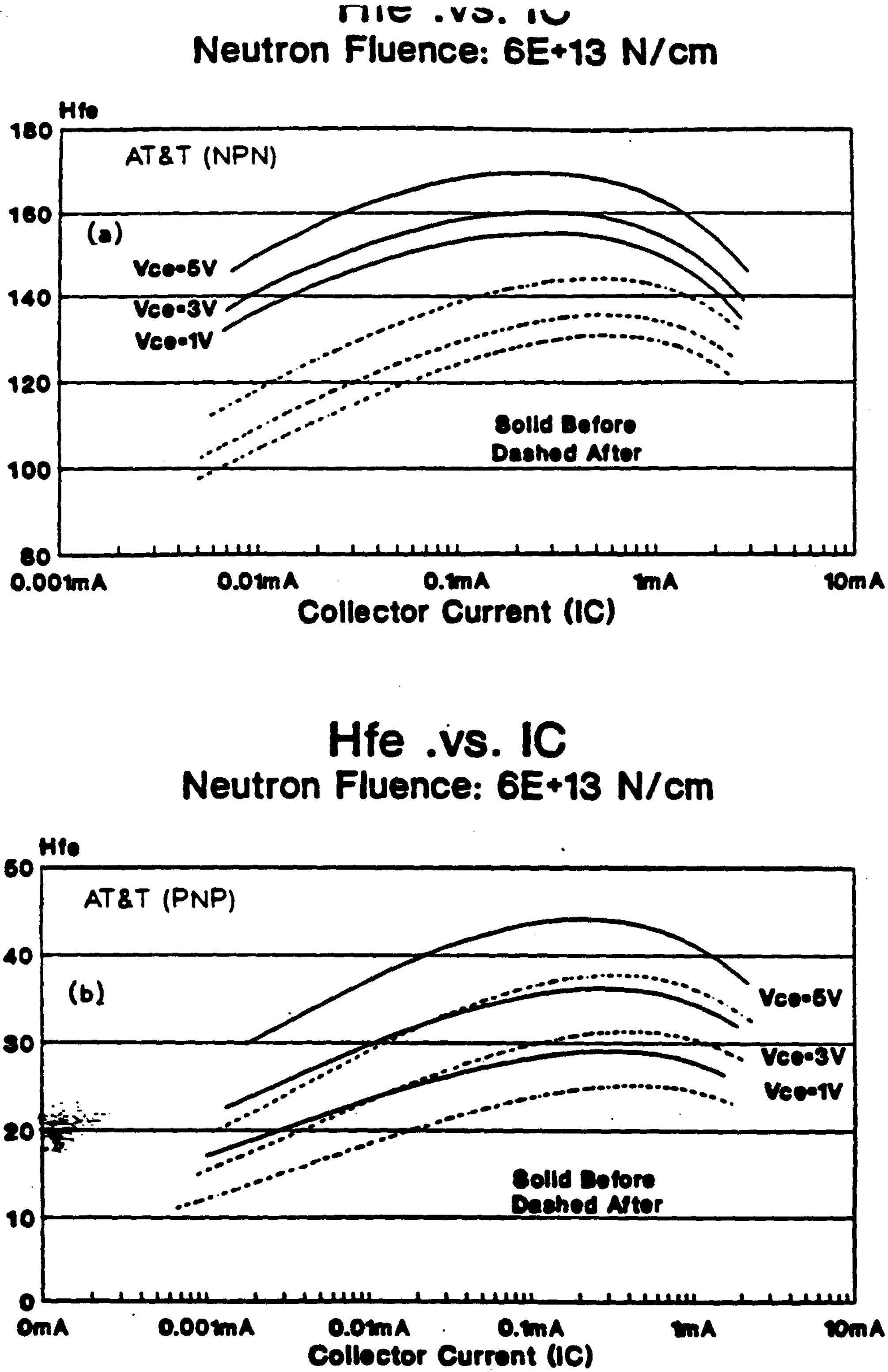

Figure 14: Beta of the AT&T CBIC-U transistors as a function of collector current before and after exposure to 6×10^{13} neutrons/cm^2.

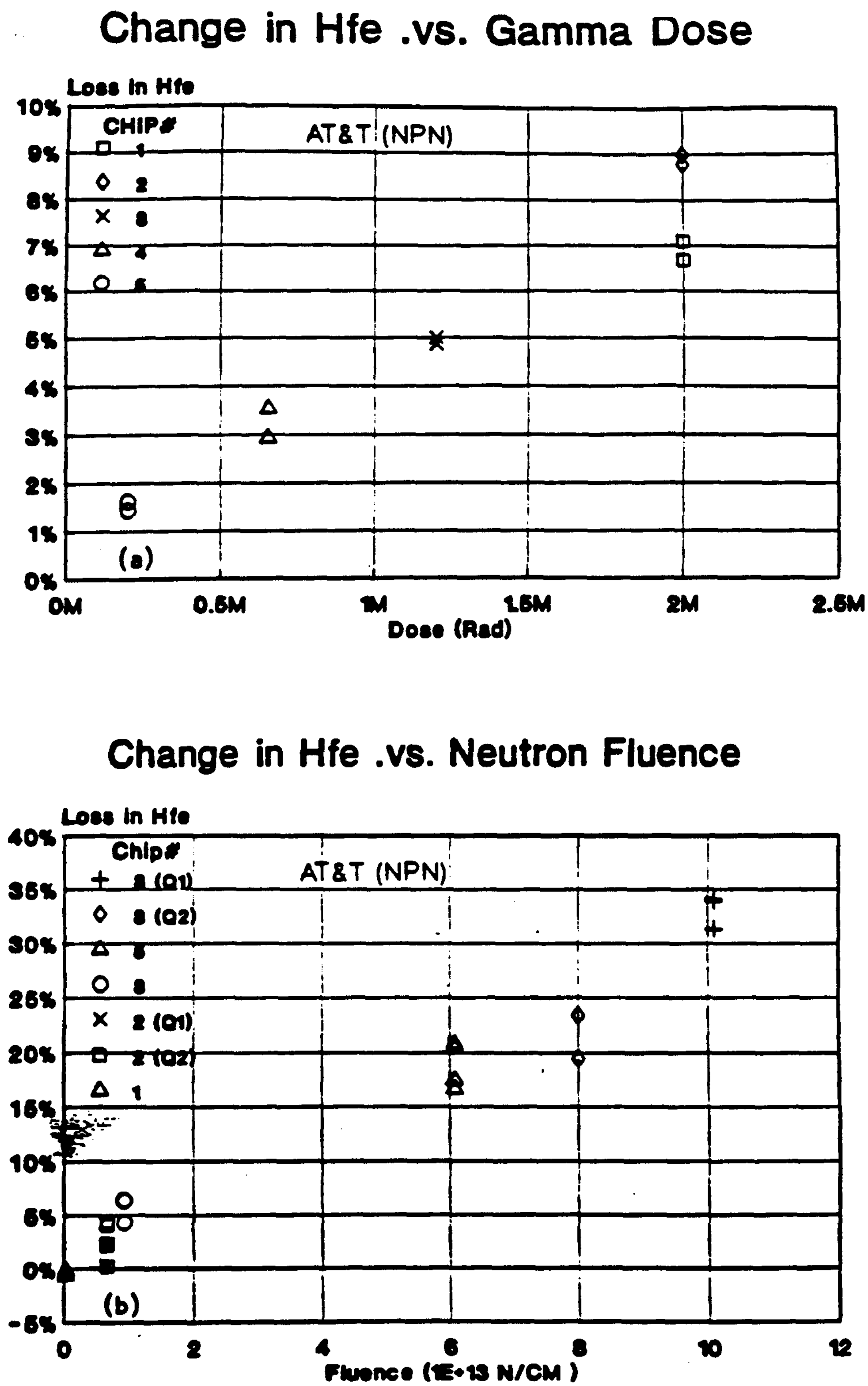

Figure 15: Percentage change in beta of the AT&T CBIC-U transistors operated at $100\mu A$ due to both n and ionizing radiation

intereference may limit our ability to take data and because we may not be aware of such limitations until full scale prototypes have been constructed, it is important that the electronics design be as robust as possible against pickup interference and as benign as possible in terms of generating such interference. This leads to a whole set of system level design decisions:

- maximal physical separation between detector input and DAQ/Trigger outputs to limit coupling
- high power supply rejection for the preamplifier and discriminator
- low ($< 300mV$) analog and digital voltage swings
- all fast signals are differential
- all non-differential signals have slow, controlled, rise and fall times
- smallest possible number of off-chip connections

The TVC/AMU is designed to be as complete a system as possible for an entire group of straws (four or eight). The preamp/../discriminator would also, of course, benefit from common integration, but, as pointed out above, bipolar technology is ideal for the functions involved and rad hard BiCMOS technologies are not yet (if they ever will be) available. Also the break from discriminator to TVC is a minimum signal point in the entire system and is, thus, an appropriate place to have an interconnection if one is necessary. For power and interference reasons, however, this interconnection is designed to be *local* (a cm. or so) and acts as a limit on satisfying the separation criteria from the list above. The set of criteria, especially the completeness criterion, has resulted in a design that handles all of the communication with the Trigger and DAQ systems in the smallest number of signals and where the only external components required are the DCC's which serve multiple TVC/AMU chips.

The block arrangement of the TVC/AMU is shown in Figure 16. The major cells are discussed in some detail below.

2.4.1 Capacitor Accuracy and Analog Design

In previous work we had fabricated and measured a CMOS Time to Voltage Converter that easily met the accuracy and linearity requirements as can be seen in the differential nonlinearity distribution, Figure 17, and the eight channel superimposed transfer function, Figure 18.

This eight channel prototype TVC design depended upon careful matching of capacitance values from one sample to the next using common centroid layouts. It became obvious in this design that while the common centroid layout gave very good matching (cf. Figure 18) channel to channel, the cost in area and layout complexity for a number of capacitors sufficient for Level 1 and Level 2 storage would be prohibitive. In fact the interconnection capacitance would dominate a sixteen capacitor version, largely defeating the matching effects of common centroid layout. Because of this, we decided to pursue a charge–measurement scheme that would, to first order, be insensitive to capacitance values.

Any capacitor memory scheme will have at least three switches around each individual capacitor as shown in Figure 19.The prototype TVC implemented eight individual capacitor storage elements with a common reset control and individual voltage outputs. By using the input switch to place charge on the capacitor at one rate and then instead of measuring the voltage on the capacitor, one were to use the output switch to remove charge at a much slower rate, it becomes possible to measure the time duration of the input current to high precision with a relatively slow comparator. If the input and output currents are ratioed to each other, then the accuracy of the measurement can be kept high even with relatively large process and device variations since both the capacitance and the absolute values of the currents ratio out of the first order time equation;

$$\Delta t_{out} = \frac{\Delta t_{in} \times i_{in}}{i_{out}} \tag{2}$$

We have adopted the ratio of $i_{in}/i_{out} \sim 150 :: 1$ in order to give about 0.1 ns resolution over a 16 ns range.

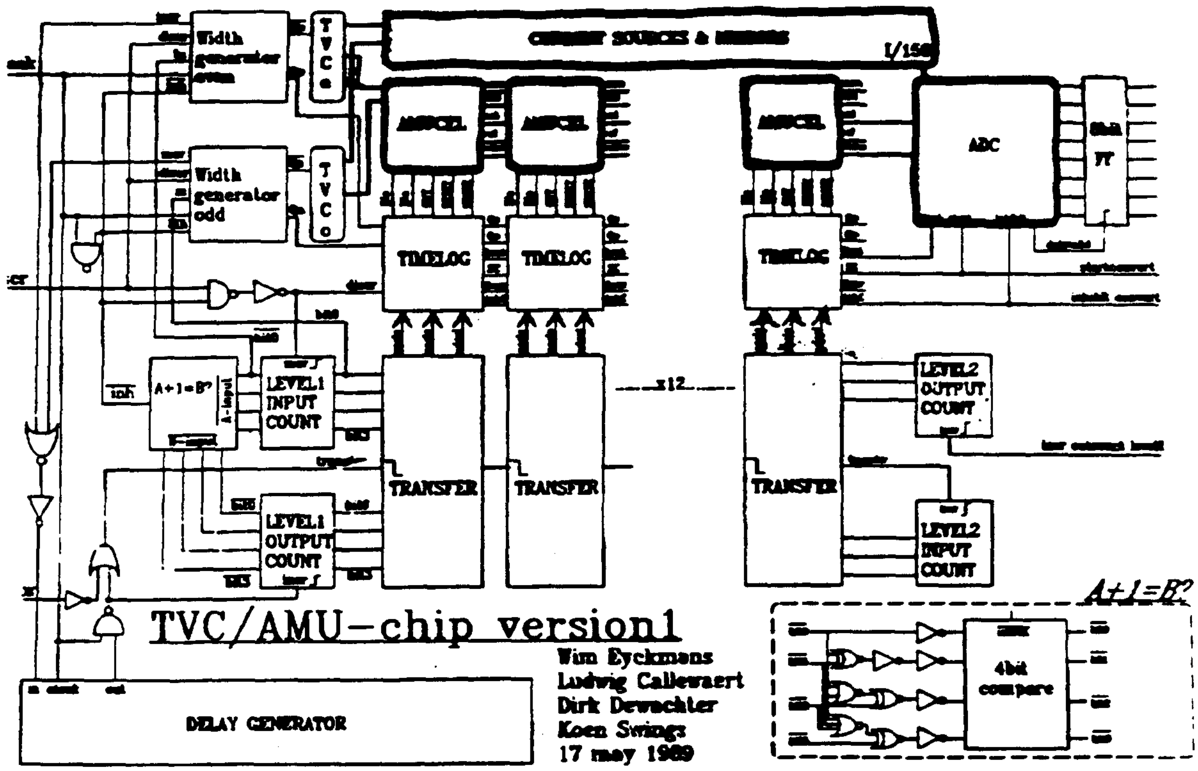

Figure 16: TVC/AMU Block Diagram. Each time-to-voltage conversion is stored in one of eight Level 1 capacitor locations (AMUCEL); there are also 4 Level 2 storage locations in this prototype version. Whenever a pulse from the discriminator occurs a 1 is loaded into the delay generator which has a delay exactly equal to the Level 1 trigger delay. A coincidence of the 1 emerging from the delay generator and a Level 1 Accept causes data to be transferred from Level 1 to Level 2 storage. Each L1 and L2 storage location has an address associated with it, in the block labelled "Transfer." The Level 1- Level 2 "transfer" is accomplished by swapping the appropriate addresses.

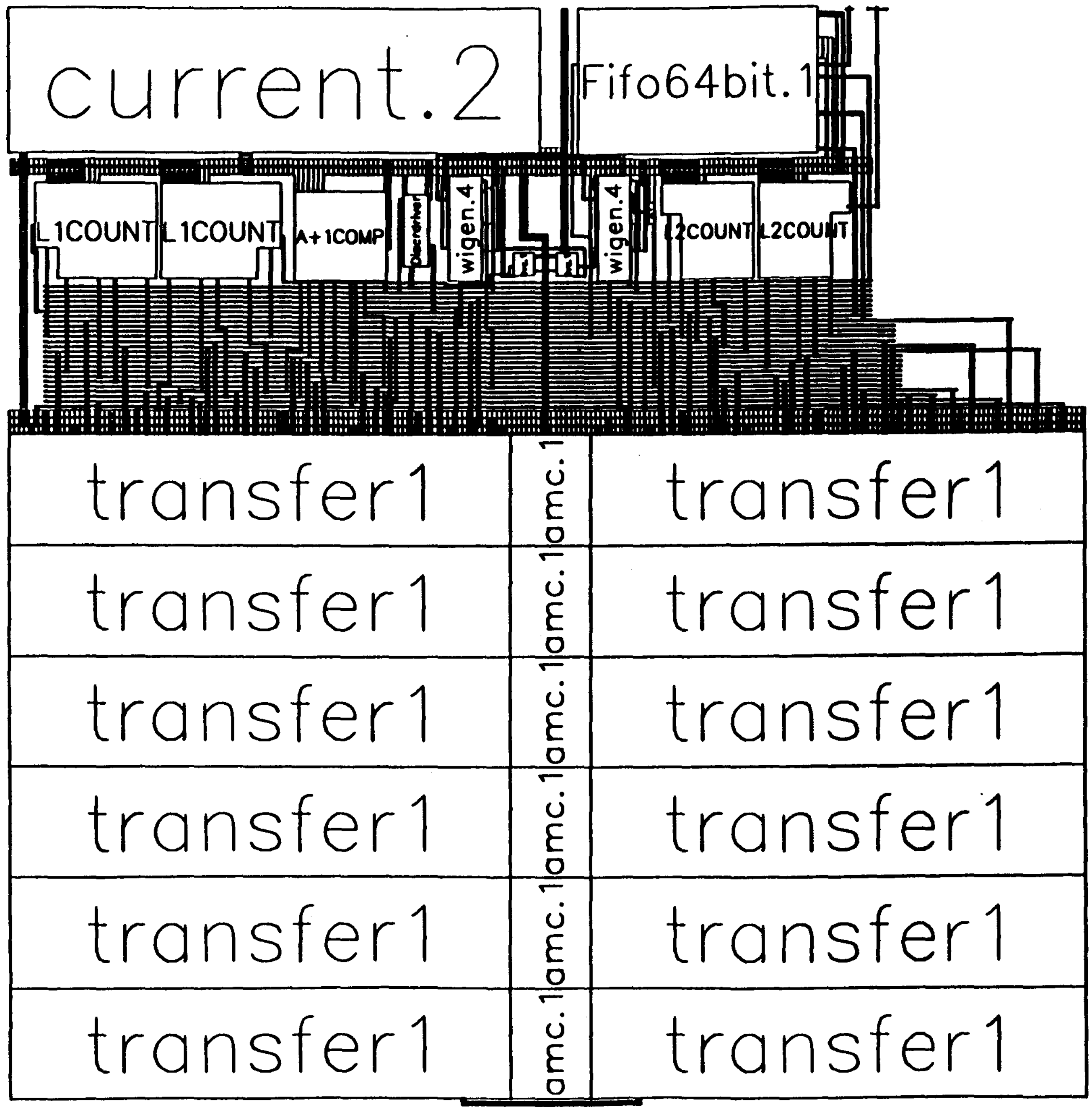

Layout of TVC/AMU

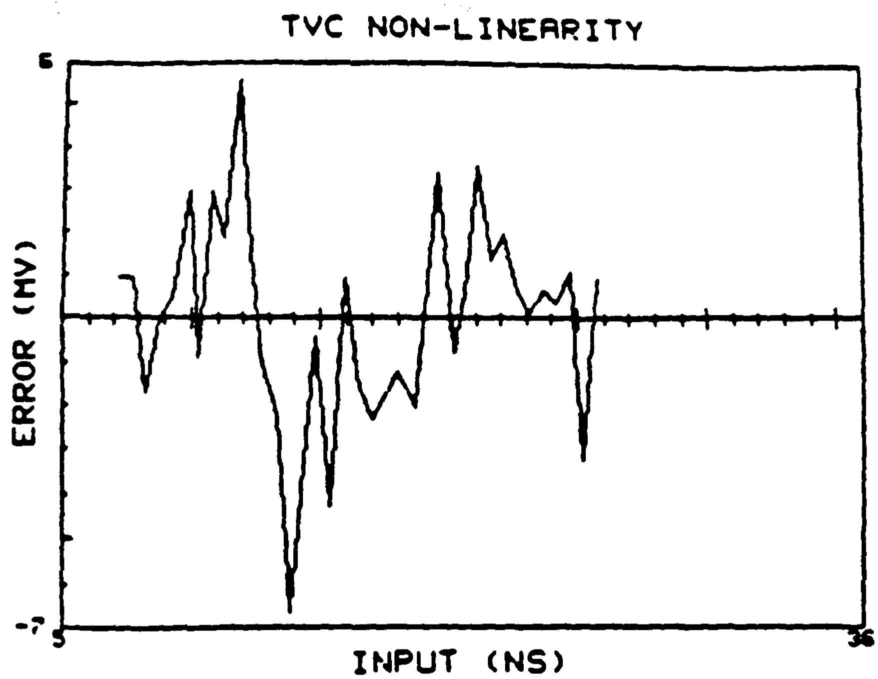

Figure 17: TVC Differential Non-Linearity from 7 to 31 ns. Note that 50 mV is equivalent to 1 ns and that the maximum peak to peak deviation is less than 250 ps.

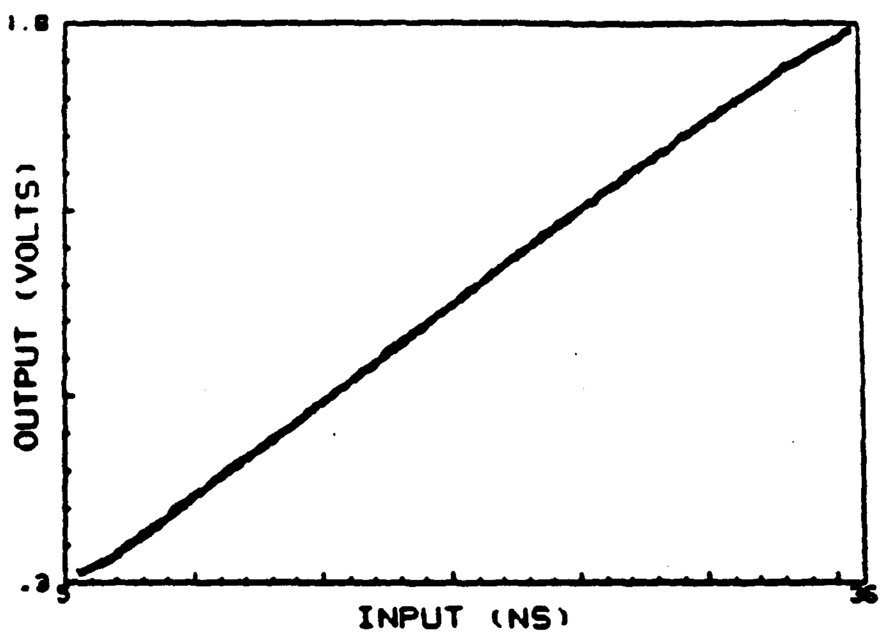

Figure 18: TVC Output Voltage vs. Input Time Difference, 8 Independent Channels Superimposed - Note that 1 ns ~ 50 mV

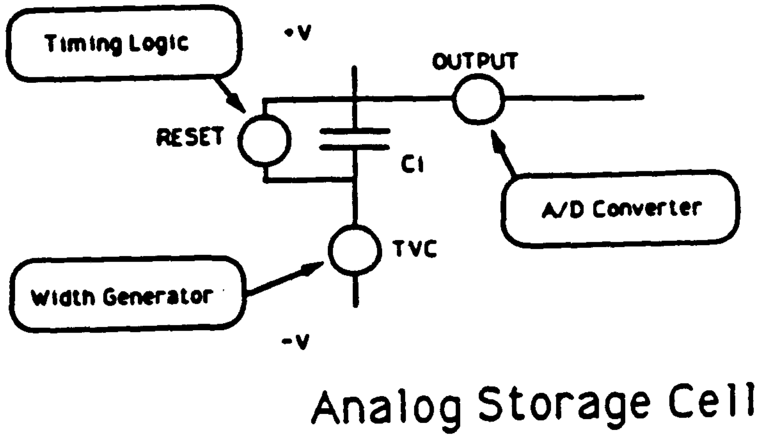

Figure 19: Input, Output, and Reset Switch Configuration

2.4.2 Level 1 Storage

For a two to three μsecond Level 1 storage time it would be necessary to provide 128 to 192 storage locations if we were to have a simple synchronous system. However, by implementing a data driven system which uses a storage location only if new data is present, many fewer locations will suffice given the relatively low occupancies of the tracking system. In the prototype TVC/AMU, we have limited the number of Level 1 locations to eight which is more than enough for a 2 μsecond delay with a 1 MHz average input rate. This design may be easily expanded to 16 or more locations in Level 1 at the cost of additional silicon real estate.

2.4.3 Level 2 Storage

While a few microseconds of synchronous storage for Level 1 is conceivable, even if awkward, many tens of microseconds is clearly outside the realm of realizeable circuits and thus Level 2 must be implemented in some data driven fashion. There are several conceivable methods of transfering information from Level 1 storage to Level 2 storage. For the TVC/AMU we have chosen to use a virtual Level 2 scheme in order to simplify the analog storage problems. The particular technique adopted is "address swapping" (as suggested by L. Calleweart and W. Eyckmans of the Catholic University of Leuven) which is logically similar to FIFO or pointer schemes, but minimizes the length of analog control signal lines - at the expense of longer control buses.

2.4.4 Time Measurement Logic

To accurately reconstruct tracks, it is necessary to know the time of arrival of the first electron at each straw anode relative to some common time that relates all of the data for a given event. The TVC/AMU operates as a common-stop time measuring device - starting on an anode discriminator pulse and stopping on the next negative going clock edge after the next positive going clock edge (Figure 20).

This scheme leaves a guaranteed minimum of one-half of a clock cycle for any time measurement and for a nominal 16 nanosecond clock means that the actual time ramp in the TVC goes from 8 to 24 nanoseconds. This minimum time allows the the TVC response to be linear in the range of interest and avoids the possible race conditions associated with a system that allows a zero minimum measuring time. The control signals that switch on or off the current in the time measuring capacitor are generated in a circuit called the Width Generator (Figure 21) which derives the required one-half to one-and-one-half clock period signals and also provides the address increment signal to the L1WA counter.

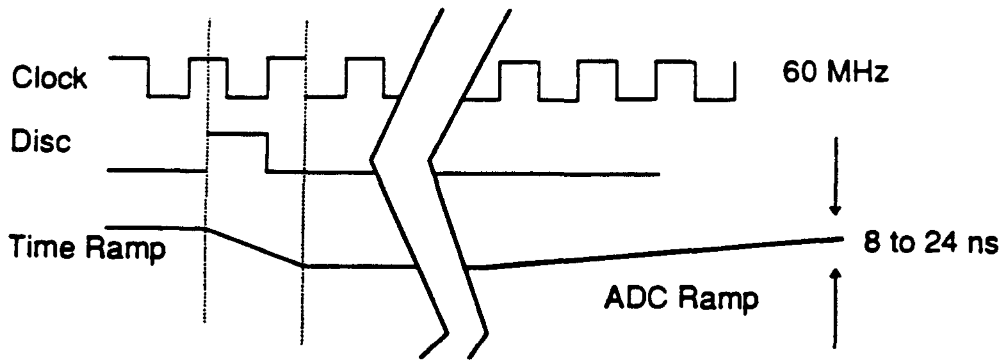

Figure 20: Timing Diagram of the TVC Measurement Cycle

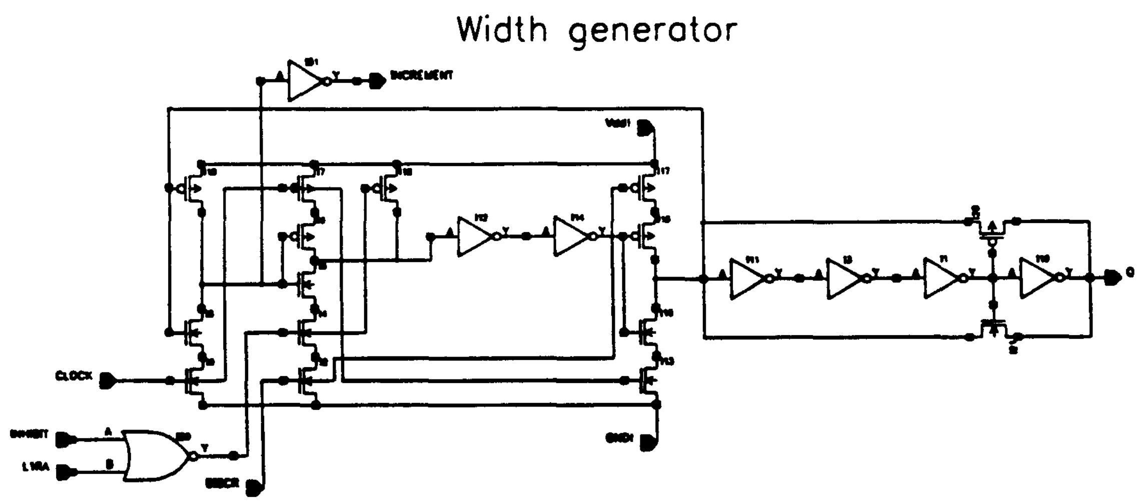

Figure 21: Width Generator Schematic

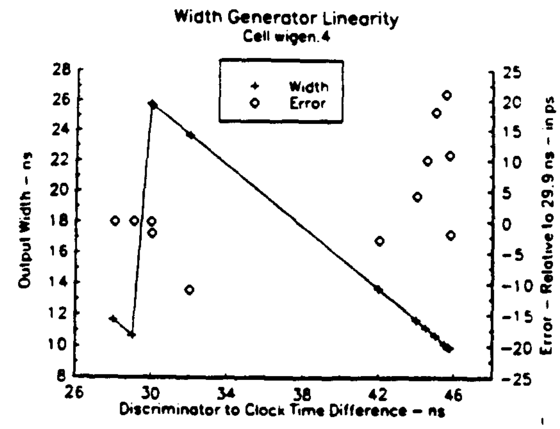

Figure 22: Width Generator Response - The connected points show the width of the generator output in nano seconds as a function of the relative time in ns between clock and discriminator pulse. The deviation from linearity is plotted in pico seconds on the right hand scale.

The Width Generator has been carefully optimized for high linearity and low propogation delay differences. Figure 22 is a simulation of the Width Generator output which shows the characteristic sawtooth shaped response in ns per ns as the relative time is varied between a discriminator pulse and the beam clock. The unconnected points show the deviation from linear response in pico seconds on the right hand scale.

2.4.5 Delay Generator

In a data driven architecture, there is no one-to-one correspondence between storage location and event time. Thus there must be some provision in the TVC/AMU to allow identification of data for a particular event with a possible Level 1 Trigger signal. A simple 64 element shift register would allow about 1 μsecond of delay with a 16 nanosecond clock period, but all 64 elements would be clocked at 60 MHz and significant power would be dissipated. We have, therefore, implemented this function as a modified serial, parallel, dynamic shift register block (Figure 23)

In this version, synchronized discriminator pulses enter at the lower left (Figure23) and are advanced upward at 60 MHz along a serial shift register of length A. Then every A clock pulses the contents of this serial shift register are loaded into A *parallel* shift registers each of length B (where $A + A \times B = N$). The parallel registers are then clocked at a rate of 60/A MHz. At the output of each of the parallel shift registers, the contents are unloaded into another *serial* shift register which is also operating at 60 MHz. Thus any individual bit of data takes N clock pulses to pass through the delay generator, but only 2A out of the N total cells are operated at 60 MHz while the bulk of the cells are running at a much lower power. The total simulated power for N=64 is about 3 mW.

This architecture can then be optimized for the lowest possible power for any given length N. Table 1 indicates the relative power dissipation for a 64 and 128 crossing delay at different ratios of A and B. It is interestin to note that the minimum power goes up roughly as $\sqrt{N}$ since the relative number of slow, low power, parallel cells can increase for larger N. This design is capable of operating well above the required

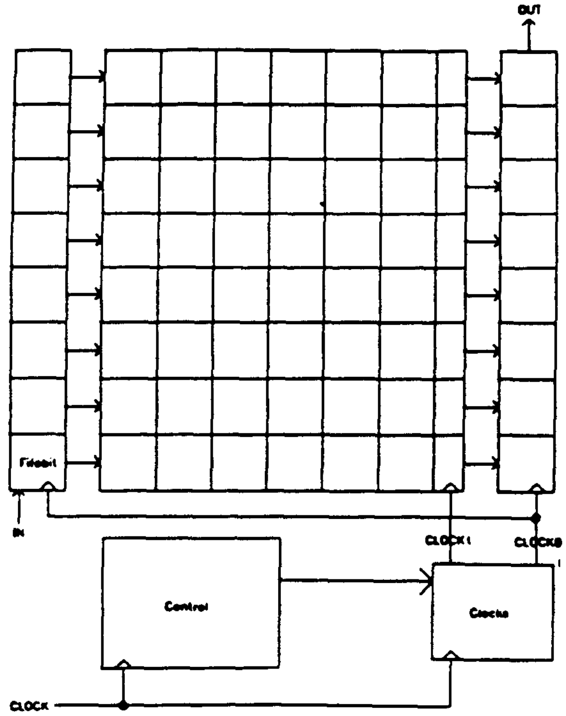

Figure 23: Delay Generator Block Diagram

60+ MHz SSC crossing frequency. It is also interesting to note that about one third of the cell area is control, divide by A, and buffer circuitry that would be shared in a multichannel version - thus the delay cell area as well as power would go up at a less than linear rate.

2.4.6 Level 1 Trigger Interface

After a delayed data pulse exits from the delay generator, it is simply *AND*ed with the Level 1 Trigger signal and the resulting signal, **L1ok** is used to provide the transfer signal that logically moves data from Level 1 to Level 2. If the Level 1 Trigger signal remains high for more than one clock period, then the same simple logic will continue to transfer any existing Level 1 data to Level 2, thus providing for the case where the detector response time is greater than one clock period (in this case the electron drift in the straw detector). In order to differentiate data from different clock cycles within any one Level 1 Trigger time, a separate small counter must keep track of clock pulses as explained below in the section on the Bunch Counter.

2.4.7 Level 2 Trigger Interface

The Level 2 Trigger is asynchronous so that a delay line is not appropriate for providing the trigger-data synchronism. Since the Level 2 Trigger is monotonic, however, it is only necessary to provide two counters (**L2WA**, **L2RA**) to keep track of Level 2 inputs and outputs. Each new entry into Level 2 increments the **L2WA** counter and each read (or reset) of Level 2 increments the **L2RA** counter. In the final version of the TVC/AMU a digital comparator will keep **L2RA** from crossing over **L2WA**. This interlock is not implemented in the test version of the TVC/AMU.

As the Level 2 Trigger is asynchronous, it must be accompanied by a timing signal (or conversely there must be a Level 2 Reject as well as a Level 2 Accept). The Level 2 Strobe is used to clock a D-Flip

N = 56			N = 112		
A	B	Power	A	B	Power
32.0	0	64.0	64.0	0	128.0
21.3	1	43.6	42.6	1	86.2
16.0	2	34.0	32.0	2	66.0
12.8	3	28.6	25.6	3	54.2
10.6	4	25.2	21.3	4	46.6
9.1	5	23.2	18.3	5	41.6
8.0	6	22.0	16.0	6	38.0
7.1	7	21.2	14.2	7	35.4
6.4	8	20.8	12.8	8	33.6
5.8	9	20.6	11.6	9	32.2
5.3	10	20.6	10.6	10	31.2
4.9	11	20.8	9.8	11	30.6
4.6	12	21.1	9.1	12	30.2
4.3	13	21.5	8.5	13	30.0
4.0	14	22.0	8.0	14	30.0
			7.5	15	30.1

Table 1: Total Delay Generator Power - 56 and 112 crossing total delays, for various Serial (A) and Parallel (B) lengths - The power figures are relative, the total power for the N=64 case is slightly less than 3 mW.

Flop with the Level 2 Accept (or Trigger) on the data input of the flip flop. For an accepted event, the ADC cycle is started, for a rejected event, the **L2RA** is simply incremented. In the prototype version, there is no additional queue to allow a second Level 2 Trigger to come in during the ADC cycle - in the final production version, this additional queue will be needed to allow Level 2 Triggers to proceed without interlocking with ADC conversion times, unless SDC decides to impose a minimum delay time between Level 2 Accepts.

2.4.8 Event Identification

During normal SSC operation, individual detector elements and systems will be involved in simultaneous input processing, data storage, data conversion, and data output. Given the non-deterministic nature of multiple asynchronous devices, the data stream out of a detector may be non-monotonic in time and space co-ordinates and it will be necessary to include in each data packet from any detector element some crossing identifier.

Trigger I.D. Counter The simplest time stamp, of course, would be a crossing counter - advancing every 16 nanoseconds. However, for Level 2 storage times of 50μseconds or more plus realistic DAQ pipeline delays of many tens of microseconds, a 13 or 14 bit crossing counter would be necessary in order to avoid ambiguity. A less marginal scheme with much longer unambiguous periods would be to count not the crossings at 60 MHz but the Level 1 Triggers at 10^3 to 10^4 Hz. Even at 10^4 Hz an eight bit Trigger I.D. Counter would remain unambiguous for 25 milliseconds. A Trigger I.D. Counter at each detector element would then keep track of the time stamping of events and only the Central Trigger System would be required to keep a long 60 MHz counter - and then only if the absolute time of day were of interest.

Bunch Counter As noted above, the Level 1 Trigger may in many cases remain true for more than one crossing. In order to completely specify the time it is necessary to have a small two bit counter,

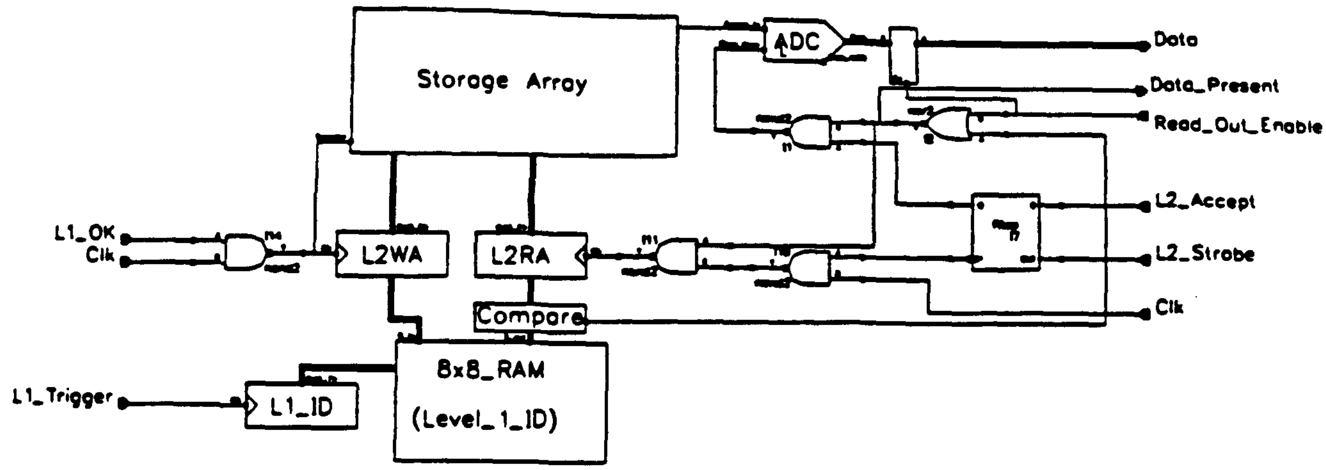

Figure 24: Level 2 Control - Block Diagram

enabled by Level 1 Trigger, and clocked by the crossing clock. This counter is enabled by Level 1 Trigger true and counts until Level 1 Trigger goes false.

Level 2 RAM Because the occupancy of a tracking system must be relatively low, most Level 1 Triggers will not have data in any given detector channel and most Level 2 Triggers will, similarly, not correspond to any data in a given channel. For Level 1 Triggers, the delayed data is *AND*ed with the trigger and no *empty* Level 1 Triggers are stored in Level 2 (but the Level 1 Trigger I.D. advances in any event). At Level 2, it is necessary to tag each piece of data with a Level 1 Trigger I.D. and then, at each Level 2 Trigger, search the on chip storage for any relevant data.

For the TVC/AMU prototype, this function will be handled off chip, but for the production design, we intend to implement a small on chip memory (Figure 24), one memory location per Level 2 location containing the relevant Trigger I.D. word and Bunch Counter value. The **L2WA** counter provides the write address for this memory and, of course, the **L2RA** provides the readout address. In order to skip over Level 2 Accepts not associated with stored data, the Trigger I.D. output of the present **L2RA** is compared with the value of the Level 2 Trigger I.D. Counter (i.e. the Trigger I.D. of the event presently being considered by the Central Trigger System; this counter is advanced by the Level 2 Strobe so that it is synchronized with the Level 1 I.D. Counter but delayed, on average, by the Level 2 decision delay). If the memory-Level 2 Trigger I.D. Counter comparison is true - that is if the chip has data associated with the event that the Central Trigger System is presently considering -then, for an event where Level 2 Accept is true, the A/D converter is started. For events where Level 2 Accept is false, the **L2RA** is simply advanced on the Level 2 Strobe. For events with data and where Level 2 Accept is true, the **L2RA** is advanced on the end of the A/D conversion cycle (i.e. as soon as the analog data can be reset).

2.4.9 ADC

The Analog to Digital Converter is implemented as a Wilkinson run-down device with a capacitor discharge current (i_{out}) ratioed (at 1/150) to the charging current (i_{in}). The capacitor voltage is then

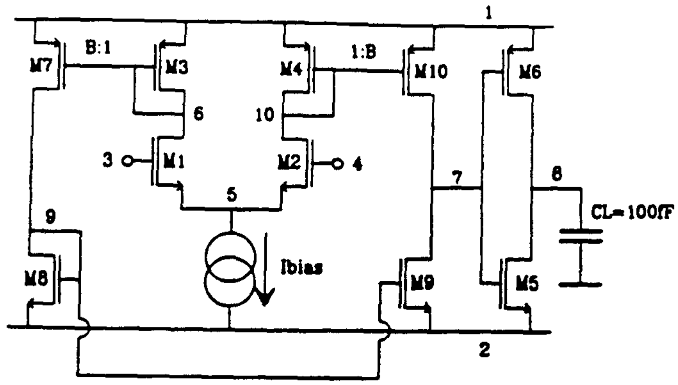

Figure 25: Comparator Schematic

viewed by a comparator which trips when the voltage reaches the reset value. A 60 MHz counter that began counting when the discharge current began flowing is stopped when the comparator trips and the counter value is loaded into an output register. This value is then the relative time of the detector *hit* in units of about 0.1 ns per least significant bit.

Comparator The requirements for the comparator are straightforward but challenging.

- The power consumption must be very low.
- The comparator must trigger on a ΔV_{in} of $\sim 5mV$.

The comparator is a conventional Operational Transconductance Amplifier (OTA) followed by a digital inverter which shields the OTA output from the load capacitance. Rather than optimize the OTA for speed alone, the required speed for the circuit (Figure 25) was set and then then the transistors were sized so that the power consumption was minimized ($< 50 - 100\mu W$) and then the circuit was checked via simulation to verify that it would function within the required delay time.

While the comparator need not respond instantly to an input crossing the threshold, the propogation delay must be stable to better than one clock cycle (16ns) in order to avoid errors. If we assume worst case process variations that would lead to ±20% propogation delays, then for a 16 ns clock we need an average propogation delay of $< 80ns$.

With the transistor dimensions below, and an $I_{bias} = 10\mu A$, the propogation delay is equal to 70 ns for a ramp input signal of 5 mV/15 ns and the average current consumption is slightly larger than either $10\mu A$ or $30\mu A$ depending upon which node is driven (a fact that we take advantage of to reduce the quiescent power of the comparator to the lowest possible value).

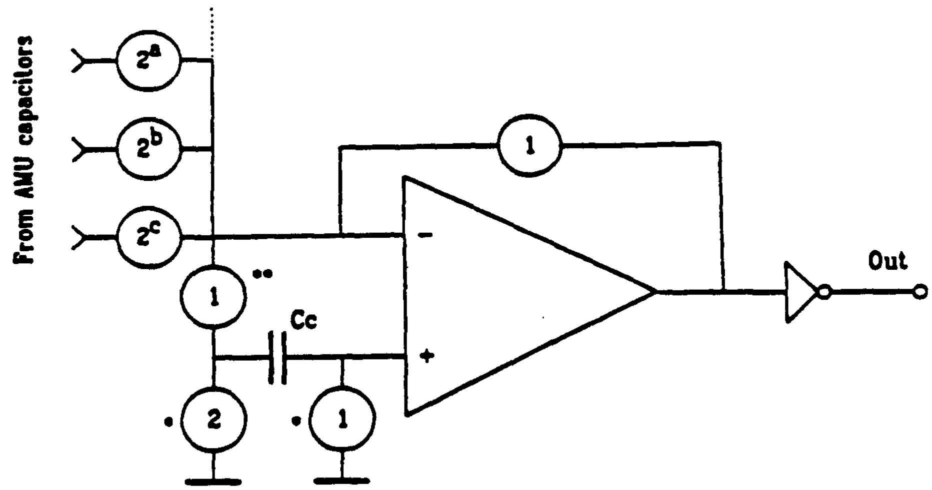

Figure 26: Comparator Offset Cancellation Circuit

Transistor	*W (μm)*	*L(μm)*
M1	5.4	1.6
M2	5.4	1.6
M3	2.4	1.6
M4	2.4	1.6
M5	2.4	1.6
M6	2.4	1.6
M7	4.8	1.6
M8	3.2	1.6
M9	3.2	1.6
M10	4.8	1.6

Offset Compensation The offset variation of the comparator must be less than one bit ($\sim 5mV$), but given minimum size CMOS transistors and normal lot to lot process variations, it is necessary to provide an active offset compensation scheme. The circuit shown in Figure 26 has a capacitor C_c which is initially connected across the comparator inputs by closing the Φ_1 switches and then opening the Φ_1 switches and closing Φ_2, thus *subtracting* the measured comparator offset voltage from the reference voltage. To settle the offset voltage to $< 1\%$, it is necessary to allow about 8 clock cycles for Φ_1. In addition, by adding a third phase at the end of conversion, it is possible to bias the comparator in a low power mode. All of this timing logic is performed by simple decoding of the single ADC counter, resulting in a simple logic block giving a 7+ bit 60 MHz Wilkinson ADC with offset compensation and extremely low power consumption.

The layout of the complete ADC is shown in Figure 27.

2.4.10 Data Output Interface

Data from the TVC/AMU prototype consists of the contents of the ADC register - measuring the time between the anode discriminator pulse and the following clock edge and the contents of the two bit Bunch Counter. The Data Present signal goes true at the beginning of the ADC cycle and the Data Valid line goes true at the end of the ADC cycle.

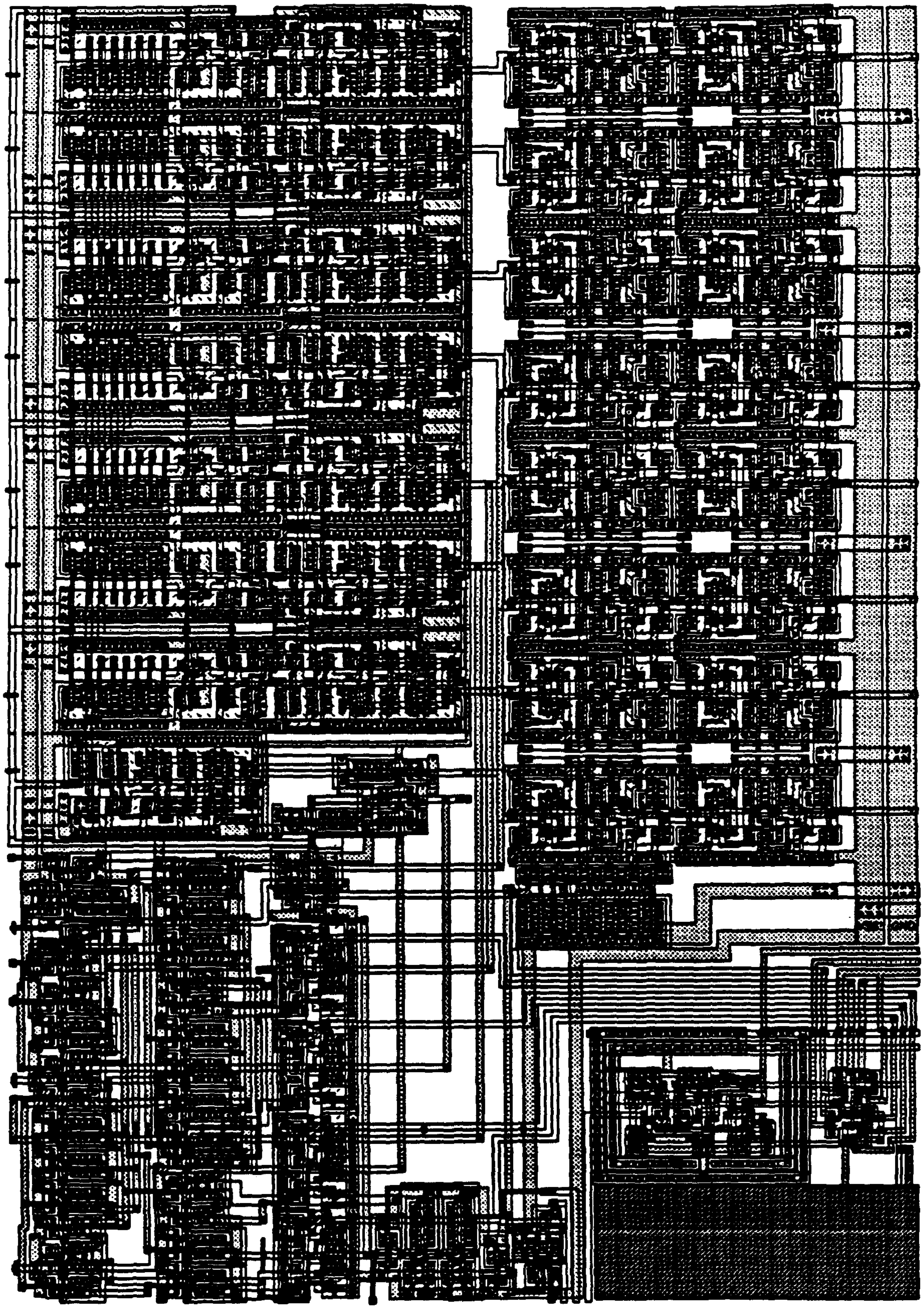

Figure 27: ADC layout with comparator, offset cancellation, latch, counter, and controls.

This arrangement is adequate for a high speed test system where the central control is able to monitor all signal lines, but for the production version a somewhat more sophisticated interaction with the Data Path (and the DAQ system in general) will be required. In general, we do not expect the upstream parts of the Data Path to have or need to have knowledge of what events have been or may have to be digitized or have knowledge of the geographic location of any subelements - all such information can be dealt with locally and should be.

For the production version, the data output must consist of the ADC and Bunch Counter information, but also a geographic address of the *hit* wire (or element), and a temporal address in the form of the Trigger I.D. Number. A fixed length packet with this information (plus necessary flags etc.) may then be assembled in a leisurely fashion with others bearing the same Trigger I.D. number to create a complete event record - this assembly can take place outside the detector with no feedback of information or requests from the DAQ to the detector. In consequence of this it is necessary that the local detector element (the TVC/AMU in this case) must keep intelligent track of all interactions with the Trigger and DAQ systems, must keep a log of possible or actual data errors, and must be down-loadable with starting values for a variety of counters and registers. In addition, it is highly desirable that the interaction with the Trigger and DAQ systems be exceptionally simple in character and detail in order that the physical connections remain uncluttered and in order that the logical connections be easily modeled and understood by all concerned.

Thus for the production version, another effective queue must be provided so that new Level 2 Accepts may arrive during digitization of some previous event - this does not add greatly to the present complexity as the function can be implemented with two additional counters and a small number of gates (analogous to the prototype Level 2 scheme). A queue will also be provided for the output data so that the next level of the Data Path (DCC) is not required to provide a deterministic response to a Data Present signal [1].

2.4.11 Data Input Interface

The present TVC/AMU has no down-loadable or presetable registers and so has no data input. The production version must not only have provision for down-loading constants, but also test patterns (to test the entire Data Path) and for reading back various error registers. Because all of these functions are slow or very slow in character, the DCC specification, which treats these problems in some detail, assumes that a simple serial link from a DCC to and through each of its local front end chips will be adequate - very analagous to the present commercial and military efforts to provide *scan-paths* for complex chips or chip sets. This interface should be common across all of the high density systems - certainly including Silicon Tracker, Straw Tracker, Forward Tracking, and Muons - but may or may not be used for the lower density, crate based systems. This interface still requires considerable effort in terms of simulation and definition before it can be finally specified.

The Threshold Control DACs for the discriminators may be included on the final TVC/AMU. The silicon area and power required for low dynamic range DACs is not large, but the extra pins may be a consideration. This part of the system design is not yet decided.

2.5 Summary and Status

At the present time we have demonstrated:

- Low power, low noise, single channel preamplifier/shapers in a radiation hard technology
- The Transfer Logic block (by far the most complex block in the TVC/AMU) operates properly at full speed (in a $2\mu m$ MOSIS test chip)

[1] The present Draft DCC specification, which is in need of a significant update, assumes a single Data Present line from a front end chip to the DCC and a single Read Out Enable from the DCC back to the front end chip as the simplest possible useful interface.

- All TVC/AMU blocks have been simulated from layouts (as well as schematics) and all blocks individually satisfy the design criteria
- The Comparator has been submitted to both UTMC and IBM for fabrication in rad hard processes
- Detailed radiation damage measurements on bipolar and CMOS technologies indicate that the TVC/AMU will work to long term doses in excess of 2 MRads

3 Straw Module Component Summary

The major components necessary for the electrical operation and readout of the straw tube module are indicated in the block schematic Fig.28 . These are described in some detail in the sections below. The Part Name and quantity per module are indicated at the right end of each sub section header.

3.1 High Voltage $R_H(200), C_{FH}(8)$

High voltage power ($\sim 2KV$ at up to a few μA per straw at $\mathcal{L}=10^{33}$) for an individual straw is brought in through a decoupling resistor, R_H, ($\sim 1M\Omega$, 1 KV) from a local HV bus which will have one or more HV filter capacitors, C_{FH} ($\sim 500pF, 2.5KV$) per module. The local HV bus will be carried on a separate physical substrate which will also mount the filter capacitors and the HV channel decoupling capacitors.

3.2 Termination

For short straws of less than 1 meter, no termination should be necessary. However, for long straws (certainly the present SDC tracker with all straws electrically longer than 2 meters), termination is probably mandatory. The proper electrical termination for a *typical* 4 mm diameter straw is about 300 Ωs in series with about 60 pF. In the positive HV design, this implies a separate HV decoupling capacitor for each straw. In terms of noise the 300 Ω resistor is an additional source of thermal noise, and significant improvement can be made in signal to noise (S/N) if an active termination is used (essentially a preamp input stage with no output). An active termination is, however, more complex mechanically and would require more power ($\sim 3mW$) per channel. For the purposes of this cost estimate we have assumed a passive termination and the cost of this termination is included in the detector cost estimate not in this electronics estimate. If noise performance were to force the use of an active termination, then that cost would have to be added to the total.

3.3 Coupling to Preamplifier $C_C(200)$

At the preamplifier it is also necessary to have a HV coupling capacitor for each channel. This capacitor should be large enough to pass significant signal (for at least one τ_m) but small enough to limit the damage caused by HV discharges into the preamplifier. The final value is likely to be about 100 pF at 2500 V. We are making the implicit assumption that the preamplifier will be sufficiently sturdy to withstand a straw discharge (at operating voltage of about 1800 V). If the preamplifier were not able to withstand likely discharges, it would be necessary to provide protective diodes and snubbing resistors at each input. The large size of such components argues strongly for including the protection necessary on chip. It is also true that additional components would add significant kT noise to the system. Radiation tests are now underway to check the hardness of possible on chip Schottky protection diodes as well as other possible devices.

3.4 Preamplifier, Shaper, Discriminator $P/S(50), D(50)$

The low noise preamplifier, shaping amplifier, and discriminator are all fabricated in a single high speed bipolar process as described above. The cost estimates are based upon quotations for quantities of high speed wafers fabricated in processes demonstrated to have adequate radiation hardness. Because of the

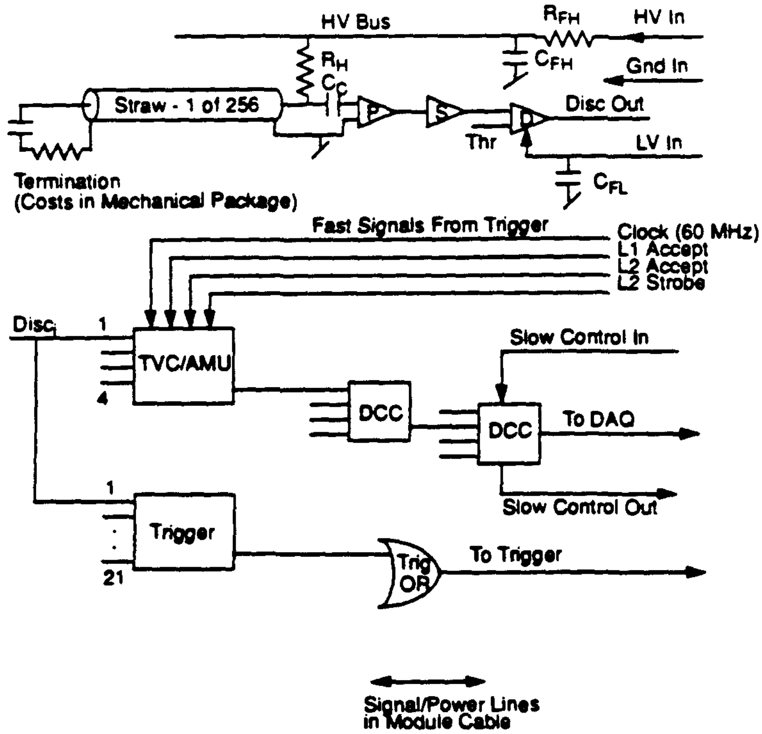

Figure 28: Block Schematic of a Straw Readout Module. Note that in this case we are describing a system with the straw anode at positive HV, it is also possible to operate the anode at ground (or near ground) potential and use a negative HV on the cathode. The negative HV scheme has some advantages in terms of the number of required HV capacitors per module but may have some disadvantages in terms of increased sensitivity to breakdown. Until further work is completed on both possibilities, we have chosen to describe the positive HV scheme both because it is somewhat more conservative and because it is, perhaps, a trifle more obvious to the reader.

speed of the discriminator output and the extreme sensitivity (a few femto-coulombs) of the input stage, coupling from input to output may be a problem in the final design. While it is possible that all three functions can be combined on a single die, to be conservative in costing and space planning we have assumed that two different die will be necessary. In any event we intend that the final configuration will have eight channels per die (with an outside possiblity of having to go down to four channels per die) and the individual die will be about 2 mm × 2 mm for the more conservative 4 channel case (this is nearly constant whether or not the discriminator is included because of input/output pad sizes).

The bipolar chip(s) will have a pin count (eight channel case) approximately as follows:

Signal (-) Inputs	8
Signal (+) Inputs	8
Ground Ref Inputs	4
Discriminator Outputs (+/-)	16
Thresholds	8
Power In	4
Power Return	4
Ground Out	4
Total	56

3.5 Time Measuring Circuit $TVC/AMU(50)$

The time to voltage conversion circuitry, analog storage, and analog to digital conversion are all contained on a single small feature size CMOS chip. If a sufficiently dense (0.5 to 0.8 μm) process can be obtained, it should be possible to pack eight channels of TVC/AMU per chip. For the purposes of this estimate, we have assumed only four channels per chip and have used preliminary quotations for radiation hard 1.2 μm processes.

The TVC/AMU will have a pin count (eight channel case) approximately as follows:

Discriminator Inputs (+/-)	16
Threshold Outputs	8
Clock Input (+/-)	2
L1 Trigger Input (+/-)	2
L2 Accept (+/-)	2
L2 Strobe (+/-)	2
L2 Strobe (+/-)	2
Resynch (+/-)	2
Reset (+/-)	2
TestTime (+/-)	2
Data Ready (+/-)	2
Grant (+/-)	2
Data Bus (+/-)	18
Slow Data In	1
Slow Clock	1
Slow Data Out	1
Slow Shift/Load	1
Slow Read/Write	1
Power In	4
Power Return	4
Total	75

3.6 Data Collection Chip $DCC(5)$

The Data Collection Chip (DCC) collects output data from a local group of TVC/AMU chips via a polling scheme and then puts data packets out to a higher level DCC (and then ultimately to some data path into the DAQ system). This tree structure continues until either all channels in a physical module are collected or the output bandwidth of the DCC is saturated. For 200 straws, a simple calculation of data rates yields the numbers shown in Table 3 which is well within the limits for the proposed DCC byte wide protocol.

Thus for 200 straws we have included four DCC chips for the first level of the tree (50 straws per DCC) and then one additional DCC on the module to serve as the top of the tree.

3.7 Trigger Formation $Trig(15)$

A fast trigger can be formed by looking for stiff (i.e. radial) tracks in any given superlayer. Jay Chapman (Michigan) has shown that a simple triplet input mean-timer circuit will work quickly enough and with great enough resolution to be interesting. While the final configuration is nowhere near certain, a possible arrangement would have 21 straw inputs per trigger chip, thus about 15 (with neighbors and overlaps) chips per module.

3.8 Low Voltage Power $C_{FL}(16)$

Low voltage DC power to the straw electronics will likely be split about ground and will require multiple analog and digital voltages. For this estimate it is sufficient to calculate the total power. At 20 mW per channel, a 200 channel module will require about 5 W or 1 A at 5 V. The 16 filter capacitors included here are arbitrary but probably close to the final number.

It is assumed in this estimate that no regulation will be done on the chamber for power reasons (low voltage linear regulators are not much more than 50 % efficient), which means that the power distribution from the regulators to the chamber must be very low impedance. The additional conductor required to maintain a low impedance connection may cause multiple scattering which would overweigh the problems associated with extra power dissipation. On the other hand both aluminum and berylium are possible and promising conductor materials and power distribution via, for instance, a berylium cable would add only very slightly to the radiation length of the tracking system. Only a detailed iteration of the design for the entire system can properly select the *best* power distribution scheme.

3.9 Cooling

The Module cooling problem is important and difficult but is not covered in any detail in this document. ORNL has completed some calculations that indicate that sufficient air flow may be introduced near the modules with a relatively small piping plant (four 1" tubes). Direct liquid cooling of the modules is possible but would introduce significant mechanical and reliability problems. More work is needed to clarify this problem.

4 Cable - Module to Crate

The cable(s) connecting the straw module with the outside world must provide:

- Power input and return
- Fast control signals in
- Slow control signals in and out
- Fast Trigger signals out

- Data out

The number and size of the power conductors are determined by the load and allowed voltage drop. The logical signals in and out of the module could be carried by optical fiber or copper conductors and copper could be either single ended or differential. Because the mass (and multiple scattering) is dominated entirely by the power cabling, the extra complexity of fibers is not attractive for any of the signal groups.

4.0.1 Optical vs. Electrical Transmission

From a pickup point of view the inherently single ended drive for fiber transmitters (unless one wished to provide a dummy transmitter to keep the currents differential) is far worse than a differential copper transmitter or a slow rise time single ended driver. From a power point of view there is nearly a factor of ten increase in transmission power required for optical rather than direct coupling just from the electro-optical conversion processes. In addition, optical receivers tend to require somewhat more power than equivalent bandwidth copper receivers unless the launched optical power is very large. Optical modulators may provide a mechanism for removing almost all of the power dissipation from the tracking region and successful demonstration of such devices may change the power part of the decision. The additional complexity of technologies and physical connections associated with optical techniques is unlikely to disappear.

4.1 Power Transmission

To provide power to a module a cable 50 mm wide with $50\mu m$ of copper would give a voltage drop of 45 mV over 3 m and 90 mV for a 6 m length for a 1 A current at 5V. This voltage drop is probably near the limit of what would be acceptable, so a full 50 mm by $50\mu m$ Cu foil mounted on thin Kapton or other flexible substrate has been assumed. This laminate would be insulated on the outside with a very thin layer of the same insulator. It is possible to imagine using aluminum or berylium rather than copper to decrease the effect of multiple scattering and conversions, but the increased difficulty of connection may make this option unattractive. So, again for reasons of conservativism, we will estimate using copper.

4.2 Number of Conductors

The logical signals for control of the module and for trigger and data output could be accomodated on the obverse side of the flat power cable described above. If all of the fast signals are differential (a *worst* case design) then the number of conductors will be approximately as described in Table 2.

If we assume that normal growth will take the 41 total above to 50 conductors, and assume that very conservative design rules of 0.5 mm conductor, 0.5 mm space are used for the signals, then our 50 conductors fit nicely onto the 50 mm wide power cable described above. Since some cable manufacturers (cf. Hughes) are capable of building cables a factor of ten denser than these estimates, there should be plenty of room for even explosive expansion in the number of conductors (not that we wish to advocate such growth), certainly enough to include extra ground conductors to allow very conservative differential transmission lines made with gnd, sig+, sig-, gnd configurations.

The other class of signals not covered in Table 2 are the fast trigger outputs. The number of signals in this category depends upon the resolution needed in matching tracking and calorimeter information. At the outer radius of the central tracker, the straw module occupies about 10 cm of circumference and if 1 cm resolution in the calorimeter is desired, then about ten fast trigger output signals need to be transfered - an additional 20 conductors. At the inner radius the angular spread is about three times as great so that as many as sixty conductors might be necessary. If trigger outputs are needed from the inner super layers, a slightly more aggressive cable technology would be required.

Signal	Conductors
Timing and Control	
Clock	2
L1 Accept	2
L2 Accept	2
L2 Strobe	2
Resynch	2
Reset	2
TestTime	2
Total T & C	14
Data Path	
Data Ready	2
Grant	2
Data Bus	18
Total Data	22
Slow Control	
Data In	1
Clock	1
Data Out	1
Shift/Load	1
Read/Write	1
Total Slow Control	5
Grand Total	**41**

Table 2: Signal count for the Module Output DCC to upstream connections. Note that the DAQ path is assumed to be Byte wide (with parity), but other path widths are possible and an optimization remains to be carried out.

5 Packaging

While there are multiple possibilities for fitting the electronics on the end of the straw modules, a system with all of the electronics mounted on a plane perpendicular to the long axis of the straw would allow all of the interconnections to be made in one plane and avoid the problems (reliability, material, and complexity) associated with mother board / daughter board schemes. However, we are attempting to fit rather a lot of functionality [2] in this area and it is useful to crudely calculate whether the density required is even feasible.

The ends of the straws themselves, for 200 straws in a module, occupy an area of $30mm \times 120mm$ for a total of $3,600mm^2$ and the area between super layers will offer at least an area of $60mm \times 120mm$ for a grand total of about $11,000mm^2$.

However, the total area required by active silicon is not small and must be considered. Using the estimates above, we see that we need the following pieces of silicon:

Active Electronics - Silicon

Chip	Ch/Chip	Chip/Mod	Size mm	Tot. Area mm^2
Bipolar - P/A	4	50	2×2	250
Bipolar - Disc	4	50	2×2	250
CMOS - TVC	4	50	6×6	2,300
Trig	21	15	6×6	550
DCC		5	8×8	350
Total				3,700

This is about 34 % active silicon. For comparison, 50 mil pitch chip carriers are 1.5 % active silicon and even large pin grid array packages (PGA) are only about 9 % silicon.

The saving grace is an emerging set of thin film technologies using IC class lithography on silicon, quartz, or ceramic substrates and polymer dielectrics. These thin film technologies have many different proprietary names and parameters, but concentrate on providing multi-chip packaging and are capable of reaching packing densities of from 30 to over 50 % depending upon the die to substrate bonding technology. In even the least exotic form with wire bonding from die to substrate, densities are around 30 % and flip chip or tab bonding offers significant additional improvements. Figure 29 shows a cartoon version of the module and cable system with active silicon area indicated by shaded blocks.

5.1 High Voltage Capacitors and Resistors

The high voltage sections of the module, of course, would not fit well into a multichip module approach and will require a separate substrate (either ceramic or plastic laminate). The HV substrate is the obvious place to have the first level interconnects from the straw anode and cathodes. The connections to the straws ought to be removable, if possible, and pin and socket, spring loaded pins to pads, and elastomeric pad to pad connectors are all possibilities. Considerable work has gone into defining this area at both Colorado (Figure 30) and ORNL and we will not go into any further details here.

The HV capacitors are a possible nuisance since they are both physically large ($\sim 3mm \times 3mm \times 2mm$) and, in some cases, composed of high Z materials.

The materials question must be addressed by a relatively extensive R&D effort to find the best materials and manufacturers, but the physical size can be accomodated at both the readout and termination ends by stacking the capacitors between two substrates with one substrate carrying the anode and cathode connections and the other carrying the HV bus and the printed decoupling resistor, R_H, on one side

[2] It might be noted that one of tese 10 × 12 cm modules is the equivalent of 25 eight channel preamp cards, 3+ amplifier shaper discriminator boards, 2+ fastbus TDC cards, and about fifty miles of Ansley cable - all operating at about 200 times the speed of present collider systems.

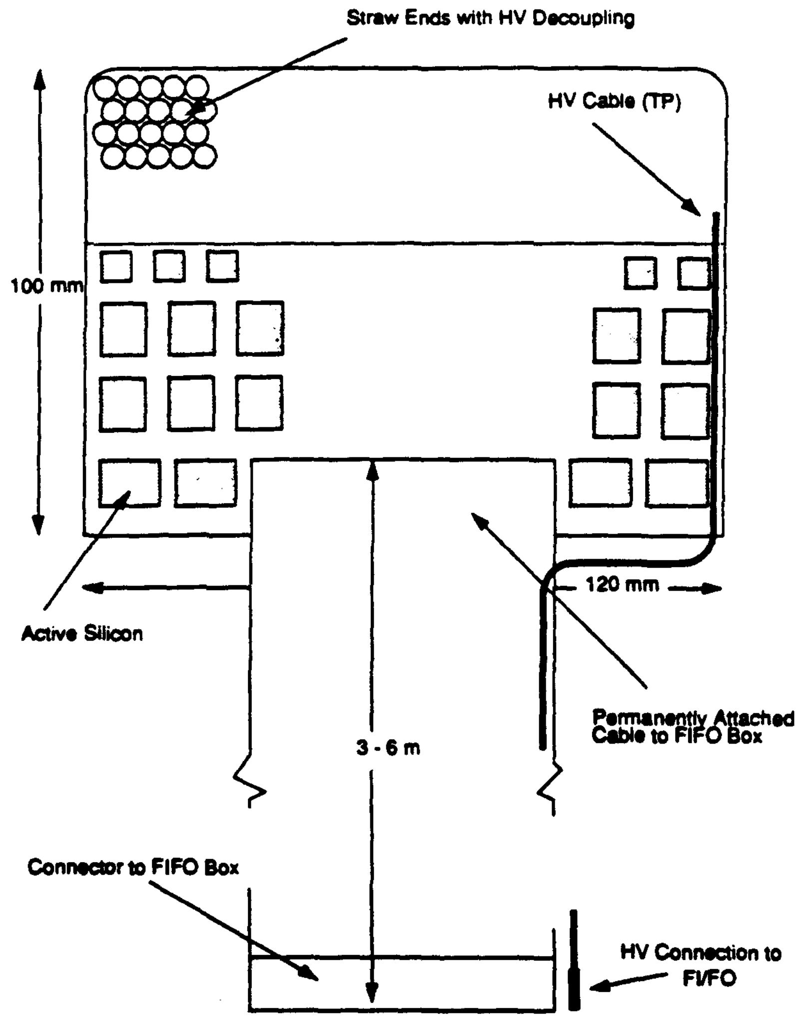

Figure 29: Approximate layout of the electronics module and attached cable.

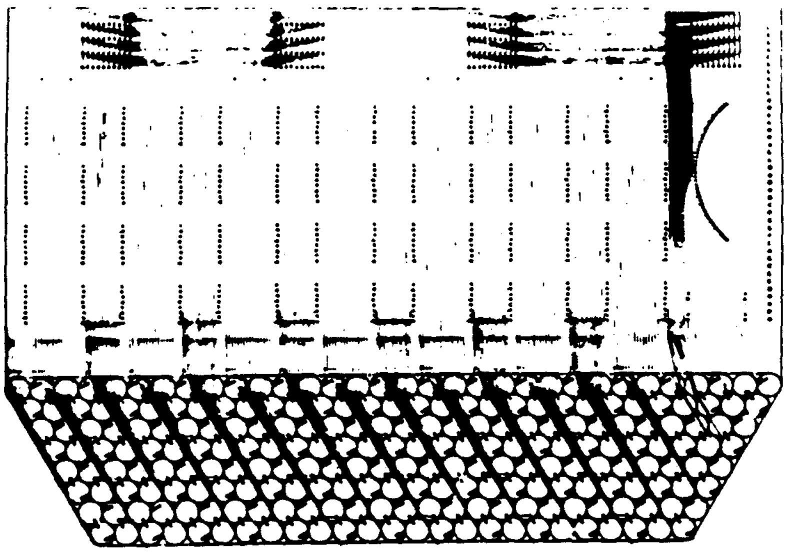

Figure 30: Placement and Layout Study for a 256 channel Module - E. Erdos, University of Colorado.

and connections to the active electronics on the other side of the substrate. The connection between the second HV substrate and the active substrate could be either permanent or removable as desired. At the termination end the active terminators could be supported on the HV substrate so no additional substrate is included in the cost or material estimate.

6 Interconnection

As is obvious from the above, interconnection technologies will play an important part in determining the final functionality of the straw readout system (as well as for other types of detectors) and a significant effort must begin immediately to qualify and develop commercial vendors of various advanced packaging technologies.

We can not attempt to cover all of the possibilities in this note, but we will describe below the basic technolgy that we are assuming for the purposes of making this cost and material estimate.

6.1 HV Substrate to Active Substrate

For simplicity we are assuming that the HV substrates form a rigid beam (separated by the HV capacitors) and that the active substrate is assembled (after separate qualification testing) to the HV assembly via a permanent soldered (or epoxied) connection or possibly an elastomeric disconnect. The part of the HV substrate in the inter super layer gap is available for low voltage decoupling networks, HV filtering, and attachment of cables – HV and the combined LV / Data cable described above.

6.2 Chip to Substrate

Chip to active substrate connections will be either wire bonds or, more likely, tab bonds (photo-lithographically produced frames carrying all of the connections to a given chip and attached via indium or gold solder bumps to both the chip and substrate pads), or full flip chip connections (where the chip is inverted and gold or indium bumps are used directly to attach the chip pads to the substrate pads). The choices are governed by density, cost, and reliability considerations (the list above is ordered by both increasing density and increasing cost - in a low volume application such as ours). [3]

6.3 Substrate to Cable

In order to keep the mass and complexity at a minimum, we are assuming that the LV / Signal cable is permanently attached to the straw electronics module and disconnects only at the Crate end. While there are a variety of possibilities for connecting the cable to the electronics module, we are assuming a very simple standard soldered connection for both the wide voltage supply connections and the multiple signal connections. There would, however, need to be some sort of sizable strain relief to prevent accidental tearing of the connections.

6.4 Cable to Crate

The cable must disconnect at the Crate in order to allow construction of the system, but the Crate is, by definition, in a relatively high density part of the detector and so any commercial connector technology (consistent with the cable design) would be appropriate. Even a standard $0.1in \times 0.1in$ pin and socket connector would have high enough density and power handling capabilities. It is also probable that an intermediate disconnect may have to be provided at about the radius of the Coil in order to facilitate replacement and maintenance of the Straw Modules. This disconnect would also use standard connector technologies.

7 Crate Level Electronics

In order to keep the material at the ends of the straws at a minimum and in order to avoid many cross connections from module to module, we have placed a minimum set of electronics and connections at the detector end. The connection to the *outside* world is via a single low mass flexible cable. In order, however, to provide reasonable power to the electronics on the detector and in order to collect signals from the detector to go to the trigger and DAQ systems the cable from the straw module must terminate fairly close to the central tracking volume. From a power point of view a cable longer than about 6 m would require local regulation at the module – increasing the cooling and density problems somewhat. From a signal transmission point of view, the differential signals should retain their integrity over distances up to 20 or 30 m. For this estimate we have assumed no local power regulation on the straw electronics module and a 3 to 6 m cable length to the Crate which would provide power regulation and conditioning.

The crate to module interface board must provide not only power but also buffer all of the signal lines in and out and provide the translation from the crate standard signal voltages to the module standards (probably low level differential) as well as the logical translation to the appropriate DAQ and Trigger formats. We estimate that 8 modules would fit reasonably on a single SDC standard 9U board - the associated logic and power conditioning should not be very dense and the total power level per board is likely to be high (60+ W) but bearable.

The entire system may either be housed in a small number of dedicated crates (four per end for a 130,000 straw system) or could be spread out in the calorimeter/shower max counter crates. There are

[3] To still the immediate reaction, high volume in the semiconductor world starts at roughly 10^6 to 10^7 identical objects - our 10^5 or 10^6 channels are getting packaged many per chip. The SSC has interesting volumes for many of the smaller (especially Rad Hard) operations, but it is nowhere near *high* volume.

advantages and costs to both arrangements in terms of detector integration, data and trigger flow, and physical installation. Two different schemes are shown in Figure 31 and Figure 32.

7.1 Inputs

The Crate Interface Card connects to cables from about 16 straw modules - in the first version that we are imagining here each Crate Interface Card handles half a wedge of the central detector for ease of trigger formation. It is possible that reliability concerns would dominate and a single Crate Interface Card would serve some more complex section of the tracker, but for simplicity we will assume a wedge based arrangement going from one module at the inner super layer to about three modules at the outer layer as shown in Fig 31.

7.2 Trigger Collection

Fast trigger signals from the modules indicate *stiff* tracks in some given angular region which is matched to the calorimeter and muon system resolution. If it is desired to use more than the outer super layer for triggering at Level 1 or 2, then signals from different super layers must be compared to see whether or not a *linked* track can be found to extrapolate toward the calorimeter. While it is possible to imagine doing segment linking directly in the Crate, the desire to have as much of the Trigger formation electronics as possible readily available probably implies that the found segments are simply forwarded by the Crate Interface Card to the standard SDC Trigger Interface Card.

7.3 Trigger Left/Right Connection

Because even stiff tracks will have some curvature and because the modules will not break at the same ϕ position at each super layer, it may be necessary to interchange signals from the outer edges of each super layer with the Crate to the left or right of the present Crate. Given that the Crate is in a relatively high density (of detector) area and that the number of signals needed per edge module is at most two or three, this extra connection should add little to the system cost. A single thirty signal (60 conductor) cable between adjacent Crates should suffice. In the case of dedicated tracking Crates, so much of the solid angle would be in a single Crate that it might well make sense to ignore the *lost* region between Crates.

7.4 Data Collection

The load imposed by the Straw Tracker on the DAQ system depends somewhat upon the organization chosen - interspersed with Calorimetry or dedicated, but Table 3 gives an approximate idea of the rates out of a module, a wedge based Crate, and an entire Straw Tracker.

7.5 Power Distribution

For the purposes of this estimate we have assumed that there is good local regulation of power at the Crate and that this power is then distributed to the individual modules via the module cables. Power input to the Crate comes from standard supplies. The Crate Interface Cards are also a consumers of power – we have assumed that there is as much power dissipated at the Crate as at all the modules which it serves, for lack of detailed designs for the internal components. Sixteen modules at five to seven Watts apiece would yield 80 to 110 Watts for a total input power of 160 to 220 Watts plus 25% for regulation and distribution drops, giving a total power demand for the system of 200 to 280 W.

7.6 Trigger and DAQ Interconnections

The system uses the SDC standard DAQ and Trigger interface cards - either one each per dedicated Crate or shared with the Calorimeter system. All of the clock and Trigger control lines are fanned out

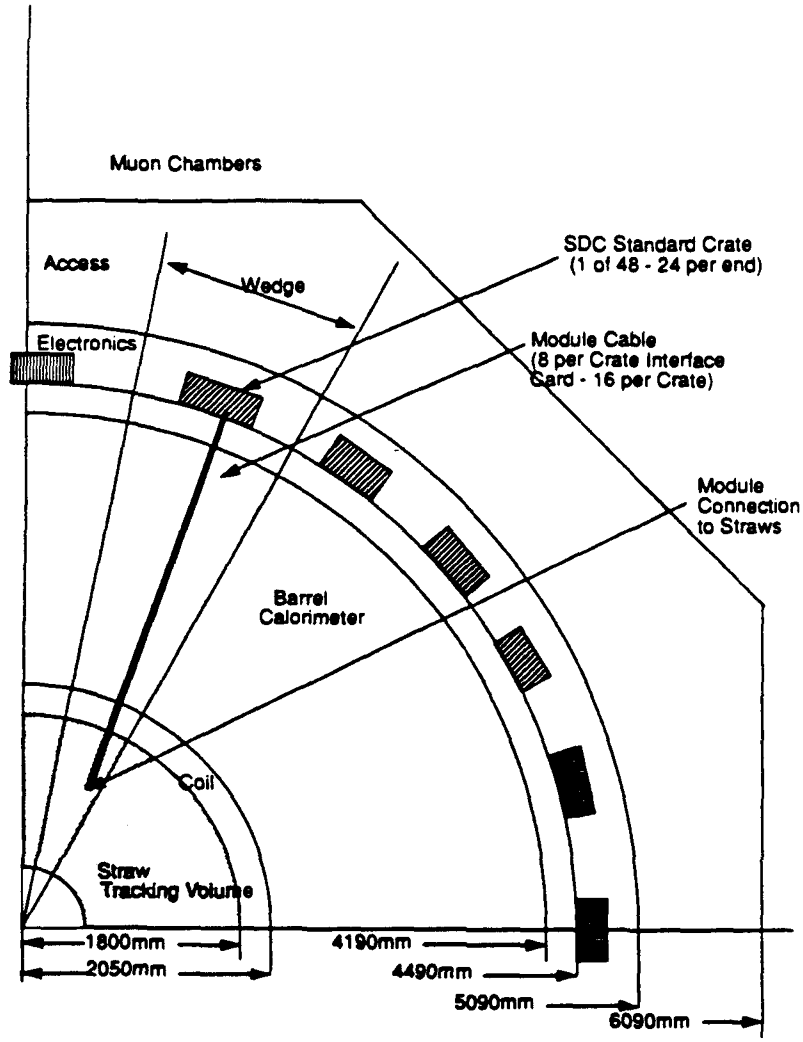

Figure 31: Module and Crate physical placement on the detector - interspersed version. In this version the Straw Crate Interface Cards are inserted in the same crates used by the Calorimeter and Shower Max detectors - one per wedge.

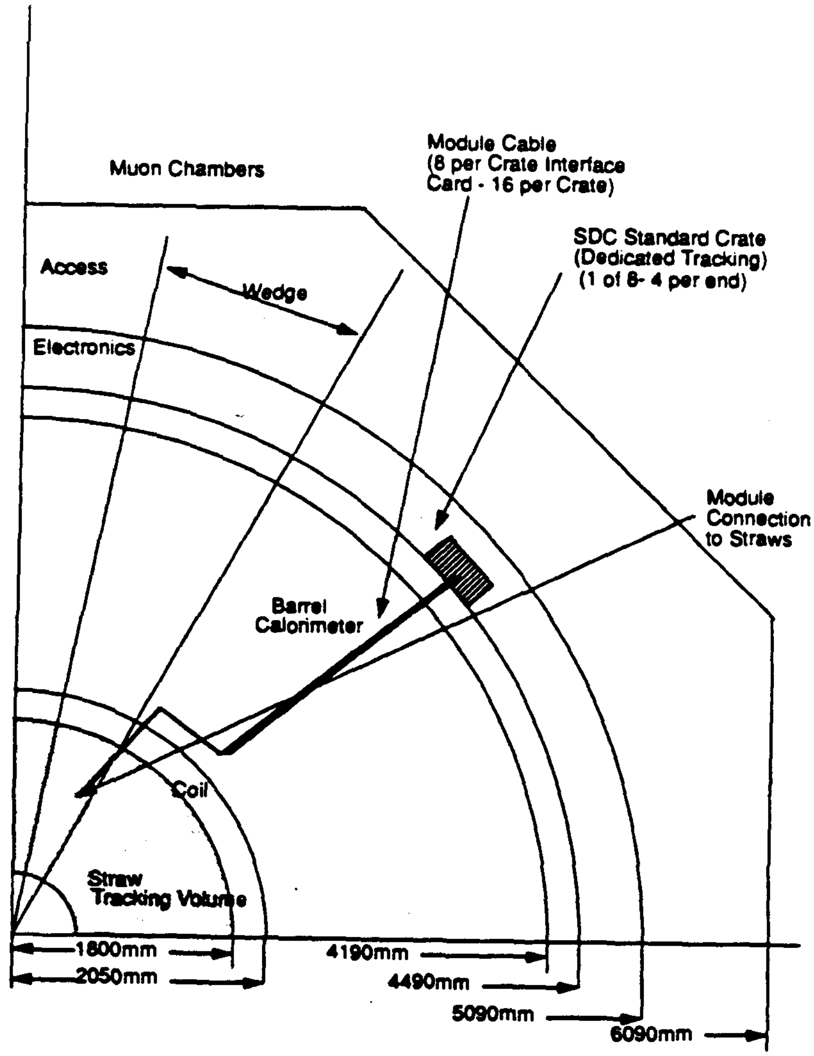

Figure 32: Module and Crate physical placement on the detector - dedicated Crate version. The assumed granularity of 8 modules per Crate Interface Card implies 8 dedicated Tracking Crates for a 130,000 straw detector - 4 Crates per each end of the barrel calorimeter.

Module Level Data Packet		
Header + Flags	6 bits (?)	
Physical Address	1 Byte	
L1 Trigger I.D.	1 Byte	
Bunch Counter	2 bits	
Fine Time	7 bits	
Total per hit	4 Bytes	1.4×10^6 Bytes per second

Crate Level Data Packet		
Header + Flags	10 bits (?)	
Module Address	4 bits	
Physical Address	1 Byte	
L1 Trigger I.D.	1 Byte	
Bunch Counter	2 bits	
Fine Time	7 bits	
Total per hit	5 Bytes	2.5×10^7 Bytes per second

Straw System Level Data Packet		
Header + Flags	10 bits (?)	
Crate Address	6 bits (?)	
Module Address	4 bits	
Physical Address	1 Byte	
L1 Trigger I.D.	1 Byte	
Bunch Counter	2 bits	
Fine Time	7 bits	
Total per hit	6 Bytes	1.4×10^9 Bytes per second

Table 3: Data Formats and Rates for the Straw Tracker System. These estimates are based upon a 60 MHz crossing rate, a very conservative 10% occupancy per crossing with a three crossing overlap and a 10,000:1 $L1 \times L2$ rejection. The system has 135,000 straws with 200 per module, 14 modules per Crate (wedge), and 48 Crates for the entire system.

SDC Straw Tracker

TVC Option | **135,000 Straws**
8/15/91 RVB | **192 Trigger Modules of 260 Straws Each**
480 Axial Modules of 175 Straws Each

WBS	Task Name	Start Date	End Date	Duratn (Days)	Effort (Days)	Total $ (EAC)
5,1,2	Straw Tracker	1-Oct-92	2-Jul-99	1,694	7,422	$8,462,577.48
5,1,2.1	Electronics Design Document	1-Oct-92	21-Jan-93	75	75	$31,638.00
5,1,2.2	Prototype Electronics	16-Oct-92	26-Apr-95	632	3,056	$1,876,066.54
5,1,2.2.1	Front End	16-Oct-92	10-Nov-94	519	1,497	$1,074,511.32
5,1,2.2.1.1	High Voltage Dist. on Modules	16-Oct-92	27-Apr-93	132	87	$73,701.56
5,1,2.2.1.1.1	Capacitors and Resistors	16-Oct-92	9-Nov-92	17	5	$3,500.00
5,1,2.2.1.1.2	At Anode HV Substrate	6-Jan-93	27-Apr-93	78	35	$26,607.56
5,1,2.2.1.1.3	Second HV Substrate	9-Nov-92	19-Mar-93	88	35	$29,746.00
5,1,2.2.1.1.4	Anode Connection	16-Oct-92	9-Nov-92	17	5	$5,603.33
5,1,2.2.1.1.5	Cathode Connection	16-Oct-92	19-Nov-92	23	7	$8,244.67
5,1,2.2.1.2	Active Components	16-Oct-92	7-Jul-94	431	922	$683,960.66
5,1,2.2.1.2.1	Preamplifier/Shaper	16-Oct-92	3-Nov-93	263	100	$113,963.16
5,1,2.2.1.2.2	Discriminator	6-May-93	14-Feb-94	193	110	$104,213.33
5,1,2.2.1.2.3	TVC/AMU	11-Jun-93	10-May-94	227	525	$299,209.09
5,1,2.2.1.2.4	DCC	11-Jan-94	7-Jul-94	123	160	$116,503.08
5,1,2.2.1.2.5	Trigger	11-May-93	10-May-94	250	0	$0.00
5,1,2.2.1.2.6	Passive Components	16-Oct-92	14-Apr-93	123	27	$15,072.00
5,1,2.2.1.3	Active Substrate	16-Oct-92	16-May-94	396	338	$225,477.37
5,1,2.2.1.3.1	Substrate	16-Oct-92	24-Aug-93	214	210	$131,011.43
5,1,2.2.1.3.2	Mounting	7-May-93	18-Aug-93	72	43	$17,984.07
5,1,2.2.1.3.3	Bonding	3-Nov-93	16-May-94	133	85	$66,481.88
5,1,2.2.1.4	Test of Module(s)	22-Mar-94	10-Nov-94	163	150	$91,371.74
5,1,2.2.2	Cable - Module to Crate	16-Oct-92	18-Aug-94	462	348	$203,930.16
5,1,2.2.2.1	Cable	16-Oct-92	8-Nov-93	267	200	$114,192.00
5,1,2.2.2.2	Connector (Crate end)	1-Dec-92	22-Mar-93	76	28	$17,627.16
5,1,2.2.2.3	Assy to Module	24-Aug-93	13-Dec-93	75	60	$35,779.00
5,1,2.2.2.4	Test of Cable Assy	29-Sep-93	18-Aug-94	222	60	$36,332.00
5,1,2.2.3	Crate	16-Oct-92	18-Aug-94	461	600	$314,246.28
5,1,2.2.3.1	Crate Mechanics	16-Oct-92	30-Mar-93	111	70	$29,142.22
5,1,2.2.3.2	Backplane	30-Mar-93	4-Oct-93	131	180	$80,390.07
5,1,2.2.3.3	Module Interface Card	26-Aug-93	18-Aug-94	245	350	$144,713.99
5,1,2.2.3.4	DAQ Interface	17-Jun-93	4-May-94	220	0	$0.00
5,1,2.2.3.5	Slow Interface - part of DAQ	17-Jun-93	4-May-94	220	0	$0.00
5,1,2.2.3.6	Crate Cooling	9-Aug-93	27-Apr-94	179	0	$0.00

WBS	Task Name	Start Date	End Date	Duratn (Days)	Effort (Days)	Total $ (EAC)
5,1,2.2.4	Low Voltage Power	16-Oct-92	4-Apr-94	366	110	$56,882.85
5,1,2.2.4.1	Regulators - 300W -DC or 400H	16-Oct-92	9-Aug-93	204	55	$32,251.11
5,1,2.2.4.2	Cabling Within Crate	17-Jun-93	24-Sep-93	69	27	$14,042.65
5,1,2.2.4.3	Cabling on Detector	30-Mar-93	4-Apr-94	255	28	$10,589.09
5,1,2.2.5	High Voltage Power	16-Oct-92	17-Aug-94	461	76	$36,193.76
5,1,2.2.5.1	HV Regulator	16-Oct-92	3-Nov-93	264	0	$0.00
5,1,2.2.5.2	Cabling - Module to Crate	3-May-94	17-Aug-94	75	38	$18,009.41
5,1,2.2.5.3	Cabling - Crate to Regulator	4-Nov-93	8-Mar-94	83	38	$18,184.35
5,1,2.2.6	System Level Tests	24-May-94	26-Apr-95	231	425	$190,302.17
5,1,2.3	Production Electronics	27-Apr-93	18-Jun-99	1,542	3,275	$6,164,033.25
5,1,2.3.1	Front End	27-Apr-93	27-May-98	1,274	1,720	$4,374,874.57
5,1,2.3.1.1	HV Dist. - Trigger Modules	27-Apr-93	22-Mar-94	225	200	$341,281.33
5,1,2.3.1.1.1	Capacitors and Resistors	27-Apr-93	12-Aug-93	75	0	$156,600.00
5,1,2.3.1.1.2	At Anode HV Substrate	1-Dec-93	22-Mar-94	75	0	$53,000.00
5,1,2.3.1.1.3	Second HV Substrate	12-Aug-93	1-Dec-93	75	0	$53,000.00
5,1,2.3.1.1.4	Anode Connection	27-Apr-93	8-Jul-93	50	0	$5,800.00
5,1,2.3.1.1.5	Cathode Connection	27-Apr-93	8-Jul-93	50	0	$5,300.00
5,1,2.3.1.1.6	Assembly of Modules	27-Apr-93	18-Mar-94	222	200	$81,581.33
5,1,2.3.1.2	HV Dist. - Axial Modules	27-Apr-93	2-Jun-94	275	300	$625,020.92
5,1,2.3.1.2.1	Capacitors and Resistors	27-Apr-93	12-Aug-93	75	0	$248,400.00
5,1,2.3.1.2.2	At Anode HV Substrate	1-Dec-93	22-Mar-94	75	0	$132,500.00
5,1,2.3.1.2.3	Second HV Substrate	12-Aug-93	1-Dec-93	75	0	$132,500.00
5,1,2.3.1.2.4	Anode Connection	27-Apr-93	12-Aug-93	75	0	$9,200.00
5,1,2.3.1.2.5	Cathode Connection	27-Apr-93	12-Aug-93	75	0	$9,200.00
5,1,2.3.1.2.6	Assembly of Modules	27-Apr-93	2-Jun-94	275	300	$115,220.92
5,1,2.3.1.3	HV Production Test	2-Jun-94	17-Feb-95	179	200	$61,414.29
5,1,2.3.1.4	Active Components	10-May-94	26-Nov-96	640	0	$1,629,720.00
5,1,2.3.1.4.1	Preamplifier/Shaper	7-Jul-94	13-Feb-95	150	0	$405,000.00
5,1,2.3.1.4.2	Discriminator	13-Feb-95	15-Sep-95	150	0	$405,000.00
5,1,2.3.1.4.3	TVC/AMU	15-Sep-95	23-Apr-96	150	0	$630,000.00
5,1,2.3.1.4.4	DCC	23-Apr-96	26-Nov-96	150	0	$148,272.00
5,1,2.3.1.4.5	Trigger	15-Sep-95	26-Nov-96	300	0	$86,000.00
5,1,2.3.1.4.6	Passive Components	10-May-94	21-Jul-94	50	0	$15,000.00
5,1,2.3.1.5	Active Substrate Trigger	17-May-94	31-May-95	260	200	$473,683.08
5,1,2.3.1.5.1	Substrate	17-May-94	20-Dec-94	150	0	$227,000.00
5,1,2.3.1.5.2	Mounting	21-Dec-94	10-Apr-95	75	0	$42,400.00
5,1,2.3.1.5.3	Bonding	13-Feb-95	31-May-95	75	0	$128,000.00
5,1,2.3.1.5.4	Assembly of Module	17-May-94	27-Dec-94	154	200	$66,283.08

WBS	Task Name	Start Date	End Date	Duratn (Days)	Effort (Days)	Total $ (EAC)
5,1,2,3.1.6	Active Substrate-Axial	17-May-94	10-May-95	246	320	$1,072,332.92
5,1,2,3.1.6.1	Substrate	17-May-94	20-Dec-94	150	0	$545,000.00
5,1,2,3.1.6.2	Mounting	21-Dec-94	10-Apr-95	75	0	$106,000.00
5,1,2,3.1.6.3	Bonding	21-Dec-94	10-Apr-95	75	0	$305,280.00
5,1,2,3.1.6.4	Assembly of Module	17-May-94	10-May-95	246	320	$106,052.92
5,1,2,3.1.7	Test of Module(s)	26-Nov-96	13-Feb-98	304	350	$138,328.70
5,1,2,3.1.8	Test of Cable/Module Assy	24-Sep-97	27-May-98	167	150	$33,093.33
5,1,2,3.2	Cable - Module to Crate	18-Aug-94	11-Apr-96	412	275	$649,840.91
5,1,2,3.2.1	Cable	18-Aug-94	13-Jan-95	100	10	$565,500.00
5,1,2,3.2.2	Connector (Crate end)	13-Jan-95	28-Mar-95	50	5	$16,500.00
5,1,2,3.2.3	Assy to Module	21-Dec-94	15-May-95	100	10	$33,750.00
5,1,2,3.2.4	Test of Cable Assy	16-May-95	11-Apr-96	227	250	$34,090.91
5,1,2,3.3	Crate	18-Aug-94	28-May-97	695	0	$596,300.00
5,1,2,3.3.1	Crate Mechanics	18-Aug-94	17-Oct-94	40	0	$16,000.00
5,1,2,3.3.2	Backplane	17-Oct-94	18-Apr-95	125	0	$48,000.00
5,1,2,3.3.3	Module Interface Card	26-Nov-96	28-May-97	125	0	$537,500.00
5,1,2,3.3.4	DAQ Interface	18-Apr-95	16-Oct-95	125	0	$0.00
5,1,2,3.3.5	Slow Interface - part of DAQ	18-Apr-95	16-Oct-95	125	0	$0.00
5,1,2,3.3.6	Crate Cooling	18-Aug-94	28-Mar-95	150	0	$19,200.00
5,1,2,3.4	Low Voltage Power	4-Apr-94	19-Oct-95	389	128	$84,800.00
5,1,2,3.4.1	Regulators - 300W -DC or 400H	4-Apr-94	28-Jun-94	60	0	$38,400.00
5,1,2,3.4.2	Cabling Within Crate	18-Apr-95	19-Oct-95	128	64	$22,200.00
5,1,2,3.4.3	Cabling on Detector	17-Oct-94	21-Apr-95	128	64	$24,200.00
5,1,2,3.5	High Voltage Power	18-Aug-94	11-Oct-96	540	102	$87,600.00
5,1,2,3.5.1	HV Regulator	18-Aug-94	17-Feb-95	125	0	$0.00
5,1,2,3.5.2	Cabling - Module to Crate	11-Apr-96	11-Oct-96	128	64	$44,200.00
5,1,2,3.5.3	Cabling - Crate to Regulator	21-Feb-95	7-Jun-95	76	38	$43,400.00
5,1,2,3.6	Crate Tests	28-May-97	27-May-98	250	250	$61,830.00
5,1,2,3.7	System Level Tests	27-May-98	14-Dec-98	139	500	$220,227.78
5,1,2,3.8	Assembly to Detector	15-Dec-98	9-Feb-99	38	150	$31,500.00
5,1,2,3.9	Full Detector Tests	9-Feb-99	26-May-99	75	150	$57,060.00
5,1,2,3.10	Commissioning	21-Jun-99	21-Jun-99	0	0	$0.00
5,1,2,4	Project Management	1-Oct-92	2-Jul-99	1,694	1,016	$390,839.68

Note that dollar and effort totals include all of the subsidiary task costs.

Conceptual Design of Straw Tube Readout with TMC

Version 1.0
Aug. 21, 1991

Yasuo Arai, Hirokazu Ikeda and Yoshiyuki Watase
KEK, National Lab. for High energy Physics

Executive Summary

This document is a conceptual design report of the readout system for the straw tubes of the central SDC tracking system. The proposed system is based on the TMC (Time Memory Cell); a VLSI time digitizer newly developed in order to meet the specific requirements imposed by the SSC experiments. A prototype 4 channel TMC chip with 1μs deep pipeline memory (TMC1004) has been successfully developed at KEK using NTT 0.8μm CMOS technology. The prototype has demonstrated the feasibility of the basic concept as well as the following performance;

time resolution	$\sigma = 0.52$ ns
power consumption	7 mW/channel (1% readout duty factor).

Amp/Shaper and Discriminator chips have also been developed at KEK using NTT bipolar process known as Super Selfaligned Transistor (SST). Prototype chips are successfully tested and used for straw-tube readout.

The present report describes the architecture of the readout system that can be accommodated physically with the current SDC detector design. The final TMC chip with the memory capability of 4μs for the level-1 trigger is proposed. The proposed readout system for the case of the 130K straw tracker is

Amp/Shaper/Discriminator chip	4ch/chip
TMC chip	4ch/chip
TMC level 2 Buffer chip	4 ch/chip
Hybrid IC	8 ch/hybrid
Data Collection Chips	256 ch/unit
Front End Board (FEB)	256 ch/board
Multi Data Buffer (MDB)	1024 ch/module
Local Buffer Crate	8 crates x 2 sides.

The data transfer rate is examined to be reasonably practical with the present-day technology. An initial attempt of the cost breakdown showed approximately $8.7M for the total readout system. Radiation damage study is under way. The preliminary analysis has indicated promising results.

In conclusion, we have successfully developed the prototype preamp/shaper, discriminator, and TMC chips. The proposed readout system meets almost all the SDC requirements with few critical paths left.

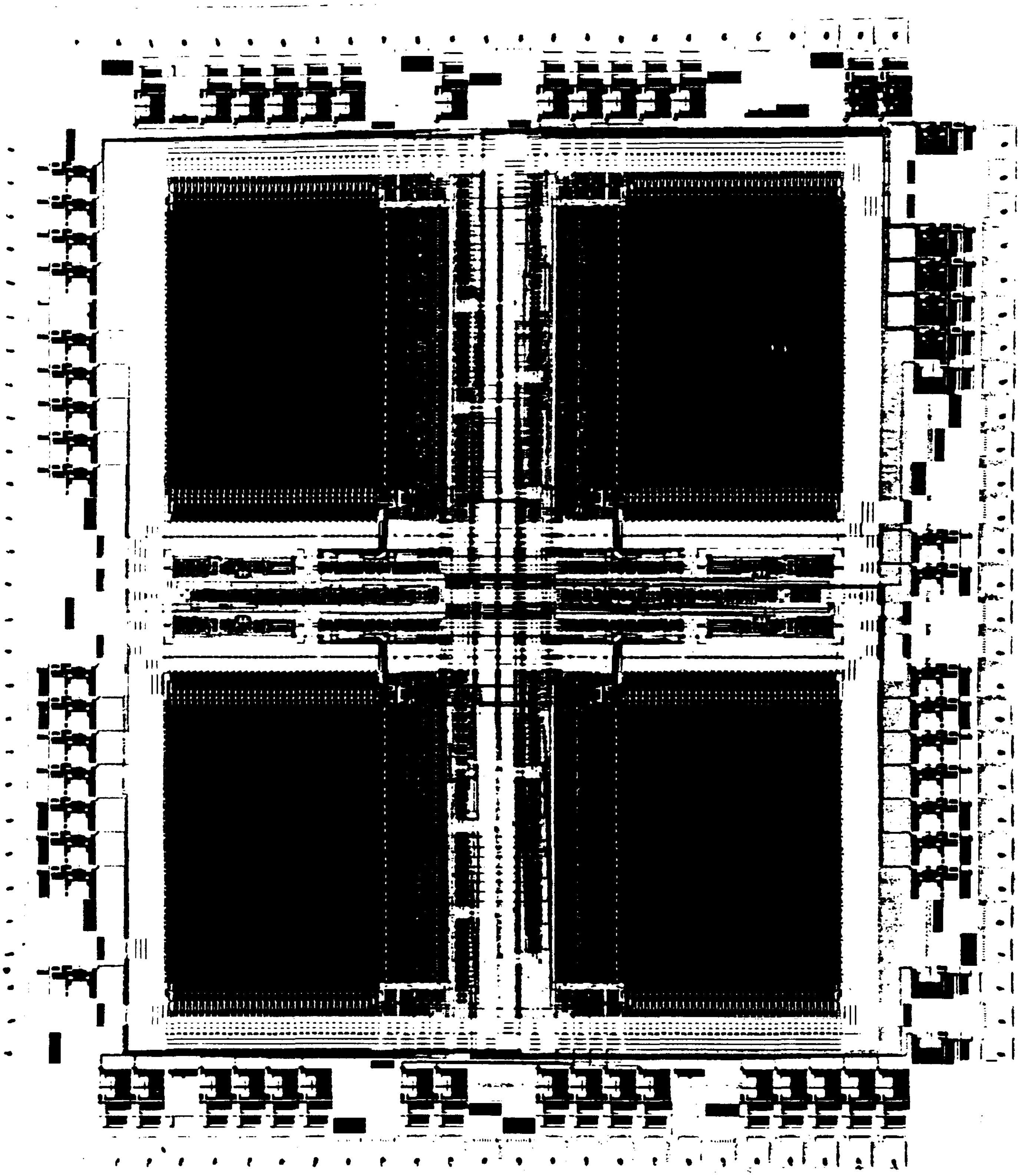

Photograph 1. TMC1004 chip

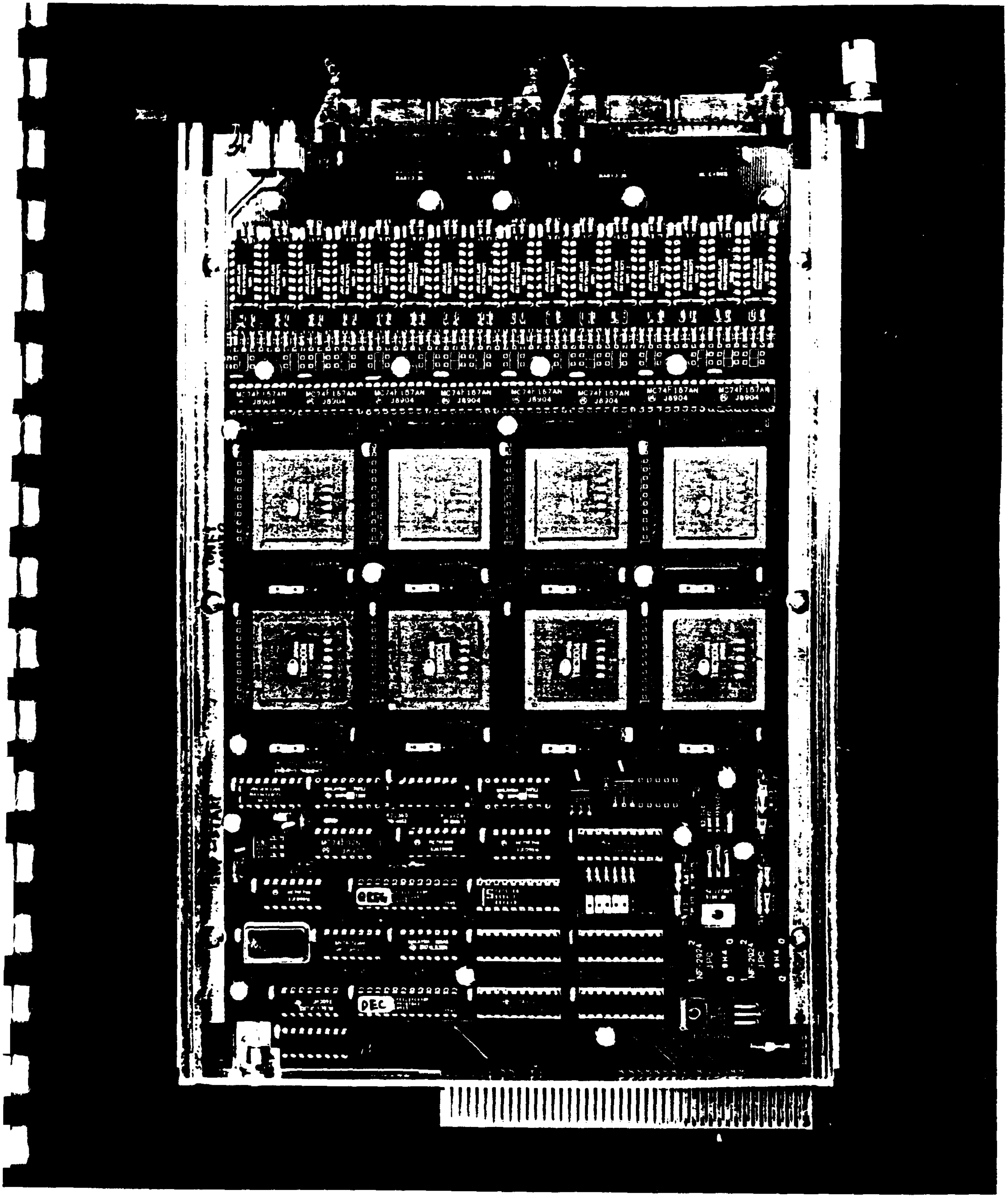

Photograph 2. CAMAC 32 ch TDC module using the TMC chip

Contents

[abbreviations]

ASIC : Application Specific IC
CSR : Control and Status Register
DCC : Data Collection Chip
DTX : Data Transmission module
FEB : Front-End Board
KEK : Kou Energy Kenkyuusho, National Lab. for HEP
LBC : Local Buffer Crate
L2B : Level 2 Buffer chip
MDB : Multi Data Buffer
NTT : Nippon Telephone and Telegram Co.
P/S/D : Preamp/Shaper/Discriminator chip
P.S. : Power Supply
SCP : Superlayer Control Processor
SDC : Solenoidal Detector Collaboration
SST : Super Selfaligned Transistor
TMC : Time Memory Cell

---

1. Introduction

We describe here a conceptual design of the readout electronics for the Straw-tube Detector. Our scheme is based on the Time Memory Cell (TMC) chip (photograph 1) which is developed at KEK with collaboration of NTT. The TMC chip is a low-power and high-density time-to-digital conversion VLSI which has enough ability for the wire chamber readout at the SSC. The prototype chip is already tested and a CAMAC module (photograph 2) which use 8 TMC chips are used for straw-tube readout [1,2,3].

In this document, we try to optimize the readout scheme to the TMC, but most of the parts except the preamp/shaper/discriminator and the TMC chips are very primitive stage. There remain many places which must be adjusted in a whole data acquisition system. There are many intensive studies for the Straw electronics by the people in Univ. of Pennsylvania [4].

Most of the electronics described here will be also applicable for the readout of muon chamber. We are trying to fulfill the requirements of both straw and muon detector to reduce the cost and development effort.

2. Conceptual Design

2.1 Requirements and Detector parameters

In the SDC, a straw-tube detector is proposed for the central tracking detector. Since the detector parameters are still not fixed, we assume following parameters for the Straw-tube detector presented at LBL meeting on Aug. 1991.

Table 1 Straw-tube detector parameters.

Superlayer	layers	angle(deg)	r (cm)	length (m)
SL1	6	0	70.4	2.8
SL2	6	3	104	3.2
SL3	8	0	134	3.9
SL4	6	-3	148	3.95
SL5	8	0	161	3.95

- Tube diameter : 4 mm
- No. of Straws/module 150 - 256 tubes
- No. of Channels : 135 k channels

Hit rate of the straw tube at the radius of 70 cm is a few MHz at a nominal luminosity of 10^{33} $cm^{-2}sec^{-1}$. The front-end electronics must work without deadtime and keep the information for 3 - 4 μs of the first level trigger decision time. The drift time of the straw tube is around 30 ns with fast gas of 100 μm/ns drift velocity. To get a spatial resolution of 150 μm, the timing error of the front-end electronics must be less than 1 ns. Furthermore, the front-end electronics must be low-power and high-density devices, because it is mounted in a very limited space. Finally the front-end electronics must survive from the radiation damage of γ rays and neutrons.

2.2 Data Flow Diagram

Figure 1 shows a data flow diagram of the proposed straw-tube detector readout system. Front-end boards (FEB) are mounted on the detector, and Local Buffer Crates (LBC) are placed outside of the barrel calorimeter. Since each straw module has 150 - 256 tubes, each board deals up to 256 channels. Assuming the data size of 4 byte/channel, 10% occupancy, and 10 kHz level 2 trigger rate, the required transfer rate at the output of the FEB is ~1 Mbyte/sec. Thus a data bus of a 2 MB/sec band width is enough for this purpose. Output data from the FEB are transmitted to a Multi Data Buffer (MDB) module outside the detector through shielded twisted pair cables. The MDB receives data from 4 FEB's. A Data Transmission module (DTX) collects the data from ten MDB's in a crate and sends it out through an optical fiber cable. The average data size transferred through the DTX is 6 kB/trigger. For level 2 trigger rate of 10 kHz, the data transfer rate becomes 60 MB/sec. Thus the transmission rate of 1Gbps is required here. Since the straw-tubes are read out at both ends of the detector, eight local buffer crates are placed at one side.

2.3 Control Path Diagram

Figure 2 shows a diagram of the control path for the front-end electronics. Each FEB has a serial network interface of 10 Mbps. The serial networks in each superlayer are linked to a Superlayer Control Processor (SCP) in electronics room at the surface. The SCP's are controlled from a host computer. The FEB includes test pulse circuits for the preamp and the TMC. All the monitoring, calibration, diagnostics are done through the serial network.

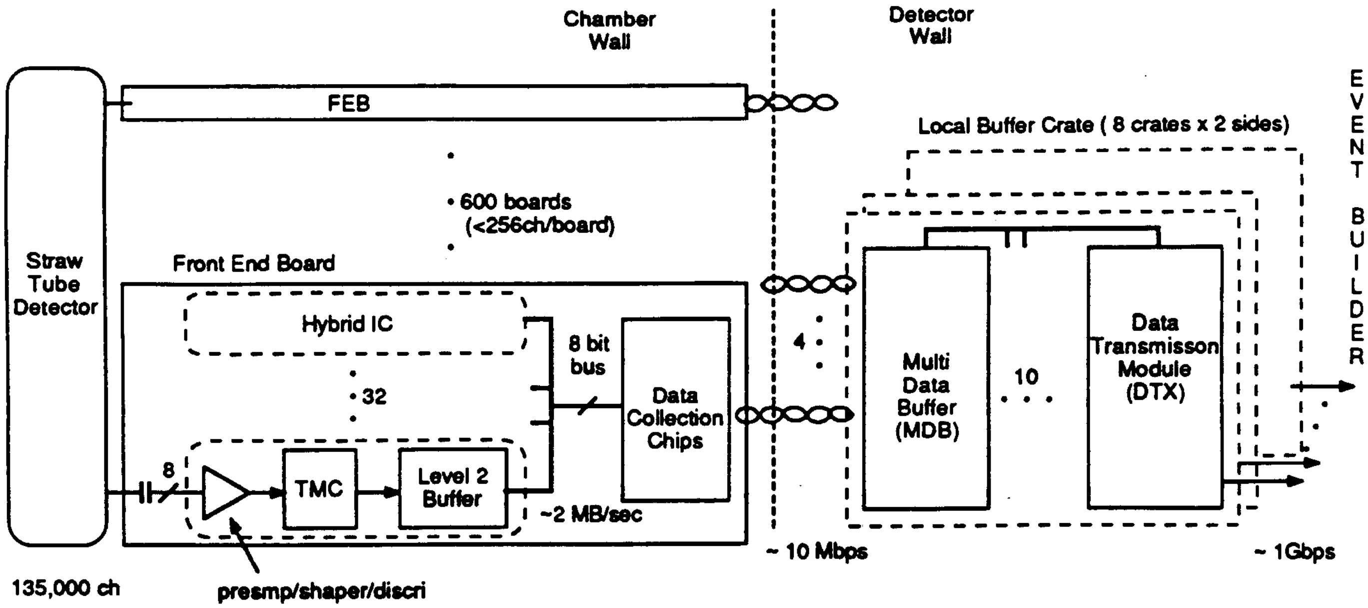

Fig.1 Data Flow Diagram of the Straw Tube

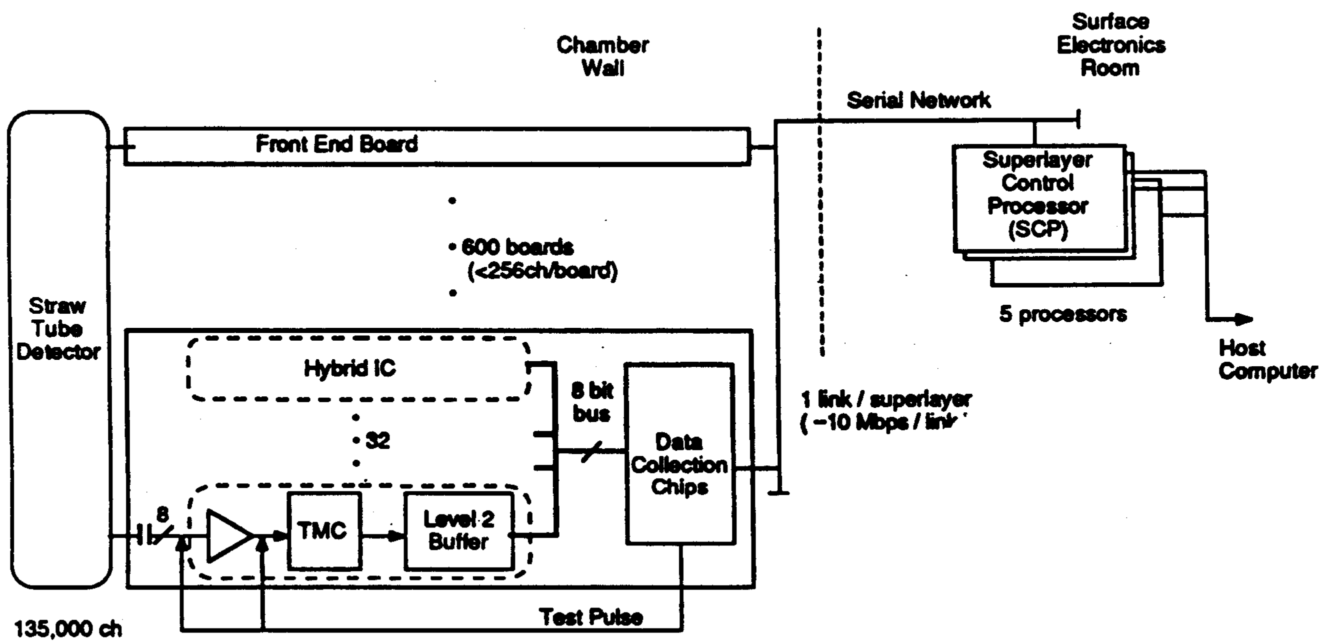

Fig. 2 Control Flow Diagram of the Straw Tube

2.4 Trigger Flow Diagram

Signals from the outer one or two superlayers are used to form track trigger signals. These trigger signals will be used with calorimeter, muon, and silicon tracker signals by checking ϕ matching. Since the straw-tubes are arranged in pointing to a beam interaction point and half-cell staggered, two types of trigger logics, time difference and time sum (mean timer), are possible.

Method of measuring the time difference within cells on a line is shown in Fig.3 -(a). The time difference is inversely proportion to the transverse momentum Pt. By changing the clipping time Tc, Pt threshold value is adjustable over a few GeV/c.

The mean timer circuit for the staggered cell is shown in Fig.3 -(b). Since the sum of straw signal timing is constant and equal to the maximum drift time, the mean timer circuit creates a pulse at fixed timing after passing the track. Although the signal has timing ambiguity depend on the z-position of the track, the ambiguity is only $< \pm 3$ ns, thus the timing from the mean timer can be used for identifying the bunch crossing.

There are several schemes to use combination of this information and compose a trigger signal. Jay Chapman (Michigan) is studying 9 cell and 8 cell track trigger circuits by using above circuit. Muon chamber and shower maximum detector will have 1024 ϕ bins, whereas the outermost superlayer has about 2600 ϕ bins. Thus it is better to combine several track trigger signals at the FEB to reduce the number of cables. We need further study to optimize the logic to be effective, reliable and flexible.

Figure 4 shows the trigger-information flow of the straw-tube detector. A key element in the above circuits is a delay line. The TMC itself is a combination of delay lines and memories, and has precise delay elements. It is natural to include the trigger circuits in the TMC, but it is also possible to implement the circuits in a separate chip. Several stiff track trigger signals which have different Pt thresholds can be used. To reduce the number of cables while keeping the several Pt thresholds, multi-value logic which has two or three different levels may be used.

More detailed Pt and track position information can be available for the level 2 trigger if necessary. We can send 500 bit information to the Global Level 2 Processor in 5 μsec by using a 100 Mbps serial line .

2.5 Functions of Each Block

2.5.1 Front End Board

Figure 5 shows a block diagram of the front-end board. The FEB includes HV decoupling capacitor, hybrid IC's, and Data Collection Chips (DCC). The Hybrid IC has 8 input channels and consists of two preamp/shaper/discri (P/S/D) chips, two TMC chips, and two Level 2 buffer chips (L2B). Those chips will be mounted on a ceramic substrate or printed circuit board by using TAB bonding, wire bonding or flip chip technique. These hybrids are connected to a simple 8 bit bus through which the DCC reads out data from the L2B and controls various functions in the front-end electronics.

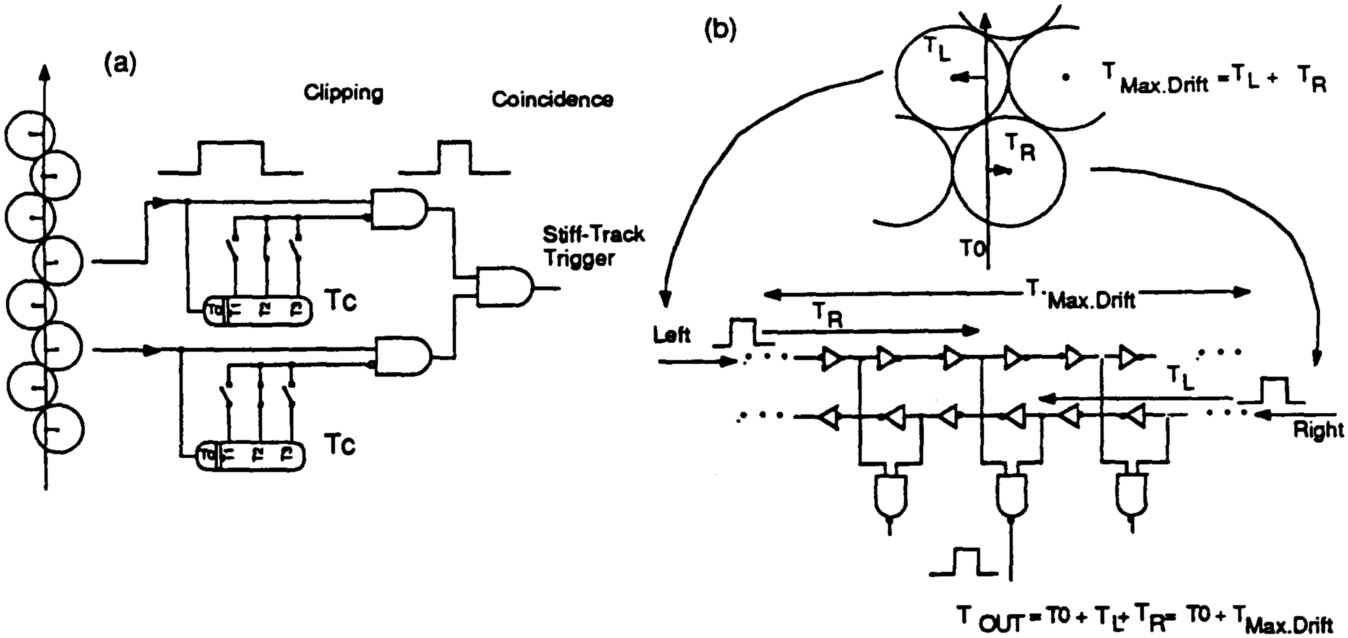

Fig.3 Basic Track Trigger Circuits. (a) Time difference circuit
(b) Mean Timer Circuit

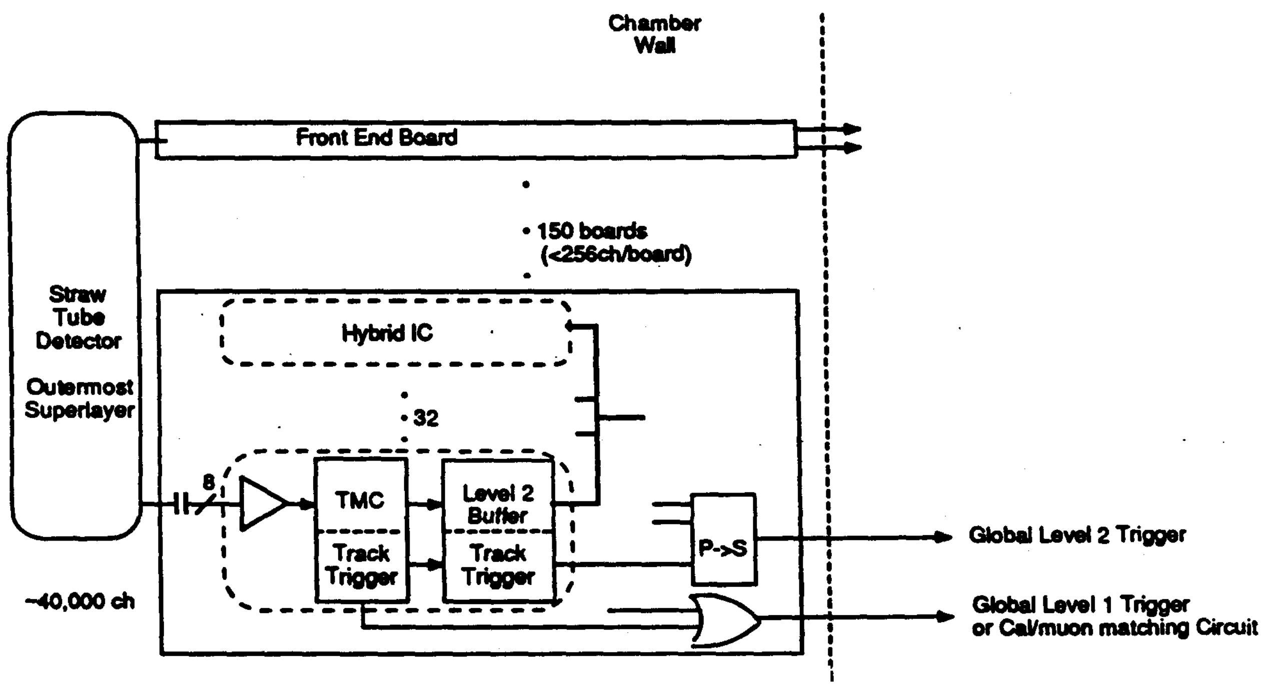

Fig. 4 Trigger Information Flow Diagram of the Straw Tube

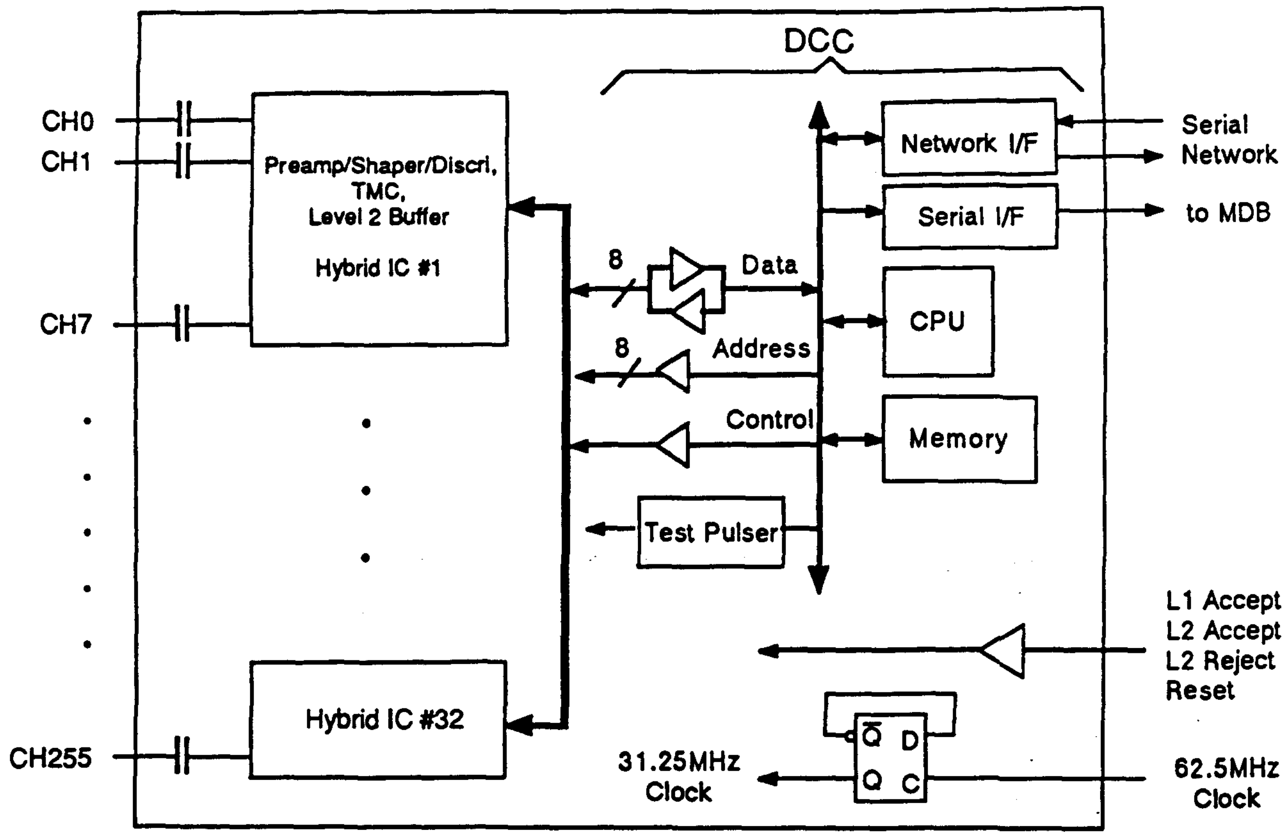

Fig. 5 Block Diagram of the Front-end Board

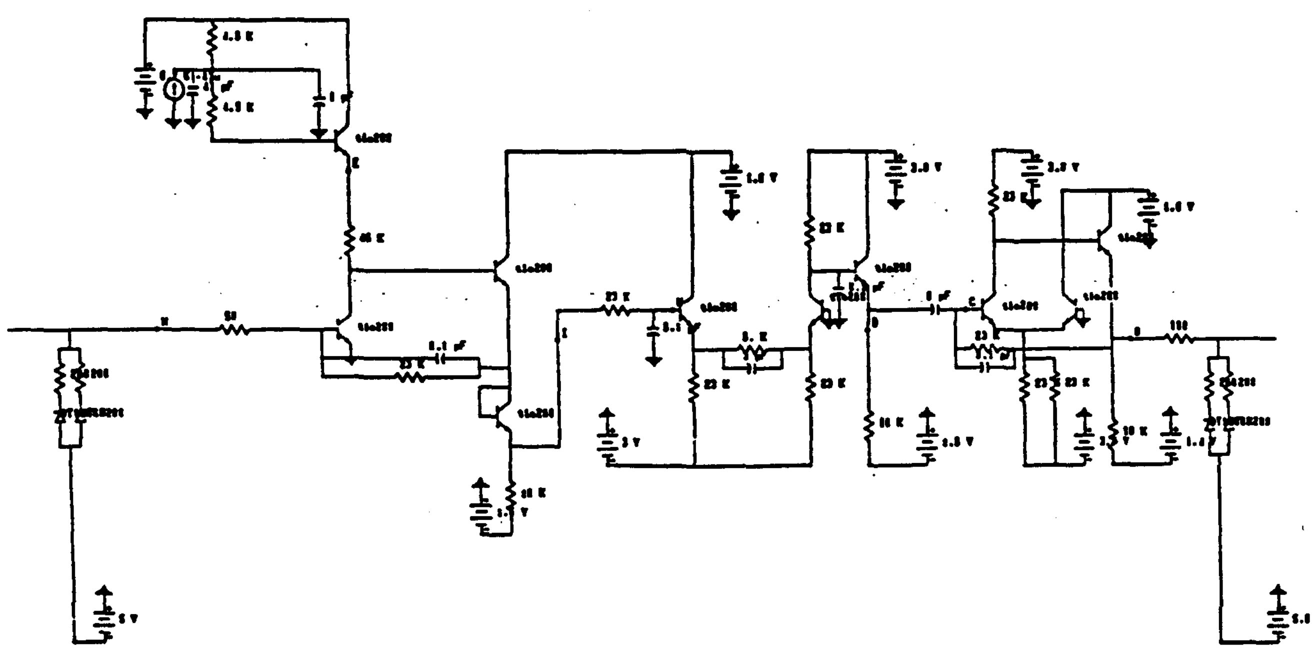

Fig.6 Schematics of the Prototype Priamp/Shaper Chips

2.5.1.1 Preamp/Shaper/Discri chip

Prototype preamp/shaper chips and discriminator chips are now being developed at KEK. The bipolar process used is NTT's Super Self-aligned Transistor (SST) with $f_T = 20$ GHz.

The preamp/shaper chip has 16 channel inputs. As shown in Fig.6, each channel has 4 integration stages, 1 differential stage, and a pole zero cancellation circuit. Two types of chip which have different time constants of 2.3 ns and 4.5 ns are designed. The gain is more than 300 mV/10^5 electron. One of the prototype preamp/shaper was tested with straw tubes by the Duke University group. Figure 7 shows the pulse shape for Fe^{55} γ-ray source.

The discriminator chip also has 16 channel inputs which contains input hysterisis circuit. The circuit diagram is shown in Fig. 8. In final chip, the preamp/shaper and the discriminator will be implemented in one chip, and will have 4 or 8 channels.

2.5.1.2 Time Memory Cell

Time Memory Cell (TMC) chip is a low-power time-to-digital converter chip which includes the first level buffer inside the chip. TMC records the history of the input signal to memory array in a digital method. The input signal is fed to the data line of CMOS memory cell, and each "write" signal to the memory cell is delayed with a variable delay element which is controlled by a feedback circuit. Table 2 summarizes the specifications of the present chip (TMC1004). The detailed explanation of the chip is given in appendix A.

Table 2.TMC1004 and TMC-SSC Specifications

	TMC1004	TMC-SSC
No. of Channels	4 channel	4 channel
Least Time Count	1 ns / bit	2 ns / bit
Time Range	1.024 μs (4 ch), 2.048 μs (2 ch) or 4.096 μs (1 ch)	4 μs
Clock Frequency	31.25 MHz	31.25 MHz
Time Resolution	$\sigma = 0.52$ ns	$\sigma = 0.75$ ns
Data Encoding	32 bit to 5+1 bit	16 bit to 4+1 bit
No. of Pins	I/O pins = 54 Power / Gnd pins = 34	I/O pins ~ 50
Supply Voltage	3.0 V	3.0 V
Power Consumption	7 mW/ch	~ 8 mW/ch
Chip size	5.0 x 5.6 = 28 mm^2	6 x 7 = 42 mm^2

Time resolution of the present chip is $\sigma = 0.52$ ns. This can be explained with a combination of the digitization error ($\sigma_{dig} = 0.29$ ns) and the TMC error ($\sigma_{TMC} = 0.43$ ns). To increase the buffer length while keeping the Si area within the acceptable level, we propose to increase the least count to 2 ns/bit instead of 1ns/bit of the present chip. If the σ_{TMC} of new chip is the same as the present

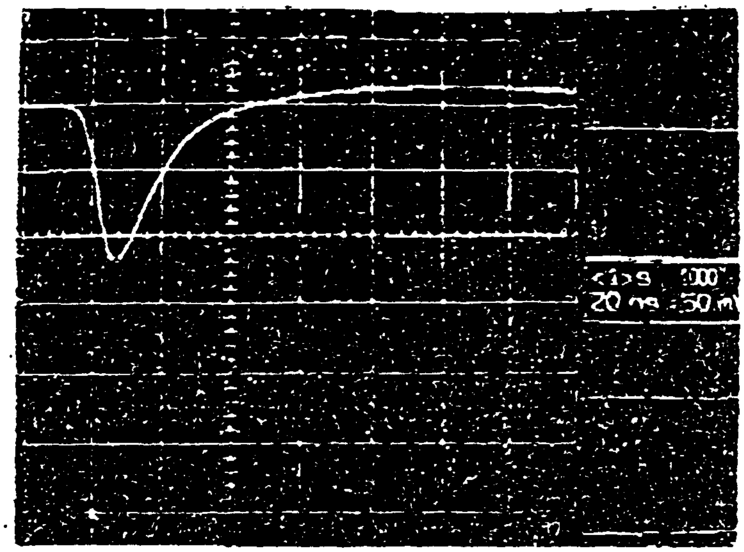

Fig.7 Output pulse shape of the prototype Preamp/Shaper for Fe^{55} γ rays.
(20ns/div and 50mV/div)

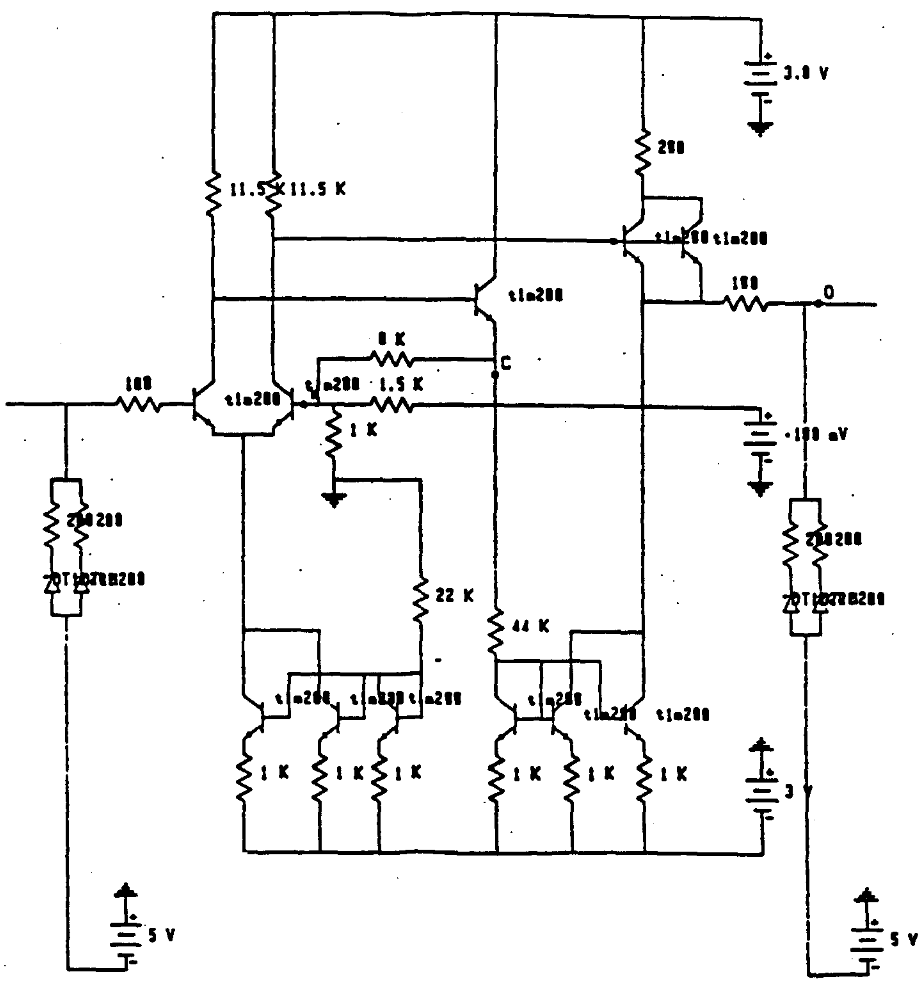

Fig. 8 Schematics of the prototype discriminator chip.

one, the time resolution will be 0.75 ns $(=\sqrt{(2ns/\sqrt{12})^2 + (0.43\ ns)^2})$. This resolution is expected to be within the requirement of the wire chamber readout.

The increase in Si area is only 50% even if we doubled the buffer length, because the control logic and pad occupy about 70% of area in the present chip. Table 2 also shows the specification of the proposed TMC-SSC chip.

Figure 9 shows a block diagram of the TMC-SSC. In the TMC-SSC, we propose to encode 16 bit data to 4 data bits plus one carry bit, and use the system clock of 31.25 MHz (32 ns period). As described in the next section, it is still possible to extract data synchronized with 16 ns trigger signal. The encoding scheme reduces required output pins and data size, and the lower clock frequency ease the chip design and reduce the power consumption.

2.5.1.3 Level 2 Buffer

Figure 10 shows a block diagram of the Level 2 Buffer (L2B). The L2B consists of an encoder logic and a buffer memory, a buffer controller, a bus interface, a TMC control logic, and a trigger control logic. The buffer controller has two pointers and the buffer works like a ring buffer. This chip is a fully digital chip using ASIC's such as gate arrays or standard cells.

In the L2B, the data from the TMC is reconstructed to drift time as shown in Fig.11. Since the maximum drift time of a straw is around 30 ns, several rows of data have to be read out from the TMC for a trigger taking into account of the uncertainty in beam crossing. The L2B reconstructs the drift time from those data. Referring to the phase synchronization of the level 1 trigger signal, the L2B recognizes starting point of the data then calculate the drift time. Although the figure shows only one hit data, but it is possible to process multi hit data.

2.5.1.4 Data Collection Chip

Data Collection Chip consists of several IC's as shown in Figure 5. The CPU moves the data from the L2B to the internal memory, and send it out through the serial I/F by adding information of a trigger number and straw address. The CPU also communicates through the serial network interface for monitoring, calibration, and diagnostic purpose. One of candidates for the CPU is a transputer which has 4 link interfaces and a high-speed external bus interface.

2.5.1.5 Power Consumption of Front-end Electronics

We estimate power consumption for the front-end electronics as shown in Table 3.

Table 3 Estimation of power consumption for the front-end electronics

P/S/D	8 mW/ch
TMC	8 mW/ch
L2B	8 mW/ch
DCC	6 mW/ch
Total	30 mW/ch

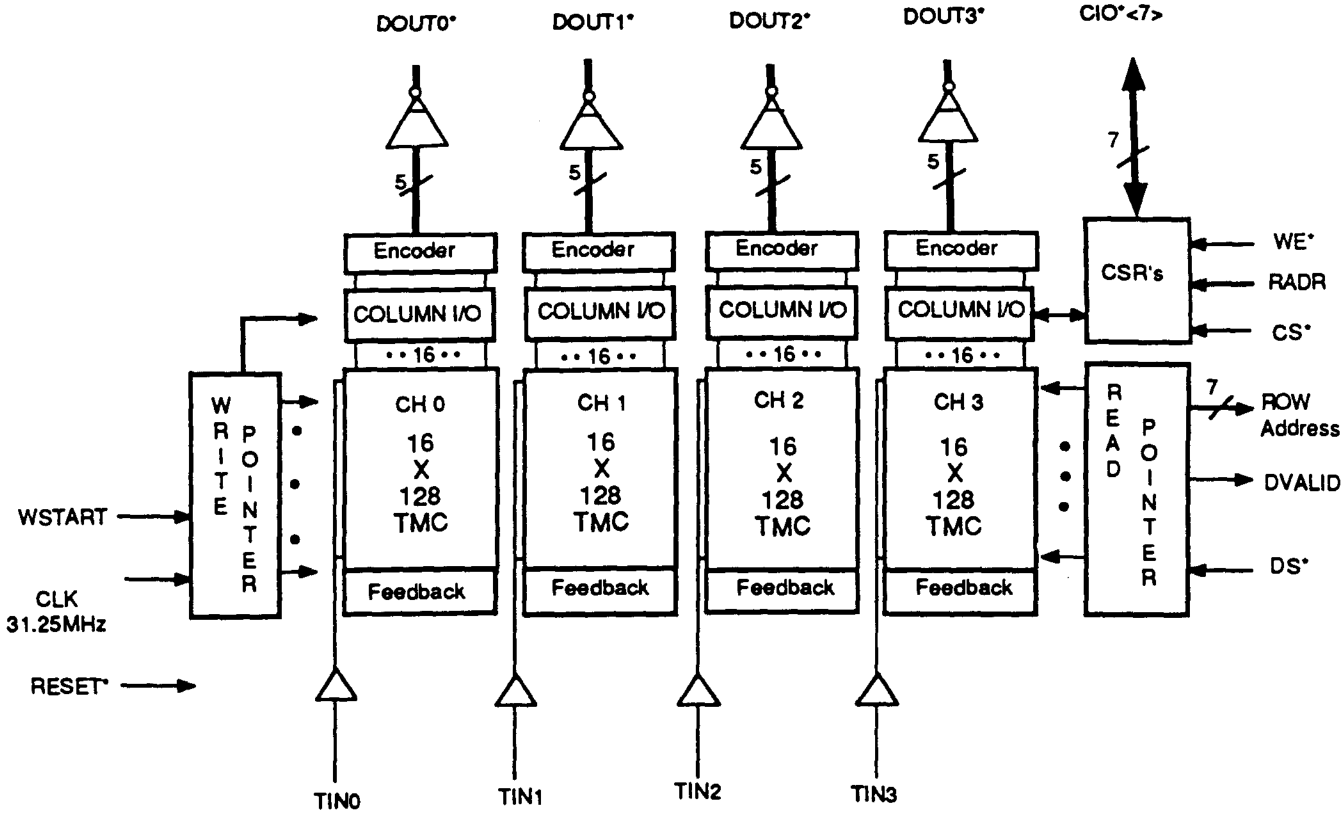

Fig. 9 TMC-SSC Block Diagram

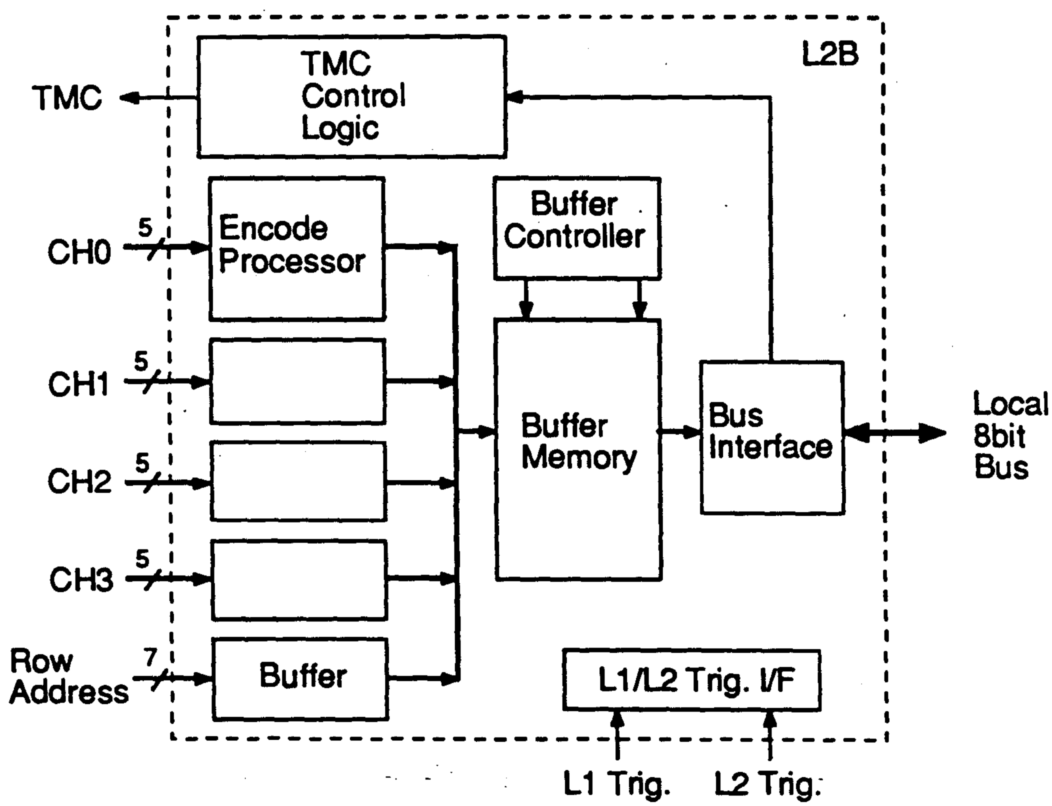

Fig. 10 Block diagram of the TMC Level 2 Buffer Chip

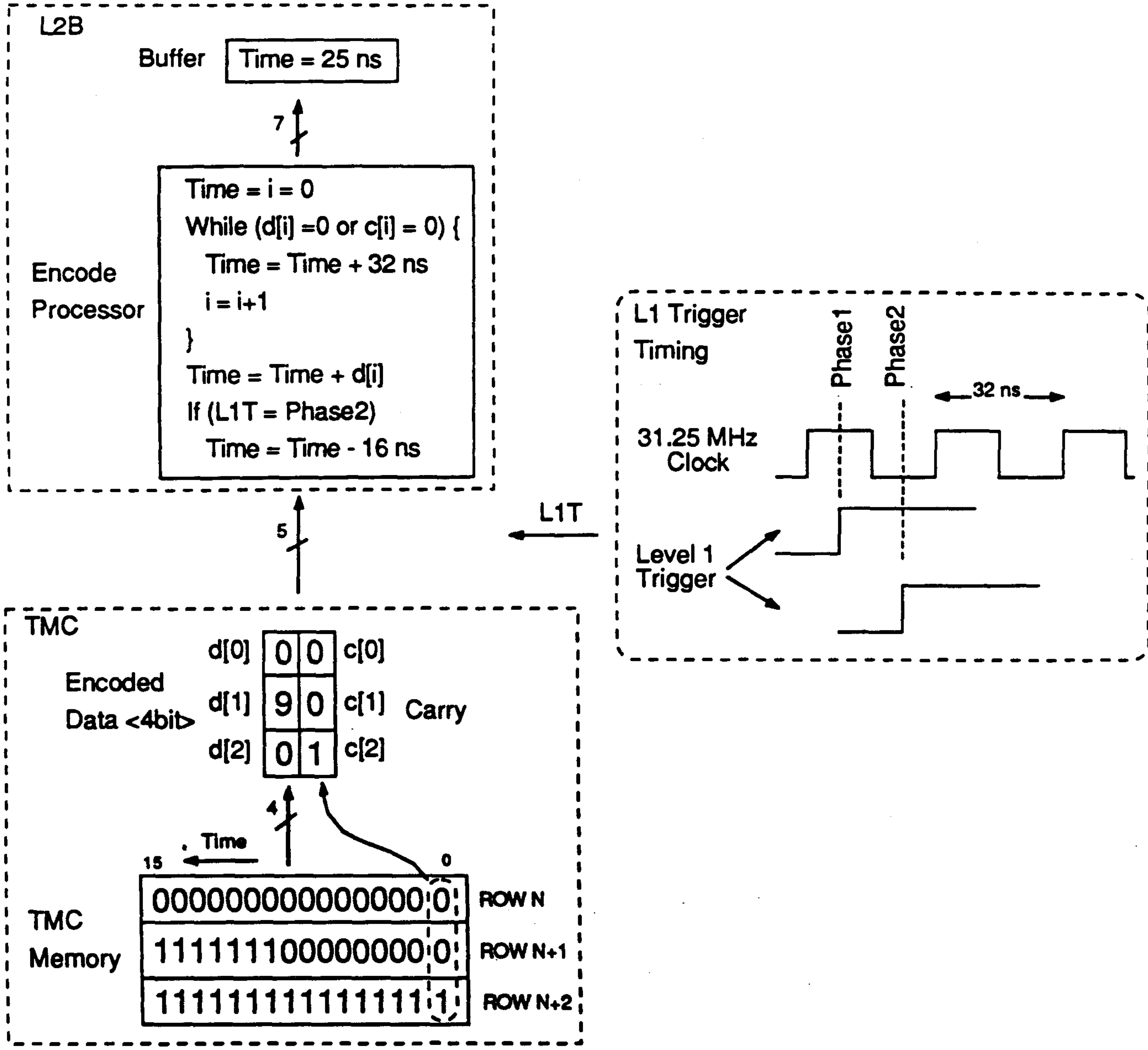

Fig. 11 TMC-SSC & L2B Data Encoding Scheme

The power consumption for the P/S/D as well as for the TMC is based on the working prototype chips. In total, we have a 2 kW heat source at one end. We think this magnitude of power consumption is manageable with a conventional cooling technique.

2.5.1.6 Higher density option

The proposed scheme of the front-end chips shown above is assuming 4 channels per chip and 8 channels in a hybrid. There is no difficulty in increasing number of input channels to 8 for the P/S/D. For the L2B, it seems possible to include 8 channel buffer in a chip, though the number of connections becomes somewhat high.

For the TMC, we have new idea which may possibly shrink the cell size by more than 30 %, and reduce power consumption. This enables us to make a 8 channels chip cost effective.

We continue to work on this option, because this reduces the cost per channels and eases the implementation of the front-end board.

2.5.2 Local Buffer Crate

The Local Buffer Crate (LBC) are placed at outside of the barrel calorimeter as described in the section of packaging. The crate contains 10 MDB modules and one DTX module. Four data cables from the FEB's are connected to one MDB module. The DTX transfers the collected data through optical fiber link with 1Gbps transfer rate.

In this crate, another module such as a clock driver, trigger driver/receiver, etc. may also be inserted.

2.6 Radiation Hardness

The radiation level induced by charged particles is about 10 krad/year at the inner most straw layer, while the neutron flux is an order of 10^{12} neutron/cm^2/year with almost no dependence on location. Thus the front-end electronics must survive for more than 100 krad and 10^{13} neutron/cm^2 radiation. Radiation damage tests are being done for both the bipolar process used in the preamp/shaper/discriminator and the CMOS process used in the TMC chip. The results of radiation damage test of the bipolar process for neutrons and γ-rays are reported in reference 5 and 6. It is shown that the process has radiation hardness up to 1 Mrad and 10^{13} neutron/cm^2.

A radiation damage test for the Co^{60} γ-ray has been done for the CMOS process. We have preliminary results. In power off condition, both PMOS and NMOS transistors show very little change up to 1 Mrad. In power on condition, PMOS shows little difference with power off condition, whereas NMOS transistors showed some degradation at the level of 100 krad.

We need further study about the radiation damage of the CMOS process.

3. Packaging and Layout

As mentioned before, front-end IC's are packaged in a hybrid as shown in Fig. 12-(a). One hybrid takes care of 8 channels. This hybrid is mounted on the FEB. Figure 12-(b) shows an

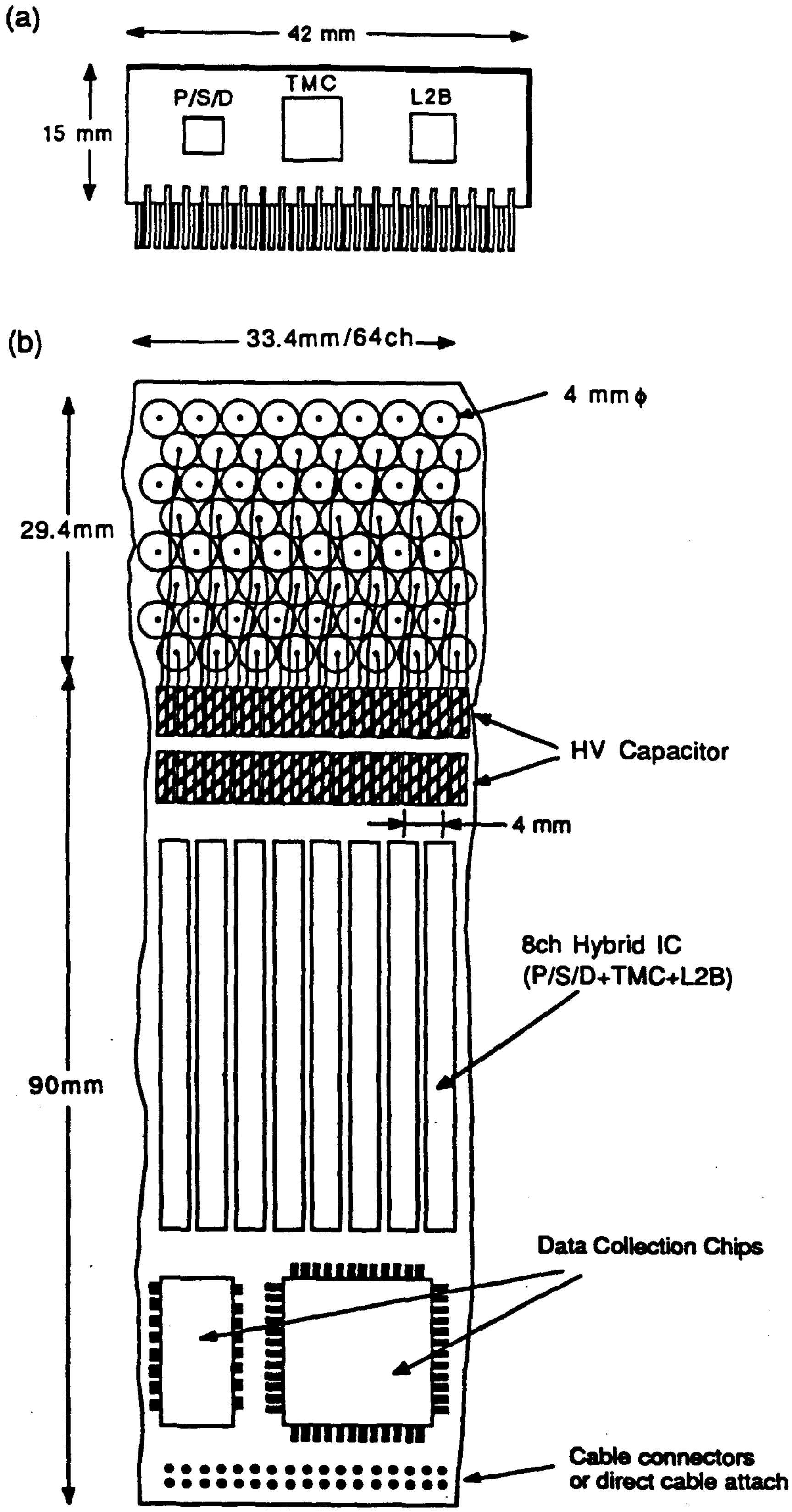

Fig. 12 Mounting Example of (a) the Hybrid IC and (b) the Front-End Board.

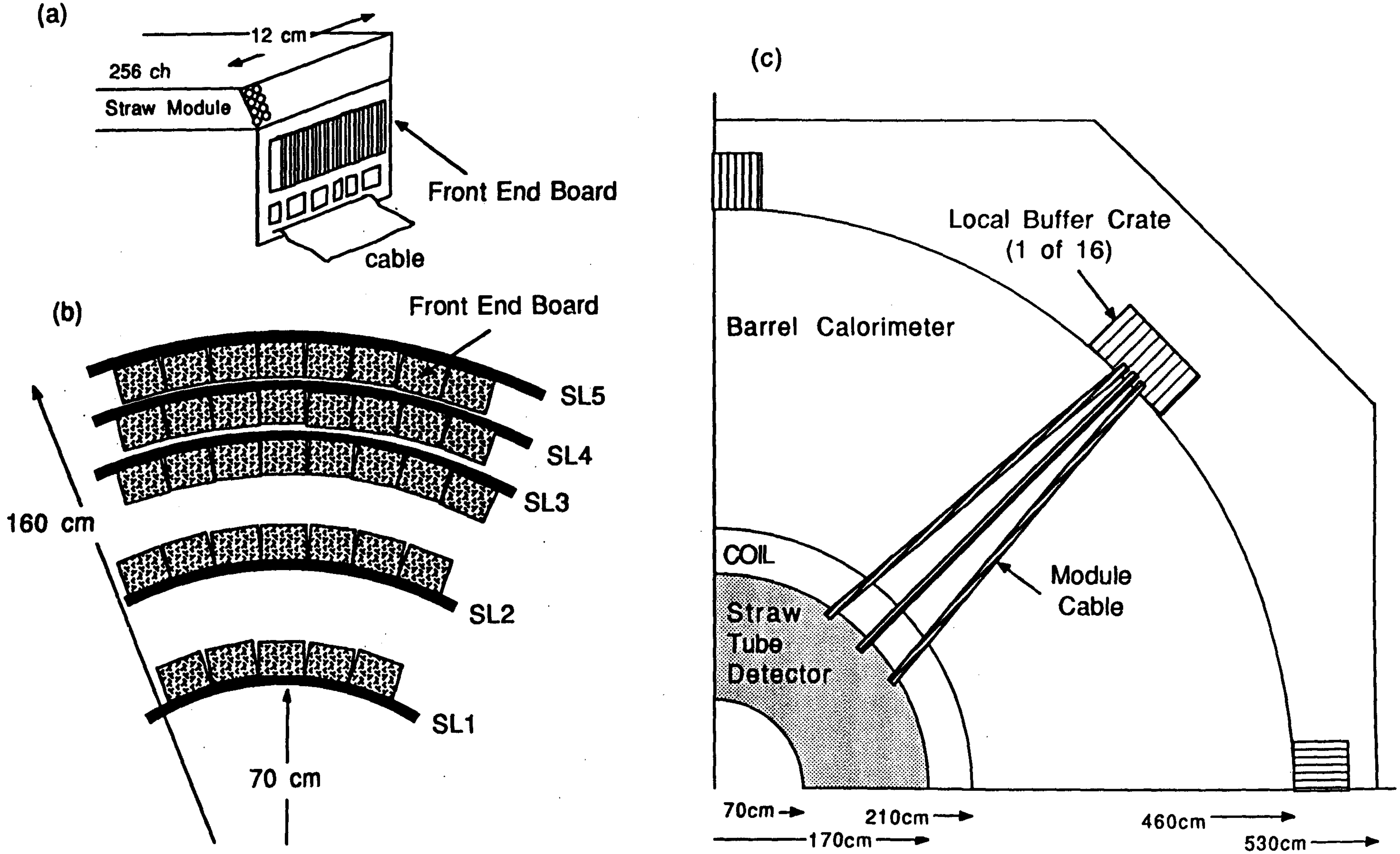

Fig. 13 Physical placement of the Front-End Boards and the Local Buffer Crates.

example of arrange around straw-tube end. Only surface copper lines from straw tube are shown. Another half lines are drawn in the real side. Since the minimum distance between superlayers is 13 cm with the current design of straw tubes, the maximum length used in the FEB is about 9 cm. As a hybrid takes 8 inputs, the pitch of the hybrid is 4 mm if it is implemented in one side. Space after the hybrid is used for the DCC's. Cables are connected with or without connector to the FEB.

Figure 13 shows the mounting scheme of the FEB to the straw superlayer structures. Since the spaces between SL1 and SL2, SL2 and SL3 are more than 30 cm, the front-end boards to the SL1 and SL2 can be mounted upside down to minimize the radiation effects and utilize maximum lever arm for tracker. The Local Buffer Crate is placed at outside of the barrel calorimeter, and module cables are connected between the MDB and the FEB.

4. Cost Estimate

Table 4 shows our cost estimate for the main parts. Cost for the FEB does not include IC's and HV capacitor listed in the table. Cost for other boards (MDB, DTX, etc.) includes all the part's cost used in the board. No R&D money is included in the table but it contains contingency. Total cost for 135k channels is about $8.7 M, or $65/channel.

Table 4 Cost estimate for the straw-tube electronics

Item	Channel/parts	Cost/parts ($)	Cost/ch ($)	Total Cost (k$)
HV Capacitor	1	3	3	405
P/S/D	4	20	5	675
TMC	4	60	15	2,025
L2B	4	40	10	1,350
Hybrid Packaging	8	60	15	2,025
DCC IC's	256	1,000	4	540
FEB*	256	1,000	4	540
Cables	256	1,000	4	540
MDB	1,024	3,000	3	405
DTX	10,240	4,000	0.4	54
LBC with P.S.	10,240	4,000	0.4	54
optical fibers	10,240	2,000	0.2	27
SCP	25,000	10,000	0.4	54
Total			64.4	8,694

(*) exclude cost of parts listed above.

5. Crucial R&D

Most crucial R&D is a radiation damage test for the front-end electronics. There is no problem for bipolar process used in the preamp, etc. The CMOS process used is relatively radiation hard compared with commercial ones, but still need further studies.

Another crucial R&D is high density readout. Although the packaging seems to be not so difficult with present technology, the system deals with small analog signal and high-speed digital signal in a very limited space. Cross-talks and oscillations must be carefully minimized or eliminated.

Most of the parts used in our scheme is based on very conservative design. Although it will take long time to develop and debugging each module, we think there is no crucial item in implementing data acquisition modules.

6. Schedule

Table 5 shows possible development schedule. Each front-end IC requires two prototype productions before the final mass production. The most of the mass production will be done in 1996. Final assembly test with straw-tube detector will be done in 1998.

References

[1] Y.Arai et al., "A CMOS 4CH x 1K Time Memory LSI with 1 ns/bit Resolution", to be published in Journal of Solid-State Circuits, March 1992.

[2] Y.Arai, "Development of TMC Chip and On-Chip Processing", Proceedings of the International Workshop on Solenoidal Detectors for the SSC, April 1990, KEK Preprint 90-54.

[3] Y.Arai, "TMC and Data Acquisition/Packaging", Proceedings of the SDC Collaboration Meeting at KEK, May 1991, page 837, SDC-91-00033.

[4] F.M.Newcomer et al., "SDC Straw Tracking Electronics Conceptual Design"

[5] H. Ikeda and N. Ujiie, "Radiation Damage of Bipolar SST due to Fast Neutrons", Nucl. Instr. and Meth. A281(1989)508.

[6] H. Ikeda and N. Ujiie, "Radiation Damage of Bipolar SST due to γ rays of ^{60}Co", Nucl. Instr. and Meth. A290(1990)462.

Table 5. Straw-tube Detector Electronics Development Schedule.

Item	'91	'92	'93	'94	'95	'96	'97	'98	'99
TMC(1st)		Design	Fabrication	Test					
(2nd)				Modify	Test				
(final)						Mass Product			
P/S/D (1st)		Design	Fabrication	Test					
(2nd)				Modify	Test				
(final)						Mass Product			
L2B(1st)		Design	Fabri	Test					
(2nd)				Modify	Test				
(filnal)						Mass Product			
Hybrid			Design	Test	Design	Test	Mass Product		
FEB				Design		Test	Mass Product		
small system test					Test				
module assembly								Assembly	Test
MDB				Design	Test	Mass Product			
DTX				Design	Test	Mass Product			
SCP					Design	Test	Mass Product		
Data Transfer test					Small System	Test		Full system	Test

[Appendix A]

A CMOS 4CH x 1K TIME MEMORY LSI WITH 1 NS/BIT RESOLUTION

Yasuo Arai, Member, IEEE, Tsuneo Matsumura, Member, IEEE, and Ken-ichi Endo

Abstract - A 4-channel 1024-bit Time-to-Digital Converter chip, which records input signals to memory cells at one nano second intervals, has been developed. To achieve one nano second precision, the chip incorporates a feedback stabilized delay element. The chip was fabricated on a 5.0 mm by 5.6 mm die using 0.8 μm CMOS technology. It dissipates only 7 mW/channel under typical operating conditions.

Y. Arai is with KEK, National Laboratory for High Energy Physics, 1-1 Oho, Tsukuba, Ibaraki 305, JAPAN

T. Matsumura and K. Endo are with NTT LSI Laboratories, 3-1 Morinosato Wakamiya, Atsugi, Kanagawa 243-01, JAPAN

(For submission to IEEE Journal of Solid-State Circuits)

I. Introduction

Particle detectors for future high energy accelerators have demanding requirements for time-to-digital conversion. A VLSI circuit designed specifically for this application is an efficient way to meet the requirements. The circuit must achieve 1 ns resolution, and it must maintain the history of the input for more than 1 μs pending receipt of a readout trigger. The readout must not create dead time. As more than 100,000 channels of the time-to-digital electronics will be mounted in the very limited space of a detector, the chip must be high density and low power. Furthermore the device must not deteriorate in the ambient flux of particles and γ rays that is present in the vicinity of the detector.

The idea of Time Memory Cell (TMC) was proposed by us and tested by making a TEG chip [1]. The cell utilizes low-power and high-density characteristics of a CMOS memory cell and gate delay time. Figure 1 shows the basic operation of the TMC. As the write signal (WL) timing in each TMC cell is delayed by 1 ns, timing information of the input lines (TIN and TIN*) is recorded to memory cells sequentially. To keep the delay time constant, the delay time of the delay element is controlled through the Vg line by a feedback circuit which refers to an external system clock period.

In an alternative approach described by Stevens et al. [2] the timing information is stored in a switched capacitor array and digitized much later. Our approach depends much less on small signal analog electronics and is therefore preferable in the detector environment where levels of radiation and electrical noise may be high.

A new TMC LSI chip (TMC1004) has been developed using an 0.8 μm CMOS process. It contains 4 channels and each channel has 1024 TMC cells (32 rows and 32 columns). The chip achieves more than 10 times the density of a 1 GHz GaAs shift register [3] while dissipating less than 1 % of the power.

II. Time Memory Cell Technique

A. Concept

A GaAs shift register clocked at 1 GHz would provide the 1 ns precision that we require, but the power dissipation of this technology is unacceptably large. Therefore we sought to accomplish our objectives in CMOS technology for which the power dissipation is intrinsically low.

In CMOS circuitry the objective of low power is further served by use of a low clock frequency and minimization of data transfers from gate to gate. The difficulty with CMOS where timing is critical is that the propagation delay of a gate may vary by more than 20 % because of fluctuations in chip processing, supply voltage, and temperature. However, the delay time of a gate which has a same physical layout is fairly uniform within a chip. We make a feedback circuit which controls delay time of the series of gates, and eliminate the process, voltage and temperature variability.

In one channel of a TMC1004 chip, 1024 TMC cells are configured as 32 rows of 32 cells. Within a row the input is written to successive cells at intervals of approximately 1 ns. The rows are successively enabled for writing by an external clock with period 32 ns.

B. Feedback circuit

The principle of our feedback circuit is analogous to the principle of a phase locked loop (PLL). Whereas a PLL stabilizes an oscillator frequency by referencing to the phase of an external clock, the TMC feedback stabilizes a variable delay element by referencing to the period of an external clock.

Figure 2 shows the schematic of the feedback circuit. When an external clock (ϕ_1) sets the flip-flops F1 and F2 at its falling edge, capacitors C1 and C2 begin to charge. The charging of C1 stops at the falling edge of the pulse from the end of the reference row. The charging of C2 stops at the next falling edge of the clock pulse (ϕ_2). Hence, the voltage difference between C1 and C2 is proportional to the time difference between the delay line and clock period. Comparator A1 checks the voltage difference and adjusts the feedback voltage (Vg). If the delay time is less than the clock period, C3 charges during a store period increasing the delay of the delay line. If the delay time is longer than the one clock period, C3 discharges reducing the delay.

C. Timing Accuracy

We give here a rough estimate of the timing accuracy attainable by the TMC circuit. There are three main sources of error; the input and clock signals, the feedback circuit, and the non-uniformity of the delay element. In the following discussion, we assume the error distribution has the Gaussian shape, and use the word "error" as the standard deviation of the distribution.

Time jitter of the input and the clock (write) signals arise when those signals pass through buffers (see Fig. 3-(a)). We assume time jitter of 50 ps for the signal passing a buffer. Since we are using about 20 buffers between input pad to a TMC cell, the total time jitter is summed in quadrature, and will be $\sqrt{20}$ x 50 ps = 0.2 ns.

The signal jitters in the write line (WL) is accumulated from the first cell to the last cell in a row. In the last cell this jitter becomes $\sqrt{32}$ x 50 ps = 0.3 ns. By averaging the jitter in a row, it becomes 0.2 ns/bit.

Although those buffers have variation of delay time caused by the change of supply voltage and temperature, the delay variation for input and clock line is cancelled each other by designing the number of buffers from input to the TMC cell to be the same.

The errors in feedback circuit come from sensitivity of the comparator and controllability of the feedback voltage (see Fig. 3-(b)). Since the input voltage of the comparator changes 1.5V for 32 ns period (= 50 mV/ns), and the comparator detects ±25 mV voltage difference from the reference voltage, the sensitivity of the comparator is ±0.5 ns / 32 ns (= ±1.5 %), so the effect of this error to each bit can be neglected. Since the adjustment of the feedback voltage is < 20mV per feedback cycle, the corresponding delay time change is less than 30 ps / cycle. Thus this error can also be neglected.

Non-uniformity of the delay element may cause difference of delay time between reference row and actual row, and causes discontinuity in data between row. If there is 5% non-uniformity in delay time of each delay element, the discontinuity will be $\sqrt{32}$ x 0.05ns = 0.3 ns. Also the non-uniformity appears as differential linearity error.

In addition to these errors, digital conversion device has digitization error intrinsically. For 1 ns digitization step the digitization error σ_{dig} is $1/\sqrt{12} = 0.29$ ns. From these considerations, it may be possible to make the device which has the timing error of $\sigma \sim 0.5$ ns.

III. Circuit Description

A. Circuit Block

A Block diagram of the TMC1004 is shown in Fig. 4. The chip has four TMC arrays, each with 32 rows by 32 columns of TMC cells. Each array has a feedback circuit. For accessing the four arrays, there are two pointers Write and Read each of which consists of a 7-bit counter and decoder. The Write Pointer is incremented in each clock (CLK) cycle which initiates a pulse in the write line of the designated row. The Read Pointer selects a row for readout and is incremented by the same clock (CLK). This scheme with two pointers and dual port cells enables read and write operations to proceed simultaneously. The four TMC arrays can be configured as 4, 2, or 1 channels by setting external pins. The 4, 2, and 1 channel modes utilize respectively the lower 5, 6 or 7 bits of the counters and retain the input history for 1, 2 and 4 μsec.

The 32 bits of row information are encoded to 6 bits at readout time so as to reduce the data size and the required number of leads to the chip.

The chip maintains various parameters in three control and status registers (CSR) which can be read as well as written.

B. Time Memory Cell

The schematic of the TMC cell is shown in Fig. 5. Each cell has one timing-information write port (TIN and TIN*) and one data-read/write port (BL and BL*). We used static memory in the TMC cell, because it may be more stable for radiations than the dynamic one. Two PMOS transistors (M1 and M2) are added to the previous design [1]. They make the write operation insensitive to the previous contents of the cell by interrupting the feedback paths during the write pulse. Transistor parameters of the delay element were selected to obtain a gate delay time close to 1 ns/bit.

The delay time of the delay element is controlled by the PMOS transistor M3. Since the input signal is latched in memory cell at the falling edge of the signal on WL', only the falling edge is controlled via the feedback voltage Vg. The transistor M3 changes the rise time of the signal at node A. At the input to the second inverter the pulse width changes and at its output the regenerated signal edge is again sharp.

C. Feedback Circuit

The operation of the feedback circuit was described in previous section. Figure 6 shows the result of simulation of the delay element. With Vg fixed the delay varies by more than ±20% with changes in power supply voltage (2.7 V ~ 3.3 V), temperature (27 °C ~ 70 °C), and transistor threshold voltage (-10% ~ +10%). With Vg controlled by the feedback circuit (1.2 V ~ 2.3 V), the delay time is kept at 1 ns.

D. Encoder

The 32-bit row data is encoded to 6 bits. Since transition times are spaced by at least 32 ns in our application, the encoder logic accommodates only one "0" to "1" transition in a row of memory. Thus the encoding reduces the output pin requirement and the amount of data without sacrificing data quality. Table 1 shows the encoding scheme. The most significant bit shows the value of the first bit of a row, and the remaining 5 bits show the position of the first "0" to "1" transition.

E. Readout Pipeline

Simultaneous reading and writing require that the operations proceed in phase so that the memory operates as a ring buffer. One row must be read out during each 32 ns interval in which a row is written. The readout cycle (memory read and encoding) is pipelined to two stages and the cycle continues while the trigger signal DS* is asserted. The data are presented on the DOUT lines.

F. Control registers

There are three CSR registers which set / show the operating mode and the settings of the pointers. Two bits of CSR#0 encode the operating mode, and four bits provide serial access to the cells of the TMC arrays. This access path is used for testing each TMC cell. The Read Pointer can be written and read via CSR#1 and the Write Pointer via CSR#2. The CSR register is accessed through the CS* and the CIO lines.

III. Measured Performance

The specifications for the TMC1004 are summarized in Table 2. Each item is discussed below.

A. Linearity

Figure 7-(a) shows the linearity curve of the TMC1004. As the chip is referencing an external quartz oscillator (31.25 MHz), the slope of the linear fit to the data (time-to-digital conversion

factor) is very stable and has the value of 1.000 ± 0.001 bit/ns without any tuning. The integral linearity error (Fig. 7- (b)) is the deviation from the ideal response function. A Gaussian fit to the integral linearity error distribution shows $\sigma = 0.31$ ns, and the maximum deviation is less than 1.5 ns.

Figure 8 shows the fine structure of the linearity curve. The first part of the row has a nearly ideal response to input, but in the latter part of the row the response is rather broad. This trend reflects the accumulation of jitter along a row and the resynchronization at the start of the next row. Making the rows shorter could reduce the integral linearity error but at the cost of increased power dissipation.

Figure 9 shows the differential linearity error. We get $\sigma = 4\%$ from Gaussian fit to the data and maximum deviation is less than 20 %. This indicates the non-uniformity of the delay element is around 4%.

We observed discontinuity in data is less than 0.5 ns for row-to-row, and less than 1 ns for TMC array-to array.

B. Stability

While the chip has non-negligible amount of integral and differential errors, its overall characteristic is very stable. Figures 10-(a) and (b) show the variation in slope with voltage and temperature for a channel. The variation is plotted as a deviation from the data point of 3.0V and 25 °C. Due to the feedback circuit, the slope is stable within 0.1% for voltage variation of 2.6 - 3.4 V and temperature variation of 15 - 55 °C.

C. Power Consumption

The most power consuming part of the chip is a sense amplifier circuit. There are 128 sense amps on a chip, one for each column of each channel. To minimize power dissipation, the DC current to the sense amps is normally held off and is raised only when a readout trigger arrives. With the feedback circuit operating, the power dissipation is about 3 mW/ch in 4 channel mode. When continuous write operation starts, the power dissipation increases to about 6.5 mW/ch. Finally, during readout the power dissipation increases by 24 mW/ch. With a readout duty factor of 1 % as expected in a typical operating environment, the average power dissipation is 6.7 mW/ch

D. Time Resolution

Figure 11 shows results of time resolution measurement. In this measurement, the deviation from ideal response line is measured and plotted. Gauss fit to the data shows $\sigma_{total} = 0.52$ ns. Assuming the σ_{total} is the quadrature sum of digitization error ($\sigma_{dig} = 0.29$ ns) and the TMC error (σ_{TMC}), we get $\sigma_{TMC} \sim 0.46$ ns. This value is in good agreement with the our rough estimate in section II.

E. Layout

Figure 12 shows the photograph of a TMC1004 chip. Four TMC arrays are arranged in quadrants. Control logic is placed in the cross shaped area separating the arrays. The chip was designed by full-custom layout, and the size is 5.0 mm by 5.6 mm.

IV. Summary

A new time-to-digital converter chip, the TMC1004, has been designed. It has 1 ns/bit least count and can record for up to 4 μs. A novel variable delay element and a feedback circuit are employed to get 1 ns accuracy. Power consumption is very low due to the CMOS static memory-like structure. Tests show that overall linearity and stability are very good. This chip is designed for time-to-digital conversion chip, but the methods used to get 1 ns timing and to record to memory can be adapted to other applications such as a memory for recording high-speed signals.

Acknowledgments

We wish to thank to N. Ieda, T. Mano and J. Yamada for their support of this project. One of the authors (Y. A.) is also grateful to Y. Watase, T. Ohsugi, T. Kondo, H. Ikeda and Y. Akazawa for their continuing advice and encouragement throughout this work.

References

[1] Y. Arai and T. Baba, "A CMOS Time to Digital Converter VLSI for High-Energy Physics", in 1988 Symposium on VLSI Circuits, Dig. Tech. Papers, Aug.1988, IEEE CAT. No. 88 TH 0227-9 pp 121-122.

[2] A. Stevens et al., "A Time-to-Voltage Converter and Analog Memory for Colliding Beam Detectors", IEEE J. Solid-State Circuits, vol. SC-24, no. 6, pp. 1748-1752, Dec. 1989.

[3] O. Sasaki et al., "1.2 GHz GaAs Shift Register IC for Dead-Time-Less TDC Application", IEEE Trans. on Nucl. Sci. Vol. 36 (1989)512.

Table 1 Data Encoding scheme

Bit Pattern	Encoded Data
3322222222221111111111 10987654321098765432109876543210	5 4 3 2 1 0
00000000000000000000000000000000	0 0 0 0 0 0
xxxxxxxxxxxxxxxxxxxxxxxxxxxxxx10	0 0 0 0 0 1
xxxxxxxxxxxxxxxxxxxxxxxxxxxxx100	0 0 0 0 1 0
:	:
10000000000000000000000000000000	0 1 1 1 1 1
11111111111111111111111111111111	1 0 0 0 0 0
(not appear)	1 0 0 0 0 1
xxxxxxxxxxxxxxxxxxxxxxxxxxxxx101	1 0 0 0 1 0
xxxxxxxxxxxxxxxxxxxxxxxxxxxx10x1	1 0 0 0 1 1
:	:
10xxxxxxxxxxxxxxxxxxxxxxxxxxxxx1	1 1 1 1 1 1

x..xx..x = 0..01..1

Table 2.TMC1004 Specifications

No. of Channels	4 channel
Least Time Count	1 ns / bit
Time Range	1.024 μs (4 ch), 2.048 μs (2 ch) or 4.096 μs (1 ch)
Clock Frequency	31.25 MHz
Time Resolution	σ = 0.52 ns
Integral Linearity Error	σ = 0.3 ns (< 1.5 bit)
Differential Linearity Error in a row	σ = 0.04 ns (< 0.2 bit)
row-to-row Discontinuity	< 0.5 bit
TMC array-to-array Discontinuity	< 1 bit
Variation of Slope (time-to-digital conversion factor)	< 0.1 % (2.6 - 3.4 V) < 0.1 % (15 - 55 °C) < 0.1 % (chip to chip)
Data Output	32 ns cycle 2 stage pipeline. 6 bit encoded output.
No. of Pins	54 I/O pins and 34 Power / Gnd pins
Supply Voltage	3.0 V
Power Consumption	7 mW/ch for 1 % readout duty factor.
Chip size	5.0 mm x 5.6 mm

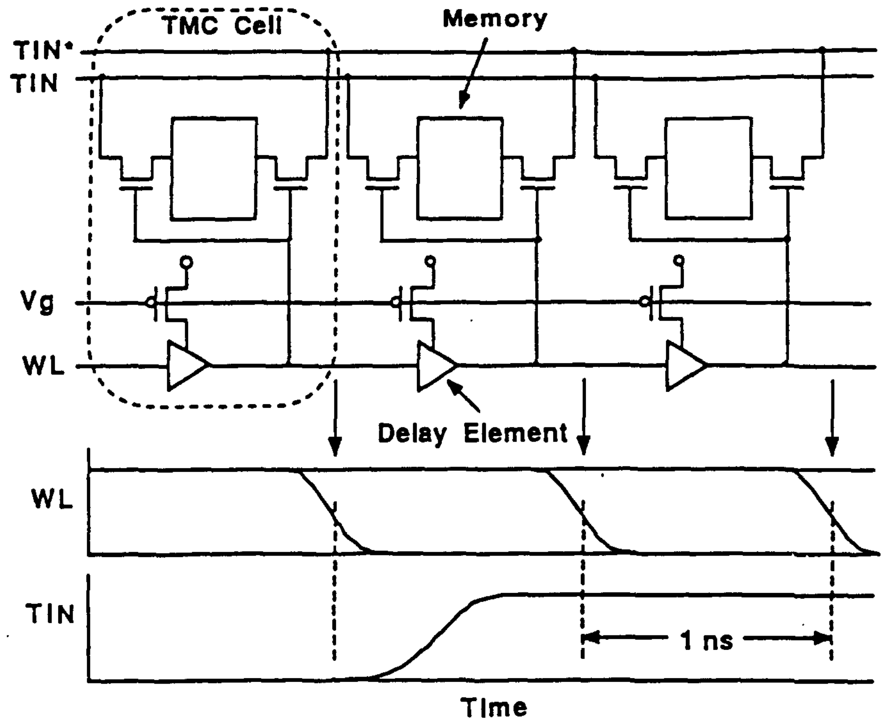

Fig. 1. Input timing write operation in the TMC cells.

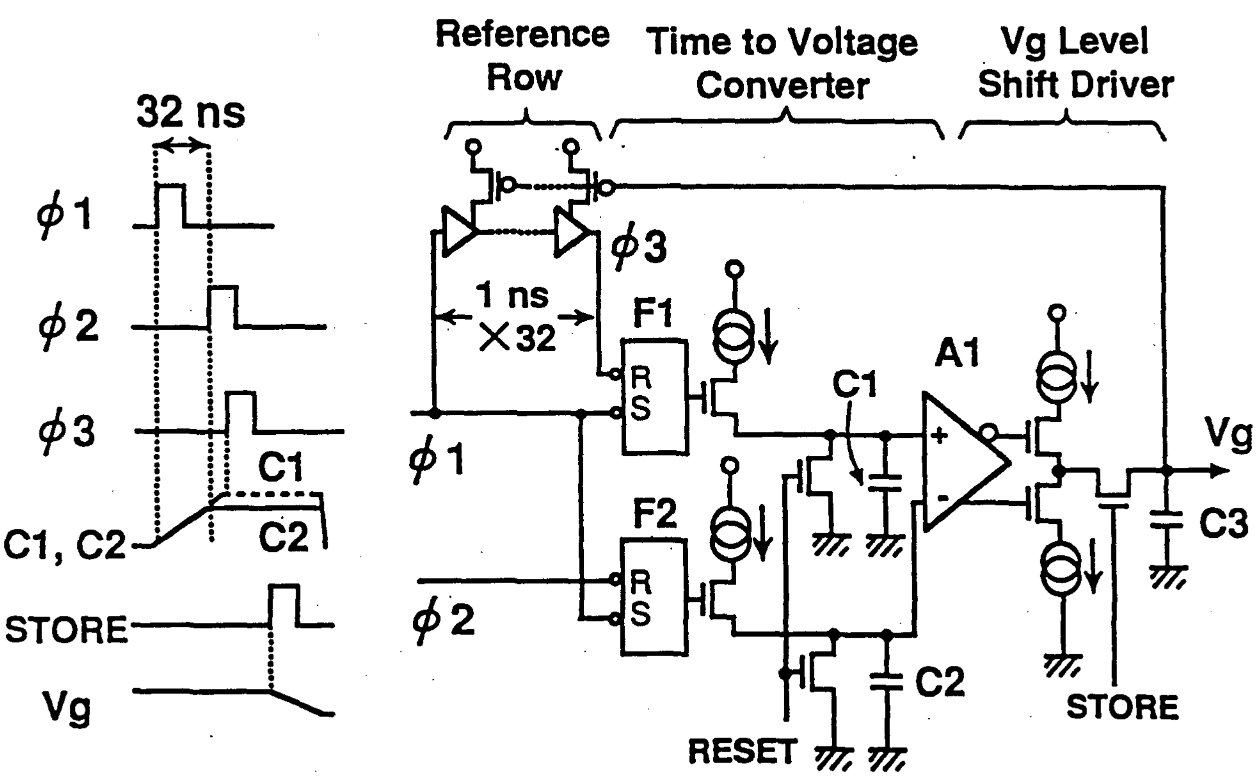

Fig.2. Feedback circuit.

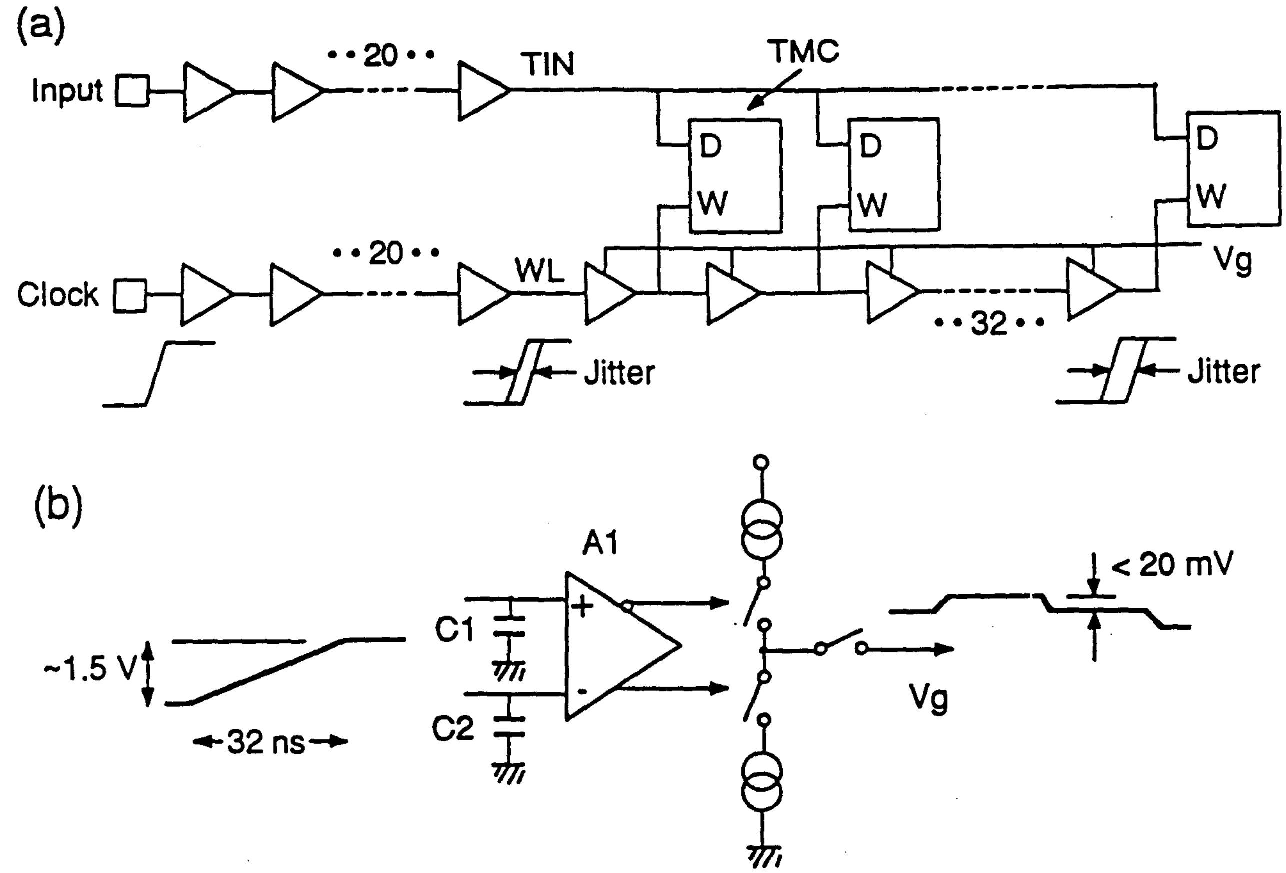

Fig. 3 (a) Signal jitter in the TMC circuit. (b) Signal Level in the feedback circuit.

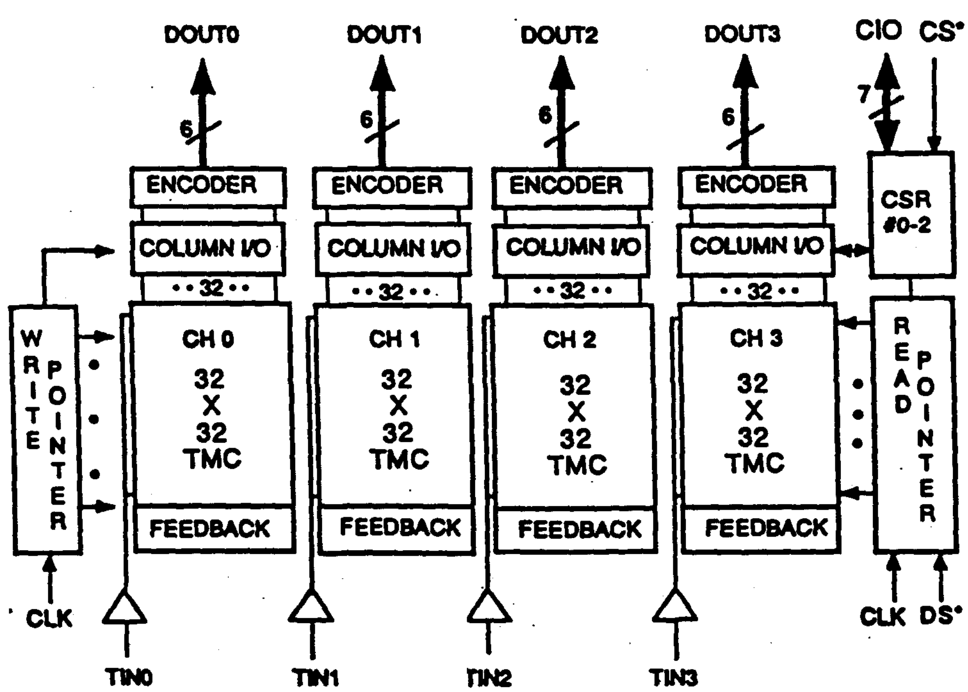

Fig. 4. Block diagram of the TMC1004.

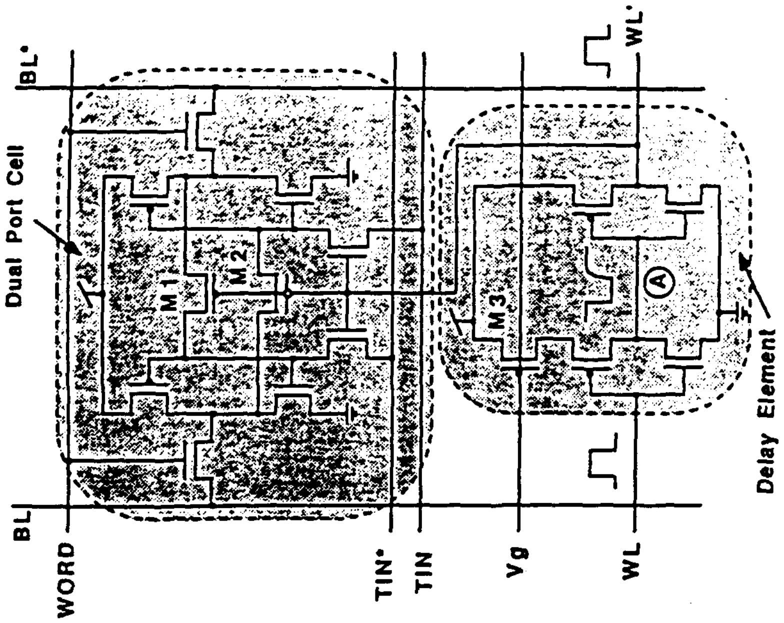

Fig. 5. TMC cell circuit.

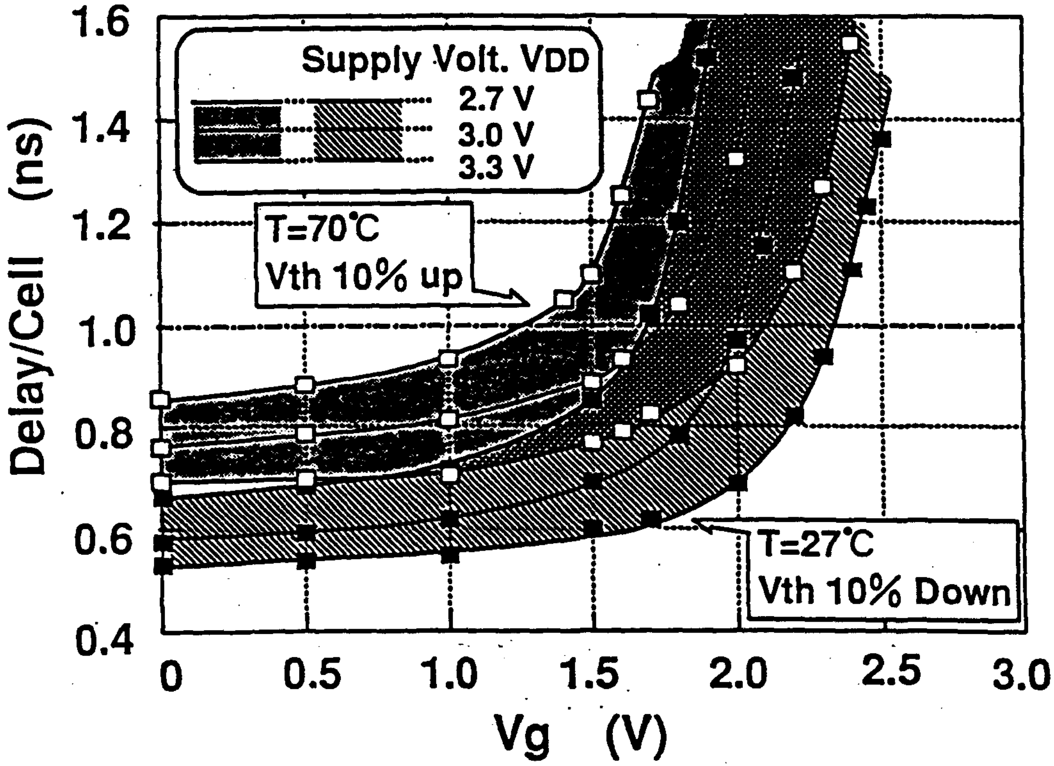

Fig. 6. Simulation of the delay time for the delay element.

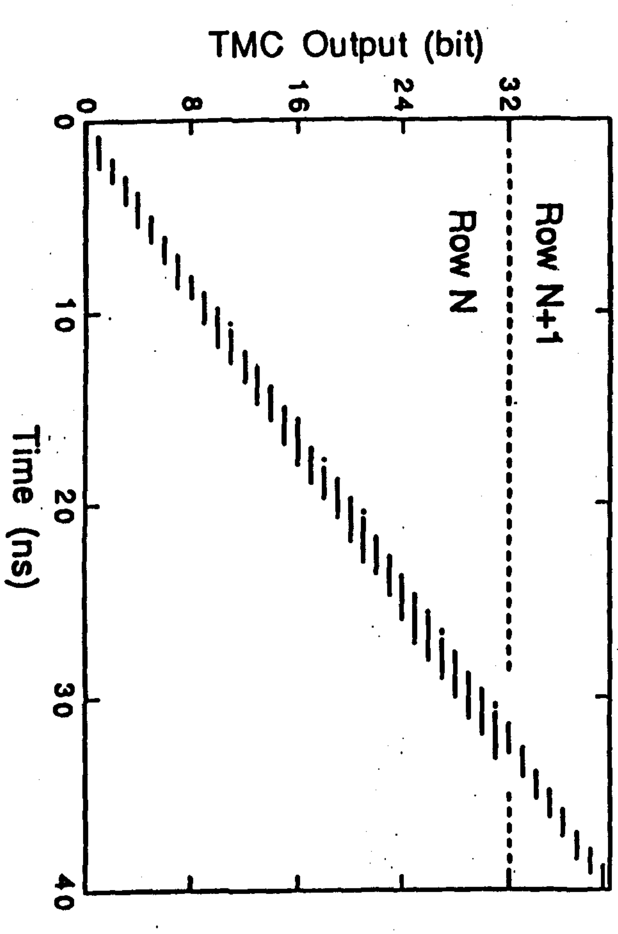

Fig. 8. Fine structure of the linearity curve. Output bits of 0 to 31 correspond to row N, and bits above 31 correspond to row N+1.

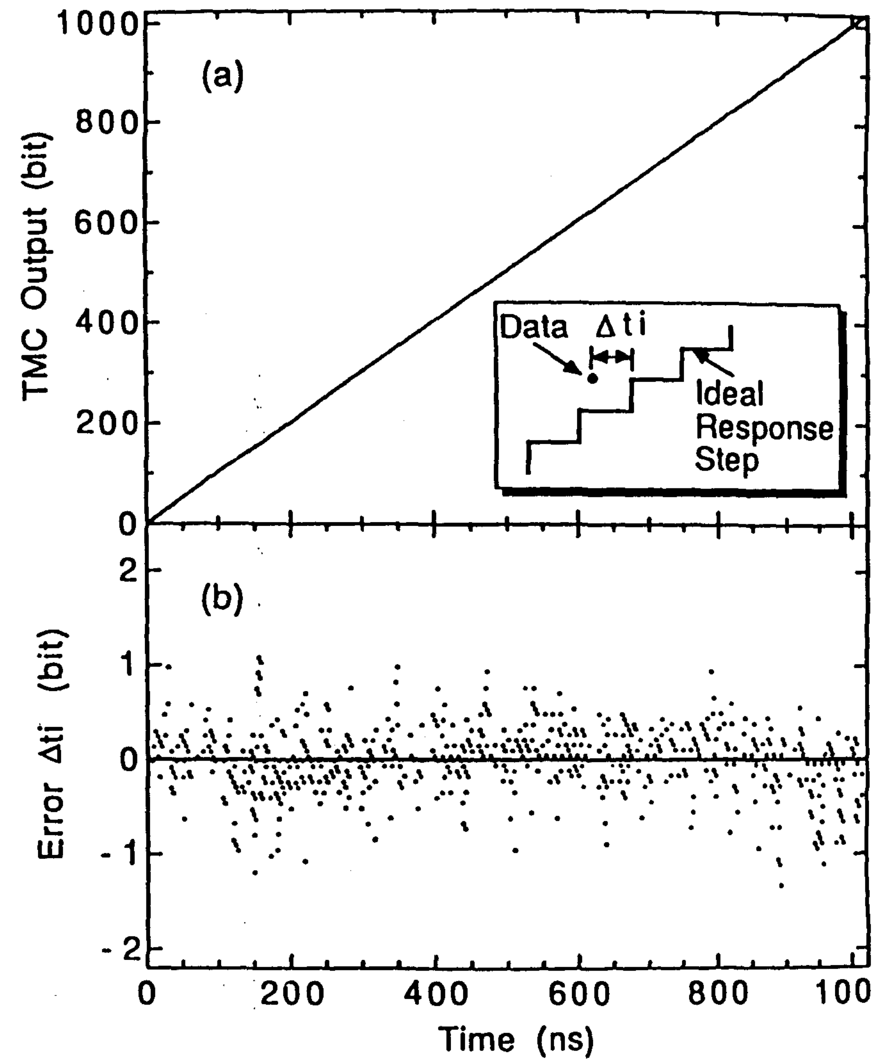

Fig. 7. (a) Linearity curve of the TMC1004. (b) Integral linearity error of the TMC1004. Da taken for 0.61 ns step and 1672 points.

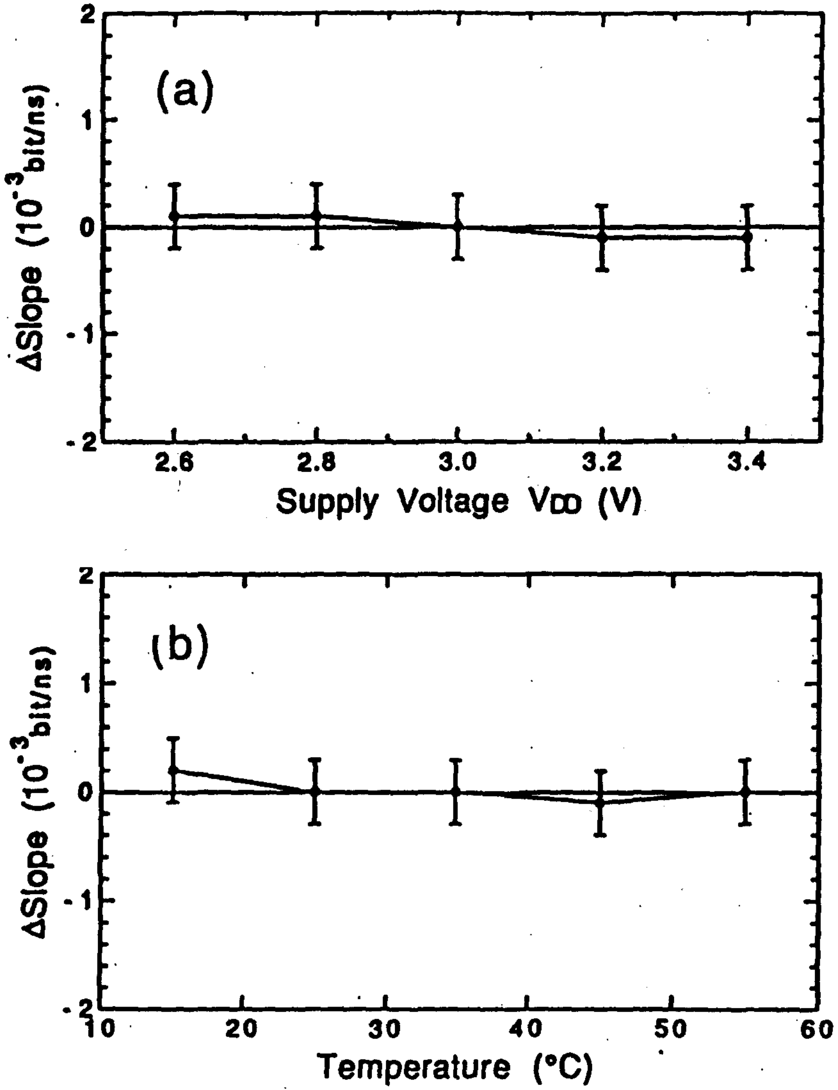

ig. 10. (a) Slope variation for supply voltages between 2.6 V to 3.4 V. (b) Slope variation for :mperature change from 15 °C to 55 °C. The data are plotted as a deviation from the data point of .0 V and 25 °C.

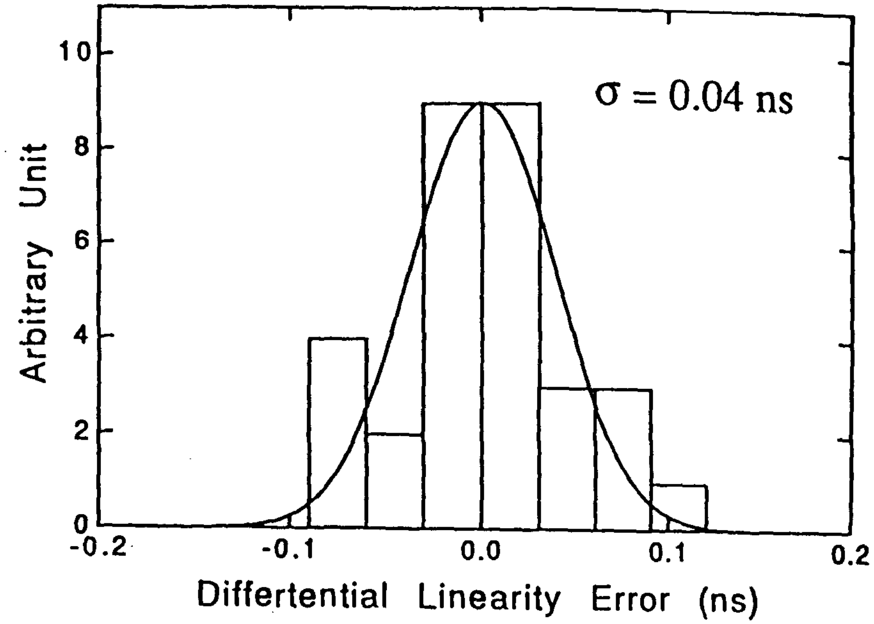

Fig. 9 Distribution of differential linearity error.

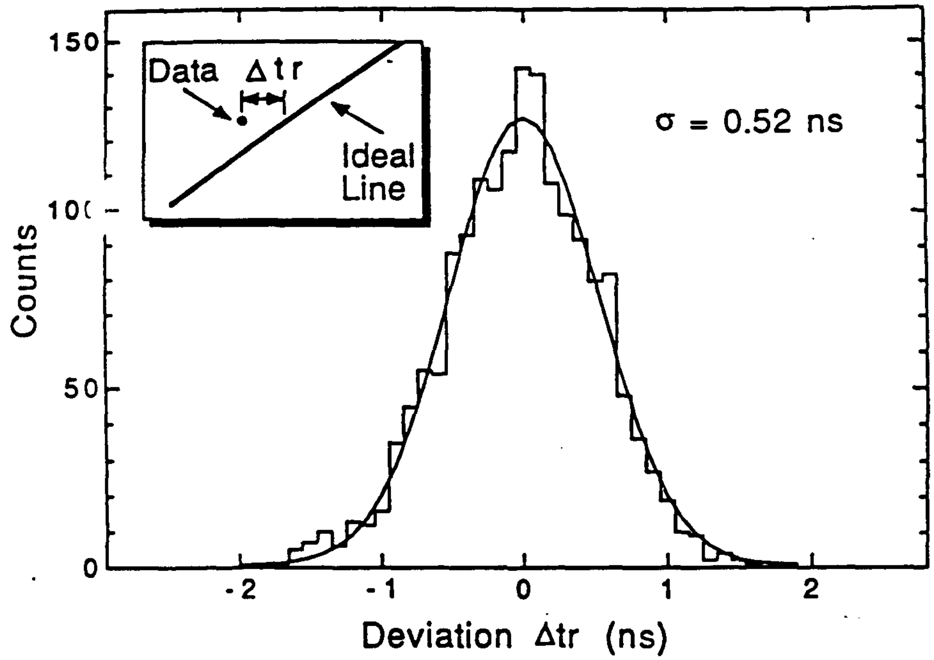

Fig. 11 Time resolution measurement. The deviation from ideal line includes both the digitization error and the TMC error.

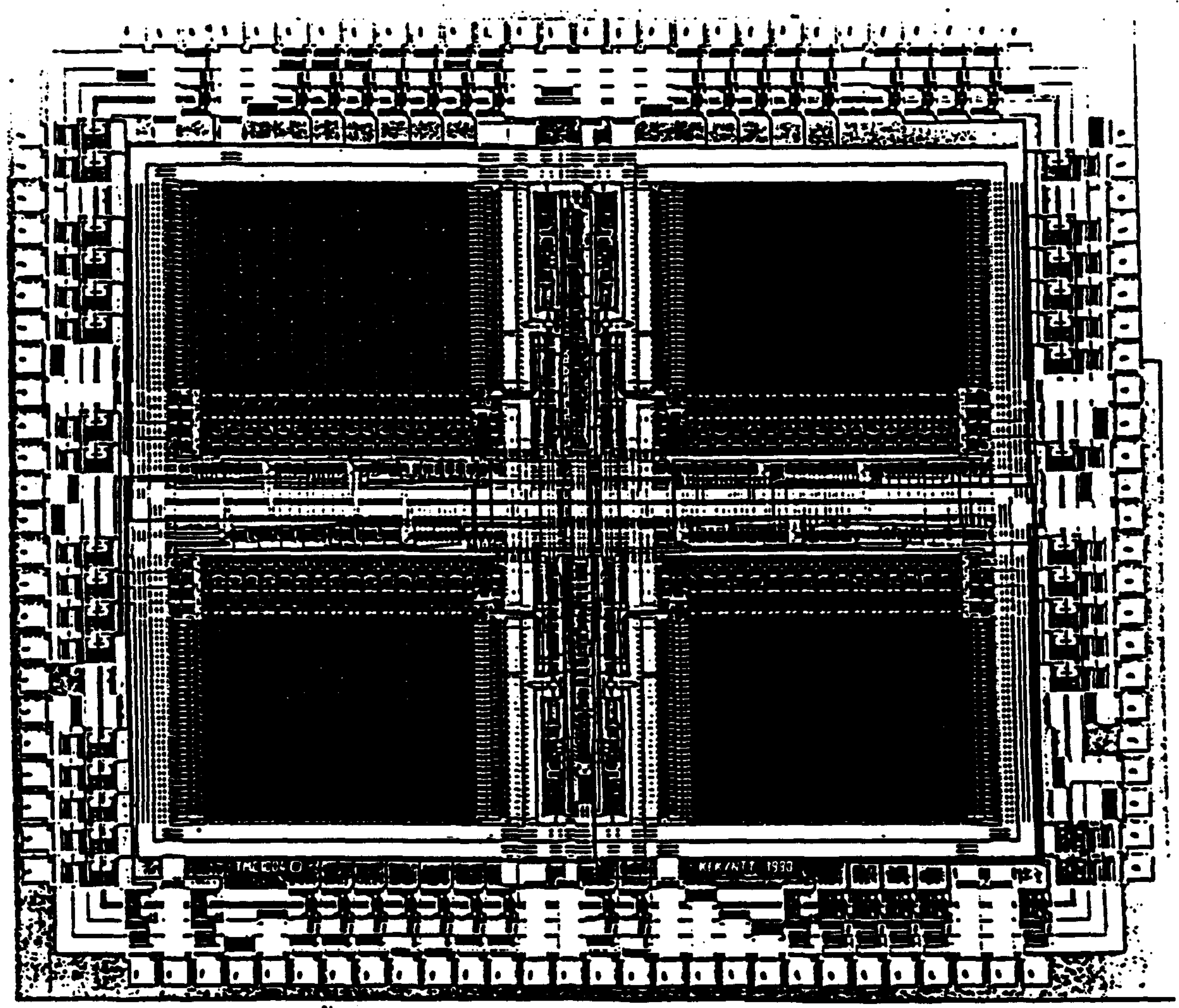

Fig. 12. Photograph of the TMC1004 chip.

of track crossings, the number of segments matching a generated track perfectly, the number containing one hit that does not belong, and the number with more than one wrongly assigned hit. For the inner superlayers, the efficiency is around 90%, if we take the strict criterion for success. If we accept one misassigned hit, the number is about 98%. Efficiency is higher for the outer superlayers, as expected from the decrease of occupancy with radius.

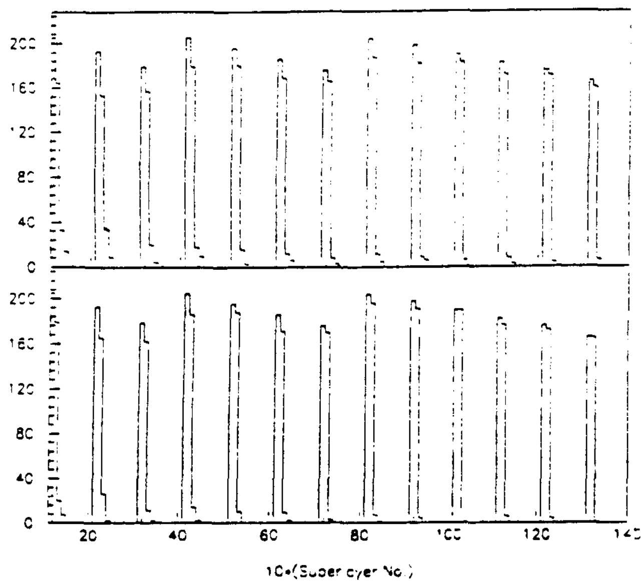

Figure 2. Segment finding efficiency and accuracy for (above) 8-layer and (below) 6-layer superlayers. For each superlayer (1-13) are plotted the reconstruction statistics described in the text.

Comparing the two histograms in Fig. 2, we find the efficiency is just as good if we have only six layers per superlayer as with eight. It should be noted here that we have not accounted for inefficiency of the cells.

A different accounting is illustrated in Fig. 3. The open histograms show the number of hits in each layer (identified with stiff tracks, as defined above); singly hatched histograms are those that have been correctly assigned to segments; doubly hatched histograms are the hits for which the correct choice of ambiguity sign was made. The performance with eight layers per superlayer is slightly better in terms of ambiguity resolution than with six.

Conclusions

We have developed a segment finding program that is quite efficient according to simulations for SSC conditions at design luminosity. Superlayers with either six or eight layers perform quite well, given that all cells are perfectly efficient (a limitation of the evaluation that will be removed in future work). These results are rather encouraging in view of the high occupancies at the smaller radii.

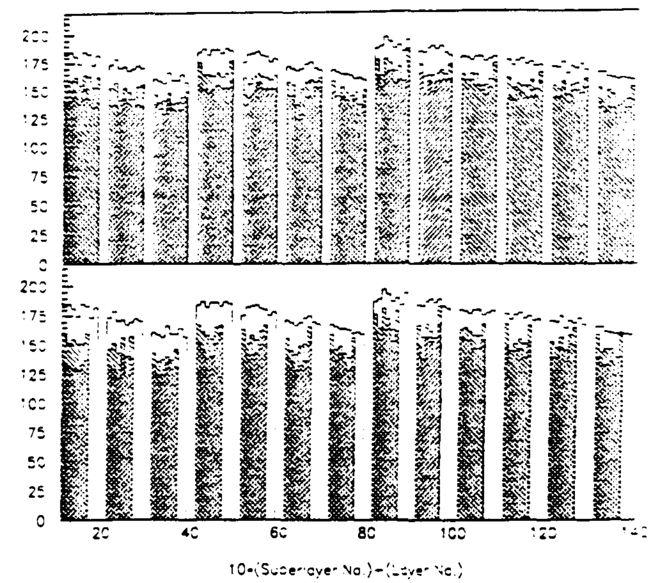

Figure 3. Linking accuracy by layer for (above) 8-layer and (below) 6-layer superlayers. Open histogram is number of layer crossings by stiff tracks; single hatched is hits correctly detected in the layer; double hatched is hits assigned the correct ambiguity sign.

*Work supported in part by the Department of Energy, contract DE-AC02-86ER40253, and by the Texas National Research Laboratory Commission.

[1] Solenoidal Detector Collaboration, Expression of Interest (1990).

[2] D. G. Cassel, et al., "Report of the Central Tracking Group", in *Proceedings of the 1986 Summer Study on the Physics of the Superconducting Super Collider*, Snowmass, CO, June 23-July 11, 1986.

[3] R. Donaldson and M. G. D. Gilchriese, *Experiments, Detectors, and Experimental Areas for the Supercollider*, Berkeley, CA, July 7-17, 1987.

[4] G. G. Hanson, B. B. Niczyporuk, and A. P. T. Palounek, "Wire chamber requirements and tracking simulation studies for tracking systems at the superconducting super collider", *Proceedings of the Wire Chamber Conference*, Vienna, Austria, February 13-17, 1989 (SLAC-PUB-4860).

[5] M. Asai, "Hit rates of the straw chamber tracker", SDC Note SSC-SDE-28 (Hiroshima Institute of Technology preprint 9001, 1990).

[6] A. P. T. Palounek, "Simulating a central drift chamber for a large solenoid detector at the SSC, using GEANT3", SLAC-PUB-4787(1988).

Segment Finding Efficiency in Superlayers

	8 layers		6 layers	
	inner	outer	inner	outer
$\epsilon_{\text{tube}} = 1 : \langle N_{hits} \rangle$	7.1		5.5	
ϵ_{seg} (perfect)	0.98 (0.89)	0.99 (0.96)	0.98 (0.92)	1.00 (0.98)
$\epsilon_{\text{tube}} = 0.95 : \langle N_{hits} \rangle$	6.8		5.2	
ϵ_{seg} (perfect)	0.97 (0.89)	0.99 (0.96)	0.96 (0.91)	0.97 (0.97)
$\epsilon_{\text{tube}} = 0.83 : \langle N_{hits} \rangle$	6.0		4.8	
ϵ_{seg} (perfect)	0.96 (0.89)	0.97 (0.94)	0.86 (0.81)	0.87 (0.86)

Segment finding efficiency in straw superlayers, as a function of the assumed tube efficiency, for 8– and 6–layer superlayers. The efficiency ϵ_{seg} allows at most one hit not originating on the track the segment is matched to. The corresponding number for no false hits is given in parentheses. Also given are the average numbers of hits included on segments, $\langle N_{hits} \rangle$.

SDC-90-00127

TRACK RECONSTRUCTION IN STRAW SUPERLAYERS*

W. T. Ford and M. Lohner
Department of Physics, University of Colorado
Boulder, Colorado 80309-0390

Abstract

We have developed a program to reconstruct track segments in dense wire drift chamber arrays. We compare our ISAJET simulations of signal and background events for SSC parameters with previous studies and report measurements of the pattern recognition efficiency for a large solenoid detector geometry. We find that the tracking is quite reliable for superlayers placed more than 50 cm from the beam axis. Without accounting for detection inefficiencies we find comparable performance for either six or eight layers per superlayer.

Introduction

We have begun a study of the reliability of track reconstruction in a combined silicon strip and wire drift chamber detector with solenoidal magnetic field under design for operation at the SSC[1]. Previous studies[2,3,4] have delineated some of the parameters for such a system. To make the pattern recognition manageable, cylindrical layers of drift cells are organized into groups (superlayers). A preliminary phase of data reduction is performed to identify strings of consecutive measurements along a track (segments), resolve right/left ambiguities, and fit for local position and direction. High particle fluxes pose the potential problems of information loss caused by pileup and confusion of the pattern recognition. Qualitative evidence that the information of interest can be extracted has been presented previously[4]. Here we discuss a quantitative study of pattern recognition at the segment finding level. One of the objectives is to establish the appropriate number of layers required in a superlayer, bearing in mind that less is better from the perspective of minimizing cost and the amount of material in the particle path.

The following sections of this paper describe the model used for simulation, the pattern recognition scheme, results and conclusions.

Event simulation and occupancy estimate

To make sure that our performance tests will be sufficiently realistic we first made some simple calculations of occupancies with the available physics process simulation programs, putting in the appropriate detector geometry but omitting detailed tracing of particle progress through the detector. Some of the omitted effects are accounted for by hand after comparison of our results with previous studies.

We use the ISAJET package to generate signal events. In the present work, these are production of Higgs bosons of mass 800 GeV/c^2 and their subsequent decay to leptons through Z^0 pairs. For the background, we ran ISAJET with the TWOJET option and a minimum transverse momentum ($p_\perp$) of 4.5 GeV/c, the value that gives a two-jet cross section equal to the total inelastic cross section extrapolated from data (about 95 mbarns). The charged particle yield is about 10 per unit of rapidity.

The detector geometry is that of the barrel straw tracker described in the SDC expression of interest[1], namely, eight superlayers at radii between 0.73 and 1.80 m and maximum half length 3.0 m, in a magnetic field of 2 T. To measure occupancy in this detector we compute the intersections of helical trajectories with the cylindrical detector surfaces. The number of crossings of one track may be zero (looper never reaches the layer), one (track exits through the coil and does not return), a few (looper traverses the superlayer, then reenters), or many (looper passes through the superlayer tangentially). We take the number of loops made before a track leaves the detector through the ends to be two, a rough average inferred from event pictures.

The integration time is taken to be 40 ns, based upon a drift cell radius of 2 mm, drift velocity of 100 μm/ns, and allowance for time-of-flight plus signal propagation delays and pulse duration. This implies that the detector integrates over 2.6 bunch crossings on average. At the design luminosity of 10^{33} cm^{-2}s^{-1} there are 1.6 interactions per crossing, so the detector sees 4.2 events per trigger. The occupancy we find from this calculation is shown by the dashed curve in Fig. 1.

An earlier study by Makoto Asai[5] can be compared with this one, if we interpolate to the approximate rapidity acceptance of SDC and correct for the slightly different straw radius. Asai's calculation used the PYTHIA event generator. The present result at 1 m superlayer radius is about ten percent higher than Asai's for primary particles only. He finds that with secondary interactions the occupancy is about two times as large. Therefore we have scaled our result to get the solid curve in Fig. 1.

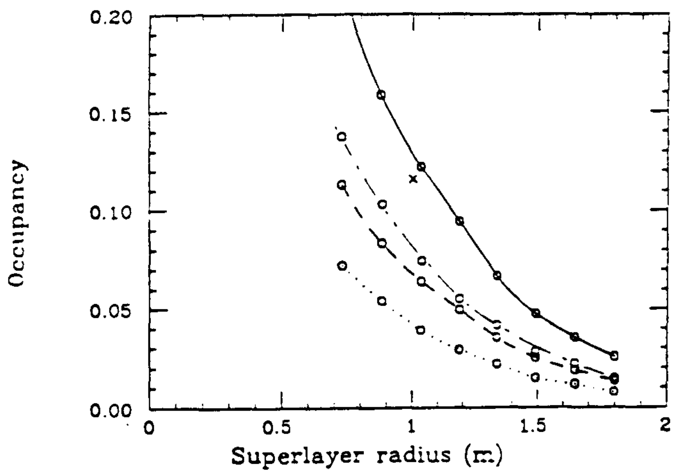

Figure 1. Occupancy vs radius in the SDC barrel straw tube tracker. The curves are: (dashed, dotted) primary charged tracks from (ISAJET,PYTHIA); (solid, dot-dashed) scaled by the factor 1.9 to account for secondary interactions.

Our calculation repeated with the PYTHIA event generator shows that the yield is about 60-70% of the ISAJET value (6.5 per unit of rapidity). The corresponding occupancy curves are included also in Fig. 1.

For the pattern recognition study discussed below we used a file of background events generated with ISAJET as described above, selecting the number of interactions from a Poisson distribution with mean of 4.2. Secondary interactions within the straw detector are included, but none in the silicon detector. The net occupancy is within the range of our present best estimates.

Pattern recognition

Each superlayer contains six or eight layers of straw tubes in a close-packed configuration. The time measurement can be converted into a simple circular contour of distance from the wire, to which the trajectory is tangent. This is true provided the time of arrival of the signal at the readout electronics is given solely by the drift time. In fact the delay from particle time of flight to the detector and propagation of the signal pulse along the wire to its end is not completely negligible: it amounts to the time equivalent of roughly 100 microns of track displacement, which is comparable to the measurement resolution from electron diffusion in the gas. Systematic variation of the pulse height may aggrevate this effect. Of course this delay is not random, and can be corrected for once a track is fully reconstructed and the axial position of the track is known. This information is not available, however, to the segment finder. It may be necessary to treat the track crossing time as a parameter to be inferred from the segment fit, along with the azimuth and direction of the track. In the present study, we have just set the resolution to 150 μm for the segment reconstruction to account for this effect.

The segment finder works as follows: one superlayer is considered at a time. A search over layers begins with the outer one (layer 8 if that is how many we have and we number from the interaction point outward). Each hit in that layer is a starting point for a candidate segment. The search continues in layers beginning with layer 1 for a hit with azimuth not too different from that of the first hit. This pair of hits is a seed for the segment; a segment is quite well determined for each of the four choices of right/left ambiguity for the seed hits.

The track is interpolated to layer 2 (or layer 3 if the second hit of the seed was found in layer 2, etc.). That layer is searched for a hit within a window of the interpolated track (both of the hit's ambiguity signs being considered). When one is found, the three hits are fed to a least-squares fit. The fit is subjected to a chi-squared test and, if passed, provides an updated set of segment parameters. The program is written so that this fit can be readily expanded to include additional parameters, such as the track crossing time, if needed. The search continues through all of the internal layers, with a chi-squared test and parameter update at each stage. When the layers and hits are exhausted, we ask are there enough hits; if so, the candidate is saved temporarily until all four right/left choices for the seed have been considered. Then the (up to four) condidates are compared. The test variable is: $(N_{layers} - N_{hits})^2 + \chi^2/\text{dof}$. The candidate with smallest test variable value is saved as a segment. Hits on the segment are excluded from further consideration as the search for more segments proceeds. The results below were obtained with the requirement of at least four hits per segment.

Performance results

For the evaluation studies we have used GEANT, with a geometry package written by Hanson, Palounek, et al.[4,6], which we shall refer to as the Large Solenoid Detector (LSD) design. There are thirteen superlayers of eight layers each, with radii between 0.57 and 1.6 m. The lengths are stepped in three groups (superlayers 1-3, 4-7, and 8-13). The straw diameters are graded from 4 mm at the inner radius to about 6 mm at the outermost. The straws run the full length of the detector.

The question we address is: given a reasonably stiff track ($p_\perp > 1$ GeV/c), which has crossed a superlayer, is it found, in the sense that we have a segment all of whose hits came from that track. The results are given in the plot of Fig. 2. For each superlayer there are four histogram bins: from left to right, these are the number